FEB - FRESENIUS ENVIRONMENTAL BULLETIN
Founded jointly by F. Korte and F. Coulston
Production by PSP - Vimy Str. 1e, 85354 Freising, Germany in
cooperation with PRT-Parlar Research & Technology
Vimy Str 1e, 85354 Freising
Copyright© by PSP and PRT, Vimy Str. 1e, 85354 Freising, Germany
All rights are reserved, especially the right to translate into foreign language or other processes - or convert to a machine language, especially for data processing equipment - without written permission of the publisher. The rights of reproduction by lecture, radio and television transmission, magnetic sound recording or similar means are also reserved.
Printed in Germany-ISSN 1018-4619

FEB-EDITORIAL BOARD

CHIEF EDITOR:
Prof. Dr. H. Parlar
Parlar Research & Technology-PRT
Vimy Str.1e
85354 Freising, Germany

MANAGING EDITOR:
Dr. P. Parlar
Parlar Research & Technology
PRT, Vimy Str.1e
85354 Freising, Germany

CO-EDITORS:

Environmental Spectroscopy
Prof. Dr. A. Piccolo
Universita di Napoli "Frederico II"
Dipto. Di Scienze Chemica Agrarie
Via Universita 100, 80055 Portici, Italy

Environmental Biology
Prof. Dr. G. Schuurmann
UFZ-Umweltzentrum
Sektion Chemische Ökotoxikologie
Leipzig-Halle GmbH,
Permoserstr.15, 04318
04318 Leipzig, Germany
Prof. Dr. I. Holoubek
Recetox-Tocoen
Kamenice126/3, 62500 Brno, Czech Republic
Prof. Dr. M. Hakki Alma
Igdir Universitesi
76000, Igdir, Turkey
Prof. Dr. A. Reichlmayr-Lais
Technical University of Munich
Arcisstraße 31
80333 Muenchen,Germany

Environmental Management
Dr. K. I. Nikolaou
Env.Protection of Thessaloniki
OMPEPT-54636 Thessaloniki
Greece

Environmental Toxicology
Prof. Dr. H. Greim
Senatkommision – DFG / TUM
85350 Freising, Germany

Environmental Proteomic
Dr. A. Fanous
Halal Control GmbH
Stahlstraße 44
D-65428 Rüsselsheim, Germany

Environmental Analytical Chemistry
Prof. Dr. M. Bahadir
Lehrstuhl für Ökologische Chemie
und Umweltanalytik
TU Braunschweig
Lehrstuhl für Ökologische Chemie
Hagenring 30, 38106 Braunschweig, Germany
Dr. D. Kotzias
Via Germania29
21027 Barza(Va), Italy
Prof. Dr. R. Kallenborn
Norwegian University of Life Sciences
Universitetstunet 3
1430 As,Norway

Environmental Education
Prof. Dr. C. Bayat
Yeni Yüzyil Üniversitesi
34010 Zeytinburnu, Istanbul, Turkey

Environmental Medicine
Prof. Dr. I. Tumen
Bandirma 17 Eylül Üniversitesi
10200 Bandirma, Turkey
Dr. J. Burhenne
Universitaet Klinikum
Im Neuenheim Feld 410
69120 Heidelberg,Germany

Advisory Board
K. Bester, K. Fischer, DCG. Muir,
R. Niessner,W.Vetter, D. Steinberg,
J. P. Lay, L. O. Ruzo

Marketing Manager
Cansu Ekici, MSC. of B.A.
PRT-Research and Technology
Vimy Str 1e
85354 Freising, Germany
E-Mail: parlar@wzw.tum.de
parlar@prt-parlar.de
Phone: +49/8161887988

Fresenius Environmental Bulletin is abstracted/indexed in:
Biology & Environmental Sciences, BIOSIS, CAB International, Cambridge Scientific abstracts, Chemical Abstracts, Current Awareness, Current Contents/Agriculture, CSA Civil Engineering Abstracts, CSA Mechanical & Transportation Engineering, IBIDS database, Information Ventures, NISC, Research Alert, Science Citation Index (SCI), Scisearch, Selected Water Resources Abstracts

CONTENTS

REVIEW

A REVIEW ON THE APPLICATION OF CARBONATION TECHNOLOGY FOR STEEL SLAG 10411
Qiang Wang, Xiaoliang Guo, Man Li

ORIGINAL PAPERS

ANALYSING INTENSITY EFFECT OF PRECOMMERCIAL THINNING ON GROWTH AND INCREMENT IN A BEECH *(Fagus orientalis Lipsky*) STAND 10427
Zafer Yucesan, Sena Karapinar

THE EFFECTS OF ADDITION MALIC ACID AND WHEY ON THE SOME PARAMETERS OF VETCH-WHEAT SILAGES 10435
Asuman Arslan Duru, Dilek Aksu Elmalı, Osman Yuksel, Harun Kutay

EFFECTS OF DIFFERENT COOKING METHODS ON PHYTOCHEMICAL CHARACTERISTICS OF CARROT (*Daucus Carota* L.) 10441
Esma Nur Gecer, Cemal Kaya

IMPLICATIONS OF VARIABILITY IN MECHANICAL CHARACTERISTICS OF RICE STRAW UNDER DIFFERENT MOISTURE, VARIETY AND LOADING RATE 10449
Shakeel Ahmed Soomro, Kunjie Chen, Altaf Ali Siyal, Abdullah Sessiz, Bakhtawar Wagan, Muhammad Sohail Memon, Zubair Ahmed Soomro, Mecha Peter, Haolu Liu, Zhenjie Yang

THE EFFECTS OF PHENOLIC, GALLOTANNIN, AND PROTEIN AMOUNTS IN PLANTS ON CONSUMPTION AMOUNT, SURVIVAL, AND PHENOLOXIDASE ACTIVITY OF *Malacosoma neustria* LINNAEUS, 1758 (LEPIDOPTERA: LASIOCAMPIDAE) LARVAE INFECTED WITH *Bacillus thuringiensis* SUBSP. *Kurstaki* 10457
Elif Fatma Topkara

FORAGE YIELD AND QUALITY OF SOYBEAN-MAIZE INTERCROPPING 10463
Ilker Inal, Derya Yucel, Celal Yucel, Rustu Hatipoglu

EFFECT OF BENZYL AMINO PURINE (BAP) AND ITS TIME OF APPLICATION ON THE DWARFISM AND FLOWER PRODUCTION OF CUT CARNATION (*Dianthus caryophyllus*) 10474
Saqib Khan Khalil, Abdul Basit, Izhar Ullah, Muhammad Sajid, Syed Tanveer Shah, Imran Ahmad, Fazal-i-Wahid, Qazi Shoaib Ali, Shamsher Ali, Imran Habib Khan, Sareer Ud Din

FABRICATION OF SEMICONDUCTOR PHOTOCATALYST AND ITS HIGH PHOTOCATALYTIC PERFORMANCE UNDER VISIBLE LIGHT IRRADIATION 10482
Guangyu Wu, Fang Ma, Ruofan Xiong, Zhouzhou Xu, Pingping Li, Jiangang Han, Weinan Xing

EXPERIMENTAL AND NUMERICAL ANALYSIS OF THE THERMAL PERFORMANCE OF NANOFLUIDS USED IN AUTOMOBILE RADIATORS 10492
Erdem Isik, Volkan Tugan

FLAVONOID CONTENTS ANTIOXIDANT AND NEUROPROTECTIVE ACTIVITIES OF CRATAEGUS MONOGYNA JACQ. LEAVES AND FLOWERS 10505
Gozde Elgin Cebe, Selin Aktar Kiremitci, M Alper Erdogan, Sibel Konyalioglu, Cigdem Yengin, Gulay Der, Emrah Kilinc

PHYLOGENETIC RELATIONSHIPS OF SOME PARDOSA (LYCOSIDAE) SPECIES 10515
Adile Akpinar, Aynur Yuncu, Derya Arslan, James Stuart Lucas, Turkan Gurer, Muhammed Ismail Varol

EFFECTS OF DIFFERENT HARVEST TIMES AND LEAF POSITIONS ON STEVIOL GLYCOSIDES CONTENT IN *Stevia rebaudiana* BERTONI UNDER MEDITERRANEAN CLIMATE CONDITIONS 10522
Kenan Turgut, Mustafa Karhan, Ahmet Hacioglu, Melis Yildiz, Narin Unal

RESEARCH ON THE COORDINATED DEVELOPMENT MODEL OF ECOLOGICAL RESOURCES AND ECONOMY IN CHANGCHUN CITY 10530
Hongxiu Cui, Wei Wang

SYMBIOTIC PROPAGATION OF THE WET MEADOW ORCHID *Anacamptis laxiflora* FOR CONSERVATION AND REINTRODUCTION 10535
Yasemin Ozdener Kompe, Haydar Karakaya, Vildan Akin Mutlu

RESEARCH ON THE INNOVATION OF ECOLOGICAL ECONOMY DEVELOPMENT PATH: BASED ON ECOLOGICAL PERSPECTIVE 10545
Huancai Peng

STUDY ON ECOLOGICAL CIVILIZATION CONSTRUCTION FROM THE PERSPECTIVE OF PUBLIC GOVERNANCE 10551
Dandan Cui, Ya Zhou

STUDY ON THE TOURISM MANAGEMENT MODE IN ECOLOGICALLY FRAGILE AREAS BASED ON BP NEURAL NETWORK 10559
Yujin Kan, Zhengbin Dou, Rong Hu

THE EFFECTS OF PICNIC AREAS ON EPIPHYTIC LICHEN DIVERSITY AT ABIES FORESTS IN ULUDAG NATIONAL PARK, TURKEY 10568
Saban Guvenc, Hulya Ozturk Kula

IMPACT OF DIFFERENT TILLAGE PRACTICES ON DISTRIBUTION OF SOIL ORGANIC CARBON AND TOTAL NITROGEN IN CLAY LOAM SOIL 10576
Tomas Zukaitis, Inga Liaudanskiene, Aleksandras Velykis

THE EFFECT ON SENSORY QUALITY OF THE STUFFED PASTA (MANTI) OF INCREASED MALONDIALDEHYDE AMOUNT WITH THE UV-C RADIATION AND STORAGE 10586
Suleyman Gokmen, Abdullah Caglar

SOIL SATURATED HYDRAULIC CONDUCTIVITY AND ITS RESPONSE TO MACROPORE AND ROCK FRAGMENT NETWORK CHARACTERISTICS IN DIFFERENT FOREST COMMUNITIES 10592
Chen Meng, Jianzhi Niu, Lingtong Du, Naiping Song

FRACTURING EFFECT OF COALBED METHANE RESERVOIRS IN BLOCK A IN THE SOUTHERN QINSHUI BASIN CHINA 10602
Chao Cao, Haibin Gao, Peng Kong, Qi Yang, Ruicheng Wang, Jian Li, Zhenguo Liu, Bingnan Wang, Cheng Jiang ,Minghao Wang

FUZZY COMPREHENSIVE EVALUATION OF DEBRIS FLOW RISK BASED ON PROBABILITY COMBINED WEIGHT 10610
Li Li, Shixin Zhang, Yue Qiang, Dongsheng Zhao, Chaoqiong Liu, Zhou Zheng, Changsi Xia

RESEARCH ON THE PLANNING METHOD OF SHARED SPACE IN OLD RESIDENTIAL DISTRICT BASED ON THE IMPROVEMENT OF ECOLOGICAL ENVIRONMENT 10625
Chao Chen, Qiang Lu

ANALYSIS OF THE EFFECT OF URBAN CHANGE ON URBAN SILHOUETTES BY ENTROPY METHOD 10633
Cengiz Acar, Alper Uzunali

EXPERIMENTAL STUDY ON PHASE DIFFERENCE DETECTION METHOD OF CORIOLIS FLOWMETER BASED ON SVD AND NUTTALL WINDOW FOURIER TRANSFORM 10643
Lei Huang, Shidong Wu, Qian Zhang, Xueyang Xing

RESEARCH ON THE RELATIONSHIP BETWEEN CHINA'S ENERGY CONSUMPTION AND ECONOMIC GROWTH BASED ON BIG DATA 10652
Yang Chen, Yu Yu

RESEARCH ON CHINA'S TOURISM MODEL FROM THE PERSPECTIVE OF BIG DATA, BASED ON THE ECOLOGICAL PERSPECTIVE 10659
Weijuan Yuan

RESEARCH ON THE SPATIO-TEMPORAL EVOLUTION OF TOURISM ECO-EFFICIENCY BY USING THE ECOLOGICAL FOOTPRINT MODEL 10665
Libo Lin

EXPERIMENTAL SIMULATION OF RIVER ENVIRONMENT TRANSFORMATION AND DEVELOPMENT 10675
Bowen Xue, Junhua Li, Yang Zhang, Linjuan Xu

HISTOPATHOLOGICAL EXAMINATION OF THE EFFECT OF BLACK SEED (NIGELLA SATIVA) OIL ON THE METHOTREXATE-INDUCED GASTROINTESTINAL MUCOSA INJURY AND HEPATOTOXICITY IN MICE 10685
Mansur Seymen Segmenoglu, Huseyin Topcuoglu

EXPERIMENTAL STUDY ON THE ACCUMULATION OF HEAVY METALS IN DIFFERENT PARTS OF FORAGE UNDER HEAVY METAL POLLUTION ENVIRONMENT 10690
Ao Sun, Huifen Deng, Fang He, Haobang Li, Yang Luo, Cheng Huan, Sheng Li, Kangle Yi, Jianbo Li

RESEARCH AND CHARACTERISTIC EVALUATION OF A NOVEL ENVIRONMENTALY FRIENDLY WATER-BASED DRILLING FLUID 10697
Yan Zhang

CORRELATION BETWEEN MENTAL RESILIENCE-MEDIATED CANCER-RELATED FATIGUE AND POST-TRAUMATIC GROWTH IN PATIENTS WITH HEAD AND NECK TUMORS 10705
Mingkun Han, Xue Yang, Yang Wang, Jing Lv

RESEARCH ON THE ROLE OF TOURISM IN ECONOMIC DEVELOPMENT: BASED ON AN ECOLOGICAL PERSPECTIVE 10712
Xiaofang Yang, Bo Dai, Zhengfa Han

ANALYSIS OF THE IMPACT OF THE ECOLOGICAL ENVIRONMENT ON THE RAILWAY CONSTRUCTION BASED ON ANALYTIC HIERARCHY PROCESS (AHP) AND PROBABILITY STATISTICS 10718
Haixia Du, Zhenzhen Li

GIS ASSESSMENT FOR GROUNDWATER QUALITY OF DISTRICT MULTAN, PAKISTAN 10728
Muhammad H Mahmood, Zahid M Khan, Muhammad Sultan, Zawar Hussain, Amman Ullah, Shazia Hanif, Yousaf R Taseer, Muhammad A Imran, Riaz Ahmad, Tallat Mehmood, Muhammad Aleem

RESEARCH ON THE EVALUATION OF ECOLOGICAL ENVIRONMENT QUALITY IN RURAL TOURISM AREAS 10738
JingYu

NUMERICAL SIMULATION OF VORTEX DRAINAGE GAS RECOVERY BASED ON ORTHOGONAL EXPERIMENT 10748
Jingming Yang, Siyang Li, Yueqi Zhang, Hao Liu, Yuhui Zhou

FISHEYE IMAGING APPROACH WITH THE SUPERVISED MACHINE LEARNING FOR THE DETERMINATION OF FRESHNESS OF FISH 10754
Hamza Feza Carlak, Kemal Kandemir, Mustafa Unlusayin

ANALYSIS OF ECOLOGICAL ADAPTABILITY OF PREFABRICATED RESIDENTIAL BUILDINGS: A CASE STUDY OF SOUTHERN ANHUI, CHINA 10763
Nan Liang, Xiaohui Fu, Qian Li, Mengxuan Yu

WATER QUALITY EVALUATION FOR IRRIGATION PURPOSE AND HYDROCHEMICAL ELUCIDATION OF SHALLOW GROUNDWATER IN HUAIBEI PLAIN: A CASE STUDY 10772
Xinyi Qiu, Linhua Sun, Weihua Peng, Kai Chen, Xiang Zhao

MODIFICATION AND PERFORMANCE EVALUATION OF INDUSTRIAL FODDER CHOPPING MACHINE 10782
Rashad A Hegazy, Wael M Moussa, Ali B El-Nagar, Ismail A Abdelmotaleb

CURRENT EPIDEMIOLOGICAL STATUS OF CUTANEOUS LEISHMANIASIS IN DIFFERENT VILLAGES OF DISTRICT MALAKAND KP PROVINCE PAKISTAN:A PERSPECTIVE STUDY 10790
Abdullah, Muddaser Shah, Muhammad Salman, Sohail Ahmad Jan, Ayesha Bibi, Zobia Afsheen, Muhammad Riaz, Muddasir Khan, Sidra Mubin, Parveen Bibi, Obaid Ullah, Attaullah

MECHANISM OF FENOXAPROP-p-ETHYL RESISTANCE IN *Avena fatua* L. POPULATIONS FROM CHINA 10797
Ninghai Lu, Guilei Hu, Geng Wang, Fanbin Kong, Kaishu Du, Baizhong Zhang, Xiling Chen

STUDY ON GREEN ENERGY-SAVING BUILDING UNDER COMPLEX ENVIRONMENT BASED ON DATA MINING 10807
Xiaoli Liu, Shuaixing Ren, Mengqi Jiang

AN EMPIRICAL ANALYSIS OF THE RELATIONSHIP BETWEEN ECONOMIC DEVELOPMENT AND ENVIRONMENTAL POLLUTION IN HENAN PROVINCE, CHINA 10815
Lei Guo

DETERMINATION OF SOME SELECTED PHARMACEUTICALS IN MARINE BIOTA: A CASE STUDY IN THE ISTANBUL METROPOLITAN AREA, TURKEY 10825
Nagihan E Korkmaz, Nuray Balkis Caglar, Abdullah Aksu

DETERMINATION OF ANTIOXIDANT CAPACITY AND CHANGES OF BIOCHEMICAL PARAMETERS ON CALVES PERSISTENTLY INFECTED WITH BOVINE VIRAL DIARRHEA VIRUS 10836
Oguzhan Avci, Sibel Yavru, Atilla Simsek, Orhan Yapici, Oya Bulut, Irmak Dik

IMPACT OF VARIOUS FUNGICIDES AGAINST BLACK SPOT SEVERITY AND INCIDENCE CAUSED BY *Diplocarpon rosae* 10841
Muhammad Zeeshan Mansha, Hafiz Muhammad Aatif, Muhammad Ijaz1, Amer Habib, Muhammad Zeeshan Mansoor, Kamran Ikram, Hafiz Tassawar Abbas, Imran Khalid

STUDY ON EVALUATION OF SOIL HEAVY METAL POLLUTION IN COPPER-SULFUR MINING AREA BASED ON TRACER METHOD 10849
Ying Chen, Chong Chen, Qiang Hao, Guoxin Li, Lijun Qian, Lihua Ou, Xiaobin Huang

EXPERIMENTAL STUDY ON THE CONSTRUCTION AND PLUGGING PERFORMANCE OF RESIN GEL SYSTEM BASED ON NANO SILICON MATERIAL: A CASE STUDY OF BLOCK MJG-60, ORDOS BASIN, CHINA 10856
Guocheng Wan, Zhixiong Xu, Xuewen Liu, Hengbo Mao, Wei Wang, Wenhua Zhao, Bo Wang, Wenjie Zhou, Mancang Dong

GAMMA RAY RADIATION RESEARCH IN BUILDING MATERIALS 10863
Aydan Altikulac

EFFECTS OF PHYSICOCHEMICAL FACTORS ON THE NITROGEN TRANSFORMATION FUNCTIONAL GENES OF MICROORGANISMS DURING THE INTERMITTENT AERATION IN POLLUTED RIVER 10871
Hua Zhang, HaiTao Tao, Jian Huang, ShanShan Xi, JinHua Wang, Tao Luo, XueFeng Cao

STUDY ON DYNAMIC UPDATING ALGORITHM OF MARINE ALGAE STATISTICAL DATABASE 10880
Lina Cui

ASSESSMENT OF SOIL EROSION INTENSITY IN THE KUTINSKA RIVER BASIN IN THE PERIOD 1971-2016 10890
Gocic Milena, Dragicevic Slavoljub, Zivanovic Stanimir, Ivanovic Radomir, Martic Bursac Natasa, Stricevic Ljiljana, Radivojevic Aleksandar, Zivkovic Jelena

OPTIMIZATION PROTOCOL FOR IN VITRO ESTABLISHMENT OF SELECTED APRICOT GERMPLASM 10899
Farhat Ali Khan, Aftab Afzal, Shazia Erum, Shabana Irum, Haji Khan, Zahid Hussain, Hassan Sher, Nadia Bostan, Fazal Rabi

COMPARATIVE EVALUATION OF STAND-ALONE HYBRID POWER SYSTEM WITH DIFFERENT ENERGY STORAGES 10908
Zafer Ozturk, Salih Tosun, Ali Ozturk, Onur Akar

STUDY ON THE COUPLING AND COORDINATED DEVELOPMENT OF TOURISM ECONOMY AND ECOLOGICAL ENVIRONMENT IN GUIZHOU PROVINCE, CHINA 10925
Wenlu Li, Li Luo

THE EVALUATION OF COORDINATED DEVELOPMENT OF AGRICULTURAL ECONOMY AND RURAL ECOLOGICAL ENVIRONMENT TAKING SINO AFRICAN COOPERATION PROJECT AS AN EXAMPLE 10933
Jiang Ou, Jie Wang

ORGANIC AMENDMENTS AND NANO-MICRONUTRIENTS RESTORE SOIL PHYSICO-CHEMICAL PROPERTIES AND BOOST WHEAT YIELD UNDER SALINE ENVIRONMENT 10941
Sobhy Sorour, Megahed Mohamed Amer, Dalia El Hag, Etab Ahmed Hasan, Mahrous Awad, Ferhat Kizilgeci, Ferhat Ozturk, Muhammad Aamir Iqbal, Ayman El-Sabagh

ECO-PHYSIOLOGICAL RESPONSE OF SELECTED FARM TREE SPECIES UNDER SALINE FIELD CONDITIONS AFTER TREATING WITH ORGANIC AMENDMENTS DURING NURSERY STAGE 10951
Muhammad Talha Bin Yousaf, Muhammad Farrakh Nawaz, Sadaf Gul, Irfan Ahmed, Muhammad Rizwan, Ghulam Yasin, Taimoor Hassan Farooq

FEATURE EXTRACTION METHOD OF ECOLOGICAL ENVIRONMENT LANDSCAPE REMOTE SENSING IMAGE BASED ON GIS TECHNOLOGY 10961
Chunjie Wang

GROWTH PERFORMANCES OVER A SLOPE RANGE IN NATURAL REPRODUCTIONS OF ANATOLIAN BLACK PINE 10970
Yunus Eser

CYTOGENETICS ANALYSES OF THE GENUS SPERMOPHILUS CUVIER 1825 (MAMMALIA RODENTIA) DISTRIBUTED IN TURKEY 10976
Safak Bulut, Cemil Arslan

A RESEARCH ON IMPROVING SEED QUALITY (PELLETING) IN TRUE POTATO OF 101 (NIF) GENOTYPE 10983
Zeynep Dumanoglu, Gulsum Ozturk

IMPACT OF CHITOSAN PMAA-NPK NANO COMPOSITE AND TRADITIONAL MINERAL-NPK FERTILIZERS ON GROWTH, YIELD AND BIOCHEMICAL PARAMETERS OF EGYPTIAN COTTON CV.GIZA 94 (*Gossypium barbadense* L.) 10989
Abdel Hamed M Omar, Mohamed E El-Menshawi, Khaled Y Farroh, Samira A F El-Okkiah, Samir A F El-Okkiah

EVALUATION OF ANTIMICROBIAL, ANTIOXIDANT AND ENZYME INHIBITORY POTENTIAL OF FIXED OIL EXTRACTED FROM STEM BARK OF *Acacia stenophylla* 11002
Nadia Khan, Arshad Iqbal, Khushnood Ur Rehman, Muhammad Hamayun, Farooq Shah, Amjad Iqbal, Anwar Hussain, Jamshaid Ahmad, In-Jung Lee

NOTICE

CONTENT AND SAFETY OF FOUR MAIN HEAVY METALS IN HARD GELATIN CAPSULE SHELL 11009
Jin Xiaoli, Wang Lei, Zhu Huanlei

GREEN REMANUFACTURING EVALUATION MECHANISM BASED ON FAULT DIAGNOSIS OF ELECTRIC SPINDLE FROM THE PERSPECTIVE OF ENVIRONMENTAL PROTECTION 11011
Haixiang Yu, Meng Wang

LETTER TO THE EDITOR

MAPPING OF HEXAVALENT CHROMIUM REMOVAL RESEARCH: A BIBLIOMETRIC ANALYSIS OF RESEARCH OUTPUTS FROM 1975 TO 2012 11025
Baogang Zhang1,*, Ye Liu1, Wenli Huang2, Jiaxin Li1, Chuanping Feng1, Weiwu Hu1

© by PSP Volume 30– No. 09/2021 pages 10411-10426 Fresenius Environmental Bulletin

REVIEW

A REVIEW ON THE APPLICATION OF CARBONATION TECHNOLOGY FOR STEEL SLAG

Qiang Wang[1,2,*], Xiaoliang Guo[1], Man Li[1]

[1]School of Civil Engineering and Architecture, Anhui University of Science and Technology, Huainan 232001, China
[2]Institute of Environment-friendly Materials and Occupational Health, Anhui University of Science and Technology, Wuhu, 241003, China

ABSTRACT

Steel slag is a solid waste discharged from the iron and steel met allurgical industry. A large amount of the accumulation occupies land, leading to the environmental pollution. Besides, the heavy metal elements in steel slag infiltrate into soil to pollute groundwater, which also brings potential threat to people's lives. Meanwhile, with human industrial and agricultural activities, the emission of carbon dioxide, a main source of greenhouse effect is increasing ceaselessly, which can cause health and environmental problems. At present, scholars at home and abroad have carried out research on the comprehensive utilization of carbon dioxide and steel slag. Carbonized steel slag is beneficial to the stability and the activity of steel slag, which is also an available way to the application for beneficial in the use of carbon dioxide. In this paper, the effects on the mechanical properties, including water content, hydration time, admixture, temperature, carbonization time, carbon dioxide concentration, forming pressure and mineral composition, as well as the and carbon sequestration effect of carbonized steel slag are analyzed. Furthermore, in view of the present situation and existing problems, this paper also introduces the research suggestion for further development and popularizing of the application of carbonized steel slag.

KEYWORDS:
Carbon dioxide fixation, Carbonized steel slag, Mechanical properties, Resource utilization

INTRODUCTION

With the rapid development of the steel industry, China has become the world's largest steel consumer, and its crude steel production accounts for 50% of the global production [1]. As a kind of waste residue produced in steel-making process of iron and steel industry, the conversion rate of steel slag is about 10%~15% per ton of steel [2-3]. In 2019, China's steel production was 996.3 million tons. According to the calculation, China's steel slag production in 2019 is about 150 million tons [4]. At present, the utilization of steel slag in developed countries such as the United States and Japan has basically reached the balance of production and use, while the comprehensive utilization rate of steel slag in China is only 20%, and nearly 90 million tons of steel slag are not effectively utilized every year, which is far lower than that in many developed countries. Moreover, a large number of steel slag is stacked and idle, which not only occupies a lot of land, but also the heavy metal ions and alkali metal ions contained in steel slag infiltrates into the soil, causing groundwater pollution and result in dust raising, which significantly affects the urban air quality and the living environment, leading to the serious social harm [5-8]. Therefore, there are more focus on the application of steel slag to protect ecological environment and promote resource recycling as well as social sustainable development [9].

In addition, with the development of global industrialization, the greenhouse effect is becoming more and more serious. Meanwhile, global warming has become the hot issue of global climate change. The increase of anthropogenic greenhouse gas emissions is one of the main causes of global warming [10-12]. Since the pre-industrial era, the carbon dioxide content in the atmosphere has increased by 39%, mainly due to the large use of fossil fuels [13]. The combustion of fossil fuels produces a lot of CO2, leading to the occurrence of greenhouse effect. With the continuous development of human industrial and agricultural activities, the emission of CO2 is also increasing year by year. In 2017, global carbon emissions increased by 1.6% [14]. The greenhouse effect caused by carbon dioxide has a great impact on natural resources, human activities, industrial production and so on. Besides, a large number of carbon dioxide emissions not only belong to the category of environmental protection, but also a development problem, which is closely related to the global green development [15-18]. Therefore, how to deal with the emission reduction and rational utilization of greenhouse gases, especially carbon dioxide, it has become a key problem.

In order to provide a sustainable method for the reuse of steel slag and carbon dioxide, was found that the absorption of carbon dioxide by minerals is a long-term carbon dioxide storage technology, that is,

using minerals rich in alkaline earth metals such as calcium and magnesium ions to react with carbon dioxide to produce high thermal stability and environment-friendly carbonate products [19-20]. In addition, it was found that steel slag has high carbonation activity in CO2 rich environment [21-23]. The carbonation reaction between steel slag and CO2 can not only absorb and solidify greenhouse gases, but also form stable carbonate products to produce strength, which can be used to prepare building materials [24-25]. Using the characteristic of a large number of carbonized active components in steel slag, the preparation of steel slag products by carbonization technology will be an effective way to improve the utilization ratio of both steel slag and CO2 utilization [26-30]. In a word, steel slag carbonization has good economic, environmental and social benefits.

MATERIALS AND METHODS

Basic properties and classification of steel slag. Steel slag is a kind of met allurgical waste containing several specific oxides, which is produced by oxidation of slag making materials (lime, fluorite, etc.). Its main chemical composition is SiO2、CaO、Fe2O3、FeO、Al2O3 and MgO. Among that, CaO content accounts for 40% to 50%.The main mineral composition of steel slag is dicalcium silicate, including (β-C2S) and (γ-C2S),(C4AF), silicates, small amounts of tricalcium silicate (C3S).In addition, it also contains a small amount of periclase, magnesium iron spinel and other minerals. The high content of inert phase [31] leads to relatively low hydration activity of steel slag. Therefore, Steel slag products have low mechanical properties, not suitable for using as building materials. Furthermore, according to the difference of alkalinity, steel slag can be divided into high alkalinity, medium alkalinity and low alkalinity steel slag [32]. The phase composition of steel slag with different basicity is different. In the high alkalinity steel slags, the round granular, leaf-like and needle-like dicalcium silicate (C2S), hexagonal-plate-like and needle-like tricalcium silicate (C3S), and irregular-shaped iron-aluminum-calcium phase and magnesium-iron solid solution are dominant. The solid solution of C2S, iron-aluminum calcium and magnesium-iron are the main components in medium alkali steel slag, and a small amount of RO phase is also found. In low-alkali steel slag, calcium ferrate and RO phase are the main ones. The high alkalinity steel slag formed under the condition of rapid cooling has higher hydration activity. Because the chemical and mineral composition of steel slag is similar to that of Portland cement clinker, which has great potential to be used in cement concrete industry.

Hydration activity of steel slag. The hydration of steel slag is a slow process. And the hydration induction period is long, which has little effect on the development of early strength, but it has a great contribution to the improvement of later strength. Besides, the early hydration reactivity of steel slag can be stimulated by high temperature and alkaline environment. The hydration activity of steel slag is relatively low and the hydration activity is obviously lower than that of cement clinker. Meanwhile, the content of Fe2O3 and FeO in steel slag is larger, but the content of CaO and SiO2 is smaller, so the content of calcium silicate in steel slag is obviously smaller than that in cement clinker. At present, there are three main methods for activation of steel slag: mechanical activation, chemical activation and thermal activation.

Mechanical activation is physical activation, which mainly uses mechanical force to improve the activity of steel slag. During the grinding process, the particles become smaller, and the specific surface area increases. Moreover, the mechanical energy is converted into the internal energy and surface energy of the new particles, and the bond energy of the crystal changes, destroying the crystal structure, causing defects, dislocation, distortion and recrystallization in the lattice of the material, forming an amorphous structure soluble in water, increasing the hydrophilic force of the steel slag, accelerating the water molecules into the particles, destroying the structure of the steel slag particles and increasing its reactivity [33]. In addition, the increase of specific surface area increases the contact area between steel slag and water per unit mass, which promotes the hydration reaction. Li Qian [34] and Xu Peng et al [35] considered that controlling the specific surface area of steel slag powder is 450~500 m2/kg which is more beneficial to stimulate the early hydration reaction activity of steel slag. And Wang [36] et al. considered that too large specific surface area of steel slag powder can improve its early activity, but it will reduce its later activity. It is generally believed that the particles with particle size less than 30μm contribute to the activity of steel slag. [32]

In the process of chemical activation Si-O and Al-O bonds are the main chemical bonds of vitreous structure in steel slag, which exist in the form of [SiO4] tetrahedron and [AlO4] tetrahedron or [AlO6] coordination polyhedron, respectively. Furthermore, steel slag produces fracture bonds during grinding. In alkaline environments, the [SiO4] tetrahedron and [AlO4] tetrahedron are depolymerized to form H3SiO4 - and H3AiO42 -, respectively. And then react with metal cations such as Ca2+、Na+ in the solution to form zeolite hydration products. Besides, the formation of these zeolite hydration products consumes the H3SiO4- and H3AlO42- of steel slag depolymerization, reducing H3SiO4- and H3AlO42- concentration in solution, which causes the Si-O and

Al-O bond to break continuously in the steel slag vitreous structure. Finally, complete dissociation of the vitreous. At present, the commonly used steel slag activators mainly include alkali metal salt, gypsum and so on. Ding Zhu [37] studied the hydration activity of water-quenched steel slag and hot-cast magnetic separation steel slag under the action of gypsum, sodium carbonate and sodium hydroxide. The results showed that water quenched steel slag had higher hydration activity, and gypsum and sodium carbonate had better excitation effect on the hydration activity of steel slag. The optimal content (mass fraction, the same as below) of gypsum and sodium carbonate is 4% and 1.5% respectively, while sodium hydroxide has no obvious excitation effect.

The mechanism of thermal activation is as follows: under autoclaved conditions, the network structure of vitreous body in steel slag is subjected to thermal stress, and its network formation bond such as Si-O bond and Al-O bond are more likely to break, which is beneficial to the depolymerization of vitreous body and the rate of hydration reaction. Moreover, the reaction activity of f-CaO was improved under high temperature, therefore, the activity of steel slag was significantly improved. Lin Zongshou [38] mixed steel slag, fly ash and gypsum evenly according to the prescribed proportion, adding water steam curing, aging, drying and grinding as pretreatment materials. When the pressure increasing, and temperature was controlled at 100℃, the pressure steaming time was 12h, the aging time was 12h, and the drying temperature was 110℃. After testing, it can be seen that the steel slag treatment material with high activity can be obtained by thermal activation.

RESULTS

Influencing factors of carbonization technology. In nature, the carbonization process is very slow, which can not be directly applied to industrial production. Therefore, in order to fix carbon dioxide on a large scale, it is necessary to strengthen the whole carbonization process. Moreover, to achieve the purpose of strengthening the carbonization process, it is necessary to select raw materials with higher carbonation fixation capacity and higher efficiency process flow. Accelerating carbonation is an innovative method that has attracted more and more attention worldwide. This method not only captures carbon dioxide, but also produces environmentally friendly building materials. Additionally, in order to capture CO2 through carbonization technology, it is necessary to study the factors affecting the reaction efficiency, such as carbonization time, temperature, CO2 partial pressure, liquid-solid ratio or humidity, and the specific surface area of the raw material used. These findings can provide basic support for most related industrial processes [39]. The relationship between the external environment and the carbonization process are shown in Table 1 and Table 2 [41] [46] respectively.

TABLE 1
Effects of external conditions on carbonization process [41]-[46]

External conditions	Effects on carbonization process
CO_2 concentration	The higher the CO_2 concentration, the higher the carbonization rate, but not the higher the strength of the carbonized products. Therefore, it is necessary to control the concentration of CO_2 to control the carbonation rate to obtain the optimal compressive strength
Relative humidity	When the relative humidity at 50 ~ 70%, the carbonization rate is the highest. If the relative humidity is too high or too low, the carbonization rate will be reduced. The diffusion rate and reaction rate of CO_2 are two contradictory factors, so it is necessary to find an optimal value of relative humidity in practical application.
Temperature	Under normal pressure, the absorption rate of CO_2 increases with the increase of temperature within 60℃, mainly because high temperature can promote the precipitation of Ca^{2+} which can reduces the solubility of CO_2 in water, so it will reduce the carbonation reaction rate. However, the carbonization reaction is an exothermic reaction, and the reaction heat promotes the production of metastable $CaCO_3$, and more stable homogeneous calcite is obtained.
Pressure	The increase of pressure can promote the increase of carbonization rate and product strength.
Time	Prolonging carbonization time is beneficial to increase the depth of carbonization reaction, and can effectively improve the strength of steel slag specimen and subsequent hydration reaction of steel slag.

TABLE 2
Effects of chemical properties of materials on carbonization process [41]-[46]

Material attributes	Law of influence
Material composition	The material is a natural inorganic substance, the mineral composition contains calcium or its silicate, can occur hydration reaction, pozzolanic reaction containing lime material or other.
PH	CO_2 can react with hydroxide in the material to form carbonate in alkaline environment.
Ca content	Carbonation reaction only occurs when available Ca exist. As a result, the higher the Ca content in the material, the better the carbonation result.
Ca/Si ratio	The higher the ratio, the higher the degree of carbonation.
Ferrate/Aluminate	Ferrate/Aluminate can promote the formation of ettringite, and its CO_2 can decompose to further produce gypsum, calcium carbonate, alumina gel.
Amount of water added	Water is the necessary medium for carbonation reaction. In the case of sufficient water, the dissolved amount of CO2 is more, but when the water is too much, it is easy to block the internal pore size of particles and hinder the diffusion of CO2 into the solid.
Specific surface area	In order to achieve the optimal carbonization effect, the material with small specific surface area needs to reduce the moisture content accordingly.
Gas permeability coefficient	The higher the gas permeability coefficient is, the more favorable the CO_2 permeability is, and the carbonation reaction process can be effectively enhanced.

Application of carbonation technology in steel slag. Carbonation is an effective means of using steel slag. By fixing carbon dioxide in steel slag artificially, it can solve the stability problem of steel slag, make it possible to apply a large amount of carbon dioxide, and absorb a large amount of carbon dioxide and alleviate greenhouse effect [47]. Steel slag has high carbonization activity, which can capture CO2, and improve the strength of steel slag products. C2S, C3S and a large number of alkaline oxides such as CaO and MgO can effectively immobilizing CO2, and forming calcium silicate hydrate, silica gel and calcium carbonate. Furthermore, the microstructure becomes denser during carbonization. It is also indicated that magnesite is most easily reacted with CO2 in steel slag, and has higher carbonization activity. Carbonization promotes the high heat release of steel slag in the process of carbonization and promotes the hydration reaction of steel slag. [48]. Additionally, carbon dioxide is stored in steel slag to prepare carbonated products, which is helpful to realize the effective utilization of secondary resources and provides material conditions for the realization of carbon fixation technology [49]. However, the carbonation efficiency of steel slag and the properties of cementitious materials prepared by steel slag are affected by its mineral composition, particle size and gradation of steel slag, raw material ratio, pre-curing and molding pressure, moisture, CO2 concentration and pressure, carbonization temperature and time [50].

Effect of chemical factors on carbonized steel slag. Effect of water addition and hydration time on carbonized steel slag. Liang Xiaojie [51] studied the carbonation effect of steel slag with different amount of water. The results show that the carbonation weight gain rate of steel slag first increases and then decreases with the increasing water addition, and there is a critical value of water addition, as shown in Figure 1. The reason for this phenomenon is that the dissolution rate of CO2 increases, the leaching efficiency of Ca2 + increases with the increase of water, besides, the carbonation weight gain rate of steel slag also increases. When the water addition exceeds the critical value, the steel slag appears bleeding and agglomeration during stirring. The steel slag are wrapped with the accumulated water, which is not conducive to the reaction. In addition, the CaCO3 particles generated by the outer layer reaction hinder the further carbonization of steel slag. Wu Haoze et al. [53] used steel slag with different particle sizes, namely, steel slag micro powder [Figure 2], steel slag coarse powder [Figure 3] and steel slag particles [Figure 4], and also studied the relationship between the carbonization weight gain rate of steel slag and the amount of water added under different particle sizes, obtained the same research results. Pan Kai [54] carried out steel slag carbonization test under different liquid-solid ratios,The test results show that the carbonation rate of steel slag increases with the increase of liquid-solid ratio. Huijgen [40] uses steel slag with particle size less than 38μm to select appropriate water-solid ratio, and the carbonation weight gain rate of steel slag is significantly improved. Johnson [61] adds 12.5% water during the forming process of steel slag specimen for carbonation curing, and the carbonation

weight gain rate and product strength are significantly improved. Therefore, the moisture content is the key factor in the carbonization process of steel slag.

Before carbonization of steel slag, hydration reaction for a period of time will also affect the carbonization effect. Liang Xiaojie [51] measured the relationship between carbonation weight gain rate and hydration time of steel slag specimens by independent hydration and carbonation reactions. The results show that a certain hydration time can promote the carbonation process, but the hydration time is not easy to be too long, otherwise it will reduce the carbonation effect of specimens and also affect the carbonation process, With the increase of hydration time, the reaction rate is faster, which promotes the carbonation reaction to generate more CaCO3 particles. However, the later generated CaCO3 forms a shell wrapped in the outer side of the steel slag, hindering the reaction. Moreover, Liu Mei [52] hydrated the steel slag for 0 h ~ 7 d and then carbonated for 2 h. It was found that the carbonation weight gain rate of the steel slag was higher in 2 ~ 6 h, but the carbonation weight gain rate of the steel slag gradually decreased after 10 h, as shown in Table 3.

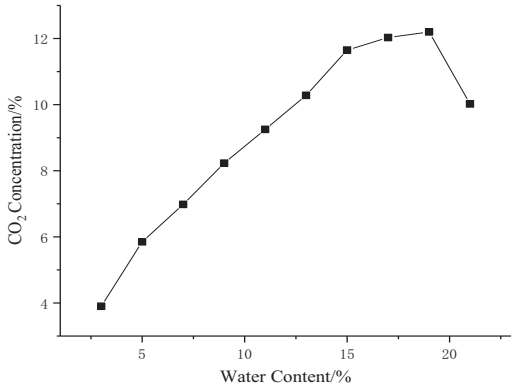


FIGURE 1
Carbonation Effect of Steel Slag Sample with Different Water Content [51]

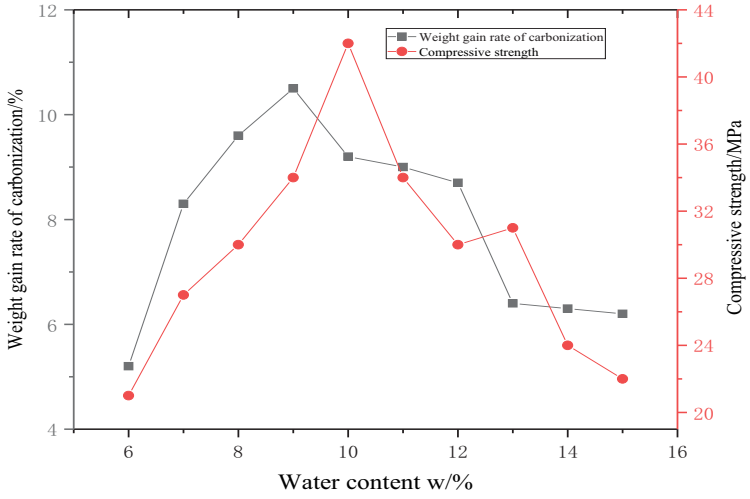


FIGURE 2
Carbonation water content of steel slag powder [53]

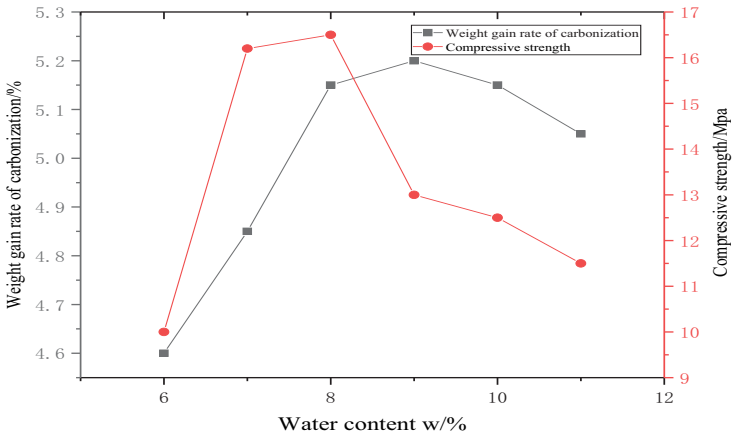


FIGURE 3
Carbonation water content of coarse steel slag powder [53]

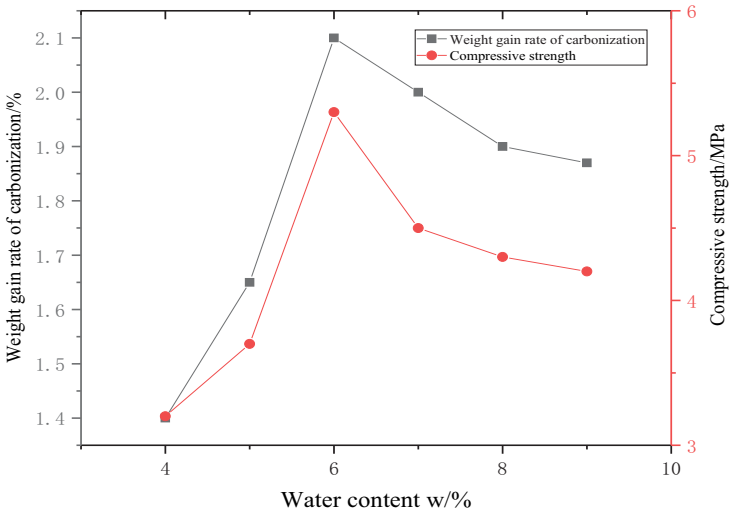


FIGURE 4
Carbonized water content of coarse steel slag particles

TABLE 3
Carbonated weight gain rate of steel slag [52]

Sample	Hydration curing time	Carbonation Time	Carbonated weight gain/ w%
1	0h	2h	9.48
2	2h	2h	10.43
3	6h	2h	10.73
4	10h	2h	10.53
5	1d	2h	10.32
6	3d	2h	10.01
7	7d	2h	9.08

Effect of Admixture on Carbonized Steel Slag. In the carbonization reaction, the addition of admixture can promote the reaction, stimulate the reaction activity of steel slag, and improve the properties of steel slag carbonization products. Through the research on the influence of admixture on the carbonation of steel slag and added seven admixtures, including CaSO4 · 2H2O, Na2CO3, NaHCO3, Na2SiO3, zeolite, rubber powder and sodium carboxymethyl cellulose into the steel slag sample for 2 h [34]. The results showed that the steel slag with NaHCO3, Na2SiO3 and sodium carboxymethyl cellulose had better carbonization than the sample without admixture. Adding three admixtures in pairs to further explore the addition of sodium carboxymethyl cellulose and CaSO4、NaHCO3 has no obvious effect on the promotion of carbonization reaction. The results indicates that the effect of admixture on carbon sequestration is not obvious, and it is likely to cause the structure of steel slag to change in an unfavorable direction, thus affecting the properties of carbonized steel slag products.

On the basis of the existing carbonization system and conditions, Shi di [56] used Shou gang steel slag as raw material and made high strength steel slag brick by the synergistic action of alkali excitation and CO2. The scholar chose Na2CO3 as activator. The experiment shows that when the solution state is Na2CO3, the carbonization effect is better than that of the solid Na2CO3, the reason is that the ionic reaction between the reactants, and the solid matter needs to be dissolved, which leads to the carbonation rate of the solid Na2CO3 is not as good as that of the Na2CO3 solution. Further tests showed that when the amount of Na2CO3 was 13.12 kg/m3, the steel slag carbonized brick has the best effect (Figure 5). Moreover hydrated lime can also be used as an activator. Cao Weida [57] found that when the mass ratio of steel slag to mature lime was 0.20, the strength of carbonized brick reached the best value, and the compressive and flexural strength was 4~5 times that of contrast brick (without hydrated lime), besides the carbonized brick mixed with activator also achieved good indexes in water absorption, drying shrinkage and stability. Chu Jian [58] found that adding gypsum in carbonated steel slag can change the aluminate to ettringite and accelerate the early hydration of silicate minerals. Zhang Feng et al [59] found that the compressive strength of steel slag concrete with 5% Cao and 15% MgO is higher. The compressive strength of concrete is 65.3MPa after 14 days carbonization, as shown in Table 4 due to the fact that Mg2+ promotes the growth of round magnesium containing calcite in the process of CaCO3 precipitation. Furthermore, the calcium magnesium carbonate products filled the pores and improved the interface structure of particles, which reduced the porosity and increased the compressive strength [75-76].

TABLE 4
Compressive Strength of Steel Slag Aggregate Concrete [59]

Sample	Mass fraction/%		Carbonation Time			
	CaO	MgO	0d	1d	3d	14d
1	20	0	9.9	31.7	41.2	48.2
2	10	10	9.4	33.5	48.4	55.9
3	5	15	10.3	38.4	54.1	65.3

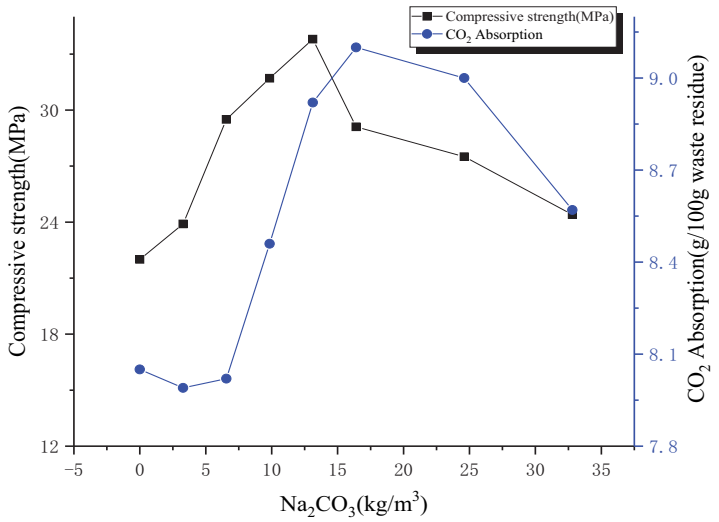


FIGURE 5
Effect of Na2CO3 content on Properties of Steel Slag Carbonized Brick [56]

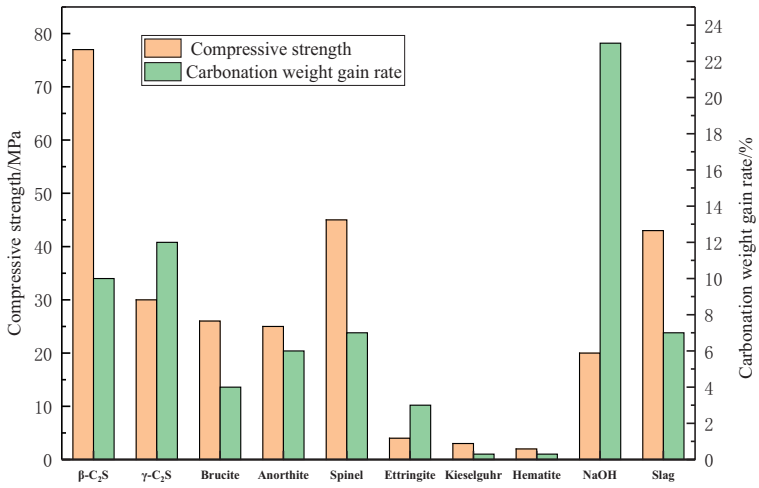


FIGURE 6
Carbonation weight gain and compressive strength of different minerals

Effect of Mineral Composition of Steel Slag on Carbonized Steel Slag. The mineral composition of steel slag affects its ability and efficiency of absorption CO2. In general, the higher the content of carbonizable components, the faster the carbonation in the early stage. Bodor et al[60] studied the carbonation of various minerals in steel slag and found that silica (Ca7MgSi4O8) is the most active phase of carbonation, followed by dicalcium silicate (β-C2S and γ-C2S) and spinel (Ca4Si2O7F2) or pyrolite (Ca2Fe2O5) and calcium iron olivine (Ca-Fe2O4). Ghouleh [21] research indicates the γ-C2S of steel slag is more active than β-C2S carbonization reaction. Fang Yanfeng et al [62] prepared the same mineral phase with steel slag by chemical reagent, meanwhile, the carbon fixation ability of different minerals under the same conditions were compared and the results show that Ca(OH)2 has the strongest ability of carbon sequestration. The carbonation effect of Ca2Fe2O5, Ca4Al2Fe2O11 and CaAl2O4 is poor (Figure 6). Berryman et al [63]. Also found that the carbonation activity of Ca2Fe2O5 is low.

Effect of physical factors on carbonized steel slag. Effect of Temperature on Carbonized Steel Slag. In a certain range, the increase of temperature can promote the movement of molecular heat and promote the chemical reaction between active substances and CO2 in steel slag. However, when the temperature reaches a certain value, the carbonization reaction will release heat. Besides, if the temperature continues to rise, it will inhibit the reaction. Liu Qian [64] compared the effects of different curing conditions on the properties of steel slag cement-based gelation materials. The results showed that the optimum curing conditions were 60℃ and carbonization for 7h, as shown in Table 5. High temperature carbonization can improve its compressive strength and increase hydration process, thus promoting carbonization reaction. Gu Hongxia [66] found that with the increase of temperature, the nitrogen adsorption rate of steel slag samples decreased after carbonization at different temperatures. The reason for this result is that with the increase of carbonization temperature, more carbonization products of steel slag are generated, filling the gap and reducing the nitrogen adsorption amount, as shown in Table 7.Additionally Gao Xiaojiao et al. [65] pressed the crushed and ground steel slag powder into a certain shape test block by adding water, and carbonized the test block with CO2 at 60℃, 90℃ and 120℃, respectively, and the changes of mass (Figure 7), volume (Figure 8) and compressive strength (Figure 9) after carbonization are analyzed. Besides, through the analysis of the results obtained the volume expansion rate and mechanical strength of steel slag samples carbonized at different temperatures for 3 days were obtained, it is found that the volume expansion rate of steel slag increases with the increase of carbonization temperature, the linear equation mechanical strength and carbonization temperature y=0.062x+33.04 (y is mechanical strength value, unit MPa, x is carbonation temperature, unit℃). Tu Maoxia [67] also proved that increasing the carbonization temperature and prolonging the carbonization time are beneficial to the strength of the specimen, and the effect of the carbonization temperature on the strength of the specimen is more significant. The results show that the higher the temperature, the higher the strength of the test block. At the same temperature, the carbonation products of steel slag increase gradually and the product is more closely connected, while the mechanical properties of the test block are improved macroscopically.

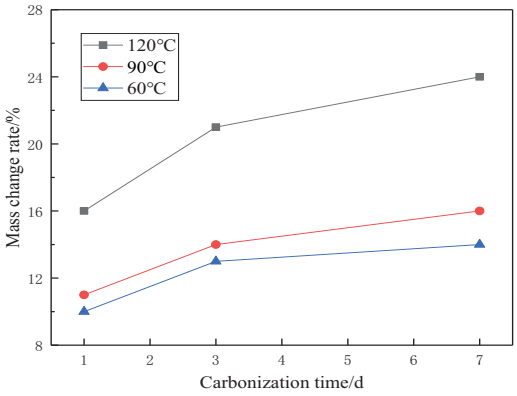


FIGURE 7
Mass change of test blocks at different carbonation temperatures [65]

TABLE 5
Relationship between curing conditions and compressive strength of steel slag cement-based cement [64]

Sample	Compressive strength/MPa					
	3d	Growth rate of compressive strength	7d	Growth rate of compressive strength	28d	Growth rate of compressive strength
S0	3.45		5.18		6.38	
H3	4.75	37.68	5.90	13.90	6.24	-2.19
H4	5.37	55.62	6.20	19.69	6.27	-1.72
C9	4.90	42.03	5.83	12.55	7.01	9.87
C10	5.55	60.87	6.30	21.62	7.41	16.14
C11	5.41	56.81	5.52	6.56	7.39	15.83
C12	4.97	44.06	5.71	10.23	7.38	15.67

Note: S0： standard maintenance; H3、H4：60℃ high temperature maintenance; C9、C10、C11、C10：60H3、H4：60℃, carbonization 7 h maintenance

TABLE 6
Ratio of pore volume of steel slag samples after carbonization at different temperatures [67]

Pore size(nm)	Uncarbonated	Temperature(℃)			
		40	60	80	90
<2	0.846	3.088	9.263	10.924	12.612
2-50	62.675	89.392	87.916	87.635	87.388
>50	36.479	7.52	2.821	1.441	0

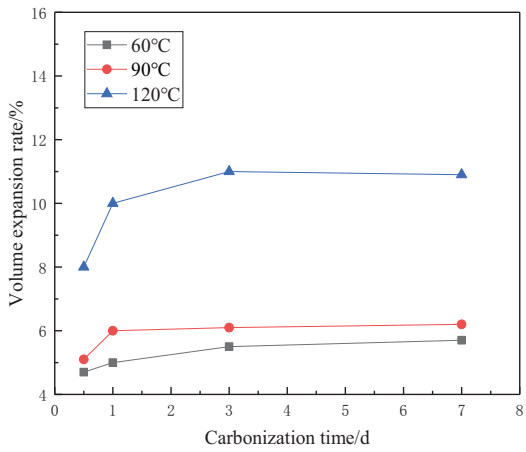


FIGURE 8
Volume expansion ratio of different carbonation temperatures [65]

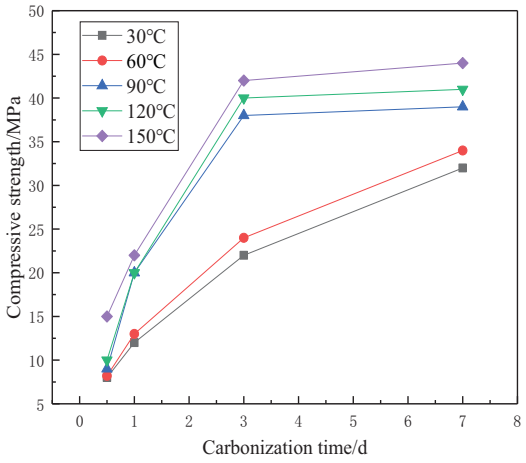


FIGURE 9
Compressive strength of different carbonation temperatures [65]

Effect of Carbonation Time on Carbonized Steel Slag. The carbonation time also has a significant effect on the carbonation depth and strength of steel slag specimens, and prolonging the carbonization age is beneficial to increase the carbonation reaction depth [68]. Some scholars have proposed that in the early stage of steel slag carbonization reaction, the conversion rate of CaO is the fastest, and 80% of the CaO will react with the CO2. With the increasing of the reaction time, the substances involved in the reaction decrease, the rate becomes slower, and the reaction tends to balance. Chang Jun [69] studied this problem and the results show that the most suitable carbonization time is 3 h, the carbonation weight gain rate is 10.79%, and the strength can reach 40.81 MPa. Ding Liang [70] studied the weight gain rate and compressive strength of carbonated steel slag specimens under different carbonization time, and found that the carbonation weight gain rate and compressive strength of the specimens increased with the increase of carbonization curing time (Figure 10). Zhao Hualei [71] obtained mortar specimens from grinding steel slag and pre-grinding slag, and their compressive strength by carbonization curing mortar specimens for different times was tested (Figure 11) (Figure 12). It is found that with the increasing carbonization time, the carbonation weight gain rate and compressive strength of the specimens increased rapidly in the early stage and slowly in the later stage, which may be CaCO3 particle filling blocked the path of CO2 diffusion into the sample interior in the steel slag pores, resulting in a decrease in the carbonization rate. Luo Naijiang [72] investigated the compressive strength and flexural strength of steel slag brick under different carbonization time.

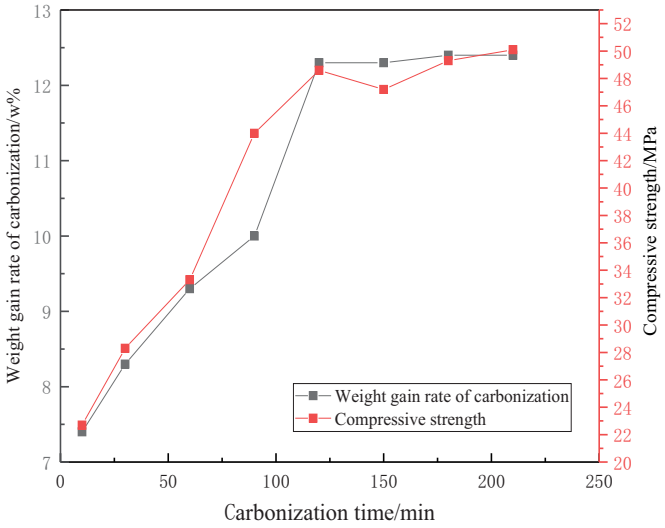


FIGURE 10
Relationship between carbonation time and carbonation weight gain and compressive strength [70]

TABLE 7
Flexural strength and compressive strength of steel slag brick under different carbonization

Carbonation Time/h	Flexural strength/ MPa		Compressive strength/ MPa	
	3d	7d	3d	7d
1	6.3	7.0	30.4	36.2
2	6.6	7.3	32.2	38.7
3	7.2	8.0	36.2	43.0
4	7.0	7.8	35.4	41.2

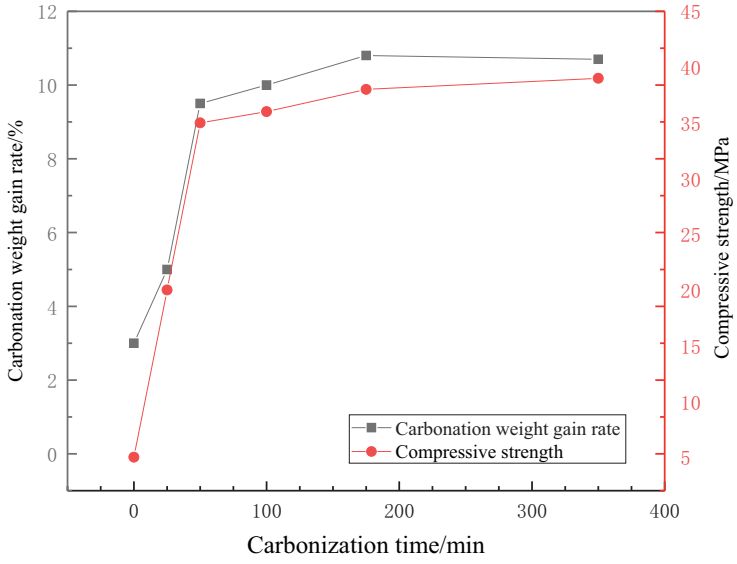


FIGURE 11
Carbonation Effect of Different Carbonation Time for Steel Slag Samples [71]

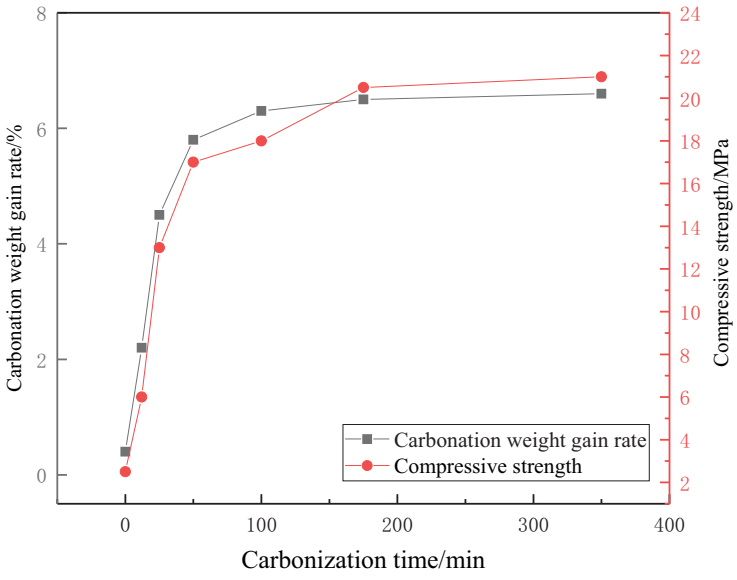


FIGURE 12
Carbonation Effect of Steel Slag Mixed Slag Sample at Different Time [73]

It found that the flexural and compressive strength of steel slag brick increased first and then decreased with the prolongation of carbonization time. The reason may be that CaCO3 is formed during the carbonization reaction, which makes the structure more compact and the increasing of the strength. However, with the carbonation reaction, the hydration products gradually participate in the reaction, which leads to the destruction of structural integrity and the decrease of strength, as shown in Table 8. Furthermore Zeng Haima [73] conducted carbonization curing for steel slag concrete specimens for 4h, 12h and 24h respectively, and obtained that

the growth rate of the compressive strength of specimens gradually tended to slow down (Figure 13). This result may be attributed to the fact that the carbonation reaction is a diffusion process of CO2 gas from the outside to the inside. With the carbonation products generated in the early carbonation reaction continuously filling the pores, the surface of the specimen becomes more dense, and the CO2 enters the inner part of the specimen slowly. Therefore, the carbonation strength increases slowly in the later stage.

Effect of CO2 concentration and forming pressure on carbonized steel slag. The porosity and diffusion rate of carbon dioxide are different with different molding pressure, and the reaction rate and carbonization effect are also different. Li Yong's [74] experiment, the design pressure range is 0~14MPa, SEM, TGA and XRD analysis of carbonized specimens. As the molding pressure increases, the carbonization effect increased first and then decreased (Figure 14). Moreover, the morphology of carbonized products has changed from typical calcite crystal to ellipsoidal calcite, which indicates that the forming pressure has a great influence on the carbonization reaction. Besides with the change of forming pressure, the water retention capacity and void ratio of the sample are different, and the velocity and the morphology of the carbonized product are different.

The diffusion and dissolution rate of CO2 in the specimen directly affect the carbonation rate [50]. Increasing the concentration and pressure of CO2 can accelerate the transmission as well as diffusion of CO2, and increase the solubility of CO2. Chu jian [58] research shows that when CO2 volume fraction is less than 20%, the carbonation effect of steel slag mortar specimen is not ideal, and when CO2 volume fraction exceeds 25%, the carbonization effect is better. Mo Liwu et al. [59] used carbon dioxide with volume fraction of 99.9% to cure steel slag products. The compressive strength of steel slag concrete carbonated for 14 days was 5.3-6.3 times higher than that of the non carbonated group after 28 days of wet curing. Meanwhile, the carbonation of f-CaO in steel slag can obviously improve the poor stability of steel slag concrete. Additionally Chang Jun[78] is made by mixing steel slag and lime from electric arc furnace, and carbonated with 0.5MPa, 100% (volume fraction) CO2 for 2h in closed container. The results show that the compressive strength of carbonated steel slag aggregate is significantly improved after carbonization. Within the accelerated carbonization treatment of steel slag brick made of steel slag sand and slag. Hu Yufen[79] it was found that with the increase of CO2 gas pressure, the weight gain of carbonation increased and the strength of the test block increased (Figure 15). Wu Haoze et al. [68] prepared mortar specimens with steel slag after grinding, and carbonized mortar specimens with CO2 at different pressures. They found that low CO2 pressure was adopted in the early stage of carbonization to avoid the formation of too much CaCO3 to block the "internal channel", and increased CO2 pressure in the later stage to promote CO2 to enter the specimen, making the specimen more carbonized fully.

In general, Increasing the pressure will accelerate f-CaO reaction with CO2 promotes the process of carbonization reaction. When f-CaO reacts too quickly with CO2, more CaCO3 is produced on the surface, which prevents CO2 from entering and leads to insufficient reaction of f-CaO inside. Moreover, to a certain extent, more CO2 dissolved into water will lead to the decrease of solution pH value, which is not conducive to carbonate precipitation.

CONCLUSION AND PROSPECT

With the increasing emission of carbon dioxide in recent years, there are more research focus on CO2 capture and storage technology in various countries. Steel slag a industrial waste, has good carbonization performance, besides, combined with carbonization technology, the performance of steel slag products can be improved, which means the better prospects for the steel slag products. In summary, some achievements have been made in the investigation of the influencing factors of carbonation technology applied to steel slag, but further research is still needed.

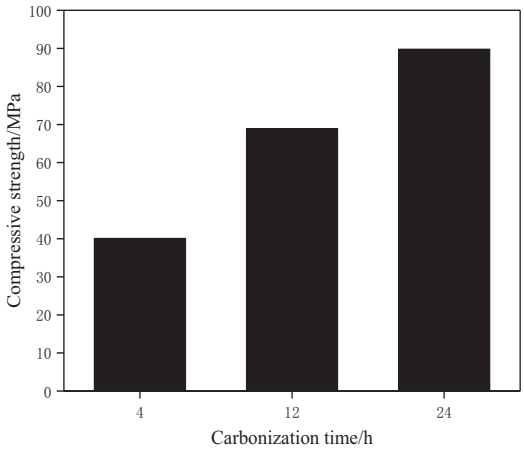


FIGURE 13
Compressive strength at different carbonization times

1. Active excitation of steel slag. At present, researchers mainly stimulate steel slag activity by physical activation, chemical activation and thermal activation. Although the single activation method has good excitation effect, it has the disadvantage of high cost. Therefore, the role of the combined activation method of physical, chemical and thermal activation and cost reduction can be the development direction of research and application of steel slag activity excitation in the future.

2. Carbonation technology is used to interfere with many external environment in steel slag, such as water content, carbonization time, CO2 concentration and forming pressure. Exploring the best conditions with a single factor is often difficult to meet the needs of the project, besides, how to ensure the accuracy of the measurement results and establish a comprehensive evaluation mechanism needs to be further studied.

3. The problem of secondary pollution of additives. The addition of chemical agents is easy to cause secondary pollution of carbonized steel slag products, and whether it will overflow toxic and cause harm to human life with the increase of time is still a problem. Moreover, the establishment of a more suitable experimental scheme and the research of green admixture are also the problems to be solved in the future research.

4. Properties of carbonized steel slag products. In recent years, the properties of carbonized steel slag products mainly focus on mechanical properties and structural properties, such as compressive strength, permeability, porosity, mass loss rate and durability. How to improve the resistance as well as humidity and heat resistance without losing the original excellent mechanical and structural properties is a major challenge to the market of carbonized steel slag technology.

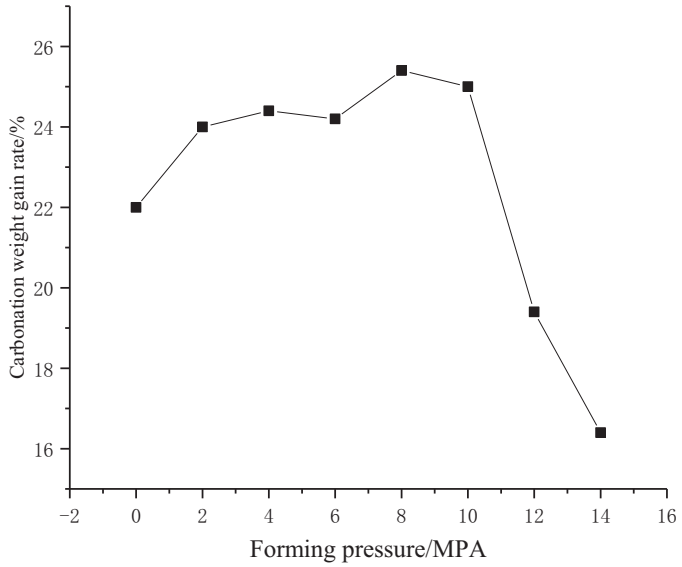


FIGURE 14
Effects of Different Forming Pressure on Carbonation [74]

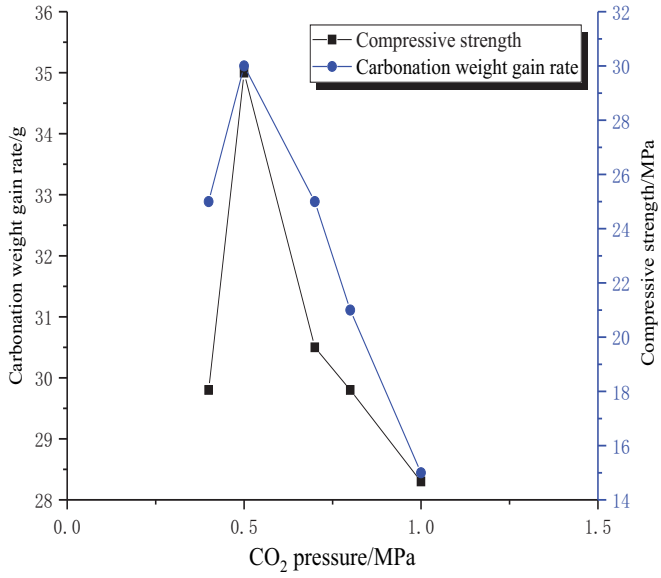


FIGURE 15
Effect of CO2 gas pressure on carbonation weight gain and test block strength

ACKNOWLEDGEMENTS

This research was funded by research foundation of the Institute of Environment-friendly Materials and Occupational Health(Wuhu), Anhui University of Science and Technology, (ALW2020YF13).

Declaration of competing interest. The authors declare that they have no known competing financial interests or personal relationships that could have appeared to influence the work reported in this paper.

REFERENCES

[1] Li, C.X., Li, B. (2019) Low carbon transformation path of China's iron and steel industry under the goal of global temperature control. Iron & Steel. 54(08), 224-231.

[2] Cheng, X.X., Yang, Q.B. (2010) Comprehensive utilization of steel slag. Fly Ash Comprehensive Utilization. (05), 45-49.

[3] Wang, Q., Yan, P.Y., Mi, G.D. (2012) Effect of blended steel slag–GBFS mineral admixture on hydration and strength of cement. Constr. Build. Mater. 35, 8–14.

[4] Gao, D., Wang, F.P., Wang, Y.T., Zeng,Y.N. (2020) Sustainable Utilization of Steel Slag from Traditional Industry and Agriculture to Catalysis. Sustainability. 12(21), 9295-9295.

[5] Wang, X., Ni, W., Li, J.J., Pascual, R. (2019) Carbonation of steel slag and gypsum for building materials and associated reaction mechanisms. Cement and Concrete Research. 125.

[6] Guo, J.L., Bao, Y.P., Wang, M. (2018) Steel slag in China: Treatment, recycling, and management. Waste Management. 78, 318-330.

[7] Zhang, X.Z., Zhao, X.X., Liu, Z.C., Wang, F.Z. (2019). Construction and Building Materials. 214, 28-36.

[8] Das, B., Prakash, S., Reddy, P.S.R., Misra, V.N. (2006) An overview of utilization of slag and sludge from steel industries. Resources, Conservation & Recycling. 50(1), 40-57.

[9] Tian, J.L., Zhang, Q. (2013) Resource utilization of steel slag in environmental pollution control. Resource Recycling, 2013(01), 55-57.

[10] Meehl, G.A.,Washington, W.M., Collins, W.D., Arblaster, J.M, Hu, A., Buja, L.E., Strand, W.G., Teng, H. (2005) How Much More Global Warming and Sea Level Rise?. Science. 307(5716), 1769-1772.

[11] Wang, W., Wang, S.P., Ma, X.B., Gong, J. (2011) Recent advances in catalytic hydrogenation of carbon dioxide. Chemical Society Reviews. 40(7), 3703-27.

[12] Datta, S.J., Khumnoon, C., Lee, Z.H., Kyung,W. (2015) CO_2 capture from humid flue gases and humid atmosphere using a microporous coppersilicate. Science. 350(6258), 302.

[13] Batarshin, V., Gulevatenko, A., Semiokhin, A. (2021) The Use and Utilization of CO2, as Part of the Fight with Greenhouse Effect. IOP Conference Series: Earth and Environmental Science. 666(3), 032018.

[14] Zhang, C., Zhang, Y.L., Zhu, M.H., Meng, B., Tu, W.F., Han, Y.f.. (2021) New way of high value utilization of CO_2: Research Progress of Fe based catalyst CO_2 hydrogenation to olefin. Chemical Industry and Engineering Progress. 40(02), 577-593.

[15] Zhu, J., Tang, D., Shao, T.S.,Wang,Q., Sun,W.. (2020) The effect of carbon dioxide treatment on micro-crack propagation of bituminous coals. Geomechanics and Geophysics for Geo-Energy and Geo-Resources. 6(4), 1-17.

[16] Yuan, J.J., Wu, C., Xu, X.X., Liu, C.. (2021) Proposal and thermoeconomic analysis of a novel combined cooling and power system using carbon dioxide as the working fluid. Energy Conversion and Management. 227, ID:113566.

[17] Anderson, J., Rode, D., Zhai, H.B., Fischbeck, P. (2021) Reducing carbon dioxide emissions beyond 2030: Time to shift U.S. power-sector focus. Energy Policy. 148(PA), ID:111778.

[18] Cupp, A.R.,Smerud, J.R.,Thomas, L.M., Waller, D.L., Smith, D.L. , Erickson, R.A., Gaikowski, M.P. (2020) Toxicity of Carbon Dioxide to Freshwater Fishes: Implications for Aquatic Invasive Species Management. Environmental Toxicology and Chemistry. 39(11), 2247-2255.

[19] Young, J.F., Berger, R.L., Breese, J. (2006) Accelerated curing of compacted calcium silicate mortars on exposure to CO2. Journal of the American Ceramic Society. 57(9), 394-397.

[20] Bukowski, J.M., Berger, R.L. (1979) Reactivity and strength development of CO2 activated non-hydraulic calcium silicates. 9(1), 57-68.

[21] Ghouleh, Z., Guthrie, R.I.L., Shao, Y.X. (2015) High-strength KOBM steel slag binder activated by carbonation. Construction and Building Materials. 99, 175-183.

[22] Mahoutian, M., Ghouleh, Z., Shao, Y.X. (2014) Carbon dioxide activated ladle slag binder. Construction and Building Materials. 66, 214-221.

[23] Boone, M.A., Nieisen, P., De, K.T., Boone, M.N., Quaghebeur, M., Cnudde, V.(2014) Monitoring of stainless-steel slag carbonation using X-ray computed microtomography. Environmental Science & Technology. 48(1), 674-80.

[24] Bao, W.J., Li, H.Q., Zhang, Y. (2007) Research progress in the carbonation and fixation of greenhouse gas CO2 minerals. CIESC Journal. 01, 1-9.

[25] Wu, H. Z., Tan, W. J., Ding, L.,Zhao, H.L., Liu, M., Pan, Z.Z, Chang, J. (2010) Building materials were prepared from steel slag carbonated with CO2 gas.China Concrete and Cement Products. 02, 24-26.
[26] Liu, S.H., Guan, X.M., Qiu, M., Feng,C.H.. (2016) The activity of the γ-C2S mineral is stimulated by accelerated carbonization. Journal of the Chinese Ceramic Society. 44(05), 658-662.
[27] Humbert, P.S., Castro-Gomes, J. (2018) CO2 activated steel slag-based materials: A review. Journal of Cleaner Production. 208,448-457..
[28] Jang, J.G., Kim, G.M., Kim, H.J., Lee,H.K.. (2016) Review on recent advances in CO2 utilization and sequestration technologies in cement-based materials. Construction and Building Materials. 127, 762-773.
[29] Said, A., Mattila, H.P., Järvinen, M., Zevenhoven, R.. (2013) Production of precipitated calcium carbonate (PCC) from steelmaking slag for fixation of CO2. Applied Energy. 112, 765-771.
[30] Li, M., Wang, Q., Yang, J.D. ,Guo,X.L., Zhou,W.J.. (2020) Strength and Mechanism of Carbonated Solidified Clay with Steel Slag Curing Agent. KSCE Journal of Civil Engineering. 1-17.
[31] Irem, Z.Y., Monica, P. (2011) Chemical, Mineralogical, and Morphological Properties of Steel Slag. Advances in Civil Engineering. 88-100.
[32] Wu, P., Liang, Z.Q., Wu, X.J. (2015) Research Progress on cementitious properties and activation of steel slag powder. China Powder Science and Technology. 21(04), 80-84.
[33] Wang, Q. (2010) Cementitious properties of steel slag and its role in the hydration and hardening process of complex binder. Tsinghua University.
[34] Li, Q. (2012) Study on Steel Slag and Blast Furance Stag-Based Cementing Meterial. HeBei University of Science and Technology. Shi jiazhuang.
[35] Xu, P., Pan, R.Y., Shen, X.D., Zhong B.Q. (2008) Effect of steel slag slag composite with different fineness on strength of cement mortar. Concrete. (12), 82-84.
[36] Wang, Q., Yang, J.W., Yan, P.Y. (2013) Cementitious properties of super-fine steel slag. Powder Technology. 245, 35-39.
[37] Di, Z., Wang, S.P., Zhang, M., Xing F. (2008) Study on activation of hydraulic activity of steel slag. Create Living. 04, 47-51.
[38] Lin, Z.S., Tao, H.Z., Tu, C.H. (2001) Study on activation method of steel slag fly ash. Journal of Wuhan University of Technology. (02), 4-7.
[39] Hou, H.G., Hamdy, M.N., Cheng, S.J.,Yao,H.S., Lu, B., Chen J.N.. (2019) Principle and optimum reaction parameters of calcium silicate accelerated carbonization process. Journal of the Chinese Ceramic Society. 47(08), 1175-1180.
[40] Huijgen, W.J.J., Witkamp, G.J., Comans, R.N.J. (2005) Mineral CO2 sequestration by steel slag carbonation. Environmental Science & Technology. 39(24), 9676-82.
[41] Bao, H., Xu, G., Wang, Q.,Yang, Y.H.,Su, Y.B.. (2021) Investigation on the Distribution Characteristics of Partial Carbonation Zone of Concrete. Journal of Materials in Civil Engineering. 33(1).ID: 04020430
[42] Wang, Y.Z., Li, Y.J., Zhang, W., Ma, X.T.,Wang, Z.Y.. (2021) The effect of Cu on NO reduction by char with density functional theory in carbonation stage of calcium looping. Fuel. 283.ID: 119332
[43] Lai, Y.J.S., Eustance, E., Shesh, T., Rittmann, B.E.. (2020) Enhanced carbon-transfer and -utilization efficiencies achieved using membrane carbonation with gas sources having a range of CO2 concentrations. Algal Research. 52, ID:102098.
[44] Chen, G.F., Lv, Y.D., Zhang, Y.Z., Yang,M.Q.. (2021) Carbonation depth predictions in concrete structures under changing climate condition in China. Engineering Failure Analysis. 119,ID: 104990.
[45] Dasol, C., Jiwoo, S., Youngjune, P. (2020) Effects of $CaCl_2$ on cyclic carbonation- calcination kinetics of CaO-based composite for potential application to solar thermo chemical energy storage. Chemical Engineering Science. ID:116207.
[46] Wang, N.N., Feng, Y.C., Guo, X. (2020) Atomistic mechanisms study of the carbonation reaction of CaO for high-temperature CO2 capture. Applied Surface Science. 532.
[47] Feng, B. (2016) Preparation and property investigation of carbonated steel slag aggregate and concrete. University of Jinan.
[48] Chang, J., Fang, Y.F., Shang, X.P. (2016) The role of β-C2S and γ-C2S in carbon capture and strength development. 49(10), 4417-4424.
[49] Wei, X.L., Ni, W., Wang, X., Li,K.Q.. (2019) Research progress of steel slag carbonization technology. Conservation and Utilization of Mineral Resources. 39(03), 99-104.
[50] Wang, A.G., He, M.C., Mo, L.W., Liu,K.W., Li, Y., Zhou, Y., Li D.S.. (2019) Research Progress on Preparation of building materials from carbonized steel slag. Materials Reports. 33(17), 2939-2948.
[51] Liang, X.J. (2012) Studies on Relationship of Carbonation with Hydration of Steel Slag and Cement. University of Jinan.
[52] Liu, M. (2010) Study on Carbonated Mechanism of Steel Slag and its Minerals, University of Jinan, Jinan
[53] Wu, H.Z., Zhang, L.J., Ye, Z.M. (2009) Effect of moisture on carbonization of steel slag. Journal of University of Jinan (Science and Technology). 23(03), 221-224.

[54] Pan, K. (2014) Research on Steel Stag for CO2 sequestration and preparation of construction materials application. Guangxi University.
[55] Hao, Y.Y., Mo, L.W., Hun, J.J. (2016) Effect of carbonation on strength and microstructure of magnesium slag mortar. Bulletin of the Chinese Ceramic Society. 35(09), 3047-3052.
[56] Shi, D. (2012) Properties and affecting factors of carbonated Steel Slag Brick. China Building Materials Academy.
[57] Cao, W.D., Yang, Q.B. (2013) Characteristics of steel slag hydrated lime carbonated brick. Journal of the Chinese Ceramic Society. 41(10), 1395-1400.
[58] Chu, J. (1998) Experimental study on converter slag carbonized brick. Coal Ash. (02), 26-28+37.
[59] Zhang, F., Mo, L.W., Deng, M. (2016) Influence of carbonation curing on strength and volume stability of steel slag concrete. Journal of the Chinese Ceramic Society. 44(05), 640-646.
[60] Bodor, M., Santos, R.M., Kriskova, L.,Elsen,L., Vlad,M.Van Gervel,T.. (2013) Susceptibility of mineral phases of steel slags towards carbonation: mineralogical, morphological and chemical assessment. European Journal of Mineralogy. 25(4), 533-549.
[61] Johnson, D.C., Macleod, C.L., Carey, P.J., Hills,C.D.. (2003) Solidification of stainless steel slag by accelerated carbonation. Environmental Technology. 24(6), 671-678.
[62] Fang, Y.F., Zhang, T.T., Chang, J. (2015) Accelerated carbonization of different minerals in steel slag. Journal of Chinese Electron Microscopy Society. 34(06), 464-469.
[63] Berryman, E.J., Williams-Jones, A.E., Migdisov, A.A. (2015) Steel slag carbonation in a flow-through reactor system: The role of fluid-flux. Journal of Environmental Sciences. 27, 266-275.
[64] Liu, Q. (2015) Effect of High temperature Carbonation Curing and Pre-carbonized Steel Slag on the Material Properties of Steel Slag-Cement Binding Materials. Beijing University of Chemical Technology.
[65] Gao, X.J., Lu, B., Jiang, W.L., Zhang,F., Jiang,R.L., Xu,N., Tao,Z.T., Fang,Y.H., Liu,J.X., Cao,Y.B., Zhang,Q.F. ,Hou,G.H.. (2016) Carbonization process of steel slag under autoclaved condition. Materials Reports. 30(04), 106-110.
[66] Gu, H.X. (2018) Research and Development of High Strength Steel Slag Brick by Carbonation Curing. Jiangsu University.
[67] Tu, M.X., Lei, Z., Lv, X.F., Zhao,H.X., Wang,L.N,Zhang,J.L.Chen,D.S.Song,W.W.,Qi, T.. (2015) CO2 fixation by carbonation of water quenched steel slag. Chinese Journal of Environmental Engineering. 9(09), 4514-4518.
[68] Wu, H.Z., Ding, L., Zheng, W.J., Chang,J.. (2011) The best carbonization system of steel slag products. Coal Ash. 23(02), 24-26.
[69] Chang, J. (2012) Effect of carbonization time on Preparation of building materials products from carbonized steel slag. The Chinese Ceramic Society. Abstract of papers of the 4th Annual Conference of Cement Branch of China Silicate Society. The Chinese Ceramic Society.
[70] Ding, L. (2010) Manufacture of steel slag water-permeable pavement brick through carbonation curing. University of Jinan.
[71] Zhao, H.L., Wu, H.Z., Chang, J., Cheng,X.. (2010) Effect of carbonation time on carbonation of steel slag. Journal of University of Jinan (Science and Technology). 24(03), 221-224.
[72] Luo, N.J., Zhu, B.G., Gu, H.G.,Cai,X., Li,y.j.,Wu,Q.S. (2020) Study on Preparation of high strength steel slag brick by carbonization curing. New Building Materials. 47(05), 71-74.
[73] Zeng, H.M., Liu, Z.C., Wang, F.Z. (2020) Effect of carbonization curing on mechanical properties and microstructure of high volume steel slag mortar. Journal of the Chinese Ceramic Society. 48(11), 1801-1807.
[74] Li, Y. (2014) Research on the Mechanism of Accelerated Carbonation of Calcium Hydroxide. Dalian University of Technology.
[75] Mo, L.W., Panesar, D.K. (2012) Effects of accelerated carbonation on the microstructure of Portland cement pastes containing reactive MgO. Cement and Concrete Research. 42(6), 769-777.
[76] Panesar, D.K., Mo, L.W. (2013) Properties of binary and ternary reactive MgO mortar blends subjected to CO2 curing. Cement and Concrete Composites. 38, 40-49.
[77] Mo, L.W., Panesar, D.K. (2013) Accelerated carbonation - A potential approach to sequester CO2 in cement paste containing slag and reactive MgO. Cem. Concr. Compos. 43, 69–77.
[78] Chang, J. (2007) Preparation of aggregate and concrete with carbonized arc furnace slag. Journal of the Chinese Ceramic Society. (09), 1264-1269.
[79] Hu, Y.F. (2015) Study on Influence Factors of carbonization of steel slag unburned brick. Shandong Science. 28(01), 97-101.

Received: **20.04.2021**
Accepted: **25.05.2021**

CORRESPONDING AUTHOR

Qiang Wang
School of Civil Engineering and Architecture,
Anhui University of Science and Technology,
Huainan 232001 – China

e-mail: wangqiang0711@163.com

© by PSP Volume 30– No. 09/2021 pages 10427-10434 Fresenius Environmental Bulletin

ANALYSING INTENSITY EFFECT OF PRECOMMERCIAL THINNING ON GROWTH AND INCREMENT IN A BEECH (*Fagus orientalis Lipsky*) STAND

Zafer Yucesan*, Sena Karapinar

Karadeniz Technical University, Faculty of Forestry, Department of Forest Engineering, 61080, Trabzon, Turkey

ABSTRACT

In this study, growth and increment values have been analysed by comparing the low and high precommercial thinning intensities. Stem analysis has been used to obtain increment data. To maximize spatial variation in the dataset, stratified random sampling has been used to layout transects. For this purpose, 6 sample plots have been taken in total in the year 2017. Each sample plot was in size of 400 square meters (20 m x 20 m). Three of six sampling plots were in part of the stand that lightly thinned. Other three sampling plots were in part of the stand that heavily thinned. Precommercial thinning with low and high intensities had been applied in years 2008 and 2009 respectively by the local directorate of forest enterprise. Obtained results showed that diameter at breast height (DBH) and basal area increments were quantitatively higher in heavily thinned sample plots. On the other hand, height and volume increment values were lower in heavily thinned sample plots. However, there were no significant differences ($p<0.05$) among lightly and heavily thinned sample plots in case of increment values. While low thinning intensity promotes height increment, high thinning intensity promotes the basal area increment. This is in line with the notion of beech has a "morphological plasticity" that can utilize the available space both horizontally and vertically

KEYWORDS:
Oriental beech, precommercial thinning, thinning intensity

INTRODUCTION

Considering the period 1973-2015 the total annual increment in the forests in Turkey has reached to 45 million 904 thousand m^3 from 28 million m^3. The main reasons of this increase are the afforestation/reforestation workings for achieving new productive forest areas and forest tending [1]. The annual average harvested wood raw material in Turkey equals to 18.314.621 m^3/year (0.82 m^3/ha/year), where the values ranges between 15.942.459 m^3/year (0.81 m^3/ha/year) in high forests and 2.372.162 m^3/year (0.87 m^3/ha/year) in coppice forests [2]. On the other hand, the annual average wood raw material demand in Turkey is nearly 40 million m^3/year [3]. Considering the amount of annual increment there is no deficit in wood raw material in Turkey. However, it is possible to say that there is a net deficit in the amount of harvested wood raw material. So, to meet the demand of the forest industry and society, appropriate silvicultural operations should be realized to increase the increment and by the way wood raw material harvest [4].

Success or failure in young stand management has long-term effects on stand development and subsequently on the profitability of forest management [5]. Precommercial thinning is the first step in stand development and is used in the age when the existing young generation has gained stand characteristics. So, precommercial thinning can be considered as one of the most important impacts on further stand development [6] and an important goal for controlling stand density to increase increment-growth and to improve stand quality in case of sustainable forestry [7, 8-10]. The timing and the intensity of precommercial thinning affect the yield and development of young stands and, furthermore, the timing and profitability of the commercial thinning [5, 11, 12].

Thinning intensity is very important for obtaining significant growth and yield after thinning. Forest yield in a unit area decreases in the year after thinning [13-15]. In many studies it has been indicated that while not thinned plots had the highest volume increment, light and moderate thinning slightly decreased the volume increment [16, 17, 18, 19-21]. For example, heavy thinning led to a greater reduction in volume increment in mixed spruce-birch stands in Finland [16]. Heavy thinning (>30% of the total volume harvested) reduced the volume increment by about 10% according to another study result [20]. However, after thinning significant increment is observed in DBH and height, as the remaining individuals in the stand have wider spaces [5, 11, 22-24].

It was reported that the high precommercial thinning intensity was excessive but, low precommercial thinning intensity was inadequate to stimulate anticipated levels of diameter growth as of 2012 (3 and 4 years after the precommercial thinning) in the studied beech stand [25]. In this context, the main

goals of this study are (1) to determine whether a different increment and growth relationship emerged in the second development period (2013-2017) after the precommercial thinning or not and (2) to evaluate the necessity of precommercial thinning recurrence in an artificial beech stand in case of thinning intensity.

MATERIALS AND METHODS

Study area. The study area is located in the Düzköy District of Trabzon City (North East of Turkey) (Figure 1). Study area is approximately 3 hectares in size and the average elevation is 1350 meters above the sea level. The main exposure is west and the site productivity is high in the study area. According to the data obtained from the nearest meteorology station in Düzköy (850m asl) average annual temperature was 8.6 °C and average annual precipitation was 853.7 mm.

Study area is an afforestation area which was constructed in 1991 with 1+0-year-old seedlings. No replacement planting has been done in the studied stand. Precommercial thinning in different intensities (Low and high) were applied by the local directorate of forest enterprise. Yücesan et al. [25] calculated the thinning intensity and stated that precommercial thinning had been started with low thinning intensity (19% of the total basal area harvested and the average harvested basal area was 4.063 m^2/ha) in the year 2008 and thinning had been continued with high intensity (40% of the total basal area harvested and the average harvested basal area was 8.079 m^2/ha) in the year 2009.

Within the scope of the study, analysis of growth and increment after precommercial thinning in the second 5 years period (2013-2017) was done by comparing the two types of precommercial thinning intensity. To maximize spatial variation in the

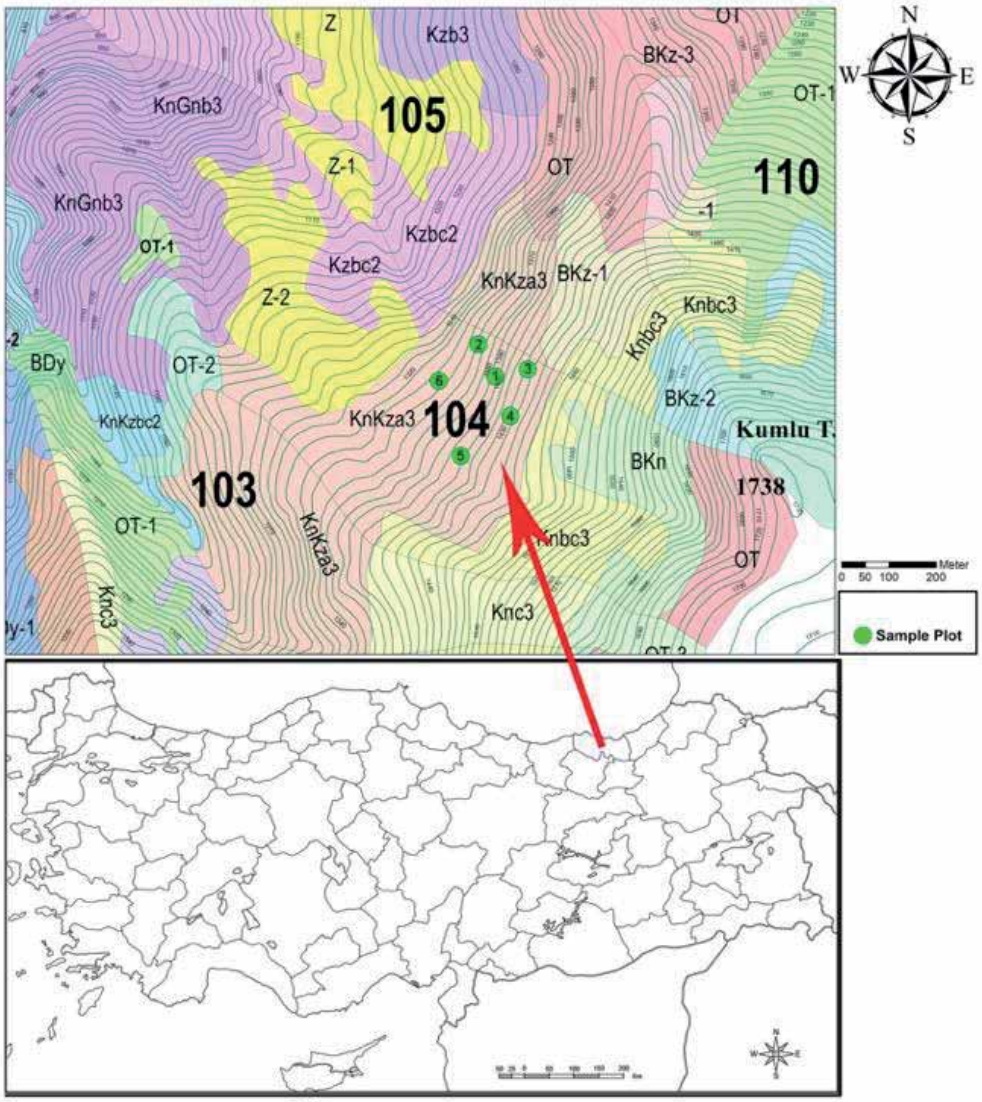


FIGURE 1
Location of the research area

TABLE 1
General characteristics of the sampling plots

Sample Plot	Elevation (m)	Aspect (Degree)	Slope (%)	DBH (cm)	Mean Height (m)	Mean Crown length (m)	Stem number (N/ha)	Coordinate (UTM)	Basal area (m^2/ha)	Volume (m^3/ha)	Form factor	Thinning intensity
1	1355	280	44	12.40±3.98	12.64	8.72	1675	538780 4523635	22.25	197.65	0.7	Low
2	1339	270	46	13.15±4.72	9.54	7.27	1325	538704 4523494	20.15	125.425	0.65	Low
3	1410	274	55	12.51±2.41	12.22	9.61	1350	538808 4523441	17.43	125.1	0.59	Low
4	1332	310	20	12.44±3.84	11.57	8.22	1475	538772 4523441	19.60	118.5	0.52	High
5	1368	326	60	12.86±3.35	12.34	8.27	1450	538666 4523258	20.30	128.075	0.51	High
6	1315	342	70	13.69±3.50	12.75	8.91	1225	538620 4523418	19.18	104.125	0.43	High

dataset, stratified random sampling was used to layout transects. Each sample plot was in size of 400 m^2 (20 m x 20 m). Three of six sampling plots were in part of the stand that lightly thinned. Other three sampling plots were in part of the stand that heavily thinned.

Methods. Slope gradient, aspect, tree coordinates in the sampling plots, breast height diameter (DBH), tree height, crown height (start of continuous green crown) etc. was measured and recorded in the sampling plots. In order to assess the effects of precommercial thinning intensity on growth in the related period (2013-2017), mean annual diameter, height, basal area and volume increments in sampling plots were calculated by using stem analysis method.

Fırat [26] and Kalıpsız [27] informed that if a tree has an average value in terms of basal area, it has an average value in terms of volume as well. So, for stem analysis, three replicates of "mean tree" selected in each sampling plot in year 2017. Stem analysis had been carried out on 18 trees in total, including 9 trees from the lightly thinned plots and 9 trees from the heavily thinned plots. To obtain stem analysis data, sample trees were felled and sectioned from 0.30 m height above ground with one-meter interval (i.e. 1.30, 2.30, 3.30, 4.30, …meters) along the entire stem. Inside and outside bark diameters for each cross-sectional sample was recorded. Two geometric mean diameters were identified for each cross section. Tree rings were measured for each disc and the age of every section was determined. The widths of each annual rings from the year 2013 to the year 2017 were measured on every disc. Then, annual diameter, height, basal area and volume increments were computed by using stem analysis method in each sampled tree. The total basal area was determined by the sum of the basal areas calculated based on the DBH of each tree. While determining the volumes of the sample trees, each tree was divided into three sections (stump, sections and top). Volumes of the stump were calculated by means of cylindrical. Volumes of the top were calculated by means of conical. Volumes of sections were determined separately by using "Smalian formula" and the total volumes of the sections were obtained. Finally, the total volume of the sampled tree was determined by the sum of the volume values of three sections. The total volume of each sample plot was calculated by multiplying average volume of the sampled trees by the number of trees in the sample plots.

The form factor was calculated by the equation given below.

$$f_{observed} = \frac{V\ Tree}{V\ Cylinder}$$

"V Tree" is the mean volume of the sample plot per hectare and "V Cylinder" is the mean volume of the cylinder at mean DBH and mean height.

Statistical methods. Test of normality was used to test whether obtained increment values have normal distribution or not. Thus, it was decided that the parametric or non-parametric test should be used. Mann-Whitney U Test was used to determine if significant differences were found among sample plots in case of thinning intensities. SPSS 15.0 statistical software was used to evaluate the obtained data.

RESULTS

General characteristics of the sampling plots, total basal area and total volume stocks per hectare and form factor values were given in Table 1. Basal area and volume values calculated on the basis of the sample trees and the sample plots were given in Table 2. Obtained results showed that the mean tree height was higher in the heavily thinned sample plots. Mean annual DBH increment did not differ significantly in case of thinning intensity but, the mean DBH value was higher in heavily thinned sample plots. On the other hand, mean basal area, mean volume and mean form factor values were higher in the lightly thinned sample plots. The numbers of standing trees in the lightly thinned

TABLE 2
Basal area and volume values in the sample trees and in the sample plots

Precommercial thinning intensity	Sampled Tree	Sample Tree					Sample Plot				
		Age	Height (m)	DBH (cm)	Basal Area (m^2)	Volume (m^3)	Sample Plot	Stem number (N/ha)	Mean Basal Area (m^2)	Total Basal Area (m^2)	Total Volume (m^3)
Low	1	27	11.0	14.2	0.0158	0.123					
	2	27	13.2	12.9	0.0131	0.167	1	1675	0.0133	0.890	7.906
	3	27	9.7	12.0	0.0113	0.064					
	4	27	12.1	15.1	0.0179	0.089					
	5	27	11.2	13.3	0.0139	0.106	2	1325	0.0152	0.806	5.017
	6	27	12.2	16.3	0.0209	0.089					
	7	27	11.2	15.0	0.0177	0.086					
	8	27	12.1	13.5	0.0143	0.111	3	1350	0.0129	0.697	5.004
	9	27	9.1	13.1	0.0135	0.081					
Mean		**27**	**10.1**	**14.0**	**0.0154**	**0.102**		**1450**	**0.0138**	**0.798**	**5.975**
High	10	27	11.7	13.8	0.0149	0.080					
	11	27	11.7	12.4	0.0121	0.093	4	1475	0.0133	0.784	4.740
	12	27	10.2	15.7	0.0193	0.068					
	13	27	11.3	12.6	0.0125	0.110					
	14	27	10.6	14.3	0.0161	0.065	5	1450	0.0140	0.812	5.123
	15	27	10.7	13.6	0.0145	0.090					
	16	27	12.0	14.2	0.0158	0.073					
	17	27	11.1	13.6	0.0145	0.072	6	1225	0.0157	0.767	4.165
	18	27	13.0	12.7	0.0127	0.110					
Mean		**27**	**11.4**	**13.7**	**0.0148**	**0.085**		**1383**	**0.0143**	**0.787**	**4.586**

TABLE 3
Annual DBH, height, basal area and volume increment values in the sampling plots

Sample plot	Sample Tree	DBH increment (cm/year)	Height increment (cm/year)	Basal area increment (m^2/ha/year)	Volume increment (m^3/ha/year)
		Low intensity			
	1	0,52	18	0.1033	1.1980
1	2	0,30	30	0.0562	0.5891
	3	0,50	2	0.0827	0.6229
	4	0,54	18	0.1144	1.2144
2	5	0,36	4	0.0688	1.0530
	6	1,02	44	0.2161	1.1240
	7	1,06	26	0.2016	0.9765
3	8	0,44	38	0.0841	1.1040
	9	0,64	6	0.1132	0.8080
Average		**0,5978**	**20,67**	**0.1156**	**0.9655**
		High intensity			
	10	1,14	18	0.1923	1.1231
4	11	0,42	24	0.0734	1.1899
	12	1,34	46	0.2549	1.1032
	13	0,26	14	0.0480	0.9300
5	14	0,86	38	0.1609	0.5838
	15	0,70	2	0.1278	0.9475
	16	1,12	20	0.1967	1.2250
6	17	0,56	2	0.1053	0.5289
	18	0,56	8	0.0982	0.8831
Average		**0,7733**	**19,11**	**0.1397**	**0.9461**

sample plots were higher. So, the total volume and the basal area

Annual height, basal area, volume and DBH increment values of the second development period (2013-2017) were given in Table 3. Obtained results showed that there was a quite difference in terms of annual DBH increment in the second development period among the sample plots. Higher mean annual DBH increment (0.60 cm/year in lightly thinned

stand and 0.77 cm/year in heavily thinned stand) was obtained in the heavily thinned sample plots.

Lower mean annual height increment (20.7 cm/year in lightly thinned stand and 19.1 cm/year in heavily thinned stand) was obtained in the heavily thinned sample plots. This situation can be interpreted that the existed wider gaps between the individuals in terms of the high precommercial thinning intensity negatively affected the competition in annual height increment.

There was a quite difference in terms of the annual basal area increment in the second development period among the sample plots. Higher mean basal area increment was obtained in the heavily thinned sample plots (0.1156 m^2/ha/year and 0.1397 m^2/ha/year in lightly and heavily thinned stands respectively). While mean annual basal area increment was higher in the heavily thinned sample plots, the mean annual volume increment was higher in the lightly thinned sample plots (0.9655 m^3/ha/year in and 0.9461 m^3/ha/year in lightly and heavily thinned stands respectively).

According to the normality test results (Table 4), it was determined that DBH, height and basal area increment values did not show normal distribution but, the volume increment values showed normal distribution. However, DBH, height, basal area and volume increment values were not significantly different ($p<0.05$) in terms of the thinning intensity (Table 5).

DISCUSSION

Non-significant but quantitatively higher annual basal area increment was obtained in the heavily thinned stands (0.1397 m^2/ha/year) than the lightly thinned stands (0.1156 m^2/ha/year). However, Yücesan et al. [25] reported that in the first period after treatment (2008-2012) annual basal area increments were similar both in lightly thinned and heavily thinned sample plots. Yücesan et al. [25] also indicated that mean annual basal area increment before thinning was higher in the heavily thinned sample plots and there were no significant differences between the basal area increments in case of thinning intensity before and after treatment. In the second period (2013-2017), higher annual basal area increments than the first period was obtained in the heavily thinned sample plots. So, the effect of precommercial thinning intensity on the basal area increment can reach to higher rate in the long-term after treatment. Umut et al. [28] clarified that, moderate and high intensity tending in beech stands at the pole stage have a great effect on diameter and basal area increments. In addition, Göktürk et al. [29] emphasized that, basal area increment has a positive correlation with tending intensity.

In terms of volume, quantitatively higher annual volume increment was obtained in the lightly thinned stands (0.9655 m^3/ha/year and 0.9461 m^3/ha/year in lightly and heavily thinned sample plots respectively). The annual volume increment values were not significantly different but, the quantitative stand volume in the lightly thinned sample plots was higher than the heavily thinned sample plots. Yücesan et al. [25] reported that the quantitative annual volume increments after precommercial thinning in the first period were higher in heavily thinned sample plots and annual height increment decreased much more in those of sampled plots. Also, Yücesan et al. [25] indicated that mean annual volume increment before thinning was higher in heavily thinned sample plots. So, depending on the long-term evaluations after precommercial thinning, it may be possible to say

TABLE 4
Results of Normality Test

	Kolmogorov-Smirnov(a)			Shapiro-Wilk		
	Statistic	df	Sig.	Statistic	df	Sig.
DBH increment	0.206	18	0.042	0.915	18	0.106
Height increment	0.124	18	0.200	0.922	18	0.138
Basal area increment	0.199	18	0.059	0.917	18	0.116
Volume increment	0.177	18	0.140	0.881	18	**0.027**

TABLE 5
Results of Mann-Whitney U Test

	DBH increment	Height increment	Basal area increment	Volume increment
Mann-Whitney U	26.000	37.500	33.000	36.000
Wilcoxon W	71.000	82.500	78.000	81.000
Z	-1.281	-0.266	-0.662	-0.397
Asymp. Sig. (2-tailed)	0.200	0.790	0.508	0.691
Exact Sig. [2*(1-tailed Sig.)]	0.222	0.796	0.546	0.730

that the annual volume increment in young beech stands was much more affected by the annual height increment.

Precommercial thinning intensity did not have significant effect on annual DBH increment in the second period (2013-2017). However, quantitative annual DBH increment reached to higher amount in the heavily thinned sample plots (0.5978 cm/year and 0.7733 cm/year in lightly and heavily thinned sample plots respectively). Yücesan et al. [25] reported that quantitative annual DBH increment among the years 2008-2012 was also higher in heavily thinned sample plots. Moreover, Yücesan et al. [25] reported that the quantitative annual DBH increment before thinning was also higher in heavily thinned sample plots. But, decreasing amount of annual DBH increment before and after precommercial thinning was in favour of the lightly thinned sample plots. Therefore, it is possible to express the increase in the annual basal area increment was directly proportional to the annual DBH increment in the second development period after thinning. Breda et al. [30] compared the first- and second-year results of forest tending at a 43-years Sessile oak (*Quercus petraea* (Matt.) Liebl.) stand and found that oak individuals had higher diameter increment in the second year after treatment. Dimeter increment increased 18% in the first 3 years, 47% in 4-6 years, 41% in 7-9 years, and 42% in 10-12 years after thinning in 12 years old Northern red oak (*Quercus rubra*) stand [31].

Lower quantitative annual height increment was obtained in the heavily thinned sample plots (20.67 cm/year and 19.11 cm/year in lightly and heavily thinned sample plots respectively). Yücesan et al. [25] reported that mean annual height increment value in the first period after treatment was higher in heavily thinned sample plots. So, the mean annual height increment values were not increased continuously in the following years. Standing trees in the stand after treatment tended to increase in diameter increment than the height increment in the second period. Moreover, lower annual height increment caused an unexpected volume increment in heavily thinned sample plots. Actually, the quantitative annual volume increment was better in the lightly thinned sample plots because of the high annual height increment.

Obtained results showed that oriental beech has a "morphological plasticity" that can utilize the available space both horizontally and vertically. Crown allometry of beech is far from constant [32]. In fact, annual volume increments have no significant differences. It is also possible to correlate the absence of a linear relationship between the diameter and the height increment with the structural composition generated in the stand by the precommercial thinning. During the thinning practices, individuals with large crown shape and thick diameters except wolf trees should be left as standing trees in the stand. These trees are capable of constructing the sufficient canopy density homogenously. However, individuals that have thin DBH and undersized canopy should not be kept as standing trees unless they are not beneficial to create storied stand structure because, in the course of growth, the individuals with underexposed growth were found to have failed to show the expected development, actually though they were enlarged with precommercial thinning [26, 33, 34]. Bontemps et al. [34] emphasized that radial growth is sensitive to the degree of competition between trees and dominant trees are usually less affected by thinning events in common beech stands. Therefore, the high number of the dominant trees in the stands where high thinning intensity applied is the reason that the effect of the thinning intensity on growth does not increase at the desired level.

It is very important to determine the stand density with the regular tending applications at the appropriate time, to increase the wood quality and well grow of the trees [35]. Odabaşı et al. [12] stated that, beech has generally reached to the thicket stage at the age of 10-15 years. In the studied stand, precommercial thinning was performed in 2008 and 2009 while the stand was 18-19 years old. So, a delay in the time of precommercial thinning should be considered. Eler [36] determined that stand age for reaching to the thicket stage has decreased after appropriate tending workings during the pre-thicket in Turkish red pine stands. Consequently, in order to achieve the correct development trend, the age factor is important in terms of forest tending and precommercial thinning should be done at the appropriate age without delay [37].

CONCLUSION

Research area subjected to precommercial thinning at the age of 18, has reached to pole and partially timber stage 8-9 years after the precommercial thinning. Development trend has reached to next development stage and it is possible to make the following evaluations; (1) delayed precommercial thinning should have an important effect on the unexpected increment values obtained in this study, (2) moderate thinning intensity should be more proper for precommercial thinning, and (3) yield is different and the increments are not caused by the differences in management.

Especially in beech stands where the wood production function is important, precommercial thinning with high intensity should be preferable. On the other hand, when the cylindrical growth tendency has a more positive effect on the stem quality, the application of the precommercial thinning with low intensity can be beneficial. More comprehensive studies on the general distribution area of the beech species can give different and significant results. There are no published volume functions for oriental

beech in Turkey. Based on this study and earlier publications we have the chance to derive volume functions that no more time-consuming stem analysis needed.

ACKNOWLEDGEMENTS

This study was carried out for a MSc thesis at Karadeniz Technical University Institute of Science and Technology. A special thanks to Prof. Dr. Ali Ömer ÜÇLER and Prof. Dr. Zafer ÖLMEZ for their contribution to the MSc thesis.

REFERENCES

[1] General Directorate of Forestry. (2018) 2018 Performance Program, Republic of Turkey General Directorate of Forestry.Available at: http://www.ogm.gov.tr/tr/e-kutuphane-sitesi/PerformansProgrami/OGM%202018%20YILI%20PERFORMANS%20PROGRAMI.pdf (Accessed date: 17 January 2019).

[2] Yücesan, Z., Hacisalihoglu, S., Kezik, U. and Karadag, H. (2019) Effects of canopy on soil erosion and carbon sequestration in a Pedunculate oak (*Quercus robur* L. subsp. *robur* L.) coppice stand during the conversion process into high forest. Austrian Journal of Forest Science. 136 (1), 45-66.

[3] Boydak, M. and Çalışkan, S. (2015) Afforestation. OGEM-VAK, CTA Ltd. Şti. Press, İstanbul. 714 pp.

[4] Bergh, J., Nilsson, U., Allen, H.L., Johansson, U. and Fahlvik N. (2014) Long-term responses of Scots pine and Norway spruce stands in Sweden to repeated fertilization and thinning. Forest Ecology and Management. 320, 118-128.

[5] Huuskonen, S. and Hyneynen, J. (2006) Timing and intensity of precommercial thinning and their effects on the first commercial thinning in Scots pine stands. Silva Fennica. 40(4), 645-662.

[6] Daume, S. and Robertson, D. (2000) A Heuristic approach to modelling thinning. Silva Fenn. 34, 237-249.

[7] Clark, A., Saucier, J.R., Baldwin, V.C. and Bower, D.R. (1994) Effect of initial spacing and thinning on lumber grade, yield, and strength of loblolly pine. For. Prod. J. 44, 14-20.

[8] Houtzagers, M.R. (2002) Thinning in discussion. Nederlands Bosbouwtijdschr. 74, 7-14.

[9] Zeide, B. (2004) Optimal stand density: A solution. Can. J. For. Res. 34, 846-854.

[10] Özçelik, R. and Eler, Ü. (2009) Effects of precommercial thinning on the development of young natural Lebanon cedar (*Cedrus libani* A. Rich) stands of western Mediterranean region of Turkey. J. Environ. Biol. 30, 179-182.

[11] Özdemir, T., Eler, Ü. and Şırlak, U. (1987) Effects of precommercial thinning for natural *Pinus brutia* stands in Antalya forest region. Republic of Turkey General Directorate of Forestry Forest Research Institute, Ankara. Technical Bulletin 184.

[12] Odabaşı, T., Çalışkan, A. and Bozkuş, F. (2007) Forest Tending, Istanbul University Press No: 4458/474, İstanbul. 192p.

[13] Eriksson, H. and Karlsson, K. (1997) Effect of different thinning and fertilization regimes on the development of Scots pine (*Pinus sylvestris* (L.)) and Norway spruce (*Picea abies* (L.) Karst.) stands in long-term silvicultural trials in Sweden (Report No.42). Uppsala: Department of Forest Yield Research, Swedish University of Agriculture (In Swedish with English summary).

[14] Karlsson, K. (2006) Impact of the thinning regime on the mean diameter of the largest stems by diameter at breast height in even-aged *Picea abies* stands. Scandinavian Journal of Forest Research. 21, 20-31.

[15] Del Rio, M., Calama, R., Cañellas, I., Roig, S. and Montero G. (2008) Thinning intensity and growth response in SW-European Scots pine stands. Ann. For. Sci. 65, 308.

[16] Repola, J., Hökkä, H. and Penttilä, T. (2006) Thinning intensity and growth of mixed spruce-birch stands on drained peatlands in Finland. Silva Fennica. 40(1), 83-99.

[17] Assman, E. (1970) The principles of forest yield study-studies in the organic production, structure, increment and yield of forest stands. Pergamon Press, Oxford. 506p.

[18] Zeide, B. (2001) Thinning and growth: a full turnaround. Journal of Forestry. 99, 20-25.

[19] Mäkinen, H. and Isomäki, A. (2004). Thinning intensity and growth of Norway spruce stands in Finland. Forestry. 77(4), 349-364.

[20] Mäkinen, H. and Isomäki, A. (2004) Thinning intensity and growth of Scots pine stands in Finland. Forest Ecology and Management. 201(2-3), 311-325.

[21] Niemistö, P., Kilpeläinen, H. and Poutiainen, E. (2018) Effect of first thinning type and age on growth, stem quality and financial performance of a Scots pine stand in Finland. Silva Fennica. 52(2), 1-21.

[22] Ceylan, B. (1988) Silvicultural Researches on first thinning in young Turkish red pine (*Pinus brutia* Ten.) stands in Muğla region. Republic of Turkey General Directorate of Forestry Forest Research Institute, Ankara. Technical Bulletin 196.

[23] Eler, Ü. (1988) Effects of thinning and preparatory cuttings on increment and growth in natural Turkish red pine (*Pinus brutia* Ten.) stands in Antalya region. Republic of Turkey General Directorate of Forestry Forest Research Institute, Ankara. Technical Bulletin. 203.
[24] Tolunay, D. (2003) Effects of forest tending on substance circulation in Scots pine (*Pinus sylvestris* L.) stands in Aladağ (Bolu) region. Journal of Istanbul University Faculty of Forestry. A53(1), 47-74.
[25] Yücesan, Z., Özçelik, S. and Oktan, E. (2015) Analysis of release cutting effects on increment and growth in Oriental beech (*Fagus orientalis* Lipsky) stand, Journal of Environmental Biology. 36(5), 1075-1082.
[26] Fırat, F. (1973) Dendrometry. Istanbul University Press No: 1890/193, İstanbul. 359 pp.
[27] Kalıpsız, A. (1993) Dendrometry. Istanbul University Press No: 3793/426, İstanbul. 91 pp.
[28] Umut, B., Dündar, M. and Çelik, O. (2000) Studies on thinning practices in young beech (*Fagus orientalis* Lipsky.) stands. Republic of Turkey General Directorate of Forestry Central Anatolia Forestry Research Institute, Ankara. Technical Bulletin. 274, 23pp.
[29] Göktürk, A., Demirci, A. and Güner, S. (2010) Thinning effects in Scots pine (*Pinus silvestris* L.) stands. Third National Blacksea Forestry Congress, 20-22 May 2010, Proceedings, Artvin. 931-940.
[30] Breda, N., Granier, A. and Aussenac, G. (1994) Effects of thinning on soil and tree water relations, transpiration and growth in an oak forest (*Quercus petraea* (Matt.) Liebl.), Tree Physiology. 15, 295-306.
[31] Ward, J.S. (2008) Crop tree release increases growth of red oak sawtimber in southern New England: 12-year results. In Proceedings of the 16th Central Hardwoods Forest Conference, April 8-9, Purdue University, West Lafayette, IN. 457-465.
[32] Dieler, J. and Pretzsch, H. (2013) Morphological plasticity of European beech (*Fagus sylvatica* L.) in pure and mixed-species stands. Forest Ecology and Management. 295, 97-108.
[33] Yücesan, Z., Özçelik, S. and Oktan, E. (2015) Effects of thinning on stand structure and tree stability in an afforested oriental beech (*Fagus orientalis* Lipsky) stand in northeast Turkey. Journal of Forestry Research. 26(1), 123-129.
[34] Bontemps, J.D., Herve, J.C. and Dhôte, J.F. (2010) Dominant radial and height growth reveal comparable historical variations for common beech in north-eastern France. Forest Ecology and Management. 259(8), 1455-1463.
[35] Mäkinen, H., Isomäki, A. and Hongisto, T. (2006) Effect of half systematic and systematic thinning on the increment of Scots pine and Norway spruce in Finland. Forestry. 79(1), 103-121.
[36] Eler, Ü. (1992) Yield Researches in Turkish red pine (*Pinus brutia*) Forests. Journal of Istanbul University Faculty of Forestry. A42(1), 177-189.
[37] Özçelik, R. (2000) Effects of stand tending on the growth and sample of *Pinus brutia* Ten. Süleyman Demirel University Journal of Forestry Faculty. 1, 41-56.

Received: **21.11.2019**
Accepted: **17.05.2021**

CORRESPONDING AUTHOR

Zafer Yucesan
Karadeniz Technical University,
Faculty of Forestry,
Forest Engineering Department,
61080 Trabzon – Turkey

e-mail: yucesan@ktu.edu.tr

© by PSP Volume 30– No. 09/2021 pages 10435-10440 Fresenius Environmental Bulletin

THE EFFECTS OF ADDITION MALIC ACID AND WHEY ON THE SOME PARAMETERS OF VETCH-WHEAT SILAGES

Asuman Arslan Duru[1], Dilek Aksu Elmali[2,*], Osman Yuksel[3], Harun Kutay[4]

[1]Department of Animal Science, Faculty of Agriculture and Natural Sciences, Usak University, Usak, Turkey
[2]Department of Animal Nutrition and Nutritional Diseases, Faculty of Veterinary, Hatay Mustafa Kemal University, Hatay, Turkey
[3]Department of Field Crops, Faculty of Agriculture and Natural Sciences, Usak University, Usak, Turkey
[4]Department of Animal Science, Faculty of Agriculture, Cukurova University, Adana, Turkey

ABSTRACT

In this study, the effects of addition malic acid, whey and the combined of whey-malic acid on the silage quality were investigated. In the study, 0.3%; 0.6% and 0.9% malic acid, whey and combinations were used. There were no significant differences in the odour, colour and structure of silages. The levels of dry matter, organic matter, crude ash, crude fiber, crude protein, neutral detergent fiber and acid detergent fiber did not differ. The pH, flieg score, and water soluble carbohydrate value of silages were significantly different. The lowest pH and highest flieg score were found in 0.9% whey and 0.9% whey+0.9% malic acid groups. Ammonia nitrogen and *Listeria* spp. were not detected. There was no difference in lactic acid bacteria. Sulfite reducing anaerobes were in one sample, and *Enterobacteriaceae* were in 4 samples. In concluation, adding 0.9% whey or 0.9% whey+0.9% malic acid may be beneficial in vetch-wheat silages.

KEYWORDS:
Malic acid, Silage quality, Whey, Vetch

INTRODUCTION

Silage is the most important roughage source for ruminants when its advantages are considered [1]. Vetch has an important place in legume family, and it is among the forage groups which are ensiled with difficulty in terms of ensiling characteristics. As their protein rate is high and carbohydrate substance is low, it is reported that vetch must be grown mixed with grains in order to keep the fermentation in a desirable level [2]. It is reported that vetch contain 16.78% crude protein, and their protein level decreases when they are planted with grains. Moreover, it is expressed that crude protein rate of silage decreases rapidly with the increase of grain level [3].

Feed materials which are medium or difficult to ensiling are required to additives for successful and high quality silage production [4]. Hence, in a study carried out by Demirel et al. [5], it is reported that the highest pH value (5.44), the lowest lactic acid level (2.34 g/kg DM) and the highest butyric acid level (2.75 g/kg DM) are found in additive-free vetch silage [5].

Whey is the by-product of cheese production. In the cheese production, whey comprises 70-80% of the total volume of milk [6]. When the high amount of this product coming out is considered, it is thought to be useful to investigate its usefulness in silage production. As a matter of fact, the studies [7, 8] show that whey has a good effect on silage fermentation quality remarkably. It was reported that the pH of the silage decreased significantly when whey was added [7]. Whey is a byproduct and is a waste stream. The use of this waste by-product in ensilage will contribute to the environment.

Organic acids are common in nature as normal elements of plant and animal tissues [9, 10]. It is reported that the addition of organic acid lowers silage pH value and causes positive effects on silage [11]. Filya and Sucu [12] indicate that a preservative based on organic acid added to the corn lowers lactic, acetic and butyric acid concentrations in silage and prevents proteolysis. Also in this research of Filya and Sucu [12], it is stated that this organic acid-based preservative inhibits the growth of yeast, mould, *Enterobacteriaceae* and *Clostridia* by showing a high level of antimicrobial activity and generally improves the aerobic stability of corn silage.

It is reported that ascorbic acid reduces silage losses by inhibiting yeast activity and completely eliminates microorganisms such as mould, *Enterobacteriaceae* and *Clostridia*, which are the cause of spoilage in silage. Moreover, it is identified that the application improves ensiling and feed value features [13].

The aim of this study was to evaluate the effects of malic acid and whey on quality of vetch-wheat silages.

MATERIALS AND METHODS

In this study, Magyar vetch-wheat mixture was used as silage material. This silage material was grown in Usak University Agriculture and Nature Sciences Faculty Implenmentation. Mix rates are as 50% magyar vetch and 50% wheat. Mixtures was harvested at the early podding stage of the legumes. Experiment groups were formed as 10 groups in total as control (untreated), 0.3% whey; 0.6% whey; 0.9% whey; 0.3% malic acid; 0.6% malic acid; 0.9 % malic acid; 0.3% whey+0.3% malic acid; 0.6% whey+0.6% malic acid; 0.9% whey+0.9% malic acid. In separate place, silage materials and additives (in the specified amounts) were mixed. In experiment, fresh whey and malic acid powder were used. Then, ensiling was made into 1 liter silo containers. Three repetitions were done for each group. Ensiling was done in the same day. Ensilage continued 56 days in laboratory conditions at room temperature.

Pysical characteristic of silages (odour, structure and colour) and quality scores were performed by six experienced panelists by using German Agriculture Organisation silage rating scale. In this scale, these scores are used 14 (no butyric acid smell, aromatic smell), 10 (little butyric acid smell, strong smell), 4 (moderate butyric acid smell, mould smell), 2 (strong butyric acid smell, NH_3 smell), 0 (strong mould smell) for odour, 4 (no distortion), 2 (a little distortion), 1 (distortion, mould), 0 (decaying) for outer view, 2 (preserves its colour the way it was ensiled), 1 (a little change in the colour), 0 (a totally different colour) for colour [14].

Immediately after the silages were opened, their pH values were measured [15]. After that, 40 g silage sample was taken. Then it was added 360 ml distilled water and shaken for 5 minutes. Mixture was drained by using Whatman no:1 paper. 100 ml were taken from the sample obtained and NH_3-N assay was performed on it by Kjeldahl distillation method. Water soluble carbohydrate values of silages were determined by phenol-sulfuric acid method [16, 17].

The dry matter, crude ash, organic matter, crude protein and ether extract substances were determined according to the methods reported in AOAC [18]. Crude fiber, neutral detergent fiber and acid detergent fiber content of silage samples were analyzed by using Fiber Analyzer (Ankom Technology Corp. Fairport, NY, USA) as decribed by Van Soest et al. [19]. The Flieg scores were calculated using formula (220+(2 x Dry matter % - 15) – 40 x pH). Quality evaluations of silages were carried out according to Flieg scores (81-100 very good, 61-80 good, 41-60 satisfactory, 21-40 medium, 0-20 poorly). Flieg scores and quality classes of silages were carried out by the method described by Kilic [20].

Each of the silages was evaluated in terms of the number of lactic acid bacteria, E*nterobacteriaceae, Listeria* spp, yeast and mould, and sulfite reducing anaerobes [21, 22].

The results were analyzed according to the One-Way Anova procedure in the SPSS package program, and the Duncan Multiple Comparison Test was applied for the differences between the groups [23].

RESULTS

It was determined that the addition of malic acid, whey and malic acid+whey to silages did not affect the physical qualities of vetch- wheat silages in the study (Table 1). Odour, structure and colour were found, respectively minimum 11.6±0.7, maximum 14.0±0.0; minimum 3.6±0.2, maximum 4.0±0.0; minimum 1.8±0.2, maximum 2.0±0.0.

TABLE 1
Physical characteristics of the silages.

Groups	Odour	Structure	Colour
Control	12.7±0.7	4.0±0.0	2.0±0.0
0.3 % malic acid	12.7±0.1	4.0±0.0	1.9±0.1
0.6 % malic acid	12.6±0.5	3.7±0.3	1.9±0.1
0.9 % malic acid	12.5±1.0	3.6±0.2	1.8±0.2
0.3 % whey	14.0±0.0	4.0±0.0	2.0±0.0
0.6 % whey	12.7±0.8	4.0±0.0	2.0±0.0
0.9 % whey	12.7±0.4	4.0±0.0	2.0±0.0
0.3 % malic acid + 0.3 % whey	12.4±0.1	3.6±0.2	1.8±0.2
0.6 % malic acid + 0.6 % whey	11.6±0.7	3.8±0.2	1.9±0.1
0.9 % malic acid + 0.9 % whey	12.5±0.4	3.7±0.2	1.9±0.1

P>0.05 The difference between the groups is not significant.

The chemical analysis results of the silages in the study and the values of the fermentation qualities are given in Table 2. Dry matter, organic matter, crude ash, neutral detergent fiber, acid detergent fiber, crude fiber, crude protein and ether extract values are no significant difference in the groups. The maximum silage pH values was detected in control group (4.39) and 0.3%MA group (4.38). Maximum Flieg score was found in 0.9%MA group (126.59). It is significant difference between the groups (P<0.001).

As a result of microbiological analyzes made in all samples in groups, *Listeria* spp. was not detected. Sulphide reducing anaerobes were found at 4.28 Log (cfu/g) level in a sample of only 0.6% malic acid group, while they were not found in all other samples. Also, *Enterobacteriaceae* 0.6% whey [3.85 Log (cfu/g)], 0.9% whey [4.11 Log (cfu/g)], 0.3% malic acid [4.20 Log (cfu/g)] and 0.9% malic acid [4.64 Log (cfu/g)] were detected only in 4 (four) sample in total.

TABLE 2
Chemical and Fermentation Characteristics of Silages.

Parameters	Control	0.3% W	0.6% W	0.9% W	0.3% MA	0.6% MA	0.9% MA	0.3% W+0.3% MA	0.6%W+0.6% MA	0.9% W+0.9% MA
DM	41.70	39.94	40.25	43.60	43.64	41.49	40.98	40.15	42.77	43.39
OM	33.90	31.82	31.90	31.84	36.35	33.37	33.57	32.35	33.98	35.03
CA	7.71	8.12	8.35	8.76	7.83	8.11	7.41	7.80	8.16	8.26
NDF	43.60	45.74	46.06	45.46	45.29	46.95	46.97	46.32	46.24	46.25
ADF	28.57	29.30	29.05	28.40	27.53	28.85	29.43	29.60	29.43	28.84
CF	27.60	27.69	28.20	28.24	26.49	27.51	28.18	28.08	28.38	26.61
CP	11.70	11.75	11.58	11.00	11.69	11.72	11.44	11.51	11.24	11.15
EE	0.21	0.24	0.26	0.22	0.26	0.21	0.23	0.21	0.27	0.26
pH*	4.39^{a}	4.14^{c}	4.14^{c}	4.14^{c}	4.38^{a}	4.29^{b}	4.24^{b}	4.27^{b}	4.28^{b}	4.12^{c}
FS*	113.01^{c}	119.48^{b}	119.76^{b}	126.59^{a}	117.24^{bc}	116.24^{bc}	117.55^{bc}	114.70^{bc}	119.28^{b}	127.04^{a}
WSC**	11.67^{a}	6.36^{bc}	6.50^{bc}	4.18^{c}	10.92^{ab}	5.77^{c}	7.50^{abc}	8.39^{abc}	5.01^{c}	4.03^{c}
NH_3-N	ND	ND	ND	ND	ND	ND	ND	ND	ND	ND

W: Whey, MA: Malic Acid, DM: Dry Matter, OM: Organic Matter, CA: Crude Ash, NDF: Neutral Detergent Fiber, ADF: Acid Detergent Fiber, CF: Crude Fiber, CP: Crude Protein, EE: Ether Extract, FS: Flieg Score, WSC: Water-Soluble Carbohydrate, ND: Not Detected

* The difference between the groups comprising different letters in the same line is significant (P<0.001)

**The difference between the groups comprising different letters in the same line is significant (P<0.05).

The number of lactic acid bacterias in the groups is given in Table 3. *Lactic* acid bacteria was detected 4.19±0.06 (minimum), 5.75±0.50 (maximum). There is no significant difference between the groups (P>0.05).

TABLE 3
Lactic acid bacteria [Log (cfu/g)].

Groups	Lactic acid bacteria
Control	5.18±0.06
0.3% malic acid	5.33±0.20
0.6% malic acid	5.72±0.54
0.9% malic acid	4.69±0.22
0.3% whey	5.41±0.09
0.6% whey	5.75±0.50
0.9% whey	5.16±0.17
0.3% malic acid + 0.3% whey	4.19±0.06
0.6% malic acid + 0.6% whey	4.55±0.81
0.9% malic acid + 0.9% whey	5.32±0.23

P>0.05 The difference between the groups is not significant.

TABLE 4
Yeast and mould levels in groups [Log (cfu/g)].

Groups	Yeast	Mould
Control	5.11**	2.60*
0.3% malic acid	5.38*	3.30**
0.6% malic acid	3.58**	3.83***
0.9% malic acid	3.79*	4.07*
0.3% whey	2.60**	ND
0.6% whey	3.10**	ND
0.9% whey	3.76**	2.6*
0.3% malic acid + 0.3% whey	ND	ND
0.6% malic acid + 0.6% whey	ND	2.6*
0.9% malic acid + 0.9% whey	ND	2.6*

ND: Not Detected, .* Positive 1 sample, ** Average of positive 2 samples, *** Average of positive 3 samples

Yeast and mould levels in groups were determined in more than one sample, and sample numbers determined by average levels are given in Table 4.

DISCUSSION

It is stated that, in the silages made of legumes, the additives can positively affect the physical qualities of silages [24]. Also, Aksu Elmali and Duru [25] report that the highest scores were obtained for all of the samples in terms of their odour, structure and colour characteristics when using 0.5% malic acid as additive. The findings obtained (Table 1) in this study are also similar to those of Aksu Elmali and Duru [25].

Legumes have been using commonly in fields for grass production from past to present. Interest in the use of legumes as silage materials have increased in the last two decades [26]. In this research performed, vetch-wheat mixture was used as a silage material, moreover whey, malic acid and combinations of both were used in different proportions as a silage additive material. According to the findings obtained (Table 2), when the silages were examined in terms of nutrient substances, the differences in dry matter, crude ash, organic matter, neutral detergent fiber, acid detergent fiber, crude protein and crude fiber substances were not considered as significant (P>0.05). Demirel et al. [5] found that dry matter, crude protein and crude fiber values in vetch silages were only significantly higher than those added corn. This difference may be due to additives used. On the contrary of the present study, Nkosi et al. [27] states that whey causes significant increases in crude protein levels. The reason for this difference may be the level of additives and the difference of silage materials used.

In a study in which organic acid was added, it was found that crude fiber value gave similar results between the groups while there was not significant difference in crude fiber values [28]. Whey addition did not affect crude fiber level in silages [27]. It is expressed that there is no significant difference in crude protein, crude ash, ether extract values in silages added whey [29]. The findings of Koc et al. [28] and Kanengoni et al. [29] are consistent with the available findings of the present study.

It is stated that the low dry matter is increased by additive applications in legume silages [24]. It is also stated that the addition of whey to silage significantly increases the dry matter level [27]. The expressions of Dumlu and Tan [24] and Nkosi et al. [27] are incompatible with this present study. The difference may be stemed from the amount or the type of additive materials and the type of legumes.

It is stated that the addition of formic acid in legume silages causes a significant decrease in the neutral detergent fiber and acid detergent fiber substances [11]. This reported difference may be due to the silage material used in the studies. In the same way, Kanengoni et al. [29] report that whey does not cause a significant difference in acid detergent fiber values.

When silages in the study are examined in terms of fermentation qualities, pH values of groups containing 0.3%, 0.6%, 0.9% whey and 0.9% whey+0.9% malic acid were found to be lower than the control and 0.3% malic acid groups ($P<0.001$). Different additives have different effects on silage pH [30, 31]. It is observed that silage pH is lowered when additives are used in legumes [24]. In a similar study, Demirel et al. [5] reported that the pH value of vetch silage was found as 5.44. As a matter of fact, in a study performed with the same silage materials, it is stated that there are significant differences between sorts in terms of silage pH [32]. It is reported that silage pH decreases significantly by the addition of organic acid [28]. It is also stated that formic acid significantly reduces the silage pH in the legume silage [11]. Similarly in other studies [7, 27, 33], silage pH is significantly reduces when whey is added as an additive to silages.

In silages made of legumes, the additive can have positive effects on the quality class of silages [24]. In this study, flieg scores of groups containing 0.9% malic acid and 0.9% malic acid+0.9% whey were found to be higher than the other groups ($P<0.001$). Similar to this study, Demirel et al. [5] point out that the flieg score is very low only in the vetch silage.

In this study, ammonia nitrogen was not found in all groups. On the other hand, Koc et al. [28] reported that there was a significant difference between their organic acid treatment groups in their study. In contrast to this study, whey is shown to increase ammonia nitrogen levels in silages [29]. Nkosi et al. [27] notes that the addition of whey to silage significantly reduces ammonia nitrogen.

It is found out while the water-soluble carbohydrate values of the groups added 0.9% whey+0.9% malic acid to their vetch-wheat silages are the lowest, water-soluble carbohydrate values of the control groups are the highest ($P<0.05$). Arslan et al. [34] point out that water-soluble carbohydrates significantly increase when the corn amount of the silage material is increased, and also the highest water-soluble carbohydrates are identified in the silages made of corn entirely. It is also stated that the legumes used reduce the ideal water-soluble carbohydrates in silages [34]. These findings are incompatible with the present study. The additives used in the present study significantly affected the amount of water-soluble carbohydrate. The reporting differences in the studies may be due to the additives used. Similar to this study, Nkosi et al. [27] states that whey added to silages significantly reduces water-soluble carbohydrates.

Koc et al. [28] reported that organic acid added to vetch-grain silages significantly increases lactic acid bacteria numbers, and organic acid addition reduces mould growth [28]. When 80%, 60% and 40% maize-soybean mixtures are ensilaged, the total amount of lactic acid bacteria in the maize silage is reported as the lowest [34]. Arslan et al. [34] reported that the leguminous increased the amount of lactic acid bacteria. In this study, it is determined that the number of lactic acid bacteria did not change significantly with respect to the groups ($P>0.05$). Yeast was not detected in 3 (three) groups with whey and malic acid combination. This difference may be due to the type and amount of the organic acid.

When silages are made of 80%, 60%, 40% corn-soybean and silages are made of completely corn, yeast is identified in the range of 0.54-1.56 Log (cfu/g) and mould is identfied 0.18-0.91 Log (cfu/g) in the silages. It is stated that legumes used in silages increase yeast and mould levels significantly [34]. Sahin et al. [35] reported that acid addition significantly reduced the number of moulds and total bacteria. Again, it is reported that an organic acid-based preservative addition inhibits the growth of yeast, mould, *Enterobacteriaceae*, *Clostridia* and *Lactobacillus* spp. in silages [12]. In this study conducted, yeast and/or mould were detected at different levels in the other groups except for 0.3% whey + 0.3% malic acid combination group.

Additives are needed when leguminous feed crops are used as silage material. It was determined that the use of 0.9% whey and 0.9% whey + 0.9% malic acid in silage production from leguminous feeds have positive effects on some quality characteristics in silages, and high quality silages can be obtained with respect to quality class. It has been concluded that the addition of 0.9% whey or 0.9%

whey+0.9% malic acid in vetch-wheat silages can make contributions to a good silage production.

ACKNOWLEDGEMENTS

This work is supported by Uşak University Scientific Projects Unit (Project No: 2013/MF016)

REFERENCES

[1] Machin, D. H. (1999) The potential use of tropical silage for livestock production with special reference to smallholders. FAO Electronic conference on tropical silage. Rome, Italy, 161.

[2] Ergun, A., Tuncer, S. D., Colpan, I., Yalcin, S., Yildiz, G., Kucukersan, M. K., Kucukersan, S., Sehu, A., and Sacakli, P. (2013) Feeds, Feed Hygiene and Technology. 5. Ed, Pozitif, Ankara, Turkey, 757. (in Turkish).

[3] Tan, M., and Serin, Y. (1996) A study on the determination of optimum mixture rates and cutting stages for different vetch+cereal mixtures. Ataturk University Journal of The Faculty of Agriculture. 27(4), 475-489.

[4] Karakozak, E., and Ayasan, T. (2010) Effect of inoculant in silages in which different forage crops and their mixtures on Flieg point and crude nutrient content. Journal of the Faculty of Veterinary Medicine, Kafkas University. 16(6), 987-994.

[5] Demirel, M., Cengiz, F., Celik, S., and Erdogan, S. (2001) A study on degradability in rumen and silage quality of mixture of corn and Hungarian Vetch grown in Van ecological conditions. Yuzuncu Yil University Agriculture Faculty Journal of Agriculture Science. 11(1), 69-78.

[6] Demirci, M., and Simsek, O. (1997) Milk Processing Technology. Hasad, Istanbul, Turkey. ISBN 975-8377-30-2. (in Turkish).

[7] Bautista-Trujillo, G.U., Cobos, M.A., Ventura-Canseco, L.M.C., Ayora-Talavera, T., Abud-Archila, M., Oliva-Llaven, M.A., Dendooven, L., and Gutierrez-Miceli, F.A. (2009) Effect of sugarcane molasses and whey on silage quality of maize. Asian Journal of Crop Science. 1(1), 34-39.

[8] Shibayama, S., Izumi, K., Morimoto, K., No, E., and Nakui, T. (2005) The effects of the addition of dry whey powder on the fermentation quality of corn silage, its intake by sheep, and its degradation in the rumen of sheep. Journal of Rakuno Gakuen University Natural Science. 30(1), 121-126.

[9] Dublecz, K. (2011) Animal Nutrition. Curriculum development for the MSc in Agricultural Engineering. Debrecen, West Hungary and Pannonia University, 1-72.

[10] Lehninger, A.L. (1975) Biochemistry. 2nd edition, Worth Publishers, New York. 584 pp.

[11] Bingol, N.T., Karsli, M.A., Bolat, D. and Akca, I. (2008) The effects of molasses and formic acid addition in sainfoin silage harvested at different maturities on silage quality and digestibility. Van Veterinary Journal. 19(2), 61-66.

[12] Filya, I., and Sucu, E. (2005) Investigations on using organic acids in the silage fermentation 1. The effect of formic acid-based preservative on the fermentation, microbial flora, aerobic stability and in situ rumen degradability characteristics of maize silage in laboratory conditions. Ankara University Faculty of Agriculture Journal of Agricultural Sciences. 11(1), 51-56.

[13] Filya, I., Karabulut, A., Degirmencioglu, T., Canbolat, O., and Kalkan, H. (2001) Improving of conservation and feed value characteristics of citrus pulps. Turkish Journal of Veterinary and Animal Sciences. 25(6), 939-945.

[14] DLG. (1987) Energy and Nutrient Requirements of Farm Animals. 4. Pigs. DLG-Verlag GmbH, Frankfurt, Germany. (in German)

[15] Polan, C.E., Stieve, D.E. and Garrett, J.L. (1998) Protein preservation and ruminal degradation of ensiled forage treated with heat, formic acid, ammonia, or microbial inoculant. Journal of Dairy Science. 81(3), 765-776.

[16] Dubois, M., Gilles, K.A., Hamilton, J.K., Rebers, P.A., and Smith, F. (1956) Colorimetric method for determination of sugars and related substances. Analytical Chemistry. 28(3), 350-356.

[17] Leventini, M.W., Hunt, C.W., Roffler, R.E. and Casebolt, D.G. (1990) Effects of dietary levels of barley-based supplements and ruminal buffer on digestion and growth by beef cattle. Journal of Animal Science. 68(12), 4334-4344.

[18] AOAC Association of Official Analytical Chemists (1999) Official Methods of Analysis. Association of Official Analytical Chemists, 16th Ed., Arlington VA.

[19] Van Soest, P.J., Robertson, J.B., and Lewis, B.A. (1991) Methods for dietary fibre, neutral detergent fibre and non-starch polysaccharides in relation to animal nutrition. Journal of Dairy Science. 74(10), 3583–3597.

[20] Kilic, A. (1986) Silo Feed. Bilgehan Basimevi, Izmir, Turkey, 357. (in Turkish).

[21] Harmon, S.M., Kautter, D.A., and Peeler, J.T. (1971) Improved medium for enumeration of *Clostridium perfringens*. Applied Microbiology. 22(4), 688-692.

[22] Harrigan, W.F. (1998) Laboratory Methods in Food Microbiology. Third Ed., Academic Pres, London, UK.

[23] SPSS. (2007) SPSS for Windows, Version 16.0. Chicago, USA.
[24] Dumlu, Z. and Tan, M. (2009) Determination of silage value of some legumes and mixtures in Erzurum conditions. Ataturk University Journal of The Faculty of Agriculture. 40(2), 15-21.
[25] Aksu Elmali, D. and Duru, M. (2012) Effects of different levels of malic acid on the some quality and micro flora of vetch (*Vicia sativa* L.) silage. Journal of Animal and Veterinary Advances. 11(10), 1651-1655.
[26] Dumlu Gul, Z. and Tan, M. (2013) Using legume forage crops for silage. Ataturk University Journal of The Faculty of Agriculture. 44(1), 189-193.
[27] Nkosi, B.D., Groenewald, I.B., Meeske, R., Motiang M.D. and Langa, T. (2013) Effects of inoculating citrus (*Citrus sinensis*) tree leaves with either bacterial or whey on the fermentation and aerobic stability of silage. African Journal of Agricultural Research. 8(9), 792-796.
[28] Koc, F., Coskuntuna, L., Ozduven, M.L., and Coskuntuna, A. (2010) The effect of organic acid usage at various temperatures on fermentation and aerobic stability of vetch-grain silages. Journal of Tekirdag Agricultural Faculty. 7(2), 159-165.
[29] Kanengoni, A.T., Nkosi, B.D., Chimonyo, M., Ndimba, B. and Dzama, K. (2016) Effects of whey, molasses and exogenous enzymes on the ensiling characteristics, nutrient composition and aerobic stability of maize cobs. South African Journal of Animal Science. 46(2), 113-120.
[30] Cetin, I. and Arslan Duru, A. (2020) Determination of some quality properties of ensiled forage turnip (*Brassica Rapa L.*) with different additives. Fresen. Environ. Bull. 29(4), 2766-2771.
[31] Guney, M., Kale, C., Temur, C., Bingol, N.T. and Aksu, T. (2018) The effect of molasses and pre-fermented lactic acid juice on silage quality and *in vitro* digestibility of sugar beet pulp+wheat straw silage. Fresen. Environ. Bull. 27(11), 7454-7459.
[32] Kavut, Y. T., Soya, H., Geren, H., Geren, H., Unsal, R., Sevim, I. and Avcioglu, R. (2012) Investigations on the herbage yield for silage and silage quality characteristics of some triticale cultivars grown under Menemen conditions. Anadolu. 22(1), 33-44.
[33] Ventura-Canseco, L.M.C., Nuñez, J.A.M., Abud-Archila, M., Oliva-Llaven, M.Á., Dendooven, L. and Gutiérrez-Miceli, F.A. (2012) Sugarcane molasse and whey as additives in the silage of lemongrass (*Cymbopogon citratus* [DC.] Stapf) leaves. Chilean Journal of Agricultural Research. 72(1), 87-91.
[34] Arslan, M., Erdurmus, C., Oten, M., Aydinoglu, B. and Cakmakci S. (2016) Determination of nutritive value of maize silages ensiled with soybean at different rate. Anadolu Journal of Agricultural Sciences. 31(3), 417-422.
[35] Sahin, K., Cerci, I. H., Guler, T., Sahin, N., Kalender, H. and Celik, S. (1999) The effects of different silage additives on the quality of sugar beet pulp silage. Turkish Journal of Veterinary and Animal Sciences. 23(3), 285-292.

Received: **10.02.2020**
Accepted: **17.05.2021**

CORRESPONDING AUTHOR

Dilek Aksu Elmali
Department of Animal Nutrition and Nutritional Diseases
Faculty of Veterinary
Hatay Mustafa Kemal University
Hatay – Turkey

e-mail: daksuelmali@hotmail.com

© by PSP Volume 30– No. 09/2021 pages 10441-10448 Fresenius Environmental Bulletin

EFFECTS OF DIFFERENT COOKING METHODS ON PHYTOCHEMICAL CHARACTERISTICS OF CARROT (*Daucus Carota* L.)

Esma Nur Gecer[1,*], Cemal Kaya[2]

[1]Department of Food Technology Zile Vocational High School, Tokat Gaziosmanpasa University, Tokat- Zile, 60400, Turkey
[2]Department of Food Engineering, Faculty of Engineering and Natural Sciences, Tokat Gaziosmanpasa University, Tokat, 60150, Turkey

ABSTRACT

Just because of phenolic compounds and antioxidant activities, colored fruits and vegetables are increasingly consumed both in Turkey and worldwide. In this study, colored carrot (*Daucuscarota L.*) cultivars were passed through different cooking processes (boiling, microwave cooking and frying) and changes in chemical and phytochemical characteristics were investigated. Total dry matter, pH, total phenolics, anthocyanins, antioxidant capacity and sugar contents of fresh and processed carrot samples were determined. Black and purple carrots had greater phenolic quantities and antioxidant capacity than the light-colored carrots. Following the cooking processes, the greatest antioxidant capacity (FRAP) (91,65 µmol TE/g DW) was observed in microwave cooking of Ereğli Siyahı. The lowest antioxidant capacity (FRAP) (1,07 µmol TE/g DW) was observed in fresh White Satin cultivar. The greatest total phenolics (56,76 mg GAE/g DW) was observed in frying of Ereğli Siyahı cultivar and the lowest value (7,47 mg GAE/g DW) was observed in boiling of Atomic Red cultivar. As compared to fresh samples, cooking processes increased antioxidant capacity of carrot samples. Such an increase was more remarkable in Ereğli Siyahı and Purple Haze cultivars.

KEYWORDS:
Carrot, cooking processes, phenolics, anthocyanins, antioxidant activity

INTRODUCTION

Antioxidants are defined as the substances significantly retarding or inhibiting oxidation. According to this definition, physiological role of antioxidant compounds is to neutralize chemical reactions including free radicals and thus to prevent cells from damages [1,2].

The bioactive phytochemicals rich in antioxidant characteristics include anthocyanins, carotenoids-like natural pigments, ellagic acid and quercetin-like phenolic substances and vitamins (A, E, C and selenium) [3,4].

Plant-originated products contain phenolic phytochemicals which are considered among strongest antioxidants and they play an important role in human health, taste, odor and color formation, color changes and enzyme inhibition, thus they are commonly used as a criterion in purity tests of various foodstuffs [5,4,6,7,8,9,10]. Plant-originated phenolic substances have a strong anti-inflammatory effects, therefore they are mostly used in inhibition of blood thrombocyte aggregation and microbial activity, in treatment of diabetic retinopathy, cholesterol-originated atherosclerosis and cardiovascular diseases and cancer [11,1,12,13,14,15]. Then, it is quite a significant issue to determine phytochemical profile and to get chemical footprint and to determine antioxidant capacity of fruits and vegetables. Such outcomes may also have significant contributions in clinical studies conducted for several diseases.

Majority of vegetables are cooked and consumed then. Cooking significantly alters texture and color parameters of vegetables, chemical composition and concentrations, bioavailability of bioactive compounds. Positive or negative effects of cooking process vary based on cooking conditions, vegetable species, nutritional and morphological characteristics of the vegetables [16,17,18]. Although herbal foodstuffs (vegetables) are recommended to be consumed fresh without any processing, bioavailability of several preservative compounds was reported to increase with cooking. However, there are still ambiguities about the effects of cooking on nutritional attributes of vegetables and such effects haven't been sufficiently quantified and qualified, yet [19,20].

Carrot has long been used as the major vegetable of winter months in Turkey. While carrot is produced as a winter vegetable in Turkey, it is produced in all seasons in the other countries of the world. Annual carrot production of Turkey was 663 882 tonnes in 2019 [21]. Carrot is consumed as fresh, boiled, garniture, vegetable juice and pickle.

This study was conducted to investigate the physical and phytochemical changes in commercially produced different color carrot cultivars after different cooking processes (boiling, frying and microwave cooking).

MATERIALS AND METHODS

Materials. Seven different carrot cultivars [Atomic Red cultivars (red color), Cosmic Purple F1 cultivars (reddish purple color), Ereğli Siyahı cultivars (black color), Parmex (Baby Carrot) cultivars (orange color), Purple Haze F1 cultivars (purple color), Yellow Stone cultivars (yellow color), White Satin cultivars (white color)] were grown in experimental fields of Tokat Gaziosmanpaşa University within the scope of the project "Determination of plant and phytochemical characteristics of different color carrots under Tokat conditions" supported by Scientific Research Projects Department of Tokat Gaziosmanpaşa University. Farmyard manure and ammonium sulphate fertilizations were performed as to have 9 kg/da N (1/2 from manure and 1/2 ammonium sulphate), 3 kg P_2O_5 and 0,7 kg K_2O. Carrots were harvested when they reached to harvest maturity. Harvested carrots were brought to laboratory in the same day. Blueline-brans (home type, 700-Watt power, 17 M x 51 model) microwave oven was used for microwave cooking. Stainless steel saucepan, distilled water or refined sunflower oil were used for boiling and frying processes.

Methods. Inedible sections of the carrots were removed. Randomly selected 20 carrots with a homogeneous and marketable size were sliced into 0.5 cm thick slices with a stainless steel knife.

Sliced carrots were divided into 4 sections of 200 g. One of these sections was analyzed as fresh and the other three sections were subjected to different cooking processes and analyzed then. Following three different cooking methods were applied to sliced carrots [22]. Each cooking process was implemented in three replicates.

Boiling: About 200 g carrot sample was boiled in a stainless steel saucepan for 10 minutes with 300 mL distilled water. Then carrots were rinsed and excess water over them was removed with the aid of a ventilator.

Microwave Cooking: About 200 g carrot sample was placed on glass plate and supplemented with 12 mL distilled water. The place was then wrapped with a stretch film and couple holes were punched over the stretch film. The place was placed into microwave oven and cooked for 15 minutes. Excess water over the samples was again removed with a ventilator.

Frying: About 25 mL refined sunflower oil was placed into stainless steel saucepan. Then, 200 g carrot samples were placed into the heated oil and fired for 5 minutes. Fried samples were cooled with a ventilator. They were washed through chloroform 3 times to remove excess oil on them. Then, chloroform over the fried samples was removed with the aid of a ventilator.

Carrot samples passed through different cooking processes were homogenized with distilled water in a homogenizator and preserved in a deep freezer at -20 °C until the time of analysis.

Analysis Methods. Total Dry Matter. Mashed carrot samples (5-6 g) were dried to a constant mass in an oven at 70ºC. Dry matter contents were expressed in "g/100g'' [23].

pH. Homogenized samples (10 g) were diluted with distilled water and pH of diluted slurry was measured with a glass-electrode WTW-brand (330/Set-1) pH-meter [23].

Total Phenolics. Total phenolics of carrot samples were determined in accordance with Folin-Ciocalteu method. Sample absorbance was read in a spectrophotometer at 750 nm wavelength. Total phenolics corresponding to resultant absorbance were then calculated with the aid of standard curved drawn with the use of gallic acid. Results were expressed in gallic acid equivalent (µg GAE/g dry weight) [24].

Antioxidant capacity (FRAP). Sample absorbance was measured in a spectrophotometer at 593 nm wavelength. Total antioxidant quantities corresponding to resultant absorbance were then calculated with the aid of standard curved drawn with the use of Trolox (10–100 µmol/L). Results were expressed in Trolox equivalent (µmol Trolox/g dry weight) [25].

Total Monomeric Anthocyanin. Sample anthocyanin analysis was conducted with the use of pH-differential method. Sample extracts were prepared with pH 1 and 4,5 buffers and absorbance readings were performed in a spectrophotometer at 520 and 700 nm wavelengths. Total anthocyanins quantity was expressed in µg/g dry weight [26].

Sugar (glucose, fructose, sucrose) Composition. Carrot samples were mixed with distilled water at 1:1 ratio, homogenized in a homogenizator, resultant pulp was centrifuged at 6000 rpm for 10 minutes. Upper clear liquid was taken, filtered through 0,45 µm membrane filter and made ready for analysis. High performance liquid chromatography (HPLC) analyses were implemented as described in Bartolome et al. [27] with slight modifications. Glucose, fructose and sucrose quantities were calculated with the aid of previously prepared standard graph and results were expressed in g/100g dry weight.

HPLC Conditions

Flow rate: 0,9 mL/min

Mobile phase: % 80 acetonitrile + % 20 deionized water

Temperature: 30 ºC

Duration: 30 minutes

Column: SS Exsil Amino, SGE (250x4,6 mm) - USA

Dedector: RI, Perkin Elmer (series-200) - Japan

Statistical Analyses. Experimental data were subjected to analysis of variance with the use of SAS statistical software. Significant means were compared with the aid of Duncan's multiple range test [28].

RESULTS AND DISCUSSION

Total Dry Matter. Total dry matter contents of carrot samples are provided in Table 1. The value was 12,10 g/100g in fresh samples, 11,54 g/100g in boiled ones, 17,88 g/100g in microwave-cooked ones and 20,68 g/100g in fired ones. Cooking processes changes total dry matter quantities of the carrot samples. As compared to fresh samples, total dry matter contents increased with microwave cooking and frying processes and such increases were found to be significant ($p<0.05$).

Greater increases in total dry matter values of frying process were attributed to greater product temperatures in this method than microwave and boiling processes, thus greater water loss in this method.

pH. Generally increasing pH values were observed after different cooking processes (Table 2). As compared to fresh samples, significant changes were observed in pH values with all three cooking processes ($p<0,05$). Besides pH-increasing effect of process water (boiling), different temperatures applied in cooking processes also increased pH values of cooked samples.

Total Phenolics. Total phenolics of carrot samples varied between 11,66-25,09 mg GAE/g DW with the greatest value from Ereğli Siyahı cultivar and the lowest value from Cosmic Purple cultivar (Table 3). The differences in total phenolics of carrot cultivars were found to be significant ($p<0,05$).

TABLE 1
Total dry matter quantities of carrot samples passed through different cooking processes (g/100g)

CULTIVARS	COOKING PROCESS				
	Fresh	Boiling	Microwave	Frying	Mean
Ereğli Siyahı	13,02 $^{b\,A\,*}$	12,13 $^{b\,AB}$	19,29 $^{a\,A}$	21,73 $^{a\,ABC}$	17,72
Purple Haze	13,68 $^{b\,A}$	13,76 $^{b\,A}$	21,20 $^{a\,A}$	22,15 $^{a\,ABC}$	19,04
Cosmic Purple	11,23 $^{c\,AB}$	10,90 $^{c\,AB}$	16,05 $^{b\,B}$	19,96 $^{a\,BC}$	15,64
Atomic Red	12,08 $^{c\,A}$	11,95 $^{c\,AB}$	19,45 $^{b\,A}$	22,48 $^{a\,AB}$	17,96
Parmex	14,13 $^{b\,A}$	12,53 $^{b\,AB}$	21,67 $^{a\,A}$	24,28 $^{a\,A}$	19,49
Yellow Stone	11,83 $^{c\,AB}$	10,29 $^{c\,B}$	15,15 $^{b\,BC}$	19,05 $^{a\,C}$	14,83
White Satin	8,77 $^{b\,B}$	9,33 $^{b\,B}$	12,88 $^{a\,C}$	15,70 $^{a\,D}$	12,64
Mean	12,10 ^{b}	11,54 ^{b}	17,88 ^{a}	20,68 ^{a}	

*The means indicated with the same small letters in the same row and the means indicated with the same capital letters in the same column are not significantly different ($p>0,05$).

TABLE 2
The pH values of carrot samples passed through different cooking processes

CULTIVARS	COOKING PROCESSES				
	Fresh	Boiling	Microwave	Frying	Mean
Ereğli Siyahı	5,72 $^{c\,E\,*}$	6,70 $^{a\,B}$	6,48 $^{b\,A}$	6,56 $^{b\,A}$	6,58
Purple Haze	5,91 $^{c\,D}$	6,52 $^{a\,C}$	6,38 $^{b\,BC}$	6,44 $^{ab\,B}$	6,45
Cosmic Purple	6,38 $^{b\,A}$	6,52 $^{a\,C}$	6,34 $^{b\,C}$	6,30 $^{b\,C}$	6,39
Atomic Red	6,23 $^{b\,B}$	6,46 $^{a\,C}$	6,30 $^{b\,C}$	6,30 $^{b\,C}$	6,35
Parmex	6,11 $^{b\,C}$	6,30 $^{a\,D}$	6,08 $^{b\,D}$	6,12 $^{b\,D}$	6,16
Yellow Stone	6,07 $^{c\,C}$	6,63 $^{a\,B}$	6,50 $^{b\,A}$	6,48 $^{b\,AB}$	6,54
White Satin	6,12 $^{c\,C}$	6,86 $^{a\,A}$	6,45 $^{b\,AB}$	6,53 $^{b\,AB}$	6,61
Mean	6,07 ^{c}	6,58 ^{a}	6,36 ^{b}	6,40 ^{b}	

* The means indicated with the same small letters in the same row and the means indicated with the same capital letters in the same column are not significantly different ($p>0,05$).

TABLE 3
Total phenolics of carrot samples passed through different cooking processes (mg GAE/g DW)

CULTIVARS	COOKING PROCESSES				
	Fresh	Boiling	Microwave	Frying	Mean
Ereğli Siyahı	25,09 $^{b\,A\,*}$	52,56 $^{a\,A}$	55,88 $^{a\,A}$	56,76 $^{a\,A}$	55,07
Purple Haze	20,37 $^{b\,B}$	33,94 $^{a\,B}$	30,18 $^{a\,B}$	29,57 $^{a\,B}$	31,23
Cosmic Purple	11,66 $^{a\,D}$	10,88 $^{a\,CD}$	10,96 $^{a\,C}$	11,77 $^{a\,D}$	11,20
Atomic Red	13,42 $^{a\,D}$	7,47 $^{a\,D}$	10,15 $^{a\,C}$	9,27 $^{a\,D}$	8,96
Parmex	18,54 $^{a\,B}$	17,71 $^{a\,C}$	17,21 $^{a\,C}$	20,08 $^{a\,C}$	18,33
Yellow Stone	19,26 $^{a\,B}$	12,22 $^{a\,CD}$	12,37 $^{a\,C}$	17,12 $^{a\,CD}$	13,90
White Satin	16,72 $^{a\,C}$	11,49 $^{a\,CD}$	11,45 $^{a\,C}$	12,42 $^{a\,CD}$	11,79
Mean	17,86 ^{a}	21,57 ^{a}	21,72 ^{a}	23,08 ^{a}	

* The means indicated with the same small letters in the same row and the means indicated with the same capital letters in the same column are not significantly different (p>0,05).

Significant increases were observed in total phenolics of dark-color carrot cultivars (Ereğli Siyahı and Purple Haze) with cooking processes (p>0,05), but the changes in total phenolics of the other carrot cultivars were not found to be significant (p>0.05). Frying was found to be more effective in preserving phenolics than the other processes. Since majority of phenolics in vegetables are water-soluble and intensified mostly in outer layers, thus they might have been lost through boiling water [29,16,30]. Total phenolics may also increase through softening or destruction of cell walls and destruction of complex phenolics after some processes [17].

Antioxidant capacity. Antioxidant capacity (FRAP values) of fresh samples varied between 1,07-20,51 µmol TE/g DW with the greatest value from Ereğli Siyahı cultivar and the lowest value from White Satin cultivar (Table 4). Except for Ereğli Siyahı, FRAP values of the other carrot cultivars were not significantly different (p>0,05). After all cooking processes, increases in FRAP values were found to be significant in two cultivars (Ereğli Siyahı and Purple Haze) (p<0,05), but were not found to be significant in the other five cultivars (p>0,05).

While the differences in mean FRAP values of boiling (22,38 µmol TE/g), microwave (22,46 µmol TE/g) and frying (22,45 µmol TE/g) processes were not found to be significant (p>0,05), mean FRAP values of all three cooking processes were significantly different from the mean FRAP values of fresh samples (p<0,05).

Present findings were complying with the results of Padmini et al. [31], but were different from the results of Sultana et al. [22].

Total Monomeric Anthocyanin. Total monomeric anthocyanins of fresh samples were 0,13 mg cy-3-glu/g DW in Ereğli Siyahı cultivar and 0,10 mg cy-3-glu/g DW in Purple Haze cultivar (Table 5). The difference in total monomeric anthocyanins of two cultivars were not found to be significant (p>0,05).

TABLE 4
FRAP values of carrot samples passed through different cooking processes (µmol TE/g DW)

CULTIVARS	COOKING PROCESSES				
	Fresh	Boiling	Microwave	Frying	Mean
Ereğli Siyahı	20.51 $^{b\,A\,*}$	89.61 $^{a\,A}$	91.65 $^{a\,A}$	86.84 $^{a\,A}$	89,37
Purple Haze	11.89 $^{b\,B}$	37.15 $^{a\,B}$	32.82 $^{a\,B}$	33.50 $^{a\,B}$	34,49
Cosmic Purple	4.06 $^{a\,C}$	6.52 $^{a\,C}$	7.89 $^{a\,C}$	7.82 $^{a\,C}$	7,41
Atomic Red	4.94 $^{a\,C}$	5.38 $^{a\,C}$	6.54 $^{a\,C}$	6.50 $^{a\,C}$	6,14
Parmex	2.06 $^{a\,CD}$	6.77 $^{a\,C}$	7.43 $^{a\,C}$	8.43 $^{a\,C}$	7,54
Yellow Stone	2.42 $^{a\,CD}$	3.54 $^{a\,CD}$	3.30 $^{a\,CD}$	5.27 $^{a\,C}$	4,04
White Satin	1.07 $^{a\,D}$	1.98 $^{a\,D}$	2.32 $^{a\,D}$	3.48 $^{a\,CD}$	2,59
Mean	6.71 ^{b}	22.38 ^{a}	22.46 ^{a}	22.45 ^{a}	

* The means indicated with the same small letters in the same row and the means indicated with the same capital letters in the same column are not significantly different (p>0,05).

TABLE 5
Total monomeric anthocyanin quantities of carrot samples passed through different cooking processes (mg cy-3-glu/g DW)

CULTIVARS	COOKING PROCESSES				
	Fresh	Boiling	Microwave	Frying	Mean
Ereğli Siyahı	0,13 $^{c\,A}$ *	1,76 $^{a\,A}$	1,73 $^{a\,A}$	1,32 $^{b\,A}$	1,60
Purple Haze	0.10 $^{b\,A}$	0.67 $^{a\,B}$	0.67 $^{a\,B}$	0.58 $^{a\,B}$	0.64
Mean	0,11 ^{c}	1,22 ^{a}	1,20 ^{a}	0,95 ^{b}	

* The means indicated with the same small letters in the same row and the means indicated with the same capital letters in the same column are not significantly different (p>0,05).

Considering the mean monomeric anthocyanin values of fresh samples (0,11 mg cy-3-glu/g DW), boiling (1,22 mg cy-3-glu /g DW), microwave (1,20 mg cy-3-glu/g DW) and frying (0,95 mg cy-3-glu/g DW) processes, it was observed that all three cooking processes increased monomeric anthocyanins and values of fresh samples were significantly different from the values of cooking processes ($p<0.05$). Increase in total monomeric anthocyanins with cooking processes were attributed to preservation of anthocyanins through deactivation of enzymes with heat treatments or preservation of Flavylium system through copigmentation of some compounds [32,33,34].

Sugar (glucose, fructose, sucrose) Composition. Total sugar content of fresh samples varied between 33,79-42,30 g/100 g DW with the greatest value from Cosmic Purple cultivar and the lowest value from Atomic Red cultivar (Table 6). While there were not any significant differences in sugar contents of Cosmic Purple, Parmex, Yellow Stone, White Satin and Ereğli Siyahı cultivars, sugar contents of Purple Haze and Atomic Red were significantly different from the others ($p<0,05$).

Considering the mean sugar content of fresh samples (38,78 g/100g DW), boiling (38,55 g/100g DW), microwave (41,84 g/100g DW) and frying (37,41 g/100g DW) processes, it was observed that sugar contents of cooking processes were not significantly different from the sugar content of fresh samples ($p>0,05$).

Türkmen et al. [16] investigated the effects of microwave and traditional cooking methods on antioxidant activity and total phenolics of pepper, zucchini, fresh bean, peas, spinach, broccoli and leaks. Total phenolics content of fresh vegetables were reported as between 183,2-344,7 mg GAE/100 g DW and total antioxidant activities were reported as between 12,2-78,2%. Following the cooking process, total antioxidant activity either increased or stay constant based on vegetable species.

In a study investigating the effects of home-cooking methods (boiling, frying, baking, pressure cooking, microwave) on antioxidant activity of the vegetables, antioxidant capacity of 20 different vegetables were investigated. Carrot, celery and green bean had increased Trolox equivalent antioxidant capacity (TEAC) values after all cooking processes [35].

Mirzaei et al. [36] applied 4 different cooking methods (boiling, pressure cooking, microwave cooking and frying) to fresh broccoli, spinach and green peppers and investigated total phenol and antioxidant activity of the vegetables. Total phenol contents of fresh vegetables varied between 882-1306 mg GAE/100 g DW, significant decreases were observed in total phenolics of spinach and broccoli with cooking and significant increases were reported in total phenolics of spinach with boiling (8%) and frying (4%). As compared to fresh vegetables, contrary to TEAC method, antioxidant activity by DPPH assay increased with all cooking methods.

TABLE 6
Total sugar content of carrot samples passed through different cooking processes (g/100g DW)

CULTIVARS	COOKING PROCESSES				
	Fresh	Boiling	Microwave	Frying	Mean
Ereğli Siyahı	40,06 $^{a\,A}$ *	36,42 $^{ab\,BC}$	39,90 $^{a\,BC}$	33,91 $^{b\,CD}$	36,74
Purple Haze	34,07 $^{a\,B}$	35,67 $^{a\,CD}$	37,69 $^{a\,C}$	36,03 $^{a\,BCD}$	36,46
Cosmic Purple	42,30 $^{a\,A}$	40,49 $^{a\,AB}$	42,16 $^{a\,BC}$	40,14 $^{a\,AB}$	40,93
Atomic Red	33,79 $^{b\,B}$	31,83 $^{b\,D}$	40,23 $^{a\,BC}$	33,11 $^{b\,D}$	35,06
Parmex	41,49 $^{b\,A}$	39,65 $^{b\,ABC}$	47,14 $^{a\,A}$	42,37 $^{b\,A}$	43,05
Yellow Stone	38,66 $^{ab\,A}$	39,90 $^{ab\,ABC}$	43,07 $^{a\,AB}$	36,49 $^{b\,BCD}$	39,82
White Satin	41,09 $^{ab\,A}$	43,66 $^{a\,A}$	42,15 $^{ab\,BC}$	38,41 $^{b\,ABC}$	41,41
Mean	38,78 ^{a}	38,55 ^{a}	41,84 ^{a}	37,41 ^{a}	

* The means indicated with the same small letters in the same row and the means indicated with the same capital letters in the same column are not significantly different (p>0,05).

Padmini et al. [31] investigated the effects of 4 different cooking method (boiling, pressure cooking, microwave cooking, stir-frying) on phenolic compounds and antioxidant activity of red beet, carrot, small onion, bitter melon, eggplant and tomatoes. It was reported that cooking methods reduced ascorbic acid and carotenoids-like antioxidant compounds and increased total polyphenol, total flavonoid and tannin quantities and antioxidant activity. In was indicated that antioxidant potential could be increased through inhibition of enzyme activity, conversion of antioxidant into more active compounds and softening tissues with minimum cooking and water use.

In another study investigating the effects of different cooking methods (boiling, frying and microwave cooking) on antioxidant activity and total phenolics of some selected vegetables (carrot, peas, spinach, cauliflower and etc.), decreasing total phenolics values were reported after boiling, frying and microwave cooking methods. Research findings revealed that all cooking methods influenced antioxidant characteristics of the vegetables. However, microwave cooking had greater negative impacts on investigated parameters of the vegetables as compared to the other cooking methods [22].

CONCLUSION

Among the fresh carrot samples, Ereğli Siyahı had the greatest total phenolics (25,09 mg GAE/g DW) and it was respectively followed by purple, yellow, orange, white and red color carrots. The lowest total phenolics was observed in Cosmic Purple cultivar (11,66 mg GAE/g DW). As compared to fresh samples, following the cooking processes, increases were observed in total phenolics of black and purple carrots and decreases were observed in total phenolics of the other color carrots. Considering the cooking processes, it was observed that the greatest increase in total phenolics (126.22%) was observed in frying process of Ereğli Siyahı cultivar and the greatest decrease (44,34%) was observed in boiling process of Atomic Red cultivar.

The greatest total monomeric anthocyanin content fresh samples was observed in Ereğli Siyahı cultivar (0,13 mg cy-3-glu/g DW). Following all cooking processes, again Ereğli Siyahı had the greatest value total monomeric anthocyanin content (1,32-1,76 mg cy-3-glu/g DW). There was a remarkable increase also in total monomeric anthocyanins content of Purple Haze cultivar after cooking processes. In both cultivars, the greatest increase was achieved through boiling and microwave cooking processes.

In fresh samples, the greatest FRAP was observed in Ereğli Siyahı cultivar (20,51 µmol TE/g DW), the same cultivar had again the greatest FRAP (86,61-91,65 µmol TE/g DW) after all cooking processes. Although not as much remarkable as Ereğli Siyahı cultivar, increases were observed in FRAP values of the other carrot cultivars as compared to initial values. Considering the cooking processes, the greatest increase in FRAP values was achieved in microwave cooking process of Ereğli Siyahı cultivar.

Present findings revealed that black and purple carrot cultivars had the greatest total phenolics, anthocyanins and antioxidant capacity and better preserved these high values after different cooking processes. Consumption of colored carrots with a high antioxidant capacity is thought to be an appropriate nutritional behavior for a healthy life.

ACKNOWLEDGEMENT

This study was financially supported by Scientific Research Projects Department of Tokat Gaziosmanpaşa University with a project number of 2010/101.

REFERENCES

[1] Huang, D., Ou, B., Prior, R.L. (2005) The chemistry behind antioxidant capacity assays. Journal of Agricultural and Food Chemistry. 53, 1841-1856.

[2] Prochazkova, D., Bousova, I., Wilhelmova, N. (2011) Antioxidant and prooxidant properties of flavonoids. Fitoterapia. 82, 513-523.

[3] Kalt, W. (2005) Effects of production and processing factors on major fruit and vegetable antioxidants. Journal of Food Science. 70(1), 11-19.

[4] Dimitrios, B. (2006) Sources of natural phenolic antioxidants. Trends in Food Science and Technology. 17, 505-512.

[5] Kim, D.O., Lee, C.Y. (2004) Comprehensive study on vitamin C equivalent antioxidant capacity (VCEAC) of various polyphenolics in scavenging a free radical and its structural relationship. Critical Reviews in Food Science and Nutrition. 44, 253- 273.

[6] Nichenametla, S.N., Taruscio, T.G., Barney, D.L., Exon, J.H. (2006) A review of the effects and mechanisms of polyphenolics in cancer. Critical Reviews in Food Science and Nutrition. 46(2), 161-183.

[7] Fernandez-Panchon, M.S., Villano, D., Troncoso, A.M., Garcia-Parrilla, M.C. (2008) Antioxidant activity of phenolic compounds: from in vitro results to in vivo evidence. Critical Reviews in Food Science and Nutrition. 48, 649-671.

[8] Kennedy, J.A. (2008) Grape and wine phenolics: Observations and recent findings. Ciencia e Investigación Agraria. 35(2), 107-120.

[9] Boeing, H., Bechthold, A., Bub, A., Ellinger, S., Haller, D., Kroke, A., Leschik-Bonnet, E., Müller, M.J., Oberritter, H., Schulze, M., Stehle, P., Watzl, B. (2012) Critical review: Vegetables and fruit in the prevention of chronic diseases. European Journal of Nutrition. 51(6), 637-663.

[10] Newair, E.F., Kilmartin, P.A., Garcia, F. (2018) Square wave voltammetric analysis of polyphenol content and antioxidant capacity of red wines using glassy carbon and disposable carbon nanotubes modified screen-printed electrodes. European Food Research and Technology. 244, 1225-1237.

[11] Kaur, C., Kapoor, H.C. (2001) Antioxidants in fruits and vegetables The millennium's health. International Journal of Food Science and Technology. 36, 703-725.

[12] Arslan, D. (2015) Effects of degradation preventive agents on storage stability of anthocyanins in sour cherry concentrate. Agronomy Research. 13, 892-899.

[13] Kasnak, C., Palamutoğlu, R. (2015) Classification and Human Health Effects of Natural AntioxidantsTurkish Journal of Agriculture - Food Science And Technology, 3(5), 226-234. (in Turkish)

[14] Todorova, M.N., Pasheva, M.G., Kiselova-Kaneva, Y.D., Ivanova, D.G., Galunska, B.Tz. (2018) Phenolics content and antioxidant activity of beverages on the Bulgarian market wines, juices and compotes. Bulgarian Chemical Communications. 50, 164-168.

[15] Zehiroğlu, C., Öztürk Sarıkaya, S.B. (2019) The importance of antioxidants and place in today's scientific and technological studies. Journal of Food Science and Technology. 56, 4757-4774.

[16] Türkmen, N., Sari, F., Velioğlu, S.Y. (2005) The effect of cooking methods on total phenolics and antioxidant activity of selected green vegetables. Food Chemistry. 93, 713-718.

[17] Bernhardt, S., Schlich, E. (2006) Impact of different cooking methods on food quality: Retention of lipophilic vitamins in fresh and frozen vegetables. Journal of Food Engineering. 77, 327-333.

[18] Waldron, K.W., Smith, A.C., Parr, A.J., Parker, M.L. (2007) New approaches to understanding and controlling cell separation in relation to fruit and vegetable texture. Trends in Food Science and Technology. 8, 213-221.

[19] Link, L.B., Potter, J.D. (2004) Raw versus cooked vegetables and cancer risk. Cancer Epidemiology, Biomarkers and Prevention. 13, 1422-1435.

[20] Clement, B.R. (2012) Food is medicine: The Scientific Evidence-Volume one London.

[21] TUIK. (2019) Crop Production Statistics, Turkish Statistical Institute. http://www.tuik.gov.tr/PreTablo.do?alt_id=1001. (Accessed date: 10.05.2020)

[22] Sultana, B., Anwar, F., Iqbal, S. (2008) Effect of different cooking methods on the antioxidant activity of some vegetables from Pakistan. International Journal Food of Science and Technology. 43, 560-567.

[23] Cemeroğlu, B. (2007) Food Analysis, Food Technology Association Publications, Ankara, 1-535. (in Turkish)

[24] Singleton, V.L., Rossi, J.L. (1965) Colorimetry of total phenolics with phosphomolybdic-phosphotungstic acid reagents. American Journal of Enology and Viticulture. 16, 144-158.

[25] Benzie, I.F.F., Strain, J.J. (1996) The Ferric Reducing Ability of Plasma (FRAP) as a measure of "Antioxidant Power": The FRAP assay. Analytical Biochemistry. 239, 70-76.

[26] Giusti, M. M., Wrolstad, R. E. (2001). Characterization and measurement of anthocyanins by UV-visible spectroscopy. Current Protocols In Food Analytical Chemistry (edited by R.E. Wrolstad, T.E. Acree & H. An). 121–129. New York: Wiley Inc.

[27] Bartolome, A.P., Ruperez, P., Fuster, C. (1995) Pineapple fruit: Morphological characteristics, chemical composition and sensory analysis of red spanish and smoot cayenne cultivar. Food Chemistry. 53, 75-79.

[28] Yıldız, N., Bircan, H. (1994) Research and Experimental Methods. Ataturk University Textbooks Series. A.U. Faculty of Agriculture Offset Facility, Erzurum, 697, 1-154. (in Turkish)

[29] [29] Barroga, C.F., Laurena, A.C., Mendoza, E.M.T. (1985) Polyphenols in mungbean (Vignaradiata (L.) Wilczek): Determination and removal. Journal of Agricultural and Food Chemistry. 33(5), 1006-1009.

[30] Rocha, N., Herzog, A., Gonzalez-Laredo, R.F., Ibarra-Perez, F.J. (2007) Antioxidant and antimutagenic activity of phenolic compounds in three different colour groups of common bean cultivars (Phaseolus vulgaris L). Food Chemistry. 103(2), 521-527.

[31] Padmini, T., Karpagavalli, B., Vijayalakshmi, R., Jesupriya Poornakala, S. (2015) Effect of cooking methods on antioxidant properties of vegetables. International Journal of Current Research. 7(12), 23466-23470.

[32] Skrede, G., Wrolstad, R.E., Durst, R.W. (2000) Changes in anthocyanins and polyphenolics during juice processing of high-bush blueberries (*Vaccinium corymbosum* L.). Journal of Food Science. 65, 357-364.

[33] Kırca, A., Ozkan, M., Cemeroğlu, B. (2007) Effects of temperature, solid content and pH on the stability of black carrot anthocyanins. Food Chemistry. 101(1), 212-218.

[34] Patras, A., Brunton, N.P., O'Donnell, C., Tiwari, B.K. (2010) Effect of thermal processing on anthocyanin stability in foods; mechanisms and kinetics of degradation. Trends in Food Science and Technology. 21, 3-11.
[35] Jimenez-Monreal, A.M., Garcia-Diz, L., Martinez-Tome, M., Mariscal, M., Murcia, M.A. (2009) Influence of cooking methods on antioxidant activity of vegetables. Journal of Food Science. 74(3), 97-103.
[36] Mirzaei, A., Delaviz, H., Mohammadi, H. (2014) The effects of cooking methods on antioxidant activity and phenol content in vegetables. World Journal of Pharmacy and Pharmaceutical Sciences. 3(7), 242-252.

Received: **12.06.2020**
Accepted: **28.05.2021**

CORRESPONDING AUTHOR

Esma Nur Gecer
Department of Food Technology
Zile Vocational High School,
Tokat Gaziosmanpasa University,
Zile 60400 Tokat – Turkey

e-mail: esma.gecer@gop.edu.tr

© by PSP Volume 30– No. 09/2021 pages 10449-10456 Fresenius Environmental Bulletin

IMPLICATIONS OF VARIABILITY IN MECHANICAL CHARACTERISTICS OF RICE STRAW UNDER DIFFERENT MOISTURE, VARIETY AND LOADING RATE

Shakeel Ahmed Soomro[1,2], Kunjie Chen[1,*], Altaf Ali Siyal[2], Abdullah Sessiz[3], Bakhtawar Wagan[2], Muhammad Sohail Memon[2], Zubair Ahmed Soomro[4], Mecha Peter[1,5], Haolu Liu[6], Zhenjie Yang[1]

[1]College of Engineering, Nanjing Agricultural University, Nanjing, 210031, China
[2]Faculty of Agricultural Engineering, Sindh Agriculture University, Tandojam, 70060, Pakistan
[3]Department of Agricultural Machinery and Technologies Engineering, Faculty of Agriculture, Dicle University, Diyarbakir, 21280, Turkey
[4]Department of Veterinary Pathology, Sindh Agriculture University, Tandojam, 70060, Pakistan
[5]Department of Agricultural Engineering, Faculty of Engineering, Egerton University, Kenya
[6]Nanjing Institute for Agricultural Mechanization, Ministry of Agriculture and Rural Affairs, Nanjing, 210014, China

ABSTRACT

Exact information of mechanical properties of straw are necessary to be executed for designing the equipment's and machineries being used for harvesting, threshing and other post-harvest practices. This study in this importance was carried out to assess the mechanical properties of rice straw as effected by different moisture, variety and loading rates, which have never been accounted before. Three different rice varieties i.e. Yue76, Qianjindao and Yue61 when harvested were collected for experimentation. Mechanical properties of rice straw were evaluated at three internodes (IN1, IN2 and IN3) down from ear, and were subject to two different moisture contents (11 and 18%) and loading rates (10 and 20 mm min^{-1}). The experimental design was subject to randomized complete block design, replicated thrice. The results revealed that the rice straw parameters and their interactions were significantly affected ($p \leq 0.05$) by different moisture content, variety and loading rate. The average values obtained were significantly different from each other, the average values for shear strength were observed to be 14.18, 9.95 and 11.99 MPA, for specific shearing energy the average values were observed to be 17.30, 13.34 and 15.93 mJ mm^{-2}, for bending strength the averages values were observed to be 11.33, 7.40 and 9.54 MPa, and for young's modulus the average values were observed to be 1.06, 0.73 and 0.99 GPa for Yue76, Qianjindao and Yue61 varieties respectively. The study revealed that shear strength and specific shearing energy increased with increasing moisture content and loading rate, where the bending strength and young's modulus decreased. The outcomes of current study revealed a wide variation between the parameters observed, which makes it necessary to assess the mechanical properties of rice straw before designing and judging the equipments and machineries being used for post-harvest operations.

KEYWORDS:
Rice straw, Moisture, Variety, Loading rate, Mechanical properties

INTRODUCTION

Being one of the prominent cereal crops in China, rice is being consume by about 65 % of its population [1]. China with 28.7% of the global rice production makes it World's leading rice producing country, which for World's food security also plays an important role [2]. Area wise China shares about 19% of its planting area for rice, where every ton of grain harvested leaves 1.35 tons of rice straw at field [3]. Crop straws currently are being used as fuel, feedstuff, fertilizer, industrial raw material and mulch to improve the soil stability [4].

Increased mechanized harvesting practices of rice and wheat crops and the commercial use of straw have led to necessarily acquire the mechanical properties of straw [5, 6]. Koloor and Borgheie [7] reported that, proper information of physical and mechanical properties of rice straws are necessarily to be executed while designing a rice harvesting machine. To better understand the behavior of material, the variation in physical properties of straw and equipment's cutting resistance are necessarily to be known [8]. Chakraverty et al. [9] reported that the cutting energy requirements, cutting force and stress applied are main factors which are necessary to be observed while judging the performance of cutting elements applied in harvester design. Information of mechanical characteristics are important for the design and analysis of the behavior of straw during the harvesting operations [10]. Cutting compression, tension, bending, shearing, and friction etc. are the important properties of cellular material, which depends on the variety, stalk diameter, maturity, moisture content and structure [11]. Physico-mechanical properties such as bending and shearing stress, and energy requirements of rice straw are important

while designing suitable cutting devices and optimising the operational parameters [12,13]. Properties such as diameter, length, variety, maturity and structure are necessary to be known to study the behaviour of straw [14].

Similar work in recent years have been reported by various researchers i.e. Chen et al. [15] on hemp stems, İnce et al. [12] on sunflower stalks, Galedar et al. [16] on alfalfa stems, Tavakoli et al. [17] on barely straw and Reza [18] on the cutting energy of rice stem by an impact shear test apparatus. But as a result of a literature survey it was observed that, the study to determine the shear strength, specific shearing energy, bending strength and young's modulus of rice straw as affected by different moisture content, variety and loading rate has never been reported before. This study was therefore carried out to fill the research gap.

MATERIALS AND METHODS

Study area. The study was carried out at the College of Engineering, Nanjing Agricultural University, Jiangsu, China. Three different varieties named Yue76, Qianjindao and Yue61, when harvested from Jiangpu Agriculture Farm were collected for determining the mechanical characteristics. Samples of the rice stems were cut from the ground level, sealed in polyethylene bags and transferred to the laboratory. First three internodes down from ear labelled as IN1, IN2 and IN3 (Figure 1a) were separated and studied removing extraneous material prior to experiment, whereas fourth lower stem was not considered as they usually are left on field [10]. Rice straw varieties were subject to two different loading rates i.e. 10 and 20 mm min^{-1} at two different moisture contents i.e. 11 and 18%. Length, thickness and diameter of each internode was measured using a digital Vernier caliper with an accuracy of 0.01mm. Moisture content in rice straw was determined by keeping the samples in oven for 24 hours at a temperature of 105 ºC [19].

Experimental setup. A TMS-Pro machine (FTC Co. USA) computer program for data acquisition (computer-controlled texture measurement system) was used for shearing and bending tests (Figure 2). Mechanical properties assessed were determined using similar procedure adopted by İnce et al. [12]; Galedar et al. [16] and Tavakoli et al. [17].

Shearing test. Shear box of steel with dimensions of 130 × 90 × 25 mm (Figure 1b) attached to compressive testing machine (TMS-Pro computer-controlled texture measurement system) was used for measuring the shear strength. The shear box with holes ranging from 2 to 7 mm was used for accommodating internodes having different diameters. Shear box attached with compressive testing machine was operated at two different loading rates i.e. 10 and 20 mm min^{-1}. The tested force was applied and recorded till specimen failure. Shear failure stress (τs) of specimen was calculated using Equation 1 [17, 20, 21]. Area under curves of shear force and displacement were integrated for determining the shearing energy. The specific shearing energy (Esp) was calculated using Equation 2 [15,16,22].

$$\tau s = \frac{F}{2A} \quad (1)$$

$$Esp = \frac{Es}{A} \quad (2)$$

Bending test. For determining the young's modulus and maximum bending strength, the sample of specimen was placed on two metallic supports which were kept at a distance of 60 mm. The load on specimen was then applied at the mid of both supports by movable driven blade. The test was conducted at two different loading rates and at different moistures on all three internodes i.e. IN1, IN2 and IN3 [16,17,21]. Equation 3 was used for calculating second moment of area (I_b) [23]. The bending strength (σ_b) was calculated using Equation 4 [23,24]. The Young's modulus (E) for a simply supported beam loaded at its centre was calculated using Equation 5 [23].

$$I_b = \frac{\pi}{4}\left[ab^3 - (a-t)(b-t)^3\right] \quad (3)$$

$$\sigma_b = \frac{F_b a l}{4 I_b} \quad (4)$$

$$E = \frac{F_b b l^3}{48 \sigma_b I_b} \quad (5)$$

Statistical Analysis. The study was planned as a randomized complete block design (RCBD) replicated thrice. Analysis of variance (ANOVA) was carried out using Statistix software (Ver. 8.1), the data was analysed at a significant level of $p \leq 0.05$ and the means were separated using Tukey's multiple range test.

RESULTS AND DISCUSSION

The analysis of variance (ANOVA) for rice straw at different moisture, variety and loading rate is presented in Table 1. The results revealed that shear strength, specific shearing energy, bending strength and young's modulus were significantly ($p \leq 0.05$) affected by moisture content (MC), variety (VR) and loading rate (LR). The interaction between VR × MC, VR × Internode (IN), VR × LR, MC × IN, MC × LR, IN × LR, VR × MC × IN, VR × MC × LR, VR × IN × LR, MC × IN × LR and VR × MC × IN × LR when observed were also statistically different ($p \leq 0.05$), except VR × LR for shear strength,

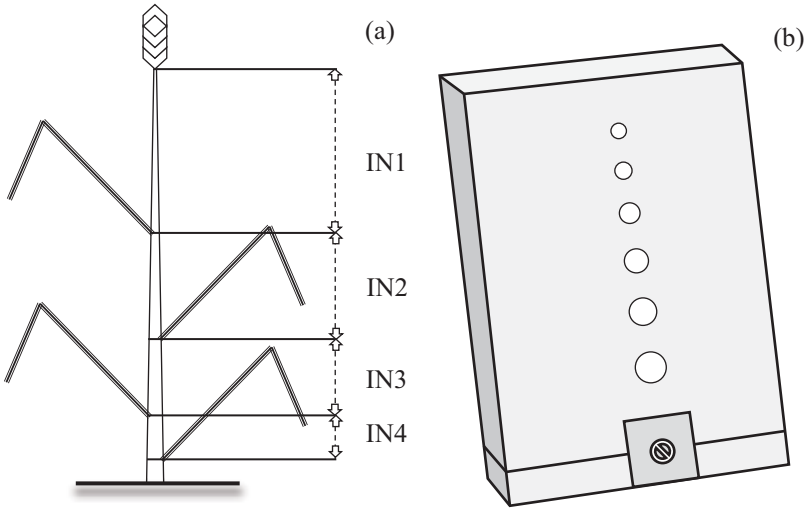


FIGURE 1
Schematic presentation of rice straw (a) and shear box (b)

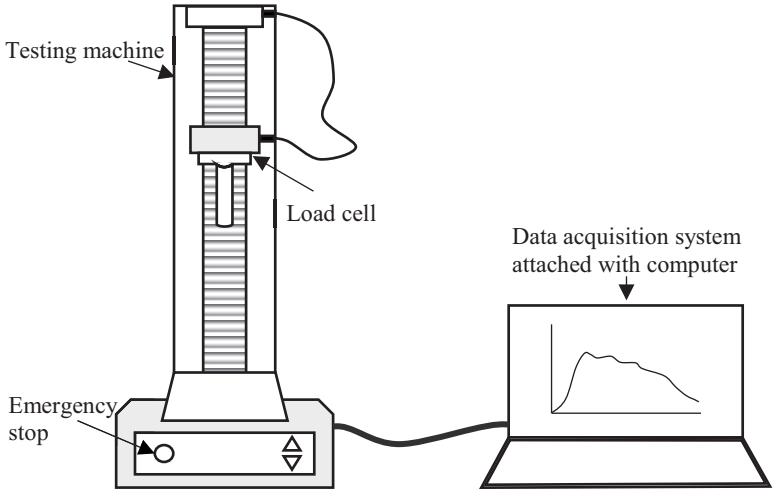


FIGURE 2
TMS-Pro computer-controlled texture measurement system

VR × MC and MC × IN for specific shearing energy, and IN × LR, VR × MC × IN, VR × MC × LR and VR × IN × LR for young's modulus.

Shear strength. The mean values of mechanical properties of rice straw for different moisture content, variety, loading rate and internode positions are presented in Table 2. It was observed that the shear strength increased with increasing moisture content, variety and loading rate for all internodes of rice straw (Figures 3a and 3b). Shear strength for Yue76 variety ranged from 11.12 MPa for IN1 at moisture of 11% and loading rate of 10 mm min^{-1} to 17.07 MPa for IN3 at moisture of 18% and loading rate of 20 mm min^{-1}, for Qianjindao the shear strength varied from 8.03 MPa at loading rate of 10 mm min^{-1} to 11.94 MPa at a loading rate of 20 mm min^{-1}, and for Yue61 the shear strength varied from 9.13 MPa at moisture of 11% and loading rate of 10 mm min^{-1} to 15.22 MPa at moisture of 18% and loading rate of 20 mm min^{-1}. Shear strength as per Tukey's multiple range test was significantly affected having different values by the treatments being applied. The values of shear strength increased towards third internode (IN3) for different moistures and loading rates. The values were greater for Yue76, followed by Yue61 and Qianjindao. Similar findings for different crops have also been reported by Annoussamy et al. [10] for wheat straw; Tavakoli et al. [20] for wheat straw and Ahmad et al. [25] for wheat straw.

Specific shearing energy. Specific shearing energy for all internodes increased with increasing moisture, variety and loading rate (Figures 4a and 4b). According to Tukey's multiple range test, the values for rice straw were different for different moisture content, variety and loading rate at all internodes (Table 2). Specific shearing energy for Yue76 varied from 14.86 mJ mm^{-2} for IN1 at 11% moisture and loading rate of 10 mm min^{-1} to 20.27 mJ mm^{-2} for

TABLE 1
Analysis of variance of rice straw as affected by moisture content, variety and loading rate.

	Source	DF	SS	MS	F
Shear strength	Variety	2	322.307	161.154	47077.60**
	Moisture	1	41.503	41.503	12124.20**
	Node	2	172.704	86.352	25226.00**
	Speed	1	21.789	21.789	6365.22**
Specific shearing energy	Variety	2	290.969	145.485	4522.19**
	Moisture	1	49.343	49.343	1533.75**
	Node	2	107.143	53.572	1665.20**
	Speed	1	118.022	118.022	3668.56**
Bending strength	Variety	2	278.577	139.288	34072.80**
	Moisture	1	12.067	12.067	2951.78**
	Node	2	101.656	50.828	12433.60**
	Speed	1	10.817	10.817	2646.14**
Young's modulus	Variety	2	2.17287	1.08643	1422.24**
	Moisture	1	0.20193	0.20193	264.35**
	Node	2	4.04934	2.02467	2650.48**
	Speed	1	0.18833	0.18833	246.55**

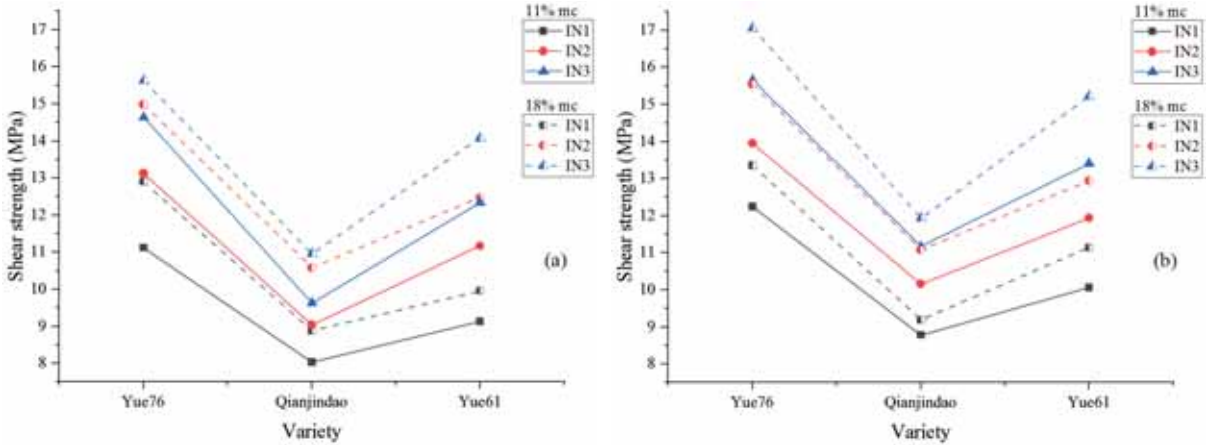


FIGURE 3
Shear strength of rice straw as affected by moisture content and variety for internodes at loading rate of 10 mm min^{-1} (a) and 20 mm min^{-1} (b).

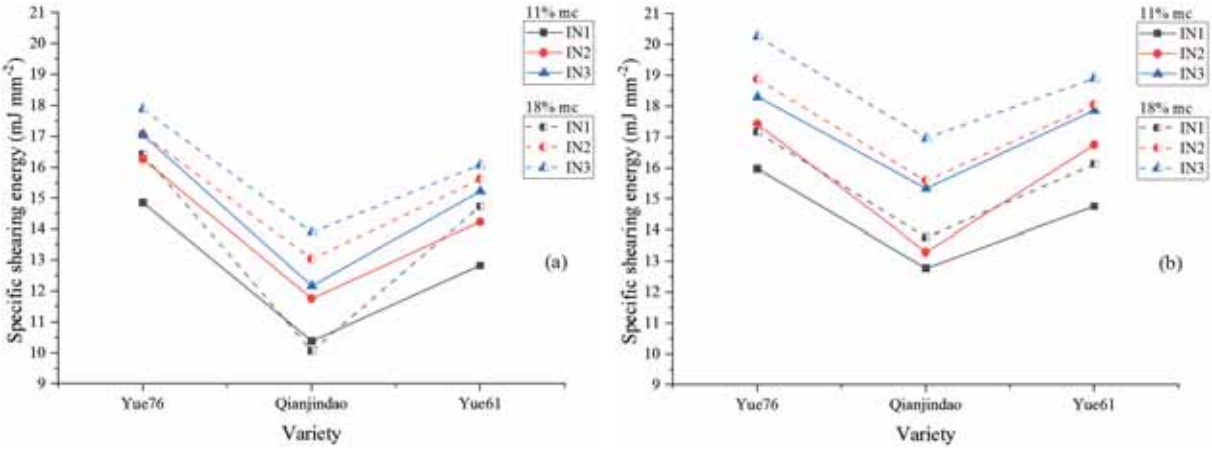


FIGURE 4
Specific shearing energy of rice straw as affected by moisture content and variety for internodes at loading rate of 10 mm min^{-1} (a) and 20 mm min^{-1} (b).

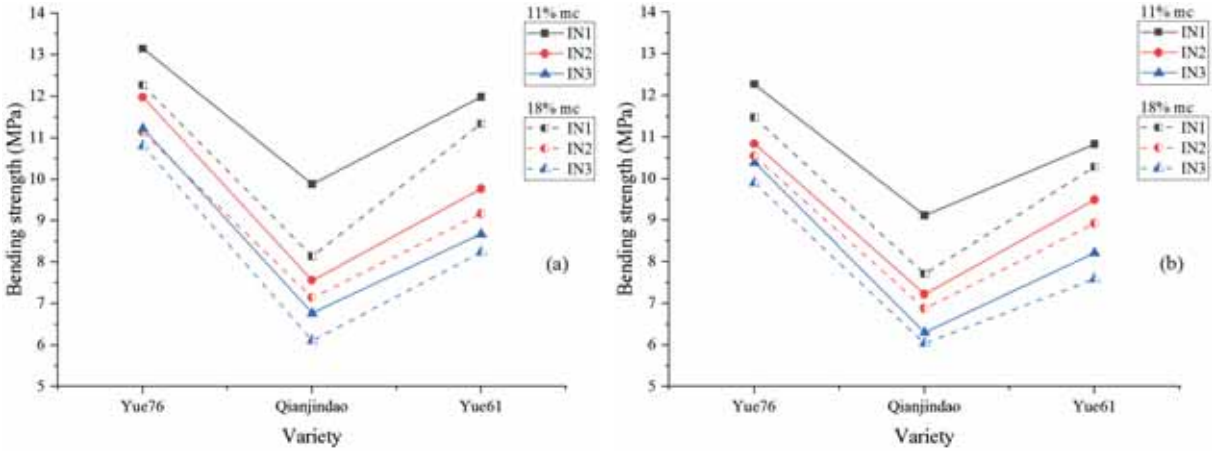


FIGURE 5
Bending strength of rice straw as affected by moisture content and variety for internodes at loading rate of 10 mm min^{-1} (a) and 20 mm min^{-1} (b).

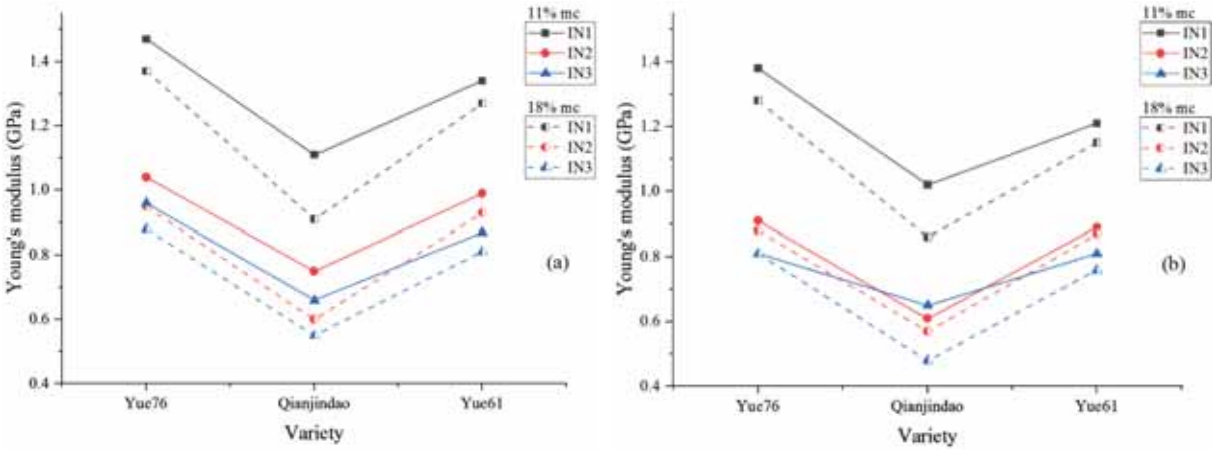


FIGURE 6
Young's modulus of rice straw as affected by moisture content and variety for internodes at loading rate of 10 mm min^{-1} (a) and 20 mm min^{-1} (b).

IN3 at 18% moisture and loading rate of 20 mm min^{1}, for Qianjindao it varied from 10.38 to 16.97 mJ mm^{-2} at moisture of 11 and 18% and loading rate of 10 and 20 mm min^{-1} respectively, and for Yue61 the specific shearing energy varied from 12.83 to 18.91 mJ mm^{-2} at moisture of 11 and 18% and loading rate of 10 and 20 mm min^{-1} respectively. The specific shearing energy with 20.27 mJ mm^{-2} unit was higher for Yue76, followed by Yue61 and minimum with 10.38 mJ mm^{-2} for Qianjindao. The specific shearing energy increased toward IN3 for all variety, moisture and loading rates. The viscous damping effect of moisture as reported by Persson [14] can be the reason for this difference. The stem with more mature fibre accumulated resulted higher shearing energy in the lower internodes Zareiforoush et al. [21]. Similiar results are in line with the findings of Chandio et al. [26] for rice and wheat straw, Tavakoli et al. [20] for wheat straw and Galedar et al. [16] for alfalfa stems.

Bending strength. Bending strength as affected by different moisture, variety and loading rate at all internodes is shown in Figures 5a and 5b. As per Tukey's multiple range test, the treatments applied had a significant effect on rice straw (Table 2), the values when observed were different for the distinct treatments. The values of bending strength decreased with increasing moisture and loading rate for Yue76, Qianjindao and Yue61 at all internodes. The vales with increasing moisture and loading rate decreased towards third internode (IN3). Bending strength for Yue76 varied from 9.90 MPa for IN3 at moisture of 18% and loading rate of 20 mm min^{-1} to 13.15 MPa for IN1 at a moisture of 11% and loading rate of 10mm min^{-1}, for Qianjindao it varied from 6.04 to 9.88 MPa at a moisture of 18 and 11% and loading rate of 20 and 10 mm min^{-1} respectively, and for Yue61 it varied from 7.59 to 11.99 MPa at a moisture of 18 and 11% and loading rate of 20 and 10 mm min^{-1} respectively. The values were higher for Yue76, followed by Yue61 and Qianjindao. This might be due the reduction in brittleness of rice straw. The results are in line with the findings of Tavakoli et al. [20] for wheat straw; Chattopadhyay

TABLE 2
Mechanical properties of rice straw as affected by moisture content, variety and loading rate.

Parameters	Variety	Moisture 11%						Moisture 18%					
		Loading rate 10			Loading rate 20			Loading rate 10			Loading rate 20		
		IN1	IN2	IN3	IN1	IN2	IN3	IN1	IN2	IN3	IN1	IN2	IN3
τs (MPa)	Yue76	11.12mn	13.13h	14.64e	12.24k	13.95f	15.66b	12.90i	14.98d	15.63b	13.36g	15.54b	17.07a
	Qianjindao	8.03v	9.04st	9.63r	8.78u	10.16p	11.17m	8.89tu	10.58o	10.96n	9.19s	11.08mn	11.94L
	Yue61	9.13s	11.17m	12.34jk	10.06pq	11.94l	13.41g	9.96q	12.47j	14.08f	11.14mn	12.94hi	15.22c
Esp mJ mm^{-2}	Yue76	14.86mn	16.27ij	17.05fg	15.97jk	17.43ef	18.31cd	16.42hij	17.07fg	17.89de	17.17fg	18.88bc	20.27a
	Qianjindao	10.38u	11.76s	12.17s	12.78r	13.30qr	15.34lm	10.07t	13.04r	13.91p	13.77pq	15.59kl	16.97fgh
	Yue61	12.83r	14.24op	15.23lmn	14.76no	16.75ghi	17.87de	14.74no	15.62kl	16.08jk	16.13jk	18.06d	18.91b
σ_b MPa	Yue76	13.15a	11.98c	11.23e	12.27b	10.84f	10.39gh	12.27b	11.14e	10.81f	11.47d	10.54g	9.90i
	Qianjindao	9.88i	7.56o	6.77q	9.12kl	7.22p	6.30r	8.14n	7.14p	6.11rs	7.71o	6.87q	6.04s
	Yue61	11.99c	9.77i	8.68m	10.83f	9.49j	8.21n	11.34de	9.17k	8.24n	10.28h	8.92l	7.59o
E (GPa)	Yue76	1.47a	1.04hijkl	0.96ijkl	1.38ab	0.91klm	0.81no	1.37bc	0.95ijklm	0.88lmn	1.28cde	0.88lmn	0.81no
	Qianjindao	1.11gh	0.75op	0.66pq	1.02hij	0.61qrs	0.65qr	0.91klm	0.60qrs	0.55st	0.86mn	0.57rst	0.48t
	Yue61	1.34bcd	0.99ijk	0.87lmn	1.21ef	0.89lmn	0.81no	1.27de	0.93jklm	0.81no	1.15fg	0.87lmn	0.76o

Means followed by different letters are significantly different from others for same parameter, τs – shear strength, Esp – specific shearing energy, σ_b – bending strength, E - young's modulus.

and Pandey [22] for sorghum stalk and İnce et al. [12] for sunflower stalk.

Young's modulus. Young's modulus as illustrated in Figures 6a and 6b decreased with increasing moisture and loading rate for all three varieties at all internodes (IN1, IN3 and IN3). Young's modulus was significantly affected by moisture, variety and loading rate (Table 1). Young's modulus was highest with 1.47 GPa for Yue76 at moisture of 11% and loading rate of 10 mm min^{-1}, where lowest with 0.48 GPa for Qianjindao at moisture of 18% and loading rate of 20 mm min^{-1}. Young's modulus of rice straw decreased towards IN3 at both moisture and loading rates. It was also observed that the first internode (IN1) was significantly greater than other two (Table 2). The average values of young's modulus were greater for Yue76, followed by Yue61 and Qianjindao. Similar decreasing trends have also been reported by Zareiforoush et al. [21] for rice straw; Chandio et al. [26] for rice and wheat straw and Tavakoli et al. [17] for barely straw.

CONCLUSION

The results of this research concluded that, the shear strength, specific shearing energy, bending strength and young's modulus when observed had significantly ($p \leq 0.05$) been affected by different moisture, variety and loading rate at all internodes. Shear strength and specific shearing energy increased with increasing moisture and loading rate for all three varieties, the highest values for shearing strength and specific shearing energy with 17.07 MPa and 20.27 mJ mm^{-2} were observed for Yue76 at IN3 at a moisture of 18% and loading rate of 20mm min^{-1}. Bending strength and young's modulus with increasing moisture and loading rate decreased for all three varieties, the highest values for bending strength and young's modulus with 13.15 MPa and 1.47 GPa were observed for Yue76 at a moisture of 11% and loading rate of 10mm min^{-1}. It was observed that for moisture, variety and loading rate the shear strength and specific shearing energy increased toward third internode (IN3), while the

bending strength and young's modulus decreased. The average values of all varieties were significantly different from each other, the values were observed to be higher for Yue76, followed by Yue61 and Qianjindao. A large variation was concluded from the findings of above study, it is strongly suggested to execute the mechanical properties of rice straw before designing or judging the performance of equipment's and machineries being used.

ACKNOWLEDGEMENT

The study was sponsored by Science and Technology Special Project of Jiangsu with Project Number SZ-YC2019002. The first author is thankful to China Scholarship Council (CSC) for providing all possible facilities during the study in China.

REFERENCES

[1] Zhang, X., Wang, D., Fang, F., Zhen, Y. and Liao, X. (2005) Food Safety and Rice Production in China (in Chinese with English Abstract). Research of Agricultural Modernization. 26, 85-88.

[2] FAOSTAT. (2013). Data base available online at http://faostat3.fao.org/home/index.html#HOME. (Accessed 26 Sept 2013)

[3] Kadam, K. L., Forrest, L. H. and Jacobson, W. A. (2000) Rice Straw as a Lignocellulosic Resource: Collection, Processing, Transportation, and Environmental Aspects. Biomass and Bioenergy. 18(5), 369-389.

[4] Liu, Z., Zu, A. and Zhao, T. (2011) Energy from Combustion of Rice Straw: Status and Challenges to China. Energy and Power Engineering. 3(3), 325-331.

[5] Yore, M. W., Jenkins, B. M. and Summers, M. D. (2002) Cutting Properties of Rice Straw. Annual Int. Meeting/ CIGR XV the World Congress. USA. 28-31 July, 1-9.

[6] Soomro, S. A., Chen, K. and Soomro, S. A. (2020) Mathematical Modelling and Optimisation of Low Temperature Drying on Quality Aspects of Rough Rice. Journal of Food Quality. 6501257, 1-10.

[7] Koloor, R. T. and Borgheie, A. (2006) Measuring the Static and Dynamic Cutting Force of Stems for Iranian Rice Varieties. Journal of Agricultural Science and Technology. 8, 193-198.

[8] Abdulla, H. M. (2007) Enhancement of Rice Straw Composting by Lignocellulolytic Actinomycete Strains. International Journal of Agriculture and Biology. 9(1), 106-109.

[9] Chakraverty, A., Singh, P. R., Raghavan, G. S. V. and Ramaswamy, H. S. (2003) Handbook of Postharvest Technology (1st Edn), Marcel Dekker Inc, New York.

[10] Annoussamy, M., Richard, G., Recous, S. and Guerif, J. (2000) Change in Mechanical Properties of Wheat Straw due to Decomposition and Moisture. Applied Engineering in Agriculture. 16(6), 657-664.

[11] Bright, R. E. and Kleis, R. W. (1964) Mass Shear Strength of Haylage. Transactions of the ASAE. 7(2), 100-101.

[12] İnce, A., Uğurluay, S., Güzel, E. and Özcan, M. T. (2005) Bending and Shearing Characteristics of Sunflower Stalk Residue. Biosystems Engineering. 92(2), 175-181.

[13] Soomro, S. A., Thebo, S. A. and Chen, K. (2018) Physico-Engineering Properties of Different Rice Varieties Grown in Sindh Province of Pakistan. International Agricultural Engineering Journal. 27(1), 275-280.

[14] Persson, S. (1987) Mechanics of Cutting Plant Material, ASAE Publications, Michigan.

[15] Chen, Y., Gratton, J. L. and Liu, J. (2004) Power Requirements of Hemp Cutting and Conditioning. Biosystems Engineering. 87(4), 417-424.

[16] Galedar, M. N., Jafari, A., Mohtasebi, S. S., Tabatabaeefar, A., Sharifi, A., O'Dogherty, M. J., Rafiee, S. and Richard, G. (2008) Effects of Moisture Content and Level in the Crop on the Engineering Properties of Alfalfa Stems. Biosystems Engineering. 101(2), 199-208.

[17] Tavakoli, H., Mohtasebi, S. S., Jafari, A. and Galedar, M. N. (2009) Some Engineering Properties of Barley Straw. Applied Engineering in Agriculture. 25(4), 627-633.

[18] Reza, T. K. (2007) Paddy Stems Cutting Energy and Suggested Blade Optimum Parameters. Pakistan Journal of Biological Sciences. 10(24), 4523-4526.

[19] ASAE (2006) ASAE Standards, 52nd Edn. Measurement–Forages. St. Joseph, MI. ASABE S358. 2. 1, 1.

[20] Tavakoli, H., Mohtasebi, S. S. and Jafari, A. (2009) Physical and Mechanical Properties of Wheat Straw as Influenced by Moisture Content. International Agrophysics. 23(2), 175-181.

[21] Zareiforoush, H., Mohtasebi, S. S., Tavakoli, H. and Alizadeh, M. R. (2010) Effect of Loading Rate on Mechanical Properties of Rice (Oryza Sativa L.) Straw. Australian Journal of Crop Science. 4(3), 190-195.

[22] Chattopadhyay, P. S. and Pandey, K. P. (1999) Mechanical Properties of Sorghum Stalk in Relation to Quasi-Static Deformation. Journal of Agricultural Engineering Research. 73(2), 199-206.

[23] Gere, J. M. and Timoshenko, S. P. (1997) Mechanics of Materials (4th Edn), Boston, Mass.: PWS Publishing Company.
[24] Crook, M. J. and Ennos, A. R. (1994) Stem and Root Characteristics Associated with Lodging Resistance in Poor Winter Wheat Cultivars. Journal of Agricultural Science. 126, 167-174.
[25] Ahmad, F., Weimin, D., Qishuo, D., Mingxing, Z., Chandio, F. A. and Arslan, C. (2015) Fuzzy Logic Model to Predict Wheat Straw Mechanical Properties under Varying Moisture Content and Loading Rate. Pakistan Journal of Agricultural Sciences. 52(4), 961-970.
[26] Chandio, F. A., Ji, C., Tagar, A. A., Mari, I. A., Arslan, C., Cuong, D. M. and Fang, H. (2013) Effect of Loading Rate on Mechanical Characteristics of Wheat and Rice Straw. Bulgarian Journal of Agricultural Science. 19(6), 1452-1458.

Received: **06.06.2020**
Accepted: **17.02.2021**

CORRESPONDING AUTHOR

Kunjie Chen
College of Engineering,
Nanjing Agricultural University
40 Dianjiangtai Road, Pukou District,
Nanjing 210031 – P.R. China

e-mail: kunjiechen@njau.edu.cn

© by PSP Volume 30– No. 09/2021 pages 10457-10462 Fresenius Environmental Bulletin

THE EFFECTS OF PHENOLIC, GALLOTANNIN, AND PROTEIN AMOUNTS IN PLANTS ON CONSUMPTION AMOUNT, SURVIVAL, AND PHENOLOXIDASE ACTIVITY OF *Malacosoma neustria* LINNAEUS, 1758 (LEPIDOPTERA: LASIOCAMPIDAE) LARVAE INFECTED WITH *Bacillus thuringiensis* SUBSP. *Kurstaki*

Elif Fatma Topkara*

Department of Biology, Science and Art Faculty, Ondokuz Mayıs University, 55139, Samsun, Turkey

ABSTRACT

This study aimed to investigate the changes in total consumption amounts, survival rates, and phenoloxidase (PO) activities in *Malacosoma neustria* (L., 1758) (Lepidoptera: Lasiocampidae) larvae infected with *Bacillus thuringiensis* subsp. *kurstaki* Berliner. *Malacosoma neustria* eggs were collected from Bafra District of Samsun, Turkey, in 2018. *Malacosoma neustria* larvae that hatched from the eggs fed on the host plants, *Coryllus maxima* Mill., *Elaeagnus rhamnoides* (L.) A. Nelson, *Quercus cerris* L. 1753, and *Crataegus monogyna* Jacq. Except for the control groups, the experiment continued by spraying *Bacillus thuringiensis* on the plants. The amounts of consumption and survival rates of both the control and infected larvae fed on *E. rhamnoides* leaves with the highest amounts of protein, phenolic, and gallotannin, were higher than in other groups. In all groups, both the consumption amounts and the survival rates decreased with a bacterial infection. When compared to the control groups, the infected groups had the higher phenoloxidase activities (except *C. monogyna*). As a result of this study, it was thought that the changes in total consumption amount, survival rates, and PO activities in larvae were related to both bacterial infection and the amounts of protein, phenolic, and gallotannin in the plants.

KEYWORDS:
Bacillus thuringiensis, Consumption, Phenoloxidase, Secondary compound, Survival

INTRODUCTION

Plants are consumed by a wide variety of organisms as the basis for terrestrial trophic chains. More than 300.000 vascular plant species are consumed by approximateyly 400.000 insect herbivores [1]. Plants and insects have co-evolved so far. Insects have adapted to plant defence properties by changing their morphological, behavioural, and biochemical properties [2]. These adaptations allow herbivores to overcome plant defences. Plants, despite being sessile organisms, are not defenceless against herbivores. Plants have developed several defence strategies to prevent pest insect damage, including morphological and biochemical defences [3, 4]. They protect themselves by morphological defences such as thorns, trichomes, and cuticles. Furhermore, the majority of secondary metabolites present in plants are highly effective chemical weapons.

Secondary compounds are essential in plant defence strategies against herbivores [4]. They can reduce insect survival, prolong their development time, reduce their size, and reduce adults fitness [5, 6]. Phenolic compounds play a vital role in the plant defence system to pest insects [7]. Phenols repel herbivores by altering the taste of plant tissues or by linking and denaturing proteins [8]. Tannins are secondary metabolites involved in plant defence against pest insects. They have astringent and bitter tastes that deter pest insects. They bind to insect midgut proteins and precipitate them using hydrogen or covalent bonds. In this way, they limit their usability to insect pests, and as a result, reduce the development and growth of the insect [9, 10]. Plant protein, on the other hand, is essential for Lepidopteran caterpillars.

Malacosoma neustria (L., 1758) (Lepidoptera: Lasiocampidae) is a significant defoliator of many plants, including apple, pear, and plum, oak and rose species, willow, poplar, aspen, and birch, particularly in eastern and central Turkey [11, 12]. For some years, their populations have reached such high numbers that they leave the trees completely leafless. Various methods have been used to combat pests, one of which is the use of biopesticides. *Bacillus thuringiensis* subsp. *kurstaki*, a Gram-positive, spore-forming bacterium, is the well-known and widely used. *Bacillus thuringiensis*

toxins (Cry) interact with protein receptors on the surface of insect midgut cells, causing pores in the cell membrane to form and, eventually, cell death [13].

The host plant selection of an insect depends on the structure and chemistry of the host plant. Plant quality is critical to the insect's survival. In nature, insects are exposed to various entomopathogens, such as bacteria, and the pathogens affect the fitness properties of insects, such as survival. Based on this knowledge, we aimed to determine how plant contents and infection affect the total consumptions, survival rates, and phenoloxidase (PO) activities of *M. neustria* larvae.

MATERIALS AND METHODS

Collection of larvae and the plants used in the study. *Malacosoma neustria* eggs were collected from the Kızılırmak Delta of the Bafra District in Samsun, Turkey, in 2018. The eggs were then placed in the climate cabin, and they were kept at 25±2°C and 70 % humidity (16 hours light/8 hours dark). The larvae that hatched from the eggs were divided into several groups and placed in plastic containers (5×10×2 cm). They were fed on *Coryllus maxima* Mill., *Elaeagnus rhamnoides* (L.) A. Nelson, *Quercus cerris* L. 1753, and *Crataegus monogyna* Jacq. leaves up to the last larval stage. The larvae were fed these plants daily. In addition, plant samples were collected daily and dried in the incubator.

Bacterial infection. A bacterial suspension with a wavelength of 600 nm (OD_{600}) of 0.189 optical density was prepared for *Bacillus thuringiensis* subsp. *kurstaki* infection. After feeding the larvae in each group for ten days in the laboratory, one ml of bacterial suspension was applied to the plant samples, and the experiment was continued for three days in the climate chamber at 27°C.

The feeding experiments. The feeding experiments were carried out in two stages. In the first stage, 400 last instar larvae, 50 in each group, were used to compare the total consumption and survival rates between the infected and control groups. In the second stage, 400 last instar larvae were used, 50 in each group, to calculate phenoloxidase activities. Except for the control larvae, the other larvae were infected with bacteria. The experiment was carried out in an incubator set at a temperature of 25±2°C and 70% humidity for 16 hours light/8 hours dark.

Plant analyses. The leaf samples were collected from the tree species where the larvae were feeding. They were put into the foils, dried for two months in the laboratory, and then dried for five days in an incubator at 50°C. The leaf samples were ground and placed in nylon bags for storage. The protein amounts of the leaf samples were determined using a semi-micro Kjeldahl with a Kjeltec Auto 1030 analyzer (Tecator, Sweden). By multiplying the nitrogen amounts by 6.25, the total protein amount of each plant was determined [15]. The total phenolic amounts of the plants were determined by using the Swain and Hillis method [16]. The amounts of gallotannin were determined using the Bate-Smith method [17].

Phenoloxidase analysis. The third legs of both the control and infected larvae were cut, and their hemolymph were taken. The phenoloxidase activity of hemolymph samples was determined using the Ashida and Söderhäll method [14].

Statistical analyses. The Log Rank test, one of the Kaplan-Meier Life Analysis tests, was used to determine the relationship between the survival rates of the control and infected groups. The ANOVA Duncan test was used to compare the total consumption amounts obtained from the feeding experiments. Two independent sample t-tests were used to determine enzyme activities.

RESULTS

Protein, total phenolic, and gallotannin amounts of plants. The protein amounts were found 14.6% for *E. rhamnoides,* 10.2% for *Q. cerris*, 11.3% for *C. maxima*, and 8.7% for *C. monogyna*. The total phenolic amounts of the leaf samples were 9.9 % in *E. rhamnoides*, 7.5% in *Q. cerris,* 9.1% in *C. maxima,* and 6.4 % in *C. monogyna*. The gallotannin amounts of the leaves of *E. rhamnoides*, *Q. cerris*, *C. maxima,* and *C. monogyna* were 5.2%, 2.6%, 4.3% and 1.8%, respectively. The highest protein, total phenolic, and gallotannin amounts were determined in *E. rhamnoides*, while the lowest ones were recorded in *C. monogyna.* The results of statistical data analysis revealed that the host plant species had a significant difference (Figure 1).

Larval survival rates. Among the control groups, the highest survival rate was in larvae fed on *E. rhamnoides* leaves (96%), while the lowest was in *C. monogyna* leaves (74%). In our study, it was found that infected groups had lower survival rates than the control groups. Among the infected groups, the highest survival rate was found in larvae fed on *E. rhamnoides* leaves (72%), while the lowest was in larvae fed on *C. monogyna* leaves (18%). Survival rates of all groups were shown in Table 1.

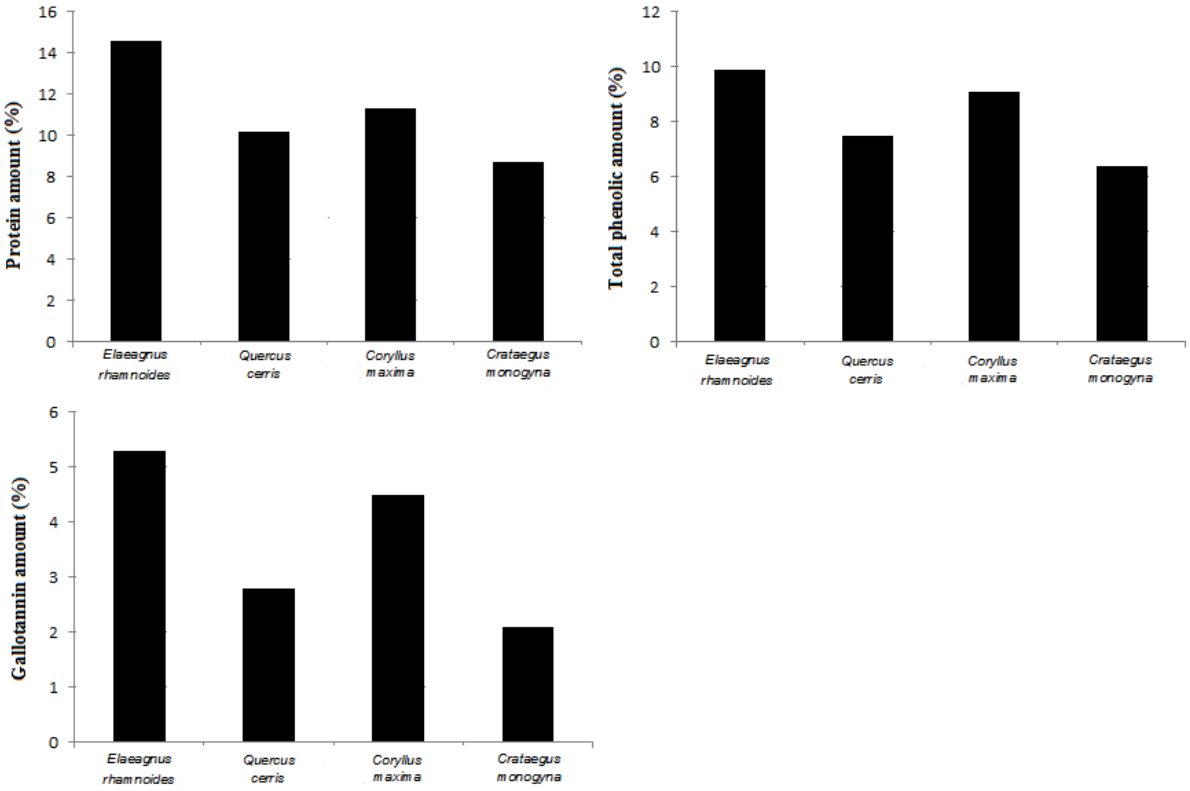


FIGURE 1
Protein, total phenolic and gallotannin amounts of plants

TABLE 1
Survival rates of *Malacosoma neustria* larvae

Plants	Total larvae number (N)		Died larvae number		Survival rate (%)	
	Control	Infected	Control	Infected	Control	Infected
Elaeagnus rhamnoides	50	50	2	14	96	72
Quercus cerris	50	50	7	24	86	52
Corylus maxima	50	50	5	18	90	61
Crataegus monogyna	50	50	13	41	74	18

TABLE 2
Total consumption amounts of *Malacosoma neustria* larvae

Plants	Total larvae number (N)	Groups	Mean±Standard error (mg)	t	*p*
Elaeagnus rhamnoides	48	Control	422.6±10.8	71.1	<0.001
	36	Infected	331.6±17.5		
Quercus cerris	43	Control	400.7±6.7	52.5	<0.001
	26	Infected	172.3±12.9		
Corylus maxima	45	Control	395.3±9.8	60.7	<0.001
	32	Infected	176.9±10.0		
Crataegus monogyna	37	Control	383.3±12,3	37.3	<0.001
	9	Infected	141.0±11.9		

TABLE 3
Phenoloxidase enzyme activities of *Malacosoma neustria* larvae

Plants	Groups	Mean±Standard error (IU/mgprotein/mlx10^3)	t	*p*
Elaeagnus rhamnoides	Control	2.1±0.01	-51.7	<0.001
	Infected	3.1±0.01		
Quercus cerris	Control	2.4±0.01	-17.4	<0.001
	Infected	2.7±0.01		
Corylus maxima	Control	2.4±0.01	-22.4	<0.001
	Infected	2.8±0.01		
Crataegus monogyna	Control	2.6±0.01	4.46	<0.001
	Infected	2.5±0.01		

Total consumption amounts. The highest total consumption amount among all control groups was found in larvae fed on *E. rhamnoides* leaves (422.6±10.8 mg; $p<0.001$). The lowest consumption amount was recorded in larvae fed on *C. monogyna* leaves (383.3±12.3 mg; $p<0.001$). Compared to the control groups, we found that the consumption amounts of all groups decreased with the bacterial infection. The lowest consumption amount in infected groups was in larvae fed on *C. monogyna* leaves (141±11.9 mg; $p<0.001$). The comparisons of the total consumption amounts of infected groups with those in the control groups regarding plants were shown in Table 2.

Phenoloxidase activities of larvae. Among the control groups, the lowest PO activity was in larvae fed on *E. rhamnoides* leaves (2.1 IU; $p<0.001$), while the highest enzyme activity was in *C. monogyna* (2.6 IU; $p<0.001$). In our study, it was found that PO activities increased with bacterial infection (except *C. monogyna*). Also, in infected groups, the highest PO activity was in the larvae fed on *E. rhamnoides* leaves (3.1 IU; $p<0.001$), while the lowest PO activity was in the *C. monogyna* (2.5 IU; $p<0.001$) (Table 3).

DISCUSSION

The quality and quantity of the host plants, as well as their properties such as secondary substance content affect the survival, ecology, behavior, fecundity, and physiology of herbivore insects [18, 19, 20]. Protein, among macronutrients, has a significant impact on herbivore performance [21, 22]. Therefore, protein is indispensable for herbivore insects. Deans et al. [23] found in a study with *Lygus hesperus* that insects fed the diet with the highest protein content survived longer. The findings of this study were consistent with those of our current research, which found that larvae fed on *E. rhamnoides* leaves with the highest protein content had the highest survival rate. The plant also had the highest amount of phenolic and gallotannin. In this case, it can be said that the protein, phenolic substance, and tannin in the plant all have a positive effect on the survival of *M. neustria*. Also, in our study, the lowest survival rate was found in larvae fed on *C. monogyna* leaves, which had the least amount of protein, phenolic substance, and gallotannin. Condensed tannins had a negative effect on the survival of *Operophtera brumata* (Lepidoptera: Geometridae) larvae [24], which contradicted the findings of our current study. One of the most crucial factors affecting the survival of herbivore insects as well as the plant content is their exposure to entomopathogens. Infection with *B. thuringiensis* has been shown to affects survival [25, 26]. With bacterial treatment, the survival rate of *Bombyx mori* larvae decreased [27]. In our study, it was also found that all infected groups had lower survival rates than control groups. This finding indicates that bacterial infection has a negative impact on larval survival.

Herbivore insects, particularly generalists, consume a wide range of foods containing protein and amino acids [28]. Among the control groups, the highest total consumption was found in larvae fed on *E. rhamnoides* leaves, which had the highest protein content. Similar findings were found in another study with *Lymantria dispar* [29]. The reason why the larvae fed on *E. rhamnoides* leaves consumed much was due to the high number of larvae that survived by feeding on this plant. Plant phenolics play a vital role in plant resistance to herbivores and pathogens. For instance, the wheat cultivars containing phenolic were less attractive to *Rhopalosiphum padi* L. (Homoptera: Aphididae) [30]. Tannins, phenolic compounds, are nutritional deterrents due to their bitter and astringent taste [31]. Besides, it was noted that *M. neustria* larvae consumed more *E. rhamnoides* in our study. The findings of our research shows that the effects of phenolics and tannins are differ between herbivore insects. The lowest consumption amount was in larvae fed on *C. monogyna* leaves, which had the least amount of protein, phenolic substance, and gallotannin. In this case, the small amount of these substances in the plant negatively affected the consumption of the larvae. In nature, larvae are exposed to microbes through feeding [32]. From this point of view, in this study where we investigated how bacterial infection affects larvae,

we found that consumption amounts of infected groups decreased compared to control groups. The reduction in consumption may mean that they may be exposed to more pathogens during this period, as well as have a longer optimum growth time.

In our study, the lowest PO activity among all control groups was found in larvae fed on *E. rhamnoides* leaves, while the highest enzyme activity was found in those fed on *C. monogyna* leaves. Insects activate immune responses to fight infection [33]. One of the first responses of the immune system to bacterial infection is the activation of the PO system in the hemolymph. PO activity can be upregulated as part of the immune defense of insects. Grizanova et al. [34] showed that PO activity in the hemolymph plasma of the *Galleria mellonella* L. (Lepidoptera: Pyralidae) larvae was induced by *B. thuringiensis* infection. In our study, the PO activities of all infected groups were found to be higher than those of control groups (except *C. monogyna*). While the larvae fed on *E. rhamnoides* leaves in the control group had the lowest enzyme activity, this activity was maximized by infection. This situation shows the effects of secondary compounds on the immune response as well as a bacterial infection.

CONCLUSION

In summary, insect herbivores must integrate the nutrient content based on carbohydrates or proteins with secondary compounds present in plants to meet nutritional requirements. In our study, it was found that the larvae fed on *E. rhamnoides* leaves with the highest amounts of protein, phenolic, and gallotannin, had the highest survival rate, and as a result, the highest consumption. Insects are the largest group of animals in the world, occupying a wide range of ecological niches. Throughout their lives, they are exposed to infections caused by viruses, bacteria, or fungi. The larvae fed on *E. rhamnoides* leaves responded to the bacterial infection with a maximum increase in PO activity. Our findings can help to clarify the interpretation of complex and dynamic plant-insect-entomopathogenic interactions, as well as the ecological roles that these interactions play.

ACKNOWLEDGEMENTS

I thank for Dr. Oğuzhan Yanar from Ondokuz Mayıs University for his contributions.

REFERENCES

[1] Schoonhoven, L.M., Van Loon, J. J. and Dicke, M. (2005). Insect-Plant Biology. Oxford University Press, Oxford. 448 pp.

[2] War, A.R. and Sharma, H.C. (2014) "Induced Resistance in Plants and Counter-Adaptation by Insect Pests, 533-549". In: Short Views Insect Biochemistry and Molecular Biology (Eds. Chandrasekar, R., Tyagi, B.K., Gui, Z.Z. and Reeck, G.R.). International Book Mission, USA. 709 pp.

[3] Zhao, L.Y., Chen, J.L., Cheng, D.F., Sun, J.R., Liu Y. and Tian, Z. (2009) Biochemical and molecular characterizations of *Sitobion avenae*-induced wheat defense responses. Crop Protection. 28, 435-442.

[4] Karban, R. (2011) The ecology and evolution of induced resistance against herbivores. Functional Ecology. 25, 339-347.

[5] Gogi, M.D., Ashfaq, M., Arif, M.J., Sarfraz, R.M. and Nawab, N.N. (2010) Investigating phenotypic structures and allelochemical compounds of the fruits of *Momordica charantia* L. genotypes as sources of resistance against *Bactrocera cucurbitae* (Coquillett) (Diptera, Tephritidae). Crop Protection. 29, 884-890.

[6] Haldhar, S.M., Bhargava, R., Choudhary, B.R., Pal, G. and Kumar, S. (2013) Allelochemical resistance traits of muskmelon (*Cucumis melo*) against the fruit fly (*Bactrocera cucurbitae*) in a hot arid region of India. Phytoparasitica. 41, 473-481.

[7] Wuyts, N., De waele, D. and Swennen, R. (2006) Extraction and partial characterization of polyphenol oxidase from banana (*Musa acuminate* grandr naine) roots. Plant Physiology and Biochemistry. 44, 308-314.

[8] Kulbat, K. (2016) The role of phenolic compounds in plant resistance. Biotechnology and Food Science. 80, 97-108.

[9] Arnold, T.M. and Schultz, J.C. (2002) Induced sink strength as a prerequisite for induced tannin biosynthesis in developing leaves of *Populus*. Oecologia. 130, 585-593.

[10] Roslin, T. and Salminen, J.P. (2008) Specialization pays off: contrasting effects of two types of tannins on oak specialist and generalist moth species. Oikos. 117, 1560-1568.

[11] Özbek, H. and Çalmaşur, O. (2005) A review of insects and mites associated with roses in Turkey. Acta Horticulturae. 690, 167-174.

[12] Özbek, H. and Çoruh, S. (2010) Egg parasitoids of *Malacosoma neustria* (Linnaeus, 1758) (Lepidoptera: Lasiocampidae) in Erzurum province of Turkey. Turkish Journal of Entomology. 34, 551-560.

[13] Adang, M.J., Crickmore, N. and Jurat-Fuentes, J.L. (2014) Diversity of *Bacillus thuringiensis* crystal toxins and mechanism of action. Advances in Insect Physiology. 47, 39-87.

[14] Ashida, M. and Söderhall, K. (1984) The prophenoloxidase activating system in crayfish. Comparative Biochemistry and Physiology Part B: Biochemistry and Molecular Biology. 77, 21-26.
[15] Monk, C. D. (1987) Sclerophylly in *Quercus virginiana* Mill. Castanea. 52, 256-261.
[16] Swain, T. and Hillis, W.E. (1959) The phenolic constituents of *Prunus domestica*. I.-The quantitative analysis of phenolic constituents. Journal of the Science of Food and Agriculture. 10, 63-68.
[17] Bate-Smith, E.C. (1977) Astringent tannins of *Acer* species. Phytochemistry. 16, 1421-1426.
[18] Schoonhoven, L.M., Jermy, T. and van Loon, J.J.A. (1998) Insect-Plant Biology. Chapman & Hall, London. 409p.
[19] Awmack, C.S. and Leather. S.R. (2002) Host plant quality and fecundity in herbivorous insects. Annual Review of Entomology. 47, 817-844.
[20] Sousa, F.F., Mendes, S.M., Santos-Amaya, O.F., Araujo, O.G., Oliveira, E.E. and Pereira, E.J.G. (2016) Life-history traits of *Spodoptera frugiperda* populations exposed to low-dose Bt maize. Plos One. 11, e0156608.
[21] Coley, P.D., Bateman, M.L. and Kursar, T.A. (2006) The effects of plant quality on caterpillar growth and defense against natural enemies. Oikos. 115, 219-228.
[22] Wallis, I.R., Edwards, M.J., Windley, H., Krockenberger, A.K., Felton, A., Quenzer, M., Ganzhorn, J.U. and Foley, W.J. (2012) Food for folivores: nutritional explanations linking diets to population density. Oecologia. 169, 281-291.
[23] Deans, C., Sword, G.A. and Behmer, S.T. (2019) First evidence of protein-carbohydrate regulation in a plant bug (*Lygus hesperus*). Journal of Insect Physiology. 116, 118-124.
[24] Tikkanen, O.P., Julkunen-Tiitto, R. (2003) Phenological variation as protection against defoliating insects: the case of *Quercus robur* and *Operophtera brumata*. Oecologia. 136, 244-251.
[25] Paramasiva, I., Krishnayya, P.V., War, A.R. and Sharma, H.C. (2014) Crop hosts and genotypic resistance influence the biological activity of *Bacillus thuringiensis* towards *Helicoverpa armigera*. Crop Protection. 64, 38-46.
[26] Jafary, M., Karimzadeh, J., Farazmand, H. and Rezapanah, M. (2016) Plant-mediated vulnerability of an insect herbivore to *Bacillus thuringiensis* in a plant-herbivore-pathogen system. Biocontrol Science and Technology. 26, 104-115.
[27] Gore, D., Rai, M. and Shinde, G. (2014) Effect of Amla extract on bacterial infection in the Silkworm, *Bombyx mori* L. Journal of Pharmacy Research. 8(5), 679-680.
[28] Lee, K.P., Simpson, S.J. and Wilson, K. (2008) Dietary protein-quality influences melanization and immune function in an insect. Functional Ecology. 22, 1052-1061.
[29] Yanar, O., Gömeç, S., Topkara, E.F., Solmaz, G. and Demir, İ. (2017) The effect of plant quality on survival of *Lymantria dispar* larvae infected by *Bacillus thuringiensis* Berliner subsp. *kurstaki.* Applied Ecology and Environmental Research. 15(3), 837-847.
[30] Leszczynski, B. (1995) The influence of phenolic compounds on the preference of winter wheat cultivars by cereal aphids. Insect Science and Its Application. 6, 157-158.
[31] Torregrossa, A.M. and Dearing, M.D. (2009) Nutritional toxicology of mammals: Regulated intake of plant secondary compounds. Functional Ecology. 23(1), 48-56.
[32] Freitak, D., Wheat, C.W., Heckel, D.G. and Vogel, H. (2007) Immune system responses and fitness costs associated with consumption of bacteria in larvae of *Trichoplusia ni*. BMC Biology. 5, 56.
[33] Wojda, W. and Taszłow, P. (2013) Heat shock affects host-pathogen interaction in *Galleria mellonella* infected with *Bacillus thuringiensis.* Journal of Insect Physiology. 59(9), 894-905.
[34] Grizanova, E.V., Dubovskiy, I.M., Whitten, M.M.A. and Glupov, V.V. (2014) Contributions of cellular and humoral immunity of *Galleria mellonella* larvae in defence against oral infection by *Bacillus thuringiensis*. Journal of Invertebrate Pathology. 119, 40-46.

Received: **30.06.2020**
Accepted: **20.06.2021**

CORRESPONDING AUTHOR

Elif Fatma Topkara
Department of Biology, Science and Art Faculty,
Ondokuz Mayıs University,
55139 Samsun – Turkey

e-mail: topkaraelif@hotmail.com

© by PSP Volume 30– No. 09/2021 pages 10463-10473 Fresenius Environmental Bulletin

FORAGE YIELD AND QUALITY OF SOYBEAN-MAIZE INTERCROPPING

Ilker Inal[1,*], Derya Yucel[2], Celal Yucel[2], Rustu Hatipoglu[3]

[1]Republic of Turkey Ministry of Agriculture and Forestry Eastern Mediterranean Agricultural Research Institute, Adana, Turkey
[2]Department of Field Crops, Faculty of Agriculture, Sirnak University, Sirnak, Turkey
[3]Department Field Crops, Faculty of Agriculture, Cukurova University, Adana, Turkey

ABSTRACT

The research was conducted to evaluate the effects of sole sowing and intercropping of maize and soybean with different sowing patterns and harvest stages on forage growth, yield and quality. A split-plot experiment in randomized block design (RCBD) was established in Adana, Turkey in 2010 and 2011 cropping seasons. Sowing patterns of the intercropping maize with soybean were 1 row maize to 1 row soybean (M1), 1 row maize to 2 rows soybean (M2), 2 rows maize to 1 row soybean (M3) in the alternate rows or 1 maize + 1 soybean (M4), 1 maize + 2 soybeans (M5), 2 maize + 1 soybean (M6) in the same row, respectively. The forage was harvested at two different growth stages of maize such as the milk and dough stages. Intercropping of maize and soybean in the same row produced a significantly higher green herbage and dry matter (DM) yields than their intercropping in the alternate rows. Our results suggested that intercropping of maize and soybean with a sowing pattern 1M-1S or 1M-2S in the same row and harvesting these intercrops at dough stage of maize could be suggested for higher DM yield with improved forage quality.

KEYWORDS:
Maize, Soybean, Intercropping, Sowing Pattern, Forage Yield, Forage Quality

INTRODUCTION

Intercropping is one of the common agricultural practices used in low input farming systems worldwide [1, 2]. Intercropping systems, especially those employing cereal crops with legumes, have several major advantages such as higher biomass yield and better land use management efficiency [3]. Generally, small farmers often shown interest and preference for intercropping as it provides an opportunity to grow diverse crops with reduced inputs, improve soil quality, reduce risk of crop failure in unfavorable seasons, and employ family labor more collectively. Maize-legume intercropping could have an economical potential to improve forage production and enhance its quality and decrease requirements for protein supplements compared with the traditional maize monocultures [4, 5]. Maize provides high dry matter yield and forage with low protein content. However, livestock need a good protein source in forage for their growth and milk production. Protein is essential for rumen bacteria, which digest the feed for ruminant animals [6]. Legumes are known to be an excellent source of protein and can be used to cover protein deficiency of cereals [7].

To optimize forage production and quality, more information is needed using different seeding ratios or planting patterns for cereal-legume intercropping [8, 9, 10]. The objective of our study was to compare the dry matter yields and forage quality of maize-soybean intercropping in different planting patterns and harvest stages under the Eastern Mediterranean climatic conditions of Turkey.

MATERIALS AND METHODS

Study site. The field study was conducted during 2010 and 2011 growing seasons (June-September) at the experimental area of Eastern Mediterranean Agricultural Research Institute, Adana, Turkey (36°51.675N, 035°20.662E with 14 m altitude above mean sea level) under typical Mediterranean climate with mild rainy winter and hot dry summer. Before planting, soil samples were collected for selected chemical and physical analysis. The soil is a non-saline clay loam, rich in calcium carbonate and slightly alkaline in pH. The soil has salinity 0.026%, pH 7.72, calcium carbonate ($CaCO_3$) 20%, organic matter 2%, sand 27.8%, clay 31.2% and silt 41% [11].

Experimental design and cultural practices. The experiment was a RCB design in split-plot arrangement. The intercropping systems [1 row maize to 1 row soybeans (M1), 1 row maize to 2 rows soybeans (M2), 2 rows maize to 1 row soybeans (M3) in the alternate rows or 1 maize + 1 soybeans (M4), 1 maize + 2 soybeans (M5), 2 maize + 1 soybeans (M6) in the same row, respectively] were the main plot. As the forage was harvested at two different stages of maize such as the milk and dough stages,

TABLE 1
Description of cropping systems and harvest times.

Cropping		Description	Plant density (plants/ha) system	
			Corn	Soybean
		Pure Sowing		
SM		Sole maize (100 % maize + 0 % soybean)	95,240	-------
SS		Sole soybean (100 % soybean + 0 % maize)		285,710
		Intercropping		
		In Alternate Rows		
M1	1M1S	Intercrop of maize (50 %) + soybean (50 %)	47,620	142,855
M2	1M2S	Intercrop of maize (33 %) + soybean (66 %)	31,747	190,473
M3	2M1S	Intercrop of maize (66 %) + soybean (33 %)	63,493	95,236
		In Same Rows*		
M4	1M1S	Intercrop of maize (50 %) + soybean (50 %)	47,620	142,855
M5	1M2S	Intercrop of maize (33 %) + soybean (66 %)	31,747	190,473
M6	2M1S	Intercrop of maize (66%) + soybean (33 %)	63,493	95,236
		Harvest Time		
H1		Harvest at milk stage		
H2		Harvest at doughy stage		

* In same rows: soybean and maize seeds were mixed before sowing then sown on the same rows and determined inner row space for intercropping applications.

the cutting-time was the sub-plot (Table 1). Each treatment combination was replicated four times.

Soybean cv. Yesilsoy and maize cv. Pioneer P31Y43 were used. Seed rates of each intercrop species were determined based on their pure sowing rates (95 plants/10 m^2 for maize and 280 plants/10 m^2 for soybeans). Plant row distance was 70 cm. Plot area was 16.8 m^2 (6 m long and four rows) for pure sowings and 33.6 m^2 (6 m long and four rows in pure sowing) for the mixtures. Chemical fertilization 50 kg ha^{-1} N and 50 kg ha^{-1} P_2O_5 were broadcasted before planting. During the vegetation period, all the plots were irrigated four times till at field moisture capacity in each irrigation.

Plant growth and sampling. While the intercropped and pure maize plots were harvested based on maize maturity (at milk or dough stage), the pure sown soybean was harvested at the end of seed filling. Plant height was measured prior to harvest. Harvested material from each of the pure grown plots was weighed to determine fresh forage yield while plant materials from mixture plots were separated into mixture components and each component was weighed separately.

A random sample of 500 g fresh forage was collected from each plot for each species and oven-dried at 55 ºC for 48 hrs to calculate for dry matter yield. Soybean ratios in the dry matter mixtures were calculated as percentage by dividing the oven-dried weight of the soybeans to the total dried weight of the mixture forage.

To evaluate the usefulness of the intercropping, the land equivalent ratio (LER) was calculated as the relative land area required for sole crop to obtain the same yield achieved in intercropping [12, 13].

LER = (yield of intercropped soybean/ yield of pure sowing soybean) + (yield of intercropped maize/ yield of pure sowing maize)When LER ≤1 implies intercropping is disadvantageous while LER>1 implies intercropping is advantageous [14].

Processing and chemical analysis. Oven-dried samples were processed (ground and 1-mm sieved) to analyze for crude protein (CP), neutral detergent fiber (NDF) and acid detergent fiber (ADF) using near infrared reflectance spectroscopy (NIRS, Foss 6500) with software package program 'IC-0904FE'-Technology. A global calibration equation was used to estimate the nutritive quality of forage corn [15]. For NIRS analysis, a sample of 0.5–1.0 g which was exposed to an electro-magnetic scanner over a spectral wavelength range of 1100 to 2500 nm (near infrared).

Digestibility of dry matter (DDM) ratio, dry matter intake (DMI) and relative feed value (RFV) were determined by the following formulas [16]:

DDM (Digestible Dry Matter)= 88.9 - (0.779 x ADF %),

DMI = Dry Matter Intake (% of BW) = 120/(NDF %),

RFV = (DDM x DMI)/1.29.

Statistical Analyses. Experimental data were analyzed using proc mixed procedure in SAS program in accordance within a split plot experiment. Significant means were compared using TUKEY test at $P \leq 0.05\%$ level [17].

RESULTS AND DISCUSSION

Corn and soybean growth and biomass production. Results showed that the factor year had significant effects on plant height of corn while it was not significantly influenced by pure sowing or intercropping with different sowing patterns. Averaged plant height of corn (284.7 cm) obtained in the second year was statistically significant higher than that

TABLE 2
Plant Heights of Pure Sowings and Mixtures of Corn and Soybean.

Treatment	Harvest Stage	Corn Plant Height (cm)			Soybean Plant Height (cm)		
		2010	2011	Mean	2010	2011	Mean
M1	H1	260.1	294.0	277.1	120.5	138.9	129.8
	H2	252.5	275.5	264.0	112.7	136.9	124.8
Mean		**256.3**	**284.7**	**270.5**	**116.6**	**137.9**	**127.3 A***
M2	H1	271.0	294.0	282.5	112.5	134.6	123.6
	H2	255.1	282.1	268.6	106.6	133.8	120.2
Mean		**263.0**	**288.1**	**275.5**	**109.6**	**134.2**	**121.9 ABC**
M3	H1	264.5	287.0	275.8	117.3	137.2	127.2
	H2	265.8	290.1	278.0	121.5	140.7	131.1
Mean		**265.2**	**288.6**	**276.9**	**119.4**	**139.0**	**129.2 A**
M4	H1	266.6	283.5	275.0	112.2	137.8	125.0
	H2	270.1	278.2	274.2	107.0	147.3	127.1
Mean		**268.3**	**280.9**	**274.6**	**109.6**	**142.6**	**126.1 AB**
M5	H1	273.1	287.5	280.3	113.3	139.8	126.6
	H2	263.1	274.7	268.9	109.2	137.8	123.5
Mean		**268.1**	**281.1**	**274.6**	**111.3**	**138.8**	**125.0 AB**
M6	H1	270.2	289.5	279.8	114.3	113.7	114.0
	H2	267.4	275.6	271.5	110.2	137.3	123.8
Mean		**268.8**	282.6	**276.4**	**112.3**	**125.5**	**118.9 BC**
Sole	H1	261.5	286.8	274.1	109.5	124.1	116.8
	H2	270.0	287.5	278.7	109.8	121.7	115.7
Mean		**265.8**	**287.1**	**276.5**	**109.6**	**122.9**	**116.3 C**
Mean (Year)		**265.1 B+**	**284.7 A**		**112.6 B+**	**134.9 A**	
			Harvest Stage Means				
H1		266.7	288.9	**277.8 A**	114.2 b	132.3	**123.3**
H2		263.4	280.5	**272.0 B**	111.0 b	136.5	**123.7**
CV (%)			**3.77**			**6.69**	

*) The means with the same capital letter in the same column are not statistically significant different from each other according to the Tukey test at P≤0.05.
+) The means with the same capital letter in the same row are not statistically significant different from each other at P≤0.05.

of the plant height (265.1 cm) in the first year (Table 2). The difference in climatically conditions, e.g. lower temperatures in June of the second years, may be reason of the higher plant height than in the first year. Two years averaged values of corn plant height changed from 270.5 cm to 276.9 cm depending on the cropping systems. Our results were not consistently similar with those of the Mut et al.[10] who reported that a lower corn plant height in sole cropping than that in the intercropping systems. Delayed harvest may also increase the plant height of corn but the increase was statistically non-significant.

Soybean plant height was significantly influenced by year and cropping systems. Plant height (134.9 cm) of soybean in the second year was higher as compared with that (112.6 cm) in the first year (Table 2). Like corn, a variation in climatic conditions between years may be resulted in significant differences in plant height of soybean. Averaged across years, the soybean plant height ranged from 116.3 cm to 129.2 cm (Table 2). Sowing pattern of M3 (2M1S in the alternate rows) had the highest soybean plant height with respect other combination of sowing patterns. Plant height in M3 was significantly higher than those in the M6 (2M1S in the same row) and in the sole soybean. Averaged plant height in sole soybean treatment was significantly lower than those in all of the intercropping combinations, with the exceptions of those in the treatments M2 and M6, respectively. A higher interspecific competition may have increased the plant height of soybean in the intercropping systems. Our results were consistent with those of the Toniolo et al. [18], who indicated a significantly lower soybean plant height in sole cropping than that in the intercropping.

Green herbage (GH) yield was significantly influenced by year, cropping system, harvest time and year x cropping system interaction, respectively (Table 3). There was a significant difference in GH yield between years with higher in the second year than that in the first year. However, the year effect on the GH yield was depended on the cropping system. The treatment of M1, M2 and M4 produced significantly higher GH yields in the second year than those in the first year. Averaged across years, the treatment of M4 (1M1S in the same row) produced significantly higher GH yield than the sole sowing and other intercrops with the exceptions of the treatments of M5 and M6. In contrast, intercrops in the same row gave significantly higher GH yields than the intercrops in alternate rows as well as pure sowings. Our results

suggested that the utilization of the ecological resources by the intercrop species in the same row was more efficient than when they are sown in the alternate rows or as a sole.

Our results did not consistent with those of the Htet et al.[19], who reported a higher GH yield of pure sowing of maize than the intercropping maize with soybean. Mut et al.[10] reported that the highest hay yield (20.66 t ha^{-1}) was achieved from the mixture of maize and soybean with the sowing rate of 50M:100S while sole maize produced lower yields than the mixtures. The GH yield based on harvest stages of maize ranged between 43.76 and 45.52 t ha^{-1} and harvest at H1 stage produced a significantly higher GH yield than the harvest at H2 stage. This may be due to higher water content of forage at H1 stage of maize than the H2 stage. Our results were in agreement with those of the Htet et al.[19].

The year, cropping system, harvest stage and year x cropping system had significant effects on dry matter (DM) yield (Table 3). Averaged DM yield was significantly higher in the 2nd year than in the 1st year, which was expected due to higher green forage yield in the 2nd year. However, effect of the year on the dry matter yield changed depending on the cropping system. While all of the intercrops and sole sowing of maize produced higher DM yield in the 2nd year than that in the 1st year, the DM yield of sole sowing of soybean did not influenced by year (Table 3). When combined years, the DM yield was significantly influenced by cropping system. The highest DM yield was obtained in the M4, like for green herbage yield; however, the DM yield in the M4 treatment was not significant different from those of other intercrops in which maize and soybean were sown in the same row. In contrast, the intercropped maize and soybean in the same row gave

TABLE 3
Green Herbage and DM Yield of Pure Sowings and Mixtures of Corn and Soybean.

Treatment	Harvest Stage	Green Herbage Yield (t ha^{-1})			Dry Matter Yield (t ha^{-1})		
		2010	2011	Mean	2010	2011	Mean
M1	H1	42.6	48.4	45.5	8.98	14.26	11.62
	H2	36.3	45.0	43.1	9.81	18.33	14.07
Mean		**39.4 d[1]**	**49.2 ab**	**44.3 C***	**9.39 ef[1]**	**16.30 b**	**12.84 C***
M2	H1	40.1	49.3	44.7	8.489	14.97	11.73
	H2	37.5	43.1	40.3	10.09	15.98	13.03
Mean		**38.8 d**	**46.2 bc**	**42.5 C**	**9.29 ef**	**15.47 b**	**12.38 C**
M3	H1	40.8	49.4	45.1	8.87	14.75	11.81
	H2	40.9	44.3	42.6	11.22	16.31	13.76
Mean		**40.8 cd**	**46.8 bc**	**43.8 C**	**10.04 de**	**15.53 b**	**12.78 C**
M4	H1	45.9	57.4	51.6	9.90	18.30	14.10
	H2	49.0	53.2	51.1	13.22	18.35	15.78
Mean		**47.4 bc**	**55.3 a**	**51.4 A**	**11.56 cd**	**18.32 a**	**14.94 A**
M5	H1	52.6	52.8	52.7	11.28	14.98	13.13
	H2	47.7	51.3	49.5	13.47	17.95	15.71
Mean		**50.1 ab**	**52.0 ab**	**51.1 AB**	**12.38 c**	**16.46 b**	**14.42 AB**
M6	H1	50.8	45.4	48.1	11.15	13.81	12.48
	H2	51.3	49.3	50.3	13.98	18.53	16.25
Mean		**51.0 ab**	**47.3 bc**	**49.2 AB**	**12.56 c**	**16.17 b**	**14.37 AB**
SS	H1	29.7	23.8	26.7	6.05	7.05	6.55
	H2	32.1	27.6	29.9	7.89	8.69	8.29
Mean		**30.9 e**	**25.7 e**	**28.3 D**	**6.97 g**	**7.87 fg**	**7.42 D**
SM	H1	47.5	51.9	49.7	1.05	14.11	12.28
	H2	42.0	44.7	43.4	11.52	17.35	14.42
Mean		**44.8 bcd**	**48.3 ab**	**46.5 BC**	**10.98 cde**	**15.72 b**	**13.35 BC**
Mean (Year)		**42.9 B+**	**46.4 A**		**10.40 B+**	**15.23 A**	
Harvest Stage Means							
H1		43.76	47.28	**45.52 A***	9.40	14.03	**11.71 B***
H2		42.08	45.43	**43.76 B**	11.40	16.43	**13.91 A**
CV (%)			**9.82**			**14.97**	

*) The means with the same capital letter in the same column are not statistically significant different from each other according to the Tukey test at P≤0.05.
+) The means with the same capital letter in the same row are not statistically significant different from each other at P≤0.05.
1) The means of different year-treatment combinations with the same lower case are not statistically significant different from each other according to the Tukey test at P≤0.05.

significantly higher DM yields than those of intercropping maize and soybean in the alternate rows as well in the pure sowings of maize and soybean. These results did not coincided with Htet et al. [19], who reported a higher DM yield of sole maize than the intercropped maize and soybeans. The results of Ijoyah and Fanen [20] reported a higher DM yield of intercropping than the sole soybean and maize, which supported our results. Harvest at the dough stage of maize gave significantly higher DM yield than that in the milk stage. Due to a higher DM content at the dough stage of maize, a higher DM yield from pure sowings and intercrops of maize and soybean was harvested at the dough stage of maize than that harvested at the milk stage.

Our results showed that year and sowing pattern of intercropping had significant effects on soybean ratio in the DM yield of intercropping. Average soybean ratio of the intercropping in the 1st year was significantly higher than in the 2nd year (Table 4). The highest soybean ratio was obtained from the treatment of M2 (1M 2S in alternate rows). The increasing sowing ratio of soybean in the intercropping increased the ratio of soybean in DM yield of the mixtures. Soybean ratios in the intercropping in which maize and soybean were sown in the alternate rows were higher than those in the intercropping in which maize and soybean were sown in the same row. Our results suggested that soybean in the intercropping can better compete with maize when it was sown in alternate rows than in the same row.

The year, sowing patterns of intercropping and year x sowing pattern did significantly affect the land equivalent ratio (LER) values. Averaged LER value was significantly higher in the 2nd year than in 1st year. However, effect of year on the LER value did significantly change depending on the sowing pattern. LER values for the treatments of M1, M2 and M4 in the second year were significantly higher than those in the first year while LER values for the other intercrops did not significantly change depending on the years. Averaged across years, the treatment of M5(1M2S in the same row) produced the higher LER value with respect the treatments of M4 and M2. In contrast, LER values in all of the intercropping combinations higher than 1. This means that intercropping of maize and soybean is advantageous compared with the pure sowings of maize and soybean (14).

Higher LER values than 1.0 for the intercropping have been also reported by Ijoyah and Fanen [20] and Kamara et al. [9]. Harvest time did not affect the LER values of the intercropping (Table 4).

Forage quality. Harvest stage and cropping system had a significant effect on neutral detergent fiber (NDF) content of forage DM. Averaged NDF

TABLE 4
Soybean ratios in dry matter yields and LER values of Mixtures of Corn and Soybean.

Treatment	Harvest Stage	Ratio of Soybean (%)			Land Equivalent Ratio (LER)		
		2010	2011	Mean	2010	2011	Mean
M1	H1	30.84	17.21	24.02	1.056	1.221	1.138
	H2	30.76	23.03	26.89	1.001	1.369	1.185
Mean		**30.80**	**20.12**	**25.46 B***	**1.028 e[1]**	**1.295 abc**	**1.162 CD***
M2	H1	40.21	32.70	36.45	1.050	1.424	1.237
	H2	45.44	38.57	42.01	1.085	1.347	1.216
Mean		**42.83**	**35.63**	**39.23 A**	**1.067 de**	**1.386 a**	**1.227 ABC**
M3	H1	19.43	13.46	16.42	0.973	1.207	1.090
	H2	19.07	12.91	15.99	1.096	1.080	1.088
Mean		**19.28**	**13.13**	**16.20 D**	**1.034 e**	**1.143 cde**	**1.089 D**
M4	H1	25.40	14.80	20.10	1.124	1.526	1.325
	H2	26.29	16.70	21.23	1.293	1.284	1.288
Mean		**25.85**	**15.49**	**20.67 C**	**1.208 bcd**	**1.405 a**	**1.307 AB**
M5	H1	30.69	22.37	26.53	1.325	1.321	1.323
	H2	28.96	20.63	24.79	1.341	1.326	1.334
Mean		**29.83**	**21.50**	**25.66 B**	**1.333 ab**	**1.323 ab**	**1.328 A**
M6	H1	15.30	10.76	13.03	1.194	1.083	1.138
	H2	15.88	12.21	14.05	1.312	1.241	1.276
Mean		**15.59**	**11.48**	**13.54 D**	**1.253 abc**	**1.162 cde**	**1.207 BC**
Mean (Year)		**27.36 A+**	**19.56 B**		**1.154 B+**	**1.286 A**	
Harvest Stage Means							
H1		26.99	18.53	**22.76**	1.120	1.297	**1.209**
H2		27.73	20.59	**24.16**	1.188	1.274	**1.231**
CV (%)			**17.62**			**17.25**	

*) The means with the same capital letter in the same column are not statistically significant different from each other according to the Tukey test at P≤0.05.

+) The means with the same capital letter in the same row are not statistically significant different from each other at P≤0.05.

1) The means of different year-treatment combinations with the same lower case are not statistically significant different from each other according to the Tukey test at P≤0.05.

content was significantly higher in the 1st year than in the 2nd year (Table 5). Dry matter yields of intercrops in the first year contained more soybean than in the second year (Table 4). Legumes contain usually lower concentration of fibers in the DM than the grasses [21]. Higher NDF content of dry matter in the first year in spite of higher soybean ratio of dry matter yields of intercrops can be explained by the rapid development and increasing rapid cell wall content of dry matter due to higher temperatures during the growing season of first year than of second year.

Averaged across years, NDF content ranged between 41.30 and 58.39 % depending on the cropping system (Table 5). The Highest NDF content was determined in the DM of sole maize while the lowest DM was determined in the DM of soybean. Intercropping of maize with soybean without depending on the sowing pattern resulted in significantly decrease in the NDF content of intercropped forage as compared with the forage of sole maize. This result is in agreement with those of Htet et al. [19]. Increasing sowing ratio of maize in the intercropping from 33.3 % (M2) to 66.6 (M3) in the alternate rows did significantly increase the NDF content of dry matter while the same increase in the sowing ratio of maize in the same row did not significantly change the NDF content of dry matter. Htet et al. [19] reported that increasing sowing ratio of soybean increased NDF content of DM of intercropped forage. The NDF content (53.68%) of dry matter of forage harvested at milk stage of maize was significantly higher than that (50.62 %) of harvested at dough stage (Table 5). Similar results have been reported by Dahmardeh et al. [22] and Htet et al.[19]. The NDF is important in ration formulation because it reflects the amount of forage that can be consumed by animals [23]. A decline in fiber concentration with increasing maturity can be attributed to the dilution effect created by increasing content of grain as maize get matured [24] or as triticale get matured in the mixture of berseem clover and triticale [25]. High quality forages have low concentration of both NDF and ADF and high digestibility [26, 27].

Years and harvest stages had a significant effect on acid detergent fiber **(**ADF) content of dry matter (Table 5). The ADF content of forage in the 1st year was statistically significant higher than in the 2nd

TABLE 5
NDF and ADF Contents of Pure Sowings and Mixtures of Corn and Soybean.

Treatment	Harvest Stage	Neutral Detergent Fibre (%)			Acid Detergent Fiber (%)		
		2010	**2011**	**Mean**	**2010**	**2011**	**Mean**
M1	H1	55.69	54.47	55.08	32.93	31.68	32.30
	H2	53.77	48.86	51.31	31.75	27.61	29.68
Mean		**54.73**	**51.66**	**53.20 BC***	**32.34**	**29.65**	**30.99**
M2	H1	52.81	52.19	52.50	31.58	31.40	31.49
	H2	49.07	48.34	48.71	29.46	28.92	29.19
Mean		**50.94**	**50.26**	**50.60 C**	**30.52**	**30.16**	**30.34**
M3	H1	58.58	52.11	55.35	34.14	29.89	32.01
	H2	53.20	54.47	53.83	29.99	30.93	30.46
Mean		**55.89**	**53.29**	**54.59 B**	**32.07**	**30.41**	**31.24**
M4	H1	54.56	52.94	53.75	31.78	30.14	30.96
	H2	53.44	47.56	50.50	31.00	28.50	29.75
Mean		**54.00**	**50.25**	**52.13 BC**	**31.39**	**29.32**	**30.35**
M5	H1	55.03	54.33	54.68	32.14	31.98	32.06
	H2	49.73	49.79	49.76	28.94	28.50	28.72
Mean		**52.38**	**52.06**	**52.22 BC**	**30.54**	**30.24**	**30.39**
M6	H1	59.26	51.12	55.19	33.83	28.20	31.01
	H2	56.71	51.88	54.29	31.85	28.63	30.24
Mean		**57.99**	**51.50**	**54.74 B**	**32.83**	**28.41**	**30.62**
SS	H1	43.50	40.41	41.95	31.41	29.49	30.45
	H2	39.04	42.27	40.65	28.04	29.03	28.53
Mean		**41.27**	**41.34**	**41.30 D**	**29.72**	**29.26**	**29.49**
SM	H1	62.32	59.52	60.92	34.93	32.94	33.93
	H2	59.10	52.63	55.87	32.14	28.16	30.15
Mean		**60.71**	**56.08**	**58.39 A**	**33.53**	**30.55**	**32.04**
Mean (Year)		**53.49 A+**	**50.80 B**		**31.62 A+**	**29.75 B**	
		Harvest Stage Means					
H1		55.22	52.14	**53.68 A***	32.84	30.71	**31.78 A***
H2		51.76	49.47	**50.62 B**	30.39	28.78	**29.59 B**
CV (%)			**6.25**			**8.23**	

*) The means with the same capital letter in the same column are not statistically significant different from each other according to the Tukey test at P≤0.05.
+) The means with the same capital letter in the same row are not statistically significant different from each other at P≤0.05.

year. Like the NDF content of the dry matter, the reason of the higher ADF content of the forage in the first year as compared with that in second year may be difference in climatic conditions between years. Averaged across years, the ADF content changed between 29.49 % and 32.04 % depending on the cropping system (Table 5). However, this change in the ADF content of DM was not statistically significant. The ADF content declined from milk stage to dough stage at harvest (Table 5). Similar results have been reported by Dahmardeh et al. [22] and Htet et al. [19]. The ADF content in sole soybean and maize decreased with the delaying the harvest from 29.72 % to 29.26 and from 33.53 % to 30.55%, respectively. A decline in fiber concentration with increasing maturity can be attributed to the dilution effect created by the increasing content of grain as corn or soybean matures [24]. Aydemir et al.[1], reported that in intercrops, CP, ADF and NDF concentrations were changed by soybean contribution, since ADF and NDF values of intercropping systems were lower than those of pure maize.

Years and cropping systems had a significant effect on crude protein ratio **(**CP). The CP ratio (9.27%) in the first year was significantly lower than that in the second year (11.24%) (Table 6). When combined years, the CP ratio varied between 7.70 and 15.89% depending on the cropping system. The highest CP ratio was obtained from sole soybean, while the lowest value was obtained from sole maize. The mean CP ratio of sole soybean was statistically significant higher than those of sole maize and all of the intercrops. On the other hand, increased sowing ratio of soybean in intercrops increased the CP content of the intercrop dry matter. Results in the present study were in agreement with other studies where legumes also increased CP ratio when in a mixture with corn [28, 29, 22, 30, 31, 19 and 32]. One of the reason of this result could be higher nitrogen availability for maize in intercropping compared with the sole crop [33, 34]. Combined analyses of years showed that the harvest time did not significantly affect the crude protein ratio of dry matter. However, effect of the harvest time on the CR ratio did significantly change in the experimental years. The CP ratio in the second year did not significantly change depending on the harvest time while harvest at milk stage of maize resulted in the higher crude protein ratio than that in the dough stage in the first year.

TABLE 6
Crude Protein and DDMR of Pure Sowings and Mixtures of Corn and Soybean.

Treatment	Harvest Stage	Crude Protein Ratio (%)			Digestible Dry Matter Ratio (%)		
		2010	**2011**	**Mean**	**2010**	**2011**	**Mean**
M1	H1	9.16	9.59	9.37	63.25	64.22	63.74
	H2	8.39	11.73	10.06	64.17	67.39	65.78
Mean		**8.77**	**10.66**	**9.72 C***	**63.71**	**65.81**	**64.76**
M2	H1	10.94	11.33	11.13	64.31	64.45	64.38
	H2	9.74	11.97	10.85	65.95	66.38	66.16
Mean		**10.34**	**11.65**	**10.99 B**	**65.13**	**65.41**	**65.27**
M3	H1	7.80	10.57	9.18	62.31	65.62	63.97
	H2	8.04	9.40	8.72	65.54	64.81	65.18
Mean		**7.92**	**9.99**	**8.95 C**	**63.92**	**65.22**	**64.57**
M4	H1	8.89	9.53	9.21	64.14	65.43	64.78
	H2	8.59	10.95	9.77	64.75	66.70	65.73
Mean		**8.74**	**10.24**	**9.49 B**	**64.45**	**66.06**	**65.26**
M5	H1	9.59	10.46	10.03	63.87	63.99	63.93
	H2	8.79	11.29	10.04	66.36	66.70	66.53
Mean		**9.19**	**10.88**	**10.03 BC**	**65.11**	**65.34**	**65.23**
M6	H1	7.60	11.10	9.35	62.55	66.94	64.74
	H2	7.90	10.55	9.22	64.10	66.60	65.35
Mean		**7.75**	**10.82**	**9.28 C**	**63.32**	**66.77**	**65.04**
SS	H1	15.79	17.50	16.65	64.44	65.93	65.18
	H2	13.67	16.60	15.13	67.06	66.29	66.68
Mean		**14.73**	**17.05**	**15.89 A**	**65.75**	**66.11**	**65.93**
SM	H1	6.68	7.98	7.33	61.69	63.24	62.47
	H2	6.81	9.32	8.07	63.87	66.97	65.42
Mean		**6.75**	**8.65**	**7.70 D**	**62.78**	**65.11**	**63.94**
Mean (Year)		**9.27 B+**	**11.24 A**		**64.27 B+**	**65.73 A**	
				Harvest Stage Means			
H1		9.55 b[1]	11.01 a	**10.28**	63.32	64.98	**64.15 B***
H2		8.99 c	11.48 a	**10.23**	65.22	66.48	**65.85 A**
CV (%)			**10.58**			**3.03**	

*) The means with the same capital letter in the same column are not statistically significant different from each other according to the Tukey test at P≤0.05.
+) The means with the same capital letter in the same row are not statistically significant different from each other at P≤0.05.
1) The means of different year-harvest stage combinations with the same lower case are not statistically significant different from each other according to the Tukey test at P≤0.05.

TABLE 7
DMI and RFV of Pure Sowings and Mixtures of Corn and Soybean.

Treatment	Harvest Stage	Dry Matter Intake (%)			Relative Feed Value		
		2010	**2011**	**Mean**	**2010**	**2011**	**Mean**
M1	H1	2.16 g-l[1]	2.22 e-k	2.19	105.8	111.1	108.4
	H2	2.25 d-k	2.47 c-e	2.36	112.1	129.5	120.8
Mean		**2.20**	**2.35**	**2.28 BC***	**109.0**	**120.3**	**114.6 BC***
M2	H1	2.28 c-k	2.30 c-ı	2.29	113.5	114.9	114.2
	H2	2.45 c-f	2.50 cd	2.48	125.3	129.0	127.1
Mean		**2.36**	**2.40**	**2.38 B**	**119.4**	**122.0**	**120.7 B**
M3	H1	2.05 ı-l	2.33 c-h	2.19	99.0	118.8	108.9
	H2	2.26 d-k	2.21 f-k	2.23	114.9	110.9	112.9
Mean		**2.16**	**2.27**	**2.21 C**	**106.9**	**114.8**	**110.9 CD**
M4	H1	2.20 f-k	2.30 c-ı	2.25	109.5	117.6	113.6
	H2	2.25 d-k	2.54 c	2.39	113.0	131.5	122.2
Mean		**2.23**	**2.42**	**2.32 BC**	**111.3**	**124.5**	**117.9 BC**
M5	H1	2.18 f-l	2.21 e-k	2.20	108.0	110.0	109.0
	H2	2.42 c-g	2.44 c-f	2.43	124.3	126.6	125.5
Mean		**2.30**	**2.33**	**2.31 BC**	**116.2**	**118.3**	**117.3 BC**
M6	H1	2.03 j-l	2.36 c-h	2.19	98.4	122.6	110.5
	H2	2.12 h-ı	2.32 c-h	2.22	105.2	119.6	112.4
Mean		**2.07**	**2.34**	**2.21 C**	**101.8**	**121.1**	**111.6 C**
SS	H1	2.76 b	2.97 ab	2.87	138.1	151.9	145.0
	H2	3.08 a	2.86 ab	2.97	159.9	147.3	153.6
Mean		**2.92**	**2.92**	**2.92 A**	**149.0**	**149.6**	**149.3 A**
SM	H1	1.93 l	2.02 kl	1.98	92.2	99.3	95.8
	H2	2.03 j-l	2.29 c-j	2.16	100.8	119.3	110.0
Mean		**1.98**	**2.16**	**2.07 D**	**96.5**	**109.3**	**102.9 D**
Mean (Year)		**2.28 B+**	**2.40 A**		**113.8 B+**	**122.5 A**	
Harvest Stage Means							
H1		2.20	2.34	**2.27 B***	108.1	118.3	**113.2 B***
H2		2.36	2.45	**2.41 A**	119.4	126.7	**123.1 A**
CV (%)			**6.68**			**9.53**	

*) The means with the same capital letter in the same column are not statistically significant different from each other according to the Tukey test at P≤0.05
+) The means with the same capital letter in the same row are not statistically significant different from each other at P≤0.05
1) The means of different treatment-harvest stage combinations with the same lower case are not statistically significant different from each other according to the Tukey test at P≤0.05

Digestibility dry matter ratio (DDMR) was significantly influenced by harvest time and years (Table 6). The value of DDMR in the second year was significantly higher than that in the first year. The DDMR is closely related to the ADF content and with increasing ADF value decreases the DDMR [35]. Therefore, higher DDMR in the second year is an expectable result due to lower ADF (Table 5).

The value of DDMR at dough stage (65.85%) was significantly higher than that at milk stage (64.15%) (Table 6).

The year, harvest stage, cropping system and year x harvest stage x cropping system had significant effects on dry matter intake (DMI) (Table 7). The DMI in the second year was significantly higher than in the first year. DMI is closely related with the NDF content of forage dry matter, and as content of dry matter increases, DMI decreases [36, 37]. For this reason, higher NDF in the first year (Table 5) resulted in the lower DMI as compared with the second year.

Due to higher averaged value of NDF for the harvest at milk stage of maize (Table 5), DMI for the harvest at the milk stage was statistically significant

lower than that at the dough stage of maize. Because of the interaction of year x harvest time x cropping system, effect of the year and harvest time changed depending on the cropping system. Averaged across years DMI varied between 2.07 % and 2.92 % depending on the cropping system (Table 7). Dry matter from the sole sowing of soybean showed significantly higher DMI than those from the sole maize and all of the intercrops while dry matter from sole maize had significantly lower DMI value than those from sole soybean and all of the intercrops.

Oba and Allen [38] stated that enhanced NDF digestibility of forage significantly increased DMI and milk yield of dairy cows. High quality forages have low concentration of both NDF and ADF and high digestibility [39, 26].

The years, cropping systems and harvest stages had a significant effect on relative feed value (RFV) (Table 7). The RFV in the second year was higher than in the first year. Lower averaged values of NDF and ADF in the second year resulted in higher RFV value as compared with that in the first year. Averaged value of RFV of forage dry matter harvested at dough stage of maize was significantly higher than that of forage dry matter harvested at milk stage. Averaged across years, RFV varied from 102.9 to 149.3 depending on the cropping system. Forage of sole soybean showed significantly higher RFV than those of sole maize and all of the intercrops while forage of sole maize had a RFV being significantly lower than those of sole soybean and all of the intercropping. The RFV is an index that combines the important nutritional factors of intake and digestibility, and as percent ADF and NDF decrease, the RFV will increase [35]. Due to ADF and NDF values for the sole soybean and sole maize shown in the Table 5, higher RFV of Soybean forage and lower RFV value of sole maize are expectable results.

CONCLUSIONS

Maize-soybean intercropping has provided an improvement on forage yield and quality. In the same rows sown intercropping was was more productive than the sole and alternative rows sowings. The higher nutritive values of forage were obtained when the harvest was made at dough stage of maize . Among all intercropped systems, the 1M1S and 1M2S (1 row maize to 1-2 rows soybean) in the same row sown were found more preferable as per nutrient composition than other intercrops.

ACKNOWLEDGEMENTS

This research was supported by the Republic of Turkey Ministry of Food, Agriculture and Livestock, General directorate of Agricultural Research and Policies, as part of Project no. TAGEM/TA/11/01/005.

REFERENCES

[1] Aydemir, K.S. (2019). Maize and soybean intercropping under different seed rates of soybean under ecological condition of Bilecik, Turkey. Int. J. Environ. Sci. Technol. 16, 5163-5170.

[2] Iqbal, M.A., Hamid, A., Ahmad, T., Siddiqui, M.H., Hussain, I., Ali, S., Ali, A. Ahmad, Z. (2019) Forage sorghum-legumes intercropping: effect on growth, yields, nutritional quality and economic returns. Bragantia. 78(1), 82-95.

[3] Dhima, K.V., Lithourgidis, A.S., Vasilakoglou, I.B., Dordas, C.A. (2007) Competition indices of common vetch and cereal intercrops in two seeding ratio. Field Crops Res. 100, 249-256.

[4] Liu, J.H., Zeng, Z.H., Jiao, L.X., Hu, Y.G., Wang, Y., Li, H. (2006) Intercropping of different silage maize cultivars and alfalfa. Acta Agron. 32, 125-130.

[5] Javanmard, A., Dabbagh-Mohammadi, A., Nasab, A., Javanshir, A., Moghadam, M. Janmohammadi, H. (2009) Forage yield and quality in intercropping of maize with different legumes as double-cropped. J. Food Agric. Environ. 7, 163-166.

[6] Ghanbari-Bonjar, A. (2000) Intercropped wheat and bean as a low-input. Wye College, University of London, Kent, UK.

[7] Gebrehiwot, L., McGrow, R.L., Assefu, G. (1996) Forage yield and quality profile of three annual legumes in the tropical highlands of Ethiopia. Trop Agr. 73, 83-98.

[8] Reta Sánchez, D.G., Espinosa Silva, J.T., Palomo, G.A., Serrato Corona, J.S., Cueto Wong, J.A. Mascorro, A.G. (2010) Forage yield and quality of intercropped corn and soybean in narrow strips. Spanish J. Agr. Res. 8(3), 713-721.

[9] Kamara, A.Y., Ttofa, A.I., Ademulegun, T., Solomon, R., Shehu, H., Kamai, N., Omoigui, L. (2017) Maize-soybean intercroppıng for sustainable intensification of cereal-legume cropping systems in Northern Nigeria. Exp. Agric. 1-15.

[10] Mut, H., Gulumser, E., Dogrusoz, M.C. Basaran, U. (2017) Forage yield and nutritive value of maize-legume mixtures. Range Mgmt. & Agroforestry. 38(1), 6-81.

[11] Yucel, C., Avcı, M., İnal, İ., Akkaya, M.R. (2016) Effect of different mixture ratios and cutting time intercropped corn/soybean on forages yield under Çukurova conditions. Project final report. Project no: TAGEM/TA/11/01/003, Publication no:12.01DATAEM.F.F30.2016.01. Adana/Turkey.

[12] Mead, R., Willey, R.W. (1980) The concept of land equivalent ratios and advantages in yields from intercropping. Exp. Agric. 16, 117-122.
[13] Sebetha, E. (2019) Maize field biomass yield and land equivalent ratio under the ınfluence of different management practices and location. Asian J. Crop Sci. 11(1), 25-31.
[14] Dariush, M., Ahad, M., Meysam, O. (2006) Assessing the Land Equivalent Ratio (LER) of two corn (Zea mays L.) varieties intercropping at various nitrogen levels in Karaj, Iran J. Cent. Eur. Agric. 7, 359-364.
[15] Jafari, A., Connolly, V., Frolich, A., Walsh, E.K. (2003) A note on estimation of quality in perennial ryegrass by near infrared spectroscopy. Irish J. Agr. Food Res. 42, 293-299.
[16] Jaranyama, P., Garcia, A.D. (2004) Understanding relative feed value (RFV) and relative forage quality (RFQ). College of Agric and Biological Sci, South Dakota State University, USDA.
[17] Littell, R.C., Milliken, G.A., Stroup, W.W., Wolfinger, R.D., Schabenberger, O. (2006) SAS for Mixed Models. Second Edition, Cary, NC, SAS Institute Inc.
[18] Toniolo, L., Sattin, M., Mosca, G. (1987) Soybean-Maize intercropping for forage. Eurosya. 5, 73-78.
[19] Htet, M.N., Soomro, N.S., Jiang bo, H. (2016) Effect of Intercropping of maize (*Zea mays* L.) and soybean (*Glycine max* L.) on green forage yield and quality evaluation. IOSR J. Agr. Vet. Sci. 9(12), 59-63.
[20] Ijoyah, M.O., Fanen, F.T. (2012) Effects of different cropping pattern on performance of maize-soybean mixture in Makurdi, Nigeria. Sci. J. Crop Sci. 1(2), 39-47.
[21] Costa, P.M., Villela, S.D.J., Leonel, F.D.P., Araújo, K.G., Ruas, R.M., Coelho, F.S., Andrade, V.R. (2012) Intercropping of corn, brachiaria grass and leguminous plants: productivity, quality and composition of silages. R. Bras. Zootec. 41, 2144-2149.
[22] Dahmardeh, M., Ghanbari, A., Syasar, B., Ramroudi, M. (2009) Effect of intercropping maize with cowpea on green forage yield and quality evaluation. Asian J. Plant Sci. 8(3), 235-239.
[23] Lithourgidis, A.S., Vasilakoglou, I.B., Dhima, K.V., Dordas, C.A., Yiakoulaki, M.D. (2006) Silage yield and quality of common vetch mixtures with oat and triticale in two seeding ratios. Field Crops Res. 99, 106-113.
[24] Coors, J.G., Albrecht, K.A., Bures, E.J. (1997) Ear-fill effects on yield and quality of silage Maize. Crop Sci. 37, 243-247.
[25] Yücel, C., Avcı, M., Yucel, H., Sevilmiş, U., Hatipoğlu, R. (2018) Effects of seed mixture ratio and harvest time on forage yield and silage quality of intercropped berseem clover with triticale. Fresen. Environ. Bull. 27(8), 5312-5322.
[26] Peterson, J.A., Belyea, R.L., Bowman, J.P., Kerley, M.S., Williams, J.E. (1994) The impact of forage quality and supplementation regimen on ruminant animal intake and performance. In: Fahley Jr., G.C. (Ed), Forage Quality, Evaluation, and Utilization. ASA, CSSA, and SSSA, Madison, Wl, 59-114.
[27] Linn, J. G., Martin, N.P. (1999) Forage quality tests and interpretations. University of Minnesota Extension service, Food and Environmental science. Available at: www.extension.umn.edu/distribution/.../DI2637.html-(Accessed 11 October 2010).
[28] Dawo, M.I., Wilkinson, M., Sanders, F.E., Pilbeam, D.J. (2007) The yield and quality of fresh and ensiled plant material from intercropping maize and bean. J. Sci. Food Agr. 87, 1391-1399.
[29] Geren, H., Avcioglu, R., Soya, H., Kir, B. (2008) Intercropping of maize with cowpea and bean: Biomass yield and silage quality. Afr. J. Biotechn. 7, 4100-4104.
[30] Baghdadi, A., Halim, R.A., Ghasemzadeh, A., Ebrahimi, M., Othman, R., Yusof, M.M. (2016) Effect of intercropping of corn and soybean on dry matter yield and nutritive value of forage corn. Legume Res. 39(6), 976-981.
[31] Erdal, S., Pamukcu, M., Curek, M., Kocaturk, M., Dogu, O.Y. (2016) Silage yield and quality of row intercropped maize and soybean in a crop rotation following winter wheat. Arch. Agron. Soil Sci. 62 (11).
[32] Yucel, C., Avcı, M., Kızılsimsek, M., Hatipoğlu, R. (2020) Yield and quality of silage from soybean-maize intercropping. Fresen. Environ. Bull. 29(2), 874-883.
[33] Eskandari, H., Ghanbari-Bonjar, A., Galavi, M., Salari, M. (2009) Forage quality of cowpea (*Vigna sinensis*) intercropped with Maize (*Zea mays*) as affected by nutrient uptake and light interception. Not. Bot. Horti. Agrobo. 37(1), 171-174.
[34] Eskandari, H. (2012) Yield and quality of forage produced in intercropping of maize (Zea mays) with Cowpea (*Vigna Sinensis*) and Mungbean (*Vigna radiate*) as Double cropped. Int. J. Sci. Basic Appl. Res. 2(1), 93-97.
[35] Linn, J.G., Martin, N.P. (1999) Forage Quality Tests and Interpretations. Available at: http://www. extension. umn.edu/ distribution/livestocksystems/DI2637.html (Accessed: date: 01 March 2020)
[36] Van Soest, P.J. (1994) Nutritional ecology of the ruminats. In Van Soet P.J. Fiber and phsiochemical properties of feeds. 2th Edn. Maizeell University Press. Ithaca and London, 140-155.
[37] Joachim, H., Jung, G. (1997) Analysis of forage fiber and cell walls in ruminant nutrition. J. Nutr. 127, 810-813.

[38] Oba, M., Allen, M.S. (1998) Evaluation of the importance the digestibility of neutral detergent fiber from forage: Effect on dry matter intake and milk yield of dairy cows. J. Dairy Sci. 82, 589-596.
[39] Hatfield, R.D. (1993) Cell wall polysaccharide interactions and digestibility. In: Forage Cell wall Structure and Digestibility (Jung, H.G., Buxton, D.R., Hatfield, R.D,. Ralph, J. Eds.), ASA, CSSA, and SSSA, Madison, WI, 285-313.

Received: **21.07.2020**
Accepted: **24.05.2021**

CORRESPONDING AUTHOR

Ilker Inal
Republic of Turkey Ministry of Agriculture and Forestry
Eastern Mediterranean Agricultural Research Inst.
Karatas Yolu 17. Km, 01370, Dogankent, Yuregir
Adana – Turkey.

e-mail: iinal@hotmail.com

© by PSP Volume 30– No. 09/2021 pages 10474-10481 Fresenius Environmental Bulletin

EFFECT OF BENZYL AMINO PURINE (BAP) AND ITS TIME OF APPLICATION ON THE DWARFISM AND FLOWER PRODUCTION OF CUT CARNATION (*Dianthus caryophyllus*)

Saqib Khan Khalil[1], Abdul Basit[1,*], Izhar Ullah[1,2], Muhammad Sajid[1], Syed Tanveer Shah[1], Imran Ahmad[1], Fazal-i-Wahid[1], Qazi Shoaib Ali[1], Shamsher Ali[1], Imran Habib Khan[1], Sareer Ud Din[1]

[1]Department of Horticulture, The University of Agriculture, Peshawar, Pakistan
[2]Department of Horticulture, Ondokuz Mayis University, Samsun, Turkey

ABSTRACT

Growth retardants like BAP have a major effect in the growth and physiology of plants. They mostly often suppress the height of stem by antagonizes the action of auxins and counteract the apical dominance and its direct application to plants fortifies cell division and growth of the dormant buds ultimately improving the plants bushiness. The experiment was conducted at the Ornamental nursery, Department of Horticulture, The University of Agriculture Peshawar during the year 2018 to evaluate the effect of Benzyl Amino Purine (BAP) and its time of application on the dwarfism and flower production of carnation using Randomized Complete Block Design with split plot arrangement. The treatments comprising of different concentration of BAP (0, 30, 60 and 90mgL^{-1}) and different time of foliar application (7, 14, 21 and 28 days after transplantation). Maximum (days to flowering, number of branches plant^{-1}, number of leaves plant^{-1}, leaf area (cm^2), number of flowers plant^{-1}, No. of petals flower^{-1} and survival percentage (%)) and minimum value of plant height (cm), fresh flower weight (g) and dry flower weight (g)) were observed when BAP was applied at 90 mg L^{-1}. Among foliar application, maximum plant height (g), number of branches plant^{-1}, number of leaves plant^{-1}, leaf area (cm^2) and No. of petals flower^{-1} were observed after 28 days of foliar application of BAP. While foliar application of BAP after 7 days had observed maximum value of days to flowering, number of flowers plant^{-1}, fresh flower weight (g), dry flower weight (g) and survival percentage (%) of carnation. Based on the findings it is concluded that BAP @ 90 mg L^{-1} and foliar application after 7 days of transplantation performed a better role in reducing the plant height and improving flower production in carnation under the agro-climatic condition of Peshawar valley.

KEYWORDS:
Apical dominance, Benzyl Amino Purine, Dianthus, Floriculture, Growth retardants, Sim

INTRODUCTION

Floriculture has a vital position in today's world and the horticulture industry due its importance in every sector of life ranging from religious occasions to weddings. The demand for floriculture products is gradually increasing day by day in the domestic as well as in the international markets. With the rapidly changing lifestyle and speedy urbanization, floriculture has gained its own commercial status [1]. Compared to other horticulture products, floriculture products need more care, high investment, up-to-date growing technology and more specific management. Therefore, as compared to other crops, the production of floriculture crops is much higher per unit area [2]. In the recent times, commercial floriculture has greatly emerged in Pakistan. The most important floriculture crops in Pakistan are seasonal flowers such as roses, petunia, pansy, marigold, carnation, chrysanthemum, antirrhinum, jasmine and statice. Pakistan is an agricultural country and its contribution to the national GDP is 21.4%. The contribution of Horticulture as a sub sector is just 11%. Floriculture has been identified as an area of high source of income for farmers in Pakistan due to its favorable agro-climatic conditions, diversity in the soil and cheap labor. Due to these factors Pakistan has the potential to develop a strong floriculture industry. The floriculture industry has flourished in big cities such as Lahore, Islamabad, Multan, Karachi, Peshawar and Faisalabad where flowers demand is high [3].

Carnation (*Dianthus caryophyllus* L.), an important cut flower belongs to the family Caryophyllaceae, indigenous to the Mediterranean region. In the international market, it ranks 3rd amongst the main ten cut flowers [4]. It is one of the main commercially grown flowers at the world level. The generic name Dianthus comes from the writings of Theophratus, who lived about 300 B.C. He proposed that the word "Dianthus" came from the Greek words: "dios" means divine (God); "anthos" means flower, that is "the flower of the Gods". Linnaeus

chose the species name "caryophyllus" after the genus of Clove, as the fragrance from Carnation is reminiscent of clove. The variety William Sim produced in 1938-39 by William Sim of North Berwick, Marine was the greatest contribution to the present Carnation industry. From that one red flowered plant, there have been mutations to several variegated forms like white, pink, orange, etc. Carnation is an important flower crop having great commercial value as a cut flower due to its excellent keeping quality, wide array of color and forms. Carnation, apart from producing cut flowers can also become useful in gardening for bedding, edging, borders, pots and rock gardens [5]. Outstanding shelf life, a variety of form and colors, capacity to survive during long distance transportation have made carnation flower a unique item in the cut flower trade worldwide [6]. Different carnations cultivars are available, but the most commonly raised are perennial, annual and border flowering carnations. Border carnation has been under cultivation since long ago. At the point when cold weather arrives, plants in chilly atmospheres hardly have adequate nutrients remaining to adapt during cool weather [7].

The most famous carnations are the perennial carnations which are the latest type, these originated in Europe around the year 1850 [8]. *Dianthus caryophyllus* and *Dianthus Chinensis* are believed to be the ancestors of perennial carnations which are used for cut flower market these are high demanding [9]. These are known as 'Sim' form which is characterized by its tall stature, thick stem with heavy flowering, it is because these characters that they are favored worldwide in the cut flower market [7,9]. Generally, carnation produces a single primary shoot that ends into a blossom bud. After the suspension of terminal development, horizontal shoots arise. They likewise bear blossom buds. A major problem which affects the business of carnation is apical dominance because it restricts the development of lateral buds, causing a limited amount of side branches and flowers [10]. Having a greater number of healthy and expanded flowers, the maximum aesthetic value can be attained [11,12]. Lately, various plant retardants have been utilized by of agribusiness for initiating more desirable plant qualities like dense and stunted growth with extended number of branches. In the floriculture industry, these characteristics are high in demand [13-15]. Carnation a highly profitable cut flower crop shows apical domination and advancement of parallel shoots and bloom generation are affected by the nearness of apical predominance [16].

Growth retardants have a major effect in the growth and physiology of plants. They most often suppress the height of stem and also affect the flowering habit of plants. The main objective of cytokinin application is to achieve healthy branched plants without detaching the apical meristem. Application of cytokinin and stunting growth chemicals treated plants may rely upon the technique utilized (foliar application or soil application). It also depends on the plant species and sometimes plant cultivar [17]. Cytokinin applied exogenously have the same effect as pinching in plants. Most of the studies showed auxins and cytokinin might control the apical dominance antagonistically. Benzyl Amino Purine (BAP) is an aromatic compound belonging to cytokinin group. Studies on BAP demonstrate that its foliar application invigorates plants to build up a well branch framework without the acts of pinching. It encourages plants to develop more axillary shoots giving a plant bushy appearance. BAP antagonizes the action of auxins and counteract the apical dominance thus playing a vital role in reducing plants height. Direct application of BAP to plants fortifies cell division and growth of the dormant buds ultimately improving the plants bushiness. Moreover, it also has positive effects on the quantity of branches and blooms with mainly having impact on plants blossoming [17-19]. Keeping in view the above prospective of carnation, an experiment was planned to study the effect of optimum level of Benzyl Amino Purine and. standardize the most suitable application time for induction of dwarfism in carnation.

MATERIALS AND METHODS

Experimental site. The present research study was conducted at Ornamental Nursery, Department of Horticulture, The University of Agriculture Peshawar Pakistan. The research site is located at 340m altitude above the sea level with a latitude of 34.01° N and longitude of 71.52° E which is considered as a subtropical region on the basis of its climate. Peshawar is well known by both its prolonged hot summers (max temp 45-47°C) and severe cool winters with a fall in temperature up to 4°C. Both the summer and winter are extreme. March is counted for highest rainfall of approximately 78mm while the lowest rainfall occurs during the month of June (8mm) with an approximate location of 1600km from north of Indian Ocean [20-22].

Experimental Description. The experiment was laid out in Randomized Complete Block Design (RCBD) with split plot arrangement having the following two factors i.e. BAP concentrations (0,30,60 and 90 mgL^{-1}) and different application time (7, 14 and 21 days after transplantation) that was replicated three times. The seedlings of carnation at two to three leaf stage were purchased from a local nursery Hayatabad region and were planted at a row to row distance of 50 cm and plant to plant distance of 25 cm. The recommended doses of fertilizers (0, 40, 80 kg ha^{-1}) were applied to the experimental field. Nitrogen was applied in the form of urea, the source of phosphorus (DAP) was used, while potash was applied in the form of Murate of potash. Split doses of urea were applied, the first dose was applied before

TABLE 1
Mean Square value of morphological and flower attributes of carnation as influenced by BAP concentration and its time of application

SOV	DF	Mean Square (MS)									
		NOBPP	NOLPP	LA	DTF	NOFPP	NOPPF	FFW	DFW	SP	PH
Replications	2	11.646^{ns}	39.396^{ns}	0.005^{ns}	51.021^{ns}	1.563^{ns}	0.25^{ns}	0.003^{ns}	0.057^{ns}	8.063ns	42.188^{ns}
Time of application (T)	3	45.472*	284.854*	0.033**	52.75*	30.965**	38.41***	0.021**	0.112**	91.806**	53.354*
Error (I)	6	6.868	51.313	0.004	10.688	3.34	2.556	0.002	0.013	14.451	10.521
BAP (B)	3	32.917***	1404.8***	0.146***	73.361**	37.688***	19.465**	0.285***	0.866**	37.361*	138.076***
T × B	9	3.269^{ns}	38.632^{ns}	0.021^{ns}	21.435^{ns}	3.743^{ns}	7.539^{ns}	0.161ns	0.353^{ns}	22.343^{ns}	29.113^{ns}
Error (II)	24	7.118	16.861	0.03	19.104	6.646	4.479	0.07	0.217	11.66	26.938
Total	47										

***: P≤0.001; **:P≤0.01;*:P≤0.05; NS: Non significant; NOBPP: Number of branches plant^{-1}; NOLPP: Number of leaves plant^{-1}; LA: Leaf area; DTF: Days to flowering; NOFPP: Number of flowers plant^{-1}; NOPPF: Number of petals flower^{-1}; FW: Fresh flower weight; DFW: Dry flower weight; SP: Survival percentage and PH: Plant height

transplanting the seedlings and the second dose was used 60 days after transplantation. Farm yard manure (FYM) was applied to the field @ 20 tons ha^{-1}. The experimental plots were prepared according to the designed layout. All the cultural practices such as irrigation, weeding, and hoeing etc. were carried out on regular basis. During the research, data was collected for different morphological (Plant height, No. of branches plant^{-1}, No. of leaves plant^{-1}, leaf area and survival percentage) and flower attributes (days to flowering, No. of flowers plant^{-1}, No. of petals flower^{-1}, fresh flower weight and dry flower weight of carnation). For statistical analysis of the data, Statistix (8.1) software was used. All the collected data for various variables were statistically analyzed using randomized complete block design with split plot arrangement and the difference between the treatments were further analyzed through least significant difference (LSD) test [23].

RESULTS AND DISCUSSION

Morphological attributes of Carnation. BAP concentration and time of application had a positive effect on number of branches plant^{-1}, number of leaves plant^{-1}, leaf area, survival percentage and plant height of carnation, whereas the interaction between BAP concentration and time of application on the morphological attributes was found non-significant (Table 1). Plant sprayed with BAP after 28 days of transplantation resulted maximum numbers of branches (20.67), number of leaves plant^{-1} (328.75), leaf area (4.66 cm^2), plant height (54.08 cm) and minimum survival percentage (91.58%) compared to plants treated with BAP application time after 7 days of transplantation that had minimum number of number of branches plant^{-1} (16.58), number of leaves plant^{-1} (322.75), leaf area (4.55 cm^2), plant height (49.83cm) and highest survival percentage (97.25%) . Regarding BAP application, the number of branches per plant increased from (16.42 to 20.42), number of leaves plant^{-1} (317.83 to 342.58), leaf area (4.45 to 4.70 cm^2), survival percentage (92.42 to 96.67 %) with increasing the concentration of BAP from 0 to 90 mg L^{-1}. Foliar application of BAP reduced the plant height when applied at higher concentrations. Application of BAP significantly reduced plant height from 55.25 to 47.42cm in untreated plant to plant received BAP @ 90 mg L^{-1} (Figure 1).

Application of BAP exhibited increase in lateral branches of plants and dominates apical dominance in *Datura* species [24]. [25] also observed a significant increase in lateral branches by the foliar spray of BAP in hibiscus. [26] also found that when BAP was applied on croton plants caused a significant increase in number of branches. The increase in number of branches plant^{-1} with the application of BAP might be attributed due to its role in invigorating vascular strand expansion and the discrimination of xylem. The spread in plant biomass and better water and nutrient uptake is a positive characteristic of BAP [27]. In petunia an increase in the number of branches was observed by the application of BAP [25, 28]. Application of BAP exhibited an increment in number of leaves plant^{-1} might be attributed due to the formation of new leaves per plant as result of apical dominance suppression. Leaves function as the core site for the production of sugar which will be further translocated to other part of the plants. These results are in accordance with the findings of [29] who reported that the application of exogenous cytokinin could increase the lateral branching of *Jatropha curcas* plant maintained under glasshouse condition. The current results are in line with those of [30] who found an increase in number of leaves in

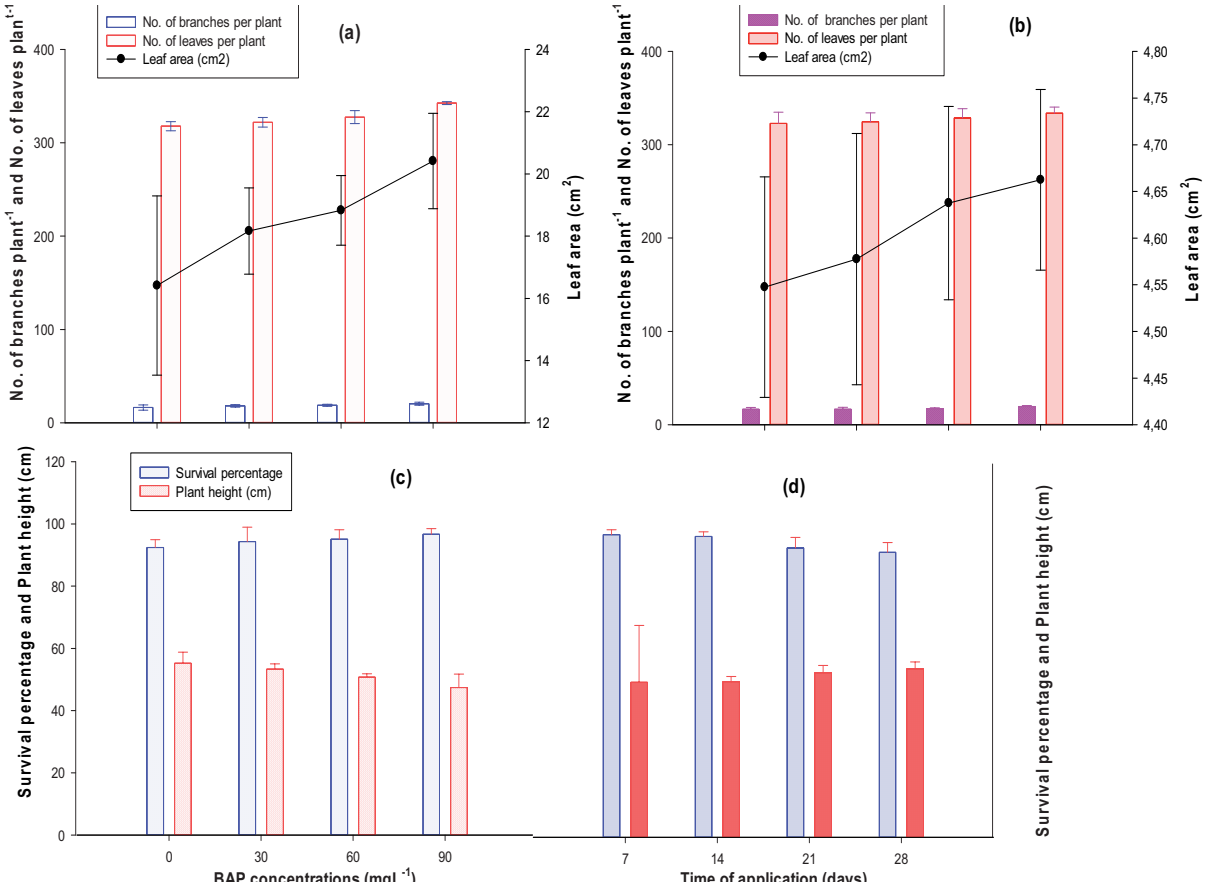


FIGURE 1

Various morphological attributes of carnation as influenced by BAP concentrations (a, c) and its time of application (b, d)

croton plants by application of BAP. The present results are supported by [31], who stated that *Matricaria chamomilla* sprayed with high concentration of BAP produced higher number of leaves plant^{-1} as compared to control. Foliar application of growth retardants in Bougainvillea plants successfully produced more lateral branches by suppressing apical dominance [32]. The current findings similar to those reported [31], who reported that *Matricaria chamomilla* applied with high concentration of BAP had higher number of leaves plant^{-1} as compared to control. An increase in leaf area might be attributed due to increase in chlorophyll content, starch contents in spongy cells and number of layers in palisade tissue [33]. These results are in line with [34] who reported an increase in leaf area from 18- 34% by application of BAP on an ornamental foliage plant *Monstera deliciosa.* Similar results were obtained in gladiolus varieties Jyotsna and Shabnum by spraying BAP during their vegetative growth [35]. In all the plants, the apical portion is responsible for the production of auxin hormone that causes apical dominance. The termination of apical bud accelerates cytokinin to activate the lateral buds and start growth which will obviously overcome apical dominance causing compact growth with controls height [36]. Benzyl amino purine is responsible for restricting the action of auxin and results in plants with controlled growth. [37] reported similar findings that BAP plays a significant role in reducing plant height. The results also correspond with [28] who reported that BAP improved the plant quality of *Salvia nemorosa* by reducing the plant height resulting in more compact plants. [38] reported that zinnia plants sprayed with BAP at 100mgL^{-1} exhibited increase in number of branches plant^{-1}, number of leaves plant^{-1}, days to flowering, number of flowers plant^{-1} and also recorded decrease in plant height, fresh weight and dry weight of carnation flower.

Flower attributes of Carnation. The analysis of the data indicated that the application of BAP concentrations and different time of application had a significant effect on the days to flowering, number of flowers plant^{-1}, number of petals flower^{-1}, fresh flower weight and dry flower weight of carnation, whereas their interaction was found non-significant (Table 1). Decrease in days to flowering of carnation plants were noted when received BAP foliar application after 7 days of transplantation. The earliest flowers were produced in (77.50) in plants received BAP application after 28 days of transplantation that was closely followed by plants received foliar application after 21 days producing flowers in (79.17)

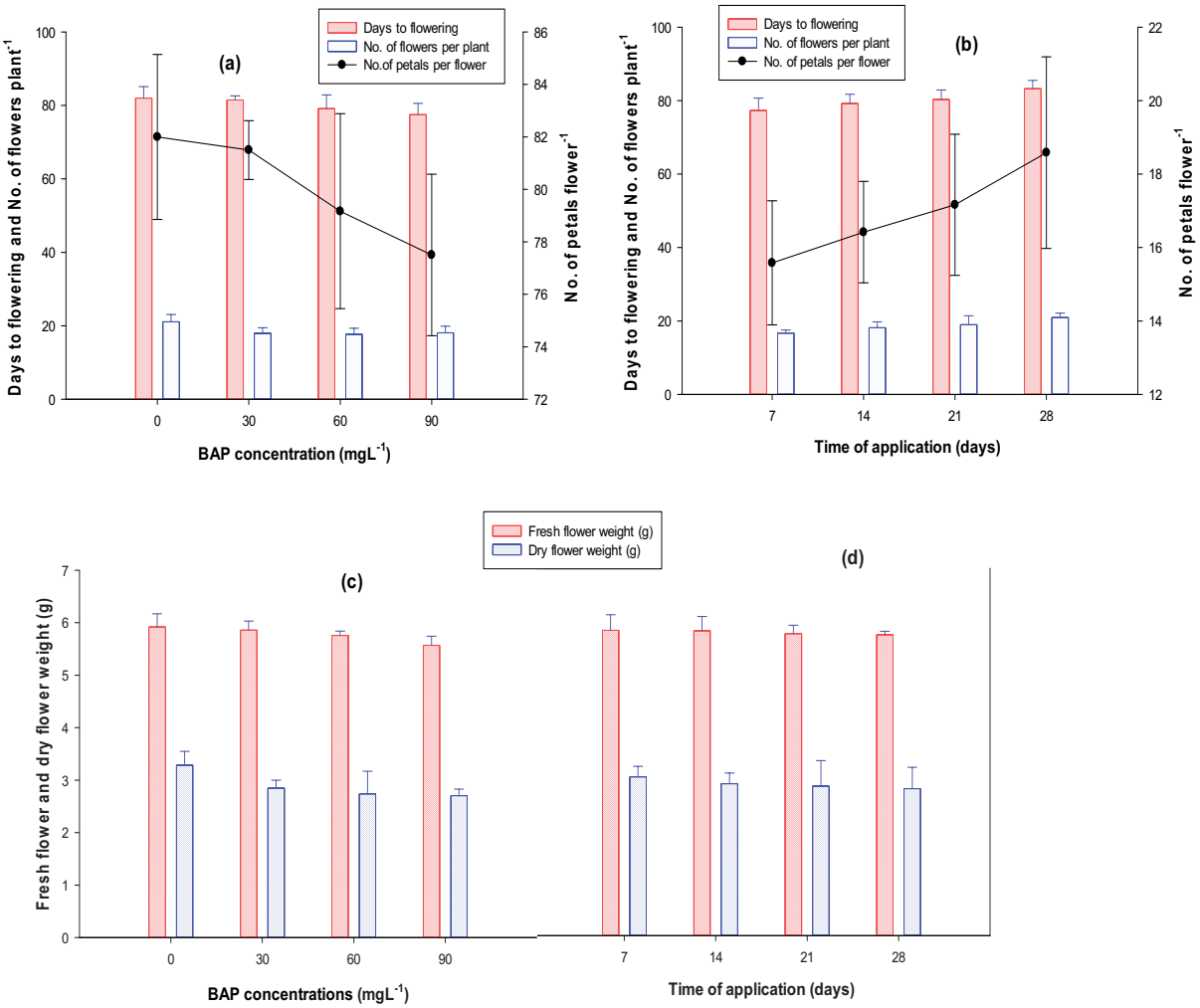


FIGURE 2
Various flowering attributes of carnation as influenced by BAP concentrations (a, c) and its time of application (b, d)

days, while maximum days (82.0) to flowering were observed in plants which received foliar application after 7 days of transplantation. The flowering of carnation was delayed when BAP concentration was increased from 0 to 90mgL^{-1}. The lowest number of days to flowering (77.33) was recorded in plants in control treatment which was at par with plants which took (79.25) and (70.33) days to flowering when received 60 and 90 mg L^{-1} BAP application, respectively. Whereas the maximum days to flowering (83.25) was taken by plants which received 90 mg L^{-1} BAP (Figure 2).

Maximum, numbers of flowers plant^{-1} (21.50), number of petals flower^{-1} (19.42) were produced when foliar application of BAP was applied after 28 days of transplantation. While the minimum number of flowers (16.92) plant^{-1} and numbers of petals flower^{-1} (15.33) were observed in plants sprayed with BAP after 7 days of transplantation. There was a significant increase in the number of flowers plant^{-1} and number of petals flower^{-1} with an increase in the concentration of benzyl amino purine from 0 to 90mgL^{-1}. Maximum numbers of flowers (20.92) and number of petals flower^{-1} (18.58) of carnation plant were obtained when BAP was sprayed at the rate of 90 mg L^{-1} as compared to control treatment (16.67,15.58) (Figure 2).

The fresh flower weight and dry weight of carnation flowers was reduced significantly when the application of BAP was delayed. The plants produced minimum fresh flower weight (5.55 g) when BAP was sprayed after 14 days of transplantation, which was closely followed by plants (5.90 g) and (5.95 g) which were sprayed after 21 and 28 days of transplantation. Whereas, the highest fresh flower weight (6.14 g) was recorded in plants which received foliar application after 7 days of transplantation. Fresh flower weight of carnation was gradually increased with the rise in benzyl amino purine concentration. Maximum value of fresh flower weight (6.24 g) was recorded in plants untreated with BAP, which was statically similar with fresh flower weight (5.83 and 5.75 g) received at 20 and 60 mg L^{-1} BAP, respectively. Whereas, the minimum fresh flower weight (5.73 g) was recorded in plants treated with 90 mg L^{-1} of BAP. The data regarding the time of

foliar application showed that the maximum dry weight of flower (3.03 g) was observed in plants received foliar application of BAP after 7 days of transplantation. While the minimum dry flower weight (2.80 g) was recorded in plants sprayed with BAP after 28 days of transplantation which was statically at par with dry flower weight (2.89 and 2.85 g) in BAP applied after 14 and 21 days of transplantation respectively. Maximum value of dry flower weight (3.28g) was recorded in control plants as compared to dry flower weight (2.70,2.84 and 2.74 g) of plants received BAP treatment at 90 mg L^{-1}, 30 and 60 mg L^{-1} respectively (Figure 2).

A variety of plant growth regulators including BAP has a positive effect on plant growth and enhances the vegetative growth [39-40]. The flowering was delayed in plant species such as *Miltoniopsis orchids* when benzyl amino purine was applied at the rate of 25 to 50milli-molar and it also enhanced vegetative shoots [41]. Early flowering was induced in *Boronia heterophylla* when BAP was sprayed at lower concentration ranging from 10-150 mg L^{-1} [42]. Different plant growth regulators including BAP enhance vegetative growth (40]. [41] reported that foliar application of BAP from 25 to 50 mM enhanced vegetative shoots in *Miltoniopsis orchids* and delayed flowering. Benzyl Amino Purine (BAP) being a member of cytokinin group boosts the flower buds to sprout by stimulating the cell division in lateral buds. The number of flowers is directly proportional to the number of lateral branches. Cytokinin suppresses the apical dominance of plants and ultimately enhances lateral shoots that leads to a greater number of flowers [43]. [44] observed maximum number flowers in plants sprayed with paclobutrazol as compared to control plants (*Jatropha curcas* significantly increased the total number of flowers in each inflorescence by application of BAP as compared to control [45]. These present results are in line with those of [46-47] who observed that early application of BAP to carnations and chrysanthemums increased the number of flowers and flowers, respectively. [48] reported that foliar application of benzyl amino purine on orchids results in increasing the inflorescence length, reduced day to flower and number of flowers per spike. [49] stated that cytokinin have critical role in the triggering of flowering process in plants. [50] reported that exogenous application of benzyl adenine increased the number of flowers in *Jatropha curcas* plants.

Hopkins and Huner (2009), reported that cytokinin are the derivatives of nitrogen-based adenine that play an important role in stimulating cell division in tissue culture. BAP is one of the aromatic cytokinin that stimulate cell division in lateral buds, which encourage flower buds to sprout.[51] observed an increase in the number of petals $flower^{-1}$ due to BAP in carnation, chrysanthemum and poinsettia respectively. BAP limits the role of auxin which ultimately increases the number of secondary branches which will obviously increase, the, number, of, flower therefore increases the yield of petals. The results are also supported by the findings of [52] that application of cytokinin is helpful in increasing the petals percentage of rose plants. [49] stated that cytokinin play a crucial role in the initiating of petals in flowering process. Application of BAP from 0 to 90mgl^{-1} progressively decreased fresh weight and dry weight of carnation flower. The present results are similar to those found by Gibson and Whipker (2003) who reported the negative effects of BAP on plant growth. They also noticed that more branches were produced as a result of high BAP application having a greater number of flowers but their quality was negatively affected as a result there were much smaller in size and had low fresh weights and dry weight.

CONCLUSIONS

It was concluded that spraying of BAP after 7 days of transplantation was found effective in reducing plant height and also improving the flower production of carnation. Benzyl Amino Purine applied at the rate of 90mg L^{-1} was effective in reducing plant height and resulted in compact plants with more lateral branches and flowers. Benzyl amino purine (BAP) could be sprayed within 14 days of transplantation to decrease plant height, delay the flowering and improve the flower production of carnation. Foliar application of 60 mg L^{-1} is recommended to control plant height and reduce logging resulting in compact plants with good vegetative and floral attributes of carnation.

REFERENCES

[1] Min. of Agric. Govt. of Ind. (2013). Indian Horticulture database. Nation. Hort. Board.

[2] Chen, J., McConnell, D. B., Henny, R. J., Norman, D. J. (2005). The foliage plant industry. Hort. Rev. 31(45), 110.

[3] Usman, M., Ashfaq, M. (2013). Economic analysis of Gladiolus (*Gladiolus Hortulanus*) Production In Punjab, Pak. J. of Agric. Res. 51(3), 317-326.

[4] Sandeep, S., Karetha, K.M., Virendra, S. (2016). Effect of pinching on growth of carnation varieties grown under protected condition. Asian J. of Hort. 11(1), 119-123.

[5] Dole, J. M., Wilkins, H. F. (2005). Floriculture principles and species, 2nd edition. Pearson prentice hall, Upper Saddle River, New Jersey. 347 pp.

[6] Kumar, V., Kumar, V., Umrao, V., Singh, M. (2012). Effect of GA3 and IAA on growth and flowering of carnation. Hort Flora Res. Spect. 89, 69. ISSN: 2250-2823.

[7] Sitch, P. (1975). Carnations for Garden and Greenhouse. John Gifford Ltd, London.
[8] Galbally, J., Galbally, E. (1997). Carnations and pinks for garden and greenhouse: their true history and complete cultivation. Timber Press, Inc., Portland, OR
[9] Hughes, S. (1993). Carnations & Pinks: The Complete Guide. Crowood Press, Marlborough, UK.
[10] Pathania, N. S., Sehgal, O.P., Gupta, Y. C. (2000). Pinching for flower regulation in Sim Carnation. J. of Orn. Hort. 3(2), 114-117.
[11] Khristov, K., Pavlov, P. (1977). Greenhouse carnation growth in relation to soil moisture and chlorcholine chloride treatment. Priroda-Bulgaria. 26(5), 88-89.
[12] Bylov, V.N., Smirnova, Z.I. (1984). Improving the quality of perpetual flowering carnation flowers during winter forcing. Bullet. Galvnogo Botan. Sada. 130, 55-58.
[13] Messinger, N. L., Holcomb, E. J. (1986). The effect of chlormequat chloride, ancymidol, BAS 106, and SD8339 on selected Dianthus cultivars. Hort. Sci. 21(6), 1397-1400.
[14] Song, C.Y., Lee, J.S. (1995). Effect of growth regulators on growth and flowering of potted camellia. J. Kor. Soc. Hort. Sci. 36, 98-106.
[15] Bañón, S., González, A., Cano, E. A., Franco, J. A., Fernández, J. A. (2002). Growth, development and color response of potted *Dianthus caryophyllus* cv. Mondriaan to paclobutrazol treatment. Scien. Hort. 94(3-4), 371-377.
[16] Cline, M. G. (1997). Concepts and terminology of apical dominance. American J. of Bot. 84(8), 1064-1069.
[17] Pobudkiewicz, A. (2008). The influence of growth retardants and cytokinins on flowering of ornamental plants. Acta Agrobotanica. 61(1).
[18] Sachs, R. M., Hield, H., DeBie, J. (1975). Dikegulac: a promising new foliar-applied growth regulator for woody species. HortSci.
[19] Taiz, L., Zeiger, E. (2010) Plant Physiology. Sunderland MA Sinauer Associates Inc.
[20] Ahmad, M., Khattak, M.R., Jadoon, S.A., Rab, A., Basit, A., Ullah, I., Khalid, M.A., Ullah, I., Shair, M. (2019). Influence of zinc sulphate on flowering and seed production of flax (*Linum usitatissimum* L.): A medicinal flowering plant. Int. J. BioSci. 14, 464-476.
[21] Basit, A., Ullah, I., Shah, S. T., Ullah, I., Alam, N., Gilani, S. A. Q. (2019). Effect of Media Amendments on Invivo Root and Shoot Organogenesis of Stevia (*Stevia Rebaudiana*). Int. J. Biosci. 14(4), 55-63.
[22] Sajid, M., Basit, A., Ullah, Z., Shah, S.T., Ullah, I., Mohamed, H.I., Ullah, I. (2020). Chitosan-based foliar application regulate the production and biochemical aspect of peach (*Prunus persica* L.) cv. Early Grand. Bull. Nat. Res. Centre. 44, 15.
[23] Jan, M. T., Shah, P., Hoolinton, P. A., Khan, M. J., Sohail, Q. (2009). Agriculture research: Design and analysis. Dept. Agronomy, KPK Agric. Uni. Peshawar, Pakistan.
[24] Mazrou, M. M. (1992). The growth and tropan alkaloids distribution of different organs of *Dataurainnoxia Mill*. Plants in relation to benzyladenine (BA) application. Minofiya J. Agric. Res. 17, 1971-1983.
[25] Eraki, M. A. (1994). The effect of gibberellic application and chelated iron nutrition on the growth and flowering of Queen Elizabeth rose plants. In The first Conf. of Orn. Hort. 2, 436-444.
[26] Abd El-Aziz, N. (2007). Stimulatory effect of NPK fertilizer and benzyladenine on growth and chemical constituents of Codiaeum variegatum L. American-Eurasian J. of Agric. & Env. Sci. 2(6), 711-719.
[27] Saadawy, F., Abdel-Moniem, A.M. (2015). Effect of some factors on growth, yield and Quality of flowers of carnation varieties grown under polyhouse. Karnataka. J. Agri. Sci. 20(4), 816-818.
[28] Carey, D.J., Whipker, B.E., McCall, I., Buhler,W. (2008). Benzyladenine Affects Growth of Petunia. A thesis submitted to the Graduate Faculty of North Carolina State University in partial fulfillment of the requirements for the degree of master of science. 131-135.
[29] Hafiz, A ., Steven,D.J., Johannes van, S. (2009) Promoting branching of a potential biofuel crop Jatropha curcas L. by foliar application of plant growth regulators. Plant Growth Regulation. 58(3), 287-295.
[30] Eid, R. A., Abou-Leila, B. H. (2006). Response of croton plants to gibberellic acid, benzyl adenine and ascorbic acid application. World J. Agric. Sci. 2(2), 174-179.
[31] Mutunga, C. M. (1998). Effect of benzyladenine, gibberellic acid, and Ethephon on growth and flower yield of chamomile (*matricaria chamomilla* L.) Plants (Doctoral dissertation).
[32] El-Quesni, F.E.M., Kandil, M.M., Mahgoub, M. H. (2007). Some studies on the effect of putrescine and paclobutrazol on the growth and chemical composition of Bougainvillea glabra L. at Nubaria. American-Eurasian J. Agric. Env. Sci. 2(5), 552-558.
[33] Reddy, T.V., Nagarajaiah,C., Vijaya, G., Raju,B., Seenappa. (1999). Effect of B99 Non anatomical changes in leaves of *China aster* (*Callistephus chinensis* L.) Ness. Mysore J. of Agri. Sciences. 33(1), 69-75.
[34] De Lojo, J., Di Benedetto, A. (2014). Biomass accumulation and leaf shape can be modulated by an exogenous spray of 6-benzylaminopurine in the ornamental foliage plant, Monstera deliciosa (Liebm.). The J. of Hort. Sci. and Biotech. 89(2), 136-140.

[35] Naveen, K.P., Reddy, Y.N., Chandrashekar, R. (2008). Effect of growth regulators on flowering and corm production in gladiolus. Indian J. of Horti. 65(1), 71-73.
[36] Sunitha, H.M., Ravi, H., Vyakaranahal, B. S., Bablad, H.B. (2007). Effect of pinching and growth regulators on plant growth, flowering and seed yield in African marigold (*Tagetes Erecta* L.). 10(2), 91-95.
[37] Sharaf-Eldien, M.N., El-Bably, S.Z., Magouz, M. R. (2017). Effect of Pinching and Spraying of Paclobutrazol on Vegetative Growth, Flowering and Chemical Composition of Zinnia elegans. Jacq. J. of Plant Prod. 8(5), 587-592.
[38] Ali, S., Basit, A., Khattak, A.M., Shah, S.T., Ullah, I., Khan, N.A., Ahmad, I., Rauf, K., Khan, S., Ullah, I., Ahmad, I. (2021). Managing the growth and flower production of zinnia (*Zinnia elegans*) through Benzyle Amino Purine (BAP) application and pinching. Pakistan Journal of Agricultural Research. 34(1), 29-40.
[39] Keever, G.J. (1994). Plant growth regulators: potential uses in the nursery industry. In Southern Reg. Comb. Proc. Nineteenth Annual Meeting, Athens, Georgia, USA. 6-9.
[40] Keever, G.J., Morrison, T.A. (2003). Multiple benzyladenine applications increase shoot formation in nandina. J. Env. Hort. 21(3),144-147.
[41] Matsumoto, T.K. (2006). Gibberellic acid and benzyladenine promote early flowering and vegetative growth of *Miltoniopsis orchid* hybrids. Hort. Sci. 41(1), 131-135.
[42] Richards, D. (1985). Effect of cytokinin application and environment on growth and flowering of *Boronia heterophylla* F. Meull. Scientia Hort. 27(3/4), 325-334.
[43] Ahmad, I., Ziaf, K., Qasim, M., Tariq, M. (2007). Comparative evaluation of different pinching approaches on vegetative and reproductive growth of carnation (*Dianthus caryophyllus*). Pak. J. Agri. Sci. 44(4), 563-570.
[44] Abd El-Aal, M. M. M., Mohamed, Y. F. Y. (2017). Effect of pinching and paclobutrazol on growth, flowering, anatomy and chemical compositions of potted geranium (Pelargonium zonal L.) plant. Int. J. of Plant & Soil Sci. 17(6), 1-22.
[45] Bang, Z.P., Xu, Z.F. (2011). Benzyladenine treatment significantly increases the seed yield of the biofuel plant *Jatropha curcas*. J. Plant Growth Regul. 30, 166-174.
[46] Katsumi, M. (1962). Physiological effects of kinetin effect on the thickening of etiolated pea stem sections. Physiologia Plantarum. 15(1), 115-121.
[47] Jeffcoat, B. (1977). Influence of the cytokinin, 6-benzylamino-9-(tetrahydropyran-2-yl)-9H-purine, on the growth and development of some ornamental crops. J. of Hort. Sci. 52(1), 143-153.
[48] Nambiar, N., Siang, T.C., Mahmood, M. (2012). Effect of 6-Benzylaminopurine on flowering of a 'Dendrobium'orchid. Australian J. of Crop Sci. 6(2), 225-231.
[49] Bonhomme, F., Kurz, B., Melzer, S., Bernier, G., Jacqmard, A. (2000). Cytokinin and gibberellin activate SaMADS A, a gene apparently involved in regulation of the floral transition in Sinapis alba. The Plant J. 24(1), 103-111.
[50] Bang, Z.P., Xu, Z.F. (2011). Benzyladenine treatment significantly increases the seed yield of the biofuel plant *Jatropha curcas*. J. Plant Growth Regul. 30, 166-174.
[51] Jeffcoat, B. (1977). Influence of the cytokinin, 6-benzylamino-9-(tetrahydropyran-2-yl)-9H-purine, on the growth and development of some ornamental crops. J. of Hort. Sci. 52(1), 143-153.
[52] Nguyen, H.V., Phan,H.A., Duong,T.N. (2006). The role of sucrose and different cytokinins in the in vitro floral morphogenesis of rose (hybrid tea) cv. “First Prize”. Plant Cell Tiss. Org. Cult. 87, 315-320.
[53] Gibson, J. L., Whipker, B. E. (2003). Efficacy of plant growth regulators on the growth of vigorous Osteospermum cultivars. HortTech. 13(1), 132-135.

Received: 17.08.2020
Accepted: 17.02.2021

CORRESPONDING AUTHOR

Abdul Basit
Department of Horticulture,
The University of Agriculture,
Peshawar – Pakistan

e-mail: abdulbasithort97@gmail.com

© by PSP Volume 30– No. 09/2021 pages 10482-10491 Fresenius Environmental Bulletin

FABRICATION OF SEMICONDUCTOR PHOTOCATALYST AND ITS HIGH PHOTOCATALYTIC PERFORMANCE UNDER VISIBLE LIGHT IRRADIATION

Guangyu Wu, Fang Ma, Ruofan Xiong, Zhouzhou Xu, Pingping Li, Jiangang Han, Weinan Xing*

College of Biology and the Environment, Co-Innovation Center for the Sustainable Forestry in Southern China, Nanjing Forestry University, Nanjing 210037, China

ABSTRACT

Recent years, photocatalytic technology is a compassionate of eco-friendly methods that has displayed significant consideration in the environmental fields. In this work, a series of high-performance Ag_2WO_4/WO_3/RGO photocatalysts (AWR) were synthesized through a facile hydrothermal approach. The products were characterized by using X-ray diffraction (XRD), scanning electron microscopy (SEM), Raman spectra, UV-vis diffuse reflectance spectroscopy (DRS), photoluminescence (PL) spectra, X-ray photoelectron spectroscopy (XPS) and Brunauer-Emmett-Teller (BET) nitrogen adsorption apparatus. The results indicated that the as-prepared Ag_2WO_4/WO_3 particles were distributed on the surface of RGO sheets and the introduction of RGO could narrow the band gap of Ag_2WO_4/WO_3. By using decontaminations of methyleneblue (MB) model reactions, the photocatalytic efficiencies of AWR photocatalysts were evaluated. The AWR photocatalysts exhibited superior photocatalytic activity under visible light irradiation. The photocatalytic activities of all AWR photocatalysts were higher than those of the WO_3, Ag_2WO_4 and Ag_2WO_4/WO_3 and about 98.15% MB was removed in 180 min. The possible mechanism of photocatalytic activity enhancement was proposed. The current work shows a design and synthesis of stable and high efficiency photocatalysts, applicable for the removal of the environmental organic pollutants.

KEYWORDS:
Photocatalyst, visible light irradiation, methyleneblue

INTRODUCTION

In the past decades, semiconductor-based photocatalysis has received growing attention as a promising and green technology for air and water purification [1]. Solar energy is believed as one of promising alternatives of fossil fuels due to its sustainability, abundance, easy accessibility, and environmentally friendly properties [2,3]. Among various methods of using solar energy, photocatalytic technology has been widely concerned in the treatment of environmental pollutants. As is well known, the photocatalysts can degrade organic pollutants into non-toxic molecules under light irradiation. The process of photodegradation involves photogenerated electrons and holes separating, migrating to the surface of photocatalyst materials, and then decomposing adsorbed organic molecules by a series of complicated redox reaction [4].

Recently, silver-based visible-light-driven photocatalytic semiconductor materials have received considerable attention owing to their excellent chemical stability, physicochemical property, and potential applications [5,6,]. However, silver-based photocatalyst has the limited quantum efficiency because of its wide band gap and the low separation rate of the photoexcited electron-hole in the using the visible light. Reduced graphene oxide (RGO) has attracted attention due to its attractive properties such as chemical and physical stability and an appropriated band edge potential to carry out redox reactions, in addition to non-toxicity and a simple and low-cost method of synthesis [7]. It has also received considerable attention recently for photoelectron-chemical and photocatalytic applications due to its extremely high specific surface area, high thermal, chemical stability, and fast electron transfer ability, which can effectively inhibit the recombination of the electron-hole pairs [8]. Thence, RGO can be as one of the most ideal supports for the separation and transfer of the photogenerated charge carriers [9]. In this work, Ag_2WO_4/WO_3/RGO photocatalyst (AWR) was synthesize by using a facile hydrothermal method. The degradation effect on the decomposition of methyleneblue (MB) under visible-light irradiation over the as-prepared photocatalyst were investigated. The present work provides a design and synthesis of stable and high efficiency photocatalysts, applicable for the removal of the environmental organic pollutants.

MATERIALS AND METHODS

Materials. Potassium permanganate ($KMnO_4$), lead acetate ($Pb(AC)_2 \cdot H_2O$), hydrogen peroxide (H_2O_2), sodium tungstate (Na_2WO_4), nitrate (HNO_3), sodium nitrate ($NaNO_3$), silver nitrate ($AgNO_3$), concentrated sulfuric acid (H_2SO_4), hydrochloric acid (HCl) and sodium bicarbonate ($NaHCO_3$) were purchased from Aladdin Chemical Reagent Co., Ltd. Methylene blue ($C_{16}H_{18}ClN_3S$, M_w=319.86 g mol^{-1}, MB) was purchased from Shanghai Chemical Reagent Co. Ltd.

Preparation of Ag_2WO_4/WO_3/RGO photocatalyst (AWR). Graphene oxide (GO) nanosheets were prepared according to the modification of Hummers' method from natural graphite [10]. GO (120 mg) was added to ultrapure water (120 mL), and then was sonicated for 3 h to obtain a GO aqueous suspension.

Na_2WO_4 (1.31 g) and $Pb(AC)_2 \cdot H_2O$ (1.51 g) were dissolved in 50 mL of ethylene glycol (EG) solution. The suspension was further stirred for 10 min and then was transferred into a Teflon-lined stainless-steel autoclave, which was heated at 160 °C for 12 h. After slow cooling to room temperature, the product was filtered and washed several times with alcohol/water mixture (V/V=1:1). The $PbWO_4$ precursor was obtained. The $PbWO_4$ precursor was firstly immersed in a certain amount of HNO_3 solution (4 mol L^{-1}) for 48 h. Then, the precipitate (H_2WO_4) was filtered, washed with distilled water, and dried in air. After then, the product was put into a quartz crucible with a cover and calcined at 500 °C for 2 h. The hollow sphere WO_3 was obtained.

A certain concentration of $AgNO_3$ solution was stirred under vigorous magnetic stirring. Subsequently, a certain amount of $NaHCO_3$ (3 mmol) was added dropwise into above aqueous. The suspension was continuously stirred for 1 h at room temperature to ensure complete reaction. The obtained products were collected by filtering and washed with distilled water and ethanol several times. Finally, sample was dried in a vacuum at 60 °C for 10 h and Ag_2CO_3 was obtained. A certain amount of GO aqueous suspension, WO_3 and Ag_2CO_3 were mixed and ground in an agate pestle for 30 min. Then, the mixture was calcined at 500 °C for 2 h and cooled to room temperature. The heterojunction structure Ag_2WO_4/WO_3/RGO photocatalyst was obtained. According to the dosage of GO in the samples, the three products with different mass content of RGO were prepared and expressed as AWR-1 (6.0%), AWR-2 (12.0%) and AWR-3 (18.0%), respectively.

The pure Ag_2WO_4 photocatalyst was prepared using mass content 1:1 of Ag_2CO_3 to WO_3. The Ag_2WO_4/WO_3 (the mass ratio of Ag_2CO_3 to WO_3=30%) product was also prepared by the same method without addition of GO.

Characterizations. X-ray diffraction (XRD) patterns of the AWR were obtained on the Shimadzu LabX-6000. X-ray Diffractometer (40 kV, 30 mA, λ= 0.154 nm) with a Cu K_α radiation source at a scanning rate of 4°/min within the range of 5-80°. Scanning electron microscopy (SEM) was performed on a field emission scanning electron microscope (HITACHI UHR FE-SEM SU8000, Hitachi, Tokyo, Japan) with the samples sputter-coated with 10 nm platinum. Raman spectra were recorded on a DXR Smart Raman spectrometer (Renishaw In Via) in the backscattering geometry with an excitation laser source (532 nm). UV-vis diffuse reflectance spectroscopy (DRS) was carried out on a Hitachi UV-3010 UV-vis spectrophotometer. $BaSO_4$ was as reference sample. The photoluminescence (PL) spectra were carried out on a Varian Cary Eclipse fluorescence spectrophotometer (Australia Varian co., LTD). The photocurrents were measured with an electrochemical analyzer (CHI660B, CHI Shanghai, Inc.). The X-ray photoelectron spectroscopy (XPS) of sample was performed on the ESCALAB250 XPS spectrometer with an Al Ka monochromatized source. The Brunauer-Emmett-Teller (BET) specific surface areas (S_{BET}) of the samples were carried out based on nitrogen adsorption and desorption isotherms (Micromeritics ASAP 2030 nitrogen adsorption apparatus, USA).

Photocatalytic degradation. The photocatalytic activity of AWR photocatalyst was evaluated by the degradation of dye (MB) aqueous solution under visible-light irradiation. 50 mg photocatalyst was added to 100 mL 1.0×10^{-5} $mol\cdot L^{-1}$ dye solution under magnetic stirring. The light source was a 250W metal halide lamp equipped with wavelength cut off filters for λ=420 nm. The photocatalytic activity of the prepared samples was performed at ambient temperature [11]. The suspensions were stirred in the dark for 30 min to reach adsorption-desorption equilibrium. After visible light irradiation, the powder was then separated by centrifugation, and the concentration of dye was determined by measuring the absorbance (465 nm) using an UV-2450 spectrophotometer. The removal efficiency of dye was calculated and photocatalytic process was modeled using pseudo first-order kinetics equation according to the following Equations (1) and (2):

$$D = \frac{C_o - C}{C_o} \times 100\% \quad (1)$$

$$\ln(C_0/C) = kt \quad (2)$$

where D is the removal efficiency; C_0 ($mg\cdot L^{-1}$) is the initial concentration of original dye solution; C

($mg \cdot L^{-1}$) is the dye concentration after light irradiation at time t (min). k is the apparent rate constant.

The reusability is an important parameter of the photocatalytic process. In order to examine the photocatalytic stability of the photocatalyst, AWR ternary plasmonic photocatalyst was filtered and washed with distilled water several times and dried in a vacuum oven at 60 °C for 12 h. The AWR photocatalyst was repeated the above cycles for five times under the same reaction conditions.

RESULTS AND DISCUSSION

Characterization. XRD patterns of pure WO_3 (a), Ag_2WO_4 (b), Ag_2WO_4/WO_3 (c), AWR-1 (d), AWR-2 (e) and AWR-3(f) photocatalysts are shown in Figure 1. From Figure 1a, the WO_3 is in good agreement with orthorhombic phase of WO_3 indexed to be the data in the JCPDS card (No. 20-1324) [12]. The diffraction peaks of Ag_2WO_4 are identical to the orthorhombic phase of Ag_2WO_4 in the JCPDS card (No. 34-0061) [13]. The pure Ag_2WO_4 (Figure 1b) displays sharp diffraction peaks at 2θ values of 16.71, 30.27, 31.63, 33.09, 45.45, 54.65 and 58.16° correspond to the planes of (011), (002), (231), (400), (402), (361) and (333), respectively. It is noteworthy that the peak intensity (2θ=31.63°) is stronger compared to other diffraction peaks. For Ag_2WO_4/WO_3 composite (Figure 1c), the diffraction peaks of Ag_2WO_4 and WO_3 are also clearly observed in comparison with bare Ag_2WO_4 and WO_3. Almost all the diffraction peaks of AWR photocatalysts (Figure 1d-f) can be assigned to Ag_2WO_4 and WO_3 obviously and no additional peaks are detected. The results indicate that the existence of RGO does not affect the growth of new crystal orientations of Ag_2WO_4/WO_3, and the AWR photocatalysts were successfully fabricated by the facile hydrothermal approach.

SEM images of RGO (a), pure WO_3 (b), Ag_2WO_4 (c), Ag_2WO_4/WO_3 (d), AWR-2 (e) and EDS spectrum of AWR-2 (f) are shown in Figure 2. As can be seen from the Figure 2a, RGO nanosheets are curled and corrugated, which is consistent with the previous report [7], while WO_3 hollow spheres sample shows the uniform particle size (Figure 2b). The pristine Ag_2WO_4 exhibits regular particle morphology with an average size of 150 nm in diameter and 20 μm in length (Figure 2c), and the surface is relatively smooth without any secondary nanostructures, indicating a high uniformity of the rod-like morphology. From Figure 2d, it could be found from that Ag_2WO_4 nanoparticles are successfully decorated on the WO_3 spheres surface and exhibits that the unique shape and the hollow sphere was not destroyed. As can be seen from Figure 2e, it seems that large amounts of Ag_2WO_4/WO_3 particles are distributed on the surface of RGO sheets, indicating a good loading between Ag_2WO_4/WO_3 and RGO. SEM images illustrate the transparent properties of the RGO substrate, where the RGO retains its two-dimensional thin sheet structure with wrinkled regions after loading of the Ag_2WO_4/WO_3. This structure might provide enough contact surface area between the RGO sheets and Ag_2WO_4/WO_3 particles and presumably facilitate charge-carrier transport. EDS spectrum (Figure 2f) shows that all the points in the selected area display the existence of Ag, W, O and C elements. The 2D-projected elemental mapping

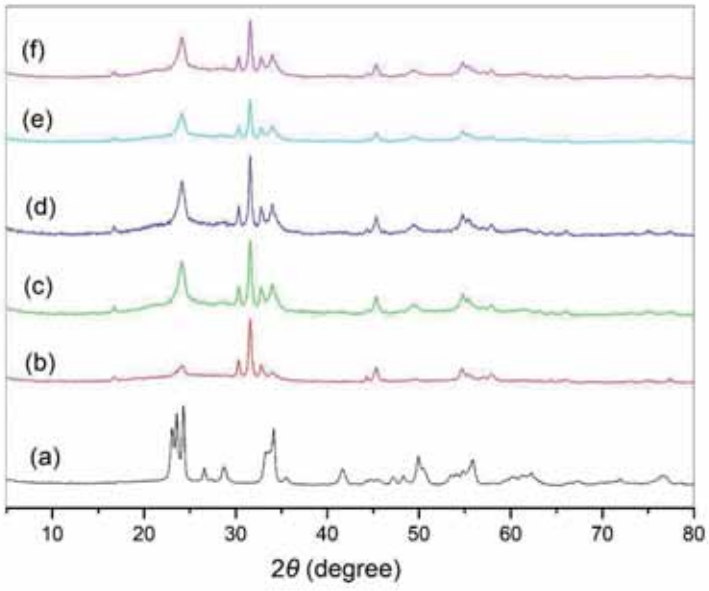


FIGURE 1
XRD patterns of pure WO_3 (a), Ag_2WO_4 (b), Ag_2WO_4/WO_3 (c), AWR-1 (d), AWR-2 (e) and AWR-1(f) photocatalysts

demonstrates the distribution of these elements throughout the AWR-2 sample.

Raman spectra of Raman spectra of RGO (a), pure WO_3 (b), Ag_2WO_4 (c), Ag_2WO_4/WO_3 (d) and AWR-2 (e) photocatalyst are shown in Figure 3. As shown in Figure 3 (a and e), two observably peaks at about 1330~1340 and 1580~1593 cm^{-1} are defined as D band and G bands of RGO in the spectra of pure RGO and photocatalyst, corresponding to the E_{2g} phonon of sp^{2-} bonded carbon atoms in a two-dimensional hexagonal lattice, as well as the defects and disorder carbon in the graphite layers, respectively [7]. As for bare WO_3, the bands centered at 808 cm^{-1} and 715 cm^{-1} are attributed to W-O stretching (Figure 3 b, d and e). The sharp peak located at about 881 cm^{-1} are observed in spectrum of pure Ag_2WO_4 and AWR-2 photocatalyst (Figure 3 c and e), which is attributed to the WO_4^{2-} symmetric stretching vibration. In addition, O-W-O stretching is revealed at the band centered at about 273cm^{-1}. For the AWR-2, all the Raman bands for RGO, Ag_2WO_4 and WO_3 can be observed confirming the presence of RGO, Ag_2WO_4 and WO_3 in the composites, which further suggests the decoration of Ag_2WO_4 and WO_3 on the RGO surface. The obtained Raman spectrum result of AWR-2 indicates that AWR-2 photocatalyst was successfully obtained.

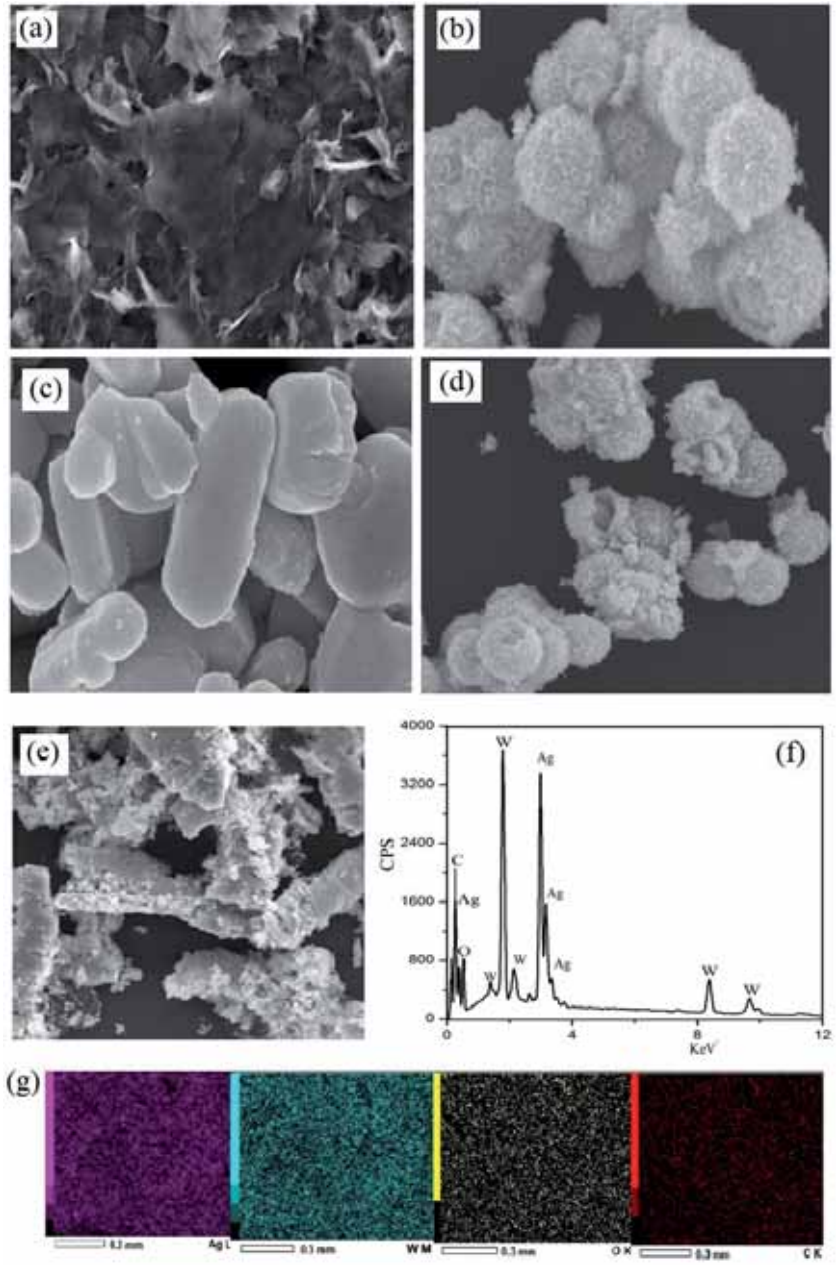


FIGURE 2
SEM images of RGO (a), pure WO_3 (b), Ag_2WO_4 (c), Ag_2WO_4/WO_3 (d), AWR-2 (e) and EDS spectrum of AWR-2 (f); The corresponding elemental mappings (g) of Ag, W, O and C elements

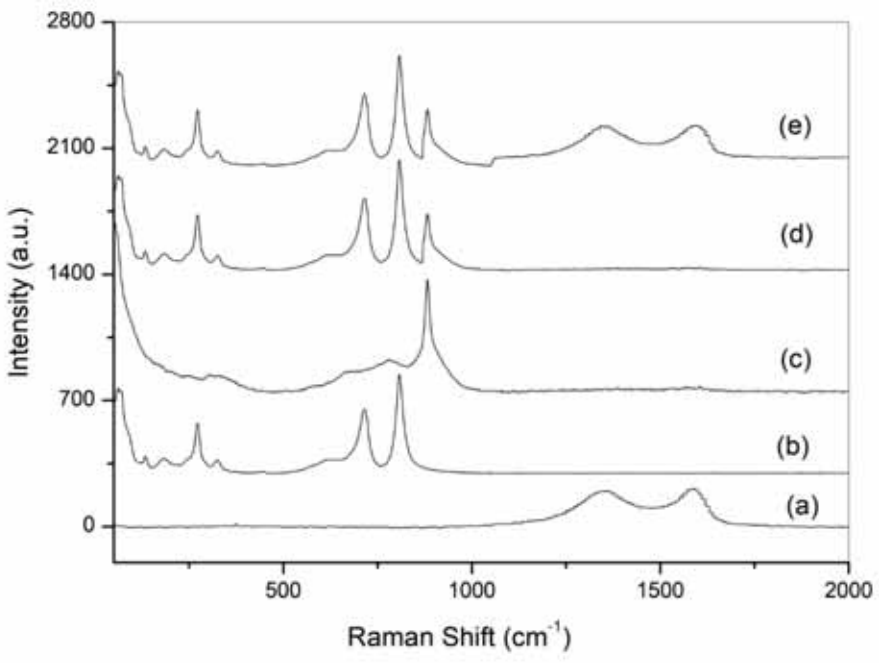


FIGURE 3
Raman spectra of RGO (a), pure WO_3 (b), Ag_2WO_4 (c), Ag_2WO_4/WO_3 (d) and AWR-2 (e)

More detailed information regarding the chemical and bonding environment of the composites are ascertained by XPS. Fig.4 shows the XPS spectra of AWR-2. From Figure 4a, the survey XPS spectrum shows the coexistence of elements, Ag, W, O and C; and no other hetero-elements were detected. As can be seen from Ag3d XPS, the peaks located at 373.66 and 368.23 eV are assigned to Ag $3d_{3/2}$ and Ag $3d_{5/2}$, respectively, further confirming the existence of Ag^+. From C 1s and O 1s XPS core level spectra, the peaks at the banding energy of 289.68 and 531.73 eV are attributed to oxygen and carbon, respectively. In the high-resolution spectrum of W 4f, the binding energy of W4f is 35.23eV, which agrees with W^{6+} ion of the sample. These results confirmed that the catalysts AWR-2 could be prepared by a facile hydrothermal method.

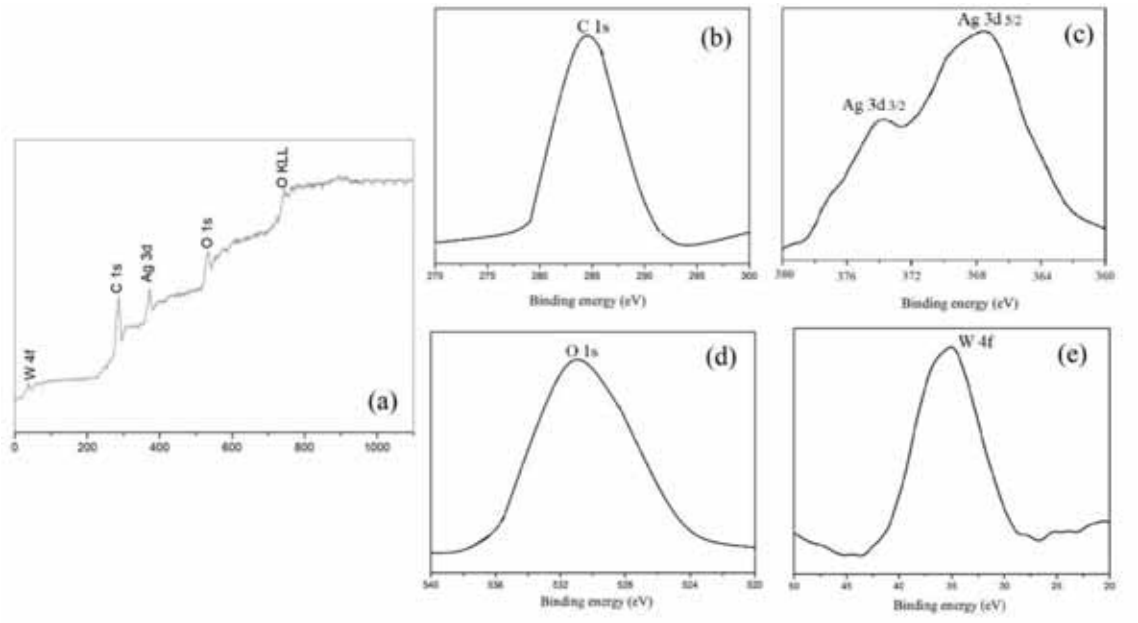


FIGURE 4
XPS spectra of AWR-2 (a), C 1s (b), Ag3d (c), O1s (d) and W4f (e)

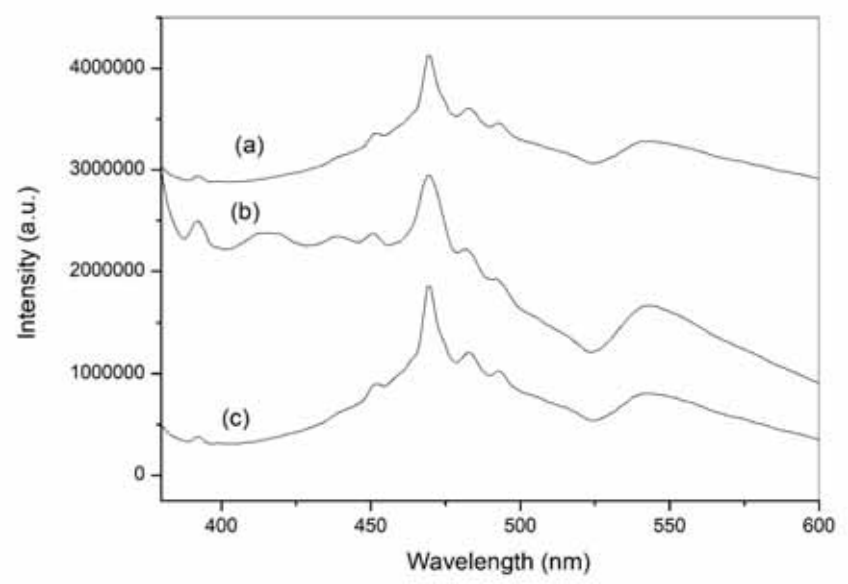


FIGURE 5
PL emission spectra of WO_3 (a), Ag_2WO_4 (b) and AWR-2 (c) photocatalysts

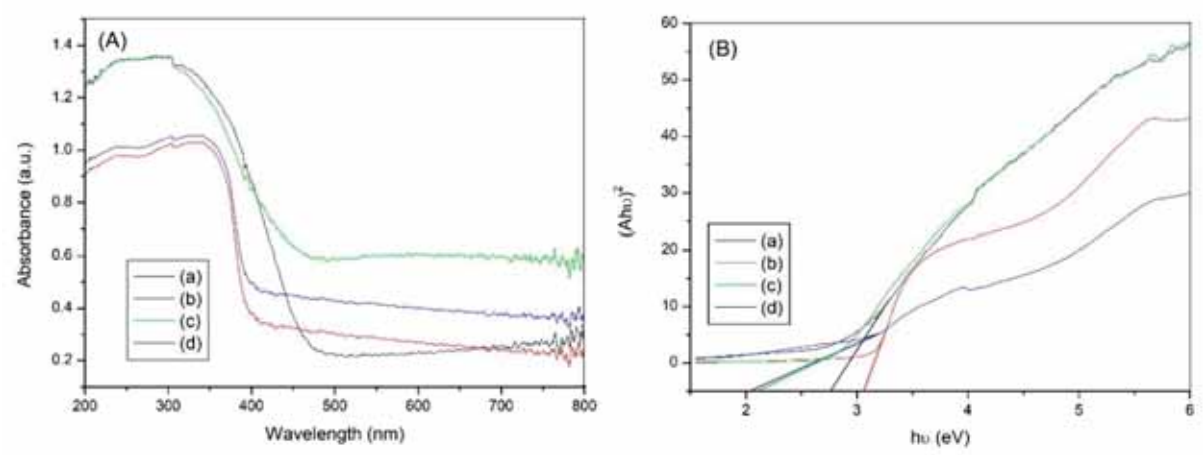


FIGURE 6
(A) UV-vis diffuse reflectance spectra of WO_3 (a), Ag_2WO_4 (b), Ag_2WO_4/WO_3 (c) and AWR-2 (d) photocatalysts; (B) Plots of $(h\nu)^2$ vs. (B) photonenergy ($h\nu$) of WO_3 (a), Ag_2WO_4 (b), Ag_2WO_4/WO_3 (c) and AWR-2 (d)

PL spectra are useful to disclose the migration, transfer, and recombination processes of the photogenerated electron-hole pairs in semiconductors. In general, the lower PL intensity indicates a decrease in the recombination rate of photogenerated charge carriers. The better separation of photogenerated electrons and holes in the AWR photocatalyst is confirmed by PL emission spectra of single Ag_2WO_4, WO_3 and AWR-2 photocatalyst; and PL emission spectra of bare WO_3 (a), Ag_2WO_4 (b) and AWR-2 (c) photocatalysts recorded with an excitation wavelength at 363 nm are shown in Figure 5. As can been from Figure 5, the strong emission peaks of the bare WO_3 and Ag_2WO_4 are located at about 469 and 470 nm, which could be attributed to a band-to-band emission. Compared with single WO_3 and Ag_2WO_4, the emission peak intensity of the AWR-2 photocatalysts decrease moderately, indicating that the recombination of photogenerated charge carriers is suppressed. The result of PL verifies that the AWR photocatalysts could effectively separate photogenerated electron-hole pairs.

The optical absorption properties of the as-prepared samples are examined by UV-vis diffuse reflectance spectra since the optical absorption behavior of a photocatalyst was essential for its photocatalytic activity, and the results are shown in Figure 6. As shown in Figure 6A, the AWR photocatalysts exhibit broad absorption in the whole visible region and its absorption intensity is strengthened. This is mainly because introduction of RGO leads to an obvious enhancement of background absorption in the range of 500-800 nm. In addition, the optical band

gap and absorption coefficient of semiconductor can be calculated by the following equation [11]: $(\alpha hv)^n=A(hv- E_g)$, where α, h, v, E_g and A are the absorption coefficient, Planck's constant, light frequency, band gap and a constant, respectively. n is a constant associated with different kinds of electronic transitions (n=0.5 for a direct allowed and n=2 for an indirect allowed). From the Figure 6B, the band gaps of WO_3, Ag_2WO_4, Ag_2WO_4/WO_3 and AWR-2 samples are about 2.75, 3.07, 2.06 and 2.04 eV, respectively. This observation indicates that the introduction of RGO narrows the band gap of Ag_2WO_4/WO_3. Therefore, the formation rate of electron-hole pairs on the photocatalyst surface/interfaces also increases substantially, resulting in the better catalytic performance.

To further obtain the pore size distributions and specific surface area of the prepared samples, N_2 adsorption-desorption measurements were performed. N_2 adsorption-desorption isotherms and pore-size distribution curves of WO_3 (a), Ag_2WO_4 (b), Ag_2WO_4/WO_3 (c) and AWR-2 (d) are shown in Figure 7. From Figure 7A, the measured BET specific surface areas of WO_3, Ag_2WO_4, Ag_2WO_4/WO_3 and AWR-2 are 13.23, 1.36, 15.21 and 18.99 $m^2 g^{-1}$, respectively. Meanwhile, the corresponding pore volume distributions of both samples were calculated by the BJH method from the adsorption branch of the isotherms. As shown in Figure 7B, average pore sizes of WO_3, Ag_2WO_4, Ag_2WO_4/WO_3 and AWR-2 are 22.3, 17.22, 20.23 and 15.28 nm, respectively. Therefore, the increase in surface area of composite material can provide more possibility for the efficient adsorption and mass transfer for the degradable dye molecules and hydroxyl radicals the photochemical reaction. This phenomenon favors for the enhancement in photocatalytic activity.

Photocatalytic activity. The photocatalytic oxidation activity of as-synthesized photocatalysts has been evaluated using MB as the model pollutant; and the results are shown in Figure 8a. For comparison, the blank test was also conducted under the

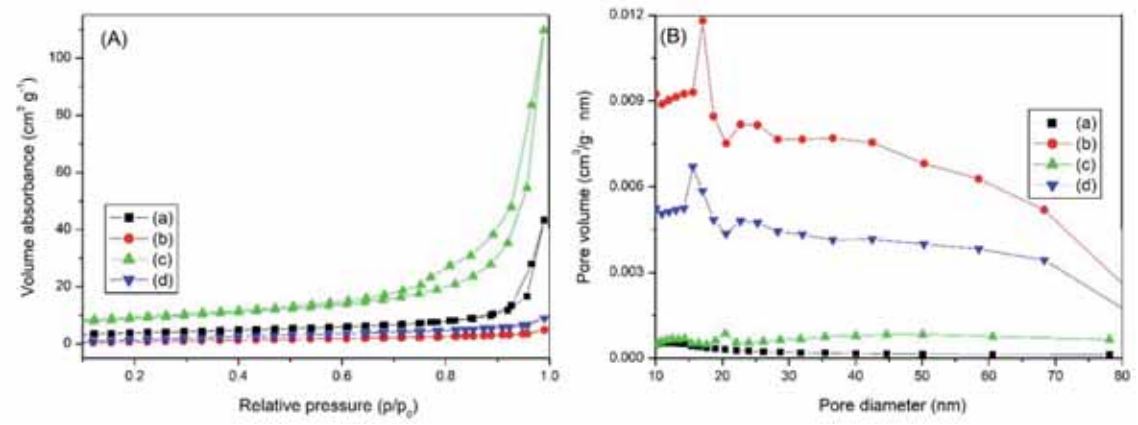


FIGURE 7
(A) N_2 adsorption-desorption isotherms and (B) pore-size distribution curves of WO_3 (a), Ag_2WO_4 (b), Ag_2WO_4/WO_3 (c) and AWR-2 (d) photocatalysts

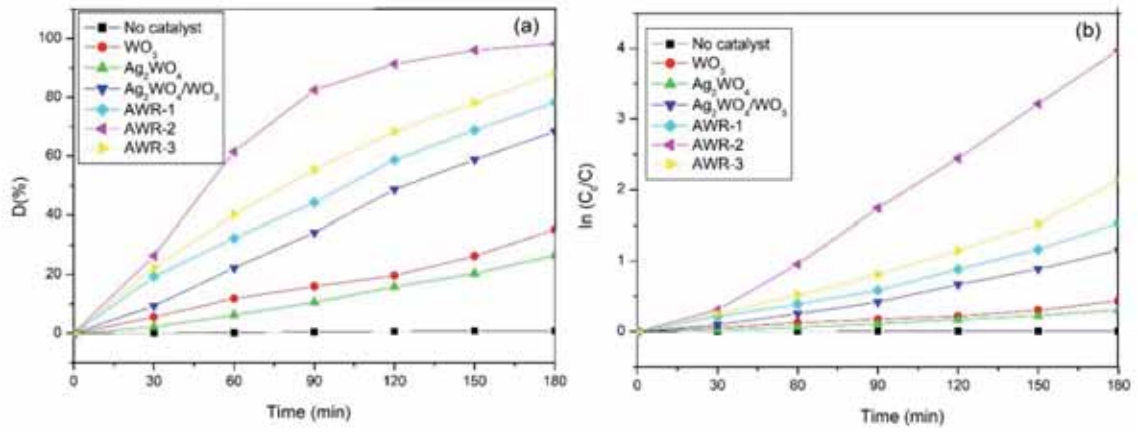


FIGURE 8
Comparison of the photocatalytic activities of samples for degradation of the MB solution

same reaction conditions. It could be seen that negligible photodegradation of MB observed when no catalyst is added. About 35%, 26% and 68% of the MB were respectively removed by WO_3, Ag_2WO_4 and Ag_2WO_4/WO_3 after 180 min of visible light irradiation. Absolutely, the photocatalytic activities of all AWR photocatalysts are higher than those of the WO_3, Ag_2WO_4 and Ag_2WO_4/WO_3 and about 98.15% MB was removed by AWR-2 in 180 min. It may be because of the formation of recombination centers of photoinduced carriers in the bulk of the catalyst [13]. The linear relationship between $\ln C_0/C$ and t of the as-prepared photocatalysts is shown in Figure 8b, which confirming that the photodegradation reaction of MB dye is fitted pseudo-first-order. According to Eq.(2) and Figure 8b, the pseudo-first-order rate constant of photodegradation are 0.0000562 min^{-1}, 0.00225 min^{-1}, 0.00172 min^{-1}, 0.00649 min^{-1}, 0.00832 min^{-1}, 0.0229 min^{-1} and 0.0115min^{-1} for no catalyst, WO_3, Ag_2WO_4, Ag_2WO_4/WO_3, AWR-1, AWR-2 and AWR-3, respectively. Clearly, the AWR-2 reveals the highest value with k. The stability of a photocatalyst is important for its assessment and application. Recycling experiments were performed to check the stability of photocatalyst. Comparison of photocatalytic performance within 5 cycles for AWR-2 photocatalyst under the same experimental condition is shown in Figure 9. As can be seen from Figure 10, the degradation of photocatalyst has no observable change even after 5 recycles. The results indicated that the prepared photocatalyst has an excellent reuse performance.

The possible mechanism. According to the above results, a proposed mechanism is shown in Figure 10. Under visible light irradiation, plasmon-excited WO_3 and Ag_2WO_4 can produce photogenerated electrons and holes. The photogenerated holes (h^+) and electrons (e^-) transfer to the surface of Ag_2WO_4/WO_3 and then drive photocatalytic oxidation reactions. O_2^{-}• radicals are produced by the reduction of O_2 molecules adsorbed on the catalyst surface by the photogenerated electrons. In addition, the reaction of H_2O and active holes generate ·OH, and both O_2^{-}• and ·OH radicals can degrade organic dye (MB) effectively. Due to the introduction of RGO and the close interfacial contact, the photogenerated electrons on the conduction band (CB) of Ag_2WO_4/WO_3 could be effectively transferred to the RGO sheets. These synergistic interaction between the SPR of WO_3 and the field around Ag_2WO_4 can force the photogenerated electrons in Ag_2WO_4/WO_3 particles under visible-light irradiation to produce photogenerated electron-hole pair separation and photogenerated charge transfer. Therefore, the formation rate of electron-hole pairs on the sample increases substantially, exhibiting excellent photocatalytic performance. Moreover, high surface area RGO sheets offer more active adsorption sites and photocatalytic reaction sites, which also favor improved photocatalytic activity. According to these results, one important conclusion can be drawn, that is, when discussing the effect of introduction graphene or RGO on the photocatalytic activities of semiconductor particles, the results should be analyzed based on specific reactions.

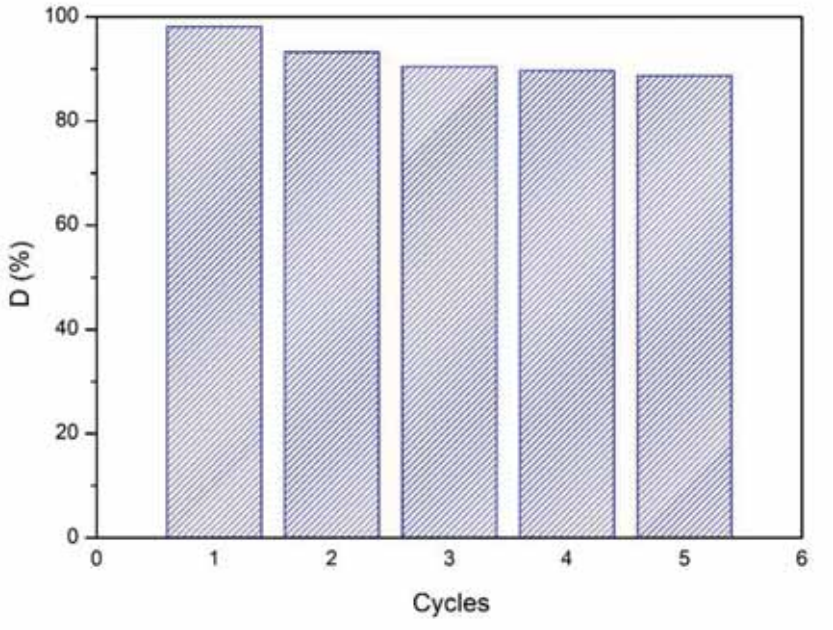


FIGURE 9
Cycling test of AWR-2 for the degradation of MB under visible light irradiation

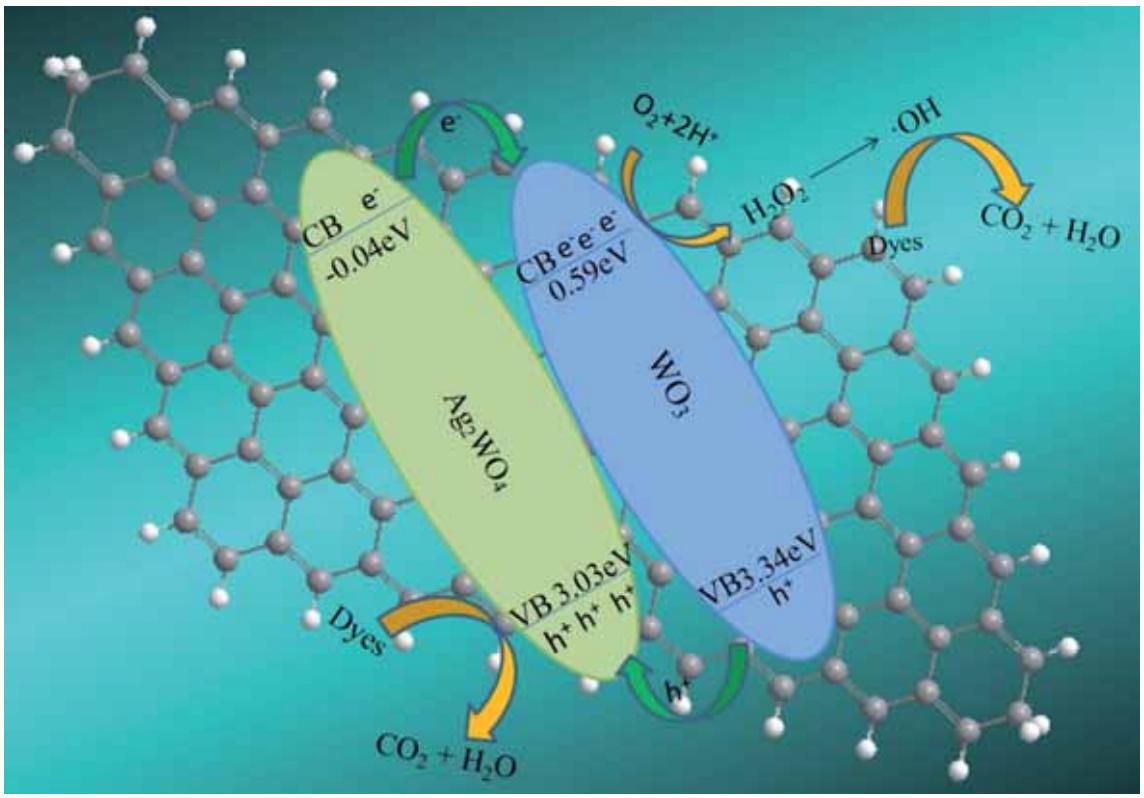


FIGURE 10
Proposed mechanism of enhanced photocatalytic activity for the AWR photocatalyst

CONCLUSION

In summary, Ag_2WO_4/WO_3/RGO photocatalysts (AWR) were synthesized with a facile hydrothermal method. The AWR photocatalyst was characterized by using XRD, SEM, Raman, Brunauer-Emmett-Teller, photoluminescence, XPS and UV-Vis DRS; and shows excellent performance in the degradation of MB under visible light irradiation. It is found that suitable content of Ag_2WO_4/WO_3 in AWR photocatalyst is crucial optimize the photocatalytic performance. Among the series of AWR photocatalysts, AWR-2 shows the highest photocatalytic activity, and degradation conversion of MB is high up to 98.15% under visible light irradiation. The enhanced photocatalytic activity of the AWR photocatalyst can be attributed to the synergy effect between Ag_2WO_4/WO_3 and RGO, which facilitates interfacial charge transfer and inhibits electron-hole recombination. This AWR photocatalyst material may have potential applications in pollutant removal as highly efficient photocatalyst.

ACKNOWLEDGEMENT

This work was financially supported by Jiangsu Planned Projects for Postdoctoral Research Funds (2020Z098), National Natural Science Foundation of China (21901119, 41471191), China Postdoctoral Science Foundation Funded Project (2019M661850), Projects of National Key Research and Development of China (2017YFC0505803), Qing Lan Project of Jiangsu Province (Qinglan 2016-15), Priority Academic Program Development of Jiangsu Higher Education Institutions (PAPD), Students Practice Innovation and Training Program of Nanjing Forestry University (2019NFUSPITP0761, 2020NFUSPITP0804, 2020NFUSPITP0807, 2020NFUSPITP0818, 2020NFUSPITP0827) and the Analysis and Test Center of Nanjing Forestry University.

REFERENCES

[1] Wu, G., Xing, W. (2019) Facile preparation of semiconductor silver phosphate loaded on multi-walled carbon nanotube surface and its enhanced catalytic performance, Journal of Inorganic and Organometallic Polymers and Materials. 29, 617-627.

[2] Xing, W., Yin, S., Tu, W., Liu, G., Wu, S., Wang, H., Kraft, M., Wu, G., Xu, R. (2020) Rational synthesis of amorphous iron-nickel phosphonates for highly efficient photocatalytic water oxidation with almost 100 % yield. Angewandte Chemie International Edition. 59, 1171-1175.

[3] Meng, Q., Lv, C., Sun, J., Hong, W., Xing, W., Qiang, L., Chen, G., Jin, X. (2019) High-efficiency Fe-Mediated Bi_2MoO_6 nitrogen-fixing photocatalyst: Reduced surface work function and ameliorated surface reaction. Applied Catalysis B: Environmental. 256, 1-41. Article ID: 117781.
[4] Lv, J., Dai, K., Zhang, J., Lu, L., Liang, C., Geng, L., Wang, Z., Yuan, G., Zhu, G. (2017) In situ controllable synthesis of novel surface plasmon resonance-enhanced $Ag_2WO_4/Ag/Bi_2MoO_6$ composite for enhanced and stable visible light photocatalyst. Applied Surface Science. 391, 507-515.
[5] Vignesh, K., Kang, M. (2015) Facile synthesis, characterization and recyclable photocatalytic activity of Ag_2WO_4@g-C_3N_4. Materials Science & Engineering B. 199(5), 30-36.
[6] Ren, H.T., Jia, S.Y., Wu, S.H., Zhang, T.H., Han, X. (2015) Phase transformation synthesis of novel Ag_2O/Ag_2CO_3/g-C_3N_4 composite with enhanced photocatalytic activity. Materials Letters. 142, 15-18.
[7] Wu, G., Xing, W. (2019) Facile and fabrication of semiconductor silver tungstate loaded on the graphene oxide surface and its effective enhanced catalytic performance. Fresen. Environ. Bull. 28(3), 2012-2021.
[8] Guo, S., Dong, S. (2011) Graphene nanosheet: synthesis, molecular engineering, thin film, hybrids, and energy and analytical applications. Chemical Society Reviews. 40(5), 2644-2672.
[9] Low, J., Cao, S., Yu, J., Wageh, S. (2014) Two-dimensional layered composite photocatalysts, Chemical Communications. 50(74), 10768-10777.
[10] Bo, C., Jing, L., Qian, X. (2014) Reduced graphene oxide grafted Ag_3PO_4 composites with efficient photocatalytic activity under visible-light irradiation, Industrial & Engineering Chemistry Research. 53(21), 8744–8752.
[11] Wu, G., Xing, W. (2019) Fabrication of ternary visible-light-driven semiconductor photocatalyst and its effective photocatalytic performance. Materials Technology. 34, 292–300.
[12] Rong, X., Qiu, F., Zhang, C., Fu, L., Wang, Y., Yang, D. (2015) Adsorption–photodegradation synergetic removal of methylene blue from aqueous solution by NiO/graphene oxide nanocomposite. Powder Technology. 275, 322-328.
[13] Qiu, F., Zhu, X., Guo, Q., Dai, Y., Xu, J., Zhang, T. (2017) Fabrication of a novel hierarchical flower-like hollow structure Ag_2WO_4/WO_3 photocatalyst and its enhanced visible-light photocatalytic activity, Powder Technology. 317, 287-292.

Received: **29.08.2020**
Accepted: **06.11.2020**

CORRESPONDING AUTHOR

Weinan Xing
College of Biology and the Environment,
Co-Innovation Center for the Sustainable Forestry in Southern China,
Nanjing Forestry University,
Nanjing 210037 – China

e-mail: xingwn@njfu.edu.cn

© by PSP Volume 30– No. 09/2021 pages 10492-10504 Fresenius Environmental Bulletin

EXPERIMENTAL AND NUMERICAL ANALYSIS OF THE THERMAL PERFORMANCE OF NANOFLUIDS USED IN AUTOMOBILE RADIATORS

Erdem Isik*, Volkan Tugan

University of Munzur, Engineering Faculty, Mechanical Engineering Department, Tunceli, Turkey

ABSTRACT

Water and ethylene glycol have been used as heat transfer fluids in automobile cooling systems for many years. However, these fluids have a low thermal conductivity coefficient. Therefore, a new heat transfer fluid, called nanofluid, has been studied recently. The aim of this study is to investigate the thermal performance of nanofluids used in automobile radiators experimentally and numerically. An automobile cooling system experimental setup was built for experimental work. ANSYS Fluent program, a Computational Fluid Dynamics software, was used in numerical analysis. In the analysis, distilled water and ethylene glycol based fluids containing Al_2O_3, CuO and MgO nanoparticles were used as nanofluids. The analyses were carried out at three different volumetric flow rates (0.232 L / s, 0.260 L / s, 0.282 L / s) and three different air velocities (1.6 m / s, 2.3 m / s, 2.9 m / s). According to the results obtained, it was observed that the convective heat transfer coefficient of nanofluids was higher than that of the base fluid under the same conditions. In addition, it was observed that the convective heat transfer coefficient of coolant fluids increases with increasing volumetric flow rate and air velocity. According to the results obtained from experimental and numerical analysis, it was observed that the convective heat transfer coefficient of nanofluids containing Al_2O_3, CuO and MgO was 21-74%, 20-47% and 1-13% higher than that of the base fluid, respectively.

KEYWORDS:
Nanofluid, Automobile radiator, Heat transfer

INTRODUCTION

Recent technological developments in the automotive sector and defense industries require the design of new cooling systems in order to use energy more efficiently. Especially in the automotive sector, intensive efforts are being made to minimize energy consumption and complex parts that are difficult to produce. While energy savings are achieved through these studies, it is also necessary to provide the desired performance.

Automobile radiator (AR) is considered to be one of the basic elements of automobile cooling systems. Heat is removed from the engine to the outside environment by means of the coolant used in ARs. The coolant circulating in the engine cooling system heats up as the engine runs. In automobile cooling systems, ethylene glycol (EG) and distilled water (DW) are generally utilized as the coolant [1]. The function of the coolant in this system is to keep the engine running at a safe temperature by moving between the AR and the engine.

Conventional coolants such as oil, DW and EG are not capable of performing the desired heat transfer because of their low thermal performance [2,3]. For this reason, various studies are being performed on a new fluid called nanofluid (NF) so as to increase the heat transfer in ARs.

The term 'nanofluid' or nanoparticle-containing fluid, was first used by Choi and Eastman [4]. NFs are new-generation heat transfer fluids obtained by adding nanoparticles in different proportions to basic heat transfer fluids such as oil, DW and EG [5-8]. NFs have a higher thermal conduction coefficient in comparison with conventional coolants [9-17, 40]. Due to the extensivity of the processes that require heating and cooling, the application area is quite wide. With successful applications being made in this regard, smaller and lighter systems that provide the same levels of cooling can be designed and the thermal performance of existing systems can be increased.

Intensive efforts are being made to use NFs in engineering applications and many studies in the literature have addressed the NFs that are used in ARs. Bhimani et al. [18] installed an experimental AR system to compare the thermal performance of DW and NFs. They examined the thermal performance of five different concentrations of TiO_2 in the range of 0.1-1.0% for volumetric flow rates in the range of 90-120 L/min. It is concluded that nanofluids can increase heat transfer efficiency by at least 45% compared to the base fluid. Hussein et al. [9] examined the convective heat transfer coefficient (CHTC) and friction factor of DW-based NF containing SiO_2 nanoparticles in an AR experimentally and numerically. Experiments were carried out by changing the

concentration in the range of 1.0-2.5% with Reynolds number (Re) of 500-1750 and volumetric flow rates of 2-8 L/min. They it is found that the friction factor decreased as the volumetric flow rate and volumetric concentration increased. Additionally, the Nusselt number (Nu) increased with the increase of the volumetric concentration and the volumetric flow rate of the fluids. It was observed that the SiO_2/DW NF could increase the heat transfer rate by about 50% compared to DW. Gaidhane and Bhosale [19] used an AR setup to compare hybrid NFs and conventional coolant fluids in terms of thermal performance. Hybrid NFs were produced using Fe_2O_3 and CuO nanoparticles and in three different concentrations of 0.5%, 1.0%, and 1.5%. According to the results obtained from the analysis, hybrid NFs used in ARs increased the total heat transfer coefficient by 21% and the CHTC by 41%. In an experimental study, Peyghambarzadeh et al. [20] analyzed the thermal performance of Al_2O_3/DW NF in an AR. Five different volumetric concentrations in the range of 0.1-1.0% were used in the experiments, which were carried out by changing the volumetric flow rate in the range of 2-5 L/min. It was concluded that even low concentrations of NFs could increase the heat transfer efficiency by up to 45% or more compared to DW. In another study, Peyghambarzadeh et al. [21] experimentally investigated thermal performance of the NFs used in ARs. In the study, DW-based NFs containing CuO and Fe_2O_3 nanoparticles at three different concentrations of 0.15%, 0.4%, and 0.65% were used. The inlet temperature of the fluids entering the radiator was set to 50 °C, 65 °C, and 80 °C, while the Re ranged from 50 to 1000 for NFs and 500 to 700 for air. According to the results obtained, the NFs could increase the total heat transfer coefficient by up to 9% compared to DW. It was further concluded that the total heat transfer coefficient was also increased by increasing the concentration and inlet velocity of the NF. Tijani and Bin Sudirman [1] used DW and EG-based NFs that contain Al_2O_3 and CuO at concentrations of 0.05%, 0.15%, and 0.30% to quantify the heat transfer properties of NFs used in ARs. The thermal performance of CuO-containing NFs is higher than that of Al_2O_3-containing NFs based on the results. Kılınç et al. [22] designed an experimental AR setup to examine the heat transfer performance of NFs. They used DW as the base fluid and graphene oxide (GO) and graphene nanoribbon (GNR) as nanoparticles for the experiments. Analysis was carried out for two different concentrations (0.01%, 0.02%), three different coolant inlet temperatures (36 °C, 40 °C, and 44 °C), and four different volumetric flow rates (0.6 m^3/h, 0.7 m^3/h, 0.8 m^3/h, and 0.9 m^3/h). According to the results obtained, as NF concentration increased, the effectiveness of the AR also increased. The highest increases that are observed in heat transfer coefficient were 6.9% and 32.0% for Go-containing NFs with concentrations of 0.01% and 0.02% compared to DW and 18.9% and 24.8% for NFs with GNR, respectively. Additionally, it was concluded that adding nanoparticles to the base fluid increased the total heat transfer coefficient and the Nu. Sokhal et al. [23] experimentally analyzed the effects of CuO/DW NF use in automobile cooling systems on heat transfer and pressure drop. The effects of fluid inlet velocity, inlet temperature, and concentration parameters on heat transfer were investigated in the experiments for NFs with concentrations in the range of 0.1-0.5%. It was observed that the concentration, temperature, and Re of the NFs increased in parallel with the Nu. It was further concluded that the pressure drop was directly proportional to the concentration and Re, and inversely proportional to the temperature of the NF. The highest increase in heat transfer was achieved as 20% for NF with a concentration of 0.5%. In another study, Canbolat and Türkan [24] carried out flow analysis to investigate the effect of pipe number, pipe diameter, airfoil number, and air velocity parameters in an AR. According to the results obtained, the thermal efficiency of the AR increased together with the number of pipes, pipe diameter, the number of airfoils, and airspeed. It was also concluded that using copper instead of aluminum as the airfoil material improved thermal performance. Elsebay et al. [25], using Al_2O_3/DW and CuO/DW NFs in an AR, conducted a numerical analysis to determine whether the radiator could be resized. The Re was changed in the range of 250-1750 for four different volumetric concentrations (1%, 3%, 5%, and 7%) and analyses were carried out. According to the results obtained, the increase in the heat transfer coefficient for Al_2O_3/DW NF compared to DW was 45% and for CuO/DW it was 38%. Based on the improvement in thermal performance, it was concluded that the size of the ARs could be reduced. Hatami et al. [26] made numerical studies to analyze the effects of DW and EG-based NFs that contain Fe_3O_4, TiO_2, Al_2O_3, and CuO nanoparticles on the cooling performance of motor radiators. Analyses were performed for four different Re (500, 1000, 1500, and 2000). The EG-TiO_2 NF showed the best cooling performance compared to other NF models. It was concluded that the rate of heat transfer and the Nu increased in parallel with the Re. Jadar et al. [27], compared the CHTC of DW with functional multi-walled carbon nanotube (f-MWCNT)-containing NF. During the experiments, the velocity of the air passing over the AR was kept constant, but the flow rate of the fluid was set to either 0.5 L/min or 2.5 L/min. According to the data obtained, the outlet temperature of the fluid and the Nu also increased in direct proportion to the volumetric flow rate. Moreover, the heat transfer performance of the f-MWCNT NF was observed to be 45% superior to that of DW. Sharma [28] experimentally investigated the effect of Al/DW NF on the rheological properties of an AR. He also studied the effect of flow rate, air velocity, volumetric concentration and inlet temperature parameters on heat

transfer. As a direct consequence of experiments performed at 318.15 K inlet temperature, the Nu was increased by 3.37% and 5.088%, respectively, according to base fluid for NF concentrations of 0.2% and 0.3%. Additionally, the friction coefficient of NFs with concentrations of 0.2% and 0.3% was observed to increase by 14.04% and 20.92%, respectively, against the base fluid. Sandhya et al. [29] studied the cooling performance in ARs of TiO_2-containing NFs with volumetric concentrations of 0.1%, 0.3%, and 0.5% based on 60% DW and 40% EG experimentally. As a result of experiments carried out by changing the Re in the range of 4000-15000, it was concluded that heat transfer performance also increased in direct proportion to NF volumetric flow rate. In addition, the inlet temperature of NFs into the radiator did not significantly affect the thermal performance. It was concluded that low concentrations of NFs can improve the heat transfer rate by 37% in comparison with the base fluid.

In this study, the thermal performance of three different NFs with 1% volumetric concentration, which is Al_2O_3/DW+EG, CuO/DW+EG ve MgO/DW+EG, was compared. CHTC and Nu of NFs were evaluated both experimentally and numerically. An automobile cooling system experimental setup was built for experimental work. ANSYS Fluent program, a Computational Fluid Dynamics software, was used in numerical analysis. In the analyzes, the effect of volumetric flow rate (0.232 L/s, 0.260 L/s, 0.282 L/s) and air velocity (1.6 m/s, 2.3 m/s, 2.9 m/s) on the CHTC of the coolants were investigated. The results obtained from the numerical analysis were compared with the experimental results.

In the next section, the materials used and the methods followed are explained. The results obtained from the analyses are then given in the form of graphs, and finally, the results obtained from the analyses are interpreted and comparisons are made.

MATERIALS AND METHODS

Experimental Study. In the experimental part of the study, an experimental AR setup was installed to study the thermal performance of NFs and the base fluid. The frame of the experimental setup consists of an AR, ventilator, circulation pump, flow meter, fluid tank, data collector, and air duct [30-32]. The laboratory image of the setup and the drawing obtained by the 3Ds Max program are given in Figure 1 and Figure 2. The double-row and circular tubular AR used in experimental analysis is shown in Figure 3.



FIGURE 1
Experimental setup

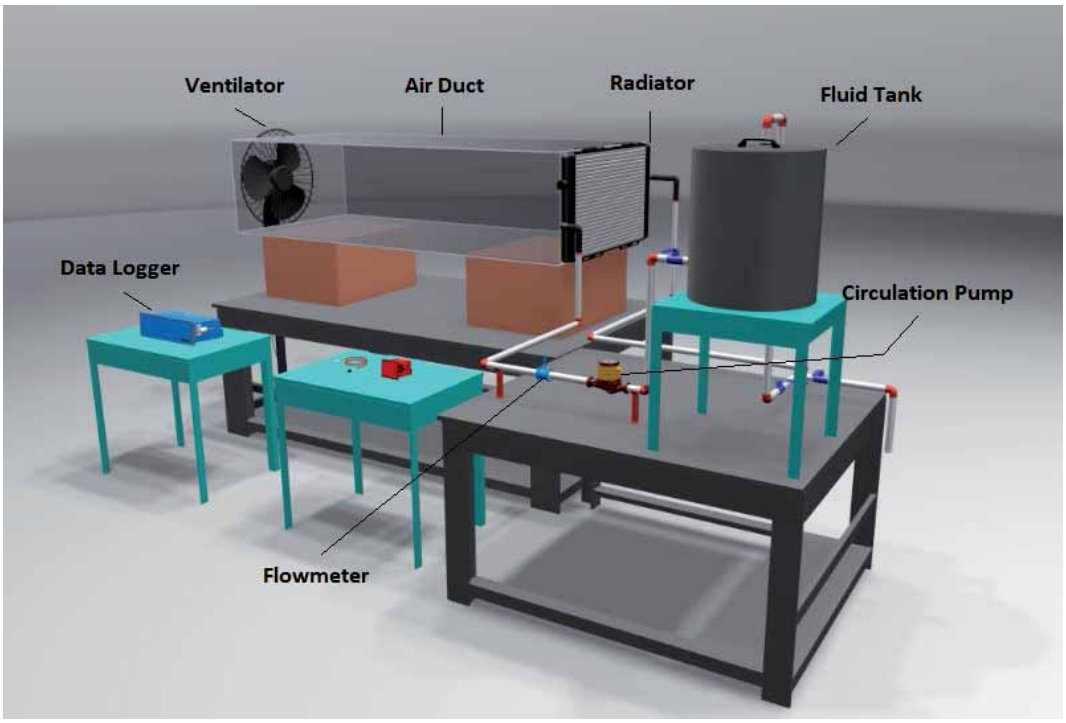


FIGURE 2
Drawing of experimental setup in 3Ds Max software



FIGURE 3
Automobile radiator used in experimental setup

The fluid tank used in the experimental study, made of stainless steel with 1750 W heater power and 16 L volume, provides heating and storage of the fluid circulating in the system. In addition, an industrial-type ventilator with 100 W power and 3 different speeds ensures that the coolant fluids are cooled by air while passing through ARs. The air duct produced from galvanized sheet, which transfers the air flow from the ventilator to the radiator, has dimensions of 0.4 m × 0.4 m × 1.2 m. A circulation pump with a length of 130 mm and connection diameter of 1□ was used to press the fluid in the tank into the system. A stainless-steel turbine-type flowmeter with a measuring range of 0.2-1.2 m^3/h and a maximum working pressure of 1.6 MPa were used to measure the volumetric flow. In this experimental setup, the fluid tank, circulation pump, flow meter, and AR were connected together using PPRC pipes and fasteners so that fluids could circulate. NFs with 99.9% purity and 1% volumetric concentration containing Al_2O_3, CuO, and MgO nanoparticles of 18 nm in size were used as coolant in the experiments.

Studies in which the thermal performances of NFs containing Al_2O_3, CuO, and MgO nanoparticles were examined separately may be found in the literature [33-35].

Numerical Analysis. Physical Model. The flow model of the AR used in the experimental study for numerical analysis was designed using ANSYS-Workbench software. The designed geometry needs to be separated into finite volumes to perform the flow analysis. In order to obtain more sensitive results, mesh was placed more closely in areas where heat transfer was intense [5, 13, 24, 35-38]. Two and three dimensional views of the designed geometry are given in Figure 4. Information about the dimensions of the AR is given in Table 1.

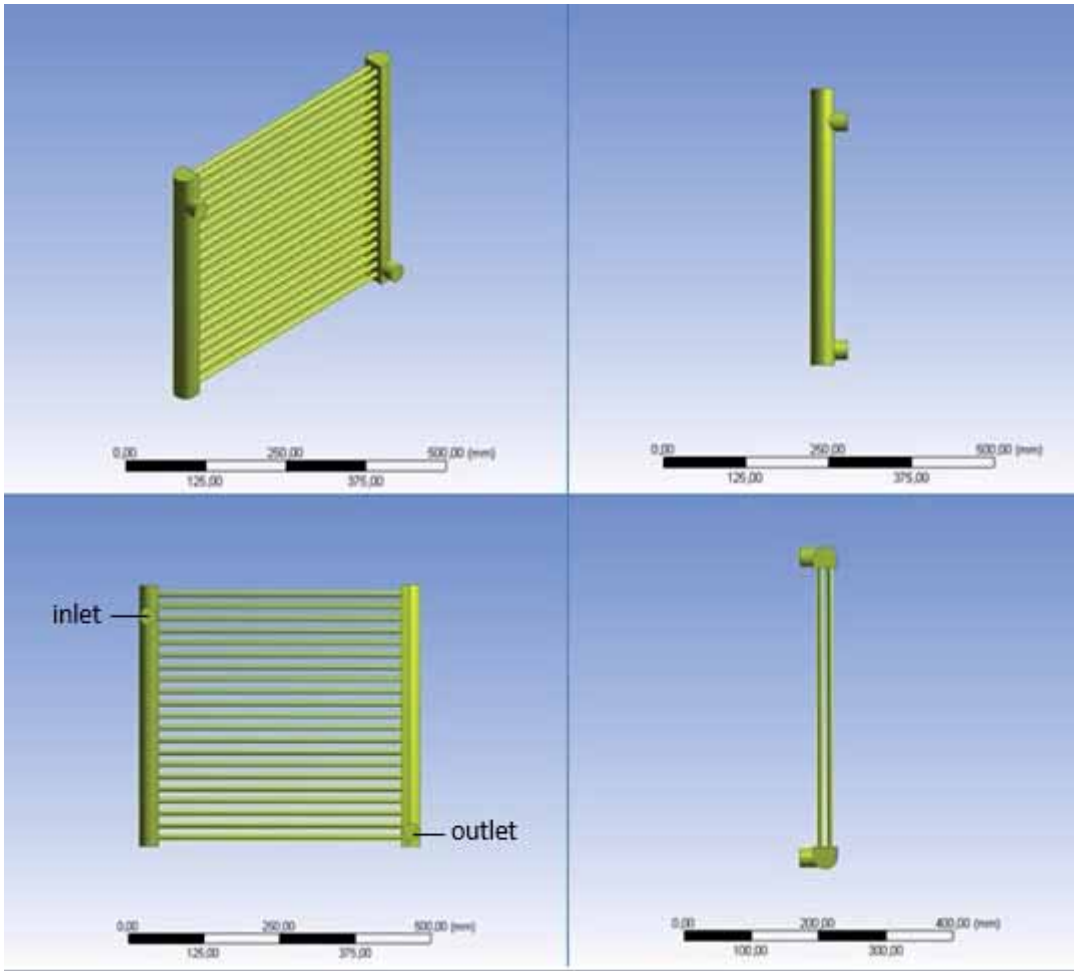


FIGURE 4
Two and three dimensional views of the model

TABLE 1
Dimensions of the automobile radiator

Radiator Dimensions	Value
Radiator length	0.464 m
Radiator height	0.4 m
Radiator width	0.036 m
Radiator inlet and outlet pipe inner diameter	0.028 m
Airfoil length	0.001 m
Airfoil height	0.019 m
Airfoil width	0.036 m
Number of Airfoil in each row	280
Inner diameter of circular tube	0.008 m
Circular tube length	0.4 m
Number of circular tubes	42

$$u_j \frac{\partial u_i}{\partial x_j} = -\frac{1}{\rho}\frac{\partial p}{\partial x_i} + \frac{\partial}{\partial x_j}\left(\nu\left(\frac{\partial u_i}{\partial x_j} + \frac{\partial u_j}{\partial x_i}\right)\right) + \frac{\partial}{\partial x_j}\left(\overline{-u_i' u_j'}\right) \quad (2)$$

$$\overline{u_i' u_j'} = -\left(\frac{\mu_t}{\rho}\left(\frac{\partial u_i}{\partial x_j} + \frac{\partial u_j}{\partial x_i}\right) - \frac{2}{3}k\delta_{ij} - \frac{2}{3}\frac{\mu_t}{\rho}\frac{\partial u_k}{\partial x_k}\delta_{ij}\right) \quad (4)$$

$$\frac{\partial}{\partial x_j}\left(\left(\mu + \frac{\mu_t}{\sigma_k}\right)\frac{\partial k}{\partial x_j}\right) - \rho\varepsilon - \rho\frac{\partial u_j}{\partial x_i}\overline{u_i' u_j'} = \frac{\partial}{\partial x_i}(u_i \rho k) \quad (6)$$

$$\frac{\partial}{\partial x_i}(u_i \rho\varepsilon) = \frac{\partial}{\partial x_j}\left(\left(\mu + \frac{\mu_t}{\sigma_\varepsilon}\right)\frac{\partial \varepsilon}{\partial x_j}\right) - \rho C_{2\varepsilon}\frac{\varepsilon^2}{k} - \frac{\varepsilon}{k}C_{1\varepsilon}\left(\rho\frac{\partial u_j}{\partial x_i}\overline{u_i' u_j'}\right) \quad (7)$$

$$C_\mu = 0.09,\ C_{1\varepsilon} = 1.44,\ C_{2\varepsilon} = 1.92,\ \sigma_k = 1,\ \sigma_\varepsilon = 1.3,\ \sigma_t = 0.85 \quad (8)$$

Government Equations. In this study, the standard k-ε turbulence model was used for the three-dimensional and steady-state flow problem. Continuity, momentum, energy conservation, turbulent kinetic energy (k) and energy dissipation (ε) equations are expressed as follows [34]:

Continuity equation:

$$\frac{\partial u}{\partial x_i} = 0 \quad (1)$$

Momentum equation: (Eq. 2)

Energy equation:

$$u_j \frac{\partial T}{\partial x_j} = \frac{\partial}{\partial x_j}\left((\alpha + \alpha_t)\frac{\partial T}{\partial x_j}\right) \quad (3)$$

$\overline{u_i' u_j'}$ that is used in Equation 2 is expressed as follows: (Eq. 4)

μ_t, that is used in Equation 4 is the turbulent viscosity and is calculated with the following equation:

$$\mu_t = \frac{\rho C_\mu k^2}{\varepsilon} \quad (5)$$

Turbulent kinetic energy (k) equation: (Eq. 6)

Energy dissipation (ε) equation(Eq. 7):

The values of the constants used in the calculations are given as follows: (Eq. 8)

Boundary Conditions. Since the thermo-physical properties of NFs were not defined in the numerical analysis software, these properties were calculated analytically and then manually defined in the program, and the necessary boundary conditions for numerical analysis were entered. The temperature was assumed to be constant at the inlet of the radiator. The inlet temperature for coolant fluids into the AR was set to 350 K. The outlet area of the radiator was defined as the pressure outlet. Three different inlet velocity of fluids into the radiator were applied: 0.376 m/s, 0.422 m/s, and 0.457 m/s. Experimental CHTC of the air obtained according to different air velocities were defined as the boundary condition to the outer surface of the AR. Ambient air temperature was defined as 290 K.

Thermophysical Properties of Nanofluids. A mixture of 50% EG and 50% DW was utilized as the base fluid for NFs. Table 2 shows the thermo-physical properties of nanoparticles and base fluid that are used in NFs.

The thermo-physical properties of NFs were calculated using the following formulas [20, 39]. Equation 9 was used to calculate the density of NFs.

$$\rho_{nf} = \phi*\rho_p + (1-\phi)*\rho_w \quad (9)$$

Here, ρ_{nf}, ρ_p and ρ_w are the density of the NF, nanoparticles and base fluid, respectively. Equation 10 was used to calculate specific temperatures of NFs.

$$(\rho* c_p)_{nf} = \phi*(\rho *c_p)_p + (1-\phi)*(\rho *c_p)_w \quad (10)$$

Here, c_{pnf}, c_{pw} and c_{pp} are the specific heat of the NF, base fluid and nanoparticles, respectively. The dynamic viscosity of the NFs is calculated as in Equation 11.

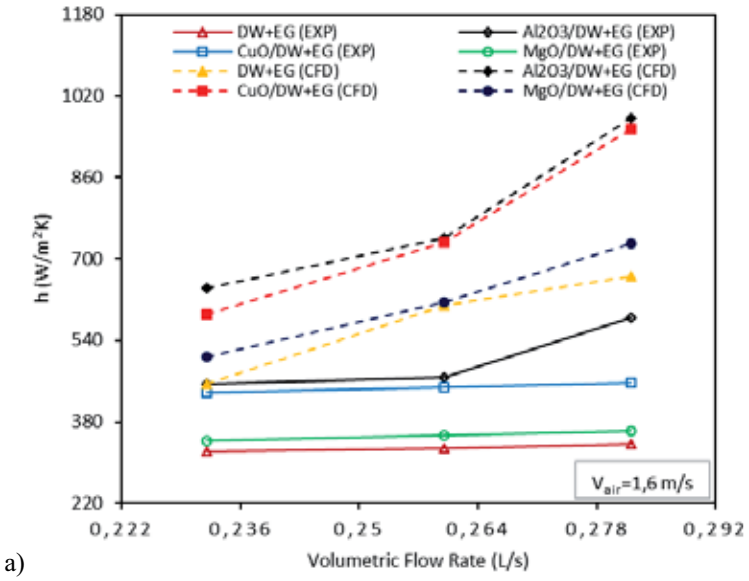
$$\mu_{nf} = \mu_w(123\phi^2 + 7.3\phi + 1) \quad (11)$$

Here, μ_w and μ_{nf} are the dynamic viscosity of the base fluid and the NF, respectively. The thermal conductivity coefficients of the NFs were calculated using the Maxwell model as in Equation 12.

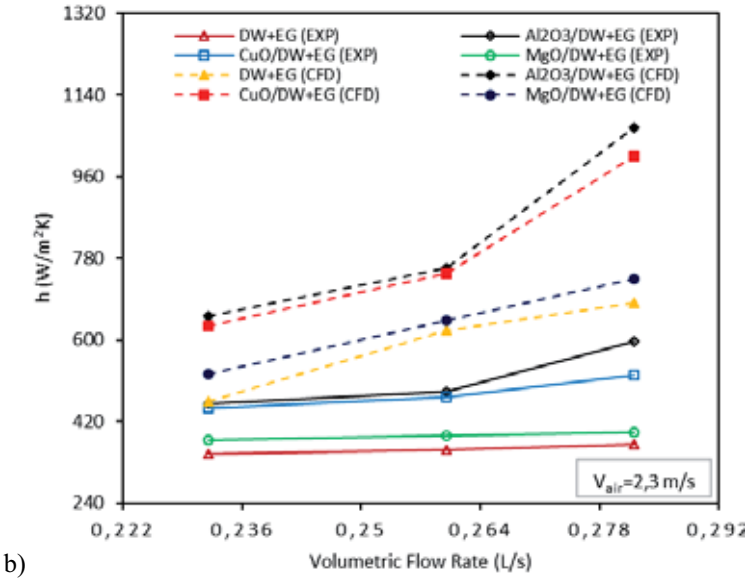
$$k_{nf} = \frac{k_p + (n-1)k_w - \phi(n-1)(k_w - k_p)}{k_p + (n-1)k_w + \phi(k_w - k_p)} * k_w \quad (12)$$

TABLE 2
Thermo-physical properties of base fluid and nanoparticles

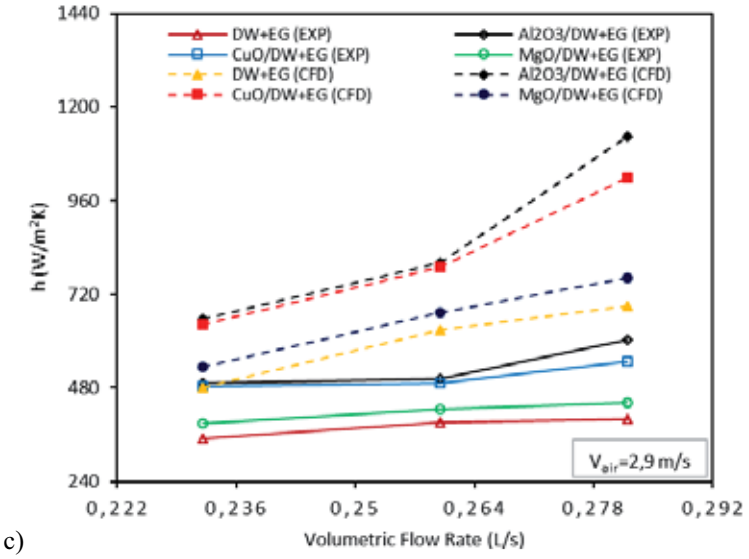
	DW+EG (50:50)	Al_2O_3	CuO	MgO
ρ (kg/m^3)	1027.01	3970	6500	3560
c_p (J/kg.K)	3570	765	535.6	955
μ (Pa.s)	0.00076	-	-	-
k (W/m.K)	0.415	46	20	45



a)

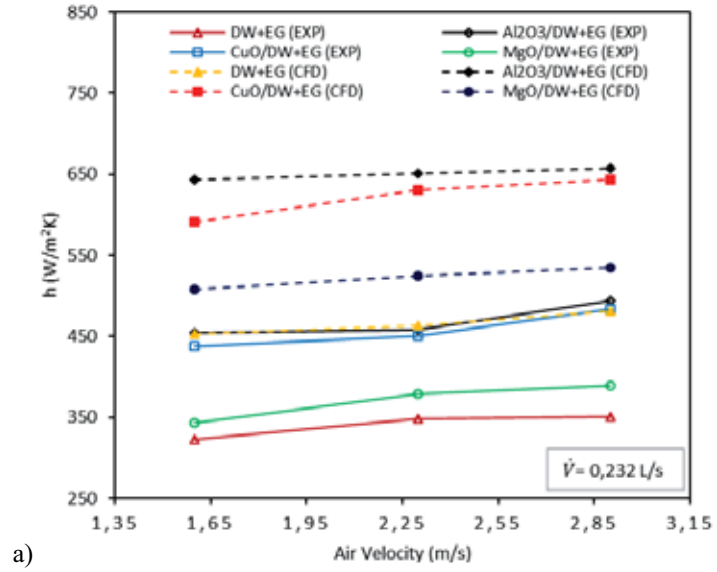


b)

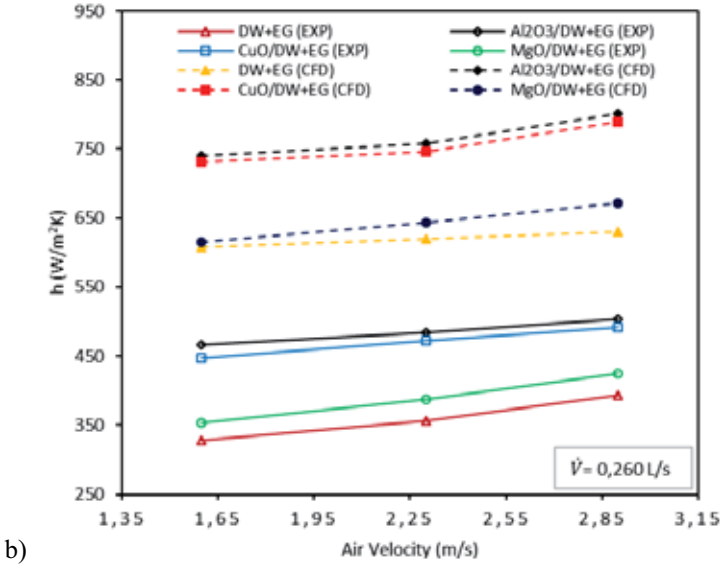


c)

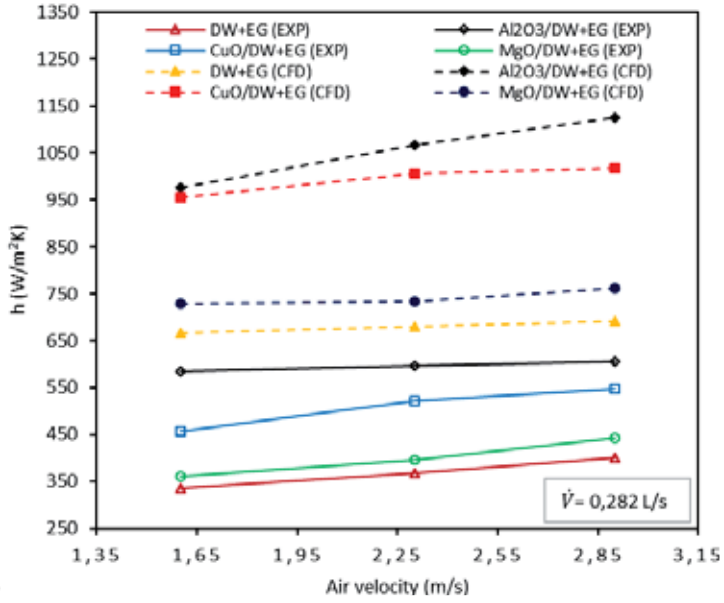
FIGURE 5
Change of CHTC with volumetric flow rate: (a) at 1.6 m/s air velocity, (b) at 2.3 m/s air velocity, (c) at 2.9 m/s air velocity



a)

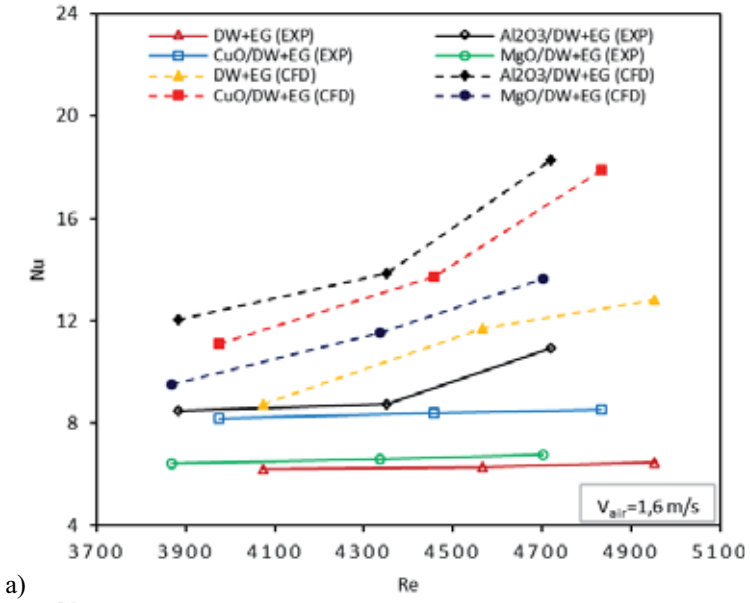


b)

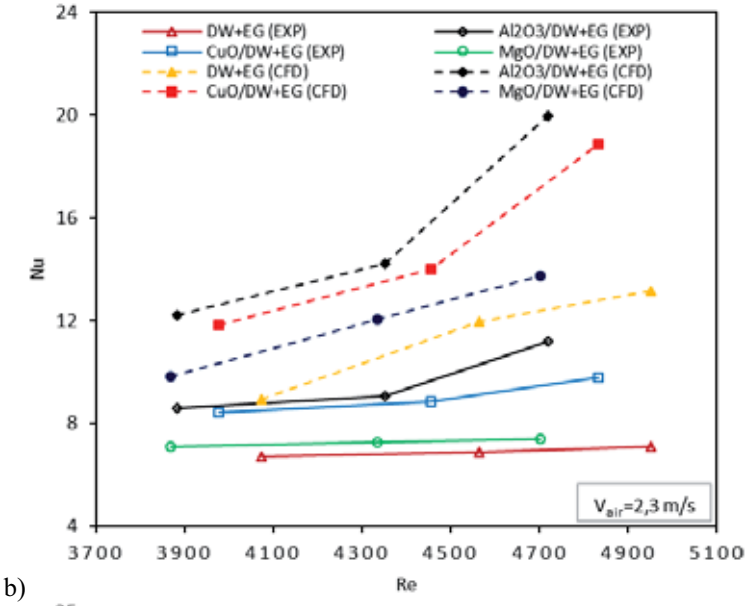


c)

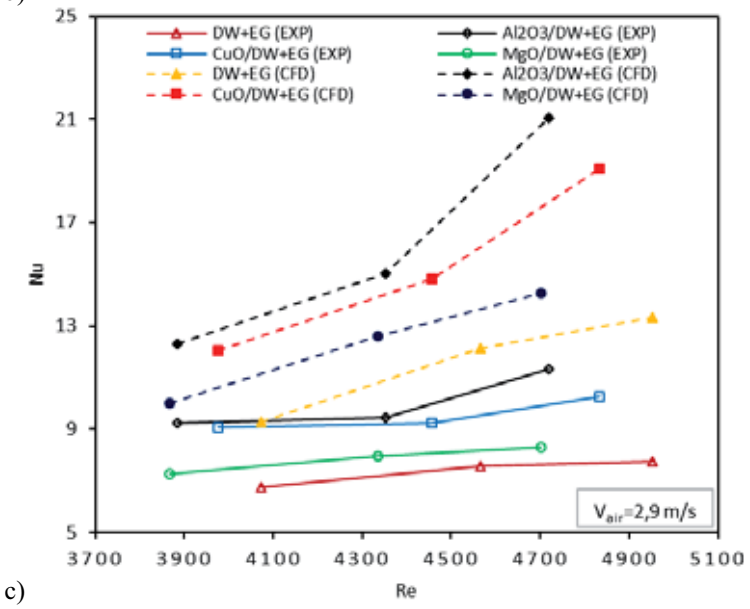
FIGURE 6
Change of CHTC of coolant with air velocity (a) at 0.232 L/s volumetric flow rate, (b) at 0.260 L/s volumetric flow rate, (c) at 0.282 L/s volumetric flow rate



a)



b)



c)

FIGURE 7
Change of Nu with Re (a) at 1.6 m/s air velocity, (b) at 2.3 m/s air velocity, (c) at 2.9 m/s air velocity

Here, n is the experimental shape factor and n = 3/ ψ is calculated. ψ, on the other hand, refers to the nanoparticle sphericity. In the Maxwell model, sphericity is assumed to be 1. k_{nf}, k_p and k_w refer to the thermal conductivity coefficients of the NF, nanoparticle, and base fluid, respectively [20,39].

Data Analysis. According to Newton's cooling law, heat transfer by convection is calculated with Equation 13 [23,39].

$$Q = h.A_S.(T_b - T_s) \quad (13)$$

T_b which represents the bulk temperature, is calculated with Equation 14.

$$T_b = \frac{T_{in}+T_{out}}{2} \quad (14)$$

The heat transfer resulting from the inlet and outlet temperature difference of the fluid is found using Equation 15.

$$Q = \dot{m}.c_p.(T_{in} - T_{out}) \quad (15)$$

Mass flow is calculated with Equation 16.

$$\dot{m} = \rho.V.A_c \quad (16)$$

Equation 17 was utilized to compute the CHTCs of coolant using the above equations.

$$h = \frac{\dot{m}.c_p.(T_{in}-T_{out})}{A_S.(T_b-T_s)} \quad (17)$$

Calculations were made using Equation 18 for the Nu found according to experimental and numerical CHTCs.

$$Nu = \frac{h.D_h}{k} \quad (18)$$

Hydraulic diameter (D_h) is calculated with Equation 19.

$$D_h = \frac{4*A_c}{P} \quad (19)$$

RESULTS AND DISCUSSIONS

In this study, the performances of the NFs are examined experimentally and numerically and the results are shown in graphics. The change of CHTC with volumetric flow rate for three different air velocities is shown in Figures 5a, 5b and 5c. In all cases, it is observed that CHTC increases with the increase of volumetric flow rate. It is clear from both experimental and numerical analyses that the CHTCs of NFs are higher than the CHTCs of the base fluid. According to the results obtained from the experimental analyses, the CHTC of Al_2O_3/DW+EG, CuO/DW+EG and MgO/DW+EG was %,28-74 %25-41 and %6-10 higher than the CHTC of the base fluid, respectively. It was observed from the results obtained from the numerical analyses that the CHTC of Al_2O_3/DW+EG, CuO/DW+EG and MgO/DW+EG was %21-62, %20-47 and %1-13 higher than the CHTC of the base fluid, respectively.

The change of the CHTC of the coolants with air velocity for three different volumetric flow rates is given in Figures 6a, 6b and 6c. In all cases, it is observed that the CHTC of the coolants increases with the increase of air velocity. For both experimental and numerical analyses, the highest CHTC was obtained for Al_2O_3/DW+EG when the volumetric flow rate was 0.282 L/s and the air velocity was 2.9 m /s.

In Figures 7a, 7b and 7c, the change of Re and Nu is given for three different air velocities. For all cases, it is obvious that Nu increases with the increase of Re. In both experimental and numerical analyses, Nu values obtained for NFs are higher than Nu values obtained for the base fluid. It was observed from the experimental results that the Nu values of Al_2O_3/DW+EG, CuO/DW+EG and MgO/DW+EG were %24-69, %21-37 and %3-7 higher than the Nu values of the base fluid, respectively. According to the results obtained from the numerical analyses, the Nu values of Al_2O_3/DW+EG, CuO/DW+EG and MgO/DW+EG were 18-58%, 16-43% and 1-10% higher than the Nu values of the base fluid, respectively.

CONCLUSION

In this study, the thermal performance of three different NFs with the same volumetric concentration was investigated experimentally and numerically. According to the data from the analyses, the following results were obtained:

- The CHTC and Nu of all fluids increased with the increase in the volumetric flow rate of coolants from 0.232 L/s to 0.282 L/s. Besides, it was observed that the CHTC of all fluids increased with the increase of air velocity from 1.6 m/s to 2.9 m/s.
- The results obtained from both experimental and numerical analyses showed that under the same conditions, the CHTC and Nu of all NFs were higher than the CHTC and Nu of the base fluid.
- According to both experimental and numerical results, the highest CHTC and Nu values were obtained for Al_2O_3/DW+EG when the air velocity was 2.9 m/s and the volumetric flow rate of the coolant was 0.282 L/s. According to the experimental results, the CHTC and Nu of Al_2O_3/DW+EG were %28-74 and %24-69 higher than the CHTC and Nu of the base fluid, respectively. According to the numerical results, the CHTC and Nu of Al_2O_3/DW+E were %21-62 and %18-58 higher than the CHTC and Nu of the base fluid, respectively.

- In all cases, it was observed that the numerical results were higher than the experimental results. This can be attributed to the losses to the environment that are ignored in numerical calculations, the simplifications made in the geometric model and the variability of the experimental environmental conditions.

Although NFs give better results in terms of the thermal performance than base fluid does, the problems that will be encountered as a result of their long-term use are not known. The sedimentation of nanoparticles in the base fluid over time is especially an important problem. For this reason, more studies are needed to minimize the sedimentation problem. In future studies, minimizing experimental errors, investigating the negative factors that may occur in the case of long-term use of NFs, choosing the correct type of nanoparticle, and determining the ideal volumetric concentration, stability, and particle size will contribute significantly to the literature.

NOMENCLATURE

A_c : Cross-section area (m^2)
A_S : Surface area (m^2)
c_p : Specific heat at constant pressure (J/kg.K)
D_h : Hydraulic diameter (m)
h : CHTC ($W/m^2.K$)
k : Thermal conductivity coefficient (W/m.K)
$\dot{m}$: Mass flow rate (kg/s)
n : Experimental shape factor
Nu : Nusselt number
P : The environment soaked by the flow (m)
Re : Reynolds number
Q : Heat transfer (W)
T_b : Bulk temperature (K)
T_{in} : Inlet temperature of fluid (K)
T_{out} : Output temperature of fluid (K)
T_s : Surface temperature (K)
V : Velocity (m/s)
Greek Symbols
$\dot{V}$: Volumetric flow rate (L/s)
ρ : Density (kg/m^3)
μ : Dynamic viscosity (Pa.s)
Φ : Volumetric concentration
ψ : Particle sphericity
Subscripts
nf : NF
p : Nanoparticle
w : Base fluid
Abbreviations
EG : Ethylene glycol
DW : Distilled water
NF : Nanofluid
AR: Automobile Radiator
CHTC : Convective Heat Transfer Coefficient

ACKNOWLEDGEMENT

This study was supported by the Scientific Research Projects Unit of Munzur University with Project Number YLMUB018-12. This article is partially produced from MSC dissertation entitled ‘‘Numerical and Experimental Analysis of The Effect of Nanofluid Use in Radiators on Thermal Performance’’ which has been executed in Mechanical Engineering Program of Munzur University Graduate School of Science Technology.

REFERENCES

[1] Tijani, A.S., Bin Sudirman, A.S. (2018) Thermos-physical properties and heat transfer characteristics of water/anti-freezing and Al_2O_3/CuO based nanofluid as a coolant for car radiator. International Journal of Heat and Mass Transfer. 118, 48-57.
[2] Peyghambarzadeh, S.M., Hashemabadi, S.H., Hoseini, S.M., Jamnani, M.S. (2011a). Experimental study of heat transfer enhancement using water/ethylene glycol based nanofluids as a new coolant for car radiators. International Communications in Heat and Mass Transfer. 38, 1283-1290.
[3] Said, Z., Assad, M. E. H., Hachicha, A. A., Bellos, E., Abdelkareem, M. A., Alazaizeh, D. Z., Yousef, B. A. A. (2019) Enhancing the performance of automotive radiators using nanofluids. Renewable and Sustainable Energy Reviews. 112, 183-194.
[4] Choi, S.U.S., Eastman, J. A. (1995) Enhancing thermal conductivity of fluids with nanoparticles. ASME International Mechanical Engineering Congress and Exposition, United States.
[5] Delavari, V., Hashemabadi, S. H. (2014) CFD simulation of heat transfer enhancement of Al_2O_3/water and Al_2O_3/ethylene glycol nanofluids in a car radiator. Applied Thermal Engineering. 73, 380-390.
[6] Ebrahimi, M., Farhadi, M., Sedighi, K., Akbarzade, S. (2014). Experimental investigation of force convection heat transfer in a car radiator filled with SiO_2–water nanofluid. International Journal of Engineering, 27(2), 333-340.
[7] Kumar, A., Subudhi, S. (2019). Preparation, characterization and heat transfer analysis of nanofluids used for engine cooling. Applied Thermal Engineering. 160, 114092.
[8] Sumanth, S., Babu Rao, P., Krishna, V., Seetharam, T. R., Seetharamu, K. N. (2018). Effect of carboxyl graphene nanofluid on automobile radiator performance. Heat Transfer—Asian Research. 47, 669-683.

[9] Hussein, A. M., Bakar, R. A., Kadirgama, K. (2014a). Study of forced convection nanofluid heat transfer in the automotive cooling system. Case Studies in Thermal Engineering. 2, 50-61.

[10] Leong, K. Y., Saidur, R., Kazi, S. N., Mamun, A. H. (2010) . Performance investigation of an automotive car radiator operated with nanofluid-based coolants (nanofluid as a coolant in a radiator). Applied Thermal Engineering. 30, 2685-2692.

[11] Naraki, M., Peyghambarzadeh, S. M., Hashemabadi, S. H., Vermahmoudi, Y. (2013). Parametric study of overall heat transfer coefficient of CuO/water nanofluids in a car radiator. International Journal of Thermal Sciences. 66, 82-90.

[12] Gulhane, A., Chincholkar, S.P. (2016). Experimental investigation of convective heat transfer coefficient of Al_2O_3/water nanofluid at lower concentrations in a car radiator. Heat Transfer—Asian Research. 46, 1119-1129.

[13] Angadi, V. M., Nagaraj, R., Hebbal, O. D. (2014). Cfd analysis of heat transfer enhancement of a car radiator using nanofluid as a coolant. International Journal of Engineering Research & Technology. 3(8), 1058-1063.

[14] Selvam, C., Raja, R. S., Lal, D. M., Harish, S. (2017). Overall heat transfer coefficient improvement of an automobile radiator with graphene based suspensions. International Journal of Heat and Mass Transfer. 115, 580-588.

[15] Elsaid, A. M. (2019). Experimental study on the heat transfer performance and friction factor characteristics of Co_3O_4 and Al_2O_3 based $H_2O/(CH_2OH)_2$ nanofluids in a vehicle engine radiator. International Communications in Heat and Mass Transfer. 108, 104263.

[16] Soylu, S. K., Atmaca, İ., Asiltürk, M., Doğan, A. (2019). Improving heat transfer performance of an automobile radiator using Cu and Ag doped TiO_2 based nanofluids. Applied Thermal Engineering. 157, 113743.

[17] Hussein, A. M., Bakar, R. A., Kadirgama, K., and Sharma, K. V. (2014b.) Heat transfer enhancement using nanofluids in an automotive cooling system. International Communications in Heat and Mass Transfer. 53, 195-202.

[18] Bhimani, V. L., Rathod, P. P., Sorathiya, A. S. (2013). Experimental study of heat transfer enhancement using water based nanofluids as a new coolant for car radiators. International Journal of Emerging Technology and Advanced Engineering. 3(6), 295-302.

[19] Gaidhane, T., Bhosale, S. (2016). Cfd analysis and experimental investigation of percentage heat transfer enhancement of cfhx with hybrid nanofluid as a coolant. International Journal of Mechanical And Production Engineering. 4(9), 1-5.

[20] Peyghambarzadeh, S. M., Hashemabadi, S. H., Jamnani, M.S., Hoseini, S.M. (2011b). Improving the cooling performance of automobile radiator with Al_2O_3/water nanofluid. Applied Thermal Engineering. 31, 1833-1838.

[21] Peyghambarzadeh, S. M., Hashemabadi, S. H., Naraki, M., and Vermahmoudi, Y. (2013). Experimental study of overall heat transfer coefficient in the application of dilute nanofluids in the car radiator. Applied Thermal Engineering. 52, 8-16.

[22] Kılınç, F., Buyruk, E., Karabulut, K. (2019). Experimental analysis of graphene based nanofluids on vehicle radiator cooling performance. Journal of the Institute of Science and Technology. 9(2), 1046-1056.

[23] Sokhal, G. S., Gangacharyulu, D., Bulasara, V. K. (2018). Influence of copper oxide nanoparticles on the thermophysical properties and performance of flat tube of vehicle cooling system. Vacuum. 157, 268-276.

[24] Canbolat, A. S., Türkan, B. (2016). Numerıcal ınvestıgatıon ınto thermal performance parameters of automobıle radıators. J. of Thermal Science and Technology. 36(2), 29-40.

[25] Elsebay, M., Elbadawy, I., Shedid, M. H., Fatouh, M. (2016). Numerical resizing study of Al_2O_3 and CuO nanofluids in the flat tubes of a radiator. Applied Mathematical Modelling. 40, 6437-6450.

[26] Hatami, M., Jafaryar, M., Zhou, J., Jing, D. (2017). Investigation of engines radiator heat recovery using different shapes of nanoparticles in $H_2O/(CH_2OH)_2$ based nanofluids. International Journal of Hydrogen Energy. 42, 10891-10900.

[27] Jadar, R., Shashishekar, K. S., Manohara, S. R., (2017). f-MWCNT nanomaterial integrated automobile radiator. Material Today: Proceedings. 4, 11028-11033.

[28] Sharma, S. (2018). Fabricating an experimental setup to investigate the performance of an automobile car radiator by using aluminum/water nanofluid. Journal of Thermal Analysis and Calorimetry. 133, 1387-1406.

[29] Sandhya, D., Reddy, M.C. S., Rao, V. V. (2016) Improving the cooling performance of automobile radiator with ethylene glycol water based TiO_2 nanofluids. International Communications in Heat and Mass Transfer. 78, 121-126.

[30] Subhedar, D. G., Ramani, B. M., Gupta, A. (2018) Experimental investigation of heat transfer potential of Al_2O_3/water-Mono ethylene glycol nanofluids as a car radiator coolant. Case Studies in Thermal Engineering. 11, 26-34.

[31] Goudarzi, K., Jamali, H. (2017). Heat transfer enhancement of Al_2O_3-ethylene glycol nanofluid in a car radiator with wire coil inserts. Applied Thermal Engineering. 118, 510-517.

[32] Contreras, E. M. C., Oliveira, G. A., Bandarra Filho, E. P. (2019). Experimental analysis of the thermohydraulic performance of graphene and silver nanofluids in automotive cooling systems. International Journal of Heat and Mass Transfer. 132, 375-387.
[33] Samira, P., Saeed, Z. H., Motahare, S., Mostafa, K. (2015). Pressure drop and thermal performance of CuO/ethylene glycol (60%)-water (40%) nanofluid in car radiator. Korean Journal of Chemical Engineering. 32(4), 609-616.
[34] Habibian, S. H., Abolmaali, A. M., Afshin, H. (2018). Numerical investigation of the effects of fin shape, antifreeze and nanoparticles on the performance of compact finned-tube heat exchangers for automobile radiator. Applied Thermal Engineering. 133, 248-260.
[35] Sumit, G.W., Ravi, H.C. (2017). Experimental study and Cfd analysis of thermal performance improvement of car radiator by MgO/water nanofluid. International Research Journal of Engineering and Technology. 4(6), 1904-1911.
[36] Kumar, R. K., Amirthagadeswaran, K. S. (2016) Experimental study and CFD analysis of copper radiator for passenger cars. International Journal of Engineering Research. 5(9), 778-782.
[37] Patel, J.R., Mavani, A.M. (2014). Effect of nanofluids and mass flow rate of air on heat transfer rate in automobile radiator by CFD analysis. International Journal of Research in Engineering and Technology. 3(6), 25-30.
[38] Deepu, D., Krishna, A.R., Jilani, S.A.K. (2014). Cfd simulation of radiator for heat transfer enhancement using nanofluids based coolant in automobiles. International Journal of Mechanical Engineering and Computer Applications. 2(5), 146-154.
[39] Ali, H. M., Ali, H., Liaquat, H., Maqsood, H. T. B., Nadir, M. A. (2015). Experimental investigation of convective heat transfer augmentation for car radiator using ZnO–water nanofluids. Energy. 84, 317-324.
[40] Abbas, F., Ali H. M., Shah, T. R., Babar, H., Janjua, M. M., Sajjad, U., Amer, M. (2020). Nanofluid: Potential evaluation in automotive radiator. Journal of Molecular Liquids. 297, 112014.

Received: **21.09.2020**
Accepted: **03.02.2021**

CORRESPONDING AUTHOR

Erdem Isik
University of Munzur,
Engineering Faculty,
Mechanical Engineering Department,
Tunceli – Turkey

e-mail: erdem@munzur.edu.tr

© by PSP Volume 30– No. 09/2021 pages 10505-10514 Fresenius Environmental Bulletin

FLAVONOID CONTENTS ANTIOXIDANT AND NEUROPROTECTIVE ACTIVITIES OF *CRATAEGUS MONOGYNA* JACQ. LEAVES AND FLOWERS

Gozde Elgin Cebe[1,*], Selin Aktar Kiremitci[2], M Alper Erdogan[3], Sibel Konyalioglu[4], Cigdem Yengin[5], Gulay Der[6], Emrah Kilinc[6]

[1]Ege University Faculty of Pharmacy Department of Pharmaceutical Botany, 35100, Izmir, Turkey
[2]Istinye University Faculty of Pharmacy Department of Pharmaceutical Botany, 34010, Istanbul, Turkey
[3]Katip Celebi University Faculty of Medicine Department of Physiology, 35620, Izmir, Turkey
[4]Ege University Faculty of Pharmacy Department of Biochemistry, 35100, Izmir, Turkey
[5]Ege University Faculty of Pharmacy Department of Pharmaceutical Chemistry, 35100, Izmir, Turkey
[6]Ege University Faculty of Pharmacy Department of Analytical Chemistry, 35100, Izmir, Turkey

ABSTRACT

Antioxidant activities of *Crataegus* species' leaves and fruits so far have been reported in literature, however, several factors ranging from plant part(s), harvest season, the species and the geographical origin of the plant extensively impede and influence these antioxidant activities. In this research, ethanolic extracts of leaves and flowers of *Crataegus monogyna* Jacq. (CRT) collected from 6 different locations (Karaman, Bolu, Sinop, Eğirdir, Elbistan, Seydişehir: CRT-1 to CRT-6) between May and June 2018 were evaluated for their flavonoid contents, antioxidant (RSA and PRAP assays) and neuroprotective capacities (SHSY5Y). Content of flavonoids epicatechin and hyperoside detected using HPLC is reported. Both CRT-3 and CRT-4 are remarkable in cycles of flavonoid content, antioxidant, and neuroprotective activities. Results show that leaves and flowers of *C. monogyna* provide considerable antioxidant protection and neuroprotective activity and can be a suitable raw material for medicine, food, and cosmetic industries.

KEYWORDS:
Antioxidant, *Crataegus monogyna*, HPLC, Neuroprotective

INTRODUCTION

Neurodegenerative disorders are very commonly observed today. It is known that compounds with antioxidant effect, such as flavonoids are effective in managing neurodegenerative disorders as well as many other diseases. It is known that *Crataegus* species contain high levels of antioxidant compounds.

Crataegus (Hawthorn) genus is represented by nearly 200 species in the world [1-3]. The species in this genus are mostly found in temperate regions such as North America, West Asia, India, China, and North Africa [4]. *C. monogyna*, belonging to the Rosaceae family, grow as bushes and trees as small as 10 m. Their flowers 8-15 mm in diameter are white or pinkish. The leaves are prickly and long, ovate, or obovate. Their fruits, 6-10 mm in diameter and hairless are red or brownish-red color, and spherical or oval shape [1, 5-7].

Only a few studies have so far been aimed at determining the chemical content, antioxidant, and antibacterial effects of some *Crataegus* species [8-14]. In *Crataegus* species fruits contain 0.1-1% flavonoids, 0.5-1.4% triterpene acids, 1-2% oligomeric proanthocyanidins (OPC) and 2-6% organic acids, while their leave and flower mixture contain 1-2% flavonoids and 1-3% OPC [15-26].

Crataegus species are known for their useful biological effects for many years. The use of *Crataegus* species in the treatment of cardiovascular diseases dates back to the 1800s. Previous studies made on heart and blood pressure disorders, diarrhea, biliary cirrhosis, insomnia, and asthma are also known [27-29].

There are monographs of leaves, flowers, and fruits of *C. monogyna* in the European Pharmacopoeia [30]. In ESCOP monographs, the leaves and flowers of the plant are registered to reduce cardiac performance [31]. Although clinical trials generate contradictory results, ethanolic extracts of moderate forms are typically used nowadays as positive inotropic, anti-arrhythmic and vasodilator agents [19, 22, 23, 32-38].

This study is aimed to determine the flavonoid contents of *C. monogyna* leaves and flowers while revealing their antioxidant and neuroprotective activities.

MATERIALS AND METHODS

Reagents: Ethanol (Carlo Erba), Quercetin (Sigma-Aldrich), Gallic acid (Fluka), (-) Epicate-

chin (Fluka), (+)-Catechin hydrate (Fluka), Rutin (Extrasynthese), Hyperoside (Extrasynthese), Formic acid (Sigma-Aldrich), Acetonitrile (Merck), Butylated hydroxytoluene (Sigma-Aldrich), DPPH (Sigma-Aldrich), Phosphomolybdic acid (Sigma-Aldrich), Sulfuric acid (Sigma-Aldrich), Sodium phosphate (Sigma-Aldrich), Ammonium molybdate (Sigma-Aldrich), SH-SY5Y (Human neuroblastoma cell line, ATCC), MTS assay (Promega, Madison, WI, USA), Cell culture medium (Life Technologies, Gibco BRL), Fetal bovine serum (Hyclone), Penicillin and Streptomycin (Invitrogen) were used.

Apparatus: Shimadzu UV-1601 UV Visible Spectrophotometer, Microplate Reader (VersaMax), Thermo Scientific Accela PDA 1250 Pump, Column; Syncronis C18 250x4.6x5µ, Elga I Purelab Classic-UV, Mill (TOPER KT 17), Heidolph Hei-VAP-Valve brand rotavapor, Speed vac (Christ RVC 2-25), Cooler (Christ LT-105), Vacuum pump (Vacuubrand RZ 2.5), HPLC-DAD (Thermo Dionex), Gradient pump (LPG-3400SD), Solvent rack (SR-3000), Autosampler (WPS-3000TSL), Column department (TCC3000SD), PDA detector (DAD-3000), Entire system and its modules (Chromeleon Client v.6.80 SR13), Thermo Scientific Syncronis C18 analytical column (250x4,6-ODS 1005), Ultrasonic bath Bandelin Sonorex RK 52 (240W, 35kHz) and NUVE MK 418 with heater (600W/1200rpm), Hanna HI 5222 pH-meter were utilized.

Plant material: Aerial parts (leaves and flowers) of fresh plants i.e. *Crataegus monogyna* were harvested from the wild at six different locations between May and June, 2018. Crude plants were dried in shade and finely powdered by a mill. Voucher specimens of the plants were kept for records in the IZEF Herbarium of Ege University, Faculty of Pharmacy (Voucher No: 6053-6058).

Ultrasound assisted extraction method: An optimized method was evaluated. The ultrasonic wave frequency was set to 20 kHz. %45 Ethanol (EtOH) was used in the extraction process lasted for 3 hours. After the extraction was completed, the solvent was removed by an evaporator. Experiments were performed in triplicates. The extracts were stored in the desiccator as to protect them from light and humidity.

HPLC method: Mobile Phase Preparation: During HPLC separation processes, two mobile phases were employed, namely aqueous 0.5% formic acid as mobile phase A (MP-A), and gradient grade (≥ 99.9%) acetonitrile for LC as mobile phase B (MP-B). Freshly prepared MP-A was filtered through 0.22µm membrane filter prior to use.

Preparation of Standard and Sample Solutions: The standards were prepared in four successive concentrations as 10.0, 25.0, 50.0 and 100.0ppm. Each level owns multi-injections (n=10) in accordance to the method validation guideline ICH Q2 (R1) [39]. Corresponding calibration graphs were obtained and used to quantify the plant sample extracts (sample codes CRT-1 to CRT-6). Dried extracts were weighed and dissolved to obtain 100 and 200ppm sample extract solutions. During these processes to obtain maximum precision and accuracy, calibrated auto-pipets with appropriate volume intervals were used. Prepared solutions were immediately put in brown amber flacons and laid in the 5^0C cooled tray of the auto sampler in order to protect standards and extracts from heat and radiation.

HPLC-DAD Analysis: Optimum gradient program designed for MP-A and MP-B in the laboratory for the present study was as follows: 0min: A (80%), 2min: A (80%), 3.5min: A (50%), 5min: A (50%), 8min: A (80%), 8.5min: A (80%). Thermostatically regulated column department was kept at 45^0C, while injection volume and flow rate were 10µL and 1.0mL/min, respectively. Once prepared, standard solutions and sample extracts were immediately put in brown amber flacon vials and laid in the appropriate rack of the sample tray which was cooled down to 10^0C. UV-Vis spectrums were collected in 200-400nm while absorbance was monitored in four different channels at; 230, 257, 270 and 367nm wavelength.

Antioxidant activity: Radical Scavenging Activity (RSA) Assay: DPPH-radical scavenging activity was tested according to the method described previously with some modifications [40]. Test samples were prepared by dissolving 0.25mg of dry extract in 4mL of ethanol. An ethanolic solution of 2diphenyl-1-picrylhydrazyl (DPPH) (1mM, 0.5mL) was then added to the samples. The absorbances were determined spectrophotometrically at 517nm. These measurements were carried out in triplicate. Butylated hydroxytoluene (BHT; 1mg/mL) was used as a positive control. The inhibition percentages were calculated as follows:

% RS A= 100 X (1-AE/AD); where AE is the absorbance of the solution when an extract was added at a particular level, and AD is the absorbance of the DPPH solution with nothing added [40].

Phosphomolybdenum-Reducing Antioxidant Power (PRAP) Assay: Phosphomolybdenum-Reducing Antioxidant Power (PRAP) of all extracts were examined using phosphomolybdic acid. The phosphomolybdenum-reducing antioxidant power of extracts was expressed as mM trolox equivalents (QE) per mg of dry weight extract. 1mL

of reagent solution containing 0.6M sulfuric acid, 28mM sodium phosphate, and 4mM ammonium molybdate was mixed with 1mL of extract solutions (0.02mg/mL) and left at 37°C for 90 min. After cooling, the absorbance of the phosphomolybdenum complex was measured at 695nm. Antioxidant capacities were expressed as trolox equivalents according to the standard curve of trolox obtained at various concentrations (0.02-0.05-0.1-0.15-0.2 mM) [41].

Cell Viability Assay Against H_2O_2-Induced Toxicity as Neuroprotective Activity: The human neuroblastoma cell line (SH-SY5Y) was maintained at 37^0C in 5% CO_2 95% humidified atmosphere. After reaching 85% confluence, cells were transferred to 96-well plates or culture dishes. For this purpose, first we examined to find proper H_2O_2 concentration for inducing toxicity.

The stock solutions of the test compounds were prepared in sterile dimethyl sulfoxide (DMSO) and these stocks were then appropriately diluted with the complete culture medium and DMSO levels which were maintained below 1% in the test concentrations [42].

H_2O_2-Induced Toxicity: H_2O_2-induced toxicity was determined as previously described [43]. Briefly, SH-SY5Y cells were seeded at a density of $2x10^3$ cells per well into 96-well plates and incubated for 24 h. After 24 h, the medium was aspirated and the cells were washed twice with sterile phosphate-buffered saline (PBS) and then treated with a range of concentrations (1, 10, 50, 100, 200, 800 and 1000µM) of H_2O_2 in sterile PBS (with Ca^{2+} and Mg^{2+}) for 1 h. After 1 h, H_2O_2 solution in the well was replaced with the warm medium and incubated for 17 h. After the 18 h exposure, the cell viability was determined using the 3-(4,5 dimethylthizol-2-yl)-5-(3-carboxy-methoxyphenyl)-2-(4-sulfophenyl)-2H-tetrazolium (MTS) assay. As a result of this test, we found the proper toxic dose for SH-SY5Y cells as 250µM of H_2O_2.

MTS Cell Viability and Proliferation Assay: SH-SY5Y cells were seeded at a density of $2x10^3$ cells/well into 96-well plates and incubated for 24 h. After 24 h, the cells were treated with synthesized compounds at a range of concentrations (1, 10 and 100 µg/mL) for 2 h. After 2 h, the medium was aspirated, and the cells were washed twice with sterile PBS and then treated with 250µM of H_2O_2 in sterile PBS (with Ca^{2+} and Mg^{2+}) for 1 h. After 1 h, the H_2O_2 solution in the well was replaced with the warm medium and incubated for 17 h. After the 18 h exposure, the cell viability was determined using the MTS assay [42, 43].

The viability and/or proliferation of cells were detected by MTS assay, after cells treatment to measure cell growth. For this assay, cells were counted using a hemocytometer and viable cells were identified by trypan blue exclusion. Viable cells were seeded in 96-well plates ($2x10^3$ cells/well). After 24 hours, drug applications were performed on the cells as described above. After treatment, a solution containing MTS and phenazine methosulphate (PMS) (20:1 v/v) was added to the cells for 2-3 h at 37°C and the viable growing cells were estimated by monitoring the absorption of the product at 490nm. All experiments were performed in triplicate and the results were reported as mean absorption ± standard deviation [42, 43].

RESULTS AND DISCUSSION

HPLC analysis of *C. monogyna* ethanolic extracts was investigated for the presence of flavonoids such as gallic acid, catechin, epicatechin, hyperoside, rutin and quercetin (Figure 1).

Of the standard substances, gallic acid, catechin, rutin and quercetin could not be detected with this method. Epicatechin amounts are 2.1774, 6.4305, 8.9521, 3.0658, ND * and 1.1339 for CRT-1 to CRT-6, respectively. Hyperoside amounts are also 17.4359, 13.6235, 4.1616, 22.477, 16.1466, 18.9015 for CRT-1 to CRT-6, respectively (Table 1, Figure 1).

The DPPH radical scavenging activity was recorded in terms of % inhibition as shown in Table 2, CRT-3 showed considerable antioxidant potential. % RSA values for CRT-1 to CRT-6 39.813 ± 0.873, 42.582 ± 0.842, 60.738 ± 0.628, 48.473 ± 1.041, 7.600 ±0.711, 47.924 ± 1.282, respectively.

TABLE 1
HPLC quantification results of the *C. monoyna* extracts

SAMPLE CODE	EPICATECHIN		HYPEROSIDE	
	t_R (min)	Concentration (µg/mL)	t_R (min)	Concentration (µg/mL)
CRT-1	3.650	2.1774	5.270	17.4359
CRT-2	3.653	6.4305	5.270	13.6235
CRT-3	3.663	8.9521	5.283	4.1616
CRT-4	3.660	3.0658	5.300	22.477
CRT-5	ND*	ND*	5.293	16.1466
CRT-6	3.663	1.1339	5.300	18.9015

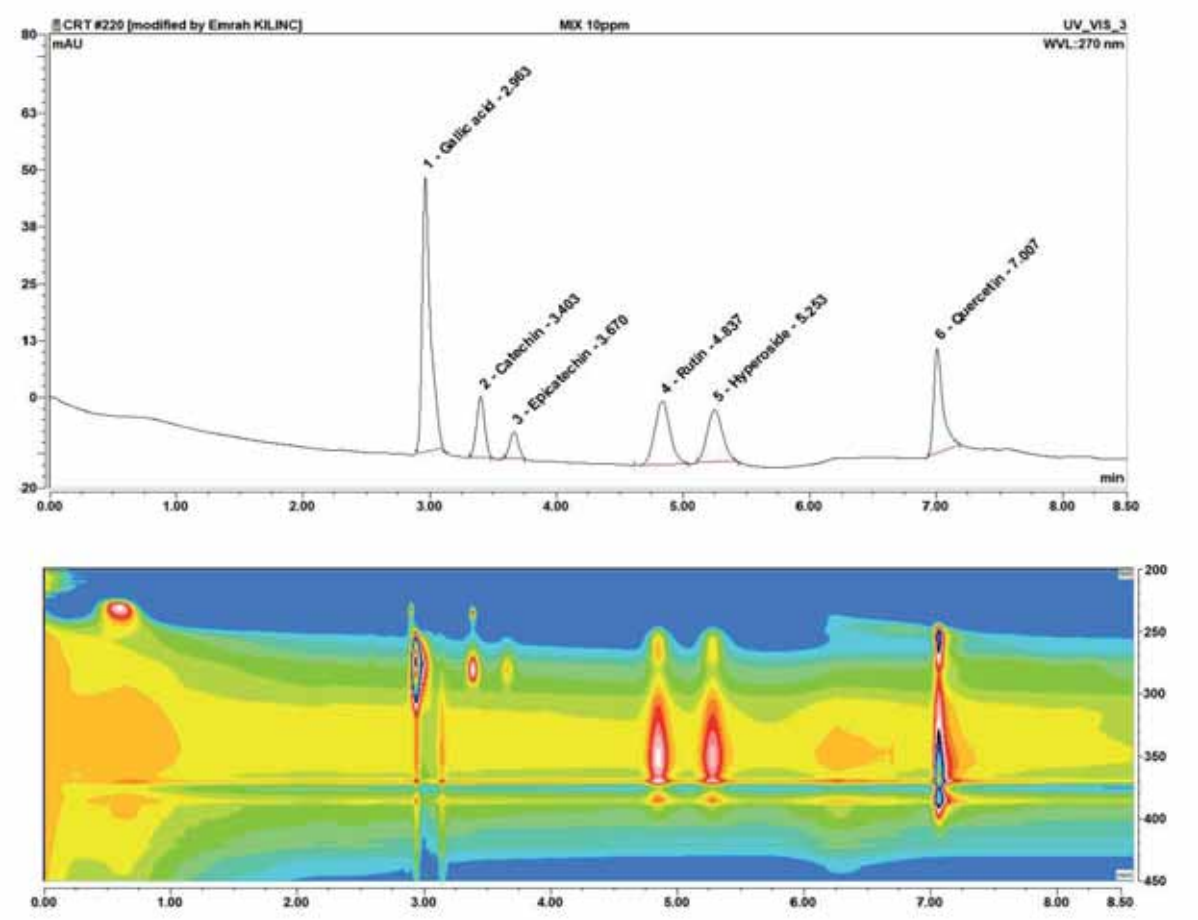


FIGURE 1
Choromatograms of all entire standards

TABLE 2
Antioxidant activity results of *C. monogyna* extracts

Number of Extracts	DPPH* RSA (Inhibition of %)	PRAP (mM Trolox/mg Dry Extract)
CRT-1	39.813 ± 0.873	2.200 ± 0.060
CRT-2	42.582 ± 0.842	2.050 ± 0.052
CRT-3	60.738 ± 0.628	1.700 ± 0.090
CRT-4	48.473 ± 1.041	3.500 ± 0.095
CRT-5	7.600 ±0.711	2.15 ± 0.070
CRT-6	47.924 ± 1.282	2.20 ± 0.044

PRAP of all extracts were examined using phosphomolybdic acid. PRAP of extracts was expressed as mM trolox equivalents (QE). Results for CRT-1 to CRT-6, 2.200 ± 0.060, 2.050 ± 0.052, 1.700 ± 0.090, 3.500 ± 0.095, 2.15 ± 0.070, 2.20 ± 0.044, respectively.

Cell viability assay against H_2O_2-induced toxicity was investigated on SH-SY5Y cells. All extracts showed increased proliferation in 1, 10, 100µg/mL concentrations (Table 3, Figure 2).

The neuroprotective activity was recorded in terms of % cell viability as shown in Table 3. The cell viability in H_2O_2 group was found to be 36.84%±2.88 and all extracts provided higher than 30% neuroprotection against H_2O_2-induced toxicity. The CRT-3 showed the highest neuroprotectivity among all concentrations.

It was found out that flavonoid compounds and oligomeric proanthocyanidins (OPCs), which are the main constituents of *Crataegus* species are responsible for their therapeutic potential. Bioflavonoids include OPCs, vitexin, quercetin and hyperoside. The effect of these compounds on the cardiovascular system has led to the development of commonly used leaf and flower extracts in Europe. Other chemical components found in *Crataegus* species are phenylethylamine (tyramine, isobutylamine, O-methoxy phenylethylamine, choline and acetylcholine), purine derivatives (adenosine, adenine, guanine, caffeic acid and amygdalin), triterpene acids and the components like ursolic acid [24, 44].

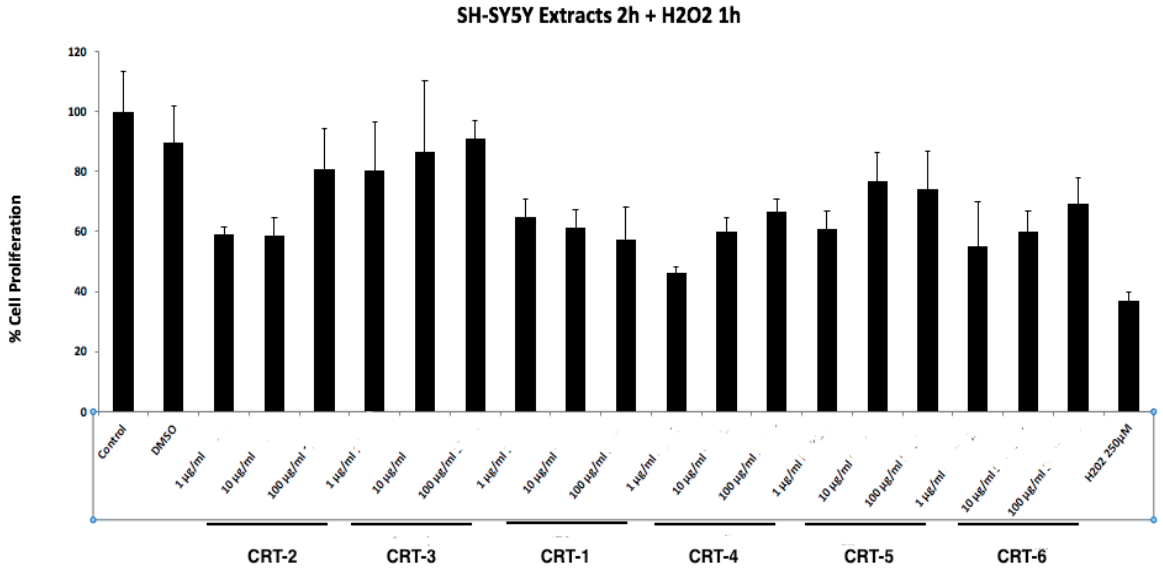


FIGURE 2
Cell proliferation results

*p < 0.05 significant difference from control cells. **p < 0.05 significant difference from H_2O_2-treated cells.
All values are means ± SDs (n = 5).

TABLE 3
Neuroprotective activity results of *C. monogyna* extracts

Compound	Conc. (µg/ml)	% Cell viability	Compound	Conc. (µg/ml)	% Cell viability
Control		**100 ± 13.39**			
DMSO		**89.64 ± 12.24**			
H202	**250µM**	**36.84 ± 2.88**			
CRT-1	1 µg/ml	64.67 ± 6.15	**CRT-4**	1 µg/ml	46.08 ± 2.25
CRT-1	10 µg/ml	61.50 ± 5.72	**CRT-4**	10 µg/ml	60.17 ± 4.42
CRT-1	100 µg/ml	57.31 ± 10.80	**CRT-4**	100 µg/ml	66.67 ± 4.08
CRT-2	1 µg/ml	59.03 ± 2.49	**CRT-5**	1 µg/ml	60.75 ± 6.12
CRT-2	10 µg/ml	58.73 ± 5.83	**CRT-5**	10 µg/ml	76.87 ± 9.69
CRT-2	100 µg/ml	80.79 ± 13.40	**CRT-5**	100 µg/ml	74.06 ± 12.60
CRT-3	1 µg/ml	80.34 ± 16.30	**CRT-6**	1 µg/ml	55.16 ± 14.95
CRT-3	10 µg/ml	86.71 ± 23.41	**CRT-6**	10 µg/ml	60.20 ± 6.80
CRT-3	100 µg/ml	90.94 ± 5.94	**CRT-6**	100 µg/ml	69.44 ± 8.29

In one of the studies, isolation of oligomeric and polymeric proanthocyanidins from acetone-water extract of *Crataegus* species prepared from leaves and flowers was carried out and their existence and structures were evidenced with the help of HPLC, MS and part NMR studies. During the seasonal development of fresh plants of *C. monogyna*, the distribution of procyanidins was monitored. The presence of oligomeric procyanidins is between 20-55 mg/g dry weight in flowers and fruits [45].

Chemical composition of the ethanolic extracts of *C. monogyna* flowers, leaves and fruits determined by GC-MS was evaluated through a survey conducted. The main classes of compounds described were monoterpenes, sesquiterpenes, aliphatic and aromatic aldehydes (benzaldehyde, 3-pyridine carboxaldehyde), ketones, alcohols, and esters (4-methoxybenzoic acid methyl ester) as well as nitrogen-containing compounds [46].

In current literature available there are not many papers published dealing with the HPLC-DAD analysis of *Crataegus* sp. Copra-Janicijevic et al. published a paper focusing on the chemical composition and antioxidant activity of some endemic *Crataegus* species of Bosnia. They have quantified gallic acid, hyperoside and caffeic acid with an isocratic HPLC-ECD method with a mobile phase of methanol-acetonitrile-water-acetic acid (20:10:70:1) and a C18 column with 200x4.6x5µm dimensions at 1.0mL/min flow rate. They have determined gallic acid in the range 0.001-0.04mg/g, which corresponds to a very low gallic acid level of 10^{-6} to $4x10^{-5}$ppm interval. This finding is similar to our findings, in which gallic acid could not be detected in six different samples. Regarding hyperoside, the paper has quantification in a range of

1.04-14.2mg/g or $1.04x10^{-3}$ to 0.0142ppm. This result displays a lower concentration range in comparison to our findings of 4.16 to 22.48ppm range. These differences in results may be due to different origins of the plant, extraction media and ECD detector choice [47].

Zheng et al., described a gradient HPLC-DAD method with a solvent system of trifluoroacetic acid (1%) as MP-A and acetonitrile/methanol (80:20) as MP-B, making separation with 250x4.6mm 5µm dimension C18 analytical column, at a 1.0mL/min flow rate and 280nm. The paper quantified seven phenolic compounds among which only two of them are the same with the current study: epicatechin and hyperoside. The publication analyzed eight plant extracts and could not detect catechin and hyperoside in five of them. They detected epicatechin in entire samples studied. According to their findings catechin was detected in the range 1.04-2.46ppm while epicatechin and hyperoside were determined in the range 0.36-21.3ppm and 0.280.96ppm, respectively. These findings represent lower concentration ranges than the findings of the current study of 1.13-8.95ppm and 4.16-22.48ppm for epicatechin and hyperoside, respectively. Similary, Zheng et al. could not detect catechin in most of their samples while detecting epicatechin in all samples. Additionally, the current study detected hyperoside in all six samples. The differences in quantification may be due to the differences in geographical locations and the extraction method, as Zheng et al. have made *in vitro* digestion rather than ultrasonic extraction and employed pepsin and HCl solution for 1 hour. These rough acidic medium parameters are likely to have reduced the antioxidant phenolic content of the samples [48].

Liu et al., published a HPLC-DAD and LC-MS paper with a solvent system composed of formic acid/water (0.5:99.5) as MP-A and acetonitrile/methanol (80:20) as MP-B and 250x4.6mm 5µm C18 as the analytical column with a flow rate of 1mL/min monitoring at 280nm. Among the studied five phenolic compounds, epicatechin and hyperoside are the common ones with the current study. Liu et al., quantified epicatechin in the range $0.87x10^{-3}$ to $11.72x10^{-3}$ppm, while detecting hyperoside in the range $0.08x10^{-3}$ to $0.80x10^{-3}$ppm. These findings represent very lower concentration ranges than our findings of 1.13-8.95ppm and 4.16-22.48ppm for epicatechin and hyperoside, respectively. These differences may be due to the scale of sample preparation process as they have diluted extracts to 25mL and used a different percent of ethanol in the extraction solvent system i.e. 80% instead of 45% as is the case for the current study. Moreover, the differences in geographical locations may play a significant role contributing to such varying results. Similar to our findings, Liu et al. also detected epicatechin and hyperoside in all their 29 samples studied [49].

Ding et al., have published a gradient HPLC-DAD method with a C18 250x4.6mm 5µm analytical column and a solvent system composed of 0.1% aqueous phosphoric acid solution as MP-A and acetonitrile as MP-B, at a flow rate of 0.9mL/min and monitoring 360nm. Among the six compounds Ding et al. quantified, only epicatechin, rutin and hyperoside are common with the current study. Instead of calculating concentration values, Ding et al. have provided contributions of the peaks to the total peak areas in bar graphs. In all 10 samples the study detected epicatechin in considerable amounts, which is also the case in the current study. Rutin was found in very low levels in only six out of 10 samples. This finding is similar to the results of the current study where we could not detect rutin in our six samples. The study was able to quantify hyperoside in seven out of 10 samples in considerably higher levels than rutin. This study obtained similar results in which hyperoside was detected in all six samples assessed [50].

Rodrigues et al., have also published a gradient HPLC-DAD and LC-MS paper having aqueous formic acid (0.1%) as MP-A and acetonitrile as MP-B with a flow rate of 0.5mL/min monitoring at 280nm. Among the 29 compounds they have identified only epicatechin is common with the current study. They have quantified epicatechin in the range $1.84x10^{-3}$ to $5.19x10^{-3}$ppm which is quite a lower range than the findings of the current study of 1.13 to 8.95ppm in our six samples. These differences may be due to some sample preparation details as a result of stirring at room temperature rather than ultrasonication. Also the extraction solvent system is totally different like methanol/water (80/20) than ethanol/water (45/55). Finally, the differences in geographical locations where plant materials were collected from may play a significant role for the differences again [51].

To evaluate the results of our research; Figure 1 displays a representative 2D chromatogram of a 10ppm mix of the 6 standards. Corresponding retention times for gallic acid, catechin, epicatechin, rutin, hyperoside and quercetin were 2.96, 3.40, 3.67, 4.84, 5.25 and 7.00 min, respectively. All peaks were separated successfully with a resolution of Rs 1.5. Below is the isoplot (3D) chromatogram of the very same standard mixture. Table 1 summarizes the quantification results of the extracts. Findings of the current study shows that samples representing different geographical locations of Turkey own variable epicatechin and hyperoside. Gallic acid, rutin, catechin and quercetin were not detected in all the samples. Remaining epicatechin and hyperoside were detected at various levels in the ranges 3.30-28,39 µg/mL and 249-23.11µg/mL, respectively. Lowest and highest levels for epicatechin were 1.13 and 8.95µg/mL for CRT-6 and CRT3, respectively. Regarding hyperoside, lowest and highest levels were 4.16 and 22.48µg/mL for

CRT-3 and CRT-4, respectively (Figure 1).

In a study by Kumar et al.; various traditional uses of *Crataegus* species are listed worldwide. *C. aronia* leaf and fruit extracts have been found to be used in the treatment of cardiovascular diseases, cancer, diabetes, and reproductive disorders in traditional Arabic medicine. In Mexico, Hawthorn extracts are known for use in treating diabetes. It has been reported that *C. pinnatifida, C. pubescens, C. cuneata, C. laevigata, C. monogyna* and *C. oxyacantha* are used in healing cardiovascular diseases as a folk medicine. *C. phaenopyrum, C. ambigua* and *C. pinnatifida* have been determined to be an edible fruit used to lower plasma lipids in Traditional Chinese Medicine. Current *in vivo* and clinical studies have proven potential cardiovascular enhancing and protective properties of *Crataegus* species [52, 53].

In vivo studies to date have shown that Hawthorn extracts exhibit a wide range of pharmacological properties such as antioxidant, positive inotropic, anti-inflammatory, antithrombocyte, vasodilator, endothelium protective, protective against ischemia/reperfusion injury, anti-arrhythmic, antihyperlipidemic and arterial blood pressure lowering effect. In addition, numerous clinical trials have shown that Hawthorn preparations are highly effective at early stages of congestive heart failure [34].

In another study on Mexican Hawthorn species, conducted with 20 different genotypes, total phenol, flavonoid and vitamin C amounts were determined for 10g of fruit. Antioxidant activity was determined by the DPPH method and expressed as the mean inhibitory concentration (IC_{50}). As a result, Hawthorn fruit has a higher phenolic content comparable to many other fruits. This feature is very important for nutraceutical use [54].

Six extracts prepared by different extraction methods from *C. monogyna* leaves and flowers were examined with TPC, DPPH, FRAP, TBARS, oxymyoglobin in terms of antioxidant activity and showed different levels of antioxidant potential [55].

In this study, % DPPH radical scavenging activity of each extract is given as % inhibition. PRAP assay results are presented as mM Trolox/mg dry extract. There is a correlation between the antioxidant activities of the extracts according to the amount of hyperoside and epicatechin. The CRT-3 extract has the highest epicatechin content and also shows the highest % DPPH inhibition. The CRT-4 extract with the highest hyperoside content also had the highest PRAP value. CRT-5 has the lowest hyperoside content and has the lowest PRAP value (Table 2).

In a study Seung-Hwan et al. investigated whether the neuroprotective effects of chlorogenic acid (CGA) ameliorated learning and memory impairment by a muscarinic antagonist, scopolamine in mice [38]. In addition, in the current study the effects of CGA on AChE, DPPH, a free radical, and thiobarbituric acid reactive substance activity assays were investigated.

In this study, the protective effects of six different extracts were evaluated in cellular oxidative stress model. Human neuroblastoma SH-SY5Y cell line is highly sensitive to oxidants; thus this cell line was used in the current study [42, 43]. Cells were treated with different concentrations (1–1000μM) of H_2O_2 and assayed for cytotoxicity after 1 h incubation. The IC_{50} value of H_2O_2 was found to be 250μM. Hence, this concentration was used for further experiments to induce oxidative stress in SH-SY5Y cells.

To avoid possible toxicity, cells were exposed to three different concentrations of extracts, then their effects on the proliferation of cells were determined. Treatments with selected concentrations alone for 2 h were not cytotoxic and did not alter cell proliferation. Next, SH-SY5Y cells were pre-treated with compounds ranging from 1 to 100μg/ml for 2 h, followed by treatment with 250μM H_2O_2 for 1 h. Cell viability was determined by the MTS assay. Following these experiments, Figure 2 and Table 3 show that selected compounds reduced H_2O_2-induced neuronal death in a dose dependent manner. The cell viability in H_2O_2 group was found to be 36.84%±2.88 and all extracts showed neuroprotection at 100μg/ml; CRT-3, CRT-5 at 10μg/ml; CRT-3 at 1μg/ml concentrations provided higher than 30% neuroprotection against H_2O_2-induced toxicity (Figure 2, Table 3).

Our results show that methodical differences may give varying results and the geographical locations may play a significant role to effect the chemical contents. As a result of this study, we found the highest level of epicatechin in CRT-3, and the highest level of hyperoside in CRT-4. At the same time, CRT-3 was found to be most effective in DPPH activity and CRT-4 was most effective in PRAP activity. In addition, on SH-SY5Y cells, 2.177 epicatechin and 17.436 hyperoside containing CRT-1 at 1μg/ml concentration provided higher than 30% neuroprotection against H_2O_2-induced toxicity.

CONCLUSION

These results show that *C. monogyna* ethanolic extracts are promising in terms of antioxidant and neuroprotective effects. Biological effects may be attributable to the presence of flavonoids in the extracts. CRT-3 has the highest amount of epicatechin, DPPH and possess neuroprotective activity while CRT-4 has the highest amount of hyperoside and exhibits PRAP activity. Our study demonstrates the importance of the flavonoid content in the local *C. monogyna* samples studied and justifies a more

extensive search for regional ethnomedical uses of the genus. It is considered that the obvious differences in the antioxidant and neuroprotective effect levels of different samples may be due to their geographical distributions and flavonoid amounts.

ACKNOWLEDGEMENTS

Authors would like to thank Prof. Dr. A. Ulvi ZEYBEK and Prof. Dr. Bayram YILDIZ for the donation and identification of the plant materials used. Many thanks to Prof. Dr. Raúl Enriquez HABIB for his technical support. This study was financially backed up by Ege University Department of Scientific Research Projects (BAP, Project numbers: 2014-TIP-086, 18/ECZ/006 and 16/ECZ/022) and Ministry of Forestry Project (15.7701) partially.

REFERENCES

[1] Browicz, K. (1972) *Crataegus* L. In: Davis, P.H. (ed.), Flora of Turkey and the East Aegean Islands. 6, Edinburgh University Press, Edinburgh. 133-147.

[2] Christensen, K.I. (1992) Revision of *Crataegus* sect. *Crataegus* and nothosect. Cataeguineae (Rosaceae-Maloideae) in the Old World. In: Anderson, C. (ed.), systematic Botany Monographs. 35. American Society of Plant Taxonomists. United States. 1-199.

[3] Dönmez, A.A. (2004) The genus *Crataegus* L. (Rosaceae) with special reference to hybridisation and biodiversity in Turkey. Turkish Journal of Botany. 28, 29-37.

[4] Kashyap, C.P., Arya, V., Thakur, N. (2012) Ethnomedicinal and phytopharmacological potential of *Crataegus oxyacantha* Linn. -A review. Asian Pacific Journal of Tropical Biomedicine. 2, 1194-1199.

[5] Dönmez, A.A. (2005) A new species of *Crataegus* (Rosaceae) from Turkey. Botanical Journal of the Linnean Society. 148, 245-249.

[6] Dönmez, A.A. (2007) Taxonomic notes on the genus *Crataegus* (Rosaceae) in Turkey. Botanical Journal of the Linnean Society. 155, 231-240.

[7] Özderin, S., Fakir, H., Dönmez, İ.E. (2015) Determination of the volatile components of Hawthorn (*Crataegus orientalis* Pall. Ex M. Bieb.) taxa, which naturally spread in Muğla-Fethiye region. International Journal of Natural and Applied Sciences. 19, 120-123.

[8] Melikoğlu, G., Bitiş, L., Meriçli, A.H. (2004) Flavonoids of *Crataegus microphylla*. Natural Product Research. 18, 211-213.

[9] Özcan, M., Haciseferogullari, H., Marakoglu, T., Arslan, D. (2005) Hawthorn (*Crataegus* spp.) fruit: Some physical and chemical properties. Journal of Food Engineering. 69, 409-413.

[10] Koçyildiz, Z.C., Birman, H., Olgaç, V., Akgün-Dar, K., Melikoğlu, G., Meriçli, A.H. (2006) *Crataegus tanacetifolia* leaf extract prevents L-NAME-induced hypertension in rats: A morphological study. Phytotheraphy Research. 20, 66-70.

[11] Sozer, U., Donmez, A.A., Mericli, A.H. (2006) Constituents from the leaves of *Crataegus davisii* Browicz. Scientia Pharmaceutica. 274, 203-208.

[12] Benli, M., Yig, N., Geven, F., Güney, K., Bingöl, U. (2008) Antimicrobial activity of endemic *Crataegus tanacetifolia* (Lam.) Pers and observation of the inhibition effect on bacterial cells. Cell Biochemistry & Function. 26, 844-851.

[13] Çalişkan, O., Gündüz, K., Serçe, S., Toplu, C., Kamiloğlu, O., Sengül, M., Ercişli, S. (2012) Phytochemical characterization of several hawthorn (*Crataegus* spp.) species sampled from the Eastern Mediterranean region of Turkey. Pharmacognosy Magazines. 8, 16-21.

[14] Özyürek, M., Bener, M., Güçlü, K. (2012) Evaluation of Antioxidant Activity of *Crataegus* species collected from different regions of Turkey. Records of Natural Products. 6, 263-277.

[15] Horvat, R.J., Chapman, G.W., Payne, J.A. (2007) Identification of volatile compounds from ripe mayhaw fruit (*Crataegus opaca, C. aestivalis* and *C. rufula*). Journal of Food Quality. 14(4), 307–312.

[16] Chang, Q., Zuo, Z., Harrison, F., Chow, M.S.S. (2002) Hawthorn. The Journal of Clinical Pharmacology. 42, 605-612.

[17] WHO Monographs on Selected Medicinal Plants (2002) 2, Geneva, 66-82.

[18] Nojima, S., Linn, C.J., Morris, B, Zhang, A., Roelofs, W. (2003) Identification of host fruit volatiles from hawthorn (*Crataegus* spp.) attractive to hawthorn-origin *Rhagoletis pomonella* flies. Roelofs Chemistry and Ecology. 29, 321-36.

[19] Svedstrom, U., Vuorela, H., Kostiainen, R., Laaksoa, I., Hiltunena, R. (2006) Fractionation of polyphenols in hawthorn into polymeric procyanidins, phenolic acids and flavonoids prior to high-performance liquid chromatographic analysis. Journal of Chromatography A. 1112, 103-111.

[20] Holubarsch, C.J., Colucci, W.S., Meinertz, T., Gaus, W., Tendera, M. (2008) Survival and Prognosis: Investigation of *Crataegus* Extract WS 1442 in CHF (SPICE) trial study group. The efficacy and safety of *Crataegus* extract WS 1442 in patients with heart failure: the SPICE trial. European Journal of Heart Failure. 10, 1255-63.

[21] Kovaleva, A.M., Goncharov, N.F., Komissarenko, A.N. (2009) GC/MS study of essential oil components from flowers of *Crataegus jackii, C. robesoniana* and *C. flabellate*. Chemistry of Natural Compounds. 45, 582-584.

[22] Liu, J.L., Yuan, J.F., Zhang, Z.Q. (2010) Microwave-assisted extraction optimised with response surface methodology and antioxidant activity of polyphenols from hawthorn (*Crataegus pinnatifida* Bge.) fruit. The International Journal of Food Science Technology. 45, 2400-2406.

[23] Liu, P., Kallio, H., Lu, D., Zhou, C., Yang, B. (2011) Quantitative analysis of phenolic compounds in Chinese hawthorn (*Crataegus* spp.) fruits by high performance liquid chromatography-electrospray ionisation mass spectrometry. Food Chemistry. 127, 1370-1377.

[24] Edwards, J.E., Brown, P.N., Talent, N., Dickinson, T.A., Shipley, P.R. (2012) A review of the chemistry of the genus *Crataegus*. Phytochemistry. 79, 5-26.

[25] Idris-Khodja, N., Auger, C., Koch, E., Schini-Kerth, V.B. (2012) *Crataegus* special extract WS®1442 prevents aging-related endothelial dysfunction. Phytomedicine. 15, 699-706.

[26] Wu, J., Peng, W., Qin, R., Zhou, H. (2014) *Crataegus pinnatifida*: Chemical constituents, pharmacology, and potential applications. Molecules. 30, 1685-1712.

[27] Hobbs, C., Foster, S. (1990) Hawthorn: A literature review. Herbalgram. 22, 19-33.

[28] Miller, A.L. (1998) Botanical influences on cardiovascular disease. Scientific Review of Alternative Medicine. 3, 422-431.

[29] Rigelsky, J.M., Sweet, B.W. (2002) Hawthorn: Pharmacology and therapeutic uses, Clinical review. American Journal of Health-System Pharmacy. 59, 417-22.

[30] European Pharmacopoeia. (2014) Hawthorn. 8, Council of Europe, Strasbourg, 57-62.

[31] ESCOP Monographs. (2009) Hawthorn. 2, Thieme Verlag, New York, 45-49.

[32] Baytop, T. (1984) Therapy with Medicinal Plants in Turkey. Publications of Istanbul University, Istanbul (in Turkish), 146-147.

[33] Fong, H.H., Bauman, J.L. (2002) Hawthorn. Journal of Cardiovascular Nursing. 16, 1-8.

[34] Wang, J., Xiong, X., Feng, B. (2013) Effect of *Crataegus* usage in cardiovascular disease prevention: An evidence-based approach. Evidence-based Complementary and Alternative Medicine. 16 pp. Article ID 149363.

[35] Zeybek, U., Haksel, M. (2011) Important Medicinal Plants and Their Usage in Turkey and the World. Zade Health Publications, Istanbul. 6-10. (in Turkish)

[36] Li, L.Z., Peng, Y., Niu, C., Gao, P.Y., Huang, X.X., Mao, X.L., Song, S.J. (2013) Isolation of cytotoxic compounds from the seeds of *Crataegus pinnatifida*. The Chinese Journal of Natural Medicines. 11, 411-414.

[37] Valko, M., Leibfritz, D., Moncol, J., Cronin, M.T.D., Mazur, M., Telser, J. (2007) Free radicals and antioxidants in normal physiological functions and human disease. International Journal of Biochemistry & Cell Biology (The International Journal of Biochemistry & Cell Biology). 39, 44-84.

[38] Seung-Hwan, K., Ha-Kyung, L., Ji-Ah, K., Sa-Ik H., Hyoung-Chun, K., Tae-Hyung, J., Young-In, P., Chong-Kil, L., Yong-Bin, K., Seok-Yong, L., Choon-Gon, J. (2010) Neuroprotective effects of chlorogenic acid on scopolamine-induced amnesia via anti-acetylcholinesterase and anti-oxidative activities in mice. European Journal of Pharmacology. 649(1-3), 210-217.

[39] Validation of Analytical Procedures: Text and Methodology; Q2 (R1). (2005) International Conference on Harmonization of Technical Requirements for Registration of Pharmaceutials for Human Use (ICH). 6.

[40] Amarowicz, R., Pegg, R.B., Rahimi-Mog Haddam, P., Barld, B., Weilc, J.A. (2004) Free radical scavenging capacity and antioxidant activity of selected plant species from the Canadian prairies. Food Chemistry. 84, 551- 562.

[41] Prieto, P., Pineda, M., Aguilar, M. (1999) Spectrophotometric quantitation of antioxidant capacity through the formation of a phosphomolybdenum complex: specific application to the determination of vitamin E. Analytical Biochemistry. 269, 337-341.

[42] Sarıkaya, G., Çoban, G., Parlar, S., Tarikogullari, A.H., Armagan, G., Erdoğan, M.A., Alptüzün, V., Alpan, A.S. (2018) Multifunctional cholinesterase inhibitors for Alzheimer's disease: Synthesis, biological evaluations, and docking studies of o/ppropoxyphenylsubstituted-1H-benzimidazole derivatives. Chemistry in Life Sciences. 351(8), 1-18.

[43] Loubid, M., Jouha, J., Tber, Z., Khouili, M., Suzeneta, F., Akssira, M., Erdogan, M.A., Aydın-Köse, F., Dagcı, T., Armagan, G., Saso, L., Guillaumeta, G. (2018) Efficient synthesis and first regioselective C-6 direct arylation of imidazo[2,1-c][1,2,4]triazine scaffold and their evaluation in H2O2-induced oxidative stress. European Journal of Medicinal Chemistry. 145, 113-123.

[44] Verma, S.K., Jain, V., Verma, D., Khamesra, R. (2007) *Crataegus oxyacantha*- A cardioprotective herb. Journal of Herbal Medicine and Toxicology. 1, 65-71.

[45] Hellenbrand, N., Sendker, J., Lechtenberg, M., Petereit, F., Hensel, A. (2015) Isolation and quantification of oligomeric and polymeric procyanidins in leaves and flowers of Hawthorn (*Crataegus* spp.). Fitoterapia. 104, 14-22.

[46] Anca Mot, C., Copolovici, D., Madosa, E., Mot, G. (2016) The chemical composition and pharmaceutical usage of Hawthorn (*Crataegus monogyna* L.) extracts. Journal of Biotechnology. 231, 4-109.

[47] Copra-Janicijevic, A., Culum, D., Vidic, D., Tahirović, A. (2018) Chemical composition and antioxidant activity of the endemic *Crataegus microphylla* Koch subsp. *malyana* K. I. Chr. & Janjić from Bosnia. Industrial Crops and Products. 113, 75-79.

[48] Zheng, G., Deng, J., Wen, L., You, L., Zhao, Z., Zhou, L. (2018) Release of phenolic compounds and antioxidant capacity of Chinese hawthorn "*Crataegus pinnatifida*" during in vitro digestion. Journal of Functional Foods. 40, 76-85.

[49] Liu, P., Kallio, H., Yang, B. (2011) Phenolic compounds in hawthorn (*Crataegus grayana*) fruits and leaves and changes during fruit ripening. Journal of Agricultural and Food Chemistry. 59, 11141-11149.

[50] Ding, X.P., Wang, X.T., Chen, L.L., Qi, J., Xu, T., Yu, B.Y. (2010) Quality and antioxidant activity detection of *Crataegus* leaves using on-line high-performance liquid chromatography with diode array detector coupled to chemiluminescence detection. Food Chemistry. 120, 929-933.

[51] Rodrigues, S., Calhelha, R., Barreira, J., Dueñas, M., Carvalho, A.M., Abreu, R.M., Santos-Buelga, C., Ferreira, I.C.F.R. (2012) *Crataegus monogyna* buds and fruits phenolic extracts: Growth inhibitory activity on human tumor cell lines and chemical characterization by HPLC–DAD–ESI/MS. Food Research International. 49, 516-523.

[52] Kumar, D., Arya, V., Ali Bhat, Z., Khan, N.A., Prasad, D.N. (2012) The genus *Crataegus*: chemical and pharmacological perspectives. Brazilian Journal of Pharmacognosy. 22, 1187-1200.

[53] Long, S.R., Carey, R.A., Crofoot, K.M., Proteau, P.J., Filtz, T.M. (2006) Effect of hawthorn (*Crataegus oxycantha*) crude extract and chromatographic fractions on multiple activities in a cultured cardiomyocyte assay. Phytomedicine. 13, 643-650.

[54] García-Mateos, R., Ibarra-Estrada, E., Nieto-Angel, R. (2013) Antioxidant compounds in Hawthorn fruits (*Crataegus* spp.) of Mexico. Revista Mexicana de Biodiversidad. 84, 1298-1304.

[55] Shortle, E., O'Grady, M.N., Gilroy, D., Furey, A., Quinn, N., Kerry, J.P. (2014) Influence of extraction technique on the anti-oxidative potential of hawthorn (*Crataegus monogyna*) extracts in bovine muscle homogenates. Meat Science. 98, 828–834.

Received: **27.11.2020**
Accepted: **13.05.2021**

CORRESPONDING AUTHOR

Gozde Elgin Cebe
Department of Pharmaceutical Botany,
Faculty of Pharmacy,
Ege University,
Izmir – Turkey

e-mail: gozde.elgin.cebe@ege.edu.tr

© by PSP Volume 30– No. 09/2021 pages 10515-10521 Fresenius Environmental Bulletin

PHYLOGENETIC RELATIONSHIPS OF SOME PARDOSA (LYCOSIDAE) SPECIES

Adile Akpinar[1,*], Aynur Yuncu[1], Derya Arslan[1], James Stuart Lucas[2], Turkan Gurer[1], Muhammed Ismail Varol[3]

[1]Department of Biology, Science and Art Faculty, University of Gaziantep, Turkey
[2]Sabanci University Nanotechnology Research and Application Centre (SUNUM), Sabanci University, Orhanli, Tuzla, Istanbul, Turkey
[3]Bolu Abant Izzet Baysal University, Medicine Faculty, Department of Medicine Biology, Turkey

ABSTRACT

In this study, 3 Pardosa species (*Pardosa proxima* (C. L. Koch, 1847), *P. tatarica* (Thorell, 1875), *P. italica* Tongiorgi, 1966) that have similar genital morphologies were analyzed by using the mitochondrial cytochrome oxidase 1 (COI) gene region. Haplotypes belonging to *P. proxima* and *P. tatarica* populations were determined. *Pardosa proxima* populations were exposed to low intraspecific mutation and exhibited a balancing selection. *P.tatarica* populations had a high mutation rate and an expanding population. The best evolutionary model that includes all samples were identified and a phylogenetic tree containing relationships between haplotypes was created. Similarities between intra and inter species were calculated. Morphologically similar species were found to be molecularly close as well. This findings show that *P. proxima* populations are not affected by environmental factors and their morphological characters are preserved. In *P. tatarica* populations, it was observed that the rate of morphological variation was high and affected by environmental factors.

KEYWORDS:
Lycosidae, Mitochondrial Cytochrome Oxidase I (COI), *Pardosa proxima, P. tatarica, P. italica*

INTRODUCTION

Among the Lycosidae, also known as wolf spiders, Pardosa (C.L.Koch, 1847) is the richest genus within the family. 536 species belonging to this genus were determined globally [1] whereas 36 species [2] have been identified in Turkey. Taxonomic studies on *Pardosa* and other spiders are generally carried out at a morphological level, both Turkey and the world. Species identifications are provided by using morphological taxonomic characters and behaviour [3, 4, 5, 6, 7]. Studies involving species identification in recent years have focused on molecular taxonomy, and universal primers were used to identify species and perform 'DNA barcoding' (8, 9,10, 11, 12, 13, 14, 15, 16]. Cytochrome C oxidase I is a mitochondrial gene region and it is used as a basis for species identifications in the animal kingdom [9]. Similarities of species and populations can be calculated by conducting DNA barcoding studies and phylogenetic studies using this gene region. DNA marker-based studies reveal relationships between taxa and these markers are used to determine genetic diversity [17, 36].

The goal of this paper is to analyse based on mitochondrial cytochrome c oxidase subunit 1 (COI) gene of three species, *Pardosa proxima, P. tatarica* and P. *italica*, which have similar genital morphologies and to calculated their inter- and intra-specific similarities. To contribute to the comparison of Pardosa species in Asian (Turkey) and European continents and to understand whether gene flow continues or not.

MATERIALS AND METHODS

Specimen collections and identifications: Spiders were collected by different methods (i.e. catching by hand, aspiratory and sweeping) between the months of February-October 2014. Specimens were collected from 33 different locations in the province of Gaziantep located in the Southeastern Anatolia Region of Turkey. (Table1). Specimens were stored in tubes containing 96-100% ethyl alcohol in the Zoology Laboratory and museum of the Department of Biology at Gaziantep University. Morphological identifications were based on reference publications on the taxonomy of Palearctic region spiders [18] with species nomenclature following the World Spider Catalog [1]. Specimens of female and male individuals who had complete genitalia development were identified at species level, whereas spiderling specimens could not be morphologically identified on species basis.

DNA extraction, PCR and sequencing: Genomic DNA was extracted from legs using the DNeasyR Blood&Tissue Kit (Qiagen) following the manufacturer's protocol and stored in a -80˚C freezer.

The mitochondrial cytochrome c oxidase subunit 1 (COI), was amplified using forward primer LCO1490 (5'-GGTCAACAAATCATAAAGATATTGG-3') [19] and reverse primer Chelicerate Reverse 2 (5'-GGATGGCCAAAAAATCAAAATAAATG-3') [11]. The PCR amplification was performed in 25 µl reactions with the following final reagent; concentrations; 1 x PCR buffer (2. 5 µl of 10 x stock), 0.2 mM dNTP mix (Qiagen, Cat No./ID: 201223 Taq PCR Core Kit (250 U) (0.5 µl of 10mM stock), 0. 4µM each of forward and reverse primers, Taq Polymerase (Qiagen, Cat No./ID: 201223Taq PCR Core Kit) (0.12 µl). The amount of genomic DNA used as a template was 2 µl for each specimen. The reaction conditions were 95 ˚C for 5 minutes; followed by 35 amplification cycles of 95 ˚C for 30 s, 52 ˚C for 40 s, 72 ˚C for 150 s; and a final elongation step for 10 minutes at 72 ˚C. PCR reactions were carried out in an Eppendorf thermocycler (Proflex).

Amplicons were separated and visualized on 1.5 % agarose gels that were stained with ethidium bromide for 15 min, following electrophoresis (45min, 100 volt). Successful PCR products were purified and then sequenced using both, forward and reverse primers.

TABLE 1
List of specimens investigated in this study, with their identification code and Genbank accession number.

Code/ haplotype	Genus	Species	COI (Genbank number)
P3/H1	*Pardosa*	*proxima* (subadult)	KX159469
P4/H2	*Pardosa*	*proxima* (♀)	KX357775
P8/H3	*Pardosa*	*tatarica* (subadult)	KX357777
P10/H4	*Pardosa*	*proxima* (♀)	KX357778
P11/H5	*Pardosa*	*proxima* (♀)	KX357779
P12/H6	*Pardosa*	*proxima* (subadult)	KX357780
P15/H7	*Pardosa*	*proxima* (♂)	KX357781
P 18/H2	*Pardosa*	*proxima* (♂)	KX357783
P 20/H1	*Pardosa*	*proxima* (♀)	KX357784
P 21/H8	*Pardosa*	*proxima* (♂)	KX357785
P 26/H9	*Pardosa*	*proxima* (♀)	KX388744
P 28	*Pardosa*	*proxima* ♂	Low quality sequence
P 31	*Pardosa*	*proxima* ♂	Low quality sequence
P33/H10	*Pardosa*	*proxima* (♀)	Low quality sequence
P 34/H1	*Pardosa*	*proxima* (subadult)	KX388745
P35/H11	*Pardosa*	*proxima* (♂)	Low quality sequence
P37	*Pardosa*	*proxima* (♀)	Low quality sequence
P38/H12	*Pardosa*	*proxima* (♀)	KX388746
P39	*Pardosa*	*proxima* (♀)	Low quality sequence
P43/H13	*Pardosa*	*tatarica* (subadult)	KX388748
P44/H14	*Pardosa*	*tatarica* (♂)	KX388749
P47/H1	*Pardosa*	*proxima* (subadult)	KX388752
P49	*Pardosa*	*proxima* (♂)	Low quality sequence
P50/H15	*Pardosa*	*tatarica* (subadult)	KX388753
P 52	*Pardosa*	*proxima* ♂	Low quality sequence
P 53	*Pardosa*	*proxima* (subadult)	Low quality sequence
P54/H16	*Pardosa*	*italica* (♀)	KX388755
P55/H5	*Pardosa*	*proxima* (subadult)	KX388756
P56/H17	*Pardosa*	*tatarica* (subadult)	KX388757
P57/H18	*Pardosa*	*proxima* (♀)	KX388758
P58	*Pardosa*	*proxima* (♀)	Low quality sequence
P 59/H19	*Pardosa*	*proxima* (♀)	KX388759
P 64	*Pardosa*	*proxima* (♂)	Low quality sequence
P79/H20	*Pardosa*	*tatarica* (♀)	KX388760

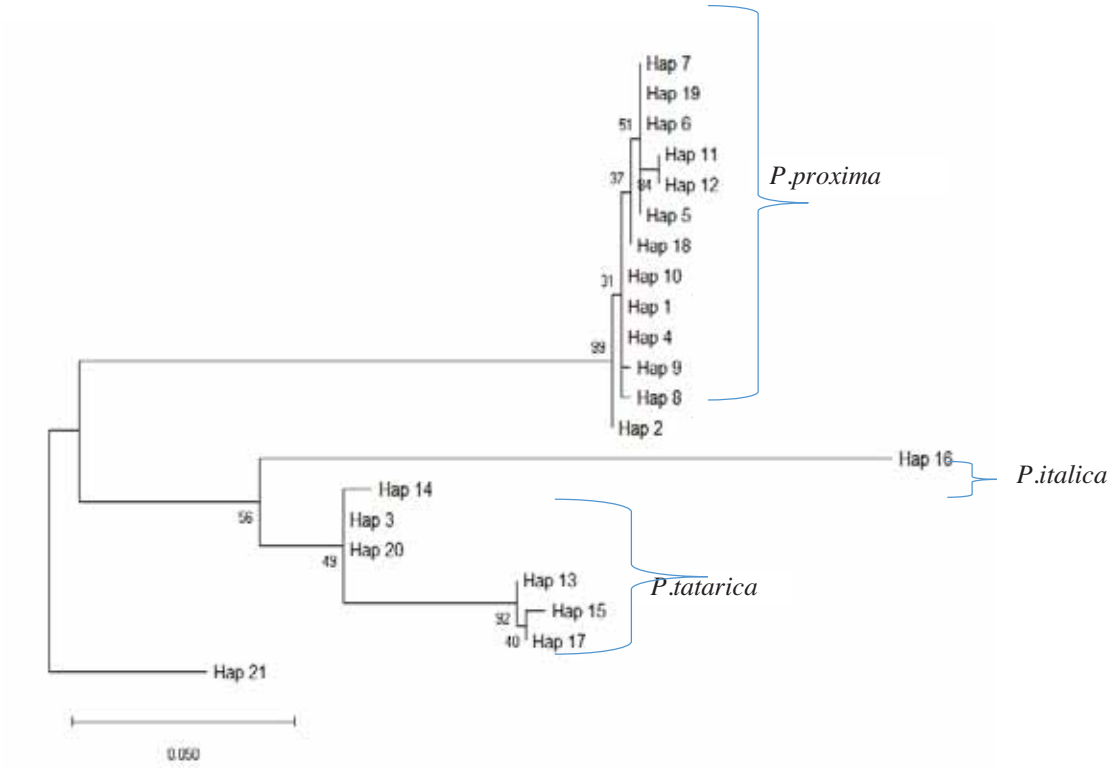


FIGURE 1
The evolutionary history was inferred by using the Maximum Likelihood method and Tamura-Nei model for the haplotypes of Pardosa species.
(Hap21: Pardosa hortensis (JN310132.1) determined as the outgroup).

Data Analyses: Primarily, sequences were viewed as chromatograms using the FinchTV (www.geospiza.com) program. Sequences were manually corrected with SeqTrace 0.9.0 [20] by adding forward and reverse primers. DNA sequences were send to Genbank and barcode numbers (Genbank numbers) were taken (Table1). Some sequences were not included in the following stages as they were not deemed high quality (<450-500bp).

Multiple alignments of sequences with Bioedit 7.2.5 [21] was performed using the Clustal W Multiple Alignment program [22].

In order to easily analyse the *Pardosa* specimens that were subjected to multiple sequencing, haplotypes of the specimens were created using DnaSP 5.10 [22] and 20 haplotypes were identified. The universal model determined as TN93+G by using the MegaX software [23, 24]. Based on this evolutionary model, a tree containing similarities between haplotypes was created (Figure 1).

TABLE 2
Tajima's D and Fu's Fs values of Pardosa proxima, P. tatarica.

Species	Tajima D	Fu'Fs
P.proxima	0,079	-0,90
P.tatarica	-0,54	2,68

In addition, the median joining network (network 5.03) was drawn to observe the gene flow between populations of the species (Figure 2) .In order to evaluate the equilibrium status of the populations, Fu's Fs test [25] and Tajima testi s D test [26] (Table 2), which are neutrality tests, were performed (DnaSP ver.5.10 software [22]).

The three species (*P.proxima, P. tatarica* and P. *italica*) belonging to the genus Pardosa were evaluated both morphologically and molecularly. 25 DNA sequence data of the species were analyzed according to mitochondrial cytochrome oxidase 1 gene region. A phylogenetic tree was created describing the relationships between species. *P. proxima* have a cosmopolitan distribution as it can live in moist, rocky and arid environments. Within the scope of this study, the highest number of specimens belonged to *P. proxima*, and intra specific pairwise distance value was calculated to be 0.005 for the species according to the K2 parameter and Gamma distribution (using MegaX). Considering the fact that the intra specific similarity ratio was less than 3% in calculations with respect to the cytochrome c oxidase 1 gene region, i.e. the mitochondrial barcode gene, and that the inter specific similarity ratio is 10-25% [9] in spiders, the observed intra specific similarity ratio was particularly low. *Pardosa italica* is not very common both globally and in Turkey [27, 18], and as with other *Pardosa* species lives in grassland areas. P.

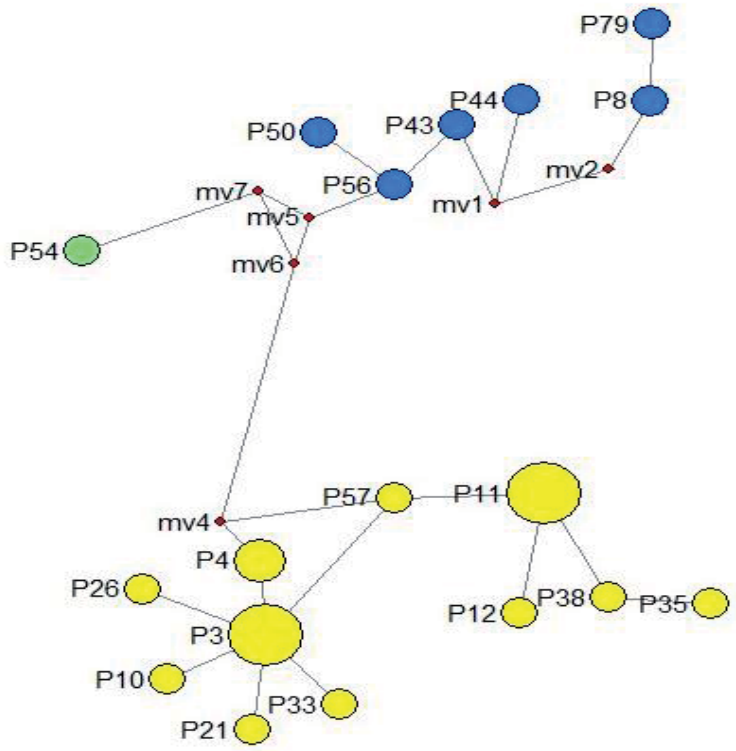


FIGURE 2
Network containing Pardosa species (P.proxima; (yellow) P4 (+P18)-P3 (+P20, P34, P47)-P21-P26-P33-P11(+P15,P55,P59)-P57-P35-P38; P.italica;(green) P54; P.tatarica; (blue) P43-P8-P44-P50-P56-P8-P79).

tatarica lives in grassland, moist and open habitats. The species is distributed in Turkey, Iran, Southern Europe, Ukraine and Caucasus [1]. The inter specific similarity ratio of these species included in the study was determined to be 0.12 on average with respect to the interspecific similarity ratio p-dist value. Accordingly, this result is consistent with the similarity ratios reported in the literature [9, 16].

In the network analysis, specimens of *P. proxima* showed a star-like structure with expansion. This indicates that gene flow continues between populations, the relationship between individuals continues and genetic drift continues. It is seen that individuals belonging to *P. tatarica* species are not fully segregated and populations are still interacting. *P. italica* is represented by a single sample (Figure 2).

Tajima's D test (Tajima, 1989) tests the deviation of populations from the standard neutral model. Statistically, when $p < 0.05$, the meaningful interpretation of the natural diversity is that the population is undergoing demographic expansion, due to population fluctuations and the change in the expected S and π parameters [28]. When $p > 0.05$, the number of rare variations in the population is low and the population can be interpreted as being passed through a bottleneck [28]. In this paper, Tajima's D values on taxon basis (Table 2), it was found that P. proxima populations were exposed to very low intraspecific mutation. This ($p > 0.05$) indicates that the populations are in neutral balance and the number of rare variations is low [28]. Populations do not increase exponentially. Negative values obtained in P. tatarica populations are interpreted as an indicator that the individuals are exposed to high levels of mutations. In addition, negative values (-0. 54) indicate a rapid increase in population [29]. In order to evaluate the equilibrium status of the populations, Fu's Fs test [25] which are neutrality tests, were performed (DnaSP ver.5.10 software [22]). Meaningful results described as $Fs < 0$ indicated that the population is expanding, while $Fs > 0$ represents the origin of the population in case of lack of allele selection pressures or exceed the bottleneck [30]. According to these tests, while P. italica populations are passing through a bottleneck, *P. proxima* populations show spread (Table2).

As seen on the tree, While *P.proxima* is similar to *P. tatarica*. The mutations observed in *P. tatarica* and *P proxima* samples are specified on the network. Mutations observed in the network show changes in P. *tatarica. P. italica* is a single example and morphologically similar to *P. tatarica. P. italica* was selected as the out group in the tree drawing.

The molecular phylogeny of the Lycosidae family is analyzed by using different nuclear and mitochondrial genes [31,5, 32]. The monophyly of the wolf family is supported by behavioral, morphological and molecular characters [33, 34]. While the family is often evaluated according to morphological characters, there is still considerable discussion over which characters are synapomorphic [32]. Analyses

made with COI data from, the *Pardosa* species strongly supported the assumption of these forming a monophyletic group [16]. In our study, NJ Phylogenetic tree data including 3 species support this result.

DISCUSSION

In this study, *Pardosa proxima, P. tatarica* and *P. italica* were analyzed molecularly for the first time and DNA sequences belonging to specimens were added to Genbank. The identification of the members of *Pardosa proxima* and *Pardosa tatarica* is not easy due to intraspecific variability of the epigyne and similarity palps in all members. It is very likely that these species were all or in part misidentification. In particularly, the deformed genital structure can cause misdiagnosis of the species. Identification of species using the COI gene region in animals both prevents misidentification and contributes to the identification of intra-species and relationships between species.

However, the ability to compare data between species was limited due to a lack of sequence in Genbank for *Pardosa* taxa found in Turkey's neighbors. This study is important to compare *Pardosa* species in Asian and European continents and to understand gene flow. The results of this research serve as a reference for subsequent molecular taxonomic studies on *Pardosa*. We think that more biological data on *Pardosa* can be increase evolutionary hypotheses. In the following period, nucleotide base length polymorphism studies can be conducted to reveal the species with high similarity ratios, and to perform intra specific studies on *Pardosa* species.

ACKNOWLEDGEMENTS

The authors are grateful to Gaziantep University, Department of Scientific Research Projects (Project number: F.E.F. 14.05) for financial support.

REFERENCES

[1] World Spider Catalog (2021). World Spider Catalog. Version 22.0. Natural History Museum Bern, online at http://wsc.nmbe.ch (Accessed on 04.2021).

[2] Danışman, T., Kunt, K.B. and Özkütük, R.S. (2021). The Checklist of the Spiders of Turkey. Version 2019, Online at http://www.spidersofturkey.info. (May-2021).

[3] Dondale, C.D., Redner, J.H. (1990). The Insects and Arachnids of Canada, Part 17. The Wolf Spiders, Nurseyweb Spiders, and Lynx Spiders of Canada and Alaska, Araneae: Lycosidae,Pisauridae and Oxyopidae. Research Branch, Agriculture Canada, Publication. 1856, 383.

[4] Töpfer-Hofmann, G., Cordes, D. and Helversen, O.V. (2000). Cryptic Species and Behavioural Isolation ın the Pardosa lugubris Group (Araneae, Lycosidae), with Description of two New Species. Bulletin of the British Arachnological Society. 11, 257-274.

[5] Murphy, N.P., Framenau, W.V., Donnellan, S.C., Harvey, M.S., Park, Y.C. and Austin, A.D. (2006). Phylogenetic Reconstruction of the Wolf Spiders (Araneae: Lycosidae) Using Sequences from the 12SrRNA, 28SrRNA, and NADH1 Genes: Implications for Classification, Biogeography, and the Evolution of Web Building Behavior. Molecular Phylogenetics and Evolution. 38, 583-602.

[6] Bayram, A., Efil, L. and Deltshev, C. (2009). Pardosa roscai (Roewer, 1951), A Spider New to the Fauna of Turkey (Araneae: Lycosidae). Turkish Journal of Zoology. 33, 463-467.

[7] Akpinar, A. and Varol, M.İ. (2013). Contributions to the Turkish Wolf Spiders (Arachnida: Lycosidae). Acta Zoologica Bulgarica. 65, 271-272.

[8] Hebert, P.D.N., Cywinska, A., Ball, S.L. and Dewaard, J.R. (2003a). Biological Identifications through DNA Barcodes. Proceeding of Royal Society London B (Biological Sciences). 270, 313-321.

[9] Hebert, P.D.N., Ratnasingham, S. and Dewaard, J.R. (2003b). Barcoding Animal Life: Cytochrome C Oxidase I Divergences among Closely Related Species. Proceeding of Royal Society London B (Biological Sciences). 70, 96-99.

[10] Arnedo, M.A., Coddington, J., Agnarsson, I. and Gillespie, R.G. (2004). From A Comb to Tree: Phylogenetic Relationships of the Comb-Footed Spiders (Araneae,Theridiidae) İnferred from Nuclear and Mitochondrial Genes. Molecular Phylogenetic and Evolution. 31, 225-245.

[11] Barrett, R.D.H. and Hebert, P.D.N. (2005). Identifying Spiders through DNA Barcodes. Canadian Journal of Zoology. 83, 481-491.

[12] Chang, J., Song, D. and Zhou, K. (2007). Incongruous Nuclear and Mitochondrial Phylogeographic Patterns in Two Sympatric Lineages of the Wolf Spider Pardosa astrigera (Araneae:Lycosidae) From China. Molecular Phylogenetic and Evolution. 42, 104-121.

[13] Blagoev, G.A., Nikalova, N.I., Sobel, C.N., Hebert, P.D.N. and Adamowicz, S.J. (2013). Spiders (Araneae) of Churchill, Manitoba: DNA Barcodes and Morphology Reveal High Species Diversity and New Canadian Records. BMC Ecology. 13, 1-17.

[14] Astrin, J.J., Höfer, H., Spelda, J., Holstein, J., Bayer, S., Hendrich, L. and Monje, J.C. (2016). Towards a DNA barcode reference database for spiders and harvestmen of Germany. PloS One. 11, e0162624.

[15] Coddington, J.A., Agnarsson, I., Cheng, R.C., Čandek, K., Driskell, A., Frick, H. and Pipan, M. (2016). DNA barcode data accurately assign higher spider taxa. Peer J. 4, e2201.

[16] Breitling, R. (2019). Barcode Taxonomy at the Genus Level. Ecologica Montenegrina. 21, 17-37.

[17] Aladadi, W., Moustafa, M.F. and Alruman, S.A. (2018). Genetic Variability among Seven Cultivars of Date Palm (Phoenix dactylifera L.) Based on Embryonic DNA of Old Fruit, Kuwait Journal of Science. 45, 108-114.

[18] Nentwig, W., Blick, T., Bosmans, R., Gloor, D., Hänggi, A., Kropf, C. (2021) Spiders of Europe. Version {no. of month}.2021. Online at https://www.araneae.nmbe.ch, (Accessed on {04.2021}.)

[19] Folmer, O., Black, M., Hoeh, W., Lutz, R. and Vrijenhoek, R. (1994). DNA Primers for Amplification of Mitochondrial Cytochrome C oxidase subunit I from Diverse Metazoan Invertebrates. Molecular Marine Biology and Biotechnology. 3, 294-299.

[20] Stucky, B.J. (2012). SeqTrace: A Graphical Tool for Rapidly Processing DNA Sequencing Chromatograms. Journal of Biomolecular Techniques. 23, 90-93.

[21] Hall, T.A. (1999). BioEdit: A User-Friendly Biological Sequence Alignment Editor and Analysis Program. Nucleic Acids Symposium Series. 41, 95-98.

[22] Thompson, J.D., Higgins, D.G. and Gibson, T.J. (1994). Clustalw: Impoving the Sensitivity of Progressive Multiple Sequence Alignment through Sequence Weighting, Position-Specific Gap Penalties and Weight Matrix Choice. Nucleic Acids Research. 22, 4673-4680.

[23] Rozas, J., Librado, P., Sanchez-Del Barrio, J.C., Messeguer, X. and Rozas R. (2010). DnaSP Version 5. http://www.ub.edu/dnasp (Accessed date: 04.2009)

[24] Nei, M., Kumar, S. (2000) Molecular Evolution and Phylogenetics. Oxford University Press, Oxford. 333.

[25] Kumar, S., Stecher, G., Li, M., Knyaz, C. and Tamura, K. (2018). MEGA X: Molecular Evolutionary Genetics Analysis across Computing Platforms. Molecular Biology and Evolution. 35, 1547-1549.

[26] Fu, Y.L. (1997). Statistical Test of Neutrality of Mutations against Population Growth, Hitch Hiking and Back Ground Selection. Genetics. 147, 915-925.

[27] Tajima, F. (1989). The Neutral Mutation Hypothesis By DNA Polymorphism. Genetics. 123, 585-595.

[28] Demir, H., Seyyar, O. (2017). Annotated Checklist of the Spiders of Turkey. Munis Entomology & Zoology. 12, 433-469.

[29] Hasan, A.U., Suguri, S., Fujimoto, C., Itaki, R.L., Harada, M., Kawabata, M. and Albino, B. (2008). Genetic diversity in two sibling species of the Anopheles punctulatus group of mosquitoes on Guadalcanal in the Solomon Islands. BMC Evolutionary Biology. 8, 318.

[30] Stephens, J.C., Schneider, J.A., Tanguay, D.A., Choi, J., Acharya, T., Stanley, S.E. and Duan, J. (2001). Haplotype variation and linkage disequilibrium in 313 human genes. Science. 293, 489-493.

[31] Li, Y.L., Kong, X.Y., Yu, Z.N., Kong, J., Ma, S. and Chen, L.M. (2009). Genetic Diversity and Historical Demography of Chinese Shrimp Fenneropenaeus Chinensis in Yellow Sea and Bohai Sea Base on Mitochondrial DNA Analysis. African Journal of Biotechnology. 8, 1193-1202.

[32] Piacentini, L.N. and Ramírez, M.J. (2019). Hunting the Wolf: A Molecular Phylogeny of the Wolf Spiders (Araneae, Lycosidae). Molecular Phylogenetics and Evolution. 136, 227-240.

[33] Planas, E., Fernández-Montraveta, C. and Ribera, C. (2013). Molecular Systematics of the Wolf Spider Genus Lycosa (Araneae: Lycosidae) in the Western Mediterranean Basin. Molecular Phylogenetics and Evolution. 67, 414–428.

[34] Polotow, D., Carmichael, A. and Griswold, C.E. (2015). Total Evidence Analysis of the Phylogenetic Relationships of Lycosoidea Spiders (Araneae, Entelegynae). Invertebrate Systematics. 29, 124–163.

[35] Cheng, D.Q., Piel, W.H. (2018). The Origins of the Psechridae: Web-building Lycosoid Spiders. Molecular Phylogenetics and Evolution. 125, 213-219.

[36] Akpınar, A., Mammadova, R. (2020). Genetic Population Structures Based on the Coi Gene of Bassaniodes pseudorectilineus (Araneae: Thomisidae). Entomological News. 129(3), 217-229.

Received: **09.12.2020**
Accepted: **02.05.2021**

CORRESPONDING AUTHOR

Adile Akpinar
Department of Biology,
Science and Art Faculty,
University of Gaziantep
Gaziantep – Turkey

e-mail: aozdemir@gantep.edu.tr

© by PSP Volume 30– No. 09/2021 pages 10522-10529 Fresenius Environmental Bulletin

EFFECTS OF DIFFERENT HARVEST TIMES AND LEAF POSITIONS ON STEVIOL GLYCOSIDES CONTENT IN *Stevia rebaudiana* BERTONI UNDER MEDITERRANEAN CLIMATE CONDITIONS

Kenan Turgut[1,*], Mustafa Karhan[2], Ahmet Hacioglu[2], Melis Yildiz[2], Narin Unal[3]

[1]Department of Field Crops, Faculty of Agriculture, Akdeniz University, Antalya, Turkey
[2]Department of Food Engineering, Faculty of Engineering, Akdeniz University, Antalya, Turkey
[3]Guney Agripark R&D Centre, Camkoy District, 21024 Str. No: 89/1 Aksu, Antalya, Turkey

ABSTRACT

The leaves of the stevia (*Stevia rebaudiana* Bertoni) plant, a perennial plant from the Asteraceae family, contain glycosides such as Stevioside, Rebaudioside A, B, C, D, E and Dulcoside A, which are sweeter than sucrose. However, among these glycosides, Stevioside (Stv) and Rebaudioside A (Reb A) give the plant the main sweetening properties. Especially, the higher the amount of Reb A in the leaves, the higher the sweetener quality of the products. This sweetener is known to be 200-300 times sweeter than sugar. Since the sweetener obtained from the stevia does not need insulin secretion during digestion, it can be used by diabetics. It is also preferred in diet products due to its zero-calorie feature. Adaptation studies carried out in Antalya conditions have shown that stevia can be cultivated perennially. It is important to know the change of Reb A amount and Reb A / Stv ratio, which are very important for the sweetener quality of the stevia leaves, according to the plant's development period (ontogenetic) and the position of the leaves in the plant. In order to determine the most suitable harvest time, trial samples were taken on 20 July, 5 August, 20 August, 5 September and 20 September 2020 and the amounts of Reb A and Stv were determined. Also, Reb A and Stv analyses were performed in the lower, middle and upper leaf samples on the same plant. It is found that the 4th harvest time (September 5th) is superior to other harvest times in terms of both high leaf yield and high SGs amount in Antalya conditions. At this harvest date, Reb A / Stv ratio, which is important for leaf quality, was found to be high as well. On the other hand, the change in Reb A / Stv ratios in lower, middle and upper leaves at different harvest times was found to be significant.

KEYWORDS:
Stevia rebaudiana, Harvest times, Leaf positions, Rebaudioside A, Stevioside

INTRODUCTION

Stevia rebaudiana Bertoni is herbaceous plant in the form of a perennial shrub from the Asteraceae family. The origin of the plant is Paraguay, and it is still cultivated in countries such as China, India, Taiwan, Thailand, Korea, Brazil, Mexico, Singapore, Indonesia and Malaysia [1]. Plant is included in the positive plants list since 2004 and steviol glycosides (SGs) were allowed to use as a sweetener in Turkey in 2013 [1]. The leaves of the stevia plant have natural sweetening properties due to the SGs it contains. The dry leaves of the plant are 20-30 times sweeter than sugar, and its extract is 200-300 times sweeter and has zero calories [2, 3]. Although plant extracts have been used in Japan since 1968 as a low-calorie sweetener in the food industry and in the treatment of diabetes in medicine, they have now become known all over the world. The findings obtained as a result of studies examining the effect of stevia extracts on human health have shown that the long-term and regular consumption of SGs by humans is safe [4, 5, 6]. Today, extracts; In addition to fruit juices, carbonated beverages, cakes, marmalade, chocolate, confectionery, ice cream, chewing gum, yoghurt, it also finds a common use in products such as toothpaste and mouthwash.

The sweet compounds found in stevia leaves are in the structure of diterpene glycosides and are called steviol glycosides (SGs). Different diterpene glycoside known as stevioside, rebaudioside A, B, C, D, E and dulcosides A, B have been identified [7]. These glycosides generally accumulate in the leaves and their amount can vary from 10% to 20% of the leaf dry weight. The amount of these ingredients that cause sweetness varies according to the variety and growing conditions. SGs yield of stevia plants are determined by their concentrations in plant parts and plant biomass; The growth of plants and biomass accumulation are significantly affected by environmental conditions [8]. The main phenological factor affecting the SGs content in the stevia plant is flowering, which is determined by day length and temperature [9], and the best time to harvest leaves is at

the beginning of flowering when steviol glycosides reach their highest level [10].

The demand for the stevia plant is increasing rapidly every year and it is estimated that it will enter the global products in the next ten years. Turkey's position particularly due to the export potential of the EU countries is also quite high. For this reason, stevia agriculture should be widespread in a planned manner in the Mediterranean climate conditions and products with market value should be produced.

The period when the plants are at the beginning of flowering is recommended as the most suitable harvest date for stevia. As stevia is a short-day plant, flowering starts from the first week of September in Antalya conditions. Therefore, this period is known as the suitable harvest period for Stevia. In this research, it was aimed to determine the most suitable harvest period for a registered stevia variety Levent 93, in Antalya coastal (Mediterranean climate) conditions. In addition, the lower, middle and upper leaves of the plants were harvested separately in different periods and the changes of SGs were investigated.

MATERIALS AND METHODS

Plant material. All field experiments were carried out in Guney Agripark R&D Centre in Antalya, Turkey. *Stevia rebaudiana* Levent 93 registered variety, which was improved at the Guney Agripark R&D Centre, was used as the trial material. Plant leaf samples were taken from plants in their third year under field conditions. Those plants were obtained from *in vitro* propagated seedlings and were grown in Antalya Kursunlu locality (119 m above sea level and 37^0 03' N; 30^0 51' E), where the Mediterranean climate prevails and Mediterranean Red Soil (Terra-Rosa) conditions. This location is characterised by a Mediterranean climate with an average total rainfall of 1062 mm and a minimum, maximum, and mean air temperature of 13.8 ^{0}C, 24.2 ^{0}C and 18.8 ^{0}C, respectively. Mediterranean climate has relatively mild winters and very warm summers. Terra-Rossa type soil characteristics of the experimental field were clay loam, with high amounts of lime, little salt, low organic matter and slightly alkaline. The stevia plots were irrigated with drip irrigation, and the weed control was done by hoeing. During the development period of the plants, 120 kg/ha nitrogen and 40 kg/ha phosphorus were given by drip irrigation.

Plants to be used in the experiment were selected from the trial plot where the land and plants were homogeneous. In this context, six plants were randomly selected and harvested at 5 different harvest times (20 July, 5 August, 20 August, 5 September, 20 September). The height of the plants was measured just before harvest. The harvested plants are divided into 3 equal parts from bottom to top and divided into lower, middle and upper leaves. The leaf samples were then dried at room temperature. Average dry leaf yield per plant was calculated by weighing the dried leaves.

Harvest times and plant development stages. 1st harvest - 20 July (Plants were in vegetative development period)

2nd harvest - 5 August (Plants were in vegetative development period)

3rd harvest - 20 August (Plants were in late vegetative development period)

4th harvest - September 5 (Plants were in the flower budding period)

5th harvest- 20 September (Plants were in blooming period)

HPLC analysis of steviol glycosides. Dry stevia leaves were crushed with a laboratory grinder (Waring, USA) and diluted 10 times by weight with ultrapure water and kept in a water bath at 40 ^{0}C for 30 minutes. Then, it was centrifuged at 2900xg force for 30 minutes at room temperature, and the clear part was first filtered through coarse filter paper and then through 0.45 µm porous membrane filter. Steviol glycoside distribution was determined under isocratic conditions using HPLC and external standard method [11]. In the analysis, the HPLC system (Shimadzu, LC 20 AD, Japan) was used with Nucleodur MN C18ec column (5 µm, 250 x 4.6 mm, ID) and SPD-M20 A (PDA-Photodiode Array) detector system. A mixture of acetonitrile (HPLC grade) and sodium phosphate buffer (pH 2.6) (32:68) was used as mobile phase. Mobile phase flow rate was determined as 0.8 mL / min, sample injection volume as 10 µl and column temperature as 40 ^{0}C. Chromatograms were obtained at 210 nm wavelength and the amount of steviol glycosides were determined quantitatively with the aid of a standard curve (Figure 1).

Statistical analyses. SAS statistical software (SAS Institute, Cary, NC, USA) was used for the data analysis. Analysis of variance was used to detect differences followed by the Duncan multiple comparison test. $P < 0.05$ was considered statistically significant.

RESULTS AND DISCUSSION

Effects of harvest times on plant height and dry leaf yield. Average plant height according to harvest times significantly increased from early harvest to late harvest (Table 1, Figure 2). Differences between the harvest times in terms of plant height were found to be statistically important. The highest plant height (97,00 cm) was obtained from the 5th harvest (20 September) and followed by the 4th harvest (90,50 cm). First harvest (20 July) gave the lowest value as 54,83 cm (Table 1). Similarly, dry leaf weights per plant were increased significantly as the

harvest was delayed. Dry leaf yield was 21,00 g per plant on the first harvest date, 30,33 g at the 2nd harvest, 32,66 g at the 3rd harvest, 42,83 g at the 4th harvest and 45,83 g at the 5th harvest. Differences between 2nd and 3rd harvests and between 4th and 5th harvests were not found statistically important. As a result, dry leaf yield increased two-fold from the 1st harvest to the 4th and 5th harvest (Table 1). These results are consistent with previous findings showing that the optimal timing for the Stevia harvest in terms of biomass yield is before flower onset [8, 9, 12]. Similarly, Tansı et al. [13] reported that the pre-flowering period is suitable for high yield of dry leaves in Cukurova conditions in Turkey. These data showed that dry leaf yield should also be considered in determining the appropriate harvest time for stevia.

TABLE 1
Plant height (cm) and dry leaf yield per plant (g / plant) according to harvest times

Harvest Times	Plant height (cm)	Dry leaf yield (g/plant)
1. Harvest (20 July)	54,83e	21,00c
2. Harvest (5 August)	66,16d	30,33b
3. Harvest (20 August)	73,33c	32,66b
4. Harvest (5 September)	90,50b	42,83a
5. Harvest (20 September)	97,00a	45,83a

Means within a column followed by different letters are statistically significant at $P \leq 0.01$ level

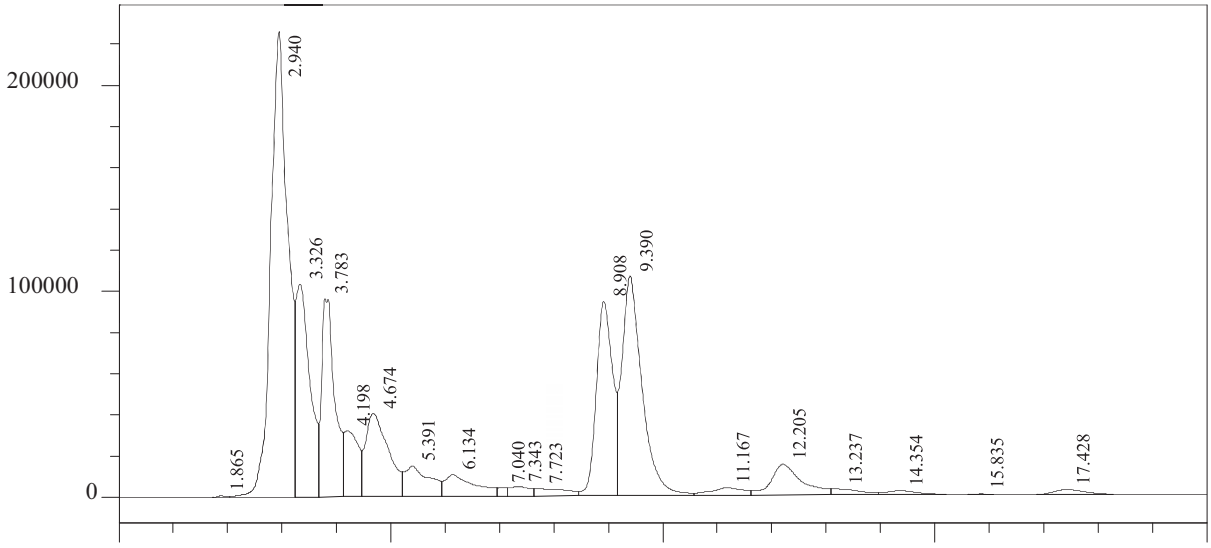


FIGURE 1
Sample chromatogram showing the distribution of steviol glycosides in dry leaf (Reb A: 8.908 mins: Stv: 9.390 mins, Reb C: 12.205 mins).

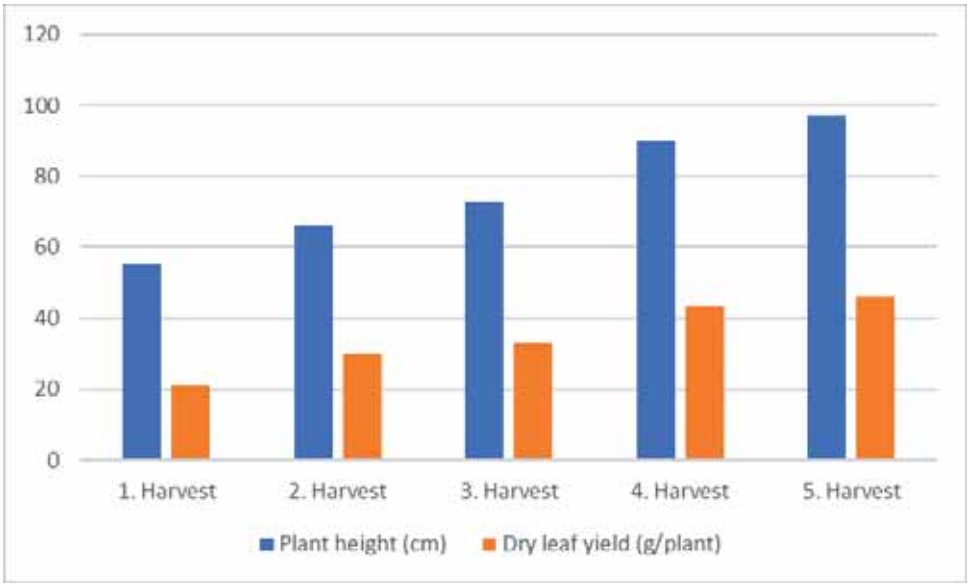


FIGURE 2
Plant height (cm) and dry leaf yield per plant (g / plant) according to harvest times.

Effects of harvest times on Reb A and Stv amounts in the leaves. HPLC analysis results obtained from dry leaves are summarized in Table 2. The findings show that there are significant differences in SGs contents of leaves at different harvest times (20 July, 5 August, 20 August, 5 September, 20 September). When the harvest times are compared, it is clearly understood that the 4th harvest time (September 5th) is superior to the other harvest times (Table 2, Figures 3 and 4). The highest average Reb A (102.19 g / kg) and average total SGs (218.91 g / kg) and a high average Reb A / Stv ratio (0.87) were obtained from 4th harvest. On the other hand, the 5th harvest date (20 September) gave the lowest amounts in all average values except the average Reb A / Stv ratio. In the fifth harvest, the average amount of Reb A decreased to 82.50 g / kg, the average Stv amount to 90.12 g / kg, and the average total SGs amount to 172.63 g / kg. As can be seen from the table, the Reb A amount, which was 102.19 g / kg in the 4th harvest, decreased to 82.50 g / kg in the 5th harvest, and the total SGs amount decreased from 218.91 g / kg to 172.63 g / kg and this corresponds to a 20% reduction in Reb A and total SGs values. On the other hand, the average Reb A / Stv ratio was found to be as high as 0.91 at the 5th harvest. As can be seen from the data, a delay of 15 days in harvest causes significant reduction of SGs content in leaves. Similarly, Serfaty et al. [8] reported that the optimum harvest time for high Stv yield in Israeli conditions is the beginning of September before flowering. In this context, due to the increase in the Stv / dry leaf ratio from June to September, the highest Stv yield was obtained in September. Tavarini and Angelini [12] observed that Reb A / Stv ratio in stevia leaves increased from July to September under Italian conditions. The decrease in diterpene glycosides after the onset of flowering has been attributed to several factors, such as the presence of aged dry leaves containing very low SGs [14], and a decrease in leaf biomass due to the generative period [15].

TABLE 2
Amount of SGs according to harvest time.

	Reb A (g/kg)	Stv (g/kg)	TSG (g/kg)	Reb A/Stv
1st Harvest	93,88c	112,17b	206,06b	0,84c
2nd Harvest	89,75d	116,26a	206,02b	0,77d
3rd Harvest	97,37b	116,57a	213,95a	0,83c
4th Harvest	102,19a	116,71a	218,91a	0,87b
5th Harvest	82,50e	90,12c	172,63c	0,91a

Means within a column followed by different letters are statistically significant at $P \leq 0.01$ level.

In the second harvest time (5 August), the Reb A / Stv ratio of 0.77, which are important for leaf quality, was lower than the other harvest dates (Table 2, Figure 3). At the first harvest (20 July), especially the Reb A amount (93.88 g / kg) and the Reb A / Stv ratio (0.84) were higher than the 2nd harvest date but remained behind the 4th and 5th harvest times. When all the results are evaluated, it is understood that the 4th harvest date (September 5), when the plants begin to bud, is the most suitable harvest date for a quality leaf harvest in Mediterranean climate conditions.

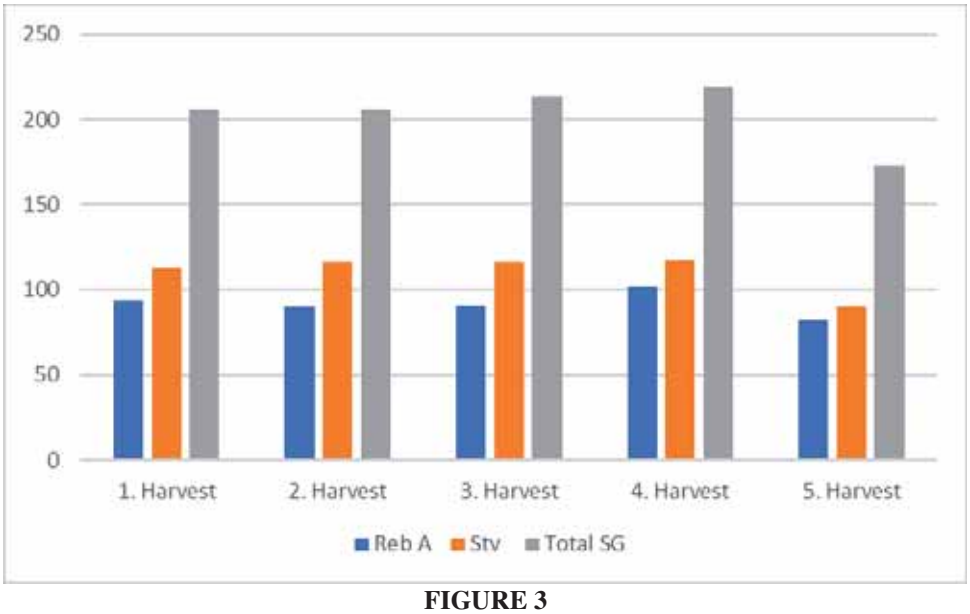


FIGURE 3
Amounts of SGs (Reb A and Stv) according to harvest times (g/kg).

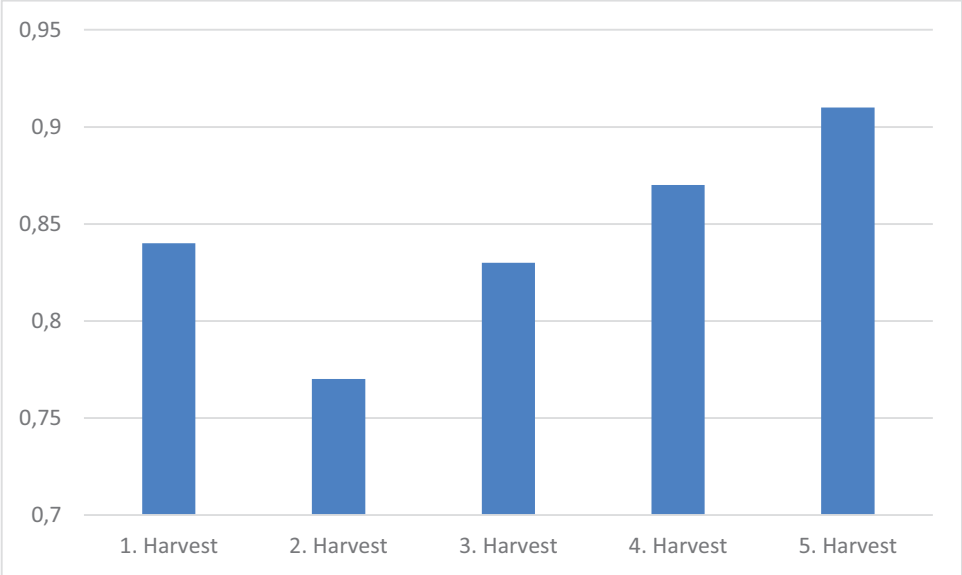


FIGURE 4
Reb A / Stv ratios according to harvest times.

Effects of leaf positions on Reb A and Stv amounts in the leaves at different harvest times. Significant differences were found in the amount of SGs when lower, middle and upper leaves were examined regardless of harvest times (Table 3). Amount of Reb A and Reb A /Stv ratio were found higher in the upper (93.75 g / kg and 0.88) and middle leaves (95.22 g /kg and 0.87), while amounts of Stv (115.04 g / kg) and TSGs (205.49 g /kg) were higher in the lower leaves. Lower leaves gave the highest amount of TSG due to high Stv content. After all, the amount of Reb A and Reb A / Stv ratio, which are very important for leaf quality, were found low in the lower leaves (Table 3). This finding can be taken into consideration in quality leaf harvesting. Bhakta and Ganjewala [16] reported that younger leaves were more active in biosynthesis and accumulation of secondary metabolites (phenolics, pro-anthocyanidins and flavonoids) than mature leaves in *Lantana camara*. They concluded that leaf ontogeny affects the biosynthesis and accumulation of secondary metabolites and thereby their biological properties. However, in the present study, amounts of Reb A and Stv varied differently according to leaf positions. This may be due to the fact that Stv is the precursor of reb A in the SGs biosynthesis pathway [17]. Variation in antioxidant contents and activities in leaves from the top to the base of three basil species (*Ocimum* spp.) were examined [18]. Sweet basil (*O. bacilicum*) leaves were rich in flavonoids from the top and middle regions. In contrast, the bottom leaves of lemon basil had the highest DPPH scavenging activity while the middle leaves had the highest activity of ferrous ion chelation.

When the SG amounts in lower, middle and upper leaves are examined according to harvest times, the highest Reb A (108.78 g / kg), Stv (122.62 g / kg) and TSGs (231.40 g / kg) amounts were found in the 4th harvest in the middle leaves (Table 4, Figure 5). On the other hand, the highest Reb A / Stv ratios were found in the upper and lower leaves (0.93 and 0.94) in the 5th harvest (Table 4, Figure 6). The lowest Reb A values were obtained from 3rd harvest lower leaves (93.28 g / kg) and 5th harvest middle leaves (73.84 g / kg); The lowest Stv amount (85.03 g / kg) and TSGs amount (158.87 g / kg) were obtained from the 5th harvest middle leaves. The lowest Reb A / Stv ratio (0.71) was found in the 1st harvest lower leaves (Table 4, Figure 6).

TABLE 3
Amount of SGs according to leaf positions.

	Reb A (g/kg)	Stv (g/kg)	TSGs (g/kg)	Reb A/Stv
Upper Leaves	93,75a	106,74c	200,50b	0,88a
Middle Leaves	95,22a	109,32b	204,55ab	0,87a
Lower Leaves	90,45b	115,04a	205,49a	0,79b

Means within a column followed by different letters are statistically significant at $P \leq 0.01$ level.

At the first harvest time (20 July), the highest Reb A amount (104.56 g / kg) was obtained from middle leaves, while the highest Stv amount (121.92 g / kg) was obtained from lower leaves (Table 4, Figure 5). Middle leaves also gave the highest TSGs (218.39 g / kg) and Reb A / Stv (0.91) values. The lowest Reb A / Stv ratio (0.71) was obtained from the lower leaves (Table 4, Figure 6). In the first harvest, middle leaves are important especially for amount of Reb A.

At the second harvest (August 5), the highest Reb A amount (93.39 g / kg) and TSGs amount

TABLE 4
Amounts of SGs in upper, middle and lower leaves at different harvest times (g/kg).

	Amount of Dry Leaf SGs (g/kg)							
	Reb A	Std. Dev.	Stv	Std. Dev.	TSGs	Std. Dev.	Reb A / Stv	Std. Dev.
1-U	89,45	1,68852	100,77	0,60132	190,23	1,55302	0,88	0,01946
1-M	104,56	2,72886	113,82	0,94750	218,39	3,25936	0,91	0,02173
1-L	87,64	1,42789	121,92	1,87798	209,57	3,30489	0,71	0,00086
Mean	93,88	8,13132	112,17	9,17237	206,06	12,54700	0,84	0,09296
2-U	93,39	8,16192	118,25	2,32735	211,64	9,29675	0,78	0,06504
2-M	91,04	1,76837	108,76	1,93577	199,81	3,34110	0,83	0,01337
2-L	84,82	1,67133	121,77	2,21043	206,60	3,83953	0,69	0,00411
Mean	89,75	5,83407	116,26	6,06454	206,02	7,50226	0,77	0,07019
3-U	100,94	4,31944	114,70	1,77144	215,64	6,08422	0,87	0,02418
3-M	97,91	1,67718	116,37	1,79010	214,28	3,40932	0,84	0,00523
3-L	93,28	1,27254	118,65	1,33546	211,93	2,59664	0,78	0,00261
Mean	97,37	4,13726	116,57	2,25322	213,95	4,20274	0,83	0,04217
4-U	97,74	4,96213	106,28	3,07412	204,02	7,83273	0,91	0,02524
4-M	108,78	7,00212	122,61	8,86669	231,39	15,82072	0,88	0,01249
4-L	100,07	0,47838	121,25	2,15556	221,32	2,24492	0,82	0,01497
Mean	102,19	6,69062	116,71	9,22043	218,91	15,02493	0,87	0,04398
5-U	87,25	0,71297	93,73	1,27961	180,98	1,56188	0,93	0,01368
5-M	73,84	5,12225	85,03	4,41723	158,87	9,51577	0,86	0,01690
5-L	86,43	5,22505	91,60	5,40110	178,03	10,50398	0,94	0,01700
Mean	82,50	7,47146	90,12	5,35537	172,63	12,65896	0,91	0,03748
U	93,75	6,70248	106,74	9,35869	200,50	14,47073	0,88	0,05961
M	95,22	13,13412	109,32	13,89077	204,55	26,74085	0,87	0,03376
L	90,45	6,18600	115,04	12,36857	205,49	15,72667	0,79	0,09056
Mean	93,14	9,29528	110,37	12,32190	203,51	19,54795	0,84	0,07542

1 (July 20), 2 (August 5), 3 (August 20), 4 (September 5), 5 (September 20); U (upper leaves), M (middle leaves), L (lower leaves); Std. Dev. (standart deviation).

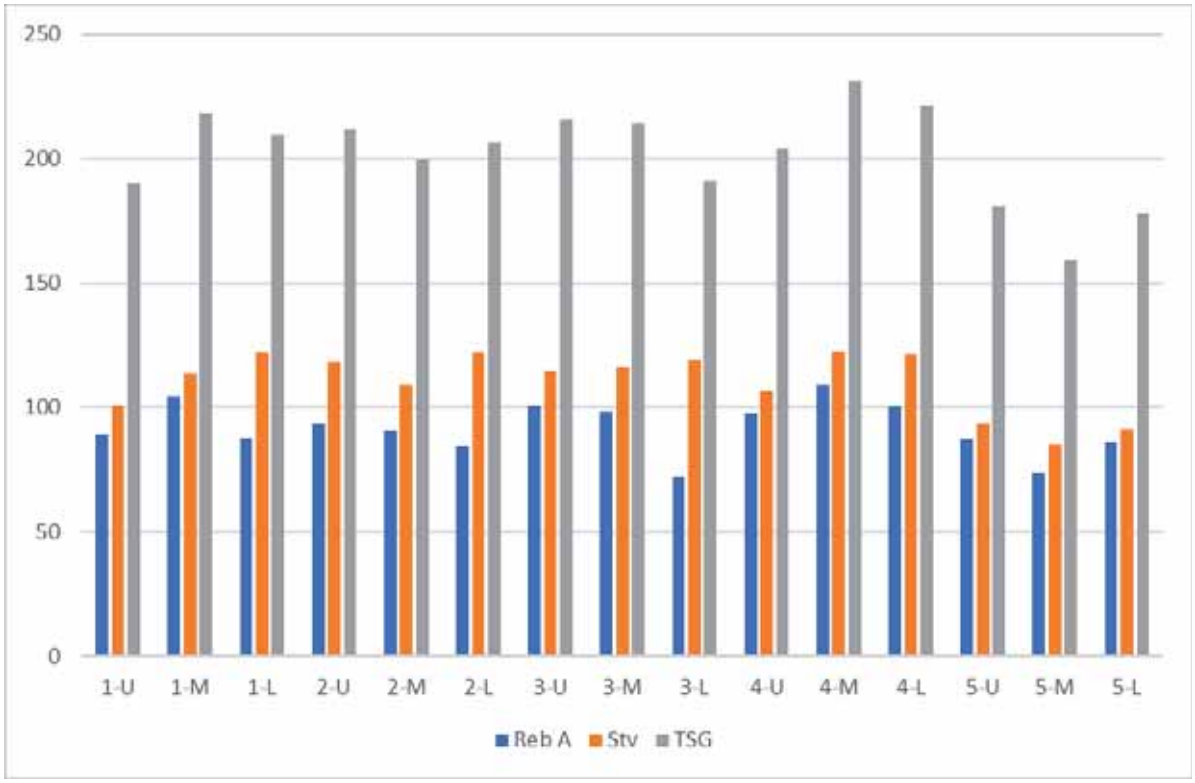


FIGURE 5
Amounts of SGs in upper (U), middle (M) and lower (L) leaves at different harvest times (g/kg).

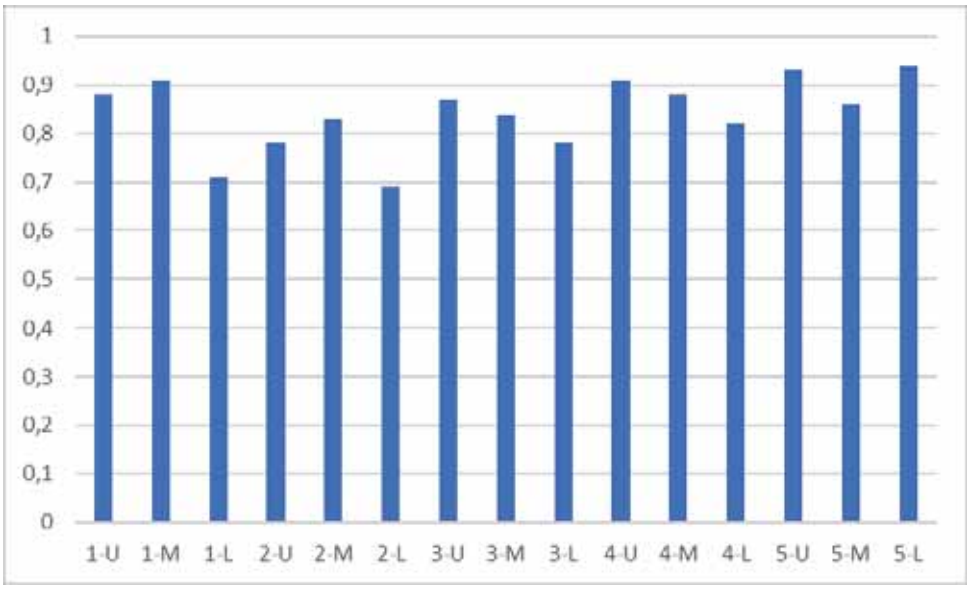


FIGURE 6
Reb A/Stv ratios in upper (U), middle (M) and lower (L) leaves at different harvest times.

(211.64 g / kg) were obtained from the upper leaves, while the highest Stv amount (121.77 g / kg) was obtained from the lower leaves. (Table 4, Figure 5). Middle leaves gave the highest (0.83) Reb A / Stv ratio, while lower leaves gave the lowest (0.69) Reb A / Stv ratio (Table 4, Figure 6).

At the third harvest time, the amount of Reb A was determined as 100.94 g / kg in the upper leaves and 93.28 g / kg in the lower leaves. On the other hand, although the amount of Stv did not show a significant change, it was found higher in the lower leaves (118.65 g / kg) compared to the upper leaves (114.70 g / kg) in contrast to the amount of Reb A. Lower leaves gave very low values (211.93 g / kg and 0.78, respectively) in terms of TSGs amount and Reb A / Stv ratio (Table 4, Figures 5 and 6).

At the fourth harvest time, the highest amounts of Reb A (108.78 g / kg), Stv (122.61 g / kg) and TSGs (231.39 g / kg) were obtained from middle leaves (Table 4, Figure 5). On the other hand, upper leaves gave the lowest amounts of Reb A (97.74 g / kg), Stv (106.28 g / kg) and TSGs (204.02 g / kg), and the highest (0.91) Reb A / Stv ratio. The lower leaves revealed the lowest (0.82) Reb A / Stv ratio (Table 4, Figure 6).

At the 5th harvest time, middle leaves had the lowest Reb A (73.84 g / kg), Stv (85.03 g / kg), TSGs (158.87 g / kg) and Reb A / Stv ratio (0.86) (Table 4, Figures 5 and 6). The highest Stv amount (93.73 g / kg) and TSGs amount (180.98 g / kg) were taken from the upper leaves. In addition, the upper and lower leaves draw attention with high Reb A / Stv ratios (0.93 and 0.94) in the 5th harvest (Table 4, Figure 6).

CONCLUSIONS

It was understood that the 4th harvest time (September 5th) was superior to other harvest times in terms of both high leaf yield and high SG amount in the Mediterranean climate conditions. At this harvest date, Reb A / Stv ratio, which is important for leaf quality, was found to be high. On the other hand, significant losses occurred in yield and quality in early harvest dates; the delay in the harvest has greatly reduced the leaf quality. These results support that a single harvest should be made in early September under Mediterranean climate conditions. On the other hand, the change in Reb A / Stv ratios in lower, middle and upper leaves at different harvest times was found to be significant. Lower leaves yielded the lowest Reb A / Stv ratio at harvest dates except for the last harvest (September 20).

ACKNOWLEDGEMENT

Statistical analyses were done by Akdeniz University Statistical Consultancy Application and Research Centre.

REFERENCES

[1] Turgut, K., Ucar E., Tutuncu B., Ozyigit Y. (2015) *Stevia rebaudiana* Bertoni could be an alternative crop in the Mediterranean Region of Turkey. Proceedings of the 8th Stevia Symposium. 43-52.
[2] Geuns, J. (2003) Stevioside. Phytochemistry. 64, 913-921.

[3] Singh, S.D., Rao, G.P. (2005) Stevia: The herbal sugar of 21st century. Sugar Tech. 7, 17-24.
[4] Koyama, E., Sakai, N., Ohori, Y., Kitazawa, K., Izawa, O., Kakegawa, K., Fujıno, A., Ui, M. (2003) Absorption and metabolism of glycosidic sweeteners of stevia mixture and their aglycone, steviol, in rats and humans. Food and Chemical Toxicology. 41, 875-883.
[5] Maki, K., Curry, L., Reeves, M., Toth, P., Mckenney, J., Farmer, M., Schwartz, S., Lubin, B., Boileau, A., Dicklin, M. (2008) Chronic consumption of rebaudioside A, a steviol glycoside, in men and women with type 2 diabetes mellitus. Food and Chemical Toxicology. 46, 47-53.
[6] Wheeler, A., Boileau, A., Winkler, P., Compton, J., Prakash, I., Jiang, X., Mandarino, D. (2008) Pharmacokinetics of rebaudioside A and stevioside after single oral doses in healthy men. Food and Chemical Toxicology. 46, 54-60.
[7] Yadav, A.K., Singh, S., Dhyani, D., Ahuja, P.S. (2011) A review on the improvement of stevia [*Stevia rebaudiana* (Bertoni)]. Canadian Journal of Plant Science. 91, 1-27.
[8] Serfaty, M., Ibdah, M., Fischer, R., Chaimovitsh, D., Saranga, Y., Dudai, N. (2013) Dynamics of yield components and stevioside production in *Stevia rebaudiana* grown under different planting times, plant stands and harvest regime. Industrial Crops and Products. 50, 731-736.
[9] Brandle, J.E., Rosa, N. (1992) Heritability for yield, leaf:stem ratio and stevioside content estimated from a landrace cultivar of *Stevia rebaudiana*. Can. J. Plant Sci. 72, 1263–1266.
[10] Kang, K.H., Lee, E.W. (1981) Physio-ecological studies on stevia (*Stevia rebaudiana* Bertoni). Korean J. Crop Sci. 26, 69-89.
[11] Shimadzu (2012) Analysis of Steviol Glycosides in Stevia Extract. Available at: https://manualzz.com/doc/8660437/l439-application-news-no (Accessed date: 25 February 2021).
[12] Tavarini, S., Angelini, L.G. (2013) *Stevia rebaudiana* Bertoni as a source of bioactive compounds: the effect of harvest time, experimental site and crop age on steviol glycoside content and antioxidant properties. J. Sci. Food Agric. 93, 2121-2129.
[13] Tansı, L.S., Samadpourrigani, E., Gedik, S., Soltanbeigi, A. (2017) Effects of different plant density and cutting Times on yield of Stevia under the Çukurova conditions. International Journal of Secondary Metabolite. 4, 355-358.
[14] Kalandia, A., Papunidze, G., Vanidze, M., Papunidze, S. (2004) HPLC of Stevia (*Stevia rebaudiana* Bertoni) diterpene glycosides. Bull. Georgian Acad. Sci. 169, 147–150.
[15] Kienle, U. (2010) Which stevia would you like? Cultivation and manufacturing perspectives worldwide. J. Verbrauch. Lebensm. 5, 241–250 (in German).
[16] Bhakta, D., Ganjewala, D. (2009) Effect of leaf positions on total phenolics, flavonoids and proanthocyanidins content and antioxidant activities in *Lantana Camara* (L). Journal of Scientific Research. 1(2), 363-369.
[17] Brandle, J.E., Telmer, P.G. (2007) Steviol glycoside biosynthesis. Phytochemistry. 68, 1855-1863.
[18] Wongsen, W., Bodhipadma, K., Noichinda, S., Leung, D. W. M. (2013) Relationship between leaf position and antioxidant properties in three basil species. International Food Research Journal. 20, 1113-1117.

Received: **30.04.2021**
Accepted: **06.06.2021**

CORRESPONDING AUTHOR

Kenan Turgut
Department of Field Crops
Akdeniz University
Antalya 07058 – Turkey

e-mail: kturgut@akdeniz.edu.tr

© by PSP Volume 30– No. 09/2021 pages 10530-10534 Fresenius Environmental Bulletin

RESEARCH ON THE COORDINATED DEVELOPMENT MODEL OF ECOLOGICAL RESOURCES AND ECONOMY IN CHANGCHUN CITY

Hongxiu Cui[1], Wei Wang[2,*]

[1]Changchun Sci-Tech University, Jilin Changchun, 130600, China
[2]Shenyang Institute of Technology, Liaoning Shenyang 113122, China

ABSTRACT

Urbanization, industrialization, and informatization are the three components of today's social and economic development, and they are of great significance. Informatization drives industrialization to a certain extent, and industrialization promotes urbanization. At the same time, urbanization is the realization carrier of informatization and industrialization. Promoting the modernization of the entire society is also an important strategy for my China's economic development. This research takes Changchun city as the research object and the coordinated development mode of ecological resources and economy as the research content. Based on the analysis of urban ecological economy, the AHP method is used to construct the ecological and economic index evaluation system. This paper evaluates the sustainable development of Changchun's ecological economy, thus providing guidance and reference value for promoting the construction of Changchun's urban ecological economy.

KEYWORDS:
Ecosystems, Economy, Evaluation index

INTRODUCTION

With the rapid development of China's economy, the level of urbanization advances by leaps and bounds, the regional expansion of urban scale and the continuous increase of urban population cause the imbalance of urban ecosystem [1-4]. In the process of urbanization, how to take the scientific development concept as the theoretical guidance, take building a resource-conserving and environment-friendly city development as the goal, set up reasonable economic development strategy and industry configuration planning, so as to realize the harmonious development of urban society, economy and environment, which is one of the important problems need to solve in the process of the urbanization [5-8].

Eco-economic city, which includes urban economy, environment and society, is a brand new urban development mode including life and production. While accelerating urban development, it organically combines society, economy, people, resources and environment [9-12]. The main features are:

(1) The essential feature of an eco-economic city is the harmony between society, economy and ecological environment, including harmony between human and human, between human and nature, as well as between society and economy;

(2) Break through the development model of traditional cities, and make urban economic operation and resource utilization more efficient;

(3) The sustainable development model guided by the concept of scientific development [13-15].

As one of China's traditional heavy industry cities, Changchun's ecosystem health is not optimistic, and the ecological pressure is increasing day by day. It is mainly manifested in two aspects:

(1) Due to the long-term predatory management and development of the ecosystem, the per capita arable land area is gradually decreasing. Urban development, energy development and transportation occupy a large amount of land, resulting in conflicts between resource supply and economic development. At the same time, due to the discharge of domestic waste and the use of pesticides and fertilizers, it has an impact on the urban ecological environment;

(2) With the ever-increasing population of Changchun City, human needs and the limited capacity of the natural environment, contradictions between rural and urban areas, have caused a certain degree of threat to the ecological health of Changchun City.

MATERIALS AND METHODS

Research area. Changchun, abbreviated as "Chang", was called Xidu and Huanglong Mansion in ancient times, and also known as "Northland Spring City". It is the capital, sub-provincial city, and core city of Changchun urban agglomeration of Jilin Province. Industrial Base. As of June 19, 2020, the city has 7 districts, 1 county, and 3 county-level cities under its jurisdiction, with a total area of 24,662

square kilometers, a registered population of 8.544 million, an urban population of 4.451 million, and an urbanization rate of 59 %. The results of the second national land survey show that the total area of the city is 20,604 square kilometers.

Changchun is located in Northeast China, in the geographic center of Northeast China, the central city of the Northeast Asian Economic Circle, bordering Songyuan City, Siping City, Jilin City and Harbin City respectively. It is a famous Chinese old industrial base and the earliest automobile industry in New China. The base and film production base are also the cradle for the development of the new China railway passenger car, photoelectric technology, applied chemistry, biological products and other industries. The famous China First Automobile Group Co., Ltd., CRRC Changchun Railway Vehicle Co., Ltd., and Changchun Film Studio, Changchun Institute of Optics, Fine Mechanics and Physics, Chinese Academy of Sciences, Changchun Institute of Applied Chemistry, Chinese Academy of Sciences, Changchun Institute of Biological Products.

Changchun is a national historical and cultural city with many historical sites, industrial heritages and cultural relics; it is also one of the four major garden cities in China, and enjoys the reputation of "Northern Spring City". Its greening rate is among the top Asian cities; it is also a pilot for "Made in China 2025" Cities, "the first batch of national urban design pilot cities", ranked among the top 50 in the world and the top 10 in China in the "Natural Index 2018-Research Cities".

Research methods. Research and analysis is conducted through questionnaires, literature analysis.

Model selection. Coordinated development degree model is studied.

RESULTS AND DISCUSSION

Research on the coordinated development model of ecological resources and economy in Changchun city. Analysis on the framework of urban ecological economic development model. According to the urban characteristics of Changchun and the development status of economic and social environment, the framework of urban ecological economic development model is set as two aspects of development stage and different types of development.

Development pattern design principles. Adhere to the principle of coordination between economic benefits, ecological benefits and social benefits to promote the virtuous circle of economy, environment and society; At the same time, we should adhere to the principle of paying equal attention to ecological environment protection and development. Based on the present and focusing on the future, we should adhere to the principle of subordinating local interests to overall interests and combining current interests with long-term interests. Adhere to the principle of combining ecological environment construction with the improvement of human living environment.

Development model framework. Stage development mode: adopt the point axis development mode, along the axis of the key lines, equipped with new growth points, so that it becomes an ecological economic city, which promotes the construction of urban ecological economic system more vigorously than the point mode; Using network development model at the same time, the Changchun high levels of industrialization, dense population and ecology economy industry, infrastructure is perfect, at this point, the ecological economic city already has a certain scale, but need to adjust the traditional economy, diffusion and transfer of part of the traditional industry, focus on developing high-tech companies and emerging industries, gradually formed on the space system of urban network.

Development framework of type model: Regional model and ecological resources and economic construction are adopted to carry out demonstration and experimental work rather than comprehensive spread out. According to different regions of Changchun, demonstrative construction of Chaoyang District with strong economic strength is carried out, and its development speed has great influence on surrounding areas.

Construction of urban ecological economy evaluation model. Determination of index weight. According to the importance of all kinds of indicators, AHP method is used to construct judgment matrix, general ranking of levels, consistency test and other steps through the hierarchical structure to calculate the direct relative importance of social population, economic development and ecological environment and the relativity of each factor's influence on sustainable development in the indicators under its ownership. The calculation method is shown in (1) and (2). The weight of a factor in a certain year is W_i, and the weight change of i factor in a certain year is ΔW_i.

$$W_i = W_{ni} + \Delta W_i \quad (1)$$

$$\Delta W_i = (\mathrm{I}_i / \sum_{i=1}^{j} I_i - \mathrm{W}_{ni} / \sum_{i=1}^{j} W_{ni}) / \mathrm{j} \ldots . (\mathrm{i} = 1,2,3 \ldots, \mathrm{j}) \ldots (2)$$

TABLE 1
Evaluation result data table.

Year/ Index	2010	2011	2012	2013	2014	2015	2016	2017
Eco-economic system	0.096	0.25	0.215	0.205	0.26	0.4	0.44	0.55
Ecological social system	0.249	0.42	0.41	0.36	0.31	0.66	0.55	1.05
Eco-environmental system	0.372	0.49	0.455	0.57	0.34	0.4	0.6	0.61
Ecological civilization system	0.21	0.26	0.22	0.28	0.3	0.37	0.62	0.55
Sustainable development capacity	0.5	0.74	0.69	0.76	0.6	0.95	1.11	1.44

Data normalization processing. Normalization processing of data is the most important step before the calculation of indicators. Data from different dimensions are normalized to eliminate the influence of dimensions. The calculation method is as follows: (3) The larger the positive index value is, the better; the smaller the negative index value is, the better.

$$\begin{cases} I_i' = \dfrac{I_i - \min(I_i)}{\max(I_i) - \min(I_i)} \\ I_i' = \dfrac{\max(I_i) - I_i}{\max(I_i) - \min(I_i)} \end{cases} \quad (3)$$

Selection of evaluation model. In this study, a comprehensive evaluation model was constructed by combining weighted sum with weighted quadrature. In the index evaluation of layer A and B, the weighted sum method is used; in the index evaluation of the lowest layer of layer C, the weighted quadrature method is used.

Evaluation on ecological economic development of Changchun city. With the data of 2010, 2011, 2012, 2013, 2014, 2015, 2016 and 2017 as the original data sources, the evaluation model constructed in 3.2 is adopted to evaluate the ecological economic development of Changchun. The evaluation result data are shown in Table 1.

The sustainable development ability and comprehensive score of Changchun at all stages are calculated. As shown in Figure 1, the fluctuation trend of ecological environment system is the largest. In 2010, Changchun's economy was in the stage of rapid development, and the contradiction between economy and environment is not revealed. By 2013 and 2014, social and environmental factors have restricted the sustainable development of Changchun City. Since 2014, the environment and society have improved to varying degrees. It can be seen that the government's policy intervention has made all walks of life in Changchun benign state of sustainable development. The enrollment rate of school-age children in Changchun City can basically reach 100%, and is supported by colleges and universities,

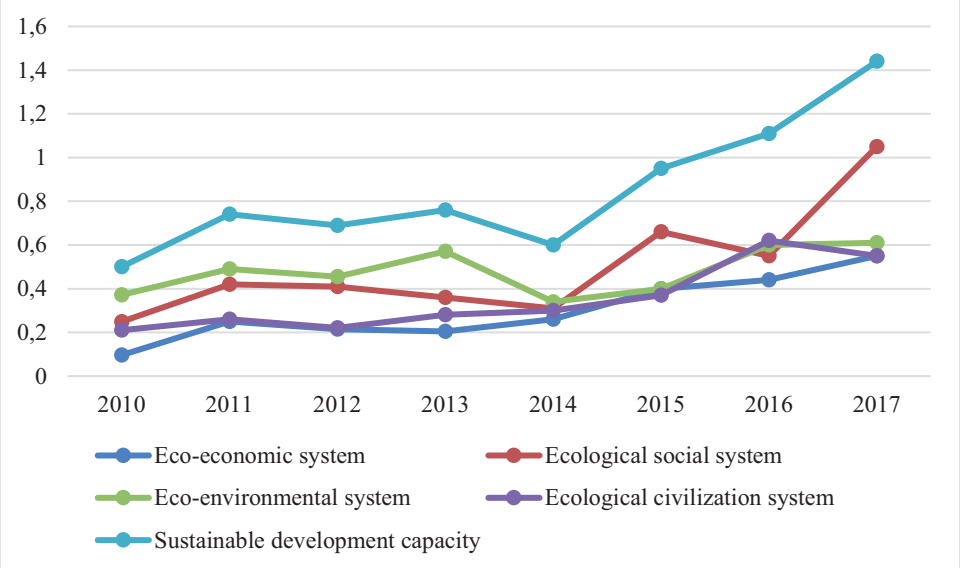


FIGURE 1
Sustainable Development Change Map of Changchun City.

scientific research institutes, and national key laboratories. The proportion of scientific and technical personnel in the population ranks among the largest and medium-sized cities in the country; The tertiary industry accounted for 6.7% of GDP in Changchun's economic indicators. The level of modernization is relatively high. The economy plays a pivotal role in the sustainable development of Changchun.

It can be seen from the figure that the ecological economic development model of Changchun City must adopt a resource-saving and economic intensive model, transform the traditional economic growth model, and shift the development momentum to relying on industrial structure adjustment, science and technology, and government management to strengthen society, The balanced and coordinated development of environment and economy will promote the construction of urban ecological economy in Changchun.

CONCLUSION

The development and health of the urban ecosystem directly affects the living standards of residents, and the degree of interference of human activities on the ecological environment is increasing day by day, which to a large extent restricts the sustainable development of economy, environment and society. The AHP method is used to calculate and analyze the ecosystem of Changchun City. The evaluation results show that the sustainable development capacity of Changchun City is on the rise, and the social, economic, and environmental systems are developing in a coordinated manner.

ACKNOWLEDGEMENTS

The study was supported by Social Science Project of the 13th Five-Year Plan of Jilin Provincial Education Department, Research on rural Entrepreneurship and its Driving Factors in Changchun Economic Circle under the background of "one main and six pairs" (Grant No. JKH20201295JY)".

REFERENCES

[1] Dong, Q.Y., Futawatari, T. (2015) A review of the progress in China's renewable energy generation, and its links with energy conservation, environmental degradation and economic growth. Fresen. Environ. Bull. 24, 405-411.

[2] Gultekin, U. (2019) Renewable electricity generation for sustainable development and environmental management in Turkey. Fresen. Environ. Bull. 28, 8171-8174.

[3] Zhou, H.Y. (2020) Incentive mechanism of low carbon economic growth quality based on fuzzy cluster analysis. Fresen. Environ Bull. 29(4), 2350-2356.

[4] He, Y., Lin, K., Zhang, F., Wang, Y., Chen, X. (2018) Coordination degree of the exploitation of water resources and its spatial differences in China. Sci. Total Environ. 644, 1117-1127.

[5] Xu, Y.P., Wang, M., Qin, M., Shi, H.X., Sui, B.W., Jia, X.Z., Lu, D.L. (2018) Study of the relationship between economic growth and environmental quality with the Kuznets curve in Guangxi, China. Fresen. Environ Bull. 27, 2818-2828.

[6] Xiong, S., Tian, Y., Ji, J., Ma, X. (2017) Allocation of energy consumption among provinces in China: a weighted ZSG-DEA model. Sustainability. 9(12), 2115-2116.

[7] Zhou, H.Y. (2020) Incentive mechanism of low carbon economic growth quality based on fuzzy cluster analysis. Fresen. Environ Bull. 29(4), 2350-2356.

[8] Pao, H., Chen, H.A., Li, Y. (2015) Competitive dynamics of energy, environment, and economy in the U.S. Energy. 89, 449-460.

[9] Tang, X., McLellan, B.C., Snowden, S., Zhang, B., Hook, M. (2015) Dilemmas for China: Energy, economy and environment. Sustainability. 7, 5508-5520.

[10] Han, S., Zhu, J. (2011) Research on the dynamic relationship of the Energy-Economy-Environment (3E) system-based on an empirical analysis of China. Energy Procedia. 5, 2397-2404.

[11] Gozgor, G., Chi, K.M.L., Lu, Z. (2018) Energy consumption and economic growth: New evidence from the OECD countries. Energy. 153, 27-34.

[12] Price, J., Keppo, I. (2017) Modelling to generate alternatives: A technique to explore uncertainty in energy-environment-economy models. Appl. Energy. 195, 356-369.

[13] Salehi, M., Jalalian, M., Siar, M.M.V. (2017) Green transportation scheduling with speed control: trade-off between total transportation cost and carbon emission. Comput. Ind. Eng. 113, 392-404.

[14] Liu, M., Yang, S.S., Zhang, K.X., Li, J.J., Liu, H.Y., Dai, Y.J. (2018) The study of smart growth of salt lake city and Nottingham city using the entropy method to explore the social, environment and economic changes. Fresen. Environ. Bull. 27, 4631-4636.

[15] Xu, S.C., Zhang, Q.Q., He, Z.X., Long, R.Y., Chen, H. (2017) Decoupling analysis of energy-related CO2 Emissions from economic growth at different stages in China. Fresen. Environ. Bull. 26, 3118-3127.

Received: **18.12.2020**
Accepted: **18.04.2021**

CORRESPONDING AUTHOR

Wei Wang
Shenyang Institute of Technology,
Liaoning Shenyang 113122 – China

e-mail: wangwei98aa12@163.com

© by PSP Volume 30– No. 09/2021 pages 10535-10544 Fresenius Environmental Bulletin

SYMBIOTIC PROPAGATION OF THE WET MEADOW ORCHID *Anacamptis laxiflora* FOR CONSERVATION AND REINTRODUCTION

Yasemin Ozdener Kompe*, Haydar Karakaya, Vildan Akin Mutlu

University of Ondokuz Mayis, Faculty of Arts and Sciences, Department of Biology, Samsun, Turkey

ABSTRACT

The study was designed to determine the diversity of mycorrhizal fungi associated with *Anacamptis laxiflora,* and to determine the symbiotic seed germination and the seedling development under *in vitro* and *in situ* conditions for reintroduction and conservation. Mycorrhizal fungi were isolated monthly from the roots of *A. laxiflora* adult individuals during the vegetation period. In addition, fungi were isolated from protocorms through in situ seed baiting. The isolates were identified as the members of *Tulasnella, Ceratobasidium, Fusarium, Phoma* and Pezizales through the sequences of ITS. Non-*Rhizoctonia* isolates did not promote germination. The isolates, AL2 and AL3 did not affect germination while AL5, AL8, AL11, AL12 and AL6 supported germination and seedling growth at different levels. Tubers were formed in symbiotic seedlings transferred to their natural habitats. The seeds inoculated with AL5 and AL6 germinated also and leaf primordium occurred in their natural habitats. Asymbiotic germination occurred in MS and VWD media with rates of 28.92% and 42.42%, respectively and no seedling development occurred. These results indicate that *A. laxiflora* has high mycorrhizal fungi diversity and the seeds have a high chance of germinating and becoming a new individual after forming a successful symbiotic association with compatible fungi in the soil.

KEYWORDS:
Anacamptis laxiflora, Orchidaceae, Mycorrhiza, Orchid reintroduction, Conservation

INTRODUCTION

Orchidaceae family includes approximately 800 genus and more than 30.000 species all around the world and dispers in almost every habitats, except regions with extreme conditions like polar regions and deserts [1]. Orchidaceae is one of the Angiosperm family, is well-known for their rarity, contains species specifically adapted to certain habitats and possesses their specific pollinators and establishes associations with mycorrhizal fungi. Decreasing the number of particularly rare and threatened orchid species is a result of loss of mycorrhizal fungi due to the habitat change or destruction [2-5].

The seed germination and population persistence are closely related to the presence and quantity of fungus (or fungi) in the soil that promote the germination of orchid seeds [3]. Moreover, while most orchids are associated with different species of fungi [6, 7], some other orchids use phylogenetically related fungi [8].

With the advancement of *in situ* seed germination techniques, studies that conducted on seed germination and early seedling development of several orchids accumulated the knowledge about orchid-fungus interaction in their natural habitats [9, 10]. For example, it was reported that *Goodyera pubescens* and *Corallorhiza odontorhiza* seeds remained in soil for six months without germination [9], *Epipactis helleborine* seed coats cracked in soil after 8-9 months [11], and *Dactylorhiza lapponica* seeds germinated without fungal symbiont in natural conditions (their own habitats), but fungi were necessary for seedling growth [12].

A. laxiflora is widely distributed in Anatolia, Greece, Aegean islands and Southern Europe countries up to an altitude of 1 to1500 m [13] and great number of individuals may be presented in one population.

This orchid tubers for medical purposes and to make a kind of tea (salep) is used in Greece, Iran and Turkey [14-16]. This study focused on *in vitro* and *in situ* symbiotic seed germination and seedling production, as well as fungal diversity of *A. laxiflora* for conservation and reintroduction.

MATERIALS AND METHODS

Plant materials for fungus isolation. The research area in which *A. laxiflora* species is spread is a Black Sea coastal city, Samsun in Turkey. Winters are cold and rainy and summers are temperate and moisty in Samsun. It is approximately 4 m above the sea level. *A. laxiflora* is a tuberous terrestrial orchid species that grows in almost any region of Turkey.

The members of *A. laxiflora* is represented in large populations in the meadows and swamps with higher groundwater levels especially in winter. Their habitats are largely submerged between November and April. Leaves and roots of the orchid develop in February, flowering in April and fruits form in June, seeds ripen and roots dry completely in July. Accordingly, fungus isolations started in February (2017) and were completed in June. Each month, three adult plants were taken randomly, all roots were examined under a microscope for the presence of the fungal coil and all the root parts containing fungus were used for isolation.

In situ seed baiting for fungus isolation. Seed packs were buried 5-6 cm away from the roots of adult individuals (approximately 5-7 cm deep). The packs were followed monthly and then the protocorms, which occurred as a result of germination in packs for 6 months after the seeds were buried, were sterilized in NaOCl (1,5%) for one minute, washed three times with sterile distilled water and a few parts were put in fungus isolation medium. Then, petri plates were incubated at 25±2°C and fungi growing into the culture medium were purified.

Fungus isolation from the roots of adult individuals. Fungus isolation was made monthly during a vegetation season. For isolation every month, all roots of three individuals were examined under the microscope for presence of fungus and all root parts containing hyphal coils were used for isolation. No isolation could made in July since the roots of plants are completely dry. Fungus isolations were made according to Clements et al. [17]. After the root parts were washed in tap water, they were sterilized for a few minutes in 1.5% NaOCl and they were washed with distilled water for three times. The roots were then cut into pieces and placed in petri dishes containing fungus isolation medium under sterile conditions. When the fungus hyphae started to grow from root parts to the medium, they were purified and stocked in PDA medium.

Seed source. *A.laxiflora* seeds were taken from the capsules of naturally pollinated plants in June 2017.

Molecular identification of the fungal isolates. DNA isolation from fungus mycelia was performed by using the CTAB (cetyltrimethyl ammonium bromide) method described by Pascual et al. [18] with some modifications. For the amplification of ITS region of the nuclear ribosomal DNA of the isolates, chromosomal DNA was isolated and the ITS region was amplified by using ITS-1 and ITS- 4 primers [19] in 50 µl rection mixture. PCR reaction mixture comprise of 1µl template DNA (1ng/µl), 5µl 10XPCR buffer, 1µl 2.5 mM dNTP mixture, 3 µl 1.5 mM $MgCl_2$, 1µl (10 pmol/µl) Primer ITS-1(5'-TCCGTAGGTGAACCTGCGG-3') and Primer ITS-4 (5′- TCCTCCGCTTATTGATATGC-3′), 0.25µl (1 units) Taq DNA polymerase, 37.75 µl sterile ddH_20 were used in the reaction mixture. The negative control was same as PCR reaction mixture except genomic DNA. Temperature profile applied for PCR was performed as a 30cycle reaction as initial denaturation at 94°C for 3 min, denaturation at 94°C for 1 min, annealing at 49°C for 2 min, extension at 74°C for 3 min, and final extension at 72°C for 7 min [20]. PCR products of the rDNA-ITS region were sequenced by Macrogen (Macrogen Inc., Seoul, Republic of Korea) by using ABI 3730 XL DNA sequencer with ITS1 and ITS4 primers. For each PCR product, sequences of both the strands were combined to generate a consensus sequence by using BioEdit version 7.2.5 software [21]. The consensus sequences of rDNA-ITS region were compared with the sequence data in GenBank by using BLASTn tool.

In vitro symbiotic germination of A. laxiflora seeds. The effects of fungal isolates on the germination of *A. laxiflora* seeds were tested in modified oat medium [17]. Pre-application for viability test of the seeds before symbiotic germination tests was conducted according to Kömpe et al. [22]. Seed packs were embedded in pots containing sterile cocopeat and they were wetted with sterile distilled water. Following 7 day-long incubation under these conditions, they were incubated in TTC (2,3,5 triphenyl tetrazolium chloride) solution at 30°C for 12 hours. After washed with sterile distilled water, seeds with red-pink embryos were evaluated alive after investigating under stereo microscope [23]. For *in vitro* symbiotic germination tests, seeds were sterilized three times in NaOCl (1.5%) solution for 15 minutes at least three times with sterile distilled water before rinsing. Then, sterile seeds were sown in modified oat medium in petri dishes. One of the fungal isolates was inoculated in each petri dish. Five repetitions were made for each isolate. Percentage of germination and developmental stages were calculated three months after seed planting. Modified oat medium without fungus, Van Waes and Deberg (VWD) [23] and Murashige-Skoog (MS) culture media [24]. were used as controls. The seeds were sown under aseptic conditions and their germination was evaluated three months later.

Transfer of seedlings from in vitro to field. In order to test the adaptation of in vitro symbiotic seedlings to the natural environment, 20 symbiotic seedlings were transferred to the natural habitat of orchids and it was determined whether they formed tubers.

In situ symbiotic germination of *A. laxiflora* seeds. Germination of *A. laxiflora* seeds was tested in pots with and without fungi placed in natural environment. AL5 and AL6 isolated from *in situ* protocorms, which showed high germination and growth in *in vitro* germination test, were used in this trial. Sterile soil mixture (soil: perlite 2:1) was filled in pots. Two of the pots were inoculated with AL5, while the other two were inoculated with AL6. Five seed packs were embedded in each pot. The pots were placed around *A. laxiflora* individuals in natural environment. As control, seed packs without fungus inoculation were embedded in the same soil mixture and they were placed close to adult individuals in their natural environment. Pots with and without fungal isolate were placed at least 100 m away from each other. This experiment set was set up on February 1th and followed until the end of spring (average temperature for February is 6.1-9 °C, average rainfall is 300 mm; average temperature for spring is 11.2-12.8°C, average rainfall is 200-300 mm). Mild irrigation was applied from time to time in April and May to provide soil moisture. Germination was evaluated in seed packs in May. Two independent experiments and 5 repetitions were made for each experiment set. Growth rate of *in vitro* and *in situ* tests was evaluated according to the index below:

0: Seed swollen
1: Seed coat cracked, rhizoid formed
2: Protocorm
3: Leaf primordium formed
4: Seedling with one or two leaves

Individuals in the second, third and fourth stages were evaluated as germination rate.

TABLE 1
ITS sequences of the taxa employed in this study, indicating isolate numbers, Month collected, GENBANK acession number, Nucleotides (bp=base pair), Description, host, percentage (ID), closest match in GenBank and references.

Isolate Number	Month collected	GenBank Acession Number	Nucleotides (bp)	Description	Host	ID(%)	Closest match in GenBank (Accession No.)	References
AL1	February	MT605397	584	Uncultured *Scutellinia (Pezizales*)	*Salix arctica*	%95	JX630686	Timling et al.2012
AL2	February	MT605384	592	Uncultured *Ceratobasidium*	*Neottia ovata*	%97	KJ188557.1	Tešitelová et al.2015
AL3	March	MT612363	640	*Tulasnella helicospora*	*Orchis patens*	%99	MT489316.1	Calevo et l.2020
AL4	March	MT605398	551	*Pezizales* sp.	*Anacamptis laxiflora*	%98	MG762599.1	Mutlu V.A and Kompe Y.O 2020
AL5	April	MT605389	500	Uncultured Ceratobasidium clone AL4b	*Anacamptis laxiflora*	%98	JF912463.1	Girlanda et al.2011
AL6	April (prot)	MT605390	608	Epulorhiza sp.H1401-17	*Cymbidium goeringii* and *Cymbidium+ faberi*	%99	FJ594926.1	Direct Submission
AL7	April	MT605400	526	Stagonosporopsis sp.	*Salix aegyptiaca*	%100	MK100222.1	Direct Submission
AL8	May	MT605391	571	Uncultured Tulasnellaceae	*Gymnadenia conopsea*	%100	KC243948.1	Tesitelova et al.2012
AL9	May	MT605401	588	*Trichoderma koningiopsis*	*Dendrobium officinale*	%99	MT111912.1	Direct Submission
AL10	May	MT605402	532	Fusarium equiseti	wheat	%100	MK780235.1	Direct submission
AL11	June	MT605392	529	Uncultured *Tulasnellaceae* clone OTUA5	orchids	%100	JX649082.1	Bailarote, et al.2012
AL12	June	MT605395	608	Epulorhiza sp.	*Cymbidium goeringii* and *Cymbidium faberi*	%99	FJ594919.1	Direct Submission

Statistical Analysis. The SPSS Statistics software (SPSS 15) was used for statistical analyses. The data of the seed germination and developmental tests repeated 5 times were analyzed by the one-way analysis of variance (ANOVA). The significant differences between per treatment was performed with the Duncan's multiple-range test ($P \leq 0.05$).

RESULTS

Fungal isolates. Twelve fungi were isolated between February and June 2017. These isolates were first grouped as Rhizoctonia-like and non- *Rhizoctonia* fungi in terms of basic morphological characteristics such as colony features, hyphae structure and absence of spore formation. Of the isolates obtained from *A. laxiflora* roots during the vegetation period, 58% (7 isolates) were *Rhizoctonia*-like fungi and 42% (5 isolates) were non- *Rhizoctonia* endophytes. ITS sequences of AL1 from non-*Rhizoctonia* endophytes were identified as *Secutellinia* (Pezizales) based on the closest match in GenBank data. Sequences of AL4, AL7, AL9, AL10 isolates were classified as Pezizales, *Stagonosporopsis* sp., *Trichoderma koningiopsis* and *Fusarium equiseti*, respectively. Other *Rhizoctonia*-like isolates AL2, AL3, AL5 sequences were identified as *Ceratobadidium*, *Tulasnella helicospora*, *Ceratobasidium*, respectively.

Sequences of AL6 obtained from the protocorms through *in situ* seed baiting and sequences of AL12 isolated from the roots in June were classified as *Epulorhiza*, and sequences of AL8 (May) and AL11(June) were classified as Tulasnellaceae. The March isolate *T. helicospora* (AL3) was first isolated from the roots of *A. laxiflora* individuals in Turkey and it showed 100% homology with the ITS sequence of *T. helicospora* from Italy.

Table 1 shows the molecular identities and similarity rates of all the isolates.

It is seen that the fungi that join the mycorrhizal union of *A. laxiflora* may differ during a vegetation year.



FIGURE 1
Coloured embryo with TZ after 7 days incubation (X10).

In vitro seed germination. Multiple germination and growth tests were conducted to test the specificity of the interaction with mycorrhizal fungi. Germination and growth tests were followed for 12 weeks and then evaluated. Viability rates of the seeds were 75% (Figure 1). Germination rates of *A. laxiflora* seeds in all tests are given in Figure 2.

Non-*Rhizoctonia* isolates did not promote germination. For this reason, it is not included in Figure 2.

Rhizoctonia-like isolates AL2 and AL3 did not promote germination. Seeds inoculated with AL5 were found to germinate with a rate of 64.84% and they developed to advanced seedling stage (stage 4) (Figure 3A). Statistical analyses showed that the other *Rhizoctonia*-like fungi AL6, AL8, AL11 and AL12 supported germination and seedling development but germination and seedling development rates were found to be significantly lower when compared with the effects of AL5. As control, the seeds were sown on fungus-free oat medium and asymbiotically on VWD and MS basic media. No germination occurred on fungus-free oat medium, while germination occurred in MS and VWD media with rates of 28.92% and 42.42%, respectively. However, no further development occurred during three months long incubation process (Figure 3C, D). Rates of developmental stages are shown in Table 2.

Fungi that do not promote germination of seeds are not included in Figure 2 and Table 2.

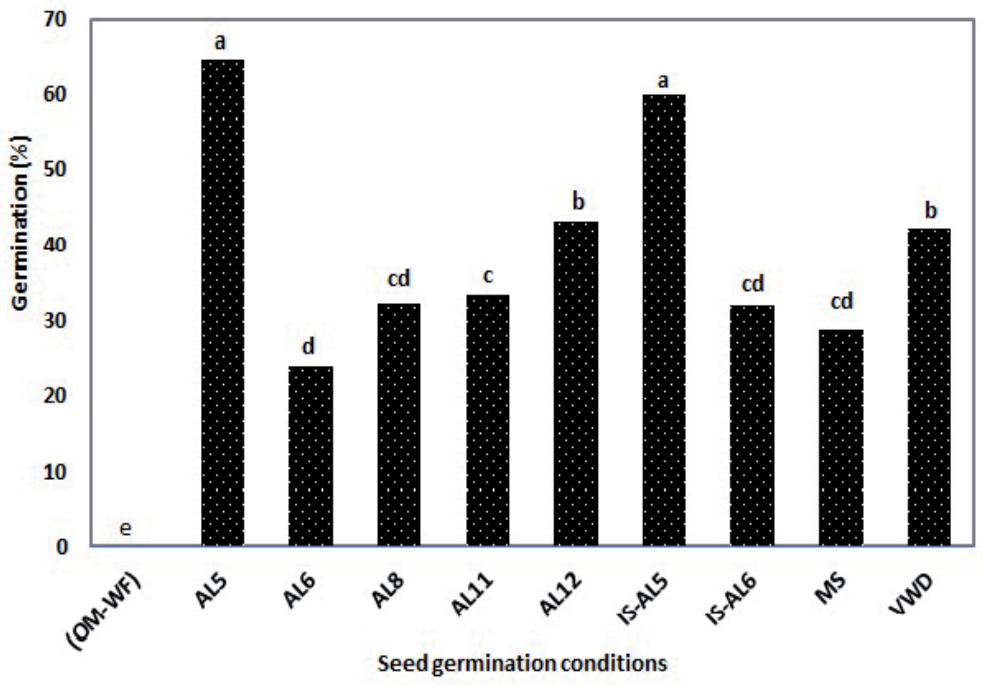


FIGURE 2
The effects of *A. laxiflora* fungi on *in vitro* and *in situ* seed germination.
Oat medium, MS and VWD media were used as control medium not containing fungus.

TABLE 2
Growth stages of *A. laxiflora*. Different rates of growth occurred in inoculation with *Rhizoctonia* like fungi in *in vitro* symbiotic medium. No photosynthetic seedling occurred under *in situ* conditions.

Fungi	Developmental stages (%)				
	0	1	2	3	4
C	100±0.00a	0.00±0.00d	0.00±0.00e	0.00±0.00b	0.00±0.00d
AL5	35.15±5.91e	11.1±3.74bc	12.48±5.13bc	17.81±3.00a	23.43±7.92a
AL6	75.96±5.98b	11.0±2.39bc	2.93±1.35de	2.19±1.63b	7.9±2.67c
AL8	67.54±9.12bc	1.79±2.5d	7.3±4.3cd	2.07±2.26b	21.27±7.25ab
AL11	66.56±3.34bc	7.15±3.74cd	3.89±1.64de	2.13±0.92b	20.38±1.69ab
AL12	56.66±5.86cd	10.76±4.4bc	11.06±2.56bc	5.13±1.31b	16.36±2.25b
IS AL5	50.4±18d	41.6±14.04a	21.00±6.85a	16.2±10.84a	0.00±0.00d
IS AL6	77.6±25.9b	17.00±7.61b	14.40±9.42b	5.2±2.94b	0.00±0.00d
IS-C	100±0.00a	0.00±0.00d	0.00±0.00e	0.00±0.00b	0.00±0.00d

n=5, ±: SD, P≤ 0.05
There is no statistically significant difference between groups with the same letters.

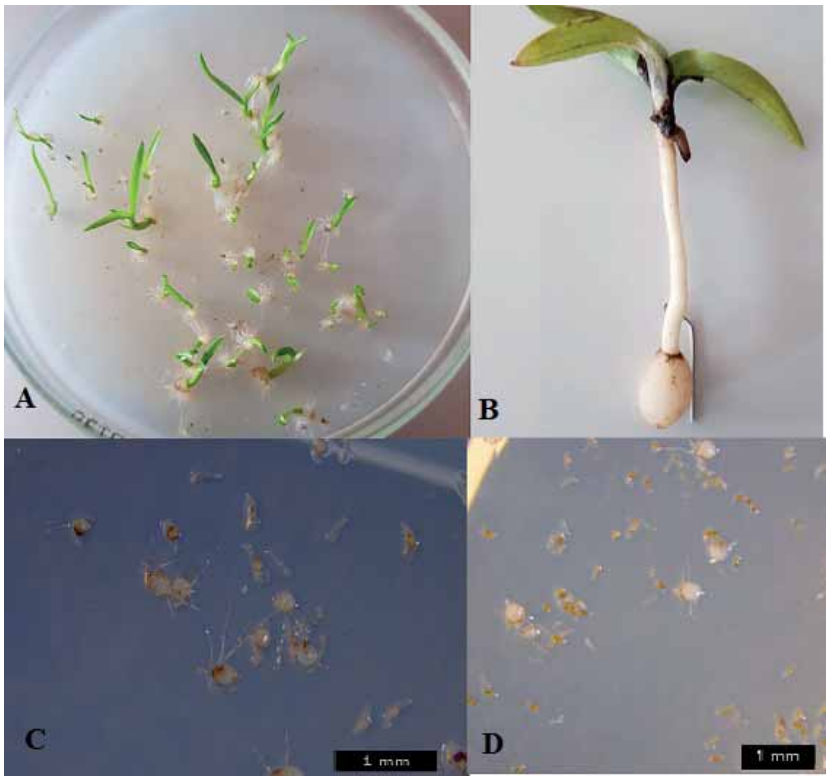


FIGURE 3

***In vitro* symbiotic and asymbiotic seed germination.**

A: Symbiotic germination with AL5, B: The first tuber to grow in their natural habitat. This is the biggest of all tubers. C: Asymbiotic germination on the MS medium D: Asymbiotic germination on the VWD medium.

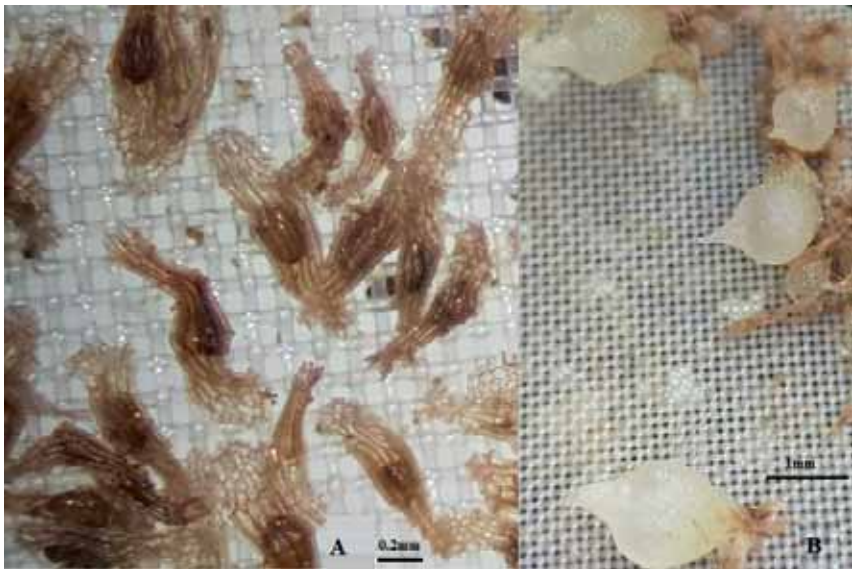


FIGURE 4

In situ symbiotic seed germination.

A: Control (without fungus), B: Symbiotic germination with AL5 under *in situ* condition.

Transfer of seedlings from in vitro to field. Fifteen out of 20 seedlings planted in the natural environment produced tubers. The length, width and weight of the tubers were determined. It was determined that tuber lengths varied between 0,7-1,3cm (mean: 0,99cm), width 0,4-1cm (mean: 0,71cm) and weight 0.3-0,8g (Mean: 0.6g) (Figure 3B).

In situ symbiotic seed germination. AL5 and AL6 were used to test whether fungi that are effective *in vitro* conditions also promote germination in natural conditions (*in situ*). The seeds inoculated with these isolates germinated with a rate of 59.85% and 32%, respectively in natural environment (Figure 2). It was found that the seeds swelled but did not

grow further in pots in which the fungus was not inoculated in *in situ* conditions (Figure 4a), while a leaf primordium developed in both isolates at the end of three months (Figure 4b).

DISCUSSION

The presence of orchids in an ecosystem depends on biotic (mycorrhizal fungi, pollination, competition) and abiotic (temperature, water, soil characteristics) factors [2]. One of the biotic factors, mycorrhizal fungi, are vital for the germination of orchid seeds *in situ* and for the persistence of generations. Symbiotic germination of orchid seeds with suitable mycorrhizal fungi is a highly advantageous method for the reintroduction of endangered orchids to their habitats and for cultivation [25, 26]. The roots of many photosynthetic orchids host various *Rhizoctonia*-like fungi (*Tulasnella, Ceratobasidium, Thanatephorus, Sebacina*). These fungi are defined as the typical fungi of orchids [27]. Accordingly, *A. laxiflora* was found to associate with various *Rhizoctonia*-like and non- *Rhizoctonia* fungi in this study. *Rhizoctonia* like fungi were identified as *Tulasnella* and *Ceratobasidium* species. Girlanda et al. [28] obtained *Sebacina* from *A. laxiflora* roots in addition to *Tulasnella* and *Ceratobasidium* in Italy and reported that *A. laxiflora* had high mycorrhizal fungal diversity and showed low mycobiont specific characteristics. As a part of this study, *Tulasnella helicospora* was isolated first time in Turkey even though the only record of this fungus in NCBI was given from Italy [29]. Although this fungus was included in polyphyletic *Rhizoctonia* group, it did not germinate the seeds of the host orchid. The germination efficiency of *T. helicospora* from Italy is unknown. This mycorrhizal fungus may probably be in interaction with adult plants like non- *Rhizoctonia* endophytes, however, studies conducted on this such an interaction are still inconclusive [3]. AL1 and AL4 of Pezizales, including macro fungi, were isolated from *A. laxiflora* roots, but had no effect on germination and seedling development of these fungi. In addition, it was found that some *Dactylorhiza* and *Orchis* species distributed in Turkey formed mycorrhizal association with fungi included in the order of Pezizales [30, 31]. Pecoraro et al. [32] reported that some macrofungal communities might affect the distribution of orchids and the continuity of habitats.

Other studies indicated that different mycorrhizal associations might be established with different fungi in different habitats of the same orchid species while more than one mycorrhizal fungus might be found in the roots of an orchid individual [6, 33, 34]. Moreover high mycorrhizal fungus diversity shows low specificity [28]. On the other hand, high fungal diversity may increase the chances of seed germination and seedling growth, and also may increase survival and stability in difficult environmental conditions [3]. Similarly, high mycorrhizal fungus diversity of *A. laxiflora* increases the chance for this species to reproduce and to form large populations. Finding out the effects of isolated fungi on the germination of orchid seeds *in vitro*, classification of orchid mycorrhizal fungi are very important for understanding the functions better, for conservation and reintroduction [35-37].

A. laxiflora is one of the orchids which has large number of individuals and can be distributed to large areas. Because its tubers are over collected and their habitats are destroyed excessively, it is considered one of the conserved orchids. In this research against the increasing extinction threats, mycorrhizal fungi of *A. laxiflora* were obtained and symbiotic germination tests were performed. All *Rhizoctonia*-like isolates except AL2 and AL3 supported germination and seedling development. It was revealed for the first time that symbiotic seedlings (with AL5) can form tubers in the wild and thus adapt to the wild nature. This result is very promising for the success of reintroduction and the protection of orchids with this application. Control tests were also conducted in fungus-free oat medium, MS medium and VWD medium. No germination occurred in oat medium, while protocorm occurred in MS and VWD asymbiotic germination medium at the end of three-month incubation period but no seedlings occurred. The seeds of temperate orchids germinate and grow slower in asymbiotic medium when compared with symbiotic conditions. This result shows that asymbiotic method is not practical for cultivation, conservation and reintroduction [12, 38, 39]. Symbiotic seedlings may be more appropriate for reintroduction to natural areas than asymbiotic seedlings since symbiotic seedlings could serve to inoculate soils with a germination promoting mycobiont [40].

In this study, after pots including soil inoculated with AL5 were transferred to natural environment, seed packs were embedded and successful germination occurred in pots in three months. No development of the protocorms into the seedling stage might be due to the relatively low temperature under natural conditions, which was relatively low (night temperature was measured 5-7°C occasionally) especially in February, March and early April. No seedlings were observed since the period of experiment was restricted to three months, however, leaf primordium formed. The absence of germination in control pots and the occurrence of germination in pots containing fungus are consistent with the findings of McCormick & Jacquemyn [4]. According to these researchers, the distribution and population size of orchids were associated with the presence and amount of compatible fungus in the soil, and in case of abundance of suitable fungus, orchid seed could germinate and became a new individual.

It is assumed that a large number of internal and external factors pose a threat for orchid diversity and that many species of orchids may extinct if these threats increase [2,5]. Conservation studies gradually become more important against such a threat. In this context, reproduction of orchids for conservation, reintroduction or agricultural purposes through symbiotic germination may be a very effective way. In addition, *in situ* symbiotic germination and seedling growth tests can also be considered and be developed as a promising practice for reintroduction and conservation.

CONCLUSION

In this study, besides revealing the variety of mycorrhizal fungi of *A.laxiflora*, it was seen for the first time in this study that *in vitro* symbiotic seedlings formed tubers and adapted to the natural environment after they were transferred to the wild environment. In addition, germination has occurred in a soil and natural environment where compatible fungi are intense. These results are promising for both reintroduction, conservation and agricultural propagation.

ACKNOWLEDGEMENTS

The authors declare that they have no known competing financial interests or personal relationships that may have affected the work reported in this article.

This research did not receive any specific grant from funding agencies in the public, commercial, or not-for-profit sectors.

REFERENCES

[1] Dressler, R. (1993) Phylogeny and classification of the orchid family. Cambridge University Press, Melbourne. 8-9.

[2] Swarts N.D., Dixon, K.W. (2009) Terrestrial orchid conservation in the age of extinction. Annals of Botany. 104(3), 543–556.

[3] McCormick, M.K., Whigham, D.F., Sloan, D., O'Malley, K., Hodkinson, B. (2006) Orchid–fungus fidelity: a marriage meant to last? Ecology 87, 903–911.

[4] McCormick, M.K., Jacquemyn, H. (2013) What constrains the distribution of orchid populations? New Phytologist 202, 392–400.

[5] Rasmussen, H.N. (1995) Terrestrial orchid: from seed to mycotrophic plant. Cambridge University Press, Cambridge. 142-172.

[6] Jacquemyn, H., Merckx, V., Brys, R., Tyteca, D., Cammue, B.P.A., Honnay, O., Lievens, B. (2011) Analysis of network architecture reveals phylogenetic constraints on mycorrhizal specificity in the genus *Orchis* (Orchidaceae). New Phytologist. 192, 518–528.

[7] Dearnaley, J.D.W., Martos, F., Selosse, M.A. (2012) Orchid mycorrhizas: molecular ecology, physiology, evolution and conservation aspects. In: Fungal Associations (Hock, B., ed.), The Mycota (Esser, K. ed.). Springer, Berlin. 9, 207-230.

[8] Ogura-Tsujita, Y., Yukawa, T. (2008) High mycorrhizal specificity in a widespread mycoheterotrophic plant, *Eulophia zollingeri* (Orchidaceae). American Journal of Botany. 95, 93–97.

[9] Rasmussen, H.N., Whigham, D. (1993) Seed ecology of dust seeds *in situ*: a new study technique and its application in terrestrial orchids. American Journal of Botany. 80, 1374–1378

[10] Whigham, D. F., O'Neill, J. P., Rasmussen, H. N., Caldwell, B. A., McCormick, M.K. (2006) Seed longevity in terrestrial orchids — potential for persistent *in situ* seed banks. Biological Conservation. 129, 24–30.

[11] Van der Kinderen, G. (1995) A method for the study of field germinated seeds of terrestrial orchids. Lindleyana. 10(2), 68-73.

[12] Øien, D.I., O'Neill, J.P., Whigham, D.F., McCormick, M.K. (2008) Germination ecology of the boreal-alpine terrestrial orchid *Dactylorhiza lapponica* (Orchidaceae). Annales Botanici Fennici. 45, 161–172.

[13] Davis, P.H. (1984) Flora of Turkey and East Aegean Islands, Vol 8. Edinburg University Press, Edinburg. 532-533.

[14] Ghorbani, A., Gravendeel, B., Naghibi, F., de Boer, H. (2014) Wild orchid tuber collection in Iran: a wake-up call for conservation. Biodiversity and Conservation. 23 (11), 2749-2760.

[15] Kreziou, A., De Boer, H., Gravendell, B. (2016) Harvesting of salep orchids in North-western Greece continues to threaten natural populations. Oryx. 50(3), 393-396.

[16] Sezik, E. (2002) Turkish orchids and salep. Acta Phamarceutica Turcica 44, 151-157.

[17] Clements, M.A., Muir, H., Cribb, P.J. (1986) A preliminary report on the symbiotic germination of European terrestrial orchids. Kew Bulletin 41, 437–445.

[18] Pascual, C.B., Toda, T., Raymondo, A.D., Hyakumachi, M. (2000) Characterization by conventional techniques and PCR of *Rhizoctonia solani* isolates causing banded leaf sheath blight in maize. Plant Pathology. 49, 108-118.

[19] White, T.J., Bruns, T., Lee, S., Taylor, J. (1990) Amplification and direct sequencing of fungal ribosomal RNA genes for phylogenetics. In: PCR protocols: a guide to methods and applications. (Innis, M.A., Gelfand, D.H., White, T.J Eds.). Academic Press, San Diego, New York, Berkeley, Boston, London, Sydney, Tokyo, Toronto. 315-322.

[20] Salazar, O., Schneider, J.H.M., Julian, M.C., Keije, J., Rubio, V. (1999) Phylogenetic subgrouping of *Rhizoctonia solani* AG2 isolates based on ribosomal ITS sequences. Mycologia. 91(3), 459-467.

[21] Hall, T.A. (1999) BioEdit: A user-friendly biological sequence alignment editor and analysis program for windows 95/98/ NT Nucleic Acids Symposium Series. 41, 95–98.

[22] Kömpe, Y. A., Mutlu, V. A., Ozkoc, I. (2020) The viability of *Anacamptis laxiflora* (Orchidaceae) seeds and the symbiotic germination. Plant Biosystems. 154(6), 800-805.

[23] Van Waes, J., Debergh, P.C. (1986) *In vitro* germination of some Western European orchids. Physiologia Plantarum. 67, 253–261.

[24] Murashige, T., Skoog, F. (1962) A revised medium for rapid growth and bioassays of tobacco tissue cultures. Physiologia Plantarum. 15, 473-497.

[25] Chen, J., Wang, H., Guo, S.X. (2012) Isolation and identification of endophytic and mycorrhizal fungi from seeds and roots of *Dendrobium* (Orchidaceae). Mycorrhiza. 22, 297–307.

[26] Nontachaiyapoom, S., Sasirat, S., Manoch, L. (2010) Isolation and identification of *Rhizoctonia*-like fungi from roots of three orchid genera, *Paphiopedilum, Dendrobium*, and *Cymbidium*, collected in Chiang Rai and Chiang Mai provinces of Thailand. Mycorrhiza. 20, 459–471.

[27] Ogura-Tsujita, Y., Yokoyama, J., Miyoshi, K., Yukawa, T. (2012) Shifts in mycorrhizal fungi during the evolution of autotrophy to mycoheterotrophy in *Cymbidium* (Orchidaceae). American Journal of Botany. 99, 1158–1176.

[28] Girlanda, M., Segreto, R., Cafasso, D., Liebel, H.T., Rodda, M., Ercole, E., Cozzolino, S., Gebauer, G., Perotto, S. (2011) Photosynthetic Mediterranean meadow orchids feature partial mycoheterotrophy and specific mycorrhizal associations. American Journal of Botany. 98, 1148–1163.

[29] Calevo, J., Voyron, S., Ercole, E., and Girlanda, M. (2020) Is the Distribution of Two Rare Orchis Sister Species Limited by Their Main Mycobiont? Diversity. 12(7), 262.

[30] Kömpe, Y. O., Mutlu, V. A. (2017) Mycorrhizal diversity in some species of *Dactylorhiza* genus (Orchidaceae). Biological Diversity and Conservation. 10(1), 55-64.

[31] Mutlu, V.A., Kömpe, Y.O. (2020) Mycorrhizal Fungi of Some *Orchis* Species of Turkey. Pakistan Journal of Botany. 52(2), 687-695.

[32] Pecoraro, L., Caruso, T., Cai, L., Gupta, V.K., Liu, Z.J. (2018) Fungal networks and orchid distribution: new insights from above- and below-ground analyses of fungal communities. IMA Fungus. 9, 1-11.

[33] Jacquemyn, H., Honnay, O., Cammue, B.P.A., Brys, R., Lievens, B. (2010) Low specificity and nested subset stracture characterize mycorrhizal associations in five closely related species of the genus *Orchis*. Molecular Ecology. 19, 4086–4095.

[34] Huang, H., Zi, X.M., Lin, H., Gao, J.Y. (2018) Host-specificity of symbiotic mycorrhizal fungi for enhancing seed germination, protocorm formation and seedling development of over-collected medicinal orchid, *Dendrobium devonianum*. Journal of Microbiology. 56, 42-48.

[35] Herrera, H., Valadares, R., Contreras, D., Bashan, Y., Arriagada, C. (2017) Mycorrhizal compatibility and symbiotic seed germination of orchids from the Coastal Range and Andes in south central Chile. Mycorrhiza. 27, 175-188.

[36] Tešitelová, T., Tešitel, J., Jersáková, J., Ríhová, G., Selosse, M. A. (2012) Symbiotic germination capability of four *Epipactis* species (Orchidaceae) is broader than expected from adult ecology. American Journal of Botany. 99, 1020–1032.

[37] Tešitelová, T., Kotilínek, M., Jersáková, J., Joly, F.X., Košnar, J., Tatarenko, I., Selosse, M.A. (2015) Two widespread green *Neottia* species (Orchidaceae) show mycorrhizal preference for Sebacinales in various habitats and ontogenetic stages. Molecular Ecology. 24(5), 1122-1134.

[38] Nikabadi, S., Bunn, E., Stevens, J., Newman, B., Turner, S.R., Dixon, K.W. (2014) Germination responses of four native terrestrial orchids from south-west Western Australia to temperature and light treatments. Plant Cell Tissue and Organ Culture. 118, 559–569.

[39] Nontachaiyapoom, S., Sasirat, S., Manoch, L. (2011) Symbiotic seed germination of *Grammatophyllum speciosum* Blume and Dendrobium draconis Rchb. F., native orchids of Thailand. Scientia Horticulturae. 130, 303–308.

[40] Johnson, T.R., Stewart, S.L., Dutra, D., Kane, M.E., Richardson, L. (2007) Asymbiotic and symbiotic seed germination of *Eulophia alta* (Orchidaceae) preliminary evidence for the symbiotic culture advantage. Plant Cell Tissue and Organ Culture. 90, 313–323.

Received: **25.04.2021**
Accepted: **17.05.2021**

CORRESPONDING AUTHOR

Yasemin Ozdener Kompe
Department of Biology
Faculty of Arts and Sciences
University of Ondokuz Mayis
Samsun 55139 – Turkey

e-mail: yasemino@omu.edu.tr

© by PSP Volume 30– No. 09/2021 pages 10545-10550 Fresenius Environmental Bulletin

RESEARCH ON THE INNOVATION OF ECOLOGICAL ECONOMY DEVELOPMENT PATH: BASED ON ECOLOGICAL PERSPECTIVE

Huancai Peng*

School of Marxism, Hunan Technology and Business University, Changsha 410205, China

ABSTRACT

Faced with the current background of anti-globalization, it is difficult for China's economic development to adapt to the needs of the times without making corresponding changes. Therefore, China urgently needs to innovate the path of economic development and realize the transformation and upgrading of all walks of life in China. This article introduces the coordinated development model and sustainable development theory. The research results show that: facing the new situation of economic development where opportunities and challenges coexist, China must grasp the direction of world economic development, and on this basis, clarify the direction of China's economic development. At the same time, it also needs to make corresponding responses in light of the new domestic development situation in China. Innovation and change ensure that the domestic economy can be better developed under the background of anti-globalization.

KEYWORDS:
Ecological perspective, Economic development, Path, Innovative research

INTRODUCTION

Although globalization is the general trend, it is obviously cyclical [1-3]. The impact of the epidemic on the global supply chain has caused countries to pay more attention to local suppliers, but in the short term they are "constrained" by various factors [4]. The conditions for the emergence of the "new world" are ready. Although concerns about "reverse globalization" began to emerge after the 2008 financial crisis (Figure 1), they are basically on the edge. However, after Trump took office in 2016, the phantom of "reverse globalization" reappeared, and after the impact of the new crown, it once again became the focus of global attention [6-9].



FIGURE 1
"Reverse globalization"

At present, China is in a critical period of building a modern economic system. In the past period of time, the high energy consumption and high pollution economic development mode has caused serious problems such as resource shortage, environmental pollution, and ecological degradation [10-12].

The coordinated development between social economy and ecological environment has always been an important topic and hotspot in sustainable development [13-15]. Coordinated development requires that regional socio-economic development and natural ecological environment conditions can promote each other and realize a coupled and coordinated common development process. In recent years, in the research on the relationship between social economy and ecological environment, it has gradually shifted from qualitative analysis to quantitative trend evaluation. Based on different conceptual models and different research perspectives, a large number of ecological environment and social evaluation model of economic coordination and coupling relationship, such as the PSR model analyzes the relationship between regional economic activities and the ecological environment from the perspective of "pressure-state-response" [16]. The Kuznets econometric model examines the relationship between economic indicators and environmental indicators. Whether there is an inverted "U" hypothesis in the relationship simulation to determine the coupling state between different regional economic systems and environmental systems, the social economy-ecological environment coupling

system dynamics model based on the traditional system dynamics model is built from the perspective of system dynamics simulation analyze the coupling dynamic process between the regional social economic system and the ecological environment system, and some scholars establish the coupling degree model of the regional economy-environment system based on the coupling theory to analyze the coordination degree of the key factors of the economy-environment system. In terms of research scale and research area, there are a lot of research results on the coupling relationship between the urbanization of key urban agglomerations, social economic system and ecological environment system in China [18-20].

The implementation of "three lines and one single" (red line for ecological protection, bottom line for environmental quality, online resource utilization and ecological environment access list) ecological environment zoning control is the implementation of the Jinping ecological civilization thought in the new era, and the modernization of the ecological environment governance system and governance capabilities Important move. It is necessary to thoroughly implement the decisions and deployments of the Party Central Committee and the State Council, speed up the preparation of the "three lines and one order" and do a good job of landing applications, and promote high-quality economic development with high-level protection of the ecological environment.

MATERIALS AND METHODS

Model selection. Coupling coordination degree model. Coupling is a physical concept, which refers to the phenomenon in which two or more systems affect each other through interaction. The natural ecosystem provides the necessary material conditions for production for social and economic development, and at the same time, the process of social and economic development has a negative feedback effect on the ecological environment. The coupling relationship between the two refers to the objective representation of the interaction relationship between the system or each element, and its main manifestation is the interaction between the system elements and the evolution process and trend of the system from low-level to high-level, simple to complex. Therefore, this study adopts the coupling coordination degree model to comprehensively evaluate the ecological environment and socio-economic development level and coupling coordination status from 2008 to 2018.

The calculation formula of coupling coordination degree is:

$$C=\sqrt{\frac{F(x)\times F(y)}{[F(x)+F(y)]^2}} \quad (1)$$

$$T=mF(x)+nF(y) \quad (2)$$

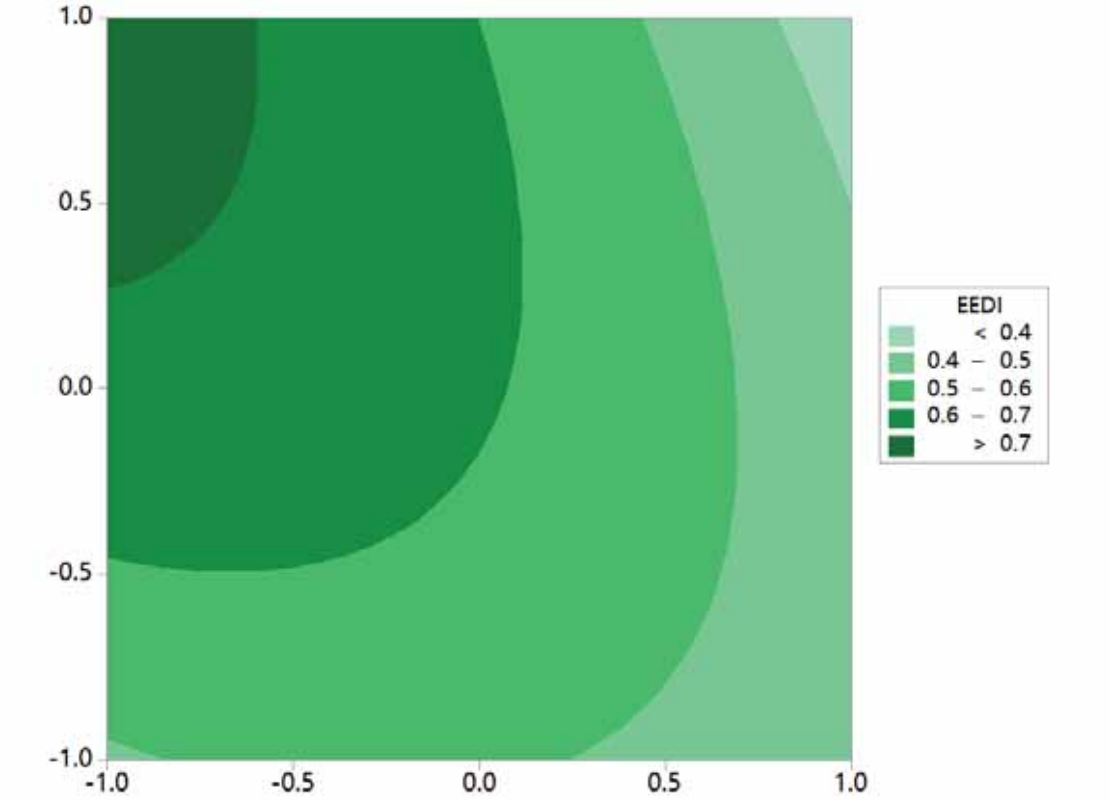
$$D=\sqrt{C\times T} \quad (3)$$

Where: F(x) is the ecological environment index, F(y) is the socio-economic index, C is the coupling degree index; T is the comprehensive development evaluation index of the two systems; D is the coupling coordination degree index of the two systems , Where m + n=1, and the values are respectively 0.5.

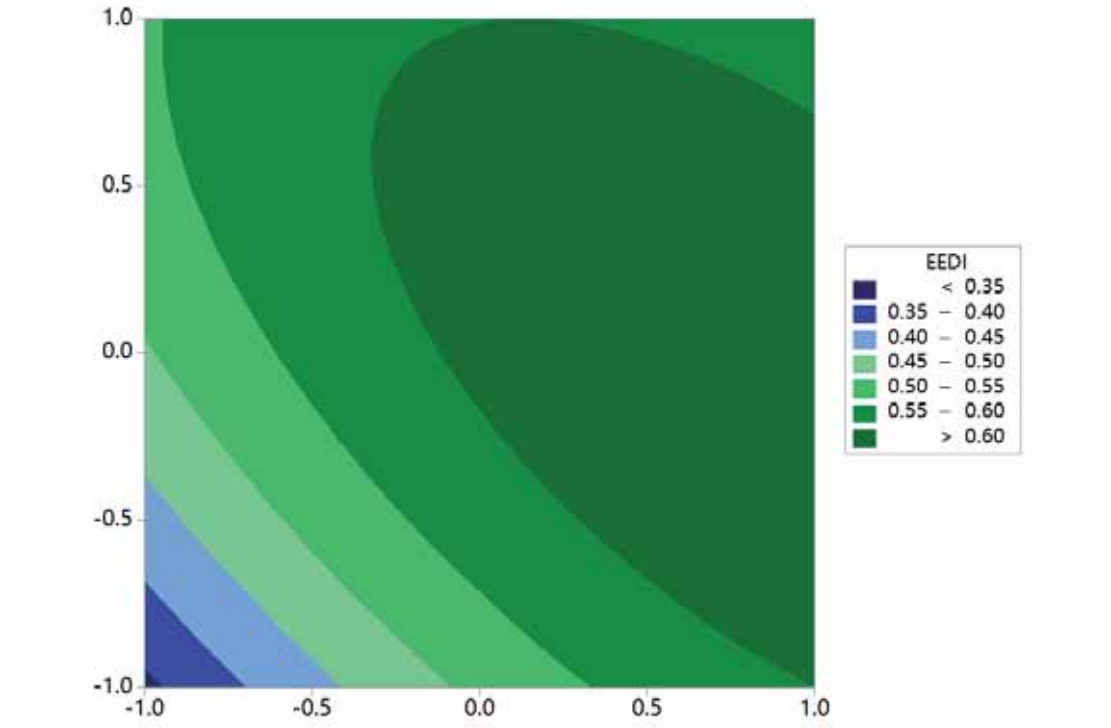
Data Sources. This study uses 2008-2018 as the research period. The data mainly comes from China Statistical Yearbook (2008-2018), China Environmental Statistics Yearbook (2008-2018), China City Statistical Yearbook (2008-2018), National Economy and Society According to statistics published in the Development Statistics Bulletin (2008-2018), pollutant discharge data mainly comes from the second national pollutant survey, and individual missing data are simulated by moving average.

RESULTS AND DISCUSSION

Analysis of Comprehensive Development Index of Ecological and Economic System. The comprehensive evaluation value of the ecological environment system showed a fluctuating and rising trend. The value of the ecological environment development index (EEDI) increased from 0.3118 to 0.6588, indicating that the ecosystem tended to improve during the study period. The structure and function of the ecosystem were continuously improved and strengthened. The index increases every year. On the whole, the ecological environment index has shown an increasing trend, especially after 2014, the growth rate of the ecological environment index has accelerated significantly. From the perspective of ecosystem classification indicators, the ecological environment level, ecological environment pressure and ecological environmental protection changes are all significant (Figure 2). The ecological environment level shows a trend of first decreasing and then increasing, while the pressure of the ecological environment shows the opposite trend. The main reason is the development of social economy, especially the implementation of resource and energy economic development strategy at the cost of the ecological environment. The increasing pressure on the ecological environment has led to a continuous decline in the level of the ecological environment, while the ecological environment protection



(a)



(b)

FIGURE 2
Results and analysis of EEDI

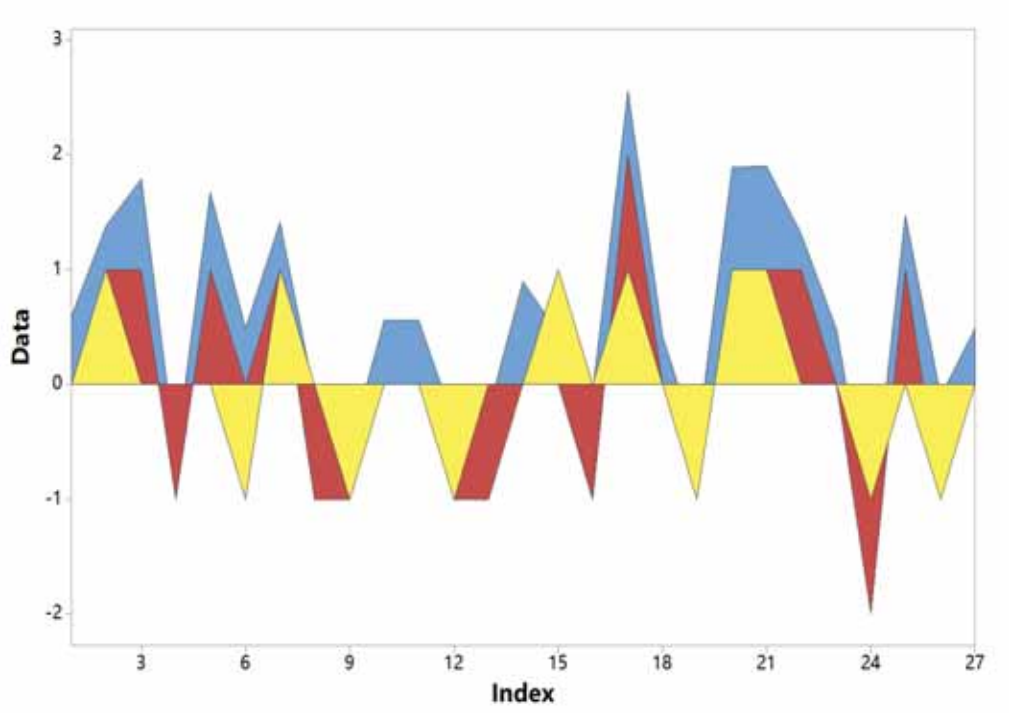


FIGURE 3
Area Graph of Coupling coordination degree

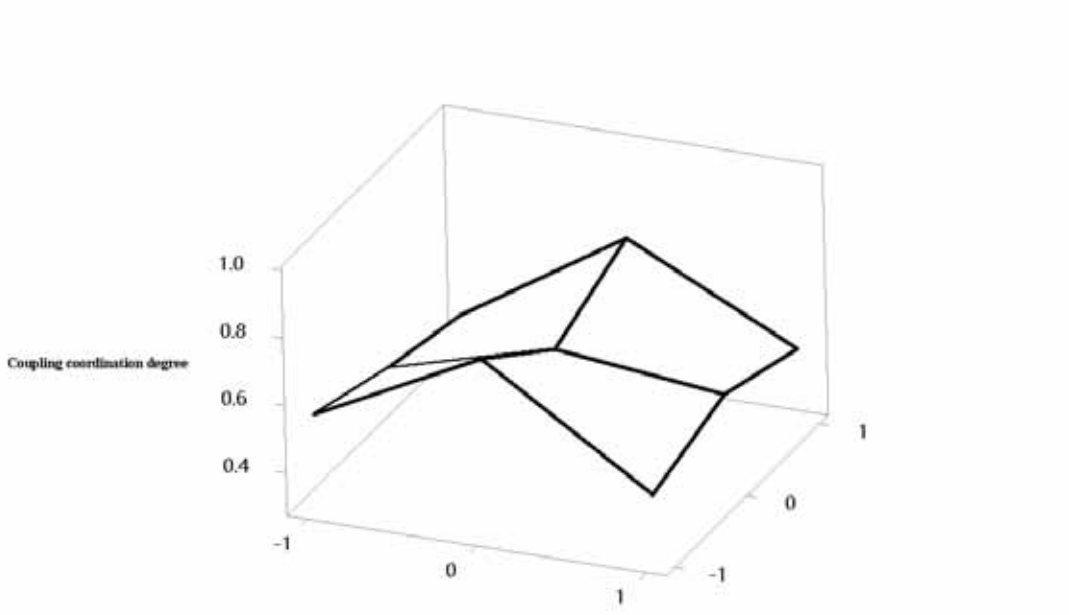


FIGURE 4
Surface Plot of Coupling coordination degree

has shown an increasing trend of changes year by year. All in all, since 2008, the rapid development of social economy and the acceleration of urbanization have not only caused the decline of the ecological environment, but also adversely affected the sustainable and healthy development of the society and economy, and realized the coordinated development of the ecological environment and the social economy to become sustainable. Development key issues that need to be solved urgently.

Analysis on the Coordinated Development of Ecological Environment and Social Economic Coupling. Based on the comprehensive evaluation index of ecological environment and social economic development, the coupling coordination degree model is used to calculate the coupling coordination degree index of the ecological environment and social economy in the study area from 2008 to 2018. During the study period, the coupling and coordination index of the ecological environment and the social economy showed an upward

trend year by year, from 0.3344 in 2008 to 0.6647 in 2018 (Figure 3 and 4), indicating that the relationship between the ecological environment and the social economy in the study area has continued to improve and tends to Coordinated development. From 2008 to 2010, the degree of coupling and coordination showed a slow upward trend. From 2011 to 2018, due to the rapid development of the two systems, the comprehensive development index rose rapidly, and the degree of coupling fluctuated accordingly, while the degree of coupling and coordination showed a rapid increase. It shows that under human intervention, the ecological environment system and the socio-economic system gradually tend to develop harmoniously, and the level of coordination continues to improve. At the same time, it further shows that the degree of coordinated development of the two systems has a strong correlation with the level of ecological environment and the level of social and economic development. The greater the index of coupling coordination degree, the higher the degree of system coupling coordination development.

Main measures and methods. Continue to promote the modernization of the ecological environment governance system and governance capabilities

Implementation of the "three lines and one single" ecological environment. Partition management and control is a relatively complex exploratory work. The preparation of "three lines and one order" and the release of results are the basic work. More importantly, the "second half of the article" is applied to the results, and the application system is continuously expanded and improved in practice. Apply the mechanism to serve the ecological and environmental protection work in the new situation.

Speed up the establishment of a national ecological environment district management and control system. Accelerate the release and storage of the results of the "three lines and one order" in various provinces (autonomous regions and municipalities), promote the sharing of the "three lines and one order" and related data systems such as pollution discharge permits, environmental assessment approvals, environmental monitoring, and environmental law enforcement, and continuously enrich and refine the "three lines One single" data support system and district management and control requirements. Establish a dynamic update and adjustment mechanism for the "three lines and one order", strengthen departmental linkage and information feedback, and continuously improve the strategic, pertinence and operability of the application of the "three lines and one order" results in practice.

Continuously improve the results application mechanism. Strengthen the application of the "three lines and one order" results in the environmental management of elements such as ecology, water, atmosphere, and soil, explore the establishment of the "three lines and one order" as the basis for environmental space management and control, and use the planning environmental assessment and project environment to assess the environmental access gates. Pollution permits are the basis for corporate operation and compliance, and the whole-process environmental management framework with law enforcement and supervision as the bottom line of environmental supervision will help win the battle against pollution. Give full play to the supporting role of the "three lines and one single" results in the "14th Five-Year Plan", and provide a basis for planning ecological environmental protection work for the regional system, planning resource development, industrial layout and structural adjustment, urban construction, and site selection for major projects. We will promptly start the drafting of the "Fourteenth Five-Year Plan for the Implementation of the Environmental Assessment and Pollution Permit Reform Implementation Plan" and actively carry out research on the revision of the "Environmental Impact Assessment Law".

Continue to promote system construction. In order to ensure the seriousness and standardization of the system, it is necessary to sort out the imperfections in the operation of the current system, check for omissions, and revise and improve relevant systems in accordance with the revision opinions and suggestions put forward by various departments to achieve a sound system and management, a well-regulated situation.

CONCLUSION

This article introduces the coordinated development model and sustainable development theory. The research results show that: facing the new situation of economic development where opportunities and challenges coexist, China must grasp the direction of world economic development, and on this basis, clarify the direction of China’s economic development. At the same time, it also needs to make corresponding responses in light of the new domestic development situation in China. Innovation and change ensure that the domestic economy can be better developed under the background of anti-globalization.

ACKNOWLEDGEMENT

This paper is supported by The 2019 Hunan Provincial Social Science Fund Key Project "Research on the Political Economy of Socialism with Chinese Characteristics for Open Development" (19WTB13).

REFERENCES

[1] Dong, Q.Y., Futawatari, T. (2015) A review of the progress in China's renewable energy generation, and its links with energy conservation, environmental degradation and economic growth. Fresen. Environ. Bull. 24, 405-411.
[2] Gultekin, U. (2019) Renewable electricity generation for sustainable development and environmental management in Turkey. Fresen. Environ. Bull. 28, 8171-8174.
[3] Broman, G.I., Robèrt, K.H. (2017) A framework for strategic sustainable development. J. Cleaner Prod. 140, 17-31.
[4] He, Y., Lin, K., Zhang, F., Wang, Y., Chen, X. (2018) Coordination degree of the exploitation of water resources and its spatial differences in China. Sci. Total Environ. 644, 1117-1127.
[5] Xu, Y.P., Wang, M., Qin, M., Shi, H.X., Sui, B.W., Jia, X.Z., Lu, D.L. (2018) Study of the relationship between economic growth and environmental quality with the Kuznets curve in Guangxi, China. Fresen Environ Bull. 27, 2818-2828.
[6] Xiong, S., Tian, Y., Ji, J., Ma, X. (2017) Allocation of energy consumption among provinces in China: a weighted ZSG-DEA model. Sustainability. 9(12), 2115-2116.
[7] Zhou, H.Y. (2020) Incentive mechanism of low carbon economic growth quality based on fuzzy cluster analysis. Fresen. Environ. Bull. 29(4), 2350-2356.
[8] Pao, H., Chen, H.A., Li, Y. (2015) Competitive dynamics of energy, environment, and economy in the U.S. Energy. 89, 449-460.
[9] Tang, X., McLellan, B.C., Snowden, S., Zhang, B., Hook, M. (2015) Dilemmas for China: Energy, economy and environment. Sustainability. 7, 5508-5520.
[10] Han, S., Zhu, J. (2011) Research on the dynamic relationship of the Energy-Economy-Environment (3E) system-based on an empirical analysis of China. Energy Procedia. 5, 2397-2404.
[11] Broman, G.I., Robèrt, K.H. (2017) A framework for strategic sustainable development. J. Cleaner Prod. 140, 17-31.
[12] Pasape, L., Anderson, W., Lindi, G. (2015) Assessment of indicators of sustainable ecotourism in Tanzania. Anatolia. 26, 73-84.
[13] Jeffery, L.R. (2015) Erratum to: Ecological restoration in a cultural landscape: conservationist and Chagossian approaches to controlling the 'coconut chaos' on the Chagos Archipelago. Human Ecology. 43, 185-186.
[14] Lee, T.H., Jan, F.H., Huang, G.W. (2015) The influence of recreation experiences on environmentally responsible behavior: the case of Liuqiu Island, Taiwan. Journal of Sustainable Tourism. 23(6), 947-967.
[15] Biglar, M., Danehkar, A., Pourebrahim, S. (2016) Application of strategic fuzzy assessment for environmental planning: Case of Bird Watch Zoning in Wetlands. Open Journal of Geology. 6, 1380-1400.
[16] Buckley, R. (2015) Understanding and managing tourism impacts: an integrated approach. Journal of Ecotourism. 10, 177-178.
[17] Zhou, H.Y. (2020) Incentive mechanism of low carbon economic growth quality based on fuzzy cluster analysis. Fresen. Environ. Bull. 29(4), 2350-2356.
[18] Pao, H., Chen, H.A., Li, Y. (2015) Competitive dynamics of energy, environment, and economy in the U.S. Energy. 89, 449-460.
[19] Tang, X., McLellan, B.C., Snowden, S., Zhang, B., Hook, M. (2015) Dilemmas for China: Energy, economy and environment. Sustainability. 7, 5508-5520.
[20] Han, S., Zhu, J. (2011) Research on the dynamic relationship of the Energy-Economy-Environment (3E) system-based on an empirical analysis of China. Energy Procedia. 5, 2397-2404.

Received: **29.12.2020**
Accepted: **24.05.2021**

CORRESPONDING AUTHOR

Huancai Peng
School of Marxism,
Hunan Technology and Business University,
Changsha 410205 – China

e-mail: penghauncai88@163.com

© by PSP Volume 30– No. 09/2021 pages 10551-10558 Fresenius Environmental Bulletin

STUDY ON ECOLOGICAL CIVILIZATION CONSTRUCTION FROM THE PERSPECTIVE OF PUBLIC GOVERNANCE

Dandan Cui*, Ya Zhou

College of Business Administration, Ningbo Polytechnic, Ningbo 315800, China

ABSTRACT

This paper sorts out and summarizes the research on ecological civilization at home and abroad. Based on Xi Jinping's ecological civilization thought, combined with the development status of Ningbo City, using the coupling development model, the evaluation system of ecological civilization construction is constructed through SPSS software. In 2018, a comprehensive evaluation was made on the level of ecological civilization construction. The research results showed that the overall level of ecological civilization construction is on the rise, and the growth rate of ecological civilization construction slowed down after 2017. Therefore, the article finally puts forward the main measures to do a good job in the construction of ecological civilization, such as improving the level of urban and rural environmental construction, building an ecological economic system with the rural economy as the main body, and improving the ecological protection system.

KEYWORDS:
Ecological civilization, Construction, Analysis, Coupling development

INTRODUCTION

Ecological civilization is a form of human civilization. It is based on respect and maintenance of nature, with the aim of harmonious coexistence between man and man, man and nature, and man and society, and the connotation of establishing sustainable production and consumption methods to guide People embark on a sustainable and harmonious development path as the focus [1-3]. Ecological civilization emphasizes human consciousness and self-discipline, and emphasizes the interdependence, mutual promotion, coexistence and harmony between humans and the natural environment. It not only pursues harmony between humans and ecology, but also pursues harmony between people, and the harmony between people is between people and people. The prerequisite for natural harmony. Ecological civilization is the result of deep reflection on traditional civilization forms, especially industrial civilization, and is a major advancement in human civilization forms and civilization development concepts, roads and models [4]. Ecological civilization refers to the sum of material and spiritual results obtained by mankind following the objective law of the harmonious development of man, nature, and society; refers to the harmonious coexistence, virtuous circle, and comprehensive development of man and nature, man and man, and man and society. A form of cultural ethics whose basic purpose is sustained prosperity. It is based on mankind's reflection on the material civilization that has dominated human society for a long time. The finiteness of natural materials determines the finiteness of human material wealth. Mankind must be freed from the singularity of material wealth and pursue the richness of spiritual life. It is possible to realize the all-round development of people. This will undoubtedly cause a fundamental change in the human society [5].

The construction of ecological civilization is not only an effective practice of my country as the largest developing country in terms of sustainable development, but also to provide Chinese ideas, Chinese solutions and Chinese contributions to global environmental governance [6-8]. The 18th National Congress of the Communist Party of my country pointed out that "increasing resource and environmental constraints" are important difficulties and challenges facing our country on the road ahead. This shows that solving resource and environmental constraints and promoting sound economic development have become a new historical mission. Judging from the specific national conditions at the current stage of our country, not only the per capita resources are far below the world average, but also the natural endowment of resources is insufficient. In recent years, environmental quality has improved, but the problem of regional ecological environmental pollution is still not optimistic; ecological protection and continuous improvement of environmental quality have become more difficult [9-12].

The 19th National Congress of the Communist Party of China further emphasized that some outstanding problems of unbalanced and insufficient development have not been resolved, and that ecological and environmental protection have a long way to go. The Party Central Committee and the State Council attach great importance to the construction

of ecological civilization. Not only did they put forward a series of new ideas, new goals, new requirements and new deployments for the construction of ecological civilization, they provided fundamental follow and action guidelines for the construction of a beautiful China, and for the first time the construction of beautiful China An important goal of a modern socialist country. The proposal of the beautiful China goal not only places the people's expectations for a better life in the future, but also reflects the Chinese Communist Party's deep understanding of the laws of human civilization and rich understanding of the goals of modernization [13-16].

The current ecological and environmental problems in my country are still very complicated. The economy needs to develop, resources need to be developed, and the living standards of urban and rural residents need to be continuously improved. However, environmental pollution risks such as air, water, and soil are high, and various phenomena such as ecosystem degradation and other phenomena coexist. Government decision-making, enterprise production, and public life are intertwined with contradictions and need to be comprehensively balanced [17-20]; they also have development consensus and require overall consideration. To solve these problems and alleviate these contradictions, it is necessary to take the development path of ecological civilization, adhere to the harmonious coexistence of man and nature, and establish and practice the development concept of "green water and green mountains are golden mountains and silver mountains"; it is also necessary to vigorously promote environmental technological innovation and promote new development. In-depth integration of technology, new methods and industrial development, promote healthy economic and social development through ecological and environmental technological innovation, and transformation of technological achievements, and effectively build a "beautiful China"; it is even more necessary to cultivate a large number of high-level ecological environment professionals with both integrity and ability, deeply participate in and lead the global ecological environment governance.

MATERIALS AND METHODS

This article mainly adopts the forms of literature research, field survey, holding seminars, questionnaire survey, etc. to obtain first-hand data, and through the introduction of models for data analysis and sorting, satisfactory results have been obtained.

Model selection. Coordination refers to the harmony of various parameters between various levels and subsystems in the system, the integration of structure and function, and the steady state of the movement of material energy between the system and the environment. System changes are inevitable, so the relationship between the internal elements of the system must also be a dynamic process of constant adjustment and change. In order to dynamically and intuitively reflect the changes in the coordination status between the systems, a quantitative model composed of one or a set of functions can be established to measure the degree of system coordination, that is, the coordination degree model.

A complex system can be parsed into a network composed of various restriction factors through various relationships. In the early research, the system is often simply divided into multiple levels, and the connections between the levels are not necessarily quantified. This article is establishing In the coordination degree model, the effective analytic hierarchy process is combined to organically combine the various levels of the system, and the factors in the system that are obviously not related to other limiting factors are eliminated. In the research process, the system elements are simplified and the system research is improved. It is more efficient, and can fully analyze the existing limiting factors more closely, so the system research based on coordination degree has obvious advantages.

RESULTS AND DISCUSSION

Currently existing problems. Over the past 30 years of reform and opening up, Ningbo's economy and society have achieved considerable development. The amount of construction land has shown a rapid growth trend, and the contradiction between the supply and demand of construction land has been prominent. Such high-intensity development, especially disorderly development, has led to a continuous increase in the regional ecological environment. It has brought a lot of pressure to the ecological environment. The scale of the city and the extent of land development and utilization exceed the bottom line of the carrying capacity of resources and environment has become a major issue affecting the construction of ecological civilization in Ningbo. In addition, the fragmentation of ecological space is prominent due to the continuous development of cities and towns and the unreasonable construction layout of industrial enterprises. The disorderly development of a large number of small and medium-sized enterprises leads to the phenomenon of villages and villages burning fires and households smoking, and there are more cases of mixed factories and residences and disorderly layout. The sprawl expansion of cities and towns has caused urban land use intensity to exceed 20% of the internationally accepted ecological livability standard, and ecological spaces such as farmland, wetlands, and forests are seriously fragmented.

In terms of the atmospheric environment, although the air quality has reached the national sec-

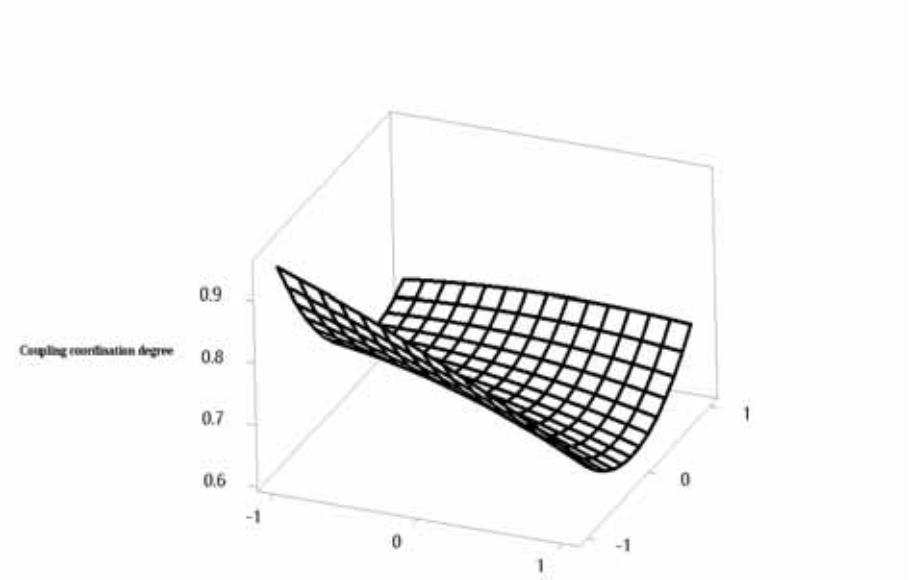
ondary standard, the foundation for steady improvement is still not strong. Structural pollution problems such as industry, energy, and transportation are still prominent. Various work has been slightly slack, and the results have been achieved. There may be repetitions. In terms of the water environment, due to various factors such as poor fluidity of the plain river network, insufficient ecological water replenishment, lagging in infrastructure construction, and the fact that illegal discharge has not been completely eliminated, the water quality is prone to fluctuate and rebound; especially in coastal waters. The overall situation is relatively poor, with four categories of inferiority as the main ones, and great efforts are needed to improve it. In terms of soil environment, the pollution status has not been fully grasped, the distribution and degree of pollution are difficult to accurately determine, the treatment and restoration technology is not yet mature, the capital demand is large, and the treatment and restoration is difficult; the city's general industrial solid waste co-processing capacity for domestic garbage has a certain gap, random disposal and dumping of solid waste still occur. At the same time, there is still a big gap between all levels and departments in learning, understanding and practicing Jinping's thoughts on ecological civilization. The transmission of ecological and environmental protection responsibilities is also diminishing to varying degrees, especially in the context of increasing downward pressure on the economy. The risk of supervision has increased; some enterprises and the public are not very aware of protecting the ecological environment, and behaviors that damage the ecological environment occur from time to time. The awareness of law-abiding needs to be further improved.

The recycling rate of industrial water in Ningbo is low, the contradiction between the carrying capacity and availability of water resources and the layout of key water-consuming industries is prominent, and the water consumption per unit of GDP remains high. However, the current urban water supply capacity is not enough to support the needs of urban planning, construction and development, and the quality of the water environment in the plain river network area cannot meet people's growing needs for a high-quality life. In addition, Ningbo's existing unreasonable water supply structure, scope and demand do not match the water supply capacity. The "single source and single line" reservoir water supply pattern has not changed. When extreme hydrological conditions and water pollution incidents emerge, the water supply dispatching capacity is limited. The foundation of emergency safety is not strong.

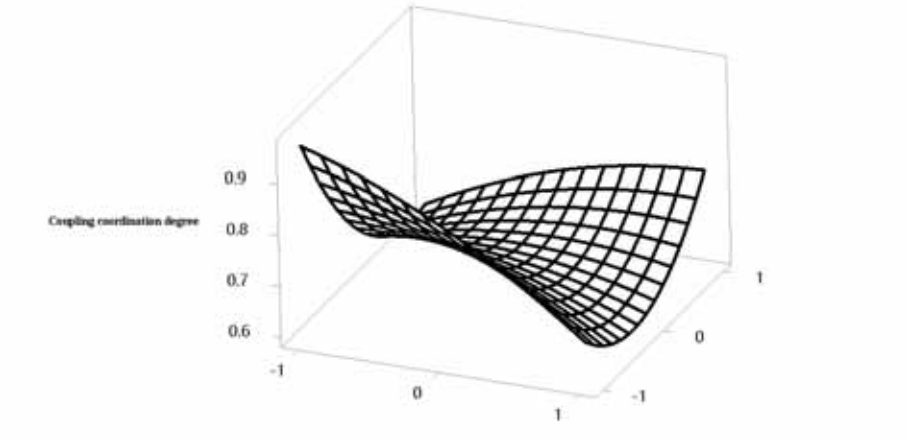
Public awareness of ecological civilization is not strong. The public's knowledge of ecological civilization is not high in depth and accuracy, and the knowledge of ecological civilization knowledge is characterized by "high understanding rate, low accuracy rate, and wide range of knowledge". The public is more concerned about their own ecological and environmental issues, but lacks understanding and attention to broader environmental issues; at the same time, although the public has certain environmental issues and phenomena, they lack the enthusiasm and autonomy to participate in environmental protection, which is widespread "blame "More lines, less" phenomenon.

Government and corporate ecological responsibility awareness needs to be strengthened. The long-term mindset and the role of supervisors have made local governments believe that they are not responsible for environmental protection; many local government officials are accustomed to holding relevant parties responsible for environmental damage in accordance with relevant laws and regulations, and neglecting their own responsibility. In particular, the emphasis on the development mode under the GDP performance evaluation system has directly led to many local governments and some officials not paying enough attention to ecological and environmental issues, the work is superficial, the initiative and enthusiasm for environmental protection are lacking, and the innovation motivation for ecological civilization construction is insufficient. Satisfied with daily routine work.

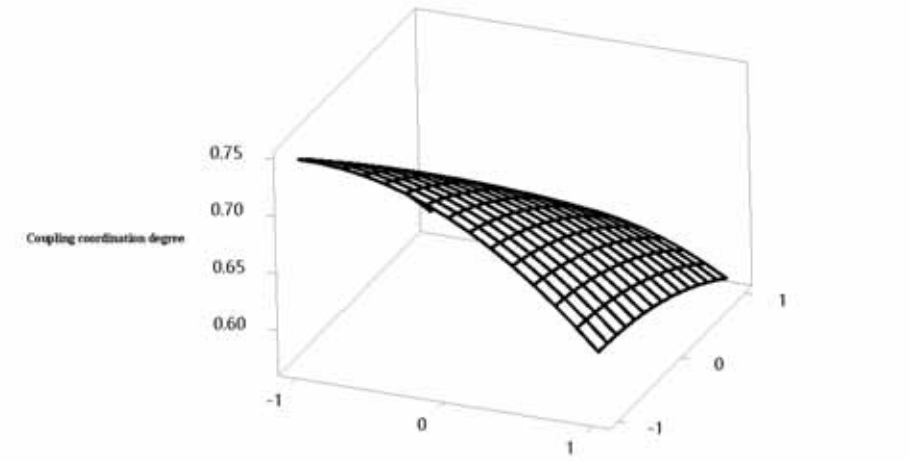
The concept of corporate ecological responsibility is generally weak. The essence of an enterprise is to produce qualified products, provide services, and maximize profits. Therefore, the level of understanding of the responsibility of ecological environmental protection is low. It is believed that the construction of ecological civilization and environmental protection responsibility are additional burdens of the enterprise. It is not a last resort and will not be taken seriously. , Some companies even pass on their so-called "extra burden" to society and the government. At the same time, some companies still have extensive production methods, and their ecological responsibility capabilities are not strong. They are only a small economic account, not a big account for ecological sustainable development. For them, shouldering ecological responsibility means that the company is responsible for preventing pollution and resource consumption. Rising costs have led to a decline in business efficiency. Some companies often choose the former between efficiency and ecological responsibility. The current laws and regulations reflect the non-severe punishment measures and the small amount of money, which further condones companies' failure to fulfill their ecological responsibilities, resulting in relatively weak corporate concepts.



(a)



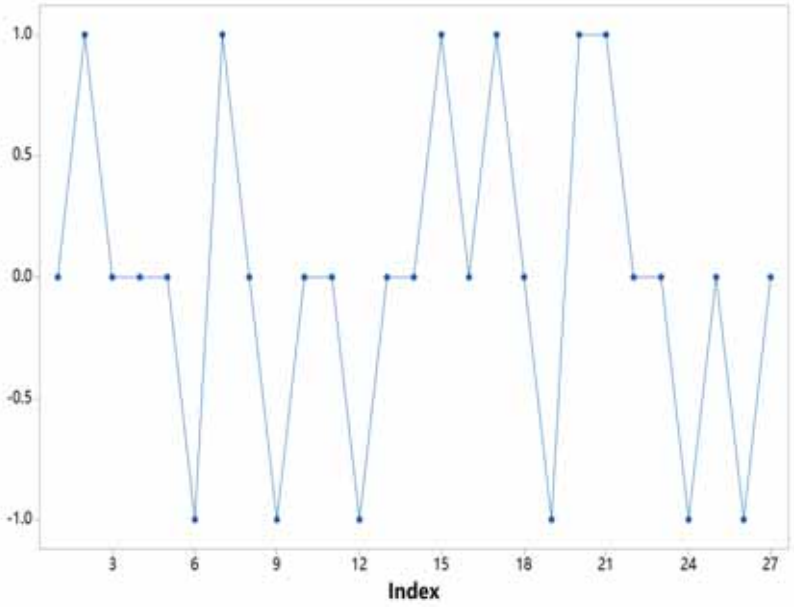
(b)



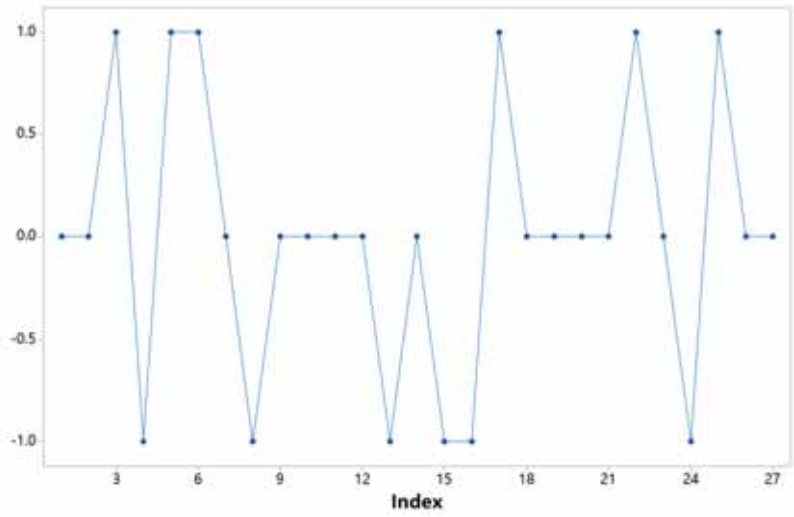
(c)

FIGURE 1
Surface Plot of Coupling coordination degree

Coordination degree model analysis. It can be seen from Figure 1 and 2 that the comprehensive index of the level of ecological civilization construction has been increasing from 2009 to 2018. In this decade, the level of ecological civilization construction in 2018 ranked first, which shows that it is gradually increasing over time. Strengthen the construction of ecological civilization. Combined with data analysis, it is found that the index development changes of the four criterion levels are almost the same as the comprehensive level of the city's ecological civilization construction, showing a rising trend. Since 2012, the ecological environment criterion level index has increased rapidly, indicating that the ecological environment has received attention and rapid development after 2012, mainly due to the impact of Zhejiang Province's policy on gradually increasing urban greening and improving urban human settlements. As a result, the green coverage rate in built-up areas and the per capita green area of parks have increased rapidly. The eco-economic criterion level index has shown an increasing trend in the past ten years, but the growth slowed down from 2013 to 2014, mainly due to the excessive energy consumption of 10,000 yuan of GDP and excessive power consumption of 10,000 yuan of GDP. After the guidance of General Secretary Xi, give full play to its own advantages, gradually accelerate the pace of economic transformation, and promote the green development by promoting ecological economy. Ecological society and ecological cultural norms have grown steadily from 2009 to 2018, urban infrastructure has been improved day by day, and the education level of residents has improved significantly.



(a)



(b)

FIGURE 2
Data statistics and analysis

Ecological civilization construction countermeasures. Improve the level of environmental construction. Social organizations should increase publicity, further strengthen the sewage recycling rate of existing urban and rural sewage plants, increase the supply capacity of recycled water, expand the scope of supply of recycled water, and apply recycled water to landscaping, urban and rural street cleaning, and mountain lakes. Vigorously promote the ecological agriculture industry, build a green agricultural base with mountains and rivers, plant organic green vegetables, reduce pollution caused by pesticides and fertilizers, and increase farmers' income; develop rural tourism and other industries that have a small environmental burden to achieve low Pollution, high-yield urban and rural development model; increase capital investment in urban and rural infrastructure, increase bus routes between urban and rural areas, reduce the use of private cars, and ensure air quality.

Construct an ecological economic system with rural economy as the main body. Social organizations should protect and transform the rural ecological environment through collective financing and government investment, and use their unique natural resources to attract external investment. On the basis of not damaging the ecological environment, establish characteristic ecological villages and seek a way for rural farmers. Sustainable development path. Depend on the farmland contracted by farmers to promote the construction of characteristic planting and breeding industries. At the same time, led by companies that process agricultural products, scientifically and rationally integrate resources, build an industrial chain with clear division of labor, professional technology, and a larger scale, thereby forming a development model in which advantageous industries drive rural economic growth. The rural tourism resources are rich, suitable for the development of tourism products in the fields of leisure agricultural park tourism, hot spring tourism, red tourism, and Xikou cultural tourism. Leading the development of tourism by leading enterprises, scientifically adjust the overall layout of the village, and rationally allocate various industrial resources in the village. Under the conditions of protecting the ecological environment, it can not only help farmers find employment, but also increase farmers' income.

Create an environmentally friendly company. A working group is formed by the person in charge of the social organization and the leaders of the environmental protection department to jointly formulate the work process and complete the filing of various legal documents, the responsibility of clean production positions, the training of employees and management personnel, the rectification and daily maintenance of environmental protection facilities, and the emission standards To improve the management level and environmental protection capabilities of various enterprises, and to organize experts and environmental supervision departments to conduct unified inspection and acceptance according to the contract period. Let enterprises be passively beaten by environmental protection in the past, and by creating environmentally friendly enterprises, they can take the initiative to enhance their market competitiveness.

Co-build a non-confrontational environmental social governance model. It is possible to sign cooperation agreements in the form of purchasing government social services to jointly explore and create a "non-confrontational environmental social governance model." Establish a five-in-one linkage working mechanism of government + environmental protection department + environmental NGO + enterprise + local residents. On the one hand, our environmental NGO supervises the performance of environmental protection and supervision functions of government departments, and on the other hand dispatches public welfare environmental protection experts to help enterprises rectify and strengthen management, and supervise and Help companies increase their awareness of complying with environmental protection laws, and achieve compliance production and emission standards. At the same time, various legal and ecological civilization publicity and education activities are carried out in the surrounding communities, schools, and villages of the company. The opinions and demands of residents are collected and returned to the government for timely disposal. Resident environmental protection supervisors are developed around the company. If the company is found to be illegally discharged, timely report Environmental protection department. Through the "non-confrontational environmental social governance model", various social conflicts caused by environmental issues have been effectively quelled. The industrial parks not only ensured normal production, but also kept the bottom line of environmental protection. In coordinating the relationship between the government, enterprises and community residents, social organizations act as a bridge as an independent third party.

CONCLUSION

This paper sorts out and summarizes the research on ecological civilization at home and abroad. Based on Xi Jinping's ecological civilization thought, combined with the development status of Ningbo City, using the coupling development model, the evaluation system of ecological civilization construction is constructed through SPSS software. In 2018, a comprehensive evaluation was made on the level of ecological civilization construction. The re-

search results showed that the overall level of ecological civilization construction is on the rise, and the growth rate of ecological civilization construction slowed down after 2017. Therefore, the article finally puts forward the main measures to do a good job in the construction of ecological civilization, such as improving the level of urban and rural environmental construction, building an ecological economic system with the rural economy as the main body, and improving the ecological protection system.

ACKNOWLEDGEMENTS

1. The general scientific research project of Zhejiang Provincial Department of education "Research on the role of social organizations in building a new pattern of community grassroots governance", Project No.:

2. Ningbo Polytechnic high level talents introduction research project "Research on the credibility evaluation of public welfare social organizations under the background of public governance", Project No.: rc201910

REFERENCES

[1] Li, N. (2019) Analysis of rural ecological environment governance and economic and social development in the background of digitization. Fresen. Environ. Bull. 28, 10076-10082.

[2] Wang, W., Chen, R.P., Zhou, Y.L. (2019) Study on environmental protection in tourist towns based on ecological theory. Fresen. Environ. Bull. 28, 8800-8805.

[3] Yang, S., Lin, A.M. (2019) Research on green development of coal industry based on ecological civilization. Fresen. Environ. Bull. 28, 5398-5401.

[4] Xiao, L., Zhao, R. (2017) China's new era of Ecological Civilization. Science. 58, 1008-1009.

[5] Lu, X.L., Li, B.Y. (2020) The Cultivation of College Students' View of Ecological Civilization from the Perspective of New Media. Journal of Hengshui University. 22(1), 90-94.

[6] Zhang, X.H., Wang, Y.Q., Qi, Y., Wu, J., Liao, W.J., Shui, W., Zhang, Y.Z., Deng, S.H., Peng, H., Yu, X.Y., Qi, H. (2016) Evaluating the trends of China's Ecological Civilization construction using a novel indicator system. Journal of Cleaner Production. 133, 910-923.

[7] Sun, X.F., Gao, L., Ren, H., Ye, Y.Q., Li, A., Stafford-Smith, M., Connor, J.D., Wu, J.G., Bryan, B.A. (2018) China's progress towards sustainable land development and Ecological Civilization. Landscape Ecology. 33, 1647-1653.

[8] Chen, Y.Y. (2019) The Choice of the Way to Cultivate College Students' View of Ecological Civilization in the New Era. Journal of Kashgar University. 40(5), 91-95.

[9] Gao, L., Bryan, B.A. (2017) Finding pathways to national-scale land-sector sustainability. Nature. 544, 217–222.

[10] Yang, Q., Yang, D. (2012) Research on the MSP Evolution Patterns of Two-oriented Society Coordinated Development in Regions of China. Procedia Environmental Sciences. 12, 777-784.

[11] Foxlee, J. (2015) Cultural landscape interpretation: The Case of the Sorry Rock Story at Uluru-Kata Tjuta National Park. Tourism Recreation Research. 32, 49-56.

[12] Pasape, L., Anderson, W., Lindi, G. (2015) Assessment of indicators of sustainable ecotourism in Tanzania. Anatolia. 26, 73-84.

[13] Jeffery, L.R. (2015) Erratum to: Ecological restoration in a cultural landscape: conservationist and Chagossian approaches to controlling the 'coconut chaos' on the Chagos Archipelago. Human Ecology. 43, 185-186.

[14] Lee, T.H., Jan, F.H., Huang, G.W. (2015) The influence of recreation experiences on environmentally responsible behavior: the case of Liuqiu Island, Taiwan. Journal of Sustainable Tourism. 23(6), 947-967.

[15] Biglar, M., Danehkar, A., Pourebrahim, S. (2016) Application of strategic fuzzy assessment for environmental planning: Case of Bird Watch Zoning in Wetlands. Open Journal of Geology. 6, 1380-1400.

[16] Buckley, R. (2015) Understanding and managing tourism impacts: an integrated approach. Journal of Ecotourism. 10, 177-178.

[17] Ven, S. (2016) Residents' Participation, Perceived Impacts, and Support for Community-based Ecotourism in Cambodia: A Latent Profile Analysis. Asia Pacific Journal of Tourism Research. 21(8), 836-861.

[18] Briassoulis, H. (2003) Crete: Endowed by nature, privileged by geography, threatened by tourism? Journal of Sustainable Tourism. 11, 97-115.

[19] Butler, R.W. (1991) Tourism, environment, and sustainable development. Environmental Conservation. 18, 201-209.

[20] Fushita, A.T., Santos, J.E., Rocha, Y.T. (2017) Historical land use/cover changes and the hemeroby levels of a bio-cultural landscape: Past, present and future. Journal of Geographic Information System. 9, 576-590.

Received: **03.01.2021**
Accepted: **03.03.2021**

CORRESPONDING AUTHOR

Dandan Cui
College of Business Administration,
Ningbo Polytechnic,
Ningbo 315800 – China

e-mail: cuidandan876@163.com

© by PSP Volume 30– No. 09/2021 pages 10559-10567 Fresenius Environmental Bulletin

STUDY ON THE TOURISM MANAGEMENT MODE IN ECOLOGICALLY FRAGILE AREAS BASED ON BP NEURAL NETWORK

Yujin Kan[1,*], Zhengbin Dou[1,2], Rong Hu[1]

[1]Nanhang Jincheng College, Nanjing, Jiangsu 211156, P.R. China
[2]Nanjing University of Aeronautics and Astronautics, Nanjing, Jiangsu 210016, P.R. China

ABSTRACT

The animal and plant resources in the tourism area are seriously affected, resulting in the reverse evolution of the ecosystem. Taking Longxi-Hongkou natural reserve as the target area, this paper takes landscape patch area, maximum patch index and connectivity as the entry points to investigate the inherent rules of pattern changes of scenic spot before and after external interference. On this basis, the ecological fragility of the area is comprehensively evaluated, and the causes are identified, in which the corresponding innovative management mode is put forward. The high-altitude area in the north of the area has the highest fragility level and is most affected by natural disasters. The management method of stable-barrier-drainage is mainly used to protect tourism resources. The central and southern regions are mainly grade I and II fragile areas, and there are many human disturbance factors. Through the establishment of natural reserve intelligence management system, the related elements of tourism are integrated continuously, the information of ecotourism activities is grasped timely and accurately, the balance of various elements of tourism resources and environment is maintained. In order to protect the ecological environment resources and increase the ability of anti-interference, we should reasonably plan tourism development and construction.

KEYWORDS:
Plant resources, natural reverse, ecological fragility, landscape, BP neural network

INTRODUCTION

With the improvement of life quality and consumption level, the tourism industry has realized the three-step development of starting, catching up and leaping at the speed of black horse, and has become a new growth point of national economy [1]. In 2019, the number of domestic and foreign tourists reached 9.736 billion, with a comprehensive contribution value of 9.89 trillion yuan, accounting for 11.34% of the total GDP, becoming a real strategic industry pillar [2, 3]. Tourism and ecological environment are interdependent and mutually promoting. Good ecological environment is the premise of tourism development. Tourism economy in turn promotes the protection and construction of ecological environment. In order to ensure the safety of the ecological environment of the viewing area, the national and local governments have also formulated relevant rules and policies to purify the tourism environment, prevent and avoid the degradation of tourism resources and the destruction of ecological environment, and ensure the sustainable development of China's tourism industry [4-7]. However, the rapid growth of ecotourism demand and the relative lack of natural environment carrying capacity are still the fundamental reasons for the destruction of ecological resources and the decline of environmental quality in tourism areas [8]. Therefore, it is urgent to innovate tourism management mode, coordinate the relationship between tourism and the natural environment, maintain the balance of various elements of tourism resources and environment.

Since from 1950s, tourism and environmental protection gradually came into the attention of scholars in various countries, and a large number of research results were achieved. Jeffrey et al. [9, 10] discussed the judgment methods and main factors of the impact of tourism on the natural environment. Timmerman et al. [11-14] put forward the method of using degree to reveal the environmental fragility, divided the level of adverse impact of external impact on tourism areas, and explored the carrying capacity and resilience of the ecosystem itself. Steven et al. [15] took the Yucatan Peninsula in southern Mexico as the research object, combined with the environmental simulation model to study its land use and plant cover, and developed a management system to promote its biodiversity in view of the unique ecological environment of the peninsula. The research on ecological fragility and tourism management in China started in 1981. Zhou et al. [16] made a preliminary discussion on the evolution of natural environment and desertification of the Mandarin Ducks Pool in Jinta County, Gansu Province. They pointed out that improper spatial distribution of water resources would cause regional ecological transition to

fragility. Qi et al. [17, 18] used the unsupervised clustering method of RBF neural network to evaluate the ecological environment fragility of the Antarctic fides peninsula with intuitive visual effect, and established the peninsula LOG-RBF ecological environment prediction model. Yu et al. [19] proposed to integrate internet and RFID technology into the construction, monitoring and management of Qingming riverside landscape garden. Combining with the elements of tourists' behavior, it attracted a lot of resources with a brand new wisdom scenic experience.

In order to better protect the natural environment resources of the tourist area, this paper selects Longxi-Hongkou nature reserve as an represent, and evaluates the current situation of the fragility of the ecological environment of the scenic spot by using the BP neural network model. The internal rule of the pattern change of the scenic spot before and after the external interference is investigated by combining the theories of systematic, ecology and sustainable development. On the basis of defining the driving mechanism for the change of ecological environment fragility, the development direction of tourism area is planned, and the countermeasures and measures for realizing the benign development of ecological environment are put forward.

MATERIALS AND METHODS

Longxi-Hongkou nature reserve, located in the north of Dujiangyan City, Sichuan Province, covers an area of 310 hectares. Geology and geomorphology are influenced by Himalayan tectonic movement with many cliffs, and the vertical height difference is 1200~4582m. They are typical alpine gorge landforms [20-22]. The climate in the study area belongs to the subtropical wet monsoon area in Sichuan Basin. The annual precipitation (about 1600~900mm) is large and the precipitation time is concentrated. Over 80% of the precipitation is concentrated in March-September. Affected by multiple factors such as topography, climate, precipitation and so on, in recent years, geological disasters such as mountain collapse, landslide and debris flow have occurred frequently, the morphosequent and vegetation cover have changed greatly, and the biodiversity has decreased [23]. The southern part is close to the Chengdu Plain Economic Zone, and human disturbance activities show a high intensity and diversification phenomenon, which seriously affects the animal and plant resources, and the ecosystem shows a reverse evolution trend [24].

On the basis of sufficient field investigation and verification, the patch area (CA), maximum patch index (LPI) and connectivity of landscape types are analyzed with the dynamic evolution of landscape pattern as the entry point. Using BP neural network method and GIS remote sensing technology, and taking the comprehensive index classification table of ecological environment fragility as the division basis [25], the RVI values in 1999, 2009 and 2019 were calculated respectively, and the ecological fragility model of the study area was established. The specific standards are shown in Table 1. On the basis of defining the driving mechanism of natural factors and human factors, innovating the tourism management mode of Longxi-Hongkou nature reserve scenic spot by means of digitalization, informatization and mobile technology. Combining the key factors and geographical location causing ecological fragility problems, giving priority to natural functions, supplemented by necessary technical measures and management measures. The corresponding management policies and suggestions are put forward to promote the coordinated development of landscape construction, ecological environment and tourism economy in Longxi-Hongkou nature reserve.

RESULTS AND DISCUSSION

Landscape status. To clarify the landscape status of Longxi-Hongkou natural reserve and grasp the rules of historical evolution and development is the prerequisite for ecological fragility assessment of the study area. BP neural network has three or more layers of neurons, which is composed of input layer, hidden layer and output layer. It has objective, general and applicable characteristics [26-29]. Therefore, this study combined with GIS remote sensing technology, objectively presents the spatial distribution pattern and dynamic evolution process of vegetation cover in the reserve through three parameters of landscape patch area (CA), maximum patch index (LPI) and connectivity, which lays a good foundation for landscape ecological fragility assessment of the reserve.

The landscape structure of Longxi-Hongkou national nature reserve can be divided into five categories: broad-leaved forest, coniferous forest, shrub land, meadowland, water area and unused land. The patch area and distribution of landscape types are shown in Figure 1. The broad-leaved forest and coniferous forest in the three periods are widely distributed. Due to the tall trees, the Wenchuan earthquake has the most serious impact on them. From 1999 to 2009, the proportion of patch area decreased by 31.27%. After 10 years of adjustment and management, the proportion of patch area increased to 82.53% in 2019, which basically restored to the level before the earthquake. The area of shrubbery and meadowland is small, accounting for less than 10% in normal period. After the earthquake, the area of trees and meadowland is exposed, and the patch area increases to 8671.32hm^2, accounting for 22.16%. With the restoration of forest landscape, the meadowland area will decrease in 2019. Frequent geological disasters, such as mountain collapse, landslide and debris flow, have caused water sources to disappear in a large

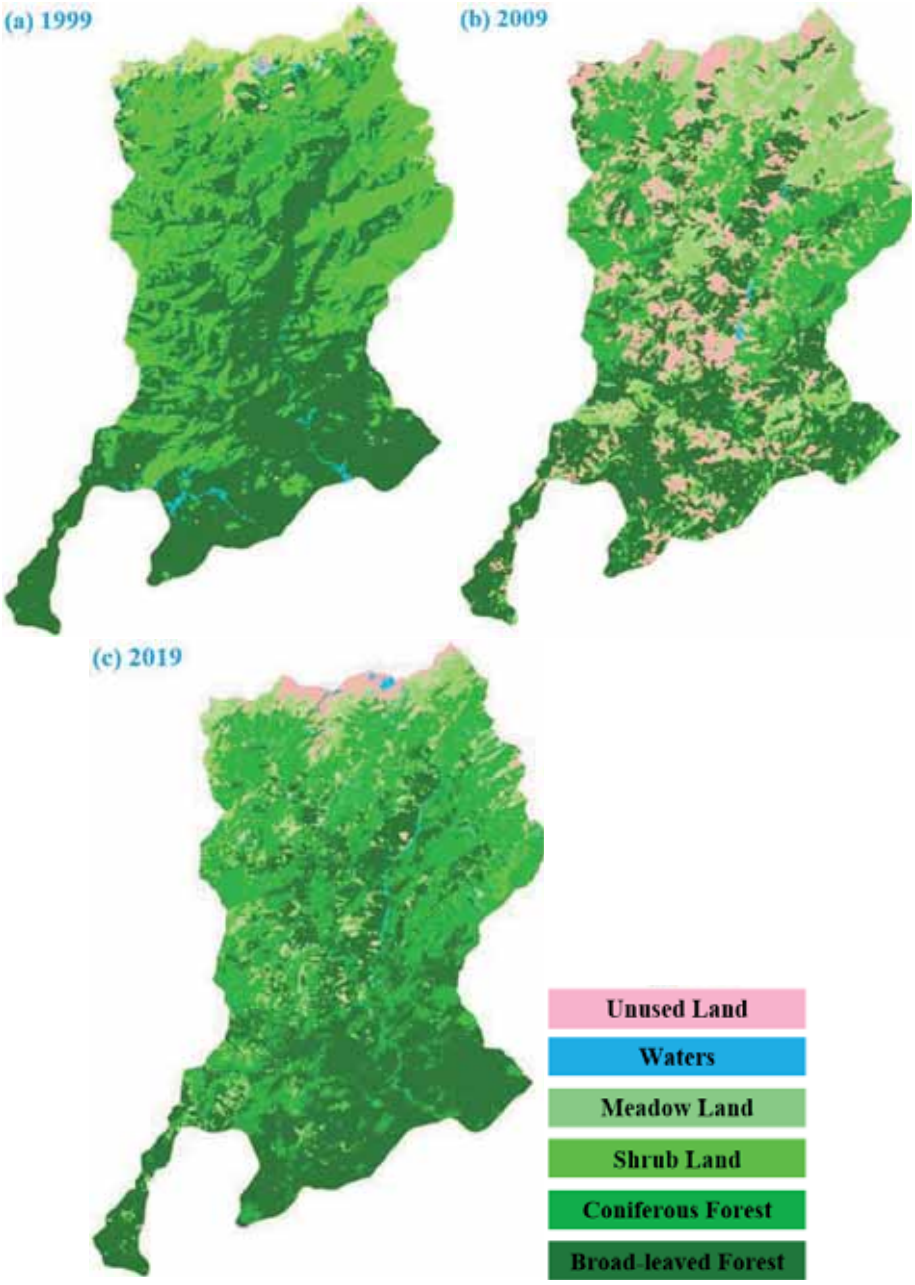


FIGURE 1
Change of patch area of landscape types in the past 20 years

area in Longxi-Hongkou national nature reserve,and unused land to increase substantially. At present, 1396.28 hm^2 bare land still exists, which is 3.23 times the area of patches before the earthquake.

Changes of LPI and connectivity index. The maximum patch index (LPI) represents the impact of the largest patch on the whole type or landscape. It can be seen from Figure 2 that during the historical evolution, the LPI value of water area changed little, except for the unused land, the index values of other landscapes showed a downward trend. The results showed that the largest patch area of broad-leaved forest, coniferous forest, shrubbery and meadowland decreased and the degree of fragmentation increased. The trend from single, homogeneous and continuous whole to complex, heterogeneous and discontinuous patch mosaics. The higher the landscape connectivity, the stronger the landscape concentration connectivity and the greater the ecosystem stability. The connectivity of landscape in the three periods is shown in Figure 3. Although the connectivity of broad-leaved forest and coniferous forest is high, the overall situation of the study area is declining year by year. Patches tend to be fractured from tightness, ecological stability deteriorates, and environmental restoration has a long way to go.

Landscape ecological vulnerability assessment. Landscape fragility of Longxi-Hongkou national reserve has changed dramatically in the past 20 years, as shown in Table 2. Broad leaved forest and coniferous forest are less fragile because of their large comprehensive patch area, high maximum plate index and connectivity. The CVI of the three years were grade I, slightly fragile, and have strong ability to maintain ecosystem stability and restore ecological environment. Shrubbery and meadowland are mostly distributed in areas with high altitude, large slope and relatively complex terrain, and their anti-interference ability is poor, especially the fragility risk of meadowland is increasing year by year. After the occurrence of earthquake, landslide, debris flow and other geological disasters, although some areas have been effectively restored, but from the CVI value, the ecological environment is still in a state of degradation. Under the erosion of rainwater, the bare land will bring sediment and gravel into the river, and some tributaries will be blocked, and the water area will be reduced. The soil after nutrient loss is not conducive to plant growth, resulting in increased landscape fragmentation and poor ecological stability.

TABLE 1
Classification of comprehensive index of ecological environment fragility

Category	Slight	Mild	Moderate	Weak	Severe
Grade	I	II	III	IV	V
RVI	0~0.2	0.2~0.4	0.4~0.6	0.6~0.8	0.8~1

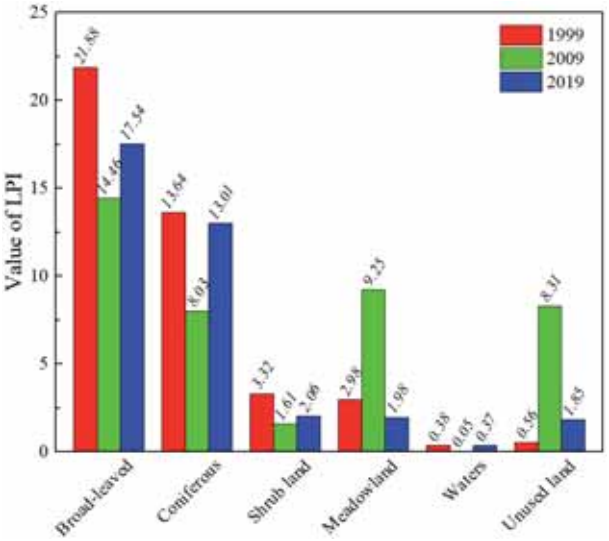


FIGURE 2
Changes of LPI in the past 20 years

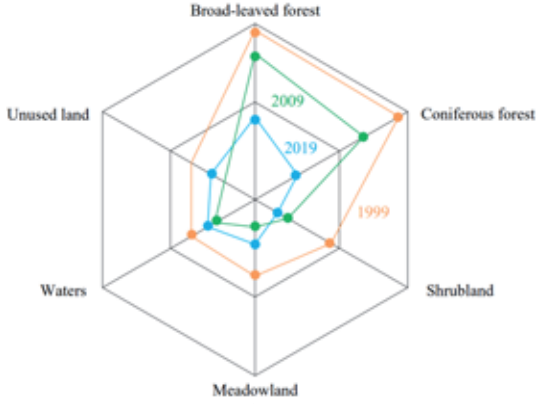


FIGURE 3
Changes of connectivity index in the past 20 years

TABLE 2
Landscape ecological fragility level

Landscape types	CVI					
	1999		2009		2019	
Broad-leaved	0.0063	I	0.0061	I	0.0089	I
Coniferous	0.0124	I	0.0298	I	0.0143	I
Shrubland	0.5932	III	1.0235	V	0.6211	IV
Meadowland	0.4831	III	0.5604	III	1.0369	V
Waters	0.1592	I	0.2014	II	0.2021	II
Unused land	0.3381	II	0.4681	III	0.4091	III

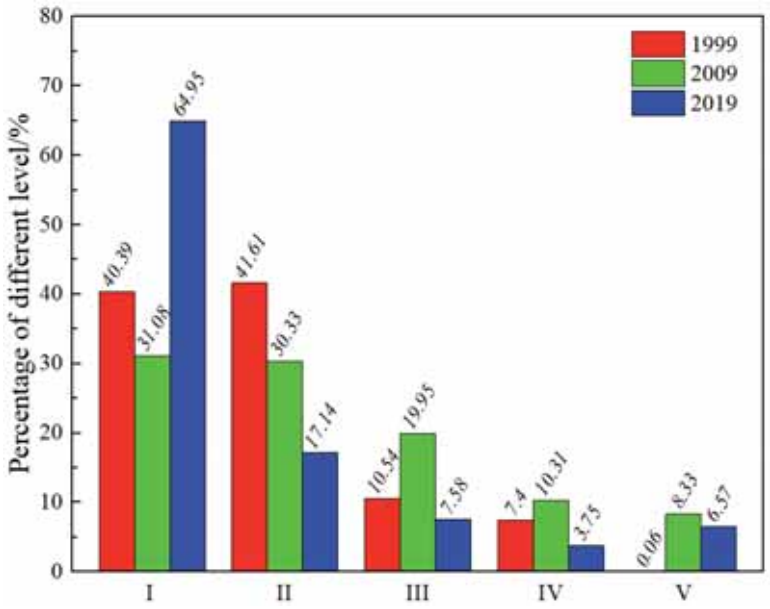


FIGURE 4
Distribution of ecological fragility in the past 20 years

Comprehensive ecological fragility assessment. The BP neural network method is used to map the ecological fragility level distribution of Longxi-Hongkou national reserve, as shown in Figure 4. In terms of spatial distribution, the study area is mainly classified as grade I slightly fragile area and grade II slightly fragile area, covering an area of 25456.37 hm^2, accounting for 82.1%. In recent years, the state and government have implemented the project of returning farmland to forest and natural protection in the middle and low latitudes, mainly planting broad-leaved forest and coniferous forest, enriching the regional structure. According to the analysis of landscape ecological fragility, deciduous forest and coniferous forest have strong anti-interference ability, so the southern and central parts of the distribution of deciduous forest and coniferous forest have high ecological self stability. Although some forests were damaged by the Wenchuan earthquake, the ecological bearing capacity of the region is strong. With the passage of time, most of the ecological environment has been well restored and the ecological service value is high. Affected by the earthquake in 2009, the area of moderately vulnerable area of grade III increased sharply, and the total proportion of fragile area of grade IV and V reached 18.64%. The ecosystem had the worst stability in 20 years. Except in 2009, the area and proportion of grade III moderately fragile area, grade IV intensity fragile area and grade V severe fragile area showed a decreasing trend. Grade III fragile areas are mainly distributed in Zhongshan and subalpine areas, and the landscape is dominated by shrubs. After the earthquake, soil and water loss is serious, especially in the vicinity of Baisha River, and some fragile areas of grade I and II evolve into moderately fragile areas of grade III. The southern part of the reserve is close to Chengdu plain economic zone. The number of tourists, digging medicine and picking bamboo shoots in the reserve increases, and the phenomenon of human disturbance is serious, resulting in a small area of grade III fragile areas scattered in the central and southern parts of the reserve. Grade IV and V fragile areas are distributed in the northern part of the reserve in a strip shape, with high altitude, steep slope and towering peaks. The limited vegetation area degenerates into meadow or unused land, the secondary disasters are obvious, the ecosystem presents the reverse succession trend, and the ecological fragility index is high.

Influencing factors of ecological vulnerability. Based on the area change of fragile area in Longxi-Hongkou nature reserve, combined with the statistics of regional influencing factors, the scale map of influencing factors of ecosystem fragility in the study area was drawn, as shown in Figure 5. Among them, the impact of natural disasters on the ecological stability of the scenic spot accounted for the largest proportion of 47%. Due to the complex terrain, changeable climate, concentrated precipitation and other factors in the study area, the geological disasters such as mountain collapse, landslide and debris flow occur frequently. The forest in the study area fell over in a large area, and the landscape presented the trend of fragmentation, which destroyed the integrity of vertical vegetation band spectrum and the balance of mountain animal and plant structure. The original stable ecosystem was in turmoil, and the environmental situation was significantly worse.

The total proportion of human activities in the fragility influencing factors is 49%. Among them, digging medicine and picking bamboo shoots, reclamation meadowland and tourism development accounted for 6%, 12% and 31% respectively. The

south of Longxi-Hongkou nature reserve is close to Chengdu Economic Zone, and the human disturbance activities are high intensity and diversified. Due to the influence of geology and geomorphology, there is less cultivated land in the nearby area, and the nearby residents reclaim meadowland on a large scale to develop agricultural production and increase economic income, resulting in the destruction of natural vegetation and the increase of exposed land area. At present, about 4.8 hm2 meadowland and woodland along the periphery of the reserve are threatened by human reclamation, and the ecological fragility is increasing. The development of tourism facilities, traffic noise and tourists' activities in the reserve also have adverse effects on the normal habitat and migration of animals. Unreasonable scenic spot planning is easy to cause overload operation. Excessive tourists rush into the scenic spot, trample on the meadowland, harden the land and affect the growth of regional plants. Some tourists lack environmental protection awareness, and litter plastic bags, waste bottles and cans, batteries and other life garbage, which often contains heavy metals, cyanide, phenol and other highly toxic substances, infiltrates into the soil and groundwater by rainwater, pollutes the soil and water quality, affects the growth of animals, plants and aquatic organisms, reduces the ecological self-purification ability and self-renewal ability of the scenic spot, and affects the fragility of the ecological environment.

Innovation management countermeasures. Natural geological disasters, such as mountain collapse, landslide and debris flow, have the greatest impact on the ecological stability of the scenic spot and are also the main reasons for the fragility of Grade IV and V. They are mostly distributed in the northern region at high altitudes. The climate in this area is cold and even glacial landscape appears with poor vegetation growth conditions. Therefore, in the management of Longxi-Hongkou natural reserve, remote sensing technology should be fully used to effectively monitor the geological disaster area, mainly biological measures, supplemented by engineering prevention measures, and three-step method of stable-barrier-drainage should be used to maintain and protect the ecological natural system. First, through landscape restoration of meadowland and shrub, plant communities with relatively high stability can be formed, and the ability of ecosystem to resist disaster disturbance can be improved. Secondly, dam is built in the valley to intercept the solid material discharged,and elevate the erosion datum surface to stabilize the foot of the slope. Furthermore, drainage structures should be built, and vegetation restoration with accumulation fans should be carried out to improve ecosystem stability.

There are many human disturbance factors in the formation of fragile areas in the central and southern regions. The development of tourism facilities causes vegetation damage, overload of tourists, and villagers digging medicine and picking bamboo shoots in the mountains have a certain impact on environmental fragility. In the management of nature reserves, we need to take into account the ecological environment, economic benefits, social development and other benefits. Strengthen the supervision of natural resources development and construction projects, continue to implement the natural protection and returning farmland to forest projects, optimize the three-dimensional multi-level composite community of forest, shrub and grass, and continuously improve the vegetation coverage in the reserve. On the basis of tourism environmental capacity, the scale of tourism development should be strictly planned, and the number of tourists entering the area should be controlled. Strengthen the propaganda of environmental protection, strengthen the intensity of ecological warning education, popularize the knowledge of ecological environment protection, establish people's ecological security concept, reduce human interference factors, and protect the ecological environment of tourist areas. At the same time, the community should be united to formulate management measures for natural resources, strengthen ecological restoration of bare surface, and plant kiwi fruit, bamboo shoots, medicinal herbs and other plants that can optimize the ecological environment and bring economic benefits, so as to combine urban new rural construction with ecological environment construction.While protecting biological resources and enriching ecological diversity, tourism should be used to promote the development of circular economy and ecological industry, so as to achieve a good situation in which ecology, economy and society go hand in hand.

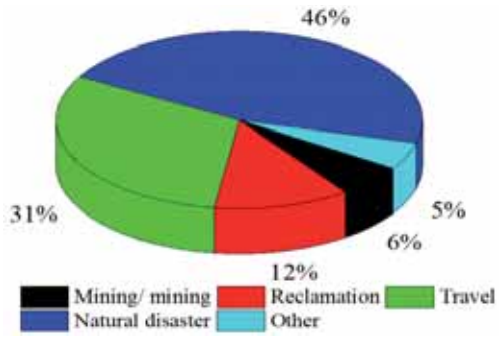


FIGURE 5
The proportion of influencing factors of ecological fragility in the study area

Improve the wisdom of tourism management. The core of wisdom tourism management is to provide wisdom tourism service mode. With the help of digitalization, informatization and mobile technology, an intelligent management system of Longxi-Hongkou nature reserve is established, which integrates the relevant elements of tourism

TABLE 3
Comparison of RVI classification area proportion after the measures

Grade	Before forecast		Natural recovery		Innovation recovery	
	Area/hm^2	Proportion/%	Area/hm^2	Proportion/%	Area/hm^2	Proportion/%
I	20139.99	64.95	20338.05	65.59	20468.67	66.01
II	5316.38	17.14	5474.808	17.65	6360.092	20.51
III	2351.94	7.58	2672.745	8.62	3101.033	10.00
IV	1164.18	3.75	817.2544	2.64	241.6838	0.78
V	2037.51	6.57	1707.146	5.51	838.517	2.70

constantly and grasps the information of ecotourism activities timely and accurately. Preventing forest fires, controlling visitor traffic, protecting animal and plant resources and monitoring environmental data are carried out through the three systems of unified data service center, biological resource management center and intelligent dispatch and command center. When an emergency occurs and the maximum capacity of the scenic spot is exceeded, timely alarm and emergency measures shall be started to realize the process management service of early warning, monitoring, analysis and decision-making. To provide tourists with intelligent and comfortable tourism services, provide intelligent management means for the department, and provide intelligent security protection for the environment of the study area.

The effect prediction of measures. With the help of BP neural network model, the RVI classification area of Longxi-Hongkou nature reserve after 10 years is counted, and the results are shown in Table 3. The improvement effect of the overall ecological fragility state of the study area shows that the innovative management measures are greater than the natural restoration. Under the action of the two methods, although the area of grade I slightly fragile area and grade II slightly fragile area in the study area has increased, the effect is more obvious after the measures. The area occupied has increased from 25812.85 hm2 to 26888.77 hm^2, increasing by 3.28%, and the ecosystem stability has been greatly improved. At the same time, the area and proportion of grade III moderately fragile area, grade IV intensity fragile area and grade V severe fragile area show a decreasing trend, especially in grade V fragile area, with the proportion declining from 5.51% to 2.7%, which indicates that the area of bare land has been greatly reduced and the ecological environment has been significantly improved. Therefore, innovative management mode, mainly based on natural function and supplemented by technical measures and management measures. The targeted restoration of landscape environment can effectively improve the protection of ecological environment resources, maintain the balance of all elements of tourism resources and environment, and promote the sustainable, rapid and healthy development of tourism.

CONCLUSIONS

To explore the innovative tourism management mode, Longxi-Hongkou nature reserve is selected as an example to evaluate the ecological fragility and influencing factors, and the spatial distribution pattern and dynamic evolution of vegetation cover are analyzed in this paper. (1) The results of ecological vulnerability show that the order of plants is as follows, broad-leaved forest > coniferous forest > shrub forest > meadowland and water area. Spatially, the study area mainly consists of grade I and grade II slightly fragile areas, grade III mainly distributes in Zhongshan and subalpine areas, and grade IV and V fragile areas distribute in strips in high altitude areas in the north. (2) Among many factors affecting ecological fragility, natural disasters such as mountain collapse, landslide and debris flow have the greatest impact on the ecological stability of the scenic spot, followed by human interference factors such as tourism, reclamation, digging medicine and picking bamboo shoots. (3) Innovating tourism management mode from three aspects, the three-step method of stabilization-barrier-drainage is used to protect tourism resources and strengthen the resistance to natural disasters. The development of protected areas should be planned rationally in conjunction with urban communities, and bare ground should be restored with economic vegetation. By comparing the fragility prediction areas before and after the measures, it can be seen that the ecological environment has been significantly improved after the innovative management.

ACKNOWLEDGEMENTS

This work was supported by the University Philosophy and Social Science Research Project of Jiangsu Province (No.2020SJA2218) and Key Projects of Graduate Education of Nanjing University of Aeronautics and Astronautics (NR2017006).

REFERENCES

[1] Kim, K., Park, O.J., Yun, S., Yun, H. (2017) What makes tourists feel negatively about tourism destinations? Application of hybrid text mining methodology to smart destination management. Technological Forecasting and Social Change. 123(10), 362-369.

[2] Kumar, V.S., Gogul, M.D., Pragadesh, S.K., Sebastin, J.S. (2016) Smart autonomous gardening rover with plant recognition using neural networks. Procedia Computation. 93(9), 975-981.

[3] Yu, Q., Yue, D.P., Wang, Y.H., Kai, S., Fang, M.Z., Ma, H., Zhang, Q.B., Huang, Y. (2018) Optimization of ecological node layout and stability analysis of ecological network in desert oasis: a typical case study of ecological fragile zone located at Deng Kou county. Ecological Indicators. 84(1), 304-318.

[4] Yin, P., Lin, Z.B., Prideaux, B. (2019) The impact of high-speed railway on tourism spatial structures between two adjoining metropolitan cities in China: Beijing and Tianjin. Journal of Transport Geography. 80(10), 102495.

[5] Mattei, F., Scardi, M. (2020) Embedding ecological knowledge into artificial neural network training: a marine phytoplankton primary production model case study. Ecological Modelling. 421(4), 108985.

[6] Chen, B.Q., Wu, Z.X., Wang, J.K., Dong, J.W., Guan, L.M., Chen, J.M., Yang, K., Xie, G.S. (2015) Spatio-temporal prediction of leaf area index of rubber plantation using HJ-1a/1b CCD images and recurrent neural network. ISPRS Journal of Photogrammetry and Remote Sensing. 102(4), 148-160.

[7] Todd, L., Leask, A., Ensor, J. (2017) Understanding primary stakeholders' multiple roles in hallmark event tourism management. Tourism Management. 59(4), 494-509.

[8] Rocha, S.J., Silva, S.D., Eleto, T.C.M.M., Jacovine, L.A., Garcia, L.H., Monteiro, G.E. (2018) Artificial neural networks: modeling tree survival and mortality in the atlantic forest biome in Brazil. Science of the Total Environment. 645(12), 655-661.

[9] Li, C.H. (2020) Biodiversity assessment based on artificial intelligence and neural network algorithms. Microprocessors and Microsystems. 79(11), 103321.

[10] Musavengane, R. (2019) Using the systemic-resilience thinking approach to enhance participatory collaborative management of natural resources in tribal communities: toward inclusive land reform-led outdoor tourism. Journal of Outdoor Recreation and Tourism. 25(3), 45-56.

[11] Chen, C.L., Chang, Y.C. (2017) A transition beyond traditional fisheries: Taiwan's experience with developing fishing tourism. Marine Policy. 79(5), 84-91.

[12] Yang, Y.J., Song, G. (2020) Human disturbance changes based on spatiotemporal heterogeneity of regional ecological vulnerability: a case study of Qiqihaer city, northwestern Songnen plain, China. Journal of Cleaner Production. 27(11), 125262.

[13] Ritchie, B.W., Jiang, Y. (2019) A review of research on tourism risk, crisis and disaster management: Launching the annals of tourism research curated collection on tourism risk, crisis and disaster management. Annals of Tourism Research. 79(11), 102812.

[14] Sun, Z.J., Shangguan, Y.X., Wei, Y., Su, B.Y., Zhou, C.Z., Hou, H. (2018) A study on antimony migration in soils using an artificial neural network model and a convection-dispersion diffusion model. Ecological Modelling. 389(9), 1-10.

[15] Duan, Y.Q., Zhang, L.D., Fan, X.Y., Hou, Q.H., Hou, X.M. (2020) Smart city oriented ecological sensitivity assessment and service value computing based on intelligent sensing data processing. Computer Communications. 160(7), 263-273.

[16] Xiang, Z. (2015) Tourism management, marketing, and development: the importance of networks and ICTs. Annals of Tourism Research. 52(5), 190-191.

[17] Hartman, S., Parra, C., De Roo, G. (2019) Framing strategic storytelling in the context of transition management to stimulate tourism destination development. Tourism Management. 75(12), 90-98.

[18] Milosevic, D., Cerba, D., Szekeres, J., Csanyi, B., Tubic, B., Simic, V., Paunovic, M. (2016) Artificial neural networks as an indicator search engine: the visualization of natural and man-caused Taxa variability. Ecological Indicators. 61(2), 777-789.

[19] Hasson, U., Nastase, S.A., Goldstein, A. (2020) Direct fit to nature: an evolutionary perspective on biological and artificial neural networks. Neuron. 105(3), 416-434.

[20] Wang, S.B., Liu, H.T., Han, Y., Chen, J., Pan, Y., Cao, Y., Meng, H., Zheng, Y.J. (2018) Low-altitude remote sensing based on convolutional neural network for weed classification in ecological irrigation area. IFAC-PapersOnLine. 51(17), 298-303.

[21] Chen, X.Q. (2017) A phenomenological explication of guanxi in rural tourism management: a case study of a village in china. Tourism Manage. 63(12), 383-394.

[22] Troumbis, I.A., Tsekouras, G.E., Tsimikas, J., Kalloniatis, C., Haralambopoulos, D. (2020) A chebyshev polynomial feedforward neural network trained by differential evolution and its application in environmental case studies. Environmental Modelling and Software. 126(4), 104663.

[23] Hu, H., Zhang, J.H., Wang, C., Yu, P., Chu, G. (2019) What influences tourists' intention to participate in the zero litter initiative in mountainous tourism areas: a case study of Huangshan national park, China. Science of the Total Environment. 657(3), 1127-1137.
[24] Sun, W., Xu, Y.F. (2016) Using a back propagation neural network based on improved particle swarm optimization to study the influential factors of carbon dioxide emissions in Hebei province, China. Journal of Cleaner Production. 112(1), 1282-1291.
[25] Kruk, M., Paturej, E., Artiemjew, P. (2020) From explanatory to predictive network modeling of relationships among ecological indicators in the shallow temperate lagoon. Ecological Indicators. 117(10), 106637.
[26] Wang, S., Hung, K., Huang, W.J. (2019) Motivations for entrepreneurship in the tourism and hospitality sector: a social cognitive theory perspective. International Journal of Hospitality Management. 78(4), 78-88.
[27] Eide, D., Fuglsang, L., Sundbo, J. (2017) Management challenges with the maintenance of tourism experience concept innovations: toward a new research agenda. Tourism Management. 63(12), 452-463.
[28] Muhammad, K., Ahmad, J., Baik, S.W. (2018) Early fire detection using convolutional neural networks during surveillance for effective disaster management. Neurocomputing. 288(5), 30-42.
[29] Guallar, C., Delgado, M., Diogene, J., Fernandez, T.M. (2016) Artificial neural network approach to population dynamics of harmful algal blooms in Alfacs bay: case studies of Karlodinium and Pseudo-nitzschia. Ecological Modelling. 338(10), 37-50.

Received: **22.01.2021**
Accepted: **30.04.2021**

CORRESPONDING AUTHOR

Yujin Kan
Nanhang Jincheng College,
Nanjing, Jiangsu 211156 – P.R. China

e-mail: xieqt006@163.com

© by PSP Volume 30– No. 09/2021 pages 10568-10575 Fresenius Environmental Bulletin

THE EFFECTS OF PICNIC AREAS ON EPIPHYTIC LICHEN DIVERSITY AT ABIES FORESTS IN ULUDAG NATIONAL PARK, TURKEY

Saban Guvenc*, Hulya Ozturk Kula

Department of Biology, Faculty of Arts and Sciences, Bursa Uludag University, Nilufer, Bursa, Turkey

ABSTRACT

The study was conducted on *Abies* trees located in Kirazlıyayla - Sarıalan camping and daily picnic areas in the Uludağ National Park. The epiphytic lichen diversity decreases due to differences in microclimate and intensive use of picnic areas by people. Relative humidity and bark surface moisture decreased due to an increase in the amount of light in picnic areas. Relative humidity in Sarıalan picnic areas significantly affects the epiphytic lichen diversity and causes a significant decrease in lichen species. Relative humidity and light are the most important factors affecting the diversity and structure of epiphytic lichen.

KEYWORDS:
Anthropogenic, diversity, epiphytic lichen, microclimate, Uludağ, National Park

INTRODUCTION

Unlike vascular plants, which take nutrients mainly from the soil through roots, lichens only depend on the atmosphere for nutrition. For this reason, they respond directly to atmospheric pollutants and they have been successfully used for biomonitoring of air pollution. Lichens are valuable bioindicators for evaluating the consequences of human activities. Epiphytic lichen diversity is strongly affected by altered microclimate resulting from changes in the forest structure and anthropogenic effects on forest ecosystems. Species diversity decreases with the intensity of management, while lichen composition also exhibited considerable variations. Nitrophytic species are clearly associated with more intensive management regimes, whereas non-nitrophytic species favored abandoned dehesas [1]. The epiphytic lichen vegetation is markedly different between the forest interior and the forest edge. It is stated that land use as compared to the changing microclimate has a stronger effect on lichen diversity along the forest interior and the forest edge [2]. The effect of edge conditions on lichen diversity depends on land-use intensity, climate, atmospheric deposition of nutrients or toxic substances, gap size, and the functional traits of the relevant epiphyte species [3]. One marked effect of the presence of hiking trail in forest was increased number of some sun-loving species and decreased number of shade-tolerant species. The presence of a hiking trail has indirectly influenced epiphytic lichen community and diversity by altering microclimate along the trail [4]. Variation in species composition in National Parks which is related to the environmental variables and habitat management was found to negatively influence species richness and alter the composition of lichen community [5]. The age of a forest stand is the main factor influencing lichen species richness [6]. Light availability and water supply are other important factors affecting the occurrence of epiphytic lichens. The lichen species richness is increased along with decreasing tree density [7]. Total species richness increases as a result of increasing number of eutrophication tolerant species that is due to the increase in land usage intensity [8]. The growth rate of epiphytic lichens is influenced by humidity, light, substrate pH, nutrient-availability and temperature [9]. In addition, the epiphytic lichen diversity is also influenced by environmental factors (humidity and light), the basic trunk of the trees, and some substrate characteristics such as bark moisture and tree size [10].

The aim of study is to analyse how picnic areas influence epiphytic lichen diversity on the trunk of *Abies* trees in Uludağ National Park.

MATERIALS AND METHODS

The study area. The Uludağ mountain is one of the largest winter sports centers in Turkey. It is the highest mountain of the Marmara region (2543 m). Uludağ was declared a National Park in 1961. Uludağ National Park is located at 40°04' N latitudes and 29°12' E longitudes which is 36 km to the south of Bursa in the southeastern part of the Marmara region of Turkey. There are different vegetation types depending on the type of climate and altitude in Uludağ Mountains. As a result of the altitudinal gradient and various geological conditions, the different vegetation types, changes from Mediterranean to Euro-Siberian, and Alpine can clearly be seen from

the bottom to the top of the mountains. While the mean annual temperature in Bursa (155 m) is 14.5 °C, it decreases to 4.8 °C in Uludağ (1878 m). The mean annual rainfall is 681.3 mm in Bursa and is 1453 mm in Uludag [11]. The mean annual temperature at Kirazlıyayla and Sarıalan plateaus which were selected as the study areas is 5.8˚C. The mean annual rainfall at Kirazıyayla is 1217.4 mm and is 1331.8 mm at Sarıalan [12].

Uludağ National Park is highly preferred by visitors for camping, hiking and daily picnic activities during summer season and it is also well known for its winter tourism. Kirazlıyayla and Sarıalan which were selected as the study areas are the most preferred plateaus by visitors for daily picnic activities. Karabelen entrance gate of Uludağ National Park is 22 km after Bursa city center by road. Kirazlıyayla and Sarıalan picnic areas are further 3 km and 10 km away by road from entrance gate, respectively. Sarıalan can also be reached by cable car. Sarıalan carries an importance for its health tourism due to the presence of exclusive picnic, travel, hiking, tent areas and plateau houses. Kirazlıyayla is generally used as a daily picnic area. The number of visitors at Uludağ National Park increases every year. In 1986, the total number of visitors was 446,093. 56.7% of them came by road and 43.2% by cable car. In 1988, the total number of visitors was 507,652 [13]. Recently, per year approximately 800,000 visitors had visited Uludağ National Park. 75% of the visitors go to the national park by road and 25% preferred by cable car.

Collection of lichen samples. The study was conducted in Kirazlıyayla and Sarıalan picnic areas located in the Uludağ National Park between 04-08 May, 2017. Lichen samples were collected from *Abies nordmanniana* (Steven) Spach subsp. *börnmuelleriana* (Mattf.) Coode & Cullen from Kirazlıyayla and Sarıalan picnic areas in Uludağ National Park (Figure 1). Four sites were selected for sampling. A total of five trees were selected from the center and edge of Kirazlıyayla picnic area (40°06′45″ N, 29°05′24″ E, 1532 m) and five trees from the control area which is 500 m away from the edge (40°06′38″ N, 29°05′23″ E, 1555 m). Similarly, five trees were selected from the center of Sarıalan camping and daily picnic area (40°08′06″ N, 29°06′33″ E, 1631 m) and five trees from the control area which is 500 m away from the edge (40°07′52″ N, 29°06′53″ E, 1630 m).



FIGURE 1
Sampling areas of lichen samples collected from Kirazlıyayla (A and B) and Sarıalan (C and D). A and C: Picnic area, B and D: Control area

Lichen samples were collected using the methods suggested by Asta et al. [14]. The sample grids were placed on the North (N), East (E), South (S) and West (W) sides 150 cm above the ground on the tree trunk. For each Uludağ fir, lichen samples were collected for a total of 20 subunits from the trunk. All lichen species found in each subunit of the sample grid were recorded. The frequency of each species was computed as the number of subunits at trunk where it was present. A sum of frequencies of all lichen species for each aspect (north, east, south and west) on each tree at trunk was calculated; four sums for each tree. The lichen diversity value (LDV) is the sum of the frequencies calculated for each aspect on a tree. The LDV of the locality was the arithmetic mean of the sums of frequencies for each sampling tree in that locality. The bark surface moisture was measured using LaserLiner DampMaster Moisture Meter. Bark surface moisture was measured for each aspect (north, east, south, and west) on each tree from the sites where five trees were located. DampMaster Moisture Meter measuring rods were measured by embedding 0.5 cm from the bark surface of the tree. In addition, the relative humidity (%) and light (10xLux) at the sampling locality were measured using with environmental tester (PCE-EM 886). Relative humidity and light were measured five times from the sites where five trees were located.

Statistical analysis. Total frequency (TF) of each epiphytic lichen species on trunk was used for statistical evaluation. The total frequency was calculated as the sum of the frequencies at that height of a species on all four aspects of each sample tree. Standard statistical analyses were conducted using IBM SPSS Statistics 23. Ordination of the 10 sample trees based on lichen species on trunk using the indirect linear model with Principal Component Analysis (PCA) in CANOCO ver. 4.5 generated diagrams of trees noted by control and picnic areas [15]. To compare species diversity and significant differences in the control and picnic areas, Paired Samples T-Test were used. Correlations between species and sampling area or environmental parameters (Bark surface moisture, Relative humidity, Light) were assessed using the Pearson correlation coefficient (2-tailed).

RESULTS

In this study, a total of 74 species were found from Kirazlıyayla and Sarıalan. A total of 58 species were found from Kirazlıyayla. Of these, only 16 were in the control area, 25 in the picnic area, and 17 were in both the control and picnic areas. A total of 57 species were found in another research area in Sarıalan. Of these, only 24 were in the control area, 12 in the picnic area, and 21 were in both the control and picnic areas (Table 1). The most common species in the control area of Kirazlıyayla were *Bryoria capillaris, Bryoria fuscescens, Evernia prunastri, Hypogymnia tubulosa, Lecanora intumescens, Parmelia sulcata, Phlyctis argena, Pseudevernia furfuracea, Ramalina farinacea, Usnea filipendula* and *U. glabrescens*, while those in the picnic area were *Candelariella xanthostigma, Hypogymnia tubulosa, Lecanora carpinea, L. chlarotera, L. cinereofusca, Lecidella elaeochroma, Melanohalea laciniatula, Pseudevernia furfuracea* and *Scoliciosporum chlorococcum*. The most common species in the control area of Sarıalan were *Bryoria capillaris, Hypogymnia tubulosa, Lecanora intumescens, Lecanora subcarpinea, Lecidella elaeochroma, Parmelia sulcata, Phlyctis argena, Pseudevernia furfuracea, Rinodina capensis* and *Usnea glabrescens*, while those in the picnic area were *Candelariella xanthostigma, Lecanora cinereofusca, L. subcarpinea, Lecidella elaeochroma* and *Melanohalea laciniatula*.

The PCA results based on lichen diversity on the trunk of sample trees in Kirazlıyayla and Sarıalan were shown in Figure 2. For Kirazlıyayla camping and daily picnic area, the first two axes of the PCA was represented 75.8% of the total variance. The first axis was associated with difference between control and picnic area. Trees in the control area were located at the left side and trees in the picnic area were on the right side of the first axis. Tree number 6 which has the lowest lichen diversity value was located at the position from edge towards the center of the picnic area, while the others were at the edge of the Kirazlıyayla picnic area (Figure 2A). For Sarıalan camping and daily picnic area, the first two axes of the PCA was represented 75.9% of the total variance (Figure 2B). Trees no 7 and 8 were close to each other on the roadside in the center of the picnic area, although trees no 9 and 10 were close to each other but they were located on the opposite side of the road in the center. Tree number 6 was farthest from the center. The lowest species diversity was found in tree no 8.

Ldv, bark surface moisture and relative humidity were decreased in picnic areas compared to control areas in both Kirazlıyayla and Sarıalan, whereas light exposure was increased. Decrease in relative humidity in picnic areas in both regions was significant, especially in Sarıalan $p<0.001$. Shannon diversity and Ldv values in Sarıalan were significantly decreased in picnic area compared to control area. This change was not significant in Kirazlıyayla (Table 2).

Bryoria capillaris, Bryoria fuscescens, Evernia prunastri, Lecanora intumescens, Parmelia sulcata, Ramalina farinacea, Usnea filipendula and *U. glabrescens* were the indicator species of the control area in both Kirazlıyayla and Sarıalan. *Biatora globulosa, Lecanora subcarpinea, Nephromopsis chlorophylla, Phlyctis argena, Ramalina* fraxine and Usnea

TABLE 1
Mean frequency values of epiphytic lichens species collected from Kirazlıyayla or Sarıalan picnic areas and control areas.

Sites	Kirazlıyayla		Sarıalan	
Sampling area	**Control area**	**Picnic area**	**Control area**	**Picnic area**
Bark surface moisture (%)	11.0	9.5	11.0	8.5
Relative humidity (%)	40.0	38.8	40.9	37.9
Light (10xLux)	1929.3	2213.4	731.8	5880.4
Shannon diversity	2.8	2.9	2.9	2.5
Lichen diversity value (Ldv)	172.0	145.2	164.0	121.2
Amandinea punctata	-	-	-	0.2
Anaptychia ciliaris	-	2.0	1.0	4.2
Arthonia radiata	-	-	0.2	0.2
Bacidia circumspecta	-	-	-	1.0
Biatora globulosa	5.6		2.4	-
Bryoria capillaris	16.6		12.4	-
B. fuscescens	9.8	0.6	6.0	-
B. nadvornikiana	4.6		1.2	-
Buellia disciformis	-	2.2	0.4	-
B. griseovirens	0.8	0.8	1.6	2.6
Caloplaca cerina	-	3.4	-	1.6
C. flavorubescens	-	3.8	-	-
C. haematites	-	2.2	-	-
C. herbidella	0.2	-	2.4	0.4
Candelaria concolor	-	1.4	-	0.4
Candelariella vitellina	-	3.2	-	-
C. xanthostigma	-	8.2	1.0	9.2
Evernia prunastri	11.6	0.8	6.2	-
Huneckia pollinii	-	-	-	0.6
Hypogymnia physodes	3.6	-	0.8	-
H. tubulosa	13.6	7.4	12.4	5.8
Lecania cyrtella	-	0.6	-	-
L. fuscella	-	-	-	1.0
Lecanora allophana	-	0.4	-	-
L. carpinea	0.2	16.4	-	-
L. chlarotera	-	7.2	-	-
L. cinereofusca	1.4	8.0	2.2	16.4
L. circumborealis	-	-	0.6	0.8
L. glabrata	-	-	0.8	-
L. hagenii	-	3.6	-	-
L. intumescens	12.4	-	11.6	-
L. saligna	-	-	0.2	0.4
L. subcarpinea	3.4	-	10.2	12.6
L. varia	-	-	1.6	-
Lecidella elaeochroma	5.4	13.6	7.8	16.0
Lepra albescens	0.6	-	0.8	-
Lepraria jackii	1.8	-	-	-
Melanelixia glabra	-	-	-	0.2
M. glabratula	2.2	0.6	1.2	-
M. subaurifera	2.2	-	1.6	-
Melanohalea elegantula	-	0.8	-	-
M. exasperatula	-	3.8	0.6	0.8
M. laciniatula	-	9.0	0.4	16
Micarea prasina	-	-	1.6	-
Nephromopsis chlorophylla	1.8	-	0.2	-
Parmelia sulcata	12.6	2.8	10.8	2.0
Parmelina tiliacea	0.6	-	-	-
Pertusaria coccodes	-	-	0.4	-
P. flavida	-	-	0.2	-
Phaeophyscia orbicularis	-	0.8	-	-

Phlyctis argena	17.0	0.2	10.8	6.6
Physcia adscendens	-	1.0	-	-
P. aipolia	-	-	-	0.2
P. leptalea	-	4.6	0.2	0.4
P. tenella	-	1.6	-	-
Physconia distorta	0.6	2.4	-	2.4
P. enteroxantha	-	2.2	-	0.2
P. perisidiosa	-	1.8	-	1.0
Pleurosticta acetabulum	1.4	2.0	-	2.2
Pseudevernia furfuracea	12.0	7.6	16.8	6.0
Ramalina canariensis	-	-	0.6	-
R. farinacea	8.6	0.6	5.2	0.2
R. fastigiata	0.4	-	-	-
R. fraxinea	1.8	0.4	0.8	-
R. pollinaria	-	1.6	0.2	-
Rinodina capensis	3.4	4.4	7.0	5.6
R. sophodes	-	0.2	2.4	3.8
Scoliciosporum chlorococcum	-	8.4	-	-
S. umbrinum	-	0.4	-	-
Usnea filipendula	7.2	-	4.0	-
U. glabrescens	7.6	-	9.6	-
U. hirta	1.2	3.6	2.0	0.6
U. rigida	0.8	-	0.4	-
Varicellaria hemisphaerica	-	-	0.4	-

TABLE 2
Paired samples correlations of species diversity and environmental parameters between control and picnic areas in Kirazlıyayla and Sarıalan camping and daily picnic area.

Species diversity and environmental parameters	Kirazlıyayla	Sarıalan
Shannon diversity	0.274	-0.827**
Lichen diversity value (Ldv)	-0.389	-0.771**
Bark surface moisture	-0.312	-0.644*
Relative humidity	-0.655*	-0.937***
Light	0.251	0.752*

* P<0.05 ** P<0.01 *** P<0.001

rigida have a high correlation for control area of Kirazlıyayla, while *Hypogymnia physodes, H. tubulosa* and *Pseudevernia furfuracea* for control area of Sarıalan. *Candelariella xanthostigma* and *Melanohalea laciniatula* have a high correlation for the picnic area in both Kirazlıyayla and Sarıalan. *Caloplaca cerina, C. flavorubescens, Lecanora carpinea* and *Scoliciosporum chlorococcum* are the only indicator species of Kirazlıyayla picnic area, whereas *Lecanora cinereofusca* and *Lecidella elaeochroma* are indicators of Sarıalan picnic area (Table 3).

DISCUSSION

Uludağ National Park is highly preferred by visitors for camping, hiking and daily picnic activities during the summer season and it is also well known for its winter tourism. Kirazlıyayla and Sarıalan which were selected as the study areas are mostly preferred plateaus by visitors for daily picnic activities. The most common species of the control area in both Kirazlıyayla and Sarıalan are *Bryoria capillaris, B. fuscescens, Evernia prunastri, Hypogymnia tubulosa, Parmelia sulcata, Phlyctis argena, Pseudevernia furfuracea, Ramalina farinacea, Usnea filipendula* and *U. glabrescens*. These species were previously detected as common in the interior of *Abies* forests in Uludag National Park [16].

The epiphytic lichen vegetation in the Uludag national park was markedly different between the control and picnic areas. Possible reasons for this difference include the presence of roads, hiking trails and camping sites in picnic areas and intense use of these areas by the public. Epiphytic lichen diversity decreases as a result of intensive use of picnic areas by people. Similarly, habitat management was found to negatively influence species richness and alter the lichen community composition. Management-induced disturbance significantly decreased lichen species richness in forest landscapes with long stand continuity [5].

It has been shown that the anthropo-zoogenic effect on the epiphytic lichen vegetation varies between individual forest stands and is related to the density of nomadic households that make summer camps around the forest [2]. Due to the burning of

charcoal and the exhaust gases from the vehicles are partially pollute the air in the picnic areas. It has been determined that the spatial distribution and abundance of lichens are inversely proportional to the concentration of CO in the air [17].

The total species richness decreases with the intensity of forest management and abandoned habitats harbor more species than the more densely managed habitats. Especially, nitrophytic species clearly associated with more intensive management regimes [1]. Therefore, it is not surprising that some nitrophytic species [18] such as *Caloplaca cerina, C. flavorubescens, C. haematites, Candelaria concolor, Candelariella vitellina, C. xanthostigma, Phaeophyscia orbicularis, Physcia adscendens, P. aipolia, P. tenella, Physconia enteroxantha, P. perisidiosa* and *Scoliciosporum chlorococcum* were found only in picnic areas in this study. Whereas, Parmeliaceae (*Bryoria, Hypogymnia, Parmelia, Pseudevernia, Usnea*) species which are abundant in the forest interior, were found with high frequency in both Kirazlıyayla and Sarıalan control areas. It has been determined that there was a significant decrease in vegetation diversity especially lichen diversity in regions close to walking paths [19].

Significant differences occur in microclimate of picnic areas compared to control areas. Relative humidity and bark surface moisture decreases due to the increase in the amount of light in picnic areas. In particular, relative humidity in Sarıalan significantly affects the epiphytic lichen diversity and causes a significant decrease in picnic areas (Table 4). *Bryoria capillaris, B. fuscescens, Evernia prunastri, Hypogymnia physodes, H. tubulosa, Lecanora intumescens, Nephromopsis chlorophylla, Parmelia sulcata, Phlyctis argena, Pseudevernia furfuracea, Ramalina farinacea, Usnea filipendula* and U. glabrescens were positively correlated with relative humidity, while *Candelariella xanthostigma, Lecanora cinereofusca, Lecidella elaeochroma, Melanohalea laciniatula* and *Physcia leptalea* were

TABLE 3
Indicator species for control and picnic areas in Kirazlıyayla and Sarıalan camping and daily picnic areas (N=10).

Kirazlıyayla		Sarıalan	
Control area	**Cor.**	**Control area**	**Cor.**
Biatora globulosa	-0.825**	*Bryoria capillaris*	-0.977***
Bryoria capillaris	-0.984***	*B. fuscescens*	-0.815**
B. fuscescen	-0.924***	*Caloplaca herbidella*	-0.720*
Evernia prunastri	-0.963***	*Evernia prunastri*	-0.827**
Lecanora intumescens	-0.853**	*Hypogymnia physodes*	-0.768**
L. subcarpinea	-0.820**	*H. tubulosa*	-0.894***
Nephromopsis chlorophylla	-0.670*	*Lecanora intumescens*	-0.892**
Parmelia sulcata	-0.851**	*Parmelia sulcata*	-0.783**
Phlyctis argena	-0.977***	*Pseudevernia furfuracea*	-0.849**
Ramalina farinacea	-0.759*	*Ramalina farinacea*	-0.840**
R. fraxine	-0.893**	*Usnea filipendula*	-0.771**
Usnea filipendula	-0.638*	*U. glabrescens*	-0.951***
U. glabrescens	-0.817**		
U. rigida	-0.633*		
Picnic area	**Cor.**	**Picnic area**	**Cor.**
Caloplaca cerina	0.773**	*Candelariella xanthostigma*	0.828**
C. flavorubescens	0.785**	*Lecanora cinereofusca*	0.946***
C. haematites	0.706*	*Lecidella elaeochroma*	0.914***
Candelariella xanthostigma	0.910***	*Melanohalea laciniatula*	0.990***
Lecanora carpinea	0.966***		
L. chlarotera	0.748*		
L. cinereofusca	0.692*		
Lecidella elaeochroma	0.725*		
Melanohalea exasperatula	0.756*		
M. laciniatula	0.862**		
Physcia leptalea	0.667*		
Physconia enteroxantha	0.718*		
Ramalina pollinaria	0.661*		
Scoliciosporum chlorococcum	0.862**		

Cor.: Correlation * P<0.05 ** P<0.01 *** P<0.001

TABLE 4
Pearson correlation coefficients of epiphytic lichen species associated with environmental parameters (bark surface moisture, relative humidity, light) in Kirazlıyayla or Sarıalan control and picnic areas.

	Kirazlıyayla			Sarıalan		
	BSM	**RH**	**Light**	**BSM**	**RH**	**Light**
Control X Picnic areas	-0.312	-0.655*	0.251	-0.644*	-0.937**	0.752*
Relative humidity	0.438	1	-0.601	0.703*	1	-0.922**
Light	-0.216	-0.601	1	-0.747*	-0.922**	1
Shannon diversity	-0.009	0.363	-0.313	0.579	0.738*	-0.597
Ldv	0.244	0.594	-0.381	0.642*	0.793**	-0.776**
Bryoria capillaris	0.195	0.641*	-0.214	0.685*	0.923**	-0.749*
B. fuscescens	0.314	0.735*	-0.411	0.595	0.809**	-0.614
Caloplaca haematites	0.029	-0.650*	0.316	0.507	0.782**	-0.742*
Candelariella xanthostigma	-0.177	-0.633*	0.085	-0.434	-0.733*	0.545
Evernia prunastri	0.246	0.675*	-0.313	0.414	0.760*	-0.641*
Hypogymnia physodes	-	-	-	0.613	0.726*	-0.560
H. tubulosa	-	-	-	0.386	0.814**	-0.628
Lecanora cinereofusca	-	-	-	-0.507	-0.808**	0.572
Lecanora intumescens	-	-	-	0.638*	0.815**	-0.686*
Lecidella elaeochroma	-0.334	-0.642*	0.661*	-0.500	-0.780**	0.537
Melanohalea laciniatula	-	-	-	-0.553	-0.904**	0.680*
Nephromopsis chlorophylla	0.472	0.667*	-0.324	-	-	-
Parmelia sulcata	0.682*	0.714*	-0.283	0.559	0.806**	-0.660*
Phlyctis argena	0.309	0.637*	-0.183	-	-	-
Physcia leptalea	-0.358	-0.658*	-0.003	-	-	-
Pseudevernia furfuracea	-	-	-	0.324	0.821**	-0.638*
Ramalina farinacea	0.316	0.768**	-0.628	0.455	0.762*	-0.625
Usnea filipendula	-	-	-	0.569	0.765**	-0.594
U. glabrescens	-	-	-	0.576	0.888**	-0.727*

Correlation with significance at the 0.05 (*) and 0.01 (**) level (2-tailed).
BSM: Bark surface moisture, RH: Relative humidity

negatively correlated. *Bryoria capillaris, Caloplaca haematites, Lecanora intumescens, Parmelia sulcata, Pseudevernia furfuracea* and *Usnea glabrescens* were negatively correlated with light, whereas *Melanohalea laciniatula* was positively correlated.

The availability of light is an important factor controlling the within stand variation of epiphytic lichens. Generally, the epiphytic lichen diversity tend to rise with increasing moisture [9]. It was also determined that the air humidity is lower and the amount of light is higher at the edge of the path than the inner regions. The paths in the forests disrupt the microclimate of the forest, and the richness of epiphytic species and the number of drooping growth forms at the edge of the path decreases compared to the inner regions [4]. In this study, fruticose lichens such as *Bryoria capillaris, B. fuscescens, Evernia prunastri, Pseudevernia furfuracea, Ramalina farinacea, Usnea filipendula* and *U. glabrescens* were found with high frequency values in the control areas. It has been determined that the epiphytic lichen diversity on *Quercus petrea* in Uludag Mountain decreased when the amount of relative humidity and light in the environment and bark surface moisture decreased [10].

CONCLUSION

Strong degradation of the picnic area in the Uludag National Park is the probable cause of the reduced epiphytic lichen diversity compared with the control area. The decrease in species richness of the picnic area is probably due to different land use regimes and related differences in microclimate, not to differences in macroclimate. The determine the factors that limititing distribution of species to preserve biodiversity will be very important in developing appropriate methods for the forest management. A better understanding by the forest managers regarding environmental variables that affect the lichen diversity will contribute to the development of sustainable forest management strategies.

ACKNOWLEDGEMENTS

This work was supported by the Unit of Scientific Research Projects of Bursa Uludağ University (Project No: KUAP (F) 2018/4).

REFERENCES

[1] Aragon, G., Lopez, R. and Martinez, I. (2010) Effects of Mediterranean dehesa management on epiphytic lichens. Science of the Total Environment. 409, 116-122.

[2] Hauck, M., Javkhlan, S., Lkhagvadorj, D., Bayartogtokh, B., Dulamsuren, C. and Leuschner, C. (2012) Edge and land-use effects on epiphytic lichen diversity in the forest-steppe ecotone of the Mongolian Altai. Flora. 207, 450-458.

[3] Hauck, M. (2014) Edge effects on epiphytic lichen diversity in the forest-steppe of the Kazakh Altai. Plant Ecology & Diversity. 7(4), 473-483.

[4] Yan, X., Bao, W. and Pang, X. (2014) Indirect effects of hiking trails on the community structure and diversity of trunk-epiphytic bryophytes in an old-growth fir forest. Journal of Bryology. 36(1), 44-55.

[5] Ardelean, I.V., Keller, C. and Scheidegger, C. (2015) Effects of Management on Lichen Species Richness, Ecological Traits and Community Structure in the Rodnei Mountains National Park (Romania). PLoS One. 10(12), e0145808.

[6] Wolseley, P., Sanderson, N., Thus, H., Carpenter, D. and Eggleton, P. (2017) Patterns and drivers of lichen species composition in a NW-European lowland deciduous woodland complex. Biodivers. Conserv. 26, 401-419.

[7] Kubiak, D., Osyczka, P. and Rola, K. (2016) Spontaneous restoration of epiphytic lichen biota in managed forests planted on habitats typical for temperate deciduous forest. Biodivers. Conserv. 25, 1937-1954.

[8] Pinho, P., Bergamini, A., Carvalho, P., Branquinho, C., Stofer, S., Scheidegger, C. and Máguas, C. (2012) Lichen functional groups as ecological indicators of the effects of land-use in Mediterranean ecosystems. Ecological Indicators. 15, 36-42.

[9] Hauck, M. (2011) Site factors controlling epiphytic lichen abundance in northern coniferous forests. Flora 206, 81-90.

[10] Öztürk, Ş., Güvenç, Ş. and Oran, S. (2019) The determination of the changes in epiphytic lichen diversity at microclimatic conditions the Quercus petraea (Mattuschka) Liebl. Forest in the Uludağ Mountains (Bursa, Turkey). Nova Hedwigia. 109(3-4), 475-487.

[11] Öztürk, M.Z. (2010) Comparative climate of Uludağ (Zirve) and Bursa Meteorology Stations. Türk Coğrafya Dergisi. 55, 13-24 (in Turkish).

[12] Tolunay, D. (1992) The relationships between climate characteristics of Uludag and air pollution, and studies on the effects of this pollution on forest society. İ.Ü. Orman Fakültesi Dergisi (Seri B) 42(3-4), 119-130. (in Turkish)

[13] Doğaner, S. (1991) A geographical approach to Mountain Tourism: Tourism in Uludağ. Coğrafya Araştırması. 3, 137-157.

[14] Asta, J., Erhardt, W., Ferretti, M., Fornasier, F., Kirschbaum, U., Nimis, P.L., Purvis, O.W., Pirintsos, S., Scheidegger, C., van Haluwyn, C. and Wirth, V. (2002) Mapping lichen diversity as an indicator of environmental quality. In: Nimis, P.L., Scheidegger, C. and Wolseley, P.A. (eds.) Monitoring with Lichens-Monitoring Lichens. Nato Science Program - IV Vol. 7, Kluwer Academic Publisher, The Netherlands. 273-279.

[15] Ter Braak, C.J.F. and Smilauer, P. (2002). CANOCO Reference Manual and Cano Draw for Windows User's Guide: Software for Canonical Community Ordination (Version 4.5). Microcomputer Power, Ithaca, New York.

[16] Öztürk, Ş. and Güvenç, Ş. (2010) The distribution of epiphytic lichens on Uludag fir (Abies nordmanniana (Steven) Spach subsp. bornmuelleriana (Mattf.) Coode & Cullen) forests along an altitudinal gradient (Mt. Uludag, Bursa, Turkey). Ekoloji. 74, 131-138.

[17] Coghill, T.G., Kostadinovic, L., Micic, R., Nuhanovic, M., Avdic, P., Jahic, M. and Stojnic, M. (2015) Lichens as specific and cost-effective biological indicators of Urban Carbon Monoxide concentration. Fresen. Environ. Bull. 24(12), 4279-4284.

[18] Wolseley, P.A., James, P.W., Theobald, M.R. and Sutton, M.A. (2006) Detecting changes in epiphytic lichen communities at sites affected by atmospheric ammonia from agricultural sources. The Lichenologist. 38(2), 161-176.

[19] Jägerbrand, A.K. and Alatalo, J.M. (2015) Effects of human trampling on abundance and diversity of vascular plants, bryophytes and lichens in alpine heath vegetation, Northern Sweden. SpringerPlus. 4, 95.

Received: **02.02.2021**
Accepted: **01.05.2021**

CORRESPONDING AUTHOR

Saban Guvenc
Department of Biology,
Faculty of Arts and Sciences,
Bursa Uludag University,
16059 Gorukle Bursa – Turkey

e-mail: saban@uludag.edu.tr

© by PSP Volume 30– No. 09/2021 pages 10576-10585 Fresenius Environmental Bulletin

IMPACT OF DIFFERENT TILLAGE PRACTICES ON DISTRIBUTION OF SOIL ORGANIC CARBON AND TOTAL NITROGEN IN CLAY LOAM SOIL

Tomas Zukaitis[1,*], Inga Liaudanskiene[1], Aleksandras Velykis[2]

[1]Institute of Agriculture, Lithuanian Research Centre for Agriculture and Forestry Instituto av. 1, Akademija, LT-58344 Kedainiai distr., Lithuania

[2]Joniskelis Research Station, Lithuanian Research Centre for Agriculture and Forestry Karpiu str. 1, Joniskelis, LT-39301 Pasvalys distr., Lithuania

ABSTRACT

Reduced tillage is one of strategies for mitigating climate change in agriculture. Enhancement of soil organic matter content by reduced or no-tillage practice and Ca-amendment application has been recognized as important strategies to combat soil degradation. Possibilities to reduce tillage clayey soil have not been sufficiently investigated in Lithuania before. Research was carried out during 2016–2018 at the Joniskelis Experimental Station of the Lithuanian Research Centre for Agriculture and Forestry on a clay loam (siltic, drainic), Endocalcary-Endohypogleyic Cambisol (CMgn-w-can) in the experiment, established in 2006. The studied treatments included: deep ploughing (DP) at 21–23 cm depth (control), ploughless tillage at 10–12 cm depth (PT), as well as ploughless tillage and aftereffect of lime sludge last incorporated in 2014 (PT+aLS) and no-till in the autumn with a cover crop for winter mulch (NT+WM). Soil samples were collected annually after the main crop harvest from three soil depth 0–10, 10–20, and 20–30 cm.

Reduced tillage systems significantly increased soil organic carbon (SOC) content in the upper (0–10 cm) soil layer by order PT+aLS > NT+WM > PT > DP and shows SOC stratification in reduced tillage systems. Water extractable organic carbon (WEOC) content was higher under PT and NT+WM treatments at 0–10 and 10–20 cm layers, however under PT+aLS the WEOC content was lower compared to DP. Cations from lime sludge stabilized mobile and labile forms of SOC, reducing WEOC content. Total nitrogen (TN) in soil was less affected by applied reduced tillage systems, amount of TN in the upper (0–10 cm) soil layer increased significantly only under NT+WM. High correlation coefficients were observed for the relationship of SOC vs TN, indicating a close relation between SOC and TN accumulation in soil; lower correlation coefficients were observed for the relations of SOC vs WEOC, and TN vs WEOC.

KEYWORDS:
Clay loam soil, lime sludge, reduced tillage, soil organic carbon

INTRODUCTION

The loss of soil organic matter due intensive tillage is recognized as one of the major threats to soil in the EU, as well as in Lithuania. Lithuania's natural conditions are characterized by a noticeable change in bioclimatic factors, which affects soil microorganisms, the amount and variety of which determine the formation and accumulation of soil organic matter. Regular mouldboard ploughing has been recognized as a key factor responsible for soil organic carbon loss, as early as 1997 Paustian et al. [1] reported that the intensive tillage has contributed 28 to 77% of organic carbon (OC) losses over time, depending on geographical location (climate) and soil type. Degradation of the soil aggregate during tillage increases the availability of SOM to soil microbes, which increases the rate of SOM mineralization and reduces its amount in the soil [2]. Conventional tillage using ploughing can reduce SOC and increase CO2 emissions from the soil, considering the increase in soil aeration. In 2015 Buragienė et al. [3] pointed that the highest soil CO2 emissions were observed for the conventional deep ploughing tillage system, and the lowest emissions were observed for the no-tillage system, autumn deep ploughing increased the soil CO2 emissions significantly by up to 8.5 times compared to no-till. Until now, yields have grown by destroying the natural potential of soil fertility, so tillage systems now must be improved.

One of the alternatives for maintaining SOM levels is the introduction of a reduced tillage systems in clay loam soils [4]. Ploughless tillage and no-tillage systems are the opposite of traditional deep ploughing, as they increase soil organic matter due to a reduced rate of mineralization and the accumulation of plant residues in the topsoil [5, 6], therefore, reduced tillage systems are recommended given their

potential to increase SOC sequestration [7]. The application of ploughless tillage and no-tillage systems tend to have higher concentrations of SOC in the topsoil compared to the SOC in the deeper soils layers [8, 9, 10, 11]. As found by Bogužas et al. [12], long-term application of various reduced tillage methods increased SOC from 19.4% to 33.9% compared to conventional deep ploughing. Tillage systems of different intensities have different effects on the distribution of SOC in separate soil layers and stratification. Conventional deep mouldboard tillage results in an even distribution of SOC throughout the 20–25 cm arable layer; on the contrary, a reduction in tillage results in higher SOC levels in the 0–10 cm and 10–20 cm soil layers compared to the deeper layers [12, 13].

Increasing SOM content through no-till (NT) and reducing soil acidity through Ca-amendment application has been recognized as an important strategy in combating soil degradation [14]. The results of previous studies showed that the combination of NT and the Ca-amendment increased soil pH and SOM content, leads to an improvement in microbial biomass and enzymatic activity [14, 15], decreased Al toxicity [14, 16], enhanced soil aggregation [17], and improved soil-water relationship [18]. Lime sludge is obtained from the beet sugar industry and produced during sugar beet juice purification process, and the main part of this by-product consists of calcium carbonate containing up to 50% of CaO [19]. It is considered an organic amendment [20] and it may be used in production of compound fertilizers as a calcium source. Sugar factory lime sludge is known to be an effective liming material with a positive effect lasting at least 9 years [21]. Results showed that application of sugar industry lime sludge significantly increased SOM (by 20% compared with control), plant available macro-nutrients (nitrogen, potassium, and especially phosphorus) and water holding capacity [22]. However, residual effect of lime sludge in improving clay loam soil properties not studied before, and there is insufficient knowledge about the interaction between the use of sugar industry lime sludge and soil tillage, and their influence on soil chemical properties.

Crop residue that acts as mulches has multiple effects on soil physicochemical properties [23]. No-till practice is often combined with the use of mulch, making it a conservative tillage. Intercrop cover plants, being left on the surface of a field as mulch, positively affect properties of soil. During the autumn and winter period, mulch crops prevent leaching of nutrients, primarily nitrates which cause groundwater contamination. Mulching also showed positive effects on nutrient retention as compared to the un-mulched plots [24]. Long-term mulching can significantly increase the content of SOM and available nutrients due to degradation of mulching materials [25, 26]. However, the increase of the amount of soil organic carbon (SOC) is regarded as the main advantage of organic mulches. The influence of mulch on soil agrochemical properties depends on the chemical composition of mulch [27]. The beneficial influence of mulch crops on organic matter content (an increase in soil organic matter) was observed already after one season of mulching [28]. However, the effect of soil management on the chemical structure of SOC has been little investigated.

Intensive crop production technologies have significantly reduced soil potential due to mineralization and declining organic matter reserves. The assessment and characterization of soil organic matter, of which soil organic carbon is a key component, is important to keep soils stable with reliably predictable yields. The main objective of study was to evaluate the long-term effect of deep ploughing, ploughless tillage and its combination with the incorporation of lime sludge and no-till in autumn with a cover crop for winter mulch on heavy clay soil chemical properties. We hypothesized that combination of reduced tillage with soil improvement practices will increase soil organic carbon and total nitrogen amount in a clay loam soil.

MATERIALS AND METHODS

Experimental site and soil description. Research was carried out during the period 2016–2018 at the Joniskelis Experimental Station of the Lithuanian Research Centre for Agriculture and Forestry, situated in the Northern part of Central Lithuania's lowland (56°21′ N, 24°10′ E) in the experiment, established in 2006. The soil of the study site is Endocalcari-Endohypogleyic Cambisol (CMg-nw-can) (Siltic, Drainic). Characteristics of the plough layer (0–30 cm) were as follows: texture – clay loam (27.03±0.83% clay, 50.24±1.11% silt, and 22.73±1.64% sand), pH – 6.6±0.2, humus content – 2.35±0.09%, total nitrogen content – 0,156%.

The experiment examined the long-term effects of conventional, reduced and no-tillage practices as well as the combinations of reduced and no-tillage with practices for soil improvement on soil chemical state. The following tillage systems were investigated: 1) deep ploughing (DP) at 21–23 cm depth – control, 2) ploughless tillage (PT) at 10–12 cm depth, 3) ploughless tillage at 10–12 cm depth and aftereffect of lime sludge last incorporated in 2014 (PT+aLS), and 4) no-till in the autumn with a cover crop for winter mulch (NT+WM). Research was conducted in the crop rotation: 1) field pea (Pisum sativum L. (Partim), 2) winter wheat (Triticum aestivum L.), 3) spring oilseed rape (Brasica napus L.) and 4) spring barley (Hordeum vulgare L.), which was spread over space and time. Cover crops were as follows: before field pea growing – a mixture of white mustard (Sinapis alba L.) and oilseed radish (Raphanus sativus L.), before spring oilseed rape

growing – a mixture of field pea (Pisum sativum L. (Partim), common vetch (Vicia sativa L.) and blue lupine (Lupinus angustifolius L.), and before spring barley growing – oat (Avena sativa L.). Post-harvest cover crop for winter mulch was sown after stubble cultivation, and was left intact in the autumn, and its frost-killed residues covered the soil. All rotational crops were fertilized with P90K60 before sowing. The field trial was laid out in a randomized single row design with four replicates. Each tilled sub-plot size was 80 m2 (16.0 × 5.0 m) of which 29.9 m2 (13.0 × 2.3 m) was harvested.

Deep ploughing (DP) was carried out with a mouldboard plough, ploughless tillage (PT and PT+aLS) – by a combined stubble cultivator. Lime sludge (7.0 t ha-1) was incorporated into the soil three times through all rotation for spring crops during the first stage of experiment (2007–2010) and once per rotation for spring barley in the second stage of experiment (2011–2014) during ploughless tillage operation (PT+aLS), last time in 2014. All rotational crops were fertilized with P90K60 before sowing.

Soil sampling and analysis methods. Soil samples were collected annually after the main crop harvest, 8 sub-samples per plot were taken randomly with a steel auger. Each soil sample core was separated into 0–10, 10–20 and 20–30 cm depth and combined across sub-samples by depth for each plot. The soil samples were air-dried, visible roots and plant residues were removed manually. Then the samples were crushed and sieved through a 2-mm sieve and homogeneously mixed. For the soil chemical analysis an aliquot of the samples was passed through a 0.25-mm sieve. The content of soil organic carbon (SOC) was determined according to Tyurin method modified by Nikitin (1999), which consists of dichromate digestion at 160°C temperature for 30 min and spectrophotometric measurement procedure at a wavelength of 590 nm using glucose as a standard. Water extractable organic carbon (WEOC) was measured by IR-detection method after UV-catalysed persulphate oxidation using ion chromatography system SKALAR (Netherlands). The total nitrogen (TN) content was determined by the Kjeldahl method using spectrophotometric measure procedure at a wavelength of 655 nm after mineralization with sulphuric acid (H2SO4). The C-to-N ratio was calculated as the ratio of SOC and TN levels in soil.

Climatic and meteorological conditions. The climatic conditions of the experimental area are characterized by the long-term (1982–2015) average annual temperature of 6.4°C and precipitation of 537mm, of which 412mm occur during the warm period (Table 1).

The year 2016 was marked by temperature-contrasting winter months, warmer and dry May (precipitation only 29.3% of long-term average), a warm summer with an especially rainy August (precipitation was 2.3 times above long-term average) and very uneven precipitation in the autumn – in September only 7.9% of long-term average, and in October and November precipitation exceeded long-term average, respectively 61.1% and 58.9%. The year 2017 was characterized by a warm winter, a very dry May (precipitation only 19.2% of long-term average), temperature close to long-term average in summer with a rainier July (precipitation was 30.9% above the long-term average), and a warm but very rainy autumn: precipitation exceeded long-term average 2.5 times in September, 45.1% in October and 22.2% in November. The year 2018 was distinguished by a warm spring, a hot summer with very dry June and July with precipitation respectively 26.7% and 66.3% of long-term average, and a warm and dry September (precipitation only 26.4% of long-term average).

TABLE 1
Meteorological conditions during experiment (2016–2018)

Month	I	II	III	IV	V	VI	VII	VIII	IX	X	XI	XII
Long-term average (mean 1982–2015)												
Temperature, °C	-4.7	-5.0	-0.6	6.6	12.2	15.5	17.7	17.0	12.1	6.6	1.5	-2.7
Precipitation, mm	31.6	26.9	27.6	33.7	44.7	60.0	72.8	63.5	50.4	45.5	41.9	38.5
2016												
Temperature, °C	-8.0	2.3	2.9	8.3	15.0	17.8	19.3	17.7	14.4	5.5	1.3	1.5
Precipitation, mm	31.4	57.9	29.8	48.4	13.1	53.6	86.0	147.7	4.0	73.3	66.6	42.5
2017												
Temperature, °C	-2.8	-1.2	4.0	5.8	12.8	16.0	17.0	17.9	14.0	9.2	3.8	1.5
Precipitation, mm	17.9	14.2	27.1	17.7	8.6	55.5	95.3	48.2	124.9	66.0	51.1	54.3
2018												
Temperature, °C	-1.3	-7.8	-1.1	10.4	16.3	17.4	20.6	20.1	15.7	8.4	1.8	—
Precipitation, mm	47.9	11.8	13.8	56.5	50.7	16.0	48.3	47.5	13.3	34.2	15.1	—

TABLE 2
Soil organic carbon and water extractable organic carbon content under different tillage practices, g kg^{-1}

Treatment	Layer, cm	SOC				WEOC			
		2016	2017	2018	Mean	2016	2017	2018	Mean
DP	0–10	13.02	12.63	14.11	13.25	0.30	0.24	0.21	0.25
	10–20	13.00	12.92	13.58	13.17	0.29	0.24	0.21	0.25
	20–30	10.95	10.02	9.94	10.30	0.25	0.23	0.20	0.23
PT	0–10	13.34	14.04*	14.72	14.03	0.32	0.27	0.20	0.26
	10–20	11.83	12.11	12.25	12.06	0.30	0.25	0.21	0.25
	20–30	10.97	8.77	7.90	9.22	0.24	0.21	0.18	0.21
PT+aLS	0–10	14.50	14.39*	15.91*	14.93*	0.26*	0.25	0.23*	0.25
	10–20	12.30	11.99	12.02	12.10	0.28	0.22	0.22	0.24
	20–30	8.85	8.22	7.53	8.20	0.21	0.21	0.15*	0.19*
NT+WM	0–10	14.64	14.33*	14.41	14.46*	0.34*	0.26	0.19	0.27
	10–20	11.69	12.18	11.65	11.84	0.28	0.23	0.21	0.24
	20–30	8.66	8.47	7.94	8.36	0.17*	0.21	0.20	0.19*
LSD_{05}	0–10	1.628	0.964	1.174	0.829	0.034	0.032	0.025	0.043
	10–20	0.739	1.017	0.955	0.490	0.044	0.032	0.019	0.036
	20–30	2.626	2.110	2.049	1.257	0.066	0.041	0.034	0.031

Note: DP – deep ploughing (control); PT – ploughless tillage; PT+aLS – ploughless tillage and aftereffect of lime sludge; NT+WM – no-tillage with winter mulch; * – significant at $P \leq 0.05$ probability level, the significance of the differences between the treatments was evaluated using the LSD.

Statistical analysis. Was done using the software SAS Enterprice, version 7.1 (SAS Institute Inc., USA). All results of SOC, TN and WEOC are the means of three field replicates. Differences among the experimental treatments were tested by the analysis of variance (one-way ANOVA). The means were compared by using least significant differences (LSD) calculated at the 0.05 probability level (Fisher's LSD test).

RESULTS AND DISCUSSION

Soil organic carbon. Soil organic carbon (SOC) is one of the most widely used soil quality indicators together with soil pH and plant available macronutrients content [29]. The results of our field experiment indicated a positive effect of reduced tillage systems on SOC content in the upper (0–10 cm) soil layer. From the data in Table 2, it is apparent that the amount of SOC in the 0–10 cm soil layer was significantly higher in all applied reduced tillage systems compared to the control DP in 2017: PT increased SOC content by 11.1%, PT+aLS – by 13.9%, and NT+WM – by 13.4%. In 2018, the amount of SOC in the upper soil layer was also higher in all reduced tillage systems compared to DP, but a significant increase (+ 12.7%) was found only under PT+aLS application, and these results are consistent with [15] research findings. The three-year (2016–2018) mean data showed that the application of DP resulted in the most even distribution of SOC in soil – the stratification coefficient of SOC between the 0–10 and 10–20 cm layers was 1.01, and between the 0–10 and 20–30 cm layers was 1.28. Although reduced tillage and especially no-till practices are known to cause pronounced SOC stratification in the arable layer [30], the use of improvers has led to greater SOC stratification: the stratification coefficient was 1.22 between the 0–10 and 10–20 cm layers, and 1.73 between the 0–10 and 20–30 cm layers under NT+WM treatment, and 1.23 and 1.82 under PT+aLS treatment, respectively. Similar results were also reported by [31] from a study conducted on a silt loam soils, which showed significantly greater SOC concentration within the top 15 cm in no-tillage system compared to mouldboard ploughing. The results of a 50-year study showed that SOM concentrations increased by 21% in the top 15 cm of soil using conventional tillage, and by 58% in the case of reduced tillage or no-till [2]. SOC increase in the upper 0–10 cm soil layer can be explained by slower crop residue decomposition with long-term soil disturbance minimization [12].

Water extractable organic carbon. The content of labile, especially water extractable organic carbon (WEOC) is a sensible indicator of SOM quality [32]. Fan et al. [33] founded that hot water extractable organic carbon content in 0–30 cm layer was 58.8% lower in cultivated than in uncultivated soils. It appears from the Table 2 that the WEOC content in the soil was higher in all study treatments in 2016 compared to the other years of the experiment. This could be explained by favourable mineralization conditions from the beginning of the vegetation and especially in the rainy second half of summer, which allowed labile organic compounds to migrate easily to deeper layers. WEOC concentration was higher at 0–10 and 10–20 cm layers under PT treatment compared to DP, which consistent with Segnini et al. [34] findings that due to less intensive tillage, the transformation of plant residues changes

with the formation of higher amounts of labile compounds. Significantly higher concentrations of WEOC were found in the 0–10 cm layer in NT+WM compared to the control DP, due to the higher amount of plant residues on the soil surface. The application of lime sludge four times during the 1st and 2nd crop rotations (last incorporated in 2014) increased the concentration of Ca cations in the soil and allowed to stabilize labile organic compounds – the concentration of WEOC under PT+aLS in the 0–10 cm layer was significantly lower compared to DP. León et al. [15] also found that Ca from lime sludge can stabilize soil aggregates, and thus may have positive cooperative effect on soil organic matter stabilization. In 2017 and 2018, due to lack of moisture and high temperature, there were unfavourable conditions for organic matter mineralization at the soil surface, and no significant differences in WEOC concentrations were found between the treatments. According to the mean data of 2016–2018, no significant differences in WEOC content were found in the 0–10 cm and 10–20 cm layers. WEOC decreased significantly only in 20–30 cm soil layer after the application of PT+aLS and NT+WM, 18% in both cases compared to DP. Like SOC, in the control DT treatment WEOC was evenly distributed in the 0–30 cm arable layer: the stratification coefficient was 1.00 between the 0–10 and 10–20 cm layers, and 1.08 between the 0–10 and 20–30 cm layers. According to the influence on WEOC stratification, applied tillage systems can be arranged in the following order: DP < PT < PT+aLS < NT+WM. Under NT+WM treatment the stratification coefficient was 1.12 between the 0–10 and 10–20 cm layers, and 1.42 between the 0–10 and 20–30 cm layers.

Total nitrogen. The distribution of soil total nitrogen (TN) under different tillage practices are not clearly understood [35], but some studies suggest that reduced tillage can improve soil quality by increasing the amount of TN as well as enhance nitrogen availability [36, 37]. The average data for the years 2016–2018, presented in Table 3, show that amounts of TN in the upper (0–10 cm) soil layer increased in all applied reduced tillage systems compared to the control DP, however, a significant difference was found only under NT+WM (+18.8% compared to DP). This can be explained by the fact that cover crops for winter mulch developed high nitrogenous biomass [38]. In 2016, TN content under NT+WM in 0–10 cm soil layer was significantly higher by 17.4 %, and in 2017 TN content under NT+WM was higher by 16.7 %, compared with DP. No significant differences in TN content were found in other two studied soil layers, and the application of PT+aLS and NT+WM demonstrated significantly lower TN concentrations in the 10–20 cm and 20–30 cm layers in 2018. The content of TN decreased significantly in the 10–20 cm layer after the application of PT+aLS and NT+WM, respectively by 12% and 14% compared to DP; and TN content under NT+WM was significantly lower by 13% in the 20–30 cm soil layer, compared with DP. Similar trends were found by Boselli et al. [39], who claimed that no-tillage increased soil TN in the topsoil layer (0–5 cm) compared with conventional tillage, and generally tended to increase TN content also in the 5–15 cm soil layer.

TABLE 3
Total nitrogen content (g kg^{-1}) and C-to-N ratio under different tillage practices

Treatment	Layer, cm	TN, g kg^{-1}				C-to-N ratio			
		2016	2017	2018	Mean	2016	2017	2018	Mean
DP	0–10	1.61	1.49	1.46	1.52	8.09	8.48	9.66	8.72
	10–20	1.66	1.53	1.42	1.53	7.83	8.44	9.56	8.61
	20–30	1.47	1.32	1.07	1.28	7.45	7.59	9.29	8.05
PT	0–10	1.67	1.65	1.56	1.62	7.99	8.51	9.43	8.66
	10–20	1.61	1.48	1.35	1.47	7.35	8.18	9.07	8.20
	20–30	1.54	1.23	0.98	1.25	7.12	7.13	8.06	7.38
PT+aLS	0–10	1.73	1.58	1.60	1.64	8.38	9.11	9.94	9.10
	10–20	1.64	1.49	1.25*	1.46	7.50	8.05	9.62	8.29
	20–30	1.44	1.20	1.20	1.28	6.14	6.85	6.28	6.41*
NT+WM	0–10	1.89*	1.74*	1.47	1.70*	7.75	8.24	9.80	8.61
	10–20	1.58	1.51	1.22*	1.43	7.40	8.07	9.55	8.28
	20–30	1.31	1.20	0.93*	1.14	6.61	7.06	8.54	7.33
LSD_{05}	0–10	0.215	0.238	0.177	0.151	1.152	1.845	1.135	1.033
	10–20	0.229	0.228	0.163	0.181	1.384	1.571	1.273	1.099
	20–30	0.318	0.213	0.237	0.211	1.130	2.253	1.456	1.028

Note: DP – deep ploughing (control); PT – ploughless tillage; PT+aLS – ploughless tillage and aftereffect of lime sludge; NT+WM – no-tillage with winter mulch; * – significant at $P \leq 0.05$ probability level, the significance of the differences between the treatments was evaluated using the LSD.

TABLE 4
Correlation relationships among soil properties

Variable	Year	n	TN	WEOC
SOC	2016	36	0.812*	0.835*
	2017	36	0.761*	0.749*
	2018	36	0.886*	0.599*
	2016–2018	108	0.707*	0.539*
TN	2016	36		0.691*
	2017	36		0.596*
	2018	36		0.565*
	2016–2018	108		0.649*

Note: n – number of observations; * – significant at $P \leq 0.05$ probability level.

TABLE 5
Simple linear regression equations

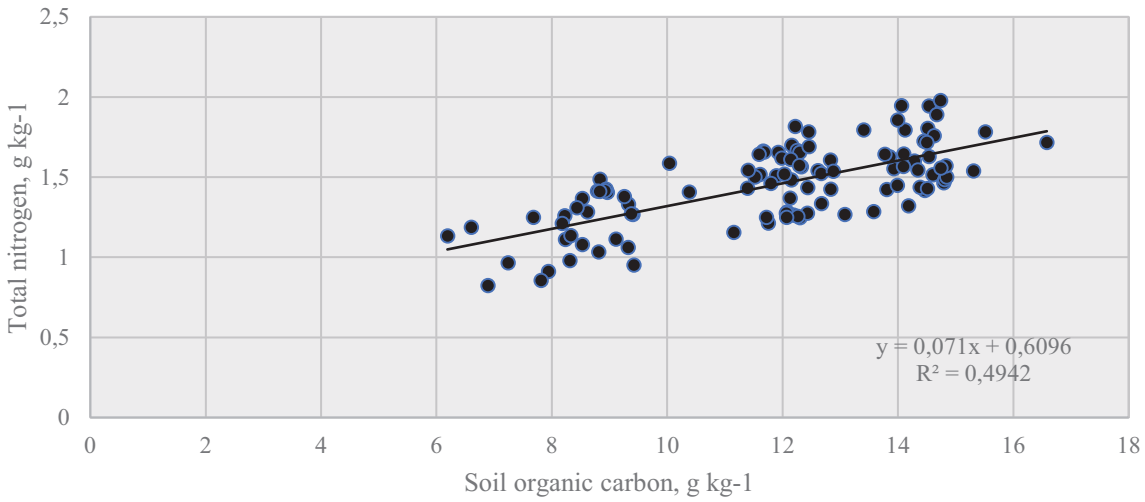
Dependent variable	Year	n	Intercept	Coefficient	Variable	R^2
TN	2016	36	0.7293	0.0733	SOC	0.659
	2017	36	0.7047	0.0637		0.580
	2018	36	0.4595	0.0689		0.786
	2016–2018	108	0.6204	0.0696		0.500
WEOC	2016	36	0.0516	0.0182	SOC	0.697
	2017	36	0.1286	0.0088		0.561
	2018	36	0.1473	0.0045		0.359
	2016–2018	108	0.1223	0.0094		0.291
WEOC	2016	36	0.9336	2.4440	TN	0.477
	2017	36	0.5228	3.9882		0.355
	2018	36	0.5757	3.5506		0.319
	2016–2018	108	0.6477	3.3958		0.421

Note: n – number of observations.

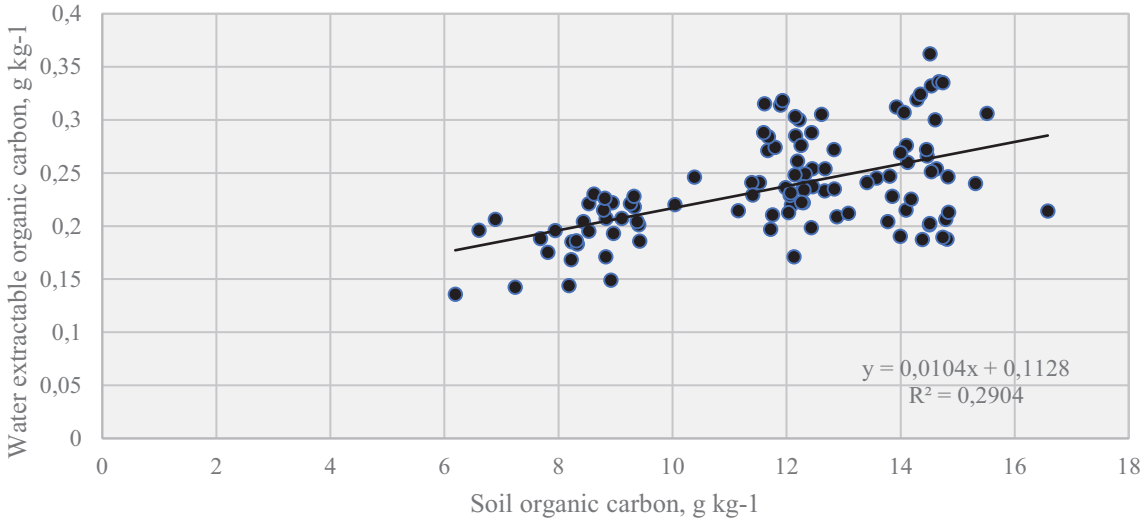
C-to-N ratio. A widely applied index of SOM mineralization is the C-to-N ratio which decreases with advancing mineralization. According to Pineiro et al. [40] in arable soils the C-to-N ratio depended on the shares on active, easily mineralizing, and passive, stable fraction in SOM. The C-to-N ratio provides information on the capacity of the soil to store and recycle nutrients [41]. The estimated soil C-to-N ratios across our experiment area varied from 6.14 to 9.94 (Table 3). The influence of tillage as well as its combinations with supplementary agronomic practices on the C-to-N ratio did not depend on the conditions of individual years in our experiment. Some authors reported that the highest C-to-N ratios were found in the 0−5 cm layer under no-till or shallow tillage, and the lowest rates in the 10−28 cm layer of the same tillage treatments [42]. The average data for the year 2016–2018 show, that lowest C-to-N ratio was under PT+aLS in 20–30 cm layer. The C-to-N ratio tended to decline with depth when tillage reduced, but the differences among the treatments were not significant. Other authors suggest that no significant differences were observed in total C, organic C, total N and C/N ratio between different tillage treatments and timing in clay soils in northern Europe and indicating that there were no differences in the quality of organic matter [43].

The correlation coefficient is a statistical method of calculating the relationship between two variables, which allows estimating the strength and direction of the relationship [44]. During the period of our experiment, the amount of SOC in the soil varied from 7.53 to 15.91 g kg-1, content of TN – from 0.93 to 1.89 g kg-1, and content of WEOC – from 0.15 to 0.34 g kg-1. According to data in Table 4, the relationship between SOC and TN was found to be linear, which is direct and strength in terms of correlation coefficient. Meanwhile, the highest correlation coefficient was established in 2018. The relationship between SOC and WEOC was also linear and direct, but the strength of the relationship differed in the individual years of the experiment: it was strong in 2016 and 2017 (r = 0.835 and r = 0.749, respectively), and moderately strong in 2018 (r = 0.599). Meanwhile, the relationship between TN and WEOC was linear, direct, and moderate in strength throughout the study years.

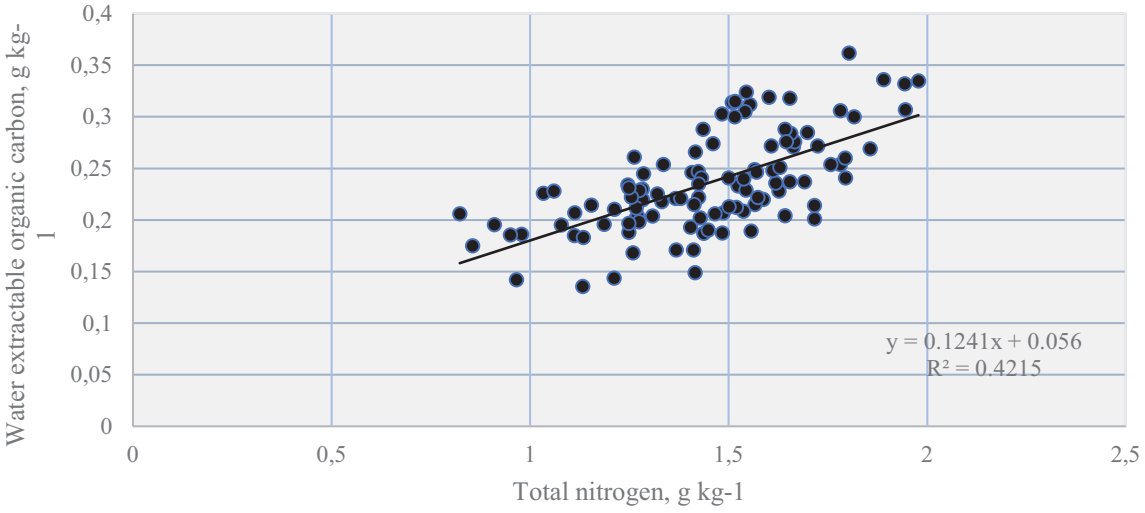
Correlation is not a causal relationship – if two variables are correlated, it does not mean that one variable causes a change in the other variable. The simple linear regression is the most used technique for determining how one variable responds to changes in another variable. Regression equations between SOC and TN (Table 5) indicate that the relationship of TN vs SOC account for 50% of the variance if we examine the data for 2016–2018, and even 78% in 2018. The relationship of WEOC vs SOC account for 29%, and WEOC vs TN – for 42% of the variance. All relationships appear linear (Figure 1).



a)



b)



c)

FIGURE 1
Relation of a) content of total nitrogen (TN) with content of soil organic carbon (SOC); b) content of water extractable organic carbon (WEOC) with SOC; and c) WEOC with TN (2016–2018)

CONCLUSION

Reduced tillage systems significantly increased soil organic carbon (SOC) content in the upper (0–10 cm) soil layer by order PT+aLS > NT+WM > PT > DP and shows SOC stratification in reduced tillage systems.

WEOC content was higher under PT and NT+WM treatments at 0–10 and 10–20 cm layers, however under PT+aLS the WEOC content was lower compared to DP. Cations from lime sludge stabilized mobile and labile forms of SOC, reducing WEOC content.

The content of TN in soil was less affected by applied reduced tillage systems, amount of TN in the upper (0–10 cm) soil layer increased significantly only under NT+WM. The ratio SOC-to-TN tended to decline with depth under applied reduced tillage systems compared to DP, but the differences were not significant.

High correlation coefficients were observed for the relationship of SOC vs TN, indicating a close relation between SOC and TN accumulation in soil; lower correlation coefficients were observed for the relations of SOC vs WEOC, and TN vs WEOC.

REFERENCES

[1] Paustian, K., Andrén, O., Janzen, H.H., Lal, R., Smith, P., Tian, G., Tiessen, H., van Noordwijk, M., Woomer, P.L. (1997) Agricultural soils as a sink to mitigate CO2 emissions. Soil Use and Management. 13 (s4), 230–244.

[2] Obour, A.K., Mikha, M.M., Holman, J.D., Stahlman, P.W. (2017) Changes in soil surface chemistry after fifty years of tillage and nitrogen fertilization. Geoderma. 308, 46–53.

[3] Buragienė, S., Šarauskis, E., Romaneckas, K., Sasnauskienė, J., Masilionytė, L., Kriaučiūnienė, Z. (2015) Experimental analysis of CO2 emissions from agricultural soils subjected to five different tillage systems in Lithuania. Science of the Total Environment. 514, 1–9.

[4] Maikštėnienė, S. (2008) Sustainable agriculture on productive soils. Lithuanian Institute of Agriculture. 344. (in Lithuanian)

[5] Lal, R. (2016) Soil health and carbon management. Food and Energy Security. 5(4), 212–222.

[6] Seddaiu, G., Iocola, I., Farina, R., Orsini, R., Iezzi, G., Roggero, P.P. (2016) Long term effects of tillage practices and N fertilization in rainfed Mediterranean cropping systems: durum wheat, sunflower and maize grain yield. European Journal of Agronomy. 77, 166–178.

[7] Somasundaram, J., Reeves, S., Wang, W., Heenan, M., Dalal, R. (2017) Impact of 47 years of no tillage and stubble retention on soil aggregation and carbon distribution in a Vertisol. Land Degradation and Development. 28(5), 1589–1602.

[8] Huang, M., Liang, T., Wang, L., Zhou, C. (2015) Effects of no-tillage systems on soil physical properties and carbon sequestration under long-term wheat–maize double cropping system. Catena. 128, 195–202.

[9] Singh, P., Heikkinen, J., Ketoja, E., Nuutinen, V., Palojärvi, A., Sheehy, J., Esala, M., Mitra, S., Alakukku, L., Regina, K. (2015) Tillage and crop residue management methods had minor effects on the stock and stabilization of topsoil carbon in a 30-year field experiment. Science of the Total Environment. 518–519, 337–344.

[10] Valboa, G., Lagomarsino, A., Brandi, G., Agnelli, A.E., Simoncini, S., Papini, R., Vignozzi, N., Pellegrini, S. (2015) Long-term variations in soil organic matter under different tillage intensities. Soil and Tillage Research. 154, 126–135.

[11] Kibet, L.C., Blanco-Canqui, H., Jasa, P. (2016) Long-term tillage impacts on soil organic matter components and related properties on a Typic Argiudoll. Soil and Tillage Research. 155, 78–84.

[12] Bogužas, V., Mikučionienė, R., Šlepetienė, A., Sinkevičienė, A., Feiza, V., Steponavičienė, V., Adamavičienė, A. (2015) Long-term effect of tillage systems, straw and green manure combinations on soil organic matter. Zemdirbyste-Agriculture. 102(3), 243–250.

[13] Horák, J., Balashov, E., Šimanský, V., Igaz, D., Buchkina, N., Aydin, E., Bárek, V., Drgoňová, K. (2019) Effects of conventional moldboard and reduced tillage on seasonal variations of direct CO_2 and N_2O emissions from a loam Haplic Luvisol. Biologia. 74, 767–782.

[14] Vazquez, E., Teutscherova, N., Almorox, J., Navas, M., Espejo, R., Benito, M. (2017) Seasonal variation of microbial activity as affected by tillage practice and sugar beet foam amendment under Mediterranean climate. Applied Soil Ecology. 117–118, 70–80.

[15] León, P., Espejo, R., Gómez-Paccard, C., Hontoria, C., Mariscal, I., Renella, G., Benito, M. (2017) No tillage and sugar beet foam amendment enhanced microbial activity of degraded acidic soils in South West Spain. Applied Soil Ecology. 109, 69–74.

[16] Gómez-Paccard, C., Mariscal-Sancho, I., Leon, P., Benito, M., González, P., Ordóñez, R., Espejo, R., Hontoria, C. (2013) Ca-amendment and tillage: Medium term synergies for improving key soil properties of acid soils. Soil and Tillage Research. 134, 195–206.

[17] Hontoria, C., Gomez-Paccard, C., Mariscal-Sancho, I., Benito, M., Perez, J., Espejo, R. (2016) Aggregate size distribution and associated organic C and N under different tillage systems and Ca-amendment in a degraded Ultisol. Soil and Tillage Research. 160, 42–52.

[18] Gómez-Paccard, C., Hontoria, C., Mariscal-Sancho, I., Pérez, J., León, P., González, P., Espejo, R. (2015) Soil–water relationships in the upper soil layer in a Mediterranean Palexerult as affected by no-tillage under excess water conditions – influence on crop yield. Soil Tillage Research. 146, 303–312.

[19] Paleckienė, R., Sviklas, A.M., Šlinkšienė, R. (2006) The role of sugar factory lime on compound fertilizer properties. Polish Journal of Environmental Studies. 16(3), 423–426.

[20] Shaheen, S.M., Rinklebe, J. (2017) Sugar beet factory lime affects the mobilization of Cd, Co, Cr, Cu, Mo, Ni, Pb, and Zn under dynamic redox conditions in a contaminated floodplain soil. Journal of Environmental Management. 186, 253–260.

[21] González-Fernández, P., Espejo-Serrano, R., Ordóñez-Fernández, R., Peregrina-Alonso, F. (2004) Comparative studies of the efficiency of lime refuse from sugar beet factories as an agricultural liming material. FAO European Cooperative Research. Nutrient and Carbon Cycling in Sustainable Plant-Soil Systems. 157–160.

[22] Kheir, A., Kamara, M. (2019) Effects of sugar beet factory lime, vinasse, and compost mixed with vinasse application on sandy soil properties and Canola productivity. Journal of Soil Sciences and Agriculture Engineering. 10(1), 69–77.

[23] Adnan, M., Asif, M., Khalid, M., Abbas, B., Hayyat, M.S., Raza, A., Khan, B.A., Mudassir Hassan, M., Khan, M.A.B., Muhammad Shakeel Hanif, M.S. (2020) Role of mulches in agriculture: A review. International Journal of Botany Studies. 5(3), 309–314.

[24] Aulakh, M.S., Khera, T.S., Doran, J.W., Singh, K., Singh, B. (2000) Yields and nitrogen dynamics in a rice–wheat system using green manure and inorganic fertilizer. Soil Science Society of America Journal. 64(5), 1867–1876.

[25] Khurshid, K., Iqbal, M., Arif, M.S., Nawaz, A. (2006) Effect of tillage and mulch on soil physical properties and growth of maize. International Journal of Agriculture and Biology. 8(5), 593–596.

[26] Jiménez, M.N., Fernández-Ondoño, E., Ripoll, M.Á., Castro-Rodríguez, J., Huntsinger, L., Navarro, F.B. (2013) Stones and organic mulches improve the Quercus Ilex L. afforestation success under Mediterranean climatic conditions. Land Degradation and Development. 27(2), 357–365.

[27] Bajorienė, K., Jodaugienė, D., Pupalienė, R., Sinkevicienė, A. (2013) Effect of organic mulches on the content of organic carbon in the soil. Estonian Journal of Ecology. 62(2), 100–106.

[28] Harasim, E., Gawęda, D., Wesołowski, M., Kwiatkowski, C., Gocół, M. (2015) Cover cropping influences physico-chemical soil properties under direct drilling soybean. Acta Agriculturae Scandinavica, Section B–Soil and Plant Science. 66(1), 85–94.

[29] Bünemann, E.K., Bongiorno, G., Bai, Z., Creamer, R.E., de Deyn, G., de Goede, R., Fleskens, L., Geissen, V., Kuyper, T.W., Mäder, P., Pulleman, M., Sukkel, W., van Groenigen, J.W., Brussaard, L. (2018) Soil quality – A critical review. Soil Biology and Biochemistry. 120, 105–125.

[30] Slepetiene, A., Kadziuliene, Z., Feiziene, D., Liaudanskiene, I., Amaleviciute-Volunge, K., Slepetys, J., Skersiene, A., Velykis, A., Armolaitis, K. (2020) The distribution of organic carbon, its forms and macroelements in agricultural soils. Zemdirbyste-Agriculture. 107(4), 291–300.

[31] Sagar, L., Singh, S. (2020) Impact of agronomic practices on soil organic carbon dynamics: A review. International Journal of Chemical Studies. International Journal of Chemical Studies. 8(4), 2173–2178.

[32] Hamkalo, Z., Bedernichek, T. (2014) Total, cold and hot water extractable organic carbon in soil profile: impact of land-use change. Zemdirbyste-Agriculture. 101(2), 125–132.

[33] Fan, R., Zhang, X., Shen, Y., Yang, X., Liang, A. (2013) Near-infrared spectroscopic assessment of hot water extractable and oxidizable organic carbon in cultivated and uncultivated Mollisols in China. Acta Agriculturae Scandinavica, Section B–Soil and Plant Science. 63(1), 37–45.

[34] Segnini, A., Carvalho, J.L.N., Bolonhezi, D., Pereira Milori, D.M.B., da Silva, W.T.L., Simões, M.L., Cantarella, H., de Maria, I.C., Neto, L.M. (2013) Carbon stock and humification index of organic matter affected by sugarcane straw and soil management. Scientia Agricola. 70(5), 321–326.

[35] Qi, J.Y., Zhang, X.Z., Li, S.S., Virk, A.L., Wang, X., Kan, Z.R., Zhao, X., Xiao, X.P., Zhang, H.L. (2021) Effects of different tillage practices on the distribution of soil total nitrogen and carbon/nitrogen ratio at different soil depths in a double rice cropping system. Archives of Agronomy and Soil Science. 67(5), 714–725.

[36] Gao, X., Lv, A., Zhou, P., Qian, Y., An, Y. (2015) Effect of green manures on rice growth and plant nutrients under conventional and no-till systems. Agronomy Journal. 107(6), 2335–2346.

[37] Nandan, R., Singh, V., Singh, S.S., Kumar, V., Hazra, K.K., Nath, C.P., Poonia, S., Malik, R.K., Bhattacharyya, R., McDonald, A. (2019) Impact of conservation tillage in rice–based cropping systems on soil aggregation, carbon pools and nutrients. Geoderma. 340, 104–114.
[38] Ugrenović, V., Filipović, V., Jevremović, S., Jeromela, A.M., Popović, V., Buntić, A., Delić, D. (2019) Effect of Brassicaceae as cover crops. Selekcija i Semenarstvo. 25(2), 1–8.
[39] Boselli, R., Fiorini, A., Santelli, S., Ardenti, F., Capra, F., Maris, S.C., Tabaglio, V. (2020) Cover crops during transition to no-till maintain yield and enhance soil fertility in intensive agro-ecosystems. Field Crops Research. 255, 107871, 1–11.
[40] Pineiro, G., Oesterheld, M., Batista, W.B., Paruelo, J.M. (2006) Opposite changes of whole-soil vs. pools C: N ratios: a case of Simpson's paradox with implications on nitrogen cycling. Global Change Biology. 12(5), 804–809.
[41] Šimon, T. (2008) The influence of long-term organic and mineral fertilization on soil organic matter. Soil and Water Research. 3(2), 41–51.
[42] Mary, B., Clivot, H., Blaszczyk, N., Labreuche, J., Ferchaud, F. (2020) Soil carbon storage and mineralization rates are affected by carbon inputs rather than physical disturbance: Evidence from a 47-year tillage experiment. Agriculture, Ecosystems and Environment. 299, 1–13.
[43] Kainiemi, V., Arvidsson, J., Kätterer, T. (2013) Short-term organic matter mineralisation following different types of tillage on a Swedish clay soil. Biology and Fertility of Soils. 49(5), 495–504.
[44] Kozak, M., Krzanowski, W., Tartanus, M. (2012) Use of the correlation coefficient in agricultural sciences: problems, pitfalls and how to deal with them. Anais da Academia Brasileira de Ciências. 84(4), 1147–1156.

Received: **02.02.2021**
Accepted: **02.05.2021**

CORRESPONDING AUTHOR

Tomas Zukaitis
Chemical Research Laboratory,
Lithuanian Research Centre for Agriculture and Forestry,
Instituto av. 1, Akademija,
LT-58344 Kedainiai distr. – Lithuania

e-mail: tomas.zukaitis@lammc.lt

© by PSP Volume 30– No. 09/2021 pages 10586-10591 Fresenius Environmental Bulletin

THE EFFECT ON SENSORY QUALITY OF THE STUFFED PASTA (MANTI) OF INCREASED MALONDIALDEHYDE AMOUNT WITH THE UV-C RADIATION AND STORAGE

Suleyman Gokmen[1,*], Abdullah Caglar[2]

[1]Department of Food Processing, Technical Vocational School, Karamanoglu Mehmetbey University, Karaman, Turkey
[2]Department of Agricultural Economics, Faculty of Agriculture and Natural Sciences, Kocaeli University, Kocaeli, Turkey

ABSTRACT

Rancidity is a process that occurs as a result of the oxidation of unsaturated fats and oils in foods and causes food to spoil when it is above a certain level. The method used to determine rancidity in foods is to be measured amount of malonaldehyde, the final product of Thiobarbutiric acid in the food. The rancidity is inevitable in foods containing fat or oil. In this study, the storage and the UV-C effect on the its sensory quality of the rancidity process consisting in stuffed pasta (mantı) including minced beef and fat, producing traditionally in Turkey was examined. According to the obtained results, it was concluded that the amount of malonaldehyde increased by UV-C radiation did not affect the sensory properties of the samples ($p < 0.05$), while the negative effect of the rancidity levels formed during storage on the sensory quality ($p < 0.05$). More research is needed on this topic.

KEYWORDS:
Mantı, UV-C, thiobarbutiric acid, storage, sensory quality

INTRODUCTION

Traditional foods are special products including cultural trends of certain areas and resulting from experience without using novel technology [1-2]. Stuffed pasta (mantı) is one of the traditional foods with high nutritive value and widely consumption in Turkey. It is a minced beef stuffed pasta product and offered for sale in fresh or in dried forms in Turkey. The basic production stages of mantı are given in below.

(1) Mortar preparation with minced beef and various spices for fillings (red and black pepper, salt and, onion)

(2) Preparation of mantı dough (wheat flour, water, egg and salt)

(3) Sheeting and cutting prepared dough,

(4) Placing to the mortar on the dough and then enclosing of dough

(5) Pre-pasteurization, freezing or drying [3-5].

In addition to industrial production flow chart for mantı was given in Figure 1.

Besides, the shelf life of mantı is short because it contains ground beef and fat or oil. Therefore, mantı is sensitive for oxidation. As a result of lipid oxidation caused by physical, chemical and biological factors, rancidity develops in foods. Since rancidity causes sensory and biological unwanted changes in foods, it is considered as a sign of food degradation. The methods utilized to determine lipid oxidation in foods are considered at either primary products or secondary products. So, the commonly utilized methods are peroxide value and Thiobarbituric acid (TBA) analyses although there are variety tests related to lipid oxidation determination in the literature [7-9]. TBA values are regarded as an indicator of putrification. Increasing TBA values shorten the shelf life of meat and meat-based food products [7-9]. Especially in these products, there is no study on whether there is a relationship between the TBA values formed during the storage process and the TBA values generated by UV-C radiation. In these 2 cases, there is also no study in the literature about the effect of increased TBA values on the sensory quality of the product. Therefore, this study aimed to determine the difference between the TBA values generated by UV-C on the sensory quality of mantı and the TBA values generated during storage.

MATERIALS AND METHODS

In this study, 10 kg bundle-type fresh mantı was used. The properties of manti were given below (Table 1).

The storage time and UV-C exposure times of the mantı were determined by preliminary trials. Thiobarbituric acid (TBA) analyzes were routinely performed in preliminary trials. Preliminary trials were continued until the TBA values formed during the storage of mantı coincided with the TBA values in the mantı exposed to UV-C radiation. Thus, the study consists of 2 stages. The first step of the study is the storage of the first group of mantı (5 kg). For this purpose, 5 kg of mantı was stored under refrigerator conditions for 24-48 and 72 hours. In the second stage, group 2 mantı samples (5 kg) were exposed to UV-C radiation for 30-45 and 60 minutes.

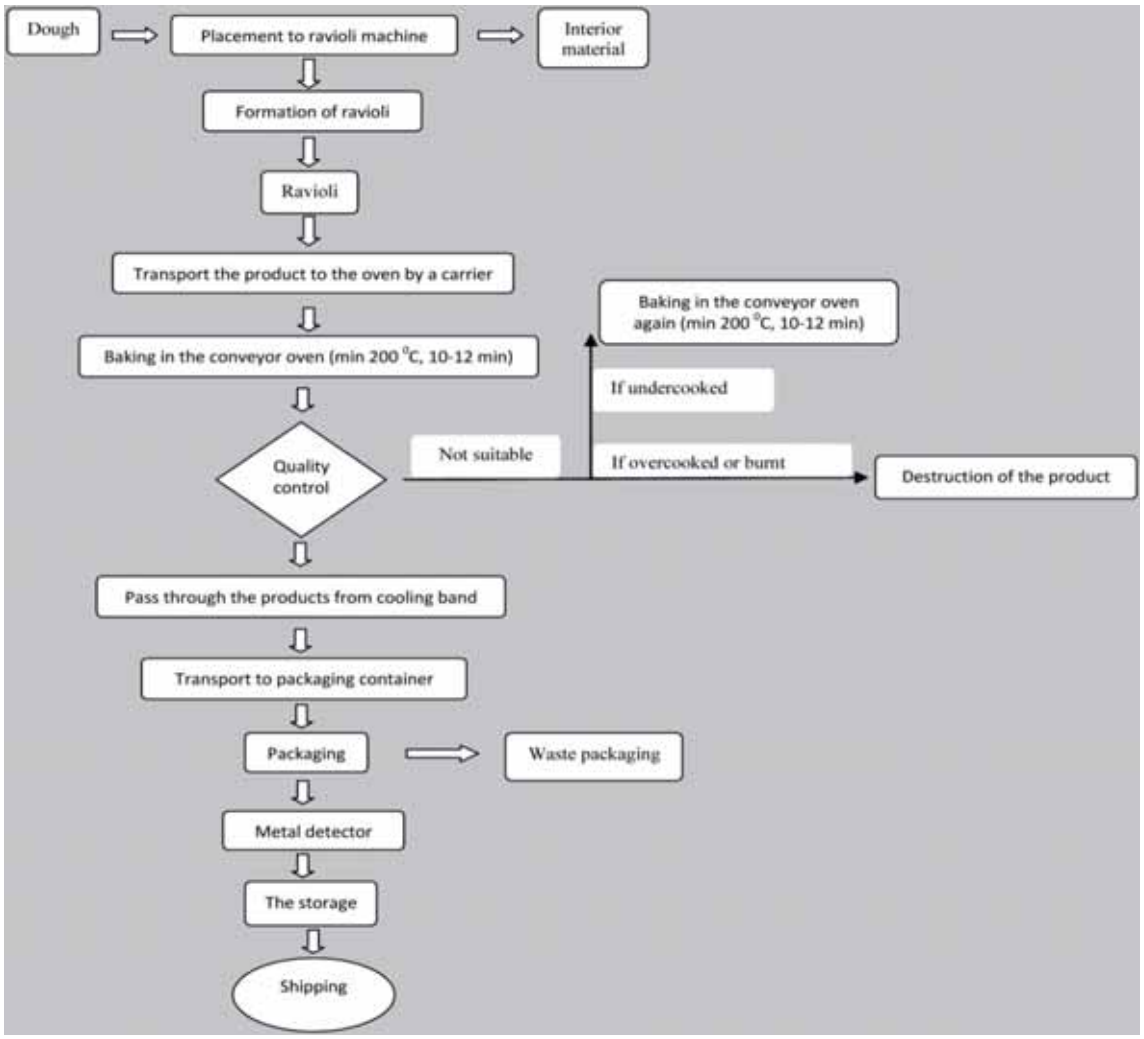


FIGURE 1
Industrial production flow chart for mantı [6].

TABLE 1
Features of Mantı samples

Moisture ratio (%)	43
Tiyobarbutiric acid value	0.21 (mg/kg)
Shape	Bundle type
Form	Fresh mantı
Weight	1 of them is about 1 g

TABLE 2
Ultraviyolet applications in mantı

UV-C applications	Time(min.)	Temperature (°C)
	30	
	45	25
	60	

UV-C radiation application to mantı samples. UV-C application was carried out in the cabin and with a UV-C fluorescent lamp. The distance between UV-C and the product is set to 25 cm. The beam intensity of UV-C was measured with a pyrometer as 1 W/m2. The features of the UV-C lamp used in the process are given below.

Properties of UV-C.

- UVC T8 15W / G13
- Scope of application
- Water, food, air, and surface sterilization
- Low mercury content, no ozone, it has the most effective radiation at 254 nm.
- Current: 0.31A- Volt: 55 V- Power: 15W

Mantı samples, which were pre-pasteurized, were exposed to UV-C radiation under the following conditions (Table 2)

Analyzes made in mantı samples were given below.

Thiobarbituric acid (TBA) analysis. Mantı (10 g) was homogenized with pure water. This mixture was transferred to Kjeldahl flask and total 100 ml mixture distilled by adding 2.5 mL 4 N HCl (Merck, Germany) and 1 mL antifoam chemical (silicon). After that, 5 mL of this collected distillate was mixed with equal volume of TBA reagent.

TABLE 3
Sensory Analysis Form

Quality Criteria	Codes														
	1	2	3	4	5	6	7	8	9	10	11	12	13	14	15
Taste															
Smell															
Aroma															
Apperance															
Mouthfeel															
General Taste															

Descriptions	1= Very bad	2= Bad	3= Intermediate	4= Good	5= Very good

Wanted Features in mantı

- Fullness in the mouth,
- The color is not in an undesirable color,
- The mantı is not dispersed,
- Not sticking,
- Its content does not come out,
- Its flavor is close to the control product.

Unwanted Features in mantı

- Weak aroma,
- Neutral taste,
- Unwanted color change,
- Unwanted foreign taste,
- Foreign smell,
- Adhesion,
- Coming out of mantı mortar.

TABLE 4
Processes applied to mantı samples and their determined TBA values

Storage time in refrigerator conditions (hour)	UV-C application time (minute)	Average Thiobarbutyric acid (TBA) values (mg/kg)
0 (Control)	0	0.21
24	30	0.43
48	45	0.68
72	60	1.50

(Merck, Germany) and then, incubated in boiling water bath at 80-90 oC for 30 minutes. The measurement was carried out by a UV- spectrophotometer at 538 nm and lipid peroxidation level was calculated according to the below equation as the equivalent of mg malondialdehyde (MDA) per kg sample [7].

TBA value (mg malonaldehit/kg sample) = 7.8 * A

Sensory analysis. Sensory analysis was carried out by 8 panelists in laboratory conditions. The panelists were provided an assessment form to evaluate each mantı for taste, smell, aroma, appearance, mouthfeel, and general taste features. A 5-point hedonic scale was used, where 5 indicates very good and 1 extremely bad for sensory properties (Table 3)**Cooking of mantı samples.** Mantı samples (500 g) with average %43 moisture contents were cooked in 2 L of potable water. When the water boiled, 500 g mantı and 1% salt were added. The mantı samples were boiled for 12-15 minutes. After that, the sample was filtered to remove water with buhner funnel and then cooled with 250 mL of cold water [4, 10].

Statistical Analyses. The difference between Thiobarbutyric Acid (TBA) values and sensory quality parameters between samples and applications was determined at 95% confidence interval using Duncan Multiple Comparison Test in JMP Statistical Analysis program.

RESULTS AND DISCUSSION

In this study, the effect of TBA values increased by storage and UV-C radiation on the sensory parameters of mantı was examined and the results obtained were given below.

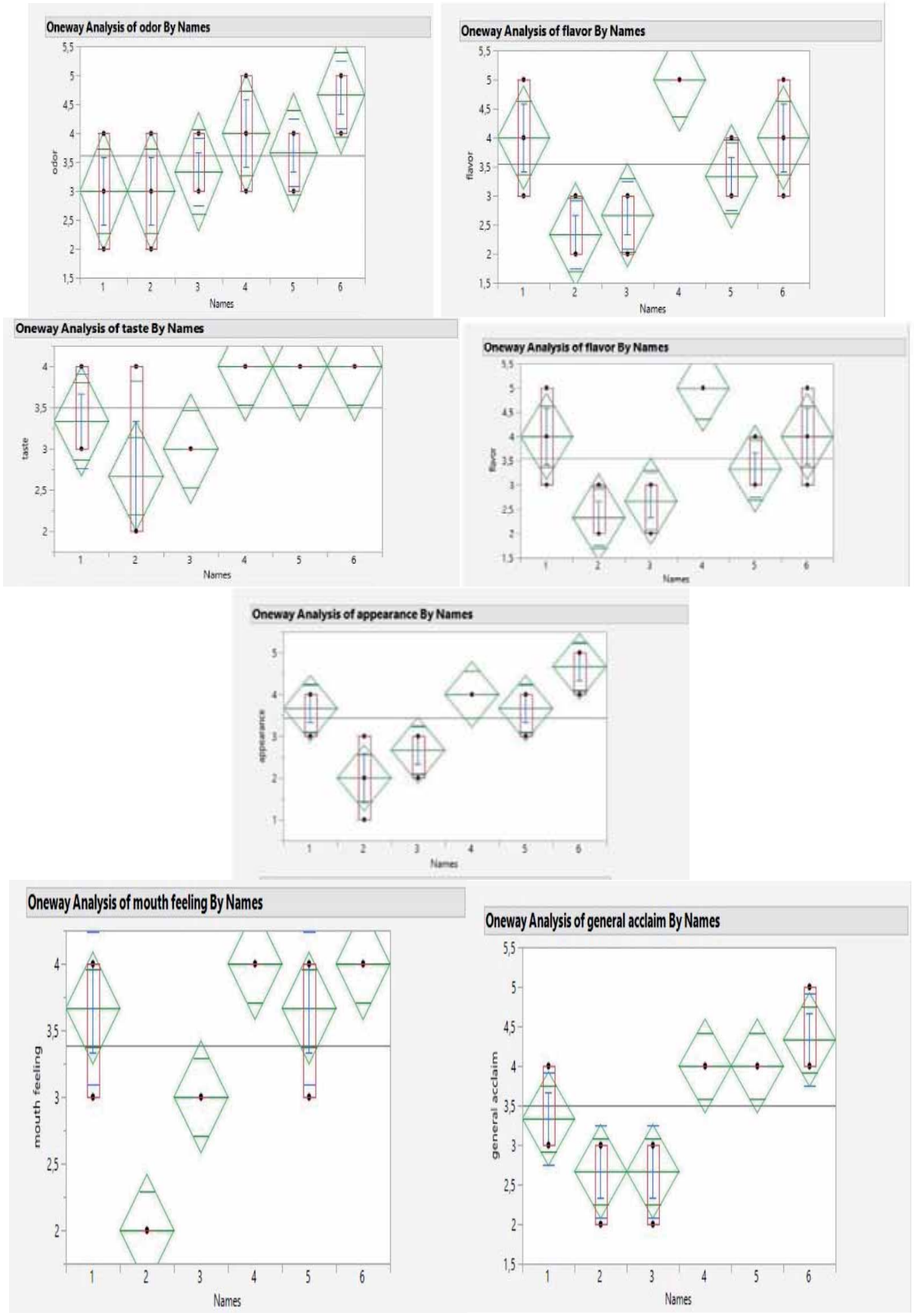


FIGURE 2
Sensory Analyses Results

1- 24 h. Storage in refrigerator conditions (hour), 2-48 h. Storage in refrigerator conditions (hour), 3-72h. Storage in refrigerator conditions (hour), 4- 30 min. UV-C application (minute), 5- 45 min. UV-C application (minute), 6-60 min. UV-C application (minute)

TBA Analysis Results. Storage times for which TBA values in mantı are equal on average and UV-C radiation exposure times were given in Table 4.

Sensory Analysis Results. In terms of taste, aroma, appearance, mouthfeel and general taste parameters, it was determined that mantı samples with TBA values formed as a result of UV-C radiation treatment were more preferred samples and it was concluded that the values obtained were statistically significant ($p < 0.05$) (Figure 2).

TBA values are used to determine lipid peroxidation in foods. As lipid peroxidation increases, TBA values increase in parallel with this [10]. However, the more increases with the storage of foods and thermal or non-thermal processes to foods, the more increase in TBA values [11]. TBA values in foods above 3 mg/kg cause the formation of unwanted flavors and aromas [12-13]. According to the Turkish Food Codex, TBA values in meat and meat-based products should not be over 5 mg/kg [5]. However, the increase in TBA values occurring in foods in each process affects the sensory properties of the products differently. In a study conducted on the subject, it was reported that preheating of mantı increased lipid peroxidation and in parallel with this, sensory quality of the mantı improved [11]. In this study, it was concluded that although the increase in TBA values in UV-C radiation application did not cause a negative change in the sensory quality of mantı samples, the prolongation of the storage time at refrigerator temperature decreased its sensory quality.

The sensory quality of mantı samples in different brands put on the market in Turkey was reported to vary [4]. Therefore, it is thought that more research should be done on the sensory quality of traditional foods such as mantı.

In another study, it was reported that Maillard reaction products formed in the cooking of ground beef and mantı positively affected the sensory quality [10, 12-14]. In parallel with this research, it was concluded that 30-45 and 60 minutes of UV-C applications did not reduce the sensory quality of the product in this study.

In a study conducted on the storage of precooked chicken meatballs at refrigerator temperature, it was reported that TBA values of meatballs that were heated in the microwave before being consumed after storage were high and that of meatballs heated in the oven were low. In the same study, it was reported that oxidative changes in meat products should be monitored routinely and storage and reheating methods affect the sensory quality [13-17]. Similarly, in our study, it was concluded that UV-C, which is one of the non-ionizing radiation types and which is a non-thermal process, does not affect the sensory quality as much as the storage process.

In addition, it has been reported that UV-C also inhibits enzymatic and microbial growth [3]. Thus, UV-C application will extend the shelf life of the food.

CONCLUSIONS

According to the results of this study, the sensory quality of the product decreased significantly during the storage of the samples. Besides it was concluded that when UV-C application was performed in certain periods of meat and meat-grain-based products such as mantı, although the TBA values increased, the sensory quality of the product did not decrease.

REFERENCES

[1] Gallegos-Infante, J.A., Rocha-Guzman, N.E., GonzalezLaredo, R.F., Ochoa-Martinez, L.A., Corza, N., Bello Perez, L.A., Medina-Torres, L., Peralta-Alvarez, L.E. (2010) Quality of spaghetti pasta containing mexican common bean flour (Phaseolus vulgaris L.). Food Chemistry. 119, 1544-1549.

[2] Cayot, N. (2007) Sensory quality of traditional foods. Food Chemistry. 101, 154-162.

[3] Gökmen, S., Kocabaş, A., Savran, İ., Sayaslan, A., Aydın, M.F., Yetim, H. (2019) Effect of infrared, ultraviolet-C radiations and vacuum drying on certain chemical and microbial characteristics of stuffed pasta (Manti). Journal of Agricultural Sciences. 25(1), 100-107.

[4] Gökmen, S., Aydın, M.F., Kocabaş, A., Sayaslan, A., Yetim, H., Çağlar, A. (2015) A study on quality criteria of commercial stuffed pasta (mantı), as traditional food. International Food Research Journal. 5, 22.

[5] Uzunlu, S., Var, I. (2016) Effect of modified atmosphere packaging on microbiological quality of mantı. Food Science and Technology Research. 22(6), 727-732.

[6] Sitti, S., Hayta, M., Yetim, H. (2009) Kayseri manti: Preparation and quality qualities. Traditional Foods Symposium. 1, Symposium Book, Van. 27-29.

[7] Kocabaş, A., Gökmen, S. (2017) Lipid Peroxidation and Its Antimicrobial Effect in Foods. Science within Food: Up-to-date Advances on Research and Educational Ideas. 164.

[8] Brewer, M.S., Ikıns, W.I.G., Harbers, C.A.A. (1992) TBA values, sensory characteristics, and volatiles in ground pork during long-term frozen storage: effects of packaging. Journal of Food Science. 57(3), 558-563.

[9] Lyon, B.G., Lyon, C.E., Ang, C.Y.W., Young, L.L. (1988) Sensory analysis and thiobarbituric acid values of precooked chicken patties stored up to three days and reheated by two methods. Poultry Science. 67(5), 736-742.

[10] Gökmen, S., Sayaslan, A., Çağlar, A. (2016) Effects of Different Drying Methods of Mantı on Hydroxymethyl Furfural (HMF) Formation and Sensory Quality. Cumhuriyet University Faculty of Science Science Journal (CSJ). 37(3), 176-186.
[11] Yücetepe, A., Güneş, G. (2016) Qualıty Of 'Mantı' (Meat-Filled Pasta Product) As Affected By Modified Atmosphere Packaging Durıng Refrıgerated Storage. Food and Health. 2, 189-198.
[12] Smıth, J.S., Alfawaz, M. (1995) Antioxidative activity of Maillard reaction products in cooked ground beef, sensory and TBA values. Journal of Food Science. 60(2), 234-236.
[13] Ji-Han, K., Hyun-Joo, J., Chi-Ho, L. (2019) Effect of aged garlic powder on physicochemical characteristics, texture profiles, and oxidative stability of ready-to-eat pork patties. Asian-Australasian Journal of Animal Sciences. 32, 1027-1035.
[14] Pikul, J., Leszczynski, P.J., Bechtel, F.A. (1984) Effects of frozen storage and cooking on lipid oxidation in chicken meat. Journal of Food Science. 49, 838-843.
[15] Johnston, M.B., Baldwin, R.E. (1980) Influence of microwave reheating on selected quality factors of roast beef. Journal of Food Science. 45, 1460-1462.
[16] Sitti, S. (2011) Effect of vacuum and modified atmosphere packaging on some of the quality characteristics of Kayseri manti (Doctoral dissertation, Master Thesis, Erciyes University (Unpublished), Turkey.
[17] Aslan, N. (2012) Effects on Quality of Dried Mantı of the Infrared Drying Method, Canakkale Onsekiz Mart University, Faculty of Engineering, Canakkale.

Received: **07.02.2021**
Accepted: **30.04.2021**

CORRESPONDING AUTHOR

Suleyman Gokmen
Department of Food Processing,
Technical Vocational School,
Karamanoglu Mehmetbey University,
Karaman – Turkey

e-mail: sugokmen42@hotmail.com

© by PSP Volume 30– No. 09/2021 pages 10592-10601 Fresenius Environmental Bulletin

SOIL SATURATED HYDRAULIC CONDUCTIVITY AND ITS RESPONSE TO MACROPORE AND ROCK FRAGMENT NETWORK CHARACTERISTICS IN DIFFERENT FOREST COMMUNITIES

Chen Meng[1,2,3], Jianzhi Niu[4,*], Lingtong Du[2], Naiping Song[1]

[1]Breeding Base for State Key Laboratory of Land Degradation and Ecological Restoration in Northwest China, Ningxia University, Yinchuan 750021, China
[2]Key Laboratory for Recovery and Restoration of Degraded Ecosystem in North-Western China of Ministry of Education, Ningxia University, Yinchuan 750021, China
[3]College of ecological environment, Ningxia University, Yinchuan 750021, China
[4]College of Soil and Water Conservation, Beijing Forestry University, Beijing, 100083, China

ABSTRACT

The macropores and rock fragments are the main factors responsible for the soil hydraulic properties. However, the characteristics of the macropores and rock fragments that determine the water flow in forest stone soil remain unclear. Intact soil columns were taken from the forest soil of northern china, and all the intact soil columns were scanned using industrial computed tomography (CT) to quantify the 3-D characteristics of the macropores and rock fragments. The Ksat of three soil layers (0-10 cm, 10-20 cm, 20-30 cm) were determined in all the samples. The results showed that the soil saturated hydraulic conductivity of mixed forest was higher than that of the pure forest; the saturated hydraulic conductivity was significantly correlated with the surface area density, volume density of the rock fragment and mean tortuosity of the macropores in a negative way, but positively correlated with the number density, surface area density, volume density of the macropores. Macropores and rock fragments co-determine the saturated hydraulic conductivity of the soil; volume and surface area of the macropores and rock fragments have the greatest influence on the saturated hydraulic conductivity of the soil which determines the soil water infiltration capacity. The effect of soil macropores on the water infiltration is greater than that of the rock fragments. It is thus justified to account for the influence of rock fragments and soil macropores on the hydraulic conductivity in related research.

KEYWORDS:
Saturated hydraulic conductivity, 3-D characteristics, Industrial CT, water infiltration, soil macropore

INTRODUCTION

Critical roles are played by the macropores, referred to as having pore size ＞0.3 mm and rock fragments, defined as crushed stone particles with particle size > 2 mm [1], on the transport of soil solutes, water, chemicals and pollutants [2-5]. Previous studies have suggested that root, soil bulk density, thickness, mechanical composition, organic matter, water content and porosity are the most important factors which determine the movement of soil water [6-12], however, these studies have neglected the influence of 3-D characteristics of the macropores and rock fragments of the soil on soil hydrological processes.

Traditional methods like dye tracing and fluid models cannot accurately obtain the 3-D characteristic parameters of macropores and rock fragment in the soil [13], and consequently further analysis of the influence of macropores and rock fragments on soil water infiltration function is not possible. Recent development of CT technology in the recent past has given an opportunity for quantification of the 3-D characteristics of the macropores and rock fragments. Various 3-D characteristic parameters of macropores like volume, surface area, number, connectivity, distribution of diameter, tortuosity, angle of the macropores can be obtained via CT scanning and further image processing technology. Simultaneously, the number, volume, diameter distribution, and surface area of the rock fragments can also be obtained from the combination of CT scanning and further image processing [14-17].

Saturated hydraulic conductivity is an important hydraulic parameter for the movement of water and solute which reflects the water infiltration and seepage characteristics. The parameters which strongly influence the saturated hydraulic conductivity are soil texture, bulk density, pore distribution and organic matter content. The saturated hydraulic conductivity having crucial influence on the distribution of soil moisture is an important parameter of

the hydrological model [18]. But till date there is no literature report on the effect of 3-D characteristics of the macropores and rock fragments on the saturated hydraulic conductivity of the soil. The primary objectives of this study were to (1) appraise the connection between the saturated hydraulic conductivity and the characteristics of soil macropores and rock fragments, and (2) analyze the main factors affecting the soil saturated hydraulic conductivity based on the 3-D structural parameters of macropores and rock fragments as obtained by the CT scan.

MATERIALS AND METHODS

Experimental site and soil sampling. The sampling point is located at a forest station near the Miyun Reservoir in Beijing, China. The research area is having a typical semi-humid and semi-dry climate, with annual rainfall of 661 mm and having annual mean temperature of 10 °C. The rock fragments are mainly derived from the Archean granite with the main type of soil being leptosols [19]. The main types of vegetation are artificial forests having 57 years, of age including Platycladusorientalis, Quercus spp., Pinustabulaeformis, Castaneamollissima, Ulmuspumila and Juglansregia, with 40% ~ 60% being the vegetation coverage rate.

We collected 18 soil samples from 2 mixed forests and 4 pure forests. One mixed forest was of Pinus tabulaeformis, Castanea mollissima and Ulmus pumila (P-C-U), while the other mixed forest was of Pinus tabulaeformis and Castanea mollissima (P-C). The pure forests were of Ulmus pumila (U), Castanea mollissima (C), Pinus tabulaeformis (J), and Pinus tabulaeformis (P). All the samples were collected from similar elevations, gradients and slope directions. Table 1 gives the basic information of soil properties and roots in all the sample points. Three intact soil columns (polyvinyl chloride pipe), having 100 mm diameter and 300 mm length, were sampled from each plot as per the details of soil column acquisition process described by Meng et al. [20].

Industrial CT scanning and image analysis. All undisturbed soil columns were scanned by an Industrial CT system (Beijing Granpect Co. Ltd., Beijing, China) having an energy level of 450 kV and 10 mA, with continuous scanning interval of 0.215 mm. After scanning and reorientation, 1024 × 1024 images were produced having a voxel size of 0.137 mm × 0.137 mm × 0.200 mm.

Commercially available software named VGStudio Max 2.2 (Volume Graphics GmbH, Heidelberg, Germany) was used for the image analysis. The region of interest (ROI) tool of VGStudio Max 2.2 was used to select the observation range after removing 5 mm at the edges and 35 mm at both the ends to avoid the impact of any artificial forces. The threshold range of the macropores and rock fragments was chosen as values lower than 75 and values greater than 165, respectively (within the range of 0–255). Threshold of the rock fragments was determined by observing the threshold of a known rock fragment in the soil column, while for the macropores it was determined by observing the threshold of an artificial macro pore [21]. These images were subsequently inspected visually to ensure that these threshold values are reasonable [20]. Next, the characteristics of the macropores (pore diameter ≥ 0.3 mm) and rock fragments (particle size ≥ 2 mm) were calculated using the Particle Analysis tool of VG Studio Max 2.2. The volume, diameter, number, and distribution of the macropores and rock fragments were obtained. The surface area of the macropores and rock fragments was estimated through Analyze Particles tool in ImageJ2x. The methodology for the calculation of angle and mean tortuosity for the macropores has been described by Meng et al. [1]. The calculation process of the characteristic parameters of the macro pore and rock fragments are shown in Figure 1.

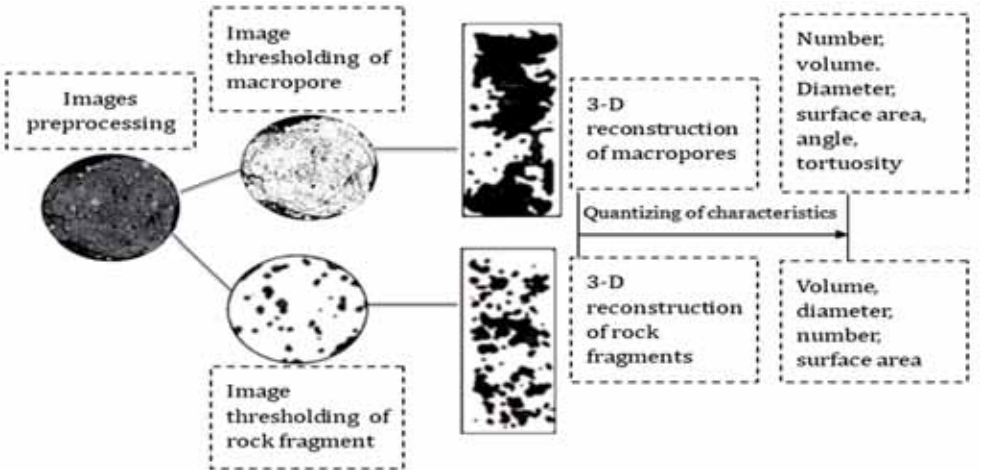


FIGURE 1
Calculation process of characteristic parameters of macropores and rock fragment.

TABLE 1
Soil properties and root length density.

Forest community	Soil depth（cm）	Soil bulk density（g·cm^{-3}）	Sand /2~0.02 mm（%）	Powder particle/0.02~0.002 mm（%）	Clay particle/＜0.002mm（%）	Organic matter（%）	Root length density（cm·cm-3）
P-C-U	0–10	1.58±0.06	65.80	34.20	0.00	5.10±0.40	5.28±0.74
	10–20	1.52±0.04	67.46	32.54	0.00	4.98±0.12	3.80±0.20
	20–30	1.54±0.03	58.06	35.80	0.00	2.11±0.11	3.31±0.22
P-C	0–10	1.62±0.07	64.20	35.80	0.00	4.84±0.33	4.49±0.96
	10–20	1.69±0.05	68.75	31.25	0.00	3.61±0.18	3.12±0.57
	20–30	1.52±0.06	85.52	14.48	0.00	1.35±0.21	2.25±0.64
U	0–10	1.66±0.08	74.71	25.07	0.22	2.58±0.41	2.13±0.98
	10–20	1.41±0.06	66.72	32.88	0.40	2.22±0.39	1.69±0.54
	20–30	1.74±0.14	67.57	32.20	0.23	0.98±0.14	1.58±0.40
C	0–10	1.56±0.16	88.85	11.15	0.00	1.60±0.34	2.60±0.34
	10–20	1.60±0.08	93.98	6.02	0.00	1.11±0.12	1.55±0.57
	20–30	1.47±0.17	91.18	8.82	0.00	0.78±0.20	1.11±0.13
J	0–10	1.55±0.06	85.58	14.42	0.00	3.41±0.12	2.35±0.55
	10–20	1.64±0.15	91.17	8.83	0.00	2.20±0.19	1.25±0.23
	20–30	1.66±0.16	89.56	10.44	0.00	1.74±0.31	1.07±0.09
P	0–10	1.49±0.04	50.51	49.49	0.00	1.88±0.04	2.48±0.29
	10–20	1.69±0.10	65.82	34.18	0.00	1.50±0.27	1.12±0.15
	20–30	1.76±0.12	50.39	49.30	0.31	1.53±0.07	0.81±0.28

Calculation of soil saturated hydraulic conductivity. In each sample point, a steel cylinder with a volume of 200 mm3 was divided into three layers (0~10 cm, 10~20 cm, 20~30 cm), with 3 repetitions on each layer. The steel cylinder was saturated by setting in the water for 12 hours. Then an infiltration experiment was carried out for all the steel cylinders using 2 cm fixed water pressure and the flow rate was recorded every minute. Darcy's law was used to calculate the saturated hydraulic conductivity of each ring cutter soil (Formula 1). In order to compare and analyze the saturated hydraulic conductivity of the soil columns measured at different temperature conditions, the saturated conductivity, Ks, was converted to the saturated hydraulic conductivity K10 at 10 ℃ (Formula 2).

$$K_s = \frac{Q \times L}{S \times t \times h} \quad \text{Formula 1}$$

Here, KS is the saturated hydraulic conductivity (cm/s), Q is the amount of water permeating through the unit cross section (ml), L is the thickness of saturated soil layer (cm), S is the cross-sectional area of the permeable steel cylinder (cm2), t is the time required for water permeation (s), and h is the water pressure height (cm).

$$K_{10} = \frac{K_s}{0.7 + 0.03K_s^\circ} \quad \text{Formula 2}$$

Here, K10 is the soil saturated hydraulic conductivity (mm/min) at 10 ℃, KS is the saturated hydraulic conductivity (mm/min) measured at the current temperature, and KS° is the water temperature (℃) measured at the current saturated hydraulic conductivity.

Statistical analyses. All the statistical analyses were performed using SPSS 22.0 and origin 9.0 softwares.

RESULTS

Saturated hydraulic conductivity of soil in different forest communities. The saturated hydraulic conductivity of soil in 0~10 cm soil layer was the highest for P-C-U (Figure 2), which was 90%, 92%, 218%, 343% and 337% higher than that of P-C, U, C, J and P, respectively. In the soil layer of 10 ~ 20cm, the saturated hydraulic conductivity of the soil of P-C-U was 111%, 56%, 179%, 160% and 191% higher than that of P-C, U, C, J and P., respectively. In general, the saturated hydraulic conductivity of surface soil of mixed forest was higher than that of the pure forest, but with deepening of the soil layer, difference between the saturated hydraulic conductivity between the mixed forest and pure forest decreased. In addition, with the deepening of soil, the saturated hydraulic conductivity of soil decreased, which was more significant in the mixed forest soil.

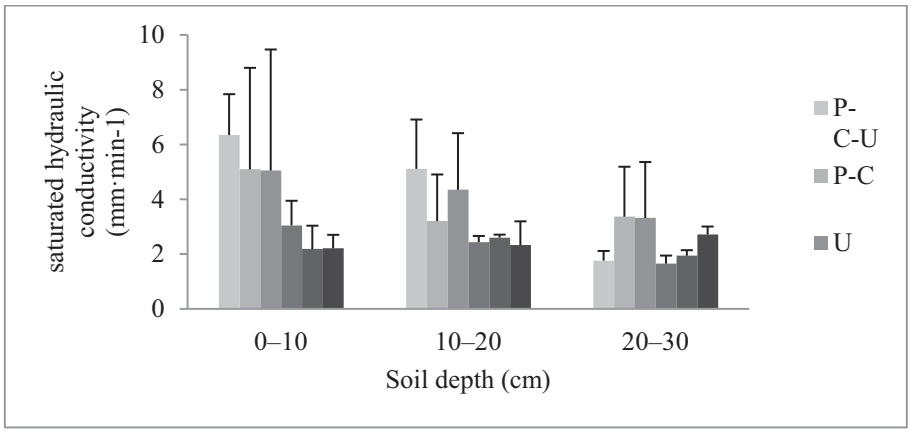


FIGURE 2
Saturated hydraulic conductivity in 3 soil layers in different forest communities

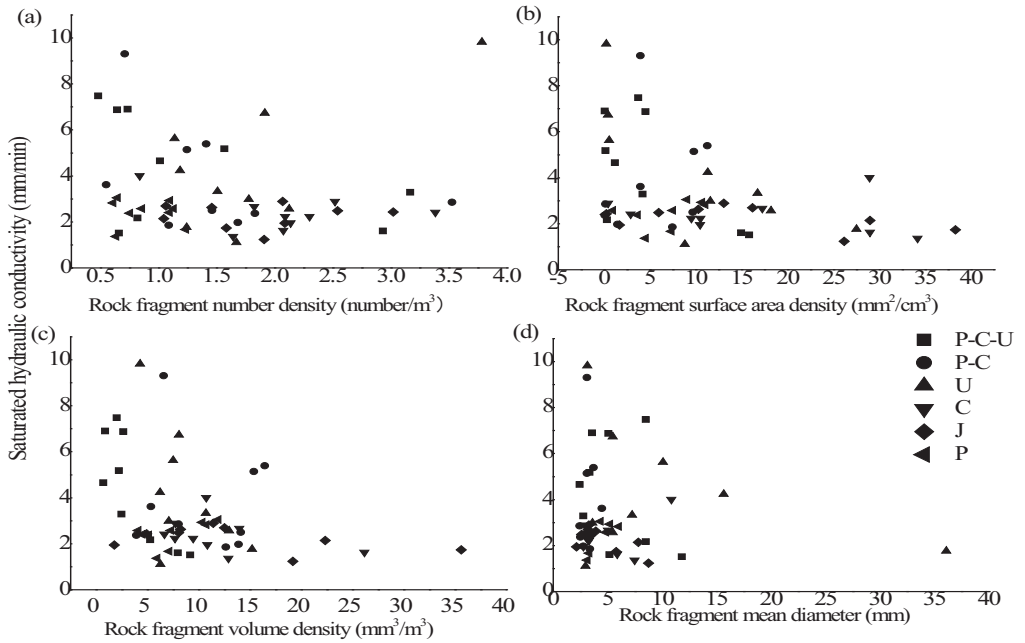


FIGURE 3
The relationship between characteristics of rock fragments and saturated hydraulic conductivity.

Selection of the characteristic factors of the rock fragments affecting saturated hydraulic conductivity. In this section, the relationship between the rock fragments characteristics and the saturated hydraulic conductivity was analyzed to understand which rock fragment characteristic factors affect the saturated hydraulic conductivity. From Figure 3(a), it was found that there was no significant correlation between the density of rock fragments and the saturated hydraulic conductivity of the soil. Figure 3(b) and Table4 indicates a negative correlation between the soil rock fragment surface area density and the saturated hydraulic conductivity of the soil. Figure 3(c) and Pearson correlation analysis (Table 2) found a negative correlation between the volume density of rock fragment with the saturated hydraulic conductivity of the soil. Figure 3(d) in combination with Table 2 show that the average diameter of the rock fragment does not show a significant correlation with the saturated hydraulic conductivity of soil.

Therefore, we believe that the number and the average diameter of rock fragment in the soil is not an important factor affecting the saturated hydraulic conductivity, but the surface area density and volume of the rock fragment are major influencing factors for the saturated hydraulic conductivity of the soil, with higher the volume content and surface area of rock fragment, lower being the saturated hydraulic conductivity of the soil.

Selection of the characteristic factors of the macropores affecting saturated hydraulic conductivity. This section compares the relationship between the macropores characteristics and saturated hydraulic conductivity of the soil, and understands the characteristic factors of the macropores that affect the saturated hydraulic conductivity of the soil.

TABLE 2
Correlation analysis of soil saturated hydraulic conductivity and characteristics of rock fragment in different soil layers.

	Soil layer	Number density of rock fragment	Surface area density of rock fragment	Volume density of rock fragment	Mean diameter of rock fragment
Soil saturated hydraulic conductivity	0-10cm	- 0.054(0832)	- 0.310(0.210)	- 0.444(0.065)	0.031(0.903)
	10-20cm	- 0.159(0.529)	- 0.262(0.294)	- 0.246(0.324)	0.416(0.086)
	20-30cm	- 0.121(0.633)	- 0.439(0.068)	- 0.149(0.554)	- 0.118(0.641)
	0-30cm	- 0.087(0.531)	- 0.372(0.006**)	- 0.342(0.11**)	- 0.069(0.620)

TABLE 3
Correlation analysis of soil saturated hydraulic conductivity and characteristics of macropores in different soil layers.

	soil layer	number density of macropores	surface area density of macropores	volume density of macropores	mean tortuosity of macropores	mean angle of macropores	mean diameter of macropores
saturated hydraulic conductivity	0-10cm	0.357(0.146)	0.699(0.001**)	0.726(0.001**)	- 0.370(0.131)	0.289(0.245)	0.336(0.173)
	10-20cm	0.332(0.178)	0.538(0.021*)	0.627(0.005**)	- 0.233(0.353)	0.419(0.083)	0.215(0.392)
	20-30cm	0.097(0.701)	0.521(0.027*)	0.517(0.028*)	- 0.086(0.734)	- 0.109(0.668)	0.115(0.649)
	0-30cm	0.404(0.002**)	0.642(0.000**)	0.663(0.000**)	- 0.313(0.021*)	0.234(0.089)	0.201(0.144)

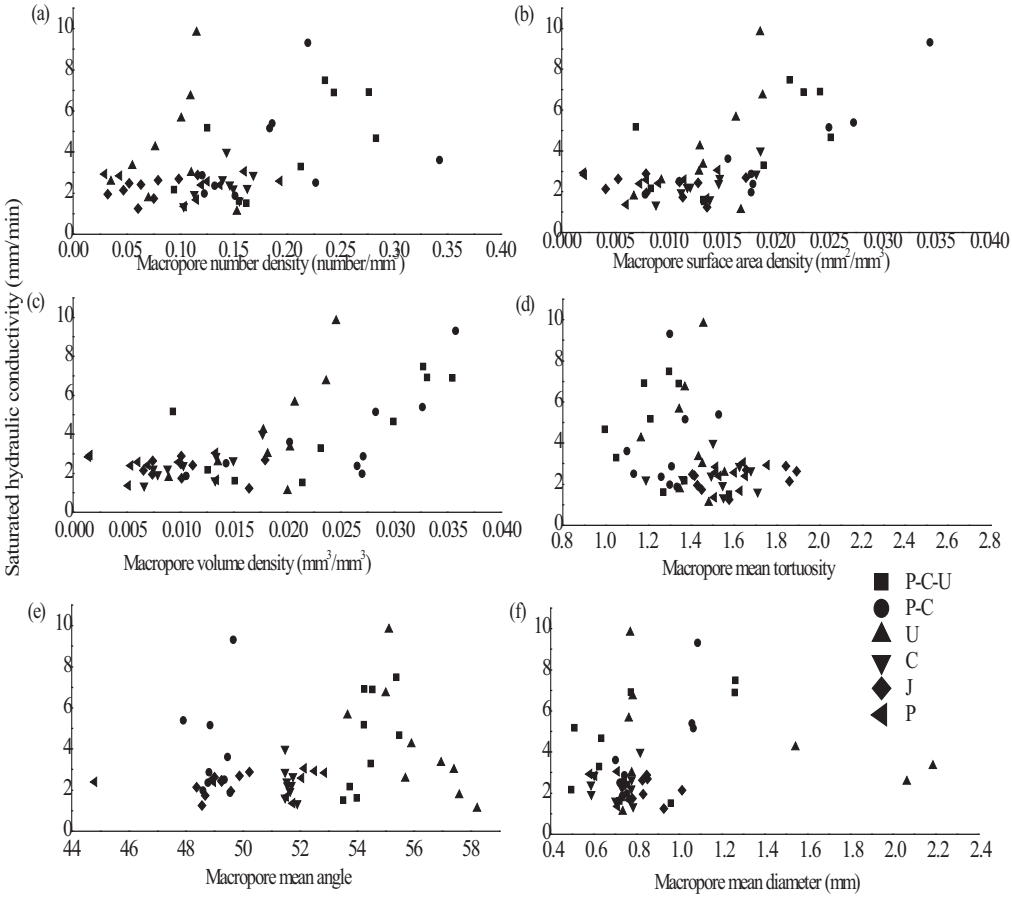


FIGURE 4
The relationship between characteristics of macropores and saturated hydraulic conductivity.

The results from Figure 4 (a) and the correlation analysis (Table 3) showed significant positive correlation between the number density of the macropores and the saturated hydraulic conductivity. It can be seen from Figure 4(b) and Table 3 that there is a positive relationship in all the soil layers between the surface area of the macropores and saturated hydraulic conductivity. From Figure 4(c) and Table 3,

it can be seen that larger the volume density of the macropores, larger is the saturated hydraulic conductivity of the soil and thus indicating a positive correlation between the volume of macropores and saturated hydraulic conductivity in all the soil layers which also showed that the correlation of 0-10cm soil was the strongest (Table 3). From Figure 4(d) and Table 3, we found that with increasing average tortuosity of the macropores, the saturated hydraulic conductivity of the soil tends to decrease, which is in confirmation with the previous research results [22]. It is believed that vertical macropores of the soil are more favorable for the rapid movement of soil moisture. From Figure 4 (e) and Figure 4 (f), it can be found out that neither the average inclination angle of macropores nor the average diameter of macropores has a significant correlation with the saturated hydraulic conductivity of the soil, which signifies that angle and diameter are not the main influencing factors of the saturated hydraulic conductivity of the soil.

Based on the comprehensive analysis, number, surface area, volume and tortuosity of the macropores were found to be the influencing factors for the saturated hydraulic conductivity of the soil.

Response of saturated hydraulic conductivity to 3-D characteristics of macropores and rock fragments. From the correlation between the saturated hydraulic conductivity of the soil and 3-D characteristics of the macropores and rock fragments, it was found that the saturated hydraulic conductivity was affected by the surface area density and volume density of the rock fragments while for the macropores, the number density, volume density, surface area density, average tortuosity were the influencing factors. We selected these parameters to further carry out multiple regression analysis on the saturated hydraulic conductivity of the soil.

It can be seen that the determination coefficients of the regression equation are lower for the relation between the saturated hydraulic conductivity of soil and the combined effect of the volume density of the rock fragments and average tortuosity of the macropores as well as the combined effect of the surface area density of the rock fragments and average tortuosity of the macropores (Figure 5). Higher determination coefficients (0.462-0.483) were observed for the regression equation of the saturated hydraulic conductivity of the soil and the combined effects of surface area density of the rock fragments and surface area density of the macropores/ volume density of the rock fragments and surface area density of the macropores / rock fragment volume density of the rock fragments and volume density of the macropores.

The regression equation determining coefficient of the three-factor combination is greater than that of the two-factor combination (Table 4). The regression equation determining coefficient for saturated hydraulic conductivity of the soil against surface area density of the rock fragment + surface area density of the macropores + volume density of macropores (0.490) is lower than that of volume density of the rock fragment + surface area density of the macropores + volume density of the macropores. It can be seen that the volume and surface area of the macropores along with the volume and surface area of the rock fragments are the most important parameters that determine the soil saturated hydraulic conductivity of the soil, among which parameters of the macropores have greater influence than the parameters of the rock fragments. Volume and surface area of the macropores have positive influence on the saturated hydraulic conductivity of the soil, whereas, the volume and surface area of the rock fragments have negative influence. Thus, the volume and surface area of the macropores together with the volume and surface area of the rock fragments determine the soil water infiltration capacity, which is found to be similar to that of the earlier reports [23].

DISCUSSION

The relationship between saturated hydraulic conductivity and the characteristics of macropores and rock fragment in six forest lands was studied and analyzed. It was found that the saturated hydraulic conductivity of the soil was influenced by many characteristic parameters of the macropores and rock fragments; among them the rock fragments hinder the infiltration of water flow. Rock fragment will also have a positive effect on the tortuosity of macropores [20]. Therefore, rock fragments not only affect the water infiltration directly, but also have indirect affect by influencing the generation of macropores [24-25]. In addition, it was also shown that the surface area density of the rock fragments is the most important factor affecting the saturated hydraulic conductivity of the soil (Table 3).

Soil macropores is an important path for the soil water infiltration. The previous method can only quantify various 3-D characteristics of the macropores but cannot quantitatively analyze the influence of 3-D structural characteristics of the macropores on the soil water infiltration performance. Judging from our research results, volume density and surface area density are the most important characteristics of the macropores, affecting the saturated hydraulic conductivity of the soil. The number density and vertical degree of macropores will also have an impact on the soil water infiltration, which is consistent with the previous research results [26-27]. The larger the average tortuosity of macroporess, more curved the macropores are. Being the main channel of water infiltration, more curved the macropores are, more curved the water transport route is, thus retarding and slowing down

the rapid infiltration of water.

Some researchers have found that when the content of rock fragments was more than 40%, the rock fragments have a positive effect on the saturated hydraulic conductivity of the soil which was contrary to the conclusion of this study [28]. As the sampling points of this study were close, the difference of rock fragment was small; it is necessary to analyze the samples with different rock contents in the future in order to compare the effect of rock fragments on the soil water infiltration more comprehensively.

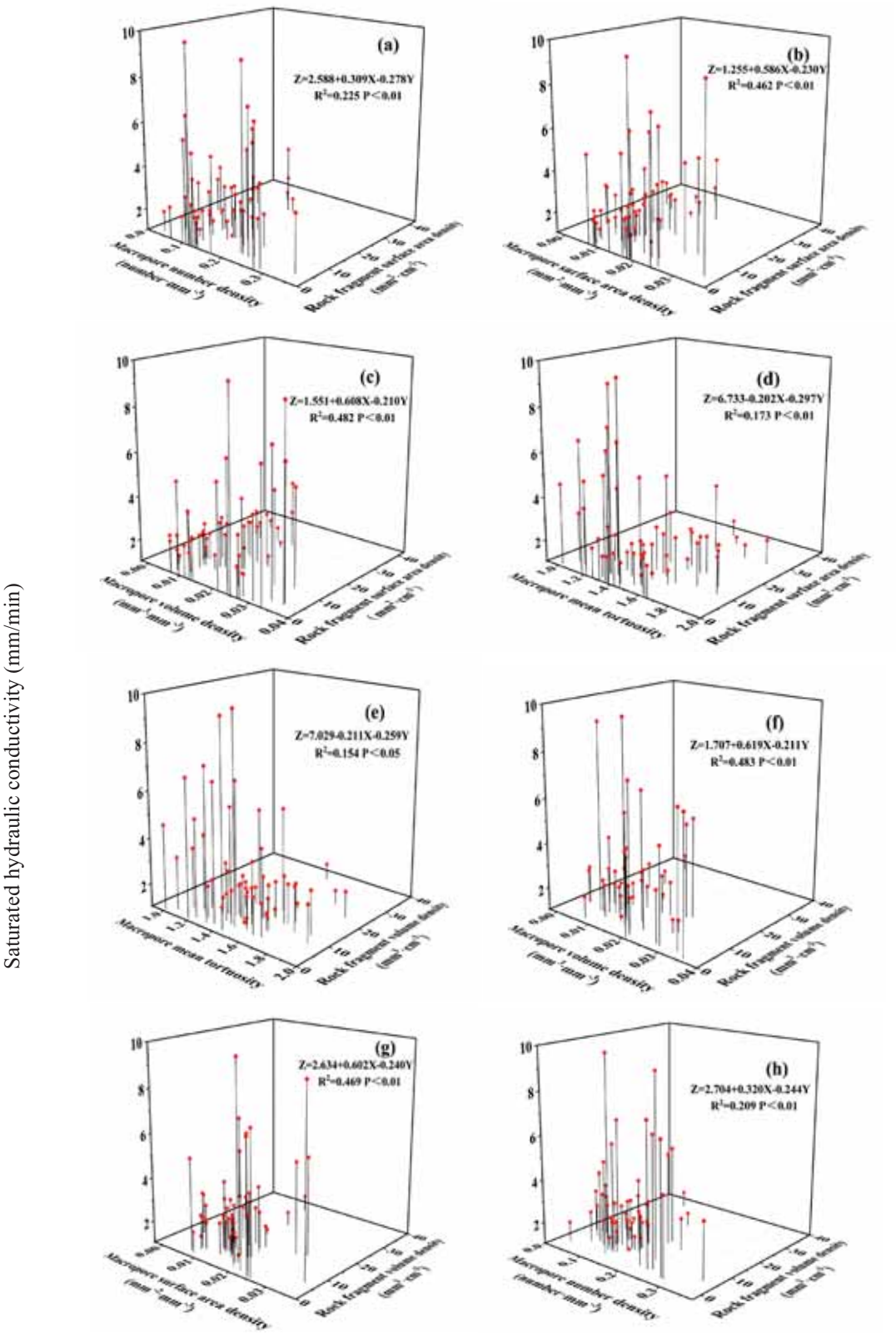


FIGURE 5

Effect of integrated structure of rock fragments and macropores on soil saturated hydraulic conductivity.

TABLE 4
Relationship between macroproe parameters, rock fragment parameters and saturated hydraulic conductivity.

regression equation	Coefficient of determination
Y=-0.21surface area density of rock fragment+0.405volume density of macropores+0.224surface area density of macropores	0.490**
Y=-0.217volume density of rock fragment+0.388volume density of macropores+0.253surface area density of macropores	0.494**

Note: Y represents soil saturated hydraulic conductivity, ** represents $p < 0.01$. * represents $p < 0.05$.

Because there were fewer samples in this study, and the saturated hydraulic conductivity of the soil is affected by many factors besides the macropores and rock fragments (such as root system, initial water content, etc.), and so the correlation between the characteristics of the macropores and rock fragments with the saturated hydraulic conductivity was not high. In future research, we need to find a better way to control the variables and increase the number of samples under the condition of cost control, so as to explore the impact of 3-D characteristics of the macropores and rock fragments on saturated hydraulic conductivity more accurately.

CONCLUSIONS

Rock fragments will have a direct impact on the soil water infiltration by reducing the effective flow section of soil, and also affect the hydrological function of the soil indirectly by affecting the formation of macropores. The surface area of macropores has a positive effect on the water infiltration by increasing the effective flow section for the soil water infiltration. The larger the number and volume of the macropores, the more the water infiltration channel in the soil, which is beneficial to the infiltration of soil water. Tortuous macropores slows down and blocks the movement of water, and thus has a negative effect on the saturated hydraulic conductivity of the soil. Macropores and rock fragments determine the infiltration capacity of the soil water. It is reasonable to consider the influence of rock fragments and soil macropores on the hydraulic conductivity, especially the volume and surface area of the macropores and rock fragments.

ACKNOWLEDGEMENTS

Funding: The research reported in this manuscript is funded by the Natural Science Foundation of China Ningxia Hui Autonomous Region (2021AAC05005), the Key R&D Program of Ningxia Hui Autonomous Region (2019BFG02010).

REFERENCES

[1] Meng, C., Niu, J., Li, X., Luo, Z., Du, X., Du, J. and Yu, X. (2017): Quantifying soil macropore networks in different forest communities using industrial computed tomography in a mountainous area of North China. Journal of Soils and Sediments. 17, 2357-2370.

[2] Katuwal, S., Norgaard, T., Moldrup, P., Lamandé, M., Wildenschild, D. and DeJonge, L.W. (2015): Linking air and water transport in intact soils to macropores characteristics inferred from X-ray computed tomography. Geoderma. 237, 9-20.

[3] Jarvis, N.J. (2007): A review of non–equilibrium water flow and solute transport in soil macropores: Principles, controlling factors and consequences for water quality. European Journal of Soil Science. 58, 523-546.

[4] Lamandé, M. and Schjønning, P. (2011): Transmission of vertical stress in a real soil profile. Part II: Effect of tyre size, inflation pressure and wheel load. Soil and Tillage Research. 114, 71-77.

[5] Wang, W.H., Wang, Q., Zhang, X.D. and Zhao, W.D. (2020): Analysis of water and salt migration characteristics of carbonate-saline soil in western jilin province. Fresen. Environ. Bull. 11(29), 9601-9613.

[6] Liang, X.H., Zhang, K.B., Wu, B. and Jia, X.H. (2020): Soil moisture dynamic of artemisia ordosica community and its relationship with plant roots at different succession stages in mu us sandy land. Fresen. Environ. Bull. 7(29), 5079-5091.

[7] Liu, B.B., Tang, C.Q., Zhang, Y.Q., Li, R.X., Tan, Y.H., Yu, G.M. and Lei, X.H. (2020) Investigation of pore throat structure and fractal characteristic of tight sandstone of chang 8 reservoir in jiyuan area, ordos basin. Fresen. Environ. Bull. 12A(28), 9865-9876.

[8] Hallett, P.D., Feeney, D.S., Bengough, A.G., Rillig, M.C., Scrimgeour, C.M. and Young, I.M. (2009): Disentangling the impact of AM fungi versus roots on soil structure and water transport. Plant Soil. 314, 183-196.

[9] Reading, L., Baumgartl, T., Bristow, K. and Lockington, D. (2012) Hydraulic conductivity increases in a sodic clay soil in response to gypsum applications: Impacts of bulk density and cation exchange. Soil Science. 177, 165-171.
[10] Sanders, E., AbouNajm, M., Mohtar, R., Kladivko, E. and Schulze, D. (2012) Field method for separating the contribution of surface-connected preferential flow pathways from flow through the soil matrix. Water Resource Research. 48, 4534-4542.
[11] Dastidar, M., Jouannet, V. and Maizel, A. (2012) Root branching: mechanisms, robustness, and plasticity. Wiley Interdisciplinary Reviews-Developmental Biology. 1, 329-343.
[12] Jomaa, S., Barry, D., Brovelli, A., Heng, B., Sander, G., Parlange, J. and Rose, C. (2011) Rain splash soil erosion estimation in the presence of rock fragments. Catena. 92, 38-48.
[13] Qiu, L., Chen, X. and Pan, J. (2013) In situ measurement of soil macropores by dye tracing and image analysis. Agro-Geoinformatics Second International Conference on IEEE. 13-17.
[14] Muñoz-Ortega, F.J., Martínez, F.S. and Monreal, F.C. (2015) Volume, Surface, Connectivity and Size Distribution of Soil Pore Space in CT Images: Comparison of Samples at Different Depths from Nearby Natural and Tillage Areas. Pure and Applied Geophysics. 172, 167-179.
[15] Timms, W., Acworth, R., Crane, R., Arns, C., Arns, J., McGeeney, D. and Cuthbert, M. (2018) The Influence of Syn-Depositional Macropores on the Hydraulic Integrity of Thick Alluvial Clay Aquitards. Water Resources Research. 54, 3122-3138.
[16] Soto-Gómez, D., Pérez-Rodríguez, P., Vázquez-Juiz, L., López-Periago, J. and Paradelo, M. (2018) Linking pore network characteristics extracted from CT images to the transport of solute and colloid tracers in soils under different tillage managements. Soil and Tillage Research. 177, 145-154.
[17] Hu, X., Lyu, Y., Liu, Y., Li, X., Sun, Z., Li, Z. and Liu, L. (2018) Exclosure on CT-measured soil macropores characteristics in the Inner Mongolia grassland of northern China. Journal of Soils and Sediments. 18, 718-726.
[18] Govindaraju, R., Corradini, C. and Morbidelli, R. (2006) A semi-analytical model of expected areal-average infiltrationunder spatial heterogeneity of rainfall and soil saturated hydraulic conductivity. Journal of Hydrology. 316, 184-194.
[19] Fao, I. and Isric, I. (2009) JRC: Harmonized World Soil Database (version 1.1). FAO, Rome, Italy and IIASA, Laxenburg, Austria.
[20] Meng, C., Niu, J., Yin, Z., Luo, Z., Lin, X. and Jia, J. (2018) Characteristics of rock fragments in different forest stony soil and its relationship with macropore characteristics in mountain area, northern China. Journal of Mountain Science. 15, 519-531.
[21] Hu, X., Li, Z., Li, X. and Liu, Y. (2015) Influence of shrub encroachment on CT-measured soil macropore characteristics in the Inner Mongolia grassland of northern China. Soil and Tillage Research. 150, 1-9.
[22] Luo, L., Lin, H. and Schmidt, J. (2010) Quantitative relationships between soil macropore characteristics and preferential flow and transport. Soil Science Society of America Journal. 74, 1929-1937.
[23] Hlaváčiková, H., Novák, V., Kostka, Z., Danko, M. and Hlavčo, J. (2018): The influence of stony soil properties on water dynamics modeled by the HYDRUS model. Journal of Hydrology and Hydromechanics. 66, 181-188.
[24] Shi, Z., Xu, L., Wang, Y., Yang, X., Jia, Z., Guo, H. and Yu, P. (2012) Effect of rock fragments on macropores and water effluent in a forest soil in the stony mountains of the Loess Plateau, China. African Journal of Biotechnology. 11, 9350-9361.
[25] Zhang, Y., Zhang, M., Niu, J., Li, H., Xiao, R., Zheng, H. and Bech, J. (2016): Rock fragments and soil hydrological processes: significance and progress. Catena. 147, 153-166.
[26] Saravanathiiban, D., Kutay, M. and Khire, M. (2014) Effect of macropores tortuosity and morphology on preferential flow through saturated soil: a lattice Boltzmann study. Computers and Geotechnics. 59, 44-53.
[27] Müller, K., Katuwal, S., Young, I., McLeod, M., Moldrup, P., DeJonge, L. and Clothier, B. (2018) Characterising and linking X-ray CT derived macroporosity parameters to infiltration in soils with contrasting structures. Geoderma. 313, 82-91.
[28] Zhou, B.B., Shao, M.A. and Shao, H.B. (2009): Effects of rock fragments on water movement and solute transport in a Loess Plateau soil. Comptes Rendus Geoscience. 341, 462-472.

Received: **08.02.2021**
Accepted: **27.03.2021**

CORRESPONDING AUTHOR

Jianzhi Niu
College of Soil and Water Conservation,
Beijing Forestry University,
Beijing 100083 – China

e-mail: niujianzhi@126.com

© by PSP Volume 30– No. 09/2021 pages 10602-10609 Fresenius Environmental Bulletin

FRACTURING EFFECT OF COALBED METHANE RESERVOIRS IN BLOCK A IN THE SOUTHERN QINSHUI BASIN CHINA

Chao Cao, Haibin Gao*, Peng Kong, Qi Yang, Ruicheng Wang, Jian Li, Zhenguo Liu, Bingnan Wang, Cheng Jiang, Minghao Wang

China United Coalbed Methane Corporation Ltd., Changzhi, Shanxi, 046600, China

ABSTRACT

The in-situ permeability of coal reservoirs is low, and hydraulic fracturing technology is generally used to create artificial fractures. However, coal reservoirs have strong heterogeneity, so the quantitative evaluation of fracturing effect is a technical problem that has not been effectively solved for a long time. In this paper, based on coalbed methane development data, fracturing data, and microseismic monitoring results, the effect of hydraulic fracturing of coal reservoirs and the factors affecting productivity were systematically studied. The research results show that the coal reservoir closure stress in the study area is distributed between 11.99-36.85 MPa, the reservoir permeability is distributed between 0.06-0.15 mD, and the coal seam has a high sand-carrying efficiency, so the fracture-forming ability is better. The microseismic monitoring results showed that the scale of cracks after stress interference increased significantly, and network cracks formed. Hydraulically affected fractures are mostly double-wing fractures, and the effect of fracture extension is ideal, which is beneficial to the production of coalbed methane. The study also found that the fluid level changes frequently during the drainage cycle. In addition, wells with a wide range of falling liquid velocity have generally low gas production. There is a certain negative correlation between the number of shutdowns and gas production. The more shutdowns, the greater the impact on gas production. The drainage and production phases of CBM wells are divided into six parts: test pumping stage, balanced water production stage, pressure holding stage, production increase stage, stable production stage, and decay stage. This research has important reference value for guiding the efficient development of coalbed methane.

KEYWORDS:
Qinshui Basin, coalbed methane, fracturing, productivity, heterogeneity

INTRODUCTION

The in-situ permeability of coal reservoirs is generally low, and hydraulic fracturing technology is usually used to create artificial fractures to improve the seepage capacity of coal reservoirs and increase the drainage area [1-4]. Compared with conventional sandstone reservoirs, coal reservoirs have the characteristics of low strength, strong heterogeneity, and well developed fracture systems, which make the hydraulic fracturing system of coal reservoirs much more complex [5-9]. For coal reservoirs with strong heterogeneity, quantitative evaluation of fracturing effect is a technical problem that has not been effectively solved for a long time [10-14].

The Qinshui Basin is currently the only large-scale basin in China that has been developed on a commercial scale. However, most coalbed methane wells have daily gas production below 1 000 m3/d. According to the rules of gas well drainage and production, the reason why CBM production is difficult to increase is closely related to the effect of CBM well reservoir fracturing [15-18]. In order to improve the effect of hydraulic fracturing in coal reservoirs, the previous have done a lot of work [19-22]. For example, the conductivity of vertical fracturing fractures in coal reservoirs has been systematically evaluated by the previous [21-24]. Some studies have discussed the main control factors for fracturing failure and analyzed the possible reservoir damage during the fracturing process. In addition, methods such as probability statistics, linear regression, numerical calculation, and fuzzy mathematics are also used to optimize fracturing construction parameters, and then the optimal scheme for proppant and fracturing fluid can be established [22-25]. However, for strong heterogeneous coalbed methane reservoirs, there are few reports in the existing references on the optimization of fracturing construction parameters and the fracturing effect.

In this paper, based on coalbed methane development data, fracturing data, and microseismic monitoring results, the effect of hydraulic fracturing of coal reservoirs and the factors affecting productivity were systematically studied. This research has im-

portant reference value for guiding the efficient development of coalbed methane.

MATERIALS AND METHODS

Geological background. The study area is located in Block A in the southern Qinshui Basin of China. According to the two-dimensional seismic data in this area, a series of NNE and SN trending faults have developed in the study area, and the structural strike is NNE trending. The tectonic units of the study area are divided into the eastern gentle slope zone, the central fold belt and the western gentle slope zone from east to west. The eastern gentle slope zone is located in the eastern part of the study area, where the faults are not developed, and the stratigraphic occurrence is gentle; there are many anticlines and synclines developed in the central fold belt, and the faults are complex; the stratum of the western gentle slope zone is buried deep and the faults are not developed.

The main exposed strata in the study area are the Lower Triassic Liujiagou Formation (T1l), Heshanggou Formation (T1h), and Quaternary (Q). The strata are typical coal-bearing strata of the Carboniferous-Permian in North China. The main strata from old to new are: Lower Paleozoic Ordovician Middle Fengfeng Formation (O2f), Upper Paleozoic Carboniferous Middle Benxi Formation (C2b), Upper Taiyuan Formation (C3t), Lower Permian Shanxi Formation (P1s) and Lower Shihezi Formation (P1x), Upper Shihezi Formation (P2s), Shiqianfeng Formation (P2sh), Mesozoic Triassic Lower Liujiagou Formation (T1l), Heshanggou Formation (T1h) and the Quaternary (Q). The study area lacks the Cenozoic Tertiary (N), and some areas lack the Lower Triassic Liujiagou Formation (T1l) and Heshanggou Formation (T1h). The target coal seam studied is 3# coal seam, with a depth ranging from 850 m to 950 m and a thickness of about 6 m. The 3# coal seam in the well area is about 30 m away from the K8 mark layer and 15m from the K7 mark layer below. The formation dip is usually less than 5°.

Methodology. (1) Drilling construction. According to the actual drilling situation combined with software simulation, it is concluded that when the drilling pressure of the PDC bit is 10-60 KN and the rotation speed is 35-80RPM, the actual drilling tool assembly will not buckle at the bottom of the well, which meets the construction requirements. The displacement of 20 L/s can meet the wellbore cleaning requirements. The overall condition of the on-site mud pump is relatively dilapidated, and its displacement cannot continue to increase, so the increase in ROP will be affected to a certain extent.

Based on the above results, combined with the coal seam collapse mechanism and field investigation on the well site, low-solid polymer drilling fluid was selected as the drilling fluid system for the drilling operation in this paper.

The construction trajectory refers to the actual axis shape of a well drilled. By tracking the wellbore trajectory during on-site construction, anomalies can be found early, and drilling construction parameters can be adjusted in advance to ensure that the wellbore trajectory meets the design requirements. The wellbore trajectory shape mainly includes the deviation line and the azimuth line. The characteristics of the deviation of S well group are shown in Figure 1.

Fracturing construction. There are 22 coalbed methane wells in the study area, and 21 fracturing wells have been completed, including 7 simultaneous fracturing (which adopts 2+2+3 mode). The specific fracturing parameters of 21 wells are shown in Table 1. Among them, the S well and T well were constructed twice to meet the design requirements.

In view of the low price of active water and the successful experience of fracturing wells in the block, all 21 wells use active water fracturing fluid (formulation: clear water + 2.0% KCL).

The closure pressure of the coal seam in the study area is about 20 MPa, and natural quartz sand is sufficient to support artificial fractures. Moreover, natural quartz sand is rich in resources and low in price, so it is reasonable to use natural quartz sand as a proppant. The proppant particle size is 16-20 mesh and 20-40 mesh.

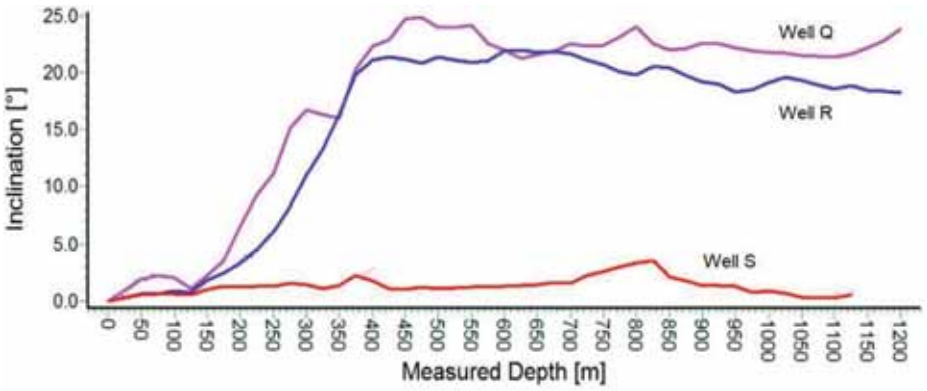


FIGURE 1
Deviation of S Well Group.

TABLE 1
Statistical results of construction parameters of fracturing wells in the study area.

Well name	Prefluid volume (m^3)	Sand-carrying fluid volume (m^3)	Displacement fluid volume (m^3)	Net liquid volume (m^3)	Sand volume (m^3)	Average sand ratio (%)	Fracture pressure (MPa)	Pressure drop (MPa)	Flowback (m^3)
A	192.60	279.10	10.80	461.33	35.29	13.00	22.89	13.4↓7.8	36.0
B	184.90	463.80	11.20	638.08	36.37	7.89	27.00	15.6↓4.7	36.0
C	199.20	248.50	11.80	441.34	30.26	12.37	35.20	21.4↓14.9	33.0
D	205.80	386.50	11.50	576.20	46.00	12.39	22.00	14.4↓10.6	94.5
E	252.46	346.16	11.48	583.27	45.82	13.89	21.59	9.25↓8.41	56.5
F	244.60	654.50	11.80	885.82	45.13	5.09	25.90	22.7↓13.1	44.7
G	226.80	360.90	12.40	573.25	45.25	13.02	35.35	18.1↓12.32	44.0
H	122.30	266.40	14.30	383.60	32.33	13.08	Not obvious	14.8↓11.1	/
I	221.10	379.20	11.90	600.18	50.20	13.23	15.80	5.5↓4.7	26.0
J	212.40	382.30	12.10	579.63	45.28	12.38	Not obvious	18.1↓10.7	23.5
K	249.80	384.20	11.10	622.1	32.09	8.56	32.90	19.6↓13.2	/
L	196.90	352.10	12.20	533.97	45.39	13.50	25.10	16.5↓9.4	39.0
M	201.60	347.10	12.40	533.98	45.20	13.68	26.50	15.0↓10.2	154
N	192.90	367.50	12.20	545.47	45.21	13.09	35.40	19.3↓14.50	98.5
O	204.90	381.70	13.50	572.54	45.93	12.54	19.00	12.6↓9.2	105.7
P	199.70	306.10	11.30	492.94	40.26	13.74	28.90	23.8↓13.9	101
Q	181.07	334.66	13.77	502.23	45.45	14.22	Not obvious	9.0↓7.3	65.0
R	197.60	369.30	12.96	552.92	45.22	12.73	33.91	14.02↓9.60	47.0
S	454.60	161.10	/	613.92	10.13	5.84	/	/	28.5
	110.60	352.40	11.80	456.81	29.99	8.79	35.50	17.3-9.8	
T	214.40	226.30	13.70	449.20	8.68	3.76	39.60	35.4↓15.4	115.0
	152.30	432.40	13.20	574.47	39.05	9.44	41.70	11.0↓9.2	

Part of the 3# coal seam contains gangue, and the lower part of the coal seam is mainly pulverized coal. The perforation section is selected from the coal seam above the gangue, and it should avoid the 0.5 m interval from the top of the coal seam. If the average borehole expansion rate is ≥30%, the 1 m bomb is selected, and the average borehole expansion rate is less than 30%, then 127 m bombs is selected. The hole density is 16 holes/m, and the phase angle is 60°.

RESULTS

G function analysis. G-function fracturing analysis was performed on one well from each of the six well groups, and the fitting results are shown in Table 2. Software analysis shows that the cracks in the east are higher than in the west, and the heterogeneity of coal seams in the east is higher than in the west. The closure stress of coal reservoirs ranges from 11.99 to 36.85 MPa. The closure stress in the eastern region is low, and the closure time is longer than that in the west. The permeability of coal reservoirs is distributed in the range of 0.06-0.15 mD, and the permeability of eastern coal is lower than that of western coal. The coal reservoir has a higher overall sand-carrying efficiency and a better effect of making fractures.

Fracturing parameters. After the fracturing construction curve is fitted, the fracture simulation results of 6 wells are obtained (Figure 2). The fracture parameters are shown in Table 3. The fracture parameters after fitting show that the fractures in the east of the study area are more developed than the west, and the length of the supporting fractures in the east is shorter than that in the west. The ground closing pressure of the formation after fracturing is 9-18 MPa, and the surface tension of the fracturing fluid is very large, so the flowback pressure of the integrated project is set at 8 MPa.

Microseismic detection. At present, a total of 7 wells have completed hydraulic fracturing ("3+2+2" mode) out of 22 wells in the study area. The fracture monitoring parameters of 7 wells are shown in Table 4 and Figure 3. From the results of microseismic monitoring, the scale of fractures increases due to stress interference, that is, the range of network fractures increases significantly. Hydraulically affected fractures are mostly double-wing

TABLE 2
Fitting results of single well G function curve.

Well name	Closing pressure	Closing pressure gradient	Ground closing pressure	Closing time	Sand carrying liquid efficiency	Net pressure	Permeability	G function curve shape	Multiple fractures
	MPa	MPa/m	MPa	min	%	MPa	mD		
J	14.86	0.0152	5.2	35.31	33.116	0.21	0.08	Multiple fractures	7
A	17.99	0.0196	8.9	29.57	82.407	1.31	0.1	Multiple fractures	8
D	20.68	0.0221	11.4	36.85	83.72	2.5	0.06	Multiple fractures	10
L	21.27	0.0222	11.8	38.88	84.827	4.42	0.15	Normal fluid loss	/
P	27.01	0.0284	17.6	11.99	71.447	1.6	0.1	Normal fluid loss	/
Q	18.44	0.0179	8.25	15.51	71.312	0.65	0.15	Normal fluid loss	/

TABLE 3
Fracture parameter results of fractured wells.

Well name	Dynamic fracture length (m)	Support fracture length (m)	Dynamic fracture height (m)	Support fracture height (m)	Fracture width (cm)	Average proppant concentration (kg/m^2)
J	107.0	80.2	37.6	28.2	2.418	23.19
A	103.3	85.1	34.6	28.5	2.936	14.55
D	104.5	86.9	19.7	16.4	4.181	33.72
L	121.9	106.9	32.6	28.6	2.833	15.26
P	106.8	102.6	23.4	22.5	4.856	18.47
Q	105.4	100.9	24.0	23.0	5.723	19.87

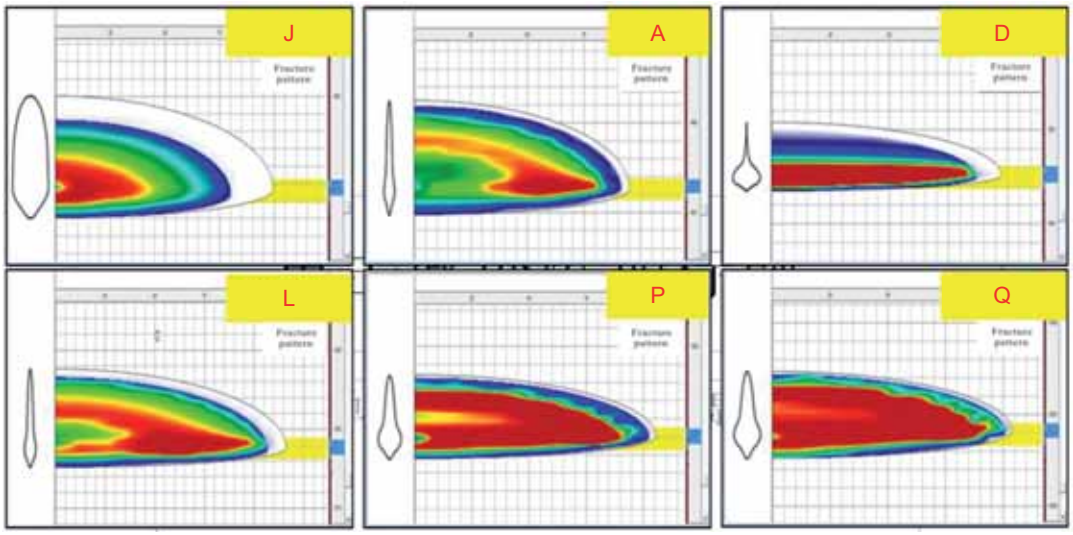


FIGURE 2
Fracture simulation results of fractured wells.

TABLE 4
Crack detection data based on microseismic monitoring.

Well name	Fracture parameter			Fracture network parameters	
	Fracture length (m)	Half-wing length	Fracture orientation	Width (m)	Height (m)
E	355	235 m (NE), 120 m (SW)	North East 70°	166	70
F	317	76 m (NE), 241m SW)	North East 39°	158	67
G	248	173 m (NW), 75m (SW)	North west 44°	103	57

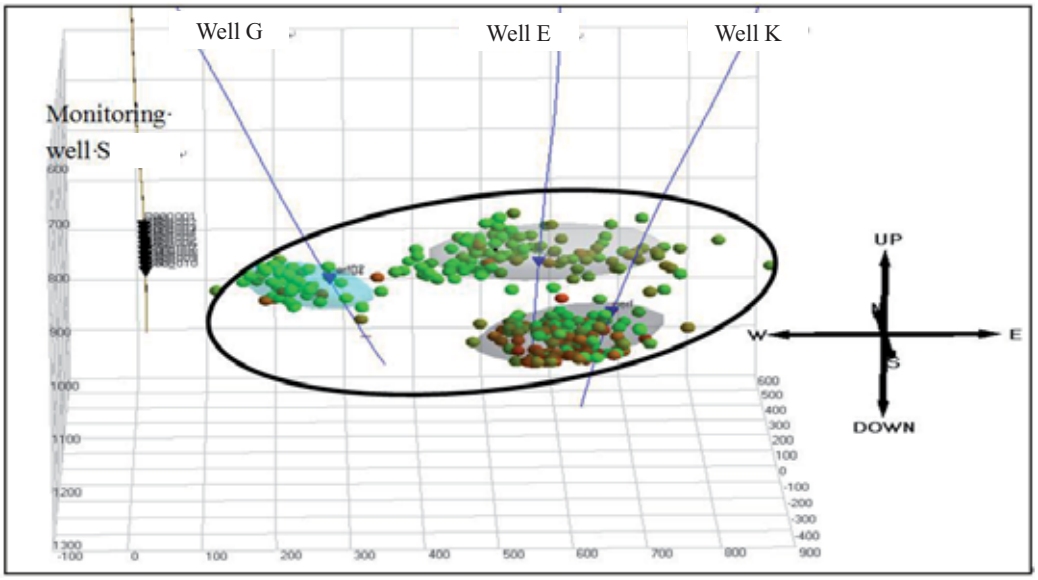


FIGURE 3
Side view of fracture detection results of synchronous fracturing wells.

fractures, and the fracture extension effect is good, which is beneficial to the production of coalbed methane.

Analysis of factors affecting drainage and production of fractured wells. The change of the phase state of coalbed methane well discharge and development causes the main controlling factors of coal reservoir conductivity to change. If the continuity of gas well discharge and production cannot be maintained, and if it is in the single-phase flow stage, the lowered fluid level will be restored. It can cause damage to the reservoir, especially to the diversion channel of the fracture in the coal reservoir. If it is in the gas/water two-phase flow stage, some of the desorbed gas may be adsorbed, which not only affects the gas production effect, but also may increase the drainage cost. The characteristics of low elastic modulus and low permeability of the coal seam determine its sensitivity to stress. If the stability of drainage and production cannot be maintained, the reservoir is vulnerable to greater damage and affects gas production.

Drainage and recovery time is a parameter that characterizes the continuous stability of CBM well drainage and production, and it is defined as the percentage of normal drainage and production days. Through the statistics of the drainage and recovery time efficiency of 14 old wells in the study area (Figure 4a), it can be seen that the drainage and recovery time efficiency of most wells is less than 80%. Wells 13 and 14 are high-yield wells. The drainage and recovery time of the two wells is also the highest among the 14 old wells. Therefore, high drainage and recovery time is a prerequisite for high production of CBM wells in this area.

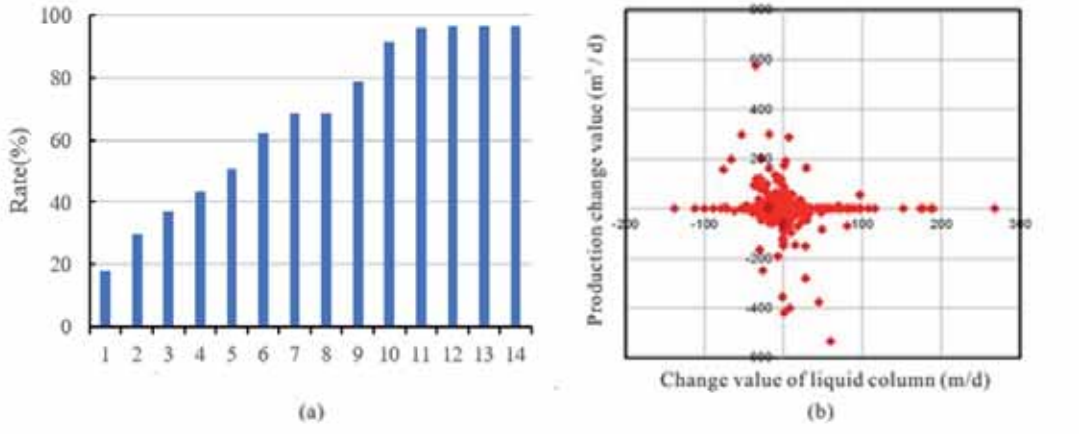


FIGURE 4
Variation characteristics of the drainage and production parameters of coalbed methane wells.
Notes: (a) Time-effect diagram of gas well discharge and production; (b) The relationship between liquid column change and gas production.

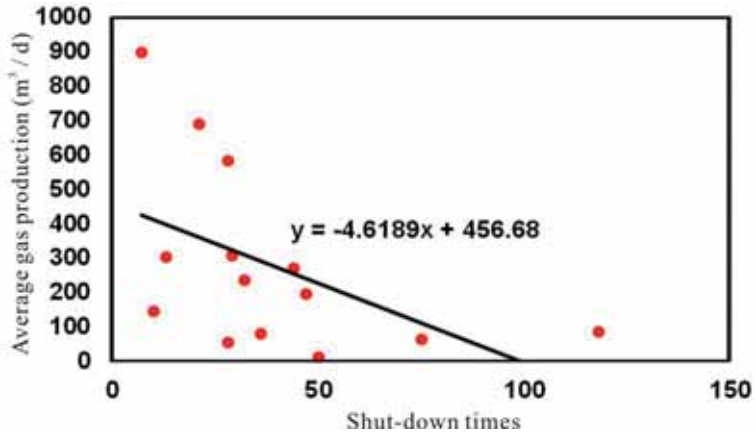


FIGURE 5
Changes in the number of shutdowns and gas production.

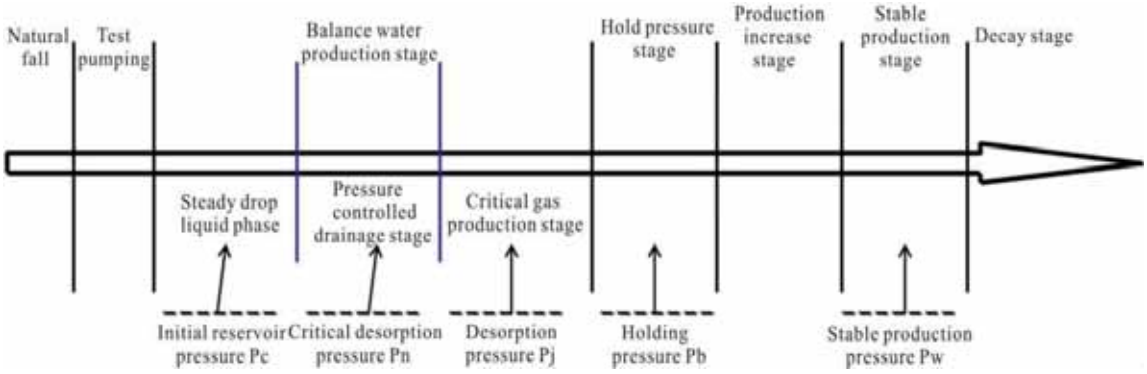


FIGURE 6
Division results of the discharge and production stages.

TABLE 5
Steady production pressure results of adjacent wells.

Well name	01	02	03	04	05	06
Stable production pressure (MPa)	1.35	0.83	0.54	0.51	0.42	0.45
Average (MPa)			0.55			

Through the analysis of the gas production situation of each well, it is found that the wells with frequent changes in the moving liquid level during the drainage and production cycle and a large range of fluctuations in the downflow rate have generally low gas production (Figure 4b). There is a certain negative correlation between the number of shutdowns and gas production. The more downtimes, the greater the impact on gas production (Figure 5).

Drainage phase division. The drainage and production of CBM wells are continuous and staged, so the drainage and production stages of gas wells are different. The traditional CBM well drainage stage is divided based on the flow pattern, and the on-site operability is greatly limited. In order to make the drainage and production system more operable, in this paper, the drainage and production stages of coalbed methane wells were divided into six stages by fully considered the production characteristics of coalbed methane wells. They are the trial pumping stage, the balanced water production stage, the pressure holding stage, the production increase stage, the stable production stage, and the attenuation stage. The results are shown in Figure 6.

In the early stage of drainage and production, the discharged water is mostly wellbore fluid, so the liquid level drops quickly and the water production is small. When the daily falling liquid level decreases and the daily liquid production gradually increases, the formation begins to supply liquid and release pressure, and the corresponding bottom hole pressure value at this time is the reservoir pressure. Desorption pressure is one of the most important parameters in the drainage process. Before coalbed methane is desorbed, that is, when the wellbore flow pressure is above the desorption pressure, the reservoir pressure relief is dominated by unidirectional flow (water). When the bottom hole pressure drops below the desorption pressure, the coalbed methane begins to desorb, and there is a two-phase flow of gas and liquid in the pores. After the CBM well sees gas, the degree of pressure relief of the reservoir determines the amount of gas suction. The difference

between the reservoir pressure and the bottom hole flow pressure determines the flow velocity. The production of coalbed methane wells is a comprehensive reflection of desorption gas volume and flow velocity. Through the statistics of the steady production pressure near the well (Table 5), it can be concluded that the average steady production pressure in this area is 0.55 MPa.

CONCLUSIONS

(1) In this paper, based on coalbed methane development data, fracturing data, and microseismic monitoring results, the effect of hydraulic fracturing of coal reservoirs and the factors affecting productivity were systematically studied. The research results show that the coal reservoir closure stress in the study area is distributed between 11.99-36.85 MPa, the reservoir permeability is distributed between 0.06-0.15 mD, and the coal seam has a high sand-carrying efficiency, so the fracture-forming ability is better.

(2) The microseismic monitoring results showed that the scale of cracks after stress interference increased significantly, and network cracks formed. Hydraulically affected fractures are mostly double-wing fractures, and the effect of fracture extension is ideal, which is beneficial to the production of coalbed methane.

(3) The study also found that the fluid level changes frequently during the drainage cycle. In addition, wells with a wide range of falling liquid velocity have generally low gas production. There is a certain negative correlation between the number of shutdowns and gas production. The more shutdowns, the greater the impact on gas production.

(4) The drainage and production phases of CBM wells are divided into six parts: test pumping stage, balanced water production stage, pressure holding stage, production increase stage, stable production stage, and decay stage. This research has important reference value for guiding the efficient development of coalbed methane.

ACKNOWLEDGEMENTS

This work was not supported by any funds. We would like to show sincere thanks to the techniques who have helped this research and all the authors of the references.

REFERENCES

[1] Tyiasning, S., Cooke, D. (2016) Anisotropy signatures in the Cooper Basin of Australia: Stress versus fractures. Interpretation. 4(2), 51-61.

[2] Wang, S., Elsworth, D., Liu, J. (2011) Permeability evolution in fractured coal: The roles of fracture geometry and water – content. International Journal of Coal Geology. 87, 13-25.

[3] Wang, Z. (2006) Advances in polygonal finite element method. Advances in Mechanics. 36(3), 344-352.

[4] Xie, J., Xu, J. (2017) Effect of key stratum on the mining abutment pressure of a coal seam. Geosciences Journal. 21(2), 267-276.

[5] Grasmueck, M., Moser, T., Pelissier, M., Pajchel, J., Pomar, K. (2015) Diffraction signatures of fracture intersections. Interpretation. 3(1), 55-68.

[6] Guo, Z., Jiang, Y., Pang, W. (2013) Distribution of ground stress on Puhe coal mine. International Journal of Mining Science and Technology. 23, 139-143.

[7] Kim, Y., Jang, H., Lee, J. (2017) Application of probabilistic approach to evaluate coalbed methane resources using geological data of coal basin in Indonesia. Geosciences Journal. 20(2), 229-238.

[8] Suman, P., Rima, C. (2011) Determination of in-situ stress direction from cleat orientation mapping for coal bed methane exploration in southeastern part of Jharia coalfield, India. International Journal of Coal Geology. 87, 87-96.

[9] Santosh, M., Feng, Z. (2020) New horizons in energy geoscience. Energy Geoscience. 1(1-2), 1.

[10] Tang, S., Zhu, B., Yan, Z. (2011) Effect of crustal stress on hydraulic fracturing in coalbed methane wells. Journal of China Coal Society. 36(1), 65-69.

[11] Yao, B., Li, D. (2012) Features and correct application of coal vitrinite reflectance index. Journal of Coal Science & Engineering. 18(4), 400-404.

[12] Li, Y., Zhou, D., Wang, W., Jiang, T., Xue, Z. (2020) Development of unconventional gas and technologies adopted in China. Energy Geoscience. 1(1-2), 55-68.

[13] Liang, J., Wang, C., Liu, Y., Gao, Y., Du, J., Feng, R., Zhu, X., Yu, J. (2014) Study on the tight gas accumulation conditions and exploration potential in the Qinshui Basin. Natural Gas Geoscience. 25(10), 1509-1517.

[14] Cao, L., Yao, Y., Cui, C., Sun, Q. (2020) Characteristics of in-situ stress and its controls on coalbed methane development in the southeastern Qinshui Basin, North China. Energy Geoscience. 1(1-2), 69-80.

[15] Aderibigbe, A., Valdes, C., Heidari, Z. (2016) Integrated rock classification in the Wolfcamp Shale based on reservoir quality and anisotropic stress profile estimated from well logs. Interpretation. 4(2), 1-18.

[16] Yang, Y., Li, X., Zhang, Y., Mei, Y., Ding, R. (2020) Insights into moisture content in coals of different ranks by low field nuclear resonance. Energy Geoscience. 1(3-4), 93-99.
[17] Armstrong, R., Wildenschild, D., Bay, B. (2015) The effect of pore morphology on microbial enhanced oil recovery. Journal of Petroleum Science and Engineering. 130, 16-25.
[18] Damaskinskaya, E., Frolov, D., Gafurova, D., Korost, D., Panteleev, I. (2017) Criterion for fracture transition to critical stage. Interpretation. 5(4), 1-8.
[19] Lungile, S., Bunt, J., Matjie, R., Piketh, S., Neomagus, H., Waanders, F. (2020) The effect of particle size on the pollution reduction potential of a South African coal-derived low-smoke fuel. Energy Geoscience. 1(3-4), 165-173.
[20] Meng, Q., Zhao, Y., Hu, Y., Feng, Z., Yu, Y. (2011) Experimental study on pore structure and pore shape of coking coal. Journal of China Coal Society. 36(3), 487-490.
[21] Meng, Z., Zhang, J., Wang, R. (2011) In-situ stress,pore pressure and stress- dependent permeability in the Southern Qinshui Basin. International Journal of Rock Mechanics & Mining Sciences. 48, 122-131.
[22] Mokhtari, M., Tutuncu, A., Boitnott, G. (2015) Intrinsic anisotropy in fracture permeability. Interpretation. 3(3), 43-53.
[23] Qiao, L., Wang, Z., Li, S., Bi, L., Xu, Z. (2017) Assessing containment properties of underground oil storage caverns: methods and a case study. Geosciences Journal. 21(4), 579-593.
[24] Cook, J., Goodwin, L., Boutt, D., Tobin, H. (2015) The effect of systematic diagenetic changes on the mechanical behavior of a quartz-cemented sandstone. Geophysics. 80(2), 145-160.
[25] Zoback, M. (2007) Reservoir Geomechanics. Cambridge: Cambridge University Press. 32-35.

Received: **21.02.2021**
Accepted: **05.05.2021**

CORRESPONDING AUTHOR

Haibin Gao
China United Coalbed Methane Corporation Ltd.,
Changzhi Shanxi 046600 – China

e-mail: 757488232@qq.com

© by PSP Volume 30– No. 09/2021 pages 10610-10624 Fresenius Environmental Bulletin

FUZZY COMPREHENSIVE EVALUATION OF DEBRIS FLOW RISK BASED ON PROBABILITY COMBINED WEIGHT

Li Li[1,*], Shixin Zhang[1], Yue Qiang[1], Dongsheng Zhao[1], Chaoqiong Liu[2], Zhou Zheng[1], Changsi Xia[1]

[1]Dept. of Civil Engineering, School of Civil Engineering, Chongqing Three Gorges University, Wanzhou, Chongqing, China
[2]Dept. of building and environmental safety, Chongqing Vocational Institute of safety &technology, Wanzhou, Chongqing, China

ABSTRACT

This paper proposes a probability-based combined method due to the subjective influence of the weight assignment process in the risk assessment of debris flow. The weight is regarded as a bounded uniform random variable, and the boundary is determined by the equal weight method, the maximum deviation method, and the entropy method. The optimal weight is obtained through the Monte Carlo simulation and used as the weight set of the fuzzy comprehensive evaluation (FCE) model. According to the formation characteristics of debris flow in Beichuan County, the loose source material reserves, the basin area, the drainage density, the basin relative relief, the shifting bed proportion, and the main channel length are selected as fuzzy factor sets. The fuzzy vector **B** calculated by the judgment matrix **F** is used to evaluate the risk of 72 debris flows in Beichuan County, Sichuan Province according to the maximum membership principle. The results show: 1) probability-based combined method is a more reasonable method of weight determination; 2) there are 33 debris flows with a high degree of danger, and Beichuan County is still facing the threat of debris flow disasters; 3) the risk degree of Xishanpogou, Yuxuegou, Subaogou and Wangjiayangou are higher than those of the method proposed by Liu and Tang. A higher assessment level is more reasonable because considering the distribution of buildings in the basin.

KEYWORDS:
Debris Flow, Risk Assessment, Fuzzy Comprehensive Evaluation, Multi-criteria Decision-making, Monte Carlo Simulation

INTRODUCTION

Debris flow is a common and extremely destructive natural geological disaster in rural areas [1]. Not only will it have a significant impact on the natural ecological environment and economic development in rural areas, but the suddenness, large flow, and strong destructive characteristics of debris flows will bring severe consequences to human production and life [2-4].

Many factors affect debris flow risk, such as the basin relative relief, gully inclination, vegetation coverage, rainfall, drainage density, loose source material reserves, etc. Therefore, the risk assessment of debris flow can be regarded as a multi-criteria decision-making problem [5]. However, considering all influencing factors will make the risk assessment process too complicated, leading to unsatisfactory results. Given this, this paper simplifies the influencing factors of debris flow hazards. According to the development characteristics of debris flow in Beichuan County after the earthquake, the loose source material reserves, the basin area, the drainage density, the basin relative relief, the shifting bed proportion, and the main channel length are selected as assessment factors.

A fuzzy-based model considering the inexact character of influential factors was proposed [6]. The fuzzy-based assessment model was applied to the Hualien area and achieved very high accuracy. The fuzzy comprehensive evaluation (FCE) model has the advantages of clear concept and objective results. It has good applicability in the risk assessment of debris flow [7]. In recent years, many types of research have improved on the FCE combined with other methods. A debris flow risk assessment model based on FCE and gray correlation analysis method was developed [8]. This method determines the relationship between 8 secondary factors and 2 main factors through the gray correlation degree, and the analytic hierarchy process was used to determine the weights of 10 influencing factors. The application in the Udonde region showed better performance. Therefore, the feasibility of the FCE method in the risk assessment of debris flow has been verified, and it has a good assessment performance.

A single weight assignment method is mostly used in the above studies, which will inevitably cause errors. Therefore, some ways of combining weights have been proposed to avoid errors caused by weight calculations. For example, a combination weighting method that considers the sensitivity of the influencing factors of large-scale debris flow was proposed [9]. This method considers both the engi-

neer's preference for the primary factors and objective information on the main factors. A fuzzy method that combines subjective weights and objective weights through game theory was proposed [10-11], and obtained more moderate weights than a single method. A combined weight method was developed and avoided the defect of excessive weight, but the simple combined strategy is subjective [12]. A fuzzy comprehensive evaluation method based on probability is proposed in this paper to solve the multi-criteria decision-making problem. It is applied to the risk assessment of debris flow in Beichuan County.

The structure of this paper is as follows: In Section 2, the study area in this paper was introduced; in Section 3, the implementation steps of equal weight method, maximum deviation method, entropy method, and probability combination method are introduced. Then use the calculated weight as the weight set of the FCE method; in Section 4, the results of the debris flow risk assessment are given; in Section 5, the performance of the probability-based combined method and the consequences of risk assessment are analyzed; finally, the conclusions were drawn.

MATERIALS AND METHODS

Beichuan County is located in Sichuan Province, China, in the Beichuan-Yingxiu fault zone. After the "5.12" earthquake, the geological conditions in Beichuan County became very fragile, and many regional debris flows were induced after prolonged rainfall. Therefore, this paper takes 72 debris flows in Beichuan County as the study object (Figure 1). The debris flows in Beichuan County are mostly concentrated in the east and south-central, and the stratum mainly covers the Quaternary loose accumulation layer.

After the "5.12" earthquake, the debris flow induced by landslides in the earthquake area has been extensively studied [13]. Many small and medium-sized landslides provide a rich source of loose deposits for the debris flow [14]. The heavy storm after the earthquake-induced many regional debris flows. Simultaneously, due to the immense relative relief of the gullies, the surface runoff converges and carries loose deposits to scour the gullies, constantly erodes the gully bed, and intensifies the debris flow development. Therefore, the debris flow in Beichuan County was mainly caused by the destruction of the initial stable terrain after the earthquake and then induced by extreme rainfall. This paper mainly focuses on the topography and hydrological conditions of the debris flow after the earthquake. It selects the 6 factors of the loose source material reserves u_1, the basin area u_2, the drainage density u_3, the basin relative relief u_4, the shifting bed proportion u_5, and the main channel length u_6 as assessment factors. The weight set is determined by the probability-based combined method. The weight is regarded as a random variable that satisfies a uniform distribution, and its boundary

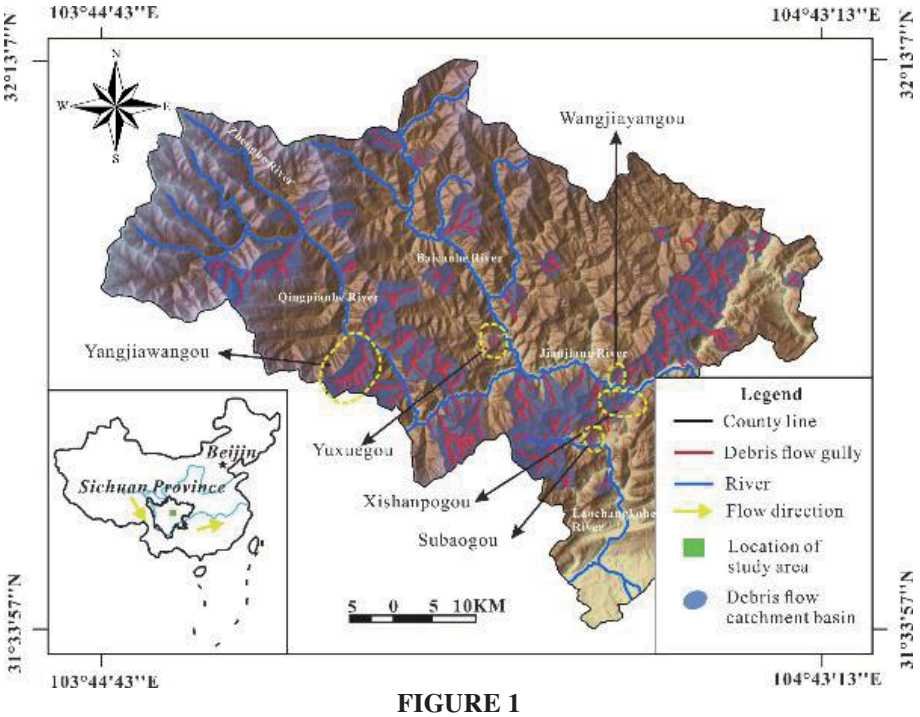


FIGURE 1
Distribution of debris flow in Beichuan County

TABLE 1
The basic data statistics table of 72 debris flows [15]

Samples	Loose source material reserves (10^3m^3)	Basin area (km^2)	Drainage density (km^{-1})	Basin relative relief (km)	Shifting bed proportion (%)	Main channel length (km)
Chaimazigou#1	0.04	2.5	8.24	1.6	0.48	2.06
Shuxuegou	39.04	13.9	2.90	1.4	0.50	4.03
Yingtaogou#1	43.65	10.3	3.78	1.4	0.72	3.89
Miaobagou	728.20	7.8	5.26	1.46	0.85	4.10
Jinlongcun	79.50	4.5	7.44	0.98	0.64	3.35
Hualingou	385.95	12.2	4.82	1.36	0.85	5.88
Wangjiashangou	104.50	1.8	7.67	1.04	0.86	1.38
Xinzhigou#1	240.45	10	5.39	1.56	0.76	5.39
Chenjiabaogou	50.20	1.9	7.16	1.1	0.48	1.36
Pijialianggou	2.40	2.4	7.42	1.14	0.23	1.78
Xishanpogou	1500	1.6	20.75	1.12	0.61	3.32
Renjiapinggou	242	0.5	14.6	0.46	0.84	0.73
Mofanggou	160.70	0.8	13.63	0.66	0.72	1.09
Miaobagou	6.60	7.5	3.81	1.38	0.39	2.86
Piankoxianggou#2	4.80	4.6	4.33	0.86	0.54	1.99
Xinzhigou#2	73.20	21.8	3.59	2.04	0.42	7.82
Honglingou	2.85	5.7	5.35	1.92	0.37	3.05
Chaimazigou#2	14.70	6.8	3.75	1.8	0.40	2.55
Qinglingou	109.30	23.2	3.23	2.3	0.61	7.49
Baishuihegou	35	10.6	4.01	1.68	0.47	4.25
Piankoxianggou#3	160.34	16	3.68125	1.04	0.51	5.89
Subaohegou	60	3.5	6.43	1.24	0.65	2.25
Shuligou	70.60	0.7	20.43	0.96	0.61	1.43
Xinigou	40.53	0.7	19.43	1	0.81	1.36
Tianbaigou	163.32	18.7	3.16	1.68	0.76	5.91
Piankoxianggou	0.89	0.9	15.11	0.72	0.43	1.36
Lijiawangou	60	1.2	12.08	0.86	0.41	1.45
Kaipingzhigou	26.20	1	13.20	0.6	0.62	1.32
Yuxuegou	1016.40	0.8	14.38	0.88	0.86	1.15
Xiatongbaogou	1967.90	15.7	3.80	1.22	0.84	5.97

Sibapinggou	378.24	21.4	3.47	1.5	0.76	7.42
Zhibeigou	199	8.7	3.25	1.36	0.60	2.83
Yangliucun	101.63	9.9	4.64	1.7	0.58	4.59
Yanghuziwangou	40.20	1.2	12.08	0.82	0.81	1.45
Zhifanggou	74	1.1	9.55	0.75	0.69	1.05
Yingtaogou#2	119.30	17.6	4.33	1.66	0.56	7.62
Sunjiagou	15.55	2.7	10.70	1.22	0.45	2.89
Chayuanlianggou	54	2.6	12.04	1.26	0.41	3.13
Hanjiashangou	67.44	0.8	15.25	0.82	0.82	1.22
Baiguoshugou	107.30	0.6	16.50	0.67	0.73	0.99
Weigou	33.54	2.2	9.50	0.74	0.57	2.09
Weigou#2	106.50	0.3	22.00	0.52	0.76	0.66
Madiwangou	3.36	0.7	29.86	0.55	0.47	2.09
Huangjiawangou	4.13	2.8	8.39	1	0.47	2.35
Jingzhuyuangou	51.80	1.1	9.00	0.59	0.46	0.99
Jiangjiagou	12.14	0.5	23.00	0.92	0.52	1.15
Maoershi	10.80	1.4	7.57	0.98	0.47	1.06
Subaogou	507	1.1	10.45	0.58	0.79	1.15
Liujiagou	120.08	1.8	7.50	1.04	0.89	1.35
Daokaimengou	15.98	3.1	8.19	0.84	0.51	2.54
Qingtangwangou	30	3.5	5.14	0.82	0.75	1.80
Huangtulianggou	114	24.6	3.29	1.22	0.64	8.10
Guanmenzigou	14.26	2.8	5.57	1.12	0.70	1.56
Shupinggou	33	4.1	8.88	1.09	0.46	3.64
Dengjiacungou	900.03	22.2	5.12	1.7	0.44	11.36
Qushanzhenggou	210	3.6	8.67	1.2	0.96	3.12
Guzhubagou	1000.10	7	5.74	1.22	0.87	4.02
Wangjiayangou	485	2.5	7.88	1	0.81	1.97
Chenjiabagou	931.24	23.1	4.28	1.2	0.66	9.88
Tudilianggou	12.21	4	6.40	1.03	0.53	2.56
Tudimiaogou	34.08	16	3.69	1.28	0.39	5.91
Guaitangou	0.08	11.7	4.05	1.08	0.21	4.74
Dapingdigou	16.80	5.4	5.59	1.46	0.40	3.02
Xiatongbaogou	98.50	22.7	3.37	1.86	0.76	7.66
Chanzipinggou	67.20	2.5	5.28	1.02	0.83	1.32

Shangyantaigou	17.50	1.5	11.67	1.24	0.9	1.75
Shuangyigou	93.30	2.8	9.82	1.3	0.78	2.75
Shilonggou	50.80	7.3	5.36	1.2	0.84	3.91
Yangjiawangou	135.57	26.4	3.20	1.8	0.67	8.46
Zhaojiawangou	14.66	2.8	8.18	1.34	0.82	2.29
Dongxigou	8.95	10.9	3.78	1.5	0.57	4.12
Maliuwangou	97.82	17.1	3.76	1.28	0.70	6.43

is determined by the calculation results of the equal weight method, the maximum deviation method, and the entropy method. The optimal weight is obtained through Monte Carlo simulation, and the optimal weight is used as the weight set in the fuzzy comprehensive evaluation method. The fuzzy vector is obtained through the operation of the judgment matrix and the weight set, and the assessment result is obtained according to the principle of maximum membership. Table 1 shows the necessary survey data of 72 debris flow gullies in Beichuan County [15].

Decision matrix and normalization. In multi-criteria decision-making problems, the weight assignment of assessment factors is essential for assessment models. Weights are often used to reflect the relative importance of various evaluation factors. The reasonable value of weights is related to the reliability and correctness of multi-criteria decision-making problems. The decision matrix is denoted as $\boldsymbol{Z}=\{z_{ij}\}_{i=1,2,\ldots,m;\ j=1,2,\ldots,n}$, m represents the number of samples (the number of debris flow gullies, i.e., 72), n is the number of assessment factors (i.e., the loose source material reserves, the basin area, the drainage density, the basin relative relief, the shifting bed proportion, and the main channel length); the weight is defined as a vector $\boldsymbol{w}=[w_1,w_2,\ldots,w_n]^T$ that satisfies the sum of 1.

Due to the different dimensions of the selected 6 assessment factors, in order to avoid affecting the results of the debris flow risk assessment and eliminate the influence between the dimensions of the assessment factors, it is necessary to normalize the decision matrix Z. The normalization equation is:

$$\tilde{z}_{ij}=\frac{z_{ij}-\min(z_{1:m,j})}{\max(z_{1:m,j})-\min(z_{1:m,j})} \quad (1)$$

Where max() represents the maximum function; min() represents the minimum function. Because the 6 assessment factors in this paper are all the greater, the value indicates the higher the risk degree, so only need to use Eq. 1 for normalization. And the larger the normalized value, the higher the danger degree.

Equal weight method. The equal weight method is the most widely used method of weight determination. When dealing with some simple problems, the equal weight method is often used to solve the multi-criteria decision-making problem. The equal weight method can be expressed as:

$$w_j=1/n \quad (2)$$

By Eq. 2, w_{EWM}= {0.17, 0.17, 0.17, 0.17, 0.17, 0.17} can be calculated. In the analytic hierarchy process, the equal weight method can be regarded as a special case of the analytic hierarchy process when it is considered that the influencing factors have equal importance to the result.

Maximum deviation method. In the multi-attribute decision-making problem, determining the weight according to the difference and importance of each assessment factor is called the maximum deviation method. The maximum deviation method stipulates that when the difference between the elements in the same row of the decision matrix is smaller, the less important the assessment factor is, the less weight is assigned. Conversely, when the difference is more generous, the evaluation factor is more important to the evaluation result and should be given greater weight. This is the essence of the maximum deviation method.

Calculate the deviation v according to the following equation:

$$v_{ij}=\sum_{k=1}^{m}\left|w_j\tilde{z}_{ij}-w_j\tilde{z}_{kj}\right| \quad (3)$$

The total deviation is defined as:

$$V_j=\sum_{i=1}^{m}v_{ij}=\sum_{i=1}^{m}\sum_{k=1}^{m}\left|w_j\tilde{z}_{ij}-w_j\tilde{z}_{kj}\right| \quad (4)$$

In the maximum deviation method, it is believed that the weight should maximize the deviation of all assessment factors, namely:

$$\max\sum_{j=1}^{n}V_j=\sum_{j=1}^{n}\sum_{i=1}^{m}\sum_{k=1}^{m}\left|w_j\tilde{z}_{ij}-w_j\tilde{z}_{kj}\right| \quad (5)$$

Using the Lagrangian method, the weight obtained by the solution is:

$$w_j = \frac{\sum_{i=1}^{m}\sum_{k=1}^{m}\left|\bar{z}_{ij} - \bar{z}_{kj}\right|}{\sum_{j=1}^{n}\sum_{i=1}^{m}\sum_{k=1}^{m}\left|\bar{z}_{ij} - \bar{z}_{kj}\right|} \quad (6)$$

The weight of the maximum deviation method is calculated as w_{MDM}={0.19, 0.21, 0.11, 0.17, 0.15, 0.18}.

Entropy method. Entropy method is an objective weighting method, and it is also a method to determine weights based on a decision matrix. Using information entropy as an intermediate tool, the weight is calculated. The entropy vector T of the assessment factor is defined as:

$$T_j = -\frac{1}{\ln m}\sum_{i=1}^{m}\frac{\bar{z}_{ij}}{\sum_{i=1}^{m}\bar{z}_{ij}}\ln\frac{\bar{z}_{ij}}{\sum_{i=1}^{m}\bar{z}_{ij}} \quad (7)$$

According to Eq. 7, the entropy weight of the assessment factor is:

$$w_j = \frac{1-T_j}{n-\sum_{j=1}^{n}T_j} \quad (8)$$

It can be seen from Eq. 7 and Eq. 8 that when the entropy value is smaller, the entropy weight is larger, the information quantity of the corresponding assessment index is more effective, and the assessment index is more important. Conversely, the greater the entropy of the indicator, the smaller the entropy weight, and the lower the importance of the indicator. Entropy weight reflects the objective characteristics of the assessment function of the indicator in objective information. The weight of the entropy method calculated by Eq. 8 is w_{EM}= {0.44, 0.25, 0.03, 0.07, 0.05, 0.16}.

Probability-based combined method and process. The 3 weight assignment methods (i.e., the equal weight method, the maximum deviation method, and the entropy method) obtain the weight of the assessment factor from different data analysis perspectives. The equal-weight method has low reliability due to its over-simplification of the assessment factor, so it needs to refer to the entropy method and the maximum deviation method. Simultaneously, only the maximum deviation method and the entropy method are used to calculate the weight, which will cause the upper and lower limits of the weight assignment of individual assessment factors to be too large. This difference is because the two methods are based on different data processing perspectives, so the equal weight method is also required to reasonably restrict the upper and lower limits of the weight.

From the definition of weight, we know that the vector $w=[w_1,w_2,...,w_n]^T$ that satisfies the sum of each element is 1 can be used as the weight. Through the results of these 3 methods, the upper and lower limits of the weight of an assessment factor can be obtained. It can be considered that the weight is a random variable that satisfies a uniform distribution within the boundary and borrows the idea of probability analysis. In summary, we propose a method of fusing the weights of different methods through probability analysis. The implementation steps of the probability-based combined method are as follows: Step 1: In the weight calculation process of equal weight method, maximum deviation method, and entropy method, the data needs to be normalized, and Eq. 1 is used to calculate the normalized decision matrix. The normalization method used in this paper is more conventional and will not be described in detail here.

Step 2: The weights of the 6 assessment factors were calculated by equal weight method, maximum deviation method and entropy method (Table 3).

Step 3: The calculated weights are regarded as uniformly bounded random variables, and the weights calculated by the 3 methods are sorted in order to obtain the upper and lower limits of the uniformly bounded variables. Figure 2 shows the weights of the 6 assessment factors obtained by the 3 methods, and the boundary conditions are:

$$w_1 \quad [0.17, 0.44]$$
$$w_2 \quad [0.17, 0.25]$$
$$w_3 \quad [0.03, 0.17]$$
$$w_4 \quad [0.07, 0.17]$$
$$w_5 \quad [0.05, 0.17]$$
$$w_6 \quad [0.16, 0.18]$$

Step 4: Randomly generate the weighted random variable samples that meet the uniform distribution within the boundary obtained in Step 3. It was denoted as $w_4=\{w_{ij}\}_{i=1,2,...,l;\ j=1,2,...,n}$, where l represents the number of samples.

Step 5: After generating 1×107 samples, the weight gradually converges within the boundary conditions, and finally the weight w_{PCM}= [0.301, 0.2093, 0.098, 0.1096, 0.1117, 0.1702] is obtained.

In the probability-based combined method, Step 4 and Step 5 are also called Monte Carlo simulation.

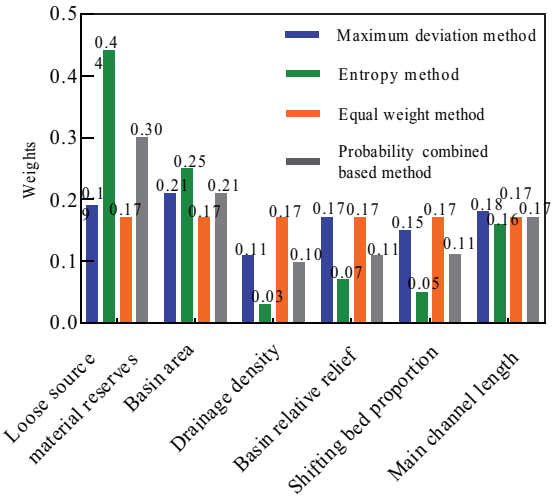


FIGURE 2
Comparison of 4 methods

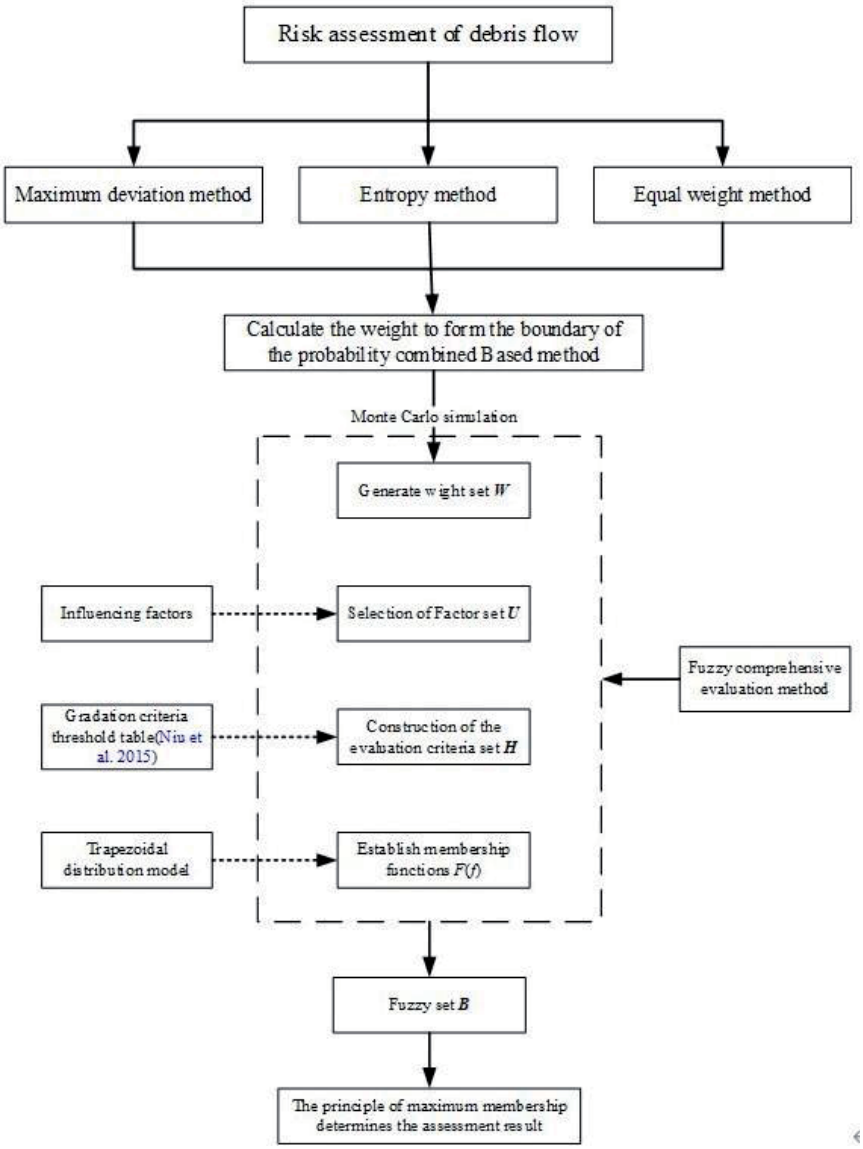


FIGURE 3
The probability combined based fuzzy comprehensive evaluation model structure diagram.

TABLE 2
Debris flow risk classification assignment table

Assessment factor	Minuscule	Sight	Moderate	Severe	High
$u_1(10^3m^3)$	<2	2~20	20~200	200~500	500~2000
$u_2(km^2)$	<0.25	0.25~3.0	3~10	10~15	15~25
$u_3(km^{-1})$	<0.5	0.5~5.5	5.5~12.5	12.5~17.5	17.5~25
u_4(km)	<0.20	0.20~0.65	0.65~1.25	1.25~1.75	1.75~3.5
u_5(%)	<7.5	7.5~22.5	22.5~37.5	37.5~52.5	52.5~100
u_6(km)	<0.5	0.5~1.0	1~2	2~7.5	7.5~15

Establishment of FCE model. This paper refers to the method of Zhang et al. [16], Jian et al. [17], and Shen et al. [18] to establish a FCE model for the risk of debris flow (see Figure 3 for the evaluation system), and optimize the weight value process based on the probability-based combined method. The assessment factors were selected according to the topography, hydrodynamic conditions, and hydrological conditions, that is, the factor set $U = \{u_1, u_2, u_3, u_4, u_5, u_6\}$={the loose source material reserves, the basin area, the drainage density, the basin relative relief, the shifting bed proportion, and the main channel length }. The risk degree is divided into 5 levels: Minuscule, Slight, Moderate, Severe, and High. Therefore, the evaluation criteria set can be expressed as $H=\{h_1, h_2, h_3, h_4, h_6\}$= {Minuscule, Slight, Moderate, Severe, High }, and establish a classification level threshold for the risk of debris flow (Table 2).

The methods for determining the membership function of fuzzy sets generally include fuzzy statistics, objective scale assistance, and assignment [19]. In this paper, the assignment method is selected to determine the membership function. According to the distribution characteristics of the assessment factors, the membership function of "trapezoidal distribution" is selected to determine the membership degree of the assessment factor U to the evaluation criteria set H. The membership function designed according to the "Trapezoidal Distribution" model is:

$$F_{h1}(u_{ij})=\begin{cases}1, u_{ij}\le e_1\\ \dfrac{e_2-u_{ij}}{e_2-e_1}, e_1<u_{ij}\le e_2\\ 0, u_{ij}>e_2\end{cases} \quad (9)$$

$$F_{h2}(u_{ij})=\begin{cases}0, u_{ij}\le e_1\\ \dfrac{u_{ij}-e_1}{e_2-e_1}, e_1<u_{ij}\le e_2\\ \dfrac{e_3-u_{ij}}{e_3-e_2}, e_2<u_{ij}\le e_3\\ 0, u_{ij}>e_3\end{cases} \quad (10)$$

$$F_{h3}(u_{ij})=\begin{cases}0, u_{ij}\le e_2\\ \dfrac{u_{ij}-e_2}{e_3-e_2}, e_2<u_{ij}\le e_3\\ \dfrac{e_4-u_{ij}}{e_4-e_3}, e_3<u_{ij}\le e_4\\ 0, u_{ij}>e_4\end{cases} \quad (11)$$

$$F_{h4}(u_{ij})=\begin{cases}0, u_{ij}\le e_3\\ \dfrac{u_{ij}-e_3}{e_4-e_3}, e_3<u_{ij}\le e_4\\ \dfrac{e_5-u_{ij}}{e_5-e_4}, e_4<u_{ij}\le e_5\\ 0, u_{ij}>e_5\end{cases} \quad (12)$$

$$F_{h5}(u_{ij})=\begin{cases}0, u_{ij}\le e_4\\ \dfrac{u_{ij}-e_4}{e_5-e_4}, e_4<u_{ij}\le e_5\\ 1, u_{ij}>e_5\end{cases} \quad (13)$$

Where u_{ij} is the actual value of the j-th assessment factor of the i-th debris flow; e_i, j=1,2,3,4,5 are the limits of each assessment level.

Calculate each element in the judgment matrix by Eqs. 9-13 to form a fuzzy comprehensive judgment matrix F:

$$\boldsymbol{F} = \begin{bmatrix} f_{11} & \cdots & f_{1v} \\ \vdots & \ddots & \vdots \\ f_{u1} & \cdots & f_{uv} \end{bmatrix} \quad (14)$$

Where u is the assessment factor; v is the risk degree; f_{uv} represents the membership degree of the u -th assessment factor to the risk degree v.

$$\boldsymbol{B} = \boldsymbol{W} \times \boldsymbol{F} \quad (15)$$

So far, the judgment matrix and weight set of the FCE have been obtained, and the fuzzy vector of each debris flow is obtained by Eq. 12. Due to the large amount of debris flow data and limited space, the judgment matrix and fuzzy vector of the debris flow on the west hillside are given:

$$\boldsymbol{F} = \begin{bmatrix} 0 & 0 & 0 & 0.33 & 0.33 \\ 0.51 & 0.49 & 0 & 0 & 0 \\ 0 & 0 & 0 & 0.57 & 0.43 \\ 0 & 0.22 & 0.78 & 0 & 0 \\ 0 & 0 & 0 & 0.82 & 0.18 \\ 0 & 0 & 0.76 & 0.24 & 0 \end{bmatrix} \quad (16)$$

$$\boldsymbol{B} = \boldsymbol{W} \times \boldsymbol{F} = (0.15 \quad 0.17 \quad 0.22 \quad 0.29 \quad 0.26) \quad (17)$$

According to the principle of the maximum membership degree, the maximum value is selected in the fuzzy vector $\boldsymbol{B}$. The risk degree corresponding to this value is the assessment level of the debris flow under the FCE method. the element in the fourth column is the maximum value of 0.29 In the fuzzy vector of the Xishanpogou, and the corresponding risk degree is the "Severe" (i.e., the final assessment result of the debris flow is the "Severe").

RESULTS

Table 3 shows the weights calculated by 4 methods, and the weights are calculated using the data in Table 1 through the decision matrix normalized by Eq. 1. The weight calculated by the equal weight method is 0.17, and the weight calculated by the maximum deviation method is 0.19, 0.21, 0.11, 0.17, 0.15, 0.18. The entropy method calculates the weights of the assessment factors to be 0.44, 0.25, 0.03, 0.07, 0.05, 0.16, respectively. The weights calculated by the method proposed in this paper are 0.30, 0.21, 0.10, 0.11, 0.11, 0.17. It can be seen from Figure 2 that the probability-based combined method and entropy method proposed all believe that the importance of u_1 is greater than the other assessment factors (the entropy method believes that the importance of u_1 is much greater than others). However, the maximum deviation method believes that the importance of basin area is greater than other assessment factors. It is worth noting that the results obtained by the 4 methods are relatively consistent only on one assessment factor (i.e., the main channel length).

TABLE 3
Weights determined by 4 weighting methods

Weight method	u_1	u_2	u_3	u_4	u_5	u_6
Equal weight method	0.17	0.17	0.17	0.17	0.17	0.17
Maximum deviation method	0.19	0.21	0.11	0.17	0.15	0.18
Entropy method	0.44	0.25	0.03	0.07	0.05	0.16
Probability-combined method	0.30	0.21	0.10	0.11	0.11	0.17

TABLE 4
The FCE method results

Risk assessment level	Minuscule	Slight	Moderate	Severe	High
Debris flows amount	5	34	13	18	2

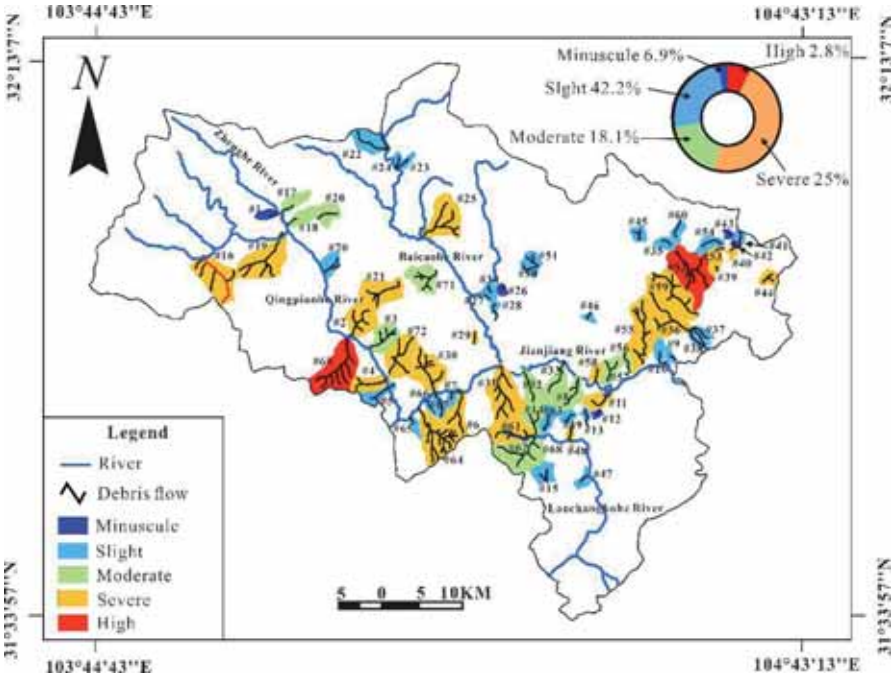


FIGURE 4
Risk level of debris flow in Beichuan County

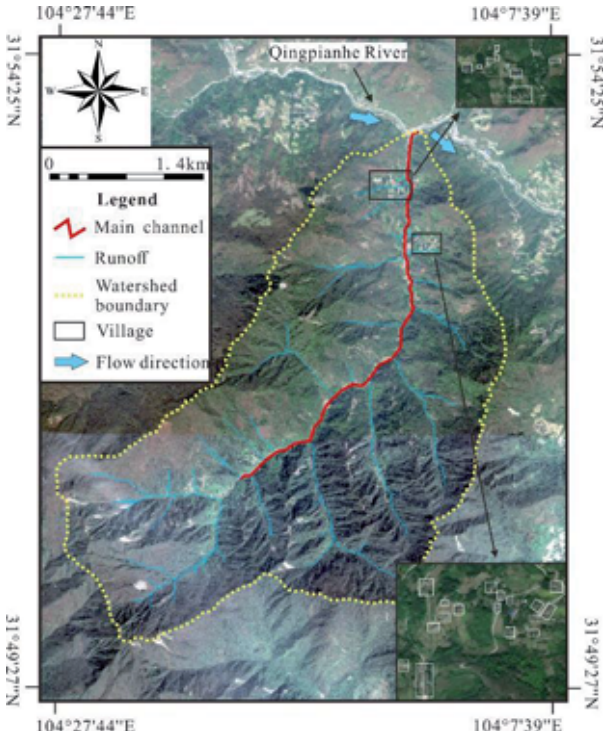


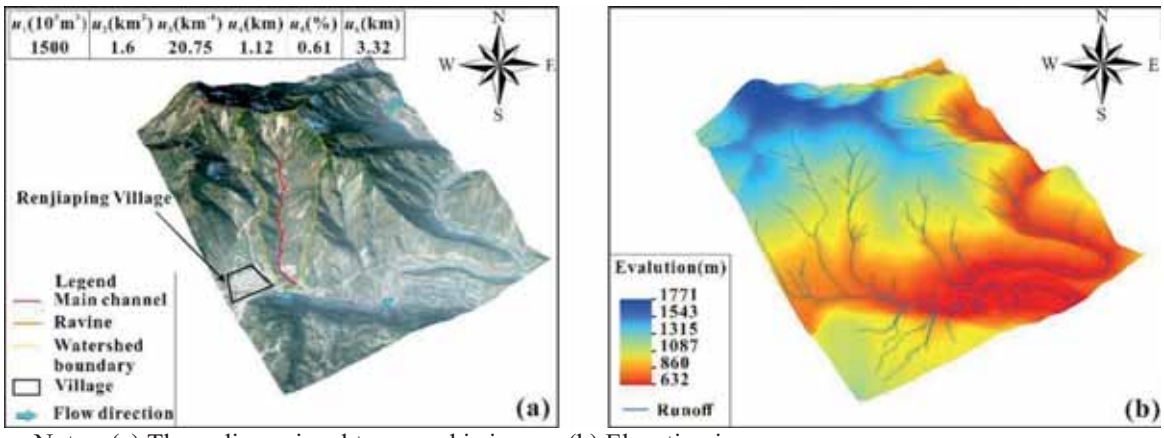
FIGURE 5
Watershed image of Yangjiawangou

Table 4 shows the FCE results of 72 debris flows. It can be seen from Table 4 that the debris flows in "Minuscule" and "Slight" account for about 54% of the debris flows in Beichuan County, those in "Moderate" account for about 18%, and those in "Severe" account for about 25%. There are 2 debris flows (i.e., Huangtulianggou and Yangjiawangou) in "High", and the most dangerous debris flow in the assessment result is consistent with the method proposed by Liu and Tang [20]. From Figure 4, the assessment level of debris flows can be seen intuitively. Simultaneously, the coincidence degree of the 72 debris flows with the survey statistics reached 87.5%. It can be seen from the assessment results that Beichuan County will be under the threat of debris flow disaster for a long time.

The formation of debris flow is determined by geographic and geomorphic conditions, loose material sources, and water source conditions. Taking the Yangjiawangou debris flow as an example (Figure 5), it can be seen from Table 5 that the basin area of Yangjiawangou is 26.4km^2, while the average basin area of the 72 debris flows is only 6.23km^2. In Yangjiawangou's judgment matrix, the membership degree given as "Severe" is as high as 1.0. The assessment results indicate that the main channel length and the basin relative relief have more significant on the risk of Yangjiawangou, and the membership degree in "Severe" reaches 0.87 and 0.97. Water source conditions are the driving factors that induce debris flow. The basin area determines the water source conditions in the basin. Therefore, for the Yangjiawangou, although the loose source material reserves are only 135.57×10^{3}m^3, the basin area in the circulation area is as high as 26.4km^2, and the water source in the basin area is sufficient. The basin relative relief and shifting bed proportion reflect the high erosion degree of the channel, the sediment and loose source materials along the way are adequately recharged. Therefore, from the perspective of hydrological and topographical conditions, the Yangjiawangou is more dangerous.

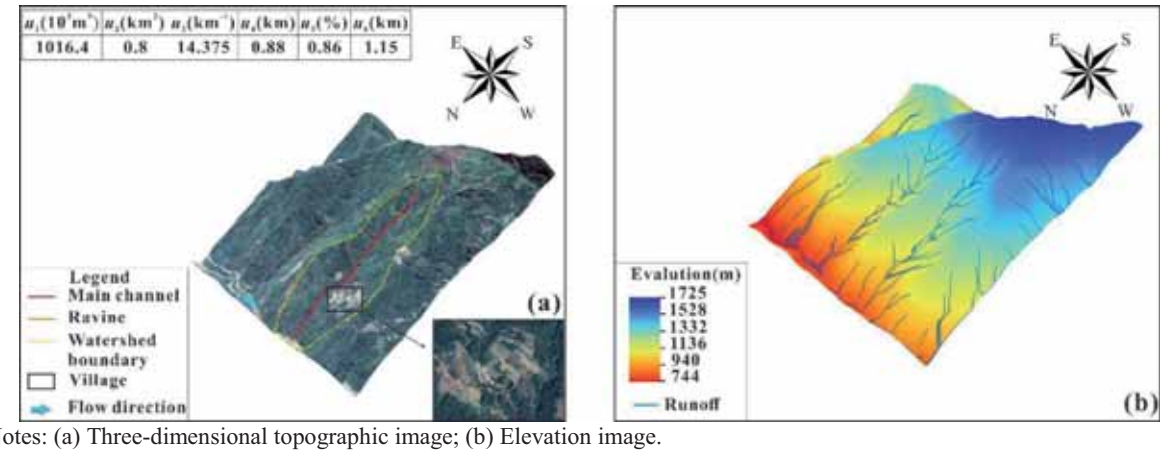
TABLE 5
Watershed image of Yangjiawangou

Assessment foctors	Field statistics	Yangjiawangou				
		Judgment matrix ***F***				
		Minuscule	Sight	Moderate	Severe	High
u_1 (10^{3}m^3)	135.57	0	0.36	0.64	0	0
u_2 (km^2)	26.4	0	0	0	0	1
u_3 (km^{-1})	3.20	0.46	0.54	0	0	0
u_4 (km)	1.80	0	0	0	0.97	0.03
u_5 (%)	0.67	0	0	0	0.69	0.31
u_6 (km)	8.46	0	0	0	0.87	0.13



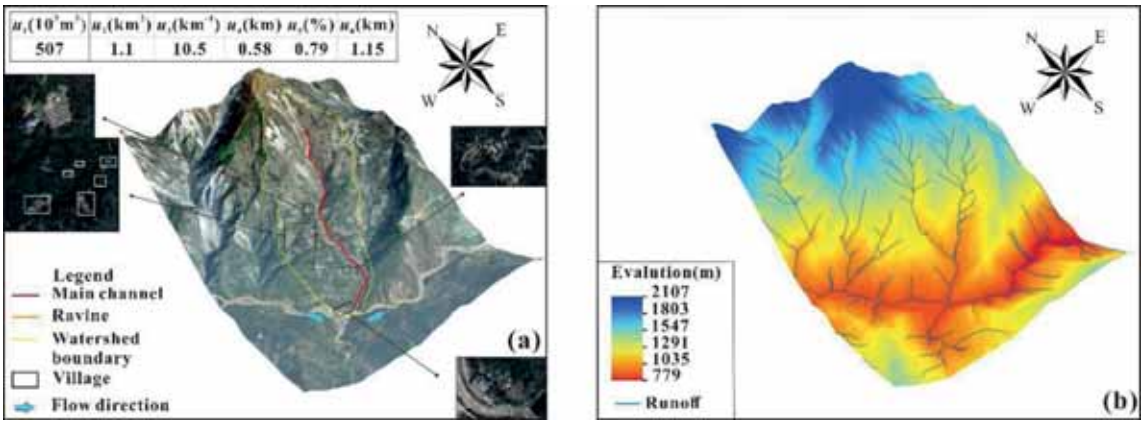
Notes: (a) Three-dimensional topographic image; (b) Elevation image.

FIGURE 6
Xishanpogou debris flow.



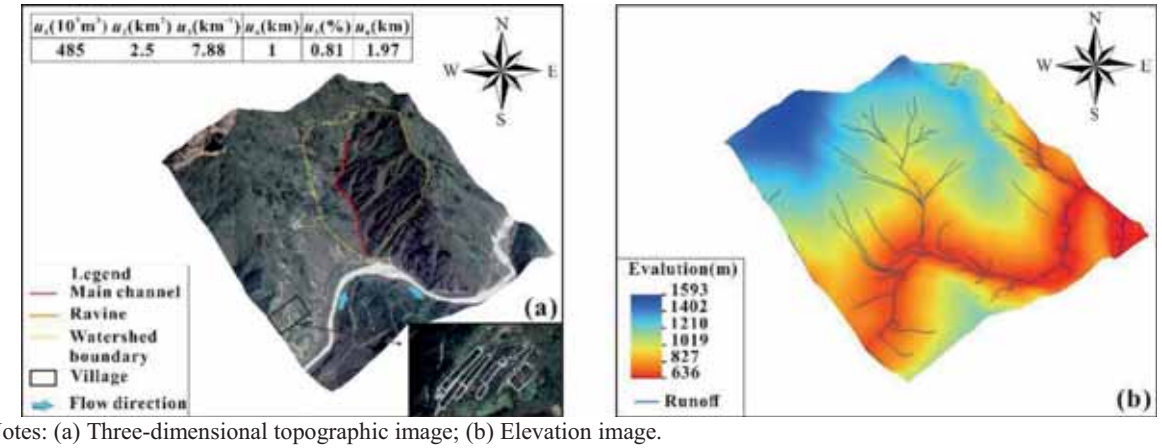
Notes: (a) Three-dimensional topographic image; (b) Elevation image.

FIGURE 7
Yuxuegou debris flow.



Notes: (a) Three-dimensional topographic image; (b) Elevation image.

FIGURE 8
Subaogou debris flow.



Notes: (a) Three-dimensional topographic image; (b) Elevation image.

FIGURE 9
Wangjiayangou debris flow.

It is worth noting that the risk of debris flow in Xishanpogou, Yuxuegou, Subaogou, and Wangjiayangou in the method proposed in this paper is higher than the method proposed by Liu and Tang [20]. The assessment levels of Xishanpogou, Yuxuegou, Subaogou, and Wangjiayangou debris flows in the proposed method are "High", "Severe", "Severe", and "Severe" respectively, and the assessment levels of Liu and Tang are all "Moderate". The three-dimensional topographic images and elevation images of the 4 debris flows are shown in Figures 6~9. The survey statistics of 4 debris flows are also shown in Figures 6~9. It can be seen from the figures that the distances between the main channel of the 4 debris flows and the nearby villages are 0.32km, 0.11km, 0.14km, and 0.86km.

Therefore, from disaster prevention and mitigation, it is reasonable to regard these 4 debris flows as a higher risk level.

DISCUSSION AND CONCLUSIONS

The weight of probability-based combined method. It could be shown from Table 3 and Figure 2, the weights of the assessment factors calculated by the 4 methods are quite different. The weights calculated only on the main channel length are consistent (the weights calculated by the equal weight method, the maximum deviation method, the entropy method, and the probability-based combined method correspond to 0.17, 0.18, 0.16, and 0.17, respectively).

As a simple weight assignment method, the equal weight method is unreliable. The equal weight method used in this paper is mainly to limit the boundary. In this paper, the equal weight method is mainly used to limit the boundary to avoid too large or too small. In the entropy method, because it is based on reflecting the degree of disorder of the data, the greater the randomness and disorder of the data, the more critical this indicator is. In this paper, the individual differences in loose source material reserves in the debris flow circulation area are substantial, with the largest being $1967\times10^3m^3$ and the smallest being only $0.04\times10^3m^3$. Therefore, the weight obtained by the entropy method in the assessment factor "loose source reserves" is 0.44. However, the weight of the assessment factor "Drainage density" obtained by the entropy method is only 0.03, which almost ignores the influence of the drainage density. This result is unreasonable. The difference between the maximum deviation method and the entropy method is that the maximum deviation method considers the deviation of the data from the average. Among the 72 debris flows in this paper, medium and small debris flows account for the majority. The weight calculated by the maximum deviation method will affect the risk assessment results of large debris flows. Given the performances of the two methods, the weight obtained by probability-based combined within the boundary conditions avoids overemphasizing the importance of a specific factor and considers the difference of the influence of each factor on the risk of debris flow.

Fuzzy method. The application of fuzzy mathematics theory in the risk assessment of debris flow has solved the hard-to quantify-problem. The FCE method is used to realize the quantitative and qualitative assessment of the of debris flow risk. In this paper, the FCE method is used to classify the debris flow risk, and the risk level is subdivided into 5 categories, namely, "Minuscule", "Slight", "Moderate", "Severe", "High". From Table 4 and Figure 4, it can be concluded that there are 72 debris flows in the study area, a total of 33 debris flows are in "Moderate" and above. And it can be seen from Figure 4 that these 33 debris flows are mainly concentrated near the Qingpianhe river in the south-central Beichuan County and the Beichuan-Yingxiu fault zone in the northeast. This result is also consistent with the distribution characteristics of the debris flow after the earthquake in Beichuan County. At the same time, the selected membership function is "trapezoidal distribution", which is simple in form and simple in calculation process. Its feasibility in the risk assessment of debris flow has been proved [8, 21]. It is worth noting that when following the principle of maximum membership degree, the membership degree of the two risk levels may be very close. For example, the membership degrees of Chaimazigou#2 in the five risk levels in this paper are: 0.123, 0.409, 0.404, 0.142, 0.003. If the principle of maximum membership is followed, Chaimazigou#2 should be classified as a "Slight" corresponding to 0.409. However, the membership degree corresponding to "Moderate" 0.404 is only 0.005 smaller than 0.409. It should be more reasonable to classify Chaimazigou#2 as "Moderate". Therefore, this paper adopts the minimum deviation optimization method to optimize the membership degree of 72 debris flows. The results in Table 4 are all optimized through minimum deviation.

(1) Based on the susceptibility characteristics of debris flow after the earthquake in Beichuan County, the loose source material reserves, the basin area, the drainage density, the basin relative relief, the shifting bed proportion, and the main channel length are selected as risk assessment factors.

(2) When the recharge water temperature is 25°C, the Probability-based combined method is proposed to optimize the weight assignment method, and the weight is regarded as a uniform and bounded random variable. Combine the weights calculated of equal weight method, entropy method, and maximum deviation method to determine boundary conditions, and implement it through Monte Carlo simulation. It avoids the influence of the methodological defects of the entropy method and the maximum deviation method on the weight assignment, and the weight obtained is more objective than using a specific weight determination method.

(3) A total of 20 debris flows in the earthquake area were "Severe" and "High", accounting for 28% of the total debris flows in Beichuan County. In the proposed method, the risk levels of debris flow in Xishanpogou, Yuxuegou, Subaogou and Wangjiayangou are higher than the method proposed by Liu and Tang.

ACKNOWLEDGEMENTS

Thanks to the Scientific and Technological Research Program of Chongqing Municipal Education Commission (Grant No. KJQN2019 01221, KJQN201901239, KJQN201901241, KJQN2020 01218, KJQN202001219), General program of Chongqing Natural Science Foundation (Grant No.cstc2019jcyj-mscm1865)，Special key program of Chongqing Technology Innovation and Application Development (Grant No.cstc2019jscx-tjsbX0015) and Open fund of Chongqing Three Gorges Reservoir Bank Slope and Engineering Structure Disaster Prevention and Control Engineering Technology Research Center (SXAPGC21 ZD01).

REFERENCES

[1] Liang, W., Zhuang, D., Jiang, D., Pan, J., Ren, H. (2012) Assessment of debris flow hazards using a Bayesian Network. Geomorphology. 171, 94-100.

[2] Perov, V., Chernomorets, S., Budarina, O., Savernyuk, E., Leontyeva, T. (2017) Debris flow hazards for mountain regions of Russia: regional features and key events. Natural Hazards. 88(1), 199-235.

[3] Su, J., Zhou, X., Fan, S. (1993) A fuzzy set evaluation method of hazard degree of debris flow. Journal of Natural Disasters. 1993(02), 83-90.

[4] Lee, D., Cheon, E., Lim, H., Choi, S., Kim, Y., Lee, S. (2020) An artificial neural network model to predict debris-flow volumes caused by extreme rainfall in the central region of South Korea. Engineering Geology. 105979.

[5] Zhou, L., Wu, X., Xu, Z., Fujita, H. (2018). Emergency decision making for natural disasters: An overview. International Journal of Disaster Risk Reduction. 27, 567-576.

[6] Lin, J., Chen, C., Peng, C. (2012). Potential hazard analysis and risk assessment of debris flow by fuzzy modeling. Natural Hazards. 64(1), 273-282.

[7] Tan, C., Ma, D., Chen, J., Zhang, W., Xu, X. (2020) Debris Flow Risk Assessment in Wudongde Reservoir Area Based on Analytic Hierarchy Process and Fuzzy Comprehensive Evaluation. In IOP Conference Series: Earth and Environmental Science. 570(4), 042053.

[8] Niu, C., Wang, Q., Chen, J., Zhang, W., Xu, L., Wang, K. (2015) Hazard assessment of debris flows in the reservoir region of wudongde hydropower station in China. Sustainability. 7(11), 15099-15118.

[9] Zhang, W., Chen, J., Wang, Q., An, Y., Qian, X., Xiang, L., He, L. (2013) Susceptibility analysis of large-scale debris flows based on combination weighting and extension methods. Nat. Hazards. 66, 1073-1100.

[10] Shi, M., Chen, J., Sun, D., Zhang, X. (2015) Assessing debris flow susceptibility in mountainous area of Beijing, China using a combination weighting and an improved fuzzy C-means algorithm. Chemical Engineering Transactions. 46, 697-702.

[11] Shi, M., Chen, J., Song, Y., Zhang, W., Song, S., Zhang, X. (2016) Assessing debris flow susceptibility in Heshigten Banner, Inner Mongolia, China, using principal component analysis and an improved fuzzy C-means algorithm. Bulletin of Engineering Geology and the Environment. 75(3), 909-922.

[12] Liang, Z., Wang, C., Han, S., Ullah Jan Khan, K., Liu, Y. (2020) Classification and susceptibility assessment of debris flow based on a semi-quantitative method combination of the fuzzy C-means algorithm, factor analysis and efficacy coefficient. Natural Hazards and Earth System Sciences. 20(5), 1287-1304.

[13] Cui, S., Wang, G., Pei, X., Huang, R., Kamai, T. (2017) On the initiation and movement mechanisms of a catastrophic landslide triggered by the 2008 Wenchuan (Ms 8.0) earthquake in the epicenter area. Landslides. 14(3), 805-819.

[14] Fan, R., Zhang, L., Wang, H., Fan, X. (2018) Evolution of debris flow activities in Gaojiagou Ravine during 2008-2016 after the Wenchuan earthquake. Engineering Geology. 235, 1-10.

[15] Wang, Y. (2009) Hazard assessment on rainstorm induced debris flows in Beichuan County of Wenchuan earthquake affected area (Doctoral dissertation, Master Thesis, Chengdu: Chengdu University of Technology (Thesis). 32-36.

[16] Zhang, W., Li, H., Chen, J. (2011) Comprehensive hazard assessment and protection of debris flows along Jinsha River close to the Wudongde dam site in China. Natural Hazards. 58(1), 459-477.

[17] Jian, S., Jun, R., Feng, X. (2016) Assessment on debris flow risk based on fuzzy comprehensive evaluation method. Journal of Catastrophology. 31(02), 171-175.

[18] Shen, S., Xie, H., Xu, Y., Zhang, M., Niu, X., Li, G. (2020) Fuzzy comprehensive evaluation of debris flow in Matun village, Laomao Mountain area, Dalian city. Arabian Journal of Geosciences. 13(2), 1-10.

[19] Běhounek, L., Cintula, P. (2005) Fuzzy class theory. Fuzzy Sets and Systems. 154(1), 34-55.

[20] Liu, X., Tang, C. (1995) Debris-Flow Risk Evaluation. Science Press: Beijing, China. 19-22.

[21] Chen, X., Cui, P., You, Y., Chen, J., Li, D. (2015) Engineering measures for debris flow hazard mitigation in the Wenchuan earthquake area. Engineering Geology. 194, 73-85.

Received: **01.03.2021**
Accepted: **02.04.2021**

CORRESPONDING AUTHOR

Li Li
Dept. of Civil Engineering
School of Civil Engineering
Chongqing Three Gorges University
Wanzhou 404100 – China

e-mail: 652344220@qq.com

© by PSP Volume 30– No. 09/2021 pages 10625-10632 Fresenius Environmental Bulletin

RESEARCH ON THE PLANNING METHOD OF SHARED SPACE IN OLD RESIDENTIAL DISTRICT BASED ON THE IMPROVEMENT OF ECOLOGICAL ENVIRONMENT

Chao Chen, Qiang Lu*

College of Humanities, Xi'an Shiyou University, Xi'an, Shaanxi, 710065, China

ABSTRACT

In order to improve the comfort and functions of the old living shared space environment, and enhance the suitability of the shared space ecological environment, in this paper, an old living area shared space planning method based on the improvement of the ecological environment is proposed. The ENVI-met model combined with one-dimensional and three-dimensional algorithms was established, and the microclimate environment was simulated through the calculation of the thermal stress relationship between vegetation and air. In addition, the shared space in the old residential area is planned from four aspects: architectural layout, activity venues, landscape greening and road organization. According to the simulation results of ENVI-met, the layout of the building and the location of the event venue were planned by "bearing the shade and embracing the sun" and side by side/staggered layout. In the end, road grades and transportation methods combined with plant morphological characteristics were used to complete road organization and landscape greening planning. The experimental results show that the shared space planned by this method can ensure the best environmental suitability and sunshine effect. After planning, its temperature drops by an average of about 1.2 °C, which can improve the comfort of the human body in the shared space.

KEYWORDS:
Ecological environment, old residential area, shared space, planning method, planning strategy, building layout

INTRODUCTION

The spatial planning method refers to the method adopted by the public sector to influence the future distribution of living space. Shared space refers to the space used by the public, which has the characteristics of publicity, openness and sociality. In addition, shared space can realize people's needs for different environments and increase the interaction between people [1]. The improvement of the ecological environment is also called the construction of the ecological environment, and its main purpose is to improve the ecological environment through environmental planning, plant planting and other means, and build a good living environment. Residential areas are the basic part of urban development, and old residential areas are part of urban residential areas, which play an indispensable role in the sustainable development of cities [2]. The development plan of the city needs to link production, living and ecological space together to realize the efficient integration of production space. Due to the long service life of the old residential area, its functional facilities can no longer meet the material and spiritual needs of current residents [3]. Therefore, under the promotion of urban development planning, its shared space planning needs to meet the needs of urban development.

For the planning of shared spaces in old residential areas, most scholars have shifted their renewal model from large-scale reconstruction to a model with protection and maintenance as the main content. There are also some scholars suggesting that full attention should be paid to building quality and energy conservation and environmental governance in the planning of shared spaces. However, Chinese scholars mainly consider economic factors, and believe that large-scale demolition of buildings for shared space planning has destroyed the historical features and urban characteristics of the original residential area to a certain extent. Some scholars pointed out that a set of relatively complete reform strategies should be put forward from the aspects of humanities, economy, and society. On the whole, the above strategies usually fail to achieve the dual requirements of ecological protection and quality of life improvement. In order to improve the comfort and functions of the old living shared space environment, and enhance the suitability of the shared space ecological environment, in this paper, an old living area shared space planning method based on the improvement of the ecological environment is proposed. This strategy can not only realize the planning and renewal of regional roads, landscapes, greening,

etc., but also meet the needs of residents for life.

MATERIALS AND METHODS

From the perspective of improving the ecological environment of the microclimate, in this paper, we systematically study the planning method of the old residential shared space based on the improvement of the ecological environment. The so-called microclimate is a means to improve the ecological environment, which has a greater correlation with human living environment and human comfort [4]. The microclimate has a very clear zoning feature, which is formed by the mutual influence of many factors. Therefore, different regions will show differentiated climatic characteristics [5]. According to the average state of atmospheric statistics, combined with the spatial scale, climate can be divided into macroclimate and microclimate [6]. Based on this, through the construction model and the proposal of planning strategy, the planning of the shared space in the old residential area is realized. Finally, taking an old residential area in X city, China as an example, the application effect of the method in this paper is verified.

Simulation software. (1) ENVI-met model structure. In microclimate research, computational fluid dynamics numerical simulation is its main simulation technology. The technology is flexible in application, the geometric shape and boundary conditions of the residential area have minimal influence on it, and the time and space resolution of the simulation results of the local area is high [7]. There is many commonly used software for computational fluid dynamics numerical simulation. In this paper, we choose ENVI-met simulation software to complete the simulation.

The ENVI-met simulation software is a three-dimensional numerical simulation software, and its simulation of the microclimate environment can be completed by calculating the thermal stress relationship between vegetation and air [8-9]. The output parameters of the software include atmospheric parameters, plant parameters, radiation parameters, building parameters, soil parameters, and outdoor thermal environment indicators.

In order to ensure the accuracy of the simulation results, the three-dimensional model and the one-dimensional model are combined to complete the establishment of the ENVI-met simulation model. The model structure is shown in Figure 1.

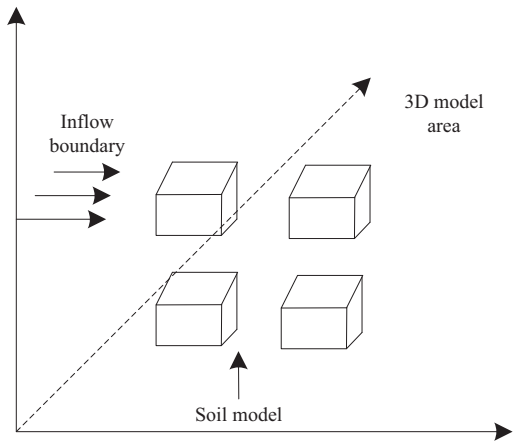


FIGURE 1
Structure of ENVI-met model.

Figure 1 shows the three necessary files required by the ENVI-met simulation model during the simulation process, which are model files, database files, and simulation configuration files. They are used to simulate the distribution of regional vegetation and buildings; the definition of stratum structure, soil type, and plant morphological characteristics; file path, initial temperature, wind field and pollution source and other sub-model settings. Through the reading and calculation of the model file, the relevant parameters of the three-dimensional model are finally output, such as atmospheric environment and soil parameters [10-11].

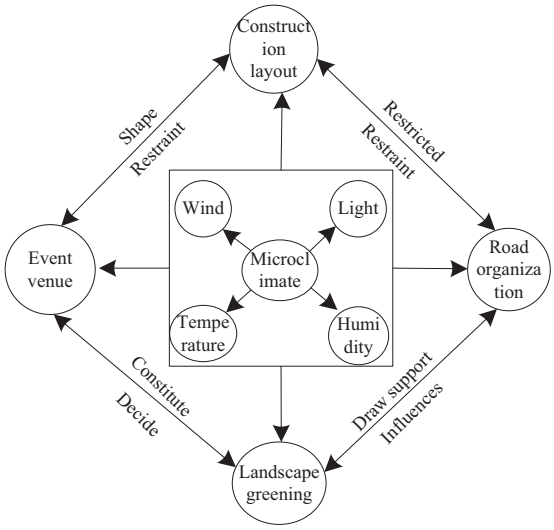


FIGURE 2
Correlation between microclimate and the elements of shared space environment.

(2) Setting of parameters in ENVI-met model. In order to improve the computational efficiency of the ENVI-met model, it is necessary to set the initial environmental parameters of the model in the simulation process. Simulation time is 48 h, 12 m high wind speed is 1 m/s, initial air temperature is

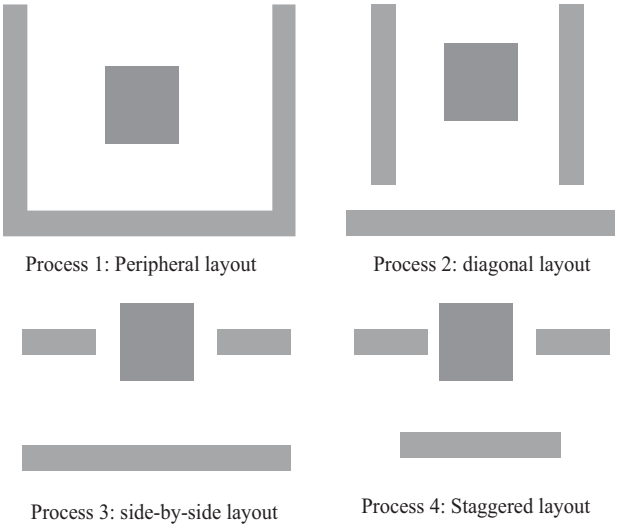


FIGURE 3
Architectural layout of isomorphic evolution.

305 k, 2 450 m height moisture content is 8 g water/kg air, 2.5 m high relative humidity is 85, initial surface temperature is 295 k. The initial surface relative humidity is 55, the temperature and humidity field is open, and the turbulent boundary field is closed forced.

Planning strategy of shared space in old residential district. (1) Shared space planning strategy. In this paper, we have completed the shared space planning of old residential areas from four aspects, namely, architectural layout, activity venues, landscape greening, and road organization [12]. The microclimate affects the environment of the shared space through different angles, and the correlation between them is shown in Figure 2.

In the process of spatial planning and layout of buildings with shared spaces, the following points should be combined:

<1> On the basis of ensuring safety, a comfortable space plan is implemented based on the residents' psychological and physical needs.

<2> The factors affecting the daily activities of residents should be analyzed, and the layout of the activity space should be completed through rational space layout planning.

<3> The greening of the shared space should be based on the climate, objective conditions and the subjective habits of residents.

(2) Planning strategy for building layout and location of event venues. The ENVI-met model is used to simulate the lighting and wind environment of different building layouts and the location of the event venue in the shared space of the old residential area. According to the relationship between building layout and microclimate, the best building layout can be determined as "bearing Shade and embracing Sun". Moreover, the location of the shared activity space is consistent with it [13-14]. Therefore, combined with scientific methods, the evolution of the planned architectural layout is shown in Figure 3.

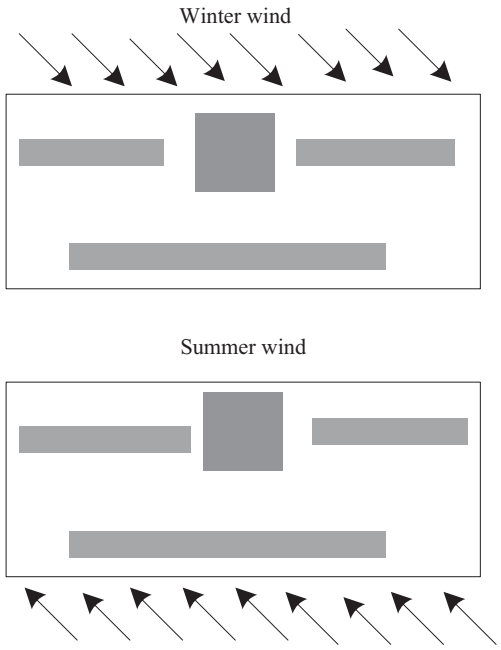


FIGURE 4
Ventilation simulation results of shared space event venues.

According to different layouts, the shared space event venue needs to meet the standards of shelter from wind in winter and ventilation in summer. Therefore, the ENVI-met model was used to analyze the coupling relationship between the layout of the building and the winter monsoon and summer monsoon. The results are shown in Figure 4.

In the simulation results, the square-shaped

area is a standard area that meets wind shelter in winter and ventilation in summer. Therefore, in the evolution of the building layout, the surrounding layout buildings are tightly enclosed, which can meet the winter wind shelter, but cannot meet the summer ventilation standards. The oblique layout cannot balance the ventilation effect of the venue. However, the side-by-side type and the staggered type meet the standards of winter shelter and summer ventilation, and can also ensure the comfort of the venue environment. Therefore, the side-by-side or staggered layout is selected as the planning layout of the shared space in the old residential area [15].

(3) Road organization and landscape planning strategy. As roads are part of the shared space environment in old residential areas, the microclimate environment will be affected by changes in the direction of road organization. The road organization is divided into residential district-level roads, residential group-level roads and inter-house roads according to their levels; there are three modes of transportation: cars, bicycles and walking [16]. With reference to the above points, on the basis of ensuring the coordination of traffic in the entire shared area, road organization should divert people and vehicles, and plan parking spaces reasonably. Then, in this paper, the road planning can be completed according to different levels or different traffic modes in the road planning process, and the result is shown in Figure 5.

After road planning, landscape greening shall be implemented. The greening of the landscape is mainly based on grass and trees, and its selection is mainly based on beauty, use and noise reduction. The difference in the height of landscape greening will affect the wind environment in the space and the sunshine environment [17-18]. Therefore, it has a regulating effect on the microclimate environment of the shared space. There are many types of landscape greening plants, and the morphology of each plant is different, and its regulating effect on the environment is also different. Tall plants can be seen as low-rise buildings, with their trunks and branches clearly differentiated. Therefore, the trunk part will not obstruct the airflow, thereby ensuring the ventilation effect of the low space [19]. The low bushes can be regarded as a wall, which can introduce wind into the space with low wind speed, so it can prevent the cold wind in winter. In addition, the reasonable planning of the landscape layout can improve the temperature and humidity of the shared space, thereby creating a comfortable shared space environment.

By studying the effects of different plants on the temperature of the shared space, it is determined that 4 green plants have better cooling effects [20-21]. That is, lawns can lower the temperature by 0.8 °C, trees can lower the temperature by 3.2 °C, shrubs can lower the temperature by 1.4 °C, and the artificial lake can lower the temperature by 1.4 °C.

In summary, the steps of the microclimate-based method for planning shared spaces in old residential areas are as follows:

<1> Adjust the architectural layout of the shared space to improve the basic climate environment of the space.

<2> Through the analysis and planning of the road organization of the event venues in the shared space, combined with the simulation effects of the winter and summer monsoons, the event venues and road organization planning strategies are determined.

<3> Combine the shapes and characteristics of different plants to determine the configuration of road landscape greening.



FIGURE 5
Road planning strategy.

RESULTS

In this paper, we take an old residential area in X City that has been established for 30 years as the research object. The area of the research object is 22,050 square meters. Because the residential area has been established for a long time, there is only a simple open-air exercise square in the area, thus the people's living comfort is poor.

In order to achieve a better planning effect of shared space, it is necessary to investigate the planning needs of the residents in the residential area. We implemented the survey methods of taking photos, visiting and surveying the residential area. Furthermore, statistics are made on its living space, the renewal history of shared space, and the living needs of the residents. The 200 most complete questionnaires and interview results were randomly selected as the target reference basis for the shared space planning of the residential area. In order to ensure the balance and validity of the results of the questionnaire, the 200 results are in different age ranges, among which the proportion of minors is 15%, the proportion of 18 to 35 years old is 32%, the proportion of 35 to 55 years old is 28%, and the proportion of 55 years old or older is 25%.

According to the results of the questionnaire, the needs of the residents in this area for shared space planning are mainly divided into two aspects: too few event venues and poor greening in scenic spots. And after actual investigation, it is found that the residential area lacks humanized design for the elderly. Therefore, when planning it, the above-mentioned requirements will be perfected.

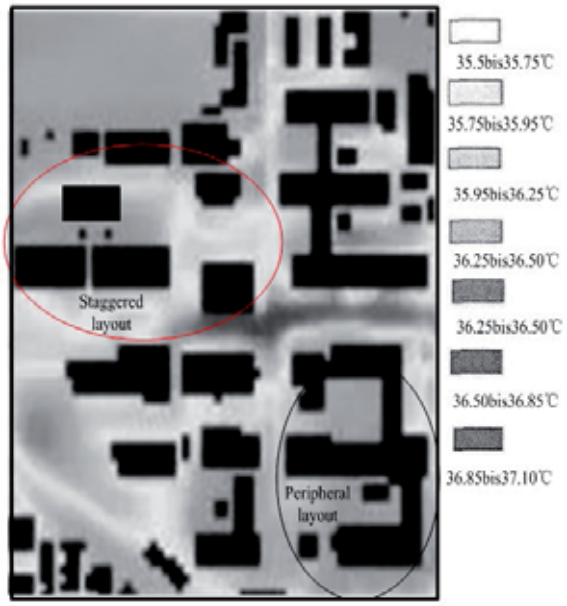


FIGURE 6
Layout simulation results.

The ENVI-met model was adopted to simulate the shared space planning of the research object. The advantages of the layout method are measured by the temperature changes around the area after different layout methods, and the simulation results are shown in Figure 6.

According to the simulation result of Figure 6, it can be seen that after the staggered layout, the ambient temperature around the shared space is lower than that after the peripheral layout. This shows that the use of staggered layout to complete the spatial planning of the shared area of the experimental subjects has the best effect.

The typical seasonal winds in summer and winter at 1.5 m elevation are selected, which are north-northwest wind and south-southeast wind respectively, and the wind speeds are 2.58 m/s and 3.08 m/s, respectively. The ENVI-met model was used to simulate the wind environment, and then tested the sunlight conditions at different venue locations (as shown in Figure 6) under different seasonal wind conditions. The result is shown in Figure 7.

According to the test results in Figure 7, it can be seen that the staggered layout has better solar illuminance, and the peripheral layout has poorer solar illuminance. This result is consistent with the temperature change results in Figure 6. This shows that the staggered layout can ensure better sunlight while realizing temperature regulation. Therefore, in this paper, the staggered layout is selected as the layout of the shared space planning of the test object.

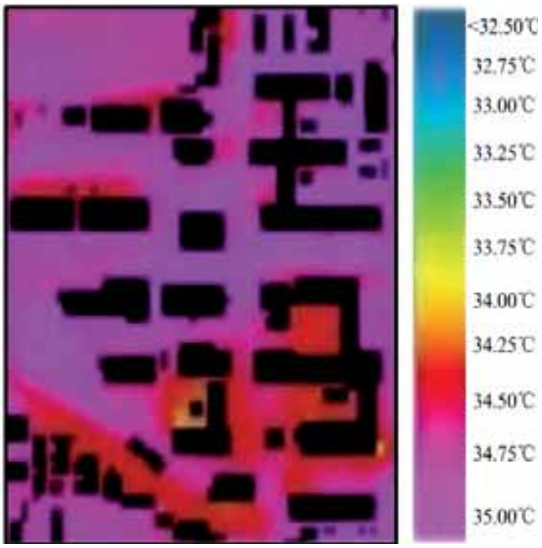


FIGURE 7
Sunshine test results.

According to the test results in Figure 6 and Figure 7, the effect of the shared space layout after simulation planning is shown in Figure 8.

The 11 locations in Figure 8 are selected as the simulation nodes of the activity site, and the microclimate environment results of each node before and after the planning are tested. While measuring

TABLE 1
Comparison of results before and after planning.

Planning situation	Location node	Wind speed (m/s)		Sunshine time (h)
		Winter	Summer	
Before planning	A	1.21	0.76	1.6
	B	0.91	0.76	1.6
	C	0.61	0.76	3.6
	D	0.61	1.76	1.6
	E	2.01	2.51	2.6
	F	1.81	0.51	1.6
	G	0.91	0.51	2.7
	H	0.91	1.51	3.5
	I	1.81	1.51	1.4
	K	0.91	0.36	1.6
	J	0.91	1.01	2.1
After planning	A	0.51	1.02	2.6
	B	0.21	1.28	4.2
	C	0.91	1.95	3.6
	D	0.61	2.05	4.1
	E	0.92	1.56	2.5
	F	0.65	1.17	2.7
	G	0.32	1.40	3.1
	H	0.93	1.55	3.6
	I	0.62	1.15	3.6
	K	0.87	1.35	2.7
	J	0.95	1.30	3.5

whether it can meet the sunshine standard of 2.5 h/d after the plan, the summer and winter monsoons at each node are respectively greater than 0.82 m/s and less than 2.68 m/s as the space planning standard. The results are shown in Table 1.

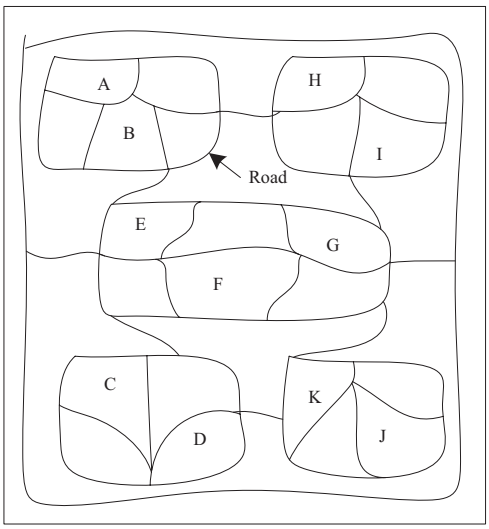


FIGURE 8
Simulation effect of shared space planning of experimental objects.

According to the simulation test results in Table 1, most of the nodes before the planning did not meet the sunshine standards and the environmental standards for summer and winter winds, and only a few node locations met the above standards. After planning, all location nodes meet all the above standards, which can ensure the environmental comfort in the shared space. This shows that the shared space environment after planning by the method in this paper is relatively comfortable.

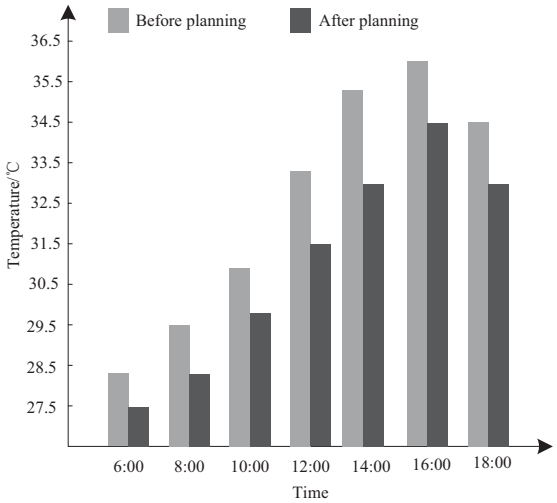


FIGURE 9
Comparison results before and after planning.

In order to measure the actual effect of the shared area planned by the method in this paper, the

comfortable temperature of the human body in the shared space at different temperatures is simulated. The location node C is randomly selected, and the human body comfort before and after planning is simulated for 12 hours in the summer. The result is shown in Figure 9.

According to the test results in Figure 9, it can be seen that the comfortable temperature of the human body after planning is better than that before planning, and the average body temperature drops by about 1.2 °C. It shows that after the method is planned in this paper, the human body comfort can be improved in the shared space. Therefore, it can also meet the life needs of the elderly and has good practicability.

CONCLUSIONS

(1) In this paper, an old living area shared space planning method based on the improvement of the ecological environment is proposed. The ENVI-met model combined with one-dimensional and three-dimensional algorithms was established, and the microclimate environment was simulated through the calculation of the thermal stress relationship between vegetation and air.

(2) In addition, the shared space in the old residential area is planned from four aspects: architectural layout, activity venues, landscape greening and road organization. According to the simulation results of ENVI-met, the layout of the building and the location of the event venue were planned by "bearing the shade and embracing the sun" and side by side/staggered layout.

(3) In the end, road grades and transportation methods combined with plant morphological characteristics were used to complete road organization and landscape greening planning. The experimental results show that the shared space planned by this method can ensure the best environmental suitability and sunshine effect. After planning, its temperature drops by an average of about 1.2 °C, which can improve the comfort of the human body in the shared space.

ACKNOWLEDGEMENTS

The work was not supported by any funds. We hope to thank all the techniques who have helped this research and all the authors of the references.

REFERENCES

[1] Liu, S., Liu, L. (2020) Research on Regional Ecological Spatial Elasticity Planning Based on Ecological Security-Taking Tengzhou City, Shandong Province as an Example. Chinese Landscape Architecture. 36(2), 11-16.

[2] Dong, J., Zuo, J., Li, C., Fan, D., Wu, Y. (2018) High-density urban ecological space planning method from the perspective of urban regeneration: Taking the special planning of the three-dimensional greening of Xiamen Island as an example. Acta Ecologica Sinica. 38(12), 4412-4423.

[3] Zhu, L., Gu, K., Fang, Y. (2019) Research on the relationship between the spatial morphology of urban residential areas and PM_(2.5) concentration based on ENVI-met. Journal of Ecological Environment. 28(8), 1613-1621.

[4] Zhao, D., Xu, J., Gao, S., Xu, H. (2020) Sponge Park Green Space Social Benefit Evaluation Based on Improved 2SFCA Accessibility Modeling-Taking Zhenjiang City Sponge City Construction Pilot Area as an Example. Ecological Economy. 36(11), 221-227.

[5] Tsoka, S., Tsikaloudaki, K., Theodosiou, T. (2019) Coupling a Building Energy Simulation Tool with a Microclimate Model to Assess the Impact of Cool Pavements on the Building's Energy Performance Application in a Dense Residential Area. Sustainability. 11(9), 1-16.

[6] Xing, Z., Yu, Q., Gu, Y., Zhou, Q., Ye, L. (2019) Research on Green Space Planning Method Based on Urban and Rural Spline Zoning. Urban Planning. 43(4), 24-40.

[7] Yu, K., Qi, S., Gong, J. (2019) Exploration of a new collaborative path of rural industry revitalization and spatial planning based on ecological adaptability. Ecological Economy. 35(03), 224-229.

[8] Favretto, A., Souza., Léa, C. (2019) A meta-analysis over geometric modeling simplifications in ENVI-met urban climate simulation. Ambiente Construído. 19(1), 143-160.

[9] Rita, L. (2019) Problems of Space Shaping in the Surroundings of Former Manors as Presented on Selected Examples in Cracow (Poland). IOP Conference Series: Materials Science and Engineering. 471(11), 112019-112019.

[10] Gao, S., Dong, Y., Zhang, L., Jiang, X., Ye, Y., Chen, J. (2019) Research on the space development management and control of national new districts based on the carrying capacity of resources and environment. Acta Ecologica Sinica. 39(24), 9304-9313.

[11] Liu, Y., Bai, Y., Ma, Y. (2020) A study on the pleasant value of green space in urban residential areas in arid oasis based on willingness to pay. Arid Zone Geography. 43(04), 1088-1097.
[12] Simon, M., Yang, J., Zheng, Y., Jonathan, R. (2019) Relevance, Mechanism, and Governance: Research on the Environmental Construction of High-density City Walkability Based on Microclimate Evaluation. International Urban Planning. 34(5), 16-26.
[13] Wang, J., Li, Z., Song, Z., Fang, Y., Liu, J., Zhai, T. (2019) Land and space planning methods and practices towards sustainable urban ecosystem management: Taking Yantai as an example. China Land Science. 33(09), 9-18.
[14] Orlov, E. (2020) Space-planning decisions of sanitary facilities of residential buildings in Russia. IOP Conference Series Materials Science and Engineering. 869, 042010.
[15] Li, K., Zhang, H., Zhao, L. (2020) Research on the optimal configuration of outdoor space landscape elements in residential areas in hot and humid areas based on empirical thermal comfort indicators. Building Science. 36(10), 158-166.
[16] Du, R., Huang, X., Hu, D. (2020) The construction of planning system for decentralized construction areas from the perspective of land and space planning. Planner. 36(19), 47-51.
[17] Li, C., Yu, M., Li, C. (2019) Research on the Renewal of Suitable Aging Landscape in Shenyang Old Residential District Based on Comfortability Optimization-Taking Xiushan District as an example. Chinese Garden. 35(1), 23-28.
[18] Kaparias, I., Wang, R. (2020) Vehicle and Pedestrian Level of Service in Street Designs with Elements of Shared Space. Transportation Research Record Journal of the Transportation Research Board. 2674(9), 036119812093362.
[19] Wang, Y., Yi, Z., Wang, F., Li, Q. (2019) The current situation and development direction of spatial planning geographic information resource sharing. Planner. 35(21), 5-10.
[20] Zhu, X., Ye, C., Li, S. (2020) Research progress of sustainable cities and their implications for territorial and spatial planning. Journal of Natural Resources. 35(9), 2120-2133.
[21] Shahhoseini, Z., Sarvi, M. (2019) Pedestrian crowd flows in shared spaces: Investigating the impact of geometry based on micro and macro scale measures. Transportation Research Part B Methodological. 122, 57-87.

Received : 07.03.2021
Accepted: 01.05.2021

CORRESPONDING AUTHOR

Qiang Lu
College of Humanities,
Xi'an Shiyou University,
Xi'an Shaanxi 710065 – China

e-mail: open1201@126.com

© by PSP Volume 30– No. 09/2021 pages 10633-10642 Fresenius Environmental Bulletin

ANALYSIS OF THE EFFECT OF URBAN CHANGE ON URBAN SILHOUETTES BY ENTROPY METHOD

Cengiz Acar[1,*], Alper Uzunali[2]

[1]Karadeniz Technical University, Department of Landscape Architecture, Trabzon, Turkey
[2]Hatay Mustafa Kemal University, Department of Landscape Architecture, Hatay, Turkey

ABSTRACT

The urban population, and consequently urban development, have increased in recent years and the urban silhouettes have been greatly affected. The aim of this study is to reveal how urban development affects urban skylines and urban identity aesthetically. The photographs of the eastern, northern and western fronts of Boztepe, an important landmark of the city of Trabzon, from the 1900s, 1950s and 2000s, were examined using the concept of entropy where the aesthetic measure could be digitized and the data were obtained. As a result of the comparisons, the positive and negative effects of urban development on urban silhouettes were digitized. It was determined that the uncontrolled development of cities negatively affected the city skylines. The impacts of the new projects are determined in advance and suggestions are given to take the necessary measures.

KEYWORDS:
Silhouette, Skyline, City Silhouette, Silhouette Analysis, Entropy, Digitization of Esthetics

INTRODUCTION

Human beings have started to migrate to cities because they think that they can easily reach basic needs such as water, electricity and heating with the developing technology and they think they can lead their lives more comfortably. As a result of this migration, the inadequacy of the establishment of the center has improved the settlement of the city. Rapid urbanization has led to irregular urbanization. Recreation areas and natural areas were destroyed and the city grew towards these regions [1]. This situation has caused green areas to transform into structural areas over time.

The impact of the increasing population in urban centers is not only the diminishing green areas. Factors such as factories established to provide employment with the increase in human population, increasing urban vehicle traffic, shelter and heating need, and increased flue smoke increased CO_2 emissions, and greatly affected the city's air and living population in the city [2-3].

Population change and consequently increased construction caused visual and aesthetic changes in the city from inside and outside. This change has taken people away from the nature they belong to, has negatively affected them psychologically and caused the existing identities of cities to be disrupted. The most important elements that make up the city identity are the topography, vegetation, historical structures and city plans specific to that city. These are the highlights of the city. The emphasis points found by the effect of urban growth have lost their value, changed or disappeared [4].

Urban identity can be strengthened by preserving its unique historical texture and natural beauties from the past. Correct city plans contribute greatly to this situation. If the planning is done correctly, both the visual quality of the people living in the city and the quality of the city identity and silhouette will increase.

According to Max Wertheimer, the human brain is programmed to perceive the simple. It detects complex images by simplifying them. Silhouette is two-dimensional and simply perceptible, unlike other methods of view. This feature makes the silhouette different and useful on large scales.

The important factors that make up the skyline of a city are the high-rise buildings that are needed in the developing cities as well as the historical, cultural and geographical development of that city. City skylines; they consist of numerous panoramas according to their viewpoints and temporal changes. Nowadays, most cities are under the influence of high-rise buildings. These buildings both negatively affect the city in terms of aesthetics and reduce the effect of natural, historical and geographical structures that are aesthetically pleasing [5].

While urban planning, historical and cultural structures and newly rising buildings directly affect the silhouette, they also affect spatial organization and habitable space designs and as a result, the silhouette is also affected.

In urban development, some countries develop their cities by considering economic reasons rather than planning aesthetics, natural and urban identity. This has often been a major problem for underdeveloped or developing countries. Even if this planning seems economical for today, it may have bad economic consequences in the future [6].

Professions such as Landscape Architecture, Architecture and City Regional Planning consider topography, building, plant organization and plant community individually or together. Urban skylines are a major factor in the formation and perception of urban identity [7].

Important factors of urban skyline are urban function, regional image formation, topography shape and the city's capacity to form a skyline [6].

City skylines are a panoramic view of topography, urbanization, urban planning and plant compositions. While each of these units has individual effects, their effects together and on each other are very important. Like tall buildings topography-structure, topography-plant, structure-plant relations affect the aesthetics of that silhouette while examining the city skylines [8-9].

Wagemans revealed what human beings are actually more aesthetically approaching and what they consider more aesthetic. In this study, the basic principles determined by the human aesthetics were used for examining the aesthetics of images and observation values were obtained with these principles [10].

Guney et al. used 2D silhouette lines and made 3D analyzes while analyzing city silhouettes with Geographical Information Systems (GIS). They stated that with this application, geospatial objects can be detected better. Guney et al. stated in the 10-year cleaning analysis of Istanbul that especially high-rise buildings affected the city to a great extent. It has been suggested that the settlement planning of the city of Istanbul can be followed in a more efficient way through 3D maps, not 2D maps [5].

Karimimoshaver and Winkemann investigated the negative aesthetic effect of high-rise buildings on urban landscape using the Analytical Network Process (ANP) method on high-rise buildings such as the Main Tower, Opernturm and the European Central Bank in Frankfurt. In order to determine the aesthetic effect, the ratio of the visible surfaces of these structures to the field of view of the observers in an area of 2500m radius was used. A pictorial questionnaire filled out by 420 participants was used to determine the effect of the aesthetics of these three buildings on the city skyline. As a result of this study, Karimimoshaver and Winkemann determined that high-rise buildings are elements that express the greatest meaning in the silhouette line and change the aesthetic value greatly. It has been observed that the individual aesthetic values of high-rise buildings and the aesthetic values of the city skyline do not match [11].

Wang and Ogawa used the fractal method for visual analysis of natural and urban areas. They stated that the reason why they preferred the fractal method is that it is a method that can be applied regardless of scale and comes from nature and naturalness. In this study, a collection of natural and urban images, the counting method for black and white photographs, and the Brownian model for color photographs are discussed [12].

Wu et al. stated that the theory proposed by Claude Shannon was widely used in information science for many years. Shannon defined entropy with a random variable as a measure of complexity based on parameters. Wu et al., using these concepts, utilize a random image generator and obtained results by processing fewer image pixels with local Shannon entropy measurement according to the global Shannon entropy measurement. In addition, this study allows image comparisons [13].

Bostancı stated that the analysis of city silhouettes can be done by combining the parameters that make up the silhouette with the entropy of Shannon, the values obtained by a kind of counting method. Silhouettes taken from certain points of the city of Istanbul were transformed into 2D and 3D linear images using Geographical Information Systems, and the images to be used to determine the entropy method parameters were obtained. As a result of this study, Bostancı reveals that silhouettes can be evaluated as numerical data using the entropy method and this assessment method works successfully [14].

Aesthetics is expresses the relationship between order and disorder. The results of qualitative studies are obtained with large sample groups and statistical studies due to the differences of opinion of the participants. The results of quantitative studies are obtained with numerical data. In this study, parameters that can be used in digitization method were created by determining the building blocks of order and irregularity. Shannon Entropy was used to process the data in the most accurate way and to determine the complexity. If the aesthetics can be digitized, the plant designs, spatial designs, accuracy and aesthetics of the city plans will be measured and the in progress projects prepared can be evaluated numerically before implementation. The effects of in progress projects that are evaluated numerically on aesthetics will be determined.

Structural development, which affects aesthetics, changes with the perspective towards the silhouette, distance and vision barriers. With this study, a natural topography that affects the central silhouette of the city to a great extent has been evaluated with images obtained from three fronts without any obstacles.

In order to observe how urban development affects the city skylines, to prevent the ongoing urban development from further disrupting the city skylines, to change the identity of the city lost through small interventions if possible and to improve the city skyline, the change of Trabzon Boztepe example over the years is examined by visual digitization method.

MATERIALS AND METHODS

Materials. The name of Trabzon city is thought to come from the colonies of Miletus who founded the city. Trapezus, which means a table because its topographic structure resembles a flat and sharp-edged table, was used. Later, each new community replaced the word in its own meaning with names that resemble the first name. For example, it was named as Trab-ıEfsun by Fatih Sultan Mehmet because of its beautiful nature and clean air during the Ottoman Empire [15].

Although the geographical conditions of the city of Trabzon are very challenging in terms of road and settlement, the settlement and trade history dates back to 2000 BC. The city was founded in 756 BC [15].

Boztepe was used as a natural observation tower to protect the city from external dangers during and before the Ottoman Empire. After the establishment of the Turkish Republic, it was used by the armed forces and NATO as a base for the military and communication center. For this reason, settlements were far from Boztepe.

After the establishment of the Republic of Turkey, the city's plans for the first time were made in 1937 by the French Urban Planner Jacques Henri Lambert. At the core of this plan are wide corridors extending from the sea to the hills in order to reduce the humid air of the city as much as possible, to ensure wind circulation and most importantly to increase the city's integrity with the sea and transportation [16].

Lambert gave great importance to the historical texture of Trabzon in his planning. In addition to planning to preserve historical buildings, he respected the architecture of the city and made the planning thinking that this architecture should be preserved [16]. With the increase in migration to cities in the 1900s, adequate control could not be achieved and the plan prepared could not be followed. Planning has changed considerably with the later revised plans.

Located in the city center of Trabzon, reflecting the gloomy character of the city and considered as one of the important places of Trabzon with its magnificent view and natural beauty, Boztepe has started to be affected by these revisions in recent years.

Boztepe, which is the liver of the city with its natural beauty and plant population, was previously used in the recreation area. Later, due to the excessive rise of urban development and the limited construction area of Trabzon, many settlements became new construction sites.

The deterioration of the naturalness of Boztepe, which directly affects the silhouette of the city of Trabzon, which is considered to be the prominent feature of the city of Trabzon, and the continuation of unplanned construction adversely affected the identity and silhouette of the city. To detect the effects of this change, similar silhouette images were found for similar year intervals. Visual effects on these silhouettes have been studied.

Methods. Aesthetic value is influenced by many factors such as the environment in which the individual live, the mood they are in, the psychological state at hand, the environmental conditions such as educational status, cleanliness, naturalness, light effects from individual characteristics such as previous good or bad experience. While the aesthetic value of the environment is directly affected by the decisions and practices made by individuals or societies about the environment, it indirectly affects emotions and experiences [17].

Aesthetic is a variable value, but there are also accepted mathematical evaluation methods. These evaluations aim to get results by digitizing the aesthetic values by taking the averages of all parameters.

Aesthetic assessment methods actually go back to many years. The most important example of this is the Golden Ratio, which appears in many places. It is known that it was used in Ancient Egypt and Ancient Greek civilizations in the 3rd millennium BC. The best-known example of this is the Mona Lisa painting. The Golden Ratio is the most perfect distribution of an object. It has been observed that human body structures and faces, many occurrences of nature, many animals and plants make up this ratio. Golden Ratio is accepted as 1,618 [18]. The Golden Ratio exists directly in nature and in many current areas. This method pioneered other aesthetic digitization methods.

Thinking that aesthetic can be solved with a mathematical formula, Birkhoff has worked on this subject and become a pioneer. As a result of the researches, he found a formula of M = O / C (Aesthetic Value = Order / Complexity) to convert the aesthetic values of the forms into mathematical data. This has led to many scientists seeking to quantify aesthetics with their formulas and studies [18-19].

The evaluation of the aesthetic qualities of cities has long been among the issues of urban design research and development. Although these evaluations are generally abstract and personal, they have been used and have proved to be successful in numerical methods. Entropy is one of them [18].

The digitization method used in the study has emerged from the concept of Entropy. Almost all known physical processes in the universe can be explained by thermodynamics, the structured discipline for the operation of complex systems [20-21]. After studies on closed and isolated systems, thermodynamic studies were developed to investigate open systems such as ecosystems [22]. Many concepts developed in thermodynamics have been used in areas such as ecology, landscape ecology, architecture and urban planning [23-24-25-26-27].

The first law of thermodynamics, also known as conservation law, states that energy is always conserved in different states. The second law of thermodynamics or the entropy law states that the beneficial energy, which is also defined as exergy or working capacity, is destroyed and entropy is produced irregularly [27]. Entropy is a thermodynamic term in physics with the symbol "S". It ıdentifies irregularity and randomness.

Entropy is the law that tells us that everything in physics will either destroy or deteriorate. As these deteriorations increase, the entropy value increases. In other words, entropy is the value of irregularity or uncertainty. For example, if the probability of an event occurring or not occurring is the same, this leads to an increase in uncertainty. This means that the entropy level is maximum. However, if an event is more likely to occur, the uncertainty decreases and the entropy value decreases.

Entropy always has energy and always tends to move towards balance [28]. According to Capra, according to the second law of thermodynamics, there is a tendency in physical phenomena from order to disorder, to ever increasing entropy [18-29]. So, the universe always prefers irregularity and turns towards it. In our opinion, this disorder may be an order for the universe.

Studies on thermodynamics and Shannon entropy have been conducted in many scientific fields [30]. Additionally, entropy is suitable for studies presenting open spatial methods [31–32].

Cities are a complex and artificial ecosystem that shapes social and ecological processes, is organized under human domination, and has managed mechanisms [33]. These mechanisms are explained in part by current concepts, theories and approaches developed by ecological disciplines [33]. Urban growth, planning and aesthetic levels can be explained by entropy, the second law of thermodynamics [34].

Shannon studied the concept of entropy, revised the theory of information and discovered a method of finding measurable numerical value. With this method, entropy became quantifiable [35]. Shannon's work on entropy has become the accepted and preferred method by many. But many scientists, except Shannon, have tried to develop the method of entropy on many concepts. Renyi was applied to calculate the biodiversity ratio, and Tsallis was applied for studies in statistical fields and was successful [35].

Shannon, who was involved in the theory of information in entropy, revisited this equation and improved the mathematical structure. He used a two-sided logarithmic formula he developed to reduce the loss of information. In this way, he managed to turn entropy into a numerical value. The unit of the resulting value is called 'bit' [19].

$$\log_2 2^N = N$$

Shannon used the ratio of the number of events in the subclasses to the number of elements in the universal set to measure the probability values of the events in the subsets and calculated the uncertainty of the future of the subset in this set. This equation shown below is defined as 'Shannon's Informational Entropy'.

$$H = -\sum p(i) \log_2 p(i)$$

According to Shannon, it takes the minimum value of "0" if the situation contains certainty, and the maximum value of "1" if the situation contains complete uncertainty.

Aesthetic evaluation methods and digitization methods were examined in determining the method of the study. Aesthetics is a unique concept and can vary from person to person. But there are certain principles that the brain perceives as aesthetic. Since the aim is to create precise numerical data, aesthetic principles and concepts that may be appropriate Shannon's information Entropy formula are discussed.

Psychological and aesthetic value of Gestalt theory was taken into consideration and it was determined that there are principles that can be digitized. In order to bring these principles into conformity with the informational entropy theory, analyzes were made through photographs and the values were obtained by combining the formula with the determined raw data.

Boztepe creates three different silhouettes from different points of the city. These silhouettes have changed greatly over time. In order to achieve the aesthetic measure of all the silhouettes of Boztepe, three different facades are considered. In order to observe the change, studies were carried out on visuals at the same angles from three different time periods at approximately fifty-year intervals. The order of application of the method is schematized in Figure 1.

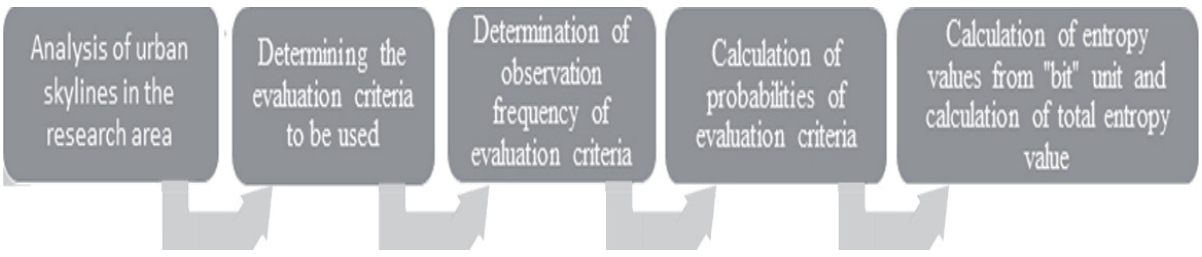


FIGURE 1
Method Diagram

RESULTS AND DISCUSSION

The purpose of evaluating by years is to observe the change of Boztepe from past to present. While doing this, the East, North and West fronts of Boztepe were used. The reason for this is that Boztepe, which has a dominant character in Trabzon, can be seen from inside the city and from the sea, and the facades that form its characteristic appearance are these three facades. While evaluating by years, fronts are evaluated with three different year intervals (-1900, -1950+, 2000+).

When the entropy value is calculated, the decimal part of the numbers obtained is taken as five digits. For example, the continuity effect for the northern front of 1900 is determined to be 0.143609027. The analysis value is accepted as 0.14461.

Over the years, the frequency of observations has increased in Boztepe, which has various structures such as roads, buildings, parks and bridges. The increase in the frequency of observation affects all parameters and decreases the bit values.

As seen Figure 2, when the values and observation frequencies are taken together, on the eastern front, although the vegetative effect has increased, the structural density has increased. This situation caused the degradation of the topography and the increase of dominant and repeat elements. Since probability is taken into account in the esthetic value calculation method, each of the values is affected by this change. As a result in Table 1, it has been observed that the bit value on this front gradually decreases every year.

East Side

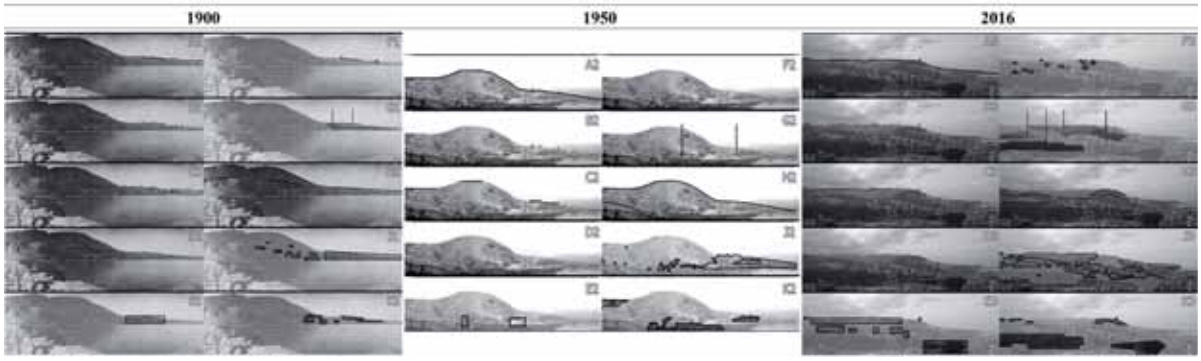


FIGURE 2
Trabzon Boztepe, East, 1900, 1950, 2016

TABLE 1
Trabzon Boztepe, East, 1900, 1950, 2016 Entropy Value

Evaluation Scales	Obs. 1900	Entropy Value 1900	Obs. 1950	Entropy Value 1950	Obs. 2016	Entropy Value 2016
Contour Effect (A)	18	0.50000 bit	22	0.50314 bit	162	0.52437 bit
Vertical Effect (B)	9	0.37500 bit	7	0.29456 bit	42	0.35120 bit
Horizontal Effect (C)	6	0.29875 bit	8	0.31872 bit	49	0.38106 bit
Color Effect (D)	5	0.26722 bit	5	0.23862 bit	8	0.11726 bit
Dominant Effect (E)	1	0.08569 bit	2	0.12619 bit	10	0.13810 bit
Repeat Effect (F)	2	0.14361 bit	0	0 bit	12	0.15742 bit
Continuity Effect (G)	2	0.14361 bit	2	0.12619 bit	4	0.06916 bit
Topography Effect (H)	3	0.19104 bit	2	0.12619 bit	12	0.15742 bit
Occupancy-Void Effect (J)	20	0.51333 bit	21	0.49666 bit	56	0.40711 bit
Herbal Effect (K)	6	0.29875 bit	17	0.46232 bit	25	0.25829 bit
Total	**72**	**2.81700 bit**	**86**	**2.69259 bit**	**380**	**2.56139 bit**

North Side

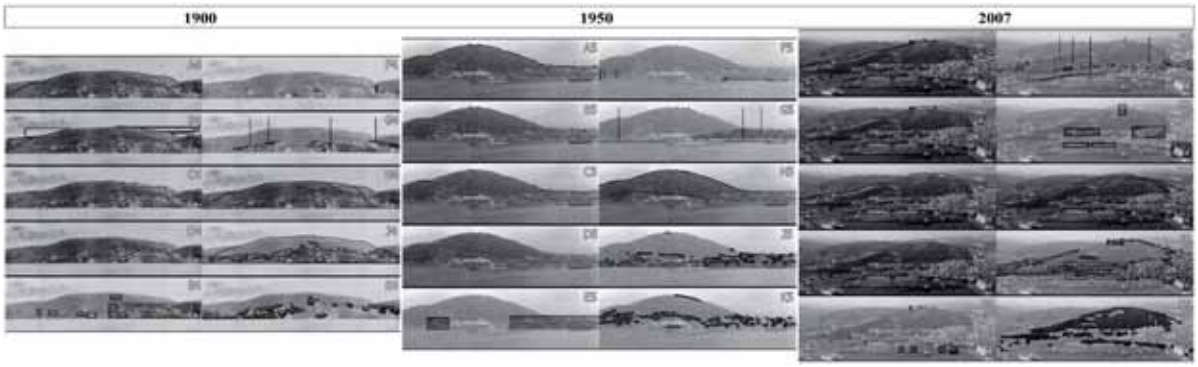


FIGURE 3
Trabzon Boztepe, North, 1900, 1950, 2007

West Side

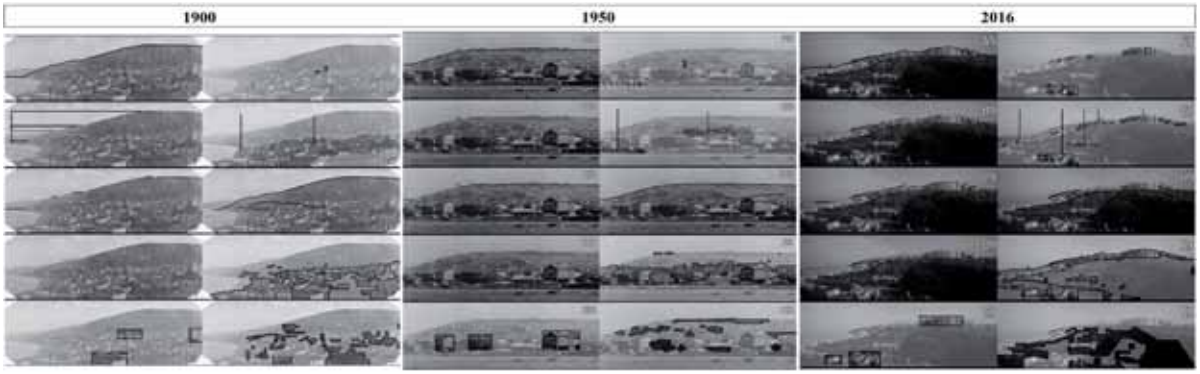


FIGURE 4
Trabzon Boztepe, West, 1900, 1950, 2016

TABLE 2
Trabzon Boztepe, North, 1900, 1950, 2007 Entropy Value

Evaluation Scales	Obs. 1900	Entropy Value 1900	Obs. 1950	Entropy Value 1950	Obs. 2007	Entropy Value 2007
Contour Effect (A)	13	0.37129 bit	78	0.52871 bit	147	0.53057 bit
Vertical Effect (B)	6	0.23451 bit	44	0.45490 bit	69	0.43267 bit
Horizontal Effect (C)	6	0.23451 bit	40	0.43725 bit	74	0.44581 bit
Color Effect (D)	5	0.20783 bit	5	0.11931 bit	8	0.11082 bit
Dominant Effect (E)	6	0.23451 bit	2	0.05912 bit	6	0.08919 bit
Repeat Effect (F)	3	0.14556 bit	3	0.08112 bit	6	0.08919 bit
Continuity Effect (G)	4	0.17841 bit	4	0.10100 bit	5	0.07753 bit
Topography Effect (H)	4	0.17841 bit	2	0.05912 bit	7	0.10026 bit
Occupancy-Void Effect (J)	42	0.52920 bit	36	0.41711 bit	49	0.36628 bit
Herbal Effect (K)	17	0.42347 bit	18	0.28614 bit	39	0.32285 bit
Total	**106**	**2.73770 bit**	**232**	**2.54378 bit**	**410**	**2.56517 bit**

As seen Figure 3, the center of Trabzon city is located on a part of the northern border of Boztepe. Therefore, between 1900 and 1950, construction increased significantly. Restoration continued in the remaining areas, and some of the old buildings were demolished and rebuilt. Therefore, the frequency of observations varied greatly between 1900 and 1950.

Considering the values and the frequency of observations together in Table 2, the graphs on the north side for the years 1950 and 2007 show almost the same level of bit values. In 1900, it was observed that the bit value was higher.

There were no large buildings on the western side of Trabzon Boztepe until 2000s. However, Trabzon, a growing city, has taken over the western edge of Boztepe because of the limited residential areas and the construction has increased exponentially. Although the frequency of observation of vegetative effect has improved over the years, it has not been enough due to the other factors brought about by this urbanization.

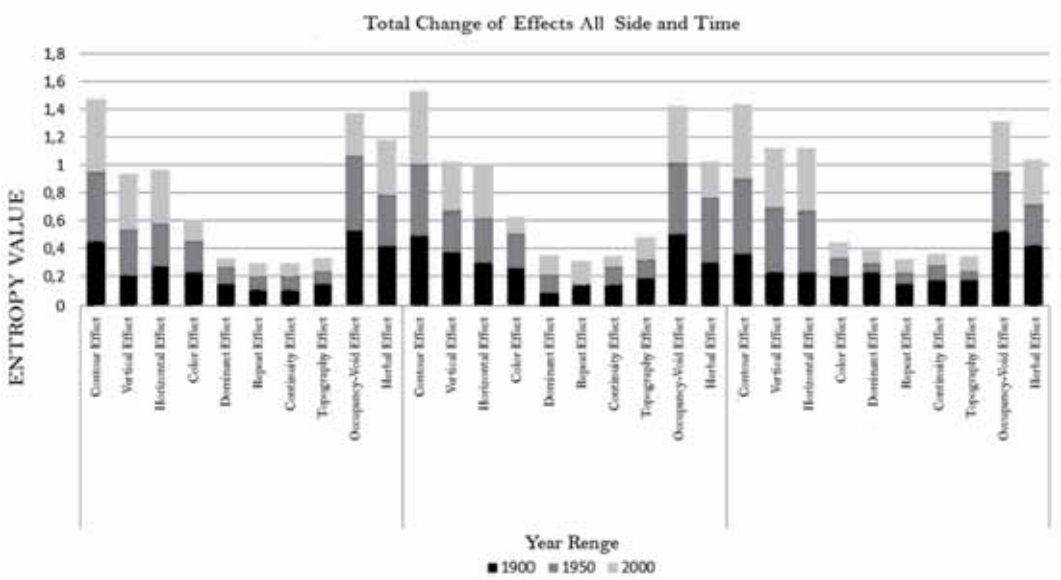


FIGURE 5
Trabzon Boztepe, Total Change of Effects All Side and Time

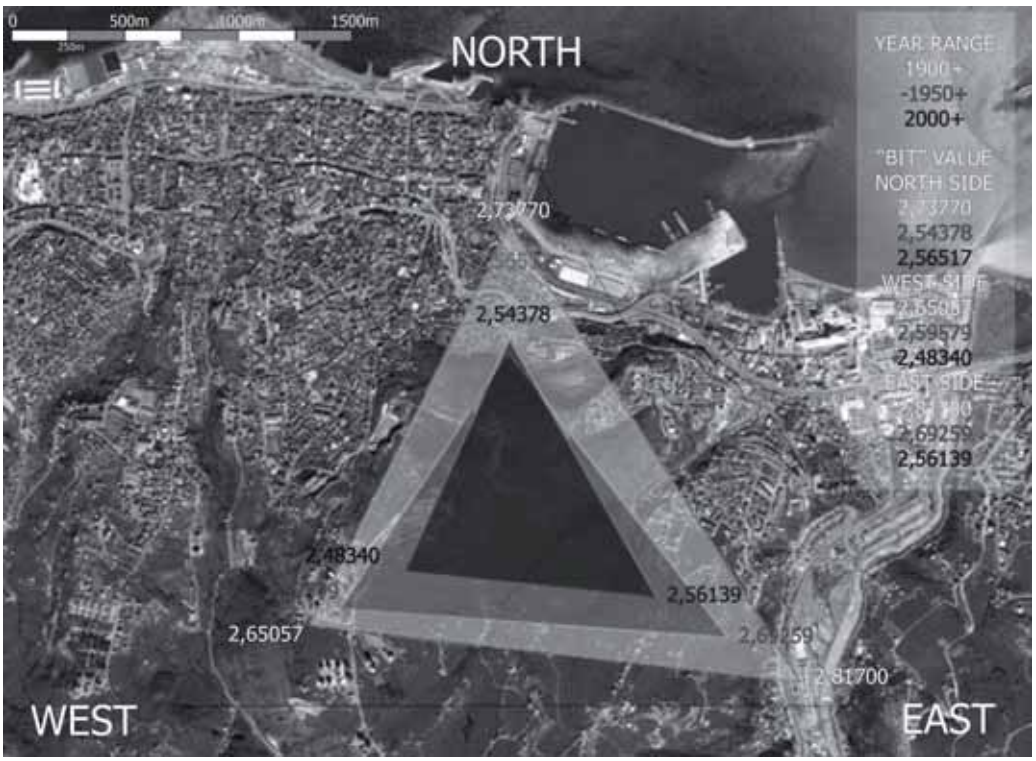


FIGURE 6
Trabzon Boztepe, Total Change of Effects All Time

As seen in Figure 4, Between 1900 and 1950, when the frequency and values of the observations are taken together, the west side bit values did not differ significantly. A great change was observed with the increase in construction in 2016. It is clear that the bit value decreases with the settlement.

When the average aesthetics of all the facades of Trabzon Boztepe are examined, aesthetics have continuously lost value since the 1900s. If urban development continues at this rate, it is predicted that the aesthetic value will gradually decrease. However, the aesthetic value can be increased numerically by making the right planning decisions in the future, increasing the visual quality of the existing construction and vegetative designs that will highlight the urban touch and are suitable for the region. In Figure 5, the change values of parameters according to years for the east, north and west directions, respectively, and in Figure 6, the total aesthetic values of Boztepe and its changes over the years can be seen.

CONCLUSIONS

The simplest method of benchmarking is to move through numerical data. This study is based on Shannon's method of digitizing aesthetics, which he developed as a result of his studies on entropy. For the method, principles appropriate to the study area were determined and the changes related to these principles were observed through photographs. The frequency of observations was adjusted to Shannon's equation and aesthetic values in terms of "bit" were obtained.

Using the digitization method, the change of Boztepe, one of the landmark points of Trabzon, from the past to the present is discussed. It has been determined how the increasing population of the city over the years affected the basic elements that make up the silhouette and what kind of a change these basic elements caused in the whole city silhouette. With the findings, the changes that occurred over the years were transformed into mathematical data. The numerical values obtained were compared with the estimates. According to the data obtained from the study;

One of the most important factors affecting aesthetics is the increase in the structural density and consequently the decrease in the bit value of the total aesthetics.

With the development of technology, the discovery of new techniques, the ease of plant care, and the understanding of the importance of the plant for society and the city, the city of Trabzon has generally progressed in terms of vegetation. However, in addition to increasing plant density, light green areas were filled with structures. According to the analysis data, the frequency of observing the vegetative effect increased as we approached to the present day, but the herbal effect density decreased.

None of the silhouettes studied from 1900 to the present day have seen a visually impressive, aesthetic and eco-friendly building or landscape. This may be the biggest deficiency of the city of Trabzon.

It is noteworthy that the Trabzon city plan is sloppy and inefficient. The poorly designed city plan caused large area losses, aesthetically affected the silhouette negatively and was functionally inadequate. It is clear that the city is not seen as a whole.

The green areas in the city center are small and scattered. There is a need for areas where people can move away from urban life and spend time with nature, but these areas should not be small and piece by piece. Within the city as much as possible, a whole natural area can contribute to the city both visually and in terms of the quality of life of the inhabitants. At the same time, these areas will greatly improve the silhouette.

The use of areas that are not suitable for construction or which are landmark for Trabzon has caused a significant change in the natural topographic lines of Trabzon.

The construction of tall buildings has gradually increased the dominant elements observed in silhouettes. The increase in observed dominant elements has an adverse effect on the whole, even if it is thought that Boztepe has increased the cue point property. In addition, high buildings cause to hide the historical texture and natural beauties.

Over time, the structural expansion of the city towards Boztepe caused the silhouette to lose its aesthetic value to a great extent.

The highest aesthetic value of the eastern facade was measured in the 1900s. However, it was the facade that lost its value at the highest rate during the year. The reason for this is that the facade, which was completely natural in the beginning, turned into a settlement in the 2000s.

Since the northern front is the front that hosts the center of the city of Trabzon, urban development has existed since the 1900s. Therefore, it was less affected by urban development, or it can be said that it was already affected by urban development in the 1900s.

With this study, the change over the years has been tried to be monitored. The evaluation of the projects to be made with 3D models can be done with this method. Before the projects are carried out, it can be predicted to what extent it will affect the silhouette.

REFERENCES

[1] Celik, K.T. (2015) Generating a Gis-Based Campus Urban Furniture Information System (CUFIS): Example of Kanuni Campus - Karadeniz Technical University. Master Thesis Karadeniz Technical University.

[2] Martinez-Zarzoso, I. (2008) The Impact of Urbanization on CO2 Emissions: Evidence from Developing Countries. Fondazione Eni Enrico Mattei. 2008.050, 1-32.

[3] Dascher, K. (2014) City Silhouette, World Climate. Annual Conference 2014: Evidence-based (Hamburg). Economic Policy. A16-V3.

[4] Gul, A. (2008) Landscape and Humanbeing Relation and Landscape Architecture. Turkish Journal of Forestry. 1, 97-114.

[5] Guney, C., Girginkaya, S.A. Cagdas, G. and Yavuz, S. (2012) Tailoring a geomodel for analyzing an urban skyline. Landscape and Urban Planning. 105, 160-173.

[6] Yusoff, N.A., Noor, A.M. and Ghazali, R. (2013) City skyline conservation: sustaining the premier image of Kuala Lumpur. ScienceDirect. 20, 583-597.

[7] Karakaya, B. (2013) Urban landscape-sustainability-city silhouette: The historic core from Edirne. Master Thesis. Trakya University.

[8] Yaran, A. (2016) Investıgatıng the aesthetıc ımpact of tall buıldıngs on urban landscape. Journal of Building Performance. 7(1), 1-8.
[9] Puspitasari, A.W. and Kwon, J. (2019) Analysis of the Visual Quality of Riverfront Skyline Through the Feature of Height and Spatial Arrangement of Tall Building. Architectural Research. 21(4), 91-98.
[10] Wagemans, J. (2013) Historical and conceptual background: Gestalt theory, Oxford Handbook of Perceptual Organization, Oxford University Press. 3-20.
[11] Karimimoshaver, M. and Winkemann, P. (2018) A framework for assessing tall buildings' impact on the city skyline: Aesthetic, visibility, and meaning dimensions. Environmental Impact Assessment Review. 73, 164-176.
[12] Wang, J.H. and Ogawa, S. (2015) Fractal analysıs of colors and shapes for natural and urbanscapes, The International Archives of the Photogrammetry, Remote Sensing and Spatial Information Sciences, 36th International Symposium on Remote Sensing of Environment, Berlin, Germany. 1431-1438.
[13] Wu, Y., Zhou, Y., Saveriades, G., Agaian, S., Noonan, J.P. and Natarajan, P. (2013) Local Shannon entropy measure with statistical tests for image randomness. Information Sciences. 323-342.
[14] Bostanci, S.H. (2015) Shannon entropy and urban skylınes, Journal of the Technical University – Sofia Plovdiv Branch, "Fundamental Sciences and Applications", International Conference on Engineering, Technologies and System TECHSYS. 21.
[15] Oksuz, M. (2005) A Sort History of Trabzon From the Very Beginning to the XIX. Century. Black Sea Studies. 5, 11-25.
[16] Bilsel, A. and Bilsel, S.G. (2010) Urban Planning Competitions, Stages of Development from the 1960s to the late 70s. Journal of the Chamber of City Planners. 50, 89-124.
[17] Hagerhall, C.M., Purcell, T. and Taylor, R. (2004) Fractal dimension of landscape silhouette outlines as a predictor of landscape preference. Journal of Environmental Psychology. 24, 247-255.
[18] Bostanci, S.H. (2008) Evaluation of the urban skylines by the entropy approach. Ph.D. İstanbul Technical University.
[19] Birkhoff, G.D. (1933) Aesthetic Measure. Publisher: Harvard University Press, Massachussets.
[20] Ying, L. (2015) Twin universes: Universal laws of thermodynamics. American Journal of Modern Physics. 4, 1-4.
[21] Bejan, A. and Errera, M.R. (2016) Complexity, organization, evolution, and constructal law. Journal of Applied Physics. 119, 1-20.
[22] Kondepudi, D. and Prigogine, I. (2015) Modern thermodynamics: From heat engines to dissipative structures. John Wiley & Sons, Ltd. 523 pp.
[23] Naveh, Z. (1987) Biocybernetic and thermodynamic perspectives of landscape functions and land use patterns. Landscape Ecology. 1, 75–8.
[24] Gobattoni, F., Pelorosso, R., Lauro, G., Leone, A. and Monaco, R. (2011) A procedure for mathematical analysis of landscape evolution and equilibrium scenarios assessment. Landscape and Urban Planning. 103(3), 289–302
[25] Ho, M.W. (2013) Circular thermodynamics of organisms and sustainable systems. Systems. 1(3), 30–49.
[26] Cushman, S.A. (2015) Thermodynamics in landscape ecology: The importance of integrating measurement and modeling of landscape entropy. Landscape Ecology. 30, 7–10.
[27] Pelorosso, R., Gobattoni, F. and Leone, A. (2017) The low-entropy city: A thermodynamic approach to reconnect urban systems with nature. Landscape and Urban Planning. 23-24.
[28] Ekinoglu, H. and Plunz, R. (2017) Modeling Spatial Wholeness in Cities Using Information Entropy Theory, A|Z ITU Journal of Faculty of Architecture. 67-81.
[29] Capra, F. (1996) The Web of Life, Publisher: HarperCollins, London.
[30] Taher Tolou Del, M.S. and Tabrizi, S.K. (2020) A methodological assessment of the importance of physical values in architectural conservation using Shannon entropy method. Journal of Cultural Heritage. 44, 135-151.
[31] Balocco, C. and Grazzini, G. (2000) Thermodynamic parameters for energy sustainability of urban areas. Solar Energy. 69(4), 351–356.
[32] Fistola, R. and La Rocca, R.A. (2014) The Sustainable City and the Smart City: measuring urban entropy first. The Sustainable City. IX, 537-548.
[33] Bai, X. (2016) Eight energy and material flow characteristics of urban ecosystems. Ambio. 45, 819–830.
[34] Girginkaya Akdag, S. and Bostanci, S.H. (2013) The ımpacts of prestıge projects on the skylıne of Istanbul. International Journal of Architectural Research. 7(2), 269-281.
[35] Zhang, F., Yao, L., Zhou, W., You, Q. and Zhang, H. (2020) Using Shannon Entropy and Contagion Index to Interpret Pattern Self-Organization in a Dynamic Vegetation-Sand Model. IEEE Access. 8, 17221-17230.

Received: **09.03.2021**
Accepted: **01.05.2021**

CORRESPONDING AUTHOR

Cengiz Acar
Karadeniz Technical University
Faculty of Forestry
Department of Landscape Architecture
Trabzon – Turkey

e-mail: cengiz@ktu.edu.tr

© by PSP Volume 30– No. 09/2021 pages 10643-10651 Fresenius Environmental Bulletin

EXPERIMENTAL STUDY ON PHASE DIFFERENCE DETECTION METHOD OF CORIOLIS FLOWMETER BASED ON SVD AND NUTTALL WINDOW FOURIER TRANSFORM

Lei Huang[1,*], Shidong Wu[2], Qian Zhang[1], Xueyang Xing[3]

[1]Mechanical and Control Engineering College, Shengli College China University of Petroleum, Dongying 257061, China
[2]FairOak Technology Inc., Hangzhou 310030, China
[3]Department of Architectural Engineering, Binzhou University, Binzhou 256600, China

ABSTRACT

Flow rate is one of the important operating parameters for monitoring of municipal sewage treatment facilities. The phase difference detection accuracy of Coriolis flowmeter determines the flow measurement accuracy. In order to study the phase difference detection method of Coriolis flowmeter, an experimental model of single straight tube Coriolis flowmeter is designed. On this basis, the phase difference processing method is improved. The signal preprocessing method is combined with FIR filter and SVD noise reduction, and then the Nuttall window discrete Fourier transform is used. Compared with other methods, the simulation results show that the phase difference is more accurate. Finally, the experimental results on Coriolis flowmeter model show that the phase difference detection method improves the phase difference detection accuracy.

KEYWORDS:
Single straight tube coriolis flowmeter, Singular value decomposition, Fourier transform with Nuttall window, Municipal sewage

INTRODUCTION

Coriolis flowmeter is a kind of instrument which can directly measures the mass flow of municipal sewage treatment facilities. Because there is no component inside the measuring tube, it does not affect the flow of fluid. And the measurement accuracy is high. The Coriolis flowmeter has been widely used for the measurement of various unconventional fluids and slurries [1-2].

The calculation of phase difference between two detecting signals of Coriolis flowmeter is the basis and one of the key points for measuring mass flow rate of Coriolis flowmeter. In terms of phase difference calculation, in the US patent USP5555190, researchers proposed the adaptive spectral line enhancement technology based on the direct IIR adaptive cavity filter, and then calculated the enhanced two-channel output signal with Goertzel algorithm [3]. Freeman proposed to use the digital phase-locked loop technology to calculate the phase difference between two sensors of the Coriolis flowmeter [4]. In the United States patent USP5734112, Bose et al. adopted the digital signal filtering methods such as adaptive filter and multi-filter, and then analyzed and calculated the frequency by using periodic spectrum, and calculated the phase difference by using discrete Fourier transform [5]. Liu et al. [6] uses the principle of neural network to make compensation calculation for the measurement of gas-liquid two-phase flow. Li et al. [7-8] presented new complex signal processing methods, Complex Bandpass Filtering (CBF), Complex Notch Filtering (CNF) and their combination (CBF-CNF). Olga L. et al. [9] adopted a neural network model to calibrate the flow of Coriolis flowmeter. Zhang et al. [10] proposed a deep learning-based signal processing method for Coriolis mass flowmeter.

The phase difference detection of Coriolis flowmeter is directly related to the mass flow measurement results, and it directly affects the measurement accuracy and application effect of Coriolis flowmeter. The common phase difference detection methods include the correlation detection method, the Hilbert transform method [11]. But the calculation amount of these methods is large, the whole period samples are needed, and the dynamic performance are poor. This research designed a phase difference detection method of Coriolis flowmeter based on SVD and Nuttall window Fourier transform. This new method does not need the whole period sampling and has high calculation accuracy.

MATERIALS AND METHODS

Introduction to Principle. (1) The principle of Coriolis flowmeter. The principle of Coriolis mass flowmeter is the Coriolis force, and it is composed of the primary instrument and the secondary instrument. The primary instrument includes a measuring tube, a driving coil, a detection coil, a shell and the other supporting structures. The secondary in-

strument includes a driving signal output part, a vibration signal processing part and a amplitude control part [12-13].

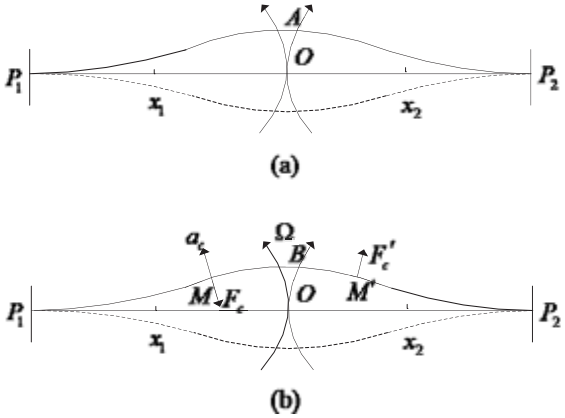


FIGURE 1
The Schematic diagram of the single straight tube Coriolis flowmeter.

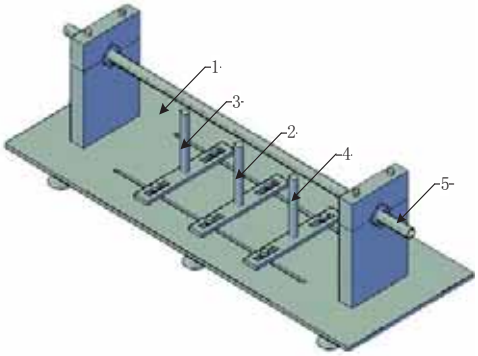


FIGURE 2
The mechanical structure of single straight tube Coriolis flowmeter.

Notes: 1. A measuring tube fixing frame, 2. A detector mounting frame, 3. The first driver mounting frame, 4. The second driver mounting frame, 5. A measuring tube.

The measuring tube is a single straight tube (Figure 1). Both the ends of the measuring tube are fixed, and the electromagnetic drive coil is installed at the middle O point. The detection coil is installed at x_1 and x_2 symmetrically. The electromagnetic drive coil provides the driving force for the measuring tube. The two detection coils detect the vibration at the installation points, and they output signals to the signal processing part.

When there is no fluid in the measuring tube (Figure 1(a)), the measuring tube is only vibrated by the driving force of the driving coil, and is not affected by the Coriolis force. The vibration at x_1 and x_2 is completely symmetric, and the output signals of the two sensors are exactly the same. When the fluid in the measuring tube flows with a velocity V (Figure 1 (b)), the measuring tube vibrates due to the driving coil. Assuming that the angular velocity of the measuring tube vibration is Ω, because the fluid in the rotating system has a velocity of V, the Coriolis acceleration at M point can be described as following equation.

$$\vec{a}_c = 2\vec{\Omega}\times\vec{V} \tag{1}$$

According to the right hand rule, it can be determined that the direction of Coriolis acceleration is perpendicular to the pipe and it is upward. This Coriolis acceleration is exerted by the pipe on the fluid, so the fluid has a reaction Coriolis force on the measuring pipe:

$$\vec{F}_c = 2m\vec{\Omega}\times\vec{V} \tag{2}$$

The direction of the Coriolis force at M point is perpendicular to the pipe and it is downward. Similarly, the Coriolis force F'_c at M' point is perpendicular to the pipe and it is upward, and it is equal to the magnitude of F_c. The original vibration at x_1 is weakened, while the original vibration at x_2 is strengthened, and the measuring tube is distorted by a twisting force. The measuring tube is subjected to two Coriolis forces, and the torsion moment can be described as following equation:

$$M = F_c r_c + F_c' r_c' \tag{3}$$

Where r_c and r'_c are the distance between the detector and the center of the measuring tube. Because $F_c = F'_c = F$, $r_c = r_c' = r$, then

$$M = 2Fr = 4mrV\Omega \tag{4}$$

When the time is t, the mass flow rate $q_m = m/t$, the liquid flow rate $V = L/t$. L is half of the length of the measuring tube. Then the Formula (4) is equal to the following equation.

$$M = 2Fr = 4r\Omega L q_m \tag{5}$$

Assume the elastic modulus of the measuring tube is K_S, and the twist angle generated by the Coriolis force is θ. The reaction moment formed by the rigidity of the measuring tube is described as following equation.

$$T = K_S\theta \tag{6}$$

Because $T = M$, the mass flow rate can be obtained from equations (5) and (6).

$$q_m = \frac{K_S}{4r\Omega L}\theta \tag{7}$$

Assume the vibration velocity of the measuring tube at the central position is V_t, the following equation can be obtained.

$$\sin\theta = \frac{V_t}{2r}\Delta t \tag{8}$$

Where, Δt is the vibration time difference between the point M to the horizontal center and the point M' to the horizontal center. Because θ is small, $\sin\theta \approx \theta$, and $V_t = \Omega L$. Then the following equation can be concluded.

$$\theta = \frac{\Omega L}{2r}\Delta t \tag{9}$$

The following equation can be obtained from equations (7) and (9).

$$q_m = \frac{K_S}{4r\Omega L} \times \frac{\Omega L \Delta t}{2r} = \frac{K_S}{8r^2} \Delta t \quad (10)$$

The mass flow rate of the Coriolis flowmeter is proportional to the time difference, and the mass flow value can be obtained as long as the time difference is detected. The time difference can be measured by the phase difference of the two detection signals installed at both ends of the measuring tube [14-15].

(2) Model of Coriolis flowmeter. Compared with other tube types, the Coriolis flowmeter model adopts the single straight pipe structure which is simple, easy to clean and has high sensitivity. The mechanical structure of the model includes a measuring tube fixing frame, a detector mounting frame, two driver mounting frame and a measuring tube (Figure 2).

The measuring tube is a steel pipe with the outer diameter of 25 mm, the inner diameter of 22 mm and the length of 890 mm. The material is 304 steel and the elastic modulus is 206 GPa. The fixed position of the measuring tube is thickened at the outer wall. The thickness of the tube wall at the thickened position is 11.5 mm which is much thicker than that of the vibration part. The thickening treatment of the fixed position can reduce the vibration propagation to both ends.

The fixing part of the vibration pipe is fixed on the fixing frame by screws. The measuring tube is fixed with a fixing frame which is equivalent to the shell part of the industrial Coriolis flowmeter. The measuring tube is tightly pressed on the fixing frame with screws. The chute on the base can realize the lateral position movement of the sensor bracket. The sensor and exciter bracket are used to fix the sensor and exciter.

The driving mode of Coriolis flowmeter adopts digital drive, and the driving block diagram is shown as Figure 3.

The driving system consists of a driver, two detectors, two signal acquisition cards and a power amplifier circuit. The sensor signal is converted into digital signal by the acquisition card for processing by PC. The excitation signal synthesized by PC is output by the acquisition card, and the exciter is excited after power amplification.

The signal acquisition cards are 9223 and 9269 of National Instruments. 9223 is the analog input card with four channel and 16 bit synchronous sampling. The highest sampling frequency can reach 1 MHz and the sampling resolution can reach 0.15 mV. 9269 is the analog output card.

The driver is an electromagnetic driver which is composed of magnet and coil. When the coil is supplied with alternating current of different frequency, the alternating magnetic field of different frequency can be generated in the coil, and it interacts with the magnet to drive the vibration of measuring tube.

The detectors are electromagnetic detectors with the same structure as the driver, but the principle is opposite. The detectors vibrate with the measuring tube, and it cut the magnetic induction line generated by the magnet to generate electromotive force inside the coil. Based on the principle of Coriolis force and the mechanical structure of the measuring tube, the deformation of the vibrating tube is the largest at 0.287 L and 0.713 L. Therefore, the two detectors are installed at 0.287 L and 0.713 L of the measuring tube respectively [15]. The relationship between the amplitude of detector output signal and vibration amplitude can be described as the following equation.

$$A_x = 96.806 A_s / f \quad (11)$$

Where, A_x is the vibration amplitude. A_s is the detector output signal amplitude. f is the vibration frequency of the measuring tube.

LM1875 integrated power amplifier is used in the power amplifier circuit. The power supply voltage is ±9 V, and the voltage magnification is 20. The bandwidth is 70 kHz which is far greater than the maximum vibration frequency 203 Hz of the measuring tube.

Phase difference detection method based on SVD and Nuttall window Fourier transform. Phase difference calculation is the core of signal processing of Coriolis flowmeter. The accuracy of phase difference calculation determines the accuracy of flowmeter measurement. Based on singular value decomposition SVD and Nuttall window Fourier transform, the new phase difference detection method firstly corrects the data by SVD method, and then it calculates the phase difference with the Nuttall window Fourier transform.

SVD method can effectively smooth the FIR filtered signal, and the Nuttall window Fourier transform method can reduce the signal leakage to get high accuracy for the phase difference calculation [16].

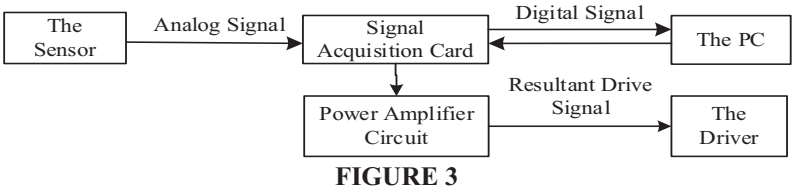


FIGURE 3
Digital drive block diagram of Coriolis flowmeter.

TABLE 1
Several cosine combination windows

Window type	The maximum side lobe peak/dB	The progressive attenuation rate of side lobe peak dB/oct
hamming	-42.7	6
Kaiser5	-119.8	6
Nuttall3a	-64.2	18
Nuttall4a	-82.6	30
Nuttall4b	-93.3	18
Nuttall4c	-98.1	6

(1) Data correction based on SVD method. The basic principle of SVD data correction method is the spatial reconstruction by using the sampled signal. SVD method can decompose the observed signal space into a series of ideal signal subspaces and noise subspaces corresponding to singular values. Several large singular values corresponding to the ideal signal subspace are reserved, and the rest singular values are all set to zero. Then the estimation formula of the ideal signal matrix can be obtained by the SVD inverse process, and the modified signal is finally reconstructed [17].

Assume the sampling data of the sensor is $x(n)$, $n = 1,2,\cdots,N$, N is the total number of data. According to the repetition rate α and the length of each data segment L, the number of data segments H can be calculated.

$$H = \frac{N-L}{L\times\alpha}+1 \tag{12}$$

Construct matrix A with i-segment signal.

$$A = \begin{bmatrix} x(1) & x(2) & \cdots & x(n) \\ x(n+1) & x(n+2) & \cdots & x(2n) \\ \vdots & \vdots & \ddots & \vdots \\ x(L-n+1) & x(L-n+2) & \cdots & x(L) \end{bmatrix} \tag{13}$$

The matrix A is decomposed by the singular value. Because the ideal sensor signal contains only one frequency waveform, two singular values are retained and the matrix A_c can be obtained by SVD inverse operation.

The de-noised signal $x_i(t)$ is obtained by connecting the elements in each row of the matrix A_c end to end. The matrix is saved from column p to row i of the matrix S which is initialized to zero, and $p = (i-1)\times L(1-\alpha)+1$.

It is saved to the i-th row of the matrix S which is initialized to zero from the p-th column. $p = (i-1)\times L(1-\alpha)+1$. Finally, the non-zero elements of each column in the matrix S are averaged to get the de-noising signal.

(2) Nuttall window Fourier transform. Nuttall window is a kind of cosine combination window which has good main lobe and fast side lobe attenuation. The discrete expression of time domain is described as follows.

$$\omega(n) = \sum_{m=0}^{M}(-1)^m a_m \cos(\frac{2\pi mn}{N}) \tag{14}$$

The characteristics of several common cosine combination windows are shown in Table 1.

Reasonable window function for Fourier transform can improve the accuracy of phase difference calculation [18-19]. The maximum side lobe peak of Nuttall4a window is -82.6 dB, and the progressive attenuation rate of side lobe peak is 30 dB/oct. Comparing the characteristics of several cosine combination windows, Nuttall4a window was selected for windowing the sensor data to meet the practical requirements. The algorithm principle of Nuttall4a window is as follows.

Window the sensor data $x(n)$, $n = 0,1,2,\cdots,N-1$ after discretization:

$$x_w(n) = x(n)\sum_{m=0}^{M}(-1)^m a_m \cos(\frac{2\pi mn}{N}) \tag{15}$$

$x_w(n)$ was transformed by Discrete Fourier Transform, and the frequency corresponding to the largest spectral line k_{max} in the Fourier transform result is the fundamental frequency of the signal. After windowed discrete Fourier transforming, the real part and imaginary part of the signal are as follows [20].

$$X_r = \sum_{n=0}^{N-1}[x(n)\sum_{m=0}^{M}(-1)^m a_m \cos(\frac{2\pi mn}{N})]\cos(n\frac{2\pi f_c}{f_s}) \tag{16}$$

$$X_i = \sum_{n=0}^{N-1}[x(n)\sum_{m=0}^{M}(-1)^m a_m \cos(\frac{2\pi mn}{N})]\sin(n\frac{2\pi f_c}{f_s}) \tag{17}$$

Where f_s is the sampling frequency. f_c is the corresponding frequency of k_{max}.

The phase of the signal is as follows [21].

$$\theta = \arctan(\frac{X_r}{X_i}) \tag{18}$$

Assume the phases of two sensor signals are θ_1 and θ_2 respectively, the phase difference is $\Delta\theta = \theta_1 - \theta_2$.

Simulation of data processing method. Based on the theoretical modeling of Coriolis flowmeter experimental system, the Simulink model is shown as Figure 4 [22-23].

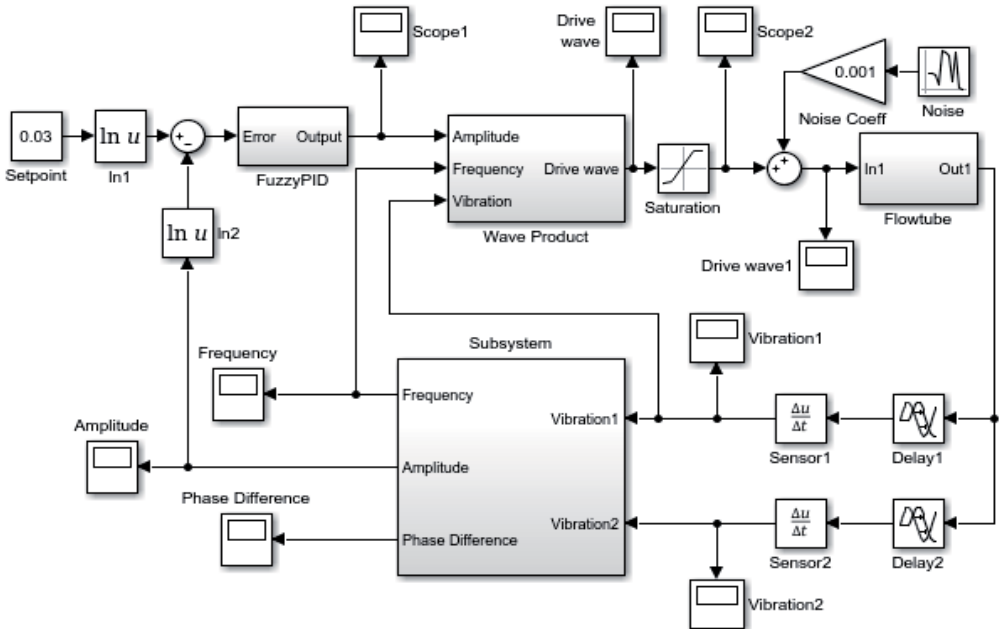


FIGURE 4
Simulink model of Coriolis flowmeter system.

TABLE 2
The calculation results of DFT and Nuttall windowed DFT.

Real value/°	Noiseless sinusoidal signals				Adding 0.0001 uniform white noise			
	DFT		Nuttall windowed DFT		DFT		Nuttall windowed DFT	
	calculation value/°	Relative error	calculation value/°	Relative error	calculation value/°	Relative error	calculation value/°	Relative error
-2.3	-2.496	0.0852	-2.300	0	-2.767	0.2030	-2.515	0.0935
-0.5	-0.528	0.0560	-0.500	0	0.61	-2.2200	-0.567	0.1340
0.5	0.523	0.0460	0.500	0	1.486	1.9720	0.466	-0.0680
1.9	1.893	-0.0037	1.900	0	2.367	0.2458	2.028	0.0674
3.4	3.320	-0.0235	3.399	0.0003	3.452	0.0153	3.346	-0.0159

(1) Comparison between DFT and Nuttall windowed DFT. The frequency of two noiseless sinusoidal signals is 116 Hz, and the amplitude is 0.023. The sampling frequency is 2300 Hz, and the sampling length N is 64. There is phase difference in the initial phase.

The calculation results of DFT and Nuttall windowed DFT (Table 2) showed that the processing result of Nuttall windowed DFT is more accurate than that of DFT. The deviation between the calculation result of Nuttall windowed DFT and the real value is within 0.001 degree without the influence of noise.

After adding 0.0001 uniform white noise, the results of Nuttall windowed DFT and DFT are greatly affected by the noise. While the two vibration signals of Coriolis flowmeter are affected by the noise during the real measurement. Therefore, FIR filtering and SVD de-noising should be used to process the signal before Fourier transform.

(2) Preprocessing with FIR filter and SVD noise reduction method. The above two signals with uniform white noise are first de-noised by FIR filtering and SVD, and then processed by DFT and DFT with Nuttall window respectively. The results are showed in Table 3.

Compared with results of Table 3 and Table 2, it can be seen that the relative error of phase difference calculated by FIR filtering pretreatment for noisy vibration signal is significantly reduced, and the relative error of DFT with Nuttall window is smaller than that of DFT.

After SVD processing of FIR filtered signal, the calculated relative error of phase difference is further reduced. Therefore, the signal should be preprocessed by FIR filtering and SVD de-noising, and then the phase difference can be calculated by Nuttall windowed DFT. This method can ensure the phase difference error is the smallest and the accuracy is the highest.

TABLE 3
The calculation results of phase difference calculation method by preprocessing of FIR filter and SVD noise reduction

/ Real value/°	After FIR filtering				SVD noise reduction after FIR filtering			
	DFT		Nuttall windowed DFT		DFT		Nuttall windowed DFT	
	calculation value/°	Relative error	calculation value/°	Relative error	calculation value/°	Relative error	calculation value/°	Relative error
-2.3	-2.3948	0.0412	-2.3179	0.0078	-2.3296	0.0129	-2.2954	-0.0020
-0.5	-0.4532	-0.0936	-0.4884	-0.0232	-0.5061	0.0122	-0.4994	-0.0011
0.5	0.4777	-0.0446	0.5087	0.0175	0.4973	-0.0054	0.5001	0.0002
1.9	1.7275	-0.0908	1.9412	0.0217	1.9148	0.0078	1.9043	0.0023
3.4	3.1260	-0.0806	3.4304	0.0089	3.3441	-0.0164	3.4079	0.0023

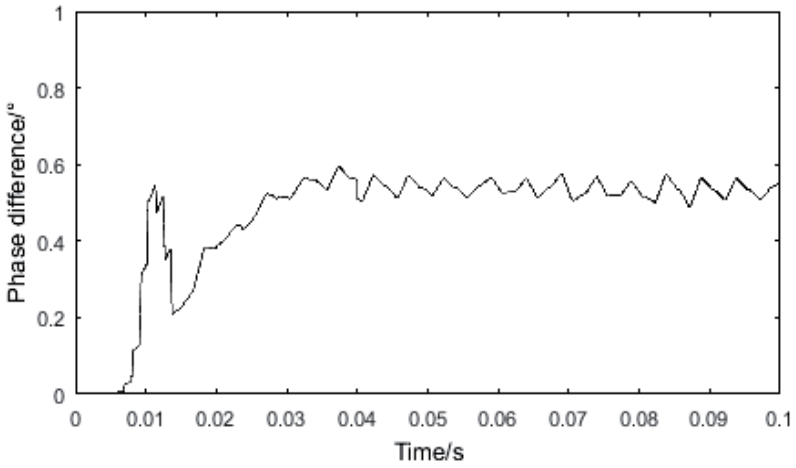


FIGURE 5
The Simulation results of the zero crossing phase detection method.

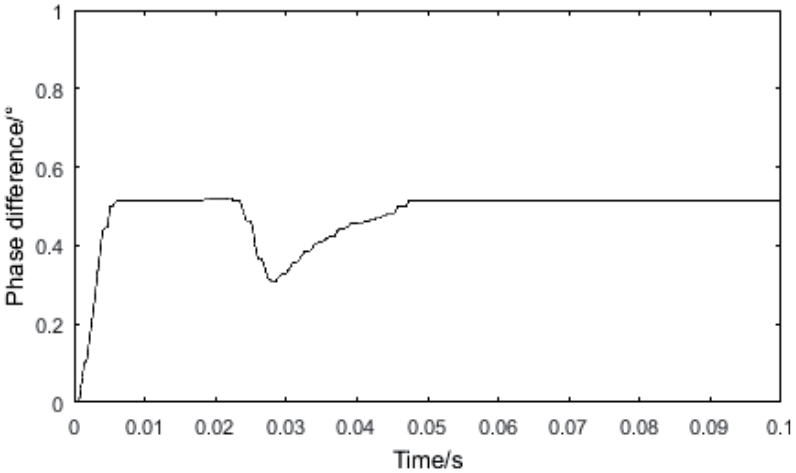


FIGURE 6
The Simulation results of the correlation function method.

(3) Comparison between the new method based on SVD and Nuttall windowed DFT and other methods. The phase difference calculation method based on SVD and DFT with Nuttall window was used to simulate. Compared with the commonly used phase difference calculation methods, such as the zero crossing phase detection method and the correlation function method, the simulation results are shown in Figure 5, Figure 6 and Figure 7. The value of phase difference is 0.5 °.

Before 0.04s, the measuring tube was in the start-up stage, and the phase difference was unstable. The variance of simulation results during the period from 0.04s to 0.1s were calculated (Table 4).

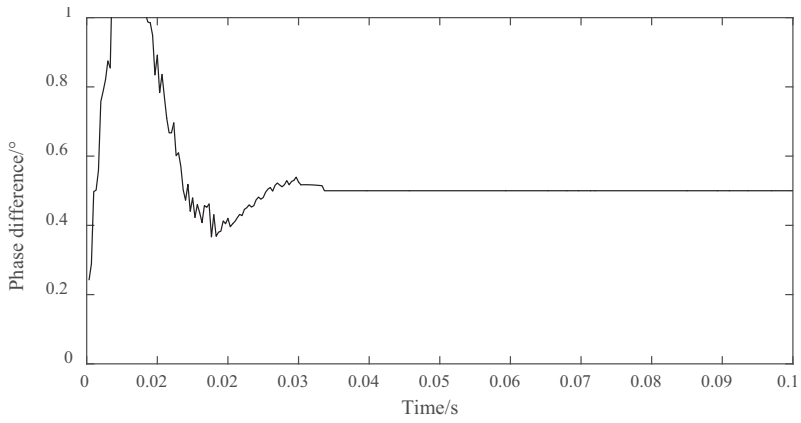


FIGURE 7
The simulation results of the new method based on SVD and Nuttall windowed DFT.

TABLE 4
Variance comparison of different phase difference calculation methods

Detection method	Variance / degree^2
Zero crossing phase detection method	0.000295
C=Correlation function method	0.000773
New method based on SVD and Nuttall windowed DFT	0.0000855

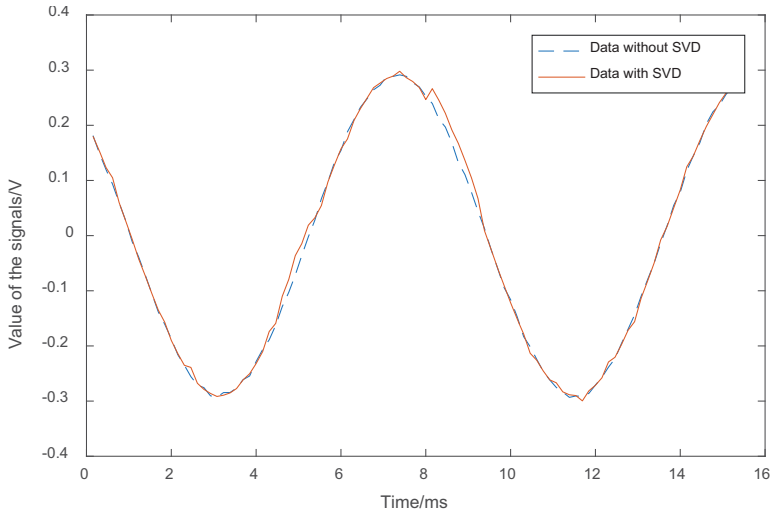


FIGURE 8
The results of SVD data correction.

The phase difference calculation method based on SVD and DFT with Nuttall window has the smallest variance and the highest accuracy.

RESULTS

The designed single straight tube Coriolis flowmeter was used for mass flow measurement. The sensor data was collected firstly, then it was filtered by FIR. The results before and after SVD correction are compared as shown in Figure 8.

After SVD processing, the signal is closer to the sine curve. The unsmooth points in the original data tend to be smooth. The flow rate of water was controlled by the flow regulator. The flow rate was measured by the Coriolis flowmeter test system (Table 5).

Foe the phase difference measurement method based on SVD and Nuttall window Fourier, the flow error under different flow rates was less than ±0.2 kg/min. If the measurement range of the Coriolis flowmeter test system was set at 0-100 kg/min, the reference error was less than ± 0.2%, and the accuracy level of the instrument could reach 0.2. The results showed that the new phase difference measurement method can improve the accuracy of phase difference measurement.

TABLE 5
Phase difference data and flow measurement error with different flow rates

Mass flow rate kg/min	Phase difference °	Mass flow rate kg/min	Error of Mass flow rate kg/min
20	-0.1195	20.0647	0.0647
40	0.6051	39.9708	-0.0292
60	1.3325	59.9570	-0.0430
80	2.0656	80.0938	0.0938
100	2.7942	100.1115	0.1115

CONCLUSIONS

The phase difference measurement method based on SVD and Nuttall windowed DFT method is adopted. Firstly, the signal is filtered by FIR to reduce the noise in the signal, and then the SVD data is modified to smooth the signal, and then the Nuttall window Fourier transform method is used to calculate the phase difference. Compared with traditional DFT, Nuttall windowed DFT can reduce the leakage phenomenon and improve the accuracy of phase difference.

ACKNOWLEDGEMENTS

The work was supported by the National Natural Science Foundation of China (51808041), Project of Natural Science Foundation of Shandong Province (ZR2019PEE005) and Binzhou University Doctoral Research Start-up Fund Project (2017Y20).

REFERENCES

[1] Vikram, A. and Edlabadkar, R. (2021) Performance evaluation of Coriolis mass flow meter in laminar flow regime. Flow Measurement and Instrumentation. 77, 101837.
[2] Meribout, M., Azzi, A., Ghendour, N., Kharoua, N., Khezzar, L. and AlHosani, E. (2020) Multiphase flow meters targeting oil & gas industries. Measurement. 165, 108111.
[3] Meribout, M., Shehzad, F., Kharoua, N. and Khezzar, L. (2020) An ultrasonic-based multiphase flow composition meter. Measurement. 161, 107806.
[4] Barbariol, T., Feltresi, E. and Susto, G. (2019) Machine learning approaches for anomaly detection in multiphase flow meters. IFAC-PapersOnLine. 52(11), 212-217.
[5] Meng, L., Li, Y., Zhang, J. and Dong, S. (2011) The development of a multiphase flow meter without separation based on sloped open channel dynamics. Flow Measurement and Instrumentation. 22(2), 120-125.
[6] Liu, R., Fuent, M., Henry, M. and Duta, M. (2002) A neural network to correct mass flow errors caused by two-phase flow in a digital Coriolis mass flowmeter. Flow Measurement and Instrumentation. 12(1), 53-63.
[7] Li, M. and Henry, M. (2018) Complex signal processing for Coriolis mass flow metering in two-phase flow. Flow Measurement and Instrumentation. 64, 104-115.
[8] Li, M., Henry, M., Zhou, F. and Tombs, M. (2019) Two-phase flow experiments with Coriolis Mass Flow Metering using complex signal processing. Flow Measurement and Instrumentation. 69, 101613.
[9] Ibryaeva, O., Barabanov, V., Henry, M., Tombs, M. and Zhou, F. (2020) A benchmark data set for two-phase Coriolis metering. Flow Measurement and Instrumentation. 72, 101721.
[10] Zhang, Y., Liu, Y., Liu, Z. and Liang, W. (2019) Developing a long short-term memory-based signal processing method for Coriolis mass flowmeter. Measurement. 148, 106896.
[11] Ruoff, J., Hodapp, M. and Kück, H. (2014) Finite element modelling of Coriolis mass flowmeters with arbitrary pipe geometry and unsteady flow conditions. Flow Measurement and Instrumentation. 37, 119-126.
[12] Zamora, M. and Henry, M. (2008) An FPGA implementation of a digital Coriolis mass flow metering drive system. IEEE Transactions on Industrial Electronics. 55(7), 2820-2831.
[13] Henry, M. (2001) On-line compensation in a digital Coriolis Mass Flow meter. Flow Measurement and Instrumentation. 12(2), 147-161.
[14] Sultan, G. and Hemp, J. (1989) Modelling of the Coriolis mass flowmeter. Journal of Sound and Vibration. 132(3), 473-489.
[15] Wang, T., Baker, R. and Hussain Y. (2006) An advanced numerical model for single straight tube Coriolis flowmeters. Journal of Fluids Engineering. 128(6), 1346-1350.
[16] Chen, N., Fan, S. and Zheng, D. (2019) A phase difference measurement method based on strong tracking filter for Coriolis mass flowmeter. The Review of Scientific Instruments. 90(7), 75003-75003.

[17] Zheng, M., Shen, F., Dou, Y. and Yan, X. (2009) Modal identification based on Hilbert-Huang Transform of structural response with SVD pre-processing. Acta Mechanica Sinica. 883-888.
[18] Wang, K., Zhang, L., Wen, H. and Xu, L. (2020) A sliding-window DFT based algorithm for parameter estimation of multi-frequency signal. Digital Signal Processing. 97, 102617.
[19] Shin, D., Kwak, C. and Kim, G. (2020) An efficient algorithm for frequency estimation from cosine-sum windowed DFT coefficients. Signal Processing. 166, 107245.
[20] Tu, Y. and Zhang, H. (2008) Method for CMF signal processing based on the recursive DTFT algorithm with negative frequency contribution. IEEE Transactions on Instrumentation & Measurement. 57(11), 2647-2654.
[21] Zhang, G., Li, D., Yao, D., Xue, L., Gao, H., Chen, Z. and Niu, Z. (2019) Numerical Analysis on Flow Characteristics of Water in Upward Dip Section of Long Distance Crude Oil Pipeline. Fresen. Environ. Bull. 28(12), 9568-9575.
[22] Jacobsen, E. and Lyons, R. (2003) The sliding DFT. IEEE Signal Processing Magazine. 20(2), 74-80.
[23] Huang, L. (2021) An improved phase difference detection method for a Coriolis flowmeter. Measurement. 172, 108862.

Received: **13.03.2021**
Accepted: **14.04.2021**

CORRESPONDING AUTHOR

Lei Huang
Mechanical and Control Engineering College,
Shengli College China University of Petroleum,
Dongying 257061 – China

e-mail: 2015016@slcupc.edu.cn

© by PSP Volume 30– No. 09/2021 pages 10652-10658 Fresenius Environmental Bulletin

RESEARCH ON THE RELATIONSHIP BETWEEN CHINA'S ENERGY CONSUMPTION AND ECONOMIC GROWTH BASED ON BIG DATA

Yang Chen[1,2,*], Yu Yu[2]

[1]School of Economics and Management, China University of Mining and Technology, Xuzhou 221000, China
[2]Department of Management Engineering, Xuzhou University of Technology, Xuzhou 221008, China

ABSTRACT

Energy is an important material basis for the survival and development of human society. Its extensive use has created huge wealth for human society and greatly improved social productivity. However, its negative limitations have also appeared simultaneously, profoundly affecting or restricting the economy. China has maintained a high economic growth rate since the reform and opening up. However, the rapid economic growth has paid a huge energy and environmental cost. Economic and social development is inseparable from the production and consumption of energy. The current development of energy resources, the maximum utilization of energy, and the development of new energy are all important issues that China's social and economic development pays attention to. This paper uses the data of GDP and energy consumption of Jiangsu Province from 2004 to 2019 to establish a coordinated development model to study the dynamic relationship between economic growth and energy consumption. The research results show that energy consumption has a positive effect on economic growth in the short term. The long-term effect is not obvious, but economic growth has a positive effect on energy consumption. Finally, suggestions to ensure the coordinated development of economic growth and energy consumption are put forward. This article supports to a certain extent national policies to reduce overcapacity, improve energy efficiency, and enhance industrial waste gas treatment capabilities.

KEYWORDS:
Energy consumption, Economic growth, Ecology

INTRODUCTION

As the largest developing country in the world, China has maintained a high economic growth rate since the reform and opening up [1-3]. However, the rapid economic growth has paid huge energy and environmental costs. Since 1990, China has greatly advocated rapid economic growth. Under the extensive economic model of development, the price of excessive consumption of resources and deterioration of the ecological environment was paid [4-6]. In 2005, the state began to pay attention to these issues and launched macro-control on high energy-consuming industries. However, until 2011, energy consumption remained relatively low. High-level growth rate, among which the growth rate changes in 2008 and 2009 have a small fluctuation. Moreover, during the observation period from 2005 to 2014, the proportion of raw coal in total energy consumption has been decreasing year by year, but it is much higher than the proportion of other energy types. The proportion of hydropower, nuclear power and wind power in total energy consumption has increased year by year [7-10]. This shows that the type of energy consumption in my country is coal. At the same time, the development and utilization of new energy is also increasing year by year, and the types are also becoming diversified [11]. However, the energy consumption structure that has always been dominated by coal will cause urgent ecological pollution problems, which will be a major obstacle to my country's green economy [12-14].

The relationship between energy consumption and economic growth is a question often studied by scholars. At different stages of economic development, these three have different relationships in reality and logic [15]. The report of the 19th National Congress of the Communist Party of China emphasized that China’s international status as the world’s largest developing country has not changed [16]. For a period of time in the future, China will still have to ensure a certain economic growth rate. This requires us to compare some energy consumption and industrial waste gas emissions [17]. Many industrial projects that can bring greater output value or are conducive to the economic growth and development of the entire society are more tolerant. In a certain period of time in the future, the contradiction between the pros and cons brought about by

the rapid development of industrialization is still one of the main contradictions that our country must handle well. The comprehensive economic strength of Jiangsu Province has always been at the forefront of China. In 2013, Jiangsu achieved a regional GDP of 5,916.18 billion yuan, an increase of 9.6% over the previous year, ranking second in China's provinces [18]. The per capita GDP is 74,607 yuan, which is US$12,047 at the average exchange rate, ranking first in China's provinces. However, like the situation in which China's economic development is in general, on the one hand, Jiangsu Province must continue to work hard on economic construction, on the other hand, it has to face the people's accusations of environmental pollution, especially air pollution. Therefore, how to deal with the relationship between environmental pollution, energy consumption and economic growth has become particularly important in the current period. Facing the increasingly severe energy and environmental problems, alleviating the excessively fast-growing energy consumption and pollution emissions, has become a long-term issue facing the sustainable development of the current and future economy [19].

The selection and processing methods of the variables involved in specific studies abroad are different, or the selected time period is different, or the methodologies used are different, and the conclusions drawn are not the same. Relevant domestic studies can all conclude that there is a balanced relationship between overall economic growth and energy consumption, but the relationship between energy consumption, environmental pollution and economic growth is not the same in different regions [20]. This paper uses the data of GDP and energy consumption of Jiangsu Province from 2004 to 2019 to establish a coordinated development model to study the dynamic relationship between economic growth and energy consumption.

MATERIALS AND METHODS

Data Sources and Variable Selection. The data from 2004 to 2019 in Jiangsu Province is used as the sample data, and the GDP of Jiangsu Province is used to represent economic growth. In order to eliminate the influence of price factors, the series data will be deflated using 2004 as the base period; statistics from Jiangsu Province The total energy consumption of the past years announced by the bureau is regarded as the annual energy consumption of Jiangsu Province (denoted by E);

Model selection. When traditional econometrics examines the relationship between variables, it is often required that the variables come from a stable random process. If the sequence is not stable, false regressions are prone to occur, resulting in serious errors in the conclusions obtained according to traditional statistical inference methods. In practice, many of the series that we have come into contact with are non-stationary and show obvious trend changes. If the regression model is directly established, the results obtained are often meaningless, and the explanatory power is lost. This paper selects the energy-economic coupling coordination degree model. This model is used to study the mutual influence and coordinated development relationship between energy and macroeconomics. Usually it is a model system composed of several models with independent functions and coupling mechanisms. The main ones are energy system models and macroeconomic models, and others are sometimes supplemented by investment decision models, population models, consumption models, and foreign trade models. Both the energy system model and the macroeconomic model can be operated and used separately to study the energy system structure and macroeconomic development issues. Through the exchange and feedback of information, the two can combine calculations and realize the coordinated research of economic growth and energy system development.

RESULTS AND DISCUSSION

Analysis of total energy consumption. During the "13th Five-Year Plan" period, Jiangsu further promoted the adjustment of industrial structure, actively optimized the energy consumption structure, vigorously implemented pollution prevention and control, and achieved certain results in carbon emission reduction. In 2019, the carbon emission intensity was reduced by about 24% compared with 2015. During the "Thirteenth Five-Year Plan" period, Jiangsu achieved a total of 30.37 million tons of coal and steel production capacity, shut down 4,454 chemical companies, and created 174 national-level green factories and 14 green parks, ranking first in the country in terms of number. By the end of 2019, all coal-fired power generation units in Jiangsu have reached ultra-low emission levels. From the perspective of energy consumption (Figure 1), due to the increasing emphasis on the energy and chemical industry in Jiangsu Province, the total energy consumption has been increasing year by year. Energy consumption has always been the main force in urban agglomerations, but in recent years it has maintained a relatively small amount of energy consumption growth, this move just responds to the call of the 19th National Congress of the Communist Party of China to "support the optimization and upgrading of traditional industries

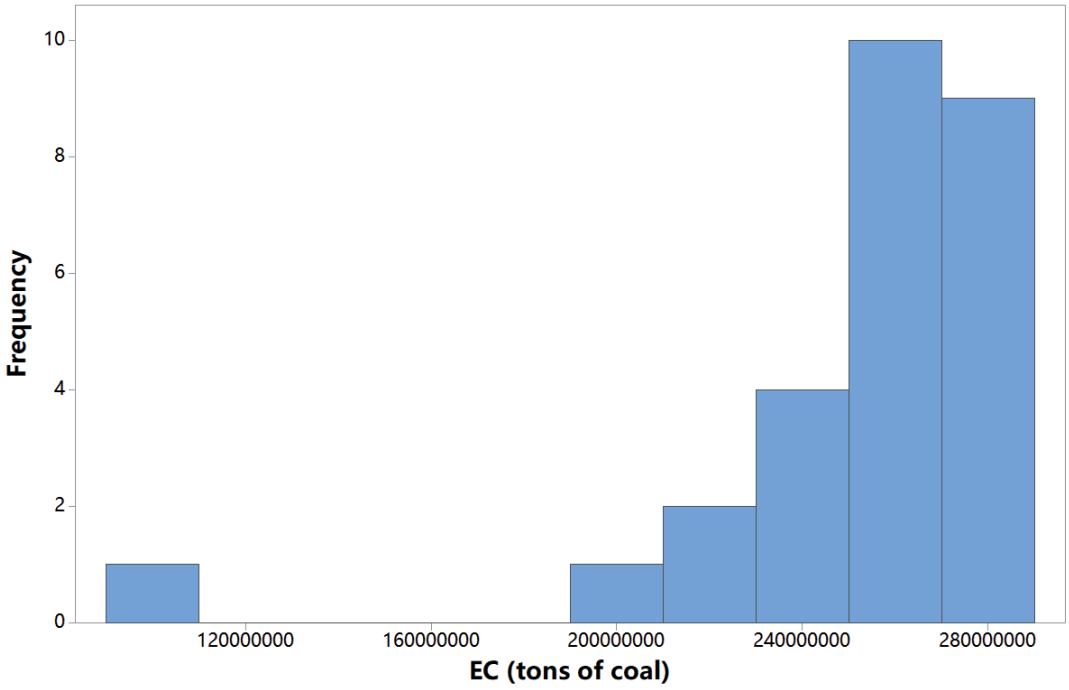


FIGURE 1
Energy consumption of urban agglomerations in Jiangsu Province from 2004 to 2019

and accelerate the development of modern service industries", and strive to achieve industrial transformation and upgrading.

Economic aggregate analysis. In 2019, our province will take effective measures to maintain stable and healthy economic development and accelerate the transformation from large to strong, high-speed growth to high-quality development. The overall strength continues to increase. The annual gross regional product value was 9.96 trillion yuan, an increase of 6.1% over the previous year. The province's per capita GDP was 123,600 yuan, an increase of 5.8% over the previous year. Fiscal revenue has grown steadily. The annual general public budget revenue was 880.2 billion yuan, a year-on-year increase of 2%; of which, tax revenue was 733.96 billion yuan, and tax accounted for 83.4% of general public budget revenue. Increased economic vitality. In the whole year, the non-public economy realized an added value of 7412.59 billion yuan, accounting for 74.4% of GDP; the added value of private and individual economy accounted for 51.2% of GDP, and the added value of private economy accounted for 55.9% of GDP. At the end of 2019, the province's industrial and commercial departments registered 3.12 million private enterprises and 6.858 million self-employed individuals.

It can be seen from Figure 2 that before 2012, the economic aggregate growth rate of urban agglomerations fluctuated greatly, reaching a peak of 55% in 2005. After 2008, due to the impact of the financial crisis, the national economic growth may have been affected. However, under the leadership of all parties, the urban agglomeration has overcome difficulties and still achieved steady economic growth; until 2019, the total economic volume of the urban agglomeration has been in a steady growth economic situation, and its GDP has increased from 155.124 billion in 2004. Yuan jumped to 9.96 trillion yuan in 2019, a 6.4-fold increase. Relatively speaking, Suzhou, Nanjing, and Wuxi have a relatively large contribution to the total economic volume of urban agglomerations, which is closely related to industrial cities and abundant energy reserves.

Economic and social development is inseparable from the influence of factors such as energy consumption, urbanization, foreign trade, and economic growth. In the traditional economic growth model, there are only two factors: labor and capital. As long as the input of labor and capital is continuously increased, the economy will continue to grow. With the continuous improvement of modern economic theory, in addition to the two factors of labor and capital, domestic and foreign scholars have also considered factors such as energy consumption, technological progress, foreign direct investment, and urbanization. Energy can be used as a major factor in the economic growth model to have an impact on economic growth. Energy is the driving force of economic growth. To a certain ex-

tent, the more energy consumed, the faster the economic growth. However, if energy is excessively consumed, this will be through the ecological environment. To curb the positive economic growth. At the same time, economic prosperity will drive the continuous development of the industry, thereby increasing the demand for energy consumption. However, with the improvement of production technology and the development of new energy sources, there is a corresponding trend of alleviation of energy consumption. Therefore, economic growth and energy consumption mutually promote and inhibit each other.

It can be seen from Figure 3 that with the development of cities, the energy consumption intensity of urban agglomerations is decreasing year by year, indicating that the economic utilization rate of energy consumption in urban agglomerations is increasing year by year. From 2000 to 2010, the energy consumption intensity of urban agglomerations has fallen sharply, indicating that the economic utilization rate of total energy consumption has increased significantly. From 2011 to 2019, the energy intensity of urban agglomerations has fluctuated smoothly, and it has begun to approach the national level. Level trend, energy consumption intensity has reached a bottleneck period. With the increase in energy consumption, the economic utilization rate of energy consumption is almost close to the level, and the increase in the economic utilization rate of energy consumption in urban agglomerations needs to be solved urgently. Compared with the trend of energy consumption per unit of GDP in the country, urban agglomerations have been much lower than the national level, indicating that the energy efficiency of urban agglomerations is relatively high, but there is still room for improvement, and it is necessary to learn advanced technology from provinces with high energy efficiency. Production and management experience, reduce the intensity of energy consumption, improve the economic utilization rate of energy consumption, and narrow the gap with the level of developed cities.

Related policies and recommendations. Do a good job in top-level design and strengthen policy guidance. Make overall plans and specific measures. Introduce a national action plan to clarify the implementation path, timetable and roadmap of "carbon peak", "carbon peak, carbon neutral". Break down the main indicators into various industries and regions, and combine the needs and affordability of economic development, put forward a plan for reaching peaks in key industries and key regions, and actively and steadily promote various tasks.

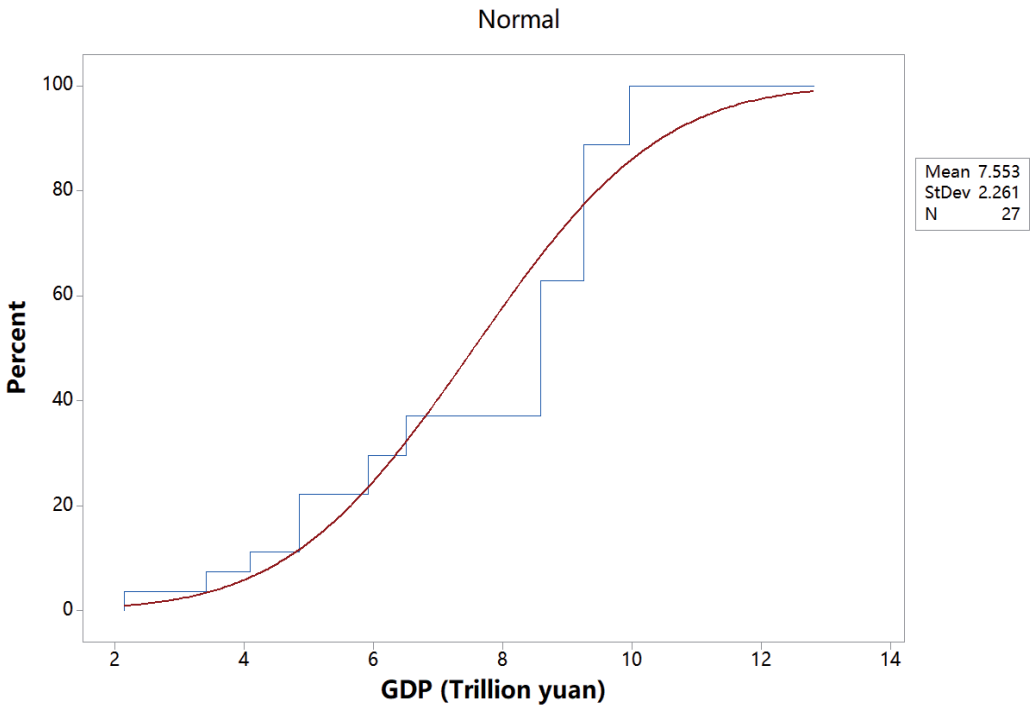
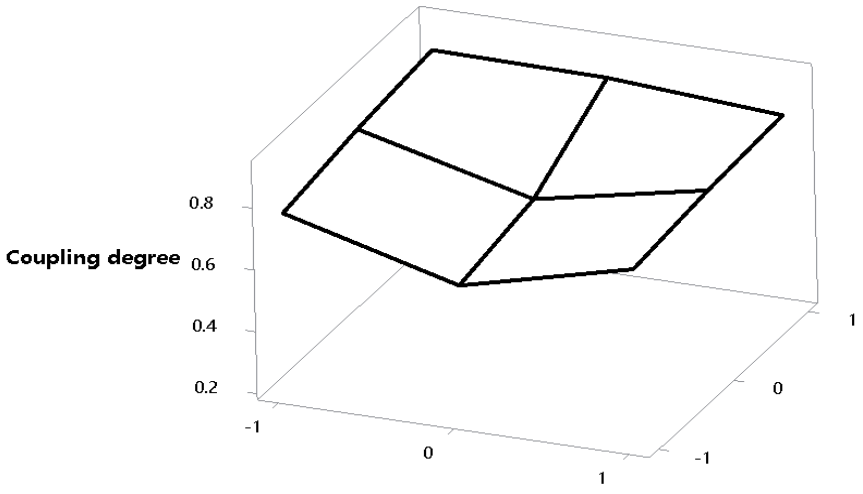
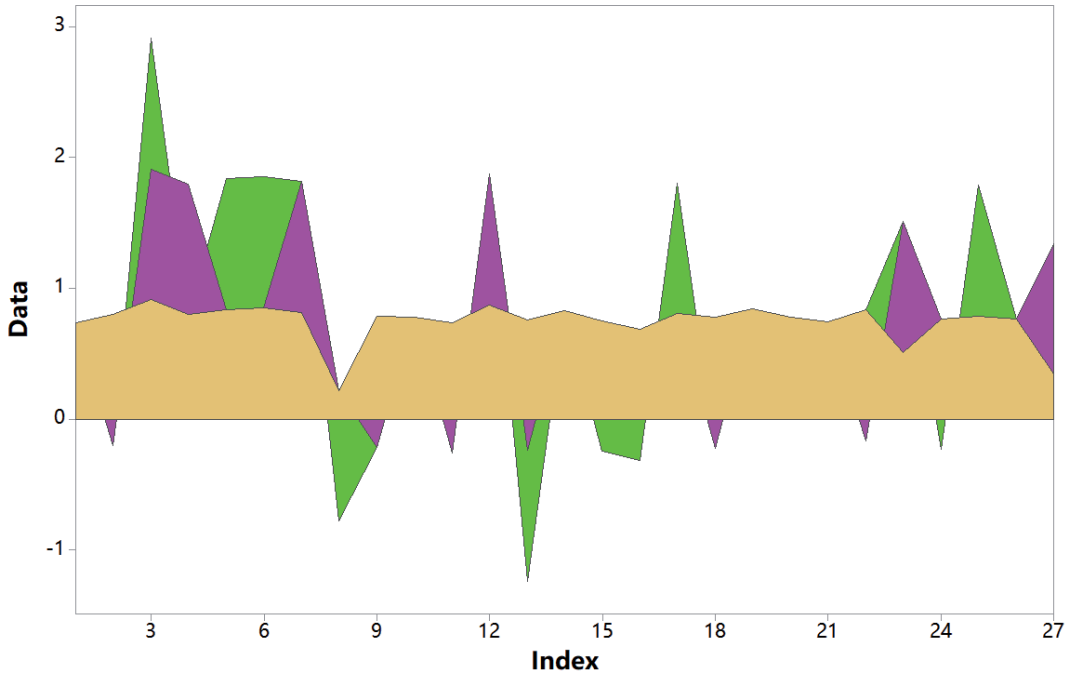


FIGURE 2
Empirical CDF of GDP (Trillion yuan)



(a)



(b)

FIGURE 3
Plot of Coupling degree

Adhere to and improve the dual control system of energy. Improve the dual control management measures, reasonably control the total energy consumption, strictly control the energy consumption intensity, and focus on the control of fossil energy consumption. Formulate demand-side response policies and measures to guide the whole process of green and low-carbon production and life behaviors of the whole society. Improve the guarantee mechanism for the consumption of renewable energy, and all users shall fairly bear the responsibility for consumption.

Strengthen the unified planning of energy and power. Carry forward the advantages of my country's power system safe operation experience, adhere to the system advantages of "unified planning, unified dispatch, and unified management" of the power grid, give full play to the role of the platform for the optimization of large power grid resources, and realize the coordinated linkage and effective connection of source, network and load. Incorporate major measures and key projects to promote the energy transition in all aspects of the power system into the national plan, coordinate and accelerate implementation.

Improve market mechanisms and price fiscal

and tax policies. Build a unified national power market, and improve the mechanism of reasonable formation of energy and power prices and cost easing. Improve the auxiliary service market transaction mechanism, and guide the thermal power unit to actively participate in system adjustment. Improve the mechanism for the formation of pumped-storage electricity prices and the allocation of capacity electricity charges, and establish an investment return mechanism for energy storage power stations. Through the price mechanism, mobilize the enthusiasm of users to save energy and reduce consumption and participate in demand-side response.

Promote the coordinated development of the carbon market and the electricity market. Based on the results of the reform of the electricity market, we will speed up the construction of the national carbon market and fully implement the market-oriented trading of carbon emission rights. Fully consider the impact of the carbon market on the electricity market, organically combine the price of electricity with the cost of carbon emissions, and play the role of mutual promotion and synergy between the two markets, improve the market competitiveness of clean energy, and let energy-using companies bear the cost of carbon emissions. Promote energy clean and low-carbon transformation.

The industry plays the role of the main body of implementation and promotes the implementation of the national plan. Power generation enterprises are vigorously developing clean energy, speeding up the implementation of flexible coal power transformation, and eliminating unqualified and backward coal-fired power generating units. Increase the proportion of flexibly adjustable power sources, build peak-shaving power sources, develop "new energy + energy storage" and solar thermal power generation, and improve system regulation capabilities. Accelerate the technological progress of carbon capture, storage and secondary utilization, and strive to achieve zero carbon emissions as soon as possible. Electricity-consuming companies actively respond to the needs of the power system, adjust their electricity consumption behavior and patterns in a timely manner, and actively consume clean energy. Industrial enterprises accelerate the promotion of green transformation, strengthen the reuse of waste heat, waste gas, and pressure, reduce energy consumption and improve energy efficiency. Relevant industries intensified the substitution of electric energy and improved the level of electrification. Strengthen independent innovation, develop and apply low-carbon energy-saving technologies and business models, promote green transportation and green buildings, and accelerate the construction of a green and low-carbon circular development economic system.

Social people take conscious actions to form a green and low-carbon production and lifestyle. Adhere to the concept that green water and green mountains are golden mountains and silver mountains, actively respond to the launch of national land greening actions, continuously increase forest area and stock, speed up the management of landscapes, forests, fields, lakes and grass systems, and enhance the carbon sequestration capacity of natural ecosystems. Consciously carry out green life creation activities, advocate simple and moderate, green and low-carbon production and lifestyles, and cultivate green, healthy and safe consumption habits. Vigorously promote the use of energy-saving and environmentally-friendly products to improve the level and efficiency of energy use.

CONCLUSIONS

This paper uses the data of GDP and energy consumption of Jiangsu Province from 2004 to 2019 to establish a coordinated development model to study the dynamic relationship between economic growth and energy consumption. The research results show that energy consumption has a positive effect on economic growth in the short term. The long-term effect is not obvious, but economic growth has a positive effect on energy consumption. Finally, suggestions to ensure the coordinated development of economic growth and energy consumption are put forward. This article supports to a certain extent national policies to reduce overcapacity, improve energy efficiency, and enhance industrial waste gas treatment capabilities.

REFERENCES

[1] Dong, Q.Y., Futawatari, T. (2015) A review of the progress in China's renewable energy generation, and its links with energy conservation, environmental degradation and economic growth. Fresen. Environ. Bull. 24, 405-411.

[2] Gultekin, U. (2019) Renewable electricity generation for sustainable development and environmental management in Turkey. Fresen. Environ. Bull. 28, 8171-8174.

[3] Broman, G.I., Robèrt, K.H. (2017) A framework for strategic sustainable development. J. Cleaner Prod. 140, 17-31.

[4] Gozgor, G., Chi, K.M.L., Lu, Z. (2018) Energy consumption and economic growth: New evidence from the OECD countries. Energy. 153, 27-34.

[5] Price, J., Keppo, I. (2017) Modelling to generate alternatives: A technique to explore uncertainty in energy-environment-economy models. Appl. Energy. 195, 356-369.
[6] Yousaf, K., Abbas, A., Zhang, X.J., Soomro, S.A., Ameen, M., Chen, K.J. (2018) Effect of multi-stage drying on energy consumption, the rate of drying, rice quality and its optimization during parboiling process. Fresen. Environ. Bull. 27, 8270-8279.
[7] Zhao, Y.B., Wang, S.J. (2015) The Relationship between Urbanization, Economic Growth and Energy Consumption in China: An Econometric Perspective Analysis. Sustainability. 7(5), 5609-5627.
[8] Lagunes-Diaz, E., Gonzalez-Avila, M.E., Diaz-Castro, S., Poujol, F., Ortega-Rubio, A. (2016) Energy consumption drivers: demand side management vs device penetration, which is stronger? implications in climate change in Arid Mexico. Fresen. Environ. Bull. 25, 3023-3029.
[9] Zhou, H.Y. (2020) Incentive mechanism of low carbon economic growth quality based on fuzzy cluster analysis. Fresen Environ Bull. 29(4), 2350-2356.
[10] Pao, H., Chen, H.A., Li, Y. (2015) Competitive dynamics of energy, environment, and economy in the U.S. Energy. 89, 449-460.
[11] Wang, S.S., Zhou, D.Q., Zhou, P., Wang, Q.W. (2011) CO_2 emissions, energy consumption and economic growth in China: A panel data analysis. Energy Policy. 39(9), 4870-4875.
[12] Pao, H.T., Fu, H.C., Tseng, C.L. (2012) Forecasting of CO2 emissions, energy consumption and economic growth in China using an improved grey model. Energy. 40(1), 400-409.
[13] Pao, H.T., Tsai, C.M. (2010) CO2 emissions, energy consumption and economic growth in BRIC countries. Energy Policy. 38(12), 7850-7860.
[14] Zhang, X.P., Cheng, X.M. (2009) Energy consumption, carbon emissions, and economic growth in China. Ecological Economics. 68(10), 2706-2712.
[15] He, Y., Lin, K., Zhang, F., Wang, Y., Chen, X. (2018) Coordination degree of the exploitation of water resources and its spatial differences in China. Sci. Total Environ. 644, 1117-1127.
[16] Xiong, S., Tian, Y., Ji, J., Ma, X. (2017) Allocation of energy consumption among provinces in China: a weighted ZSG-DEA model. Sustainability. 9(12), 2115-2116.
[17] Tang, X., McLellan, B.C., Snowden, S., Zhang, B., Hook, M. (2015) Dilemmas for China: Energy, economy and environment. Sustainability. 7, 5508-5520.
[18] Xu, Y.P., Wang, M., Qin, M., Shi, H.X., Sui, B.W., Jia, X.Z., Lu, D.L. (2018) Study of the relationship between economic growth and environmental quality with the Kuznets curve in Guangxi, China. Fresen Environ Bull. 27, 2818-2828.
[19] Han, S., Zhu, J. (2011) Research on the dynamic relationship of the Energy-Economy-Environment (3E) system-based on an empirical analysis of China. Energy Procedia. 5, 2397-2404.
[20] Soytas, U., Sari, R. (2009) Energy consumption, economic growth, and carbon emissions: Challenges faced by an EU candidate member. Ecological Economics. 68(6), 1667-1675.

Received: **17.03.2021**
Accepted: **14.04.2021**

CORRESPONDING AUTHOR

Yang Chen
School of Economics and Management,
China University of Mining and Technology,
Xuzhou 221000 – China

e-mail: chenyang897@hotmail.com

© by PSP Volume 30– No. 09/2021 pages 10659-10664 Fresenius Environmental Bulletin

RESEARCH ON CHINA'S TOURISM MODEL FROM THE PERSPECTIVE OF BIG DATA, BASED ON THE ECOLOGICAL PERSPECTIVE

Weijuan Yuan*

Yellow River Conservancy Technical Institute, Kaifeng 475000, China

ABSTRACT

In recent years, under the guidance of the concept of "green water and green mountains are golden mountains and silver mountains", rural eco-tourism has developed rapidly and has gradually become an important engine and booster for poverty alleviation and rural revitalization. This paper introduces the sustainable development theory and the green development system model. The research results show that: the current tourism development is out of the ecological green development path, and the ecological investment is obviously insufficient; the level of green welfare, the influence of green policies and the level of green development are constantly improving. And the actual green investment intensity and the dynamic optimal green investment intensity are constantly approaching. We should achieve unified planning; give full play to characteristics and strengthen brands; strengthen the construction of ecological civilization, strengthen the awareness of ecological civilization, and realize the sustainable development of eco-tourism under the premise of maintaining ecological civilization.

KEYWORDS:
Ecological tourism, Resources, Ecological civilization, Sustainable development

INTRODUCTION

The advancement of human civilization has brought about improvements in production efficiency, but has also created unprecedented pressure on the ecological environment [1-3]. Ecological economic system refers to a composite system with a certain structure and function formed under the mutual influence of the ecological and economic systems [4]. Any economic activity has a corresponding ecological economic system. The contradiction between economic and social development and environmental protection is related to the country's sustainable development and people's happiness, and it has always been the focus of attention of all countries [5]. While the development of traditional industrial civilization brings opportunities, it also gradually restricts social development and becomes a block in the way of national development. At this stage, the main direction of China's socialist construction is the construction of ecological civilization [6]. The construction of ecological civilization is an inevitable requirement for social development and an inevitable requirement for the overall development of human beings. Only by building an ecological civilization can sustainable development be achieved [7-10]. As a practical approach to the construction of ecological civilization, ecotourism is the key to the development of tourism industry and environmental protection.

Ecotourism is a subject that encompasses ecology and tourism. The purpose of ecotourism is to develop tourism under the guidance of ecological knowledge [11-13]. Ecological sustainable development is an important part of sustainable development, and it is also a long-term plan related to sustainable social and economic development that cannot be ignored. The term "eco-tourism" was first proposed by the World Conservation Union (IUCN) in 1983. In 1993, the International Ecotourism Association defined it as a tourism activity that has the dual responsibility of protecting the natural environment and maintaining the lives of local people [14-16]. Ecotourism refers to the responsible tourism behavior in a certain natural area. In order to enjoy and appreciate the historical and existing natural and cultural landscapes, such behavior should not interfere with the natural area, protect the ecological environment, and reduce the negative impact of tourism. Provide beneficial social and economic activities for the local population [17].

In the early days, eco-tourism was marketed as a tourism product. After the concept of sustainable development was put forward in the early 1990s, eco-tourism was considered to be the basic means and way to achieve sustainable tourism. Countries around the world apply the basic principles of sustainable tourism to the development of eco-tourism, highlight the protection of the ecological environment and characteristic culture in the development of tourism, and evaluate the social, economic, environmental and social effects of eco-tourism based on the criteria of sustainable development [18-20].

At present, eco-tourism is in a stage of rapid growth worldwide, and its development momentum is very strong. It is estimated that the average annual growth rate of eco-tourism is 20% to 25%, which is much higher than the average growth rate of the world tourism industry. Due to the great differences in the conditions of tourism resources, economic development levels, and social and cultural traditions of various countries in the world, there are also great regional differences in the eco-tourism models adopted [21]. Western economically developed countries have reached a certain level in tourism environmental management, and have more advanced governance technologies. Ecotourism emphasizes the protection of traditional cultures that are on the verge of disappearing. The tourism industry in the Asia-Pacific region is developing rapidly, and the problem of the tourism environment has become increasingly prominent, focusing on controlling the deterioration of the tourism environment [22]. Seashores, islands, and natural ecological areas are areas that implemented sustainable tourism strategies earlier. In their development strategies, ecotourism is an important means to achieve sustainable tourism goals. African countries pay more attention to the protection of primitive natural ecosystems. Although the eco-tourism development model of various countries in the world is still in the early stage of development, it has provided a good reference for the development of eco-tourism [23].

This paper introduces the sustainable development theory and the green development system model to study sustainable development of ecotourism.

MATERIALS AND METHODS

Green development system model construction. Modeling process of system dynamics. Using system dynamics to understand and solve system problems, modeling is a continuous cycle process between the virtual world represented by the model and the real world represented by actions, rather than a linear arrangement of various steps. The model has to undergo frequent and continuous questioning, testing and refinement.

RESULTS AND DISCUSSION

Index interannual change analysis. Figures 1 to 4 show the inter-annual changes of tourism consumption index, tourism environmental service index, green eco-tourism policy index and green ecotourism development index. By observing the interannual changes of these indexes rather than individual measures, we can more clearly show the development status of the economy, resources and environment over the years, and compare the degree of correlation between the indexes. It can be seen from the figure that the correlation between the green policy index and the consumption index is weak, and the change of the green policy index has a small impact on the change of the consumption index. Judging from China's current national conditions, the overall income of consumers is at a lower-middle level, and the demand for green tourism products is relatively small. In particular, the issue of consumer safety is worrying. The change trends of the tourism environmental service index and the green policy index are basically the same. The environmental index and the green policy index show a strong correlation. The level of tourism products and services is greatly affected by national policies, but the fluctuation range of the green policy index is weaker than that of the environmental service index. This shows that the green support in China's national policy the strength is not enough. Since the Green Policy Index only involves investment measures for environmental pollution control, this shows that China's environmental governance efficiency is relatively low, China's environmental pollution has not been curbed or improved, its environmental governance capacity is relatively low, and its environmental governance efficiency is still less than three points of that of developed countries. First, it has become particularly urgent to improve the level of green technology research and development and improve the government's environmental management capabilities.

Path to Realize the Sustainable Development of Ecotourism. Relying on the government's unified planning. The development of eco-tourism must be developed in a unified manner under the rational planning of the government and the ideology of protecting the ecological environment. The resources and environment must not be destroyed, and comprehensive development must be achieved. The development of eco-tourism projects must be planned in a unified manner, strictly managed, guided by the theory of sustainable ecological development, and fully create an atmosphere of harmony between man and nature, and create a scenic spot where man and nature are in harmony. At the same time, in order to meet the requirements of environmental tourism, relevant construction must follow the principles of scientific and orderly development, and any form of development must not harm nature. This requires a full assessment of the environment first, so that we can understand the environmental capacity of the tourist area and better obtain local materials to create a unique eco-tourism scenic spot. If the development of tourism exceeds the capacity of the environment itself, it will cause serious damage to the environment, making it difficult to effectively protect and manage, or even to manage. The local government should scientifically plan the development of the tourism industry from the perspective of ecological civilization, formulate relevant

strategies, and cooperate with scientific research institutions of universities to popularize ecological civilization and tourism management knowledge to the public to promote the development of local tourism economy.

Give full play to the characteristics and strengthen the brand. The model of eco-tourism should not be limited to sightseeing tours. It should also have an innovative spirit, develop leisure, entertainment and accommodation according to the characteristics of each region, highlight regional cultural characteristics, and tap local folk customs and ethnic characteristics resources. In the selection of tourist attractions, innovation must be combined with local characteristics, local materials must be selected, and the pursuit of harmony between man and nature and harmony between man and nature must be pursued.

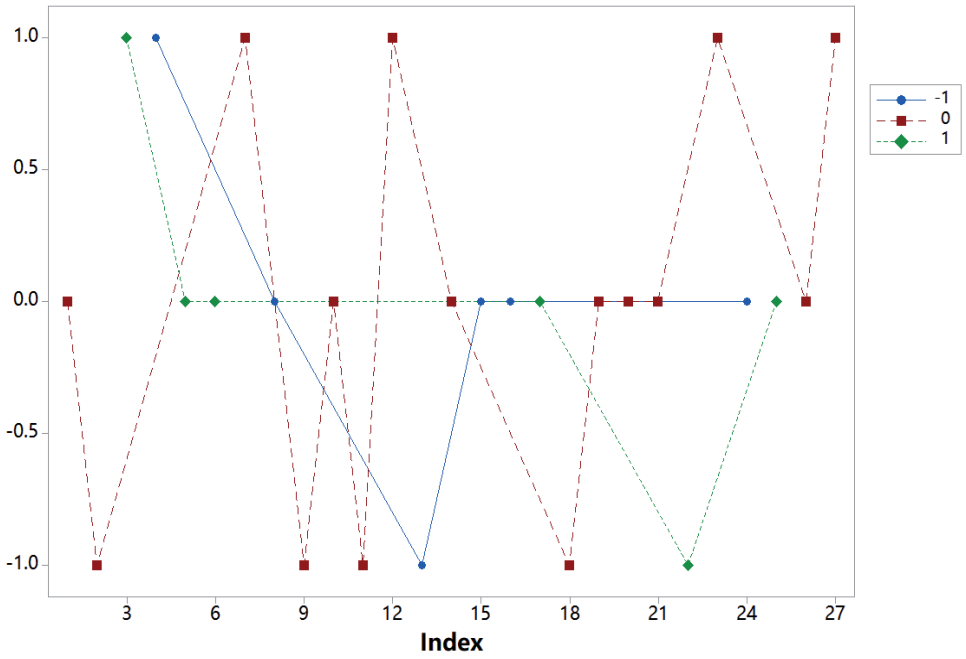


FIGURE 1
Time Series Plot

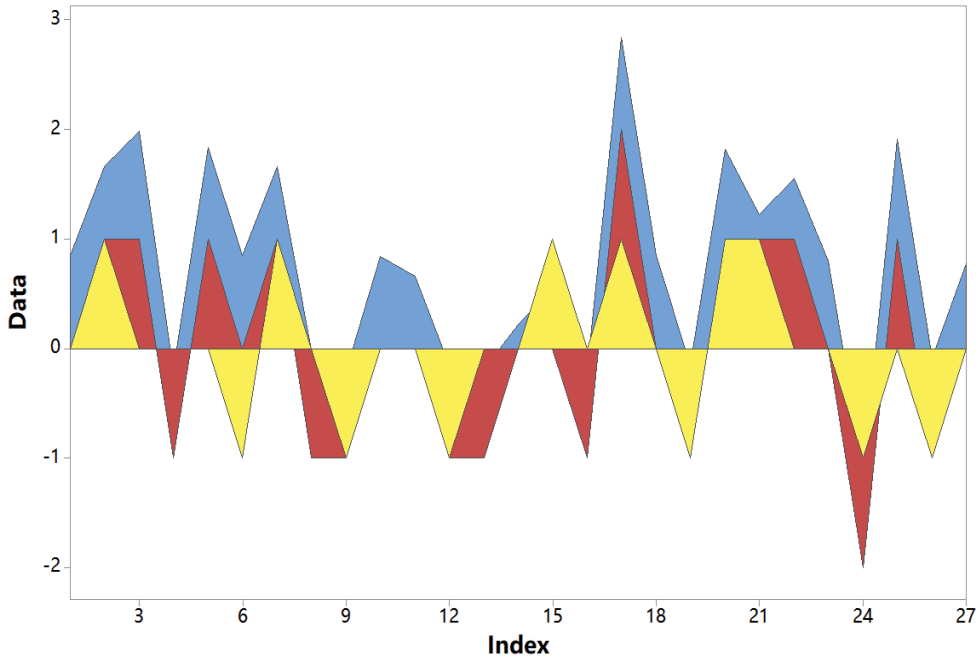


FIGURE 2
Area Graph of Tourism environmental service index

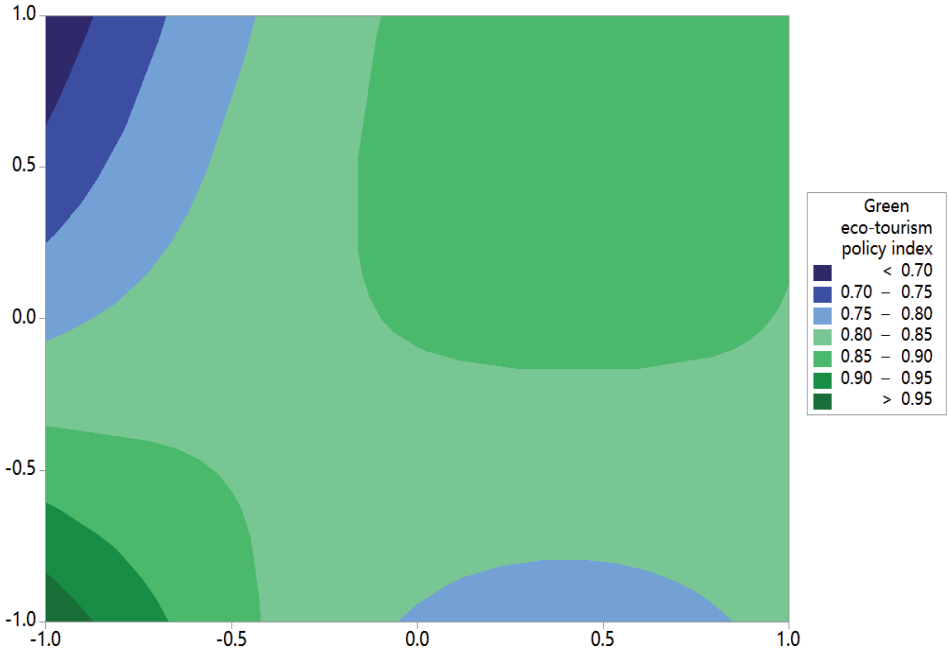


FIGURE 3
Contour Plot of Green eco-tourism policy index

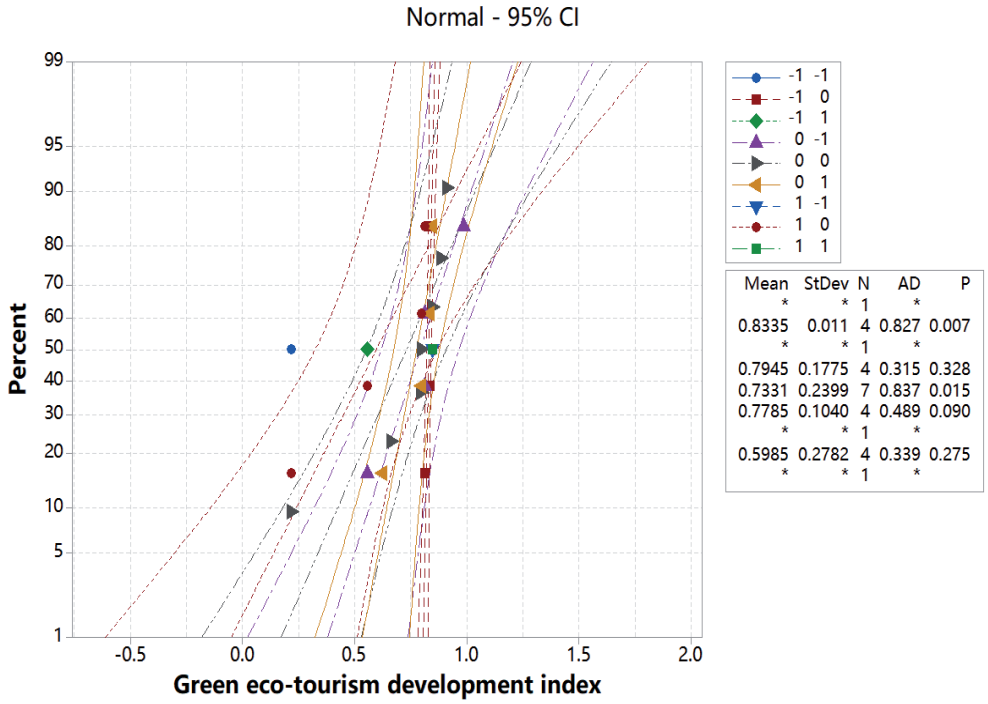


FIGURE 4
Probability Plot of Green eco-tourism development index

Strengthen the construction of ecological civilization and strengthen the awareness of ecological civilization. It is necessary to grasp regional characteristics from the perspective of ecological civilization, objectively analyze the problems in the ecological environment, and fully implement the concept of sustainable development. Combine policy guidance with tourism development and construction, and increase investment in eco-tourism. It is necessary to strengthen ecological environmental protection, realize the organic combination of ecological tourism and environmental protection, and realize common development and progress. To promote the development of green economy. Establish a modern green economic industrial system with the

theme of openness, innovation and green development. At the same time, it can attract local residents and foreign investors to participate in the construction of eco-tourism facilities, further improve infrastructure, and increase public participation.

Although the strategic thinking of environmental protection and sustainable development has gradually taken root in the hearts of the people, there will be people who despise environmental protection and pay more attention to economic benefits because of the problems left over from the times. This requires strengthening the popularization of local people's awareness of ecological civilization and strengthening the management of professional managers, and conducting professional and systematic business training on their environmental awareness, skill level, and professional ethics. Improve relevant environmental protection facilities, such as setting up warning signs to remind tourists to protect the ecological environment, setting up relevant regulations to restrain tourists' uncivilized behavior, and strengthening tourists' awareness of environmental protection.

Increase publicity, scientific marketing. With the progress of society and the rapid development of the Internet, the Internet has become the mainstream way of propaganda. To catch the ride on the Internet, you must first establish your own eco-tourism official website, with your own official account, official account, etc. With the development of the Internet, the publicity method should also change from the original single text publicity to colorful picture publicity and dynamic video publicity. Actively learn from the regions and organizations that have achieved successful experience. In addition, to improve the quality of eco-tourism, it is necessary to continuously improve its own ecological protection capabilities and the level of eco-tourism development.

Strengthen legal and policy guidance. South Korea formally promulgated the "Low-Carbon Green Growth Basic Law" in January and August. South Korea's "Basic Law on Green Growth" not only responded to the responsibility of global greenhouse gas emission reductions, but more importantly, it promoted South Korea to the first place after the "Han River Miracle". The second round of epoch-making economic transition period. The South Korean government adopts a green growth strategy in which legislation, policies, and planning go hand in hand. In contrast, my country still has a long way to go in terms of the understanding, legislation and practice of green development. The law is the greatest invention of mankind. It allows mankind to learn how to restrain itself. Law is a binding criterion that regulates the behavior of the whole society, and it is a manifestation of mature and institutionalized policies. Although China has no special laws on green development at this stage, there are no lack of relevant laws to promote green development. As a "soft law" policy, although it does not have the mandatory binding force of the law, as a guide to standardize the behavior of the whole society, it has a calling, guiding and stimulating function. By formulating a policy framework, it provides new ways to create economic value and solve environmental problems, and open up innovative economic growth opportunities, and put forward behavior guidelines and specific goals for the whole society to promote green development.

CONCLUSIONS

This paper introduces the sustainable development theory and the green development system model. The research results show that: the current tourism development is out of the ecological green development path, and the ecological investment is obviously insufficient; the level of green welfare, the influence of green policies and the level of green development are constantly improving. And the actual green investment intensity and the dynamic optimal green investment intensity are constantly approaching. We should achieve unified planning; give full play to characteristics and strengthen brands; strengthen the construction of ecological civilization, strengthen the awareness of ecological civilization, and realize the sustainable development of eco-tourism under the premise of maintaining ecological civilization.

REFERENCES

[1] Kiper, T., Uzun, O., Topal, T.U. (2016) A method approach for identifying thematic footpaths in ecotourism: kiyikoy pabucdere and kazandere basins. Fresen. Environ. Bull. 25, 6139-6150.

[2] Li, L., Hong, X.F., Wang, J. (2018) Spatial effects of technology innovation on energy-related carbon emissions: a spatial panel approach. Fresen. Environ. Bull. 27(12), 8053-8061.

[3] Wang, W. (2019) Analysis of three relations in rural tourism development of China Guizhou under the strategic background of rural vitalization. Fresen. Environ. Bull. 28, 2733-2738.

[4] Dong, Q.Y., Futawatari, T. (2015) A review of the progress in China's renewable energy generation, and its links with energy conservation, environmental degradation and economic growth. Fresen. Environ. Bull. 24, 405-411.

[5] Gultekin, U. (2019) Renewable electricity generation for sustainable development and environmental management in Turkey. Fresen. Environ. Bull. 28, 8171-8174.

[6] Yao, H.Q., Liu, B. (2020) Study on the problems of rural tourism eco-environment and its countermeasures. Fresen. Environ. Bull. 29, 1489-1492.
[7] Wang, Q.Y., Li, M., Yang, Y.L. (2019) Study on the issues of rural tourism eco-environment and governance strategy. Fresen. Environ. Bull. 28, 10083-10088.
[8] Kim, K.H., Park, D.B. (2016) Relationships among Perceived Value, Satisfaction, and Loyalty: Community-Based Ecotourism in Korea. Journal of Travel & Tourism Marketing. 34(2), 1-21.
[9] Oviedo-García, M.Á., Castellanos-Verdugo M., Vega-Vázquez, M., Agüera, F.O. (2017) The Mediating Roles of the Overall Perceived Value of the Ecotourism Site and Attitudes Towards Ecotourism in Sustainability Through the Key Relationship Ecotourism Knowledge-Ecotourist Satisfaction. International Journal of Tourism Research. 19(2), 203-213.
[10] Jamrozy, U., Lawonk, K. (2017) The multiple dimensions of consumption values in ecotourism. International Journal of Culture Tourism & Hospitality Research. 11(1), 18-34.
[11] Hatak, I., Floh, A., Zauner, A. (2015) Working on a dream: sustainable organisational change in SMEs using the example of the Austrian wine industry. Review of Managerial Science. 9(2), 285-315.
[12] Lagunes-Diaz, E., Gonzalez-Avila, M.E., Diaz-Castro, S., Poujol, F., Ortega-Rubio, A. (2016) Energy consumption drivers: demand side management vs device penetration, which is stronger? Implications in climate change in Arid Mexico. Fresen. Environ. Bull. 25, 3023-3029.
[13] Zhou, H.Y. (2020) Incentive mechanism of low carbon economic growth quality based on fuzzy cluster analysis. Fresen. Environ. Bull. 29(4), 2350-2356.
[14] Pao, H., Chen, H.A., Li, Y. (2015) Competitive dynamics of energy, environment, and economy in the U.S. Energy. 89, 449-460.
[15] Wang, S.S., Zhou, D.Q., Zhou, P., Wang, Q.W. (2011) CO2 emissions, energy consumption and economic growth in China: A panel data analysis. Energy Policy. 39(9), 4870-4875.
[16] Pao, H.T., Fu, H.C., Tseng, C.L. (2012) Forecasting of CO2 emissions, energy consumption and economic growth in China using an improved grey model. Energy. 40(1), 400-409.
[17] Tang, X., McLellan, B.C., Snowden, S., Zhang, B., Hook, M. (2015) Dilemmas for China: Energy, economy and environment. Sustainability. 7, 5508-5520.
[18] Xu, Y.P., Wang, M., Qin, M., Shi, H.X., Sui, B.W., Jia, X.Z., Lu, D.L. (2018) Study of the relationship between economic growth and environmental quality with the Kuznets curve in Guangxi, China. Fresen. Environ. Bull. 27, 2818-2828.
[19] Butler, R.W. (1991) Tourism, environment, and sustainable development. Environmental Conservation. 18, 201-209.
[20] Cobbinah, P.B. (2015) Contextualizing the meaning of ecotourism. Tour. Manag. Perspect. 16, 179-189.
[21] Sayyed, M.R.G., Mansoori, M.S., Jaybhaye, R.G. (2013) SWOT analysis of Tandooreh National Park (NE Iran) for sustainable ecotourism. Proc. Int. Aca. Ecol. Environ. Sci. 3(4), 296-305.
[22] Liu, C., Li, J., Pechacek, P. (2013) Current trends of ecotourism in China's nature reserves: a review of the Chinese literature. Tour. Manag. Perspect. 7, 16-24.
[23] Lenao, M., Basupi, B. (2016) Ecotourism development and female empowerment in Botswana: a review. Tour. Manag. Perspect. 18, 51-58.

Received: **22.03.2021**
Accepted: **16.05.2021**

CORRESPONDING AUTHOR

Weijuan Yuan
Yellow River Conservancy Technical Institute,
Kaifeng 475000 – China

e-mail: yunwenjuan8889@163.com

© by PSP Volume 30– No. 09/2021 pages 10665-10674 Fresenius Environmental Bulletin

RESEARCH ON THE SPATIO-TEMPORAL EVOLUTION OF TOURISM ECO-EFFICIENCY BY USING THE ECOLOGICAL FOOTPRINT MODEL

Libo Lin*

Management School, Inner Mongolia University for Nationalities, Tongliao, Inner Mongolia 028000, P.R. China

ABSTRACT

As an emerging industry, tourism has a very important impact on the development of ecological economy. Therefore, it is of great significance to accurately evaluate the tourism ecological efficiency. Based on the ecological footprint analysis method, this paper constructs a calculation model of ecological efficiency, and analyzes the changes of tourism overall characteristics, including six elements from time and space by taking Yunnan Province of China as an example. The results reveal that although the ecological efficiency of tourism in Yunnan Province has fluctuated in recent ten years, it is on the rise as a whole, and the effective utilization of environmental resources is increasing. Spatial distribution is unbalanced, showing the characteristics of high abdomen and low surrounding, and the ecological efficiency of the northern region is higher than that of the southern region. The overall utilization rate of catering and transportation is low, which is less than half of the industrial ecological efficiency, and it needs to be further optimized and improved. The ecological efficiency of catering in Kunming and Xishuangbanna is higher, and the utilization rate of traffic ecological environment in Xishuangbanna, Honghe and Lijiang is higher. The ecological efficiency of housing, tourism, shopping and entertainment are far higher than the overall efficiency of the industry. Through the analysis, it can be seen that diet, transportation and shopping have a greater response to ecological efficiency. To improve the eco-efficiency, it is necessary to increase tourism revenue and reduce environmental energy consumption.

KEYWORDS:
Ecological footprint, ecological efficiency, environmental resources, tourism, spatial and temporal characteristics, countermeasures

INTRODUCTION

With the development of society, tourism has gradually developed from the edge of the national economy into a national strategic pillar industry [1]. Yunnan Province, as a big tourism province, has gorgeous natural scenery, including Lijiang ancient city, Yulong Snow Mountain, Erhai, Xishuangbanna tropical rain forest and other scenic spots, attracting countless Chinese and foreign tourists. Tourism income of Yunnan Province in 2019 was 113.52 billion yuan, an increase of 204.376 billion yuan compared with 2018, an increase of 22.73 % year on year, accounting for 7.1 % of GDP of the province, effectively promoting economic development [2-5]. Although promoting the economic development of commerce, transportation, catering services and other industries, overload tourism has also brought non-negligible pressure to the location [6]. The problems of ecological destruction, resource shortage and environmental pollution are becoming more and more serious, and the gap between the comprehensive development level of ecological environment and the development level of tourism is gradually widening. In order to make up for this shortcoming, Yunnan provincial government has formulated a series of policies to coordinate the relationship between tourism economic development and ecological environment protection, strengthen supply-side reform, and deeply optimize resource allocation, so as to improve the overall ecological efficiency of tourism industry [7-9]. Therefore, in the tourism environment of promoting quality and efficiency, how to accurately evaluate the tourism ecological efficiency and explore the countermeasures to improve the tourism ecological efficiency is an urgent problem to be solved in the innovation of tourism development mode.

In the early 21st century, it was introduced into the tourism industry and became an important indicator to evaluate the sustainability of tourism development [10]. On the basis of clarifying the ecological system structure of the Seychelles Reserve, Scholars combined with the results of the tourism ecological footprint model, interpreted the correlation between economic efficiency and environmental safety of the tourism industry, and discussed the advantages and disadvantages of different methods [11,12]. By used the data sets of 103 regions in Qinling in recent five years, Yang et al. [13] evaluated the ecological efficiency competitiveness of tourist attractions by using parametric and non parametric methods, stochastic production function method and

data envelopment analysis method. By comprehensively considering the problems existing in the tourism function, some people simulated the inherent economic process of the region, and emphasized the adjustment of national tourism industry planning on the basis of national administrative decision-making, so as to improve regional tourism ecological efficiency and core competitiveness of economic development [14-17]. Zhan et al. [18] analyzed the ecological efficiency of different scale types of tourism operation system, and put forward the best way to improve tourism ecological efficiency and management suggestions. Langnel et al. [19] built a tourism ecological footprint model from two aspects of resource consumption and waste absorption according to the practical survey results, which provided a scientific theoretical basis for the follow-up evaluation of ecological and economic efficiency. The Super-SBM DEA model was used to measure the tourism ecological efficiency of forest parks [20]. Through the Dagum Gini coefficient and a variety of convergence test methods, the spatial disequilibrium situation and convergence characteristics of different regions are described, and suggestions for reversing the regional gap of ecological efficiency are put forward [21,22].

In order to promote the harmonious development of tourism economy and ecological environment, this paper makes an in-depth analysis of ecological efficiency based on the tourism industry in Yunnan Province. In which, we constructs an ecological efficiency calculation model based on ecological footprint analysis. According to the measurement results, the overall trend of tourism industry from two aspects of time and space are analyzed, including the dynamic change rules of six tourism elements (catering, housing, transportation, tourism, shopping and entertainment).

MATERIALS AND METHODS

Yunnan Province is located in Southwest China, covering an area of 394,100 square kilometers, with a permanent population of 48.583 million. In addition to the Han nationality, there are 15 ethnic minorities with a population of more than 6,000, which is the province with the most ethnic groups [23]. The terrain is divided into east and west regions. The eastern part is the eastern and central Yunnan plateau, and most of them are low mountains and round hills. High mountains and canyons in the west, the terrain is grim, the formation of strange, magnificent mountain glacier landscape [24, 25]. The rich national culture and unique topography have created a unique folk natural landscape in Yunnan Province. There are more than 200 scenic spots and attractions in the province, 12 national scenic spots, 134 national scenic spots above level A, and 6 national historical and cultural cities, which deeply attract Chinese and foreign tourists [26]. In 2019, Yunnan received 14.849 million overseas visitors and 799.778 million domestic visitors, an increase of 4.8% and 17.4% respectively compared with 2018. The rapid growth of the number of tourists and tourism income, not only led to the rapid development of infrastructure, accelerate the interaction of capital, logistics, personnel, but also caused the ecological environment pollution problem is becoming more and more serious, the comprehensive development level of ecological environment and tourism development level gradually widen the gap.

Tourism ecological efficiency is a bridge between economy and ecology, which aims to maximize economic benefits and minimize the impact on ecological environment [27]. The specific method is as follows: (1) Calculating the tourist ecological footprint value of Yunnan Province. (2) Counting tourism industry catering, housing, transportation, tourism, shopping and entertainment six parts of the consumption income in the past ten years [28]. (3) Constructing a tourism eco-efficiency model based on the ecological footprint method, and tourism ecological efficiency is equal to the ratio of tourism income to ecological footprint. The calculation results of ecological footprint of Yunnan Province from 2010 to 2019 is shown in Table 1.

TABLE 1
Ecological Footprint value of Yunnan Province from 2010 to 2019 (hm^2)

Years	Catering	Housing	Traffic	Tourism	Shopping	Entertainment	Total
2010	2534285	8061	1889188	6408	4940	14258	4465726
2011	2170583	8005	1968455	6407	7228	14983	4179138
2012	2763233	8475	2562955	6489	11114	16281	5368180
2013	3488787	8599	3434888	7472	8586	17041	6978090
2014	3667665	7547	4135077	6969	13836	18823	7856278
2015	4318972	7518	4637100	7265	16014	19514	9016679
2016	5001590	7566	5033433	13733	39522	27601	10125087
2017	7135050	7765	5839311	13603	42565	23840	13060155
2018	8674804	6404	7900244	15550	57632	25712	16674514
2019	7723076	5264	7477488	15550	71645	36759	15326764

RESULTS AND DISCUSSION

Calculation of ecological efficiency of tourism industry. On the basis of tourism ecological footprint method, combined with single index method and index system method, taking ecological footprint as input index and tourism income as output index, that is, tourism eco-efficiency is equal to the ratio of tourism income to ecological footprint. The tourism ecological efficiency model based on ecological footprint method is constructed, and environmental factors are included in the evaluation index of tourism ecological efficiency, so as to reflect the degree of sustainable development of tourism in the study area [29, 30]. The higher the value of tourism ecological efficiency is, the richer the tourism benefits are obtained under unit environmental consumption, and the higher the degree of sustainable development is. On the contrary, tourism income per unit of environmental consumption is low and the degree of sustainable development is poor [31]. The calculation results of ecological efficiency in Yunnan Province is shown in Table 2.

Overall dynamic analysis of tourism ecological efficiency. The change of tourism ecological efficiency in Yunnan Province from 2010 to 2019 is shown in Figure 1. Although the tourism ecological efficiency in Yunnan Province has fluctuated in the past decade, it has an overall upward trend, and the effective utilization of environmental resources has been increasing. In 2011, the growth rate of ecological efficiency was the largest, with an increase of 38.2%. The main reason is that Yunnan Province implemented tourism "Second Undertaking", relying on scenic spots to set up rural holiday pilot to promote consumption, and the tourism income increased by 19932.7248 million yuan compared with 2010. During the period of 2012~2018, although the tourism ecological efficiency has declined in some years, with the maximum decline rate of 5.7%, it has basically maintained a stable and rising trend. Under the influence of the theme publicity activities of "Wisdom·Travel to Yunnan", the ecological efficiency rose from 29243.2 yuan/hm2 to 34568.4 yuan/hm2 in 2019. The growth effect was obvious and the effective utilization rate of resources was greatly improved.

TABLE 2
Ecological efficiency of Yunnan Province from 2010 to 2019 (yuan/hm^2)

Years	Catering	Housing	Traffic	Tourism	Shopping	Entertainment	Total
2010	4810	1703698	6590	1577433	2407214	507476	15169
2011	7443	2209792	8147	2032234	2119166	622079	20965
2012	7172	2634137	7896	2532331	2185706	722475	20718
2013	7203	3292255	7472	2788803	2151385	875434	19541
2014	8686	4755114	7868	3789622	2246047	1004578	22507
2015	9248	5985108	8807	3838700	2112989	1222659	24124
2016	9988	7635741	10133	3792518	1876239	1433351	28131
2017	10300	9082859	10949	4068845	1690808	1558781	28610
2018	10747	15376669	9237	4347062	1437021	1881895	29243
2019	11793	19110434	14093	6027508	1279563	1731831	34568

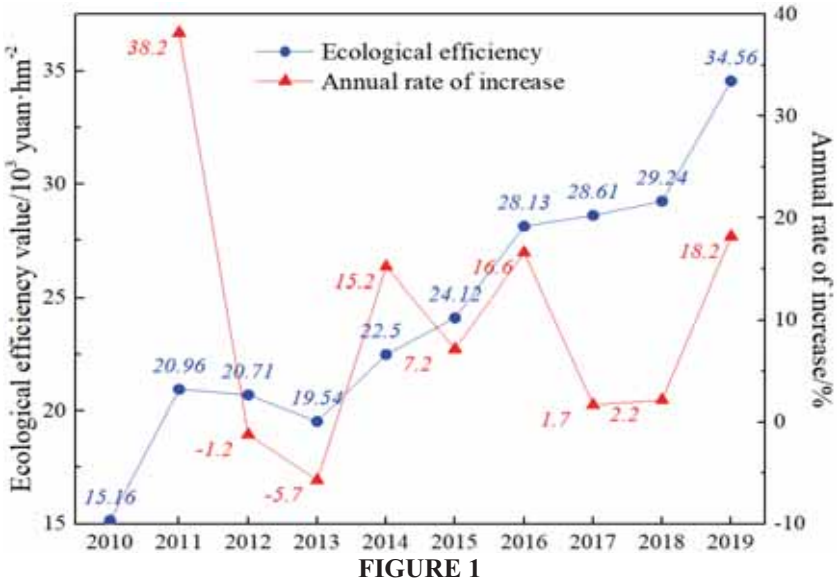


FIGURE 1
Change of tourism ecological efficiency in Yunnan Province from 2010 to 2019



FIGURE 2
Distribution of ecological efficiency value of tourism core cities in Yunnan Province

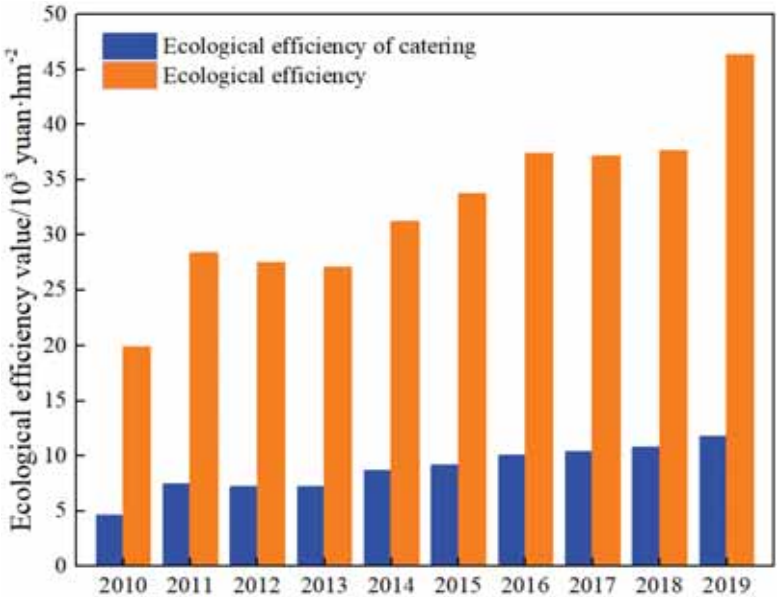


FIGURE 3
Change of ecological efficiency of catering in Yunnan Province from 2010 to 2019

The spatial output of regional ecological efficiency in Yunnan Province is unbalanced, showing the characteristics of high abdomen and low surrounding, and the ecological efficiency in the northern region is higher than that in the southern region, as shown in Figure 2. They are mainly concentrated in five core cities, from high to low: Kunming (37227.5 yuan/hm2), Lijiang (37037.6 yuan/hm2), Dali (36872.9 yuan/hm2), Xishuangbanna (36601.8 yuan/hm2) and Honghe (34568.4 yuan/hm2), which are higher than the total ecological output value of tourism industry in the whole province.The output level of ecological efficiency in other cities is generally low, at 27290.6 yuan/hm2. The core city is rich in tourism resources, the number of tourists visiting to the core cities is increasing year by year, the facilities and service level of the scenic spot are constantly improving, the growth rate of tourism consumption income is far higher than the consumption rate of the ecological environment, the tourism ecological efficiency is in a healthy and efficient state, and the industrial development space is becoming mature. The surrounding cities due to the small number of scenic spots, and the visibility is not high, infrastructure needs to be improved, the number of visitors to visit is less. Although the intervention on the environment is smaller, due to the meager consumption income, the output of tourism ecological efficiency is lower than the overall level of tourism industry, which is unhealthy and inefficient. Profit space and tourism resources need to be improved.

Dynamic analysis of ecological efficiency of tourism catering. Form Figure 3, it can be seen that the ecological efficiency of tourism catering in Yunnan Province shows a slow rising trend from 2010 to 2019, from 4810.6 yuan/hm2 in 2010 to 11793.9 yuan/hm2 at present, with an average annual growth rate of 14.5%. However, the overall utilization rate of the environment is low, less than half of the industrial ecological efficiency, and the input and output need to be further optimized. In the catering structure, meat food is far more complex than fruits and vegetables because of its feeding, transportation, processing and other production links, so the utilization rate of the ecological environment is relatively small. At the beginning of 2014, the outbreak of avian influenza in more than 35 countries in the world led to the killing of millions of poultry and the rise in the price of meat food. Some consumers' dietary structure inclined to fruits and vegetables that had little impact on the ecological environment. As a result, the ecological efficiency of catering increased by 1482.7 yuan/hm2 compared with 2013, and the utilization rate of the environment increased by 21%. Therefore, under the level of ensuring the quality and structure of tourists' diet, tourists can be appropriately guided to reduce meat consumption, increase fruit and vegetable consumption, reduce ecological occupation, and improve the ecological efficiency of catering.

Draw the distribution map of tourism catering ecological efficiency of each city, as shown in Figure 4. Among the core cities, Kunming as the capital of Yunnan Province, tourists from other provinces to Yunnan are mostly transited in the city. Catering service facilities, a wide range of food. Xishuangbanna takes more food locally in tourism consumption, which reduces the cost of goods and increases the profit space.Therefore, the catering ecological efficiency of Kunming and Xishuangbanna is higher than that of Yunnan Province, which is 12355.5 yuan/hm2 and 12636.3 yuan/hm2 respectively. In the diet structure of Lijiang, Dali and Honghe, the output of meat is relatively high, and the consumption income of tourism catering is lower than the consumption rate of the ecological environment, resulting in the low ecological efficiency of catering.The rest of the cities have high ecological efficiency of catering, but the number of tourists is small, the income of tourism catering is low, and the potential of resource development is large, which is in an unhealthy state of high efficiency.

Dynamic analysis of ecological efficiency of tourism transportation. After fitting the tourism traffic ecological footprint and consumption income of Yunnan Province from 2010 to 2019, it can be seen that the two indicators show an upward trend in recent ten years, and the growth rate of traffic income is greater than that of ecological footprint. Therefore, the ecological efficiency of tourism transportation fluctuates and increases, and the utilization of environmental resources is gradually strengthened, as shown in Figure 5. Especially in 2019, three new high-speed railways, three intercity railways and six ordinary railways were built and opened. Compared with 2018, the traffic income increased by 324.1 × 108 yuan, and the ecological efficiency increased from 9237.1 yuan/hm2 to 14093.4 yuan/hm2, an increase of 52.6%. Although the traffic ecological efficiency has increased significantly in recent two years, there is still a big gap compared with the overall level. The highest proportion is only 43.4 % of the overall industrial level, and the utilization rate of the ecological environment needs to be further improved.

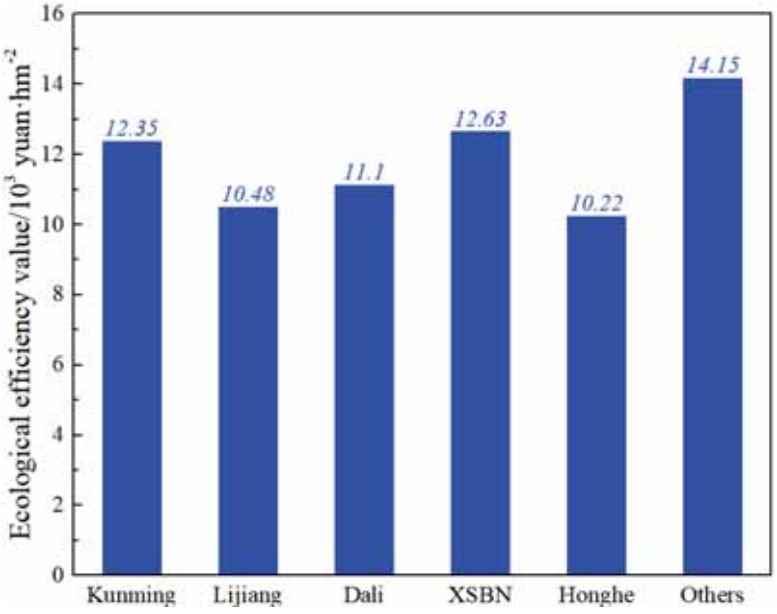


FIGURE 4
Distribution of tourism catering ecological efficiency in cities of Yunnan Province

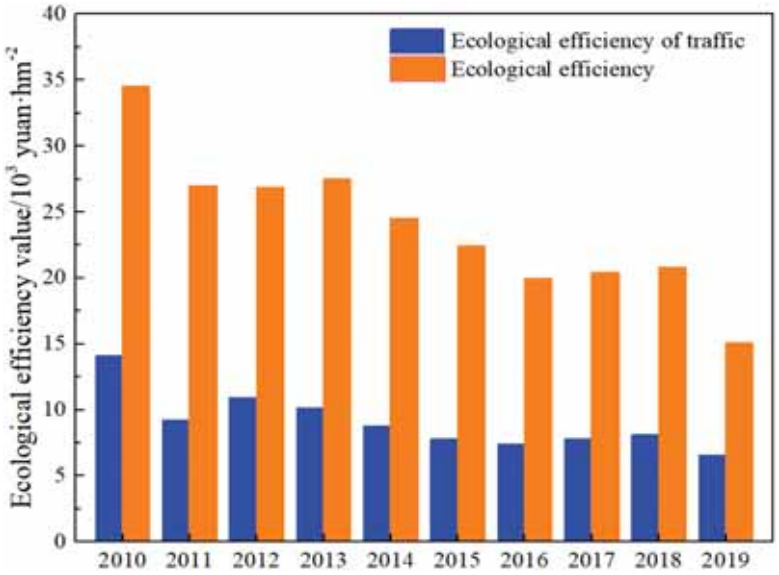


FIGURE 5
Change of ecological efficiency of transportation in Yunnan Province from 2010 to 2019

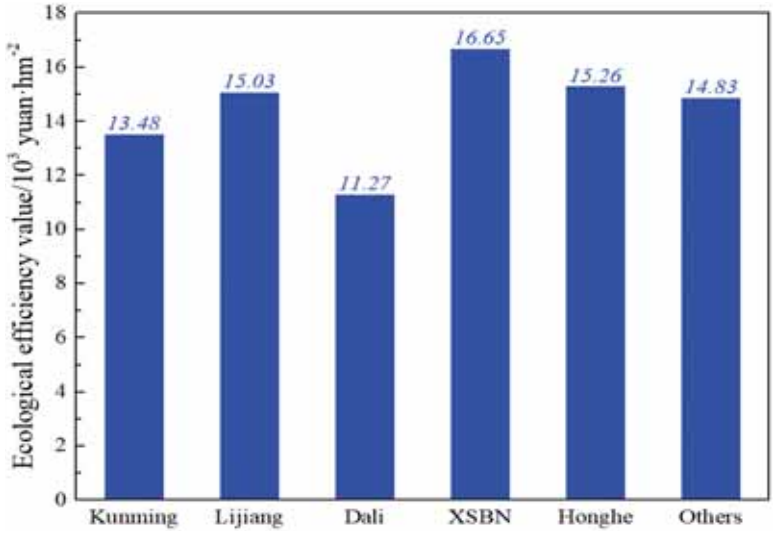


FIGURE 6
Distribution of tourism traffic ecological efficiency of cities in Yunnan Province

Change of ecological efficiency of transportation in Yunnan Province from 2010 to 2019. It can be from Figure 6 that in the spatial distribution of tourism traffic ecological efficiency of cities in Yunnan Province, Kunming and Dali, as the core cities, have a large scale of development and high level of economic development. However, overloaded passenger flow has a greater impact on traffic pressure and ecological environment, resulting in low ecological efficiency values. The utilization rate of ecological environment in Xishuangbanna, Honghe and Lijiang is higher, which is 19218.2 yuan/hm2, 15267.8 yuan/hm2 and 15032.9 yuan/hm2 respectively. It shows that the development structure of tourism transportation in this area is reasonable, and the development of scenic spots can promote the construction of transportation infrastructure. In other cities, the number of scenic spots above 4A level is less, the number of tourists is limited, the impact on the ecological environment is correspondingly smaller, and the ecological efficiency value is in an unhealthy and virtual high state.

Dynamic analysis on ecological efficiency of housing, tourism, shopping and entertainment. The ecological efficiency of housing, tourism, shopping and entertainment in tourism elements of Yunnan Province is far higher than the overall efficiency level of the industry, as shown in Figure 7. Among them, housing has the highest utilization rate of environmental resources, which is more than 500 times of the comprehensive level, followed by tourism projects. With the development of economy, people pay more and more attention to the enjoyment of spirit. The promotion of holiday tourism makes the utilization rate of hotel rooms increase, the consumption income and the ecological efficiency of housing increase year by year, and the average annual growth

rates are 113% and 102.2% respectively. Yunnan is an important province of Chinese herbal medicine industry in China, and the planting area of Chinese herbal medicine ranks first in the country. In 2014, the 'Top 10 Famous Medicinal Materials' brand enterprises increased publicity and triggered a shopping boom, but the increase in consumption income was far less than the increase in ecological footprint. Therefore, although the shopping ecological efficiency has been in an efficient state, it shows a decreasing trend. The ecological benefits of tourism and entertainment in Yunnan Province are increasing year by year, with an average annual growth rate of 26.8%, which is 30-60 times of the total level of the industry and is in a healthy and efficient state. The spatial distribution of ecological efficiency of housing, tourism, shopping and entertainment is consistent with that of catering, which is mainly affected by the regional economic development and the number of scenic spots. The article is no longer detailed.

Countermeasures to improve tourism ecological efficiency. According to the calculation formula, ecological efficiency is directly proportional to tourism income, and inversely proportional to environmental energy consumption. Through the analysis, it can be seen that the response of catering and shopping to ecological efficiency is more obvious, which has a larger room for improvement; Catering and transportation have a greater impact on environmental energy consumption. Therefore, the utilization rate of the ecological environment can be improved by increasing the consumption income of the six elements of tourism, and reducing environmental energy consumption.

Increase tourism revenue. The unique three-dimensional climate in Yunnan Province has laid the foundation for the growth of wild vegetables and fruits. Many wild vegetables and fruits have unique flavor and sweet taste, which are loved by domestic tourists. In the catering structure, fruits and vegetables have a relatively small impact on the ecological environment. Under the condition of ensuring the diet structure and quality, it can further increase the consumption of wild vegetables and fruits by tourists and improve the ecological efficiency of tourism. At present, the wild vegetables and fruits in Yunnan Province are mainly primary processing, but the fine processing and deep utilization are relatively weak, which greatly affects the value-added of resources. By expanding channels, improving technology, fine processing, extend the industrial income chain. At the same time cultivate leading enterprises, improve brand effect, promote food consumption income, improve tourism ecological benefits. In terms of the ecological efficiency of tourism shopping, the higher the annual productivity of the bio-productive land purchased by tourists, the smaller the consumption of the environment. Therefore, we can start from improving the quality of goods, enriching the types of goods, and updating the styles of goods.

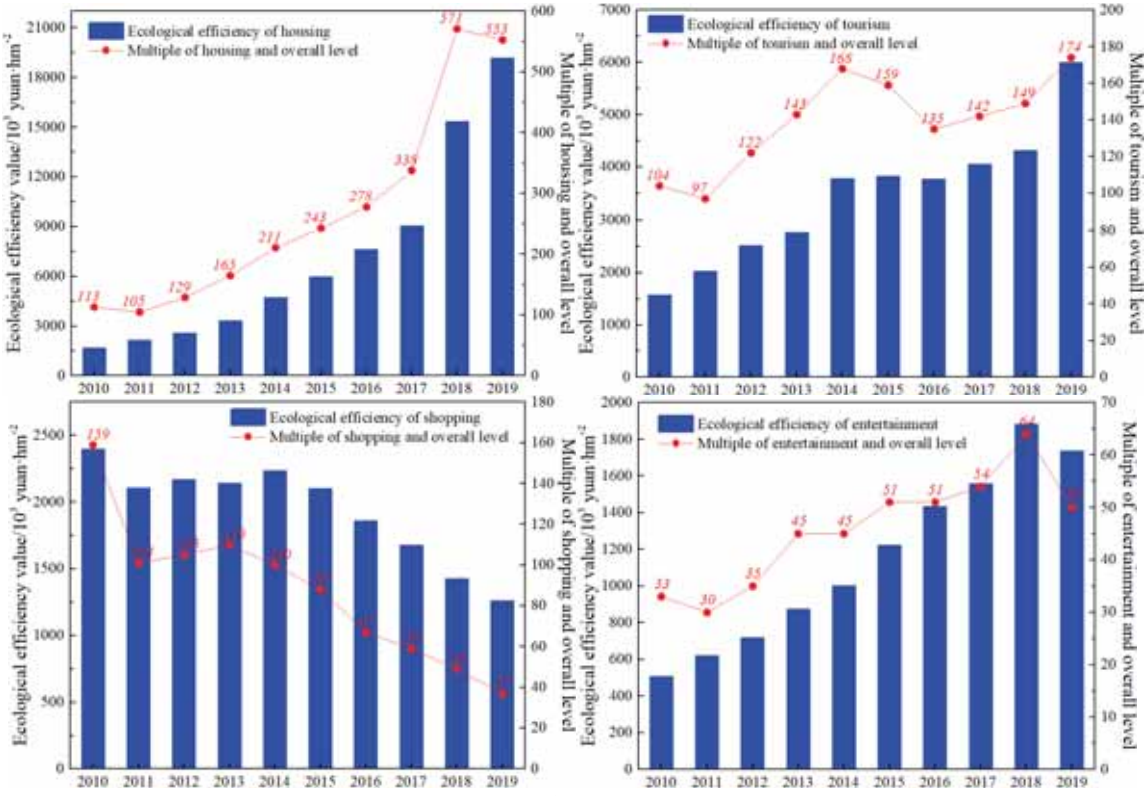


FIGURE 7
Change of ecological efficiency of housing, tourism, shopping and entertainment in Yunnan Province from 2010 to 2019

Reduce environmental energy consumption. Reducing environmental energy consumption is another important means to improve tourism ecological efficiency. Catering and transportation are indispensable parts in the process of tourism, which have the greatest impact on the ecological environment. Tourism catering consumption is the most basic consumption of tourists. If the environmental impact of this part is reduced, the circular economy development mode can be implemented from hotels. Technically, it helps hotels and restaurants to fundamentally save resources and reduce energy consumption by extending the length of catering food supply, reforming key energy consumption equipment and using waste. For example, the breakfast time in the hotel should be appropriately delayed to adapt to the habit of some customers getting up late, reduce the waste of food resources while increase the satisfaction of tourists; After the transformation of the boiler and heating equipment in the hotel, the affordable heavy diesel can be used to replace the 0# diesel, so as to reduce the production costs and increase the profit margins. By encouraging and guiding tourists to travel greenly and environmentally, public transport can be chosen as much as possible to reduce the use of private cars. For the traffic in scenic spots, the ecological fragile areas can be avoided by reasonable planning to reduce the impact on the environment; For smaller scenic spots, encourage tourists to walk in, energy saving and consumption reduction at the same time can also strengthen physical fitness; For larger scenic spots, green and pollution-free new energy vehicles such as bicycles can be selected. Through the above measures, the utilization rate of ecological resources by catering and transportation can be improved to effectively improve the ecological efficiency of tourism.

CONCLUSIONS

Taking Yunnan Province of China as an example, an tourism ecological efficiency model is constructed to investigate the spatio-temporal evolution characteristics of tourism eco-efficiency. The change law of tourism eco-efficiency is evaluated from time and space according to the measurement results, and the main influencing factors are found out. The main conclusions can be obtained: (1) In recent ten years, the overall ecological efficiency of tourism in Yunnan Province has fluctuated, but the overall trend is on the rise, and the effective utilization degree of environmental resources is increasing. The spatial distribution of ecological efficiency is unbalanced, showing the characteristics of high abdomen and low surrounding, and the ecological efficiency in the northern region is higher than that in the southern region. (2) In terms of time, the ecological efficiency of catering industry and transportation industry is rising slowly, but the overall utilization rate of the environment is low, less than half of the industrial ecological efficiency, and the input and output need to be further optimized. In terms of space, the efficient areas of catering industry are concentrated in Kunming and Xishuangbanna, while the utilization rate of transportation industry in Xishuangbanna, Honghe and Lijiang is higher. The ecological efficiency of tourism housing, tourism, shopping and entertainment are far higher than the overall efficiency level of the industry. Among them, the ecological efficiency of tourism shopping is decreasing, in an unhealthy and efficient state. (3) The response of catering, transportation and shopping to ecological efficiency is obvious, and there is a large space for improvement. Through these three aspects, we can increase the utilization rate of the ecological environment and promote the sustainable development of tourism in Yunnan Province.

ACKNOWLEDGEMENTS

The research is supported by the National Social Science Fund Project (20MBZ116).

REFERENCES

[1] Ren, L.J., Li, J., Li, C., Dang, P.Y. (2021) Can ecotourism contribute to ecosystem? Evidence from local residents' ecological behaviors. Science of the Total Environment. 757(2), 143814.

[2] Li, P., Ryan, C., Cave, J. (2016) Chinese rural tourism development: transition in the case of Qiyunshan, Anhui. Tourism Management. 55(8), 240-260.

[3] Huang, H., Chen, B., Ma, Z.Y., Liu, Z.H., Zheng, S.L., Yu, W.W., Liao, J.J., Hu, W.J., Du, J.G., Chen, G.C. (2017) Assessing the ecological security of the estuary in view of the ecological services-a case study of the Xiamen estuary. Ocean & Coastal Management. 137(3), 12-23.

[4] Bello, M.O., Solarin, S.A., Yuen, Y.Y. (2018) The impact of electricity consumption on CO2 emission, carbon footprint, water footprint and ecological footprint: the role of hydropower in an emerging economy. Journal of Environmental Management. 219(8), 218-230.

[5] Dong, H.W., Li, P., Feng, Z.M., Yang, Y.Z., You, Z., Li, Q. (2019) Natural capital utilization on an international tourism island based on a three-dimensional ecological footprint model: a case study of Hainan province. China. Ecological Indicators. 104(9), 479-488.

[6] Wells, E.C., Zarger, R.K., Whiteford, L.M., Mihelcic, J.R., Koenig, E.S., Cairns, M.R. (2016) The impacts of tourism development on perceptions and practices of sustainable wastewater management on the Placencia Peninsula, Belize. Journal of Cleaner Production. 111(1), 430-441.

[7] Liu, L.N., Lei, Y.L., Ge, J.P., Yang, K.J. (2018) Sector screening and driving factor analysis of Beijing's ecological footprint using a multi-model method. Journal of Cleaner Production. 191(8), 330-338.
[8] Patterson, M., Mcdonald, G., Hardy, D. (2017) Is there more in common than we think? Convergence of ecological footprinting, emergy analysis, life cycle assessment and other methods of environmental accounting. Ecological Modelling. 362(10), 19-36.
[9] Dancette, R., Sebastien, L. (2019) The actor in 4 dimensions: a relevant methodology to analyze local environmental governance and inform ostrom's social-ecological systems framework. MethodsX. 6(7), 1798-1811.
[10] Shahzad, U., Fareed, Z., Shahzad, F., Shahzad, K. (2020) Investigating the nexus between economic complexity, energy consumption and ecological footprint for the United States: new insights from quantile methods. Journal of Cleaner Production. 279(1), 123806.
[11] Tang, C.C., Wu, X.F., Zheng, Q.Q., Yu, N. (2018) Ecological security evaluations of the tourism industry in ecological conservation development areas: a case study of Beijing. Journal of Cleaner Production. 197(10), 999-1010.
[12] Ruan, W.R., Li, Y.Q., Zhang, S.N., Liu, C.H. (2019) Evaluation and drive mechanism of tourism ecological security based on the DPSIR-DEA model. Tourism Management. 75(12), 609-625.
[13] Yang, Y., Ling, S., Zhang, T., Yao, C.X. (2018) Three-dimensional ecological footprint assessment for ecologically sensitive areas: a case study of the southern Qinling Piedmont in Shaanxi, China. Journal of Cleaner Production. 194(9), 540-553.
[14] Michailidou, A.V., Vlachokostas, C., Moussiopoulos, N., Maleka, D. (2016) Life cycle thinking used for assessing the environmental impacts of tourism activity for a greek tourism destination. Journal of Cleaner Production. 111(1), 499-510.
[15] Marti, L., Puertas, R. (2020) Analysis of the efficiency of African countries through their ecological footprint and biocapacity. Science of the Total Environment. 722(6), 137504.
[16] Angelstam, P., Barnes, G., Elbakidze, M., Marais, C., Marsh, A., Polonsky, S., Richardson, D.M., Rivers, N., Shackleton, R.T., Stafford, W. (2017) Collaborative learning to unlock investments for functional ecological infrastructure: bridging barriers in social-ecological systems in south Africa. Ecosystem Services. 27(10), 219-304.
[17] Ulucak, R., Apergis, N. (2018) Does convergence really matter for the environment? An application based on club convergence and on the ecological footprint concept for the EU countries. Environmental Science & Policy. 80(2), 21-27.
[18] Zhan, L., Lei, Y.L., Li, L., Ge, J.P. (2019) Interprovincial transfer of ecological footprint among the region of Jing-Jin-Ji and other provinces in China: A quantification based on MRIO model. Journal of Cleaner Production. 225(7), 304-314.
[19] Langnel, Z., Amegavi, G.B. (2020) Globalization, electricity consumption and ecological footprint: an autoregressive distributive lag approach. Sustainable Cities and Society. 63(12), 102482.
[20] Wang, F., Yu, F.Y., Zhu, X.H., Pan, X.L., Sun, R.M., Cai, H.R. (2016) Disappearing gradually and unconsciously in rural China: Research on the sunken courtyard and the reasons for change in Shanxian County, Henan Province. Journal of Rural Studies. 47(10), 630-649.
[21] Kourgialas, N.N., Karatzas, G.P., Dokou, Z., Kokorogiannis, A. (2018) Groundwater footprint methodology as policy tool for balancing water needs in water scarce islands - the case of Crete, Greece. Science of the Total Environment. 615(2), 381-389.
[22] Lin, W.P., Li, Y., Li, X.D., Xu, D. (2017) The dynamic analysis and evaluation on tourist ecological footprint of city: take Shanghai as an instance. Sustainable Cities & Society. 37(2), 541-549.
[23] Cano-Orellana, A., Delgado-Cabeza, M. (2015). Local ecological footprint using principal component analysis: a case study of localities in Andalusia (Spain). Ecological Indicators. 57(10), 573-579.
[24] Bi, M.L., Xie, G.D., Yao, C.Y. (2020) Ecological security assessment based on the renewable ecological footprint in the Guangdong-Hong Kong-Macao greater bay area, China. Ecological Indicators. 116(9), 106432.
[25] Liu, J., Zhang, J.F., Fu, Z.B. (2017) Tourism eco-efficiency of Chinese coastal cities-analysis based on the dea-tobit model. Ocean & Coastal Management. 148(11), 164-170.
[26] Popova, E., Vousden, D., Sauer, W.H.H., Mohammed, E.Y., Allain, V., Downey-Breedt, N., Fletcher, R., Gjerde, K.M., Halpin. P.N., Kelly, S., Obura, D., Pecl, G., Roberts, M., Raitsos, D.E., Rogers, A., Samoilys, M., Sumaila, U.R., Tracey, S., Yool, A. (2019) Ecological connectivity between the areas beyond national jurisdiction and coastal waters: safeguarding interests of coastal communities in developing countries. Marine Policy. 104(6), 90-102.

[27] Monz, C., Antonio, A., Lawson, S., Barber, J., Newman, P. (2016) The ecological implications of visitor transportation in parks and protected areas: examples from research in US national parks. Journal of Transport Geography. 51(2), 27-35.
[28] Baabou, W., Grunewald, N., Ouellet-Plamondon, C., Gressot, M., Galli, A. (2017) The ecological footprint of Mediterranean cities: awareness creation and policy implications. Environmental Science & Policy. 69(3), 94-104.
[29] Long, X.Y., Yu, H.J., Sun, M.X., Wang, X.C., Xie, W., Wang, C.D., Li, W.Q., Wang, Y.T. (2020) Sustainability evaluation based on the three-dimensional ecological footprint and human development index: a case study on the four island regions in China. Journal of Environmental Management. 265(7), 110509.
[30] Muniz, I., Garcia-Lopez, M.A. (2019) Urban form and spatial structure as determinants of the ecological footprint of commuting. Transportation Research. 67(2), 334-350.
[31] He, J., Wan, Y., Feng, L., Ai, J.Y., Wang, Y. (2016) An integrated data envelopment analysis and emergy-based ecological footprint methodology in evaluating sustainable development, a case study of Jiangsu province, China. Ecological Indicators. 70(11), 23-34.

Received: **22.03.2021**
Accepted: **30.04.2021**

CORRESPONDING AUTHOR

Libo Lin
Management School,
Inner Mongolia University for Nationalities,
Tongliao, Inner Mongolia 028000 – P.R. China

e-mail: haojie93@126.com

© by PSP Volume 30– No. 09/2021 pages 10675-10684 Fresenius Environmental Bulletin

EXPERIMENTAL SIMULATION OF RIVER ENVIRONMENT TRANSFORMATION AND DEVELOPMENT

Bowen Xue[1,2], Junhua Li[2,*], Yang Zhang[2], Linjuan Xu[2]

[1]School of Water Conservancy, North China University of Water Resources and Electric Power, Zhengzhou 450046, China
[2]Key Laboratory of Yellow River Sediment Research, Yellow River Institute of Hydraulic Research, Yellow River Conservancy Commission, Zhengzhou 450003, China

ABSTRACT

Alluvial rivers have different patterns and follow their own laws in terms of river bed form, sediment movement and river evolution. Due to the different influences on human, the governing principles and specific engineering measures are also very different. First, on the basis of extensive research, this article analyzes the causes of river winding from a microscopic point of view and puts forward the influencing factors of different river forms. In addition, through the large flume experiment, the development process of the sedimentation area with the change of the river type was studied, and the following four conclusions were drawn: 1) The sediment deposition process is fan-shaped expansion; 2) The wandering frequency and amplitude increase with the increase of the flow rate; 3) As the pattern changes, rivers develop alternately, forming a stable, unstable and extremely unstable law.; 4) River is easy to change when the ratio of transverse and longitudinal gradient exceeds two. This paper has focused on the discriminant index of river transformation. The study on the evolution of river patterns and the discriminant indicators has not only theoretical but also practical significance.

KEYWORDS:
River patterns, River simulation, Discriminant indicators, Flume experiments

INTRODUCTION

In the large and complex natural river system, there are a lot of factors affecting the revolution and development of rivers. On the macro level, the affecting factors include river geology, geomorphology, hydrology, meteorology and human disturbance. While on the microscopic scale, the factors are river boundary conditions, water and sediment characteristics, and water conservancy facilities [1].

At the same time, as conditions change, natural rivers usually take on ever-changing forms. Therefore, this paper analyzes the reasons for the formation of curved rivers and simulates the development process of rivers through flume experiments, laying a foundation for a better understanding of the transformation and development of rivers, and is of great significance to the understanding and management of specific rivers [2-3].

Rivers can be divided into mountain rivers and plain rivers according to its geographical location, and the incoming water-sediment and riverbed boundary conditions are quite different, which makes the river fluvial process complex and varied. Even for the same river, different riverbed forms and different evolution laws would occur in different river reaches [4]. Thus, different river patterns would finally form. With respect to the division of plain river patterns, scholars home and abroad had conducted a lot of research. In western countries, the river pattern classification is widely used, of which river are divided into three patterns of meandering rivers, braided rivers, and straight rivers. In China, we use different methods instead. Based on their method, rivers are divided into wandering rivers, anabranching rivers, meandering rivers, and straight rivers [5-7].

River bending reasons or mechanism has always been a continually debating issue in scientific community. Based on the minimum variance theory, from the aspects of circulation and dynamic instability, silt-clay content of bed materials and the relationship between valley and river slopes have been deeply studied by many experts [8-12].

The river bending can be regarded as the joint result of secondary circulations and nonequilibrium sediment transport, meaning that any irregular shape sediment of riverbed or riverbank with a certain size could make the flow path deflect on different degrees [8-10]. On the basis of mechanical analysis on the side wall sediment particles and with vortex energy theory, the critical incipient motion condition of the side wall sediment particles is provided. The curvatures of a river bend are largely controlled by the energy of river flow, the flow rate, and the channel slope [11]. River meandering is a natural fluvial process to compensate the energy loss so that the river could keep itself moving forwards. The meandering channel process can result in a rise in the upstream water level, consequently increasing the potential energy in the chan-

nel reach, leading to a rising in the downstream channel slope and the increasing of the kinetic energy [12].

In short, the shapes of rivers are all meandering. Based on the flat shapes, the natural rivers could often be divided into different river patterns like straight, meandering, braided and wandering ones. And the formation is mainly due to the internal and external causes [13]. The internal cause is that the river flow entropy or the energy dissipation rate tends to be a minimum value, which is the root reason for the formation of different river patterns. The external causes are the various constrained conditions of flow including river water-sediment conditions and riverbed boundary conditions, which is the important condition for the formation of different river patterns. As the water-sediment condition changes, the flat shapes of different river patterns could also accordingly adjust. When the river adjusts to a critical value, the river pattern then changes [14-15]. To natural rivers, the river regime of unstable river is easy to be adjusted and the certain pattern river of stable river regime under the certain water-sediment condition is expected to form. In this paper, river development process is simulated with a large-scale experiment and the river regime water-sediment discriminated index of a stable river pattern is proposed.

MATERIALS AND METHODS

River patterns transformation index. In natural, climate changes, tectonic changes, and human activities all may lead to river patterns transformation, and this transformation is mutual.

The wandering strength parameter Θ is introduced to reflect the swinging strength of the wandering rivers: Θ>5, wandering rivers; Θ<2, non-wandering rivers; Θ=2~5, transitional rivers.

Considering both of the static and dynamic characteristics of alluvial rivers and conducting multiple regression analysis with lots of measured data, the calculation formula of river pattern discrimination coefficient is required φ : φ <0.01‰, wandering rivers; 0.01‰< φ <0.5‰, anabranching rivers; 0.5‰< φ <5‰, meandering rivers; φ >5‰, straight rivers.

According to large amounts of measured data, formula (1) with X_* and Y_* which can be used to reflect the longitudinal and transverse stability index of riverbed is proposed:

$$X_* = \frac{1}{J}\left[\frac{\rho_s - \rho}{\rho}\frac{d_{50}}{h}\right]^{1/3} \tag{1}$$

$$Y_* = \left(\frac{h}{B}\right)^{2/3} \tag{2}$$

Where, J is riverbed gradient. h is water depth, and B is river width; D_{50} is the median particle size of bed sand. ρ and ρ_s are densities of water and sand, respectively. The riverbed stability index Z_w is obtained by combining formula (1) and (2):

$$Z_w = \frac{1}{J}\left[\frac{\rho_s - \rho}{\rho}\frac{D_{50}}{h}\right]^{1/3}\left(\frac{h}{B}\right)^{2/3} \tag{3}$$

Combined with the above two formula would get the riverbed stability index Z_w : $Z_w < 5$,wandering rivers; $5 < Z_w < 15$, anabranching rivers; $Z_w > 15$, meandering rivers.

Foreign scholars also have done a lot of work on river patterns transformation index. And the most famous was formula (4):

$$J = 0.0125Q^{-0.44} \tag{4}$$

Based on the formula of Leopold-Wolman and with measured data, formular (5) is acquired:

$$\frac{J}{F_r} = \frac{h}{B} \tag{5}$$

In summary, during the process of river transformation, there is absolutely a critical value. River pattern transformation is the mutation occurs when external conditions slowly change until it reaches the critical value.

Experimental models and conditions. As the formation and transformation of river patterns is extremely complex, model-based testing has become a common technique for related research. However, most of the relevant studies based on river natural model tests are all about river patterns. In these model tests, river channels in the initial conditions are usually given. Normally a straight river channel is dug and the elevation of the channel import and export are controlled in advance so the gradient is constant [16]. However, in this way of settling initial condition, the formed channel pattern is single, which means the required river pattern is only wandering, meandering or straight. Besides, research on river transformation and development is little at present, which affects people's

understanding of river natural development process [17].

This study tends to conduct studies on river natural development laws based on river spatial and temporal natural shaping model when river flows out of the valley, of which the downstream is still ocean. When sediment carried by the import flow comes across the ocean, the water velocity would decrease and the sediment would deposit. As time goes on, the deposition surface would gradually uplift and the plains would also form. With the formation of plains, a new river channel would be molded by river itself. Since this whole process is shaped all by water flow itself, the river gradient ratio is also naturally formed. Therefore, during the long-distance river forming process, different river patterns would occur [18-19].

In order to be able to simulate the alluvial plain formation process and the river natural shaping process, the test flume size is required to be as large as possible to decrease the effect of channel boundary on river shaping process. In this test, the total length of the channel is 32 meters. The deposition area is 30 meters long and 7.5 meters wide. The entire flume circulatory system includes two mixing tanks, orifice box, inlet water forebay, retrograded pool, waste canal, and flow monitoring system. The main characteristics of the flume circulatory system are: the big mixing tank is connected with the orifice box, the orifice box is connected with the test flume, and the waste canal is connected with the small mixing tank. When the muddy water flows through the overflow weir and enters the waste canal, the muddy would flow back to the small mixing tank. And when the small mixing tank is almost filled with muddy water, sediment would be added into the small mixing tank in order to get the proper sediment concentration [20-22]. Then the muddy water with appropriate sediment concentration would be pumped into the big mixing tank. Until then the whole flume circulatory system forms. The main boundary conditions of the model are: the import boundary is the mountain and the downstream of the import reaches is the river deposit area. The river deposit area of fluvial river is totally filled with fresh water without any sediment. After the river deposit area, there settles the overflow weir and the waste canal to guarantee a stable outlet water elevation. The flume floor plan is showed in Figure 1.

In this paper, hydraulic parameters include import sediment concentration, sedimentation thickness, water depth, topography of each section, and the river flow velocity would be observed.

Two different generalization test groups under different water-sediment conditions will be conducted. In the beginning of both the two test groups, the flume is filled with clear water and the water depth of which is both 17cm. The water-sediment condition of the group 1 is low flow with low sediment. During the first 246 hours, the flow rate in the import is 1l/s and the sediment concentration is 50kg/m^3. But in the left hours, the flow rate in the import is 2l/s and the sediment concentration is 80kg/m^3. In the group 2, it lasts for 56 hours with the flow rate in the import is 3l/s and the sediment concentration is 120kg/m^3. In both the two groups, the tail water level is always fixed. During the model test, the water elevation would be real time measured with the measuring pins settled on the right of the flume. The sediment concentration of mixing tank, import, the waste canal, and the whole sediment deposition and topography of flume would also be real time measured. And would be real time measured.

Besides, coal ash from Zhengzhou heat-engine plant is adopted as the model sand and the median size is 0.042 meter. The detailed test scheme is listed as Table 1.

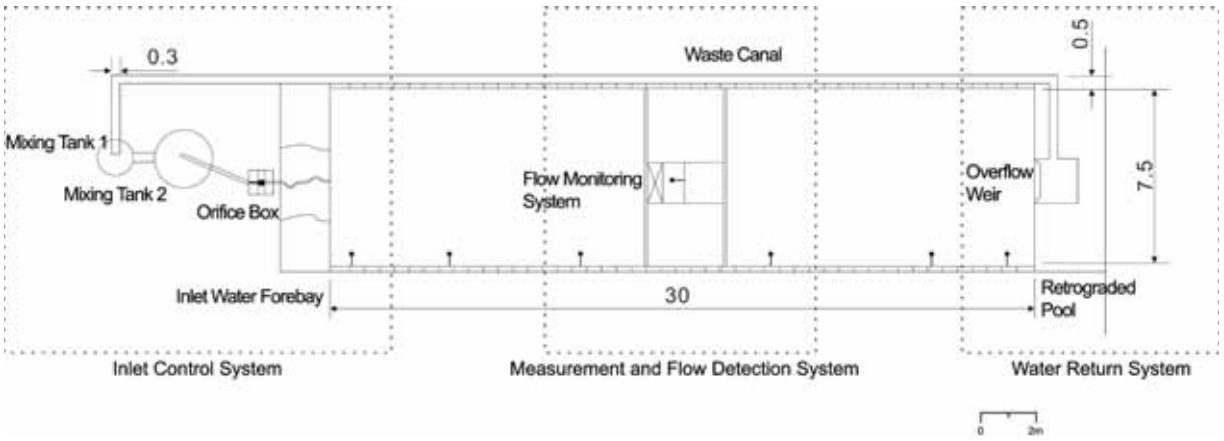


FIGURE 1
Flume floor plan.

TABLE 1
Approach of river spatial and temporal natural shaping model research

Number	Duration (h)	Flow rate in the import (l/s)	Sediment concentration (kg/m^3)	Water level in the downstream (cm)	Median size of model sand (mm)
Group 1	246	1	50	17	0.042
	64	2	80	17	0.042
Group 2	56	3	120	17	0.042

RESULTS

When water with sediment passes through the simulated valley river which is the channel import and flows into the channel slowly, sediment begins to deposit and spread forward. As the experiment proceeds, the sediment in the deposition area gradually forms alluvial fan and meanwhile the channel initially comes into shape (Figure 2).

Judging from the whole process, the sediment deposition rises above water in 66 hours. Consequent to sedimentation, regional channel is shaped 2 meters away from the import. The 1.5-meter-long channel is firstly formed in the simulated valley export then swings and deposits forward. As the experiment time reaches 110 hours, the river regime begins to adjust. Before the adjustment, the main channel is on the right of the flume. However, the river regime quickly changes after 110 hours and the newly formed main channel starts to move to the left (Figure 3).

Based on the test, sediment deposition moves forward in the shape of fan before the formation of the channel. During the preliminary period of developing process, the river regime will definitely wander in order to consume water energy after it passes through the mountain. It is also the wandering river regime that prompts the new formed river channel to move forward and the sediment deposit along both banks.

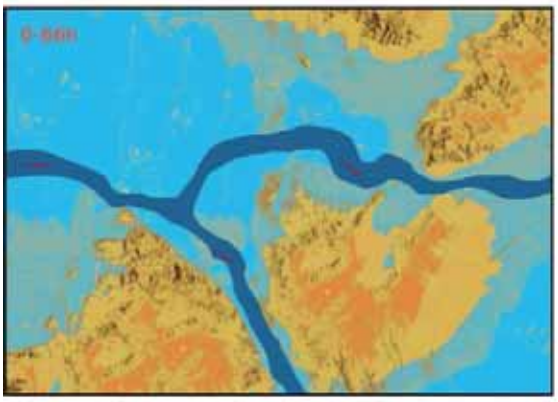


FIGURE 2
Test gradual development of the river.

The main channel formed in 133 hours is on the left side of the flume. At this moment, the river channel had been stable for about half an hour, until the river course suddenly changes and continues to turn to the left. It can be seen that the river regime is being adjusted. After the test for 145 hours, a river bend is formed, and the river turns to the right side of the flume. But at 150 hours, the main channel is already on the left. And until 154h, when the formed river course gradually becomes longer and longer, the main river course proceeds completely along the left bank of the flume (Figure 4).



FIGURE 3
The channel is gradually forming.

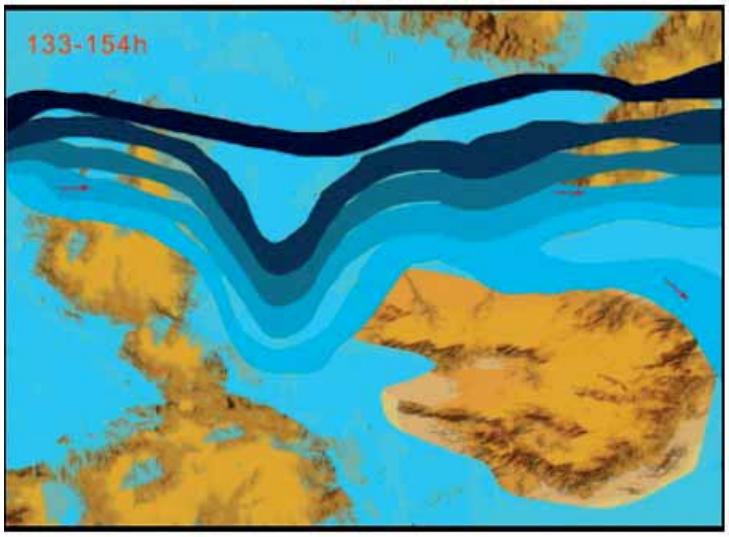


FIGURE 4
The increased transverse ratio of the channel resulting in the main stream wandering.



FIGURE 5
After adjustment to stabilize the river regime.

With the test going, the main channel formed at 160h begins to deposit. At 162h, it begins to expand. Two hours later, the river channel turns to the right side and a 90-degree river bend is formed. After 175 hours of the test, the main channel becomes narrow and deep. The river width is 0.7 meter and the downstream river narrows to 0.4 meter (Figure 5).

After 212h of the test, the river regime of the former half part is relatively straight, while the latter half part moves forward in diffusion. At 214h, a quite straight channel is formed but turns narrow and deep after about one hour. Another hour later, the river channel continues to expand. At 310h (Figure 6), the former 20m of the channel is wandering but the latter10m is fixed. The width is about 1m.

As the test lasts, the sediment deposits gradually and the channel is completely shaped. Compared with the group 1, the flow rate and sediment concentration of the group 2 increases. The deposition and diffusion rate are also greater. After 2.5 hours of testing, the sand has spread to the tailgate of the passage. When the test lasts for 3.5 hours, the sediment will rise above the water surface. After 9.5 hours, the river channel is 4 meters long and is stable for the next two hours. After 17 hours, the river swung to the left side of the channel, and the river was 14 meters long. After the test lasts for 36 hours, the river swings completely to the right. When it lasts for nearly 38 hours, the river begins to widen and its shape is in a critical state of adjustment. After 56 hours, the channel is fully formed.

Although the water-sediment conditions of two groups are different, and river development time, sedimentation rate, and swinging frequency are also significantly different, the river natural development and the cyclical adjustment laws are basically the same.

River natural development follows the following rules. First, sedimentation in the deposition zone diffuses and promotes with a shape of fan and gradually rises along the flow direction. Secondly, to some extent, river begins to silt out of water and an early but short channel forms in front of the flume. Thirdly, sediment-laden flow promotes and sediment silts in the early channel, which causes the transverse slopes on both sides increased. Furthermore, the transverse enters the critical adjustment status, river channel begins to expand and the

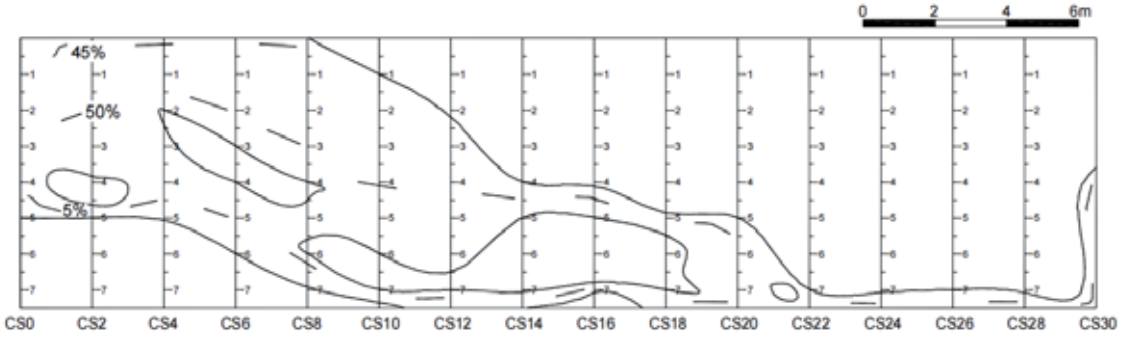


FIGURE 6
River regime at 310h.



FIGURE 7
River natural development pattern sketch.

TABLE 2
Hydraulic parameters statistics of different river patterns in group 1

River Regime	Discharge Q ($10^{-3}m^3/s$)	Width B (m)	Average water depth h(m)	Froude Number Fr	Longitudinal Shrinking Slope J	J/Fr	h/B
Stable	1	0.3	0.0181	0.4379	0.0072	0.0164	0.0603
	1	0.3	0.0197	0.3861	0.0121	0.0315	0.0656
	1	0.35	0.0124	0.6587	0.0105	0.0160	0.0355
	1	0.35	0.0306	0.1701	0.0137	0.0807	0.0876
	1	0.45	0.0084	0.9148	0.0095	0.0104	0.0188
	1	0.4	0.0099	0.8138	0.0095	0.0117	0.0247
	1	0.5	0.0067	1.1781	0.0144	0.0122	0.0133
	1	0.3	0.0188	0.4120	0.0074	0.0179	0.0628
	1	0.3	0.0196	0.3885	0.0074	0.0192	0.0653
	1	1	0.0054	0.8050	0.0107	0.0132	0.0054
Unstable	1	0.4	0.0180	0.3307	0.0208	0.0629	0.0450
	1	0.85	0.0157	0.1909	0.0102	0.0536	0.0185
	1	0.85	0.0097	0.3912	0.0099	0.0252	0.0115
	1	0.65	0.0155	0.2547	0.0084	0.0329	0.0238
	1	0.9	0.0089	0.4215	0.0096	0.0228	0.0099
	1	0.65	0.0138	0.3029	0.0079	0.0260	0.0212
	1	2.5	0.0053	0.3312	0.0067	0.0202	0.0021
	1	0.8	0.0188	0.1555	0.0070	0.0448	0.0234
	1	1.85	0.0106	0.1577	0.0111	0.0703	0.0057
Extremely Unstable	1	5.3	0.0044	0.2068	0.0067	0.0323	0.0008
	1	5.6	0.0072	0.0926	0.0063	0.0680	0.0013
	1	6.8	0.0145	0.0270	0.0067	0.2473	0.0021
	1	6.2	0.0080	0.0723	0.0067	0.0930	0.0013
	1	3.9	0.0077	0.1214	0.0070	0.0578	0.0020
	1	3.5	0.0027	0.6378	0.0065	0.0102	0.0008
	1	3.2	0.0043	0.3583	0.0066	0.0184	0.0013
	1	3.6	0.0348	0.0137	0.0069	0.5082	0.0097

mainstream swings to the side. Finally, the river regime adjustment is completed, and the newly formed river is stabilized again. As the river wanders and swings, sediment deposits on both sides. That is, with the development of river channels, plains on both sides of river are gradually formed. The river development rule is showed in Figure 7.

During the first stage of river development cycle, the river morphology is often stable, the early narrow channel at this time is straight or meander-

ing and the river regime is relatively regulated. Then, during the second stage, with the channel sedimentation, the elevation increases, the channel begins to expand, and the river is in the unstable status. Furthermore, during the third stage, the channel expands to a large range, the mainstream begins to gradually adjust, and the river regime starts to wander and is extremely unstable. Finally, a new straight river channel forms and the river regime returns to stable again.

With a large amount of measured data, a formula to tell different river patterns like straight, meandering, braided and wandering is received.

Based on the statistics and analysis of hydraulic parameters of the two groups' river development cycles, the formula of Parker is considered to be used to distinguish the river regime status. For the unstable status, items on the left of the formula are larger than the right ones. And the lager the value times is, the greater the river regimes wanders. For the stable status, items on the left of the formula are smaller than the right ones. And the smaller the value times is, the straighter the river channel would be. Hydraulic parameters statistics of different river patterns in two groups are shown in Table 2 and Table 3 and the summary diagram of different river regimes is shown as Figure 8.

TABLE 3
Hydraulic parameters statistics of different river patterns in group 2

River Regime	Discharge Q ($10^{-3}m^3/s$)	Width B (m)	Average water depth h(m)	Froude Number Fr	Longitudinal Shrinking Slope J	J/Fr	h/B
Stable	2.983	0.45	0.0056	5.1137	0.0056	0.0011	0.0123
	2.983	0.3	0.0234	0.8864	0.0048	0.0054	0.0781
	2.983	0.4	0.0160	1.1771	0.0028	0.0024	0.0400
	2.983	0.6	0.0100	1.5981	0.0024	0.0015	0.0166
	2.983	0.6	0.0129	1.0818	0.0076	0.0070	0.0215
	2.983	1.35	0.0141	0.4194	0.0008	0.0020	0.0105
	2.983	0.47	0.0313	0.3654	0.0054	0.0148	0.0667
	2.983	0.5	0.0292	0.3829	0.0052	0.0136	0.0583
	2.983	0.5	0.0280	0.4068	0.0051	0.0124	0.0560
	2.983	0.5	0.0176	0.8162	0.0047	0.0058	0.0352
	2.983	0.5	0.0312	0.3466	0.0048	0.0140	0.0623
Unstable	2.983	0.7	0.0356	0.2029	0.0637	0.3142	0.0508
	2.983	2.4	0.0155	0.2060	0.0014	0.0066	0.0065
	2.983	0.6	0.0193	0.5946	0.0322	0.0542	0.0321
Extremely Unstable	2.983	2	0.0333	0.0786	0.0280	0.3562	0.0166
	2.983	6	0.0097	0.1662	0.0056	0.0337	0.0016
	2.983	2.3	0.0340	0.0661	0.0162	0.2448	0.0148

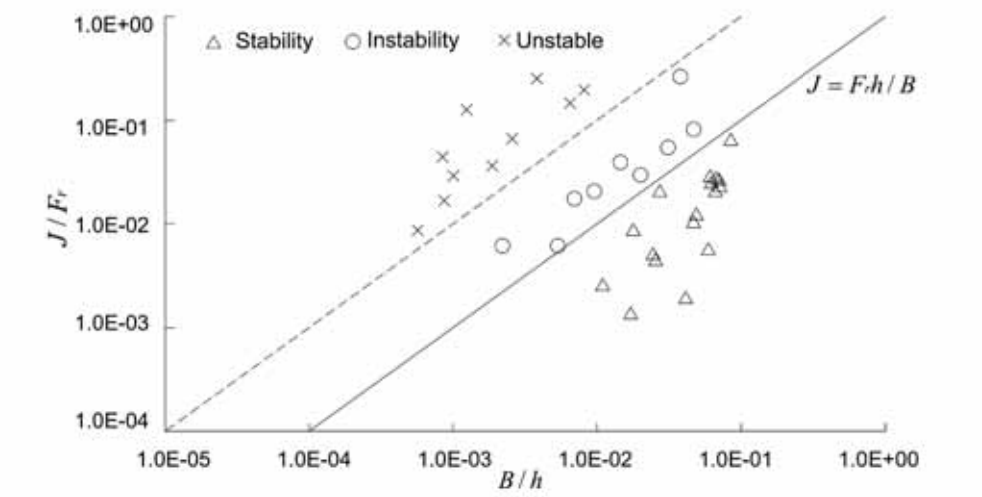


FIGURE 8
Summary diagram of different river regimes.

TABLE 4
Hydraulic parameters statistics calculated with Zhang Hongwu formula

River Patterns	Discharge Q ($10^{-3}m^3/s$)	Width B (m)	Average water depth h(m)	Longitudinal Shrinking Slope J	D_{50} (mm)	X_*	Y_*	Z_w
	1	0.3	0.018	0.0072	0.042	190.95	0.1537	29.36
	1	0.3	0.020	0.0121	0.042	109.42	0.1626	17.79
	1	0.35	0.012	0.0105	0.042	147.24	0.1080	15.91
	1	0.35	0.031	0.0137	0.042	83.54	0.1972	16.47
	1	0.45	0.008	0.0095	0.042	185.66	0.0706	13.11
	1	0.4	0.010	0.0095	0.042	175.92	0.0848	14.92
	1	0.3	0.019	0.0074	0.042	182.74	0.1580	28.86
	1	0.3	0.020	0.0074	0.042	178.80	0.1621	28.99
	2.983	0.45	0.006	0.0056	0.042	361.69	0.0534	19.32
Meandering	2.983	0.3	0.023	0.0048	0.042	263.31	0.1826	48.09
	2.983	0.4	0.016	0.0028	0.042	501.56	0.1170	58.66
	2.983	0.6	0.010	0.0024	0.042	696.94	0.0651	45.35
	2.983	0.6	0.013	0.0076	0.042	201.47	0.0774	15.59
	2.983	0.47	0.031	0.0054	0.042	210.82	0.1644	34.67
	2.983	0.5	0.029	0.0052	0.042	223.15	0.1504	33.55
	2.983	0.5	0.028	0.0051	0.042	233.85	0.1464	34.23
	2.983	0.5	0.018	0.0047	0.042	292.35	0.1074	31.40
	2.983	0.5	0.031	0.0048	0.042	235.24	0.1572	36.97
	2.983	0.8	0.017	0.0041	0.042	334.35	0.0777	25.96
	1	1	0.005	0.0107	0.042	191.79	0.0308	5.90
	1	0.4	0.018	0.0208	0.042	65.85	0.1265	8.33
	1	0.85	0.016	0.0102	0.042	140.13	0.0699	9.79
Anabranching	1	0.85	0.010	0.0099	0.042	170.47	0.0508	8.66
	1	0.65	0.016	0.0084	0.042	171.60	0.0828	14.22
	1	0.9	0.009	0.0096	0.042	179.77	0.0461	8.29
	1	0.65	0.014	0.0079	0.042	189.75	0.0767	14.55
	1	3.6	0.035	0.0069	0.042	158.25	0.0454	7.18
	1	1.85	0.011	0.0111	0.042	147.12	0.0321	4.72
	1	5.3	0.004	0.0067	0.042	327.71	0.0088	2.89
	1	5.6	0.007	0.0063	0.042	294.69	0.0119	3.50
	1	6.8	0.014	0.0067	0.042	220.35	0.0165	3.64
	1	6.2	0.008	0.0067	0.042	267.10	0.0118	3.16
	1	3.9	0.008	0.0070	0.042	259.18	0.0157	4.08
Wandering	1	3.5	0.003	0.0065	0.042	392.80	0.0085	3.33
	1	3.2	0.004	0.0066	0.042	335.41	0.0121	4.06
	2.983	2	0.033	0.0280	0.042	39.87	0.0651	2.60
	2.983	6	0.010	0.0056	0.042	300.23	0.0138	4.14
	2.983	2.3	0.034	0.0162	0.042	68.48	0.0602	4.12
	2.983	0.7	0.036	0.0637	0.042	17.12	0.1372	2.35
	2.983	0.6	0.019	0.0322	0.042	41.52	0.1010	4.19

Also, based on the formula of Zhang Hongwu, relevant parameters of different river patterns has been counted and acquired the riverbed stability index, which could further validate the adaptability of the formula. Hydraulic parameters statistics calculated with Zhang Hongwu formula is listed in Table 4 and is shown in Figure 9.

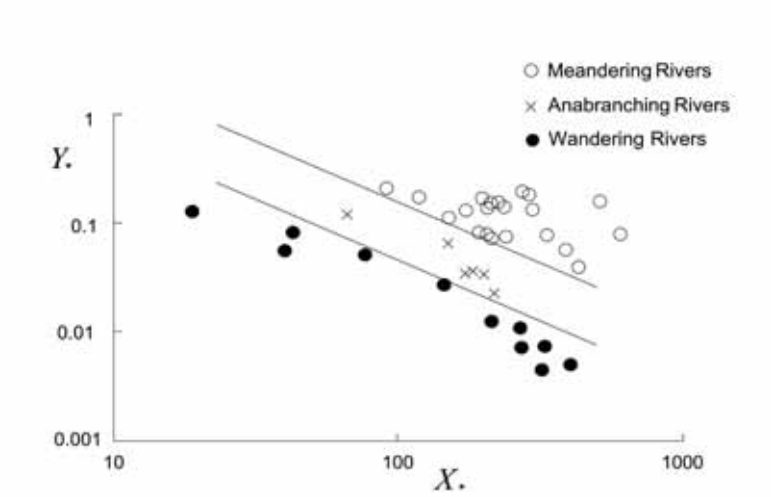


FIGURE 9
The stabilities of different river patterns in the model test.

CONCLUSION

(1) The cross-sectional morphological adjustment of the sedimentary area is fan-shaped in the form of siltation. No matter in whatever water and sand, the river will naturally wander and sway when flowing out of a mountain as long as it is not restricted. If the water and sediment conditions are large, the frequency and amplitude of river wandering and swinging will rise significantly. The amount of sediment directly affects the rate of river deposition.

(2) The simulation test of river development shows that : 1)in the natural process of river development, deposition zone moves forward in the form of fan-shaped siltation and meanwhile elevates ; 2) with sediment deposition gradually rising above water, the preliminary and short river is formed in the mountain pass; 3) continuous siltation of the initial river promotes the water level, which to some extent leads to sediment brought onto both river banks; 4) when the transverse slope begins to increase, the river starts to broaden and enters the critical state of adjustment, bringing about its one-side swing; 5) whiling swinging to one side, the river gradually produces new river in low-lying areas through washing, which tends to maintain bending stability. The process repeats in cycle during which the river experiences alternately stable, unstable, and very unstable development.

(3) The test hydraulic parameters demonstrate that $\frac{J}{F_r} \Big/ \frac{h}{B}$ can be considered as the discriminant index to judge whether a river is stable or not. The lager the value, the greater the river will wander. The smaller the value, the straighter the river channel will be.

ACKNOWLEDGEMENTS

This work was not supported by the national natural science foundation of China (42041006), and the special basic research fund for central public research institutes (HKY-JBYW-2020-15, HKY-JBYW-2018-03).

REFERENCES

[1] Ordu, S., Demir, A. (2009) Analysis of river water quality via geographic information systems: a case study. Fresen. Environ. Bull. 18(12), 2282-2288.
[2] Thomas, R., Nicholas, A.P., Quine, T.A. (2007) Cellular modelling as a tool for interpreting historic braided river evolution. Geomorphology. 90(3-4), 302-317.
[3] Altun, L., Yilmaz, M., Karagul, R., Okatan, A. (2009) Seasonal variations of water quality in rivers of the Düzce watershed (Turkey). Fresen. Environ. Bull. 18(5), 553-559.
[4] Guralnik, B., Matmon, A., Avni, Y., Porat, N., Fink, D. (2011) Constraining the evolution of river terraces with integrated OSL and cosmogenic nuclide data. Quaternary Geochronology. 6(1), 22-32.
[5] Feng, Y., Sun, Q., Peng, G., Ren, N., Zhang, Z. (2009) Polycyclic aromatic hydrocarbons in surface water from the Songhua river of China. Fresen. Environ. Bull. 18(12), 2388-2395.
[6] Lei, D., Deng, H., Xu, H., Lei, D., Ping, W., Ridder, D.D. (2010) Adsorption characteristics of phosphate from aqueous solutions by sponge iron: isotherm, kinetics, and thermodynamics studies. Fresen. Environ. Bull. 19(11), 2548-2561.

[7] Wang, J., Pei, Y., Yang, Z., Lin, C. (2011) Characteristics and applications of a heterotrophic nitrifying-aerobic denitrifying bacterium isolated from an urban river. Fresen. Environ. Bull. 20(1), 114-120.
[8] Constantine, J.A., Dunne, T., Ahmed, J., Legleiter, C., Lazarus, E.D. (2014) Sediment supply as a driver of river meandering and floodplain evolution in the Amazon Basin. Nature Geoscience. 7(12), 899-903.
[9] Leheny, R.L., Nagel, S.R. (1993) Model for the evolution of river networks. Physical Review Letters. 71(9), 1470-1473.
[10] Yang, S., Carlson, K. (2003) Evolution of antibiotic occurrence in a river through pristine, urban and agricultural landscapes. Water Research. 37(19), 4645-4656.
[11] Brauer, G., Deacon, H.J., Zipfel, F. (1992) Comment on the new maxillary finds from Klasies River, South Africa. Journal of Human Evolution. 23(5), 419-422.
[12] Padalko, Y.A., Chibilyov, A.A. (2017) Problems of riverbed evolution in the basin of the Ural River. Doklady Earth Sciences. 475(2), 968-971.
[13] Formann, E., Habersack, H.M., Schober, S. (2007) Morphodynamic river processes and techniques for assessment of channel evolution in Alpine gravel bed rivers. Geomorphology. 90(3-4), 340-355.
[14] Tsai, H., Hseu, Z.Y., Huang, W.S., Chen, Z.S. (2007) Pedogenic approach to resolving the geomorphic evolution of the Pakua river terraces in central Taiwan. Geomorphology. 83(1/2), 14-28.
[15] Cobbett, R., Israel, S., Mortensen, J., Joyce, N., Crowley, J. (2017) Structure and kinematic evolution of the Duke River fault, southwestern Yukon. Canadian Journal of Earth Sciences. 54(3), 322-344.
[16] Lin, C.M., Zhuo, H.C., Gao, S. (2005) Sedimentary facies and evolution in the Qiantang River incised valley, eastern China. Marine Geology. 219(4), 235-259.
[17] Tournoud, M.G., Perrin, J.L., Gimbert, F., Picot, B. (2010) Spatial evolution of nitrogen and phosphorus loads along a small Mediterranean river: implication of bed sediments. Hydrological Processes. 19(18), 3581-3592.
[18] Ward, I., Nanson, G.C., Head, L.M., Fullagar, R., Price, D.M., Fink, D. (2005) Late Quaternary landscape evolution in the Keep River region, northwestern Australia. Quaternary Science Reviews. 24(16-17), 1906-1922.
[19] He, H., Qian, Y., Jie, Z., Tian, Y.Q., Chen, R.F. (2008) Modelling complex flood flow evolution in the middle Yellow River basin, China. Journal of Hydrology. 353(1-2), 76-92.
[20] Thomaz, A.T., Christie, M.R., Knowles, L.L. (2016) The architecture of river networks can drive the evolutionary dynamics of aquatic populations. Evolution. 70(3), 731-739.
[21] Allen, L.G., Gibbard, P.L. (1993) Pleistocene evolution of the Solent River of southern England. Quaternary Science Reviews. 12(7), 503-528.
[22] Bunn, H.T. (1994) Early pleistocene hominid foraging strategies along the ancestral Omo River at Koobi Fora, Kenya. Journal of Human Evolution. 27(1-3), 247-266.

Received: **23.03.2021**
Accepted: **18.04.2021**

CORRESPONDING AUTHOR

Junhua Li
Yellow River Institute of Hydraulic Research Zhengzhou Henan 450003 – China

e-mail: junhua778899@163.com

© by PSP Volume 30– No. 09/2021 pages 10685-10689 Fresenius Environmental Bulletin

HISTOPATHOLOGICAL EXAMINATION OF THE EFFECT OF BLACK SEED (*Nigella sativa*) OIL ON THE METHOTREXATE-INDUCED GASTROINTESTINAL MUCOSA INJURY AND HEPATOTOXICITY IN MICE

Mansur Seymen Segmenoglu[1,*], Huseyin Topcuoglu[2]

[1]Osmaniye Korkut Ata University, Faculty of Health Sciences, Department of Nursing, Osmaniye, Turkey
[2]Adana Veterinary Control Institute, Pathology Laboratory, Adana, Turkey

ABSTRACT

Black seed (*Nigella sativa*) oil is one of the herbal product which used for therapeutic purposes. We aimed to investigate the effects of black seed oil on irritated gastrointestinal mucosa and liver. 21 healthy swiss albino mice were randomly divided into three groups: control group, group-2, group-3. The MTX (20 mg/kg) was given intraperitoneally as a single dose on the 1st day to the group-2 and group-3. Black seed oil (4 ml/kg) was administered by gavages into the stomach daily for 7 days to the group-3. No pathology was observed in control group. In gastric mucosa histopathology, no pathology was observed in the gastric mucosa of group-2 and group-3. In the histopathological examination of the intestinal mucosa, significant hyperplasia and mononuclear cell infiltrations were observed in the intestines of the mice forming the group-2, characterized by an increase in villous epithelial cells. In the intestines of group-3, marked hyperplasia was observed, characterized by an increase in villous epithelial cells, and no other pathognomic findings in group-2 were observed. In liver histopathology, vascular congestion, sinusoidal enlargement, mononuclear cell infiltrations in periportal areas and local degenerative changes were observed in group-2 and group-3. According to the data we obtained in our study, black seed oil has no irritating side for stomach and intestinal mucosa, and it was also seen that it has a protective and therapeutic effect. However, it was also observed in this study that the black seed did not affect the damaged liver and did not have a healing effect.

KEYWORDS:
Black seed oil, gastrointestinal, hepatotoxicity, histopathology, methotrexate

INTRODUCTION

One of the basic concepts of ecology is the environment. Environment is the whole of the factors affecting the organism and living environment, therefore environment is important for plants [1]. When we examine plant ecology, that is, the relationship of plants with other living organisms and environmental factors [2], we see that plants form the basis of conventional medicines and the source of modern medicines [3].

Nigella sativa (NS) is a plant whose effects on vitality activities of body and therapeutic power have been studied and its effects have been accepted [4]. NS is species of the Ranunculaceae Family. The part used as food is the seed of this plant formed in a capsule. NS seeds contain essential oil (0.38-0.49%), fixed oil (30-40%), protein (20-30%), saponin, melantin, nigellin and tannin [5]. NS seeds are unsaturated and rich in essential fatty acids [6]. It is known that p-cymene, γ-terpinene, α-pinene, β-pinene, α-thujen, carvacrol are also presence in the structure of essential oil with timoquinone, dithymoquinone, thymohydroquinone and thymol, which are the main pharmacologically active components [6-8]. It is one of the medicinal herbs that are widely used as antihypertensive, antidiabetic, anticancer, analgesic, anti-inflammatory, bronchial dilatator, diuretic, stomach and liver protective and antioxidant [4, 9, 10].

Methotrexate (MTX) is a folic acid analog that inhibits cell proliferation [11-13] and used in the treatment of various cancer types, autoimmune and chronic inflammatory diseases. It has been determined that methotrexate can cause important disorders in the liver [14], digestive system [15], lungs, skin and central nervous system, along with the bone marrow and kidneys [13].

In this study, we aim to investigate the effects of black seed oil against irritation caused by methotrexate on stomach, intestine and liver tissue of swiss albino mice.

MATERIALS AND METHODS

In this study, 21 healthy swiss albino mice (aged 12 weeks), provided from Adana Veterinary Control Institute Experimental Animals Unit were

used. The mice were fed with the pellet diets as ad libitum and were kept in a light-dark cycle for 12 hours a day and at a temperature of 24ºC ± 3ºC. They were acclimatized for 7 days before the study started.

In the 2nd week, they were randomly divided into three groups: Group-1 is control group (n=7); Group-2 is MTX-treated group (Methotrexate 50 mg/5ml, Koçak Farma, Turkey) (n=7); Group-3 is the MTX and NS oil treated group (*Nigella sativa* oil, 50 ml, Defne Doğa, Turkey) (n=7). Pellet feed + water was administered to the group-1. The MTX (20 mg/kg) was given intraperitoneally as a single dose on the 1st day and pellet feed+water daily for 7 days to the group-2. The MTX (20 mg/kg) was administered intraperitoneally as a single dose on the 1st day; NS oil (4 ml/kg) was administered by gavages into the stomach daily for 7 days and pellet feed+water daily for 7 days to the group-3. 24 hours after the last NS oil given, anesthesia was provided with ketamine (40 mg/kg) and the animals were decapitated. Following the necropsy, the gastrointestinal mucosa and the liver tissue samples were collected for histopathological evaluation and fixed in 10% neutral buffered formalin solution. The tissue samples were processed routinely, embedded in paraffin. Sections (5 mm) were taken from paraffin-embedded tissues, stained with haematoxylin-eosin (HE) and examined microscopically (Olympus CX41).

The present research performed with the principles of laboratory animal care and national laws on animal use. The research was authorized by the Animal Research Ethics Committee of Adana Veterinary Control Institute (2019-5/808).

RESULTS AND DISCUSSION

In the histopathological examination of the gastric mucosa, no pathology was found in the gastric mucosa of the groups 1, 2 and 3.

In the histopathology of the intestinal mucosa, no any pathology was found in the control group mice (figure 1), but it was seen marked hyperplasia characterized by the increase of villous epithelial cells and mononuclear cell infiltration in the lamina propria in the MTX group mice (figure 2). Significant hyperplasia characterized by an increase in villous epithelial cells was observed in the intestines of mice given black seed oil (figure 3). Other than that, no pathological finding was observed.

In the liver, no any pathological finding was found in the mice of the control group (figure 4). Vascular congestion, sinusoidal enlargement, mononuclear cell infiltration in periportal areas, bile duct hyperplasia and local degenerative changes were noted in the livers of MTX group (figure 5) and Black Seed oil group mice (figure 6).

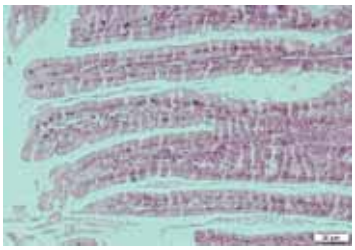


FIGURE 1
Histological appearance of intestinal mucosa of control mice with no any pathology. A section of group-1, H.E., bar=50 µm

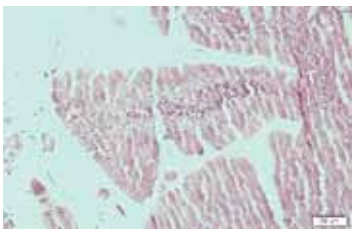


FIGURE 2
Histopathology of intestinal mucosa of group-2 mice. Marked hyperplasia in the villous epithelial cells, H.E., bar=50 µm

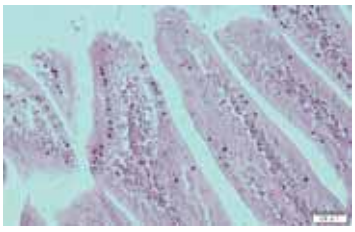


FIGURE 3
Histopathology of intestinal mucosa of group-3 mice. Significant hyperplasia in the villous epithelial cells, H.E., bar=50 µm

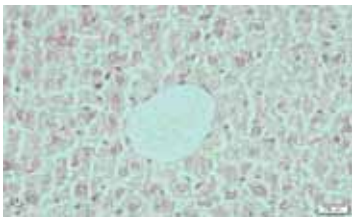


FIGURE 4
Microscopic view of liver of control mice with no any pathology. A section of group-1, H.E., bar=20 µm

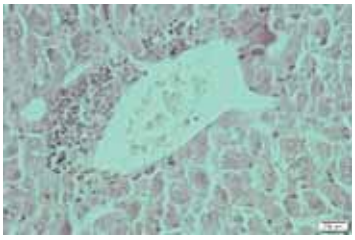


FIGURE 5
Histopathology of liver of group-2 mice. Mononuclear cell infiltration in periportal area, H.E., bar=20 µm

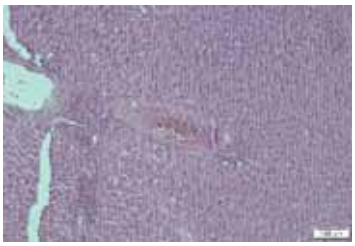


FIGURE 6
Histopathological appearance of liver of group-3 mice. Mononuclear cell infiltration in periportal area and degenerative changes, H.E., bar=100 µm

Methotrexate (MTX) is an immunosuppressive agent commonly used in the treatment of diseases such as cancer, psoriasis, multiple sclerosis and rheumatoid arthritis in human [15, 16]. Inflammation of the stomach and intestinal mucosa, hemorrhage and peptic ulcers are known side effects of MTX affecting the digestive system mucosa, in addition to this, it is rarely seen in fatal mucosal necrosis caused by MTX [15]. MTX is also known for its toxicity in kidney and liver tissues, although the treatment area is large, its most important side effect is on the liver tissue [14]. Various studies and case reports in which low and high doses of MTX have been applied have reported that damage to the stomach and intestinal mucosa of humans has been reported [15, 17]. In a study in which three rheumatoid arthritis patients were evaluated according to different treatment options, it was observed that patients who used MTX in different doses for at least three days a week had damage to the mouth and gastrointestinal tissue and developed diarrhea. It was also reported that there was no gastrointestinal tissue damage in the patient who received high doses once a week, although oral findings were observed [18]. In this study, although there was no damage to the gastric mucosa due to MTX given once, marked hyperplasia characterized by the increase of villous epithelial cells in the intestines and mononuclear cell infiltrations in the lamina propria were observed. This study shows the effect of MTX on the stomach similar to Teke and Özen [18]'s single dose study, although the research subjects are different, including human and mice, it contains differences with the studies of Tsukada et al. [15] and Peker et al. [17]. The effect of MTX on the intestines also coincides with the studies of Tsukada et al. [15] and Peker et al. [17] and differs with the findings of Teke and Özen [18].

In the liver studies conducted with rats, it was observed that the damaging of radial structure of the remark cords, enlargement of the sinusoids, vascular congestion and mononuclear cell infiltration especially in the portal areas in the liver with a single administration of 20 mg/kg MTX [11]. In a study, two different groups were formed in which MTX was administered, vascular congestion, sinusoidal dilatation, mononuclear cell infiltration in the periportal area and hepatocytes with a small number of heterochromatic nuclei and a decrease in the glycogen content of hepatocytes were found in the livers of the group given MTX once. It was noted that the liver of the group given MTX twice a week increased morphological changes compared to the first group. Vascular congestion and sinusoidal dilatation were more common together with periportal inflammation, hepatocyte formations with heterochromatic nuclei, fibroblast activation in the portal areas, and depletion of glycogen storage of hepatocytes were seen [16]. In a study conducted after 4 years of MTX therapy in patients with rheumatoid arthritis, signs of liver fibrosis were found in varying degrees [19]. In this study, vascular congestion, sinusoidal enlargement, mononuclear cell infiltration in periportal areas, bile duct hyperplasia and degenerative changes were observed in the livers of MTX group. However, there are no signs of fibrosis seen in humans, suggesting that fibrosis may occur as a result of prolonged exposure to MTX.

Medicinal plants have been used to treat diseases for centuries, one of the most common of which is black seed (*Nigella sativa*) oil and seeds [4]. Black seed is widely used in the treatment of many diseases with its protective and antioxidant features such as stomach and liver protection, blood pressure stabilizer, antidiabetic, immune system regulator, anticarcinogenic, analgesic and many other features [3, 4].

In a study, it stated that different groups formed by giving black seed oil (10 ml/kg, gavage) and timoquinone (10 mg/kg, p.o) inhibited lesions occured by only giving ethanol, and that black seed oil significantly reduced the ulcer index compared to ethanol [20]. In another study, the effects of black seed oil on gastritis caused by stress in hypothyroidal rats were examined. It was revealed that black seed oil applications significantly decreased the volume of gastric juice, the number of gastric lesions and the size of gastric lesions, and also significantly increased gastric tissue protein compared to the operated and stressful groups [9]. In a study investigating the effects of different doses of black seed extract on rats with indomethacin-induced gastric damage, they found that indomethacin-induced hemorrhagic lesions, erosions, and infiltration of polymorph nuclear leukocytes were significantly reduced in groups treated with black seed [21]. In this study, no any pathological finding was found in the gastric mucosa. There is no different situation in the gastric mucosa of mice given black seed oil and in the gastric mucosa of control and MTX group mice. Besides being curative, black seed oil did not have an irritating effect on stomach mucosa. In the intestines of mice given black seed oil, prominent hyperplasia characterized by an increase in villous epithelial cells was observed. However, other pathological findings encountered in MTX group mice were not seen.

CONCLUSION

As a result, studies have shown that the black seed plant, which has been accepted as a medicinal plant for years, does not irritate the stomach and intestinal mucosa, but has a protective and therapeutic effect. However, it was also noted in this study that black seed did not have a curative effect on the damaged liver. This situation should not create a negative judgment about black seed, on the contrary, similar scientific studies should be increased and more scientific data should be obtained about these and similar plants.

ACKNOWLEDGEMENTS

We would like to thank Adana Veterinary Control Institute Directorate and staff for supporting our work. In addition, we also thank to pathologist Prof. Dr. Ahmet Aydoğan.

REFERENCES

[1] Ceyhan, E., Kahraman, A. and Önder, M. (2012) The impacts of environment on plant products. International Journal of Bioscience, Biochemistry and Bioinformatics. 2(1).

[2] Yousaf, Z. and Ramazan, H. (2017). Introductory Chapter: Plant ecology. Traditional approaches to recent trends. Intechopen. Chapter. 1.

[3] Yimer, E.M., Tuem, K.B., Karim, A., Ur-Rehman, N. and Anwar, F. (2019) *Nigella sativa* L. (black cumin): A promising natural remedy for wide range of illnesses. Evidence-Based Complementary and Alternative Medicine. Hindawi. 16.

[4] Ahmad, A., Husain, A., Mujeeb, M., Khan, S.A., Najmi, A.K., Siddique, N.A., Damanhouri, Z.A. and Anwar, F. (2013) A review on therapeutic potential of *Nigella sativa*: A miracle herb. Asian Pacific Journal of Tropical Biomedicine. 3(5), 337-352.

[5] Kaya, M.S., Kara, M. and Özbek, H. (2003) The effects of black cumin (*Nigella sativa*) seeds on CD3+, CD4+, CD8+ cells of human immune system and total number of leucocytes. Genel Tıp Dergisi. 13(3), 109-112.

[6] Randhawa, M.A. and Al-Ghamdi, M.S. (2002) A review of the pharmaco-therapeutic effects of *Nigella sativa*. Pakistan Journal of Medicine Research. 41, 77-83.

[7] Bulca, S. (2014) The composition of black cumin and use of black cumin and other essential oils as antioxidant in food technology. Journal of Adnan Menderes University Agricultural Faculty. 11(2), 29-36.

[8] Benkaci-Ali, F., Baaliouamer, A., Meklati, B.Y. and Chemat, F. (2007) Chemical composition of seed essential oils from Algerian *Nigella sativa* extracted by microwave and hydrodistillation. Flavour Fragrance Journal. 22, 148-153.

[9] Abdel-Sater, K.A. (2009) Gastroprotective effects of *Nigella sativa* oil on the formation of stress gastritis in hypothyroidal rats. International Journal of Physiology, Pathophysiology and Pharmacology. Short Communication. 1, 143-149.

[10] Sıcak, Y. and Eliuz, E.A.E. (2019) Chemical content and biological activity spectrum of *Nigella sativa* seed oil. KSU Journal of Agriculture and Nature. 22(6), 928-934.

[11] Kocaman, N. and Dabak, D.Ö. (2019) Investigation of the protective effects of silymarin on the methotrexate-induced hepatotoxicity in rats. Fırat Medical Journal. 33(2), 67-72.

[12] Kremer, J.M., Maini, R.N. and Romain, P.L. (2009) Major side effects of low-dose methotrexate. Uptodate. 17.1.

[13] Oğuz, Y., Eyileten, T., Karaman, M., Ay, S.A. and Yılmaz, M.İ. (2011) Methotrexate-induced pancytopenia in two patients with renal dysfunction. Turkish Nephrology, Dialysis and Transplantation Journal. 20(1), 93-95.

[14] Armağan, İ. (2015) The role of oxidative stress in methotrexate-induced damage in liver and kidney of rats. SDU Medical Faculty Journal. 22(4), 151-155.

[15] Tsukada, T., Nakano, T., Miyata, T. and Sasaki, S. (2013) Life-threatening gastrointestinal mucosal necrosis during methotrexate treatment for rheumatoid arthritis. A case report. Gastroenterology. 7, 470-475.

[16] Kocaman, N. and Çolakoğlu, N. (2013) Effects of Repeated Doses Administration of Methotrexate on Rat Liver Tissue. Fırat Medical Journal. 18(3), 141-145.

[17] Peker, A., Yarkıcı, H. and Akar, H. (2018) Gastrointestinal bleeding secondary to use of high-dose methotrexate: A case report. Journal of Surgery and Medicine. 2, 151-153.

[18] Teke, H.Ü. and Özen, M. (2014) Low-dose methotrexate induces pancytopenia in rheumatoid arthritis patients: are the risk factors predictors for physicians?: A case report. Turkish Journal of Physical Medicine and Rehabilitation. 60, 54-7.

[19] Albrecht, K. and Müller-Ladner, U. (2010) Side effects and management of side effects of methotrexate in rheumatoid arthritis. Clinical and Experimental Rheumatology. 28, 95-101.

[20] Kanter, M., Demir, H., Karakaya, C. and Özbek, H. (2005) Gastroprotective activity of *Nigella sativa* oil and its constituent, thymoquinone against acute alcohol-induced gastric mucosal injury in rats. World Journal Gastroenterology. 11(42), 6662-6666.

[21] Paseban, M., Niazmand, S., Soukhtanloo, M. and Meibodi, N.T. (2020) The preventive effect of *Nigella sativa* seed on gastric ulcer induced by indomethacin in rat. Journal Herbmed Pharmacology. 9(1), 12-19.

Received: **23.03.2021**
Accepted: **17.05.2021**

CORRESPONDING AUTHOR

Mansur Seymen Segmenoglu
Department of Nursing,
Faculty of Health Sciences,
Osmaniye Korkut Ata University,
Osmaniye – Turkey

e-mail: mansurseymen@gmail.com

© by PSP Volume 30– No. 09/2021 pages 10690-10696 Fresenius Environmental Bulletin

EXPERIMENTAL STUDY ON THE ACCUMULATION OF HEAVY METALS IN DIFFERENT PARTS OF FORAGE UNDER HEAVY METAL POLLUTION ENVIRONMENT

Ao Sun[1], Huifen Deng[2], Fang He[1], Haobang Li[1], Yang Luo[1], Cheng Huan[1], Sheng Li[1], Kangle Yi[1], Jianbo Li[1,3,*]

[1]Hunan Institute of Animal Husbandry and Veterinary Medicine, Changsha 410131, China
[2]Hunan Biological and Electromechanical Polytechnic, Changsha 410127, China
[3]Hunan De Nong Animal Husbandry Group Co. Ltd., Huayuan 416400, China

ABSTRACT

The use of agricultural fertilizers can cause serious pollution of heavy metals in the soil. In addition, it can also lead to unsafe factors such as heavy metal residues in the forage feed produced, which affects the health of livestock in the animal husbandry industry, and ultimately affects human health. Research on the accumulation of heavy metals in different parts of forage under heavy metal pollution is very important to the safety and environmental protection of forage feed. In order to solve this problem, in this paper, we systematically studied the accumulation characteristics of heavy metals in forages in soils with different concentrations of heavy metal cadmium, and proposed a calculation formula for the content of heavy metals in forages. Through experiments, the average concentration of metal cadmium accumulation in the whole forage in different experimental fields was obtained. The measurement results found that the cumulative cadmium concentration of the three forages in experimental field 1 (soil cadmium concentration of 1.68 mg/kg) was lower than 1.0 mg/kg, which was a low concentration. The results of the accumulation of heavy metal cadmium in different parts of the stems and leaf roots of the three forage grasses showed that the cadmium concentration in the stems and leaf roots of bonnet, sweet sorghum and hybrid elephant grass showed a trend of first increasing and then decreasing with the increase of soil cadmium content. In addition, the cadmium concentration in the leaves of the forage grass is the least accumulated, followed by the roots and stems. A comprehensive comparison of the cadmium accumulation of the three commonly used forages found that the cadmium accumulation concentration of the stems, leaves and roots of bonbon is far lower than that of sweet sorghum and hybrid elephant grass, so its safety index is the highest.

KEYWORDS:
Heavy metal pollution, experimental field, bullvain, cadmium concentration, heavy metal accumulation

INTRODUCTION

With the continuous development of industrial and agricultural technology and economy, the extensive use of agricultural fertilizers has made soil pollution by heavy metals more and more serious. Heavy metal pollution seriously affects the industrial development of herbivores in animal husbandry. As people continue to pay attention to food safety, the green safety of edible crops and animal husbandry has become the focus of attention and research of the majority of scholars [1-3].

In the process of livestock breeding, forage safety is the primary factor. The accumulation of heavy metals in different parts of the forage under heavy metal pollution affects the green safety of feed production, which in turn affects the health quality of livestock and the safety of human diet. The previous have done a lot of research on the accumulation of heavy metals in pasture. For example, Andrew et al. proposed a direct heavy metal pollution migration model between soil and plants, and analyzed the migration law of heavy metals through specific examples [4]. Jiang et al. analyzed the migration laws of soil, plants, and food chains in complex polluted farmland [5]. However, existing studies have not fully studied the accumulation of heavy metals in different parts of forage under heavy metal pollution, which is very important to the safety and environmental protection of forage feed.

In this paper, we systematically studied the accumulation characteristics of heavy metals in forages in soils with different concentrations of heavy metal cadmium, and proposed a calculation formula for the content of heavy metals in forages. Through experiments, the average concentration of metal cadmium accumulation in the whole forage in different experimental fields was obtained. Through experiments and comparisons, the distribution of heavy metal cadmium accumulation in the roots of the stems, leaves and roots of bonnet, sweet sorghum and hybrid elephant grass has been clarified. This study can provide a basis for the selection of high-quality forage grass.

MATERIALS AND METHODS

Experiment location and experiment method. With the development of social economy, agricultural technology has made considerable progress. However, the rapid development of agricultural fertilizers and other technologies has caused more and more serious soil pollution, especially heavy metal pollution. For animal husbandry, the quality of pasture has a great influence on the good quality of aquaculture products. In this paper, a heavy metal forage accumulation experiment was carried out on a pasture in Hunan, China, and the experimental results can provide reference for the optimization of forage [6-7].

(1) Experiment location and object. The experiment site was selected in a ranch in Hunan, China. The climate in this area is humid all year round, and the annual average sunshine hours is about 1 600 hours. The average annual temperature in the experimental area is relatively high, the annual average temperature is between 15-18 ℃, the annual average precipitation is between 1 200-1 700 mm, the rainfall is relatively abundant, and the soil is fertile. These temperature and climate factors provide good external conditions for the experiment [8-9]. In order to study the accumulation of heavy metals in different parts of the forages, in this paper, we selected three commonly used feeding forages, namely bonbon, sweet sorghum and hybrid elephant grass as the research objects. The results of the measured heavy metal cadmium concentration and soil pH value of the five experimental fields are shown in Table 1.

(2) Experimental steps. In order to ensure the accuracy of the experiment, strict experimental procedures have been formulated, as shown in Figure 1.

As can be seen from the experimental steps of heavy metal accumulation in forages in Figure 1, the experimental steps mainly include sample planting, collection of experimental samples, sample pretreatment, heavy metal detection and analysis. First, the three research objects of forages were planted evenly in experimental fields with different concentrations of cadmium and heavy metals, and cultivated under uniform and normal external conditions. Water, temperature and other conditions are kept consistent, so the influence of other external factors is eliminated [10]. The forages are sampled after they are mature, and 1 m2 of the same forages in the test field are randomly and uniformly collected, the soil and other impurities on the surface are removed, and they are placed in clean fresh-keeping bags and labeled. Then, all samples of the three forages were pretreated, washed with clean water, and dried. Forage grass of the same species is divided into four equal parts, one part is processed as a whole and crushed into powder, and the other three parts are divided into root, stem and leaf. They were used to analyze the accumulation of heavy metal cadmium in the whole forage and the three parts of stems, leaves and roots.

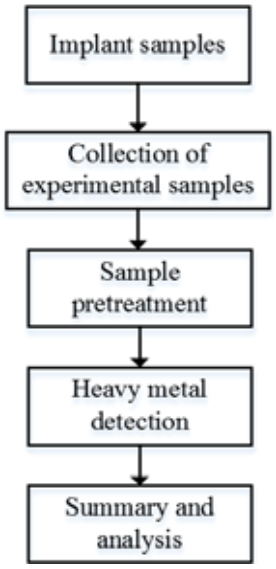


FIGURE 1
Basic steps of forage heavy metal accumulation experiment.

TABLE 1
Measurement results of the concentration of heavy metal cadmium in the experimental field.

Serial number	Concentration of heavy metal cadmium (mg/kg)	Soil PH value
Experimental field 1	1.68	5.35
Experimental field 2	2.42	5.38
Experimental field 3	2.99	5.29
Experimental field 4	5.34	5.31
Experimental field 5	9.37	5.32

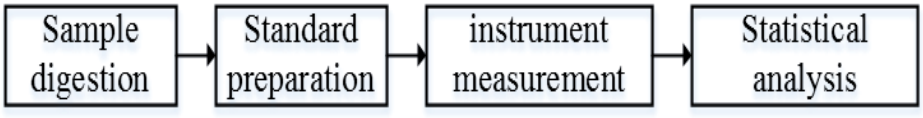


FIGURE 2
Basic steps of measuring heavy metal accumulation in forage.

Heavy metal accumulation measurement method. In this paper, the detection of heavy metals in forage grass adopts atomic fluorescence spectroscopy. Atomic fluorescence spectroscopy determines the content of the element to be measured by measuring the fluorescence emission intensity of the atomic vapor of the element to be measured under the excitation of radiant energy. At present, this method has been widely used. It has the advantages of accurate measurement and less interference, and has been widely used in various aspects such as medicine and agriculture [11-12]. In this paper, the AFS-830 dual-channel atomic fluorescence spectrometer is selected in the measurement process, combined with the computer system, digestion furnace and other tools to measure the heavy metal cadmium in the forage [13-15]. The measurement of heavy metal cadmium adopts the national standard of "Graphite Furnace Atomic Absorption Spectrometry", and the specific measurement steps are shown in Figure 2.

The measurement steps of forage heavy metal accumulation mainly include four steps, which are the digestion and treatment of forage samples, the preparation of heavy metal standards, instrumental measurement and statistical analysis. The digestion of the forage sample is an important part of the whole measurement process, that is, the forage sample is mixed with nitric acid and perchloric acid for soaking treatment. After being placed for a certain period of time, it is heated and dissolved in a digestion furnace to prepare a sample digestion solution for subsequent measurements [16-18]. After the sample is digested, the heavy metal standard application solution needs to be made before the measurement. Then use an atomic fluorescence photometer to measure the prepared sample. The calculation formula of heavy metal content in forage grass is shown in formula 1 [19-20].

$$X = \frac{(C - C_0) \times V \times 1000}{M \times 1000 \times 1000} \quad (1)$$

In the above formula, X is the content of heavy metal cadmium measured in the forage, mg/kg; C is the measured concentration of the forage sample digestion solution, ng/ml; the concentration of the measuring reagent used for C0, ng/ml; V is the total volume of the digestive juice of the measurement sample, ml; M is the weight of the measured forage sample, g. The concentration of the heavy metal cadmium in the measured forage can be calculated by formula 1.

RESULTS

Analysis on the accumulation of heavy metals in the whole forage. In this paper, we conducted experiments on the accumulation of heavy metal cadmium in pastures in five experimental fields. Through the above-mentioned experimental methods and procedures, the accumulation of heavy metal cadmium in three forages of bonbon, sweet sorghum and hybrid elephant grass was determined. The soils of the five test plots contained different concentrations of heavy metal cadmium, and the pH value of the test plots was almost the same, thus eliminating the interference of other factors. Each experimental field was planted with equal amounts of three experimental forages, and the average concentration of metal cadmium accumulation in the whole forages of different experimental fields was measured. The results are shown in Table 2.

According to China's standard for cadmium content in feed materials, considering the safety and reliability of forage farming, forage cadmium concentration Cd less than 1.0 mg/kg is defined as a low enrichment concentration, which is the standard for forage feeding. Pastures below the standard are considered safe pastures. Through the cumulative measurement results of the heavy metal cadmium concentration in the Table 1, it is found that the soil cadmium concentration in the experimental field 1 is 1.68 mg/kg, and the cadmium cumulative concentration of the three forages in the experimental field is lower than 1.0 mg/kg, which is a low enrichment concentration. Test field 2 only had a low enrichment concentration of bullvain, and test field 5 had the highest soil cadmium concentration value, which was as high as 9.37 mg/kg. In order to more clearly analyze the change law of cadmium accumulation in different cadmium concentration test fields for different forages, the curve of the heavy metal cadmium accumulation concentration change of different forages as shown in Figure 3 was drawn.

TABLE 2
Measurement results of the concentration of heavy metal cadmium in the experimental field.

Serial number	Test field parameters		Overall cadmium content of forage (mg/kg)		
	Cadmium concentration (mg/kg)	PH value	Verbena	Sweet sorghum	Hybrid elephant grass
Experimental field 1	1.68	5.35	0.14	0.65	0.65
Experimental field 2	2.42	5.38	0.42	4.41	3.23
Experimental field 3	2.99	5.29	1.94	9.44	5.77
Experimental field 4	5.34	5.31	1.54	3.09	2.73
Experimental field 5	9.37	5.32	0.19	0.64	0.84

TABLE 3
Accumulation of heavy metals in different parts of three pastures.

Serial number	Test field parameters		Cadmium concentration in verbena (mg/kg)			Cadmium concentration in sweet sorghum (mg/kg)			Cadmium concentration in hybrid elephant grass (mg/kg)		
	Cadmium concentration(mg/kg)	PH value	Stem	Leaf	Root	Stem	Leaf	Root	Stem	Leaf	Root
Experimental field 1	1.68	5.35	0.46	0.11	0.18	0.89	0.38	0.68	0.8	0.53	0.63
Experimental field 2	2.42	5.38	0.87	0.28	0.49	7.11	2.56	3.56	4.01	2.57	3.12
Experimental field 3	2.99	5.29	3.28	1.34	2.64	17.34	6.16	7.81	7.67	3.85	5.80
Experimental field 4	5.34	5.31	2.65	1.12	2.04	4.83	2.44	2.61	3.26	2.42	2.50
Experimental field 5	9.37	5.32	0.88	0.08	0.18	1.10	0.25	0.57	1.24	0.35	0.92

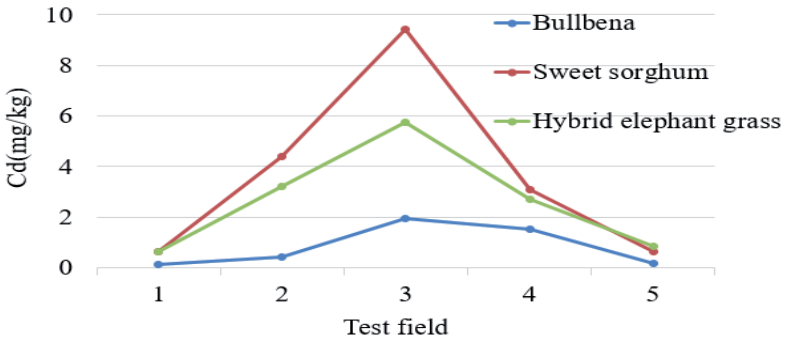


FIGURE 3
Changes of cumulative concentration of heavy metal cadmium in different pastures.

It can be seen from Figure 3 that the cumulative concentration of cadmium in the three forages of bonbon, sweet sorghum and hybrid elephant grass showed the same trend of change. As the concentration of cadmium in the soil of the experimental field increased, it showed a trend of first increasing and then decreasing. With the increase of cadmium concentration, the cumulative concentration of forage decreases, this is because the concentration of heavy metals is too high, which seriously affects the normal growth of forage. At the same time, under the same experimental field conditions and the same soil cadmium concentration, the cumulative cadmium concentration of the three pastures differed greatly. The highest cumulative concentration is sweet sorghum, then hybrid elephant grass and hybrid grass, and the cumulative concentration of cadmium in hybrid grass is much lower than the other two pastures. This shows that when considering the accumulation of heavy metals, the safety index of Verbena is higher.

Analysis of heavy metal accumulation in different parts of forage. Through the above heavy metal accumulation test method, the concentration of cadmium accumulation in the stems, leaves and roots of three forage grasses in different cadmium content test fields was tested respectively. The statistical results are shown in Table 3.

It can be seen from Table 3 that the cadmium concentration in the stems, leaves and roots of different pastures varies greatly. Among the three forage grasses, the cadmium concentration in the stems accumulated the most, followed by the roots, and the leaves accumulated the least. In the case of bullvain, the accumulation of cadmium in the stems was much higher than that in the roots and leaves in the five experimental fields with different cadmium content, and the accumulation of cadmium in the leaves was the least. In the experimental field 1 with a cadmium concentration of 1.68 mg/kg, the concentration of stems, leaves and roots were all lower than 1.0 mg/kg, which was a low enrichment concentration. The cumulative cadmium concentration in the leaves was 0.11 mg/kg, and the cumulative cadmium concentration in the leaves of the bullvain was the lowest. In order to analyze the difference of cadmium concentration in different parts of the forage more intuitively, the curve of the cadmium concentration in the stems, leaves and roots of hornbeam, sweet sorghum and hybrid elephant grass with the soil cadmium concentration was drawn. The results are shown in Figure 4, Figure 5 and Figure 6.

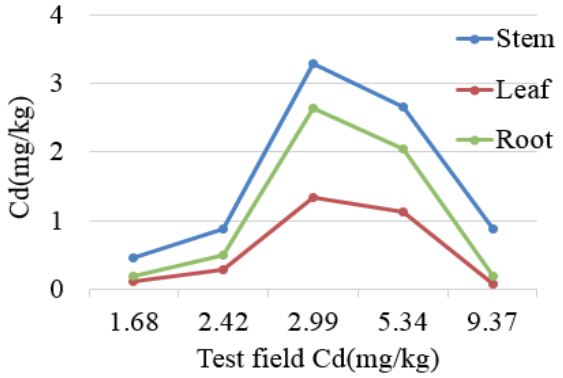


FIGURE 4
Changes of cumulative concentration of cadmium in stems, leaves and roots of verbena.

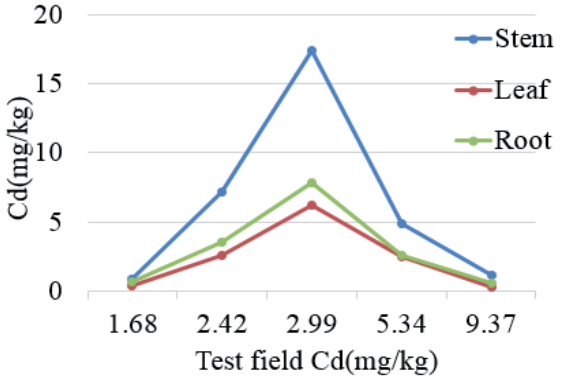


FIGURE 5
Changes in the cumulative concentration of cadmium in the stems, leaves and roots of sweet sorghum.

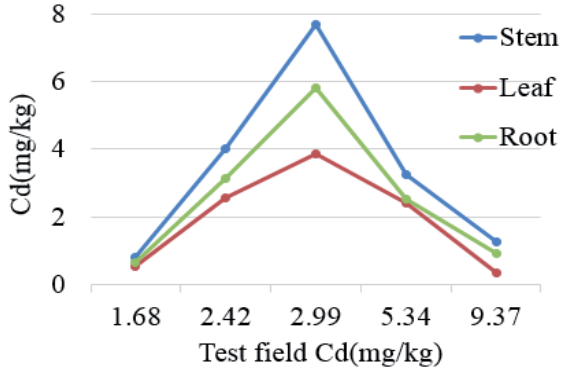


FIGURE 6
Changes in the cumulative concentration of cadmium in the stems, leaves and roots of hybrid elephant grass.

It can be seen from Figure 4 that the cumulative concentration of cadmium in the stems, leaves, and roots of Verbena vulgaris showed a trend of first increasing and then decreasing with the increase of soil cadmium content. The cumulative concentration of cadmium in the leaves of bonbon is lower than that in the rhizome, indicating that the bonbon leaves are more suitable for animal breeding. At the same time, it is found from the curve that the cumulative concentration of heavy metal cadmium is less than 1.0 mg/kg in experimental field 1, experimental field 2 and experimental field 5. In experimental field 3, the cumulative concentration of cadmium in bullwhip stem is higher than the heavy metal cadmium content in experimental field soil. This indicates that in this range, the accumulation of heavy metals in forage vervain is the highest, and it is not suitable for animal breeding.

It can be seen from Figure 5 that the cumulative concentration of cadmium in the stems, leaves and roots of sweet sorghum also increased first and then decreased with the increase in soil cadmium content. At the same time, the cadmium accumulation concentration of the three parts of the stem, leaf and root of sweet sorghum was also lower than that of the rhizome. It can also be found from the curve in Figure 5 that only the experimental field 1 has a cumulative concentration of heavy metal cadmium lower than 1.0 mg/kg, and its low concentration range is lower than that of Verbena. At the same time, it was found that the cumulative concentration of each part of sweet sorghum was higher than that of Verbena. Especially in Experimental Field 3, the cadmium concentration in the stems of sweet sorghum was accumulated as high as 17.34 mg/kg, which seriously polluted the quality of forage.

It can be seen from Figure 6 that the cumulative concentration of cadmium in the stem, leaf and root of hybrid elephant grass is similar to that of sweet sorghum. However, its cumulative concentration of cadmium is lower than that of sweet sorghum, but higher than that of Verbena. For example, in Experimental Field 3, the cumulative concentration of cadmium in the stems of hybrid elephant grass reached 7.67 mg/kg, which was much higher than that of Verbena but lower than that of sweet sorghum.

A comprehensive comparison of the cadmium concentration changes in different parts of bonnet, sweet sorghum and hybrid elephant grass, it can be seen that the cumulative concentration of cadmium in the stems, leaves, and roots of the three forage grasses all increased first and then decrease with the increase of cadmium content. In experiment field 3 (soil cadmium concentration of 2.99 mg/kg), the cumulative cadmium concentration of the three forage stems, leaves and roots reached the maximum. Excessive cadmium concentration in the soil results in an excessively high accumulation of heavy metals in forages, which seriously pollutes the quality of forages. At the same time, a comprehensive comparison of the cadmium accumulation of the three commonly used forages found that the cadmium accumulation concentration of the stems, leaves and roots of bonbon is far lower than that of sweet sorghum and hybrid elephant grass. This shows that for the three commonly used forages in this paper, the vervain is superior to the other two in terms of heavy metal accumulation, especially the accumulation of the leaf parts of the vervain is the lowest and the pollution is the least.

CONCLUSIONS

(1) In this paper, we systematically studied the accumulation characteristics of heavy metals in forages in soils with different concentrations of heavy metal cadmium, and proposed a calculation formula for the content of heavy metals in forages. Through experiments, the average concentration of metal cadmium accumulation in the whole forage in different experimental fields was obtained.

(2) The measurement results found that the cumulative cadmium concentration of the three forages in experimental field 1 (soil cadmium concentration of 1.68 mg/kg) was lower than 1.0 mg/kg, which was a low concentration. The results of the accumulation of heavy metal cadmium in different parts of the stems and leaf roots of the three forage grasses showed that the cadmium concentration in the stems and leaf roots of bonnet, sweet sorghum and hybrid elephant grass showed a trend of first increasing and then decreasing with the increase of soil cadmium content.

(3) The cadmium concentration in the leaves of the forage grass is the least accumulated, followed by the roots and stems. A comprehensive comparison of the cadmium accumulation of the three commonly used forages found that the cadmium accumulation concentration of the stems, leaves and roots of bonbon is far lower than that of sweet sorghum and hybrid elephant grass, so its safety index is the highest.

ACKNOWLEDGEMENTS

Authors acknowledge the funding provided by 'Application and Demonstration of High Quality Beef Cattle Efficient and Safe Breeding Technology (2018YFD050170)', 'Study and application of three-way cross combination screening and supporting production technology of meat black goat (2019NK4194)' , 'Research and Application of High Yield Cultivation and High Efficiency Utilization Technology of High Quality Forage Grass in Central Hunan(2020NK4243) ' and 'Safety assessment of food crops and forage (XiangNongLian (2018)NO.70). The construction of modern agricultural industrial technology system in Hunan Province (Xiangcai nongzhi 2019[97])

REFERENCES

[1] Huang, Y., Huang, Y., Yu, G., Diao, W., Sun, Q. (2011) Research progress on absorption and accumulation of heavy metals in vegetables. The Yangtze River Vegetable. 1(10), 1-6.

[2] Jiang, X., Xu, X., Yu, Y., Zhang, C. (2006) Preliminary study on the biological enrichment of heavy metals in vegetables. Chinese Vegetables. 2(7), 8-10.

[3] Aschbacher, P., Thacke, E. (1974) Metabolic Fate of Oral Diethylstilbestrol in Steers. Journal of Animal Science. 39(6), 1185-1192.

[4] Lagana, A. (1991) General and Selective Isolation Procedure for High Performance Liquid Chromatographic Determination of Anabolic Steroids in Tissues. Journal of Chromatography. 58(8), 89-98.

[5] Bohemen, H., Janssen, V., Leak, W. (2003) The influence of road infrastructure and traffic on soil, water, and air quality. Environmental Mangement. 31(1), 50-68.

[6] Hjortenkrans, D., Bergback, B., Haggerud, A. (2006) New Metal Emission Patterns in Road Traffic Environments. Environmental Monitoring and Assessment. 117(3), 85-98.

[7] Li, J., Liu, J., Zhang, H. (2010) Broad Specificity Indirect Competitive Immunoassay for Determination of Nitrofurans in Animal Deeds. Analytica Chimica Acta. 6(7), 1-6.

[8] Arsova, G., Hajrulai, M., Stojanovska, B. (2012) In-house Validation and Quality Control of Commercial Enzyme-linkedimm Unosorbnet Assays for Screening of Nitrofuran Metabolites in Food of Animal Origin. Mac. Vet. Rev. 35(1), 13-21.

[9] Wen, B., Liu, Y., Wang, P. (2012) Toxic Effects of Chlortetracycline on Maize Growth, Reactive Oxygen Species Generation and the Antioxidant Response. Environ. Sci. 24(6), 1099-1105.

[10] Liu, X., Nie, J., Wang, Q., Xu, X. (2001) Research progress in phytoremediation of heavy metal contaminated soil. Journal of Gansu Agricultural University. 36(3), 8-15.

[11] Li, H., Ma, W., Zhao, X. (2007) Remediation of Heavy Metals in Contaminated Soil by Plants is Briefly Discussed. Jilin Agricultural Sciences. 32(1), 35-39.

[12] Zhang, C., Li, H., Xia, L., Li, D. (2005) Effects of Cadmium and Zinc on Seed Germination and Seedling of Alfalfa. Acta Agriculturae Boreali-Sinica. 20(1), 96-99.

[13] Yang, H. (2011) Law and application of soil heavy metal enrichment by crops. Green Science and Technology. 11(4), 162-164.

[14] Zhang, X., Xia, H., Li, Z. (2009) Phytoremediation of Heavy Metal Contaminated Soil by Forage. Journal of Ecology. 28(8), 1640-1646.

[15] Zhang, G., Jiang, X., Cui, Y. (2005) Progress in Research and Application of Vetiver. Pratacultural Science. 22(1), 73-78.

[16] Hu, Y., Yang, X., Yang, F., Sun, D. (2009) Determination of Heavy Metal Content in Several Compositae Plants in Copper Mine Area. Resource Development & Market. 25(7), 596-598.

[17] Wang, X., Wu, Y. (1998) Study on the Absorption characteristics of Heavy Metal Compound Pollutants by Different Crops. Agricultural Environmental Protection. 17(5), 193-196.

[18] Wei, S., Zhou, Q., Wang, X. (2004) Study on Plants with Heavy Metal Superaccumulation around the Pit Mouth of a Lead-zinc Mine. Technology and Equipment for Environmental Pollution Control. 5(3), 33-39.
[19] Yang, Q., Ren, Z. (2007) Effects of Sewage Irrigation on Accumulation and Distribution of Heavy Metals in Soil and Vegetables. China Rural Nongli Hydropower. 1(5), 74-75.
[20] Zhou, J., Le, J., Ji, X., Wei, D. (2010) Flue Gas Emission and Soil Heavy Metal Pollution from Nongli Hydroelectric Smelters in Rural China. Journal of Hubei Second Normal University. 1(12), 52-54.

Received: **24.03.2021**
Accepted: **30.04.2021**

CORRESPONDING AUTHOR

Jianbo Li
Hunan Institute of Animal Husbandry and Veterinary Medicine,
Changsha 410131 – China

e-mail: kkkkanty@163.com

© by PSP Volume 30– No. 09/2021 pages 10697-10704 Fresenius Environmental Bulletin

RESEARCH AND CHARACTERISTIC EVALUATION OF A NOVEL ENVIRONMENTALY FRIENDLY WATER-BASED DRILLING FLUID

Yan Zhang*

CNPC Engineering Technology R&D Company Limited, Beijing 102206, PR China

ABSTRACT

With the continuous deepening of exploration and development and the increasingly stringent environmental protection regulations, environmental protection in the entire process of oil and gas exploration and development has become an issue that has to be carefully considered. As the blood of drilling, environmentally friendly drilling fluid systems need to pay special attention to environmental protection issues. In this paper, aiming at the technical problems of environmentally friendly water-based drilling fluids, natural polymer-based flow regulators are prepared by modifying natural polymers. The rheological properties and fluid loss properties of the 4% base slurry, and the temperature resistance, biodegradability, biological toxicity, and inhibitory properties of the flow regulator are evaluated. With the new flow regulator as the key treatment agent, a new environmentally friendly water-based drilling fluid system is designed, and the rheological performance, fluid loss performance, and environmental performance of the system are evaluated. The results show that the newly prepared flow regulator can effectively increase the dynamic shear force of the drilling fluid system, and at the same time has certain fluid loss reduction performance and good environmental protection performance. The constructed environmentally friendly water-based drilling fluid system has good rheological properties, and the temperature resistance can be up to 150°C, showing good field application potential.

KEYWORDS:
Environmental protection, water-based drilling fluid, flow regulator, biological toxicity, temperature resistance

INTRODUCTION

With the continuous deepening of oil and gas exploration, the impact of oil and gas development activities on the environment has gradually improved. In the gradual process, the drilling fluid with the greatest impact on the environment needs special attention. Countries all over the world have higher and higher requirements for environmental protection, and a large number of environmental protection regulations are released every year, and the requirements for the environmental performance of drilling fluids are also getting higher and higher [1]. While improving its temperature resistance, it is often difficult to take into account its environmental protection performance [2-4]. Solving the environmental protection problem of drilling fluid can better protect the environment and improve quality and efficiency.

Patel et al. [5] and others developed a high-performance water-based drilling fluid system named Ultradrill. This drilling fluid system has been widely used abroad. The main treatment agents include Ultrahib, Ultracap, PAC-LV, XC, Ultrafree, environmentally friendly lubricants, etc. The drilling fluid system has also been used in China's Dagang, Zhanjiang and other oil fields with good results. Xu et al. [6] et al. developed a natural heteropolysaccharide environmentally friendly drilling fluid treatment agent using domestic gum as a raw material, and used it as a key treatment agent to optimize the construction of an environmentally friendly drilling fluid system with good rheological properties at 120°C. In recent years, many scholars at home and abroad have conducted a lot of research on hydroxyethyl cellulose (HEC) modified water-soluble polymers and developed a lot of flow regulators for drilling fluids based on HEC [7-12].

Most of the existing environmentally friendly water-based drilling fluid systems have poor temperature resistance (<140°C), and there is an urgent need to develop a drilling fluid system with better temperature resistance. In this paper, cellulose is used as a raw material to prepare an environmentally friendly flow regulator for drilling fluids through graft copolymerization to provide a solution for the source control of drilling fluids. Then, it is used as a key treatment agent to develop a new environmentally friendly water-based drilling fluid system and applied in the Bohai Bay area.

MATERIALS AND METHODS

Materials. The following chemical materials are mainly used in the experiment: including sodium

hydroxide, absolute ethanol, urea, cellulose, sodium carbonate, deionized water, acrylamide, 2-acrylamide-2-methylpropanesulfonic acid (AMPS), ammonium persulfate. The instruments used in the experiment are: six-speed rotary viscometer, normal temperature medium pressure filter loss instrument, GJ-3S digital display high-speed mixer, all purchased from Shandong Meike Instrument Co., Ltd. Three-necked flasks, beakers, measuring cylinders, and glass stoppers which are all purchased from the corresponding glassware manufacturers. JA2003 electronic balance, purchased from Changzhou Depu Textile Technology Co., Ltd. Microtox M500 biological toxicity detector, purchased from Shanghai Aishengte Environmental Protection Technology Co., Ltd. The biochemical oxygen demand tester and chemical oxygen demand tester were purchased from Jiangsu Shengaohua Environmental Protection Technology Co., Ltd.

Methods. (1) Preparation of cellulose flow regulator. We disperse 5g of cellulose into 150ml of cellulose dissolving solution (12% urea and 7% NaOH), freeze at -18°C for 4 hours, take out the sample to melt and centrifuge at 1000 rpm for 20 minutes to obtain a uniform cellulose solution. Then, we place the cellulose solution in a 60°C water bath, add 0.4g of ammonium persulfate, and stir at constant temperature for 30 minutes, add 2g of acrylamide and 2g of AMPS successively, and fully stir and polymerize for 4h. Finally, the mixture obtained by the reaction is cooled to room temperature, a large amount of absolute ethanol is added, and the product was purified, dried and ground in vacuum at 40° C to obtain the flow regulator LX-8.

(2) Preparation of drilling fluid experiment slurry. 1) Preparation of water-based drilling fluid base slurry: we add 16g sodium bentonite and 0.8g anhydrous sodium carbonate to 400ml of water, stir with a high-speed mixer for 1h at a speed of 12000r/min, then stand for 48h for hydration to get 4% water-based drilling fluid base slurry [13].

2) Preparation of water-based drilling fluid experiment slurry: We add different concentrations of drilling fluid treatment agents to 4% of the base slurry. After each treatment agent is added, stir at high speed for 10 minutes and then add the next treatment agent until all the treatment agents are added.

(3) Testing of rheological properties of drilling fluid. A six-speed rotary viscometer is selected to test the rheological properties of the prepared experimental slurry. At the same time, after the drilling fluid is heated at 150°C for 16 hours, the rheological properties of the drilling fluid after the hot rolling are tested, and the relevant viscosity calculation formula is used to obtain the rheological parameters of drilling fluids include apparent viscosity, plastic viscosity, dynamic shear, etc. [14-15].

(4) Biodegradability of drilling fluid. The biochemical oxygen demand tester is used to test the biochemical oxygen demand (BOD5) of the drilling fluid, the chemical oxygen demand tester is used to test the chemical oxygen demand (CODCr) of the drilling fluid, and the biodegradability of the drilling fluid is obtained according to the ratio method (BOD5/CODCr) [16-18].

RESULTS

Comprehensive performance evaluation of LX-8. (1) Evaluation of rheological properties and fluid loss properties. The rheology of drilling fluid refers to the characteristics of fluid flow and deformation under the action of external force. This characteristic is usually described by the rheological curve, apparent viscosity, plastic viscosity, dynamic shear force, and static shear force of the drilling fluid [19]. The rheology of drilling fluid plays a vital role in solving the problem of carrying cuttings, suspending cuttings and barite, increasing the ROP, maintaining the wellbore rules and ensuring downhole safety.

We add LX-8 to 4% water-based drilling fluid base slurry at a concentration of 0.3%, stir at 10000r/min for 30 minutes to prepare experimental slurry 1. The rheological properties and fluid loss properties of slurry 1 before and after hot rolling at 150°C for 16 hours are measured. Then, we calculate the apparent viscosity (AV), plastic viscosity (PV), dynamic shear force (YP), etc. of experimental slurry 1, and evaluate the influence of LX-8 to the fluid loss performance and rheological properties of slurry 1. The experimental results are shown in Table 1.

From the experimental results in Table 1, it can be seen that after the 4% water-based drilling fluid base slurry is hot rolled at 150°C, the dynamic shear force decreases significantly, indicating that the high temperature hot rolling destroys the rheological properties of the base slurry. Before hot rolling, after adding 0.3% LX-8, the apparent viscosity, plastic viscosity, and dynamic shear force of the experimental slurry have been greatly improved, and the dynamic shear force has been significantly increased. At the same time, the filtration loss of the experimental slurry has also been compared. As the viscosity of the drilling fluid increases, the water molecules are bound by the mud cake formed by the drilling fluid, the kinetic energy of the water molecules decreases, and the fluid loss decreases. After hot rolling, the apparent viscosity, plastic viscosity, and dynamic shear force of the experimental slurry decreased to a certain extent than before hot rolling. Due to the high

temperature degradation, part of the molecular chain of LX-8 is degraded and destroyed, causing the viscosity of the experimental slurry to decrease slightly. Compared with hot rolling, the fluid loss of drilling fluid also increased due to the decrease of viscosity.

(2) The effect of LX-8 dosage on the rheological properties and fluid loss of drilling fluid. The evaluation of rheological properties and fluid loss performance shows that LX-8 can greatly increase the dynamic shear of drilling fluid, but the optimal concentration needs to be determined through laboratory experiments. By adding different concentrations of LX-8 to the 4% water-based drilling fluid base slurry, the rheological properties and fluid loss properties of the experimental slurry before and after hot rolling at 150°C are tested, and the influence of the dosage on the rheological properties of the drilling fluid is analyzed. The results are shown in Figure 1.

LX-8 is a cellulose modified flow regulator. Due to the grafting effect, its molecular chain is longer, and the presence of amide groups and other adsorption groups makes it possible to form a grid structure in the drilling fluid, which enhances the drilling viscosity and dynamic shear of the liquid system. With the increase of the concentration of LX-8, the apparent viscosity, plastic viscosity, and dynamic shear force of the experimental slurry gradually increase, and the fluid loss gradually decreases. The proper concentration prevents the rheological properties of the drilling fluid from being poor due to excessive viscosity and affecting the drilling operation [20].

TABLE 1
The rheological and filtration performance of fluid with LX-8

LX-8 concentration/%	Testing conditions	AV /(mPa·s)	PV /(mPa·s)	YP/Pa	YP/PV	FL_{API} /mL
0	Before hot rolling	6	4	2	0.5	32
	After hot rolling	5	4	1	0.25	39
0.3	Before hot rolling	24	11	13	1.18	13.6
	After hot rolling	20	10	10	1.0	14.8

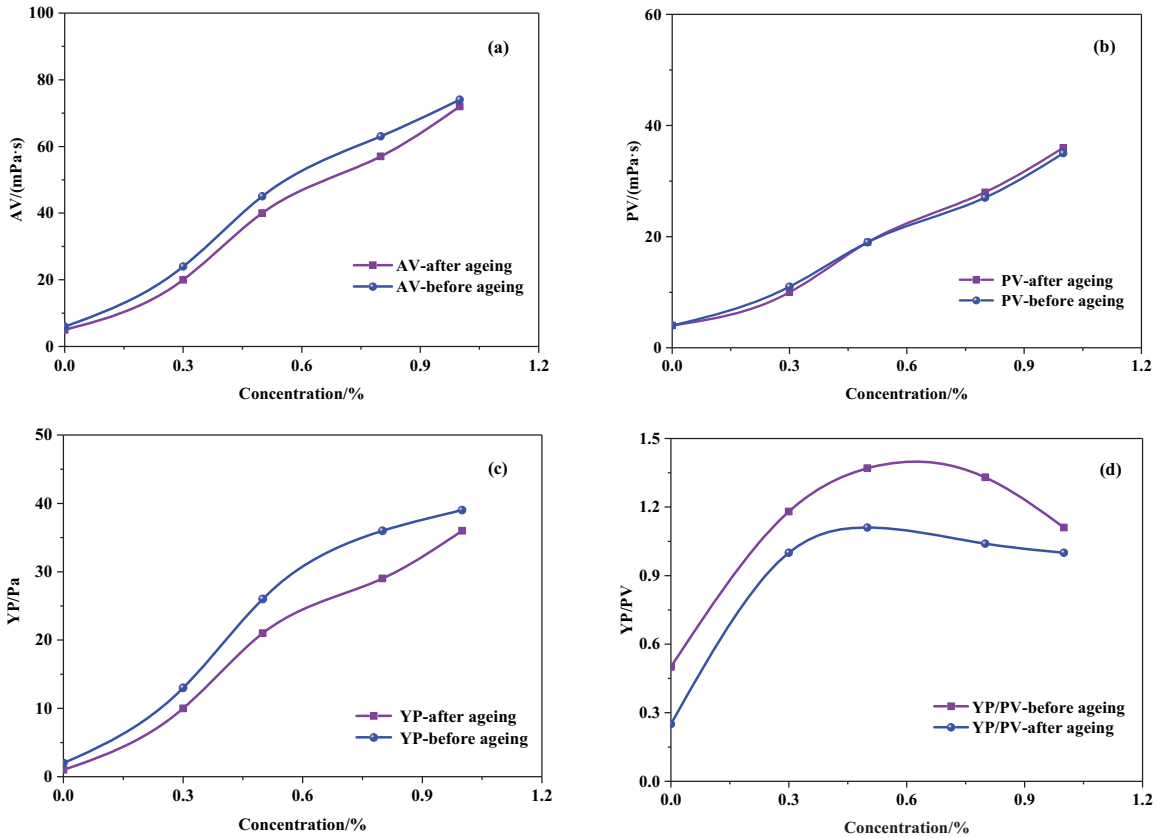


FIGURE 1
The rheological performance of fluid with different LX-8 addition.

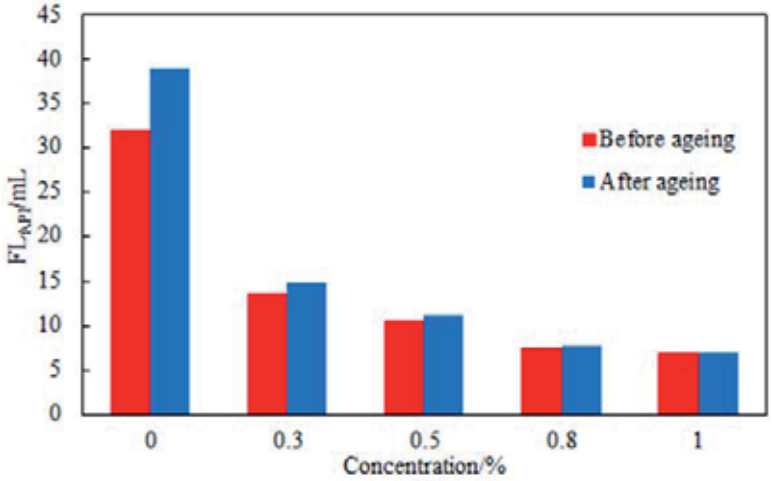


FIGURE 2
The filtration loss of fluid with different LX-8 addition.

TABLE 2
The rheological and filtration performance of fluid with different temperature

Temperature/°C	AV /(mPa·s)	PV /(mPa·s)	YP/Pa	YP/PV	FL_{API} /mL
Room temperature	24	11	13	1.18	13.6
120	23	11	12	1.09	14.2
150	20	10	10	1.00	14.8
160	14	9	5	0.56	18.4

It can be seen from the experimental results in Figure 2 that the fluid loss of the experimental well decreases with the increase of the LX-8 concentration, but after the concentration exceeds 0.5%, the fluid loss reduction rate changes little, indicating that LX-8 has an effect on fluid loss. The influence of the amount becomes smaller after its concentration is greater than 0.5. At the same time, it can be seen from Figure 1a that when the concentration of LX-8 is 0.5%, the dynamic plastic ratio of the experimental pulp is the largest. According to relevant research experience, combined with the experimental results of the rheological properties of the experimental pulp, the concentration of LX-8 is 0.5%.

(3) Temperature resistance of LX-8. Poor temperature resistance is the main reason why natural polymer drilling fluid treatment agents are difficult to be applied on a large scale in high temperature wells. By introducing monomers with strong temperature resistance into the cellulose, the molecular chain of the product is enlarged, and the temperature resistance of the prepared flow pattern regulator is improved. By comparing the performance of LX-8 after hot rolling at different temperatures, the temperature resistance of LX-8 is explored, and the dosage of LX-8 is fixed at 0.3%. The experimental results are shown in Table 2.

It can be seen from the data in Table 2 that under the same concentration, with the increase of the hot rolling temperature, the YP/PV of the experimental slurry before and after the hot rolling gradually decreases within 150°C, but the amplitude of the change is small, and the change of the fluid loss is also small. When the hot-rolling temperature is 160°C, the YP/PV of the experimental slurry is reduced to 0.56, and the apparent viscosity is reduced by 41.67% compared with that before the hot-rolling. Compared with the base pulp, YP/PV still has a 50% increase, but compared with the experimental pulp after hot rolling at 150°C, YP/PV drops by 44%. It shows that the temperature resistance of LX-8 can reach 150°C, but lower than 160°C.

(4) Environmental performance of LX-8. 1) Biological toxicity. Biotoxicity test is carried out based on the GB/T18420.2-2009 "Biological Toxicity of Pollutants in Offshore Petroleum Exploration and Development Part 2: Test Methods" and GB/T18420.1-2009 "Biological Toxicity of Pollutants in Offshore Petroleum Exploration and Development Part 1: Classification". The luminescent bacteria method is used to test the biological toxicity EC50 of LX-8. The experimental results show that the EC50 value of the LX-8 solution is 3.2×10^4mg/L, which is higher than the allowable discharge value of 2.0×10^4mg/L.

2) Biodegradability. Determination of CODCr: According to the National Standard of the People's Republic of China GB11914-89 "Water Quality Determination of Chemical Oxygen Demand by Potassium Dichromate Method", the chemical oxygen demand of LX-8 is determined. Determination of BOD5: According to the National Standard of the People's Republic of China HJ505-2009 "Water quality—Determination of biochemical oxygen demand after 5 days (BOD5) for dilution and seeding method" (Water quality—Determination of biochemical oxygen demand after 5 days (BOD5) for dilution and seeding method), we incubate the sample in a dark place at 20±1°C for 5 days. Then, we determine the mass concentration of dissolved oxygen in the water samples before and after the incubation. From the difference between the mass concentrations of dissolved oxygen before and after the incubation, we calculate the amount of dissolved oxygen consumed per liter of sample, expressed as BOD5.

According to the above measurement method, the biodegradability of LX-8 is evaluated. The BOD5 and CODCr values of LX-8 are tested indoors, and the BOD5/CODCr values of LX-8 are calculated. The experimental results show that the BOD5/CODCr value of the flow regulator LX-8 is 18.6%, and the biodegradability evaluation result is relatively easy to degrade.

Development and performance evaluation of a new environmentally friendly water-based drilling fluid system. (1) Development of environmentally friendly water-based drilling fluid system. With LX-8 as the key treatment agent, combined with on-site requirements, a new environmentally friendly water-based drilling fluid system is constructed. Environmentally friendly water-based drilling fluids need to meet discharge standards in terms of biological toxicity, biodegradability, chroma, pH, etc. Therefore, light-colored treatment agents with good environmental performance are preferred. Based on the optimization of existing treatment agents for environmentally friendly drilling fluids, combined with the performance of the treatment agents, the construction of an environmentally friendly drilling fluid system is carried out. The preferred environmental protection drilling fluid treatment agents are: environmental protection fluid loss reducer LS-3, environmental protection starch fluid loss reduction agent DF-150, environmental protection coating agent HLS-3, environmental protection flow regulator LX-8, environmental protection inhibition and prevention collapse agent NF-25, environmental protection blocking film forming agent CMJ-1, environmental protection inhibitor SSJ-3.

Through indoor formulation optimization experiments, the new environmentally friendly water-based drilling fluid formulation is as follows: 1% environmentally friendly fluid loss reducer LS-3 + 1% Environmental protection starch filtrate reducer DF-150+ 0.3% environmental protection coating agent HLS-3+0.5% environmental protection flow regulator LX-8+ 2% environmental protection inhibition anti-collapse agent NF-25+1% environmental protection blocking film formation CMJ-1+1% environmental protection inhibitor SSJ-3.

(2) Evaluation of rheological properties and fluid loss performance of environmentally friendly water-based drilling fluid system. The rheological properties and fluid loss properties of the drilling fluid system before and after hot rolling at 150°C are evaluated. The experimental results are shown in Table 3.

It can be seen from the experimental data in the table that the environmentally friendly water-based drilling fluid system has good rheological properties. After being heated at 150°C, the apparent viscosity, plastic viscosity, dynamic shear, and filtration loss of the drilling fluid do not vary significantly. The initial cut and final cut can be better maintained, and the dynamic plastic ratio is reasonable, which can effectively carry cuttings and keep the borehole unobstructed [21]. The fluid loss of the drilling fluid system is low, and the invasion of the formation is correspondingly small, which is beneficial to the protection of the reservoir. The high-temperature and high-pressure fluid loss more easily reflects the percolation of the experimental slurry under formation conditions. The evaluation results show that the high-temperature and high-pressure fluid loss of the environmentally friendly drilling fluid system is low.

TABLE 3
Experimental results of rheological properties and fluid loss performance of the environmentally friendly water-based drilling fluid system

Conditions	AV /(mPa·s)	PV /(mPa·s)	YP /Pa	YP/PV	Initial cut/Final cut /(Pa/Pa)	FL_{API} /mL	FL_{HTHP} /mL
Before hot rolling	62	43	19	0.44	10/20	3.2	14
After hot rolling	58	40	18	0.45	12/22	3.4	

TABLE 4
Experimental results of environmental performance evaluation of environmentally friendly water-based drilling fluid system

BOD_5 /(mg·L^{-1})	COD_{Cr} /(mg·L^{-1})	BOD_5 /COD_{Cr}	EC_{50} /(mg·L^{-1})
832	3840	0.2167	4.6×10^4

TABLE 5
Environmental protection water-based drilling fluid cuttings rolling dispersion experiment

System	Initial weight /g	Final weight after rolling /g	Recovery /%
Water	30.21	4.33	14.33
Environmentally friendly water-based drilling fluid	30.35	28.16	92.78

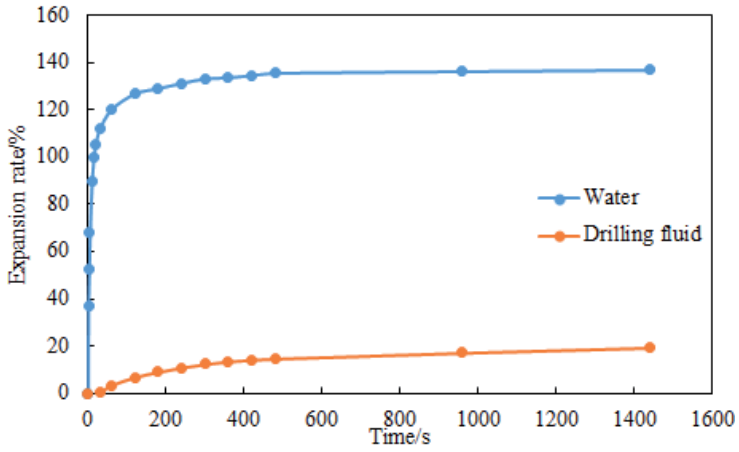


FIGURE 3
Swelling rate of shale of environmentally friendly water-based drilling fluid and water.

(3) Environmental performance evaluation of environmentally friendly water-based drilling fluid system. According to the corresponding environmental performance evaluation method, the environmental performance of the constructed environmentally friendly water-based drilling fluid system is evaluated. The experimental results are shown in Table 4.

It can be seen from the results that the constructed environmentally friendly water-based drilling fluid system has an EC_{50}value greater than 25000 mg/L, is non-toxic, has a BOD_5/COD_{Cr} value greater than 15, and is easily biodegradable. The environmentally friendly water-based drilling fluid system meets the domestic discharge standards.

(4) Evaluation of shale inhibition performance of environmentally friendly water-based drilling fluid system. In drilling engineering, the clay minerals in the shale formation will hydrate and swell and disperse in contact with water, causing instability of the borehole wall. Drilling fluid inhibition refers to the inhibition of hydration expansion and dispersion of shale formations. We select a rock sample from a certain block and use the rolling recovery rate evaluation experiment to evaluate the shale inhibition performance of the environmentally friendly water-based drilling fluid. The experimental results are shown in Table 5.

It can be seen from the experimental data in Table 5 and Figure 3 that the rock sample in this block with a high content of clay minerals has a low rolling recovery rate of water. The rolling recovery rate in water is only 14.33%. In the environmentally friendly water-based drilling fluid, the rolling recovery rate of this rock sample can reach 92.78% which is over 5 times the value from water. The swelling rate of the shale immersed in water is 136.82%, while that in the environmentally friendly drilling fluid system is only 19.41%, indicating that the environmentally friendly water-based drilling fluid system has good suppression performance and can be used in formations with high suppression performance requirements.

Field application of environmentally friendly water-based drilling fluid system. The environmentally friendly water-based drilling fluid system has been used in 10 wells in the Bohai Bay area. No complications occurred during the construction of the completed experimental wells. The maximum temperature of the well bottom of the wells has reached 155℃, and the completion electrical survey does smoothly. Among the 10 wells under

construction, 9 are successful in one electrical test, with a 90% success rate of electrical test and a 100% pass rate of wellbore quality. The drilling fluid experiment achieves satisfactory results.

CONCLUSIONS

(1) The flow regulator LX-8 based on cellulose modification has good rheological properties in drilling fluids, has obvious effect of increasing shear force, and has a certain effect of reducing fluid loss. The optimal addition amount of LX-8 is 0.5%. The temperature resistance test of LX-8 shows that the temperature resistance of LX-8 can reach 150°C, and the environmental protection performance of LX-8 is good.

(2) With LX-8 as the key treatment agent, combined with the optimization of related environmentally friendly drilling fluid treatment agents, a new environmentally friendly water-based drilling fluid system is developed. The formula of the system is as follows: 1% environmentally friendly fluid loss reducer LS-3 + 1% Environmental protection starch filtrate reducer DF-150+ 0.3% environmental protection coating agent HLS-3+0.5% environmental protection flow regulator LX-8+ 2% environmental protection inhibition anti-collapse agent NF-25+1% environmental protection blocking film formation CMJ-1+1% environmental protection inhibitor SSJ-3. The performance evaluation results show that the temperature resistance of the system can reach 150°C, the rheological performance, fluid loss performance and shale inhibition performance are good. The drilling fluid system can effectively carry and remove the cuttings, and the environmental performance is excellent. The EC50 value is higher than 2.5×10^4mg/L, which is much higher than the allowable limit of biological toxicity.

(3) Field tests in the Bohai Bay area show that the environmentally friendly water-based drilling fluid system can smoothly carry out drilling operations in relevant blocks without complications and has good field application effects.

ACKNOWLEDGEMENTS

This work was not supported by any funds. And the author wants to show sincere thanks to all the techniques who have contributed to this research.

REFERENCES

[1] Cui, X., Li, S., Xu, H., Zhang, Z., Zhao, X., Gao, Z. (2018) Late Quaternary Paleoenvironmental Reconstruction, Using Benthic Foraminifera and Ostracoda, of Marine Sedimentary Beds On the Southern Coast of Laizhou Bay, Bohai Sea, China. Journal of Foraminiferal Research. 48(2), 87-99.

[2] Al-Hameedi, A., Alkinani, H., Dunn-Norman, S., Albazzaz, H., Mohammed, M. (2019) Insights into Eco-Friendly and Conventional Drilling Additives: Applications, Cost Analysis, Health, Safety, and Environmental Considerations. Symposium: Asia Pacific Health, Safety, Security, Environment and Social Responsibility. SPE. 195398-MS.

[3] Huang, H. (2004) Ultra drill, a new water based drilling fluid with safety and environmental protection. Drilling Fluid and Completion Fluid. 21(6), 4-7.

[4] Gu, S., Wang, C., Jiang, B., Tan, Y., Li, N. (2012) Field test of rock burst danger based on drilling pulverized coal parameters. Disaster Advances. 5(4), 237-240.

[5] Zhao, N., Lu, N., Chen, C., Li, H., Yue, T., Zhang, L., Liu, Y. (2017) Mapping temperature using a Bayesian statistical method and a high accuracy surface modelling method in the Beijing–Tianjin–Hebei region, China. Meteorological Applications. 24(4), 571-579.

[6] Xu, C., Wu, F., Zhang, J., Tan, T., Yang, X. (2006) Application of new environmental friendly heteropolysaccharide drilling fluid in Jiangsu Oilfield. Drilling Fluid and Completion Fluid. 23(1), 19-23.

[7] Bai, D., Khin, C., Chen, S., Tsai, C., Chen, B. (2005) Interaction between a nonionic surfactant and a hydrophobically modified 2-hydroxyethyl cellulose. Journal of Physical Chemistry B. 109(11), 4909-4916.

[8] Ismail, A., Alias, A., Sulaiman, W., Jaafar, M., Ismail, I. (2017) Drilling fluid waste management in drilling for oil and gas wells. Chemical Engineering Transactions. 56, 1351-1356.

[9] Elkatatny, S. (2019) Assessing the Effect of Micronized Starch on Rheological and Filtra-tion Properties of Water-Based Drilling Fluid. In SPE Middle East Oil and Gas Show and Conference. Society of Petroleum Engineers. 133-139.

[10] Wei, J., Yu, H., He, J., Tuo, D. (2018) Preparation and property evaluation of crosslinked carboxymethyl starch filter loss reducing agent. Oilfield Chemistry. 1, 3.

[11] Adesina, F., Anthony, A., Gbadegesin, A., Esseoghene, O., Oyakhire, A. (2012) Environmental Impact Evaluation of a Safe Drilling Mud. SPE. 152865-PP.

[12] Singh, A., Nath, L., Guha, M. (2011) Microwave assisted synthesis and characterization of Phaseolus aconitifolius starch-g-acrylamide. Carbohydrate Polymers. 86(2), 872-876.
[13] Dow, M., Florence, A. (2012) Chloride-free Inhibitive Water-Based Fluid Significantly Improves Environmental Acceptability for Rain Forest Locations While Maintaining Drilling Performance. SPE. 156824.
[14] Wang, D., Wang, J., Song, Z., Zhuang, J., Zhao, Y. (2018) Preparation and Properties of a Novel Inorganic Silicon Modified Sodium Carboxylmethyl Starch Filtra Reducer. Petroleumical Technology. 39(04), 440-443.
[15] Zhou, G., Qiu, Z., Zhong, H., Zhao, X., Kong, X. (2021) Study of Environmentally Friendly Wild Jujube Pit Powder as a Water-Based Drilling Fluid Additive. ACS Omega. 6(2), 1436-1444.
[16] Wang, Y., Jiang, B., Lan, J., Xu, N., Sun, J., Meng, L. (2020) Synthesis and properties of a high-performance environment-friendly micro-nano filtration reducer. RSC Advances. 10(70), 43204-43212.
[17] Patidar, A., Sharma, A., Joshi, D. (2020) Formulation of cellulose using groundnut husk as an environment-friendly fluid loss retarder additive and rheological modifier comparable to PAC for WBM. Journal of Petroleum Exploration and Production Technology. 10(8), 3449-3466.
[18] Aramendiz, J., Imqam, A. (2020) Silica and Graphene Oxide Nanoparticle Formulation To Improve Thermal Stability and Inhibition Capabilities of Water-Based Drilling Fluid Applied to Woodford Shale. SPE Drilling & Completion. 35(2), 164-179.
[19] Aramendiz, J., Imqam, A. (2019) Water-based drilling fluid formulation using silica and graphene nanoparticles for unconventional shale applications. Journal of Petroleum Science and Engineering. 179, 742-749.
[20] Zhong, H., Kong, X., Chen, S., Grady, B., Qiu, Z. (2021) Preparation, characterization and filtration control properties of crosslinked starch nanospheres in water-based drilling fluids. Journal of Molecular Liquids. 325, 115221.
[21] Shao, X., Pu, X. (2018) Research Status and Development Trend of Environmental Protection Drilling Fluid. Chemical World. 59(9), 545-551.

Received: **24.03.2021**
Accepted: **30.04.2021**

CORRESPONDING AUTHOR

Yan Zhang
CNPC Engineering Technology R&D Company Limited,
Beijing 102206 – PR China

e-mail: zhangyandr@cnpc.com.cn

© by PSP Volume 30– No. 09/2021 pages 10705-10711 Fresenius Environmental Bulletin

CORRELATION BETWEEN MENTAL RESILIENCE-MEDIATED CANCER-RELATED FATIGUE AND POST-TRAUMATIC GROWTH IN PATIENTS WITH HEAD AND NECK TUMORS

Mingkun Han[1,2,3,4], Xue Yang[5], Yang Wang[1,2,3,4], Jing Lv[5,*]

[1]College of Otolaryngology Head and Neck Surgery, Chinese PLA General Hospital, Beijing 100853, China
[2]National Clinical Research Center for Otolaryngologic Diseases, Beijing 100853, China
[3]Key Lab of Hearing Science, Ministry of Education, Beijing 100853, China
[4]Beijing Key Lab of Hearing Impairment for Prevention and Treatment, Beijing 100853, China
[5]The Second Medical Center & National Clinical research Center for Geriatric Diseases, Chinese PLA General Hospital, Beijing 100853, China

ABSTRACT

To explore the mediating effect of mental resilience between post-traumatic growth and cancer-related fatigue (CRF) in patients with head and neck tumors.

A total of 282 patients with head and neck tumors diagnosed in our hospital from January 2019 to October 2020 were selected as the research objects. The mental resilience, CRF and post-traumatic growth scores were investigated by questionnaire, and the mediating effect structural equation model was established to analyze the relationship among them.

The total scores of mental resilience, CRF and post-traumatic growth of patients with head and neck tumors were (52.32±9.12) points, (35.51±8.34) points and (64.36±8.44) points, respectively. Besides, CRF had negative correlations with mental resilience and post-traumatic growth, and mental resilience was positively related to post-traumatic growth ($P<0.05$). The mediating effect of mental resilience in the path between CRF and post-traumatic growth was -0.43, taking up 30.50% of the total effect.

Mental resilience acts as a mediator in the path between CRF and post-traumatic growth. In the clinical intervention of patients with head and neck tumors, clinicians should try their best to alleviate the burden of patients to help them cope with cancer optimistically and actively, increase their resilience and promote their post-traumatic growth.

KEYWORDS:
Mental resilience, Cancer-related fatigue, Post-traumatic growth, Head and neck tumors, Alleviate burden

INTRODUCTION

Head and neck tumors, common malignancies, are regarded as the most traumatic tumors. As a type of serious stressor, cancer brings physiological pain and causes severe psychological burden to patients [1]. Faced with side effects during the treatment of head and neck tumors using different methods, patients are prone to suffering from depression, loss of sense of security, cancer-related fatigue (CRF) and other psychological problems, which may exert indirect or direct impacts on the disease outcome and further affect the quality of life and even the survival outcome of patients [2]. Hence, actively promoting the ability of patients to cope with the traumatic event (cancer) is conducive to the prognosis recovery of the disease. Post-traumatic growth is an index reflecting individual's ability to self-regulate trauma. In other words, it refers to the positive transformation experienced by the individual after the internal struggle against the psychological changes induced by the trauma [3].

CRF refers to a persistently uncomfortable, physical, emotional and/or cognitive subjective fatigue or feeling of exhaustion. It is also one of the most common discomfort experienced by cancer patients, which is related to tumor or tumor treatment and disproportionate to recent activities and affects daily life. Besides, CRF not only affects the quality of life of patients, but also leads to the interruption of anti-cancer treatment and reduces the survival rate in severe cases. Some studies in China and foreign countries have confirmed that cancer patients exhibit a high level of CRF and a certain level of post-traumatic growth [4]. In recent years, from a positive point of view, researchers have found that mental resilience, as the coping ability of individuals to maintain or restore their mental health in face of stress events, can evaluate the positive mental state of individuals [5]. The better the mental resilience of cancer patients is, the higher their post-traumatic growth level will be [6]. In addition, the depression level of

cancer patients with better mental resilience is relatively low, which is negatively correlated with CRF [7]. Previously, the relationship among mental resilience, CRF and post-traumatic growth of patients with head and neck tumors have rarely been reported. In this study, therefore, this relationship was explored, and it was assumed that mental resilience might be a positive psychological quality significantly influencing the relationship between CRF and post-traumatic growth. Moreover, the correlation among them was investigated by constructing a structural equation model, which provided reference for clinical evaluation, rehabilitation and the improvement of the quality of life of patients with head and neck tumors.

MATERIALS AND METHODS

Clinical data. There were 282 research objects in total that were randomly selected using a random number table. They were patients with head and neck tumors admitted and treated in the Department of Oncology and Department of Critical Care Medicine from January 2019 to October 2020 in our hospital, including 189 males and 113 females aged 29-76 years old, with an average of (58.29±8.42) years old. Among them, there were 76 cases of oral cancer, 152 cases of nasopharyngeal carcinoma, 49 cases of head skin cancer and 25 cases of other cancers. According to the cancer stage, there were 21 cases in stage I, 103 cases in stage II, 126 cases in stage III and 52 cases in stage IV.

This research was approved by the Ethics Committee of our hospital. All subjects were informed of the relevant rights and risks, voluntarily participated in the research and signed the informed consent.

Inclusion and exclusion criteria. Inclusion criteria were as follows: 1) patients diagnosed with malignant head and neck tumors confirmed by pathological sections or cytological diagnosis, 2) those whose Kamofsky Performance Status (KPS) score ≥60 points, and 3) those who were able to consciously and clearly express their willingness and accept questionnaire survey.

Exclusion criteria were set below: 1) patients with history of mental and neurological diseases or consciousness disorders, 2) those with history of dependence on alcohol and psychotropic drugs, 3) those with severe cognitive impairment or audio-visual impairment, 4) those complicated with other malignant tumors, 5) those who could not control their serious complications, or 6) those who died during research or quit the research for other reasons.

Collection of questionnaires. According to the calculation using the relevant principles of scale design and psychometrics, the sample size should be 5-10 times as large as the scale variables. 290 questionnaires were distributed in total, and 282 valid questionnaires were collected, with an effective collection rate of 97.24%. All members of the research team who participated in the questionnaire survey received unified training, and they explained the content of the scale and the guidance for filling in it to the subjects. Then the subjects filled in the questionnaire by themselves, and those who could not fill in it by themselves for other reasons were assisted by the research members by inquiring and recording one by one in a unified way. Next, the research members collected and checked the questionnaires on the spot, registered and coded the valid questionnaires, filled in the missing items and amended the wrong items in time to ensure the authenticity and completeness of the questionnaires.

Connor-Davidson resilience scale (CD-RISC). CD-RISC was written by Connor and Davidson based on the trait theory. In this study, CD-RISC (2001) revised by Yu and Zhang [8] was adopted. The Cronbach α coefficient of the total scale was 0.907, and the internal consistency coefficients of each dimension were 0.867, 0.835 and 0.826, respectively. This scale consisted of a total of 25 items, including optimism (4 items), strength (8 items) and tenacity (13 items). Each item was scored using the 5-Point Likert Scale (0-4 points), which represented "never" to "almost always" accordingly, with a total score of 100 points. The higher the score was, the higher the mental resilience level of patients would be.

Brief fatigue inventory (BFI). Evaluation using BFI manifested that Cronbach's α coefficient was 0.916, and this scale was composed of 9 items. Each item was scored 0-10 points, with 0 being no fatigue or interference and 10 being the most fatigue or severest interference. The first three items were used to individually assess the current fatigue degree, general fatigue degree in the past 24 h and the highest degree of fatigue of patients, and the last six items were utilized to evaluate the impact of fatigue on patients' life in the past 24 h, including general activities, emotions, walking ability, normal work, contact with others and life appreciation. The impact of fatigue on life was scored 0-90 points, and the higher the score was, the higher the degree of fatigue would be [9].

Posttraumatic Growth Inventory (PTGI). In this study, the scale translated and edited by Wang et al. [10] in 2011 based on the original version compiled by Tedeschi was adopted. The Cronbach α coefficient of the total scale was 0.900, and the test-retest reliability was 0.826. This scale consisted of 5 dimensions, namely, interpersonal dimension (6 items), new possibility dimension (3 items), personal

strength dimension (4 items), mental change dimension (3 items) and life appreciation dimension. Using 6-Point Likert Scale, each item was scored 0-5 points, indicating "no change at all", "very little change", "little change", "some changes", "many changes" and "obvious changes". The total score was 0-105 points, and the higher score indicated stronger post-traumatic growth ability.

Statistical analysis. Epidata 3.1 software was employed for data entry, and SPSS 19.0 and AMOS 20.0 were adopted for data analysis. Measurement data in conformance with normal distribution were expressed as mean ± standard deviation, and inter-group comparison was conducted using independent samples t-test. Count data were expressed as frequency or percentage, and $\chi 2$ test was utilized for comparison between groups. Moreover, the correlation among indexes were determined via Pearson's correlation analysis, multivariate regression analysis and mediating effect model. Lastly, the Bias-Corrected Bootstrap method was adopted for detection, and $P<0.05$ on both sides showed a statistically significant difference.

RESULTS

Total scores of mental resilience, CRF and post-traumatic growth. The total scores of mental resilience, CRF and post-traumatic growth were (52.32±9.12) points, (35.51±8.34) points and (64.36±8.44) points, respectively (Table 1).

Mental resilience and post-traumatic growth levels of patients with different characteristics of head and neck tumors. According to the scores of different payment methods, cancer stages, caregivers and treatment methods, the mental resilience and post-traumatic growth of patients with head and neck tumors exhibited statistically significant differences ($P<0.05$). In addition, the post-traumatic growth level also showed a significant difference in the score of different disease duration ($P<0.05$) (Table 2).

Correlations among mental resilience, CRF and post-traumatic growth. Significantly negative correlations were detected among CRF, mental resilience and post-traumatic growth (r=-0.723, -0.724, $P<0.001$), and an obvious positive relation was discovered between mental resilience and post-traumatic growth (r= 0.707, $P<0.001$) (Table 3).

Regression analysis results of mental resilience, CRF and post-traumatic growth. Regression analysis was carried out with CRF as an independent variable, post-traumatic growth as an dependent variable and mental resilience as an intermediate variable. Equation 1 shows that CRF can directly affect the post-traumatic growth level of patients (β=-0.428, $P<0.001$). Equation 2 displays that CRF negatively affects the mental resilience of patients (β=-0.929, $P<0.001$). Equation 3 illustrates that mental resilience positively influences the post-traumatic growth level of patients (β=0.549, $P<0.001$). Moreover, Equation 4 reveals that CRF and mental resilience simultaneously affect post-traumatic growth (β=0.698, -0.353, $P<0.001$), and the regression equation was shown as follows: post-traumatic growth =34.287 + 0.698 × mental resilience - 0.353 × CRF (Table 4).

TABLE 1
Total scores of mental resilience, CRF and post-traumatic growth ($\bar{x} \pm s$)

Item	Dimension (n)	Total score of dimension	Average score
Mental resilience	25	52.32±9.12	2.28±0.62
Optimism	4	8.01±7.52	2.02±0.64
Strength	8	18.43±6.21	2.25±0.62
Tenacity	13	26.22±10.35	2.14±0.64
CRF	9	35.51±8.34	3.67±1.10
Post-traumatic growth	20	64.36±8.44	3.25±0.82
Interpersonal relationship dimension	6	20.72±5.64	3.25±0.91
New possibility dimension	3	10.34±4.12	3.37±0.82
Personal strength dimension	4	15.21±4.03	3.72±1.14
Mental change dimension	3	7.75±2.23	2.55±0.82
Life appreciation dimension	4	13.21±4.61	3.24±0.71

TABLE 2
Mental resilience and post-traumatic growth levels of patients with different characteristics of head and neck tumors ($\bar{x} \pm s$)

Variable	Variable stratification	Mental resilience score	P	Post-traumatic growth score	P
Gender	Male (n=179)	52.51±7.52	0.765	64.56±7.43	0.964
	Female (n=103)	52.33±8.45		64.41±7.56	
Age	≤60 years old (n=184)	52.28±9.15	0.415	64.35±7.28	0.717
	>60 years old (n=98)	53.11±8.12		64.89±7.07	
Place of residence	Rural areas (n=131)	52.21±8.42	0.234	64.18±8.12	0.249
	Urban areas (n=151)	52.55±7.32		65.34±7.12	
Marital status	Married (n=206)	52.36±7.76	0.782	64.57±8.11	0.728
	Unmarried (n=76)	52.51±8.25		64.72±7.34	
Degree of education	Junior high school and below (n=77)	53.13±7.28	0.824	65.24±7.29	0.893
	Senior high school and junior college (n=109)	52.41±7.32		64.89±8.07	
	Bachelor degree or above (n=96)	52.35±8.12		64.38±7.45	
Monthly income	< 3000 yuan (n=95)	52.38±7.32	0.748	64.55±8.41	0.684
	3,000-6,000 CNY (n=91)	52.56±7.08		64.36±7.32	
	> 6000 CNY (n=96)	52.32±7.08		64.52±7.45	
Payment method	Self-funding (n=77)	51.23±7.15	0.028	63.08±7.34	0.025
	Medical insurance and partial public expenses (n=205)	52.87±7.23		65.11±7.21	
	Rural cooperative medical care (n=64)	52.43±7.35		64.74±7.43	
	Partial public expense (n=30)	51.11±7.45		64.12±7.34	
Tumor type	Oral cancer (n=66)	52.45±7.23	0.587	64.61±8.14	0.863
	Nasopharyngeal carcinoma (n=142)	52.32±8.22		64.23±7.22	
	Head skin cancer (n=49)	52.25±7.44		64.34±7.16	
	Other cancers (n=25)	52.62±7.62		64.71±7.37	
Cancer stage	Stage I-II (n=114)	52.92±7.14	0.029	64.96±6.92	0.038
	Stage III-IV (n=168)	51.26±6.41		63.21±7.22	
Metastasis	Yes (n=106)	52.24±6.35	0.574	64.41±6.45	0.724
	No (n=176)	52.34±6.23		64.58±6.45	
Duration of disease	≤1 month (n=87)	52.58±7.14	0.128	64.82±7.11	0.029
	1 month to 1 year (n=107)	52.41±7.32		63.65±7.25	
	≥1 year (n=112)	52.67±7.51		63.18±8.24	
Caregiver	Spouse (n=173)	53.22±7.25	0.026	64.45±7.12	0.024
	Parents and children (n=98)	52.67±7.32		64.62±8.14	
	Others (n=35)	51.22±7.23		63.11±7.43	
Treatment method	Radiotherapy + chemotherapy (n=111)	52.51±7.23	0.030	65.17±7.56	0.012
	Operation + radiotherapy/chemotherapy (n=102)	53.12±7.09		64.45±7.23	
	Operation + radiotherapy + chemotherapy (n=93)	51.24±7.11		63.23±7.18	

TABLE 3
Correlations among mental resilience, CRF and post-traumatic growth

Item	Score ($\bar{x} \pm s$)	CRF	Post-traumatic growth	Mental resilience
CRF	35.51±8.34	1	-0.724	-0.723
Post-traumatic growth	64.36±8.44	-	1	0.707
Mental resilience	52.32±9.12	-	-	1

P<0.001, -: blank.

TABLE 4
Regression analysis results of mental resilience, CRF and post-traumatic growth

Equation	Dependent variable	Constant and independent variable	Coefficient of regression	Standard deviation	*t*	P
Equation 1	Post-traumatic growth	Constant	91.783	0.012	16.893	<0.001
		CRF	-0.428	0.021	-3.478	0.002
Equation 2	Mental resilience	Constant	97.265	0.017	11.287	<0.001
		CRF	-0.929	0.015	-4. 673	<0.001
Equation 3	Post-traumatic growth	Constant	37.298	0.017	11.684	<0.001
		Mental resilience	0.549	0.045	13.982	<0.001
Equation 4	Post-traumatic growth	Constant	34.287	0.021	5.897	<0.001
		Mental resilience	0.698	0.026	10.982	<0.001
		CRF	-0.353	0.021	7.546	<0.001

TABLE 5
Mediating effect of mental resilience in the path between CRF and post-traumatic growth

Path	Point estimated value	Standard deviation	Percentage (%)	Z	P	95%CI
CRF → Post-traumatic growth (total effect)	-1.41	0.24	100.00	6.12	<0.001	-2.54~-0.43
CRF → Post-traumatic growth (direct effect)	-0.82	0.35	58.16	4.85	<0.001	-1.63~-0.56
CRF → mental resilience → post-traumatic growth	-0.43	0.13	30.50	3.62	0.003	-0.44~-0.19

Mediating effect of mental resilience in the path between CRF and post-traumatic growth. The structural equation model of mediating effect was established with CRF fatigue as a predictor, mental resilience as a mediator and post-traumatic growth as an effect variable. Subsequently, this structural equation model was analyzed by Bootstrap method, and the fitting indexes were good ($\chi 2$=9.354, $\chi 2$/DF=0.720, P=0.305), indicating that the model fits well. The total effect of CRF on post-traumatic growth was -1.41, and the direct effect was -0.82. Besides, the mediating effect of mental resilience was -0.43, taking up 30.50% of the total effect (Table 5).

DISCUSSION

It has been shown that post-traumatic growth effectively facilitates the cancer patients to cultivate positive attitude, which is beneficial to the improvement of patients' quality of life [11]. In this study, it was discovered that the total score of post-traumatic growth of patients with head and neck tumors was (64.36±8.44) points, which was at the medium level and close to the score of post-traumatic growth of breast cancer patients reported by Su and Fang [12]. According to a previous study [13], age, nationality, education level, trauma exposure, and the damage degree of trauma events all affect the post-traumatic growth level to some extent. In addition, this study revealed that different payment methods, cancer stages, caregivers, treatment methods and disease duration exert certain effects on the post-traumatic growth score of patients. Based on analysis, the reasons might be as follows: 1) Patients with medical insurance needed to bear lighter economic burden, so they might generate less negative emotions. 2) The lower cancer stage indicated the better prognosis, which increased the patients' confidence in healing. 3) Spouse and children gave more support and care,

which was beneficial to patients treated with many methods and having longer disease duration. 4) Patients experienced relatively severe side effects such as hair loss and digestive tract symptoms related to radiotherapy and chemotherapy, which aggravated the discomfort and negative psychology of patients in the treatment process, and made them lose confidence in the cure of diseases.

During treatment, various influencing factors bring different psychological burdens to patients, resulting in differences in their growth level [14]. Relative to general fatigue, CRF is characterized by rapid onset, high severity, long duration, unpredictability, and failure to be relieved by rest or sleep, which seriously affects patients' self-care ability and quality of life. It was discovered from the results of this study that the total score of CRF in patients with head and neck tumors was (35.51±8.34) points, which displayed a negative association with post-traumatic growth. The direct effect of CRF on post-traumatic growth in the structural equation model was -0.82, suggesting that the higher level of CRF represented the lower post-traumatic growth level of patients, and that CRF is able to stunt post-traumatic growth to some extent.

The research results of Li et al. [15] illustrated that there was a negative correlation between mental resilience and CRF in patients with advanced non-small cell lung cancer, and the higher the level of mental resilience was, the lower the CRF level would be. In the meantime, the two interacted with each other. In other words, mental resilience protected patients' psychological status, which was conducive to improving patients' CRF, and the lower level of patients' CRF could reduce the level of mental resilience. In the present study, a remarkably negative correlation was detected between mental resilience and CRF in patients with head and neck tumors. The multiple regression equation demonstrated that CRF was included in the regression equation as an independent variable affecting the mental resilience of patients. The successful establishment of the equation represented that CRF could effectively predict the mental resilience level of patients with head and neck tumors. The level of mental resilience, a coping mechanism of the body, can also affect the post-traumatic growth level of patients. In the current research, the score of patients' mental resilience was at a medium level, which had a positive correlation with the post-traumatic growth level. Furthermore, the regression equation successfully constructed with mental resilience as an independent variable confirmed that patients with a higher level of mental resilience had a higher growth level after experiencing the traumatic event (head and neck tumors). This might be related to the fact that patients with a higher level of mental resilience can cultivate more positive attitude, which is conducive to correctly dealing with traumatic events in adversity. The research of Ergun et al. [16] also manifested that subjects with a high level of mental resilience could better extricate themselves from traumatic events.

Moreover, it was found from the constructed structural equation model that mental resilience acted as a mediator in the path between CRF and post-traumatic growth of patients with head and neck tumors, and its effect accounted for 30.50% of the total effect, which can predicted the post-traumatic growth level to some extent. It can be inferred that CRF can negatively predict the post-traumatic growth level and positively predict the post-traumatic growth level through mental resilience. Patients with a low level of CRF were able to actively adjust the stress and anxiety caused by CRF, so as to increase their mental resilience. The protective factors in mental resilience helped patients strengthened their ability to break through difficulties and resist pressure in the face of severe traumatic events, thus indirectly increasing their post-traumatic growth level. Hence, understanding the source of patients' burden is beneficial to the enhancement of their mental resilience and the formulation of corresponding nursing measures. This can help them relieve their anxiety and depression, strengthen the enthusiasm of physiological rehabilitation activities and promote their post-traumatic growth.

To sum up, this study proves that the mental resilience of patients with head and neck tumors exerts a partial mediating effect in the path between CRF and post-traumatic growth through the structural equation model of mediating effect. In the clinical intervention, the burden of patients should be relieved as much as possible to help them confront cancer optimistically and actively, improve mental resilience and promote post-traumatic growth.

ACKNOWLEDGEMENTS

Ethical approval. This research was approved by the Ethics Committee of our hospital. All subjects were informed of the relevant rights and risks, voluntarily participated in the research and signed the informed consent.

Consent for publication. Informed consent was obtained from all individual participants included in the study.

Availability of data and material. The datasets used or analysed during the current study are available from the corresponding author on reasonable request.

Funding. None

REFERENCES

[1] Von Wilmowsky, C., Traxdorf, M., Adler, W., Neukam, F.W., Iro, H., Nkenke, E., Kesting, M., Wurm, M. (2019) Survival benefit for patients treated in a certified head and neck tumor center. European Review for Medical and Pharmacological Sciences. 23, 2863-9.

[2] Oeser, A., Gaebel, J., Dietz, A., Wiegand, S., Oeltze-Jafra, S. (2018) Information architecture for a patient-specific dashboard in head and neck tumor boards. International Journal of Computer Assisted Radiology and Surgery. 13(8), 1283-90.

[3] Wolf, M., Da, K.F. (2019) Post-traumatic growth impairment following pediatric distal radius fractures resulting in an ulnar variance: A case report. Der Orthopade. 48(6), 531-5.

[4] Oeki, M., Takase, M. (2019) Coping Strategies for Self-perceived Burden Among Advanced Cancer Patients. Cancer Nurs. 3 (1), e12942.

[5] Catabay, C.J., Stockman, J.K., Campbell, J.C., Tsuyuki, K. (2019) Perceived stress and mental health: The mediating roles of social support and resilience among black women exposed to sexual violence. Journal of Affective Disorders. 259, 143-9.

[6] Abraham, R., Lien, L., Hanssen, I. (2018) Coping, resilience and posttraumatic growth among Eritrean female refugees living in Norwegian asylum reception centres: A qualitative study. International Journal of Social Psychiatry. 64(4), 359-66.

[7] Durbin, A., Nisenbaum, R., Kopp, B., O'Campo, P., Hwang, S.W., Stergiopoulos, V. (2019) Are resilience and perceived stress related to social support and housing stability among homeless adults with mental illness? Health & Social Care in the Community. 27(4), 1053-62.

[8] Yu, X., Zhang, J. (2007) Factor analysis and psychometric evaluation of the Connor-Davidson Resilience Scale (CD-RISC) with Chinese people. Social Behavior and Personality: an International Journal. 35(1), 19-30.

[9] Gebremariam, G.T., Anshabo, A.T., Tigeneh, W., Engidawork, E. (2018) Validation of the amharic version of the brief fatigue inventory for assessment of cancer-related fatigue in ethiopian cancer patients. Journal of Pain and Symptom Management. 56(2), 264-72.

[10] Wang, J., Chen, Y., Wang, Y.B., Liu, X.H. (2011) [Revision of the Posttraumatic Growth Inventory and testing its reliability and validity]. Journal of Nursing Science. 26(14), 26-8.

[11] Brooks, S., Amlôt, R., Rubin, G.J., Greenberg, N. (2020) Psychological resilience and posttraumatic growth in disaster-exposed organisations: overview of the literature. BMJ Military Health. 166(1), 52-6.

[12] Su, Y., Fang, G.Z. (2018) Correlations between posttraumatic growth, body image and sexual adjustment in breast cancer patients. Journal of Nursing Science. 33(19), 72-5.

[13] Carlier, Y., Desmoineaux, P., Lenoir, H., Vidil, A. (2019) Prospective comparative analysis of arthroscopic débridement for primary and posttraumatic elbow osteoarthritis. Orthopaedics & Traumatology: Surgery & Research. 105(8), S217-20.

[14] Cui, C., Wang, K., An, J., Jin, C. (2017) Current status and influencing factors of post-traumatic growth in maintenance hemodialysis. International Journal of Nursing Sciences. 4(4), 362-6.

[15] Li, H.Y., Zhang, J., Lv, M.M., Zhang, J.P. (2019) [Mediating effect of resilience in relationship between self-perceived burden and depression in patients with advanced non-small cell lung cancer]. Chinese Journal of Behavioral Medicine and Brain Science. 28(7), 597-602.

[16] Ergün, G., Gümüş, F., Dikeç, G. (2018) Examining the relationship between traumatic growth and psychological resilience in young adult children of parents with and without a mental disorder. Journal of Clinical Nursing. 27(19-20), 3729-38.

Received: **24.03.2021**
Accepted: **01.05.2021**

CORRESPONDING AUTHOR

Jing Lv
The Second Medical Center & National Clinical research Center for Geriatric Diseases,
Chinese PLA General Hospital,
Beijing 100853 – China

e-mail: 154525125@qq.com

© by PSP Volume 30– No. 09/2021 pages 10712-10717 Fresenius Environmental Bulletin

RESEARCH ON THE ROLE OF TOURISM IN ECONOMIC DEVELOPMENT: BASED ON AN ECOLOGICAL PERSPECTIVE

Xiaofang Yang[1,*], Bo Dai[1], Zhengfa Han[2]

[1]Shangrao Normal University, Shangrao 334001, China
[2]Yong In University, 134 Cheoin-gu, Yongin-si, Gyeonggi-do, 031-332-6479, Korea (17092)

ABSTRACT

Eco-tourism is a special form of conventional tourism, which emphasizes the use of tourism activities to obtain economic benefits on the basis of protecting natural and cultural eco-tourism resources. Now that the tourism industry is developing rapidly, the continuous development and utilization of eco-tourism resources can better promote the development of regional tourism economy. Based on analysis and investigation, this paper establishes a quantitative evaluation index system and evaluation model for ecotourism development, uses analytic hierarchy process to determine the weight of each evaluation index, introduces a coupling coordination degree model, and obtains a quantitative evaluation result. The research results show that the degree of coupling and coordination between ecotourism and economy is maintained between 0-1, and the stability is good. In order to create a better tourism environment, it is necessary to establish a reasonable development goal for the tourism industry, optimize the overall industrial structure, enable the coordinated development of tourism and the economy, and enhance the support of external hardware. At the same time, it is necessary to grasp the internal soft power of development. Strengthen government guidance and macro-control, support and cooperate with the development of tourism.

KEYWORDS:
Tourism, Economic development, Coupling coordination degree, Analytic hierarchy process

INTRODUCTION

According to statistics from the World Trade Organization and the international tourism industry, in recent years, due to the impact of economic development and the relative stability of the international situation, the scale of customers in the tourism industry in my country has continued to expand, and per capita consumption expenditure has also increased year by year, as shown in Table 1. Therefore, in a relatively stable development situation, an opportunity for the development of combining tourism and environmental protection has been given, and China and other countries in the world also regard tourism as the main source of economic income for foreign development [1-4]. At the same time, many countries believe that the rapid development of the tourism industry driven by tourism at this stage can gradually become a new and modern development industry. This industrial structure can effectively reduce the cost of production [5-7]. It only needs to realize the growth of the tourism industry by means of cultural propaganda expenditure. Effective development. For this reason, with the development of multiple angles, the current international tourism industry has gradually become one of the economic territories that various countries are competing for [8-11]. The main factors affecting the development and progress of the world tourism industry are: the current rapid development of the world economy and the relatively stable international political situation; the convenience of international travel and the cancellation of foreign restrictions by various countries; and the gradual integration of various tourism resources and facilities [12-16]. The integration of tourism resources with information equipment and infrastructure; the excavation and development of various characteristic tourist destinations; the sales and promotion of various surrounding tourist materials, etc.

The long-term development of national tourism is inseparable from the strong support of relevant national policies [17-20]. Only national policy constraints can ensure the reasonable development of tourist destinations and ensure that natural and cultural resources will not be excessively consumed. The government can also use propaganda to deepen the protection of tourism development sites, reduce resource waste and resource consumption in tourism culture, and reduce pollution to the natural environment. Government units collect some taxes to further reduce and restrain the waste of tourism resources in the tourism industry.

TABLE 1
Tourism development (2015-2019)

Year	User scale (100 million person-times)	Per capita consumption expenditure (yuan)
2015	36.1	14491.0
2016	40.0	15717.0
2017	44.4	17111.0
2018	50.0	18322.0
2019	55.4	19853.0

MATERIALS AND METHODS

Analytic hierarchy process. The analytic hierarchy process was proposed by Saaty, an American operations researcher and professor at the University of Pittsburgh in the early 1970s. The analytic hierarchy process must first hierarchize the problem to form a multi-level structural model, systematically reduce the objects for decision-making to the lowest level, and then rank the relative advantages and disadvantages relative to the highest level (target).

Model selection. Coupling coordination degree model. The coupling coordination degree model is used to analyze the coordinated development level of things. Coupling degree refers to the interactive influence between two or more systems to achieve a dynamic relationship of coordinated development, which can reflect the degree of mutual dependence and mutual restriction between systems. Coordination degree refers to the degree of benign coupling in the coupling interaction relationship, which can reflect the quality of coordination.

RESULTS AND DISCUSSION

Problems in the tourism industry. The surrounding tourism promotion ability is weak. Tourism is not only an industry within a scope and a city, but for the country, it is also one of the important industries that can promote economic development. Foreign tourists have discovered the beautiful scenery and traditional cultural connotations of tourist destinations. With the attention and deliberate promotion of the government and related units, these distinctive tourism and cultural products have become the core and important resource content of promoting the development of tourism. The emphasis is on the publicity of environmental protection undertaking sites, while ignoring the promotion of tourism in other regions, resulting in concentrated but non-decentralized tourism. This is not only not conducive to the promotion of traditional culture and the promotion of natural scenery, but also speeds up to a certain extent, this has resulted in the consumption of tourism resources in the places where environmental protection was developed, resulting in a lot of waste of tourism resources (Figure 1).



FIGURE 1
Waste of tourism resources.

Unreasonable allocation of tourism resources and environment. Tourism is an important part of my country's economic development. It can use its own advantages to drive the development of various industrial structures and enhance the development speed of other industries. With the gradual improvement of economic development, the resulting problem of unreasonable construction of supporting facilities for the tourism industry has gradually been exposed. Among them, the lack of public transportation facilities and tourist guide publicity are important reasons that restrict the development of the tourism industry. Many hotels and hotels established during the environmental protection period to promote the development of tourism have gradually been put aside after environmental protection. The large economic income gap has brought a certain impact on the accompanying service industry of the tourism industry.

Low level of tourism service. The tourism industry itself is a systematic service industry. With the deepening of environmental protection, how to increase the intensive management below the tourism industry has become the main content of the development of the tourism industry. However, it is precisely the lack of a certain service management method that causes the level of service under the promotion of environmental protection to continue to be low. At this stage, my country is only systematically promoting environmental protection related content in the process of carrying out environmental protection publicity. The publicity and management of other extended industries under the background of environmental protection is relatively lacking, resulting in relatively weak tourism service management capabilities and service quality. relatively low. Due to the rapid increase in the number of tourists, the service personnel and service equipment cannot meet the overloaded number of tourists, and finally the quality of tourism services is relatively low.

Quantitative evaluation results and the Coordinated Development of Tourism and Economy. From the quantitative evaluation, it is known that from the evaluation results (the full score of all items is 5), the ecotourism environmental value is higher, with a score of 4.11, indicating that the ecological environment of the tourist area is good: the natural environment and ecosystem are better, and the tourism value is higher (Figure 2). It can be used as the basis for future tourism development; while the basic conditions for social development are in a general state, with a score of 3.55, indicating that if the tourism industry is to be further developed, corresponding measures must be taken in terms of transportation infrastructure construction, population and service facilities, and regional cultural background. However, tourism development is still in its infancy, with an evaluation score of only 2.58. The main reason is that the infrastructure is relatively backward, but tourism development still has a certain potential for development. In general, the overall score of eco-tourism development evaluation is 3.62, indicating that the eco-tourism industry is at a development stage above the middle level. To achieve greater development in the future, it needs to be further improved in terms of basic conditions for social and economic development and tourism infrastructure (Figure 3).

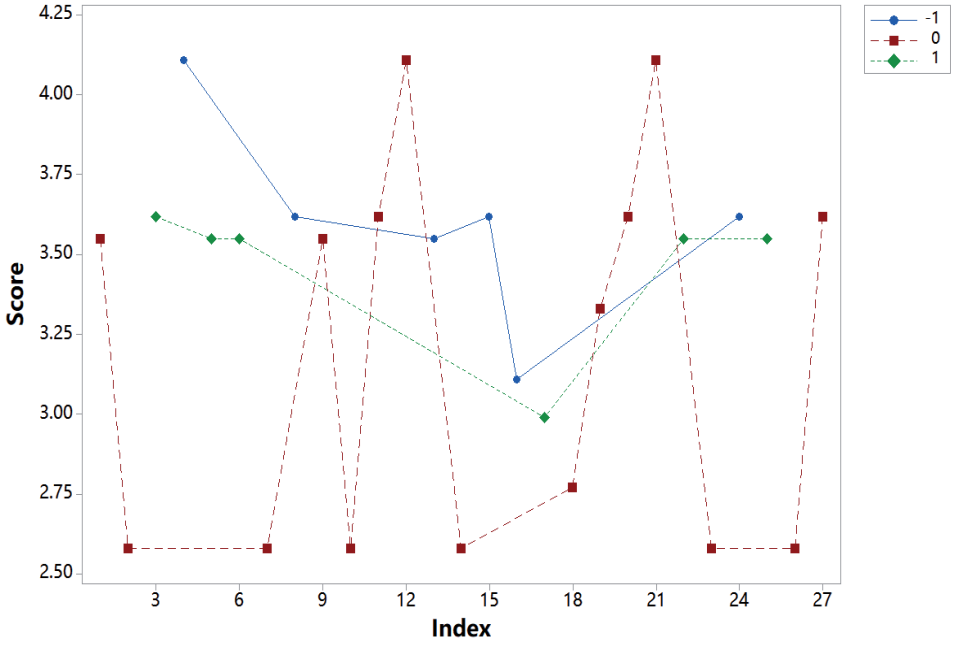


FIGURE 2
Time Series Plot of Score.

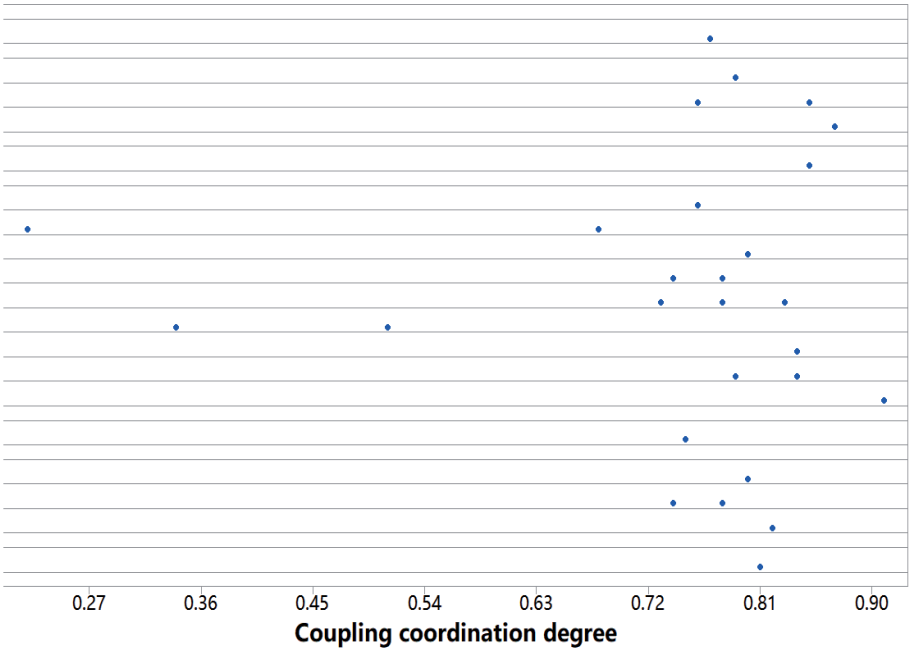


FIGURE 3
Dotplot of Coupling coordination degree.

Countermeasures to promote the sustainable development of tourism. Strengthen the promotion of surrounding tourism. Enhancing the promotion of surrounding tourism can not only promote tourism development, but also promote the rapid development of tourism in other regions during the environmental protection period. One is to use the network platform to promote environmental protection culture and tourism at the same time to promote the local customs and cultural characteristics of the surrounding areas. With the continuous penetration of informatization methods and the continuous promotion of multiple media methods, while deepening environmental protection and cultural tourism, a variety of new media methods can also be used to integrate my country's traditional cultural characteristics and cultural connotations from other regions on the network information platform. Make promotion to effectively promote the development of tourism in other regions of our country. The second is to establish tourism and cultural facilities related to environmental protection in surrounding areas. Most regions in my country have their own unique cultural backgrounds and tourism characteristics. In order to promote the spirit of environmental protection in our country, let more people know about our country's environmental protection, enhance the promotion of environmental protection, and improve the tourism industry in the surrounding areas For development, it is possible to establish tourism sites related to environmental protection in the surrounding areas of the development area to increase the influence of environmental protection while increasing the promotion of surrounding tourism. The third is to plan an infectious surrounding tourism publicity plan. A tourism promotion plan with distinctive characteristics can effectively attract more tourists to participate in the tourism activities around the environmental protection development area. By understanding the surrounding tourist attractions, it also deepens the understanding of the environmental protection development area. Give full play to the role of surrounding tourism and realize the effective promotion of surrounding tourism.

Optimize the allocation of tourism resources and environment. The optimal allocation of tourism resources can effectively enhance the development of the tourism industry and improve the quality of the tourism industry. In order to deepen the development of China's tourism industry under the promotion of environmental protection, one is to speed up the construction of tourism resources and the environment and improve the quality of tourism facilities. In order to better realize the construction of tourism resources and the environment, and give full play to the advantages of tourism, in the process of implementing tourism facilities, we must not only focus on the construction of quantity and speed. We must pay more attention to quality under the premise of ensuring the speed. The second is to consider the quantity management of tourism resource construction during the environmental protection period in light of actual conditions. At this stage, my country's tourism industry is developing rapidly. On this basis, many basic facilities are gradually improved, and many characteris-

tic tourist areas have set up a wide range of tourist hotel facilities. The construction of these facilities can fully meet the current tourism needs, and can meet the accommodation needs even during the environmental protection period. Therefore, the construction of tourism resources and environmental facilities based on actual time is very important. The third is to accelerate the planning and construction of public transportation infrastructure. Under the influence of environmental protection, the application of public transportation is much higher than the use of private transportation. In many tourist areas in my country, the construction of public transportation facilities is not yet complete, which has led to a relatively low evaluation of travel quality by many travelers. Speeding up the construction of public transportation in tourist areas is not only conducive to the development of environmental protection, but also enhances the development of tourism culture in the area.

Improve the level of tourism service management. High-quality services allow many tourists to feel the enthusiasm and quality of work of our people while experiencing the culture of environmental protection. As a service industry, it is necessary not only to deepen the management of tourism services during the environmental protection period, but also to optimize service concepts and enhance service quality in daily life. The state should add service windows during the environmental protection period. The new service windows must not only meet the needs of tourists from many countries, but also help them solve emergencies that may arise. Due to the large difference between foreign communication methods and my country's domestic communication methods, different simultaneous translation mechanisms must be provided in the additional service windows to ensure the different needs of tourists from different countries. Promote the consumption of environmental protection services in the form of discount vouchers. During the travel period, many people face the phenomenon of not receiving attentive services. Therefore, service personnel can distribute certain coupons to ease the emotions of tourists.

CONCLUSIONS

This paper establishes a quantitative evaluation index system and evaluation model for ecotourism development, uses analytic hierarchy process to determine the weight of each evaluation index, introduces a coupling coordination degree model, and obtains a quantitative evaluation result. The research results show that the degree of coupling and coordination between ecotourism and economy is maintained between 0-1, and the stability is good. In order to create a better tourism environment, it is necessary to establish a reasonable development goal for the tourism industry, optimize the overall industrial structure, enable the coordinated development of tourism and the economy, and enhance the support of external hardware. At the same time, it is necessary to grasp the internal soft power of development. Strengthen government guidance and macro-control, support and cooperate with the development of tourism.

REFERENCES

[1] Yao, H.Q., Liu, B. (2020) Study on the problems of rural tourism eco-environment and its countermeasures. Fresen. Environ. Bull. 29, 1489-1492.

[2] Li, L., Hong, X.F., Wang, J. (2018) Spatial effects of technology innovation on energy-related carbon emissions: a spatial panel approach. Fresen Environ Bull. 27(12), 8053-8061.

[3] Wang, W. (2019) Analysis of three relations in rural tourism development of China Guizhou under the strategic background of rural vitalization. Fresen. Environ. Bull. 28, 2733-2738.

[4] Dong, Q.Y., Futawatari, T. (2015) A review of the progress in China's renewable energy generation, and its links with energy conservation, environmental degradation and economic growth. Fresen. Environ. Bull. 24, 405-411.

[5] Gultekin, U. (2019) Renewable electricity generation for sustainable development and environmental management in Turkey. Fresen. Environ. Bull. 28, 8171-8174.

[6] Kiper, T., Uzun, O., Topal, T.U. (2016) A method approach for identifying thematic footpaths in ecotourism: kiyikoy pabucdere and kazandere basins. Fresen. Environ. Bull. 25, 6139-6150.

[7] Wang, Q.Y., Li, M., Yang, Y.L. (2019) Study on the issues of rural tourism eco-environment and governance strategy. Fresen. Environ. Bull. 28, 10083-10088.

[8] Dekhili, S., Achabou, M.A. (2015) The perception of ecotourism. Semantic profusion and tourists' expectations. Rimhe Revue Interdisciplinaire Management Homme & Entreprise. 19(5), 3-20.

[9] Sayyed, M.R.G., Mansoori, M.S., Jaybhaye, R.G. (2013) SWOT analysis of Tandooreh National Park (NE Iran) for sustainable ecotourism. Proc. Int. Aca. Ecol. Environ. Sci. 3(4), 296-305.

[10] Pasape, L., Anderson, W., Lindi, G. (2015) Assessment of indicators of sustainable ecotourism in Tanzania. Anatolia. 26, 73-84.

[11] Bălteanu, A.D., Dincă, A.I., Surugiu, C., Dumitraşcu, M., Micu, D., Felciuc, M. (2008) Ecotourism and Environmental Change in the Romanian Carpathians. Global Environmental Research. 12(2008), 161-172.
[12] Bhattacharya, A.K., Saksena, V., Banerjee, S. (2006) Environmental auditing in ecotourism: a study on visitors' management in Van Vihar National Park, Bhopal, M.P. (India). Indian Forester. 132(2), 1-3.
[13] Machado, Á.L.D.M., Conto, S.M.D. (2013) Environmental practices to minimize environmental impacts of ecotourism: information managers of travel agencies of Rio Grande do Sul. Cultur Revista De Cultura E Turismo. 2013, 31-46.
[14] Dong, H.M. (2010) Study on sustainable development of ecotourism in the Northern Piedmont in the Qinling Mountains. Journal of Sustainable Development. 3(1), 104-108.
[15] Li, Y.H., Xiang, B. (2014) Research Progress in the Ecotourism Environmental Carrying Capacity. Advanced Materials Research. 869-870, 781-785.
[16] Pao, H.T., Fu, H.C., Tseng, C.L. (2012) Forecasting of CO2 emissions, energy consumption and economic growth in China using an improved grey model. Energy. 40(1), 400-409.
[17] Tang, X., McLellan, B.C., Snowden, S., Zhang, B., Hook, M. (2015) Dilemmas for China: Energy, economy and environment. Sustainability. 7, 5508-5520.
[18] Xu, Y.P., Wang, M., Qin, M., Shi, H.X., Sui, B.W., Jia, X.Z., Lu, D.L. (2018) Study of the relationship between economic growth and environmental quality with the Kuznets curve in Guangxi, China. Fresen. Environ. Bull. 27, 2818-2828.
[19] Butler, R.W. (1991) Tourism, environment, and sustainable development. Environmental Conservation. 18, 201-209.
[20] Cobbinah, P.B. (2015) Contextualizing the meaning of ecotourism. Tour. Manag. Perspect. 16, 179-189.

Received: **25.03.2021**
Accepted: **28.04.2021**

CORRESPONDING AUTHOR

Xiaofang Yang
Shangrao Normal University
Shangrao 334001 – China

e-mail: yangxiaofang889@163.com

© by PSP Volume 30– No. 09/2021 pages 10718-10727 Fresenius Environmental Bulletin

ANALYSIS OF THE IMPACT OF THE ECOLOGICAL ENVIRONMENT ON THE RAILWAY CONSTRUCTION BASED ON ANALYTIC HIERARCHY PROCESS (AHP) AND PROBABILITY STATISTICS

Haixia Du*, Zhenzhen Li

School of Mathematics and Statistics, Zhengzhou Normal University, Zhengzhou Henan 450000, China

ABSTRACT

Eco-environmental impact assessment is a process of comprehensively analysing the characteristics of the ecological environment and development and construction activities and their interaction. This article summarizes the current situation of the ecological environmental impact assessment of railway construction projects, points out its unreasonable points, and proposes new methods for assessment. At the same time, it studies the formulation principles of the comprehensive evaluation index system of railway ecological environmental impact, establishes reasonable evaluation indicators, and aims to explore a method that can quantify the ecological impact evaluation which is highly operable and comparable. We use the improved analytic hierarchy process (AHP) to determine the weights, reducing the error that may be caused by artificially determining the weights. The experiment designed a sample combination consisting of n samples, and there is a measured index matrix X (m×n), and passed c Level standard evaluation suppresses m indicators. Using the constructed probability and statistics method, the pattern recognition model and the probability and statistics method, we input of the integrated unit system as l (t × c) fuzzy matrix, and determine the corresponding grade standard. Theevaluation value is 0.53, and the evaluation grade is 3. Judging from the current research situation of some scholars, there are more qualitative evaluations on ecological impacts, but less quantitative evaluations. Considering that an index system should be established based on the characteristics of railway construction itself, and railway projects should be divided into subgrade engineering, bridge engineering, tunnel engineering, etc., each project should be refined into each process, and the characteristics of each process should be analyzed to extract factors affecting the environment. We establish an indicator system, which includes (1) water pollution control, (2) noise pollution control, (3) air pollution control, (4) solid waste control, (5) damage to the ecological environment, (6) the health of construction workers affects. Based on the research data of ecological environmental impact assessment of construction projects at home and abroad, this paper analyzes the relationship between railway construction and the ecological environment in detail in accordance with the characteristics of the railway ecological environmental impact, and finds out the possible negative impacts on the ecological environment. The jury is composed of 10 experts. According to the specific situation and relevant information, combined with various indicators, the judgement set P = [A, B, C, D, E] is judged, indicating that the magnitude of the impact is on the environment. The review weighting coefficient matrix is F. At the same time, the comprehensive evaluation evaluates the railway ecological project, making the ecological environment impact assessment project more scientific and reasonable. The results show that this method is also suitable for solving other similar problems.

KEYWORDS:
AHP, probability and statistics method, railway construction, ecological environment

INTRODUCTION

With the continuous expansion of the scope and scale of economic activities, the adverse environmental impacts caused by railway construction and development, industrial development, and natural resource development and utilization have become more and more prominent [1]. Environmental impact assessment, also known as environmental impact quality prediction assessment, refers to the impact on surrounding environmental areas before major project construction, planning, urban construction and development. Regional planning and other activities that may affect the environment are carried out in a certain area for the investigation, prediction and evaluation [2]. Too much attention is paid to the speed and quantity of development and environmental management during the construction phase is neglected, causing excessive damage to the ecological environment and other issues [3]. The mountainous terrain is complex and the ecological environment is

fragile. Due to the high linear standard of the mountain railway, the mountain body will inevitably be filled and excavated, which will lead to a series of ecological environmental problems such as the destruction of native vegetation and animal habitats, soil erosion, and local environmental degradation. The environmental damage and pollution caused by railway projects are mainly manifested as non-polluting ecological environmental impacts, generally vegetation damage, local landform damage, soil erosion, natural resource impacts, etc. [4]. High filling and deep excavation in the construction of railway projects directly destroys the surface vegetation, changes the original appearance, and piles up a large amount of spoil, which will cause a series of environmental problems, such as soil erosion, landslides, debris flows, deterioration of local microclimate and destruction of biological chains, etc. This leads to serious ecological degradation after the construction of the railway project [5].

At present, the evaluation of ecological environment is carried out by a combination of qualitative description and quantitative analysis [6]. Developed countries such as the United States, Japan, UK, France, Germany, etc., after years of hard analysis and research, have come to the relevant norms and standards for ensuring natural economic benefits in the various stages of railway survey, design, and construction, as well as on the use and protection of natural resources, plants and various natural characteristics, protection of historical sites and landscapes, etc. [7]. The country's environmental assessment began with the survey and evaluation of urban environmental pollution in the 1970s [8]. The comprehensive evaluation of the impact on the ecological environment is a multi-level, multi-objective, multi-task system engineering, which increases the difficulty of the work [9]. Chen et al. [10] used the comprehensive evaluation index method to evaluate the ecological environmental impact of expressways. Liang et al. [11] used the clustering method of probability statistics to perform cluster analysis on different counties and cities, and evaluate the ecological environment of the reservoir area. Peng et al. [12] proposed a semi-quantitative matrix to express the prediction method of the impact of railway construction projects on the ecological environment. The Netherlands, Germany, the UK, France, and other countries not only require the basic design standards and principles in environmental landscape design, but also require that the proportion of ecological investment in the total construction investment should be specified in accordance with national conditions. Ecological investment mainly includes water, sound, air, and other environmental factors investment. Ren [13] discussed the prediction and evaluation method of the impact of railway construction projects on the ecological environment. Due to the obvious temporal and spatial differences of the ecological environment and lack of a unified quantitative standard, its comprehensive evaluation is still in the initial stage [14].

This paper mainly focuses on the following aspects: (1) Analyze the factors affecting the ecology of railway construction projects. (2) Establish a mathematical comprehensive evaluation model of probability statistical methods suitable for railway ecological environmental impact evaluation. (3) Use a combination of qualitative and quantitative methods to make a comprehensive impact assessment of railway construction projects. (4) Take corresponding measures to prevent and control the problems reflected in the evaluation, to achieve the purpose of ecological protection. The basic project will use new methods and technical indicators to analyze and study the impact of the railways' ecological effects, and comprehensively apply the comprehensive evaluation of the analytic hierarchy process and the probability and statistics method to the railway ecological environment impact assessment, to be able to contribute to the ecological construction of the railway. By comparing and learning several common weight determination methods, this article uses a combination of subjective and objective weights for calculation to make the results more accurate. The subjective weight uses the improved AHP analysis method, which eliminates the process of consistency checking in the traditional AHP analysis method, and the calculation is simpler, and the result is more reasonable. The objective weight uses the gray relational analysis method, which is more objective. After studying and comparing several evaluation methods, the article applies the gray theory, which has the characteristics of solving the problem of poor information and small samples. Finally, the gray clustering method is used to establish a comprehensive evaluation model of railway green construction environmental protection.

MATERIALS AND METHODS

Based on the current status of railway green construction at home and abroad and environmental protection evaluation indicators and evaluation methods, this paper conducts the following research on the impact of railways on the environment during the construction phase: We put forward the concept of railway green construction, and learn about environmental bearing ability theory, sustainable development theory, comparative analysis of the advantages and disadvantages of several weight determination methods and evaluation models, and determine the comprehensive evaluation method used in this article. According to the extracted environmental factors, a qualitative and quantitative evaluation index system is constructed, and the rating standards and evaluation levels of the indicators are determined according to the current norms and standards.

Combining with the evaluation index system constructed in this paper, a comprehensive evaluation model of railway green construction environmental protection based on gray theory is established. The improved analytic hierarchy process and grey relational analysis method are used to determine the combination weight, and the grey clustering method is used for comprehensive evaluation. In order to verify the scientificity and rationality of the comprehensive evaluation model proposed in this article, five bid sections of a certain section of the high-speed rail are selected for example verification, and conclusions are drawn, which can lay the foundation for the next step of research.

(1) AHP and the theoretical basis of probability and statistics. AHP was proposed by the American mathematician T. L Saaty in 1977. It is a combination of qualitative and quantitative decision-making methods [15]. The steps to solve the problem can be summarized into the following four steps: Step 1: Analyze the relationship between the factors in the system and establish the hierarchical structure of the system; Step 2: Perform pairwise comparisons, and construct the judgment matrix A for pairwise comparison according to Table 1. Step 3: Calculate the relative weight of the compared element to the standard from the judgment matrix; and check the consistency of the judgment matrix. [16] Let w be the sorting weight vector of the n-order matrix, when A is the consistency judgment matrix:

$$w = (w1, w2, , wn)^T \tag{1}$$

We multiply the above formula with w= (w1, w2,…,w-n) T to the right, and get A-w = n-w, which shows that w is the eigenvector of A and the eigenvalue is n. After normalizing the feature vector, the required weight vector can be obtained. Therefore, the calculation of weights can be attributed to the problem of calculating the eigenvalues and eigenvectors of the judgment matrix. When comparing complex things and various factors in pairs, it is impossible to achieve complete agreement, which will inevitably include a certain degree of inconsistency, and lead to deviations in eigenvalues and eigenvectors. Therefore, the consistency check of the judgment matrix should be carried out. We define its inconsistency quantity index CI as:

$$CI = (\max[a,b] - k)/(k-1) \tag{2}$$

$$\sum_{i=1}^{k}\sum_{j=i+1}^{k-1} w_{ij} = w^* \tag{3}$$

CR is the consistency ratio, including two sets (i.e., factor set a, evaluation set b) and k, i,j = 1, when w-i-j ≤ 0.1, the judgment matrix has satisfactory consistency, otherwise it does not have satisfactory consistency, and certain corrections are needed. Step 4: Calculate the total ranking weight of each level to the system and perform the ranking. Finally, get the total ranking of each plan for the total goal, that is, get the weight vector. If the upper level A contains m factors A1, A2,..., Am, the total ranking weights of the levels are al, a2,..., am, and the next level B contains n factors B1, B2,..., Bn. For the factor A-j, the weights of the single rank order are b1, b2,..., bn, and the total rank weight of the B level is given by the formula. It can be seen that the traditional analytic hierarchy process is the method of applying the feature vector to find the corresponding feature vector and obtain the weight vector of the element of this layer relative to an element of the previous layer. Then, according to the principle of hierarchical synthesis, the weight vector of each layer element to the overall goal is calculated. But when the judgment matrix does not satisfy the consistency test, the traditional EM solution method cannot answer the question of which item of the comparison matrix is the key to its inconsistency, and it is difficult to correct it.

$$A = \begin{bmatrix} w1 \\ w2 \\ wn \end{bmatrix} \begin{bmatrix} 1/w1 & 1/w2 & \ldots & 1/wn \end{bmatrix} \tag{4}$$

The linear programming method given in this paper is a two-stage solution method. The main purpose of the first stage is to find the consistency constraint range, and then use the obtained range to find the weight vector in the second stage. First, we define i-j as the error value of i, satisfying x(i)-x(j) = u. If the judgment matrix A is a consistency matrix, then i-j = w(i,j). Our goal is to construct a consistent comparison matrix as much as possible, that is, for all i and j, ln i tends to zero. y(i,j) = w, ln y = u. The linear programming model of the first stage is as follows:

$$\begin{cases} x(i) - x(j) - y(i,j) = \log u(i,j) \\ w(i,j) > u(i,j) > y(i,j), i < j \end{cases} \tag{5}$$

Taking natural logarithms on both sides of equation (2) can get constraint equation (4), constraint equation (5) can get the larger of y-i-j and y-j-i, that is, get all the overestimated elements and their overestimated values. When a-i-j>1,the i factor is more important than the r factor, that is, w-i>w-j, the constraint condition formula (6) can be obtained. For all U, there is r-k>a-j-k and there is q so that y(k)>a-j-q, showing that the n factor is more important than the U' factor, that is, w-i>w-j, the constraint equation (7) can be obtained. Therefore, when the judgment matrix is inconsistent, the item that affects the consistency can be found in the solution process and corrected.

$$U = w^* r, r = [r1, r2, ..., rk] \tag{6}$$

$$U' = \int_{k=1}^{n} u^* y(k) / \int_{k=1}^{n-1} y(k) \tag{7}$$

The linear programming model in the first stage must have an optimal solution V. V is the optimal consistency target to be found, which defines a consistency constraint range for the linear programming

in the next step. Our goal is not only to find the optimal solution V, a11 is the number of evaluation factors, and a-n-n is the number of evaluation set elements., but also to make every deviation as small as possible.

$$V = \begin{bmatrix} a11 & a12 & a13 \\ a21 & a22 & a23 \\ a31 & a32 & ann \end{bmatrix} \quad (8)$$

$$p(k) = \max(u / m(k-1), u / m) \quad (9)$$

Equation (10) can ensure that only the solution that satisfies the optimal value p(k) is an effective solution, and other conditions are the same as before. The decision variables obtained by the above model need to be converted into u/m weight vectors. Then we normalize the sum to (k-1).

(2) Variables need to be converted to weights. Due to the shortcomings in the statistical methods and traditional methods, it is necessary to adopt new rating methods to evaluate ecological projects [16]. In the daily comprehensive evaluation of the ecological environmental impact of railway construction projects, generally based on the characteristics of the railway, a combination of qualitative and quantitative methods is adopted to evaluate key projects and propose corresponding ecological environmental protection measures [17]. The evaluation results are also quite consistent. In practice, there are a large number of probability and statistical methods, and there are many factors that are difficult to determine the boundary and difficult to quantify, and the evaluation results may be distorted [18].The experience and knowledge of the environmental assessment staff determine the accuracy and rationality of the ecological environment impact prediction. In the comprehensive evaluation, the weight is very important, and it reflects the occupancy of each influencing factor in the comprehensive decision-making process [19]. Therefore, in order to improve the rational component of the weight determination and obtain more realistic evaluation results, a new method can be used for model construction. The model algorithm flow is shown in Figure 1.

As a qualitative and quantitative decision-making tool, AHP has been widely used. If a certain judgment matrix does not meet the consistency, the calculated weight does not meet the decision-making requirements, and certain corrections are needed [20]. This paper proposes two new methods of consistency correction based on the convex combination of the disturbance deviation matrix, named the convex combination correction method. The research content of the new method of judgment matrix testing can be applied to the risk assessment of the impact of railway construction on the ecological environment, and then the relationship between the disturbance matrix and the inconsistency of the judgment matrix is studied. Two types of convexity based on the disturbance deviation matrix are proposed. The elements to be corrected are determined by determining the element with the largest disturbance in the disturbance matrix and the column vector with the smallest cosine value between the vectors. The new method is verified by examples and compared with the traditional correction method, and the results are better. The effect, the specific model framework is shown in Figure 2.

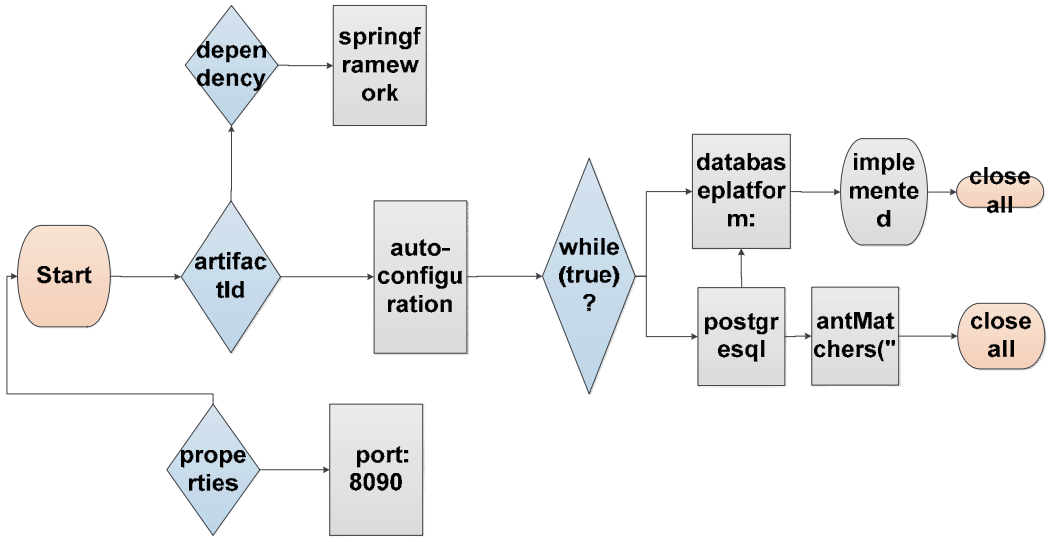


FIGURE 1
Environment model algorithm based on AHP and probability statistics.

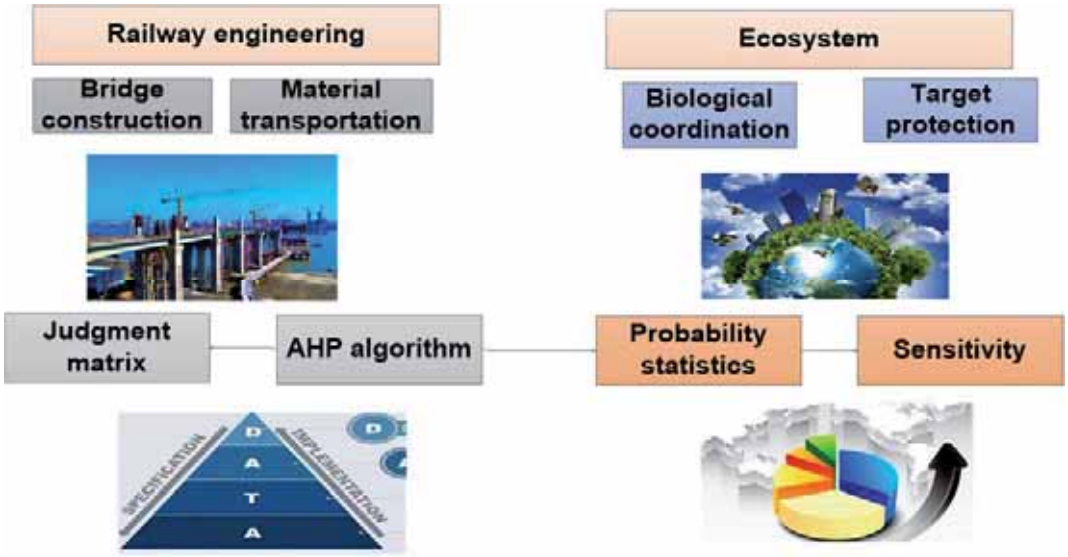


FIGURE 2
A model framework for the impact of railway construction on the ecological environment based on AHP and probability statistics.

TABLE 1
Probability and statistics method parameter evaluation

Number of indicators	Evaluation factor	Numerical value	Reference	Result value
Railway location	latitude Longitude	12.3	10	11.6
ecosystem	pollution index	29	34	25
Regional Humanities	Management Index	87	79	82
Construction cost	Input costs	33.1%	24.3%	35.3%

(3) Probability and statistics method parameter optimization. In the AHP problem, the consistency of the judgment matrix determines the rationality and scientificity of the decision result. Usually, the proposed average random consistency index is used for testing. However, the method is only suitable for situations with fewer decision-making attributes. The reason is that the method only gives the critical value of the judgment matrix within the 15th order. In practical applications, we found that in a multi-factor and big data environment, the reliability of the method has certain defects, and it is not suitable to be used. In response to this defect, we expressed the judgment matrix as the product of the consistency matrix and the disturbance matrix. Through the study of the relationship between the two, we proposed a new consistency test method based on probability statistics and hypothesis testing. The specific parameter evaluation method is shown as Table 1.

First, the improved Analytic Hierarchy Process (AHP) is used to determine the weights. AHP combines quantitative and qualitative methods to express and process people's subjective judgments in a quantitative form, to minimize the abuses caused by personal subjective assumptions and make the evaluation results more reliable. Then, the multi-layer complex system is divided into a basic unit system and a comprehensive unit system. The basic unit system refers to a number of basic factors as the input of the unit system. We usethe probability and statistics method to evaluate the pattern recognition theory model.tThe comprehensive unit system refers to the unit system whose input is composed of the output of several basic unit systems, and the linear weighted average operators are used. It can be evaluated reasonably and accurately through the comprehensive evaluation model of probability and statistics. The specific data results are shown in Figure 3.

According to the central limit theorem of probability theory, if a random variable is superimposed by a large number of small, independent random factors, then this variable can be considered to obey a normal distribution. Since the establishment of the judgment matrix is random, the judgment matrix can be regarded as a certain random disturbance from the consistency matrix. According to the definition of the Z product, the disturbance element can be known, which can be regarded as being randomly and independently given within a certain range. According to the theorem, when the element in the disturbance moment matrix is close to 1, the consistency requirement is met, and according to the subjective consistency in people's decision-making process, the perturbation element can be made to obey a certain mean value of normal distribution.

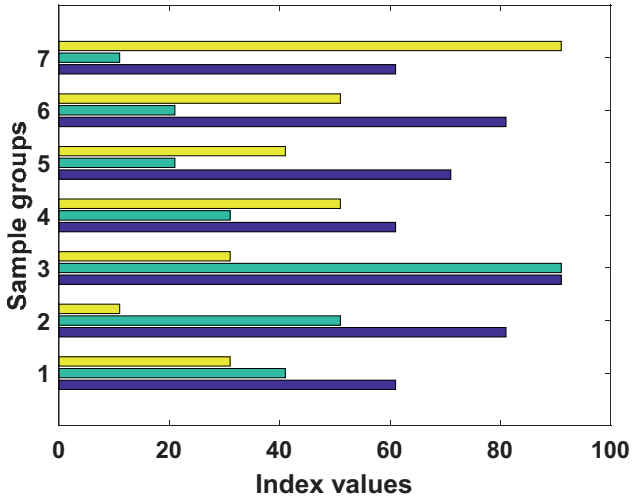


FIGURE 3
Indicator distribution of environmental sample group.

TABLE 2
Characteristic value of evaluation index in railway construction stage

Influencing factors	Material transportation	Eigenvalues S1	Eigenvalues S2	Eigenvalues S3
Construction workers	Regional regeneration	0.66	0.42	0.76
Construction workers	Biological resources	0.31	0.51	0.52
Material transportation	Environmental awareness	0.27	0.24	0.39

RESULTS

(1) Evaluation index design for railway construction stage. This paper proposes a comprehensive assessment of environmental quality based on variable weights and probability statistics. First, according to the requirements of national standards or internationally recognized definitions, the indicators of environmental quality, such as pollution index, emission quantity, vegetation coverage, and ecological resources, are graded. This paper divides the specified scope of each indicator into 10 grades according to the national standard or internationally recognized definition. Table 2 shows the distribution of eigenvalues of evaluation indexes during railway construction. Since these 10 levels are all qualified environments, during the assessment process, if the out-of-range is very small, the excess part can be regarded as the 11th level. For the frequency deviation, the national standard stipulates that the absolute value of the frequency deviation under normal conditions shall not exceed 2%, and the span is 0.02 divided into 10 levels, and the part exceeding 0.2% is regarded as the 11th level.

We use the method of probability statistics to obtain the probability pk at each level in the evaluation time period, and calculate the probability of each indicator at each level to obtain a matrix R(n×m), where n represents the number of environmental quality indicators considered, m indicates that each indicator is divided into m levels. If a 10-level system is adopted for the limit range in the quantification of the sub-item environmental quality indicators, the evaluation of the normalized environmental quality index will also adopt the 10-level system, and the cases exceeding the 10 levels will be evaluated as unqualified to maintain the consistency of the classification.

(2) AHP combination weight calculation. Using the improved analytic hierarchy process, the weight vector w=[0.303 0.061 0.303 0.061 0.152 0.061 0.061] can be derived. It can be seen from Table 2 that w1=w3, which is reasonable because a13=1. However, it can be seen from the formula that w2=w4=w6=w7 is unreasonable. It can be judged that the main source of inconsistency is related to elements 2, 4, 6, and 7, and then carefully observe the formula, a24=1, a46=1/ 2. A67=1/2, indicating that the order of importance from strong to weak is: 7,6,2, but a26=4, a47=2, indicating that 6,7 is more important than 2,4, which is obviously unreasonable. We multiply R and the weight vector A of each index obtained by the improved analytic hierarchy process to obtain the matrix V, and apply the weighted aver

TABLE 3
Measurement of the environmental impact index of railway construction

Quantification method	Index distribution	Index 1	Index 2	Index 3	Index 4
Average topography	Mineral quality	0.03	0.023	0.01	0.015
PM index	Vegetation coverage	0.7	0.65	0.4	0.3
Scoring by experts	Location index	0.5	0.8	0.6	0.44
Output ratio	Technology accounted for	0.4	0.32	0.48	0.6

age method to the matrix V to obtain the environmental quality assessment result V'. The specific distribution is shown in Figure 4.

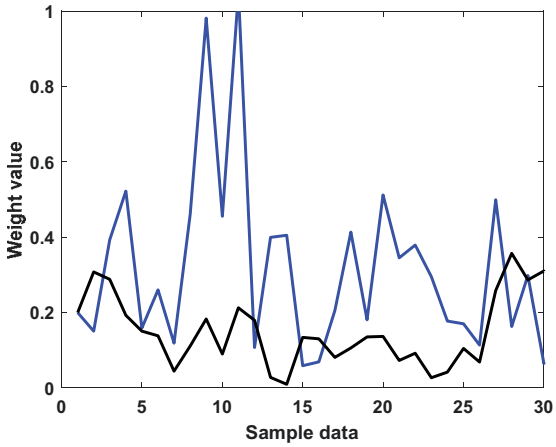


FIGURE 4
Fitting of environmental sample weights based on probability statistics.

According to the specified C-level standard value, the basic unit system is evaluated by the probability and statistics method to identify the model, and the relative membership vector of sample j to each level can be obtained, and the evaluation results of the basic unit system after considering the standards of all levels. The pattern recognition model of probability and statistics is used to discuss the basic unit system respectively, and the relative membership degree vectors of the 4 influencing factors on the 4 standard levels are obtained. The specific values are shown in Table 3.

(3) Environmental model simulation and analysis. A certain railway passes through 8 stations (7 intermediate stations and 1 overpass station). There are 81 bridges and 60.5 tunnels. The ratio of bridges to tunnels is as high as 91.6%. The total length of the tunnel is 231.7 kilometers, and the total length of the bridge is 95.3 kilometers. The total amount of spoil is 35 million cubic meters, which is equivalent to length, 1000 meters in width and 40 meters in height. If these spoils are not properly and effectively disposed, it will cause soil erosion and damage to the surrounding ecological environment. A total of 6542 mu of cultivated land and 688 mu of forest land were requisitioned for the main line. Because the line passes through the collapsible loss area and has frequent activities along the seismic zone, the intensity is high, which brings great difficulties to construction and environmental protection. The following applies the comprehensive evaluation method of multi-level and multi-objective complex system probability statisticsto evaluate the suitability of its ecological part of the environmental impact assessment. The improved AHP method determines the index weights. There are many complex factors in the ecological evaluation of new railway projects, such as sensitive areas, land use, protective measures, construction personnel and other factors that are interrelated, affect each other, and restrict each other, which can usually be based on the needs of the research problem. According to the requirements of AHP, a three-layer hierarchical structure is established, which is composed of target layer A, constraint factor B and sub-restraint factor C. The specific error distribution is shown in Figure 5.

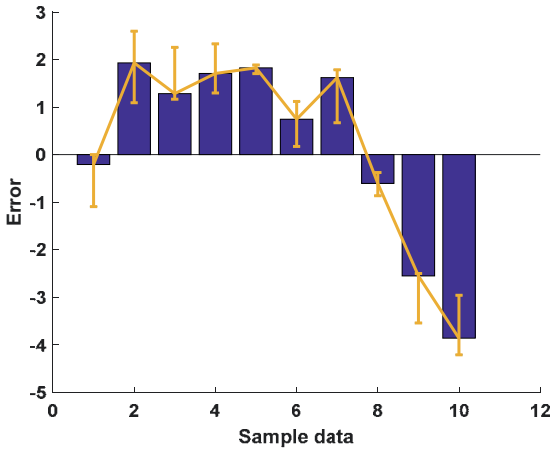


FIGURE 5
Error distribution of environmental sample data.

BLTJ-8 is the longest roadbed construction mileage among the 12 bidding sections, and the environmental protection evaluation is biased towards water pollution control, solid waste pollution control

and the impact on the ecological environment. BLTJ-6 has the longest bridge construction mileage, and the environmental protection evaluation focuses on noise pollution control, water pollution control and air pollution control. BLTJ-2 has the longest tunnel construction mileage, and the environmental protection evaluation focuses on noise pollution control, the impact on the ecological environment and the health impact on the constructors. BLTJ-3 and BLTJ-9 are the relatively long total mileage among the 12 bids, and comprehensive evaluation of all aspects of environmental protection is carried out. The numerical value of the green construction environmental protection evaluation index during the construction of the five tender sections was counted. Due to the complexity of the construction process and the diversity of the construction situation, it is difficult to collect data. Some of the data are measured data, and some of the data are scored and estimated by experts. The suitability of the evaluation of the ecological environmental impact of railway construction is a concept of probability statistical methods with clear connotation but unclear extension. Multi-objective probability statistical method pattern recognition model can be used to evaluate the basic unit system. The resulting model evaluation is shown in Figure 6. We use the following relative membership degree formula to change the matrices X(m ×n), Y(m ×c) into the corresponding measured indicators, the relative membership matrix R(m ×n) and the standard relative membership matrix S (m ×c) can be derived .

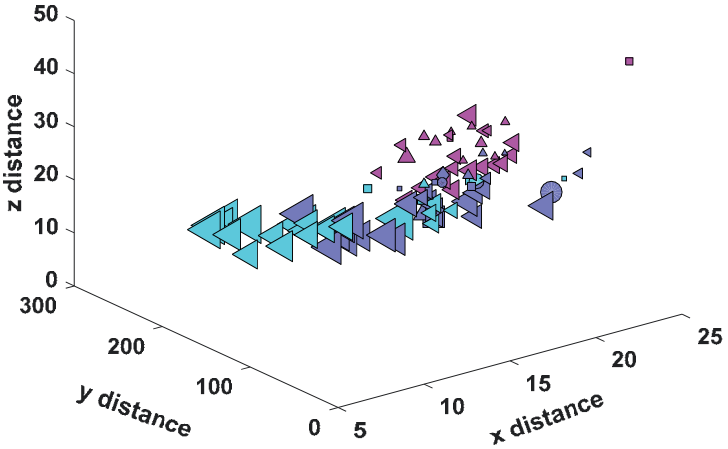


FIGURE 6
Environmental model spatial distribution based on AHP and probability statistics.

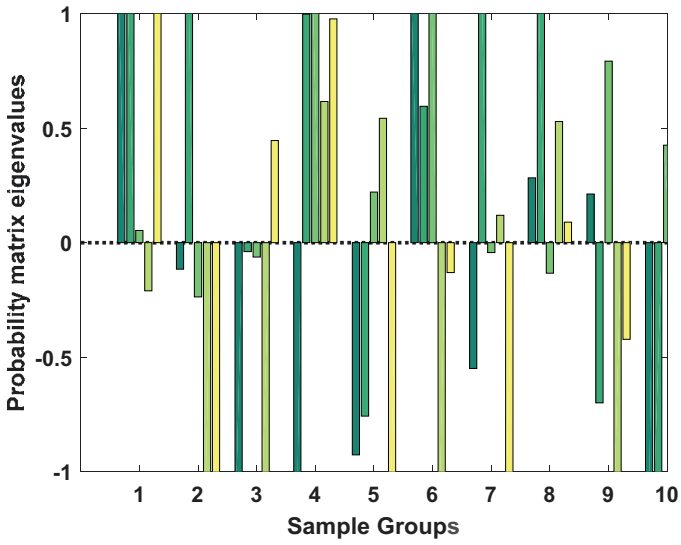


FIGURE 7
Histogram of eigenvalues of environmental sample matrix based on probability statistics.

Since the optimal relative degree of membership h-j is not much different, there is a large error in identifying the level attribution using the principle of maximum degree of membership. Therefore, the characteristic value of the level variable h-j can be used in the evaluation to judge the level attribution of the railway ecological environmental assessment project. Practice has proved that using the characteristic value of the grade variable h-j as the evaluation index, the calculated h-j of the ecological environmental assessment project corresponds to the grade division. The ecological environmental assessment of the railway construction project is close to grade II, which is more appropriate.

The experiment uses the weighted average method to obtain the evaluation result, which is the final evaluation result of environmental quality. According to the quantitative evaluation of environmental quality indicators in Figure 7, the environmental quality is good. Therefore, it can be concluded that the railway green construction environmental protection evaluation grades of the first tender (BLTJ-2), the second tender BLTJ-3) and the third tender (BLTJ-6) are “qualified”, the evaluation level of the fourth bid section (BLTJ-8) and the fifth scale (BLTJ-9) is "medium". From the probability matrix obtained from the analysis and processing of the original measured data, although most of the environmental quality indicators considered are within the limit range, due to the impact of the railway cost load, there are only a few factors that destroy the ecological environment. It is reasonable to keep exceeding the standard, so the environmental quality is good.

CONCLUSION

(1) Based on the methods of AHP and probability statistics and combining the characteristics of the railway construction stage, this paper constructs the concept of the influence model of railway construction on the ecological environment. The weights are determined by the combination of qualitative and quantitative analytic hierarchy process. For the m index weights w-i-j of sample j, m- i = w-j = 1 is satisfied, which makes the weight assignment more scientific and reasonable, and can better reflect the railway construction degree of various factors to the status of the ecological environment. According to the principles of AHP, indicators with greater weight have greater impact on the ecological environment. Starting from the principle of focusing on key points, it is obvious that factors that have a large impact on the ecological environment should be given priority.

(2) By comparing and learning several common weight determination methods, this paper adopts the method of combining subjective and objective weights for calculation to make the results more accurate. The subjective weight uses the improved AHP analysis method, which eliminates the process of consistency checking in the traditional AHP analysis method, and the calculation is simpler, and the result is more reasonable. The objective weight uses the gray relational analysis method, which is more objective. From the above calculations, key considerations should be given to the combination of weights greater than 0.1, such as rare species, nature reserves, spoil ground settings, protective measures, tunnels, landslides, mudslides, construction units, environmental awareness, waste water, and waste solids treatment measures.

(3) In this paper, through the inconsistency of the judgment matrix, it is convenient to find the items that affect the consistency in the judgment matrix, so as to obtain a reasonable weight. During the construction of railway roadbeds, bridges, and tunnels, the impact on nature reserves should be minimized. The protection measures for the reserves should be complete. Reliable measures should be taken to protect rare species, and the impact of construction on nature reserves and rare species should be minimized. On this basis, the method of probability and statistics is used to comprehensively evaluate the environmental quality. The ecological environmental assessment of the railway construction project is close to grade II, which is more appropriate.

ACKNOWLEDGEMENTS

This work was not supported by any funds. The authors would like to show sincere thanks to those techniques who have contributed to this research.

REFERENCES

[1] Schade, B., Rothengatter, W. (2004) The economic impact of environmentally sustainable transport in Germany. European Journal of Transport and Infrastructure Research. 4(1), 147-172.

[2] Ying, M., Yang, X., He, J., Guo, Y., Rong, J., Dong, Z. (2013) A new assessment model for pollutant removal using mulch in bioretention processes. Fresen. Environ. Bull. 22(5A), 1507-1515.

[3] Huang, D., Zhang, T., Zhao, C. (2018) Research on the financial impact of ecological environment information disclosure on heavy polluting enterprises. Ekoloji. 27(106), 1055-1063.

[4] Bahceci, I., Topkaya, B. (2008) Landfill site selection using GIS methods. Fresen. Environ. Bull. 17(11), 1859-1867.

[5] Suckling, D.M., Walker, J., Wearing, C.H. (1999) Ecological impact of three pest management systems in New Zealand apple orchards. Agriculture Ecosystems & Environment. 73(2), 129-140.
[6] Memisoglu, T., Colak, H.E. (2018) Spatial clustering of environmental pollution risk areas using kernel density analysis in the valleys of Trabzon, Turkey. Fresen. Environ. Bull. 27(6), 4357-4366.
[7] Li, X., Liang, C., Zhao, X. (2012) Assessment of potential impact of tunneling on the groundwater in Epi-Fissure-Karst-Zone and ecological environment. Environmental Earth Sciences. 66(3), 967-976.
[8] Lange, J.H., Thomulka, K.W., Sites, S. (2003) Airborne concentrations of asbestos during removal of pipe/boiler insulation using glovebags with and without containments. Fresen. Environ. Bull. 12(5), 431-434.
[9] Witte, W. (2000) Ecological impact of antibiotic use in animals on different complex microflora: environment. International Journal of Antimicrobial Agents. 14(4), 321-325.
[10] Behbahani, H., Yaghoubi, H., Rezvani, M.A. (2012) Development of technical and economical models for widespread application of magnetic levitation system in public transport. International Journal of Civil Engineering. 10(1), 13-24.
[11] Kaldellis, J.K., Kokala, A., Kapsali, M. (2010) Natural air pollution deposition impact on the efficiency of PV panels in urban environment. Fresen. Environ. Bull. 19(12), 2864-2872.
[12] Dixon, A.M., Simon, M., Burkitt, T. (2003) Assessing the environmental impact of two options for small-scale wastewater treatment: comparing a reedbed and an aerated biological filter using a life cycle approach. Ecological Engineering. 20(4), 297-308.
[13] Kim, J.W. (2006) The environmental impact of industrialization in East Asia and strategies toward sustainable development. Sustainability Science. 1(1), 107-114.
[14] Schumann, A.H. (1994) German perspectives of the environmental impact of water resource developments. Surveys in Geophysics. 15(3), 279-287.
[15] Al-Mahish, M., Brizmohun, R. (2021) Food production environment and maize international prices: an evidence from Mauritius poultry sector. Fresen. Environ. Bull. 30(3), 2959-2966.
[16] Koprivnikar, J. (2010) Interactions of environmental stressors impact survival and development of parasitized larval amphibians. Ecological Applications. 20(8), 2263-2272.
[17] Gilliland, M.W., Risser, P.G. (1977) The use of systems diagrams for environmental impact assessment: procedures and an application. Ecological Modelling. 3(3), 183-209.
[18] Yadav, P., Samadder, S.R. (2018) Environmental impact assessment of municipal solid waste management options using life cycle assessment: a case study. Environmental Science and Pollution Research. 25(1), 838-854.
[19] Sharp, R.R. (2002) Environmental and health impacts due to biodiesel exhaust gas. Fresen. Environ. Bull. 11(10), 823-828.
[20] Gaudi, S., Mancini, L. (2019) Epigenetics in the Mediterranean area: genome-pollution interaction. Fresen. Environ. Bull. 28(6), 4970-4973.

Received: **28.03.2021**
Accepted: **01.05.2021**

CORRESPONDING AUTHOR

Haixia Du
School of Mathematics and Statistics,
Zhengzhou Normal University,
Zhengzhou Henan 450000 – China

e-mail: duhaixia521@126.com

© by PSP Volume 30– No. 09/2021 pages 10728-10737 Fresenius Environmental Bulletin

GIS ASSESSMENT FOR GROUNDWATER QUALITY OF DISTRICT MULTAN, PAKISTAN

Muhammad H Mahmood[1], Zahid M Khan[1], Muhammad Sultan[1,*], Zawar Hussain[1], Amman Ullah[1], Shazia Hanif[2], Yousaf R Taseer[3], Muhammad A Imran[4], Riaz Ahmad[5], Tallat Mehmood[6], Muhammad Aleem[1]

[1]Department of Agricultural Engineering, Bahauddin Zakariya University, 60800 Multan, Pakistan
[2]Department of Agricultural Engineering, Muhammad Nawaz Shareef University of Agriculture, Multan, Pakistan
[3]Department of Building and Architectural Engineering, Bahauddin Zakariya University, Bosan Road, Multan 60800, Pakistan
[4]School of Environmental and Municipal Engineering, Xi'an University of Architecture and Technology, 710055 Shaanxi, Xi'an, China
[5]College of Engineering, Nanjing Agricultural University, Nanjing 210031, China
[6]Office of the Assistant Director Agriculture (Water Management), Punjab Agriculture Department, Officers Colony, Jauharabad, Khushab 41000, Pakistan

ABSTRACT

Groundwater is a major source of freshwater for agricultural and domestic purposes. For conservation of freshwater resources, the identification and management of groundwater quality is essential. Increased exploitation of groundwater and rapid urbanization is causing deterioration of groundwater quality. This study focused on the groundwater quality of District Multan, Pakistan by selecting eighty-three sites and sampling of sixteen groundwater quality parameters including pH, temperature, color, dissolved oxygen (DO), turbidity, electrical conductivity (EC), total dissolved solids (TDS), chlorides, calcium (Ca), magnesium (Mg), total alkalinity (TA), copper (Cu), iron (Fe), nickel (Ni), lead (Pb) and cobalt (Co). Presence levels of all these parameters were incorporated in geographic-information-system (GIS) and their spatial distribution was mapped through interpolations using inverse-distance-weighting (IDW) technique. The results indicated that DO was <3 mg/L in southwest and southeast of study area. Forty-four locations had high turbidity (5-86.68 NTU). TDS concentrations (>1000 mg/L) was found in northeast and southeast. The EC was high (1500 to 3000 µS/cm) in northeast and southeast. The observed level of iron was high (0.3 to 2.63 mg/L) in southeast and north side. Fifty-four locations had higher Pb concentrations (0.01 to 0.268 mg/L) and concentrations of Co (0.1 to 0.19mg/L) in drinking water source. Some of the parameters show very high level at few sampling sites which may not represent the entirely specified region.

KEYWORDS:
Drinking water source, Sampling, Groundwater quality maps, Heavy metals, Physico-chemical characteristics, Inverse distance weighted, GIS tools

INTRODUCTION

Groundwater is a critically important natural resource of any nation and the quality as well as availability of fresh groundwater is becoming a global issue. Groundwater is being used as a major source of urban and rural water supply, but the groundwater is rapidly contaminating due to different anthropogenic activities like urbanization, industrialization, and extensive agricultural practices [1–4]. If such trends continue, the precious groundwater resource may even become unfit for domestic and commercial uses [5]. The deterioration of physical, chemical and biological characteristics of groundwater occurs mainly due to the contaminated municipal, commercial and industrial discharges to the groundwater [6]. Additional sources of contamination include non-point (agricultural, and urban runoff) and point (sewage, and industrial effluent) sources [7–9].

Rapid urbanization, development and consequently increased utilization of groundwater for drinking and other purposes and disposal of mostly untreated industrial and domestic wastewaters are impacting the availability and quality of both the surface and ground water [10–12]. In view of relatively huge amounts of groundwater that are daily pumped for industrial, agricultural, and domestic purposes. The long-term aquifer recharge and quality management is critically important for sustained use of this valuable national resource. To perform efficient water quality management, the information on water quality status and its changing trends with respect to permissible limits is necessary to devise policy guidelines and their implementation [13-14].

Geographic-information-system (GIS) is an important tool for integrated spatial data with other information [15]. It allows to analyze the data spatially and to represent the information for resources development in term of environmental protection. This capability of GIS makes it powerful tool for groundwater quality assessment using measured values of water quality parameters. The GIS can also be

used beneficially for groundwater monitoring than the traditional methods as it can store different data layers, perform spatial & temporal analysis, modeling and much more applications to conceive a conceptual result. Many studies have been conducted for groundwater assessment by the GIS are available in literature [16-20].

MATERIALS AND METHODS

Study Area. The Multan District is spread over an area of 3221 square kilometers and has population of 2,060,000 lives in urban areas [21]. By population the district Multan (30º 11'52''N and 71º 28'11''E) is a fifth largest city of the country. It comprises of four tehsils namely Multan City, Multan Saddar, Shujabad and Jalapur Pirwala. For assessment of groundwater quality, the following five Towns (Autonomous Municipalities) covering two Tehsils (sub district management bodies) namely Multan Saddar and Multan City out of four Tehsils of District Multan were selected for sampling:

1. Bosan Town
2. Shah Rukan e Alam Town
3. Shershah Town
4. Mumtaz Abad Town
5. Multan Cantonment

Households in the Multan District pump groundwater through bore wells for drinking purposes and due to non-monitoring of drinking tap water the water pollution is becoming a major issue. The Pakistan council of research in water resources (PCRWR) in 2006 collected the water samples from 16 different locations of Multan city out of which sample of tube well water, water supplies and hand pumps were seven, two and seven, respectively. Out of all these sixteen locations none of source was supplying safe drinking water for health. Physico-chemical analysis of these samples revealed the presence of coliform bacteria, arsenic, iron, calcium, and turbidity more than the world health organization (WHO) prescribed permissible limits. Sojhla in 2011 conducted a study on drinking water quality in different areas of Multan. During study, the samples were taken from Tahir-Pur, Nawab-Pur, Bhinda Sandila, Muhammad-Pur Ghota, Basti Laar, Chak Nos. 4, 5, 14 & 7 Faiz. All the samples were tested by the PCRWR lab for various water quality tests. The results of water samples indicated that water used by the community was not safe for drinking, but it was also the cause of diseases like hepatitis-C & gastroenteritis and many other diseases.

Therefore, keeping in view, the drastic results of world bank and the PCRWR reports, this research work is focusing on detail analysis of groundwater samples for various physico-chemical parameters (essential inorganic and toxic inorganics) including heavy metals and the spatial distribution of these water quality parameters by the GIS based inverse-distance-weighted (IDW) interpolation technique.

Sample Analysis. The groundwater samples five autonomous towns (comprising Multan Saddar and Multan City Tehsil) of the District Multan were taken at random as per sampling procedure. The parameters like hydrogen ions concentration (i.e., pH), temperature, color, dissolved oxygen (DO), turbidity, electrical conductivity (EC), total dissolved solids (TDS), total alkalinity (TA) and chlorides were analyzed in the laboratory. All the water sample were also analyzed/tested for metals like calcium (Ca), magnesium (Mg), copper (Cu), iron (Fe), nickel (Ni), lead (Pb), and cobalt (Co). For the determination of metals in sample water atomic absorption spectrometer (AAS) of thermo scientific (iCE 3000) series was used.

Water Quality Maps. The data used for the mapping water quality and other supporting maps were developed from the results of samples that were collected from predetermined locations of existing water wells. The sampling locations were integrated with the water data for the generation of spatial distribution maps of selected water quality parameters.

The present study used the IDW method for spatial interpolation of water pollutants or other parameters. This method uses a defined or selected set of sample points for estimating the output grid cell value. It determines the cell values using a linearly weighted combination of a set of sample points and controls the significance of known points upon the interpolated values based upon their distance from the output point thereby generating a surface grid as well as thematic isolines. Important water quality parameters and their distribution patterns were studied in Multan also with the help of cartographic techniques. Thus, the GIS enables us to present the cause and effect relationship visually.

RESULTS AND DISCUSSION

The H^+ Ion Concentration (pH). It was measured that three sample locations situated in Tehsil Multan Saddar and one sample location situated in Tehsil Multan City has low pH (6.45 to 7.0) as shown in the Figure 2(a). The sample locations of Tehsil Multan Saddar have high pH (8.0 to 8.52). All remaining samples have pH value from 7.0 to 8.4 (within the permissible limits). It is one of the crucial operational water quality parameters. A careful pH control is needed at every stage of water treatment to make sure water clarification and disinfection.

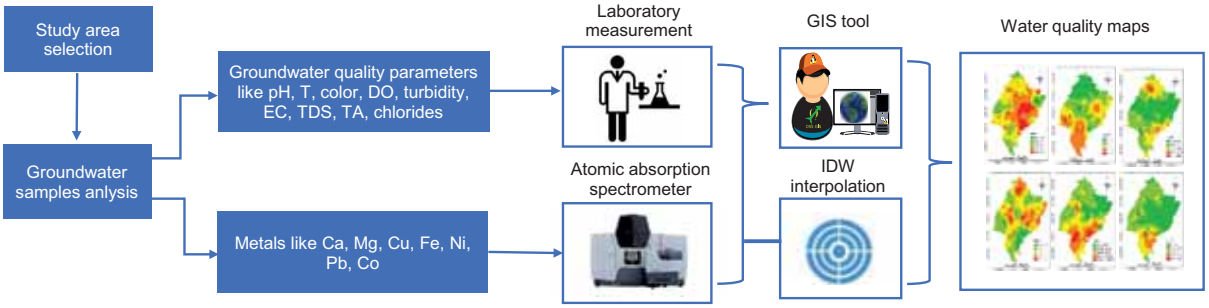


FIGURE 1
Flow chart summarizing the process of groundwater quality assessment.

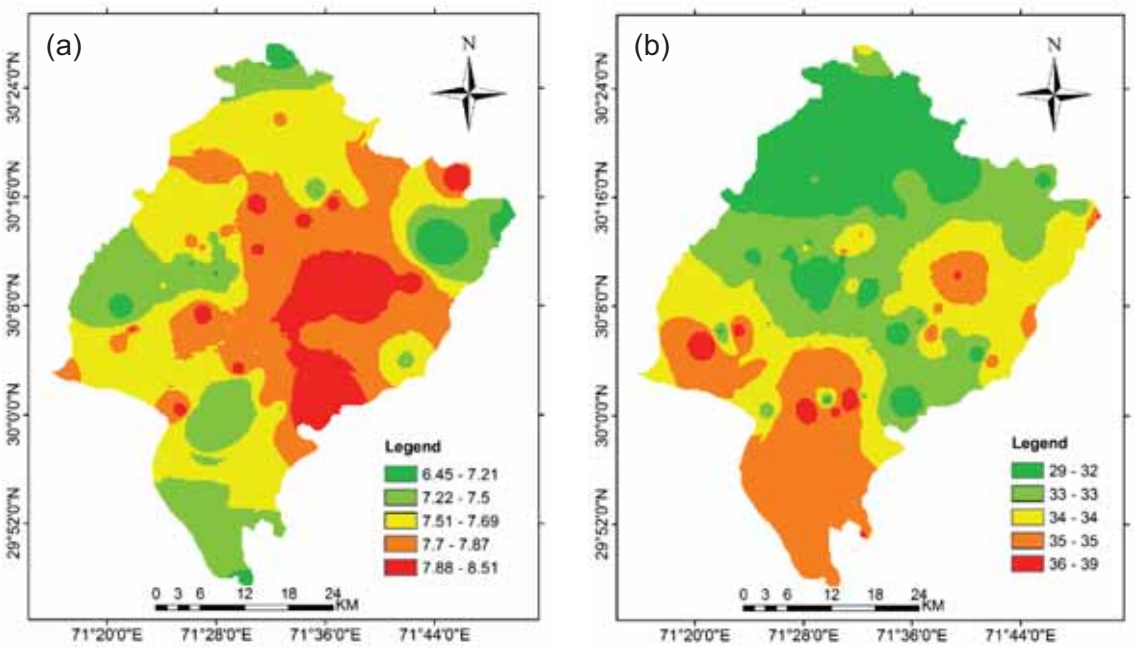


FIGURE 2
(a) Concentration of H^+ ions in groundwater, and (b) distribution of temperature of groundwater.

Temperature. The water temperature of all samples ranges from 29°C to 38°C as spatial distribution of temperature over the entire area is shown in Figure 2(b). No water sample fall within the permissible limit (i.e., 15°C) as recommended by the environmental protection division (EPD), government of British Columbia. The WHO has not recommended guideline value for water temperature because it has no health problems at levels found in drinking water. However, the different water temperature ranges may affect its acceptability for users. Therefore, no water sample has such a value which is harmful for water quality.

Color. The color in surface and groundwater results primarily from the presence of natural organic matter, particularly aquatic humic matter. The color level less than 15 TCU (pt/co or Hz) is permissible for drinking purposes as per the drinking water quality standards (DWQS) of WHO [22]. A glass containing water with the color level greater than 15 TCU can be detected by naked eye.

The spatial trend of high color levels can be visualized from Figure 3(a). It was measured that the most of sample locations situated in southwest direction have high color level (15 to 181 TCU) with greater spatial distribution and sample locations situated in northeast and northwest have also have high color level but with low spatial extent. High color level might be due presence of metals (iron, lead, copper), corrosion products, pipe sedimentation, manganese, impurities and leaching of the industrial effluent to groundwater.

Dissolved Oxygen (DO). The dissolve oxygen (DO) concentration of water supply (domestic) should not below the 3 mg/L as per water quality control emission regulations. Uzaira et al. [23] stated that the standard value of dissolved oxygen is 3 mg/L. The DO of water is primarily affected by the source, temperature of raw water, treatment process or chemical/biological process takes place in the water distribution system [23].

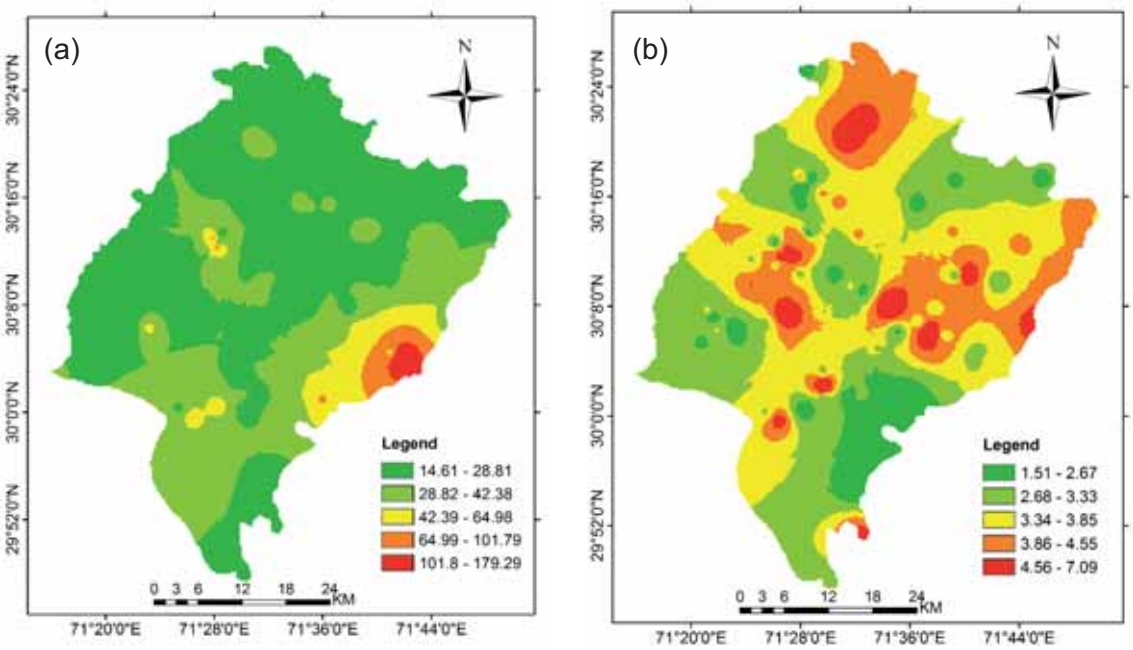


FIGURE 3
Concentration of (a) color, and (b) dissolved oxygen (DO) in groundwater.

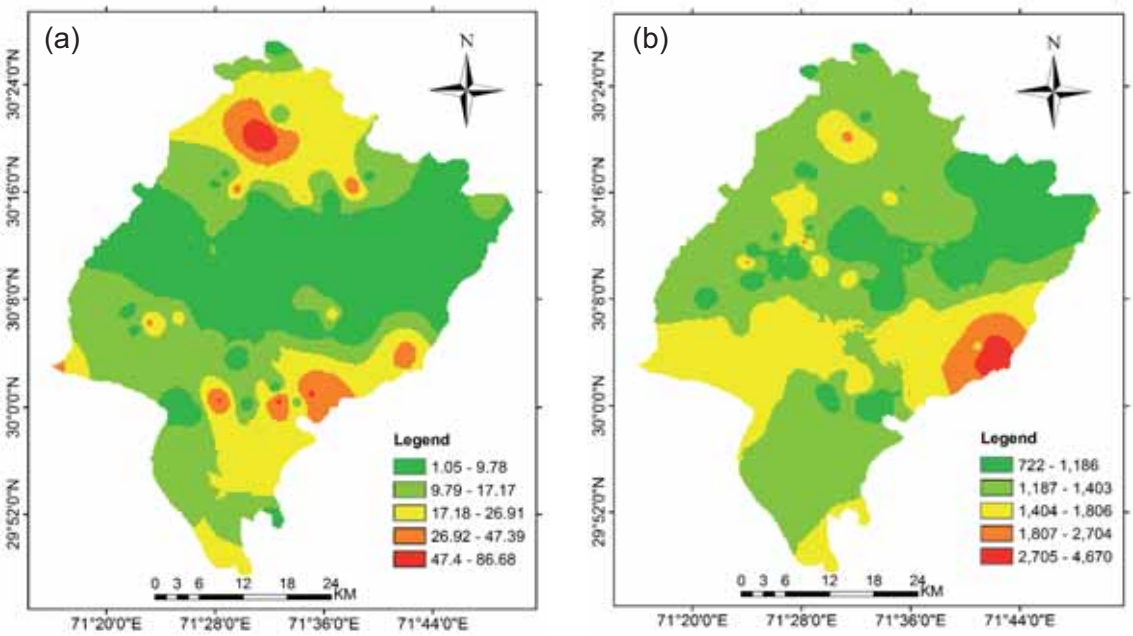


FIGURE 4
Concentration of (a) turbidity, and (b) electrical conductivity (EC) in groundwater.

It was measured that minimum value of the DO is 1.5110 mg/L and maximum value is 7.085 mg/L. Areas where the DO level of drinking water is below the standard limit (3 mg/L) are highlighted with dark green hot spots while the areas with high DO levels are highlighted with red hot spots and within the permissible limits are shown as light green hot spots in the Figure 3(b).

Turbidity. The high turbidity water level (5.0 to 86.7 NTU) of the research area can be spatially examined over entire study area as represented in Figure 4(a). The remaining sample locations mostly situated northeast and northwest have level of turbidity less than 5 NTU. The water of said areas is suitable for drinking purposes based on turbidity level recommended by the WHO [22]. All the remaining sites have high turbidity (5 to 86.7 NTU) and water of these areas is not acceptable for drinking purposes as it crosses the WHO permissible limits. The high turbidity level may be due to the presence of inert clay in groundwater, and it may also be due to the chalk particles and the precipitation of insoluble reduced iron.

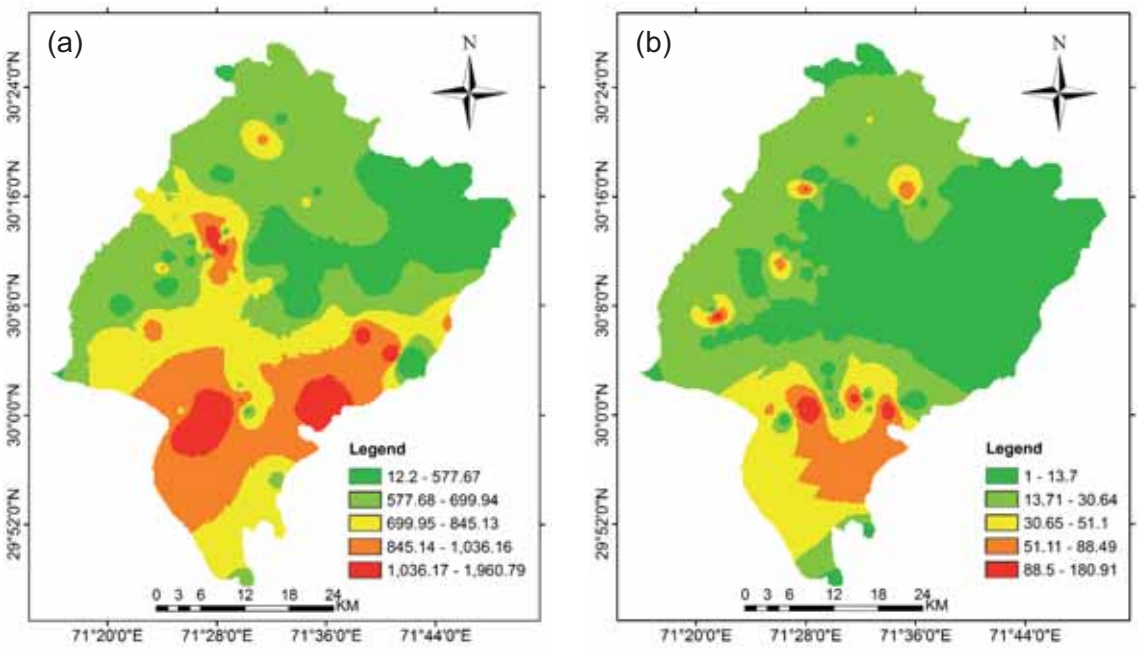


FIGURE 5
Concentration of (a) total dissolved solids (TDS), and (b) chlorides in groundwater.

Electrical Conductivity (EC). It is the measure of ability of an aqueous solution to carry an electric current and this ability depends on the presence of ions; on their total concentration, mobility, and valence; and on the temperature of measurement. The EC value of the research area ranges from 720 µS/cm to 4700 µS/cm as shown in Figure 4(b). The WHO classified that the EC value less than 1500 µS/cm is considered as permissible and EC value from 1500 to 3000 µS/cm is considered as not permissible whereas EC value greater than 3000 µS/cm is considered as hazardous. It is measured that the water the water sample of some site in southeast of the study area has hazardous EC value of about 4700 µS/cm.

Total Dissolved Solids (TDS). The solids refer to the matter suspended or dissolved in water. Solids may affect water or quality adversely in number of ways. As per the DWQS of WHO [22], level of TDS < about 600 mg/L is considered good, TDS level 600 to 1000 mg/L is considered as permissible, and level of TDS > 1000 mg/L is considered not acceptable for drinking purposes. The spatial distribution of the TDS over entire study area is obvious from Figure 5(a). The water of locations situated in southwest and southeast have the TDS value greater than 1000 mg/L with greater spatial distribution whereas northwest and southeast location also have TDS value greater than 1000 mg/L. The high TDS level may be due to the salt's intrusion from soil thick mantle, weathered rock media and long contact time of groundwater with the body of aquifer [24]. The water which has high TDS level may produce adverse physiological reaction in the transient users and also become a reason of gastrointestinal disorder [25].

Chloride. The recommended level of chloride in water is less than 250 mg/L as the higher level (>250 mg/L) affect the taste of water [26]. It was measured that the water of all the sample locations has chloride level within the permissible limits (>250 mg/L) as per the DWQS of WHO [22] as it is apparent from Figure 5(b). According to the Turkish standards institutions (TSE), the recommended level of chloride is 25 mg/L and maximum contamination level is 600 mg/L. Keeping in view the TSE the spatial variation map is classified in two layers i.e. dark green (14.6 to 25 mg/L) and light green (25.0 to 180.4 mg/L) to bifurcate the different chloride levels of the study area to understand the concentration of chloride over the entire area. Furthermore, the DWQS of WHO reported that the levels of chloride found particularly in the drinking water has no health effects [22].

Calcium (Ca). Calcium (Ca) is necessary in plants and animal nutrition and is an essential component of bones, shells, and plants structures. Presence of the Ca in water supplies results from passage over deposits of limestone, dolomite, gypsum and gypsiferous shale. The highest desirable limit of Ca in groundwater is less than 75 mg/L whereas the highest permissible limit is 75 to 200 mg/L [27]. It has been found that the Ca mineral contents in the drinking water of most Asian countries ranges from 2 to 80 mg/L [28].

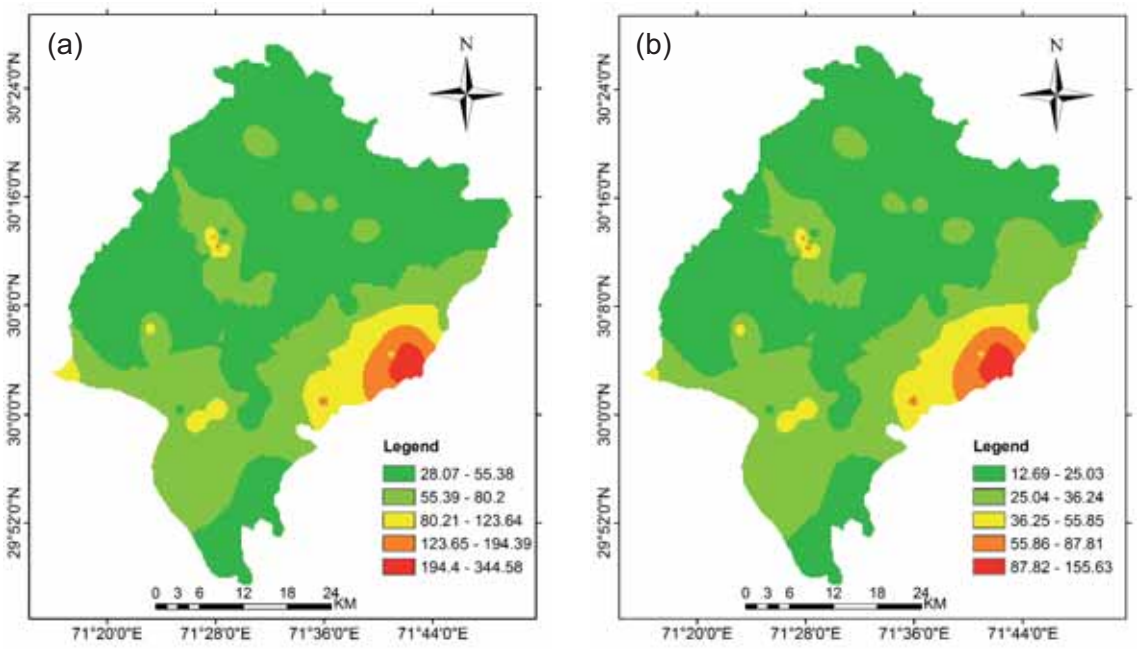


FIGURE 6
Concentration of (a) calcium (Ca) , and (b) magnesium (Mg) in groundwater.

The huge variation in the Ca spatial distribution can be observed from Figure 6(a) as most of the sample location (about seventy) sample locations has Ca level within the maximum desirable range (<75 mg/L). The location situated in southeast of the study area have Ca level within the maximum permissible level (75 to 200 mg/L) with higher spatial extent whereas the study locations of north, northwest and southwest less spatial distribution of the Ca. However, only one sample location situated in southeast direction has higher level of the Ca which is greater than 200 mg/L.

Magnesium (Mg). Magnesium (Mg) is an essential element in chlorophyll and in red blood cells. Some salts of Mg are toxic by ingestion on inhalation. Concentration greater than 125 mg/L also can have cathartic and diuretic effect [22]. The maximum desirable level of the Mg in water is 50 mg/L whereas the maximum allowable level is 150 mg/L [27]. The results of 24 study locations of Punjab (India) revealed that there was big variation of the Mg over the entire area as it ranges from 5 to 235.6 mg/L [29].

It was measured that the water studied locations has Mg within the most/maximum desirable range (12 to 50 mg/L) as shown green in Figure 6(b). Whereas the sample location in southeast has Mg level within the maximum permissible/allowable range of 50 to 150 mg/L as marked by orange hot spots. Only some sample location also situated in southeast of the study area has crossed the allowable Mg level.

Total Alkalinity (TA)as CaCO3. Alkalinity is a measure of water capacity to neutralize the acids. The recommended value of alkalinity level of water is 200 mg/L [22]. The high alkalinity level (>200 mg/L) might be because of organic matter decay and also the mineral and rocks weathering. Figure 7(a) represents the spatial variation of alkalinity over the study area. It was measured that the water of all the sample locations have alkalinity level within the allowable limits except the water of only two sample located in has alkalinity level greater than WHO permissible level (200 mg/L).

Copper (Cu). The desirable oral intake of copper (Cu) is 2 to 3 mg/L whereas the maximum tolerable Cu intake level is 10 mg/L, exceeding this limit results in gastrointestinal effects. The water Cu level greater than 1 mg/L causes the yellowing sanitary ware and its level greater than 2.5 mg/L can affect the color and taste of water [22].

The recommended guideline value for Cu in drinking water is 2 mg/L. The concentration range of Cu in drinking varies from ≤0.005 to > 30 mg/L and it is mainly because of corrosion of Cu plumbing. It was measured that the water of all the sample locations have Cu level within the acceptable range as maximum value is 0.463mg/L represented in Figure 7(b).

Iron (Fe). The daily requirement of iron (Fe) is 10 to 50 mg/L depending upon the various factors like gender and age. The permissible level of Fe in drinking water is 0.3 mg/L. The Fe can be found in the range of 0.5 mg/L to 50 mg/L in fresh natural water [22].

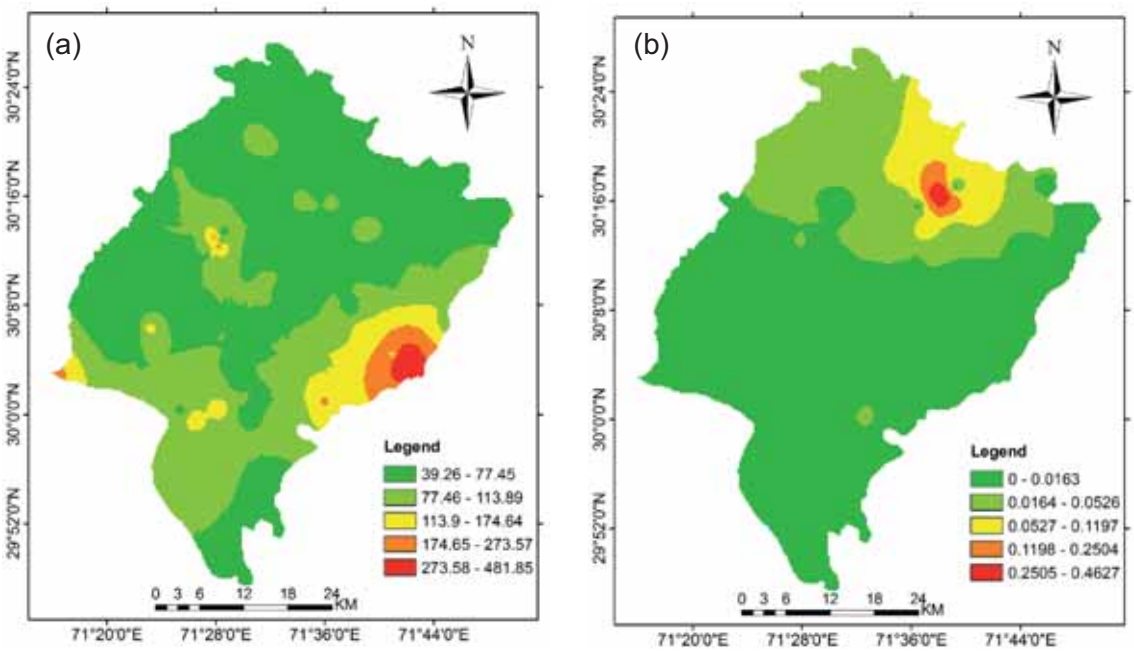


FIGURE 7
Concentration of (a) total alkalinity, and (b) copper (Cu) in groundwater.

The level of Fe in water samples of study area varies up to 2.63 mg/L and it has been divided into two categories as shown in Figure 8(a). It has been measured that the water from sample locations of red spots have Fe level greater than 0.3 mg/L as shown in Figure 7(a). The remaining study areas have Fe level within the WHO permissible range (i.e., 0.3 mg/L).

Nickel (Ni). Main source of nickel (Ni) intake is food for non-smoking population and water is minor source of daily oral nickel intake. The daily intake of Ni is 12 µg/kg and recommended permissible level of Ni in drinking water defined by the WHO is 0.07 mg/L [22]. It is obvious from Figure 8(b) that most of study areas have no issue regarding Ni concentration in the water. It was measured that only three water sample locations situated in north and northwest of the study area have greater Ni concentration of 0.334 mg/L as compared to permissible limits. Whereas all the remaining study locations/sites have Ni level in the water below the permissible limits.

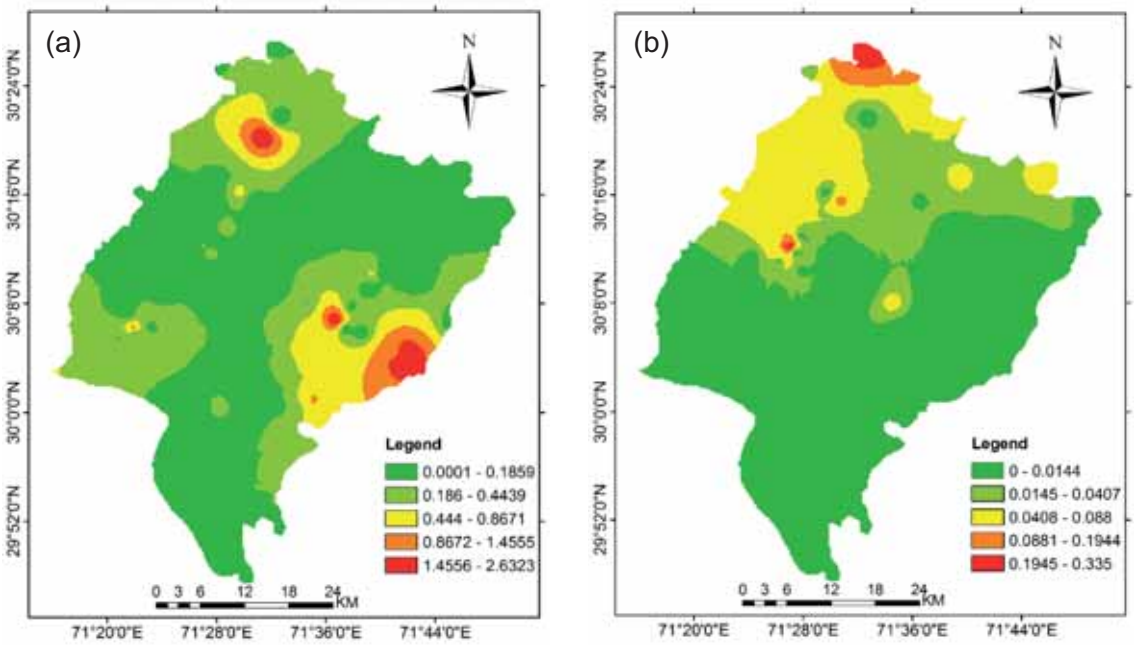


FIGURE 8
Concentration of (a) iron (Fe), and (b) nickel (Ni) in groundwater.

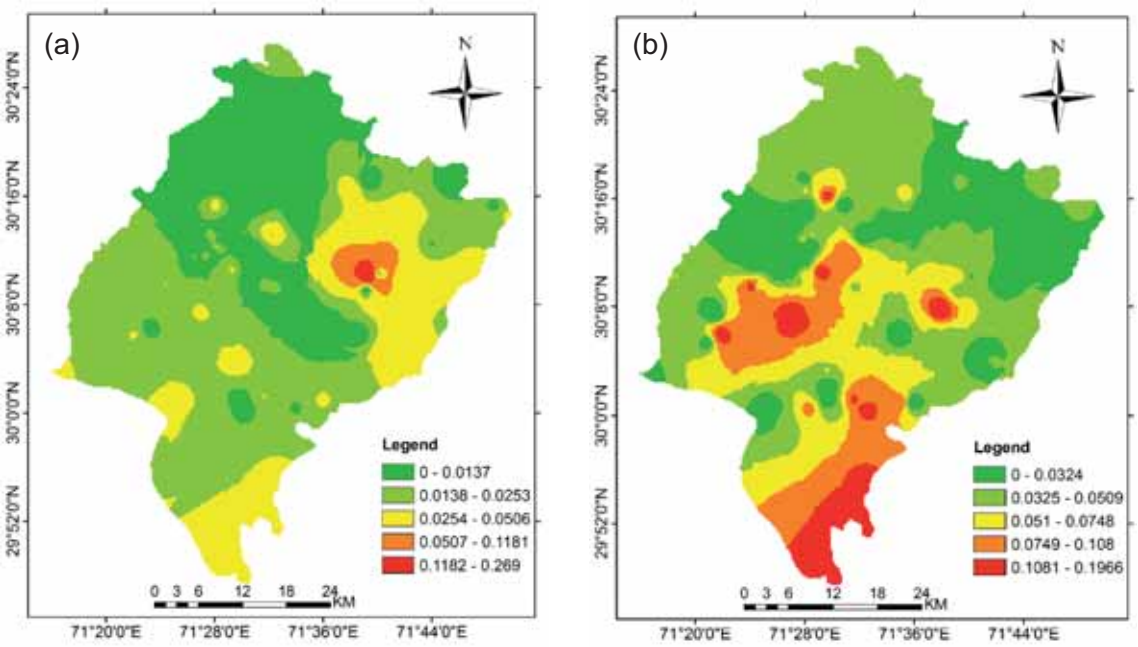


FIGURE 9
Concentration of (a) lead (Pb), and (b) cobalt (Co) in groundwater.

Lead (Pb). Naturally, the lead (Pb) metal is found in environment and manufacturing products. The Pb emission sources include the fuel used in road vehicles and emission of Pb from industrial sources. In batteries, Pb is particularly used for lead acid battery production and generally used in alloys & solders. The Pb can be present in tap drinking water as it dissolves by natural sources [22]. The guideline value of the Pb in drinking water is 0.01 mg/L.

The most of study areas are affected by high Pb concentration as obvious by red hot spots in Figure 9(a). It was measured that about twenty-nine water sample locations have Pb level within the WHO permissible limits, whereas all the remaining fifty-four research area have Pb level range of 0.01 to 0.268 mg/L in water.

Cobalt (Co). Cobalt (Co) is generally rare metal, obtained in the result of byproduct of the other metals like Cu and it naturally occurs in water, soil, plants, rocks, air and animals. The maximum desirable level of Co in drinking water is 0.1 mg/L [30]. The WHO has not recommended any guideline value for Co concentration in drinking water. The spatial distribution is made as per United States, environmental protection agency (EPA) recommended permissible level of Cu in drinking water as shown in Figure 9(b).

It was measured that the water of sample of sixteen locations marked with red hot spots have Co level greater than permissible limits. The water sample of remaining sixty-seven locations has Co level within permissible limits.

CONCLUSIONS

Freshwater resources are very limited and are decreasing day by day due to population growth and urbanization. Groundwater is main source of fresh water but due to various sources like uncontrolled hazardous waste disposal, landfills, chemicals, and untreated wastewater disposal continuously degrading the groundwater quality. This study explores groundwater quality assessment of District Multan from viewpoints of sixteen groundwater quality parameters like pH, temperature, color, DO, turbidity, EC, TDS, chlorides, Ca, Mg, TA, and heavy metals like Cu, Fe, Ni, Pb, and Co. The study included groundwater sampling of eighty-three locations spread over five municipalities in two Tehsils of Multan. The GIS software was used to see spatial distribution map of presence levels of sixteen water quality parameters by adopting IDW technique. The following conclusions were drawn:

1. Southwest and southeast side of study area had low DO levels of 1.5 to 2.9 mg/L indicating poor environmental acceptability and health.
2. Forty-four tested locations showed high turbidity of 5 to 86.68 NTU spread over larger area.
3. High EC levels of 1500 to 3000 µS/cm was found in southeast of study area indicating presence of dissolved ionic salts in the groundwater.
4. Northeast and southeast side of study area had high TDS levels of greater than 1000 mg/L.
5. Southeast and north side of study area had high Fe concentrations of 0.3 to 2.63 mg/L.
6. Three tested locations had high Ni concentrations of 0.334 mg/L.
7. Fifty-four tested locations had higher Pb concentrations of 0.01 to 0.268 mg/L in drinking water

source.

8. The southern locations of study area had high Co concentration of 0.1 to 0.19 mg/L.

ABBREVATIONS

AAS	Atomic absorption spectrometer
Ca	Calcium [mg/L]
Co	Cobalt [mg/L]
Cu	Copper [mg/L]
DO	Dissolved oxygen [mg/L]
DWQS	Drinking water quality standards
EC	Electrical conductivity [µS/cm]
EPD	Environmental protection division
Fe	Iron [mg/L]
GIS	Geographic-information-system
IDW	Inverse-distance-weighted
Mg	Magnesium [mg/L]
Ni	Nickle [mg/L]
NTU	Nephelometric turbidity unit
Pb	Lead [mg/L]
PCRWR	Pakistan council of research in water resources
TA	Total alkalinity [mg/L]
TCU	True color unit
TDS	Total dissolved solids [mg/L]
TSE	Turkish standards institutions
WHO	World health organization

ACKNOWLEDGEMENTS

This research work has been carried out in the Department of Agricultural Engineering, Bahauddin Zakariya University, Multan-Pakistan.

REFERENCES

[1] Nussinovitch, A., and Dagan, O. (2015) Hydrocolloid liquid-core capsules for the removal of heavy-metal cations from water. Journal of Hazardous Materials. 299, 122–131.

[2] Sellamuthu, V., Mariyappan, V.P., Rafi, M., and Vallel, K.L.K. (2011) Assessment of groundwater quality for irrigational use in Cumbum valley, Madurai district, Tamilnadu, India. Nature Environment and Pollution Technology. 10, 207–212.

[3] Ahamed, J.A. (2013) A comparative evaluation of groundwater suitability for drinking and irrigation purposes in Pugalur area, Karur district, Tamilnadu, India. Scholars Research Library Archives of Applied Science Research. 5(1), 213–223.

[4] Khan, R.A., Zain, S.M., Juahir, H., Yusoff, M.K., and Hanidza, T.T. (2012) Using Principal Component Scores and Artificial Neural Networks in Predicting Water Quality Index. Chemometrics in Practical Applications IntechOpen, Rijeka, 271-288.

[5] Ehirim, C., and Nwankwo, C. (2010), Evaluation of aquifer characteristics and groundwater quality using geoelectric method in Choba, Port Harcourt, Archives of Applied Science Research, 2(2), 396–403.

[6] Sharma, S., and Bhattacharya, A. (2017) Drinking water contamination and treatment techniques. Applied Water Science. 7(3), 1043–1067.

[7] Ali, I., Peng, C., Lin, D., Saroj, D.P., Naz, I., Khan, Z.M., Sultan, M., and Ali, M. (2019) Encapsulated green magnetic nanoparticles for the removal of toxic Pb2+ and Cd2+ from water: Development, characterization and application. Journal of Environmental Management. 234(December 2018), 273–289.

[8] Amjed, M.A., Peng, C., Dai, M., Chang, Q., Ali, I., Sultan, M., Naz, I., Farooq, M., and Kashif, M. (2020) Recent updates on the solar-assisted biochar production and potential usage for water treatment, Fresen. Environ. Bull. 29, 5616–5632.

[9] Arsalan, M., Khan, Z.M., Sultan, M., Ali, I., Shakoor, A., Mahmood, M., Ahmad, M., Shamshiri, R., Ali Imran, M., and Khalid, M. (2021) Experimental investigation of a wastewater treatment system utilizing maize cob as trickling filter media. Fresen. Environ. Bull. 21, 148–157.

[10] Kumar, B. R., Prasad, M. L., Rao, D. S., and Rao, K. R. S. S. (2013), Bioremediation of Sewage using Specific Microbial consortium and Biogenic Filter materials. Biotechnology. 2(11), 10–15.

[11] Amiri, V., Rezaei, M., and Sohrabi, N. (2014) Groundwater quality assessment using entropy weighted water quality index (EWQI) in Lenjanat, Iran. Environmental Earth Sciences. 72(9), 3479–3490.

[12] Ali, I., Peng, C., Khan, Z.M., Naz, I., Sultan, M., Ali, M., Abbasi, I.A., Islam, T., and Ye, T. (2019) Overview of microbes based fabricated biogenic nanoparticles for water and wastewater treatment. Journal of Environmental Management. 230, 128–150.

[13] Dahiya, S., Singh, B., Gaur, S., Garg, V. K., and Kushwaha, H. S. (2007), Analysis of groundwater quality using fuzzy synthetic evaluation, Journal of Hazardous Materials. 147(3), 938–946.

[14] Fang, Y., Peng, C., Yang, K., Zhang, Y., Lopez-Valdivieso, A., Dai, M., Ali, I., Sultan, M., Naz, I., Asghar, N., Mahmood, M., and Raza, H. (2020) Adsorptive removal of cationic toxic dyes from aqueous solution: Adsorbents development and performance investigation. Fresen. Environ. Bull. 29, 6072–6081.
[15] Nampak, H., Pradhan, B., and Manap, M.A. (2014) Application of GIS based data driven evidential belief function model to predict groundwater potential zonation. Journal of Hydrology. 513, 283–300.
[16] Baskar, M. (2020) GIS-based Assessment of Groundwater Quality for Drinking and Irrigation by Water Quality Index. International Journal of Current Microbiology and Applied Sciences. 9(3), 2361–2370.
[17] Jha, M.K., Shekhar, A., and Jenifer, M.A. (2020) Assessing groundwater quality for drinking water supply using hybrid fuzzy-GIS-based water quality index. Water Research. 179, 115867.
[18] Elubid, B.A., Huag, T., Ahmed, E.H., Zhao, J., Elhag, K.M., Abbass, W., and Babiker, M.M. (2019) Geospatial distributions of groundwater quality in Gedaref state using geographic information system (GIS) and drinking water quality index (DWQI). International Journal of Environmental Research and Public Health. 16(5), 1–20.
[19] Yetis, A.D., Kahraman, N., Yesilnacar, M.I., and Kara, H. (2021) Groundwater Quality Assessment Using GIS Based on some Pollution Indicators over the Past 10 Years (2005–2015): a Case Study from Semi-Arid Harran Plain, Turkey. Water, Air, and Soil Pollution. 232(1).
[20] Makki, Z.F., Zuhaira, A.A., Al-Jubouri, S.M., Al-Hamd, R.K.S., and Cunningham, L.S. (2021) GIS-based assessment of groundwater quality for drinking and irrigation purposes in central Iraq. Environmental Monitoring and Assessment, 193(2).
[21] World Statistical Data (2021) Population stat. Available at: https://populationstat.com/pakistan/multan. (Accessed: 12-Feb-2021).
[22] World Health Organization, (WHO) (2017) Guidelines for drinking-water quality, 4th edition, incorporating the 1st addendum, 2017. Available at: https://www.who.int/publications/i/item/9789241549950. (Accessed: 12-Feb-2021).
[23] Iqbal, U., Qasim, H., Khan, A.K., Rashid, R., Nasreen, S., Mahmood, Q. and Khan, J. (2009) Surface and ground water quality risk assessment in district Attock Pakistan. World Applied Sciences Journal. 7(8), 1029–1036.
[24] Dar, I.A., Sankar, K. and Dar, M.A. (2011) Spatial assessment of groundwater quality in Mamundiyar basin, Tamil Nadu, India. Environmental Monitoring and Assessment. 178(1–4), 437–447.
[25] Pius, A., Jerome, C. and Sharma, N. (2012) Evaluation of groundwater quality in and around Peenya industrial area of Bangalore, South India using GIS techniques. Environmental Monitoring and Assessment. 184(7), 4067–4077.
[26] Lehtonen, J., Hassinen, J., Honkanen, R., Kumar, A.A., Viskari, H., Kettunen, A., Pahimanolis, N., Pradeep, T., Rojas, O.J. and Ikkala, O. (2019) Effects of Chloride Concentration on the Water Disinfection Performance of Silver Containing Nanocellulose-based Composites. Scientific Reports. 9(1), 1–10.
[27] World Health Organization. (2009). Calcium and magnesium in drinking water: public health significance. World Health Organization. 1-194. https://apps.who. int/iris/handle/10665/43836. Accessed on: 16 May, 2021.
[28] World Health Organization. (2009). Potassium in drinking-water: background document for development of WHO guidelines for drinking-water quality. 4th Edition, World Health Organization, Geneva, Switzerland. https://apps.who.int/iris/handle/ 10665/70171. Accessed on: 16 May, 2021.
[29] Kumar, M., Singh, S. and Mahajan, R.K. (2006) Trace level determination of U, Zn, Cd, Pb and Cu in drinking water samples. Environmental Monitoring and Assessment. 112(1–3), 283–292.
[30] US EPA (2018) 2018 Edition of the Drinking Water Standards and Health Advisories, 2018. Available at: https://www.epa.gov/sites/production/files/2018-03/documents/dwtable2018.pdf. (Accessed: 11-Feb-2021).

Received: **28.03.2021**
Accepted: **01.05.2021**

CORRESPONDING AUTHOR

Muhammad Sultan
Department of Agricultural Engineering
Bahauddin Zakariya University
Multan 60800 – Pakistan

e-mail: muhammadsultan@bzu.edu.pk

© by PSP Volume 30– No. 09/2021 pages 10738-10747 Fresenius Environmental Bulletin

RESEARCH ON THE EVALUATION OF ECOLOGICAL ENVIRONMENT QUALITY IN RURAL TOURISM AREAS

JingYu*

School of Commercial, HuangGang Normal University, Huanggang Hubei 438000, China

ABSTRACT

Economic development cannot be done at the cost of destroying the environment. The environmental construction and economic construction must be carried out simultaneously to create a green ecological environment. This paper takes rural tourism areas as an example to evaluate the quality of the ecological environment and propose the problems of the ecological environment in rural tourism areas and the optimization measures through data analysis. This study uses the hierarchical analysis method (AHP) to build an ecological travel environment quality evaluation system that meets the characteristics of rural tourism areas and determines 40 specific evaluation indexes and factor weights by constructing a judgment matrix for two-by-two comparisons, based on expert surveys. At the same time, the evaluation grade standard and fuzzy evaluation standard of ecological environment quality of rural tourism were determined, and the fuzzy comprehensive evaluation method (FCE) was applied to carry out empirical research. The subsystems of natural, economic, and social environment are analyzed separately first, and then the development status of each subsystem and the main influence factors of each subsystem are derived, after which the composite system is evaluated comprehensively. The overall ecological environment quality of rural tourism area is on the rise, the foundation is weak, and the ecological environment quality is not high. There are deficiencies in ecological protection, town greening construction, science and education, and social security, which need to be improved. Finally, in response to the problems of ecological environment construction in rural tourism areas, countermeasures are proposed to strengthen ecological environment construction and protection, strengthen town green construction, increase education investment, implement national population policy to control population growth, and promote the development of special industries to encourage entrepreneurship and employment. Combined with the actual situation, the evaluation results are more reasonable, indicating that the evaluation model is representative, relevant, and universal.

KEYWORDS:
Rural tourism, Ecological environment, Environmental quality, Fuzzy evaluation

INTRODUCTION

In the context of rapid socio-economic development, the high-quality conflicts between humans and the ecological environment are becoming increasingly prominent. The impact of human productive activities and lifestyles on the ecosystem is increasing. As a result, various ecological and environmental problems have emerged, which have an impact on the sustainable development of human beings. In terms of social development, the emphasis has been placed on the quality of life of the population, and great efforts have been made to improve the social public infrastructure and enhance the livelihood security of the population, resulting in a significant improvement in the living standards of the people [1]. At the present stage, rural tourism areas have achieved better development in terms of economic and social development and natural environment monitoring, but the current research work related to ecological environment quality assessment of rural tourism areas is still in its infancy, and there are great differences in research methods because of differences in research purposes, focus, and direction, and there is a lack of methods that can comprehensively and objectively analyze the ecological environment quality of rural tourism areas [2]. It is important to objectively recognize and understand the status and changes of ecological environment quality in rural tourism areas, and to carry out research on the ecological environment quality assessment for the construction of ecological rural tourism. Evaluation of ecological environment quality in rural tourism areas is an important guarantee to achieve the goal of green development and strive to build a beautiful countryside [3]. It is an effective measure to comprehensively monitor the ecological countryside process and regulate the development of ecological environmental quality more intuitively.

Faced with the gradual improvement of ecological environment content, international research on the ecological environment quality evaluation index system has also appeared in different fields, different

levels, and different measures of the division. Mikayilov J., Mukhtarov S., Mammadov J., analyzed the suitability development of Manuka city in New Zealand from three dimensions: urban environment, economy, and society, and selected indicators from the following elemental layers: the sense of belonging, the stability of the community, quality of buildings [5]. Agnieszka Xu Z., Sun B., developed a system of indicators to evaluate urban ecological environment from three perspectives: resource, economic, and social resilience [6]. Kóródi M., Dávid L., used hierarchical analysis to assess the quality of the ecological environment in three semi-enclosed coastal areas and constructed a system of 11 indicators based on bimolecular and physicochemical elements to obtain an assessment of the ecological quality by calculating weight [7]. Atun R., Nafa H., Türker Ö., constructed the Mediterranean submarine cave ecosystem using a structural operational theory model and based on this ecosystem, a quality index framework (EBQI) was developed for assessing the ecological environmental quality of Mediterranean submarine caves and their surroundings [8].

At this stage, there are more evaluation indexes on ecological environment construction, but few of them are combined with rural tourism areas and quality aspects. Rural tourism areas are significantly different from other areas in terms of the natural ecological system, economic system, social system, etc. Therefore, this paper focuses on the concept of ecological environment quality and analyzes the current development status of ecological environment quality construction in rural tourism areas [9]. The evaluation model of the ecological environment quality of rural tourism areas is evaluated. The evaluation of ecological environment quality of rural tourism area can reflect its ecological environment quality construction and development status scientifically and truly, which can highlight the problems existing in the process of ecological environment quality construction in the rural tourism area, reflect the effect of ecological environment quality management work, and prompt governments at all levels to strengthen ecological environmental protection and governance, improve the ecological environmental protection level and level, improve the quality of residents' living environment, promote sustainable development, and make the construction of ecological environment quality more reasonable.

MATERIALS AND METHODS

(1) Principle of ecological environment quality evaluation construction. Rural tourism area refers to rural tourism activities with a certain number of large-scale and geographically more concentrated rural houses, building facilities, and farmers or fishermen's families as the receiving unit, with rural tourism resources such as idyllic landscape, natural ecology, rural culture, and agricultural production, life and rural settlement landscape as the main tourist attraction, sightseeing, dining, experience, entertainment, learning, shopping, leisure and vacation as the rural tourism activities.

The evaluation of ecological environment quality must be based on the principle of scientific development, which mainly includes scientific ideas, scientific theories, and scientific systems. Firstly, the article should be conceived with scientific thought as the guide. According to the nature and laws of things, we use scientific thought to reflect the characteristics and features of the evaluated things objectively, correctly, systematically, and comprehensively [10]. Secondly, the content construction should be based on scientific theories. According to the disciplinary background of ecotourism, we sort out the relevant theoretical studies on ecological environment quality, such as landscape ecology theory, ecotourism planning theory, tourism carrying capacity theory, and use them as the basis for in-depth research on the theoretical system of ecological environment quality evaluation in rural tourism areas [10]. Thirdly, the selection of indicators should be aimed at the scientific system. The relevance and representativeness of the indicator system should be fully considered when selecting the comprehensive evaluation layer, and the scientifically and system activeness of the indicators should be fully considered when selecting the element evaluation layer and factor evaluation layer. We select the indicator system with the characteristics of rural tourism area and construct a more scientific and reasonable evaluation model. Table 1 lists the principles of ecological environment quality evaluation.

TABLE 1
Principles of ecological environment quality evaluation construction

Serial number	Evaluation Principles	Detailed description
1	Scientific principle	Index system is based on scientific theory
2	The principle of wholeness	The indicator system is an organic whole
3	Geographical principle	Different ecological environments are different
4	Practicality principle	Quantitatively reflect the actual situation
5	Forward-looking principle	In line with the planning of rural tourism area

Both qualitative and quantitative methods, as two research methods for analyzing problems, have their characteristics in terms of use and processing. Qualitative methods mainly analyze things descriptively using subjective empirical judgments, while quantitative methods analyze problems quantitatively through mathematical models and operations. If we use qualitative methods alone, we will lack scientific and accurate data analysis, and on the contrary, quantitative research without qualitative analysis is also blind. The qualitative analysis provides the direction for quantitative analysis and quantitative analysis provides the basis for qualitative analysis [11]. Therefore, only by organically combining qualitative and quantitative analysis can we achieve a more scientific and reasonable analysis and research of things. In this paper, we use qualitative analysis methods to screen evaluation indexes and construct an evaluation model for ecological tourism resources of small towns. At the same time, a more mature and reliable quantitative evaluation method is used to calculate the index weight, and the results are combined with the empirical analysis of Hinge Town. By combining qualitative and quantitative methods, we hope to achieve a more scientific and reasonable evaluation model and an objective and comprehensive evaluation of the research object.

In this paper, based on insisting on the theoretical basis of ecology and tourism as the guidance, we find out the individuality and commonality of the ecological environment quality evaluation index of rural tourism area through field investigation, and organically combine theory and practice to construct the ecological environment quality evaluation of rural tourism area. The specific approach is as follows: firstly, the ecological environment quality evaluation of small rural tourism areas should be based on scientific theory as the guiding basis, and the ecological environment conditions, ecological tourism resources conditions, and tourism capacity conditions should be fully considered in the index screening process. Secondly, according to the results of the field survey and combined with the actual situation of ecological environment quality of rural tourism area and the characteristics of rural tourism area itself for dimensional screening, we determine the comprehensive evaluation layer of ecological environment quality of rural tourism area [12]. Thirdly, according to the analogy standard, the progressive relationship between each element evaluation layer and comprehensive evaluation layer is scientifically constructed. Finally, based on the relevant national standards and industry norms, the factor evaluation layer is screened and the evaluation system is constructed.

(2) Ecological environment quality evaluation index system constructions. An indicator system is defined as a structured system that comprehensively reflects the "signs" of various aspects of things, and has three functions: first, to describe and reflect the level or status of development of various aspects at any point in time and within a period; second, to evaluate and monitor the trend of development of various aspects; third, it is a comprehensive measure of the characteristics of each aspect through the summary of the status of each aspect [13]. There are two methods to construct the index system, the first is the itemized statistical method, which specifies the development criteria for the current level of each element and evaluates the distance between the current level and the criteria, and the other method is to construct a system of quantitative criteria. In this case, the uniqueness of the development criteria is clarified, the distance between the current status quo level and the criteria is determined through a quantitative system, and the status quo and development are evaluated separately.

In this paper, the entropy method is used to assign indicators. The entropy method is a commonly used, which has been widely accepted and recognized by experts and scholars in environmental science, socio-economics, and other fields. The entropy method comes from information theory, which uses information entropy to characterize the degree of system disorder, and the amount of information provided by the indicator value determines the assignment result [14]. Because of this feature, entropy value is also often used in statistics to determine the degree of data dispersion, and in general, the degree of dispersion of an indicator determines the weighting [15]. The entropy value method can well reflect the utility value of data information entropy, and the calculated results are more credible than those from the hierarchical analysis method. Assuming that the multi-attribute evaluation matrix H with m evaluation indicators and n objects is as follows.

$$H = \begin{bmatrix} P_{11} & P_{12} & P_{1n} \\ P_{21} & P_{22} & P_{2\mathrm{n}} \\ P_{m1} & P_{m2} & P_{mn} \end{bmatrix} \quad (1)$$

Data normalization. The matrix H is normalized to obtain the new matrix F. For the indicators with positive evaluation benefits, the calculation is done according to equation (2):

$$F_{mn} = \frac{P_{mn} - \min(P_{mn})}{\left|\max(P_{mn}) - \min(P_{mn})\right|} \quad (2)$$

For indicators with negative evaluation benefits, the calculation is done according to equation (3).

$$F_{mn} = \frac{\max(P_{mn}) - P_{mn}}{\left|\max(P_{mn}) - \min(P_{mn})\right|} \quad (3)$$

Based on the above equation, the normalization matrix is obtained as follows.

$$F = f(mn) * \lambda * f_{mn}, m \subseteq [1, m], n \subseteq [1, n] \quad (4)$$

Calculate the contribution of the m-th scenario in the n-th attribute.

$$H_{mn} = f_{mn} \Big/ \sum_{1}^{m}\sum_{1}^{n} f_m * f_n \quad (5)$$

Calculate the entropy value of the m-th indicator, where β=1/log2n.

$$B_n \subseteq [0,1], \sum_{1}^{n} b_n \subseteq [0,1] \quad (6)$$

$$A_m = \beta \log_2 H_{mn} \sum_{1}^{m}\sum_{1}^{n} h_m * h_n \quad (7)$$

The indicator weights are calculated as in equation (8), where

$$B_n = \lambda * \frac{\sqrt{1 - A_m}}{\left| \sum_{1}^{m} A_m - \sum_{1}^{n} A_n \right|} \quad (8)$$

Through the hierarchical analysis method, a hierarchical structure model is established to construct a judgment matrix. We determine the weights of indicators at each level, carry out the hierarchical single ranking and its consistency check respectively, and finally carry out the hierarchical total ranking consistency check to verify its rationality (Figure 1). Firstly, the index set and evaluation set of the evaluated object are determined. Then the weights of each factor and their affiliation degrees are determined respectively, to obtain the fuzzy judgment matrix. Finally, the fuzzy operation on each vector is performed and its normalization is processed to obtain the fuzzy comprehensive evaluation results.

(3) Motion intelligent detection system design implementations. An accurate and reasonably comprehensive evaluation requires a scientific evaluation index system, so it is especially important to establish a feasible evaluation index system.The duplication of indicators should be screened scientifically and reasonably [16]. In the initial selection of indicators, this paper selects the two methods of literature reference and theoretical analysis, to obtain the indicator system under comprehensive conditions which is also in line with the connotation of ecological quality and relevant theoretical basis. Finally, combining with the actual situation of rural tourism area, the initial selection of indicators is revised to obtain the initial selection of indicator system.

In this paper, the ecological environment quality evaluation of rural tourism area is divided into five evaluation levels: the comprehensive score of ecological environment quality evaluation is ≥90 for the fifth-grade quality evaluation; 70~89 for the fourth-grade quality evaluation; 50~69 for the third-grade quality evaluation; 30~49 for the second-grade quality evaluation; 20~29 for the first-grade quality evaluation; ≤20 for the unearned quality evaluation [17]. The ecological environment quality evaluation is also divided into three different levels of quality: ordinary level ecological environment quality, excellent level ecological environment quality, and special level ecological environment quality (Table 2).

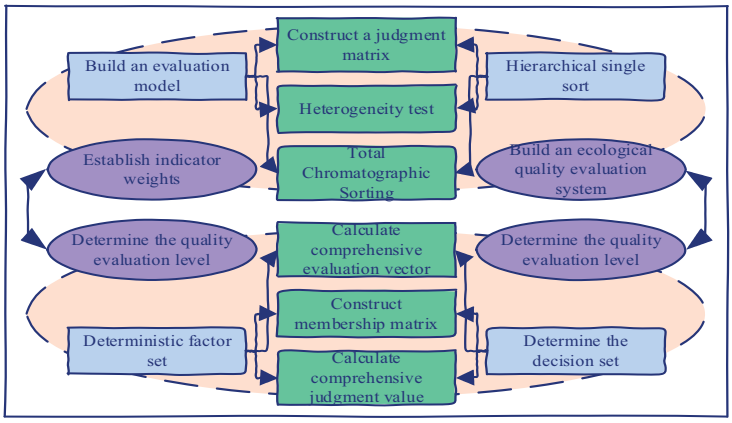


FIGURE 1
Determination of indicator weights and quality evaluation levels.

TABLE 2
Ecological environment quality evaluation grade standard of rural tourism area

Evaluation type	Evaluation grade	Evaluation score	Evaluation grade
Type 1	Level 5	≥90	Good grade
Type 2	Level 4	70~89	Good grade
Type 3	Level 3	50~69	Good grade
Type 4	Level 2	30~49	Ordinary
Type 5	Level 1	20~29	Ordinary
Type 6	Unrated	≤20	None

TABLE 3
Preliminary discrete information table for ecological quality evaluation

	A1	A2	A3	A4	A5
M1	2	3	1	1	2
M2	3	2	2	3	1
M3	3	3	1	2	2
M4	1	2	1	3	2
M5	2	1	3	2	1

The data of the established evaluation information table were discredited using the k-means algorithm commonly used in rough set calculations, which transformed the knowledge base of continuous attributes into a decision table. The sample data are imported into SPSS software for processing. Since SPSS software comes with a standardization function, there is no need to standardize the index data intentionally [18]. The sample data were discrete categorized according to the k-means algorithm, and the data were discredited using k-means of SPSS software. The standardized data were imported into the software according to classification. And the indicators divided by each criterion layer were obtained separately from the data discretization information table [19]. According to the discretization processing method, the preliminary discretization of ecological environment quality evaluation is shown in Table 3.

RESULTS

(1) Statistical analysis of ecological environment quality. In the design of the questionnaire, the options were categorized according to a five-level scale: extremely important, important, average, unimportant, and extremely unimportant whose scores were 5, 4, 3, 2, and 1, respectively, or extremely good, good, average, bad, and extremely bad whose scores were 5, 4, 3, 2, and 1, respectively. For statistical purposes, the larger of the score is more important or better. The evaluation is based on the data obtained from the survey. The importance and performance averages of the 40 evaluation indicators were calculated separately (Figure 2). The natural environment of rural tourism areas at the beginning of development is superior and well received by tourists, but in the process of development, and even at the more mature stage of development, the natural environment gradually changes qualitatively due to the development and use of rural tourism or the influx of tourists. The quality of the natural environment will be lower than at the beginning of the development, which is a major problem that needs attention in the development of rural tourism.

In this study, the questionnaire information was collated and analyzed using SPSS statistical software, and the mean and plural percentages of the importance of each indicator were used as the basis for judging their importance, and the plural percentages and the magnitude of the coefficient of variation were used as the basis for judging the concentration of expert opinions. The statistical results are shown in Figure 3. After analysis, there are 33 indicators with coefficients of variation between 0-0.315 for each indicator, which are consistent. Referring to the opinions of experts, all of them will be retained. It is found that the indicator waterfront greenery richness, whose plural and mean values are larger, will be retained after professional discussion. Finally, the optimization indicator service reception facilities perfect degree and the perfect degree of tourism facilities will be integrated and modified as the perfect degree of tourism service facilities.

In general, there is still room for improvement in the quality level of management and services in rural tourism areas. The quality of environmental hygiene in rural tourism areas needs to be maintained and improved by rural tourism areas and tourists together. The rural tourism area should strengthen the relevant management, standardize the hygiene behavior of the businesses in the area, and establish a certain reward and punishment system to maintain the environmental health of the rural tourism area. At the same time, the cleaning and processing of garbage generated by tourism activities can be targeted to solve [20]. In the clean-up of garbage, the number of staff can be increased to make garbage timely processing. In the treatment of garbage, we should follow the principle of classification and recycling, and strive to establish a scientific and reasonable garbage disposal system, so as not to cause pollution to the ecological environment. Of course, as the civilized quality of domestic tourists is not high, in this regard, rural tourism areas should strengthen guidance and persuasion, establish a civilized and hygienic image or establish a certain reward and punishment system to improve the environmental protection awareness of tourists. The quality of environmental hygiene is related to the service quality of rural tourist areas, moreover, it is a performance of civilized behavior and environmental awareness improvement. Only the two-pronged approach of scenic spots and tourists can protect and maintain the quality of environmental hygiene on one side.

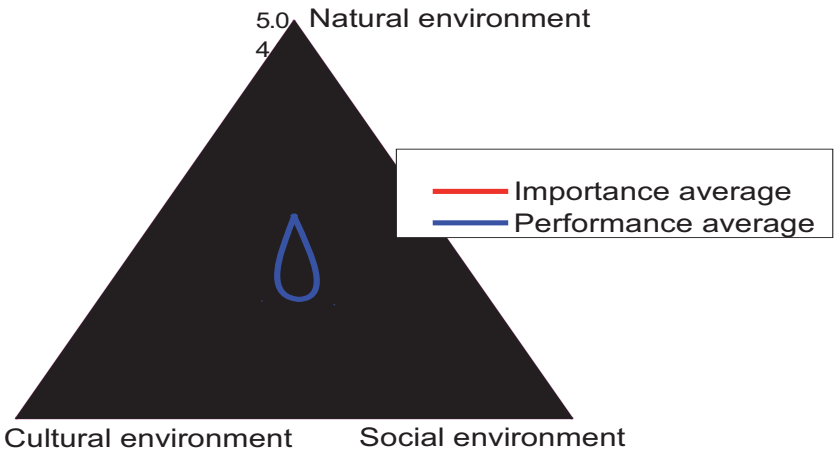


FIGURE 2
Statistical results of evaluation indicators.

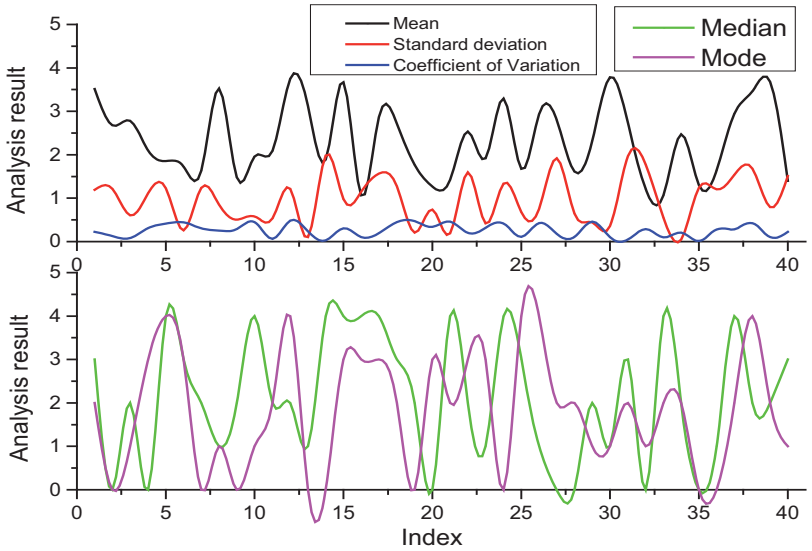


FIGURE 3
The judgment of the importance of evaluation indicators.

(2) Ecological environment quality evaluation analyses. Since the geography and landscape of rural tourism areas are complex and varied, this study selects different rural tourism areas as evaluation units based on various zoning methods and divides rural tourism areas into three specific areas for evaluation according to different ecological environments. The economic development and ecological environment quality construction of the three regions show their different characteristics due to their different locations, topography, and natural environment.

As can be seen from Figure 4, the scores of the economic environmental quality subsystem of rural tourism zones 1, 2, 3, 4, and 5 in 2020 are 0.9132, 0.9246, 0.9151, 0.9821, and 0.9214, respectively, which are 8.34%, 16.14%, 14.29%, 28.33%, and 41.64% higher compared to 2016. From 2016-2020, the economic environmental quality of the studied rural tourism areas all improved. The increase in rural tourism areas 1, 2, and 3 being slower compared to the other 2 areas, the economic environmental quality of rural tourism area 4 also improved very significantly compared to 2016, and the increase in rural tourism area 5 was the most significant in the study, far exceeding the other rural tourism areas. In terms of the natural environment quality subsystem, rural tourism areas 1, 2, 3, 4, and 5 have scores of 0.8955, 0.9124, 0.9169, 0.9017, and 0.8452 in 2020, respectively, with the four fetches of rural tourism areas 1, 2, 3, and 4 improving their natural environment quality compared to 2016 by 4.97%, 4.1%, 11.15%, and 6.96%, respectively. This shows that rural tourism area 3 has made more efforts to build the natural environment quality during 2016-2020, while rural tourism area 5 has decreased by 5.97% compared to 2016 natural environment quality, which means that rural tourism area 5 needs to be improved on the side of natural environment quality. Comparing the social environment quality in 2016, these five areas have 12.41%, 7.58%, 18.35%, 37.48% and 19.57% improvement in 2020, especially rural tourism area 4 has made a very great effort in social environmental quality.

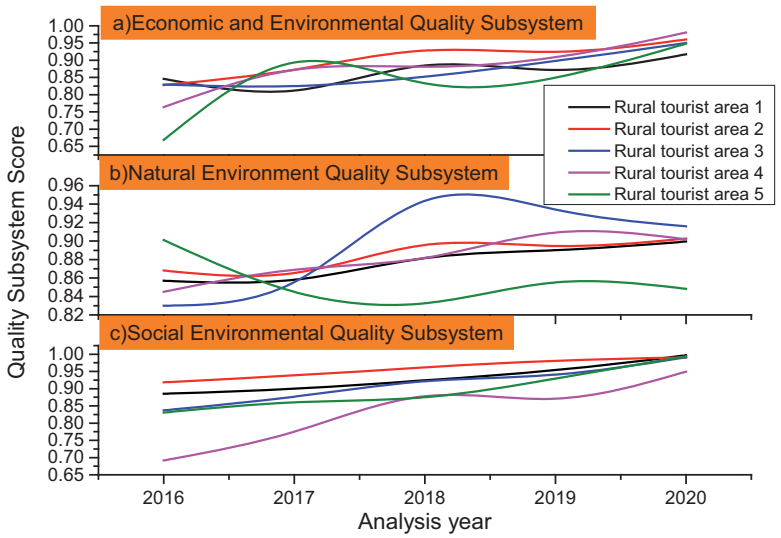


FIGURE 4
Ecological environment quality score of rural tourism area.

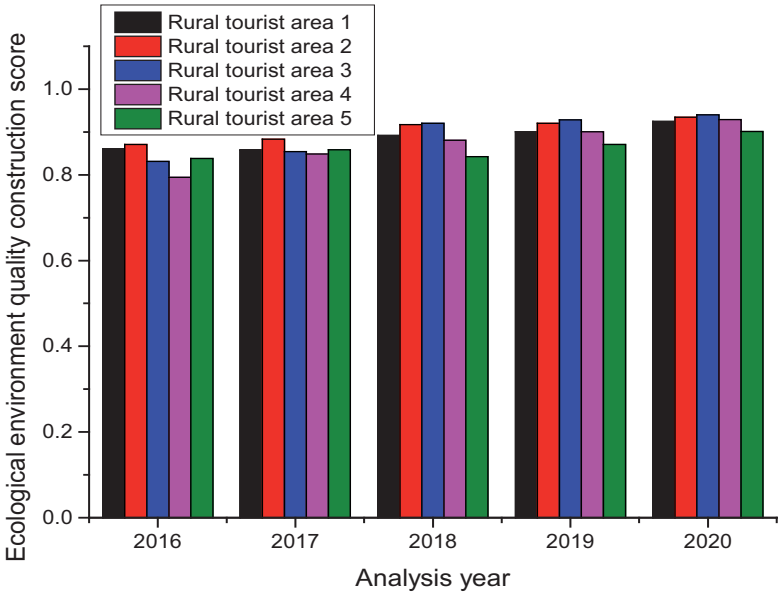


FIGURE 5
Level of ecological quality construction.

From Figure 5, we can see that the ecological environment quality construction of rural tourism areas 3 and 4 in 2016 is in a relatively backward state in the studied area, but from 2017 to 2020, the two areas of rural tourism areas 3 and 4 have very significant progress and improvement in the ecological environment quality construction. The ecological environment quality construction of rural tourism areas 1 and 2 has been rising gently from 2016-2020, and the ecological environment quality construction of rural tourism area 5 has improved slightly in 2017 but dropped significantly in 2018. After that, it improved year by year from 2018-2020. It can be seen that the ecological environment quality construction level from 2016-2020 in the studied area has been significantly improved, and the ecological environment quality construction score increases year by year, indicating that the ecological environment quality construction has achieved significant results in the past 5 years.

(3) Motion detection analyses. The statistical software SPSS was used to analyze the 40 index factors in the whole index system. The eigenvalues and contribution rates of the index factors were obtained from the principal component analysis, which is shown in Figure 6, and according to the principle that the eigenvalue is greater than 2 and the corresponding cumulative contribution rate is more than 86.24%, the first two principal components meet the requirements, the first principal component eigenvalue is 26.183, the second principal component eigenvalue is 2.16, and the cumulative contribution rate is 94.12.

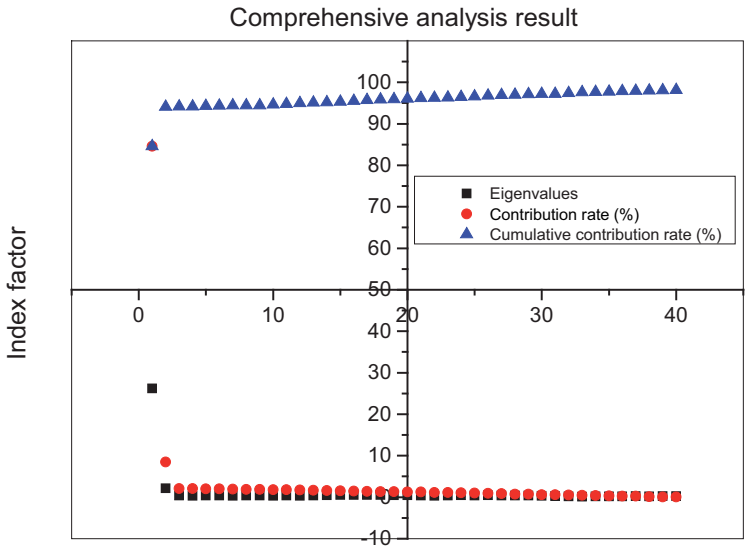


FIGURE 6
Principal component analysis eigenvalues and contribution rates.

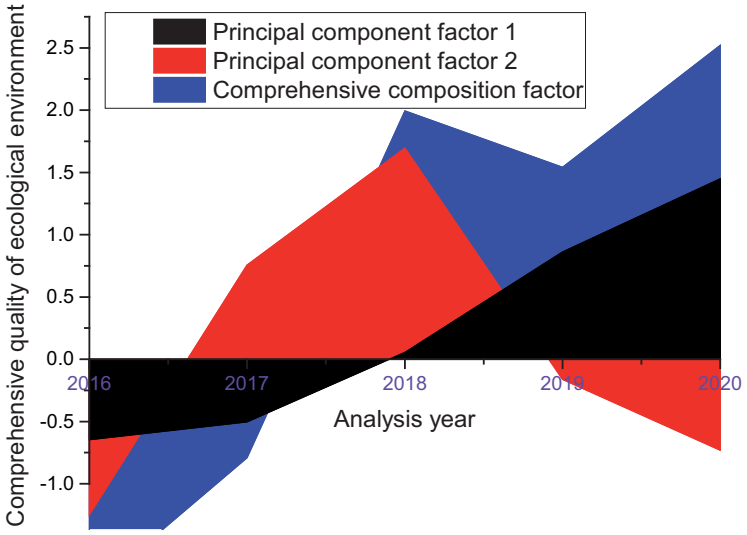


FIGURE 7
Principal component factors and composite factor scores.

The trend of changes in the comprehensive quality of the ecological environment in rural tourism areas is shown in Figure 7. From 2016 to 2020 the comprehensive score of ecological environment quality of Dan rural tourism area continues to rise, showing a good development trend. However, there are certain fluctuations in the scores of the first principal component and the second principal component, the first principal component in 2016 to 2018 shows a decline, and then shows the slow growth during 2018-2019. The second principal component increased rapidly from 2016 to 2018 and decreased significantly from 2018 to 20120. This shows that the quality of the ecological environment is generally good, but it is still unstable and needs to be continuously strengthened and improved.

According to the results of principal component analysis, the ecological environment of rural tourism area has a good development trend, but the foundation is weak, the ecological environment quality level is still low. The ecological protection, town greening construction, science, and education as well as social security and other aspects need to be optimized and improved [21]. Because of the actual situation of ecological environment construction in rural tourism areas, countermeasures and suggestions are put forward for the existing problems. In recent years, the rural tourism area has seen rapid socio-economic development, and the town has been expanding with a new look. The economic development brought the destruction of the ecological environment. In response to this problem, effective measures should be taken to protect mountains and forests, strengthen afforestation, protection, and restoration of mountains and farmland, adhere to the principle of protection first, and implement ecologi-

cal engineering construction [22]. We need to optimize the layout of urban land and reduce the encroachment on arable land and forest land. In addition, we need to strengthen arable protection, improve the quality of arable land, focus on the protection of the red line of arable land. What's more, we must strengthen the protection of forest resources and biodiversity, reduce the impact of human activities on ecology, establish and improve the system of environmental information publication, vigorously implement ecological creation projects, and gradually build several ecological civilization demonstration parks and villages.

The main body of management of eco-tourism scenic spots in rural tourist areas mainly involves eco-tourism resources, tourism developers, tourism operators, etc. For the management of ecotourism resources in rural tourist areas, we must adhere to the management principles of protection first and development equally, pay attention to the original protection of hot spring resources, delimit core areas, and scientifically select development areas. We must develop ecotourism resources while protecting the resource in the development process to achieve sustainable utilization. For the management of tourism developers in rural tourist areas, it is necessary to implement the management strategy of planning first and long-term planning. In terms of the development and planning of tourism resources, the design and planning of tourism routes, and the marketing planning of tourism products, it is necessary to adhere to local conditions, harmony between people and land, and nature. The concept of the unity of human beings enhances the comprehensive benefits of tourism development and minimizes the negative impact of tourism development on ecological resources and the ecological environment. For the management of ecological operators in rural tourist areas, it is necessary to adhere to the people-oriented and service-oriented management philosophy. It is necessary to formulate relevant management strategies based on the characteristics of ecological tourism development, cultivate and build a professional management team, strengthen the management quality process, and improve the efficiency of management functions. At the same time, tourism operators need to design tourism routes and update tourism products according to the actual conditions of the tourism area, and continuously improve the experience of eco-tourists, and ensure that the tourism resources of the scenic area are not damaged and the tourism operation activities are carried out normally.

CONCLUSIONS

(1) Based on the review of literature research, this paper determines the index screening principles and index screening sources of ecological environment quality evaluation system of rural tourism area and constructs a comprehensive evaluation layer of ecological environment quality of rural tourism area from four research dimensions, such as construction conditions of rural tourism area, ecological environment conditions, ecological tourism resources conditions and tourism capacity conditions, based on the research subject and its scientific connotation. At the same time, the article identifies the indicators of industrial form, beautiful environment, facilities and services, ecological environment quality, ecological environment protection, resource element value, and resource influence according to national standards, analogous standards, and normative documents to build the element evaluation layer. Finally, the article determines 40 specific evaluation indexes according to the hierarchical structure progression relationship, and initially establishes an evaluation index system with the characteristics of rural tourism area which is also in line with the ecological environment quality evaluation standards.

(2) The article adopts the fuzzy mathematical four-point scoring method to design the evaluation questionnaire and calculates the final score by combining the index weights determined by the hierarchical analysis method in the previous paper, which is calculated in a bottom-up calculation order, that is, the fuzzy comprehensive evaluation of ecological environment quality of rural tourism area according to 40 specific factor evaluation indexes, and the comprehensive score of the valid questionnaire is calculated by using the fuzzy comprehensive evaluation method. The scores of factor evaluation layer are calculated according to the weights in the previous section, and the scores of factor evaluation layer and comprehensive evaluation layer are calculated according to the weights in the previous section, and finally the scores of comprehensive evaluation layer are added to calculate the comprehensive score of ecological environment quality of rural tourism area, and the grade of ecological environment quality of rural tourism area is determined according to the evaluation grade standard.

(3) This paper actively draws on relevant standards and research results to innovate the research content, fully considers the conditions of rural tourism areas, ecological environment conditions, ecological environment quality, and tourism capacity conditions. However, for the systematic selection of specific evaluation indicators, further optimization is still needed. In terms of evaluation methods, this paper mainly selects more mature and reliable research methods such as hierarchical analysis method, expert questionnaire survey method, and fuzzy comprehensive evaluation method for quantitative research, which ensures the credibility of the model and data. The empirical analysis of ecological environment quality for rural tourism areas in different regions still needs further research.

ACKNOWLEDGEMENTS

This work was supported by the research on targeted poverty alleviation in Dabie Mountain Area from the perspective of global tourism (202015104).

REFERENCES

[1] Nip, M.J., Haes, H. (1995) Ecosystem approaches to environmental quality assessment. Environmental Management. 19(1), 135-145.
[2] Steube, C., Richter, S., Griebler, C. (2009) First attempts towards an integrative concept for the ecological assessment of groundwater ecosystems. Hydrogeology Journal. 17(1), 23-35.
[3] Liu, W.X., Coveney, R.M., Chen, J.L. (2003) Environmental quality assessment on a river system polluted by mining activities. Applied Geochemistry. 18(5), 749-764.
[4] Salas, F., Marcos, C., Neto, J.M., Patricio, J., Perez-Ruzafa, A., Marques, J.C. (2006) User-friendly guide for using benthic ecological indicators in coastal and marine quality assessment. Ocean & Coastal Management. 49(5/6), 308-331.
[5] Atique, U., Iqbal, S., Khan, N., Qazi, B., Sherzada, S. (2020) Multivariate assessment of water chemistry and metals in a river impacted by tanning industry. Fresen. Environ. Bull. 29(4A), 3013-3025.
[6] Blocksom, K.A., Johnson, B.R. (2009) Development of a regional macroinvertebrate index for large river bioassessment. Ecological Indicators. 9(2), 313-328.
[7] Simaika, J.P., Samways, M.J. (2011) Comparative assessment of indices of freshwater habitat conditions using different invertebrate taxon sets. Ecological Indicators. 11(2), 370-378.
[8] Wu, B., Rui, Z., Cheng, S.P., Ford, T., Zhang, X.X. (2011) Risk assessment of polycyclic aromatic hydrocarbons in aquatic ecosystems. Ecotoxicology. 20(5), 1124-1130.
[9] Innes, J.P., Pascoe, S. (2010) A multi-criteria assessment of fishing gear impacts in demersal fisheries. Journal of Environmental Management. 91(4), 932-939.
[10] Harris, J.H. (1995) The use of fish in ecological assessments. Australian Journal of Ecology. 20(1), 65-80.
[11] Hua, Z., Dai, B., Li, G., Chu, K., Li, Y. (2011) Offshore ecosystem health assessment: a case study of Jiangsu offshore area, China. Fresen. Environ. Bull. 20(7), 1598-1610.
[12] Schultink, G. (2000) Critical environmental indicators: performance indices and assessment models for sustainable rural development planning. Ecological Modelling. 130(1-3), 47-58.
[13] Su, L., Liu, J., Christensen, P. (2011) Spatial distribution and ecological risk assessment of metals in sediments of Baiyangdian wetland ecosystem. Ecotoxicology. 20(5), 1107-1116.
[14] Kalashnik, N.A. (2008) Chromosome aberrations as indicator of technogenic impact on conifer stands. Russian Journal of Ecology. 39(4), 261-271.
[15] Thapa, B., Pant, R.R., Thakuri, S., Pond, G. (2020) Assessment of spring water quality in Jhimruk River Watershed, Lesser Himalaya, Nepal. Environmental Earth Sciences. 79(22), 1-14.
[16] Convery, J.J. (1994) Challenges to environmental engineers. Waste Management. 14(8), 661-670.
[17] Baas, J., Kooijman, B. (2010) Chemical contamination and the ecological quality of surface water. Environmental Pollution. 158(5), 1603-1607.
[18] Muthu, S.S., Li, Y., Hu, J.Y., Mok, P.Y. (2012) Quantification of environmental impact and ecological sustainability for textile fibres. Ecological Indicators. 13(1), 66-74.
[19] Duian, L. (2017) Comparative assessment of heavy metals in agricultural soils under different land uses: a case study from China. Fresen. Environ. Bull. 26(8), 5323-5330.
[20] Terzopoulou, E., Voutsa, D. (2015) Quality assessment of surface water at the basin of Strymonas River, Northern Greece. Fresen. Environ. Bull. 24(12C), 4771-4782.
[21] Sun, Q., Liu, Z. (2020) Impact of tourism activities on water pollution in the West Lake Basin (Hangzhou, China). Open Geosciences. 12(1), 1302-1308.
[22] Pu, J., Zhao, X., Miao, P., Li, S., Tang, W. (2020) Integrating multisource RS data and GIS techniques to assist the evaluation of resource-environment carrying capacity in karst mountainous area. Journal of Mountain Science. 17(10), 2528–2547.

Received: **28.03.2021**
Accepted: **01.03.2021**

CORRESPONDING AUTHOR

Jing Yu
School of Commercial,
HuangGang Normal University,
Huanggang Hubei 438000 – China

e-mail: yujing110803@163.com

© by PSP Volume 30– No. 09/2021 pages 10748-10753 Fresenius Environmental Bulletin

NUMERICAL SIMULATION OF VORTEX DRAINAGE GAS RECOVERY BASED ON ORTHOGONAL EXPERIMENT

Jingming Yang[1], Siyang Li[2,*], Yueqi Zhang[3], Hao Liu[4], Yuhui Zhou[1]

[1]School of Petroleum Engineering, Yangtze University, Wuhan 430000, China
[2]Changqing Drilling Company, CNPC Chuanqing Drilling Engineering Company Limited, Xi'an 710016, China
[3]Changqing Oilfield Company, PetroChina, Xi'an 710016, China
[4]Operation Zone of Jiqing Oilfield, Xinjiang Oilfield, PetroChina, Jimsar 831700, China

ABSTRACT

The phenomenon of liquid loading accumulation will affect the normal production of gas wells, shorten the production cycle and even stop production. The drainage and gas production technology with eddy current tools can effectively solve the problem of gas well fluid accumulation. In order to make the eddy current tool work efficiently and normally, it is necessary to analyze the influencing factors reasonably. Taking X gas well in Sulige gas field as an example, combined with the practical application in the field, taking the four factors of spiral wing height, wing width, spiral flange number and rotating fluid diameter as the research object, the influence of various factors on drainage and gas production effect is analyzed and evaluated by Fluent fluid simulation software, which can guide and apply to the field practice.

KEYWORDS:
Liquid loading, Eddy current tool, Orthogonal experiment, Fluent, Gas field

INTRODUCTION

In the process of shale gas production, the problem of liquid accumulation in gas wells is common in the process of gas well development. Selecting effective drainage gas production technology is the key to prolong the production cycle and enhance oil recovery [1]. Eddy current drainage gas production technology is a new drainage gas production process. When the irregular gas-liquid two-phase turbulent fluid enters the eddy current tool, the acceleration makes the heavy liquid swing to the pipe wall, and the fluid moves upward along the tool, which turns into a regular spiral two-phase laminar flow. Thus, the gas well drainage capacity is improved and the tubing pressure loss is reduced [2-3]. In recent years, the domestic research on eddy current tools is gradually deepening. Li Jun et al. [4] made in-depth research on the internal structure and size of eddy current tool by using fluent commercial software, which laid the foundation for the future eddy current numerical simulation research. Fengcuiju et al. [5] studied the factors influencing the construction effect of the drainage and gas production process of eddy current tools in gas reservoir, The results show that the drainage effect of vortex tools is positively correlated with the volume fraction of liquid, but when the volume fraction of liquid is less than 10%, the drainage effect is not obvious. Xu Jianning et al. [6] analyzed the influencing factors of vortex drainage gas recovery based on orthogonal test, five factors (air velocity, water content, helix angle, diameter of swirling fluid and wing height of swirling body) are selected in the orthogonal test, and the analysis of influencing factors of swirling tool is not comprehensive enough. This paper starts with the influencing factors of eddy current tools, analyzes the main factors of the effect of the vortex tool production, selects the factors that have not been studied and not fully studied, the factors selected are divided into different levels by orthogonal test table, and then the screening analysis is carried out. The results of eddy current tools are evaluated by fluent, and the optimal size structure combination is obtained.

MATERIALS AND METHODS

Working principle of eddy current tool. The key component of eddy current tool is swirling fluid, the swirling fluid consists of two parts: a solid cylinder and a protruding spiral wing fixed on the outside of the cylinder, the reason why it is called the key core component is that it can change the flow pattern of the gas-liquid two-phase fluid entering the vortex tool through the annulus between the swirling fluid and the tubing (Figure 1). Thus, it can change the direction of fluid movement, increase the flow velocity and transform the gas-liquid two-phase turbulent flow into spiral flow [7].

Its working principle is to separate the fluid medium flowing into the solid cylinder and the oil pipe by the spiral guide vane, and make it flow along the spiral guide vane, which is accelerated by the reduction of the flow section. To achieve the purpose of changing the flow path of the mixed fluid medium,

so as to improve the overall flow speed and gas carrying capacity of the fluid medium. According to the theory of fluid mechanics, centrifugal force will be produced after flowing through the spiral guide vane, which can effectively transform the gas-liquid two-phase turbulent flow into spiral orderly flow [8-9]. When the fluid passing through the vortex tool generates centrifugal force due to the existence of swirling fluid, the density of the fluid medium in the pipe decreases gradually from the pipe wall to the pipe center. Eddy current tools can transform various irregular and inefficient turbulent flows such as bubble flow and elastic flow into regular spiral stratified flow, the liquid phase and gas phase flow upward along the pipe wall and near the center of the pipe respectively, thus forming a gas-liquid two-phase swirl in the pipe.

The basic properties of orthogonal table. Orthogonal array has the basic properties of orthogonality, comprehensive comparability and balanced dispersion,Orthogonal array is the basic tool of experimental design, This table is a kind of mathematical table (i.e. orthogonal table) which is generated by combining mathematical theory based on the concept of sample equilibrium distribution. It is a mathematical experimental method evolved from Hadamard matrix and orthogonal Latin square. The core idea of orthogonal table is equilibrium distribution, and the most representative part of the test is used to replace the whole experiment, the analysis of small part of the test results replaces the analysis of all tests, so as to achieve an idea and method to understand all the tests. However, it is precisely because the nature of orthogonal test itself is to replace the whole test with partial test, so it is certainly impossible to make a comprehensive analysis of the influence effect of various factors at all levels, just like the whole test. Although there are some shortcomings in orthogonal experimental design, it can determine the relatively optimal level combination through some experiments.

Determination factors and scheme design. According to the variable structure size of the model and the actual situation, the factors that may affect the drainage and gas recovery effect of the vortex tool are selected, and each factor takes five values. If we comprehensively analyze the influence of these four factors on the vortex tool drainage gas recovery, the experimental design and calculation will be huge. In order to simplify the process, it is the most suitable choice to use orthogonal test method to analyze [10-12].

It is necessary to optimize the orthogonal design, assuming that the parameters of the bottom hole velocity, holdup rate and small droplet diameter are certain, the initialization is carried out in the boundary condition of fluent. Four factors of size and structure are selected, including helix wing height h, helix wing width b, helix diameter D and helix number n (helix length is fixed), as shown in the Table 1.

The numbers of four factors, namely, height h, width b, diameter D and number of spiral rings n, are specified as A, B, C and D respectively. Capital letters are used to represent the corresponding five levels. For example, the structural dimensions of the vortex tool are: helix wing height h is 1 mm, helix wing width B is 2 mm, helix diameter D is 40 mm, and helix number n is 1. Because the experiment is a four factor and five level orthogonal design experiment, according to the standard orthogonal table L25(56), the experimental scheme is designed, and these 25 groups of design schemes are modeled by the proe software described. Draw 3D model of rotating fluid in 25 kinds of eddy current tools with different structural parameters, and some models are shown in the Figure 2.

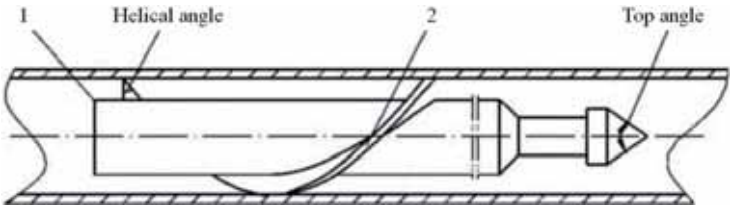


FIGURE 1
Structure diagram of scroll gearbox.

1 - inner column; 2 – blade.

TABLE 1
Values of orthogonal experiment factors.

/	Wing height h/mm	Wing width b/mm	Diameter D/mm	Number of wings n
1 level	1	2	40	1
2 level	3	5	55	5
3 level	2	6	45	3
4 level	1.5	3	35	2
5 level	2.5	4	50	4

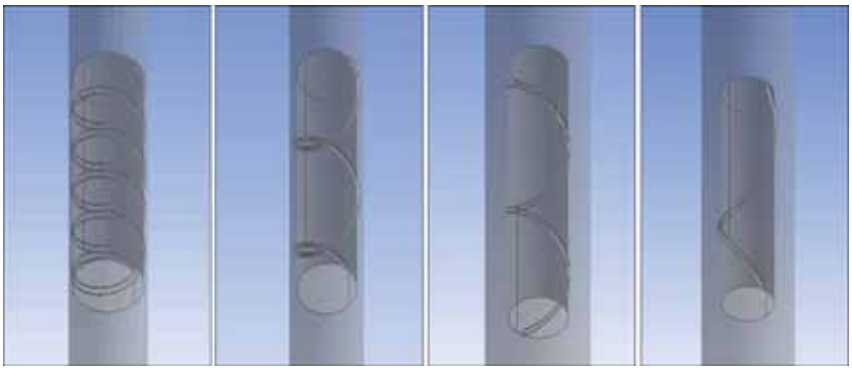


FIGURE 2
3D model of swirling fluid of some eddy tools.

RESULTS

The function of vortex tool is to transform gas-liquid two-phase turbulence into stratified swirling flow, and improve the lifting ability of gas carrying liquid by changing the flow state of fluid. The change of pressure drops and liquid holdup is the main basis to evaluate the effect of gas-liquid cyclone separation, so it is selected as the evaluation index of this orthogonal experiment [7, 13].

These 25 sets of design schemes are modeled by the proe software introduced, and the 3D models of swirling fluid in 25 kinds of vortex tools with different structural parameters are drawn, the 25 sets of swirling fluid geometric models were placed in the tubing model with an inner diameter of 62mm and a total length of 1500mm to simulate the basin. In combination with the production data of Sulige gas field, Under the production condition, the oil pressure changes in the range of 1MPa~3.5MPa. The wellhead oil pressure is 3.2MPa. According to the field measured data, the pressure at 3500 meters underground is about 9.4 MPa, the casing pressure changes in the range of 4.9MPa~9.8MPa, the average daily gas production of a month is 5996m3. According to the boundary condition, the velocity at the entrance is about 0.33m/s, the volume fraction of liquid phase is 0.00355, the droplet diameter is 0.001mm. Analyze the gas-liquid two-phase flow process, study the liquid drainage effect of these 25 groups of vortex tools, and compare the liquid holdup difference between inlet and outlet.

After 25 groups of simulation results are obtained by ANSYS FLUENT software, the difference of liquid holdup between inlet and outlet of tubing model is compared, so as to analyze the drainage effect of each group. 25 groups of orthogonal test schemes and their results are shown in the Table 2.

It can be seen from Figure 2 that the smaller the liquid holdup difference, the better the drainage effect. It is not difficult to see that the liquid holdup difference of No. 10 eddy current tool is the smallest, only 0.0014%, and the drainage effect is the best; The second is No.7 and No.3 vortex tools, the difference of liquid holdup is 0.0061%, and the drainage effect is the second. The worst drainage effect is No.15 vortex tool, the difference of liquid holdup is 1.5732%, followed by No.21, No.13 and No.2 vortex tools, the difference of liquid holdup is more than 1%, indicating that the liquid carrying efficiency is not ideal after use.

The orthogonal test table was analyzed by DOE software [14-15], according to the results of variance analysis in the Table 2, it is not difficult to see that the level change of factor C has a high degree of influence on the experimental design results. That is: the diameter of swirling fluid D has the most significant effect on the drainage effect. Keeping the other three factors (wing height, wing width and number of wing rings) unchanged, another four groups of eddy current tools with different diameters were established by proe and compared with the original No. 10 eddy current tool, The new experiment consists of five sets of eddy current tools. According to the specific model parameters, the images are as Figure 3.

Each eddy current tool model is meshed by mesh and then imported into fluent to define the boundary conditions for numerical simulation. According to the cross section of the volume fraction distribution of the four groups of eddy current tools, it can be seen that the gas-liquid mixture flow has obvious gas-liquid separation after passing through the eddy current tool. In order to more intuitively compare the practical application effect of each group of eddy current tools [16-17]. We compare four groups of liquid volume fraction distribution cross sections at y = 1.4m, as shown in the Figure 4. At the same time, calculate the difference of the liquid holding rate between the inlet and outlet of each oil pipe model, draw the curve diagram of the liquid holding rate of five groups of eddy current tools according to the comparison data of the difference of the holding rate, as shown in Figure 4.

According to the analysis in Figure 4, it is not difficult to see that the liquid holdup difference of gas-liquid two-phase flow before and after passing through No. 10 and No. 29 vortex tools is the smallest, which is 0.0014% and 0.0335% respectively, The maximum difference of liquid holdup before and after 27 eddy current tool is 0.7452%, and the best level combination is 10 eddy current tool, That is to

say, the optimal scheme is: the height of helix wing is 3mm, the width of helix wing is 4mm, the diameter of helix body is 40mm, and the number of helix turns is 5.

TABLE 2
Comparison of orthogonal test scheme and test index.

Test number	Wing height h/mm	Wing width b/mm	Diameter D/mm	Number of wings /n	Liquid holdup difference of test indexes/%
1	1	2	40	1	0.0622
2	1	5	55	5	1.1854
3	1	6	45	3	0.0302
4	1	3	35	2	0.2641
5	1	4	50	4	0.1932
6	3	2	55	3	0.8127
7	3	5	45	2	0.0061
8	3	6	35	4	0.5703
9	3	3	50	1	0.5701
10	3	4	40	5	0.0014
11	2	2	45	4	0.9355
12	2	5	35	1	0.5801
13	2	6	50	5	1.1732
14	2	3	40	3	0.1126
15	2	4	55	2	1.5732
16	1.5	2	35	5	0.6062
17	1.5	5	50	3	0.8415
18	1.5	6	40	2	0.6692
19	1.5	3	55	4	0.1552
20	1.5	4	45	1	0.5741
21	2.5	2	50	2	1.4363
22	2.5	5	40	4	0.2773
23	2.5	6	55	1	0.5223
24	2.5	3	45	5	0.7575
25	2.5	4	35	3	0.2415

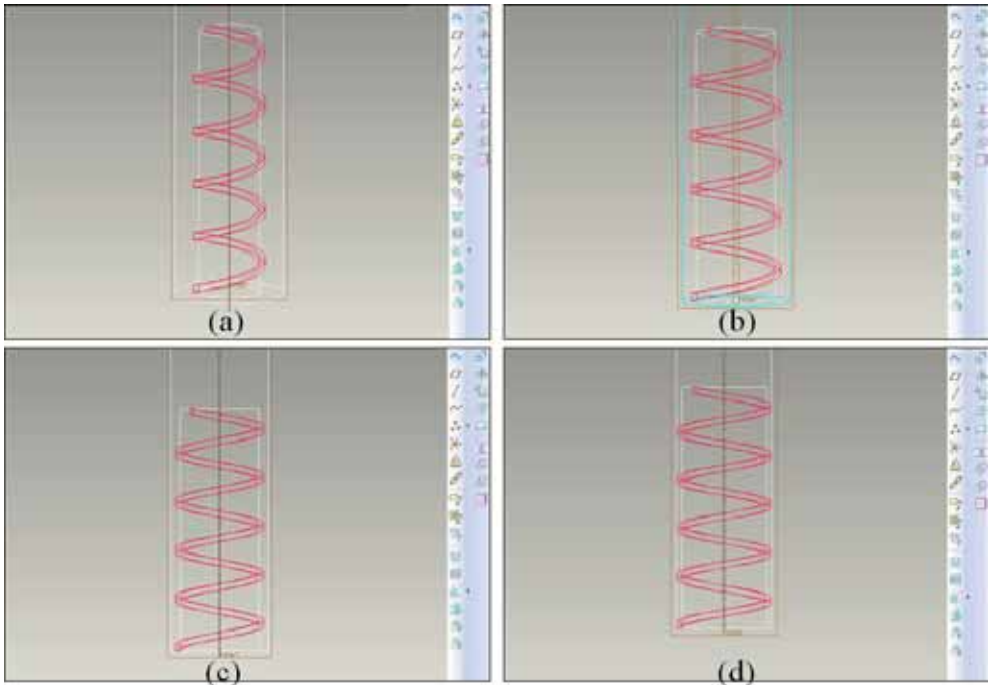


FIGURE 3
Four sets of eddy current tools with different diameters.
(a) The diameter of the rotating fluid is 35mm, (b) The diameter of the rotating fluid is 45mm, (c) The diameter of the rotating fluid is 50mm, (d) The diameter of the rotating fluid is 55mm.

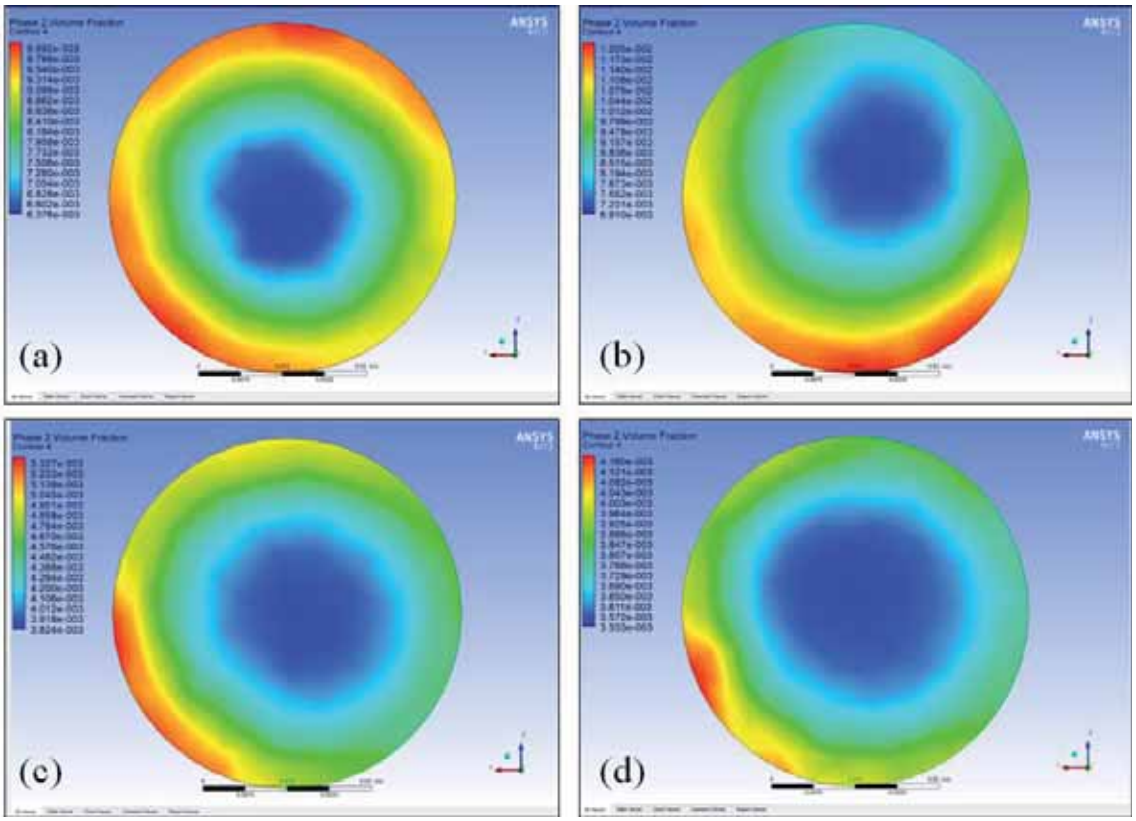


FIGURE 4

Cross section of liquid volume fraction distribution of four sets of eddy current tools at y = 1.4m.

(a) Cross section of vortex tool No.26, (b) Cross section of vortex tool 27, (c) Cross section of vortex tool 28, (d) Cross section of vortex tool 29.

CONCLUSIONS

1. Through 3D modeling, model meshing and numerical simulation of gas-liquid two-phase mixed fluid flow field before and after passing through the eddy tool, by observing the velocity distribution and volume fraction distribution of two-phase fluid before and after passing through the eddy current tool. It is found that the numerical simulation of different specifications of the vortex tool drainage effect is good, can appear obvious gas-liquid separation phenomenon, so as to carry on the orthogonal experiment comparative analysis.

2. The core size of eddy current tool can be calculated accurately by range analysis. Through the variance analysis, the diameter D of swirling fluid in the swirling tool has the most obvious influence on the drainage effect of the whole swirling drainage gas production system, and this factor should be considered more in actual production and processing.

3. By using the standard orthogonal table of six factors and five factors, 25 representative eddy current tool models are simulated. The difference of liquid holdup between the inlet and outlet of the model is selected as the test index, the structure size of the eddy current tool is selected as the four parameters of the orthogonal test, and five levels are selected for each factor. Then, the numerical simulation is carried out by fluent, and the liquid holdup difference of gas-liquid two-phase flow before and after passing through the vortex tool is compared. The optimal size structure combination is determined by analysis: the height of helix wing is 3mm, the width of helix wing is 4mm, the diameter of spiral body is 40mm, and the number of spiral rings is 5.

ACKNOWLEDGEMENTS

This work was not supported by any funds. We would like to show sincere thanks to those techniques who have contributed to this research.

REFERENCES

[1] Yang, T. (2012) New technology and application of vortex drainage gas recovery in gas wells. Natural Gas Industry. 32(8), 63-66.

[2] Yang, X., Wei, Y., Xiao, S., zhao, L. (2013) Exploration and research of downhole vortex tool drainage gas recovery in Sulige gas field. Drilling and Production Technology. 36(6), 125-127.

[3] Zhu, Q., Zhang, J., Xie, F., Liu, Q. (2013) Application of vortex drainage gas production technology in Sichuan gas field. Natural Gas Technology and Economy. 1, 37-39.

[4] Li, J., Li, N., Li, J., Wang, F. (2013) Numerical simulation of vortex drainage gas recovery technology. Oil drilling and Production Technology. 6, 65-68.
[5] Feng, C., Wang, C., Zhang, H. (2013) Analysis of influencing factors on the drainage effect of vortex tools in natural gas wells. Petroleum Machinery. 1, 78-81.
[6] Xu, J., Shao, L., Liang, H., Zhu, D. (2014) Analysis of influencing factors of vortex drainage gas recovery based on orthogonal test. Petroleum Field Machinery. 11, 52-56.
[7] Ren, L., Jia, R., Cao Z., Su, D. (2015) Research progress of influencing factors of fluid discharge effect of downhole eddy current tools. Mechanical Research and Application. 3, 49-51.
[8] Krish, M. (2009) Investigation of Swirl Flows Applied to the Oil and Gas Industry. SPE Projects Facilities & Construction. 4(1), 1-6.
[9] Shao, L. (2015) Research on Optimization Design of vortex tools for low pressure and low production gas wells. Xi'an: Xi'an University of Petroleum (Thesis). 32-38.
[10] Dougherty, G., Fehn, B., Smith, T. (2007) Apparatus and method for creating a vortex flow: US. US. 7160024 B2.
[11] Li, P., Xu, M., Wang, F. (2011) Proficient in CFD engineering simulation and case practice. People's Posts and Telecommunications Press, Beijing. 48-51.
[12] Zhang, Y., Liu, D., Han, L. (2019) Experimental Study on the Influence of Loading Rates on Kaiser Effect of Different Lithologic Rocks for In-situ Stress Determination During Oil & Gas Exploration. Fresen. Environ. Bull. 28(12), 9495-9502.
[13] Zhi, Y. (2017) Research and application of agent model for oilfield production optimization based on DOE method. Yangtze University, Faculty, Wuhan.
[14] Huang, B., Li, X., Fu, C., Wang, Y., Cheng, H. (2019) The mechanism of drainage gas recovery and structure optimization of an internal vortex tool in a horizontal well. Journal of Natural Gas Science and Engineering. 67, 233-241.
[15] Chao, Z., Xw, B., Tz, A., Xu, Z., Sg, C., Hu, B. (2019) Dynamic analysis for two-phase vortex flow and optimization of vortex tools to unload liquid from gas wells - sciencedirect. Journal of Petroleum Science and Engineering. 173, 965-974.
[16] Du, J., Li, K., Yu, X., Li, X., Liu, Y., Zhang, Z. (2020) A new method for gas well liquid accumulation predicting based on convolutional neural network environment. Fresen. Environ. Bull. 29(7), 5487-5496.
[17] Wu, X., Zhou, C., An, Y., Liu, X., Cen, X. (2016) Dynamic analysis of a liquid droplet and optimization of helical angles for vortex drainage gas recovery. Natural Gas Industry B. 3(4), 339-345.

Received: **19.03.2021**
Accepted: **25.05.2021**

CORRESPONDING AUTHOR

Siyang Li
Changqing Drilling Company
CNPC Chuanqing Drilling Engineering Company Limited
Xi'an 710016 – China

e-mail: lisiy1016@126.com

© by PSP Volume 30– No. 09/2021 pages 10754-10762 Fresenius Environmental Bulletin

FISHEYE IMAGING APPROACH WITH THE SUPERVISED MACHINE LEARNING FOR THE DETERMINATION OF FRESHNESS OF FISH

Hamza Feza Carlak[1,*], Kemal Kandemir[1], Mustafa Unlusayin[2]

[1]Electrical and Electronics Engineering, Akdeniz University, Antalya, 07058, Turkey
[2]Faculty of Fisheries, Akdeniz University, Antalya, 07058, Turkey

ABSTRACT

One of the most important selective specification in determining the quality of fish is its freshness. In this study, the fast and sensitive alternative technique is proposed as the fish freshness detection. 120 different images of 20 red mullet fish images were taken with an interval of 8 hours in two days. The segmentation of fisheyes according to a fully automatic computerized vision was acquired from the digital images of fish samples. Three different methods have been proposed to identify the fish freshness after the segmentation process. The first method is the local binary pattern (LBP) method. The distance between histograms obtained by this method was examined and compared with Chi-Square Divergence, Kullback-Leibler Divergence, and Correlation methods. Next, the discrete wavelet transform was performed. The energy densities of these wavelet transforms were investigated. The data obtained from these methods provide a strategic framework for the assessment of fish freshness. Then, the histograms obtained from the LBP method were educated with supervised machine learning. As a result of the tests, the freshness situation of 18 fish was determined within 20 red mullet fish.

KEYWORDS:
Fish freshness, image processing, local binary pattern, wavelet transform, machine learning

INTRODUCTION

The freshness of the fish can be measured by sensory, physical, chemical, and microbiological methods [1]. One or more of these methods can be used for freshness control. Sensory evaluation of fish products will always be critical in terms of quality. Chemical tests may be widely used when it is as efficient and cost-effective as sensory testing [2]. Sensory evaluation in the fish industry is currently the most important method for freshness. Sensory analysis of fish and fish products to determine the quality level in the production and marketing process is a parameter widely used by the government or industry [3], [4]. Sensory methods are still important in evaluating the freshness of fish and fishery products, considering all the developments in the analysis methods in recent years [5]. They are the most commonly used methods for the sensory testing of seafood. These are based on the specific properties of fish (skin, eyes, gills, tissue, etc.) and quality assessment of fish in the entire fish industry [6]. After the mortality, some sensory changes occur in the smell, appearance, taste, and texture of the fish. Post-mortem change in fish shows three stages, such as death stiffness, autolysis, and putrefaction [7]. These events follow each other. However, they cannot be separated from each other by precise lines. The type, age, and sex of the fish can be effective in this change process, as well as the form of fishing, catching season, temperature, method of death, the hygienic structure of catching equipment, and the post-mortem procedures are also highly effective. In sensory analyses, decisions made by individuals may show differences. Different parts of a fish are examined in the sensory analysis. One of them is the fisheye [8]. For example, the eyes of fresh fish are transparent and bright. As the fish lose their freshness, the eyes become dull and lose their brightness. Blood is seen around. However, this blood should not be confused with the one created by hitting the nets while catching a fish. As the fish loses water during staling, tissue fragments detached from the pupil increase the viscosity of the eye fluid, and the optical fracture of the eye fluid increases. This method may be applicable to most of the fish species.

Color change in various regions of food samples can be considered as an essential parameter in determining food quality. The colorimetric technique can be used as a decisive feature in the grading of freshness of a fish [9]. Although some of the studies have been carried out to assess fish freshness, there is still a need to develop systems that analyze image freshness and machine learning-based fish freshness [10]. Image processing applications had been reported in the food processing sector. Wang et al. applied a fisheye regression model for freshness control [11]. Regression Modelling and the relationship between the change of energy of the image and the

value (pH, electrical conductivity, TVBN) were analyzed. In Isaac et al. study, based on the visual images of computerized fish samples, fish-based gills were divided into views [12]. Majid Dowlati et al. [13] evaluated the fish freshness by tracking color changes in fish eyes using the machine vision technique during the storage.

Image processing and machine learning, which is a non-destructive and safe technique, can be useful as capturing images using a camera without causing physical, biological, or chemical changes. This technique increases the reusability of the sample. This study proposes a fully automatic, efficient, and non-destructive image processing methods and machine learning to predict the freshness of the fish sample. In this study, images of red mullet fish were recorded with a digital camera at certain time intervals for two days at the ideal room temperature. Images were taken from the top of the fish upright and fixed at a certain distance. From the images obtained, the fish's eye tissue contains the maximum discriminatory information required for the freshness identification. Therefore, the eye of the fish is considered as the area of interest (ROI) for feature extraction. To obtain the ROI, segmentation is applied to the fish images. Tissues were compared using local binary patterns (LBP) for tissue change in the fisheye due to freshness analysis. LBP is a widely used method in the face, iris, and tissue recognition [14], [15]. The discrete wavelet transformation of the eye of the fish was performed as the second method. The energy density of these wavelet transforms was investigated. As a third method, LBP histograms were trained by supervised machine learning. The trained evaluator confirmed the results of all these three methods. In this study, the freshness detection of the fish is aimed at using eye images by image processing and machine learning algorithms as a fast technique approach.

MATERIALS AND METHODS

Image processing and machine learning procedures for the assessment of the proposed fish freshness system is depicted in Figure 1. In the first step, the eyes of the fish were selected with a segmentation algorithm. Then, three different methods were applied. Firstly, the local binary pattern (LBP) method was implemented for the selected pixels. Then, distance calculations were obtained between LBP histograms. After that, a discrete wavelet transform was applied to the selected pixels. Lastly, LBP histograms were implemented in a machine learning algorithm, and the freshness estimation was carried out.

Materials. Fresh Red mullet, Mullus barbatus L., 1758 samples from Uncalı Fish market were purchased in Antalya (Turkey). 20 red mullet fish samples were used in the experiments. These samples were transported to the laboratory in Styrofoam with ice.

Data Recording Procedure. Images of red mullet fish were obtained at different time intervals for 2 days. In 2 days, 6 photos were taken with an interval of 8 hours. During these procedures, red mullet fish were kept at an ideal room temperature. The camera is located at the top of fishes 90 degrees within a fixed distance (Figure 2.).

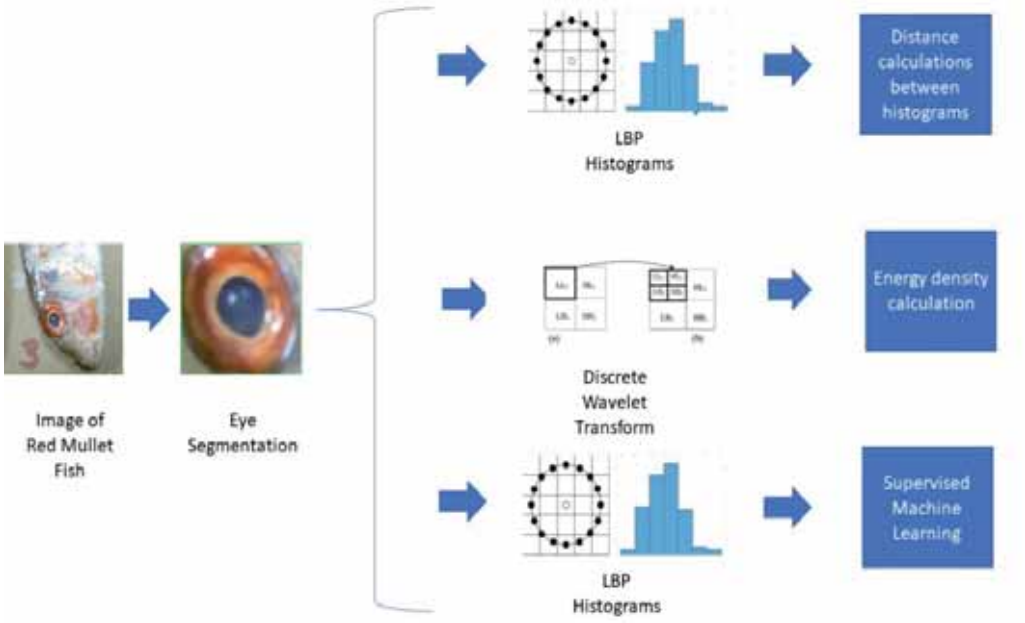


FIGURE 1
Image processing and machine learning procedures for the assessment of the proposed fish freshness system.



FIGURE 2
Fish images are captured in this controlled medium using a digital camera.



FIGURE 3
The region of interest (ROI) of the fisheye region is obtained from the raw image data.

Eye Segmentation. In the eye segmentation process, the eye region of the fish from a fish image was determined. This process consists of 3 steps: these steps, respectively, image filtering, eye localization, image normalization. First, GaussianBlur and medianBlur filters were applied to determine the eye localization. The eyes of the fish were determined by using a haar cascade eye classifier in the filtered images. Then, the detected fisheye image was normalized. The eyes of the fish were determined by using a haar cascade eye classifier in the filtered images (Figure 3.). The detected fisheye image was normalized. The general 2D formula of Gaussian Filter is given with the Eq. 1.

$$G(x,y) = \frac{1}{2\pi\sigma^2} e^{-\frac{x^2+y^2}{2\sigma^2}} \quad (1)$$

Where, x is the distance from the origin in the horizontal axis, y is the distance from the origin in the vertical axis, and σ is the standard deviation of the Gaussian distribution.

Local Binary Pattern (LBP). The local binary pattern is a very powerful method of defining the texture of a digital image. LBP is widely used in face recognition, iris recognition and tissue recognition [14], [15]. In this study, changes in the eye tissue of fish were determined by using the local binary pattern method. The LBP consists of sequential binary comparisons between neighbouring pixel values of a centre pixel. The original LBP method is based on the assignment of binary values by comparing the pixel value in the middle of the 3x3 matrix by selecting them as the threshold level. If the value of the neighbouring pixel is greater than or equal to the center pixel, the neighbouring pixel will be 1 and if it is smaller, it will be 0. Thus, an 8-bit LBP code is generated for a neighbourhood [16]. However, matrices of 3 × 3 may not be effective to capture dominant features. Therefore, the length of the matrices should be determined depending on the data. Instead, LBP definitions are made circularly [17]. There are two parameters to be defined here. These are determined as the number of sample points P and the radius measure R of the symmetrical circular neighbourhood which can express mathematically with the Eq. 2.

$$LBP_{P,R}(x_c, y_c) = \sum_{p=0}^{P-1} s(i_p - i_c)2^p \quad (2)$$

Where (x_c, y_c) refers to the location of the pixel and the gray level of the central pixel. i_c and i_p are respectively gray-level values of the central pixel and P is the surrounding pixel in the circle neighborhood with a radius R, s(x) is the binarization function and defined as the Eq. 3.

$$s(x) = \begin{cases} 1, & if \ \ x \geq 0 \\ 0, & if \ \ x < 0 \end{cases} \quad (3)$$

If 5 is accepted as a central pixel, the neighbouring pixel becomes 1 because 6 is greater than 5. When we do this for the value of 1, the neighbouring pixel becomes 0 because the value of 1 is less than 5. This process will continue until the neighbouring pixels which are chosen are finished.

Wavelet Transform. Wavelet transform which is a multiresolutional analysis technique [18] was widely used for the tissue analysis [19], [20]. However, it is rarely used as a feature in the eye pattern. In this study, the wavelet transform was used as a feature extractor to differentiate differences in the eye tissue of fish. Throughout the study, tissue-based recognition methods were analysed using the characterization method of Haar, Daubechies and reverse biorthogonal wavelet transforms. These wavelet transforms were compared according to their energies.

The image is decomposed into approximated and detailed components using the 2-D scale function and the 2-D wavelet functions:

$$\varphi_{j,m,n}(x,y) = 2^{\frac{j}{2}}\varphi(2^j x - m, 2^j y - n) \quad (4)$$

Where $\varphi_{j,m,n}(x,y)$ is a scaling function, m and n are translations of the scaling function. (Formula 5)

$$\psi^i_{j,m,n}(x,y) = 2^{\frac{j}{2}}\varphi^i(2^j x - m, 2^j y - n), i = \{H,V,D\} \quad (5)$$

$\psi^i_{j,m,n}(x,y)$, indicates the direction-sensitive wavelet function. Image analysis by two-dimensional discrete wavelet transform is described as Eq. 6 and Eq. 7. (Formulas 6 and 7)

$$W_\varphi(j_0,m,n) = \frac{1}{\sqrt{MN}}\sum_{x=0}^{M-1}\sum_{y=0}^{N-1} f(x,y)\varphi_{j,m,n}(x,y) \quad (6)$$

$$W^i_\psi(j,m,n) = \frac{1}{\sqrt{MN}}\sum_{x=0}^{M-1}\sum_{y=0}^{N-1} f(x,y)\varphi^i_{j,m,n}(x,y), i = \{H,V,D\} \quad (7)$$

f (x,y) shows the function of the image density. The size of the image is MxN. Here N=M=2j, j = 0,1,2,…, J-1. m,n = 0,1,2... , 2j – 1. j0 specifies the random start scale. j approximates component at scale Wφi (j0, m, n) with identified. $j \geq j_0$ three-way detail for component Wψi (j, m, n) with identified.

The high-scale to low-scale separation by 2-D discrete wavelet transform is shown in the Eq. 7. LL (corresponding to W) indicates approximate components. HH, HL, LH. (It corresponds to WψD, WψH, and WψV) specifies detailed components. The second level separation is extended on the LL1 component as the above process.

Energy is defined as the sum of the squares of values. Thus, the energy of an image is the sum of the squares of the pixel values, the energy in the wavelet transformation of an image is the sum of the squares of the conversion coefficients. The energy is found by the energy density by dividing the MxN size of the image.

Chi-Square Divergence, Kullback-Leibler Divergence and Correlation Methods. Chi-Square divergence is a statistical method that helps to determine whether there is a remarkable difference between the two histograms. The similarity or difference between the two histograms can be obtained with this method.

Chi-Square divergence is calculated using the Eq. 8.

$$d(H_1,H_2) = \sum_I \frac{(H_1(I)-H_2(I))^2}{H_1(I)} \quad (8)$$

Where H (I) is the histogram, d (H1, H2) shows the Chi-Square Divergence between two histograms.

Kullback-Leibler divergence is a measure of the similarity or difference between two possibilities relative to each other. We can see the relationship between histograms in Eq. 9

$$d(H_1,H_2) = \sum_I H_1(I) log(\frac{H_1(I)}{H_2(I)}) \quad (9)$$

Where d (H1, H2) shows the Kullback-Leibler divergence between the two histograms.

Correlation is a statistical method used to show the relationship between the two histograms. The similarity between the two histograms may be examined with this method using Eq. 10.

$$d(H_1,H_2) = \frac{\sum_I (H_1(I)-\underline{H_1})(H_2(I)-\underline{H_2})}{\sqrt{\sum_I (H_1(I)-\underline{H_1})^2 \sum_I (H_2(I)-\underline{H_2})^2}} \quad (10)$$

Here, $\underline{H_k} = \frac{1}{N}\sum_I (H_1(I) - \underline{H_1})^2$ (11)

RESULTS AND DISCUSSION

In this study, three different methods have been proposed for the determination of fish freshness.

Local Binary Pattern Application. The first method uses local binary pattern histograms. For each fish, histograms of the images taken at different times compared to the first image of this fish. Chi-Square Divergence, Kullback-Leibler Divergence, and Correlation methods were used to compare the similarities between two fish images taken at different times. Tissue differences between the images taken at different times were observed.

Firstly, histograms obtained from fisheye images were compared with Chi-Square Divergence method. As a result of this comparison, histogram distributions between the images of the same fish taken at different times were observed to be different. This was implemented for each 20 fish. The median and mean values of the fish images were calculated using the following equation. They increased during the waiting period of the fish (Figure 4a). Moreover, there is a significant change between the mean values of third and fourth group of images (Table 1). This may be used as a marker of the spoiling of the fish. Similarly, histograms are compared using the Kullback - Leibler Divergence method. As a result of this comparison, histogram distributions between the images of the same fish taken at different times were

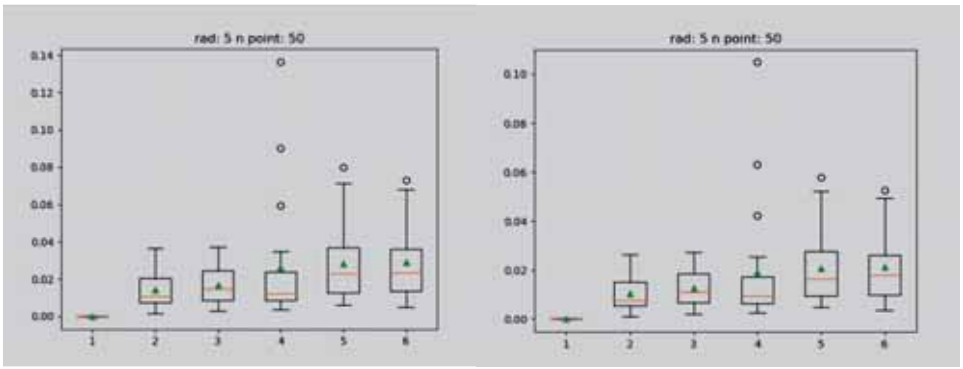
observed to be different (Figure 4b). The results were obtained according to the median and mean values of the fish images. As it can be seen from Table 2, the dramatic difference of mean values taking place in the fourth group images is the scaler of spoiling process.

TABLE 1
The average and geometric mean values of histogram data obtained with Chi-Square Distance method. The images were taken in 6 different time periods in 2 days.

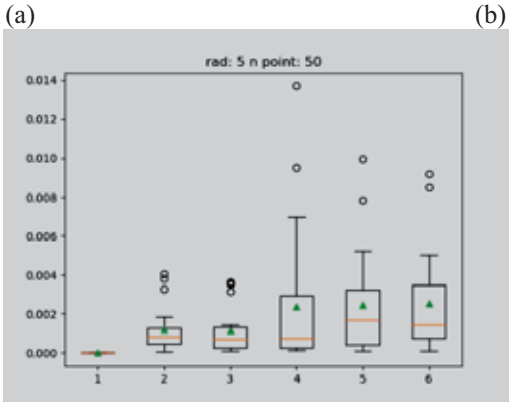
Kullback-Leibler Distance Method	Mean value	Geometric mean value	Amount of increase of mean values (%)
First Group Images	0.0	0.0	
Second Group Images	0.0105	0.0083	
Third Group Images	0.0126	0.0101	20
Fourth Group Images	0.0192	0.0116	**52.3810**
Fifth Group Images	0.0206	0.0160	7.29
Sixth Group Images	0.0213	0.0161	3.40

TABLE 2
The average and geometric mean values of histogram data obtained with Kullback - Leibler method. The images were taken in 6 different time periods in 2 days.

Chi-Square Distance Method	Mean value	Geometric mean value	Amount of increase of mean values (%)
First Group Images	0.0	0.0	
Second Group Images	0.0144	0.0113	
Third Group Images	0.0169	0.0135	17.36
Fourth Group Images	0.0261	0.0158	**53.85**
Fifth Group Images	0.0281	0.0216	7.66
Sixth Group Images	0.0291	0.0217	3.56



(a) (b)



(c)

FIGURE 4
Histograms of the fisheye images are compared according to Chi-Square Divergence
(a), Kullback-Leibler Divergence (b), and the Correlation methods (c). The maximum differences of mean values in all images occur in between third and fourth group of images for all methods. Orange straight lines on box plots show the median and green triangles correspond to the mean values.

TABLE 3
The average and geometric mean values of histogram data obtained with Correlation method. The images were taken in 6 different time periods in 2 days.

Discrete Wavelet Transforms	Haar Function (Mean values)	db1 Function (Mean values)	rbio1.1 Function (Mean values)
First Group Images	0.00016	0.000155	0.000145
Second Group Images	0.00013	0.000130	0.000130
Third Group Images	0.00011	0.000109	0.000109
Fourth Group Images	0.00014	0.000137	0.000137
Fifth Group Images	0.00013	0.000128	0.000128
Sixth Group Images	0.00012	0.000127	0.000127

TABLE 4
A discrete wavelet transform is implemented on fish images. Haar, Daubechies and Reverse Biorthogonal functions are used as the discrete wavelet transform functions. Energy densities are calculated and presented in the table according to the captured times of the picture.

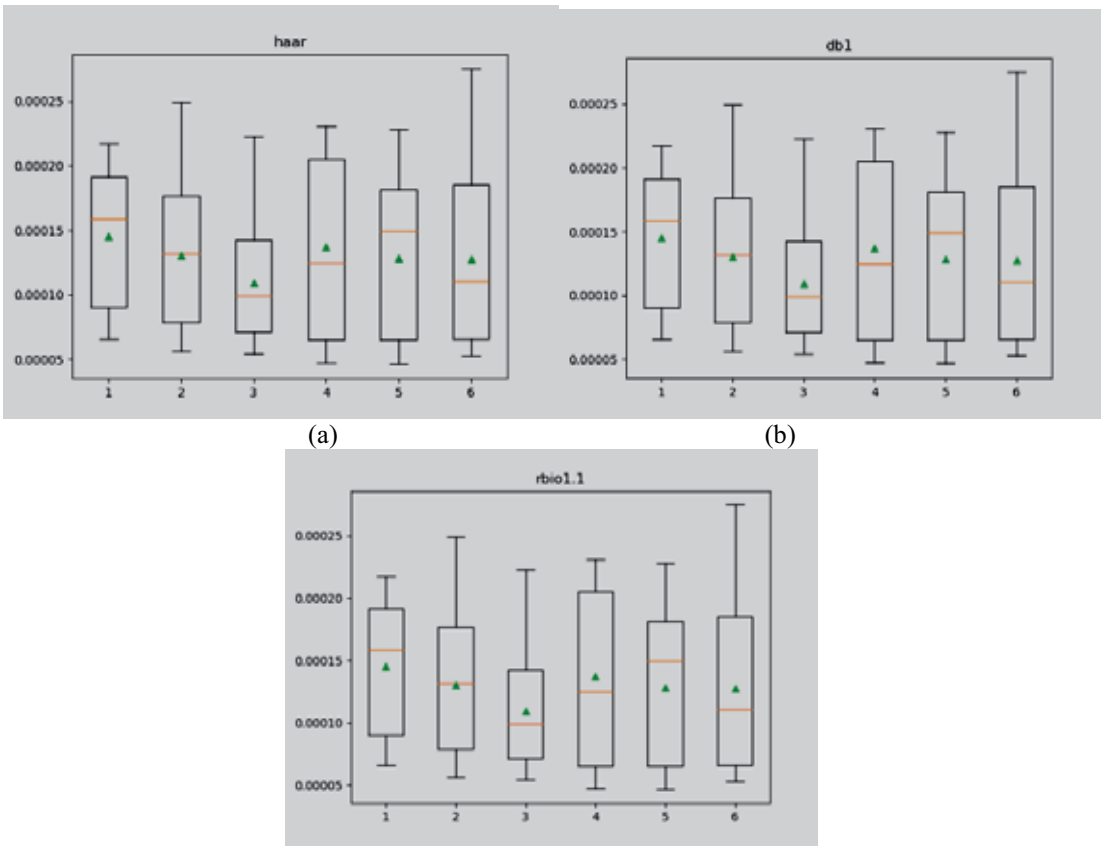
Correlation Method	Mean value	Geometric mean value	Amount of increase of mean values (%)
First Group Images	0.0	0.0	
Second Group Images	0.0012	0.0007	
Third Group Images	0.0012	0.0007	0.0
Fourth Group Images	0.0024	0.0009	**100**
Fifth Group Images	0.0025	0.0013	4.17
Sixth Group Images	0.0025	0.0014	0.0

Moreover, the correlation between histograms showed that the correlation values between the images taken at different times of the same fish are different. This was done separately for 20 fishes. The median and mean values increased due to the waiting duration of the fish (Figure 4c). The maximum differences of mean values in all images occur in between third and fourth group of images as happening in other two methods (Table 3).

The p values of this method were calculated as 0.001, 0.001, 0.003. $P > 0.05$ is the probability that the null hypothesis is true. A p-value less than 0.05 is statistically significant. Since the p-values of the proposed method satisfy $p < 0.05$ condition, they are statistically significant.

Discrete Wavelet Transform Application. The discrete wavelet transform was applied to fisheye images as the second method. The energies of the discrete wavelet transform were calculated. The main wavelet functions in wavelet transforms were selected Haar (Figure 5a), Daubechies 1 (Figure 5b), and Reverse Biorthogonal 1.1 functions (Figure 5c). They are implemented respectively on each 20 fish samples. The results were obtained according to the median and mean values of energy densities of the fish images. The mean values reduced from the first to the third group of images. However, these decreases stopped at the fourth group images. They made a peak, and then they start to fall again (Table 4). Oscillation of the mean values of the energy densities is the indicator of the spoiling process. Therefore, we may understand that the freshness of the fish was loosened at the fourth group images.

Machine Learning Method Application. The neural network method was implemented as an additional modality to determine the fish freshness by training LBP histograms of fisheye tissue with the supervised machine learning algorithm. The feed-forward artificial neural network model, which is supervised learning is used as the machine learning type. LBP histograms are used as the input data for the machine learning training and testing procedures. LBP histograms of 120 images obtained by 20 different fishes captured six times per day are considered as the input data of the study. 100 randomly selected data of these 120 histograms were used as the training data. The remaining 20 data were allocated as the test data. For this study, the "trainbr" function was selected as the learning function. "trainbr" is a network training function. The function updates the weight and bias values according to Levenberg-Marquardt optimization. Also, logarithmic sigmoid (logsig), elliot symmetric sigmoid (elliotsig), and tangent sigmoid (tansig) transfer functions were selected as the transfer functions for the study. The accuracy of determination of the fish freshness by the machine learning application is shown in Figure 6. The freshness situation of 18 fish was determined correctly in 20 red mullet fish with the machine learning application. The accuracy of the assessment of fish freshness is acquired as 90 % (for 20 samples). The expert in this field confirmed the results.



(a) (b)

(c)

FIGURE 5

Discrete wavelet transform is applied on fish images.

Haar (a), Daubechies (b), Reverse Biorthogonal (c) functions are applied and energy densities are acquired. The calculations are presented in the figure according to the time distribution of the image. Orange straight lines on box plots show the median and green triangles correspond to the mean values.

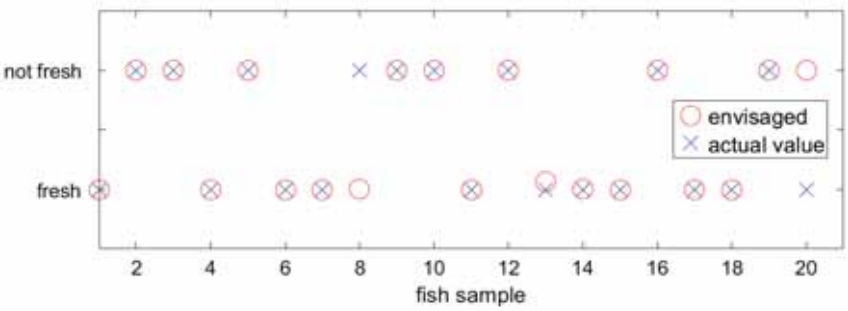


FIGURE 6

The accuracy of determination of the fish freshness by the machine learning application is shown in the figure. X corresponds to an actual value, and the circle is the prediction of the algorithm. When the circle and X matches, it means a correct evaluation.

In this study, non-destructive image processing and machine learning techniques have been proposed as a freshness assessment method. The fisheye region was selected to find the pattern of the distortion in fish samples. A pattern change was observed in the fisheye tissue within the time. The LBP histogram was extracted using three different LBP methods of the fisheye tissue as the first method. The distances between the histograms were calculated. It is used as a frame to determine the freshness of the fish, depending on the distance averages. The maximum increase of mean values occurs between the third and fourth groups of images in all three different LBP methods. This dramatic increase denotes that the fishes start to spoil, and this may be used as the indicator of fish freshness.

The second method, the Discrete Wavelet Transform, was used as a separate frame to determine the freshness of the fish depending on the average energy density obtained by calculating the energy density by performing a discrete wavelet transformation of the fisheye tissue. Three different

wavelet functions were used, and the energy density variations occurred in the same image groups which is the fourth group image. This process denotes that the fourth group fishes were different from the first three groups of images. So, this may be used as an indicator of the freshness. The result of the Discrete Wavelet Transform method is precisely consistent with the LBP method.

CONCLUSIONS

Sensory, physical, chemical, and microbiological methods have been used to detect fish freshness as the existing systems. The results of sensory methods may vary from person to person. In this method, there is no possibility of damaging the fish since there is no contact with the fish. In this way, the freshness of the fish can be determined by consumers.

Moreover, most of these methods require an experimental environment for the determination of freshness. The test environment means extra time, sensors, and space. On the other hand, this method only needs a regular camera which may be found on a smart mobile phone. Thanks to this method, the fish freshness detection is less costly and more comfortable to apply.

There is no gold standard for the determination of fish freshness. This technology, which may be the technology of the future, will be used in the development of quality indices for seafood, both consumer and industrial. Therefore, it will meet the needs of the consumer in this regard. It is thought that this technique has a significant potential for the determination of fish quality and may be more widespread in practice than possible.

In the applications already made in terms of quality assurance in the seafood processing industry, high labor costs, inconsistency and variability of human control have revealed the need for objective measurement. Fisheye imaging and image processing techniques, which promise superior speed and accuracy, and freshness controls in seafood can provide many significant advantages over other known methods. Requirements have increased in this regard. With this application, it is possible to provide better quality assurance regarding the freshness of fisheries thanks to its fast and objective use.

In the meantime, the applied methods are often used in classification structures. In this work, the classification part is done by applying artificial intelligence. One of the most critical features of this method is its high accuracy rate (90 % for 20 samples).

As a future study within the scope of the research, it is thought that the algorithm of deep learning will be developed depending on the number of data being increased. It is aimed to increase the accuracy of fish freshness detection by extracting distinguishing features with Convolutional Neural Network (CNN) based algorithms. Besides, different fish species can also be added into the system, resulting in common distinguishing features between fish species. In this way, the developed algorithm may be used to detect fish freshness for all fish species.

ACKNOWLEDGEMENT

Declaration of competing interest. The authors declare that they have no known competing financial interests or personal relationships that could have appeared to influence the work reported in this paper.

REFERENCES

[1] Huss, H.H. (1995) Quality and quality changes in fresh fish. FAO Fisheries Technical Paper. 348. Rome.

[2] Rehbein, H. and Oehlenschlager, J. (2009) Fishery Products: Quality, Safety and Authenticity, Wiley-Blackwell. Oxford, UK. 411-420.

[3] Olafsdóttir, G., Martinsdóttir, E., Oehlenschlager, J., Dalgaard, P., Jensen, B., Undeland, I., Mackie, I., Henehan, G. and Nielsen, H. (1997) Methods to evaluate fish freshness in research and industry. Trends Food Science Technology. 8, 258–265.

[4] Council Regulations, EC No 2406/96 of 26 November 1996. Laying Down Common Marketing Standards for Certain Fishery Products. Official Journal of the European Communities. No. L-334/2. (23.12. 1996).

[5] Martinsdóttir, E., Schelvis, R., Hylding, G. and Sveinsdóttir, K. (2009). Sensory evaluation of seafood: methods. In: Fishery Products: Quality, Safety and Authenticity. Rehbein, H. and Oehlenschlager, J. (eds), Wiley-Blackwell, Oxford, UK. 425–443.

[6] Howgate, P., Johnston, A. and Whittle, K. (1992). Multilingual Guide to EC Freshness Grades of Fishery Products. Torry Research Station and MAFF, Aberdeen, UK.

[7] Botta, J.R. (1995). Evaluation of Seafood Freshness Quality. VCH. 180.

[8] Yoshizawa, M., Yamamoto, Y., O'Quin, K.E. and Jeffery, W.R. (2012) Evolution of an adaptive behavior and its sensory receptors promotes eye regression in blind cavefish. BMC Biology. 10(1), 108.

[9] McCaig, T.N. (2002). Extending the use of visible/near-infrared reflectance spectrophotometers to measure colour of food and agricultural products. Food Research International. 35, 731–736.

[10] Gümüş, B., Balaban, M.Ö. and Ünlüsayın, M. (2011). Machine Vision Applications to Aquatic Foods: A Review. Turkish Journal of Fisheries and Aquatic Sciences. 11, 171-181.
[11] Wang, F., Zang, Y., Wo, Q., Zou, C., Wang, N., Wang, X. and Li, D. (2013, January). Fish freshness rapid detection based on fisheye image. In: Proc. SPIE 8761, PIAGENG 2013: Image Processing and Photonics for Agricultural Engineering. 87610A, Sanya, China.
[12] Issac, A., Dutta, M.K. and Sarkar, B. (2017). Computer vision-based method for quality and freshness check for fish from segmented gills. Computers and Electronics in Agriculture. 139, 10–21.
[13] Dowlati, M., Mohtasebi, S.S., Omid, M., Razavi, S.H., Jamzad, M. and De La Guardia, M. (2013) Freshness assessment of gilthead sea bream (Sparus aurata) by machine vision based on gill and eye color changes. Journal of Food Engineering. 119(2), 277-287.
[14] Guillaume, H., Rodriguez, Y. and Marcel, S. (2006, April). Local binary patterns as an image pre-processing for face authentication. 7th International Conference on Automatic Face and Gesture Recognition (FGR06). IEEE, Southampton, UK. 9-14.
[15] Sun, Z., Tan, T. and Qiu, X. (2006). Graph matching iris image blocks with local binary pattern. International Conference on Biometrics. Springer, Berlin, Heidelberg. D. Zhang and A.K. Jain (Eds.). 366–372, Springer-Verlag Berlin Heidelberg.
[16] Huang, D., Shan, C., Ardabilian M., Wang Y. and Chen L. (2011). Local binary patterns and its application to facial image analysis: a survey. IEEE Transactions on Systems, Man, and Cybernetics, Part C (Applications and Reviews). 41(6), 765-781.
[17] Ojala, T., Matti, P. and Mäenpää, T. (2002). Multiresolution gray-scale and rotation invariant texture classification with local binary patterns. IEEE Transactions on Pattern Analysis & Machine Intelligence. 7, 971-987.
[18] El-Latif, A., Eman, I., Taha, A. and Zayed, H.H. (2020) "A passive approach for detecting image splicing based on deep learning and wavelet transform." Arabian Journal for Science and Engineering. 1-8.
[19] Zhou, J., Luo, T., Li, M., Guo, S. and Oing, T. (2010, September). Using 2D Haar Wavelet Transform for Iris Feature Extraction. Asia Pacific Conference APCIT 2010, Xi'on China.
[20] Isnanto, R.R. (2015). Wavelet Types Comparison for Extracting Iris Feature Based on Energy Compaction. Journal of Physics: Conference Series. 622, 1. IOP Publishing.

Received: **29.03.2021**
Accepted: **11.05.2021**

CORRESPONDING AUTHOR

Hamza Feza Carlak
Electrical and Electronics Engineering
Akdeniz University
Antalya 07058 – Turkey

e-mail: fezacarlak@akdeniz.edu.tr

© by PSP Volume 30– No. 09/2021 pages 10763-10771 Fresenius Environmental Bulletin

ANALYSIS OF ECOLOGICAL ADAPTABILITY OF PREFABRICATED RESIDENTIAL BUILDINGS: A CASE STUDY OF SOUTHERN ANHUI, CHINA

Nan Liang*, Xiaohui Fu, Qian Li, Mengxuan Yu

School of Architecture and Civil Engineering, Anhui Polytechnic University, Wuhu, Anhui, 241000, China

ABSTRACT

In order to improve the ecological adaptability of prefabricated residential buildings in southern Anhui, China, in this paper, a new ecological adaptability analysis method of prefabricated residential buildings was proposed. The design of prefabricated residential buildings in terms of site selection, layout, structure, materials, and climate design are analyzed, and the design structure mechanism is analyzed with the concept of ecological adaptability. On this basis, the ecological adaptability analysis index is set. In addition, the final ecological adaptability analysis result is obtained through the comprehensive calculation of the ecological adaptability index of the prefabricated residential buildings. According to the prefabricated building data of residential buildings in southern Anhui, it can be found that the current prefabricated residential buildings in this area have high adaptability to daylighting, but the ventilation and warmth remain to be improved. Finally, in view of the sustainable development of ecological buildings in southern Anhui, the following strategies were proposed, that is, rational residential resource adaptability strategies, strengthening of residential building intensification, and material-saving paths for residential buildings.

KEYWORDS:
Prefabricated building, Southern Anhui residential, ecological adaptability, ecological building

INTRODUCTION

The southern Anhui region of China has a special geographical location and climatic conditions, which determine the unique architectural types and styles of this area, that is, residential buildings. At present, the development of southern Anhui in China is relatively mature, and related disciplines such as ecological environment have been integrated into the field of urban planning in theory and thinking. The continuous improvement of urban planning integrates multiple disciplines such as regional ecology and architectural ecology. From a practical perspective, the current ecological planning and construction of human settlements in southern Anhui is being actively and effectively carried out. Eco-city planning, sponge city construction, the formulation of urban green building evaluation standards, low-energy building design, and even mandatory building energy-saving calculations have greatly improved the regional ecological environment [1]. However, there are still some lags in the research on the ecological adaptability of urban human settlement environment planning [2]. In addition, the architectural ecology in southern Anhui is also relatively vague, which does not meet the requirements of the sustainable development of modern cities. Assembled residential buildings are widely used in residential building space due to their advantages of energy saving, environmental protection, short construction period, etc. In order to improve the ecological adaptability of prefabricated residential buildings in southern Anhui, China, in this paper, a new ecological adaptability analysis method of prefabricated residential buildings was proposed.

MATERIALS AND METHODS

Prefabricated residential building design. In this paper, taking southern Anhui as an example, we analyze the current situation of residential building design in southern Anhui, combining the local geographical environment and climate characteristics. From module to module, and then to component, the structure of prefabricated residential buildings is designed [3]. We first divide the module according to the function of the living space, and then determine the assembly module, and finally split the assembly module into individual assembly parts (Figure 1).

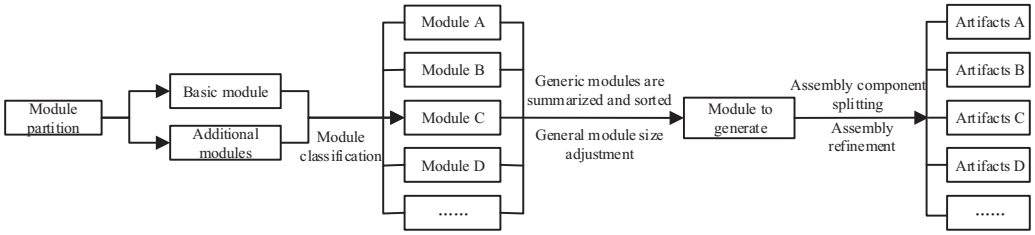


FIGURE 1
Design process of prefabricated residential buildings.

(1) Site selection and layout of residential buildings in southern Anhui. For the traditional settlements in southern Anhui, relatively stable small ecological areas were mainly formed in the early stage of reclamation [4]. It is dominated by the main entrances and exits of the settlement, and the main street often determines the future development trend of the settlement [5]. The buildings are arranged along the street, and each building unit is connected in series along the street. Such a combination of buildings conforms to the current status of towns and cities, and is relatively easy to be accepted by local residents. As the nature of residents' work changes, so will the residential houses in southern Anhui. From the perspective of the spatial distribution of the building structure, scattered independent houses may be transformed into clusters of multi-storey apartments to realize the combination and transformation of buildings, thereby forming a centralized living environment.

(2) Reasonable selection of assembly structure and materials. The load-bearing structure in the prefabricated building is composed of beams and columns passing through nodes, and its architectural space structure is flexible and easy to use [6]. The prefabricated building system has the characteristics of flexible space division, clear height of indoor space, strong seismic performance, low overall cost, suitable for hoisting, and high degree of industrialization [7]. The combined

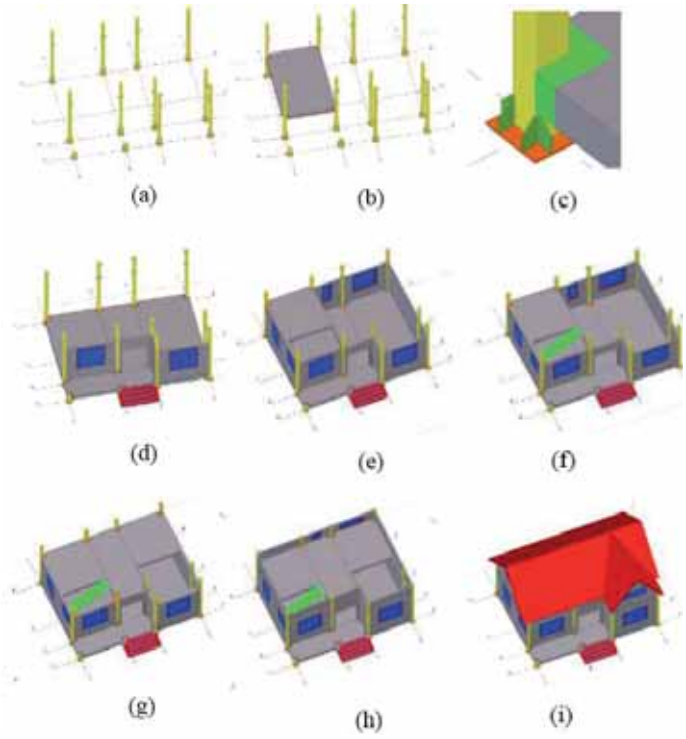


FIGURE 2
Assembly process.

Notes: (a) Steel column installation; (b) Installation of integrated parts of bottom wall frame beam combined floor slab; (c) Installation of the integration node; (d) Bottom composite wall panel installation; (e) Installation of two-story wall frame beam-combined floor integrated parts; (f) Integrated staircase installation; (g) Installation of two-story composite floor integrated parts; (h) Two-story composite wall panel installation; (i) Combined roof installation.

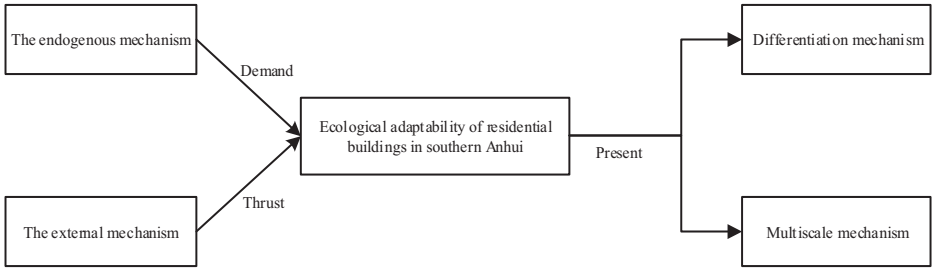


FIGURE 3
Ecological adaptability mechanism of residential buildings in southern Anhui.

building system is composed of wall frame columns, cold-formed thin-wall steel beams, lightweight aggregate concrete composite floor, cold-formed thin-wall steel beams, and lightweight aggregate concrete composite wall panels. The specific assembly process is shown in Figure 2.

(3) Design of building climate. The thermal state of the building is the result of the combined effect of indoor and outdoor climate factors. The comfort of the microclimate environment of the external space of the building is affected by its external wind environment and thermal environment. While the comfort of the microclimate environment directly affects the activities and behaviors of users [8]. By optimizing the wind environment and thermal environment of the building, the climate environment of the outer space of the building can be improved, and a pleasant microclimate environment can be created. The internal microclimate refers to the use of a shell to isolate a building from the external environment [9]. The relative indoor climate of the area where the building is located is the energy flow of the indoor environment composed of wind, solar, rain, and plants. The external environment temperature changes with the change of the envelope structure and the indoor temperature, and the envelope structure is of great significance as a dynamic regulation system for indoor and outdoor heat exchange. This adjustment is divided into dynamic adjustment and static adjustment. The variable adjustment of the movable sun visor is called "dynamic" adjustment [10]. The architectural climate design is a complete process from analysis, design, evaluation, to dynamic cyclic adjustment. Biological climate maps, heat and humidity index analysis, shading analysis maps, etc. can all be used as tools [11]. Cooling, shading, passive solar, natural ventilation, etc. are all achievable, thus forming a climate design plan for combined residential buildings.

Ecological adaptation mechanism. The ecological adaptability mechanism of southern Anhui residential buildings refers to the main related factors for studying the ecological adaptability of southern Anhui residential buildings. This research can have a deeper understanding and grasp of its internal operation mode [12]. The ecological adaptability mechanism in the architectural design of southern Anhui residential buildings is shown in Figure 3.

Among the inherent characteristics of ecological adaptation, two aspects are worthy of attention. First of all, ecological adaptability emphasizes the study of the role of natural and human factors in ecological types. Southern Anhui has special geographical features such as mountains, dampness and heat, rain and dew, and planning is a type of typical artificial activity, which includes planning layout and effective control. The connection between the two is an important process for studying the benign ecological development of rural areas in southern Anhui [13]. Ecological adaptation theory believes that the higher the degree of conformity between the adaptability of organisms and the local environment, the greater the ecological benefits obtained. The external promotion mechanism of ecological adaptability of southern Anhui's human settlement environment planning mainly includes policy guidance mechanism, innovation support mechanism, technical support mechanism and public participation mechanism. There are differences in the ecological adaptability of the rural human settlement environment planning in southern Anhui, which is mainly due to the imbalance of their own conditions and development in different areas of southern Anhui. Recognizing this imbalance and difference is the correct choice for making ecological adaptation plans for human settlements [14]. In addition, the ecological adaptation countermeasures in the planning of human settlements are naturally constantly adjusted and adapted.

Realization of ecological adaptability. In the process of introducing ecological adaptability in Southern Anhui's human settlement environment planning, although the methods and paths for implementing ecological adaptability are different, the basic goals are the same. In different regions, dif-

ferent types, and different development conditions, the ways to achieve ecological adaptability are different [15]. Promoting rationalization, achieving ecologicalization and improving adaptability are the main ecological adaptation goals of the rural human settlement environment planning in southern Anhui. Ecological adaptability can be divided into three types: climate ecological adaptation, soil ecological adaptation and biological ecological adaptation. Among them, the ecological adaptation indicators include building shape coefficient, building shadow area and so on. The expression of the building shape coefficient index is:

$$S = \frac{F_0}{V_0} \quad (1)$$

In the formula, F_0 and V_0 represent the external surface area of the building in contact with the outdoor atmosphere and the volume of the building, respectively. Thermal environment indicators are generally divided into two categories: simple indicators and comprehensive indicators [16]. The calculation formula of operating synthesis temperature t_{op} is:

$$t_{op} = 0.5t_a + 0.5t_r \quad (2)$$

The parameters t_r and t_a in formula 2 represent the average radiant temperature outside the building and the measured air temperature inside the prefabricated building, respectively, and the variable t_g is the black bulb temperature. The calculation formula for the above variables and air flow rate is:

$$\bar{t}_r = \left[\left(t_g + 273 \right)^4 + 2.5 \times 10^8 \times v^{0.6} \times \left(t_g - t_a \right) \right]^{\frac{1}{4}} - 273 \quad (3)$$

Comparing the comprehensive value of the environment through different surface temperature, relative humidity and average radiation temperature can reflect the indoor thermal environment more comprehensively. In addition, the thermal comfort index can also be used to measure the adaptability of the building's indoor thermal environment. At present, people are beginning to use a large number of air-conditioning equipment to adjust the temperature of the indoor micro-environment, but the air-conditioning equipment does consume non-renewable energy conditions in the actual operation process, which is extremely unfriendly to the environment and fails to fundamentally solve the climate question [17]. In architectural design, it is necessary to integrate the building with the surrounding environment, so as to make full use of the clean energy provided by the environment to realize the sustainable development of the environment [18].

RESULTS

Analysis results of ecological adaptability of residential buildings in southern Anhui. In this paper, we have analyzed the climate and ecological adaptability of residential buildings in southern Anhui from three aspects: thermal environment, wind environment and light environment. Among them, the analysis results of the thermal insulation of the enclosure structure of the prefabricated residential buildings in southern Anhui are shown in Table 1.

TABLE 1
Analysis results of thermal insulation of enclosure structure of prefabricated residential buildings in southern Anhui.

Area	Temperature (℃)			Annual average relative humidity (°C)	Building insulation and heat storage methods	
/	Annual average temperature	Average summer temperature	Average winter temperature	/	Wall material (brick/soil/stone)	Wall method (Solid/hollow/sandwich)
Huangshan	9.9	23.5	-6.0	43.3	Brick	Solid
Wuhu	7.8	21.2	-6.9	48.0	Brick + adobe	Sandwich
Maanshan	7.8	21.1	-6.9	52.0	Brick	Solid
Tongling	8.5	21.0	-5.2	51.0	Brick	Solid
Xuancheng	8.2	22.3	-4.8	45.0	Brick	Solid
Chizhou	8.3	23.1	-5.5	47.0	Brick + adobe	Sandwich

TABLE 2
Adaptation results of sunlight and natural ventilation in prefabricated residential buildings in southern Anhui.

Area	Wind direction		Natural ventilation in summer	Openness		Gate location	Sunshine data		Relationship between courtyard and sunshine	
/	Dominant wind direction in summer	Dominant wind direction in winter	Building orientation	Main house openness	Side room openness	/	Annual sunshine hours (h)	Incident angle on winter solstice (°)	Building type	Building shading method
Huangshan	NE	NE	From west to east			Middle door	3 246.7	26.37	Mouth type	With an arbor
Wuhu	SW	SW	From north to south			Middle door	3 056.4	26.75	Slotted	With a verandah
Maanshan	NW	NW	From west to east			Middle door	3 085.0	27.57	Mouth type	With a verandah in main room
Tongling	NE	NE	From west to east	Closed doors and windows		Side door	2 200.0	28.57	H narrow courtyard	With a verandah in main room
Xuancheng	SW	SW	From east to west			Middle door	3 030.0	27.47	H narrow courtyard	With a verandah in main room
Chizhou	NW	NW	From north to south			Side door	3 015.6	26.74	Multi-entry courtyard	With verandahs in many rooms

In the same way, the analysis results of sunlight adaptation and natural ventilation adaptation can be obtained, as shown in Table 2.

Comprehensively integrating the site selection, orientation, layout, structural system, heating method, and wind protection and ventilation of prefabricated residential buildings in southern Anhui, the analysis results of ecological adaptability can be obtained. In addition, the analysis results are imported into the calculation of quantitative indicators of ecological adaptability, and then the quantitative results can be obtained. Judging from the current analysis of ecological adaptability of buildings, the annual average temperature of buildings is less than 10 ℃, that is, the thermal insulation effect of buildings has not reached the expected effect. From the perspective of daylighting and ventilation, closed doors and windows are mainly used, so the degree of ventilation is poor, but the daylighting is high. At present, the ecological adaptability of prefabricated residential buildings in southern Anhui still has a large space for improvement.

Analysis of indoor thermal insulation, radiation intensity and relative humidity test results of residential buildings in southern Anhui. The indoor thermal insulation, radiation intensity and relative humidity of a residential building in southern Anhui were tested. The test time is September 15, 2020, the test time period is 0:00-24:00, and the

test point is the south-facing bedroom of a residential building in southern Anhui. The specific test results are shown in Figure 4 to Figure 6.

According to the test results in Figure 4 to Figure 6, it can be seen that for the south-facing bedroom, the indoor temperature of the prefabricated residential building reached the highest at 12:00 noon. During the whole day, the relative humidity does not change much. Therefore, in terms of temperature and humidity, it can be considered that the prefabricated residential buildings in southern Anhui have a higher sense of comfort and have better adaptability to the ecological environment. However, the highest radiation intensity appeared indoors at about 16:00, which was about 250W/m^2. This shows that the radiation protection of the building needs to be improved.

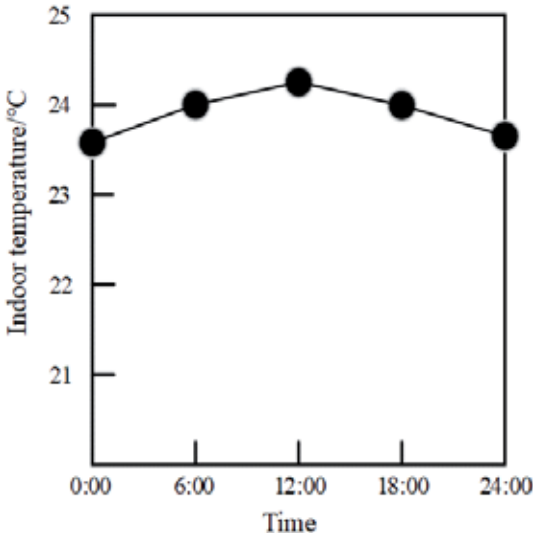


FIGURE 4
Test results of thermal insulation of prefabricated residential buildings in southern Anhui.

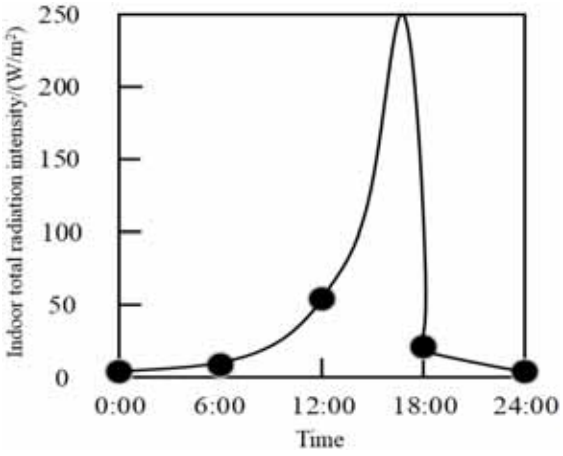


FIGURE 5
Test results of radiation intensity changes of prefabricated residential buildings in southern Anhui.

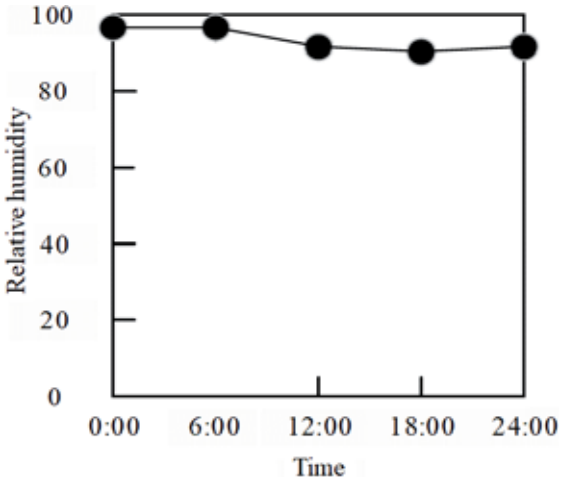


FIGURE 6
Relative humidity test results of prefabricated residential buildings in southern Anhui.

Strategies to improve the ecological adaptability of prefabricated residential buildings. Based on the current development status of ecological adaptability of prefabricated residential buildings in southern Anhui, in order to further improve the ecological adaptability of buildings, the following strategies are proposed.

(1) Strategies for adaptation of residential resources. The rammed earth wall has great adaptability to the climate due to the high thermal conductivity of the raw earth material. For a general 30 cm rammed earth wall, the thermal conductivity is within a certain range, and the attenuation coefficient can reach 80%. At this time, the calculated thermal resistance is not large. The research results show that the temperature conductivity coefficient of rammed earth materials is small, and the heat storage coefficient is large. Therefore, it cannot be simply evaluated and restricted from the perspective of thermal resistance. The heat storage and delay functions of thermal materials can give the wall of this material excellent climate adaptability [19]. In summer, the heavy rammed earth wall will absorb and store heat during the day, and at night will gradually release the heat absorbed during the day, which plays the role of cooling in summer. In winter, the thickness of the wall ensures that heat will not be lost. This natural cooling and heating system not only greatly saves cooling and heating costs, but also saves energy. The installation of solar energy equipment in prefabricated residential buildings in southern Anhui adopts three methods: direct absorption, sunlight room absorption, and heat collection and storage wall absorption. The key to solar energy utilization is to store heat and reduce heat loss [20]. In terms of thermal engineering, increasing the area of the solar collector is undoubt-

edly the most direct and effective method. And in reducing heat dissipation, the structural level of the enclosure structure and the choice of interior decoration materials play a vital role. Therefore, for the utilization of solar energy, increasing the area of the outer wall and choosing materials with good thermal inertia for indoor decoration can improve the heat preservation and heat storage properties of the enclosure structure.

(2) Strengthening of the intensification of residential buildings. We have made a detailed plan for the specific layout of residential buildings in southern Anhui. For the concentrated newly built houses around the old houses, the phenomenon of excessive expansion of the regional land caused by them needs to be remedied. It needs to target space shrinkage to realize the modernization of regional functions [21]. While taking the above strengthening measures, it is necessary to use land intensively, pay attention to the protection of cultivated land, and use hillside land with caution in accordance with the overall planning of construction land [22].

(3) Material-saving path of residential building. For the recycling of construction waste, it can generally be divided into recycling, landfill and other methods. Recycling, transforming, and transforming discarded building materials can make them put back into use, so it makes more sense than dismantling or discarding them directly [23]. Building materials such as relatively complete bricks and tiles, suitable stones, and debris can be recycled and reused and re-made, and then reused in construction or landscape engineering. When backfilling, it is difficult to recover recyclable waste materials, and for materials that are completely unusable, appropriate simple landfill treatment can be carried out at appropriate locations. To make full use of local materials, it is not only simply using traditional materials in southern Anhui, but also actively introducing locally produced light-weight, high-strength and other new energy-saving materials. In addition, it is necessary to analyze the types of local materials in order to judge specific strategies when using them [24]. In addition, we have also conducted research on common soil, stone, wood building materials and grass plant fibers in southern Anhui. Both soil and stone materials are non-renewable resources, and the over-exploitation of traditional materials such as clay solid bricks will damage the land and mineral resources.

CONCLUSIONS

(1) In order to improve the ecological adaptability of prefabricated residential buildings in southern Anhui, China, in this paper, a new ecological adaptability analysis method of prefabricated residential buildings was proposed. The design of prefabricated residential buildings in terms of site selection, layout, structure, materials, and climate design are analyzed, and the design structure mechanism is analyzed with the concept of ecological adaptability.

(2) According to the prefabricated building data of residential buildings in southern Anhui, it can be found that the current prefabricated residential buildings in this area have high adaptability to daylighting, but the ventilation and warmth remain to be improved. The indoor temperature of prefabricated residential buildings in southern Anhui reached the highest at 12:00 noon, and the indoor temperature throughout the day was between 23.5 °C and 24.5 °C. This shows that the building has good thermal insulation properties, and the relative humidity is relatively stable throughout the day. However, its radiation intensity is up to 250 W/m^2, indicating that the radiation resistance of prefabricated buildings in southern Anhui needs to be strengthened.

(3) Finally, in view of the sustainable development of ecological buildings in southern Anhui, the following strategies were proposed, that is, rational residential resource adaptability strategies, strengthening of residential building intensification, and material-saving paths for residential buildings.

ACKNOWLEDGEMENTS

This work was financially supported by the Key Research Project Fund of Humanities and Social Sciences in Anhui Universities “Expression of Traditional Design Vocabulary Based on Prefabricated Houses in Southern Anhui under the Background of Rural Revitalization” (No. SK2020A0232), the Key Research Project Fund of Humanities and Social Sciences in Anhui Universities “Research on Decoration Design and Structural Design of Huizhou Ancient Dwellings” (No. SK2018A0119), the Youth Project of Anhui Philosophy and Social Science Planning Project “Study on the Path of Improving Human Settlements in Huizhou Traditional Villages” (No. AHSKQ2019D086), and the Key Research Project Fund of Humanities and Social Sciences in Anhui Universities “Research on the Inheritance and Contemporary Application of Huizhou Traditional Residence Design Wisdom” (No. SK2020A0233).

REFERENCES

[1] Zhou, C., Yao, Z., Hu, Y., Hu, Z. (2020) Application Scheme Of Fiber Bragg Grating Sensor In Prefabricated Building. IOP Conference Series Earth and Environmental Science. 525(1), 121-132.

[2] El-Abidi, K., Ofori, G., Zakaria, S., and Abdul-Aziz, A. (2019) Using Prefabricated Building to Address Housing Needs in Libya: A Study based on Local Expert Perspectives Arabian. Journal for Science and Engineering. 44(10), 8289-8304.

[3] Ma, H., Zhang, H., and Chang, P. (2020) 4D-Based Workspace Conflict Detection in Prefabricated Building Constructions. Journal of Construction Engineering and Management. 146(9), 04020112.

[4] Xie, L., Chen, Y., Xia, B., and Hua, C.(2020) Importance-Performa.nce Analysis of Prefabricated Building Sustainability: A Case Study of Guangzhou. Advances in Civil Engineering. 1, 1-17.

[5] Sebaibi, N., Boutouil, M. (2020) Reducing energy consumption of prefabricated building elements and lowering the environmental impact of concrete. Engineering Structures. 213, 110594.

[6] Gonzalez-Libreros, J. H., Bertolazzi, A., Turrini, U., and Pellegrino, C. (2020) Assessment of an Existing Reinforced-Concrete Prefabricated Building: The Case of the Procédé Camus. Journal of Architectural Engineering. 26(3), 40-55.

[7] Liu, H., He, Y., Hu, Q., Guo, J. (2020) Risk management system and intelligent decision-making for prefabricated building project under deep learning modified teaching-learning-based optimization. PLoS ONE. 15(7), 235-246.

[8] Luo, L., Jin, X., Shen, G. Q. (2020) Supply Chain Management for Prefabricated Building Projects in Hong Kong. Journal of Management in Engineering. 36(2), 05020001.1-05020001.15.

[9] Jiang, W., Shi, K. (2020) Pricing and Advance Ordering Strategy for Prefabricated Building Assembler. IOP Conference Series: Materials Science and Engineering. 780(6), 062032.

[10] Li, X. (2020) Research on investment risk influence factors of prefabricated building projects. Journal of Civil Engineering and Management. 26(7), 599-613.

[11] Zou, D., Sun, C. (2020) Analysis for Thermal Performance and Energy-Efficient Technology of Prefabricated Building Walls. International Journal of Heat and Technology. 38(1), 269-273.

[12] Nan, C., Jie, Z. (2020) Estimation of Environmental Damages of Cement Building and Environmental Benefits of Prefabricated Building: A Case Study Based on a Residential Project in Henan Province, China. Nature Environment and Pollution Technology. 19(2), 721-728.

[13] Novalic, A., Zejnilovic, E. (2019) Spatial Configuration Of Dwelling Units In Multi-Storey Residential Buildings: The Case Of Apartments Built In Sarajevo 2008-2018. Spatium. 41, 32-40.

[14] Liu, S., Shi, L., Zhang, H., Wang, C. (2019) Green Design Strategy of Village and Town Residential Buildings under the Background of New Urbanization. IOP Conference Series: Materials Science and Engineering. 592(1), 121-132.

[15] Akl, M., Sheta, S., and Hegazy, I. (2020) Population Density and Solar Radiation Effect on the Residential Buildings Forms: Case Study of the Graduates Villages at El -Burullus Lake. Bulletin of the Faculty of Engineering Mansoura University. 40(1), 1-11.

[16] Andrade, J., Luís, B. (2019) Assessing buildings' adaptability at early design stages. IOP Conference Series: Earth and Environmental Science. 225(1), 012012.

[17] Li, G., Xu, Y., Fan, Y. (2019) The Design of Sustainable Retrofitting Strategies and Energy-efficiency Optimization for Residential Buildings. IOP Conference Series: Materials Science and Engineering. 556, 54-66.

[18] Gamayunova1, O., Radaev, A., Petrichenko1, M., Dmitrieva, E. (2019) The increase in energy efficiency of residential buildings of military towns. E3S Web of Conferences. 110(22), 02144.

[19] Erkal, A. (2019) Impact of Traffic-Induced Vibrations on Residential Buildings and Their Occupants in Metropolitan Cities. Promet - Traffic - Traffico. 31(3), 271-285.

[20] Au-Yong, C., Chua, S., Ali, A., Tucker, M. (2019) Optimising maintenance cost by prioritising maintenance of facilities services in residential buildings. Engineering Construction & Architectural Managemen. 26(8), 1593-1607.

[21] Umar, G., Yusuf, D., Mustapha, A. (2019) Theory and Design for the Contemporary Residential Buildings: A Case Study of Kano Metropolis, North-western part of Nigeria. International Journal of Environmental Studies. 7(1), 1-8.

[22] Badawy, M., Elnawawy, O., Mohamed, E. (2020) The Cost of Late Payments in Residential buildings in Arabian Countries. International Journal of Scientific and Engineering Research. 11(3), 1392-1398.

[23] Rosado, P., Levinson, R. (2019) Potential benefits of cool walls on residential and commercial buildings across California and the United States: Conserving energy, saving money, and reducing emission of greenhouse gases and air pollutants. Energy and Buildings. 199, 588-607.
[24] Pichandi, R., Murugavel, K., Karthick, A., Sudhakar, K. (2020) Performance evaluation of building-integrated photovoltaic systems for residential buildings in southern India. Building Services Engineering Research and Technology. 41(4), 492-506.

Received: **01.04.2021**
Accepted: **01.05.2021**

CORRESPONDING AUTHOR

Nan Liang
School of Architecture and Civil Engineering,
Anhui Polytechnic University,
Wuhu Anhui 241000 – China

e-mail: nanliangahpu@163.com

© by PSP Volume 30– No. 09/2021 pages 10772-10781 Fresenius Environmental Bulletin

WATER QUALITY EVALUATION FOR IRRIGATION PURPOSE AND HYDROCHEMICAL ELUCIDATION OF SHALLOW GROUNDWATER IN HUAIBEI PLAIN: A CASE STUDY

Xinyi Qiu[1,2], Linhua Sun[1,2,3,*], Weihua Peng[1,3], Kai Chen[1,2], Xiang Zhao[1,2]

[1]School of Resources and Civil Engineering, Suzhou University, Anhui 234000, China;
[2]School of Earth and Environment, Anhui University of Science & Technology, Anhui 232001, China;
[3]Key Laboratory of Mine Water Resource Utilization of Anhui Higher Education Institute, Suzhou University, Anhui 234000, China

ABSTRACT

Shallow groundwater is essential for irrigation in Huaibei Plain, China, as the area is one of the most important grain bases. Therefore, 22 shallow groundwater samples were collected in the area, and their major ion concentrations and suitability for irrigation were evaluated using various indices (sodium adsorption ratio, Kelly's ratio, sodium percent, residual sodium carbonate, magnesium hazard, and permeability index). Moreover, Piper diagram, Gibbs diagram, ion ratio and principal component analysis (PCA) were applied in hydrochemical elucidation. The results indicated that the most of the water samples were unsuitable for irrigation because of high Na+, Mg2+, and HCO3- contents. The major hydrochemical type of shallow groundwater was Na-Mg-HCO3. The ion composition of groundwater was controlled by water-rock interaction, with dominantly controlled by silicate weathering and followed by carbonate dissolution. Na+ mainly weathered from the silicate weathering, and a few were derived from halite dissolution and ion exchange reaction. Mg2+ also mainly weathered from silicate weathering. HCO3- mainly originated from the reaction of dissolved CO2 in water with silicate. According to the PCA results, the hydrochemistry of 2/3 samples were controlled by natural processes and 1/3 of them have been influenced by human activities.

KEYWORDS:
Shallow groundwater, water quality assessment, water–rock interaction, hydrochemistry

INTRODUCTION

Agriculture is the foundation of existence and human development of the base. The Huaibei Plain is one of the important grain bases in China. Agriculture has always been the pillar industry of economic development in the area, and groundwater is used as the main water source of agricultural activities [1]. As an important source for domestic, industrial and agricultural irrigation purposes, groundwater is less susceptible to pollution from human activities than surface water. However, once groundwater is extremely difficult to treat once polluted because of its concealment [2]. Groundwater pollution has become a serious issue. It has been reported that 90% of China's shallow groundwater is polluted, and an alarming 37% is so foul that it cannot be treated for use as drinking water [3]. In China, 76.1% of 2833 monitoring wells are severely polluted. [4]. In addition, according to the China Eco-Environment Status Bulletin, 14.9% of 329 water sources failed to satisfy the drinking water standard in 2018 [5].

Current studies on groundwater pollution focus on source analysis [6-8], hydrochemical evolution [9-10], and health risk [11-12]. For instance, Zhang et al. [6] used isotope mixing model to analyze the main sources of NO3- pollution and found that NO3- mainly was derived from chemical fertilizer and soil organic nitrogen in groundwater. Zuo et al. [10] applied factor analysis and other methods to analyze the influencing factors of shallow fluorinated groundwater in Liaohe River Plain in the coastal area of Northeast China. They found that the main factors affecting fluorine-containing groundwater were fluorine leaching and regional hydraulic gradient.

Within Huaibei Plain, Suzhou is an important agricultural city; Groundwater quality assessment [13-14] and heavy metal pollution detection [15-16] had been carried out. Qiu et al. [13] used sodium percent (Na%) and sodium adsorption ratio (SAR) as irrigation indexes to analyze the suitability of shallow groundwater in Huaibei for irrigation. They found that the groundwater in the area had slight sodium salt and high salinity hazard. Qiu et al. [15] analyzed the heavy metal pollution status of shallow groundwater in Huaibei and found that the area had relatively high Sr and Mn and relatively low Cr, Ni, Cu, Zn, Cd, and Pb. However, studies on the water quality assessment and hydrochemical elucidation of shallow groundwater for irrigation in this area were limited and insufficient for the protection and management of local groundwater.

This study was performed to evaluate the quality and elucidate the properties of shallow groundwater in Suzhou City for irrigation purpose. The objectives of this study were as follows: (1) to evaluate the quality of shallow groundwater in the area for irrigation purpose; (2) to elucidate the hydrochemical profile of the groundwater. This study is important to identify the priority pollutants in groundwater that influence water quality for irrigation and understand their source apportionment.

MATERIALS AND METHODS

Study area. The study area is located in Yongqiao District of Suzhou City and bordered by Tuohe River in the northeast, Huihe River in the southwest, and Taoyuan coal mine in the south (Figure 1). With the area is located between 116° 55′ and 117° 05′ E longitude and between 33° 30′ and 33° 41′ N latitude and has a total area of 134.69 km2. The region is characterized by temperate semi-humid monsoon climate with hot summer and dry, cold winters. The annual average temperature is approximately 14.4 °C, and the highest temperature is approximately 40.3 °C. The temperature and precipitation data of Suzhou City show that the annual average precipitation and evaporation are 858.1 and 1589.4 mm, respectively, and precipitation is concentrated in June to August. Surface waters, such as Tuohe River and Xinbianhe River, pass through the study area, and a railway runs through the area from southeast to northwest.

Shallow groundwater in the Chengxi water source area, which belongs to the porous water-bearing group of loose rocks, was studied. In accordance with the burial situation of underground water and the alternation between precipitation and surface water, the loose layer of the Chengxi water source area was divided into the first aquifer (FA), first weakly permeable layer, second aquifer (SA), and third aquifer.

This research was mainly carried out in the FA and SA. The FA is composed of silty sand, sub-sand, local fine sand, and silt, as well as a mixture of limestone and dolomite with a buried depth of more than 30 m. The SA is composed of fine sand, medium fine sand, silt, and local coarse sand. This aquifer also contains a small amount of limestone and dolomite with a buried depth of 30–100 m.

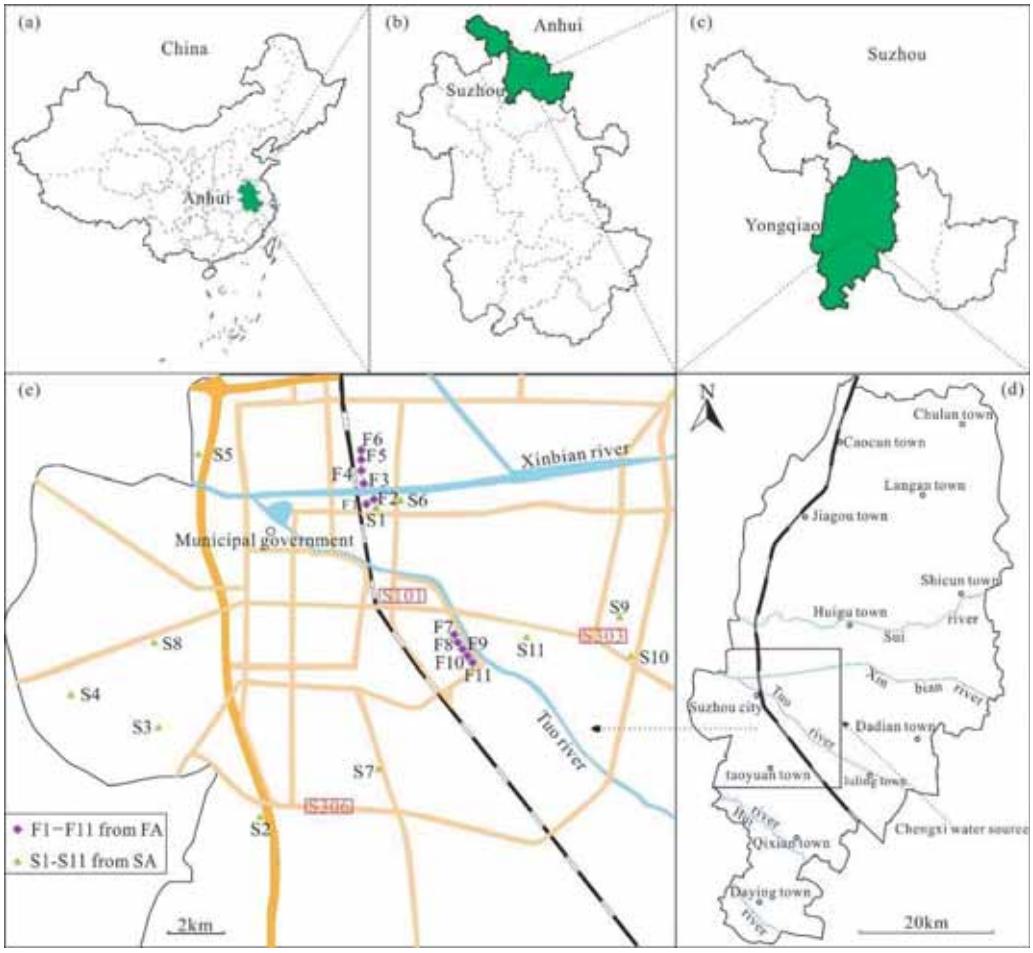


FIGURE 1
Location of the study area

Sampling and analyses. According to the hydrogeological conditions of the Chengxi water source in Suzhou City [14], 22 shallow aquifer samples were collected in October, 2019. FA and SA have 11 samples each, which are recorded as F1-F11 and S1-S11, respectively (Figure 1e). The samples were collected in polyethylene bottle cleaned in the laboratory, and the locations and other information were recorded during sampling. All samples were filtered by 0.45 μm microporous membrane and used for hydrochemical elucidation. Ten ions were tested, including K+, Na+, Ca2+, Mg2+, F-, Cl-, NO3-, PO43-, SO42-, and HCO3-. HCO3- was determined using acid titration [14], and the other ions were tested by ion chromatography (Diane, ICS-600-900). The charge balance errors (%E) of cation and anion in all samples were calculated to verify the accuracy of the test results using Equation (1), as follows:

$$\%E = (\sum C - \sum A)/(\sum C + \sum A) \quad (1)$$

Where C represents cations, and a represents anions. The calculated results showed that the %E of all samples was within 5% (mean value 2.24%).

Data processing and analyses. (1) Evaluation method of groundwater irrigation suitability. The species and content of ions in irrigation water influence plant metabolism [17]. High ion levels in water can inhibit plant growth and reduce crop productivity [18]. In this study, the quality of groundwater for agricultural purpose was systematically evaluated using SAR (Sodium adsorption ratio), Kelley's ratio, Na% (sodium percent), residual sodium carbonate (RSC), magnesium hazard (MH), and permeability index (PI) [17-18].

SAR. SAR is an important parameter in determining the suitability of groundwater irrigation; SAR is evaluated using the equation [17-18]:

$$SAR = Na+/\sqrt{(Ca2+ + Mg2+)/2} \quad (2)$$

Kelley's ratio. Kelley's ratio can also be used to calculate the suitability of water for irrigation and to estimate whether the Na+ content of groundwater is harmful to crops. Kelley ratio is evaluated using the equation [18]:

$$\text{Kelley's ratio} = Na+/(Ca2+ + Mg2+) \quad (3)$$

Na%. Na% is also an interpretation of sodium concentration and defined by the equation [17-18]:

$$Na\% = (Na+ + K+) \times 100/(Ca2+ + Mg2+ + Na+ + K+) \quad (4)$$

RSC. RSC reflects the concentrations of CO32− and HCO3−. Groundwater with high RSC value has high alkali content, which is not conducive to agricultural irrigation. RSC is calculated by the equation [17-18]:

$$RSC = (CO32- + HCO3-) - (Ca2+ + Mg2+) \quad (5)$$

MH. Irrigation water with high MH value has high alkalinity, which reduces crop yield. MH is calculated by the equation:

$$MH = (100 \times Mg2+)/(Mg2+ + Ca2+) \quad (6)$$

PI. PI is a measure of soil permeability. If soil is irrigated for a long time, the accumulation of soil ions (Na+, Mg2+, Ca2+, CO32−, and HCO3−) gradually increases, and higher osmotic pressure is formed in and out of the plants, which lead to crop reduction. PI is calculated by the equation:

$$PI = 100 \times (Na+ + \sqrt{HCO3-})/(Ca2+ + Mg2+ + Na+) \quad (7)$$

(2) Chloro-alkaline indexes. Chloro-alkaline indexes (CAI) can be used to reflect the direction and intensity of alternating cation adsorption in groundwater and is calculated through the equations [19]:

$$CAI\text{-}I = (Cl- - Na+ - K+)/Cl- \quad (8)$$

$$CAI\text{-}II = (Cl- - Na+ - K+)/(SO42- + HCO3- + NO3-) \quad (9)$$

If CAI-I and CAI-II are negative, then Ca2+ and Mg2+ positively replaced Na+ and K+, respectively. If CAI-I and CAI-II are positive, then Na+ and K+ positively replaced Ca2+ and Mg2+, respectively.

(3) Data analysis. Microsoft Excel 2010 and IBM SPSS Statistics 25.0 were used to perform data treatment and statistical analysis. One-way ANOVA (LSD method) was performed to identify the differences in ion concentrations between the two aquifers. OriginPro 2018 was used to plot graphs. R language was used for principal component analysis (PCA).

RESULTS AND DISCUSSION

Ion contents. The statistical results of the samples are shown in Table 1. In FA, the average concentrations of cations and anions are in the order Na+>Mg2+>Ca2+>K+ and HCO3->SO42->Cl-> NO3-> PO43->F-, respectively. In SA, the average concentrations of cations and anions are in the order Na+>Mg2+>Ca2+>K+ and HCO3->SO42->Cl-> PO43-> NO3->F-, respectively. In these two aquifers, the dominant cation and anion are Na+ and HCO3-, respectively. Na+ and HCO3- in SA are higher than those in FA, whereas all the other ions in FA are higher than those in SA.

A coefficient of variation (CV) < 0.1 indicates that the influence of anthropogenic sources is small, whereas CV>0.9 indicates that the influence of anthropogenic sources is great [20]. Ca2+, F-, and NO3- in FA and K+, Ca2+, NO3- and SO42- in SA have CV>0.9; therefore, these ions may be greatly affected by anthropogenic sources. One-way ANOVA shows that all the ions between the two aq-

uifers with the exclusion of Cl- and NO3- had no remarkable difference (Figure 2). Therefore, the different of ions between the two aquifers were not separated in detail in the following analysis.

Evaluation of irrigation water quality. The results of Kelley ratio and Na% (Table 2) respectively show that 59.09% and 36.36% of water samples are unsuitable for irrigation. RSC indicates that 68.18% of water samples are unsuitable for agricultural irrigation because of high HCO3- concentration. MH shows that 95.45% of water samples are unsuitable for irrigation because of high Mg2+ concentration. PI shows that 72.23% of water samples are unsuitable for irrigation. Thus, a majority of shallow groundwater in the area is unsuitable for irrigation.

Hydrochemical types and control mechanisms. (1) Hydrochemical types. Piper triangular diagram is widely used in identifying hydrochemical types [21]. The diagram intuitively presents the relative content of various main ions and hydrochemical types. The diagram (Figure 3) indicates that the water samples in FA and SA have similar distribution spatial evolution. The cations are aggregated in one side of the Na-Mg axis; thus, Na+ and Mg2+ are the main cations in shallow groundwater. The anions gather together on the side of HCO3-; thus, HCO3- is the main anion in groundwater.

TABLE 1
Statistical analysis of groundwater chemical indicators

	FA (n=11)					SA(n=11)				
	Min	Max	Mean	SD	CV	Min	Max	Mean	SD	CV
	mg/L	mg/L	mg/L	%		mg/L	mg/L	mg/L	%	
Na^+	51.23	127.58	84.59	21.72	0.26	41.45	157.62	109.17	34.47	0.32
K^+	0.90	15.04	4.39	4.27	0.97	1.40	20.60	3.99	5.34	1.34
Mg^{2+}	17.27	66.01	39.88	14.56	0.37	17.54	47.21	32.99	8.89	0.27
Ca^{2+}	0.72	80.23	23.09	23.37	1.01	2.48	88.05	17.07	23.68	1.39
F^-	0.01	0.83	0.31	0.29	0.95	0.01	0.83	0.44	0.23	0.53
Cl^-	8.22	87.08	34.61	29.02	0.84	10.91	76.32	31.12	18.55	0.60
NO_3^-	0.01	74.42	8.19	21.16	2.58	0.44	3.50	0.86	0.86	1.00
HCO_3^-	126.31	634.58	393.87	141.71	0.36	167.80	553.24	392.01	131.07	0.33
SO_4^{2-}	8.09	114.70	44.43	35.02	0.79	5.81	179.88	34.26	48.83	1.43
PO_4^{3-}	1.75	1.80	1.77	0.02	0.01	1.72	1.79	1.74	0.02	0.01

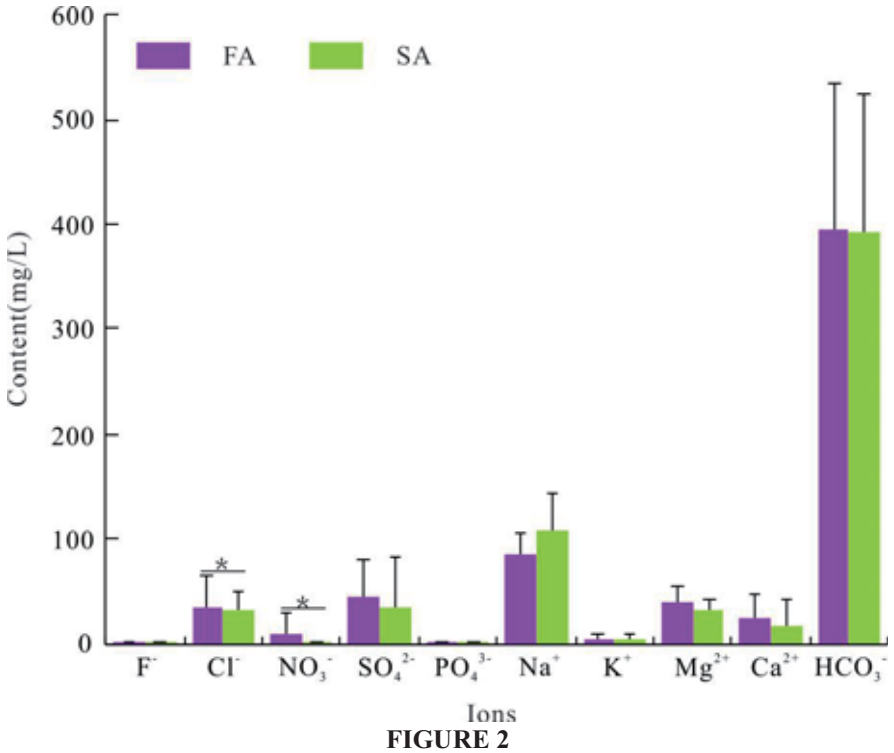


FIGURE 2
Plot of ion content
(Mean ± SD, n = 11; FA: First aquifer; SA: Second aquifer; * represents significant difference at 0.05 level)

TABLE 2
Statistical analysis and evaluation results of irrigation water quality indexes

Irrigation parameters	Statistical analysis		Evaluation results			
				Water class	Number of samples	Percentage (%)
SAR	Range	1.5–5.66	<10	Excellent	22	100%
	Average	3.18	10–18	Good	-	-
			18–26	Doubtful	-	-
			> 26	Unsuitable	-	-
Kelley Ratio	Range	0.37-2.60	< 1	Suitable	9	40.91%
	Average	1.25	> 1	Unsuitable	13	59.09%
Na%	Range	27.40-72.50	< 20	Excellent	-	-
	Average	52.73	20–40	Good	5	22.73%
			40–60	Permissible	9	40.91%
			60–80	Doubtful	8	36.36%
			> 80	Unsuitable	-	-
RSC	Range	-1.60-6.94	<1.25	Suitable	4	18.18%
	Average	2.94	1.25-2.5	Moderate	3	13.64%
			>2.5	Unsuitable	15	68.18%
MH	Range	39.99-98.47	< 50	Suitable	1	4.55%
	Average	79.93	> 50	Unsuitable	21	95.45%
PI	Range	51.92-106.84	< 25	Suitable	-	-
	Average	83.32	25–75	Moderate	6	27.27%
			> 75	Unsuitable	16	72.73%

TABLE 3
Statistics of hydrochemical types

Source of water	Numbers	Hydrochemical types	Numbers	Percentage
FA	F3、F6、F8-F11	Na-Mg-HCO_3	6	54.55%
	F5、F7	Mg-Na-HCO_3	2	18.18%
	F1	Mg-Ca-Na	1	9.09%
	F2	Mg-Na-Ca	1	9.09%
	F4	Na-Mg-Ca	1	9.09%
SA	S2-S9	Na-Mg-HCO_3	8	72.73%
	S10-S11	Mg-Na-HCO_3	2	18.18%
	S1	Na-Ca-Mg	1	9.09%

Table 3 further shows that Na–Mg–HCO3 is the dominant water type in FA and SA and accounts for 54.55% and 72.73% of the water types, respectively.

(2) Control mechanisms. Gibbs diagram utilizes the ratio relationships, Na+/(Na+ + Ca2+) and Cl-/(Cl- + HCO3-), which can effectively provide prominence to the water chemistry mechanism of the control area [22-23]. The mechanism of hydrochemical control can be divided into precipitation dominance, rock dominance, and evaporation crystallization. Figure 4 shows that the hydrochemical action of groundwater is dominated by water–rock interaction.

The mixed diagrams of Ca2+/Na+-Mg2+/Na+ and Ca2+/Na+-HCO3-/Na+ [24] can be further subdivided into water-rock interaction. Figure 5 shows that although the water samples in FA deviate from the silicate weathering region more than those in SA, some water samples in FA and SA are concentrated in the silicate weathering region and deviate from the carbonate dissolution region. Therefore, groundwater ions are mainly affected by silicate weathering, and few ions are weathered from carbonate dissolution.

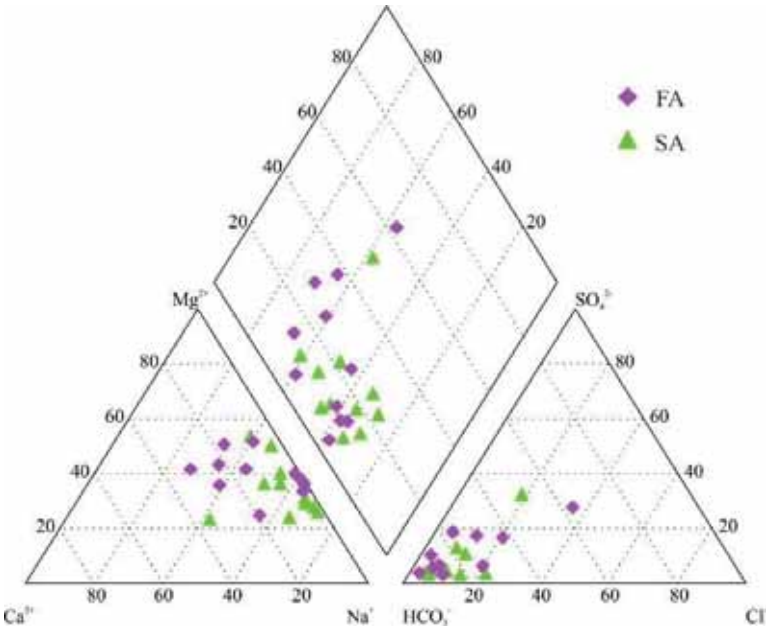


FIGURE 3
Piper diagram of groundwater

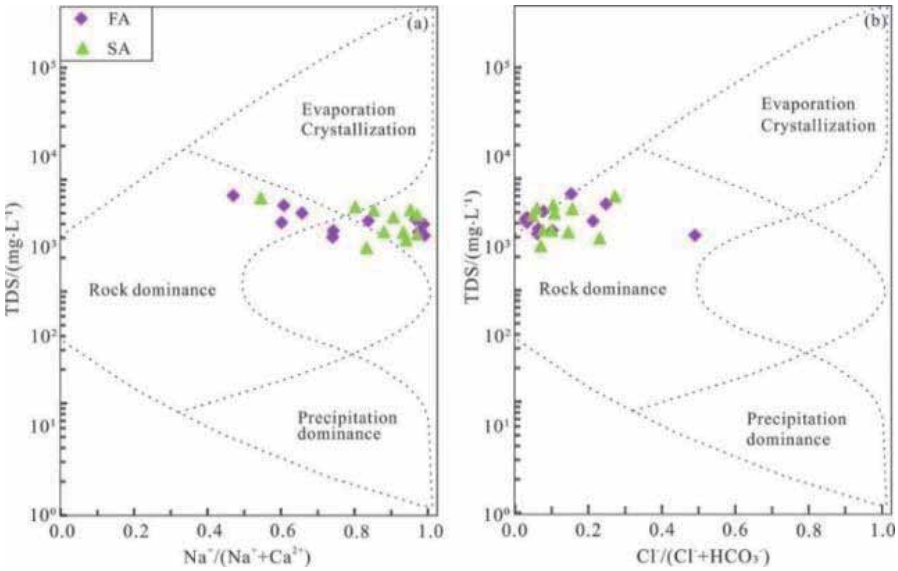


FIGURE 4
Gibbs diagram of groundwater

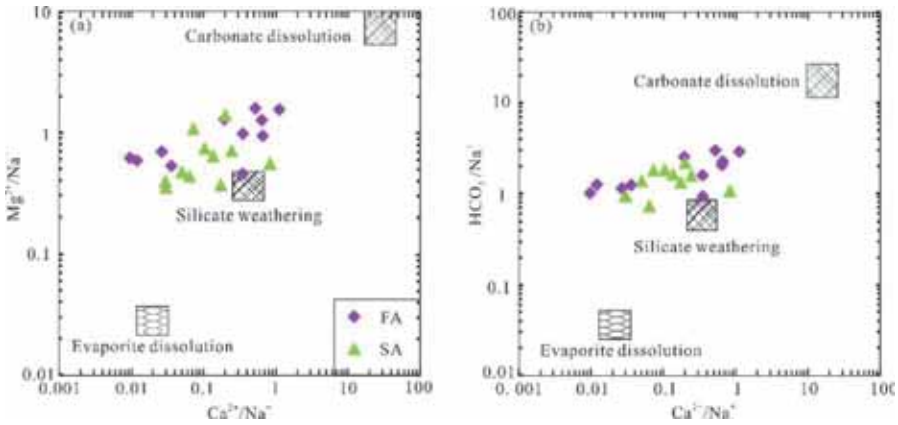


FIGURE 5
Plot of Ca^{2+}/Na^{+}-Mg^{2+}/Na^{+} and Ca^{2+}/Na^{+}-HCO_3^{-}/Na^{+}

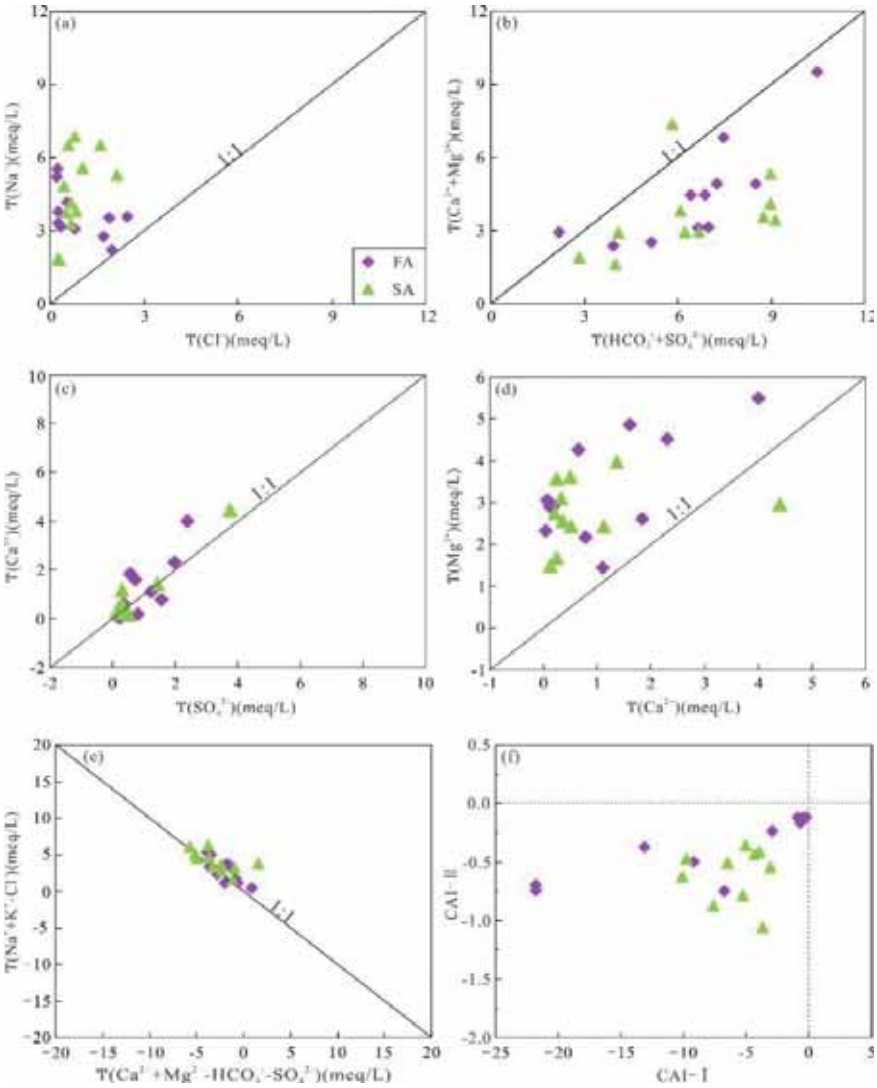


FIGURE 6
Proportional ionic relation

Ion source analysis based on ion ratio. Ion ratio can be used to infer the material source and formation process of groundwater and further provide prominence to the temporal and spatial evolution mechanisms of hydrochemical components [25-27]. Figure 6 shows the various ion ratios.

The possible sources of Na and K in natural waters are usually atmospheric precipitation, halite dissolution, and the weathering of Na-bearing silicate minerals [19]. In atmospheric precipitation, T (Na+)/T(Cl-) is approximately 0.86 [19]. Na only weathers from halite dissolution, and T (Na+)/T (Cl-) is 1 in halite dissolution [27]. If T(Na+)/T(Cl-) is higher than the sea-water value of 0.86 and the halite value is 1, then the source of most Na is different from atmospheric precipitation and halite dissolution [20]. In the present study, T (Na+)/T(Cl-) ranges from 1.22 to 22.5 and has a mean value of 7.75. Figure 6(a) shows that the computed T(Na+)/T(Cl-) is distributed above the straight line of T(Na+)/T(Cl-) = 1 and located very close to the Na+ axis. These results indicated that, besides halite dissolution and atmospheric precipitation, a great part of Na present in the studied groundwater weathered from Na-bearing silicate minerals.

In natural groundwater, Ca2+, Mg2+, HCO3-, and SO42- are mainly derived from the dissolution of carbonate, calcium magnesium sulfate, and silicate [25]. The proportional relationship between T (Ca2+ + Mg2+) and T(HCO3− + SO42-) can be used to determine whether HCO3- is obtained from silicate and carbonate dissolution in groundwater [24]. Figure 6(b) shows that most of the groundwater samples in FA and SA are under the straight line of T(Ca2+ + Mg2+)/T(HCO3- + SO42-) = 1, which indicates the relative excess of HCO3- and SO42-. Most sampling points are located on both sides of the line of T (Ca2+)/T (SO42-) = 1 in Figure 6(c); thus, only HCO3- is relatively excess. Silicate dissolution produces Na+ and substantial HCO3- during rock dominance. Therefore, HCO3- might mainly stem from the reaction of soluble CO2 with silicate in water.

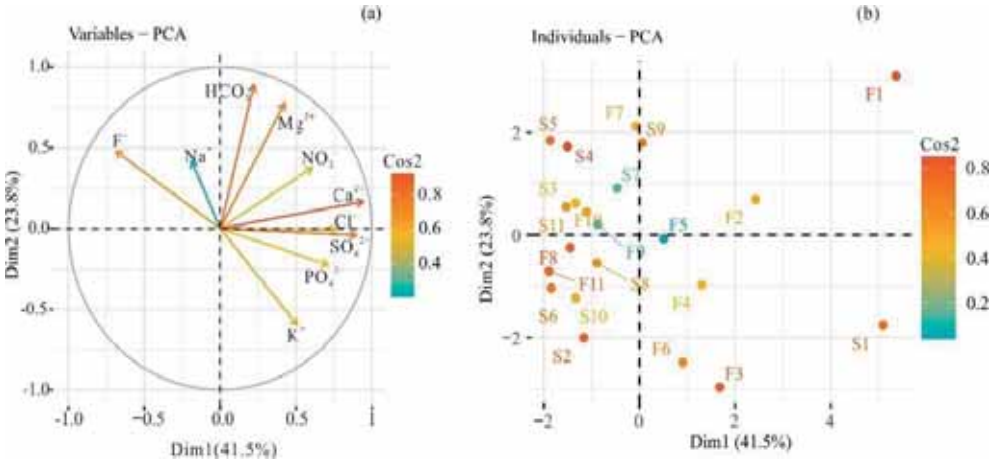


FIGURE 7
(a) Variable load diagram and (b) scatterplot of principal component score

Ca2+ and Mg2+ usually originate from carbonate or silicate dissolution in groundwater [19]. If T(Mg2+)/T(Ca2+) = 1, then Ca2+ and Mg2+ stem from dolomite or carbonate dissolution; if T(Mg2+)/T(Ca2+) > 1, then Mg2+ stems from silicate dissolution. Figure 6(d) shows that most of the water samples are above the line of T(Mg2+)/T(Ca2+) = 1. Therefore, Mg2+ stems from silicate dissolution.

The proportional relationship between T(Ca2+ + Mg2+ - HCO3- - SO42-) and T(Na+ + K+ - Cl-) can be used to determine whether cation exchange occurs in groundwater [26]. Figure 6(e) shows that the groundwater samples in FA and SA fall on both sides of the 1:1 straight line. This result indicates the existence of cation exchange in groundwater. CAI can infer the direction of cation exchange in groundwater. Figure 6(f) shows that the groundwater samples in FA and SA are located at the negative half axis of CAI-I and CAI-II. Therefore, positive cation exchange occurred in the groundwater samples.

Principal component analysis. PCA is a dimensionality reduction mode that combines the relevant original variables into new unrelated combination factors to highlight important variables [28]. The results obtained using the R language software are shown in Figure 7. Two PCA dimensions (principal components 1 and 2) were extracted from the graph. The components can reflect 64.5% of the original data. The majority of the ions are concentrated in the first and fourth quadrants (Figure 7a). The 22 samples were divided into four quadrants (Figure 7b).

Figure 7(b) shows that the ions of samples F1–F6 and S1 are located in the first and fourth quadrants. These two quadrants included NO3-, Ca2+, Cl-, SO42-, PO43-, and K+, as show in Figure 7(a). Under natural circumstances, minerals usually do not produce NO3- in groundwater [29]. Therefore, NO3- is obtained from domestic sewage, industrial and mining activities, and other anthropogenic sources. These results agree with the CV analysis. Therefore, the seven samples were mainly affected by anthropogenic sources. Figure 1 also shows that the seven samples are distributed near the urban area.

The second quadrant is mainly contributed by F- and Na+, and F- is the main contributor. The ion ratio source analysis indicated that Na+ was obtained from silicate dissolution (Figure 6a). Although the correlation between F− and Na+ is relatively low, a certain correlation evidently exists between them. Therefore, the main natural source of F- and Na+ was affected. The study area in Figure 1 shows that the sample points in the second quadrant are far away from the urban area and accord with these conclusions. The samples have no major ion contribution in the third quadrant; therefore, the location of samples was mainly affected by natural source. As a result, except for S1 and F1–F6, the other samples were mainly affected by natural sources.

CONCLUSIONS

SAR, Kelley's ratio, and other irrigation indexes were used for evaluating the suitability of groundwater in the Chengxi water source area for irrigation. Meanwhile, the main chemical composition of groundwater was analyzed using Piper diagram, Gibbs diagram, ion ratio, and PCA. The main conclusions were as follows:

(1) The evaluation of irrigation indexes showed that most of the water samples in the study area were unsuitable for irrigation because of high Na+, Mg2+, and HCO3- levels.

(2) The main hydrochemical type of groundwater in study area was Na–Mg–HCO3. The Gibbs diagram showed that the ion composition was controlled by water–rock dominance in groundwater. The ion ratio indicated that the hydrochemical composition of groundwater was affected by silicate weathering, and a small part samples was affected by carbonate dissolution. Na+ and Mg2+ were weath-

ered from silicate. HCO3− originated from the reaction of dissolved CO2 in water with silicate. The calculation results of CAIs showed that cation exchange exists in groundwater, and Na+ and K+ were replaced by Ca2+ and Mg2+, respectively.

(3) PCA results showed that the S1 and F1–F6 samples were affected by anthropogenic sources, and the other samples were controlled by natural sources.

ACKNOWLEDGEMENTS

This work was financially supported by Natural Science Research Project of Universities in Anhui Province (KJ2020ZD64; KJ2020A0740), and Doctoral Scientific Research Foundation of Suzhou University (2019jb15).

REFERENCES

[1] Wang, S.Q., Shao, J.L., Song, X.F., Zhang, Y.B., Huo, Z.B. and Zhou, X.Y. (2008) Application of MODFLOW and geographic information system to groundwater flow simulation in North China Plain, China. Environmental Geology. 55(7), 1449-1462.

[2] Zhou, Y.H., Li, P.Y., Xue, L.L., Dong, Z.H. and Li, D. (2020) Solute geochemistry and groundwater quality for drinking and irrigation purposes: a case study in Xinle City, North China. Geochemistry. 80(4), 125609.

[3] Qiu, J. (2011) China to Spend Billions Cleaning Up Groundwater. Science. 334(6057), 745.

[4] Cai, H., Mei, Y.D., Chen, J.H., Wu, Z.H., Lan, L. and Zhu, D. (2020) An analysis of the relation between water pollution and economic growth in China by considering the contemporaneous correlation of water pollutants. Journal of Cleaner Production. 276, 122783.

[5] MEEC (Ministry of Ecology and Environment of China). (2018) China's Eco-environment status Bulletin 2017. Ministry of Water Resource of China (in Chinese).

[6] Hussain, R., Wei, C.H. and Luo, K.L. (2019) Hydrogeochemical characteristics, source identification and health risks of surface water and groundwater in mining and non-mining areas of Handan, China. Environmental Earth Sciences. 78(14), 402.

[7] Zhang, H., Xu, Y., Cheng, S.Q., Li, Q.L. and Yu, H.R. (2020) Application of the dual-isotope approach and Bayesian isotope mixing model to identify nitrate in groundwater of a multiple land-use area in Chengdu Plain, China. The Science of the Total Environment. 717, 137134.

[8] Wang, Y.J., Peng, J.F., Cao, X.F., Xu, Y., Yu, H.W., Duan, G. and Qu, J.H. (2020) Isotopic and chemical evidence for nitrate sources and transformation processes in a plateau lake basin in Southwest China. The Science of the Total Environment. 711, 134856.

[9] Zhang, X.Y., Miao, J.J., Bill, X.H., Liu, H.W., Zhang, H.X. and Ma, Z. (2017) Hydrogeochemical characterization and groundwater quality assessment in intruded coastal brine aquifers (Laizhou Bay, China). Environmental Science and Pollution Research. 24(26), 21073-21090.

[10] Zuo, R., Liu, X., Yang, J., Zhang, H.K., Li, J., Teng, Y.G., Yue, W.F. and Wang, J.S. (2019) Distribution, origin and key influencing factors of fluoride groundwater in the coastal area, NE China. Human and Ecological Risk Assessment: An International Journal. 25(1-2), 104-119.

[11] Yu, G.M., Wang, J., Liu, L., Li, Y., Zhang, Y. and Wang, S. S. (2020) The analysis of groundwater nitrate pollution and health risk assessment in rural areas of Yantai, China BMC Public Health. 20, 437.

[12] Su, H., Kang, W.D., Xu, Y.J. and Wang, J.D. (2017) Assessing Groundwater Quality and Health Risks of Nitrogen Pollution in the Shenfu Mining Area of Shaanxi Province, Northwest China. Exposure and Health. 10(2), 77-97.

[13] Qiu, H.L., Gui, H.R., Cui, L., Pan, Z.G. and Lu, B. (2019) Hydrogeochemical characteristics and water quality assessment of shallow groundwater: a case study from Linhuan coal-mining district in northern Anhui Province, China. Water Science & Technology Water Supply. 19(5), 1572-1578.

[14] Chen, K., Sun, L.H., Liu, Q., Cao, W.M. and Tang, J. (2019) Quality evaluation and its controlling factor analyses of shallow groundwater in the urban area of Suzhou, Anhui Province, China. Fresen. Environ. Bull. 28(9), 6801-6807.

[15] Qiu, H.L. and Gui, H.R. (2019) Heavy metals contamination in shallow groundwater of a coal-mining district and a probabilistic assessment of its human health risk. Human and Ecological Risk Assessment: An International Journal. 25(3-4), 548-563.

[16] [16] Qiu, H. L., Gui, H. R. and Song, Q. X. (2018) Human health risk assessment of trace elements in shallow groundwater of the Linhuan coal-mining district, Northern Anhui Province, China. Human and Ecological Risk Assessment: An International Journal. 24(5), 1342-1351.

[17] Karunanidhi, D., Vennila, G., Suresh, M. and Subramanian, S. (2013) Evaluation of the groundwater quality feasibility zones for irrigational purposes through GIS in Omalur Taluk, Salem District, South India. Environmental Science and Pollution Research. 20(10), 7320-7333.

[18] Arumugam, K. and Elangovan, K. (2009) Hydrochemical characteristics and groundwater quality assessment in Tirupur Region, Coimbatore District, Tamil Nadu, India. Environmental Geology. 58(7), 1509-1520.
[19] Zhu, B.Q., Wang, X.M. and Rioual, P. (2017) Multivariate indications between environment and ground water recharge in a sedimentary drainage basin in northwestern China. Journal of Hydrology. 549, 92-113.
[20] Nagaraju, A., Thejaswi, A. and Sun, L.H. (2016) Statistical Analysis of High Fluoride Groundwater Hydrochemistry in Southern India: Quality Assessment and Implications for Source of Fluoride. Environmental Engineering Science. 33(7), 471-477.
[21] Guo, Q.N., Zhang, J.M., Hu, Z.L. and Zhou, Z.W. (2020) Hydrochemical and Isotopic Evolution of Groundwater Flowing Downstream of the Daqing River (Liaodong Bay, China). Journal of Coastal Research. 36(3), 608-618.
[22] Wang, H., Jiang, X.W., Wan, L., Han, G.L. and Guo, H.M. (2015) Hydrogeochemical characterization of groundwater flow systems in the discharge area of a river basin. Journal of Hydrology. 527, 433-441.
[23] Gibbs, R.J. (1970) Mechanisms controlling world water chemistry. Science. 170, 1088-1090.
[24] Zhu, B., Yang, X., Rioual, P., Qin, X.G., Liu, Z.T., Xiong, H.G. and Yu, J.J. (2011) Hydrogeochemistry of three watersheds (the Erlqis, Zhungarer and Yili) in northern Xinjiang, NW China. Applied Geochemistry. 26(8), 1535-1548.
[25] Ghobadi, M.H., Stakhri, M.D.A. and Mirarabi. A. (2018) Investigating the hydrogeological properties of springs in a karstic aquifer in Dorfak region (Guilan Province, Iran). Environmental Earth Sciences. 77, 96.
[26] Senarathne, S., Jayawardana, J.M.C.K., Edirisinghe, E.A.N.V. and Chandrajith, R. (2021) Influence of regional climatic on the hydrogeochemistry of a tropical river basin—a study from the Walawe river basin of Sri Lanka. Environmental Science and Pollution Research. 28, 15701-15715.
[27] Das, P., Maya, K. and Padmalal, D. (2021) Hydrochemistry, geothermometry and origin of the low temperature thermal springs of South Konkan region, India. Geothermics. 90, 101997.
[28] Mohammad, N.H., Khalidur, R., Tajmunnaher. and Mohammad, R.B. (2020) Assessment of ground water quality in the vicinity of Sylhet City, Bangladesh: a multivariate analysis. Sustainable Water Resources Management. 6, 88.
[29] Hu, J., Long, Y.C., Zhou, W., Zhu, C.B., Yang, Q., Zhou, S.Q. and Wu, P. (2020) Influence of different land use types on hydrochemistry and heavy metals in surface water in the lakeshore zone of the Caohai wetland, China. Environmental Pollution. 267, 115454.

Received: **05.04.2021**
Accepted: **02.05.2021**

CORRESPONDING AUTHOR

Linhua Sun
School of Resources and Civil Engineering,
Suzhou University,
Anhui 234000 – China

e-mail: sunlinh@126.com

© by PSP Volume 30– No. 09/2021 pages 10782-10789 Fresenius Environmental Bulletin

MODIFICATION AND PERFORMANCE EVALUATION OF INDUSTRIAL FODDER CHOPPING MACHINE

Rashad A Hegazy[1,*], Wael M Moussa[2], Ali B El-Nagar[2], Ismail A Abdelmotaleb[1]

[1]Agric. Eng. Dept., Faculty of Agriculture, Kafrelsheikh University 34511, Egypt
[2]Rice Mechanization Center (RMC), Agric. Eng. Research Institute (AEnRI), Agricultural Research Center (ARC), Giza, Egypt

ABSTRACT

Star forage chopper machine (SFCM) was modified and tested to reduce the power required and to improve forage cutting efficiency, also, it will reduce the environmental and health impacts by replacing diesel-based farm machines with electrically operated ones. Power transmission assembly, rotating cutter head knives and straw outlet position modified, and newly constructed feed rollers were added and positioned to control plant material chopping process. The performance of SFCM was evaluated based on its ability to chop rice straw and cotton stalks under three different feed rates 0.8, 1.2 and 1.5 t/h four different knife speed, 78.6 (750), 91.1 (1000), 115.2 (1250) and 136.2 (1500) m/s (rpm). Minimum cut lengths were 1.35 and 1.27 cm for rice straw and were achieved by using the highest feed rate of 1.5 t/h with the maximum of knife speed 136.2 m/s with using toothed blades and normal (flail) blades respectively. At higher feed rates, either power required cutting rice straw or cotton stalks increased with increasing knife speed under the two types of new knifes. Minimum power required to cut rice straw were 1.81 and 1.76 kW and were achieved by using feeding rate of 0.8 t/h with knife speed of 78.6 m/s for toothed blades and normal (flail) blades respectively. Rice straw and cotton stalks cutting efficiency decreased with increasing feeding rates and increased with increasing knife speeds. Specific energy for cutting rice straw and cotton stalks decreased with increasing feeding rates and decreased also with increasing knife speeds.

KEYWORDS:
Animal feed, crop residue, chopping power

INTRODUCTION

Agricultural residues are the most abundant biomass and animal feed resources in Egypt. Due to the size of agricultural production, a large volume of residues is generated from this sector each year, the total residue produced for all the selected residue types was estimated to be around 30 Mtonnes/year. A large portion of these residues consists of those from cereals (67.6 percent), with wheat straw making up the largest share (37.7 percent), followed by maize stalk (16.6 percent) and rice straw (10.7 percent) [1]. Around 52 % chopping; by hand with a machete; by using a hand-operated chopper; an engine-driven chopper or an engine-driven chuff cutter. Both electric and petrol-driven motors are used widely to power mechanical choppers and chaff cutters too [3]. Chopping is a prerequisite for either use, and or reducing the shearing force has been considered as one of the most effective approaches to save energy [4]. A feed chopper is mechanical device used to cut and properly processes the straw or hay into small pieces to mix it together and fed to cattle. This improves animal digestion and prevents animal from rejecting any part of their food. In addition, it improves feed intake and thus might be a viable option to help cows cope with less nutrient-dense feeds [5, 6]. Therefore, to increase the productivity and reduce the physical effort required for running the machine, improved and motorized machineries came into existence to support farmers and animal feed processors. Presently fodder-cutting machines are electric driven as well as hand operated or engine driven [7].

[8] Recommended using engine-driven feed choppers as they proved their effectiveness in terms of different chopping efficiency, output capacity and conservation of moisture and content in crop stalks. Engine-driven chopper has been developed by [9] for chopping of maize stalk and grass. The machine was designed with feed chopper, rotating drum with swinging knives, casing with fixed knives welded on it, a screen and stands as main components. The test result showed that the optimum drum speed and feed rate values for both maize stalk and grass were 1200 rpm and 40 kg h-1 respectively. The average size reduction percentage using these optimum combinations was 92.0% and 79.5% for maize stalk and grass respectively. [10] Conducted field experiments to evaluate the performance of a modified thresher machine for chopping two types of crop residues namely rice straw and cotton stalks. They concluded that the optimum operation conditions for cutting rice straw was at cutting rotor speed of 19.6 m/s, stalks moisture content of 10.45 %, and using swinging knives and for cutting cotton stalks was at cutting rotor speed of 27.5 m/s, stalks moisture content of 8.37 %, and using rotating knives. [11] Constructed

and evaluated a fodder-bales chopper in terms of chopping productivity and efficiency and required power. Results cleared that the maximum machine productivity values were 785.5 and 830.7 kg/h, the maximum required power values were 20.86 and 22.64 kW, and the maximum chopping efficiency values were 96.8 and 97.4% when the chopper used with wheat straw and rice straw bales respectively by using combined knives with hammers at drum speed of 1040 rpm.

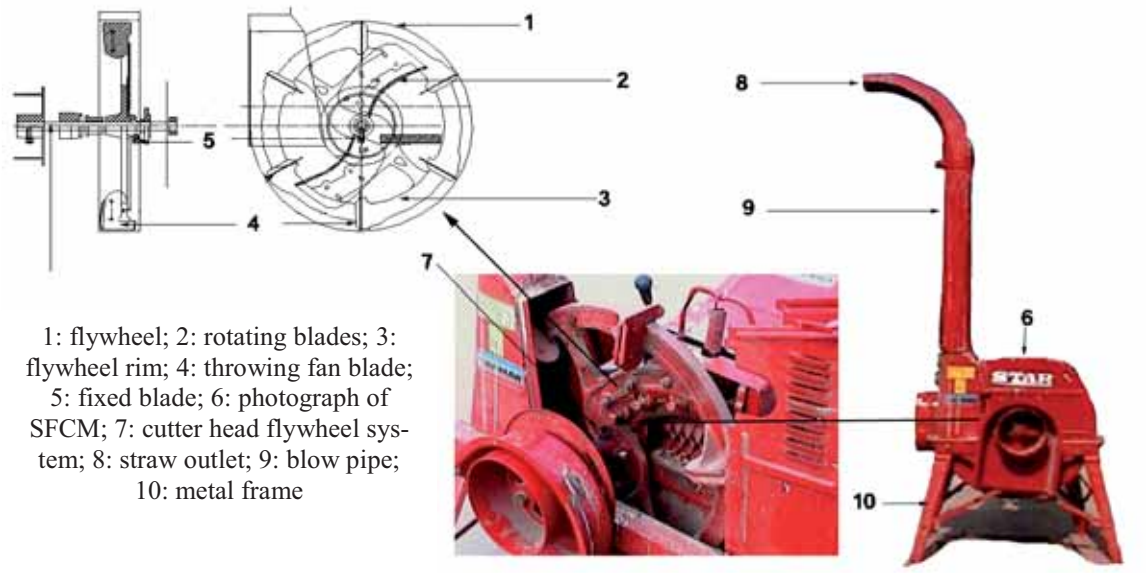
[12] Determined the optimum machine working conditions for making a good silage from fodder beet tubers using small local prototype forage chopper machine. The highest recorded actual capacity and machine efficiency were 3.412 Mg/h and 88.41% respectively. In addition, minimum recorded total losses and energy required were 7.65%, 0.767 kW.h/Mg respectively. From literature review, it is recommended to work further to modify, promote and to adapt fodder choppers. Therefore, this research work was aimed at demonstrating and evaluate a modified engine driven feed chopper, which is star forage chopper machine (SFCM) for reducing power requirement and to improve the cutting efficiency.

MATERIALS AND METHODS

Star forage chopper machine (SFCM) was modified at private engineering workshop and tested at Rice Mechanization Research Center (RMRC), Meet El-Deeba, Kafr El-Sheikh Governorate, Egypt during 2018. The present research was carried out to change SFCM that was used only for chopping maize stalks to be suitable for chopping more residual materials such as rice straw and cotton stalks with using electricity as the power source to run the modified SFCM.

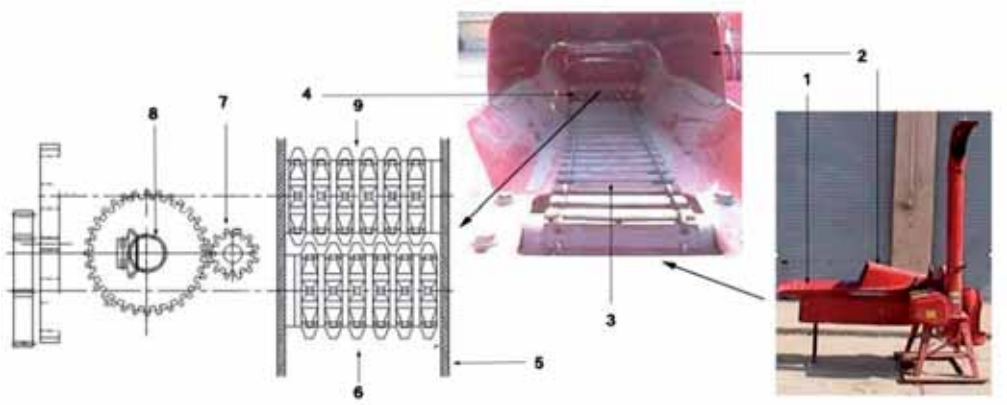
Star forage chopper machine (SFCM) is a stationary flywheel chopper machine. The machine consists primarily of a feed chain, upper and lower feed rollers, a stationary lower blade, a cutter and a throwing fan. The straw is fed via the feed chain into the feed rollers, pressed and moved forward by them, then cut into pieces by the combination of upper and lower blades, and it is finally blown by the fan to the storage site or containers. The power is coming from the source (often a tractor) by flat belt to the plane pulley fixed on the main axial of the machine. The cutter head flywheel system consists of two types of knives; first type is rotating flat and logarithmic curved edge knife, where, two knives fixed on arms of the flywheel with 180o between each other and they rotate in clockwise direction. Second type is fixed flat and straight edge knife and only one knife is fitted at 4 cm down the level of the flywheel axis (Figure 1). SFCM has flat pulley rotate by tractor as power source, so the machine rotate with one speed for cutting (770 rpm) with high slippage between belt and pulley and low power transmission efficiency. The overall dimensions of developed machine were 157 x 87.5 x 163 cm as length, width and height respectively.

SFCM' feeding system consists of; trough as feeding inlet for the material intended to be cut, the material slides on the floor by forward moving of conveyer; conveyor driven by pentagonal wheel; conveyer roll on the back of the trough; pentagonal wheel turned by chain and two sprockets to move the conveyor from back side to forward direction; powered feeding drums fixed in the entrance of the feeding gate. The feeding system movement is correlated to the cutting system movement with help of bevel and spur gears and quick coupling components under feeding gears ratio (Figure 2).



1: flywheel; 2: rotating blades; 3: flywheel rim; 4: throwing fan blade; 5: fixed blade; 6: photograph of SFCM; 7: cutter head flywheel system; 8: straw outlet; 9: blow pipe; 10: metal frame

FIGURE 1
Star forage chopper machine (SFCM).



1: inlet feeding trough; 2: feeding gate; 3: conveyor; 4: feeding drums; 5: guide plates; 6: lower feed drum; 7: spur gear; 8: bevel gear; 9: upper feed drum

FIGURE 2
Feeding system, movement mechanism and feeding drums.

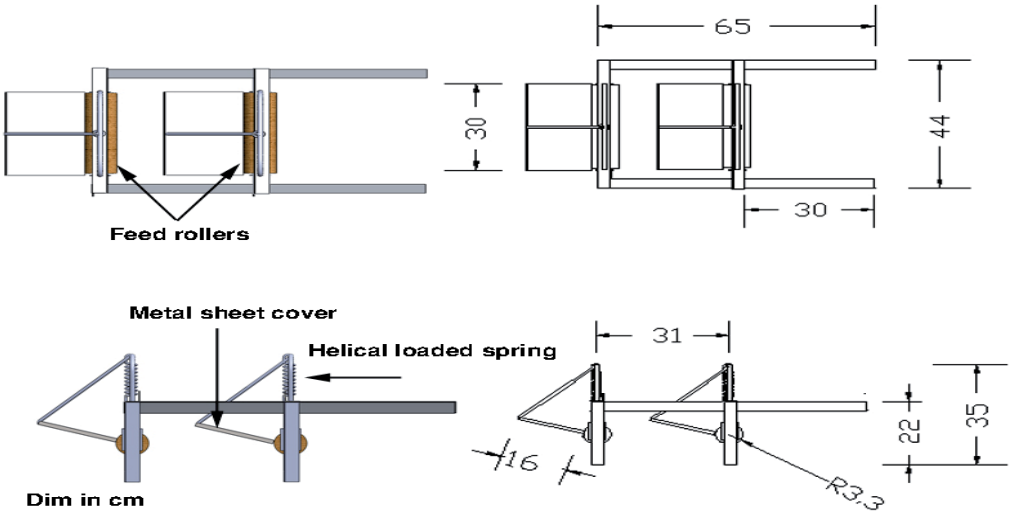


FIGURE 3
Feed rollers

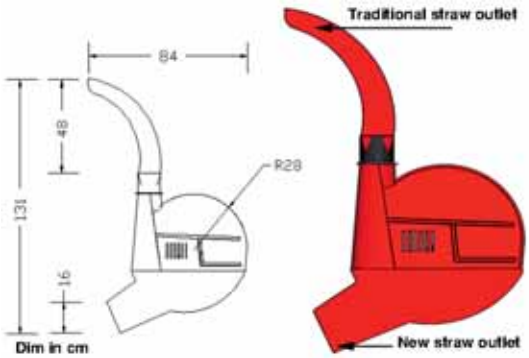


FIGURE 4
New straw outlet position

Feeding rollers are positioned and are adapted to control plant material to be chopped forward. Two-30 cm wide cylindrical feed rollers were used to gather, compress and advance the crop into the feeding drums. These feed rollers have adjustable clearance by moving vertically with help of helical loaded springs according to amount and volume to be fed into the hopper. A metal sheet cover was fixed in front of each roller to direct the feed to the feed rollers (Figure 3).

Lower straw outlet position has been made to collect chopped material directly after cutting to

shorten the distance and reduce the energy required to move chopped material though the blow pipe and the upper straw outlet (Figure 4).

Two types of new knives, to guarantee the best possible chopping quality, replaced traditional curved rotating knives that are attached in the cutter head flywheel. The new knives are pressed out of steel strap. Longitudinal operating edges are sharpened with making one of them in form of triangular toothed blades, and the other as sharp flat edge blade for longer time cutting operation. Six openings is drilled out on the head of each knife for proper fixing. The finished product goes through thermal processing for enhancing its strength and wear resistance. New cutter head knives shape and specifications are listed in Figure 5 and Table 1.

New power transmission assembly is done mechanically and made up based on an electric motor, belt, shaft and pulley. Tensioner is used to tighten the belt to make a better grip between the pulley and the belt. The electric motor is connected to pulleys of different sizes either driver or driven with belts. Electric motor (5 kW - 1490 r.p.m) was installed with special chasse on machine chasse. By stacking pulleys (drive pulley and driven pulley) of two different diameters on top of one another, four different speed options created just by sliding the belt onto a different set of pulleys. Each set of pulleys is paired such that the belt length and the distance between the pulleys' pivots stay the same while the speed ratio changes (Figure 6). Based on the used different pulleys' sizes, knife speeds were 78.6 (750), 91.1 (1000), 115.2 (1250) and 136.2 (1500) m/s (r.p.m). The speed of the feed rolls has fixed relative speed to the cutter head. All modified parts, systems were adjusted properly, and the modified SFCM fixed on a frame with final dimensions of 157 x 87.5 x 193 cm as length, width and height respectively (Figure 7).



FIGURE 5
New cutter head knives

TABLE 1
New cutter head knives' specifications

Characteristic	value
Weight, kg	0.22
Number of mounting holes, N	6
Mounting holes diameter, cm	1.8
Thickness, cm	5
Length, cm	25
Width, cm	13
Blades	normal flail/toothed
Material	steel

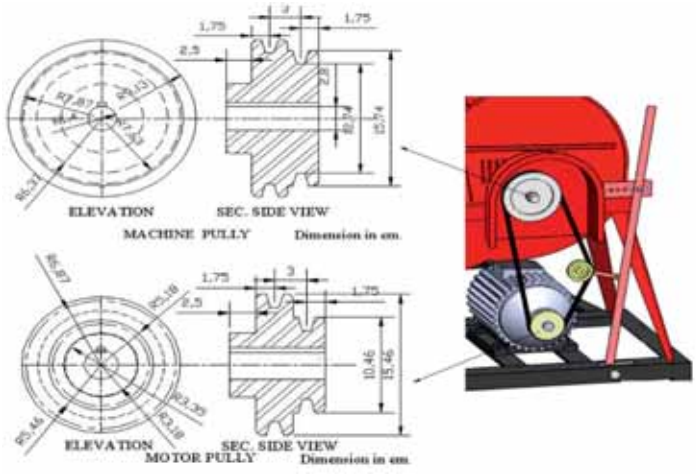


FIGURE 6
New power transmission assembly

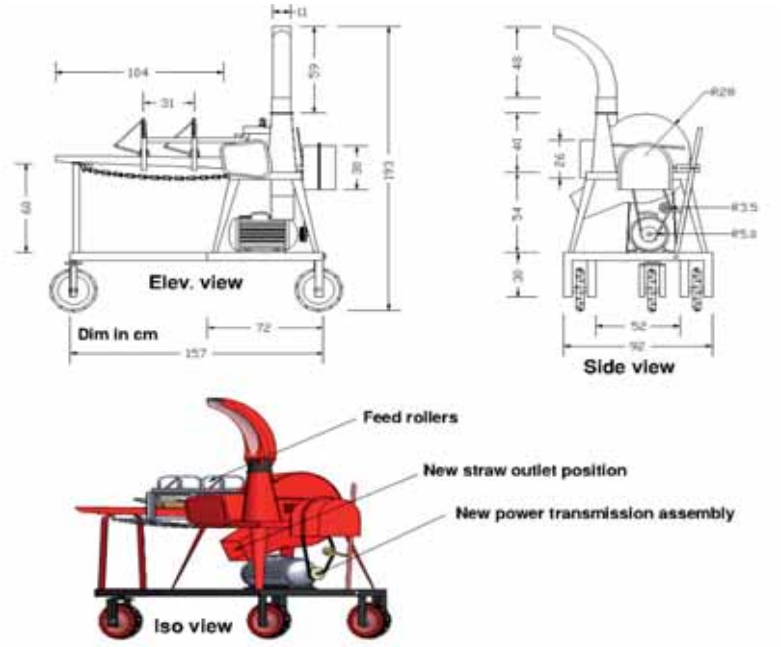


FIGURE 7
Modified SFCM and its final geometry

TABLE 2
Characteristics of used residual material

Characteristic	Cotton stalks	Rice straw
Stem original length, cm	From 90 to 170	Normal length from 85 to 100, after combine harvester from 35 to 45
Average stem diameter, cm	From 0.70 to 1.5	From 0.25 to 0.40
Mass of stalk, g	From 35 to 190	From 15 to 75
Moisture content, %	From 12.25 to 22	From 9 to 15.3
Tensile strength, MPa	12.54 to 30.12	From 30.20 to 50.47
Compressive strength, MPa	7 to 17	8.5 to 13
Bulk density, kg/m^3	165 to 190	165 to 220

Modified SFCM was evaluated against its ability to maintain the desirable residue cutting length, save the power and specific energy required, achieving better cutting efficiency and productivity with the ability to reduce the operating costs. Study variables were three feeding rates (0.8, 1.2 and 1.5 t/h), four different knife speed, 78.6 (750), 91.1 (1000), 115.2 (1250) and 136.2 (1500) m/s (r.p.m), and two types of residual material (rice straw and cotton stalks) with two different knife; blades (normal flail and toothed blades). Moisture content and characteristics of used residual material were recorded and are presented in Table 2. Theoretical length of chopped residual material, power and specific energy required, cutting efficiency and productivity and operating costs for modified SFCM were calculated and recorded.

RESULTS AND DISCUSSION

Average cut lengths of rice straw and cotton stalks were measured and presented in Figure 7. At lower feeding rate (0.8 t/h), increasing knife speed from 78.6 to 136.2 m/s decreased rice straw cut length from 5 to 6 cm and from 5.9 to 4.8 cm with using toothed blades and normal (flail) blades respectively. While the length of cotton stalks reduced from 6.5 to 5.5cm and from 6.2 to 5.4 cm with using toothed blades and normal (flail) blades respectively. Also at higher feed rates, cut length for rice straw and cotton stalks reduced with increasing knife speed under the two types of new knifes. Minimum cut lengths were 1.35 and 1.27 cm for rice straw and were achieved by using the highest feed rate of 1.5 t/h with the maximum of knife speed 136.2 m/s with using toothed blades and normal (flail) blades respectively. Similar cut lengths of cotton stalks were also obtained under same conditions, where, the cut lengths were 1.50 and 1.40 cm with using toothed blades and normal (flail) blades respectively (Figure 8).

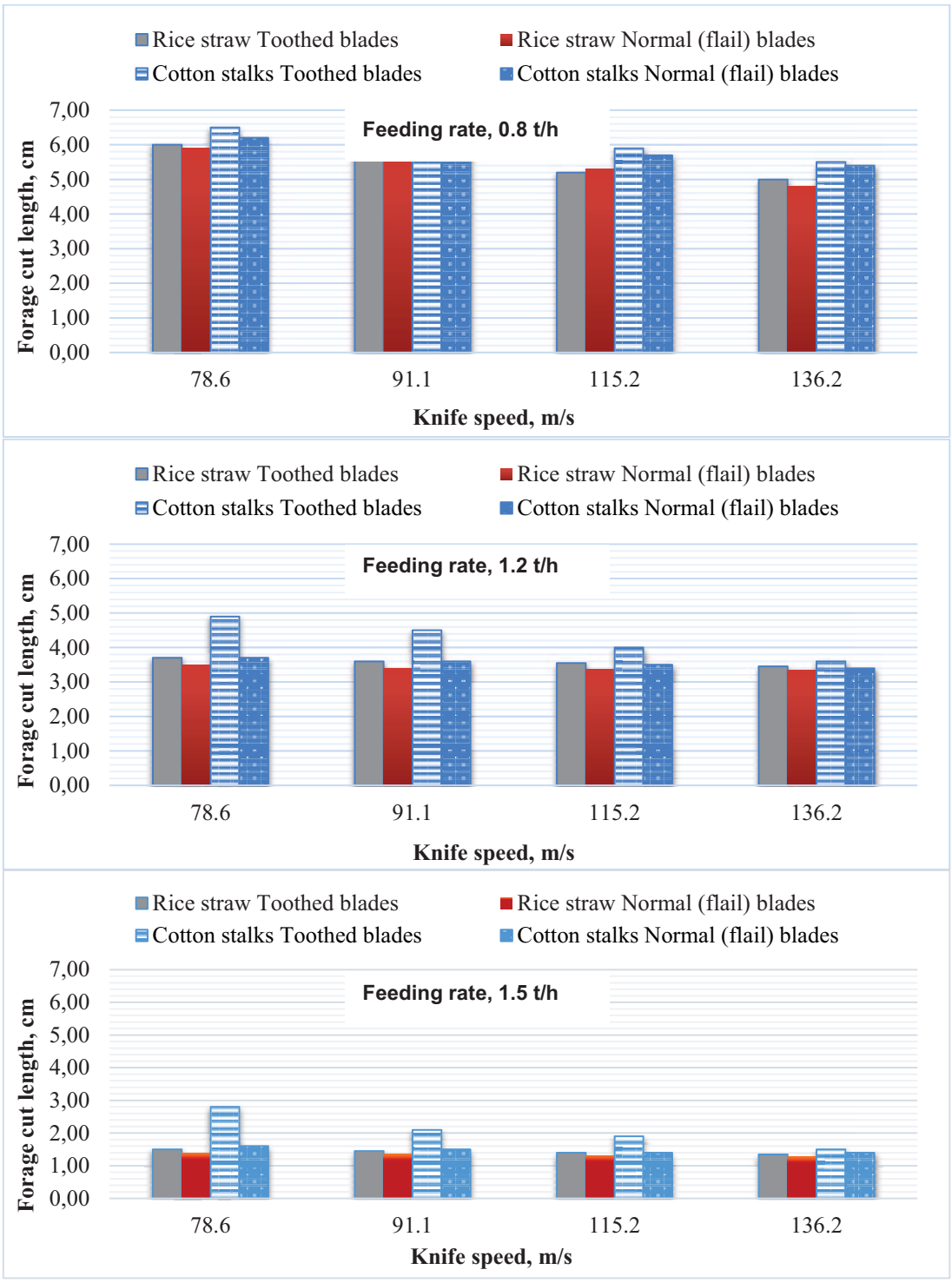


FIGURE 8
Effect of feed rate, knife speed and type on cut length of rice straw and cotton stalks

Increasing knife speed from 78.6 to 136.2 m/s increased the power required to cut rice straw residues from 1.81 to 2.64 kW and increased the power required to cut cotton stalks from 1.76 to 2.42 kW with using toothed blades and normal (flail) blades respectively at 0.8 t/h feeding rate. At higher feed rates, either power required to cut rice straw or cotton stalks increased with increasing knife speed under the two types of new knifes. Minimum power required to cut rice straw were 1.81 and 1.76 kW and were achieved by using the lowest feeding rate of 0.8 t/h with the lower knife speed of 78.6 m/s with using toothed blades and normal (flail) blades respectively. Minimum power required to cut cotton stalks were also obtained under same conditions, where, power required were 1.8 and 1.85 kW with using toothed blades and normal (flail) blades respectively (Figure 9).

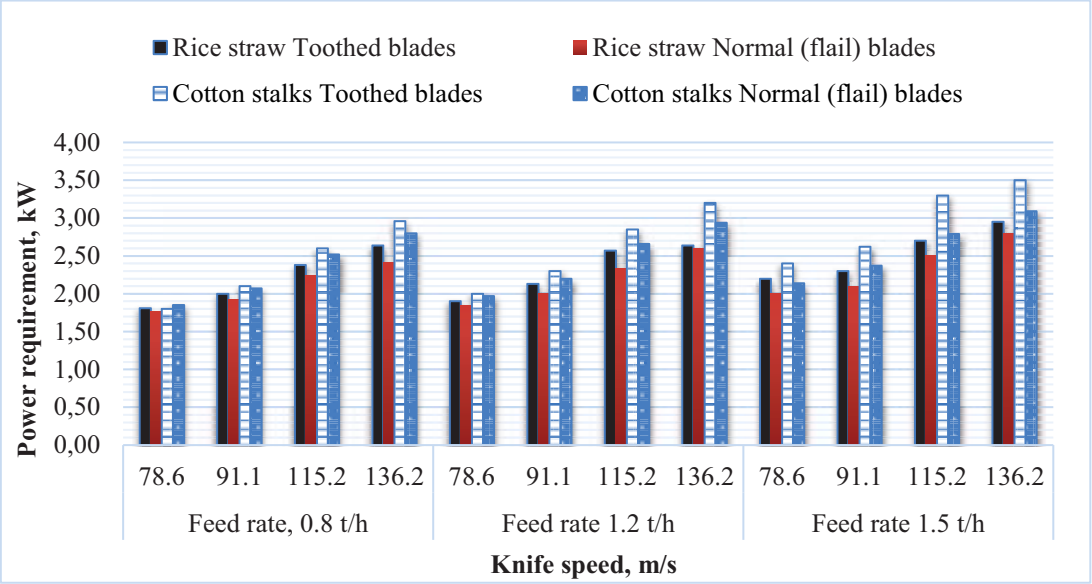


FIGURE 9
Effect of feed rate, knife speed and type on power required for cutting rice straw and cotton stalks

TABLE 3
Rice straw and cotton stalks cutting efficiency and calculated specific energy.

Feed rate, (t/h)	Knife speed, m/s	Toothed blades	Normal (flail) blades	Toothed blades	Normal (flail) blades
		Cutting efficiency, %			
0.8	**78.6**	**63.0**	**66.5**	**72.6**	**74.5**
	91.1	64.8	68.2	73.9	75.8
	115.2	66.7	70.2	75.4	77.2
	136.2	67.9	72.2	76.9	78.5
1.2	**78.6**	**62.0**	**65.4**	**71.0**	**73.9**
	91.1	63.3	67.2	72.3	75.1
	115.2	64.8	69.1	74.0	76.6
	136.2	65.9	71.0	75.3	77.7
1.5	**78.6**	**60.8**	**64.3**	**70.0**	**73.2**
	91.1	61.5	66.1	71.2	74.5
	115.2	62.3	68.0	72.9	75.9
	136.2	64.3	69.3	74.1	76.9
		Specific energy, kW.h/t			
0.8	**78.6**	**1.65**	**1.6**	**2.34**	**2.31**
	91.1	1.6	1.5	2.3	2.3
	115.2	1.5	1.4	2.2	2.2
	136.2	1.4	1.3	2.2	2.1
1.2	**78.6**	**1.2**	**1.1**	**1.7**	**1.7**
	91.1	1.1	1.1	1.7	1.6
	115.2	1.1	1.0	1.6	1.5
	136.2	1.0	0.9	1.5	1.4
1.5	**78.6**	**0.5**	**0.8**	**0.8**	**1.2**
	91.1	0.5	0.7	0.7	1.1
	115.2	0.4	0.6	0.6	1.0
	136.2	0.3	0.6	0.6	0.9

CONCLUSION

Modified SFCM was able to chop the proposed two types of residues (rice straw and cotton stalks) with suitable uniformity in cut lengths. Using the modified chopper gives small-scale animal feed processors the chance to cut the fodder with minimum possible lengths when they operate Modified SFCM at higher feeding rates and higher knife speeds. Both new knifes can be used to achieve good operational parameters. However, it is important to consider the higher power required during the use of SFCM at higher feeding rates and higher knife speeds. Increasing the knife speeds help to obtain higher values of cutting efficiency but increasing the feeding rates will decrease it, so matching between suitable knife speeds and higher feed rates is required. To achieve minimum required specific energy, it is better to consider higher feeding rates and higher knife speeds when power is available and the attention is directed to the production amount.

REFERENCES

[1] Food and Agriculture Organization (FAO). (2017) Sustainable Bioenergy Options from Crop and Livestock Residues: BEFS Assessment for Egypt. FAO's Climate and Environment Division. Food and Agriculture Organization of the United Nations (FAOUN), Rome. P:1–169. Available at: http://www.fao.org/3/a-i6684e.pdf. (Accessed 21 May 2019).

[2] Nakhla, D.A., Hassan, M.G., El Haggar, S. (2013) Impact of biomass in Egypt on climate change. Natural Science. 5(6), 678–684.

[3] Lukuyu, B.A. (2015) Chopping of green fodder and forages. Feed Intervention TechSheet 32, TechFit. CGIAR Research Program on Livestock and Fish. P:1–12. Available at: https://cgspace.cgiar.org/bitstream/handle/10568/75596/Techsheet32.pdf?sequence=3&isAllowed=y. (Accessed 16 July 2019).

[4] Van-Dam, V., Quoc-Huy, N., Thanh-Toan, N., Huu-Cong, N., Quoc-Tuan, N., Van-Du, N. (2020) Multi-objective optimisation of cutting force and cutting power in chopping agricultural residues. Biosystems Engineering. V(191), 107–115.

[5] Umer, A.T. and Usmane, I.A. (2020) Demonstration of Improved Elephant/Napier grass (Pennisetum purpureum) Technologies for Animal Feed Resources in Dire Dawa and Harari Region rural areas: Glob. J. Ecol. 5, 014–017.

[6] Kahyani, A., Ghorbani, G.R., Alikhani, M., Ghasemi, E., Sadeghi-Sefidmazgi, A., Beauchemin, K.A. (2019) Performance of dairy cows fed diets with similar proportions of undigested neutral detergent fiber with wheat straw substituted for alfalfa hay, corn silage, or both. J. Dairy Sci. 102, 10903–10915.

[7] Sankpal, N., Power, V., Patil, S., Salunke, K., Pandit, S.V. (2017) Design and Modification of Chaff Cutter Machine. International Journal of Innovative Research in Science, Engineering and Technology 6(4), 5675–5683. Available at: http://www.ijirset.com/upload/2017/april/126_DESIGN.pdf. (Accessed 23 March 2020).

[8] Umer, A.T., Usmane, I.A., Nur, J., Umer, A. (2020) Engine driven feed chopper technology demonstration for animals' feed preparation in the selected districts of AGP-II in Harari region and Dire Dawa Administration. J. Food Sci. Nutr. 6(1), 011–014.

[9] Tekeste, S. and Biweta, W. (2012) A Design Study of a Motor-Driven Chopper for Chopping Crop Residue and Hay. The IUP Journal of Mechanical Engineering. V(3), 68–75, Available at: https://ssrn.com/abstract=2179499.

[10] Basiouny, M. A., El-Yamani, A.E. and El-Shazely, A.E. (2015) Modifying of a Local Thresher for Chopping Crop Residues. J. Soil Sci. and Agric. Eng., Mansoura Univ. 6(1), 143-163.

[11] AL-Gezawe, A.A., Abd El-hamid, S.G. and Ghandour, A. (2016) Development of a Fodder Bales Chopper. Misr J. Ag. Eng. 33(4), 1255–1272.

[12] Hassan, M.A. (2019) Performance Evaluation of a Small Machine for Chopping Fodder Beet. J. of Soil Sciences and Agricultural Engineering, Mansoura Univ. 10(10), 579–587. Available at: https://jssae.journals.ekb.eg/article_59499_632669794372eacbc97899a35004f304.pdf. (Accessed 28 August 2020).

Received: **05.04.2021**
Accepted: **16.05.2021**

CORRESPONDING AUTHOR

Rashad Aziz Hegazy
Agric. Eng. Dept.,
Faculty of Agriculture,
Kafrelsheikh University
34511 – Egypt

e-mail: rashad.hegazy@agr.kfs.edu.eg

© by PSP Volume 30– No. 09/2021 pages 10790-10796 Fresenius Environmental Bulletin

CURRENT EPIDEMIOLOGICAL STATUS OF CUTANEOUS LEISHMANIASIS IN DIFFERENT VILLAGES OF DISTRICT MALAKAND KP PROVINCE, PAKISTAN: A PERSPECTIVE STUDY

Abdullah[1,*], Muddaser Shah[2,3], Muhammad Salman[1], Sohail Ahmad Jan[4], Ayesha Bibi[5], Zobia Afsheen[1], Muhammad Riaz[1,6], Muddasir Khan[1], Sidra Mubin[7], Parveen Bibi[2], Obaid Ullah[3,8], Attaullah[9]

[1]Department of Health and Biological Sciences, Abasyn University Peshawar, Khyber Pakhtunkhwa (KP), Pakistan
[2]Department of Botany Abdul Wali Khan University Mardan, Pakistan
[3]Natural and Medical Sciences Research Center, University of Nizwa, Birkat Al Mauz 616, Nizwa
[4]Department of Bioinformatics and Biosciences, Capital University of Science and Technology, Islamabad, Pakistan
[5]Department of Human Nutrition and Dietetics, Women University Mardan, Pakistan
[6] Department of Zoology, Government Degree College Lakarai, District Mohmand, Khyber Pakhtunkhwa (KP), Pakistan
[7]Department of Botany, Hazara University Mansehra, Pakistan
[8]Department of Chemistry, University of Malakand, Chakdara, KP, Pakistan
[9]Center for Human Genetics, Hazara University Mansehra, KP, Pakistan

ABSTRACT

The current study was aimed to investigate the epidemiological status cutaneous leishmaniasis, in endemic regions of district Malakand KP province of Pakistan. The prospective study was conducted during July 2020 to December 2020 in different villages of district Malakand KP province. A total of 278 CL active lesions samples were collected by applying cotton on the lesion site with 100% of ethanol and then punctured via disposable blood lancet. The blood or tinged fluid was then poured on the slide. Microscopy on Giesma stained slides were done of all collected lesion samples. The data were analyzed by using Chi square tests, SPSS version 23.0. A major portion (54%; n=151) of age group 1-15 years were more effected with CL. The highest prevalence 54% was found in males followed by females 46%. The statistical analysis revealed a significant association (p value = 0.02) between the various age groups and gender with 5% significance level. No association between the lesion and gender was observed. The mean age was found to be 18.63±15.91 years. It is concluded that CL infection is health threatening issue for local population of District Malakand. Current study could be helpful for health authorities to take instant action against this negligible disease. Additionally, the healthcare department should arrange sessions and awareness campaigns for locals.

KEYWORDS:
Cutaneous leishmaniasis, Leishmania, Epidemiological status, Malakand, PCR

INTRODUCTION

The Cutaneous type of leishmaniasis (CL) is an endemic disease in Khyber Pakhtunkhwa, Pakistan caused by Leishmania tropica and L. major [1-5]. Globally, this form of leishmaniasis is considered as 9th prevalent skin disease [6]. Mostly in humans, it is found in immune-suppressed people while these parasites are widespread in the endemic localities of the world accompanied by sand-fly vectors [7, 8]. Over twenty species of leishmania are responsible for infection in endemic centers of the world such as Europe, Southern America, Africa, the Middle East, Asia, and the Mediterranean area. There are three types of species which cause infection in human including Visceral leishmaniasis (VL) or kala-azar, CL (cutaneous leishmaniasis) and MCL (mucocutaneous leishmaniasis) [9, 10]. Studies reported that parasites of the leishmanial (proamastigotes) are transmitted by female sand-flies of the genus Phlebotomus to humans [10, 11]. The sandfly sucks the host's blood from its skin and proamstigotes in the saliva are injected into the host [11].

CL is globally the most prevalent clinical form of leishmaniasis, 90 % of all CL cases occur in only seven countries: Afghanistan, Algeria, Brazil, Iran, Peru, Saudi Arabia, and Syria [4]. In Pakistan, there are 37 different types of leishmanial species (Phlebotomus), and the prevalence ratio in some areas is about 65% [12]. The vector propagation of the sand-fly is high winter season (Sep-Nov), the majority of cases are reported in these months. Likewise, the highest prevalence of CL has been recorded in the regions located above sea level (1500-1800 meters) [13]. A few techniques of a laboratory can detect parasites of leishmaniasis such as parasitological, molecular, and immunological methods. PCR is

turning to be a ′gold standard′ method which is effective in diagnosis as compared to microscopy for leishmaniasis [14].

Over one decade thousands of CL cases are reported from different areas Khyber Pakhtunkhwa province of Pakistan, including Timirgara (15), Dir (16), Kohat, Surgul, [14] Dargai, [17], Peshawar [18], Waziristan [19], and Karak, etc. [20-22]. The present study was designed to focus on the investigation of the epidemiological status of recent outbreaks of cutaneous leishmaniasis in District Malakand KP province, Pakistan. The data were collected from CL-positive patients to examine CL lesions.

MATERIALS AND METHODS

Study area. A prospective study was conducted from July 2020 to December 2020 at different villages in district Malakand including Kharkay kalay, Dargai, Meherdai, Wartir, Sakhakot (Jaded,bandajat and Khas), Gukhel, Badraga, Koper, and Heroshah (Figure 1). According to Tehsil headquarter (THQ), Dargai information these villages were chosen for the study of CL infection. All patient details such as name, age, sex, complete address, profession, lesion's nature (active, dry, wet), lesion's number, site of lesion, travel history, type of house, presence of animals, and previous disease history were also documented on a questionnaire.

The procedure of CL tissue collection. Before taking the sample the contaminated site was sterilized by applying cotton with 100% of ethanol and then punctured via disposable blood lancet. The blood or tinged fluid was then poured on the slide. The specimens were then transferred to Talha Clinical Laboratory Dargai for further examination of microscopy.

Staining Slides. The leishmanial suspected smears were fixed by dipping in absolute methyl alcohol and air-dried the slides. The smears were stained with buffered water (1:20) diluted Giemsa for 10 minutes. The stain was washed gently through rinsing distilled water. All the stained slides were air-dried and were kept ready for microscopic examination [23].

Microscopy. The smear slides were kept under a microscope for direct detection of cutaneous leishmaniasis amastigotes. Initially, the slides were observed under a 10X lens. Drop cedar wood oil was poured on the slide and observed under an oil immersion lens. Complete scanning of the smear slides was done under an oil immersion lens for the detection of cutaneous leishmaniasis. Amastigotes form of cutaneous leishmaniasis was found in infected body parts of the patients during microscopic examination of the smear (Image 1). Positive reports were assembled and were used for further analysis by applying different tools.

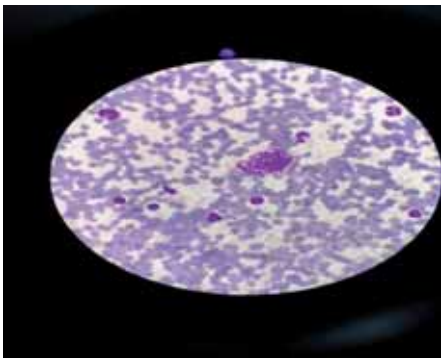


IMAGE 1
Smear shows Amastigotes

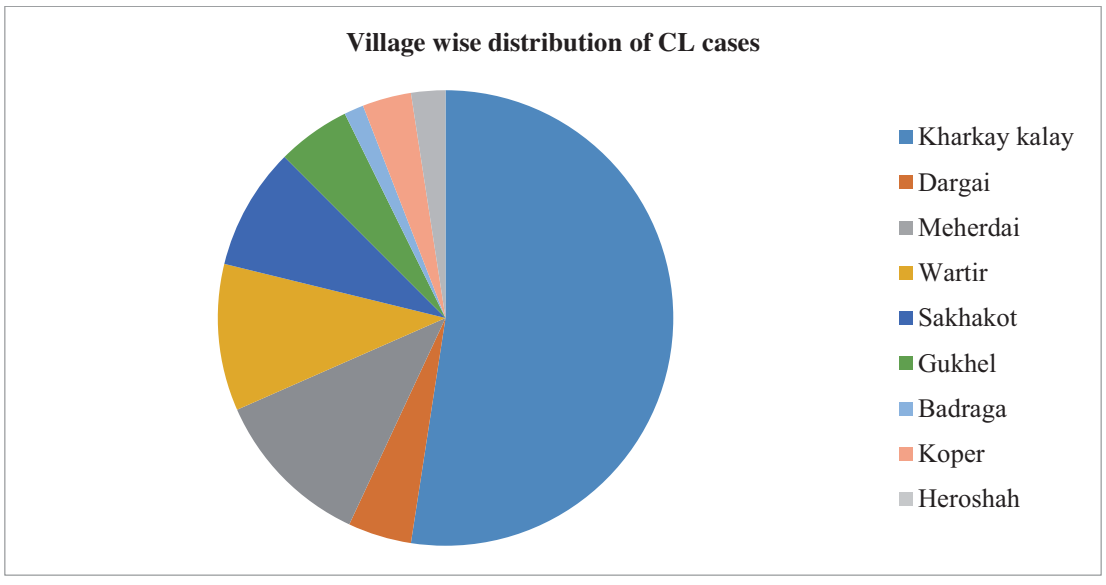


FIGURE 1
Village wise distribution of CL cases

Statistical analysis. The data were analyzed by using Chi square tests, SPSS version 23.0. A p-value less than <0.05 was considered as significant. The association between variable such as gender and age group and gender and lesions were tested. The level of significance (5%) was adopted in the test.

RESULTS

Village wise distribution of CL prevalence. A total of 278 individuals (Active CL lesions) were recorded from 11 villages of district Malakand via questionnaire. The highest prevalence was in Kharky kali (52%), followed by Meherdi (11%), Wartair (10%) and Sakhakot (Khas, jaded and bandajat) with 9% (Figure 1).

Age and gender-wise distribution of CL prevalence. Table 1 and 2 indicates gender and Age-wise prevalence of CL, the highest percentage of infection was found in age group 1-15 years (151\278; 54%) and least infection rate was found in in age group over 46 old individuals. On the other hand, male populations were more effected of CL (142\278; 54%) infection, as compared to females (136\278; 46%).

Lesion specific site distribution. Lesions were predominantly occurred on exposed parts of the body, like face, legs, hands and lips. The highest ratio was found in facial regions (50%), followed by legs (20%), hands (17%) and other body parts (13%) Table 3 & Figure 2.

Distribution of CL lesions by number. Table 4 presents the classification of infected population by number of lesions. The maximum number of patients (54%) carried 1 lesion.83 (30%) patients had two lesions whereas, 16% of infected population carried multiple lesions. Though, single bite was more frequently occurred and every lesion was ulcerated and some of them had a super infection due to bacterial infection.

Lesions duration based prevalence. As Table 5 depicted, there were huge number of patients with lesions 1-3 months duration with prevalence ratio of 55.3%, followed by 26.9% in 4-6 months old lesions. Patients with greater than 6 month's lesions duration yielding prevalence rate of 17%.

The statistical analysis revealed a significant association (p value = 0.02) between the various age groups and gender with 5% significance level. No association between the lesion and gender was observed. The mean age was found to be 18.63±15.91 years.

TABLE 1
Gender-wise frequency of cutaneous leishmaniasis

Gender	No.cases	Microscopy Positive Percentage	No.cases	RT- PCR Positive Percentage
Male	142	54%	28	56%
Female	136	46%	22	44%
Total	278	100%	50	100%

TABLE 2
Age-wise frequency of cutaneous leishmaniasis

Group #	Age groups	No. cases	Microscopy Positive Percentage
1	1-15	151	54%
2	16-30	83	30%
3	31-45	24	8.63%
4	>46	20	7.55%
	Total	278	100%

* The statistical analysis revealed a significant association (p value = 0.02) between the various age groups and gender with 5% significance level

TABLE 3
Distribution of lesions CL on different parts of body infected individuals

Body sites	Infected Individuals	Percentage
Facial regions	139	50
Legs	55	20
Hands	47	17
Other body parts	36	13

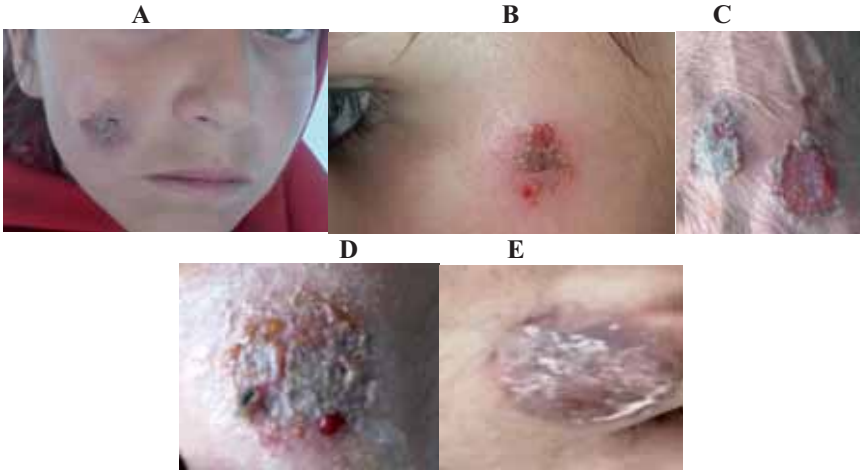


FIGURE 2
The photos shows the lesions on different parts of the body. Photo presents "a" ulcerative lesion on 7 years female face along with 4 years male child on facial in photo "b". "c" CL lesion visible on foot of 45 years male. "d" photo CL lesion is visible 37 male's hand and neck lesion is also visible in "e" photo.

TABLE 4
Distribution of CL with respect to lesions number

One lesion	Two lesion	Multiple Lesion
150	83	44
54%	30%	16%

TABLE 5
Distribution of patients with respect to duration of lesions

Duration in month	Infected individuals	Percentage
1-3	154	55.3
4-6	75	26.9
>6	49	17.6

DISCUSSION

According to published literature, CL is broadly spread in infection-free areas of Pakistan and constantly scattering in various regions of the country [25, 26, and 27]. It is recommended that infection-free regions with nearby CL endemic regions are at huge risk [17]. Concerning this district, Malakand is at a high-risk area for CL owing to sharing borders with endemic regions like Upper and Lower Dir. Therefore, a current study was aimed to determine the current status of CL in different villages in district Malakand KPK, province. We observed the highest incidence of active lesions in different parts of the body (Table 3 & Figure 2) in the native population of the study area. Similarly, the native shared their accommodation with migrants (IDPs) of the hilly areas who visited with their cattle which may promote vector-borne parasitic diseases. In 2013, WHO published a report and claimed that more than 1 million IDPs are settled in different districts of KP province [30]. Amongst the 3 main forms of leishmaniasis, cutaneous leishmaniasis, and visceral leishmaniasis are more prominent in Pakistan. According to previous studies, Zoonotic and Anthroponotic CL is endemic in many regions of the country [2, 18].

We observed the highest incidence of CL in village Kharki (54.5%), followed by village Meherdi with 12.5% of the total prevalence (Figure 1). A previously conducted study in tehsil Dargai revealed the highest ratio (60%) in the local population [17]. The reason behind higher prevalence in prevalent villages is maybe their congested population and, migration of people (IDPs) from the other area where CL is endemic.

The current study also revealed the highest prevalence (54%; 1-15) in the age group of the young population. Similar results were investigated by Din et al in the young age group [22]. Similarly, the study conducted in 2009, investigates the higher prevalence in the young age group [26]. Our investigations and previous studies revealed that CL is a prominent and health-threatening skin infection in various parts of the country [24]. Formerly, a study was conducted in 2001 in Multan reported more than hundreds of cases whereas in 2006 thousands of cases were documented in Pakistan [23, 28]. The present study recorded the maximum number of cases in the male population (54%) as compared to a female domain (46%), other studies also reported the

highest prevalence in males which is correlated to our findings [17, 18, 22]. In a 2016 study, another study revealed the highest (57%) prevalence in males as compared to females [27]. Males are more socially active than females and spent most of the time outdoor [14]. Similarly, a study conducted in Nepal observed the maximum cases in males 9.9%, than females 8.3% [29].

The current study observed the least number of active lesions in the adult age group which proved their acquired immunity [31]. The statistical analysis revealed a significant association (p-value = 0.02) between the various age groups and gender with a 5% significance level.

The present investigative study recorded several lesions of Cutaneous leishmaniasis in patients where maximum individuals were found to had a single lesion (57%), our results are in a correlation with the previously reported studies in this regard [22,23]. The infected individuals were observed in several reports across the country with a single lesion such as in the Khyber agency with the highest ratio 78.1% [31], Quetta with 65.5% [23], in Karak 58% [33], and in Kohat 65.1% [4]. The present study examined the majority of lesions on uncovered body parts particularly; the facial regions followed by legs, hands, and other body parts. The highest frequency of CL has been reported in exposed parts of the body in various studies [16, 17, 19 and 20].

Our study also observed a duration-based study of an active skin lesion with which lesion 1-3 month duration yield higher prevalence (55.3%), our findings are similar to a previously conducted study in the same region in 2013 by Jamal et al [17]. Similarly, in 2009 the study was conducted in Sindh revealed the same findings that correlate with our results [26].

CONCLUSION

From current epidemiological data, it is concluded that CL infection is a health-threatening issue for the native population of District Malakand. Furthermore, this is the first-ever study to use PCR for the detection of CL in District Malakand. The current study could be helpful for the department of disease control cell in the district Malakand to notice particular areas through this study and take positive steps for its control. It is recommended that the age group 1-15 should be protected to minimize the rate of infection. It is also recommended that PCR should be used for the detection of Leishmaniasis due to its highly sensitive rate than microscopy.

ACKNOWLEDGEMENTS

Abdullah and M. Shah equally contributed in this research, and all the authors would like acknowledged technicians of Talha Clinical Laboratory for their support and provide us Lab for this study. The authors are highly obliged to Dr. Ikram Muhammad to critically review the whole manuscript.

REFERENCES

[1] Azizi, K., Rassi, Y., Javadian, E., Motazedian, M.H., Rafizadeh, S., Yaghoobi Ershadi, M.R. and Mohebali, M. (2006). Phlebotomus (Paraphlebotomus) alexandri: a probable vector of Leishmania infantum in Iran. Annals of Tropical Medicine & Parasitology. 100(1), 63-68.

[2] Hussain, M., Munir, S., Jamal, M.A., Ayaz, S., Akhoundi, M. and Mohamed, K. (2017). Epidemic outbreak of anthroponotic cutaneous leishmaniasis in Kohat District, Khyber Pakhtunkhwa, Pakistan. Acta Tropica. 172, 147-155.

[3] Kassi, M., Kassi, M., Afghan, A.K., Rehman, R. and Kasi, P.M. (2008). Marring leishmaniasis: the stigmatization and the impact of cutaneous leishmaniasis in Pakistan and Afghanistan. PLoS Negl. Trop. Dis. 2(10), e259.

[4] Hussain, M., Munir, S., Ayaz, S., Khattak, B.U., Khan, T.A., Muhammad, N. and Kasbari, M. (2017). First report on molecular characterization of Leishmania species from cutaneous leishmaniasis patients in southern Khyber Pakhtunkhwa province of Pakistan. Asian Pacific Journal of Tropical Medicine. 10(7), 718-721.

[5] Hayat, M., Ahmad, I., Afaq, U., Munir, S., Anees, M., Hussain, T. and Hussain, M. (2013). Prevalence and molecular diagnosis of cutaneous leishmaniasis in local population of Dir District, Khyber Pakhtunkhwa, Pakistan. Int. J. Pharm. Sci. Rev. Res. 21, 359-64.

[6] Alvar, J., Vélez, I.D., Bern, C., Herrero, M., Desjeux, P., Cano, J. and WHO Leishmaniasis Control Team. (2012). Leishmaniasis worldwide and global estimates of its incidence. PloS One. 7(5), e35671.

[7] Chaudhary, R.G., Bilimoria, F.E., Katare, S. (2008) diffuse cutaneous leishmaniasis: co-infection with human immunodeficiency virus (HIV). Indian J. Dermatol. Venereol. Leprol. 74, 641.

[8] Kimutai, R., Musa, A.M., Njoroge, S., Omollo, R., Alves, F., Hailu, A., Khalil, E.A., Diro, E., Soipei, P., Musa, B. and Salman, K. (2017) Safety and effectiveness of sodium stibogluconate and paromomycin combination for the treatment of visceral leishmaniasis in eastern Africa: results from a pharmacovigilance programme. Clin. Drug Investig. 37, 259–272.

[9] Bailey, M.S. and Lockwood, D.N. (2007). Cutaneous leishmaniasis. Clinics in Dermatology. 25(2), 203-211.

[10] Clem, A. (2010) A current perspective on leishmaniasis. J. Glob. Infect. Dis. 2, 124.

[11] Ve´lez, I.D., Colmenares, L.M., Mun˜oz, C.A. (2009) Two cases of visceral leishmaniasis in Colombia resistant to meglumine antimonial treatment. Revista do Instituto de Medicina Tropical de Sa˜o Paulo. 51, 231–236.
[12] Durrani, A.Z., Durrani, H.Z., Kamal, N. (2012) Prevalence of Leishmania in sand fly in Pakistan. Pakistan Journal of Zoology. 44.
[13] Durrani, A.Z. (2011) Prevalence of cutaneous leishmaniasis in humans and dogs in Pakistan. Pakistan Journal of Zoology. 43.
[14] Khan, I., Hussain, M., Ul Akbar, N., Ahmad, H., Ahmad, W. and Waqar, M. (2013). Prevalence of cutaneous leishmaniasis in Surgul village of district Kohat, Khayber Pakhtunkhwa. International Journal of Advancements in Research & Technology. 2(12), 141-7.
[15] Rowland, M., Munir, A., Durrani, N., Noyes, H. and Reyburn, H. (1999). An outbreak of cutaneous leishmaniasis in an Afghan refugee settlement in north-west Pakistan. Transactions of the Royal Society of Tropical Medicine and Hygiene. 93(2), 133-136.
[16] Rahim, F., Jamal, S., Raziq, F., Uzair, M., Sarwar, B., Ali, H. and Sherin, M. (2003). An outbreak of Cutaneous Leishmaniasis in a village of district Dir, NWFP. Journal of Postgraduate Medical Institute (Peshawar-Pakistan). 17(1).
[17] Jamal, Q., Shah, A., Ali, N., Ashraf, M., Awan, M.M. and Lee, C.M. (2013). Prevalence and comparative analysis of cutaneous leishmaniasis in Dargai Region in Pakistan. Pakistan Journal of Zoology. 45(2).
[18] Mumtaz, S., Munir, A.H., Asghar, M. and Naheed, N. (2016). Frequency and types of leishmaniasis in Khyber Pakhtunkhwa (KPK). J. Medical Sci. 24(3), 136-140.
[19] Hussain, M., Munir, S., Khan, T.A., Khan, A., Ayaz, S., Jamal, M.A. and Kasbari, M. (2018). Epidemiology of cutaneous leishmaniasis outbreak, Waziristan, Pakistan. Emerging Infectious Diseases. 24(1), 159.
[20] Rahman, H.U. and Rehman, A.U. (2018). Cutaneous leishmaniasis in Dir Lower District, North-West Pakistan: epidemiology and treatment response. Journal of Pakistan Association of Dermatol. 27(4), 353-362.
[21] Zeb, I., Ali, A., Nawab, J., Khan, M.Q., Kamil, A. and Tsai, K.H. (2020). Cutaneous Leishmaniasis in Male Schoolchildren in the Upper and Lower Dir Districts of Khyber Pakhtunkhwa, and a Review of Previous Record in Pakistan. Acta Tropica. 105578.
[22] Nawaz, M., Din, M., Khan, A., Khan, A., Ali, M., Din, S.U. and Aslam, K. (2020). Epidemiological features of cutaneous leishmaniasis endemic in hilly areas of district Karak, Khyber-Pakhtunkhwa province of Pakistan. J. of Parasitic Dis. 1-5.
[23] Khan, S.J., Muneeb, S. (2005). Cutaneous leishmaniasis in Pakistan. Dermatol. J. Onl. 11(1), 1-4.
[24] De Almeida Ferreira, S., Almeida, G.G., de Oliveira Silva, S., Vogas, G.P., Fujiwara, R.T., De Andrade, A.S.R. and Melo, M.N. (2013). Nasal, oral and ear swabs for canine visceral leishmaniasis diagnosis: new practical approaches for detection of Leishmania infantum DNA. PLoS Negl. Trop. Dis. 7(4), e2150.
[25] Hossain, F., Ghosh, P., Khan, M.A.A., Duthie, M.S., Vallur, A.C., Picone, A. and Mondal, D. (2017). Real-time PCR in detection and quantitation of Leishmania donovani for the diagnosis of Visceral Leishmaniasis patients and the monitoring of their response to treatment. PloS One. 12(9), e0185606
[26] Bhutto, A.M., Soomro, F.R., Baloch, J.H., Matsumoto, J., Uezato, H., Hashiguchi, Y. and Katakura, K. (2009). Cutaneous leishmaniasis caused by Leishmania (L.) major infection in Sindh province, Pakistan. Acta Tropica. 111(3), 295-298.
[27] Ali, A., Rehman, T.U., Qureshi, N.A., Rahman, H.U. (2016). New endemic focus of cutaneous leishmaniasis in Pakistan and future epidemics threats. Asian Pacific Journal of Tropical Disease. 6(2), 155-159.
[28] Marco, J.D., Bhutto, A.M., Soomro, F.R., Baloch, J.H., Barroso, P.A., Kato, H., Uezato, H., Katakura, K., Korenaga, M., Nonaka, S. and Hashiguchi, Y. (2006) Multilocus enzyme electrophoresis and cytochrome b gene sequencing–based identification of Leishmania isolates from different foci of cutaneous leishmaniasis in Pakistan. Amer. J. Trop. Med. Hyg. 75, 261-266.
[29] Rijal, S., Uranw, S., Chappuis, F., Picado, A., Khanal, B., Paudel, I.S. and Boelaert, M. (2010). Epidemiology of Leishmania donovani infection in high-transmission foci in Nepal. Tropical Medicine & International Health. 15, 21-28.
[30] Organization WHO. (2013) Global tuberculosis report 2013. World Health Organization.
[31] Qureshi, N.A., Ali, A., Rashid, U. and Ali, N. (2016). Prevalence of Leishmania tropica in school boys of Khyber agency, FATA near Pak-Afghan border. Acta Tropica. 164, 90-94.
[32] Hayat, M., Ahmad, I., Afaq, U., Munir, S., Anees, M., Hussain, T. and Hussain, M. (2013). Prevalence and molecular diagnosis of cutaneous leishmaniasis in local population of Dir District, Khyber Pakhtunkhwa, Pakistan. Int. J. Pharm. Sci. Rev. Res. 21, 359-64.
[33] Ul Bari, A., Hasshim, R., Mahmood, K., Muhammad, I., Shahbaz, N. and Tariq, K.M. (2016). Clinico-epidemiological pattern of cutaneous leishmaniasis in armed forces personnel fighting war against terrorism in Khyber Pakhtunkhwa Province and Fata regions. J. Pak. Assoc. Dermatol. 21(1), 10-15.

Received: **05.04.2021**
Accepted: **16.05.2021**

CORRESPONDING AUTHOR

Abdullah
Department of Health and Biological Sciences,
Abasyn University,
Peshawar – Pakistan

e-mail: abdullah4us.71@gmail.com

© by PSP Volume 30– No. 09/2021 pages 10797-10806 Fresenius Environmental Bulletin

MECHANISM OF FENOXAPROP-p-ETHYL RESISTANCE IN *Avena fatua* L. POPULATIONS FROM CHINA

Ninghai Lu, Guilei Hu, Geng Wang, Fanbin Kong, Kaishu Du, Baizhong Zhang*, Xiling Chen

Henan Institute of Science and Technology, Xinxiang 453003, People's Republic of China

ABSTRACT

To explore resistant mechanism of wild oat to fenoxaprop-p-ethyl, the susceptibility of Acetyl-CoA Carboxylase (ACCase) from 24 wild oat populations to fenoxaprop-p-ethyl, the level of gene expression and mutation site of ACCase were conducted. In vitro ACCase activities were solated and measured by enzyme-linked immunosorbent assay kit (ELISA) assays, the results indicated that the IC50 value of the ACCase of the most unsusceptible to fenoxaprop-p-ethyl in the wild oat population from Yexian2017 (W24) was 7206.557-fold compared to that of the ACCase of the most susceptible to fenoxaprop-p-ethyl in the wild oat population from Queshan (W11). The level of gene expression of ACCase was significantly higher in the resistant populations than in the relative susceptible populations, and was significantly more suppressed in the relative susceptible populations than in the resistant populations by quantitative Real-time PCR (qPCR). The mutations point of ACCase, Ile-1781-Leu, Trp-1999-Cys, Trp-2027-Cys, Ile-2041-Asn, Asp-2078-Gly, Cys-2088-Arg to have been published were not found in the populations tested by multiple sequence alignment with a model complete ACCase sequence of Alopecurus myosuroides. These findings suggest that ACCase plays a critical role in the development of wild oat resistant mechanism to fenoxaprop-p-ethyl.

KEYWORDS:
Avena fatua, Acetyl-CoA Carboxylase (ACCase), Fenoxaprop-p-ethyl Resistance, Mutation Points

INTRODUCTION

Wild oat (Avena fatua L.) also called oat grass, belongs to the Gramineae Avena and matures one or two years [1], is as malignant weed that harms wheat, oilseed rape, and other crops in China, and has developed serious resistance to herbicides all over the world [2]. At present, A. fatua is controlled by using chemical herbicides. The herbicide varieties that effectively control wild oat are relatively less. The only inhibitors are metsulfuron-methyl and fenoxaprop-p-ethyl. Fenoxaprop-p-ethyl is a kind of aryloxyphenoxypropionate herbicide (AOPP). Its mode of action is by inhibiting the activity of Acetyl-CoA Carboxylase (ACCase) (ACCase) in grassy weeds and then blocking normal fatty acid synthesis in plants [3]. As a highly effective herbicide, it has been widely used in wheat fields to prevent grassy weeds, such as wild oat. However, both long-term and single use of fenoxaprop-p-ethyl in wheat fields have caused resistance to wild oat. In addition, fenoxaprop-p-ethyl only acts on ACCase, so weeds are easily able to develop resistance [4]. Fenoxaprop-p-ethyl belongs to the high-risk level in the resistant risk classification, in which weeds will typically develop resistance after continuous use for a year [5, 6]. Recently, it has been difficult to control in wheat fields by using only fenoxaprop-p-ethyl. However, the resistance of wild oat to fenoxaprop-p-ethyl has been seldom reported, especially the resistance mechanism.

Carboxylation of acetyl-CoA includes mainly two processes which are involved with carboxylation of biotin and transfer of carboxylation reaction respectively [7], the ACCases of plants comprise homogeneity (ACCase I) and heterogeneity (ACCase II), they are both responsible for catalysing acety-CoA to malony-CoA [8]. Homomeric ACCase localizes in cytosol as a pivotal enzyme to the step of fatty acid synthesis reaction. Heteromeric ACCase used to be in cytosol, its production malony-CoA is mainly utilized for elongating fatty acid chain and for synthesizing metabolite associated with flavonoids, resistance-endowing [9]. However, there are 2 special cases in cellular distribution of the two isoenzymes. The first one is that the chloroplast of rape has not only homomeric ACCase and heteromeric ACCase. The second one is that the ACCase of gramineous plants are all classified as homogeneity whether they present in cytosol or in plastid [10].

Target-site herbicide resistance (TSR) and non-target-site herbicide resistance (NTSR) are the main mechanisms of weed resistance to herbicides. TSR involves a target-site mutation that affects the target enzyme sensitivity and results in much lower or higher expression levels of the target enzyme. Studies of NTSR have mainly included osmosis, reduced herbicide absorption and conduction, metabolic detoxification, shielding effects and buffer functioning

to increase herbicide resistance and herbicide heightening [11]. ACCase is used as the target of AOPP. Weeds develop resistance to AOPP mainly due to mutations of ACCase; but the overexpression of ACCase in weeds also results in the development of resistance to herbicides [12]. Sorghum halepense had developed resistance to enoxaprop-p-ethyl and sethoxydim due to the overexpression of ACCase gene [13, 14].

Previous studies of the resistance mechanism to ACCase herbicides in resistant Avena spp. populations revealed that ACCase gene mutation can confer the resistance to weed frequently [15-18]. Ile-1781-Leu, Trp-1999-Cys, Trp-2027-Cys, Ile-2041-Asn, Asp-2078-Gly and Cys-2088-Arg are now known mutation sites of ACCase to be associated with resistance to fenoxaprop-p-ethyl in wild oat [1, 19-21]. Therefore, the susceptibility of Acetyl-CoA Carboxylase (ACCase) from 24 wild oat populations to fenoxaprop-p-ethyl, digital gene expression (DGE) profiling, the level of gene expression, and mutation site of ACCase were conducted in A. fatua. It would provide a theoretical basis for understanding the molecular mechanisms of weed resistance.

MATERIALS AND METHODS

Cultivation of seedlings of wild oat. Seed information of wild oat collected from Henan Province were distributed in Table 1. The greenhouse potting methods were adopted [22]. The seeds of different populations of wild oat were sown into pots with a surface area of 75 cm2. The soil surface with the unused herbicide was mixed with a proportion of grass biochar, sifted and cultured in the greenhouse. Rearing conditions were 20°C in the daytime and 15°C at night, 75±5% relative humidity, and a 12:12 h light: dark photoperiod. Seeds of wild oat collected from Henan Province were distributed in 24 populations.

TABLE 1
Wild oat information used in the study

Populations	Abbreviation	Collection time
Xiangxian (Xuchang)	W1	2016.6
Huojia (Xinxiang)	W2	2016.6
Huixian (Xinxiang)	W3	2016.6
Wuzhi (Jiaozuo)	W4	2016.6
Xiuwu (Jiaozuo),	W5	2016.6
Xunxian (Hebi)	W6	2016.6
Fugou (Zhuokou)	W7	2016.6
Wuyang (Luohe)	W8	2016.6
Lankao (Kaifeng)	W9	2016.6
Heshan (Hebi)	W10	2016.6
Queshan (Zhumadian)	W11	2016.6
Qixian (Hebi)	W12	2016.6
Suiyang (Shangqiu)	W13	2016.6
Zhaoling (Luohe)	W14	2016.6
Huaiyang (Zhoukou)	W15	2016.6
Xihua (Jiaozuo)	W16	2016.6
Dengfeng (Zhengzhou)	W17	2016.6
Suiping (Zhumadian)	W18	2016.6
Linying (Luohe)	W19	2016.6
Sheqi (Nanyang)	W20	2016.6
Xihua (Zhoukou)	W21	2016.6
Yanling (Xuchang)	W22	2016.6
Tangyin (Anyang)	W23	2016.6
Yexian (Pingdingshan)	W24	2016.6
Yexian (Pingdingshan)	W25	2017.6

Chemicals. The active compound of fenoxaprop-p-ethyl (95.8%) used were supplied by Noposion (Shenzhen, China). Triton X-100 was obtained from Sigma-Aldrich Co. (Saint Louis, USA). Flavine adenine dinucleotide (FAD), thiamine pyrophosphate (TPP), phenylmethanesulfonyl fluoride (PMSF), sodium pyruvate (C3H3NaO3), alpha naphthol (α-naphthol), Tris (hydroxymethyl) aminomethane hydrochloride (Tris-HCl) and polyvinylpyrrolidone (PVP) were obtained from Sigma-Aldrich (USA). Creatine (C4H9N3O2), sodium hydroxide (NaOH), Coomassie brilliant blue–G250, monopotassium phosphate (KH2PO4), magnesium chloride (MgCl2), ethylenediaminetetraacetate acid (EDTA), and bovine serum albumin (BSA) as well as an ACCase-ELISA kit were purchased from Beijing Tongzheng Biological Company (Beijing, China). HiPure Plant RNA Mini Kit, HiPure Plant DNA Mini Kit and HiPure Gel Pure DNA Mini Kit produced by Magen were used to isolated total RNA, genomic DNA and purify the production of PCR, respectively. Taq-Plus PCR Forest Mix (2x) from NOVA (China) was the reagent for PCR. The kit HiScript® II QRT SsuperMix for qPCR and chamQ™ SYBR® qPCR Master Mix, which are used for cDNA synthesis and quantitative Real-time PCR (qPCR) separately, are bought from company Vazyme (Nanjing, China). Peptone, yeast powder and agar powder purchased from AOBOX (Beijing, China) were used make LB culture medium. The Ampicillin purchased from Gentihold (Beijing, China) was applied in Escherichia coli transformation experiment as the bacterial inhibitor.

Instruments and equipment. An ultraviolet and visible spectrophotometer (UV2102PC, Multi Wavelength Fluorescence Spectrophotometer, China), refrigerated centrifuge (5417R, Eppendorf, Germany), and a VMax Microplate Reader (Molecular Devices) with SoftMax Pro 5.4 software were used in the analyses. The primary herbicide sprayer was an atomizer with an auto spray device (Model: ASP-1098, Spray-head: ST110-01, Pressure: 0.2 MPa). The PCR program ran in the Analytik Jena Gradient PCR Instrument (9701 series, Germany) and productions of PCR were validated in the electrophoresis equipment (Beijin Junyi-dongfang Equipment Co.Ltd, Voltage: 100v, time: 20 min). The Bio-Rad CFX 96 (USA) was used for qPCR. An constant temperature incubator shaker produced by Jie Rui Er (Jiangsu, China) was used to cultivate Escherichia coli.

IN VITRO ACCASE SUSCEPTIBILITY OF DIFFERENT WILD OAT POPULATIONS TO FENOXAPROP-P-ETHYL

Enzyme preparations. Buffer solution: 100 mmol/L Tris-HCl (pH 8.3), 300 mmol/L glycerinum, 5 mmol/L DTT, 2 mmol/L EDTA, 0.5 mmol/L PMSF, and 0.01% (v/v) Triton X-100. First, take 3 g of aerial portions at the 3-leaf stage, tear them in pieces and put them into a prechilled mortar. Grind into a powder in liquid nitrogen, transfer the contents to a 50 mL centrifuge tube, wash the mortar with cold buffer solution in another 50-mL centrifuge tube and place the tube in the refrigerator at 4°C for two hours. Second, primary product to be disposed in two steps. First, put the abovementioned homogenate into a high-speed freezing centrifuge at 4000×g at 4°C for 30 min, discard the sediment, and then, retain liquid supernatant. Second, continue to centrifuge at 20000×g at 4°C for 30 min, discard the sediment, and then, retain the liquid supernatant containing the protein. Transfer the supernatant to a 1.5-mL centrifuge tube to standby for application. Regarding the sample treatment and requirement of the tissue sample, centrifuge the sample for 30 min (4000 r/min). Retain the liquid supernatant for immediate measurement or place it in a -20°C refrigerator for later use. Note that the sample does not contain NaN3 because it affects the activity of haptoglobin-related protein (HRP).

The ACCase activity of wild oat. The test of the ACCase activity depended on mothod of the ELISA-ACCase according to Webb et al [23]. With slight modification. The kit was based on the double antibody-sandwich method for testing the ACCase activity. The spectrophotometric (OD) values were recorded by a Vmax microplate reader at a wavelength of 450 nm. The protein content was determined by the method of [24] using bovine serum albumin as a standard. ACCase activity was expressed as U/mg protein/h. The herbicide was applied at a dose rate of 1, 10, 100, 1000, and 10000 mg/L each sample according to preliminary experiments. The inhibition rate was calculated according to ACCase activity. The herbicide concentration required to reduce ACCase activity by 50% (IC50) was calculated, and the IC50 values and the comparative analysis were calculated using a software SPSS 15.0 according to the inhibition rate of ACCase activity.

Fenoxaprop-p-ethyl treatment. A whole-plant assay modified was conducted according to Ryan [25]. Plants thinned and planted in the field (20 plants per pot) at the 3-leaf stage (20 cm plant height), were treated with fenoxaprop-p-ethyl by atomizing with an auto spray device (Model: ASP-1098, Spray-head: ST110-01, Pressure: 0.2 MPa). The herbicide was applied at a an IC50 concentration containing 0.05% (v/v) Triton X-100 according to the results of a whole plant assay, the amount of spouting liquid was 450 L/ha. Water alone containing 0.05% (v/v) Triton X-100 was used as a control. Each treatment was repeated 3 times. Foliar parts were collected for gene stability analyses at 24 h after treatment and stored at –80°C for RNA extraction.

TABLE 2
Primer design for qPCR

Gene name	Sequence (5′–3′)	Tm (°C)	Efficiency (%)	Product Length (bp)	R^2
18S	F: TGCACCACCACCCATAGAAT	59.00	97.2	102	0.99
	R: CTGCGGCTTAATTTGACCCA	58.83			8
ACCase	F: ACCTGCAACCGTGGATTAAG	59.99	99.8	127	0.99
	R: AGCTAGAGCAAGCAGCAAGG	60.06			9

The role of ACCase expression in fenoxaprop-p-ethyl resistance. Relative expression of ACCase gene of wild oat from 3 resistant populations and 1 susceptible population (W11), and ACCase expression of wild oat from the 4 populations treated by fenoxaprop-p-ethyl at their own IC50 concentration in 3-leaf stage were determined. Each treatment was repeated for 3 times. *18S* was selected as the reference gene [26], an ACCase sequence from RNA-seq of wild oat was used to design primers by primer 3.0 (http://bioinfo.ut.ee/primer3-0.4.0/). The primers used were listed in Table 2.

Quantitative Real-Time PCR (qPCR). RNA isolated with using TRIzol reagent (Invitrogen, Carlsbad, USA) according to the manufacturer's instructions. The concentration and quality of RNA was test by NanoDrop 2000 (Thermo Scientific, USA). RNA samples with an A260/A280 ratio ranging from 1.8 to 2.0 and an A260/A230 ratio >2.0 were used for cDNA synthesis. Total RNA (1μg) was reverse transcribed into first-strand complementary DNA using a PrimeScript RT reagent kit with gDNA Eraser (Takara, Dalian, China) according to the manufacturer's instructions and stored at –20°C.

ROX's Platinum SYBR Green qPCR SuperMix-UDG kit (Invitrogen) was used for qPCR and implementing on an Applied Biosystems 7500 Real-Time PCR system (Applied Biosystems, Foster City, CA). The reactions were performed in a 20 μl volume of a mixture containing 1 μl of cDNA template, 10 μl of SYBR Green qPCR SuperMix-UDG, 0.3 μl of each primer, and 8.7 μl of nuclease-free water. The thermocycling program was as follows: 50°C for 2 min, 95°C for 2 min, and 40 cycles of 95°C for 15 s, and 55°C for 30 s. To acquire a high specificity amplification, a melting curve analysis between 65 to 95°C, was constructed at the end of each PCR run. And it based on a 2-fold dilution series of cDNA (1:5, 1:10, 1:10, 1:10, 1:20, and 1:40). The corresponding qPCR efficiencies (E) were calculated refer to the formula $E= 10^{-1/slope} - 1$ [27]. Each sample was prepared as 3 biological replicates, and each reaction was analysed with 2 technical replications.

MUTATION POINT DETECTION

DNA extraction, PCR amplification, and cloning. DNA was isolated from 3-leaf stage issue of 1 relative susceptible populations and 7 relative unsusceptible populations using HiPure Plant DNA Mini Kit. 20 plants was tested in each population selected as mutation point detection. As the complete ACCase sequence is unknown, so PCR primers was designed from Alopecurus myosuroides (GeneBank accession No. AJ310767) and the region of PCR product in the wild oat plastids ACCase carboxyl transferase domain with 5 known and potential ACCase resistance mutation sites, lle-1,781- Leu, Trp-1,999-Cys, Trp-2,027-Cys, lle-2041-Asn, and Asp-2,078-Gly. The PCR was conducted in 25 μL volume that consist of 12.5 μL Taq-Plus PCR Forest Mix (2x) (NOVE, Jiangsu, China), 0.5 μL forward primer: CTGAATGAAGAAGACTATGGTCG, 0.5 μL reverse primer: TCCTCTGACCTGAACTTGATCTC, 1 μL DNA, 10.5 μL dd H_2O. The PCR was run with the following profiles: 94℃ for 2 min; 25-35 cycles for 30 sec, 60℃ for 30 sec, 72℃ 2 min; 72℃ 5 min. The PCR products was purified from agarose gels using HiPure Gel Pure DNA Mini Kit. The DNA that it had been purified was connected with pGEM-Teasy vector by T4 DNA Ligase as follows: 3 μL PCR product, 5 μL 2 x T4 Ligase buffer, 1 μL pGEM-Teasy vector, 1 μL Ligase. All of operations above were on the ice and the action was at 4℃ overnight for the maximum number of transformants.

The transformation of ligation product consists mainly of following steps: First, centrifuging the ligation reactions briefly and adding 2 μL of each ligation reaction to a sterile 1.5 mL tube on ice; Second, placing the competent cells in an ice bath until just thawed (5 minutes) and mixing cells by gently flicking the tube; Third, transferring carefully 50 μL cells to the ligation reaction tubes from Step 1, then flicking gently the tubes and incubating on ice for 30 minutes; Fourth, heat-shocking the cells for 45-50 seconds in a water bath at exactly 42℃ without shaking and returning immediately the tubes to ice for 2-3 minutes; Fifth, adding 950 μL room temperature liquid LB medium (without ampicillin) to the ligation reaction transformations and incubating for 1.5 hours at 37℃ with shaking (150-200 rpm); Sixth, plating 100 μL transformation culture onto solid duplicate LB/ampicillin/ IPTG/X-Gal plates; Finally, incubating plates overnight at 37℃.

ACCase gene sequencing and alignment. Selecting white colonies and transferring it into liquid LB medium (including ampicillin) continue to incubate for 18 hours at 37℃ with shaking (220 rpm) ,

TABLE 3
The susceptibility of ACCase to fenoxaprop-p-ethyl on different populations of wild oat

Populations	SLOPE±S.E	IC_{50} (mg/L)(95% FL)	X^2	Df	R^2
Xiangxian (W1)	0.08±0.016	115.315 (24.337-447.658)	7.039	13	0.971
Huojia (W2)	0.07±0.023	69.285 (43.449-149.531)	4.050	13	0.922
Huixian (W3)	0.05±0.014	3966.196(4511.583-5253.136)	1.573	13	0.844
Wuzhi (W4)	0.12±0.038	2.725 (1.716-6.723)	2.889	13	0.868
Xiuwu (W5)	0.09±0.034	98. 781 (65.103-155.183)	1.282	13	0.925
Xunxian (W6)	0.10±0.040	12.065 (7.904-70.572)	3.527	13	0.965
Fugou (W7)	0.07±0.037	7656.177 (5962.964- 8554.205)	6.218	13	0.932
W8(Wuyang)	0.13±0.039	1.255 (0.986-8.655)	12.939	13	0.909
W9(Lankao)	0.10±0.013	1140.105 (1244.703-5456.843)	7.550	13	0.878
Heshan (W10)	0.30±0.018	13.805 (5.630-29.448)	16.850	13	0.969
Queshan (W11)	0.17±0.037	1.134 (0.525-6.959)	14.761	13	0.943
Qixian (W12)	0.27±0.023	36.828 (11.222-83.391)	11.625	13	0.827
Suiyang (W13)	0.20±0.044	166.126 (31.72 5-209.475)	2.466	13	0.925
Zhaoling (W14)	0.38±0.032	7.140 (2.949-22.873)	31.076	13	0.939
Huaiyang (W15)	0.23±0.065	10. 797 (2.668-17.5 65)	5.102	13	0.946
Wenxian (W16)	0.11±0.015	560. 584 (229.352-883.867)	6.978	13	0.858
Dengfeng (W17)	0.16±0.037	507. 665 (117.969-781.807)	7.065	13	0.923
Suiping (W18)	0.16±0.030	130.537 (83.338-476. 601)	5.700	13	0.991
Linying (W19)	0.10±0.024	2736.872 (1454.222-2563.884)	0.819	13	0.927
Sheqi (W20)	0.08±0.032	133.274 (50.615-186.894)	20.564	13	0.937
W21(Xihua)	0.21±0.064	5111.930 (4495.158-5918.343)	4.998	13	0.908
Yanling (W22)	0.13±0.045	166.984 (105.604-372.714)	32.600	13	0.939
Tangyin (W23)	0.05±0.013	400.835 (186.5252-638.301)	3.640	13	0.901
Yexian2017 (W24)	0.06±0.020	8172.236 (6454.222-9591.452)	2.109	13	0.901
Yexian2016 (W25)	0.08±0.019	1339.554 (807.785-1800.296)	1.792	13	0.992

then it was sequenced by a gene corporation named Beijing Genomic Institute, BGI (Beijing, China). These sequences were analysis and alignment by using a software, DNAMAN with a model ACCase sequence (Alopecurus myosuroides Gene Bank Accession No. AJ310767) due to the lack of complete wild oat ACCase sequence [28].

Statistical analysis. Statistical and bioassay analyses were performed by using Microsoft Excel (2010). IC50 values were calculated by SPSS (15.0). ACCase activity of different wild oat populations was determined by an unpaired t-test ($P < 0.05$), and ACCase gene expression level was performed according to the one-way ANOVA, followed by Tukey's multiple comparison test ($P < 0.05$) with InStat Version 3.0 software (GraphPad Software, San Diego, CA).

RESULTS

In vitro ACCase susceptibility of different wild oat populations to fenoxaprop-p-ethyl. In vitro ACCase susceptibility of different wild oat populations to fenoxaprop-p-ethyl was shown in Table 3. The results indicated that the most unsusceptible ACCase to fenoxaprop-p-ethyl was found in the wild oat population from W24, its IC50 value was

8172.236 mg/L, the next unsusceptible ACCase to fenoxaprop-p-ethyl were from W7, W21(Xihua), W3 and W19, their IC50 values were 7656.177, 5111.930, 3966.196, and 2736.872 mg/L, respectively. The most susceptible ACCase to fenoxaprop-p-ethyl was found in the wild oat population from QW11, its IC50 value was 1.134 mg/L. The IC50 of the most unsusceptible ACCase to fenoxaprop-p-ethyl of wild oat population from W24, which was 7206.557-fold greater than that of the most susceptible ACCase to fenoxaprop-p-ethyl of the wild oat population from W11. In addition, the susceptibility of ACCase to fenoxaprop-p-ethyl of the wild oat from W24 is less than that from W25; the IC50 values were 8172.236 and 1339.554 mg/L, respectively, with an 6.101-fold difference.

In vivo ACCase activity of different wild oat populations. The ACCase activity of different wild oat populations was shown in Figure 1. The ACCase activity of the wild oat population from W13 was the highest at 3.278 U/h/mg protein. The next highest ACCase activity were from W14, W16, W12 and W19, their ACCase activities were 3.245, 3.234, 3.123 and 3.101 U/h/mg protein, respectively. The ACCase activity of the wild oat population from W10 was the lowest, which was 0.664 U/h/mg protein. Among them, the highest ACCase activity of wild oat population from W13was 4.936-fold that of the lowest population from W10. In addition, the ACCase activity of wild oat from W24 was higher than that from W25, which were 2.492 and 1.356 U/h/mg protein, respectively, a 1.838-fold difference.

Mutation point detection. Eight populations were selected for mutation point detection by multiple sequences alignment and a complete ACCase sequence from *Alopecurus myosuroides* (Gene Bank Accession No. AJ310767), which has high homology with wild oat, was used for the alignment stander. There was no amino acid mutation in six possible sites, it indicated that the resistant mechanism of these populations in the assay to fenoxaprop-p-ethyl wasn't caused by the 6 known amino acid mutations. However, the other sites, Glu-1797-Gly, Thr-1805-Ser, Pro-1829-Leu, Thr-1833-lle, Met-1859-Thr, Asp-1904-Gly, Asn-1913-Asp, Phe-1935-Ser, Gln-2009-Arg, Thr-2092-Ala may be possible amino acid mutations (Figure 2).

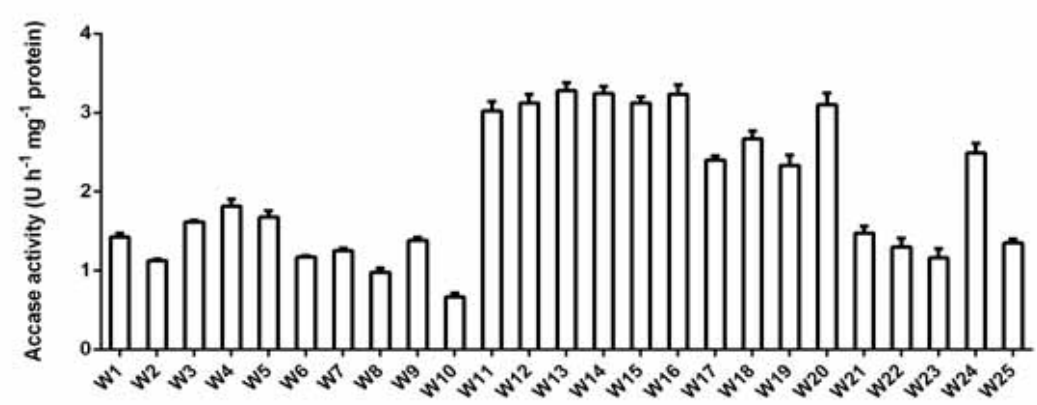


FIGURE 1
In vivo ACCase activity of different wild oat populations.

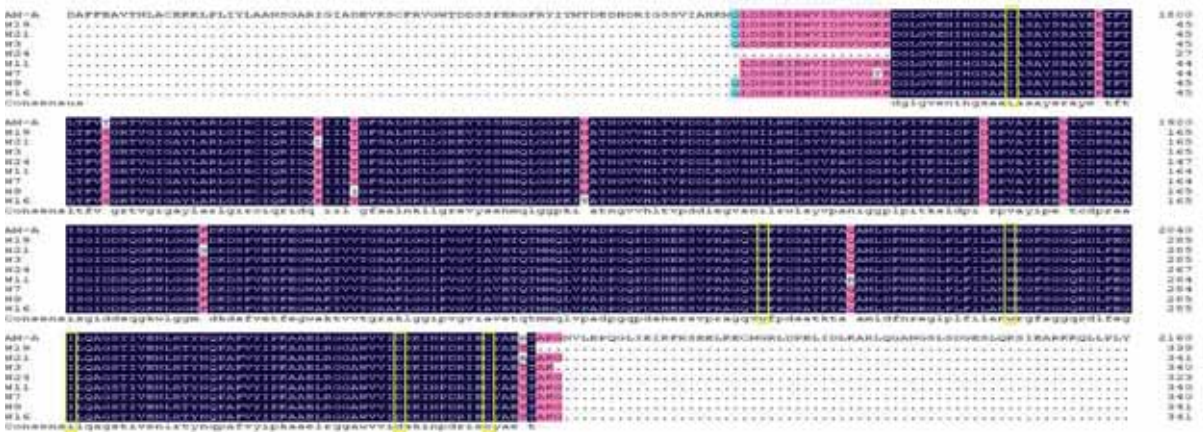


FIGURE 2
Alignment of the deduced amino acid sequences of ACCase
Yellow frames represent that 6 possible amino acid mutation site which had been published. AM-A means model ACCase sequence (*Alopecurus myosuroides*). W11 is the most susceptive population, the other 7 are relative resistant population.

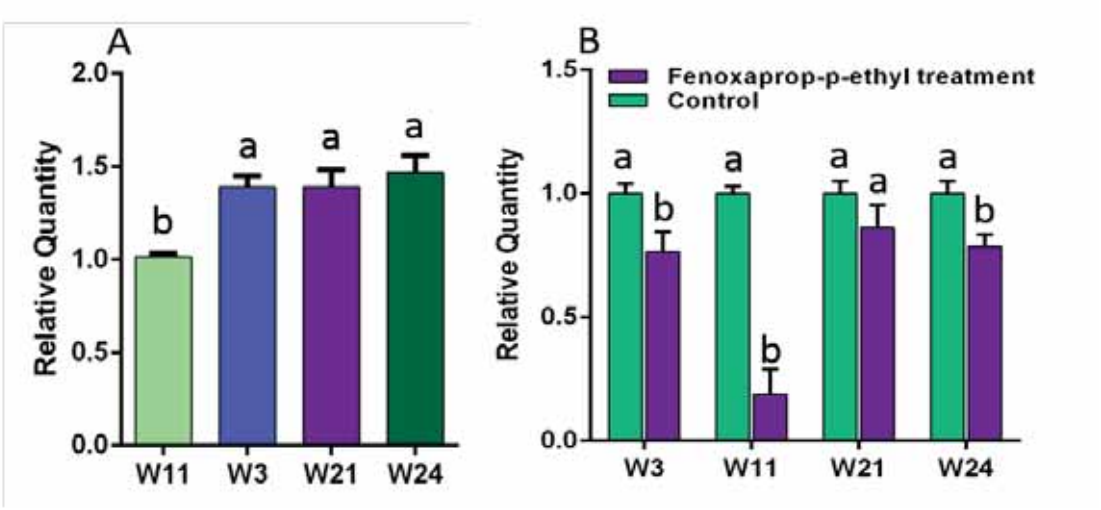


FIGURE 3

Relative expression of ACCase gene in 3 resistant populations and a susceptible population (W11).

(A) Relative expression of ACCase gene in the 4 populations; (B) Relative expression of ACCase gene in the 4 populations treated by fenoxaprop-p-ethyl compared to their own control. Date are means ± tandard error (S.E) of 3 replicates, and *18S* was used as a reference gene. The relative expression was calculated using $2^{-\triangle\triangle Ct}$ method base on the value of the control expression, which was ascribed an arbitrary value of 1. W11 is the most susceptive population, the other 3 are relative resistant populations.

The role of ACCase expression in fenoxaprop-p-ethyl resistance of wild oat from some populations. In order to validate role of ACCase expression in fenoxaprop-p-ethyl resistance, ACCase was selected based on a complete ACCase sequence from *Alopecurus myosuroides*. ACCase expression of wild oat in the 3 resistant populations from W3, W21, and W24, and 1 relative susceptible population from W11 were determined. The results indicated that overexpression of ACCase gene of wild oat in the 3 resistant populations from W3, W21, and W24 compared to 1 relative susceptible population from W11, with 1.39-, 1.44-, 1.47-fold higher in W3, W21, and W24 than that in W11 (Figure 3A); In addition, the ACCase expression of wild oat from W3, W11, Xihua, and W24 treated by fenoxaprop-p-ethyl, was suppressed by 0.24-, 0.81-, 0.14-, and 0.21-fold compared to the control (Figure 3B).

DISCUSSION

Fenoxaprop-p-ethyl is the main ACCase inhibition herbicide, which used to manage weeds in wheat fields, some species, i.g. Alopecurus japonicas, Beckmannia syzigachne, and A. fatua have developed different levels of resistance to fenoxaprop-p-ethyl because of its wide usage [29-33]. ACCase is the only target of fenoxaprop-p-ethyl, so the susceptibility of ACCase in plants to fenoxaprop-p-ethyl in vitro or in vivo could reflect a relationship between the plant biotype and its susceptibility to the herbicide. In this study, susceptibility of ACCase in 24 different populations of wild oat to fenoxaprop-p-ethyl was conducted in vitro. The results indicated that the IC50 value of the ACCase of the most unsusceptible to fenoxaprop-p-ethyl in the wild oat population from W24 was 7206.557-fold compared to that of the ACCase of the most susceptible to fenoxaprop-p-ethyl in the wild oat population from W11. This is somewhat accordance with the previous research of Echinochloa crus-galli, 106-fold difference of ACCase sensitivity between quizalofop–ethyl-resistant and-susceptible barnyardgrass[34]. This indicated that ACCase sensitivity of wild oat could play a critical role in the resistance to fenoxaprop-p-ethyl.

Point mutations of ACCase could result in resistance of wild oat to the herbicide, thus 6 point mutations of ACCase loci published [1, 19, 35-37] were determined in the 8 wild oat populations from the 7 relative susceptible and the 1 relative unsusceptible populations to fenoxaprop-p-ethyl, these genetic loci mutations can lead to the different levels of resistance. Amino acid mutations in 1999, 2027, 2041 and 2096 loci of the ACCase of weed species have resulted in resistance to one or more AOPP herbicides but not to cyclohexanedione (CHD) or phenylpyrazoline (PPZ) herbicides, and amino acid mutations in 1781, 2078 and 2088 loci of the ACCase of weed species have led to resistance to all ACCase-inhibiting herbicides [38, 39]. However, our results indicated that 6 published resistance-related amino acid mutation sites weren't found in the populations texted in the eight wild oat populations. However, the other sites, Glu-1797-Gly, Thr-1805-Ser, Pro-1829-Leu, Thr-1833-lle, Met-1859-Thr, Asp-1904-Gly, Asn-1913-Asp, Phe-1935-Ser, Gln-2009-Arg, Thr-2092-Ala may be possible amino acid mutations, so the resistance of wild oat to the herbicide may be caused by other amino sites mutation, ACCase or detoxification enzymes.

In order to explore the relationship expression of ACCase genes and resistance to fenoxaprop-p-

ethyl. Gene expression of ACCase down-regulated in the fenoxaprop-p-ethyl treatment compared to the control of wild oat was used to compared its expression in 3 resistant populations and the relative susceptible population treated by fenoxaprop-p-ethyl for 24 hours. Forthermore, overexpression of ACCase genes were also observed in the resistant populations compared to the the relative susceptible population. The results showed that ACCase expression in the resistant populations were significantly less suppressed than the susceptible populations of wild oat. This is somewhat accordance with the previous researches, differential overexpression of ACCase in weeds of resistacne to ACCase-inhibiting herbicides and the susceptible populations could lead to resistance to herbicides [40-42]. This proved that the resistant mechanism of wild oat to fenoxaprop-p-ethyl is related to overexpression of ACCase gene.

CONCLUSION

Overexpression of ACCase could play a critical role in the resistant mechanism of wild oat to fenoxaprop-p-ethyl. The 6 published resistance-related amino acid mutation sites weren't found in the populations tested in the 8 wild oat populations. Resistant mechanisms of wild oat still need further validation, such as other point mutation detection of ACCase and detoxication enzymes.

ACKNOWLEDGEMENTS

This work is supported by the Key Science and Technology Program of Henan (Agriculture) (212102110441), the Key Scientific Projects of Institutions of Henan (21A210008), and Project of Plant Protection Key Discipline of Henan Province (1070202190011005), Provincial University Student Innovation and Training Program of Henan (S2020104670S).

Disclosure Statement. Competing financial interests: The authors declare no competing financial interests.

Ninghai Lu and Guilei Hu are contributing equally to this study

REFERENCES

[1] Christoffers, M.J., Berg, M.L. and Messersmith, C.G. (2002) An isoleucine to leucine mutation in acetyl-CoA carboxylase confers herbicide resistance in wild oat. Génome. 45, 1049-105

[2] Cavan, G., Cussans, J. and Moss, S. (2001) Managing the risks of herbicide resistance in wild oat. Weed Science. 49, 236-240.

[3] Devine, M.D. and Shukla, A. (2000) Altered target sites as a mechanism of herbicide resistance. Crop Protection. 19, 881-889.

[4] Delye, C. (2005) Weed resistance to acetyl coenzyme A carboxylase inhibitors: an update. Weed Science. 53, 728-746.

[5] Chen, G., Xu, H., Zhang, T., Bai, C. and Dong, L. (2018) Fenoxaprop-P-ethyl resistance conferred by cytochrome P450s and target site mutation in Alopecurus japonicus. Pest Management Science. 74, 1694-1703.

[6] Pornprom, T., Mahatamnuchoke, P. and Usui, K. (2006) The role of altered acetyl-CoA carboxylase in conferring resistance to fenoxaprop-P-ethyl in Chinese sprangletop (Leptochloa chinensis, (L.) Nees). Pest Management Science. 62, 1109-1115.

[7] Konishi, T., Shinohara, K., Yamada, K. and Sasaki, Y. (1996) Acetyl-CoA carboxylase in higher plants: most plants other than Gramineae have both the prokaryotic and the eukaryotic forms of this enzyme. Plant Cell Physiology. 37, 117–122.

[8] Schulte, W., Töpfer, R., Stracke, R. and Martini, N. (1997) Multi-functional acetyl-CoA carboxylase from Brassica napus is encoded by a multigene family: indication for plastidic localization of at least one isoform. Proceedings of the National Academy of Sciences of the United States of America. 94, 3465-3470.

[9] Shorrosh, B.S., Dixon, R.A., Ohlrogge, J.B. (1994) Molecular cloning, characterization, and elicitation of acetyl-CoA carboxylase from alfalfa. Proceedings of the National Academy of Sciences of the United States of America. 91, 4323-4327.

[10] Sasaki, Y., Kozaki, A., Hatano, M. (1997) Link between light and fatty acid synthesis: thioredoxin-linked reductive activation of plastidic acetyl-coa carboxylase. Proceedings of the National Academy of Sciences. 94, 11096-11101.

[11] Powles, S.B., Preston, C., Bryan, I.B. and Jutsum, A.R. (1997) Herbicide resistance: impact and management. Advances in Agronomy. 58, 57–93.

[12] Zhang, X.Q. and Powles, S.B. (2006) The molecular bases for resistance to acetyl co-enzyme A carboxylase (ACCase) inhibiting herbicides in two target-based resistant biotypes of annual ryegrass (Lolium rigidum). Planta. 223, 550-557.

[13] Parker, W.B., Somers, D.A., Wyse, D.L., Keith, R.A., Burton, J.D., Gronwald, J.W. and Gengenbach, B.G. (1990) Selection and characterization of sethoxydim- tolerant maize tissue cultures. Plant Physiology. 92, 1220-1225.

[14] Bradley, K.W., Wu, J., Hatzios, K.K. and Esjr, H. (2015) The mechanism of resistance to aryloxyphenoxypropionate and cyclohexanedione herbicides in a johnsongrass biotype. Weed Science. 49, 477-484.
[15] Maneechote, C., Holtum, J.A.M., Preston, C. and Powles, S.B. (1994) Resistant Acetyl-CoA Carboxylase is a Mechanism of Herbicide Resistance in a Biotype of Avena sterilis ssp. ludoviciana. Plant & Cell Physiology. 35, 627-635.
[16] Seefeldt, S.S., Fuerst, E.P., Gealy, D.R., Shukala, A., Irzyk, G.P. and Devine, M.D. (1996) Mechanisms of resistance to diclofop of two wild oat (Avena fatua) biotypes from the Williamette Valley of Oregon. Weed Science. 44, 776–781.
[17] Shukla, A., Dupont, S. and Devine, M.D. (1997) Resistance to ACCase-Inhibitor Herbicides in Wild Oat: Evidence for Target Site-Based Resistance in Two Biotypes from Canada. Pesticide Biochemistry & Physiology. 57, 147-155.
[18] Cocker, K.M., Coleman, J.O.D., Blair, A.M., Clarke, J.H. and Moss, S.R. (2000) Biochemical mechanisms of cross-resistance to aryloxyphenoxypropionate and cyclohexanedione herbicides in populations of Avena spp. Weed Research. 40, 323–334.
[19] Liu, W., Harrison, D.K., Chalupska, D., Gornicki, P., O'Donnell, C.C., Adkins, S.W., Haselkorn, R. and Williams, R.R. (2007) Single-site mutations in the carboxyltransferase domain of plastid acetyl-coa carboxylase confer resistance to grass-specific herbicides. Proceedings of the National Academy of Sciences of the United States of America. 104, 3627-32.
[20] Cruz-Hipolito, H., Osuna, M.D., Dominguez-Valenzuela, J.A., Espinoza, N., Prado, R.D. (2011) Mechanism of resistance to accase-inhibiting herbicides in wild oat (Avena fatua) from latin America. Journal of Agricultural & Food Chemistry. 59(13), 7261-7.
[21] Beckie, H.J., Warwick, S.I., Sauder, C.A. (2012) Acetolactate synthase (ALS) inhibitor-resistant wild buckwheat (Polygonum convolvulus) in Alberta. Weed Technology. 26, 156-160.
[22] Li, R., Zhang J. and Chen, G. (2010) Advance of study on identification of weed herbicide resistance. Chinese Agricultural Science Bulletin. 26, 289–292.
[23] Webb, S.R., Hall, J.C. (2000) Monoclonal-based ELISA for the identification of herbicidal cyclohexanedione analogues that inhibit graminaceous acetyl coenzyme-A carboxylase. Journal of Agricultural and Food Chemistry. 48, 1210-1218.
[24] Bradford, M.M.A. (1976) Rapid sensitive method for the quantization of microgram quantities of protein utilizing the principle of protein binding. Analytical Biochemistry. 25, 248-254.
[25] Ryan, G.F. (1970) Resistance of common groundsel to simazine and atrazine. Weed Science. 18, 614–616.
[26] Liu, J., Li, P., Lu, L., Xie, L., Chen, X. and Zhang, B. (2018) Selection and evaluation of potential reference genes for gene expression analysis in Avena fatua. Plant Protection Science. 55, 61-71.
[27] Pfaffl, M.W. (2001) A new mathematical model for relative quantification in real-time RT-PCR. Nucleic Acids Research. 29, e45.
[28] Brown, H.M. (1990) Mode of action, crop selectivity and soil relations of the sulfonylurea herbicides. Pest Management Science. 29, 263-281.
[29] Zhang, C.X., Ni, H.W., Wei, S.H., Huang, H.J., Liu, Y. and Cui, H.L. (2009) Current advances in research on herbicide resistance. Scientia Agricultura Sinica. 42, 1274-1289.
[30] Guo, F. (2011) The resistacne of Japanese foxtail (Alopecurus japonicus Steud.) and wild oat (Avena fatua L.) to fenoxaprop-p-ethyl and clodinafop-propargyl. Chinese Academy of Agriculatural Sciences. Beijing. (Doctoral Thesis).
[31] Guo, F. (2012) The sensitivity of different wild oat Avena fatua populations to fenoxaprop-P-ethyl and clodinafop-propargyl. Acta Phytophylacica Sinica. 39, 87-90.
[32] Zhang, C.X., Ni, H.W. and Wei, S.H. (2013) Herbicide-resistant weeds and their management. Plant Protection. 39, 99-102.
[33] Bi, Y. (2013) Resistance of Alopecurus japonicus to fenoxaprop-p-ethyl and mesosulfuron-methyl in winter wheat fields. Shandong Agricultural University, Shandong Taian.
[34] Huan, Z., Xu, Z., Lv, D., Wang, J. (2013) Determination of ACCase sensitivity and gene expression in quizalofop–ethyl-resistant and -susceptible barnyardgrass (Echinochloa crus-galli) biotypes. Weed Science. 61, 537-542.
[35] Yu, Q., Nelson, J.K., Zheng, M.Q., Jackson, M. and Powles, S.B. (2007) Molecular characterisation of resistance to als-inhibiting herbicides in Hordeum leporinum biotypes. Pest. Management Science. 63, 918-927.
[36] Hochberg, O., Sibony, M. and Rubin, B. (2009) The response of ACCase-resistant Phalaris paradoxa populations involves two different target site mutations. Weed Research. 49, 37-46.
[37] Kaundun, S.S. (2010) An aspartate to glycine change in the carboxyl transferase domain of acetyl CoA carboxylase and non-target-site mechanism (s) confer resistance to ACCase inhibitor herbicides in a Lolium multiflorum population. Pest Management Science. 66, 1249-1256.
[38] Powles, S.B. and Yu, Q. (2010) Evolution in action: plants resistant to herbicides. Annual Review of Plant Biology. 61, 317-347.

[39] Collavo, A., Panozzo, S., Lucchesi, G., Scarabel, L. and Sattin, M. (2011) Characterisation and management of phalaris paradoxa resistant to ACCase-inhibitors. Crop Protection. 30, 293-299.
[40] Dong, Z., Zhao, H., He, J., Huai, J., Lin, H., Zheng, J., Liu, Y., Wang, G. (2011) Overexpression of a foxtail millet Acetyl-CoA carboxylase gene in maize increases sethoxydim resistance and oil content. African Journal of Biotechnology. 10, 3986-3995.
[41] Heckart, D.L., Schwartz, B.M., Raymer, P.L., Parrott, W.A. (2016) Synonymous mutation gene design to overexpress ACCase in creeping bentgrass to obtain resistance to ACCase-inhibiting herbicides. Transgenic Research. 25, 465-476.
[42] Laforest, M., Soufiane, B., Simard, M.J., Obeid, K., Page, E. and Nurse, R.E. (2017). Acetyl-CoA carboxylase overexpression in herbicide-resistant large crabgrass (Digitaria sanguinalis). Pest Management Science. 73, 2227-2235.

Received: **06.04.2021**
Accepted: **22.05.2021**

CORRESPONDING AUTHOR

Baizhong Zhang
College of Natural Resources and Environment,
Henan Institute of Science and Technology,
Eastern HuaLan Avenue,
Xinxiang 453003 – China

e-mail: baizhongok@163.com

© by PSP Volume 30– No. 09/2021 pages 10807-10814 Fresenius Environmental Bulletin

STUDY ON GREEN ENERGY-SAVING BUILDING UNDER COMPLEX ENVIRONMENT BASED ON DATA MINING

Xiaoli Liu*, Shuaixing Ren, Mengqi Jiang

The Architectural Engineering College, Guangdong Polytechnic of Science And Technology, Zhuhai, Guangdong 519000, China

ABSTRACT

Recently, the development of urbanization in China has great impact not only on resources but also on the environment. To greatly improve the high-rise green energy-saving building under complex environment, this paper introduced a data mining algorithm for solving the problems of environment. First, multiple data from high-rise green energy-saving building are collected. Then, the statistical and quantified operations will be done for the collected data. After quantified the collected data, the Apriori algorithm for data mining and analysis from the quantified data is used. Based on the experimental result, we analyzed the essence of green construction technology, concrete construction technology content and control factors, and created a green construction evaluation system. The existing problems in the high building construction under the complex environment of our country is also discussed. Finally, the application of exterior envelope, constant temperature and humidity and oxygen system as well as new energy utilization system is studied.

KEYWORDS:
Complex environment, Environmental protection, Green energy-saving building, Apriori algorithm

INTRODUCTION

In the progress of science and technology, the economy is changing, and people's consumption consciousness has also changed in the direction [1]. From a relatively stable environment to a dynamic equilibrium environment, from a simple single environment to a complex and changeable environment, it is an inevitable trend for the construction part of the construction [2-4]. In particular, the architectural category of engineering objects has changed in space, and engineering construction has been progressively promoted from surface construction to high-altitude construction. Therefore, the construction environment is becoming more and more complex [5-7]. The only constant theme is "change", and the speed of change will be faster and faster. Under the guidance of modern science and technology and economic level, more and more advanced energy-saving technologies have been used in super high-rise buildings, such as all glass curtain walls, energy saving and new energy use of electrical equipment, energy saving and water saving and reuse of water, and even the cooperative operation of all kinds of energy-saving technologies [8]. It can better solve the current situation of high energy consumption and high consumption materials in the construction industry. Measures to match environmental protection and energy saving in super high rise projects can guarantee and enhance the external conditions and humanization of the project, so as to realize the harmonious coexistence of the occupants and the environment [9].

Driven by the continuous scientific research and progress of many experts and practice workers in our country, more and more decision-making theories and methods will be tested in the field of engineering practice under the background of the continuous development of the technology of the construction industry in China [10-13]. Such as: the application of analytic hierarchy process in investment decision of water conservancy projects by Chen Guoqiao, Guangzhou Water Conservancy Society; the application of utility function in multi-objective decision making by the Golden branch of Shanghai Jiao Tong University and Zhang Li; Wang Baojun and Song Hongbin's decision making method of engineering bidding based on Fuzzy Mathematics in Tianjin University; Li Xican and Song Yan's multi-objective multilevel system multidimensional fuzzy decision theory model. The research results are concentrated in two aspects: one is to apply the theory of modernization and the applicable method of engineering to the actual operation of the project; on the other hand, it combines the existing theories and methods with the specific circumstances of our country, and improves the existing theories and methods.

MATERIALS AND METHODS

Construction of high level green energy-saving building evaluation system. Construction content and control factors of construction technology. The basic connotation of green construction is the efficient use of resources, new green construction technology and environmental protection and coordination management of construction site. In the construction technology, it will improve the low construction efficiency, avoid the waste of excessive energy resources in the construction stage and reduce the pollution to the environment and the surrounding area. It is also necessary to achieve the lowest local ecological impact through a series of technical measures, so as to emphasize the efficient use of energy resources and the protection of the environment. Under the high level complex environment, the main contents of green construction are as follows:

(1) Reduce the consumption and saving of resources;

(2) Use environmentally friendly materials and instruments;

(3) Prevent the pollution of the environment;

(4) Use advanced technology and efficient management to control the green construction process.

In complex environment, the goal of high level green construction is to achieve energy saving, land saving, water saving, timber saving and protection environment, but in the process of implementation, specific elements should be controlled to achieve the expected goal. Through the comprehensive analysis and evaluation of the previous research literature, the control objectives and requirements of green construction are simplified in the process of research, which are summarized as the protection of the environment, the saving and rational use of resources and materials, the use and saving of the energy and the land. As shown in Figure 1.

Green construction evaluation system. In complex building environment, the green construction evaluation system is to identify whether the construction process meets the requirements. Both the ongoing and upcoming projects need to undergo this overall assessment project. After evaluation, the construction process can be improved according to the results to ensure the green characteristics and circulation of the project. Generally speaking, the system of evaluating green construction is mainly divided into the general evaluation stage, the list of the factors of evaluation, the establishment of evaluation index and the grade of evaluation. The process of green construction evaluation starts from the construction stage of foundation stage, foundation engineering, structural engineering, equipment decoration and installation, and the specific requirements of green construction. The actual situation of the enterprise and the project is combined, the relevant indicators are determined on the basis of self-examination at various departments. In turn, we should follow different aspects such as the selection of evaluation elements, the batch of evaluation and the setting of evaluation stage. The concrete evaluation system for green construction can be illustrated in Figure 2.

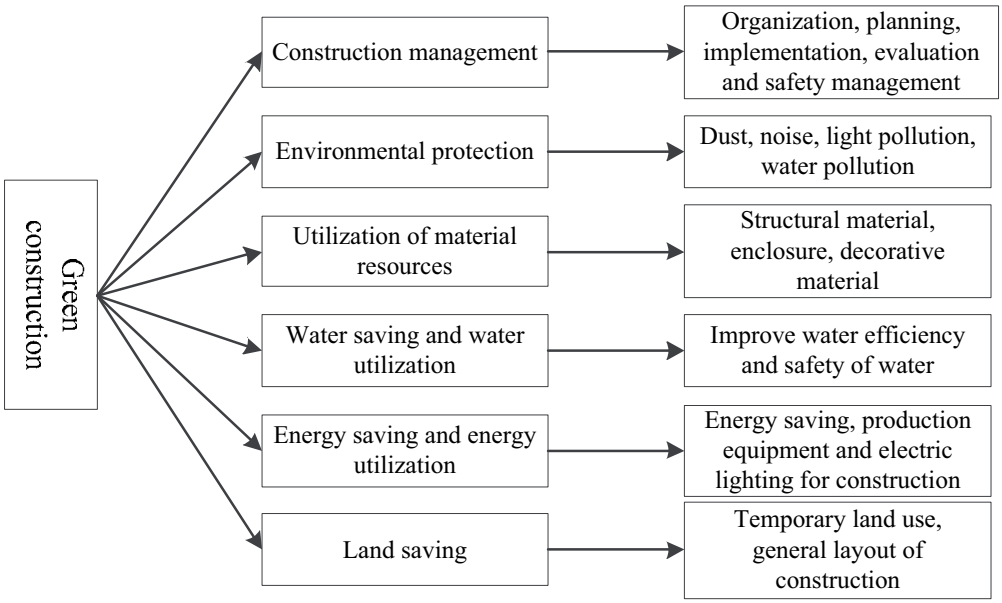


FIGURE 1
Key elements of green construction

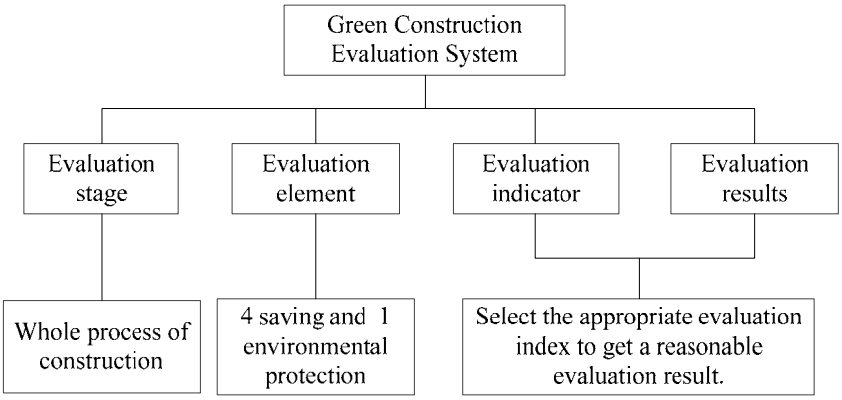


FIGURE 2
Green construction evaluation system

It is the choice of evaluation index to decide whether the construction process meets the requirements of green construction and whether it meets the expected green construction expectation. The weight and reference value of a green project is the evaluation index. Therefore, this part takes the evaluation index as the breakthrough point, and elaborates the evaluation system of green building in detail. Figure 3 shows the general process of green construction evaluation.

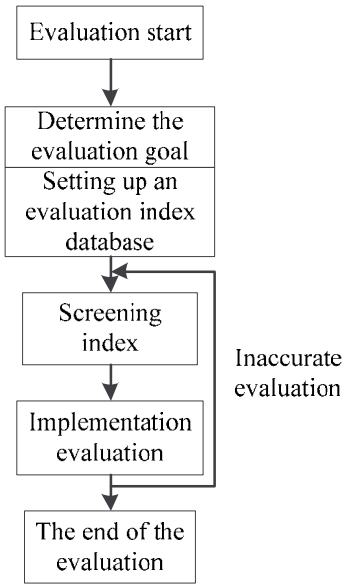


FIGURE 3
Evaluation process of green construction

Because of the lack of the corresponding fixed index of construction evaluation and the complexity of the operation and management of this process, so far, there has not been a unified tool to evaluate the construction process. Referring to China's "green Olympic Architecture Evaluation System", "green construction evaluation standard for Construction Engineering", and other major standard standards, the index system used in China's concrete green building evaluation system is summarized. Investment, management and training, environmental safety, energy consumption and employee health can be selected as evaluation indicators. Construction of environmental impacts, energy consumption, materials and resources, water resources and many other indicators are shown in Figure 4. In the process of the use of the real green construction evaluation system, the units and related personnel should choose the corresponding indicators in a reasonable category, because a fair and reasonable evaluation of green construction cannot be separated from the correct data and fair indicators.

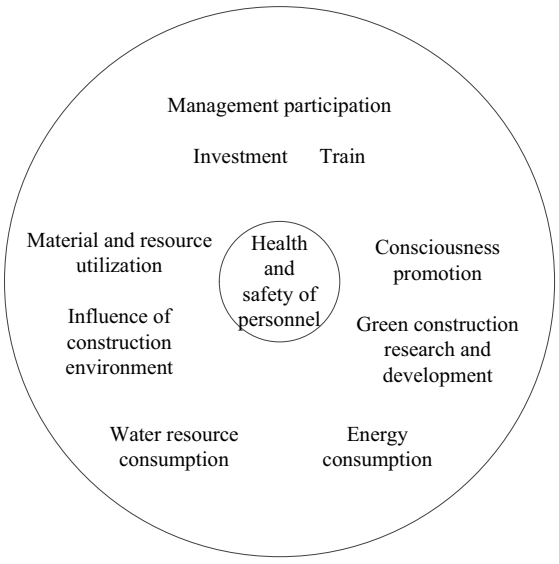


FIGURE 4
Evaluation index of conventional green construction

RESULTS AND DISCUSSION

Innovation and application of related technologies in the construction of high level green energy-saving buildings. Frame of outer enclosure structure. Starting from improving indoor comfort

and adjusting the living environment, building energy efficiency is regarded as a system containing comprehensive design to reduce building energy consumption. Building energy efficiency design must be an integrated system design, not only a single technical means, but also at the expense of indoor comfort. On the contrary, starting from improving indoor comfort, people adopt advanced and mature technology, carry out a series of optimization design combined with China's national conditions, and achieve high efficiency naturally.

(1) Thermal insulation of external wall. The external thermal insulation system is like a warm coat. In summer, we should minimize indoor and outdoor heat transfer in order to reduce direct solar radiation to the interior. In winter, we need to do a good job in indoor heat preservation. It is necessary to reduce the heat loss in the room. The heat transfer coefficient of the enclosure structure can be greatly reduced and the thermal resistance of the enclosure structure can be increased through the technology of extruded polystyrene board, breathing curtain wall and dry hanging stone, rock wool, thermal insulation and so on.

The heavy stone facade highlights the high-end product positioning of the project. By adding the flowing air layer in the middle of the stone and structure concrete, the heat conduction can be weakened effectively after the direct sunlight, thus reducing the indoor temperature. The air layer is a 135 millimeter level fire resistant rock wool insulation layer, and the final one is the 200 millimeter thick concrete layer (Figure 5). The heat transfer coefficient of the external wall is 0.38 $W/m^2 \cdot K$, and the smaller the heat transfer coefficient, the better the heat preservation performance.

(2) Outer window. When it comes to building energy consumption, we cannot fail to talk about the insulation performance of windows, which mainly consist of two kinds of materials, window frames and glass. Through market research, a more energy-efficient combination of aluminum frame and hollow Low-E glass can effectively prevent heat transfer.

The broken bridge aluminum alloy usually has two layers inside and outside, and the middle part is made up of non-conductive high strength nylon. It has good effect on air tightness and water tightness, and has good heat breaking performance. It can avoid various kinds of permeation of air. Compared with the high thermal conductivity of general aluminum alloy, it is better to keep warm in winter or in summer (Figure 6). In addition, the original advantages of aluminum alloy, such as easy extrusion molding, easy processing, high corrosion resistance and so on still exist, which better meet the needs of consumers.

The project can be selected according to the specific position of the house. For example, in the house along the street, the design of a high performance broken bridge aluminum window frame and double Low-E glass system can effectively reduce the noise impact of the surrounding traffic on the interior of the house. It has solved the boycott mentality of the customers in the house purchase, and has increased the economic value of the project.

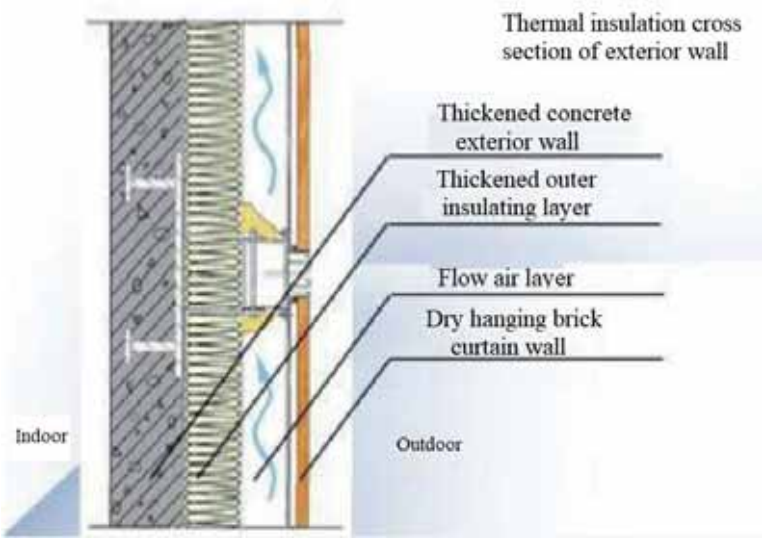


FIGURE 5
Dry hanging stone facade

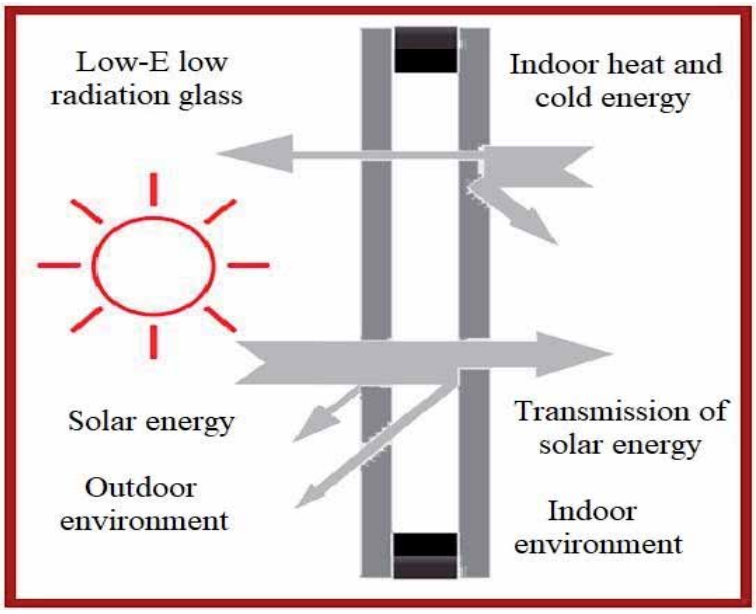


FIGURE 6
Energy saving principle of aluminum alloy outer window for broken bridge

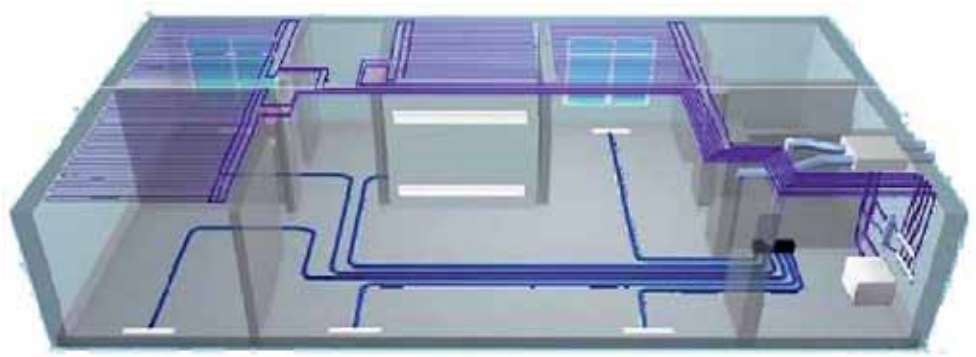


FIGURE 7
Capillaries in constant temperature system

The establishment of constant temperature and constant oxygen system. (1) Constant temperature system. In order to break the traditional way of cooling and heating, the heat radiation tube is embedded under the concrete floor or ceiling. In summer, the cold water of 18 to 21 centigrade is poured into the tube, and the hot water of 28 to 31℃ is entered in winter. The temperature of the room is controlled at 20-26℃, and the heat is spread to every corner of the room in the form of radiation (Figure 7). The radiation system greatly improves the comfort of people while greatly reducing the energy consumption of the traditional air conditioning system. Through the synchronous intelligent control system, the power of the air conditioning system can be adjusted with room temperature. The system uses low temperature hot water and high temperature cold water as the cold and heat source to meet the principle of saving energy. The efficiency of the air conditioner is more than 30% higher than that of the traditional air conditioner.

The capillary network system is made up of 4.3 * 0.8 mm PPR plastic capillary through a specific arrangement of grids. The distance between the grids is 10 mm~30 mm. The capillary network system mainly plays the role of collecting, distributing and transporting liquid, just like human capillaries and blood. In the grid, the flow rate of liquid is between 0.05-0.2 m/s, while the flow rate of human capillary is basically the same. In winter, the capillary network radiates heat through low temperature water. In summer, the cold water injected into the capillary network is mild and radiates into the interior. Because the outer surface of the capillary network is large, the heat transfer area is large, and the heat transfer speed is faster than the traditional method. Therefore, the heat transfer efficiency is higher.

(2) Total replacement fresh wind system. The application of the total replacement fresh air system ensures that the room is all fresh air in 24 h. The treated fresh air will be sent into the room at 0.2-0.3

m/s speed through the indoor air inlet. The new wind lake is formed on the ground and filled with every corner of the room. The new wind is sent back continuously to form alternative use. The humidity of the total displacement system can be kept stable, the utilization rate of new wind is high, and the operation cost is low. The fresh air unit has humidification dehumidification module and high efficiency plate type full heat recovery machine. The heat recovery rate is above 60%, the air conditioning load can be reduced by 30%, and the energy saving effect is remarkable.

In this project, the ground air supply system is designed. Because carbon dioxide is heavier than air, the lower the oxygen content is, the better the ventilation effect is when the fresh air system is installed on the ground. When the wind speed is low, the indoor air will not disturb the indoor air and avoid eddy current and turbulence, so the indoor air temperature is more uniform in the horizontal direction. The vertical temperature is stratified, the higher the layer height, the more obvious the change of temperature. The upward flow of hot air can not only take away excess heat, but also remove the dirty air from the roofs of the kitchen and toilet, and fresh air from the surface of the wall can be sent out of fresh air. Fresh air can be directly transported to the mouth and nose of the human body, providing good air quality for indoor human activities.

Integration of new energy utilization system. (1) Ground source heat pump. Ground source heat pump (GSHP) system is a new environmental protection energy utilization system using shallow geothermal energy for heating and cooling (Figure 8). In winter, heat is transferred from underground soil to buildings through buried pipes, and indoor heat is transferred to underground soil in summer. At the same time, the underground cooling capacity is transferred to the building to form a cold and hot circulation system, thus ensuring the indoor temperature requirements. Because the temperature of the surface of the surface is relatively stable all the year round, the temperature difference between the soil and the air is generally 17°C. Winter is higher than ambient air temperature and summer is lower than ambient air temperature. It is a good source of heat pump and air-conditioning. This temperature characteristic makes the ground source heat pump run by 40% to 60% higher than the traditional air conditioning system, so it can save 50% of the operating cost, so we call it the energy-saving air conditioning system. Compared with the air source heat pump, the pollutant discharge of ground source heat pump can also be reduced by more than 40%, which is reduced by more than 70% compared with that of electric heating. Moreover, the ground source heat pump system has many advantages, such as multi-function, low maintenance cost and long service life.

In any case, the initial investment of buried pipeline system is much higher than that of the traditional air conditioning system. In order to meet the total calculation load of the building, the initial investment of buried pipeline system will be more, but the operation cost will be greatly reduced. As part of the system operates under load, the use of hybrid power system will greatly save energy. The composite energy system is made up of three parts, namely, ground source heat pump, cooling tower and boiler system. After the completion of the ground

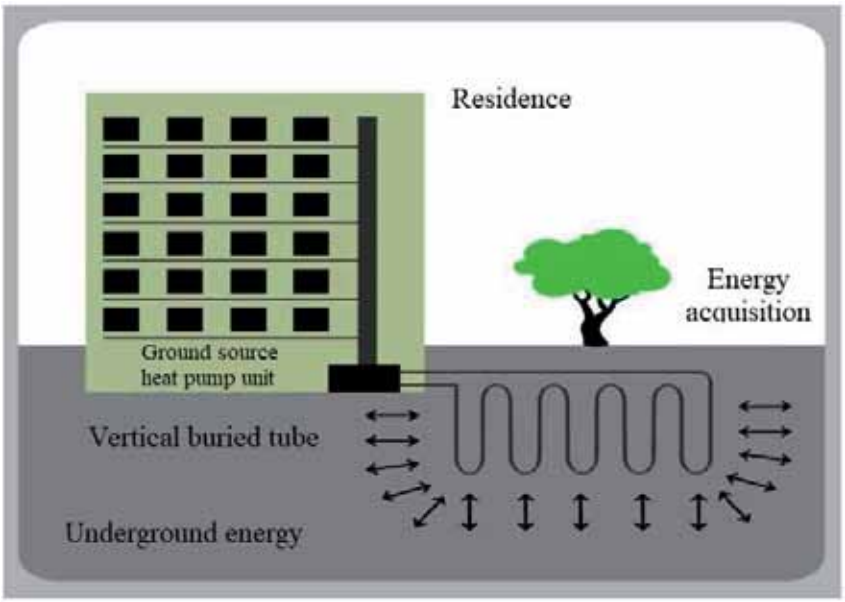


FIGURE 8
Ground source heat pump



FIGURE 9
Natural light leading-in

source heat pump, it can solve the total load of over 80% throughout the year. This method will greatly reduce the input of initial cost. This not only makes the system more safe and reliable, but also balances the endothermic and exothermicof the soil to avoid the balance between the heat absorption and release of the soil.

(2) Natural light leading-in. There are many ways to use solar energy in buildings, such as solar water heaters, photovoltaic power generation and solar energy direct utilization (light tube lighting) system. The daylight tube lighting system has been widely recognized and applied as an efficient and clean energy saving technology.

The light tube lighting system can capture and collect sunlight through the outdoor lighting device, and transfer it into the light guide tube for transmission. Finally, the light beam installed at the indoor roof will illuminate the light evenly (Figure 9). This system can reduce the lighting energy consumption of more than 80% in the daytime and more than 10% of the air conditioning refrigeration energy consumption.

At present, the material used for light tube is mainly aluminum optical reflection material. The total reflectivity of this material is greater than 99%. There are three kinds of bending tubes, which are 30 degrees, 60 degrees and 90 degrees respectively, and the service life is >25 years. The angle of the guide tube should not be too large, because the angle of the light source is very large, and the length of the guide tube should not be too long. It is not difficult to know that there is a positive correlation between the angle of the guide tube and the cost and length of the light guide tube.

The light guide lighting system can be used in various building sites, but it is mainly used for long-span buildings, stadiums, offices, underground space and so on. Combined with the product planning of this project, it is suggested that the natural light introduction system should be designed at the top level of the kindergarten.

CONCLUSION

Sustainable development is not a new subject, but its implementation is subject to various obstacles. Economic development, scientific and technological progress, the accelerated process of urbanization, the development and utilization of various resources are in the stage of sustainable development. Social development is the precondition of economic development. If the economic level cannot take the road of sustainable development, the society will gradually lose the foundation of survival. The sustainable development of the social economy needs the common sustainable development of environment and ecology. The development trend of the real estate industry in this century not only embodies environmental protection and energy saving, but also meets the growing demand of the people. The concept of green real estate is put forward under the trend of development and become the goal of real estate. Therefore, environmental protection and energy conservation are the basic tasks of green real estate projects. In actual operation, green real estate can be truly developed only by taking into account the social and economic benefits and satisfying the requirements of all kinds of industries involved and all kinds of demands of the consumers.

ACKNOWLEDGEMENT

This work was supported by Special Fund for the Innovation Strategy of Science and Technology of Guangdong Province in 2021 (Special Fund for "Climbing Program") (Grant No. Pdjh2021b0772).

REFERENCES

[1] Jiang, H.Y. (2020) Research on information design of green ecological building on ecological perspective. Fresen. Environ. Bull. 29, 5004-5011.
[2] Li, H.S. (2020) Analysis of application advantages in interior design based on traditional building information modeling technology. Fresen. Environ. Bull. 29, 5564-5569.
[3] Wong, I., Baldwin, A.N. (2016) Investigating the potential of applying vertical green walls to high-rise residential buildings for energy-saving in sub-tropical region. Building & Environment. 97, 34-39.
[4] Wang, L., Han, X. (2012) Energy saving and environmental protection of high-rise building under the background of green construction technology analysis of. Hunan Agricultural Machinery. 39(11), 260-261.
[5] Alwan, Z., Jones, P., Holgate, P. (2017) Strategic sustainable development in the uk construction industry, through the framework for strategic sustainable development, using building information modelling. Journal of Cleaner Production. 140(1), 349-358.
[6] Zhao, X., Jian, Z., Wu, G., Huang, C. (2018). A bibliometric review of green building research 2000 – 2016. Architectural Science Review. 62(1), 1-15.
[7] Wang, Y. Y., Ren, H., Ji, F. R. (2018). Cooperative innovation evolutionary game analysis of industrialized building supply chain. Applied Mechanics and Materials. 878, 213-218.
[8] Sui, Q., Wang, C.J. (2013) Analysis of the Application of Double Envelope Enclosure in the Energy-Saving Design of High-Rise Buildings. Applied Mechanics Materials. 361-363, 352-356.
[9] Ke, Z. T., Xia, Q. L. (2009) Study on coordination development of ecological-environment and economy based on coupling model: a case study of Wuhan city. Fresen. Environ. Bull. 28(5), 4007-4012.
[10] Chen, Y., Hong, T., Piette, M.A. (2017) Automatic generation and simulation of urban building energy models based on city datasets for city-scale building retrofit analysis. Applied Energy. 205, 323-335.
[11] Ma, J., Cheng, J.C.P. (2016) Estimation of the building energy use intensity in the urban scale by integrating GIS and big data technology. Applied Energy. 183, 182-192.
[12] Kammen, D.M., Sunter, D.A. (2016) City-integrated renewable energy for urban sustainability. Science. 352, 922-928.
[13] Gong, M., Zhu, W. (2012) Green Building Performance Analysis of High-Rise Residence in Steel Structure Residence System. Advanced Materials Research. 461, 83-87.

Received: **06.04.2021**
Accepted: **17.05.2021**

CORRESPONDING AUTHOR

Xiaoli Liu
The Architectural Engineering College,
Guangdong Polytechnic of Science and Technology,
Zhuhai Guangdong 519000 – China

e-mail: xiaoliliu@email.cn

© by PSP Volume 30– No. 09/2021 pages 10815-10824 Fresenius Environmental Bulletin

AN EMPIRICAL ANALYSIS OF THE RELATIONSHIP BETWEEN ECONOMIC DEVELOPMENT AND ENVIRONMENTAL POLLUTION IN HENAN PROVINCE, CHINA

Lei Guo*

Henan Logistics Vocational College, Zhengzhou Henan 450000, China

ABSTRACT

After the reform and opening up, the economic growth in China has achieved world-renowned achievements. However, looking back at the process of the economic development, we have followed a path of economic growth at the expense of high investment in resources and environmental destruction, which has led to an increasingly tense relationship between the economy and the environment. We analyze and study how to improve the level of environmental protection, change our real-life situation of focusing on development and light pollution, and the tendency to rely solely on administrative fees to protect the environment, thereby promoting the harmonious relationship between the economy and the environment. This paper collects the economic and environmental data of Henan Province from 2000 to 2020, establishes an indicator system for economic development and environmental quality, uses principal component analysis to eliminate relevant indicators, and constructs an environmental Kuznets curve with characteristics of Henan Province to analyze the relationship between economic development and environmental quality in Henan Province. The results show that the environmental Kuznets curve of Henan Province conforms to the typical inverted U shape of developed countries, that is, environmental pollution does show a trend of rising first and then falling with the increase of per capita income.

KEYWORDS:
Henan Province, economic development, environmental quality, principal component analysis, environmental Kuznets curve

INTRODUCTION

The tremendous changes in today's world have made us clearly see that mankind has gradually stepped into an era of industrial civilization in which we conquer nature, plunder resources, and seek survival and development at the expense of the ecological environment, and gradually step into an era of protecting the environment, building the environment, and rebuilding the harmony between man and nature [1-2]. With the increasingly tense relationship between development and environmental contradictions, foreign scholars have launched investigations and studies on the relationship between environmental protection and sustainable economic development.

Since the 21st century, many foreign researchers have used different research methods to empirically test the existence of the environmental Kuznets curve based on different data sources in various regions [3-6]. Herman E Daly (2001) believes that the natural resources that exist in various natural life forms are limited, and that human irrational activities will make the regeneration system unable to heal. In the book "Beyond Growth: The Economics of Sustainable Development" Regarding sustainable development as a brand-new concept, its core lies in the increase in quality, not just the increase in quantity, and calls on people to change the traditional backward economic form since the industrial revolution, and gradually form a green, pollution-free, and ecologically destructive cycle forward mode [7].

Robert (2002) puts social development and pollution control at the same important position, believes that there is no absolute contradiction between environment and social development, and calls on the government to use environmental protection technology to conduct unified management of the use of natural resources at a macro level [8]. Roca (2011) collected and analyzed a variety of economic and environmental data in Spain. Through linear regression simulation of the relationship between each data and residents' income, the simulation results showed that the relationship between SO2 emissions and income follows the typical EKC curve established by developed countries [9]. Lenzen JD (2002) designed an indicator system for the development level of the environment-economy-energy system, placed the selected indicators in each independent system to analyze the relationship between the environment-economy-energy system and measured the coordinated state of the relationship between the systems [10]. Song (2008) conducted a statistical analysis of the dynamic environmental data of most

provinces in China and found that the relationship between the emissions of major industrial pollutants and the gross domestic product shows a typical Kuznets hypothesis relationship in developed countries [11]. Fodha and Zaghdoud (2010) studied the relationship between industrial pollution and economic growth in Tunisia, and verified that there is a U-shaped relationship between industrial pollution and economic growth in Tunisia [12]. Boulding (2010) analyzed the relationship between the economic system and the environmental system and pointed out that unreasonable human economic activities will cause serious damage to the global environment and called for the establishment of a brand-new economic development model, which is to protect nature while economic development and realize the circular sustainable development of economy and environment [13]. Li Keguo (2009) measured the inevitable connection between the development of social production and the concentration of pollution from a holistic perspective and pointed out that the continuous deterioration of the social environment is cognitively disdainful of the laws of natural ecology [14]. Wu Yuping (2002) constructed an EKC model between Beijing's economic growth and the level of environmental pollution and concluded that the relationship between the two shows a significant inverted U-shaped Kuznets curve [15]. Wu Kaiya (2003) explored the relationship between the per capita GDP of Anhui Province and the amount of industrial wastewater, exhaust gas, and solid waste emissions, and used the correlation analysis method to study the degree of correlation between index data and constructed a EKC curve model with local characteristics [16].

With the acceleration of the economic development of Henan Province, the accumulated environmental problems have seriously threatened the sustainable development of the economy. This paper collects the economic and environmental data of Henan Province from 2000 to 2020, establishes an indicator system for economic development and environmental quality, uses principal component analysis to eliminate relevant indicators, and constructs an environmental Kuznets curve with characteristics of Henan Province to analyze the relationship between economic development and environmental quality in Henan Province.

MATERIALS AND METHODS

(1) Evaluation index system. We generally divided the system into economic system and environmental system. The economic system usually contains the following indicators, namely, the overall economic situation, industrial structure, production vitality, economic efficiency, development speed, etc. There are four environmental subsystems: atmospheric environmental index, water environmental index, solid waste environmental index, and ecological protection and destruction index. According to research needs, this paper selects 11 economic development and environmental quality indicators. Through these indicators, the relationship between economic development and environmental quality in HenanProvince is studied, and an indicator system is constructed as shown in Table 1.

(2) Choice of Evaluation Method. The analysis method of the relationship between economic development and environmental quality is still in the exploratory stage. At present, there are two main analytical methods: one is to calculate the comprehensive index of each system by establishing an index system between the economic development system and the environmental system, and then use the coordination degree model to measure the coordination relationship between the two [17-18]. However, the analysis of the research results is more general, that is, simple coordination and incoordination. The other is to construct an indicator system between the economic development system and the environmental system, and then use the principal component analysis method to replace the indicators with strong correlations, get the energy indicators that better reflect the relationship between the two, finally choose the gray correlation model to measure the coordination correlation between key economic indicators and key environmental indicators, and establish an economic environment evaluation model [19]. This paper uses modern statistical analysis methods and principal component analysis to eliminate relevant economic environmental indicators. It is found that per capita GDP and industrial wastes are the main component indicators of Henan Province. On this basis, the environmental Kuznets curve is selected to simulate, respectively. The EKC model between Henan's per capita GDP and industrial wastewater, waste gas, and solid waste more vividly describes the relationship between economic development and environmental quality.

RESULTS AND DISCUSSION

(1) Current economic situation. 1) Changes in total economic growth. Judging from the data compiled by the Henan Provincial Bureau of Statistics and the Henan Financial Yearbook, the GDP of Henan Province has maintained a steady upward trend, from 505.299 billion yuan in 2000 to 5,499.07 billion yuan in 2017. In just 20 years, the economy has grown by about 11 times. From 2019 to 2020, the slow GDP growth is mainly due to the impact of the new crown epidemic. The change in GDP per capita is shown in Figure 2. Overall, per capita GDP has increased significantly, from 5,450 yuan per capita in 2000 to 56,388 in 2020, an increase of more than

TABLE 1
Evaluation index system of the relationship between economic development and environmental quality in Henan Province

Indicator system	Specific index content
Economic development system	X1 GDP per capita
	X2 fiscal revenue
	X3 Investment in fixed assets
	X4 Gross industrial output value
	X5 Per capita consumption level
Environmental quality system	Y1 Industrial wastewater discharge
	Y2 Industrial waste gas emissions
	Y3 Amount of solid waste generated
	Y4 Total smoke and dust emissions
	Y5 Output value of comprehensive utilization of Three Wastes
	Y6 Comprehensive utilization of solid waste

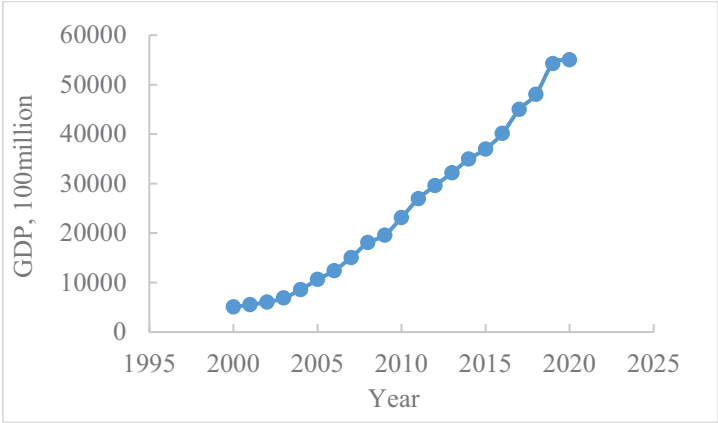


FIGURE 1
The changes of GDP in Henan Province from 2000 to 2020.

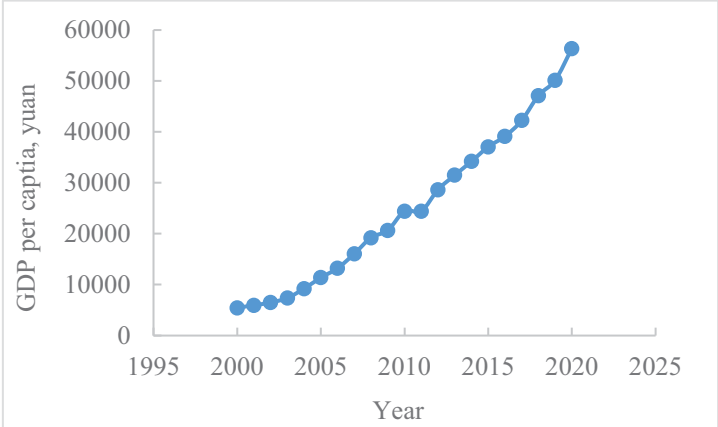


FIGURE 2
The changes of GDP per captia in Henan Province from 2000 to 2020.

10 times (Figure 2).

From 2000 to 2020, the economic growth rate of Henan Province has experienced complex fluctuations. From Figure 3, it can be roughly divided into several periods: First, from 2000 to 2004, the growth rate is between 9%-13.7%, reflecting the rapidly changing environment of the economic situation. From 2005 to 2007, the growth rate is relatively stable, at around 14.5%. From 2008 to 2019, the economic growth rate declines slowly. The significant decline in the growth rate in 2020 is mainly due to the covid epidemic.

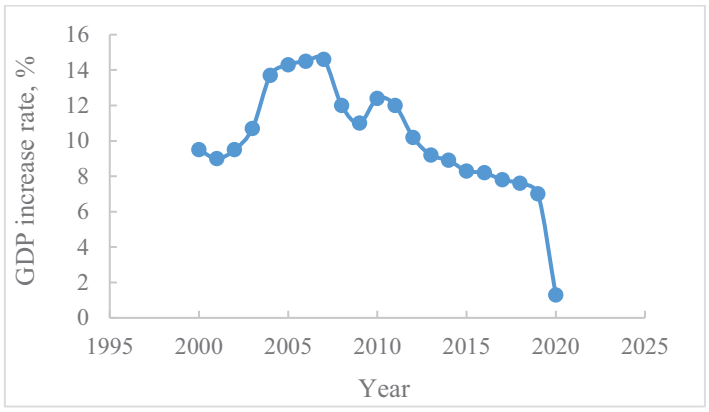


FIGURE 3
The increase rate of GDP in Henan Province.

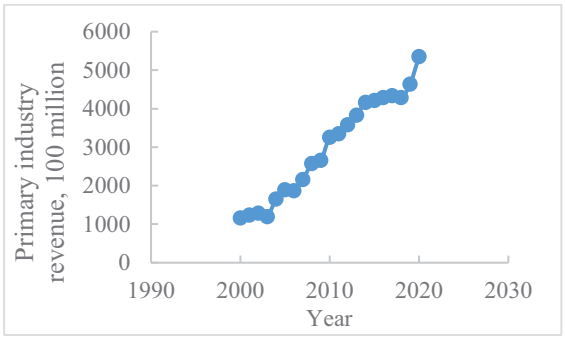


FIGURE 4
The changes of the primary industry revenue from 2000-2020.

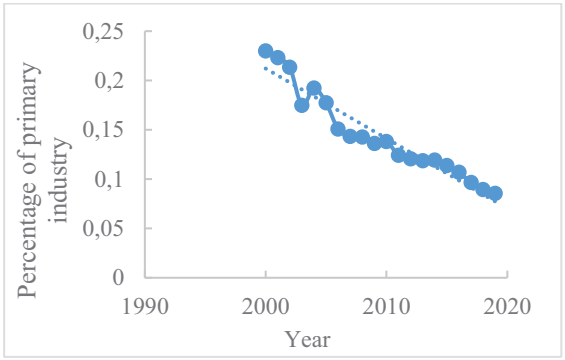


FIGURE 5
The percentage of primary industry from 2000-2020.

2) Evolution characteristics of the industrial structure of Henan Province. The industrial structure upgrade specifically includes three aspects: one is to gradually establish a new industrial structure dominated by the tertiary industry; the other is to lengthen the industrial chain within each industry and increase the added value; the third is to use labor and capital-intensive industries. The main trend is constantly changing to focus on technology and knowledge-intensive industries. Henan has realized the necessity of the transformation and the upgrading of the industrial structure and has begun to put it into action, but some problems have appeared in the process of transformation and upgrading.

In the past ten years, the total contribution of Henan's primary industry to the economy has doubled, but its proportion has continued to decline. It can be seen from Figure 3 that the actual value created by the primary industry has increased from 265.878 billion yuan in 2008 to 433.449 billion yuan in 2017. The total output value has nearly doubled in ten years. From Figure 4, it can be seen that the proportion of output value has increased from ten years ago. Nearly 15% of the company's investment has dropped to less than 10% in 2017, a decrease of about 5%, and the adjustment and optimization of the internal structure will be gradually realized (Figure 5). Henan, as an important food production base, has a higher share of agriculture than most parts of the country. However, after more than ten years of economic development, Henan has actively adjusted its industrial structure under the good momentum of rising agricultural total. The proportion of agriculture has maintained an overall downward trend for many years, reflecting that the adjustment of Henan's industrial structure has achieved initial results.

The industrial industry has developed rapidly since the founding of the country's industrialization, and its share of GDP has generally maintained an upward trend. Since 2011, the share of the secondary industry has begun to decline. It reflects the continuous advancement of Henan's industrial transformation and upgrading plan, which has achieved initial results in recent years. As can be seen from Figures 6 and 7, the actual GDP of the secondary industry has increased from 828.283 billion yuan in 2007 to 1,927.582 billion yuan in 2017, with the highest proportion reaching 57.284%, which has become an important factor in stimulating economic growth and boosting people's income. After 2011, due to the rise of resources and labor costs, coupled with increasingly surplus production capacity and insufficient effective demand, the development space of the industry is gradually compressed, and the proportion of the secondary industry begins to decline. By 2017, the proportion of the secondary industry dropped to 47.679%.

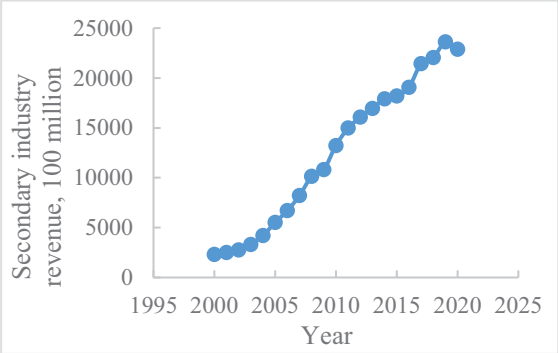


FIGURE 6
The changes of the secondary industry revenue from 2000-2020.

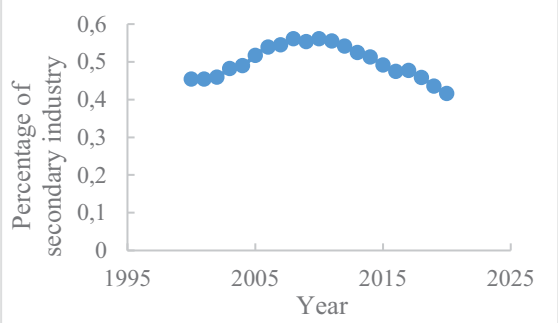


FIGURE 7
The percentage of secondary industry from 2000-2020.

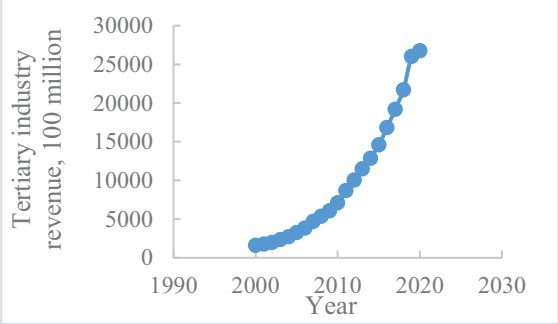


FIGURE 8
The changes of the tertiary industry revenue from 2000-2020.

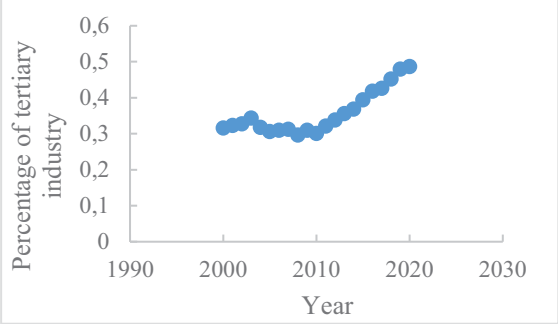


FIGURE 9
The percentage of secondary industry from 2000-2020.

Fundamentally, with the support of policies, the tertiary industry in Henan has been developing rapidly. With the broad development prospects, enterprises and individuals have devoted themselves to the construction of the tertiary industry mainly based on the service industry. It can be seen from Figure 8 that the tertiary industry in Henan Province gradually approached the share of the secondary industry in the national economy after 2012, reaching 42.675% in 2017, which has become another growth pole of economic development. Henan has established multiple logistics centers in Zhengzhou, Luohe and Xinyang in terms of circulation. The transportation network covers all parts of the country, and the post and telecommunications system basically achieve full coverage of the province. Radio, television, health, tourism, and information consulting industries have developed vigorously. To shrink, the tertiary industry is comparable to the secondary industry in terms of financing amount, development scale, or number of employees. However, industry still occupies the leading position, and the secondary industry is still the most important industry for driving Henan's economic growth.

(2) Current situation of the environment. The environment of a country or region is an important foundation and carrier of economic and social development, and environmental quality is one of the key factors affecting economic development. With the rapid economic development of Henan Province, the environmental problems have become more and more serious. According to the actual situation in Henan Province, the destruction of environmental quality is mainly caused by the discharge of the three industrial wastes. Therefore, the current situation of environmental quality is mainly introduced from these three aspects.

In recent years, the Henan Provincial Government has paid more attention to environmental issues. In terms of ecological construction and environmental pollution prevention and control, a series of environmental protection policies and measures have been adopted and great progress has been made. At the same time, relying on the investigation and management of industrial pollution sources and strengthening environmental supervision and management and technical management methods can be used to effectively control the increase in the total discharge of pollutants and reduce the total discharge of major pollutants. The government strengthened the supervision of environmental protection work, coupled with raising people's environmental awareness. Overall, there are still many environmental problems in Henan Province. In order to better understand the environmental status of Henan Province, starting from the actual situation of Henan Province's environmental quality, the changes in Henan Province's environmental quality are mainly analyzed from three aspects: solid waste, wastewater and exhaust gas.

1) Industrial wastewater discharge. The total amount of wastewater discharged from industrial production in Hebei Province is relatively large. From 2000 to 2010, the amount of industrial wastewater discharged continuously increases, increasing the pressure of urban environmental pollution and severely restricting the healthy and sustainable development of Henan's economy and society. In addition, due to the unreasonable use of chemical fertilizers and pesticides in the agricultural production process, groundwater pollution and soil acidification are formed, and the backward scientific and technological equipment and imperfect infrastructure in agricultural production have caused serious environmental pollution in the rural areas of Henan Province. This series of problems have been reduced the overall environmental quality level of Henan Province.

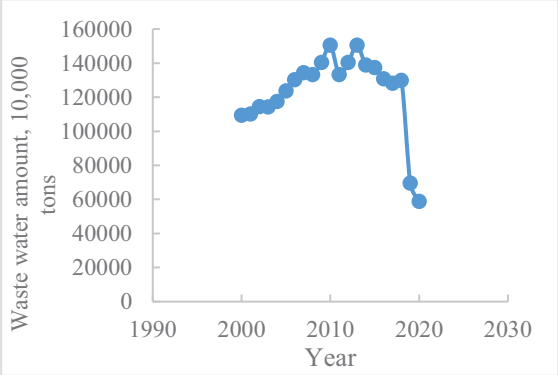


FIGURE 10
The wastewater production from 2000-2020.

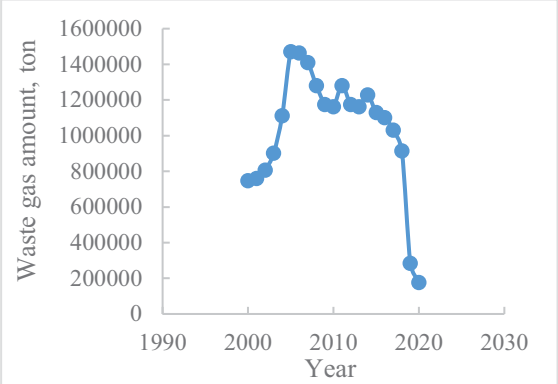


FIGURE 11
The waste gas production from 2000-2020.

Looking at the overall trend, after 2013, with the implementation of various government measures, the discharge of industrial wastewater begins to decrease. Since 2018, the discharge of industrial wastewater has been significantly reduced. For example, in 2018, the amount of industrial wastewater discharged in Henan Province was 1,298 million tons. By 2019, the discharge amount suddenly dropped to 69,500, a reduction rate of more than 40% (Figure 10).

2) Air quality status. Exhaust gas refers to gas pollution that is toxic and harmful to human health due to unreasonable social production and living activities of human beings. The vast majority of air pollution comes from human waste gas emissions from production and life. Air pollution sources mainly include emissions from production enterprises, automobile exhaust, construction smoke and so on. Waste gas emitted by factories is the most important source of air pollution, and industrial waste gas pollution data are easier to obtain. According to data, the main industrial waste gas in Henan Province is sulfur dioxide.

It can be seen from Figure 11 that the industrial waste gas emissions in Henan Province begin to rise slowly from 2000 to 2005, and in 2005, the industrial waste gas emissions slowly decline. From 2010 to 2015, industrial waste gas emissions change in waves. After 2015, industrial waste gas emissions continue to decrease. After 2018, industrial waste gas emissions have dropped rapidly. For example, in 2018, industrial waste gas emissions are 915,002 tons. By 2019, this value has become 284,700, a reduction rate of more than 60% (Figure 11).

3) Status of solid waste. According to the source of solid waste discharge, it is divided into three categories: industrial production solid waste, agricultural production solid waste, and household waste.

It can be seen from Figure 12 that from 2000 to 2020, the amount of industrial solid waste produced in Henan Province has remained at a relatively high level. Since 2004, the amount of solid waste produced has continued to rise. It is showing a trend of rapid rise. By 2008, the amount of industrial solid waste generated is close to 200 million tons. In 2013 alone, the amount of industrial solid waste generated is 429.83 million tons, more than seven times that of 2000. It can be seen that the state of solid waste pollution in Henan Province is not very optimistic. Beginning in 2014, solid waste emissions began to slowly decline. From 2018 to 2019, solid waste dropped from 382.64 million tons to 189.65 million tons, a drop of more than 50%.

(3) EKC model establishment. The number of principal components can be selected according to the characteristic roots of the correlation coefficient matrix. The characteristic roots of the correlation coefficient matrix are just equal to the variance of the principal components, and the variance is one of the important criteria for judging the information contained in the variable data. There are three criteria for determining the number of principal components according to the λ value of the principal component score: First, we only take the principal components with the initial characteristic root score $\lambda \geq$principal component. The second is the principal component

corresponding to the lambda value whose cumulative percentage reaches more than 95%. The third is to determine the number of principal components according to the mutation point of the characteristic root value change. The experimental results show that the economic system only selects per capita GDP as the object of analysis and research, which can not only cover the information of economic development and reflect the level of economic development but will not cause research bias and loss of accuracy. Regarding environmental quality indicators, the main component indicators of the environmental system in Henan Province, we select industrial wastewater emissions, industrial waste gas emissions, and industrial solid waste generation that have a large cumulative contribution rate. This is also in line with the reality of environmental pollution in Henan Province.

The EKC model is a model that reflects the relationship between income and environmental pollution. It reflects the relationship between the level of income and the level of environmental pollution. After the screening of the main components, this paper collates the data of per capita GDP and industrial wastes from 2000 to 2020, and uses correlation analysis to construct a regression model of the relationship between economic development and environmental quality, and simulates per capita GDP and industrial wastes through the Kuznets cubic curve equation, and the derived EKC model. Then, the relationship between economic development and environmental quality in Henan Province is fully explained. The analysis shows that the traditional economic development model of Henan Province has led to a decline in environmental quality and an increase in pollution levels, and economic development is facing huge environmental pressure. The discharge of industrial wastewater and industrial waste gas has been alleviated.

1) Analysis of the relationship between per capita GDP and wastewater pollution. The relationship between Henan's per capita GDP and industrial wastewater discharge is quite similar to the typical EKC curve in developed countries.

It can be observed from Figure 13 that the relationship between Henan's per capita GDP and industrial wastewater discharge exceeds the turning point of the EKC curve, but then it does not fall all the time, showing an upward trend. The theoretically calculated value of GDP per capita corresponding to the turning point is about 28,000 yuan, indicating that the industrial wastewater discharge is basically under control in the short term and is beginning to develop in a benign manner. This is not the same as the inverted U shape of the typical EKC curve, which means that with the increase of income in Hebei Province, the degree of environmental pollution has intensified. When the economic development reaches a certain level, it reaches the critical point, that is, the per capita GDP is 28,000 yuan. As per capita income continues to grow, it will improve, and the quality of the environment will be greatly improved. It is found through the figure that the sewage discharge volume has begun to decline.

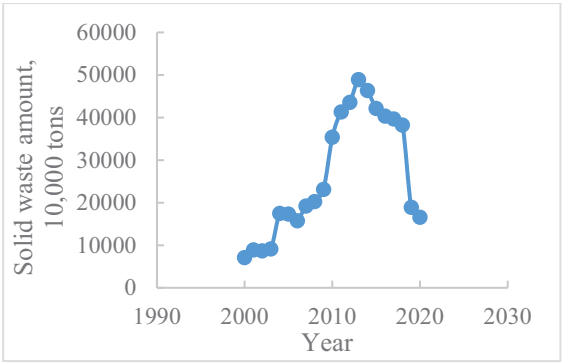


FIGURE 12
The solid waste production from 2000-2020.

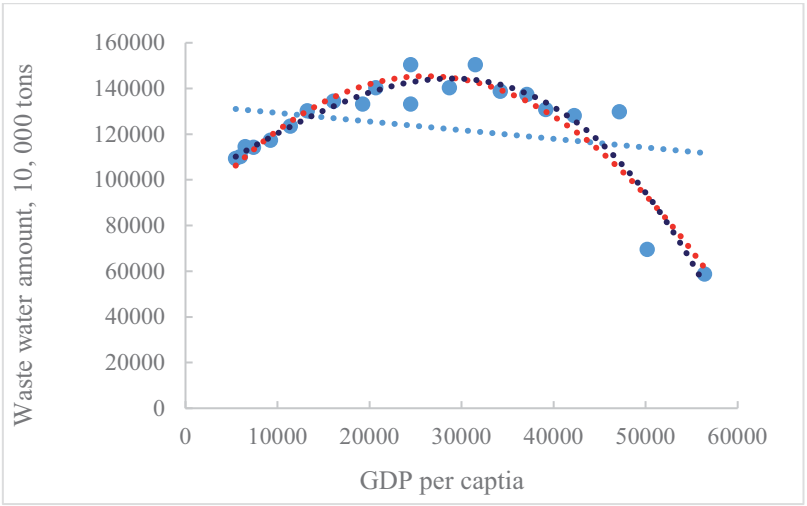


FIGURE 13
EKC curve between per capita GDP and industrial wastewater discharge in Henan Province.

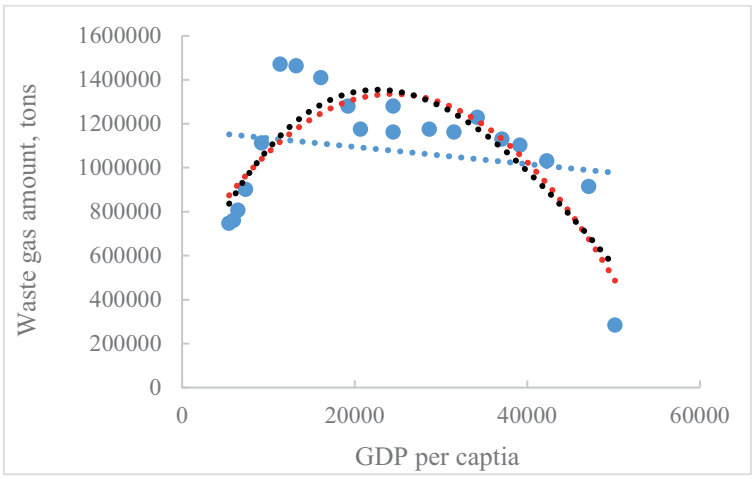


FIGURE 14
The EKC curve of Henan Province's per capita GDP and industrial waste gas emissions.

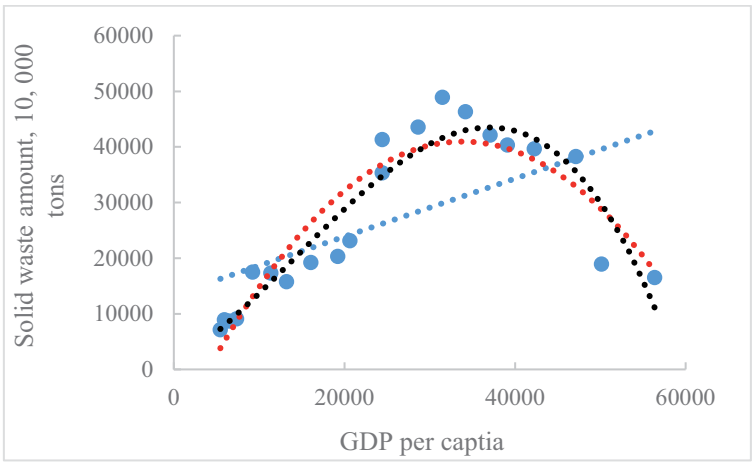


FIGURE 15
EKC curve of per capita GDP and solid waste discharge in Henan Province.

2) Analysis of the relationship between GDP per capita and waste gas pollution. Through the simulation of the relationship between Henan Province's per capita GDP and industrial waste gas from 2000 to 2020, it is found that the waste gas curve of Hebei Province does not completely conform to the typical EKC curve of developed countries. It is specifically expressed as part of the typical curve, that is, industrial waste gas and per capita GDP. The rising part of the relationship and the half-falling part over the turning point. This shows that in the past 20 years, with the continuous deepening of the economic development of Hebei Province and the continuous increase of per capita income, the discharge of industrial wastewater has a relatively downward trend, and the environmental pollution caused by the discharge of wastewater has been curbed to a certain extent. The side reflects the positive trend of the relationship between economy and environment (Figure 14).

Figure 14 depicts the EKC curve of the relationship between Henan's per capita GDP and industrial waste gas emissions, showing an inverted U shape, and the relationship between per capita GDP and waste gas emissions breaks through the inflection point of the EKC curve. The per capita GDP corresponding to the turning point is about 25,000 yuan. The annual GDP per capita in 2011 is 24,446 yuan, indicating that from 2000 to 2011, with the economic development of Henan Province, industrial waste gas pollution gradually increases. After 2011, waste gas emissions show a gradual signs of going down with the increasing economic growth.

3) Analysis of the relationship between per capita GDP and solid waste discharge. By simulating the relationship between Henan Province's per capita GDP and industrial solid waste from 2000 to 2020, it is found that the solid waste curve of Henan Province is specifically a typical EKC curve (Figure 15).

It can be observed from Figure 15 that the relationship between Henan's per capita GDP and industrial wastewater discharge exceeds the turning point of the EKC curve, showing a downward trend. The theoretical calculation value of per capita GDP corresponding to the turning point is about 37,000 yuan (per capita GDP in 2015 is 37,012 yuan), indicating

that the industrial wastewater discharge is basically under control in the short term and is beginning to develop in a benign manner. This is the same as the inverted U shape of the typical EKC curve, which means that with the increase of income in Henan Province, the degree of environmental pollution has intensified. When the economic development reaches a certain level, after reaching the critical point of per capita GDP of 37,000 yuan, the environmental pollution situation will change. With the continuous growth of per capita income and improvement, the environmental quality has been greatly improved.

CONCLUSIONS

(1) From an overall point of view, there is a significant correlation between economic growth in Henan Province and changes in industrial structure, and the two have interactive effects. On the one hand, industrial restructuring has promoted economic growth. First, the adjustment of industrial structure optimizes the allocation of resources, so that limited and scarce resources can be allocated to more critical industries that are more beneficial to the development of the national economy; second, the adjustment of industrial structure can enable the first developed industries to take the lead in adopting advanced technologies, thereby driving other industries; finally the development of emerging industries can provide more employment opportunities, ultimately achieving economic growth. On the other hand, economic growth has also accelerated the transformation and upgrading of the industrial structure. Economic development increases people's disposable income, which brings about changes in demand and leads to the development of new industries that adapt to demand. In addition, economic development increases social investment capacity and the speed of technological change, which will also accelerate the transformation of industrial structure.

(2) This paper simulates the relationship between the main economic development indicators and environmental quality indicators after the principal component analysis, and then draws the three environmental Kuznets between the per capita GDP of Henan Province and industrial wastewater, industrial waste gas, and industrial solid waste. It is found that the three EKC curves in Henan Province show a typical inverted U shape, that is, the amount of environmental pollution does rise first and then decline with the increase of per capita income.

(3) The relationship between economic development and environmental quality is a systematic project. Based on the consideration of manpower, material resources, time, and other factors in this study, this article only analyzes and studies the overall situation of Henan Province, and does not study the situation of each city in the province separately. In the future, we will conduct research on various cities in Henan Province to gain a deep understanding of the relationship between Henan's economic development and environmental quality.

ACKNOWLEDGEMENTS

This work was not supported by any funds. The authors would like to show sincere thanks to those techniques who have contributed to this research.

REFERENCES

[1] Shen, S., Yang, C., Wang, Y., Yang, D. (2015) Spectral characteristics of dissolved organic matter (DOM) in surface sediments from an urban river with different outfalls. Fresen. Environ. Bull. 24(1), 56-62.

[2] Sarkodie, S.A. (2018) The invisible hand and EKC hypothesis: what are the drivers of environmental degradation and pollution in Africa? Environmental Science and Pollution Research, 25(22), 21993-22022.

[3] Allard, A., Takman, J., Uddin, G.S., Ahmed, A. (2018) The N-shaped environmental Kuznets curve: an empirical evaluation using a panel quantile regression approach. Environmental Science and Pollution Research. 25(6), 5848-5861.

[4] Smorkalov, I.A., Vorobeichik, E.L. (2011) Soil respiration of forest ecosystems in gradients of environmental pollution by emissions from copper smelters. Russian Journal of Ecology. 42(6), 464-470.

[5] Zhou, T., Yuan, F., Fan, Y., Zhang, D., Cooke, D., Zhao, G. (2008) Granites in the Sawuer region of the west Junggar, Xinjiang Province, China: geochronological and geochemical characteristics and their geodynamic significance. Lithos. 106(3-4), 191-206.

[6] Filloy, J., Grosso, S., Bellocq, M.I. (2015) Urbanization altered latitudinal patterns of bird diversity-environment relationships in the southern Neotropics. Urban Ecosystems. 18(3), 777-791.

[7] Fooks, J.R., Messer, K.D. (2010) Maximizing conservation and in-kind cost share: applying goal programming to forest protection. Journal of Forest Economics. 18(3), 207-217.

[8] Maqbool, S., Zameer, M.N. (2018) Corporate social responsibility and financial performance: an empirical analysis of Indian banks. Future Business Journal. 4(1), 84-93.

[9] Lin, W.T. (2010) The control of environmental pollution and optimal investment and employment decisions. Optimal Control Applications and Methods. 8(1), 21-36.

[10] Tsai, M.S., Hsu, F.Y. (2009) Application of grey correlation analysis in evolutionary programming for distribution system feeder reconfiguration. IEEE Transactions on Power Systems. 25(2), 1126-1133.
[11] Chen, M., Lu, D., Zha, L. (2010) The comprehensive evaluation of China's urbanization and effects on resources and environment. Journal of Geographical Sciences. 20(1), 17-30.
[12] Selden, T.M., Song, D. (1994) Environmental quality and development: is there a Kuznets curve for air pollution emissions? Journal of Environmental Economics and Management. 27(2), 147-162.
[13] Rodhe, H. (1990) A comparison of the contribution of various gases to the greenhouse effect. Science. 248(4960), 1217-1219.
[14] Kwon, Y.D., Yamauchi, H. (1993) Agricultural policy adjustments in the Korean rice economy. Agricultural Economics. 9(4), 335-346.
[15] Anderson, K., Giesecke, J., Valenzuela, E. (2009) Distorted agricultural incentives and Australian economic development. World Economy. 32(3), 351-384.
[16] Sun, L., Fulginiti, L.E., Peterson, E.W. (2010) Accounting for agricultural decline with economic growth in Taiwan. Agricultural Economics. 36(2), 181-190.
[17] He, L., Turvey, C. (2009) Financial repression in China's agricultural economy. China Agricultural Economic Review. 1(3), 260-274.
[18] Fragoso, R., Marques, C., Lucas, M.R., Martins, M.B., Jorge, R. (2011) The economic effects of common agricultural policy on Mediterranean montado/dehesa ecosystem. Journal of Policy Modeling. 33(2), 311-327.
[19] Wilson, O.J. (1995) Rural restructuring and agriculture-rural economy linkages: A New Zealand study. Journal of Rural Studies. 11(4), 417-431.

Received: **06.04.2021**
Accepted: **05.05.2021**

CORRESPONDING AUTHOR

Lei Guo
Henan Logistics Vocational College,
Zhengzhou Henan 450000 – China

e-mail: wyshguo@163.com

© by PSP Volume 30– No. 09/2021 pages 10825-10835 Fresenius Environmental Bulletin

DETERMINATION OF SOME SELECTED PHARMACEUTICALS IN MARINE BIOTA: A CASE STUDY IN THE ISTANBUL METROPOLITAN AREA, TURKEY

Nagihan E Korkmaz*, Nuray Balkis Caglar, Abdullah Aksu

Department of Chemical Oceanography, Institute of Marine Science and Management, Istanbul University, Vefa, 34134 Istanbul, Turkey

ABSTRACT

This paper presents data on eleven pharmaceuticals of different classes (nonsteroidal anti-inflammatory drugs, blood lipid regulators, antiepileptics and hormones) in biota (mussels, macroalgae, fish muscle tissue) from the Golden Horn Estuary, Turkey. An ultrasonic extraction method was used to extract pharmaceuticals from the biota. The solid-phase extraction (SPE) method was used for clean-up. High-performance liquid chromatography (HPLC) with a DAD detector was used to quantify the pharmaceuticals. All target compounds were detected in at least one of the samples. Gemfibrozil (56–9135 ng/g) was the most frequently detected compound in all biota samples. Five pharmaceuticals were detected in the macroalgae samples at a maximum concentration of 7221 ng/g for gemfibrozil. Additionally, nine of the pharmaceutical compounds were detected in several or all of the seven fish species. The highest concentration of 17α-ethinylestradiol detected in *Mullus barbatus* was 1258 ng/g. The concentrations of diclofenac (4694 ng/g), naproxen (1570 ng/g), ibuprofen (5098 ng/g), 17β-estradiol (2364 ng/g), clofibric acid (1296 ng/g), and gemfibrozil (9135 ng/g) were considerably higher in mussels than in other biota species. The accumulation potential of pharmaceutical compounds was higher in mussels than in other biota species.

KEYWORDS:
Pharmaceuticals, Fish species, *Mytilus galloprovincialis*, *Ulva laccuta*, Golden Horn Estuary, Istanbul

INTRODUCTION

Pharmaceuticals are a group of emerging pollutants that have attracted much attention in recent years because of their widespread use and potentially harmful effects on the environment and human health [1, 2]. The presence of such micropollutants in the aquatic environment stems from their large consumption in agriculture and aquaculture, human and veterinary medicine and the inability of these compounds to be fully treated in many wastewater treatment plants [3, 4]. Long-term exposure to environmental pharmaceuticals that are biologically active, even at low concentrations, can be hazardous to aquatic organisms [3, 5]. For example, the presence of 1 μg/L diclofenac impairs liver and kidney cell function in fish [6]. Mussels are useful bioindicators because they are common in aquatic ecosystems, have a sedentary lifestyle, feed by filtering water, are highly adaptable and tolerate high concentrations of pollutants [7, 8]. In addition, macroalgae can be used as indicator organisms, as they widely occur in all coastal environments and can efficiently accumulate pollutants [9]. Fish are good indicators of aquatic environmental contaminants because of their ability to absorb contaminants found in water through their gills and ingest contaminated organisms [10].

The Golden Horn Estuary is located in the northeastern Marmara Sea. The Galata Bridge is the most important fishing area in Istanbul. Before 1994, the estuary was contaminated with industrial wastewater [11]. Since that year, cleaning activities have been conducted regularly. However, uncontrolled inputs still cannot be averted in this area. The aim of this study was to determine the levels of pharmaceuticals (diclofenac, fenoprofen, ibuprofen, ketoprofen, naproxen, gemfibrozil, clofibric acid, estrone, 17β-estradiol, 17α-ethinylestradiol and carbamazepine) in various organisms (fish muscle tissue, macroalgae and mussels). To the best of our knowledge, this is the first study to document the levels of pharmaceutical compounds in the biota of the Golden Horn Estuary.

MATERIALS AND METHODS

Chemicals and reagents. Target pharmaceutical compounds that were high purity grade (>95% or higher) were purchased from Sigma-Aldrich (Athens, Greece). The main properties of these pharmaceuticals are shown in Table 1. Acetonitrile and methanol were HPLC-gradient grade and purchased from Merck (Darmstadt, Germany). Potassium dihydrogen phosphate was supplied by Fluka. Solid-phase extraction (SPE) cartridges [Cleanert PEP (500 mg/6 mL)] were acquired from Agela Technologies (Torrance, USA).

Study Area. The Golden Horn Estuary is located in the northeastern Marmara Sea. It has a surface area of 2.6 km^2, length of 7.5 km, width of 200–900 m and maximum depth of 36 m [19, 20]. The estuary has a two-layered stratification: the upper layer has less saline Black Sea water (18–20 ppt), and the lower layer has highly saline Mediterranean water (38 ppt) [21]. Mussels were sampled from the Galata Bridge (GB) (41.02° N, 28.97° E), Unkapanı (UNK) (41.02° N, 28.96° E), and Kasımpaşa (KSP) (41.03° N, 28.95° E) stations. Macroalgae were sampled from the Eyüp-Sütlüce (ES) (41.04° N, 28.94° E) station in the estuary. The locations of the four sampling stations are also shown in Figure 1.

TABLE 1
The main properties of the focal pharmaceutical compounds

Compounds	Use	Molecular Formula	Molecular weight (g mol^{-1})	pK$_a$	Log K$_{ow}$
Diclofenac	NSAID	$C_{14}H_{11}Cl_2NO_2$	318.1	4.15[12]	4.51[12]
Ibuprofen	NSAID	$C_{13}H_{18}O_2$	206.3	4.4[13]	4[13]
Ketoprofen	NSAID	$C_{16}H_{14}O_3$	254.3	4.45[12]	3.12[12]
Naproxen	NSAID	$C_{14}H_{14}O_3$	230.3	4.15[12]	3.18[12]
Fenoprofen	NSAID	$C_{15}H_{14}O_3$	522.6	4.5[14]	3.1[14]
Carbamazepine	Antiepileptic	$C_{15}H_{12}N_2O$	236.3	13.90[14]	2.77[14]
Estrone	Hormone	$C_{16}H_{22}O_2$	270.4	10.3[15]	3.13[16]
17β-Estradiol	Hormone	$C_{18}H_{24}O_2$	272.4	10.6[15]	4.01[16]
17α-ethinylestradiol	Hormone	$C_{20}H_{24}O_2$	296.4	10.4[15]	3.67[16]
Gemfibrozil	Lipid regulator	$C_{15}H_{22}O_3$	250.3	4.7[17]	4.77[17]
Clofibric acid	Lipid regulator	$C_{10}H_{11}ClO_3$	214.7	3.18[18]	2.84[18]

NSAID: Nonsteroidal anti-inflammatory drug

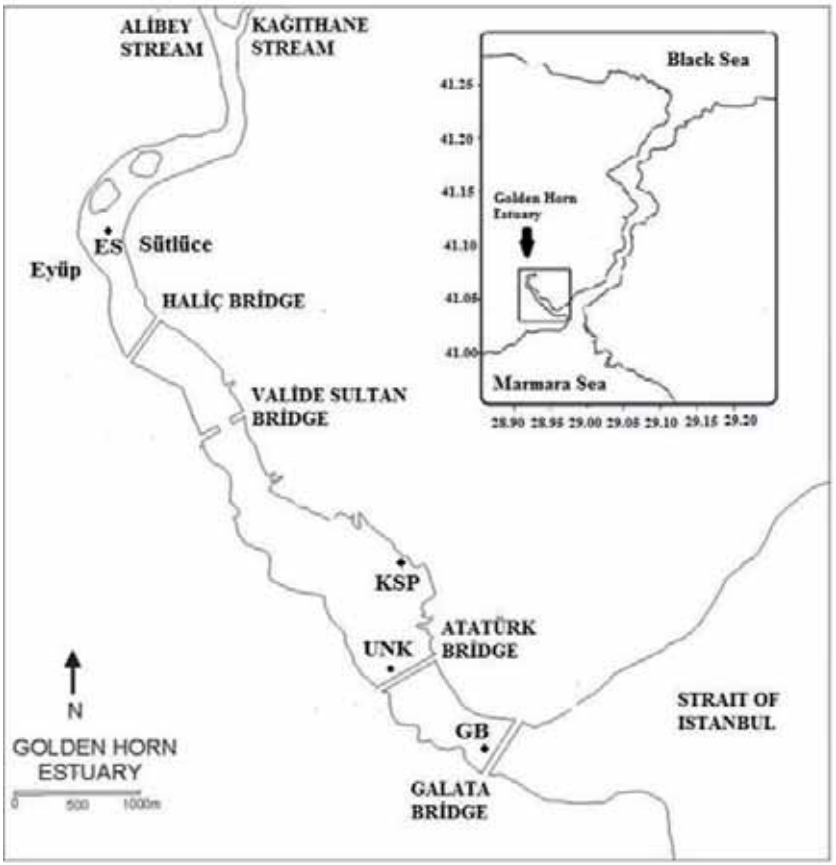


FIGURE 1
Sampling stations along the Golden Horn Estuary.

Sample collection. Mussels (*Mytilus galloprovincialis*) were sampled at the GB, UNK, and KSP stations, and macroalgae (*Ulva laccuta*) were collected from the ES station. Twenty samples of each species were collected in a hand net on the boat. Fifteen samples of each fish species (*Mullus barbatus, Trachurus meditterraneus, Diplodus annularis, Lithognathus mormyrus, Spicara maena, Sardina pilchardus,* and *Mugil cephalus*) were purchased from fishermen who had collected these fish at the Galata Bridge. All samples were collected in April 2019. Basic information on the biota samples is summarized in Table 2. These samples were wrapped in aluminum foil and stored in a deep freezer until they were brought to the laboratory. The contaminants on the outer shells of the mussels brought to the laboratory were cleaned with a clean knife. The shells were then washed with distilled water, and the soft parts of the mussels in their shells were cleaned with pure water. The muscle tissue of fish brought to the laboratory were separated from their internal organs and then divided into groups of five as homogeneous. All samples were stored at –20°C until analysis.

Sample preparation and extraction. Biota samples were lyophilized and homogenized. The extraction method used by Xie et al. was modified and applied [22]. Twenty-five g samples were extracted with 75 mL of acetonitrile, and ultrasonic extraction was performed for 30 min. The samples were then kept in the dark for one night, and the solution was decanted. Next, 50 mL of acetonitrile/water (8/2, v/v) was added to the samples, ultrasonic extraction was performed for 30 min, and the solution was decanted after being kept in the dark overnight and mixed with the first extraction. The supernatant was evaporated in the rotary evaporator. The supernatant volume was 10 mL with acetonitrile/water (8/2, v/v). The SPE method was used for clean-up. Cartridges were conditioned with 10 mL of methanol and 10 mL of ultrapure water. Next, the samples (10 mL) were loaded onto the cartridges, and the cartridges were washed with 10 mL of distilled water. The cartridges were eluted with 10 mL of methanol and 10 mL of acidic methanol. Eluents were evaporated by an evaporator. The eluent volume was finished with 5 mL of acetonitrile/water (1/1, v/v) and then filtered with 0.22-µm syringe filters.

Instrumental analysis. An HPLC 1100 Series device with a DAD detector was used for the chromatographic analysis of pharmaceuticals in biota samples. Pharmaceuticals were analyzed by a C18 (250 × 4.6 mm i.d., 5 µm) column. Acetonitrile and 25 mM potassium dihydrogen phosphate were used as the mobile phases. The flow rate was set at 1.2 mL/min. The gradient elution program followed that of Camacho-Muñoz et al. [23].The detection

TABLE 2
Basic information on biota samples.

Common name	Latin name	Habitat	Feeding habits	Food items
Red mullet	*Mullus barbatus*	Demersal fish, inhabits sandy, muddy, or gravel floors	Carnivorous	Polychaete worms, bivalve mollusks and crustaceans
Horse mackerel	*Trachurus meditterraneus*	Benthopelagic fish, inhabits the benthos, also occurs in surface waters	Carnivorous	Sardines, anchovies, and small crustaceans
Annular seabream	*Diplodus annularis*	Demersal fish, inhabits rocky, sandy bottoms and seagrass beds	Carnivorous	Benthic invertebrates, crustaceans, worms and mollusks
Striped seabream	*Lithognathus mormyrus*	Benthopelagic fish, inhabits sea grass meadows and sandy muddy seabeds	Carnivorous	Worms, mollusks and small crustaceans
Blotched picarel	*Spicara maena*	Inhabits seabed over sandy and muddy bottoms	Omnivorous	Crustacean, mollusks and zooplankton
European pilchard	*Sardina pilchardus*	Coastal pelagic fish, a migratory, largely coastal species	Filter feeding	Planktonic crustaceans, larger planktonic animals
Black mullet	*Mugil cephalus*	Euryhaline fish, found in salty or freshwater	Omnivorous	Zooplankton, algae
Mussel	*Mytilus galloprovincialis*	Fixed on hard substrates in nearshore habitats	Filter feeding	Algae, detritus and organic material
Macroalgae	*Ulva lactuca*	Attached to boulders and bedrock		

TABLE 3
Method detection limits (MDL), method quantification limits (MQL) and average recoveries (R, n=3) of biota samples.

Compounds	MDL (ng/g)	MQL (ng/g)	R (%)
Carbamazepine	8.79	29.3	85
Clofibric acid	12.2	40.6	70
Gemfibrozil	9.03	30.1	82
Estrone	15.2	50.8	96
17β-estradiol	26.6	88.7	82
17α-ethinylestradiol	16.3	54.5	88
Fenoprofen	9.21	30.7	90
Ketoprofen	18.9	63	65
Ibuprofen	4.57	15.2	75
Diclofenac	10.5	35	91
Naproxen	4.96	16.5	61

wavelengths of the studied compounds ranged from 220–300 nm [24]. For quality control, ten procedural blanks were prepared and analyzed. The linear response range of the detector was determined using an external standard multipoint calibration technique. Regression coefficients for all compounds were >0.99. Individual recovery rates of the compounds were calculated to determine the accuracy. For the biota samples, MDL (method detection limit) and MQL (method quantification limit) were calculated using the ratio of LOD (limit of detection) and LOQ (limit of quantification) values of the instrument multiplied by the final volume of the extract injected into the HPLC device to the average dry weight of the biota (25 g). Values of MDL, MQL and recovery (R) are shown in Table 3

RESULTS AND DISCUSSION

The occurrence of pharmaceutical compounds was detected in biota samples collected from the Golden Horn Estuary in April 2019. The concentrations of the focal pharmaceuticals in biota samples ranged from <4.57 to 9135 ng/g dw (Table 4). Gemfibrozil, which had average concentrations of 56 and 9135 ng/g, was the major pollutant in the biota samples. This indicates that gemfibrozil was the most widespread pharmaceutical in the collected samples.

The pharmaceutical compound with the highest concentration in fish muscle tissue was 17α-ethinylestradiol (1258 ng/g in *Mullus barbatus*). In addition, *M. barbatus* had the most pharmaceutical compounds. Diclofenac (864 ng/g), ibuprofen (206 ng/g), estrone (206 ng/g), 17β-estradiol (1247 ng/g), 17α-ethinylestradiol (1258 ng/g), clofibric acid (87 ng/g), gemfibrozil (624 ng/g) and carbamazepine (836 ng/g) were detected in *M. barbatus* muscle tissue (Table 4 and Figure 2). *M. barbatus* has a high lipid content (8.12 ± 0.27/100 g) and is thus considered a high-fat fish [25]. High lipid content results in a higher capacity to accumulate hydrophobic compounds [7, 26]. Therefore, the fact that large amounts of pharmaceutical compounds were observed in *M. barbatus* is to be expected. Diclofenac was detected in the muscle tissue of all fish species except for *D. annularis*, and the highest values were observed in *S. maena* (935 ng/g) and *M. barbatus* (864 ng/g) (Table 4, Figure 2). Many studies have documented physiological and behavioral effects in fish exposed to diclofenac. Diclofenac exposure has been shown to induce cytological changes in rainbow and brown trout tissues (kidney and gills) in aquatic environments [27, 28]. Mehinto et al. reported that diclofenac caused tissue damage in rainbow trout [29]. Fenoprofen was detected in three fish species: *M. cephalus* (37.41 ng/g), *T. meditterraneus* (33.31 ng/g), and *S. pilchardus (*62.3 ng/g). Although polar compounds do not have a high potential for bioaccumulation, they can pose a risk to aquatic organisms because they are constantly released and persist in the environment [30]. The detection of fenoprofen in biota in this study stemmed from its continuous entry into the receiving environment. Ketoprofen and naproxen were below the MDL or MQL in fish muscle tissue. Generally, pharmaceutical residues are discharged from organisms exposed to pharmaceutical pollution because of their rapid elimination [31]. These compounds might not accumulate in fish because of their rapid elimination in aquatic environments. Ibuprofen was detected in the muscle tissue of all fish species, and the highest value was observed in *T. meditterraneus* (821 ng/g). Estrone and 17β-estradiol were only detected in *M. barbatus* muscle tissue (206 ng/g and 1247 ng/g, respectively). 17α-ethinylestradiol was detected in the muscle tissue of *M. cephalus* (74 ng/g), *S. pilchardus* (119 ng/g), and *M. barbatus* (1258 ng/g) (Table 4, Figure 2). Because of their relatively high lipophilicity and persistence, most estrogen compounds can

bioaccumulate in aquatic organisms [32]. This is consistent with the high values of 17α-ethinylestradiol detected in fish. The detection of estrone and 17β-estradiol in only a few species can be explained by the fact that they decomposed more rapidly in the aquatic environment compared with synthetic hormone. Clofibric acid was only observed in the muscle tissue of *M. barbatus* (87 ng/g). Gemfibrozil was detected in the muscle tissue of all fish species; the highest concentration was observed in *M. cephalus* (1059 ng/g). The concentration of carbamazepine was 53.5 ng/g and 836 ng/g in *S. pilchardus and M. barbatus* muscle, respectively (Table 4, Figure 2). Clofibric acid (log K_{ow} 2.84) and carbamazepine (log K_{ow} 2.77) are moderately hydrophobic; thus, they were detected in fewer fish species and in lower amounts compared with gemfibrozil (log Kow 4.77).

The most abundant pharmaceutical compound in *Ulva laccuta* was gemfibrozil (7221 ng/g). Other detected pharmaceuticals in macroalgae were diclofenac (1167 ng/g), ibuprofen (946 ng/g), clofibric acid (40.7 ng/g), and carbamazepine (98.5 ng/g) (Figure 3). Macroalgae occur in all coastal environments and efficiently accumulate pollutants [9]. This property makes them suitable indicator organisms for monitoring coastal pollution (e.g., pharmaceutical pollution).

TABLE 4
Concentration of pharmaceutical compounds (ng/g, dw) in fish muscle tissue, mussels and macroalgae.

Species	Diclofenac	Fenoprofen	Ketoprofen	Naproxen	Ibuprofen	Estrone	17β-estradiol	17α-ethinylestradiol	Clofibric acid	Gemfibrozil	Carbamazepine
Mugil cephalus (n=5)	102±1.41	37.4±4.60	<MDL	<MDL	76±0.067	<MDL	<MDL	74.0±2.10	<MQL	1059±5.45	<MDL
Lithognathus mormyrus (n=5)	142±2.53	<MDL	<MDL	<MQL	138±3.48	<MDL	<MDL	<MQL	<MDL	430±6.40	<MDL
Trachurus meditterraneus (n=5)	75±2.96	33.3±3.75	<MDL	<MQL	821±5.20	<MDL	<MQL	<MQL	<MDL	154±5.80	<MDL
Sardina pilchardus (n=5)	378±5.1	62.3±1.83	<MDL	<MDL	99.9±1.89	<MDL	<MQL	119±4.10	<MQL	543±1.10	53.5±0.33
Mullus barbatus (n=5)	864±6.3	<MDL	<MQL	<MQL	206±4.50	206±6.3	1247±5.5	1258±4.30	87±6.10	624±5.30	836±5.40
Spicara maena (n=5)	935±5.7	<MDL	<MQL	<MDL	208±4.60	<MDL	<MDL	<MQL	<MDL	416±2.96	<MQL
Diplodus annularis (n=5)	<MQL	<MDL	<MDL	<MDL	104±3.8	<MDL	<MDL	<MDL	107.9±5	56±4.8	<MDL
Ulva lactuca	1167	<MDL	<MDL	<MDL	946	<MDL	<MDL	<MDL	40,7	7221	98.5
Mytilus galloprovincialis (collected from GB)	3434	<MDL	344	633	4440	1913	2364	612	128	1612	<MDL
Mytilus galloprovincialis (collected from UNK)	281	403	64	<MQL	836	318	1030	1102	1296	4513	806
Mytilus galloprovincialis (collected from KSP)	4694	502	<MDL	1570	5098	<MDL	1883	738	922	9135	233

MDL: Method Detection Limit; MQL: Method Quantification Limit.

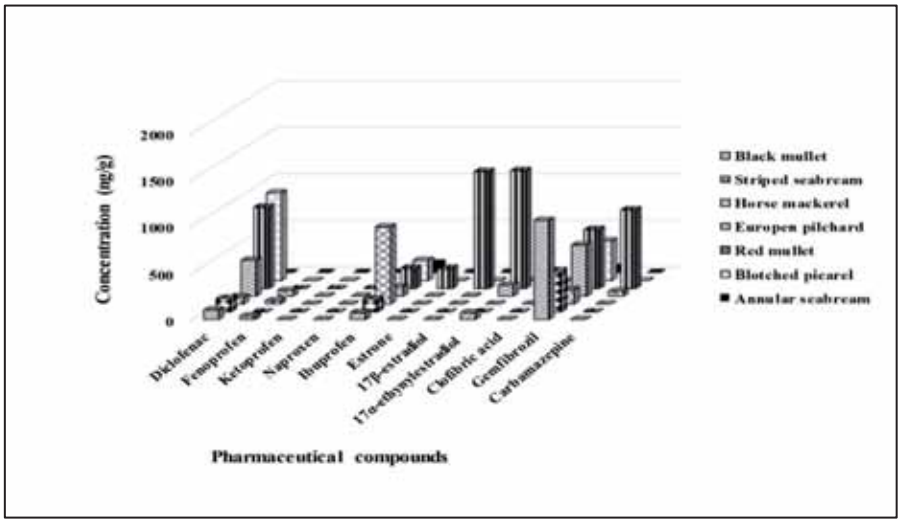


FIGURE 2
Concentrations of pharmaceutical compounds in the muscle tissue of seven different fish species.

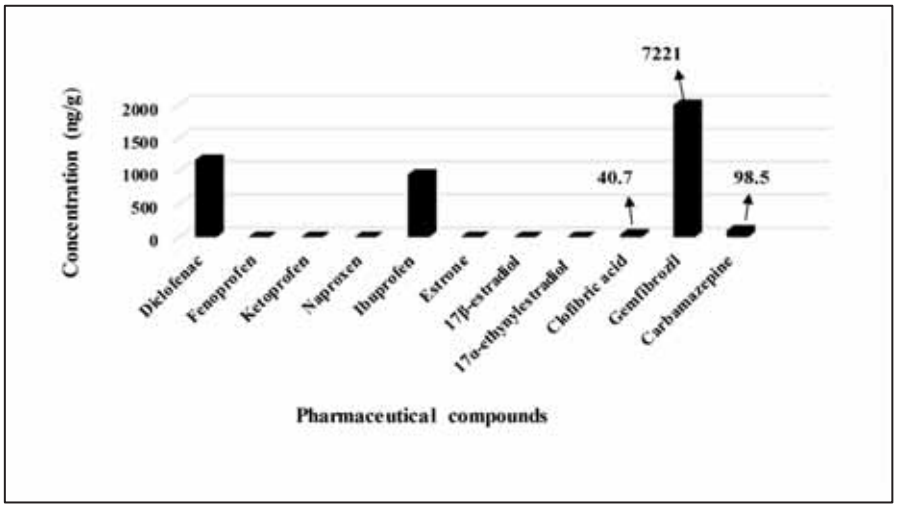


FIGURE 3
Total pharmaceutical compound concentrations in macroalgae (*Ulva laccuta*) collected from the ES station in the Golden Horn Estuary.

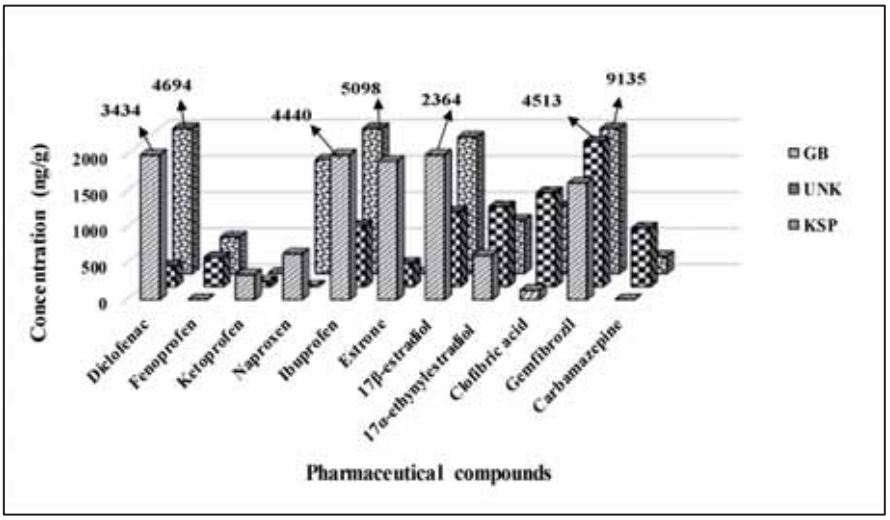


FIGURE 4
Concentrations of pharmaceutical compounds in mussels *(Mytilus galloprovincialis)* collected from the GB, UNK and KSP stations in the Golden Horn Estuary.

TABLE 5
Summary of pharmaceutical compound concentrations in biota (fish muscle tissue, mussels, macroalgae) in other studies.

Location	Pharmaceutical compound levels									References
	DCF	KTP	NPX	IBF	CBZ	GFZ	E1	E2	EE2	
Mussel (ng/g)										
Taihu Lake, China	<LOD–4.12			<LOD				<LOD–12.1		[36]
Adriatic Sea	<LOD–16.1	<LOD		<LOD–9.39						[7]
Latvia		<LOD		<LOD–1363						[37]
San Francisco Bay			<LOQ	<LOQ	1.3–5.30					[38]
Hong Kong							<LOD–10.7	<LOD–18.5	<LOD–9.7	[39]
China								21.6–235	49.7–138	[40]
Adriatic and Tyrrhenian Sea	<1.4–170			<8–143.7	35–280					[41]
Pearl River, China						<LOD				[22]
This study	281–4694	<MDL–344	<MQL–1570	836–5098	<MDL–806		<MDL–1913	1030–2364	612–1102	
Fish muscle tissues (ng/g)										
Mar Menor Lagoon, Mediterranean	1.30				6.3					[42]
Taihu Lake, China	<LOD–13			<LOD–40	<LOD–4.1					[43]
Xiangjiang River, China							<LOD–6.98		<LOD	[44]
Basque Estuaries, Bay of Biscay								15.2	26.9	[45]
This study	<MQL–935	<MDL	<MDL	76–821	<MDL–836		<MDL–206	<MDL–1247	<MDL–1258	
Macroalgae (ng/g)										
Norway, Italy, Portugal, Spain					<MDL					[46]
Pearl River, China							<LOD–30			[35]
Saudi Red Sea					<LOD–1.70					[31]
This study	1167	<MDL	<MDL	946	98.5		<MDL	<MDL	<MDL	

LOD: Limit of Detection; LOQ: Limit of Quantification; MDL: Method Detection Limit; MQL: Method Quantification Limit; DCF: Diclofenac; KTP: Ketoprofen; NPX: Naproxen; IBF: Ibuprofen; CBZ: Carbamazepine; GFZ: Gemfibrozil; E1: Estrone; E2: 17β- estradiol; EE2: 17α-ethinylestradiol.

Mussels (*M. galloprovincialis)* had the highest concentrations of pharmaceutical compounds among all organisms. The highest value was observed for gemfibrozil (9135 ng/g), which was collected from the KSP station. Additionally, the concentrations of ibuprofen (4440 ng/g, 5098 ng/g) and diclofenac (3434 ng/g, 4694 ng/g) in mussel samples at some stations were higher than those of other pharmaceutical groups (Figure 4). These filter-feeding organisms filter large amounts of seawater. Consequently, they can accumulate dissolved chemical compounds in water at concentrations two to five times greater than concentrations in seawater [33, 34]. Mussels accumulated most of the selected pharmaceutical pollutants at higher amounts compared with other biota samples.

A comparison of our results with the concentrations of pharmaceuticals detected in biota (fish muscle tissue, mussels and macroalgae) in other studies is shown in Table 5. The values of diclofenac, gemfibrozil, 17β-estradiol and 17α-ethinylestradiol in biota in our study were well above those reported in other studies. To the best of our knowledge, there has been no study to date that has examined the worldwide distribution of fenoprofen and clofibric acid in fish muscle tissue, mussels and macroalgae. The data provided in our study represent a valuable contribution to the international literature. Gemfibrozil was

the most abundant pharmaceutical compound in fish muscle tissue, followed by ibuprofen, diclofenac, 17α-ethinylestradiol, and 17β-estradiol (Figure 2). In macroalgae, gemfibrozil was also the most abundant pharmaceutical compound, followed by diclofenac, ibuprofen, carbamazepine, and clofibric acid (Figure 3). In mussels, gemfibrozil was the most common, followed by diclofenac, ibuprofen, carbamazepine, and clofibric acid (Figure. 4). The concentrations of ketoprofen detected in mussel and fish species in our study are considerably lower than those reported (40–2208 ng/g) by Xie et al. [22]. The concentrations of naproxen in mussels are higher than those reported by other studies and similar to those in other fish species. Comparison of the concentrations of ibuprofen in the biota samples of our study and samples from other studies revealed that our concentrations were either similar or higher to those reported by Xie et al. [22]. The concentrations of estrone determined in biota are far above those reported in other studies. In macroalgae, the value of 30 ng/g reported in the study of J. Yang et al. [35] is quite high compared with the value (<LOD) obtained in our study (Table 5).

CONCLUSION

The presence and abundance of commonly used pharmaceuticals in biota collected from the Golden Horn Estuary in 2019 were studied. Gemfibrozil, which is a lipid regulator, was detected in all biota samples, and its concentration was often high. This indicates that gemfibrozil is more commonly consumed by people living around the Golden Horn Estuary. Ibuprofen and diclofenac were also detected in the muscle tissue of most fish species. *M. barbatus* was the fish species that harbored the most pharmaceutical compounds. The concentrations of pharmaceutical compounds were higher in *M. galloprovincialis* samples than in other biota samples. When endocrine-disrupting compounds are taken into the body, they can disrupt the reproductive systems of living things by imitating natural hormones. These compounds have been found to increase the frequency of genderless births and sex disorders, decrease sperm count, lead to femininity in male organisms and the development of male characteristics in female organisms in many animal species [47-53]. Thus, characterizing the concentrations of pharmaceuticals in biota is important for evaluating risks to the environment and human health.

ACKNOWLEDGEMENT

We thank the Scientific Research Projects Coordination Unit of Istanbul University (Project No: 31466) for supporting this study. We also thank the Istanbul Metropolitan Municipality, Environmental Protection and Control Department for allowing us to use their ships to collect samples.

REFERENCES

[1] Bu, Q., Wang, B., Huang, J., Deng, S., Yu, G. (2013) Pharmaceuticals and personal care products in the aquatic environment in China: A review. Journal of Hazardous Materials. 262, 189-211.

[2] Daughton, C.G., Ternes, T.A. (1999) Pharmaceuticals and personal care products in the environment: agents of subtle change? Environmental Health Perspectives. 107(6), 907-938.

[3] Boxall, A.B., Rudd, M. A., Brooks, B. W., Caldwell, D. J., Choi, K., Hickmann, S., Innes, E., Ostapyk, K., Staveley, J. P., Verslycke, T., Ankley, G. T., Beazley, K. F., Belanger, S. E., Berninger, J. P., Carriquiriborde, P., Coors, A., Deleo, P. C., Dyer, S. D., Ericson, J. F., Gagné, F., Giesy, J. P., Gouin, T., Hallstrom, L., Karlsson, M. V., Larsson, D. G., Lazorchak, J. M., Mastrocco, F., McLaughlin, A., McMaster, M. E., Meyerhoff, R. D., Moore, R., Parrott, J. L., Snape, J. R., Murray-Smith, R., Servos, M. R., Sibley, P. K., Straub, J. O., Szabo, N. D., Topp, E., Tetreault, G. R., Trudeau, V. L., Van Der Kraak, G. (2012) Pharmaceuticals and personal care products in the environment: what are the big questions? Environmental Health Perspectives. 120(9), 1221-1229.

[4] Santos, L.H.M.L.M., Araújo, A. N., Fachini, A., Pena, A., Delerue-Matos, C., Montenegro, M.C.B.S.M. (2010) Ecotoxicological aspects related to the presence of pharmaceuticals in the aquatic environment. Journal of Hazardous Materials. 175(1), 45-95.

[5] Fent, K., Weston, A.A., Caminada, D. (2006) Ecotoxicology of human pharmaceuticals. Aquatic Toxicology. 76(2),122-159.

[6] Triebskorn, R., Casper, H., Heyd, A., Eikemper, R., Köhler, H. R., Schwaiger, J. (2004) Toxic effects of the non-steroidal anti-inflammatory drug diclofenac. Part II: cytological effects in liver, kidney, gills and intestine of rainbow trout *(Oncorhynchus mykiss).* Aquatic Toxicology. 68(2), 151-166.

[7] Mezzelani, M., Gorbi, S., Da Ros, Z., Fattorini, D., d'Errico, G., Milan, M., Bargelloni, L., Regoli, F. (2016) Ecotoxicological potential of non-steroidal anti-inflammatory drugs (NSA IDs) in marine organisms: Bioavailability, biomarkers and natural occurrence in *Mytilus galloprovincialis.* Marine Environmental Research. 121, 31-39.

[8] Regoli, F., Pellegrini, D., Cicero, A. M., Nigro, M., Benedetti, M., Gorbi, S., Fattorini, D., D'Errico, G., Di Carlo, M., Nardi, A., Gaion, A., Scuderi, A., Giuliani, S., Romanelli, G., Berto, D., Trabucco, B., Guidi, P., Bernardeschi, M., Scarcelli, V., Frenzilli, G. (2014) A multi-disciplinary weight of evidence approach for environmental risk assessment at the Costa Concordia wreck: Integrative indices from Mussel Watch. Marine Environmental Research. 96, 92-104.

[9] Torres, M.A., Barros, M.P., Campos, S.C.G., Pinto, E., Rajamani, S., Sayre, R.T., Colepicolo, P. (2008) Biochemical biomarkers in algae and marine pollution: A review. Ecotoxicology and Environmental Safety. 71(1), 1-15.

[10] Huerta, B., Rodriguez-Mozaz, S., Lazorchak, J., Barcelo, D., Batt, A., Wathen, J., Stahl, L. (2018) Presence of pharmaceuticals in fish collected from urban rivers in the U.S. EPA 2008–2009 National Rivers and Streams Assessment. Science of The Total Environment. 634, 542-549.

[11] Kinaci, C., Inanc, B., Aydin, A. F., Yuksel, E., Sevimli, M. F., Arikan, O., Topacik, D. (2004) Quality of the bottom sediment prior to dredging in the Golden Horn of Istanbul. Journal of Environmental Science and Health, Part A Toxic/Hazardous Substances and Environmental Engineering. 39(2), 365-374.

[12] Kim, I., Tanaka, H. (2009) Photodegradation characteristics of PPCPs in water with UV treatment. Environment International. 35(5), 793-802.

[13] Patel, A., Bell, M., O'Connor, C., Inchley, A., Wibawa, J., Lane, M.E. (2013) Delivery of ibuprofen to the skin. International Journal of Pharmaceutics. 457(1), 9-13.

[14] National Center for Biotechnology Information (NCBI) (2021) https://pubchem.ncbi.nlm.nih.gov. (Accessed March 20, 2021).

[15] Adeel, M., Song, X., Wang, Y., Francis, D., Yang, Y. (2017) Environmental impact of estrogens on human, animal and plant life: A critical review. Environment International. 99, 107-119.

[16] Aydin, E., Talinli, I. (2013) Analysis, occurrence and fate of commonly used pharmaceuticals and hormones in the Buyukcekmece Watershed, Turkey. Chemosphere. 90(6), 2004-2012.

[17] Westerhoff, P., Yoon, Y., Snyder, S., Wert, E. (2005) Fate of Endocrine-Disruptor, Pharmaceutical, and Personal Care Product Chemicals during Simulated Drinking Water Treatment Processes. Environmental Science & Technology. 39(17), 6649-6663.

[18] Salgado, R., Oehmen, A., Carvalho, G., Noronha, J.P., Reis, M.A. M. (2012) Biodegradation of clofibric acid and identification of its metabolites. Journal of Hazardous Materials. 241-242, 182-189.

[19] Alpar, B., Burak, S., Doğan, E. (2005) Environmental and Hydrological Management of the Golden Horn Estuary, Istanbul. Journal of Coastal Research. 21(4), 646-749.

[20] Ozturk, M., Basturk, A., Ozturk, I., Kinaci, C., Topacik, D., Sevimli, M.F. (1998) Application studies of Golden Horn's Rehabilitation Project. In: Symposium of Sewerage and Sea Pollution Management in Metropolises. Ozturk, I., Sarikaya, H.Z., Okus, E. (Eds.), Istanbul, Turkey. 30-34. (in Turkish).

[21] Müftüoglu, A.E. (2008) Hydrodynamic structure of the bays and the estuary of the Sea of Marmara. Ph. D. thesis, Istanbul University Institute of Marine Sciences and Management, Istanbul, Turkey. (in Turkish).

[22] Xie, H., Hao, H., Xu, N., Liang, X., Gao, D., Xu, Y., Gao, Y., Tao, H., Wong, M. (2019) Pharmaceuticals and personal care products in water, sediments, aquatic organisms, and fish feeds in the Pearl River Delta: Occurrence, distribution, potential sources, and health risk assessment. Science of The Total Environment. 659, 230-239.

[23] Camacho-Muñoz, D., Martín, J., Santos, J. L., Aparicio, I., Alonso, E. (2009) An affordable method for the simultaneous determination of the most studied pharmaceutical compounds as wastewater and surface water pollutants. Journal of Separation Science. 32(18), 3064-3073.

[24] Debska, J., Kot-Wasik, A., Namiesnik, J. (2005) Determination of nonsteroidal antiinflammatory drugs in water samples using liquid chromatography coupled with diode-array detector and mass spectrometry. Journal of Separation Science. 28(17), 2419-2426.

[25] Prato, E., Biandolino, F. (2012) Total lipid content and fatty acid composition of commercially important fish species from the Mediterranean, Mar Grande Sea. Food Chemistry. 131(4), 1233-1239.

[26] Ruhí, A., Acuña, V., Barceló, D., Huerta, B., Mor, J.R., Rodríguez-Mozaz, S., Sabater, S. (2016) Bioaccumulation and trophic magnification of pharmaceuticals and endocrine disruptors in a Mediterranean river food web. Science of The Total Environment. 540, 250-259.

[27] Hoeger, B., Köllner, B., Dietrich, D.R., Hitzfeld, B. (2005) Water-borne diclofenac affects kidney and gill integrity and selected immune parameters in brown trout *(Salmo trutta f. fario).* Aquatic Toxicology. 75(1), 53-64.

[28] Schwaiger, J., Ferling, H., Mallow, U., Wintermayr, H., Negele, R.D. (2004) Toxic effects of the non-steroidal anti-inflammatory drug diclofenac. Part I: histopathological alterations and bioaccumulation in rainbow trout. Aquatic Toxicology. 68(2), 141-150.

[29] Mehinto, A.C., Hill, E.M., Tyler, C.R. (2010) Uptake and biological effects of environmentally relevant concentrations of the nonsteroidal anti-inflammatory pharmaceutical diclofenac in rainbow trout *(Oncorhynchus mykiss)*. Environmental Science & Technology. 44(6), 2176-2182.

[30] Daughton, C.G. (2002) Environmental stewardship and drugs as pollutants. Lancet. 360(9339), 1035-1036.

[31] Ali, A.M., Rønning, H.T., Sydnes, L.K., Alarif, W.M., Kallenborn, R., Al-Lihaibi, S.S. (2018) Detection of PPCPs in marine organisms from contaminated coastal waters of the Saudi Red Sea. Science of The Total Environment. 621, 654-662.

[32] Matozzo, V., Gagné, F., Marin, M.G., Ricciardi, F., Blaise, C. (2008) Vitellogenin as a biomarker of exposure to estrogenic compounds in aquatic invertebrates: a review. Environment International. 34(4), 531-545.

[33] Baršienė, J., Lehtonen, K.K., Koehler, A., Broeg, K., Vuorinen, P.J., Lang, T., Pempkowiak, J., Šyvokienė, J., Dedonyte, V., Rybakovas, A., Repečka, R., Vuontisjärvi, H., Kopecka, J. (2006) Biomarker responses in flounder *(Platichthys flesus)* and mussel *(Mytilus edulis)* in the Klaipėda-Būtingė area (Baltic Sea). Marine Pollution Bulletin. 53(8), 422-436.

[34] Norling, P., Kautsky, N. (2008) Patches of the mussel *Mytilus sp.* Are islands of high biodiversity in subtidal sediment habitats in the Baltic Sea. Aquatic Biology. 4, 75-87.

[35] Yang, J., Li, H., Ran, Y., Chan, K. (2014) Distribution and bioconcentration of endocrine disrupting chemicals in surface water and fish bile of the Pearl River Delta, South China. Chemosphere. 107, 439-446.

[36] Xie, Z., Lu, G., Liu, J., Yan, Z., Ma, B., Zhang, Z., Chen, W. (2015) Occurrence, bioaccumulation, and trophic magnification of pharmaceutically active compounds in Taihu Lake, China. Chemosphere. 138, 140-147.

[37] Ikkere, L.E., Perkons, I., Sire, J., Pugajeva, I., Bartkevics, V. (2018) Occurrence of polybrominated diphenyl ethers, perfluorinated compounds, and nonsteroidal anti-inflammatory drugs in freshwater mussels from Latvia. Chemosphere. 213, 507-516.

[38] Klosterhaus, S.L., Grace, R., Hamilton, M.C., Yee, D. (2013) Method validation and reconnaissance of pharmaceuticals, personal care products, and alkylphenols in surface waters, sediments, and mussels in an urban estuary. Environment International. 54, 92-99.

[39] Xu, E.G., Ho, P.W.L., Tse, Z., Ho, S.L., Leung, K.M.Y. (2016) Revealing ecological risks of priority endocrine disrupting chemicals in four marine protected areas in Hong Kong through an integrative approach. Environmental Pollution. 215, 103-112.

[40] Chiu, J.M.Y., Po, B.H.K., Degger, N., Tse, A., Liu, W., Zheng, G., Zhao,D.M., Xu, D., Richardson, B., Wu, R.S.S. (2018) Contamination and risk implications of endocrine disrupting chemicals along the coastline of China: A systematic study using mussels and semipermeable membrane devices. Science of The Total Environment. 624, 1298-1307.

[41] Mezzelani, M., Fattorini, D., Gorbi, S., Nigro, M., Regoli, F. (2020) Human pharmaceuticals in marine mussels: Evidence of sneaky environmental hazard along Italian coasts. Marine Environmental Research. 162,105137.

[42] Moreno-González, R., Rodríguez-Mozaz, S., Gros, M., Pérez-Cánovas, E., Barceló, D., León, V. M. (2014) Input of pharmaceuticals through coastal surface watercourses into a Mediterranean lagoon (Mar Menor, SE Spain): sources and seasonal variations. Science of the Total Environment. 490, 59-72.

[43] Xie, Z., Lu, G., Yan, Z., Liu, J., Wang, P., Wang, Y. (2017) Bioaccumulation and trophic transfer of pharmaceuticals in food webs from a large freshwater lake. Environmental Pollution. 222, 356-366.

[44] Zhou, X., Yang, Z., Luo, Z., Li, H., Chen, G. (2019) Endocrine disrupting chemicals in wild freshwater fishes: Species, tissues, sizes and human health risks. Environmental Pollution. 244, 462-468.

[45] Bizarro, C., Ros, O., Vallejo, A., Prieto, A., Etxebarria, N., Cajaraville, M.P., Ortiz-Zarragoitia, M. (2014) Intersex condition and molecular markers of endocrine disruption in relation with burdens of emerging pollutants in thicklip grey mullets *(Chelon labrosus)* from Basque estuaries (South-East Bay of Biscay). Marine Environmental Research. 96, 19-28.

[46] Álvarez-Muñoz, D., Rodríguez-Mozaz, S., Maulvault, A.L., Tediosi, A., Fernández-Tejedor, M., Van den Heuvel, F., Kotterman, M., Marques, A., Barceló, D. (2015) Occurrence of pharmaceuticals and endocrine disrupting compounds in macroalgaes, bivalves, and fish from coastal areas in Europe. Environmental Research. 143(Pt B), 56-64.

[47] Andersson, C., Katsiadaki, I., Lundstedt-Enkel, K., Orberg, J. (2007) Effects of 17alpha-ethynylestradiol on EROD activity, spiggin and vitellogenin in three-spined stickleback *(Gasterosteus aculeatus).* Aquatic Toxicology. 83(1), 33-42.
[48] Berg, C., Halldin, K., Fridolfsson, A.K., Brandt, I., Brunström, B. (1999) The avian egg as a test system for endocrine disrupters: effects of diethylstilbestrol and ethynylestradiol on sex organ development. Science of The Total Environment. 233(1-3), 57-66.
[49] Hallgren, P., Sorita, Z., Berglund, O., Persson, A. (2012) Effects of 17α-ethinylestradiol on individual life-history parameters and estimated population growth rates of the freshwater gastropods *Radix balthica* and *Bithynia tentaculata.* Ecotoxicology. 21(3), 803-810.
[50] Larcher, S., Yargeau, V. (2013) Biodegradation of 17α-ethinylestradiol by heterotrophic bacteria. Environmental Pollution. 173, 17-22.
[51] Martyniuk, C.J., Gerrie, E.R., Popesku, J.T., Ekker, M., Trudeau, V.L. (2007) Microarray analysis in the zebrafish *(Danio rerio)* liver and telencephalon after exposure to low concentration of 17alpha-ethinylestradiol. Aquatic Toxicology. 84(1), 38-49.
[52] Notch, E.G., Miniutti, D.M., Mayer, G.D. (2007) 17α-Ethinylestradiol decreases expression of multiple hepatic nucleotide excision repair genes in zebrafish *(Danio rerio).* Aquatic Toxicology. 84(3), 301-309.
[53] Pojana, G., Gomiero, A., Jonkers, N., Marcomini, A. (2007) Natural and synthetic endocrine disrupting compounds (EDCs) in water, sediment and biota of a coastal lagoon. Environment International. 33(7), 929-36.

Received: **06.04.2021**
Accepted: **05.05.2021**

CORRESPONDING AUTHOR

Nagihan E Korkmaz
Department of Chemical Oceanography
Institute of Marine Science and Management
Istanbul University
Vefa 34134 Istanbul – Turkey

e-mail: nagihan.ersoy@istanbul.edu.tr

© by PSP Volume 30– No. 09/2021 pages 10836-10840 Fresenius Environmental Bulletin

DETERMINATION OF ANTIOXIDANT CAPACITY AND CHANGES OF BIOCHEMICAL PARAMETERS ON CALVES PERSISTENTLY INFECTED WITH BOVINE VIRAL DIARRHEA VIRUS

Oguzhan Avci, Sibel Yavru, Atilla Simsek, Orhan Yapici, Oya Bulut, Irmak Dik*

Department of Virology, Faculty of Veterinary Medicine, University of Selcuk, Konya, Turkey

ABSTRACT

The aim of this study was to investigate determination of antioxidant capacity and changes of biochemical parameters [Albumin, ALP (Alkaline phosphatase), ALT (Alanin transaminase), AST (Aspartate aminotransferase), cholesterol, CK-MB (Creatine kinase), GGT (Gama-glutamil transferase), T-Protein, Triglycerine, BUN (Blood Urea Nitrogen)] on calves persistently infected (PI) with Bovine viral diarrhea virus (BVDV) in Konya. Blood samples (both sera and leukocyte) will be taken from the PI calves. Obtained samples will be screened for BVDV antigen and antibodies, antioxidant capacity and changes of biochemical parameters with the use of a commercially available Enzyme Linked Immunosorbent Assay (ELISA) kits. Independent T test will be performed for comparing results between PI calves and a control group. $P<0.05$ value will be considered significance level. A statistically significant difference was found between ALB, ALP, Cholesterol, CK-MB, TP values ($P<0.05$) while there was no statistically significant difference MDA and TAC values between control and study group ($p>0.05$). It can be communicable that persistently BVDV infection has been damage the heart, duodenum and liver, although affecting lipid metabolism and lipid peroxidation. In conclusion the fact that the PI animals to be detected are to be removed from farms is of economic importance both our province and others. In addition, changes in biochemical parameters and antioxidant capacities in persistent infected animals will give some information about the pathogenesis of the infection.

KEYWORDS:
Biochemical parameters, persistently infected, BVDV, MDA, TAC

INTRODUCTION

The agent in the *Pestivirus* genus of the F*laviviridae* family [1] contains single-stranded RNA with positive polarity. Bovine Viral Diarrhea-Mucosal Disease (BVD-MD) is a multisystematic viral infection with variations such as clinical and pathological reproductive disorders, congenital anomalies, abortion, immune tolerance, persistent-infected calf births, premature embryo deaths, and mummification with huge losses in the bovine industry around the world [2, 3]. Virions have four structural proteins, three of which are membrane glycoproteins with a diameter of 40-60 nm and one is a capsid protein. The reference strain of BVDV is the National Animal Disease Laboratory (NADL, 4).Different strains of BVDV may show similarity antigenically, whereas immunological differences may be seen. BVDV has two biotypes as cytopathic (CPE) and non-cytopathic (NCP) [5]. Cytopathogenic BVDV is characterized by rounding of cells, vacuolization, shedding of cells, and cell death in cell cultures. BVDV creates a cytopathological effect (CPE) in cell cultures within 2-3 days. NCP biotype of BVD, on the other hand, shows no effect on cell cultures. Calves that have a very healthy appearance but are born as PI are responsible for the continuous spread of the infection to other animals in the herd and the continuity of the infection within the organization. Also, if they are exposed to re-infection with a cp BVDV biotype while continuing their lives, the Mucosal Disease (MD) form of infection will occur and these animals will be observed to die suddenly in a short time [2].

This study was carried out to determine the biochemical parameters, oxidative stress, and total antioxidant capacity of calves breeding in the Konya region and determined to be persistent-infected with BVDV.

MATERIALS AND METHODS

Animals. Preparation of blood serum samples. Blood samples taken into sterile kaolin tubes with the help of a holder (blood samples were collected from 600 calves from 25 different organizations) were taken under the cold chain and brought to the laboratories of Selcuk University Veterinary Faculty Veterinary Virology Department. Blood

samples were centrifuged (Hettich, Germany) at 2500 rpm for 15 minutes to obtain serum. The serum obtained as a result of the centrifugation procedure was transferred to 1.5 ml sterile eppendorf tubes with the help of a sterile pipette and inactivation was carried out by keeping it in a water bath at 56 °C for 30 minutes. The other part of the blood remaining in the tube was removed through medical waste bags without causing any harm to the environment. Serum samples prepared were frozen at -20°C until the time to be tested. The samples were thawed at the time of examination and tested by ELISA for the presence of BVDV antibodies as well as MDA and TAC.

Preparation of leukocyte samples. The blood samples taken into sterile tubes with anticoagulants were brought to Selcuk University Veterinary Faculty Veterinary Virology Department laboratories under the cold chain and then subjected to centrifugation procedure at 2500 rpm for 15 minutes. While the plasma was removed with the help of a sterile pipette, the leukocyte layer was transferred to 10 ml sterile tubes containing Phosphate Buffer Saline (PBS), which was previously prepared in our laboratory. Leukocytes taken into tubes with PBS were subjected to the centrifugation procedure at 2500 rpm for 15 minutes, and this procedure was repeated 2 more times to wash the leukocytes. Washed leukocytes were transferred to 1.5 ml sterile eppendorf tubes. Leukocyte samples were examined on the same day for antigen presence by direct ELISA method.

Animals determined to be antigen positive and antibody-negative in the 1st sampling were sampled for a 2nd time 20 days later and retested for the presence of both antigen and antibody.

ELISA Kits. While the prepared blood samples were examined for the presence of antibodies specific to BVDV by commercially available indirect ELISA (Biox BIOK283, Belgium), commercial direct ELISA kits (Biox BIOK258, Belgium) were used for antigen assay. The procedure was carried out per the instructions indicated in the kits.

Commercially available kits were used to determine oxidative stress in serum samples of persistent-infected animals obtained in the study. For this purpose, serum malondialdehyde (MDA-586TM, OxisResearch, Cat no: 21044, USA) kit, Total Antioxidant Capacity (TAC, SunRed, Cat no: 201609, China) kit were used. The tests were carried out as per the kit procedures. The values obtained were determined by calculating the ELISA reader (MWGt Lambda Scan 200, Bio-Tek Instruments, Winooski, VT, USA) absorbance values.

Measurement of biochemical parameters. The biochemical parameters [Albumin, ALP (Alkaline phosphatase), ALT (Alanine transaminase), AST (Aspartate aminotransferase), cholesterol, CK-MB (Creatine kinase), GGT (Gamma-glutamyl transferase), T-Protein, Trigliserin, BUN (Blood Urea Nitrogen) were measured using a blood gas analyzer (Instrumentation Laboratory, Milan, Italy).

Statistical analysis. The results of this study amongst PI calves and control groups were calculated by using an independent T-test (SPSS 19.0 for windows). The difference was considered significant when $P<0.05$.

RESULTS

600 blood samples collected from 25 different organizations in the Konya region were tested for BVDV antigens and antibodies by ELISA. Animals determined to be antigen positive and antibody-negative in the 1st sampling were sampled for a 2nd time 20 days later and retested for the presence of both antigen and antibody. 6 animals were determined as antigen-positive and antibody-negative in the 2nd sampling, and these animals were considered to be persistent-infected with BVDV. 6 calves determined to be negative in terms of the presence of both antigen and antibodies were determined as the control group in the 1st sampling. Serum samples of the animals that were considered as the persistent-infected and control group were measured in terms of biochemical parameters. The results of biochemical parameters are presented in Table 1, and the results of MDA and TAC are presented in Table 2. CK-MB, ALP, total protein, and albumin levels of the persistent-infected group was found to be higher than the control group ($P<0.05$).

DISCUSSION

In this research, the CK-MB level of the persistent-infected group was found to be higher than the healthy animals ($P<0.05$). CK-MB level, which is used as a specific marker in determining heart damage in humans, is also used in ruminants [6, 7, 8]. CK-MB enzyme level, which is a heart-specific subtype of the creatine kinase (CK) enzyme, reaches a peak level within the first 24 hours after heart damage [9]. It has been stated that some viral diseases such as Foot and Mouth Disease (FMD) may develop serious cardiac damage in bovine and this damage may cause death [10]. Similarly, it can be stated that persistent BVDV infection in calves may cause chronic cardiac degeneration and should be taken into consideration in diagnosis and treatment.

TABLE 1
Serum biochemical values of control and persistent-infected calves (Mean + SD).

Parameter	Control	Persistent-infected
CK-MB (U/L)	66.33±14.12[b]	602.00±258.94[a]
ALP (U/L)	118.16±17.62[b]	286.00±50.34[a]
ALT (U/L)	21.50±9.84	20.66±2.23
AST (U/L)	51.66±13.63	71.16±4.56
GGT (U/L)	11.50±3.09	8.00±3.16
TP (g/L)	4.46±0.53[b]	6.98±0.27[a]
Albumin (g/dL)	1.91±0.197[b]	2.93±0.18[a]
BUN (mg/dL)	7.33±1.70	4.50±0.99
Cholesterol (mg/dL)	522.16±81.99[b]	681.83±47.78[a]

Ck-MB: Creatine Kinase-MB, ALP: Alkaline Phosphatase, ALT: Alanine Aminotransferase, AST: Aspartate Aminotransferase, GGT: Gamma Glutamyl Transferase, TP: Total protein, ALB: Albumin, BUN: Blood urea nitrogen. a, b, Different letters on the same line are statistically significant (P<0.05).

TABLE 2
Results for MDA and TAC parameters in control and persistent-infected calves (Mean+SD)

Parameter	Control	Persistent-infected
MDA (µM)	0.0842±0.005[a]	4.02±0.69[a]
TAC (µM)	0.0717±0.005[a]	4.56±0.68[a]

a: Same letters on the same line indicate that there is no difference (P>0.05).

ALP, ALT, total protein, and albumin levels of the persistent-infected group were measured higher than the control group in this research (P<0.05) (Table 1). It was found that the statistically different total protein and albumin levels were within the reference values reported for bovine [11]. ALP level is used to define bile duct damage, while the ALT level is used to define liver cell damage [12, 13]. It is known that bile and liver damage can develop in viral diseases and related blood parameters defining the damage are increased [14, 15, 16, 17]. Considering the ALP and ALT elevations, it can be stated that the BVDV agent may cause damage to the bile duct and liver, and liver-sparing vitamin-amino acid supplements may be useful in treatment.

In this research, the cholesterol level was found to be higher in persistent-infected bovine than the healthy group (P<0.05) (Table 1). It has been reported that there may be changes in serum cholesterol levels in some viral [18, 19] or bacterial [20] infections. Considering the increased level of cholesterol, it can be stated that persistent BVDV infection in bovine may affect lipid metabolism.

Although no statistical difference (P> 0.05) was found in this research, the MDA and TAC levels in the persistent-infected bovine were determined to be very different from the healthy ones (Table 2). MDA is a biomarker used to determine lipid peroxidation developing in living organisms [21, 22]. The total activity of substances with antioxidant properties against free radicals in living organisms is defined by the Total antioxidant capacity (TAC) [23, 24]. The viral infections were stated to cause oxidative stress [22, 25, 26, 27, 28, 29, 30]. It can be stated that persistent BVDV infection can cause lipid peroxidation and TAC can be induced to prevent the development of the peroxidation. Besides, antioxidant supplementation may be considered in the treatment of persistent BVDV infections.

As a result, it can be stated that persistent BVDV infections may cause heart, bile duct, and liver damage, that it may affect lipid metabolism and cause lipid peroxidation. Therefore, it can be stated that the relevant organ damage parameters can be considered in the diagnosis and the addition of antioxidant vitamins or amino acids to the treatment may be useful.

It is of utmost importance that the programs to be prepared for the control and eradication of the infection caused by the Bovine Viral Diarrhea Virus are implemented by adopting throughout the country, not regionally. Thus, the current persistent infection rates of bovine farms should be determined and it should be questioned whether they use vaccines for protection from infection. When the control and eradication programs carried out by various countries in the struggle against BVDV are checked, it is observed that they are carried out in 3 different stages. 1- Determining the condition of the herd in terms of BVDV, 2- Determining the existing individuals and controlling the persistent infection, if the herd is infected with BVDV, 3- Continuing this in the organizations free from BVDV. Since the control and eradication with BVDV in cattle farms in some Northern European countries such as Norway program is carried out, in 2006, it was announced that they were free from BVDV infection.

When the results of the studies conducted in our country are considered, the presence of BVDV in all regions of our country has been revealed by serological and virological tests. As per the results of the current research, the presence of BVDV infection in our city was once again revealed. Considering that

intensive bovine breeding stands out throughout our country, it is inevitable that BVDV struggle programs will step forth. However, in our country where animal husbandry is very important, there is no preventive program being carried out to struggle with the infection caused by BVDV.

Also, considering the animal movements in our country and because the PI animals detected in the management sampled in our province were removed from the herd and the spread of BVDV infection both within our province and between provinces was evaluated, it is inevitable that it contributes positively to the bovine breeding sector in Konya and also supports the struggle against disease in the region. Also, it is thought that it contributes to the national economy by reaching the purpose of reducing economic losses caused by BVDV infection.

ACKNOWLEDGEMENTS

This study is supported by SUPABK (17401075). The abstract was presented at the International Congress on Domestic Animal Breeding Genetics and Husbandry (ICABGEH) the Congress Czech Republic, 2019.

REFERENCES

[1] Heinz, F., Collett, M., Purrchell, R., Gould, E., Howard, C., Houghton, M., Moorman, R., Rıce, C. and Theıl, H.J. (2000) Family Flaviviridae. In: Van Regnmortel MHV, Fanqute CM, eds. Virus taxonomy, Proceedings of the Seventh Report of International Committee on Taxonomy of Viruses. Wisconsin. Academic. Press. 859–878.

[2] Lanyon, S.R., Hill, F.I., Reichel, M.P. and Brownlie, J. (2014) Bovine viral diarrhoea: pathogenesis and diagnosis. Vet. J. 199, 201-209.

[3] Diao, N.C., Gonga, Q.L., Lia, J.M., Zhao, D., Li, D., Zhao, B., Ge, G.Y., Li, D.L., Shi, K. and Du, R. (2020) Prevalence of bovine viral diarrhea virus (BVDV) in yaks between 1987 and 2019 in mainland China: A systematic review and meta-analysis. Microb. Pathog. 144, 04-85.

[4] Kahrs, R.F. (2001) Viral Diseases of Cattle. Blackwell Publishing. 120-121.

[5] Ran, X., Chena, X., Maa, L., Wen, X., Zhai, J., Wang, M., Tong, X., Hou, G. and Ni, H. (2019) A systematic review and meta-analysis of the epidemiology of bovine viral diarrhea virus (BVDV) infection in dairy cattle in China. Acta Trop. 190, 296–303.

[6] Avcı, O., Yavru, S. and Bulut, O. (2013) Plasmabiochemical values in sheep with foot and mouth disease. Eurasian. J. Vet. Sci. 29, 216-219.

[7] Bozukluhan, K., Atakisi, E. and Atakisi, O. (2013) Nitricoxide levels, total antioxidant capacity in cattle with foot and mouth disease. Kafkas Univ. Vet. Fak. Derg. 19, 179-181.

[8] Corum, O., Dik, B., Bahçivan, E., Er, A., Yazar, E., and Eser- Faki, H. (2016) Cardiac safety of gamithromycin in ewes. Eurasian. J. Vet. Sci. 32, 242-245.

[9] Hallen, J. (2012) Troponin for the estimation of infarct size: what have we learned? Cardiology. 121, 204-212.

[10] Tunca, R., Sozmen, M., Erdogan, H., Citil, M., Uzlu, E., Ozen, H. and Gokce, E. (2008) Determination of cardiac troponin I in the blood and heart of calves with Foot and Mouth Disease. J. Vet. Diagn. Inves. 20, 598-605.

[11] Kaneko, J.J., Harvey, J.W. and Bruss, M.L. (2008) Clinical biochemistry of domestic animals. California: Academic. Press. 873-905.

[12] Russell, K.E., and Roussel, A.J. (2007) Evaluation of the ruminant serum chemistry profile. Vet. Clin. North. Am. Food. Anim. Pract. 23, 403-426.

[13] McGill, M.R. (2016) The Past and Present of Serum Amınotransferases and The Future of Lıver Injury Bıomarkers. EXCLI J. 15, 817-828.

[14] Teitelbaum, J.E. and Daghistani, R. (2007) Rotavirus causes hepatic transaminase elevation. Dig. Dis. Sci. 52, 3396-3398.

[15] Arıcı, S. (2008) Toksic Hepatitis. Pamukkale. M. J. 1, 113-119.

[16] Bowden, T.R., Babiuk, S.L., Parkyn, G.R., Copps, J.S. and Boyle, D.B. (2008) Capripoxvirus tissue tropism and shedding: a quantitative study in experimentally infected sheep and goats. Virology. 371, 380-393.

[17] Altay, D. (2016) Aminotransferase Levels in Children. Fırat Tıp Derg. 21, 113-119.

[18] Jang, E.S., Won, J.E., Jung, J.I., Lee, S.H., Kim, J.W. and Jeong, S.H. (2011) The effect of antiviral therapy on serum cholesterol levels in chronic hepatitis C. Gut Liver. 5, 356-362.

[19] Fernandez-Rodrıguez, C.M., Lopez-Serrano, P., Alonso, S., Gutierrez, M.L., Lledo, J.L., Perez-Calle, J.L., Temino, R., Cacho, G., Nevado, M., Casas, M.L., Gasalla, J.M. and Bonet, B. (2006) Longtermreversal of hypocholesterolaemia in patients with chronic hepatitis C is related to sustained viral response and viral genotype. Aliment. Pharmacol. Ther. 24, 507-512.

[20] Nassajı, M. and Ghorbanı, R. (2012) Plasma lipid levels in patients with acute bacterial infections. Turk. J. Med. Sci. 42, 465-469.

[21] Özler, M., Oter, S. and Korkmaz, A. (2009) The use of ozone gas for medical purposes. TAF Prev. Med. Bull. 8, 59-64.

[22] Sezer, K. and Keskin, M. (2014) Role of the free oxygen radicals on the pathogenesis of the diseases. F.U. Sag. Bil. Vet. Derg. 28, 49-56.

[23] Güler, T., Celebi, N., Sürer, H., Yılmaz, F.M., Güler, S., Sipit, T., Duranay, M. and Yücel, D. (2004) Serum total antioxidant status in pulmonary tuberculosis patients. Turkiye Klinikleri J. Med. Sci. 24, 618-623.
[24] Sırmatel, F., Duygu, F., Celik, H., Selek, S., Sırmatel, O., Gursoy, B. and Eris, F.N. (2009) Evaluation of total oxidative level and total antioxidant capacity in cases with chronic viral hepatitis. Klimik Dergisi. 22, 92-96.
[25] Akaite, T. and Maeda, H. (2000) Nitric oxide and virus infection. Immunol. 101, 300-308.
[26] Reıter, R.J., Tan, D.X., Saınz, R.M., Mayo, J.C., Lopez- Brillo, S. (2002) Melatonine: reducing the toxicity and increasing the efficacy of drugs. J. Pharm. Pharmacol. 54, 1299-1321.
[27] Farinati, F., Cardin, R., Bortolami, M., Burra, P., Russo, F.P., Rugge, M., Guido, M., Sergio A. and Naccarato, R. (2007) Hepatitis C virus: from oxygen free radicals to hepatocellular carcinoma. J. Viral Hepat. 14, 821-829.
[28] Cıragil, P. (2014) The role of oxidative stress in viral hepatitis. Mersin Univ. Saglık Bilim. Derg. 7, 93-99.
[29] Gümüşova, S.O. and Memis, Y.S. (2014) The Efficacy of Melatonin in Some Viral Infections. Atatürk Univ. Vet. Bil. Derg. 9, 50-54.
[30] Kocatürk, M., Tvarijonaviciute, A., Martinez-Subiela, S., Tecles, F., Eralp, O., Yılmaz, Z., Ceron, J.J. (2015) Inflammatory and oxidative biomarkers of diseases everity in dogs with parvoviral enteritis. J. Small Anim. Pract. 56, 119-124.

Received: **07.04.2021**
Accepted: **05.05.2021**

CORRESPONDING AUTHOR

Irmak Dik
Department of Virology,
Faculty of Veterinary Medicine,
University of Selcuk,
Konya – Turkey

e-mail: irmakdik@selcuk.edu.tr

© by PSP Volume 30– No. 09/2021 pages 10841-10848 Fresenius Environmental Bulletin

IMPACT OF VARIOUS FUNGICIDES AGAINST BLACK SPOT SEVERITY AND INCIDENCE CAUSED BY *Diplocarpon rosae*

Muhammad Zeeshan Mansha[1], Hafiz Muhammad Aatif[1,*], Muhammad Ijaz[1], Amer Habib[2], Muhammad Zeeshan Mansoor[1], Kamran Ikram[3], Hafiz Tassawar Abbas[4], Imran Khalid[5]

[1]College of Agriculture, Bahauddin Zakariya University, Bahadur Sub Campus, Layyah, 31200, Punjab, Pakistan
[2]Department of Plant Pathology, University of Agriculture, Faisalabad, 38000, Punjab, Pakistan
[3]Department of Agricultural Engineering, Khwaja Fareed University of Engineering and Information Technology, Rahim Yar Khan, 64200, Punjab, Pakistan
[4]Faculty of Agriculture, Department of Plant Pathology, Lasbela University of Agriculture, Water and Marine Sciences, Uthal, Balochistan, Pakistan
[5]Faculty of Agriculture and Environment, The Islamia University of Bahawalpur, Punjab, Pakistan

ABSTRACT

Rose (*Rosa indica* L.) falls in Rosaceae family comprising genera in hundreds with thousands of species viz. shrubs, herbs and trees. Globally, rose has a paramount importance due to its contribution in medicinal and cosmetic industry, while also valuable for its aesthetic aspect. Current study was carried out in randomized complete block design (RCBD) under factorial arrangements with three replications at field area of College of Agriculture, Bahadur sub-campus, Layyah, Punjab, Pakistan. Results revealed that Antracol with its 300 ppm concentration significantly minimized the severity (%) and incidence (%) of black spot of rose followed by Acrobat MZ, whereas, Companion exhibited minimum impact against targeted malady as compared to rest of the fungicides over control. In crux, results of given study exhibited that Antracol with its 300 pmm concentration can be used to inhibit the impact of black spot malady in rose.

KEYWORDS:
Rose Black spot, *Diplocarpon rosae*, Black spot, Fungicide

INTRODUCTION

Rose (*Rosa indica* L.) is the important profit-making crop belonging to the Genus Rosa and the family Rosaceae, contains almost 200 species and over 18,000 cultivars [1]. The rose is known as a King of Flowers. Even before the record of human civilization, rose flowers were grown-up. Roses are grown on vast area in various parts worldwide for glamorous purposes. There are about 120 rose species including the well-liked and aromatic Rosa damascene, Rosa cent folia and Rosa gullied. The two key varieties used for the profitable production of the oil required are Rosa cent folia and Rosa damascene, selected by a large number of perfumers [2].

145 countries observe floriculture and expenditure pattern is in billions but Pakistan's contribute to take away, worldwide market 3% while India defenses 25th in global trade with Export having development rate of 12-15% in floriculture, somewhere near about floriculture goods of 50% are contribute via Netherlands. Because as is concerned Pakistan, this manufacturing is still in preschooler position, floriculture deal in Pakistan for the supply of roses crop about 50% [3]. Considering only the Netherlands two years flower sales, during 2007, 3243 million cut rose stems, and in 2008, 3415 million stems were sold ($10 billion), respectively [4]. Rose has always been Pakistan's favorite flower and has a special place in our society, as there is hardly any event where roses are not shown. Rose production in Pakistan has great prospects, as it has an agricultural financial system with various climatic conditions. Cut roses are already growing on 526 ha in the province of Punjab according to a survey [5].

Flowers grown in the country are widely used and limited amounts have been exported into the Middle East, although other flowers have been worn out [6]. [7] said that due to a lack of knowledge of floral cultivation causes for small-scale farming of flowers in agriculture are a major problem, and clearly recognized that the country's environment is the most relevant.

Rose is so used in so many ways. They are cultivated as ornamental products, rose oil used in perfume production, used as room refreshers, rose water for various medicine uses, relieved from the soothes of the mind, rose petals were used as an antiseptic ingredient in the eye wash. Vitamins such as vitamins A, C, D, E and B3 enrich the food. Rosy water is used for skin beauty in face masks to preserve the skin pH and regulate extra oil. When you use a cup of rose water to highlight the hair, it produces good hair and is used in jams, jellies and rose soup. The rose is a symbol of love and calmness and is also used as a gift for welcoming parties, weddings and religious events [7].

Fungal diseases include leaf spot, Black mold,

Black spot, Botrytis blight, Brown canker, Powdery mildew, Cercospora leaf spot, common canker of stalk, Crown cancer, Downy mildew, Fungal Cancers, Graft cancer, Rust, Anthracnose, Verticillium, and Powdery mildew. Pathogenic ascomycete belonging to the Dermateaceae family, *Diplocarpon rosae* [8]. On some wild rose and rose cultivars D. rosae may be found. This disfigures and decreases the vigor of susceptible plants, because they are also fungicidally sprayed [9]. Black spot disease in ornamental roses in especially the hot and wet climates, is economically significant and devastating [10]. Initiated by rainfall-splashed pathogen spores overwintered by dropping leaves, disease outbreaks in early season. Characteristic dark spots, chlorosis and dropping early on grow infected leaves. If left unprocessed, the disease can lead to a reduction in plant strength, reduced flowering, aesthetics compromised and potential plant break-up [11]. The rose plants are used for landscaping and are cultivated in gardens, because of their esthetic interest. Fluffy black spots on the leaves and yellowing and defoliation lead to a decline in market value and the landscape management of roses [12].

MATERIALS AND METHODS

Collection and transplantation of Rose. In the current study, Abracadabra (fragrant rose germplasm) was taken from Green Valley nursery of Layyah, Pakistan and transplanted in well-drained sandy loam soil with pH between 6-7, favorable for rose cultivation, at the research area of BZU, Bahadur Sub Campus, Layyah during 2019-20. The experiment was laid out in Randomize Complete Block Design (RCBD) under factorial arrangements with three replicates containing 15 plants in each replication. Row to row distance was 75 cm and plant to plant was 60 cm.

Preparation and application of various fungicides against black spot disease incidence and severity. The crop was observed carefully for initiation of the disease under natural inoculum. Spray of each treatment was given immediately after disease appearance for disease severity (%) study, whereas, treatments applied before disease appearance for disease incidence (%). Three concentrations (100 ppm, 200 ppm, 300 ppm) of five fungicides viz. Acrobat MZ, Antracol, Myclobutanil, Amistar Top and Companion were evaluated for their efficacy against black spot disease. Data regarding disease severity (%) [13] and disease incidence (%) [14] was recorded according to following scale (Table 1) and formula 1 respectively after 15, 30 and 45 days of treatment application.

Statistical Analysis. Data collected from each experiment were analyzed using Statistix v. 8.1 software. Least significant difference (LSD) test at 5% probability level was applied to compare the treatment means.

RESULTS

Impact of various fungicides against black spot (*Diplocarpon rosae*) severity (%) of Rose. Application of various treatments (Tr) viz. Acrobat MZ, Antracol, Myclobutanil, Amistar Top and Companion along with respective concentrations (C) i.e. 100 ppm, 200 ppm and 300 ppm minimized the disease severity (%) significantly ($p \leq 0.05$) with respect to different days (15, 30, 45). Maximum reduction in disease severity was assessed in case of Antracol (18.03%) followed by Acrobat MZ (25.25%), Myclobutanil (35.87%), Amistar Top (44.17%) and Companion (47.98%) over control (55.96%). In case of used concentrations, disease severity was higher in 100 ppm (40.07%) as compared to 200 ppm (37.00%), whereas, 300 ppm concentration reduced the disease severity up to 36.57%. Disease severity was minimum after 15 days (34.38%) of treatment application followed by 30 days (37.74%) and 45 days (41.50%) (Table 2).

TABLE 1
Rating scale for disease severity (%)

Scale	Disease severity	Symptom description
1	0%	Leaflet with no black spot symptoms
2	1-20%	Leaflet with black spots having size less than 5 mm. No yellowing of leaflet and no premature defoliation.
3	21-40%	Leaflet with black spots having less than 5 mm size along with yellowing and/or defoliation symptoms
4	41-60%	Leaflet with black spots having 5-10 mm size with no yellowing and/or defoliation symptoms
5	61-80%	Leaflet with black spots of 5-10 mm along with yellowing and/or defoliation symptoms
6	81-100%	Leaflet with black spots of more than 10 mm along with yellowing and/or defoliation symptoms

$$\text{Disease incidence } (\%) = \frac{\text{Plant with disease symptoms}}{\text{Total plants observed}} \times 100 \quad (1)$$

Interactive effect between Tr × C, Tr × D, C × D and Tr × C × D revealed their significant ($p \leq 0.05$) impact in black spot severity (%) reduction. Antracol with its 300 ppm concentration, in Tr × C interaction, showed maximum reduction in disease severity followed by Acrobat MZ, Myclobutanil, Amistar Top and Companion, whereas, disease severity (%) was maximum in case of control (Figure 1). Interaction between Tr × D exhibited that disease severity was minimum after 15 days of Antracol application followed by 30 and 45 days, whereas, maximum severity was assessed in case of control. Similar trend was observed in other applied treatments (Figure 2). Interactive effect of C × D showed reduction in disease severity (%) after 15 days of 300 ppm treatment application, over 200 ppm and 300 ppm, followed by 30 and 45 days (Figure 3). Interaction between Tr × C × D exhibited that Antracol with 300 ppm concentration efficiently reduced the severity of disease, as compared to 200 ppm and 100 ppm, after 15 days of application over 30 and 45 days. Similar but increasing trend in disease severity was observed in other used treatments (Figure 4).

TABLE 2
Impact of various fungicides applied at different concentrations on disease severity (%) at different days.

Factors	Disease Severity %	LSD (Tr) ($p \leq 0.05$)
Treatment (Tr)		
Acrobat MZ	25.25 E	0.22**
Antracol	18.03 F	
Myclobutanil	35.87 D	
Amistar Top	44.17 C	
Companion	47.98 B	
Control	55.96 A	
Concentration (C)		**LSD (C) ($p \leq 0.05$)**
100 ppm	40.07 A	0.15**
200 ppm	37.00 B	
300 ppm	36.570 C	
Days (D)		**LSD (D) ($p \leq 0.05$)**
15	34.38 C	0.15**
30	37.74 B	
45	41.50 A	
	LSD ($p \leq 0.05$)	
Tr × C	0.19**	
Tr × D	0.38**	
C × D	0.27**	
Tr × C × D	0.67**	

Any two means within a column followed by same letters are not significant at $p \leq 0.05$. * = Significant at $p \leq 0.05$; ** = Significant at $p \leq 0.01$.

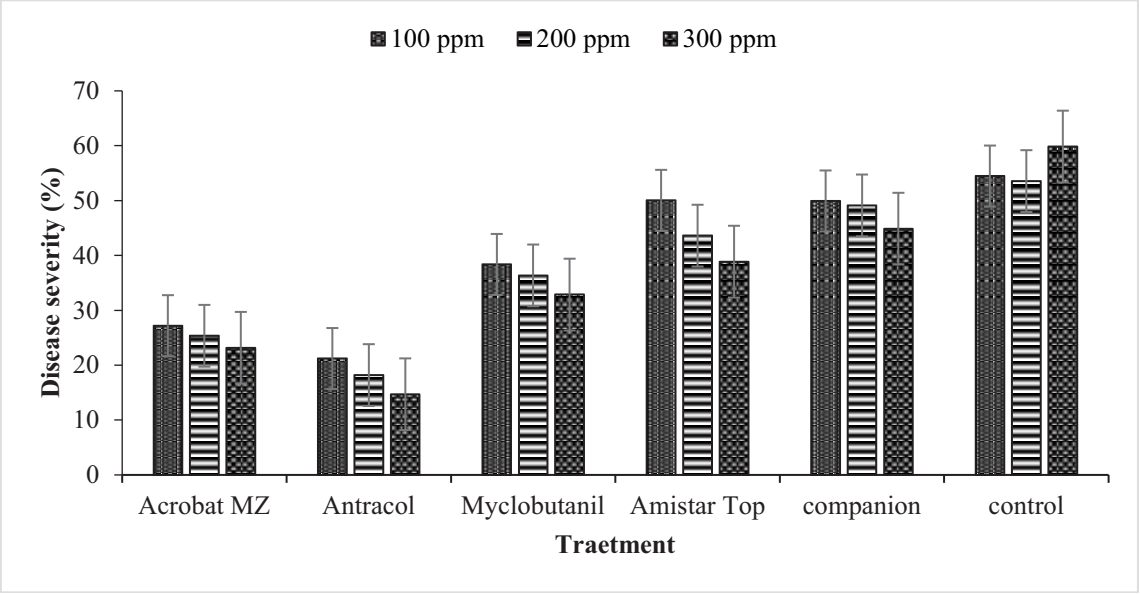


FIGURE 1
Interaction between treatments and concentrations on disease severity (%) of black spot

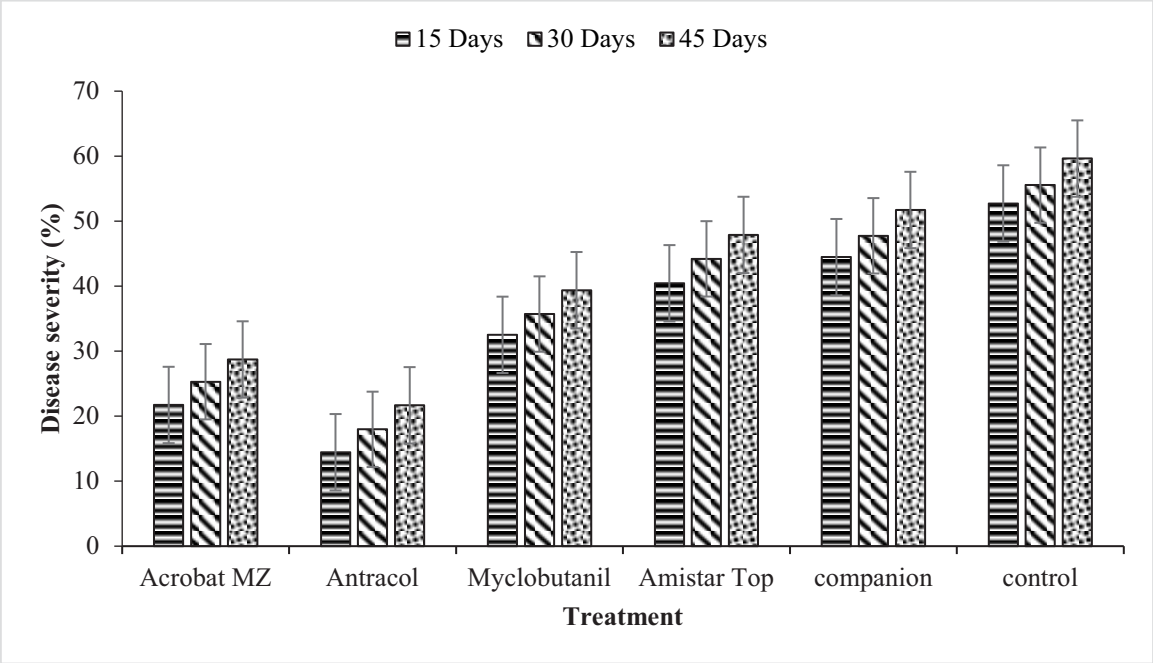


FIGURE 2
Interaction between treatments and days on disease severity (%) of black spot

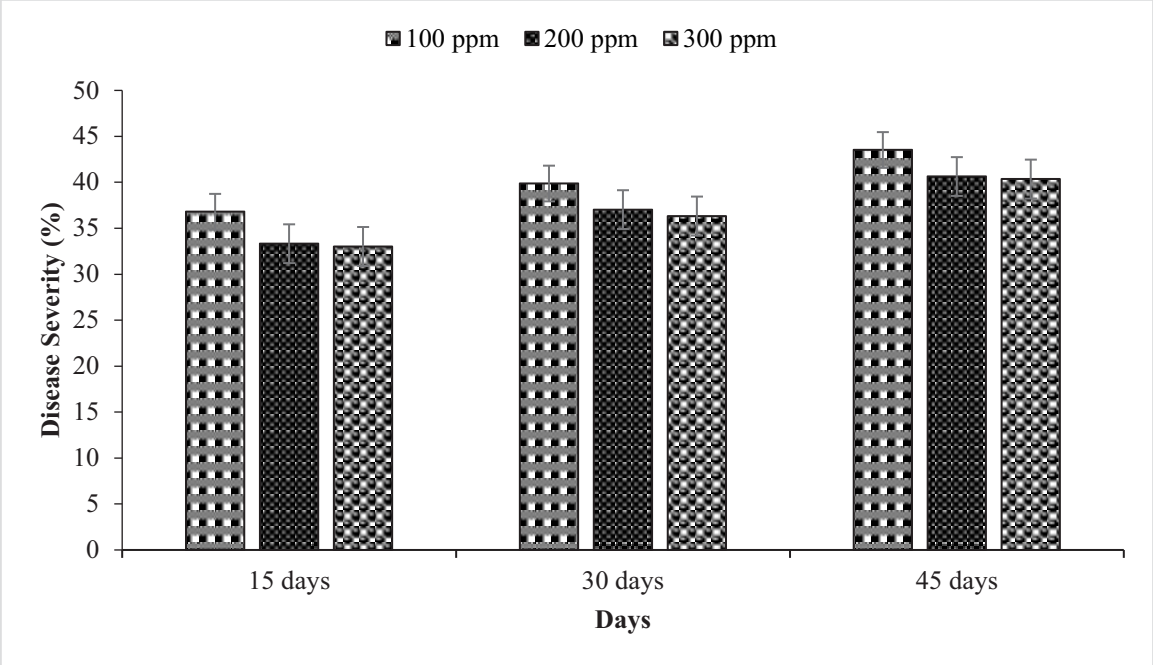


FIGURE 3
Interaction between days and concentrations on disease severity (%) of black spot

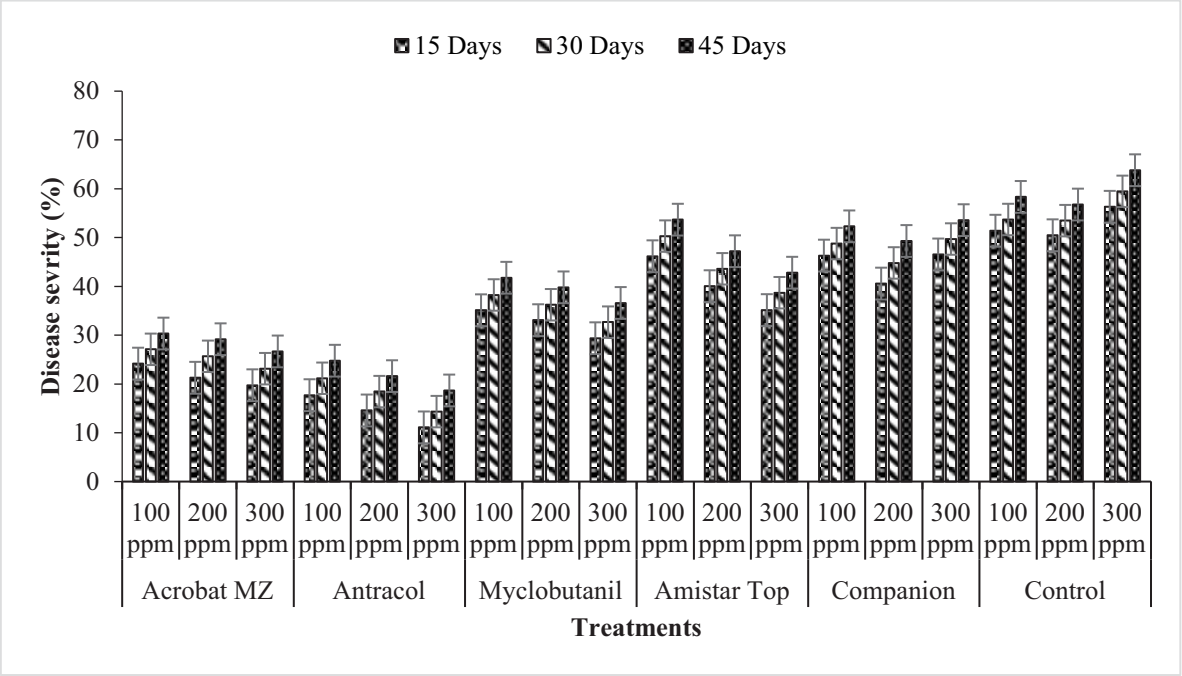


FIGURE 4
Interaction between treatments, concentrations and days on disease severity (%) of black spot

Impact of various fungicides against black spot (*Diplocarpon rosae*) incidence (%) of Rose. Various treatments application (Tr) viz. Acrobat MZ, Antracol, Myclobutanil, Amistar Top and Companion with their particular concentrations (C) i.e 100 ppm, 200 ppm and 300 ppm reduced the incidence (%) of disease significantly ($p \leq 0.05$) with respect to different days (15, 30, 45). Maximum reduction in disease incidence was assessed in case of Antracol (13.62%) followed by Acrobat MZ (19.57%), Myclobutanil (31.40%), Amistar Top (40.05%) and Companion (46.98%) over control (76.29%). In case of used concentrations, disease incidence was higher in 100 ppm (39.90%) as compared to 200 ppm (37.80%), whereas, 300 ppm concentration reduced the disease incidence up to 36.26%. Disease incidence was minimum after 15 days (36.86%) of treatment application followed by 30 days (37.77%) and 45 days (39.32%) (Table 3).

TABLE 3
Impact of various chemicals and their concentrations on disease incidence with respect to different days.

Factors Treatment (Tr)	Disease incidence %	LSD (Tr) ($p \leq 0.05$)
Acrobat MZ	19.57 E	
Antracol	13.62 F	
Myclobutanil	31.40 D	0.17**
Amistar Top	40.05 C	
Companion	46.98 B	
Control	76.29 A	
Concentration (C)		**LSD (C) ($p \leq 0.05$)**
100 ppm	39.90 A	
200 ppm	37.80 B	0.12**
300 ppm	36.26 C	
Days (D)		**LSD (D) ($p \leq 0.05$)**
15	36.86 C	
30	37.77 B	0.12**
45	39.32 A	
	LSD ($p \leq 0.05$)	
Tr × C	0.31**	
Tr × D	0.30**	
C × D	0.21**	
Tr × C × D	0.52**	

Any two means within a column followed by same letters are not significant at $p \leq 0.05$. * = Significant at $p \leq 0.05$; ** = Significant at $p \leq 0.01$.

Interaction between Tr × C, Tr × D, C × D and Tr × C × D showed their significant ($p \leq 0.05$) impact in black spot incidence (%) reduction. Antracol with its 300ppm concentration, in Tr × C interaction, showed maximum reduction in disease incidence followed by Acrobat MZ, Myclobutanil, Amistar Top and Companion, whereas, disease incidence (%) was maximum in case of control (Figure 5). Interactive effect of Tr × D revealed that disease incidence was minimum after 15 days of Antracol application followed by 30 and 45 days, whereas, maximum incidence was observed in control. Similar trend was observed in other applied treatments (Figure 6). Interaction between C × D showed reduction in disease incidence (%) after 15 days of 300 ppm treatment application, over 200 ppm and 300 ppm, followed by 30 and 45 days (Figure 7). Interactive effect of Tr × C × D showed that Antracol with 300 ppm concentration effectively minimized the incidence of disease, as compared to 200 ppm and 100 ppm, after 15 days of application over 30 and 45 days. Similar but increasing trend in disease incidence was observed in other used treatments (Figure 8).

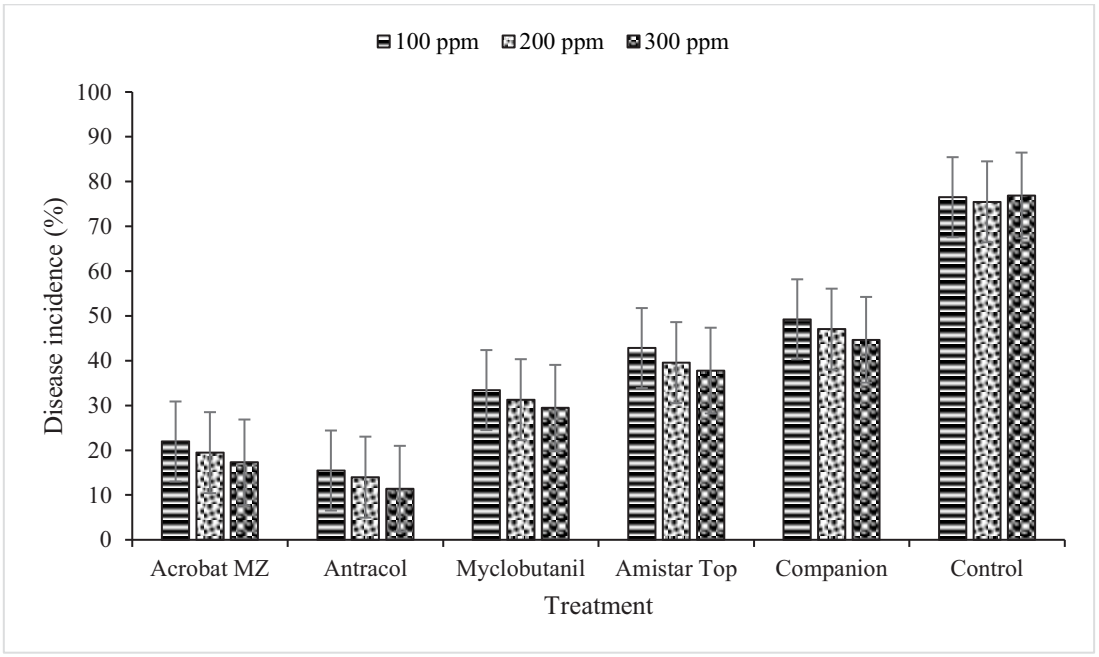


FIGURE 5
Interaction between treatments and concentrations on disease incidence (%) of black spot

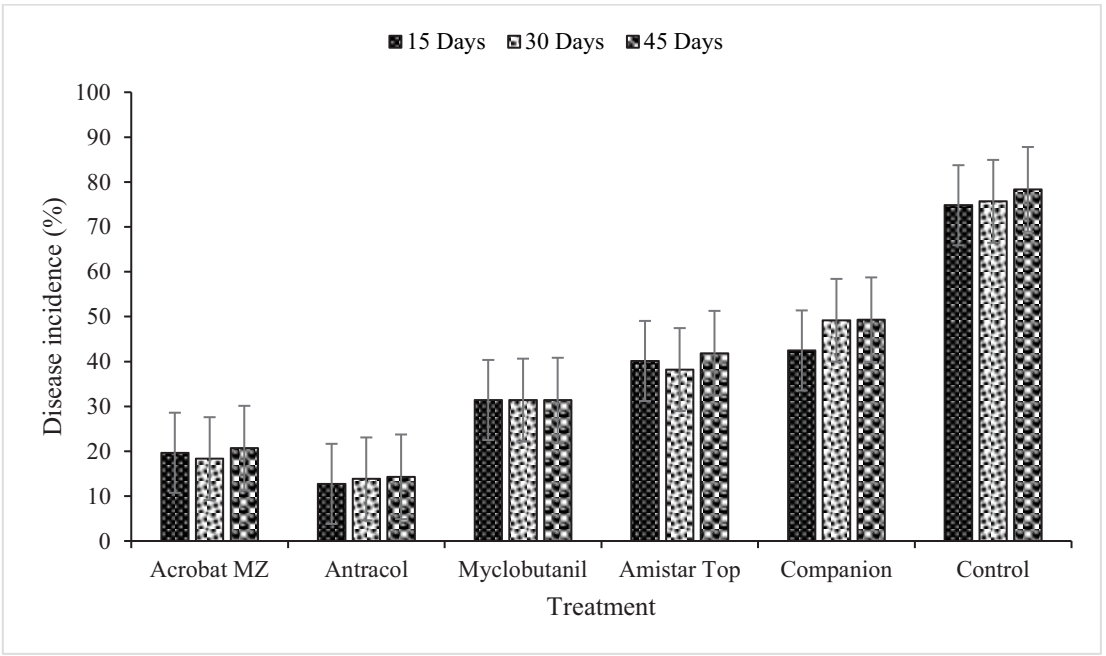


FIGURE 6
Interaction between Treatment and days on disease incidence (%) of black spot

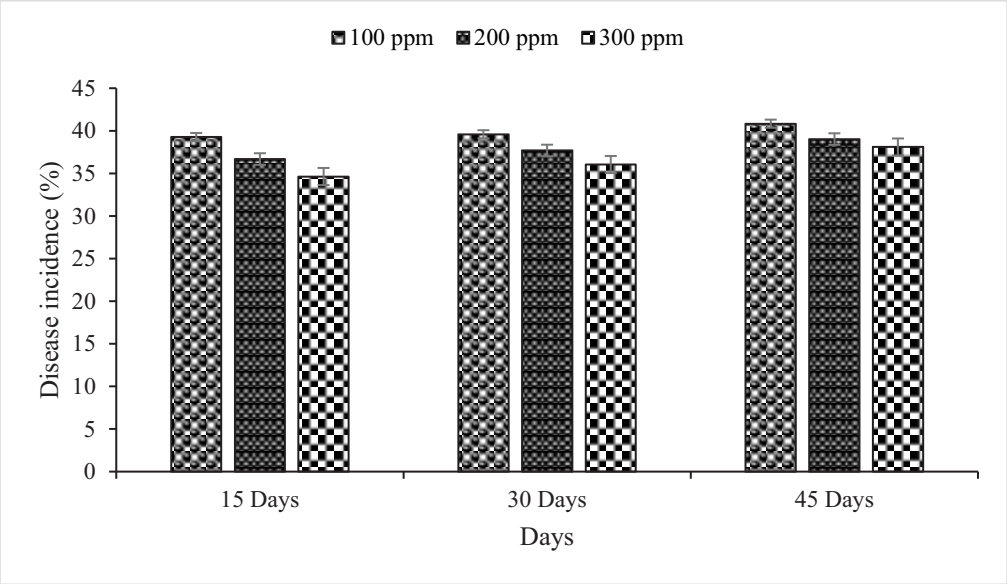


FIGURE 7
Interaction between Days and concentration on disease incidence (%) of black spot

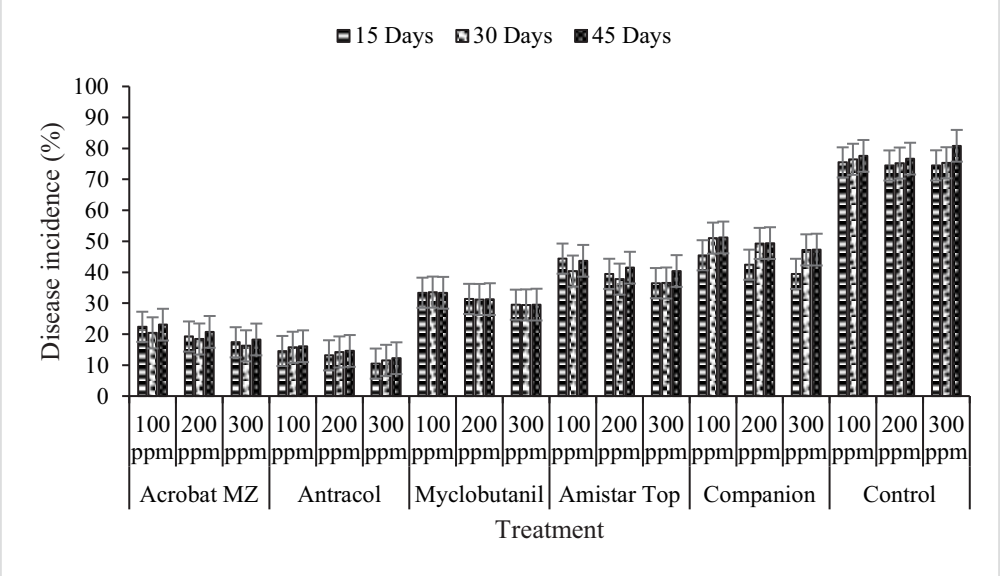


FIGURE 8
Interaction between treatments, concentrations and days on disease incidence (%) of black spot

DISCUSSION

Five different fungicides were tested for their efficacy against black spot disease severity and incidence of rose. Among all the fungicides Antracol along with 300 ppm concentration gave best results and maximum inhibited the disease followed by Acrobat MZ, while the least control of disease is shown by Companion over control. Systemic fungicides, by having similar mode of action, intrusive in production of energy in the cell of fungi viz. restriction in transfer of electron at quinol oxidation (Qol) site in the complex of cyto chrome bcl, consequently inhibiting the production of ATP. In fungi, sterol inhibitors restrict the structure formation of cell wall, consequently restrict the fungal ability of reproduce and develop [15]. These results are in line with of [13] who also found fungicidal impact on germination (%) of conidia on the leaves on exact day that were treated was explained on third of interval each. Pyraclostrobin restrict the conidial germination on sprayed leaflets. Strobilurins reduced the lesion size in sprayed leaves against marssonia blotch of apple. Mentioned fungicides were in close line with benzimidazoles and dodine, these fungicides not only restrict the production of conidia but also reduced the disease development and vice-versa. Apple leaves exhibited reduction in production, sprayed with pyraclostrobin, azoxystrobin, carbendazim, dodine, tebunazole, difenoconazole, mancozeb and metiram, of conidia (57.22-88.93%) under poly house environment [16]. Similar results were also documented

in field trials [17]. Protectant fungicidal spray, during summer, in 7-10 days interval may be effective against black spot malady. Fungicides Amistar top, Companion and Myclobutanil were suggested for the control of disease of rose.

CONCLUSION

In crux, systemic fungicides viz. Acrobat MZ, Antracol, Myclobutanil, Amistar Top and Companion are effective with 300 ppm concentration against disease severity (%) and disease incidence (%) reduction in rose. These fungicides effective when applied at regular intervals for restriction of black spot of rose.

ACKNOWLEDGEMENTS

We are highly thankful to College of Agriculture, BZU, Bahadur Sub Campus, Layyah, Punjab, Pakistan for research facilities and KFUEIT, Rahim Yar Khan, Pakistan for provision of technical and research help.

REFERENCES

[1] Gudin, S. (2000). Rose Genetics and Breeding. Plant Breeding Reviews. 17, 159–89.
[2] Khan, M.A. and Younis, A. (2007). Phyto-Chemical Analysis and Exploitation of Hetrosis for Essential Oil Contents in Rose Species. M.Sc. Thesis Submitted in Institute of Horticultural Sciences, Univ. Agric. Faisalabad.
[3] Sidhu, S. (2005). Proceedings of Seminar On "Diversification in Floriculture Trends and Avennues" held at University of Arid Agriculture, Rawalpindi.
[4] Evans, A. (2009). Rose imports. Floriculture Intl. 19, 42–43.
[5] Khan, M.A. (2005). Development of commercial floriculture in Asia and Pacific: Issues, challenges and opportunities. Proceedings of the National Seminar on Streamlining, Production and Export of Cut-Flower and house plants. Saeed, A. (Ed.), Hort. Foundation. Pak., 2nd -4th March. 29–42.
[6] SMEDA. (2009) Online Available: https://smeda.org/index.php?option=com_rseventspro&view=calendar&layout=day&date=09-03-2009. (Accessed on 13-03-2021).
[7] Leghari, S.J., Soomro, F.A., Leghari, Z., Maher, P.A., Minhas, A.A. and Soomro, A.A. (2015). Causes of Low-Level Farming of Flowers in Indus Valley. Am. Res. Thoughts. 1, 2636-2646.
[8] Nauta, M.M. and Spooner, B.M. (2000). British Dematiaceous: 4B. *Dermateoideae* gerna B-E. Mycologist. 14, 21–8.
[9] Drewes-Alvarez, R. (2003). Black Spot. In: Roberts, A., Debener, T., Gudin, S., eds. Encyclopedia of Rose Sciences. Oxford, UK: Elsevier Science. 148-53.
[10] Horst, R.K. and Cloyd, R.A. (2007). Compendium of Rose Diseases. APS Press, St. Paul, MN. 96.
[11] Henn, A. (2010). The Plant Doctor – Black Spot and Powdery Mildew of Rose. Extension, Mississippi State University. Online Available: http://extension.msstate.edu/sites/default/files/publications/publications/p2827.pdf (Accessed date: 20-10-2015).
[12] Drewes-Alvarez, R. (2003). Black spot. In: Roberts A, Debener T, Gudin S, eds. Encyclopedia of Rose Sciences. Oxford, UK: Elsevier Science. 148–53.
[13] Gachomo, E.W. (2005) Studies of the life cycle of *Diplocarpon rosae* Wolf on roses and the effectiveness of fungicides on pathogenesis. Inaugural Dissertation. 1-147.
[14] Iqbal, Z. (2004) Studies on malformation of mango inflorescence. Thesis, Bahauddin Zakaria University Multan. 1-193.
[15] Nene, Y. and Thapliyal, P.N. (1979) Fungicide in Plant Disease Control. Oxford and IBH Publishing House, New Delhi. 01-163.
[16] Kumar, A. and Sharma, J.N. (2015) Evaluation of pre-symptom activity of fungicides against *Marssonina coronaria* causing premature leaf fall in apple. Indian phytopathology. 68 (3), 293-296.
[17] Mangandi, J. and Peres, N.A. (2009) Black spot of rose. University of Florida IFAS Extention, Publication #PP26800. Online Available: http://edis.ifas.ufl.edu/pp268. (Accessed date: 2009)

Received: **07.04.2021**
Accepted: **05.05.2021**

CORRESPONDING AUTHOR

Hafiz Muhammad Atif
Department of Plant Pathology,
College of Agriculture,
Bahauddin Zakariya University,
Bahadur Sub Campus,
Layyah 31200 Punjab – Pakistan

e-mail: aatif.pak@bzu.edu.pk

© by PSP Volume 30– No. 09/2021 pages 10849-10855 Fresenius Environmental Bulletin

STUDY ON EVALUATION OF SOIL HEAVY METAL POLLUTION IN COPPER-SULFUR MINING AREA BASED ON TRACER METHOD

Ying Chen[1,2], Chong Chen[1,2,*], Qiang Hao[1,3], Guoxin Li[1,2], Lijun Qian[1,2], Lihua Ou[1,2], Xiaobin Huang[1,2]

[1]The Engineering & Technical College of Chengdu University of Technology, Leshan 614000, China
[2]Southwestern Institute of Physics, Leshan 614000, China
[3]School of Ocean and Earth Science, Tongji University, ShangHai 200000, China

ABSTRACT

A series of metal sulfide deposits are developed in the lakeside area of the middle and lower reaches of the Yangtze River in China, of which copper-sulfide deposits are one of them. Copper-sulfur mines will produce heavy metal pollution in the surrounding soil, so the study of the enrichment law of heavy metal elements in the soil has important reference value for formulating reasonable heavy metal pollution prevention and control measures. In this paper, taking copper-sulfur mines in the middle and lower reaches of the Yangtze River in China as an example, the tracer method was used to study the enrichment characteristics and sources of heavy metal pollution element copper in soil. Research results show that the sources of copper and sulfur in the soil in this area include copper-sulfur mine tailings, waste ore, organic and inorganic sulfur in the soil, and biological effects. The sulfur content in the soil around the copper-sulfur mine is close to the sulfur content of the ore by 20%~30%, indicating that the sulfur in the soil basically comes from tailings and waste ore; the copper content in the soil is also high, therefore, the pollution effect of the mine on the soil is obvious. The main sources of copper enrichment in the soil include acidic high-salinity water, water leaching the soil, and vegetation. Among them, acidic high-salinity water and water leaching of the soil are the main factors that cause copper enrichment in the soil, and the copper enrichment caused by the vegetation is relatively low.

KEYWORDS:
Tracer method, copper-sulfur mining area, heavy metal pollution, soil, source

INTRODUCTION

In copper-sulfur mining, the sulfide that was originally under reducing conditions is exposed to a large area of oxidation conditions with free oxygen and water [1-3]. Sulfides, especially disulfides such as pyrite are very easy to oxidize, while chalcopyrite and sphalerite cannot be oxidized directly [4-5]. Chalcocite can react with ferrous sulfate to produce iron sulfate and natural copper [6-8]. The surrounding rock of the copper-sulfur mine pit can form sulfurous acid and sulfuric acid, and can further produce a certain neutralization reaction with the surrounding rock [9-10]. The pH value of copper-sulfur mine water is generally acidic water of 2~4, and it contains a large amount of heavy metal ions mainly Cu, Fe, and Zn. It can be seen that the mine water is a source of pollution [11-13]. For mining under the lake water, the lake water will inevitably be polluted similarly to mine pits. Due to the high content of SiO_2, FeS_2, and copper in copper-sulfur ore and surrounding rocks, soil and atmospheric dust pollution during mining, ore transportation, and dumping cannot be underestimated [14-15].

A series of polymetallic sulphide deposits are developed in the lakeside zone of the middle and lower reaches of the Yangtze River in China, and most of them require open-pit mining, of which copper-sulfur deposits are one of them [15-17]. Due to the proximity of such deposits to cities, it is particularly important to discuss the generation of pollution sources, the formation of pollution pathways and the protection of natural environment in the process of its mining and selection [18-19]. The mining conditions of copper-sulfur deposits are complex and highly polluting, so special attention should be paid to the protection of the soil surrounding the mining area. In this paper, taking copper-sulfur mines in the middle and lower reaches of the Yangtze River in China as an example, the tracer method was used to study the enrichment characteristics and sources of heavy metal pollution element copper in soil. This research has important reference value for formulating reasonable heavy metal pollution prevention and control measures in copper-sulfur mining areas.

MATERIALS AND METHODS

Geological background. The study area is located in Area A in the middle and lower reaches of the Yangtze River in China, where large copper-sul-

fur mines are developed, and more than 75% of industrial ore bodies are located in bedrock (Figure 1). This area has a subtropical rainy, warm and freezing climate.

The exposed stratum in the mining area is shown in Figure 1. The copper-sulfur mining area in the study area is located in the wing of a syncline structure, with a dip angle of 30-75°, and its strike is in the NEE-SWW direction. The most important fault in the mining area is also a normal fault along the bedding gravity, and the normal fault is the largest in the Middle Carboniferous limestone. The thickness of cataclastic rock is often greater than 15 m, which is the main channel for ore liquid activity, and it is also the most important ore storage structure.

Characteristics of mineral development in the study area. The magmatic rocks in the study area are mainly Yanshanian granodiorite porphyry and quartz porphyry, and they are distributed in an elliptical shape. Among the mineral types, the accessory minerals are mainly magnetite and apatite, and the sulfide content is generally higher. The ore-forming heavy metal elements Cu, Zn, Ag, As, W, and Mo are relatively high. The main wall rock alterations include skarnization, silicification, and pyrite mineralization [7, 20]. And these subvolcanic rocks are often accompanied by intrusive structural breccia and blasting breccia. The main sulfides in the study area are copper-sulfur ore, pyrite, and chalcopyrite, followed by chalcocite, sphalerite, tetrahedrite, and silverite. Non-metallic minerals are mainly clay.

Tracer method. The working test samples were mainly collected from the internal ore body of the copper-sulfur mine in the study area. The measurement objects are sulfur and copper. By measuring the accumulation of various heavy metal elements in the vegetation soil around the copper-sulfur mining area and the pH value of the leachate, the enrichment law and source of heavy metal elements in the soil have been clarified.

RESULTS

The soil type in the study area belongs to subtropical red soil, which is widely distributed in hilly areas. The parent rock is mainly acid mixed rock, and there are biotite plagioclase gneiss, granite, quartz slate, sandstone and shale. From the chemical point of view, the content of organic matter in the red soil in this area is not high, mainly distributed between 0.5% and 2.5%, and most of the various bases are leached. The content of copper in the soil of copper-sulfur mining area is relatively high. If the copper content in the uncontaminated area is taken as the background value, the average background value of copper in the red soil of the study area is 36 mg/kg. The average copper background value in vegetation is 45 mg/kg. In the process of mineralization, some parent rock components contain high flux. During the process of soil formation, the copper content in the soil increases through the migration and accumulation of copper.

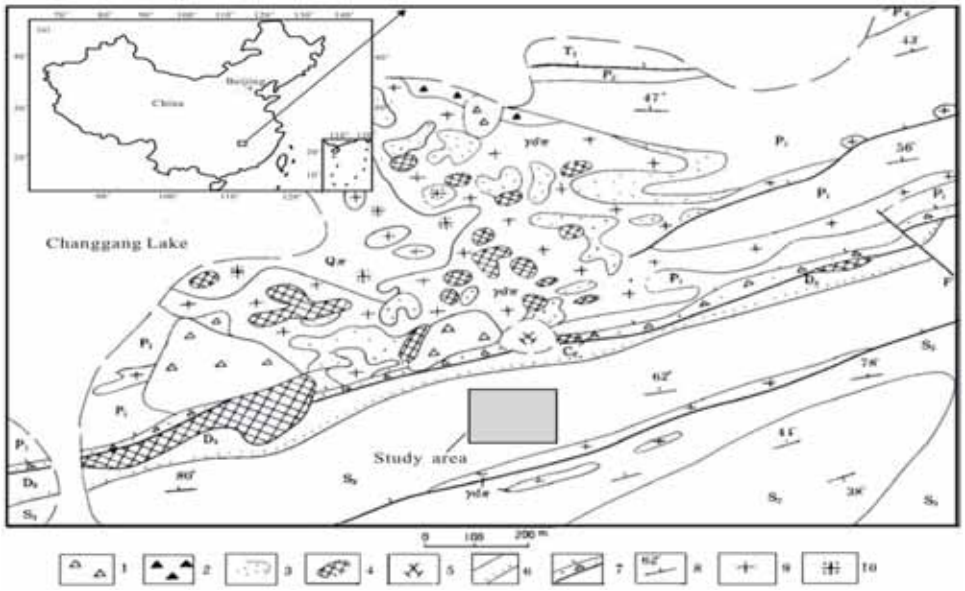


FIGURE 1
Geological map of the copper-sulfur mining area.

Notes: 1. Karst cave collapsed breccia; 2. Intrusive structural breccia; 3. Skarn and ore body; 4. Iron cap and ore body; 5. Old mine pit; 6. Stratum boundary; 7. Bedding gravity sliding fault And sliding rocks; 8. Stratigraphic occurrence; 9. Yanshanian granodiorite porphyry; 10. Yanshanian quartz porphyry; S2. Middle Silurian shale intercalated with sandstone; S3. Upper Silurian sand shale Interbedded; D3. Upper Devonian quartz glutenite (including Lower Carboniferous); C2. Middle Carboniferous breccia limestone; P1. Lower Permian limestone; P2. Upper Permian limestone intercalated with shale; T1- 2. Middle-Lower Triassic argillaceous limestone intercalated with shale.

Characteristics of various heavy metal elements in copper-sulfur ore. The sources of copper and sulfur in the soil in this area include copper-sulfur mine tailings, waste ore, organic and inorganic sulfur in the soil, and biological effects. Generally speaking, sulfur in surface water comes from sulfur carried by atmospheric precipitation and sulfate dissolved in soil and rocks. In this area, sulfur in water also comes from the dissolution of sulfide minerals in tailings and waste ore. SO_4^{2-} in water is not easily affected by adsorption, precipitation and other factors, so the range of influence of SO_4^{2-} is usually greater than that of heavy metals Pb, Zn, and Cu. However, this area is a coal-producing area, and the stratum contains gypsum salt layers [21-22]. Affected by the high-sulfur coal and gypsum salt layer, the SO_4^{2-} content in the main stream and the tributary stream are equivalent, and the SO_4^{2-} content in the river water has little change.

The test results show that the sulfur content in the soil around the copper-sulfur mine is the highest, which is close to the sulfur content of the ore by 20% to 30%, which shows that the sulfur in the soil basically comes from tailings and waste ore. Therefore, the pollution effect of mines on the soil is obvious.

Copper has two stable isotopes, 63Cu and 65Cu, and their proportions in nature are 69.17% and 30.83%, respectively. The measurement results of copper isotopes in the soil in the study area showed that the copper content in the soil around the copper-sulfur mine was also higher than the normal level. This indicates that copper will also pollute the soil, especially crops, to a certain degree in this area. Therefore, we further analyzed the accumulation process or reason of the heavy metal element copper in the soil.

Copper enrichment caused by acidic high-salinity water. After the minerals such as chalcopyrite ($CuFeS_2$) and chalcocite (Cu_2S) are exposed to the surface, they are extremely unstable in the solution containing free oxygen in the oxidation zone. Chemical action and biochemical action with the participation of microorganisms will produce acidic water with high metal content such as sulfuric acid and copper sulfate and high total salinity. The reaction equation is [6, 23] (Formula (1))

The hot and rainy subtropical climate in this area is conducive to this process. In addition, ore mining, transportation, ore accumulation and other activities have significantly accelerated and strengthened the process. The high-salinity acidic water formed in the oxidation zone of sulfide deposits enters the soil in the form of surface runoff, underground runoff, irrigation, etc., and becomes an important way for copper to enter the soil.

In order to study the characteristics of copper accumulation in the soil and its influencing factors, a simulation experiment was carried out with the soil in the study area. In the experiment, the total irrigation amount is equivalent to 2 000 m3/mu of polluted field irrigation. The results show that the cumulative amount of copper in the soil is related to the concentration of copper in the solution and the acidity state. From the perspective of the influence of solution concentration, when the copper concentration in the copper-containing solution flowing through the soil is low, they can all be absorbed and maintained by the soil. The increase in copper in the soil layer is equivalent to the product of the volume of the solution entering the soil and the copper concentration. However, if the copper concentration in the solution exceeds a critical value, all the copper flowing through the soil will not be absorbed and retained, but a part of it will migrate with the water.

From the perspective of acidity, after the copper-containing acidic water flows through the soil column, the pH value of the leachate is a comprehensive reflection of the soil acidity, the acidity of the incoming copper-containing solution and the soil buffering performance. Experiments show that when the pH of the filtrate is less than 5, it is often accompanied by a certain degree of copper migration with water. It is worth noting that when the soil presents a strong acid reaction, the accumulation process of copper in the soil is different from the process in most soils in this region. Under the action of the solution with lower copper concentration, the leaching of copper occurs in the soil at the beginning, and then there will be its accumulation process (Table 1).

$$4CuFeS_2 + 17O_2 + 10H_2O \rightarrow 4Cu^{2+} + 4Fe(OH)_3 + 8SO_4^{2-} + 8H^+ \quad (1)$$

TABLE 1
Accumulation characteristics of copper in strong acid soil.

Cumulative irrigation amount (square/mu)		200	400	600	1000	1400	1800	2200
Cumulative amount of copper (mg/kg)	Irrigation copper concentration 1 mg/L	-72.23	-0.89	1.54	1.79	1.69	1.75	1.81
	Irrigation copper concentration 10 mg/L	-54.82	17.93	19.56	20.13	19.56	20.12	20.14
PH value of leachate	Irrigation copper concentration 1 mg/L	2.73	2.93	3.2	3.3	3.4	3.5	3.4
	Irrigation copper concentration 10 mg/L	2.71	2.94	3.1	3.3	3.5	3.5	3.5

Notes: The soil pH is 3.25 and the total copper content is 700 mg/kg.

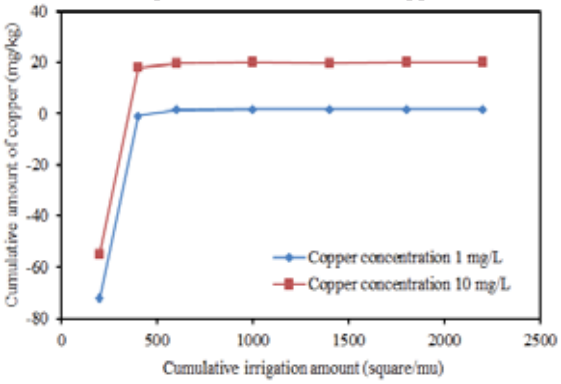


FIGURE 2
Relationship between the cumulative amount of copper in the strong acid soil and the cumulative irrigation amount.

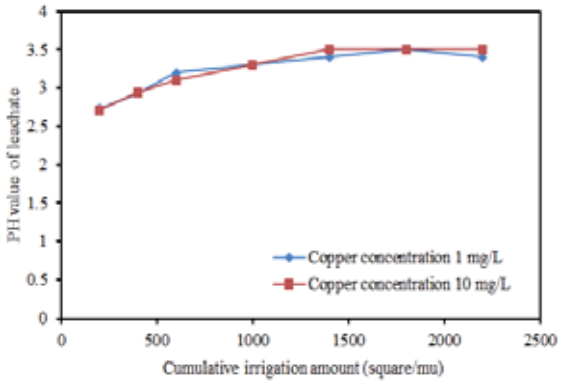


FIGURE 3
Relationship between pH value of leachate and cumulative irrigation volume in strong acid soil.

The relationship between the cumulative amount of copper in the strongly acidic soil and the cumulative irrigation amount is shown in Figure 2. With the increase of cumulative irrigation, the cumulative amount of copper increased very rapidly at first, and then the increase was greatly reduced. The relationship between the pH value of the leachate in the strongly acidic soil and the cumulative irrigation volume is shown in Figure 3. It can be found that the pH value of leachate in the strongly acidic soil gradually increases with the increase of the cumulative irrigation volume.

For most of the soil in the study area, when the copper-containing solution whose concentration exceeds a certain limit value, the retention of copper in the soil shows an exponential upward trend. When the copper concentration in the soil increases to a certain critical value, if the solution continues to enter, the soil retention of copper will increase very slowly. The copper actually retained in the soil is restricted by the amount of water entering the soil, the copper concentration in the solution, and the physical and chemical properties of the soil. It can be calculated according to the index model [17]:

$$S_t = S_m(1 - e^{-kcw}) \quad (2)$$

In the formula (2), St is the soil absorption concentration; Sm is the maximum absorbing capacity of the soil; k is a parameter related to soil properties; c is the copper concentration in the irrigation water; w is the irrigation volume.

The test results are consistent with the field survey results. A large area of soil in the study area will be affected by this factor. The contaminated soil studied in this article mainly refers to the resulting soil with high copper content.

Copper enrichment caused by water leaching soil factors. The retention time and intensity of copper in the soil are largely affected by the acidity of the soil and the leaching solution. In uncontaminated soil, the copper content in the water-soluble, substitutional and calculated soluble state is very low, so the difference is not much. Under the influence of the leaching solution, the leaching effect of copper is very insignificant or does not occur, which has little effect on the accumulation of copper in the soil. For example, when H_2SO_4 was used to adjust the pH value of the eluent to 4~6, no copper leaching in the soil layer was detected.

It is worth noting that in the subtropical copper-sulfur mining areas studied, the soil is relatively acidic under natural conditions, and its sensitivity to acid pollution is also relatively strong. Under the long-term influence of acidic water produced in the oxidation zone of sulfide deposits, the soil will be simultaneously affected by copper pollution and acid pollution. At this time, the proportion of active copper in the soil increases. After the leaching liquid interacts with the soil, if the pH value is within a certain range, the characteristic of copper in the soil will be filtered out.

Measurement results of copper leaching loss in soil under clear water conditions is shown in Table 2. The results showed that the stronger the soil acidity, the more obvious the leaching effect.

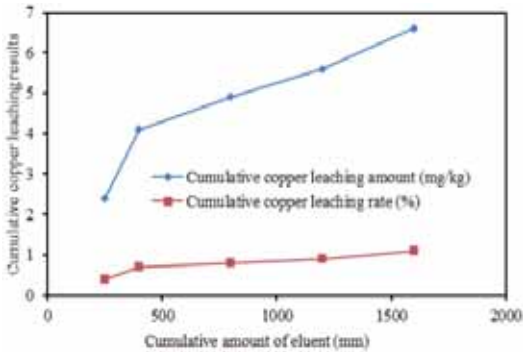


FIGURE 4
Relationship between the cumulative amount of eluent and the cumulative amount of copper leached under the condition of pH=5.2.

The relationship between the cumulative

amount of eluent and the cumulative amount of copper leached under the condition of pH=5.2 is shown in Figure 4. As the cumulative amount of eluent increases, the cumulative amount of copper leached gradually increases. As the cumulative copper leaching amount changed from 2.2 mg/kg to 6.6 mg/kg, the cumulative copper leaching rate increased from 0.4% to 1.1%.

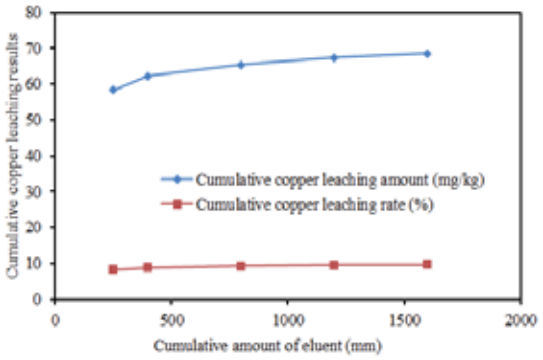


FIGURE 5
Relationship between the cumulative amount of eluent and the cumulative amount of copper leached under the condition of pH=3.4.

The relationship between the cumulative amount of eluent and the cumulative amount of copper leached under the condition of pH=3.4 is shown in Figure 5. As the cumulative amount of eluent increases, the cumulative amount of copper leached gradually increases. As the cumulative copper leaching amount changed from 58.3 mg/kg to 68.5 mg/kg, the cumulative copper leaching rate increased from 8.3% to 9.8%.

The test results show that when the contaminated soil is leached with clean water without or containing copper, the pH of the leachate is less than 5, and the leaching effect of copper is significantly enhanced. In the contaminated soil in the copper-sulfur mining area, leaching has an effect on reducing the accumulation in the soil layer under certain conditions. The retention time and accumulation process of copper in the soil in this area should be well taken into consideration.

Copper enrichment caused by vegetation factor. In order to determine the amount of copper harvested in the soil when crops are harvested, the enrichment coefficient of heavy metals is calculated. The enrichment coefficient refers to the ratio of the total amount of heavy metals in the crops per unit area to the total amount of heavy metals in the soil. The enrichment coefficient of crops has a complicated relationship with the copper content in the soil. Copper is an essential trace element in the process of crop production and development. The absorption of copper by crops is governed by its growth process to a certain extent, and it is rarely affected by the copper content in the soil environment. Only when the copper content in the soil reaches a certain limit, will the excessive accumulation of copper in the crops be made, thereby hindering its normal growth.

The farmland in the study area is mainly planted with double-cropping rice. According to the actual field survey results, when the copper concentration in the soil is 180-200 mg/kg, the enrichment factor is 0.000 2 to 0.000 3. It can be seen that the output of this process is very low, and its effect on the total accumulation of copper is not significant.

In summary, the high copper content in the parent rock or the high concentration of copper-containing water in the oxidation zone of the sulfide deposit enters the soil, which is the main reason for the increase in the copper content in the soil of the copper-sulfur mining area. In strongly acidic soils contaminated with copper, we should pay attention to the process of leaching with water to make copper migrate and export. The copper enrichment caused by the vegetation is relatively low.

CONCLUSIONS

(1) In this paper, taking copper-sulfur mines in the middle and lower reaches of the Yangtze River in China as an example, the tracer method was used to study the enrichment characteristics and sources of heavy metal pollution element copper in soil.

(2) Research results show that the sources of copper and sulfur in the soil in this area include copper-sulfur mine tailings, waste ore, organic and inorganic sulfur in the soil, and biological effects. The sulfur content in the soil around the copper-sulfur mine is close to the sulfur content of the ore by 20%~30%, indicating that the sulfur in the soil basically comes from tailings and waste ore; the copper content in the soil is also high, therefore, the pollution effect of the mine on the soil is obvious.

TABLE 2
Measurement results of copper leaching loss in soil under clear water conditions.

Cumulative amount of eluent (mm)		250	400	800	1 200	1 600
Experimental soil (pH=5.2)	Cumulative copper leaching amount (mg/kg)	2.4	4.1	4.9	5.6	6.6
	Cumulative copper leaching rate (%)	0.4	0.7	0.8	0.9	1.1
Experimental soil (pH=3.4)	Cumulative copper leaching amount (mg/kg)	58.3	62.3	65.4	67.4	68.5
	Cumulative copper leaching rate (%)	8.3	8.9	9.3	9.6	9.8

Notes: The copper content under pH=5.2 conditions is 600 mg/kg, and the copper content under pH=3.4 conditions is 700

mg/kg.

(3) The main sources of copper enrichment in the soil include acidic high-salinity water, water leaching the soil, and vegetation. Among them, acidic high-salinity water and water leaching of the soil are the main factors that cause copper enrichment in the soil, and the copper enrichment caused by the vegetation is relatively low.

ACKNOWLEDGEMENTS

We acknowledge the Engineering & Technical College of Chengdu University of Technology. This work was supported by the Academy Foundation [C122018032], the National Land and Space Application Research Center [C222019002]. Thank my colleagues for their help in my writing process. At the same time, I would like to thank Dr. Qiang Hao of Tongji University for helping me test the samples and giving me guidance in the process of writing.

REFERENCES

[1] Crerar, D., Barnes, H. (1976) Ore solution chemistry: Sotubilities of chalcopyrite and chalcocoite assemblages in hydrothermal solution at 200℃ to 350℃. Econ. Geol. 71, 772-794.

[2] Zhao, Y., Zhang, T., Tian, Z., Wu, D., Liang, K., Han, J. (2020) Research Progress on Phytoremediation Technology of Heavy Metal Contaminated Soil around Mining Area. Urban Geology. 15(1), 22-33.

[3] Candela, P., Holland, H. (1986) A mass transfer model fo rcopper and molybdenum in magmatic hydrothermal system: The origin of porphyry-type ore deposit. Econ. Geol. 81, 1-19.

[4] Ji, K., Wu, X., Zhang, G. (1989) The ore source, hydrothermal and heat source of hydrothermal deposits and the distribution of deposits. Beijing: Science and Technology Press. 1-131.

[5] Jiang, B., Zhang, B., Wang, X., Zhang, Q. (2020) Heavy Metal Pollution and Potential Risk Assessment of Soil in Fushun Western Open-Pit Mining Area. Journal of Northeastern University (Natural Science). 41(4), 568-574.

[6] Gao, Y., Zhang, R., Ye, C., Liu, C., Dai, G., Fan, L. (2020) Ecological risk assessment of heavy metal pollution in soil of a lead-zinc mine area in Danzhai County, Guizhou Province, China. 39(3), 928-936.

[7] Lu, J., Hua, R., Jiang, S. (2004) A study on copper iso tope compositions of Dexing porphyry Cu-Au deposit of Jiangxi, China. Geochimica et Cosmochimica Acta. 68(11), A302.

[8] Zhang, L., Liu, J., Chen, Z. (2012) The evolution of hydrogen and oxygen isotopes in the water-rock system of Dexing Copper Mine, Jiangxi. Chinese Journal of Geology. 31(3), 250-263.

[9] Zhang, J., Xu, Y., Chen, H., Ke, Y. (2020) Comparative Study of the Accumulated Effect of Heavy Metals on Soil and Wheat in Xiaoqiuling Gold Mining Area. Northwestern Geology. 53(3), 284-294.

[10] Sun, Y., Wang, X., Jiao, K., Duan, L., Lv, Z. (2020) Research Progress of Nitrogen Pollution Isotope Tracing in Freshwater Environment. Ecology and Environment Sciences. 29(8), 1693-1702.

[11] Tuli, J. (1985) Nuclear waller cards. Natural Nuclear Data Center, Brookhaven National Laboratory. 35-37.

[12] Cheng, J., Cai, S., Huang, M. (2021) Analysis on Speciation and Risk Assessment of Heavy Metals in Soils and Surface Sediments of Maoshi Molybdenum mining Area in Guizhou. Research of Soil and Water Conservation. 28(1), 353-359.

[13] Clayton, R. (1986) High temperature iso to pe effects in the early solar system. Reviews in Mineralogy. 16, 129-139.

[14] Guo, Q., Shi, X., Wang, H., Xu, H., Wu, J. (2019) Numerical analysis of the influencing factors for estimating DNAPL residual by the partitioning interwell tracer tests. Hydrogeology and Engineering Geology. 46(6), 165-172.

[15] Shields, W., Goldich, S., Gamer, E. (1965) Natural variations in the abundance ratio and atomic weight of copper. J. Geophys. Res. 70(2), 479-491.

[16] Walder, A., Freedman, P. (1992) Isotope ratio measurements using a double focusing magnetic sector mass analyzer with an inductively coupled plasmation source. J. Anal. At. Spectrom. 7, 571.

[17] Halliday, A., Lee, D., Christensen, J. (1995) Recent developments in inductively coupled plasma magnetic sector multiple collector mass spectrometry. Int. J. Mass Spec. Ion Proc. (146/147), 21-33.

[18] Huang, C., Huang, L. (2021) A review of pollution status and countermeasures of heavy metal pollution in Guangxi Manganese mining areas. Energy Environmental Protection. 35(1), 1-5.

[19] Cao, R., Fan, M., Huang, X., Hu, J., Qin, F., Zhang, Z. (2017) Application progress of isotope tracer technique for clarifying the origins of heavy metals in atmospheric particulate matter. Environmental Pollution and Control. 39(2), 212-216.

[20] Jiang, J., Dong, F., Liu, R., Yuan, Y. (2017) Applicability of Bayesian inference approach for pollution source identification of river chemical spills: A tracer experiment based analysis of algorithmic parameters, impacts and comparison with Frequentist approaches. China Environmental Science. 37(10), 3813-3825.

[21] Jiang, S., Woodhead, J., Yu, J. (2001) Preliminary determination of Cu isotopic composition of the Jinman hydrothermal vein copper deposit in Yunnan. Chinese Science Bulletin. 46(17), 1468-1471.
[22] Li, H., Chen, J., Cai, M. (2014) Using Isotopes to Trace Sources of the Heavy Metal Contaminations of the River: For Example the Zinc Isotopes of the Seine River. Bulletin of Mineralogy, Petrology and Geochemistry. 33(6), 941-949.
[23] Li, Z., Huang, T., Pang, Z., Xiong, D., Li, Y., Tian, J., Li, X., Ma, M., Hao, Y. (2019) study on groundwater baseline quality, monitoring indicators and contamination tracing methods related to shale gas development: A case study in the Fuling gasfield in SW China. Journal of Engineering Geology. 27(1), 170-171.

Received: **08.04.2021**
Accepted: **05.05.2021**

CORRESPONDING AUTHOR

Chong Chen
The Engineering & Technical College of Chengdu University of Technology,
Leshan 614000 – China

e-mail: chenyinggeology@126.com

© by PSP Volume 30– No. 09/2021 pages 10856-10862 Fresenius Environmental Bulletin

EXPERIMENTAL STUDY ON THE CONSTRUCTION AND PLUGGING PERFORMANCE OF RESIN GEL SYSTEM BASED ON NANO SILICON MATERIAL: A CASE STUDY OF BLOCK MJG-60, ORDOS BASIN, CHINA

Guocheng Wang[1], Zhixiong Xu[2], Xuewen Liu[3], Hengbo Mao[4], Wei Wang[5], Wenhua Zhao[6], Bo Wang[7], Wenjie Zhou[7], Mancang Dong[8,*]

[1]No.5 Oil Production Plant, Changqing Oilfield Company, PetroChina, Xi'an Shaanxi, 710018, China
[2]No.3 Oil Production Plant, Changqing Oilfield Company, PetroChina, Yinchuan Ningxia, 750006, China
[3]No.9 Oil Production Plant, Changqing Oilfield Company, PetroChina, Yinchuan Ningxia, 750001, China
[4]No.12 Oil Production Plant, Changqing Oilfield Company, PetroChina, Qingyang Gansu, 744505, China
[5]Changqing Downhole Technical Operation Company of CNPC Chuanqing Drilling Engineering Co., Ltd., Xi'an 710021, China
[6]The First Gas Production Plant, SINOPEC North China Petroleum Bureau, Yulin Shaanxi, 719002, China
[7]Shaanxi Hongfeng Petroleum Engineering Technology Co., Ltd, Xi'an Shannxi, 710007, China
[8]Fuxian Oil Production Plant, Yanchang Petroleum (Group)., Ltd., Fuxian Shaanxi, 716000, China

ABSTRACT

Based on the reservoir characteristics and the serious seepage loss of oil displacement fluid in the process of reservoir oil and gas exploitation in Block MJG-60, Ordos Basin, a new type of resin material with nano silicon (ODE) is designed, and a new type of nano silicone gel plugging system suitable for Block MJG-60 is constructed. The plugging rate and filtration volume are used as indexes to investigate the influence of the types of resin materials, the content and properties of nano silicone resin (ODE), and the core length on the plugging ability of resin gel plugging system. It is concluded that the plugging rate of nano silicone gel plugging system is 98.2% under the same conditions, which is much higher than 74.2% of commercial common resin gel system AB. The filtration capacity of the two resin gel systems is 9.5ml and 16.4ml, respectively. Among the four factors, the content of nano resin is the biggest factor that can affect the plugging ability of the gel system. When applied to Block MJG-60, the plugging ability could reach 98.9%, and the filtration capacity of the gel system is only 7.3ml, which can significantly improve the plugging ability of the oil field, providing basic data reference for improving working fluid filtration and reservoir plugging.

KEYWORDS:
Ordos Basin, Block MJG-60, reservoir plugging, nano silicone, gel oil displacement agent, reservoir reconstruction

INTRODUCTION

Many oil and gas exploitation blocks in Ordos Basin, such as Block MJG-60, have the characteristics of high porosity, wide distribution of fractures, and high permeability [1-5]. Because of the above reservoir characteristics, the working fluid filtration is large in oil and gas development, and the fracture sealing capacity is weak. Due to the high-water content of long-term development, the reservoir has many defects [6-9], which leads to the phenomenon of fluid pointing and water channeling in the oil and gas flooding gel system, leading to the reduction of oil recovery rate in oil and gas block in Ordos Basin.

Based on the above defects in the injection and production process of Block MJG-60in Ordos Basin, profile control and water plugging operations are mostly used to alleviate and control reservoir seepage and filtration problems [10-12]. Water plugging is an important part of the technology. Gel, microspheres, and inorganic salts are widely used, and the gel system is the most widely used [13-16]. Among them, the gel system is mostly made of resin material, which has many characteristics such as simple operation, low cost, temperature resistance, shear resistance and excellent plugging effect, and is widely used in profile control and water plugging of oil and gas reservoirs, especially in many oil and gas production blocks in Ordos Basin [17-22]. However, the temperature resistance and shear resistance of the resin gel system studied by colleges and universities are relatively poor, and the mechanical strength is the only way to maintain its shear resistance. Based on the resin gel system currently studied, it is of great practical significance to improve the injection and production capacity of Block MJG-60 in Ordos Basin to meet the plugging needs of each block in Ordos Basin.

In this study, a kind of resin material ODY was prepared based on the synthesized nano silicon material. The nano silicone resin gel system was constructed. The effect of the gel system on the core sealing capacity of low permeability reservoir was

explored under different factors. The physical simulation experiment was carried out to verify the core sealing capacity of Block MJG-60 in Ordos Basin, which provides basic data and reference for finding the gel freezing system suitable for the blocking capacity.

MATERIALS AND METHODS

Construction of nano silica gel system. (1) Test reagents and instruments. The experimental reagents needed for the synthesis of nano silica phenolic resin include 2,6-naphthalene diphenol (chemical purity, 99.9%), nano silica and hydroxyethyl methacrylate (chemical purity, 98.9%); acetaldehyde, toluene, cyclohexane, and deionized water purchased by Aladdin reagent company (chemical purity, 99.2%).

The experimental instruments include: cdm-2015 rotary evaporator provided by Shanghai Yarong biochemical instrument Co., Ltd., agitator bsy-291 provided by Shanghai Yiyi mechanical and Electrical Equipment Co., Ltd., dat-20 constant temperature water bath oil bath pot (Shanghai Kuncheng Scientific Instrument Co., Ltd.), amt-31 vacuum drying oven (Changzhou lino drying engineering machinery Co., Ltd.), and beaker, measuring cylinder and glass instruments purchased from Taizhou Yunyao Medical Equipment Co., Ltd.

(2) Synthesis method of nano silica phenolic resin. 14.5 g of 2,6-naphthalene diphenol and 50 ml of toluene wew added into a 100 ml three port flask, stir evenly, pour 7.4 g of hydroxyethyl methacrylate into the flask, and add 10 ml of deionized water and 2 ml of toluene 2 g nano silica powder into a 250 ml three port flask containing dried solid. Then, 150 ml cyclohexane is poured, heated at 55 °C, and stirred for 30 min. Finally, the mixture is taken out, dried at 150 °C to obtain pale yellow solid granular material, namely nano silica phenolic resin (Figure 1).

(3) Preparation of nano silica phenolic resin gel. We take 1L sealed pressure vessel, pour into a certain quality of nano silicon resin, deionized water, various chemicals and polyacrylamide, and then seal it, mix it continuously, and keep it for standby at room temperature.

Sealing performance of nano silica phenolic resin gel system. (1) Sealing parameter measurement device of nano silica phenolic resin gel system. Figure 2 shows the core plugging rate measuring device, which is modified from the conventional oil displacement device based on the conventional oil field working fluid. As the most important data index to characterize the plugging ability of the gel system, the plugging rate can be obtained by measuring the permeability of the reservoir core after the modification of the gel system.

Like other oil displacement equipment, the plugging rate measuring equipment also includes five parts as shown in Figure 2. The mixing system, temperature and pressure fine-tuning system, pressure system and data processing system are auxiliary systems, which are responsible for the preparation of gel system, the stability of test environment and the calculation and characterization of later data. As the most important part of the plugging rate, the detailed structure of the core displacement system is shown in Figure 2b. The core with a certain length and diameter is added into the core holder, and a confining pressure is filled. The nano silicone gel system enters from the inlet at a certain speed, and continuously accumulates the pressure until it breaks through the maximum principal stress of the core and flows out from the end of the core holder. At this time, the breakthrough pressure is recorded as the maximum wind pressure P1. The average flow velocity and pressure difference Δ P are calculated after flowing for 15 min according to the current flow velocity, so as to calculate the permeability and plugging rate.

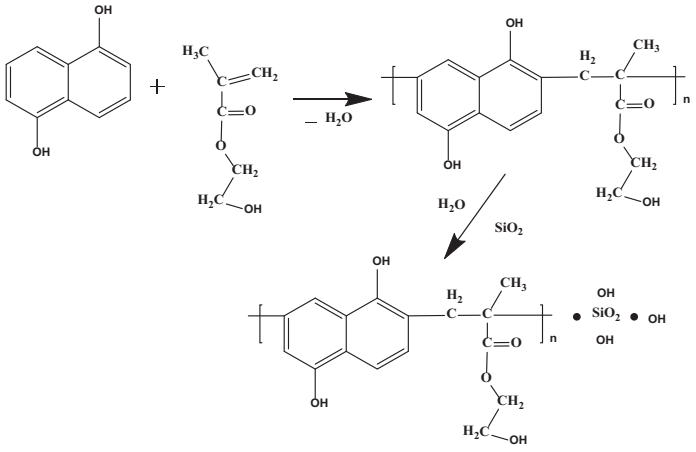


FIGURE 1
Preparation method of nano silica phenolic resin.

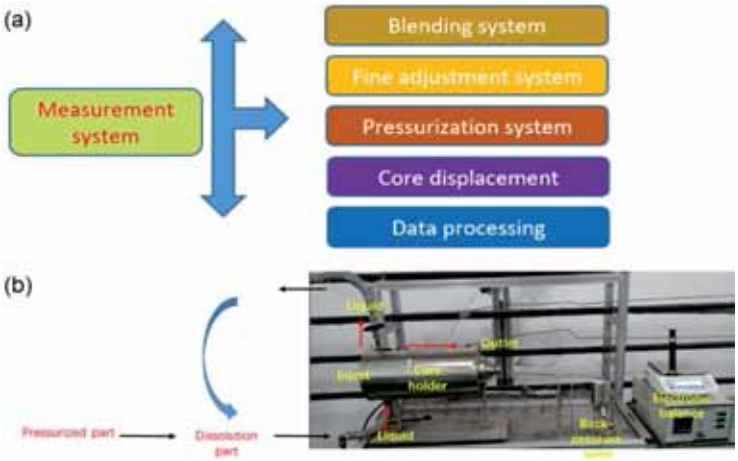


FIGURE 2
Plugging performance measuring device of nano silica phenolic resin ODY gel system.

(2) Filtration volume of gel system. The method for measuring the filtration volume of the gel system is: Based on the measuring device shown in Figure 2, deionized water is injected around the core holder to set the confining pressure, and the nano silicone gel system is injected at a certain flow rate. After a period, the gel system can break through the maximum principal stress of the core and flow out of the core. After 15 minutes of flow, the flow volume can be observed, and the filtration volume V_{max} of gel system can be measured.

(3) Core plugging rate. The sealing capacity of the nano urea formaldehyde resin gel system to the reservoir rocks is mainly based on the plugging rate. In this study, according to the industrial standard sy-t5358-2016, the initial permeability K_1 of natural rock core with different permeability is determined after treatment, and the core is saturated with crude oil. The treated core is placed in the core holder and flows through the resin gel system. The pressure to the outlet and the flow rate of the outflow fluid will not change any more. The permeability K_2 is obtained by Formula 1. The permeability of its gel system to the core is calculated according to Formula 2.

$$K = \frac{QL\mu}{\Delta PA} \quad (1)$$

$$\kappa = \frac{K_1 - K_2}{K_1} \times 100\% \quad (2)$$

Formula 2 is the core plugging rate; K_1 is the initial permeability, $\times 10^{-3}$ μm^3; K_2 is the late core permeability, $\times 10^{-3}$ μm^3.

RESULTS

Based on the gelling system plugging measuring equipment constructed in Figure 2, this study explores the influence of nano silicone phenolic resin ODY gelling system on core plugging performance parameters such as plugging rate and filtration volume when different factors change. The gelling system constructed by commercially available common resin is taken as reference to show the excellent plugging ability of nano silicone resin on core.

Influence of phenolic resin types on core plugging. Under the experimental conditions of 20 cm core length, 130 °C, 20 MPa, 0.2% resin concentration and permeability of 18×10^{-3} um^2, the effects of different phenolic resin types on core plugging rate and filtration volume are discussed.

As shown in Table 1, the influences of the nano silica phenolic resin ODY and market resin freeze-gel system on the plugging rate and filtration volume of the reservoir core are shown in Table 1. When the resin concentration of the two systems is 0.2%, the plugging rate of the prepared nano silica phenolic resin ODY gel system to the core is 98.2%, which is much higher than 74.2% of the commercial common resin gel system AB system. The core filtration volume of ODY and AB resin gel system is 9.5ml and 16.4ml, respectively. The nano silica gel system has significantly improved the core sealing ability, which helps to reduce the serious problems of the loss of the gel during the flooding.

TABLE 1
Influence of phenolic resin ODY and AB resin gel system on core plugging rate and filtration loss

Type	Factors	Plugging rate /%	Filtration rate /ml
ODY	0.2%	98.2%	9.5
	120℃	98.7%	8.9
AB	0.2%	74.2%	16.4
	120℃	75.3%	16.1

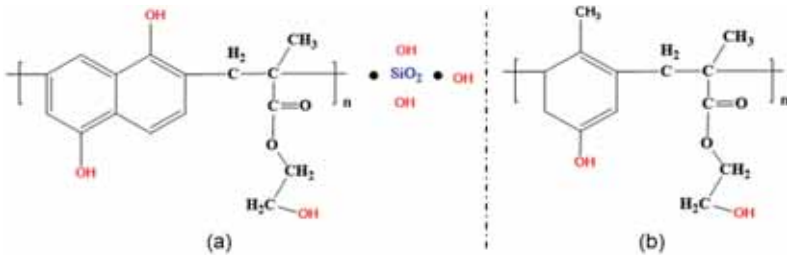


FIGURE 3
The difference of hydroxyl -OH distribution between resin ODY and resin AB.

No matter the change of resin concentration or temperature, ODY shows greater core sealing ability and smaller gel system filtration volume than AB, depicting better working fluid sealing ability for core. The main reason is that there are more hydroxyl groups in the resin than in the polyacrylamide hydrogen bonds. A lot of hydroxyl groups are formed around the nano silicon, so there are more amide groups in the part of nano silicon, which increases the ability to attract amide groups (Figure 3).

Effect of nano silica on the concentration of phenolic resin. Under the experimental conditions of 20cm core length, 130 °C, 20 MPa and permeability of 18×10^{-3} um^2 permeability, the effects of different resin concentrations in gel system on core plugging rate and filtration volume are discussed.

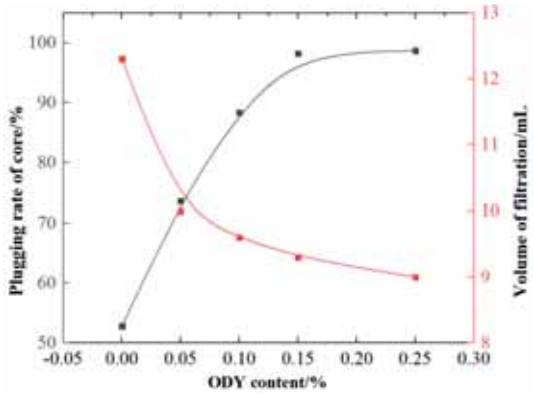


FIGURE 4
Effect of concentration of nano silica phenolic resin ODY on core plugging rate and filtration volume.

The relationship curve between resin concentration and plugging rate and filtration volume in gel system is shown in Figure 4. In Figure 4, with the increasing of the concentration of nano silicone resin in the resin gel system, the plugging rate of the core increases obviously, while the filtration volume of the core decreases obviously. The results show that the change of core plugging rate and filtration volume of nano silicone ODY gel system presents an obvious reverse trend. The increase of plugging ability leads to the decrease of fluid filtration volume of gel system, and the ability of core fracture blocking is significantly enhanced.

With the increase of the concentration of nano silicone resin, less gel fluid can not flow out through the core fracture, and the loss is significantly reduced, which is conducive to the pressure of oil displacement fluid to the maximum principal stress of the reservoir, so as to realize the fracture expansion and increase the sweep efficiency. When the concentration of nano silicone resin in the gel system increases from 0 % to 0.25%, the core plugging rate increases from 52.8% to 98.7%, while the filtration volume of the gel system decreases from 12.1 ml to 9.2 ml. With the increasing concentration of nano silicone resin, it shows excellent plugging and anti-filtration ability to reservoir rocks.

The reasons for the excellent core sealing performance are as follows: when there is no nano silica resin, the gel system cannot be formed. At this time, only the interaction between polyacrylamide and water molecules forms the intermolecular hydrogen bond, and each polyacrylamide molecule is bonded. The plugging rate is still 52.8% and the filtration volume is still 12.1ml when the concentration is 0 (Figure 5). However, with the increase of the concentration of nano silicon resin, polyacrylamide can not only hydrolyze and bind with each other, but also the amide group in the acyl ammonia molecule can combine with a large number of hydroxyl OH of nano silicon resin ODY to lose a molecule of water, thus forming hydrogen bond. The hydrogen bond increases with the increase of ODY concentration of nano silicon resin. The micro grid in the system shows a higher density, the filtration volume is reduced, and the plugging capacity is enhanced.

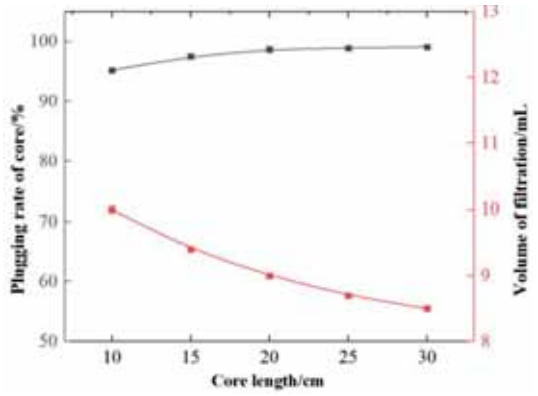


FIGURE 6
Effect of different core length on plugging rate and filtration volume.

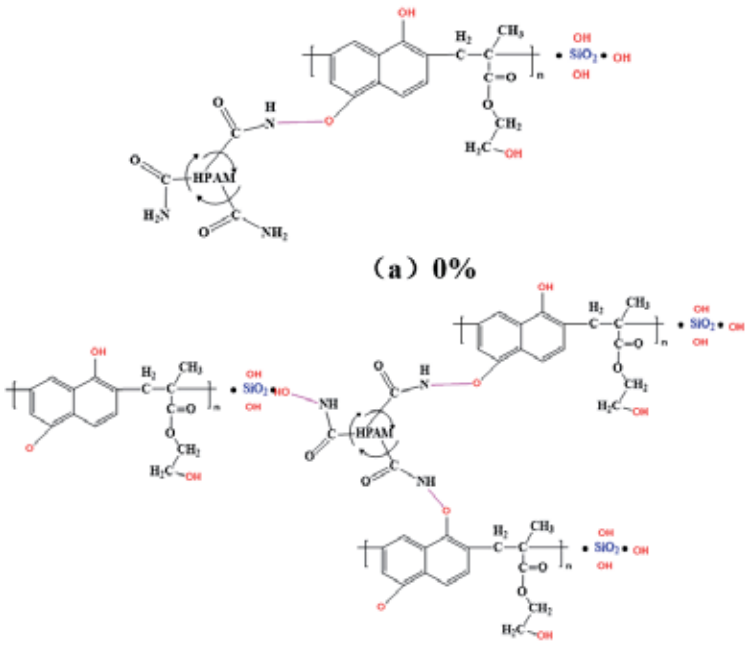


FIGURE 5
Schematic diagram of hydrogen bond formation between resin ODY and polyacrylamide.

Influence of core length on core plugging performance. The effects of core length (10cm, 15cm, 20cm, 25cm and 30cm) on core plugging rate and filtration volume are studied in a nano silicone gel system with 0.25% nano silicone concentration, 130 °C, 20 MPa and permeability of 18 × 10^{-3} μm^2.

As shown in Figure 6, the plugging performance of nano silicone gel system is tested by selecting cores with different lengths. With the increasing of core length, the plugging rate increases slightly, while the filtration volume decreases slightly. However, the change trend of plugging rate and filtration volume is obviously lower than that caused by the concentration of nano silicone resin. When the core length is less than 20cm, the plugging rate of the core increases significantly with the increase of the core length, and the filtration volume of the nano silicone gel system in the core decreases significantly. When the length of the core is higher than 20cm, the plugging rate of the gel system on the core is gradually gentle, and there is no obvious change. The filtration volume is no longer greatly reduced and stabilized.

The main reason is as shown in Figure 7. When the core length is short, because of the existence of confining pressure, the nano silicone gel system can only flow laterally, and the shorter core can be completely swept in a relatively short time, and then it is easier to flow out through the core holder outlet, resulting in poor sealing ability. However, when a long core is encountered, even if the gel system particles do not seal the core fracture near the entrance, the probability of sealing the core fracture behind the fracture increases significantly, thus reducing the filtration volume of the gel fluid and improving its sealing ability. It can be seen from Figure 6 that when the core length is 20cm, it can have excellent plugging ability.

Field test. Based on the above physical model test data of plugging performance of nano silicone gel system, this study selects Block MJG-60 of Ordos basin for field plugging test. The reservoir conditions of this block are as follows: well depth is 2500m, porosity is 14%, permeability is 18 × 10^{-3} μm^2, injection pump pressure is 18Mpa, casing pressure is 17Mpa, single day injection volume of resin gel system is 20m^3, and the continuous injection days are 30 days. The water yield, plugging rate, maximum pump pressure and permeability data of Block MJG-60 are shown in Figure 8.

As shown in Figure 8, when Block MJG-60 is injected, the water output of the reservoir is large. The plugging rate is close to 50%, which is far lower than 95% of the industry standard. The maximum pump pressure is small, and the working fluid can not hold pressure in the oil and gas reservoir. The permeability is large, and the sealing of reservoir fractures cannot be completed. But after 10 days of using nano silica resin ODY gel system, the water output, plugging rate, maximum pump pressure and permeability are improved obviously. The water output is only 0.6m^3, the pump pressure is obviously increased, the permeability decreases rapidly, and the plugging rate reaches over 98%. The results are consistent with the physical model test data under this condition. The ODY gel system can be used for Block MJG-60 sealing.

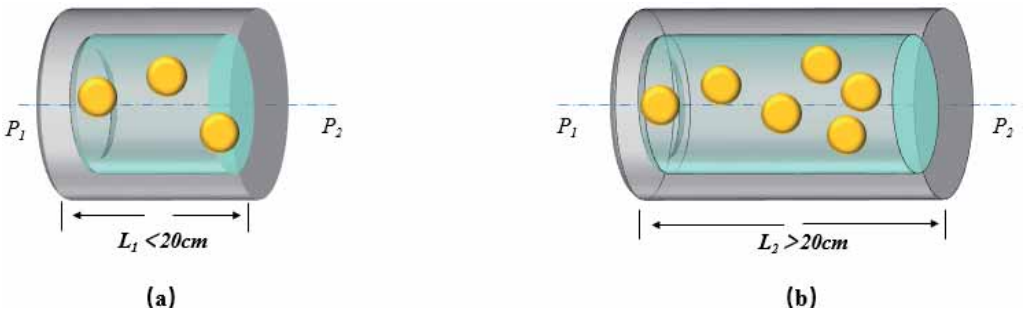


FIGURE 7
Fracture sealing ability of gel particles with different core lengths.

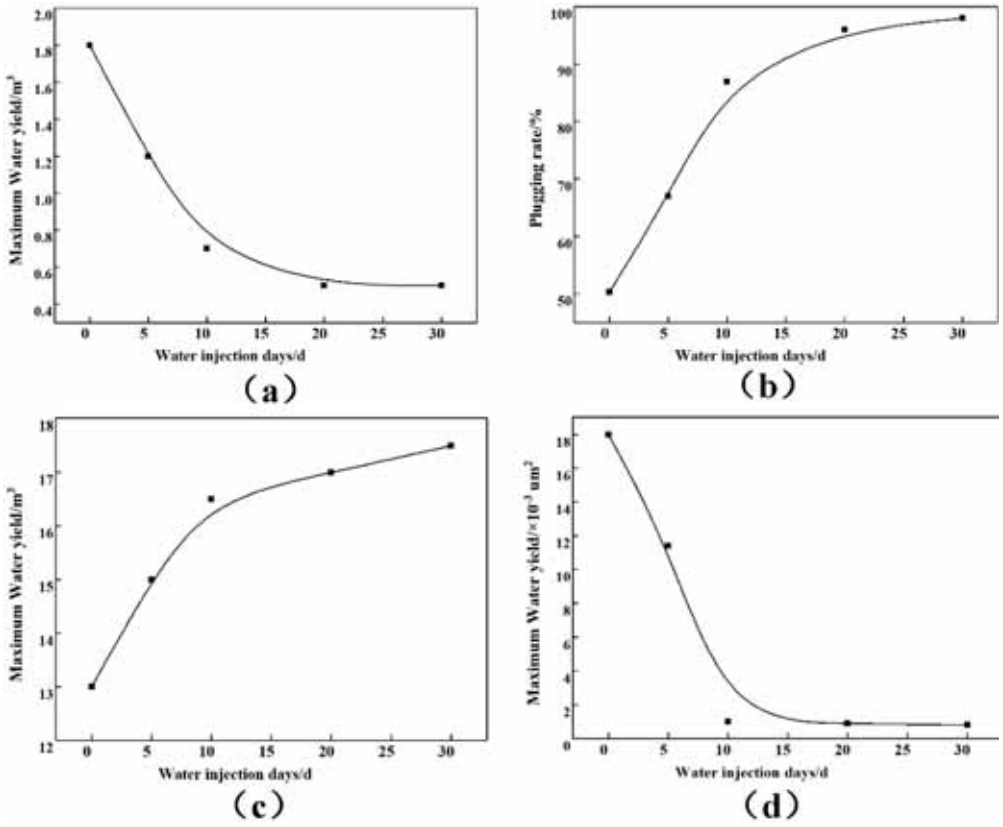


FIGURE 8
Field data of Block MJG-60 with nano silicone gel system.

CONCLUSIONS

(1) The results show that the ODY can form a temperature resistant and shear resistant gel sealing system with polyacrylamide, and its sealing capacity for reservoir fractures is significantly higher than that of commercial resin AB. The plugging rate increases obviously, and the filtration volume decreases obviously.

(2) There are more hydroxyl groups on the surface of nano silicone resin, which can hydrolyze with amide group in polyacrylamide, form intermolecular hydrogen bond, increase the interaction between molecules, and increase the system forming ability. The temperature resistance, shear resistance and plugging performance are mainly adjusted by the micro grid density constructed by intermolecular hydrogen bonds. The larger the grid density is, the stronger the plugging ability is.

(3) The field data of Block MJG-60 in Ordos Basin are in good agreement with the physical model test data, and the plugging rate is over 98%, which can be used to achieve excellent plugging capacity on site.

ACKNOWLEDGEMENTS

This work was not financially supported by any funds. We want to show sincere thanks to all the techniques who have helped this research and all the authors of the references.

REFERENCES

[1] Fu, S., Wang, W., Li, X., Xi, S., Hu, X., Zhang, Y. (2021) Volume fracturing and drainage technology of low pressure marine shale gas reservoir in Ordos Basin. Natural Gas Industry. 41(03), 72-79.

[2] Li, H., Li, Y., Guo, Z. (2021) Pore characteristics of Ordovician rocks in southern Ordos Basin. Contemporary Chemical Industry. 50(03), 669-672.

[3] Sun, X., Liang X., Wang S., Lu, Y. (2014) Experimental study on the rheology of CO_2 viscoelastic surfactant foam fracturing fluid. Journal of Petroleum Science and Engineering. 119(1), 104-111.

[4] Li, Q., Jiang, Z., You, X. (2016) Heterogeneity characteristics and main controlling factors of lacustrine deep water turbidite reservoir in Shang 847 block, Huimin Sag. Petroleum Geology and Recovery Efficiency. 23(05), 44-49.

[5] Zhang, H., Wang, R., Li, X. (2021) Stress field simulation of Chang 7 formation in Ansai area, Ordos Basin. Science Technology and Engineering. 21(04), 1342-1349.

[6] Wang, S., Xiao, L. (2021) Characteristics of Chang 71 reservoir in xin'anbian area, Ordos Basin. Petroleum Geology and Engineering. 35(01), 47-51.

[7] Zhang, J. (2013) Logging response characteristics and evaluation of heterogeneous heavy oil reservoir. Petroleum Geology and Recovery Efficiency. 20(03), 41-45.

[8] Wu, X. (2018) Production variation of Daqing placanticline oilfield after fine water drive potential tapping measures in ultra-high water cut stage. Petroleum Geology and development in Daqing. 37(05), 71-75.

[9] Yan, M., Zhao, J., Cao, Q., Wu, H., Huang, Y. (2021) Reservoir characteristics of Permian Shihezi Formation in Linxing area, Ordos Basin. Lithologic Reservoirs. 33(2), 49-58.

[10] Gong, Q., Wei, X., Xin, D. (2021) Research progress of water shutoff and profile control agent in Oilfield. Petrochemical Industry Application. 40(1), 10-13.

[11] Han, J., Zhao, Y., Yang, L. (2020). Research status and development trend of profile control and plugging agent for Oilfield. Yunnan Chemical Technology. 47(12), 14-16.

[12] Zhang, J., Yang, B., Li, Y., Wu, R. (2020) Application of oil well reverse profile control (water shutoff) technology in low permeability oilfield, Journal of Yanan University (Natural Science Edition). 39(03),61-64.

[13] Li, B., Shi, D., Lv, Q., Bai, H., Zheng C., Xu J. (2018) Experimental study on rheological properties of thinkened CO_2 in liquid and supercritical state. Petroleum Science and Technology. 36(22), 1913-1919.

[14] Yu, L., Li, Y., Gong, H. (2016). Viscoelastic branched precrosslinked gel particle flooding for enhanced oil recovery after polymer flooding in heterogeneous reservoirs. Petroleum Geology and Recovery Efficiency. 23(1), 113-118.

[15] You, Q., Yu, H., Wang, Y. (2009) Research progress of deep profile control technology in domestic oilfield. Fault-Block Oil Gas Field. 16(4), 68-71.

[16] Yu, L., Li, Y., Gong, H. (2015). Evaluation of plugging properties and profile control ability of precrosslinked gel particles. Petroleum Geology and Recovery Efficiency. 22(5), 107-112.

[17] Guo, Y., Ma, S., Ni, B. (2004) Synthesis of sulphonated polyacrylamide used as oil displacement agent and study on its performance. Journal of Xi'an Petroleum University. 3(01), 29-31.

[18] You, Q., Yu, H., Wang, Y. (2009) Research progress of deep profile control technology in domestic oilfield. Fault-Block Oil Gas Field. 16(4), 68-71.

[19] Wang, X. (1988) Polymer profile control and injectability test in Gangxi experimental area of Dagang Oilfield. Oil Drilling & Production Technology. 7, 77-79.

[20] Zhong, H., Kong, X., Chen, S., Grady, B., Qiu, Z. (2021) Preparation, characterization and filtration control properties of crosslinked starch nanospheres in water-based drilling fluids. Journal of Molecular Liquids. 325, 115221.

[21] Cui, Q. (2015) Application status and development trend of profile control and water shutoff technology. Science Guide. 3, 246-247.

[22] Wang, G., Wu, J., Zhang, Y., Zhang, P., Guo, L. (2020) Preparation of gel water plugging and profile control agent controlled by low temperature and time. Applied Chemical Industry. 49(9), 2229-2232.

Received: **08.04.2021**
Accepted: **05.05.2021**

CORRESPONDING AUTHOR

Mancang Dong
Fuxian Oil Production Plant,
Yanchang Petroleum (Group). Ltd.,
Fuxian Shaanxi 716000 – China

e-mail: dongmancang_year@163.com

© by PSP Volume 30– No. 09/2021 pages 10863-10870 Fresenius Environmental Bulletin

GAMMA RAY RADIATION RESEARCH IN BUILDING MATERIALS

Aydan Altikulac*

Mugla Sitki Kocman University, Ula Ali Kocman Vocational School, 48640, Ula, Mugla, Turkey

ABSTRACT

Building materials used in the construction industry, such as marble, granite, ceramics, travertine, and cimstone, are of crustal origin and contain natural radiation. While these materials act as a source of natural radiation inside the building, they actually serve as a shield by blocking external radiation. Therefore, these building materials can also be considered as radiation-shielding materials. In the first part of this study, activity concentrations of radioactive isotopes in materials used in construction industry were determined via gamma spectrometry. The activity concentrations of ^{226}Ra, ^{232}Th and ^{40}K radioactive isotopes in marble samples were measured as 10.5,14.3 and 584.6 Bqkg^{-1}, respectively. In granite samples, the activity concentrations of radioactive isotopes were found to be 72.3, 63.5, 1024.7 Bqkg^{-1}, respectively. In ceramic samples , the activity concentrations of radioactive isotopes were found to be 39.8, 68.5, 1338.7 Bqkg^{-1}, respectively. In the experiment performed using travertine samples, the activity concentrations of radioactive isotopes were calculated to be 5.9, 9.9 and 1338.7 Bqkg^{-1}, respectively. The activity concentrations of radioactive isotopes in cimstone samples were measured as 6.78, 26.9 and 649.7 Bqkg^{-1}, respectively. Radium equivalent activity caused by these activities was 21.6, 101.46, 32.29, 91.7, and 47.51 Bqkg^{-1} for marble, granite, travertine, ceramic, and cimstone, respectively. The second part of the study focused on the use of building materials as shielding materials. Mass attenuation coefficient μ/ρ (cm^2/gr), and half value layer (HVL) values, representing the radiation interaction with the material used for shielding, were examined individually for marble, granite, travertine, ceramic, and cimstone samples. The attenuation coefficients were measured for gamma energies from ^{152}Eu, ^{137}Cs, and ^{60}Co sources. The obtained experimental data were compared with the theoretical values calculated using WinXCom software, and the results were found to be compatible.

KEYWORDS:
Natural radioactivity, radiation shielding, mass attenuation coefficient, building material, XRF

INTRODUCTION

Radiation is a phenomenon that exists in the earth's crust, air, and water. People are continuously exposed to terrestrial and cosmic radiations that constitute natural radiation sources as a result of internal and external irradiations, depending on the geological structure of the region where they live and the quality of their lives. Because people spend most of their time in closed buildings such as homes and workplaces, it is important to know the radiation dose they are exposed to and determine the level of radiation in buildings. Studies show that the amount of radiation inside a building is relatively small compared to the amount of radiation outside a building, and the dose rates of radiation absorbed inside the building particularly depend on the location of the building and the type of construction material used. In buildings with a stone, brick, or concrete exterior, gamma rays from external sources are greatly absorbed by the walls, while the dose rate absorbed inside the buildings depends on the activity concentration of natural radionuclides in the construction materials used [1]. In the literature, there are studies for the investigation of radioactivity in the construction industry [2-16]. With the rapid development of nuclear technology worldwide, nuclear activities have increased, causing the development of anti-radiation measures to be inevitable. However, in medicine, it is impossible to completely abandon radiation, which is used in diagnostics and treatment and provides benefit in this aspect. Therefore, in the field of medicine, methods have been developed to reduce the harmful effects of radiation while utilizing its beneficial effects. The most effective way of protection from the harmful effects of gamma rays emitted by radiation sources is shielding. The material that is used in shields to reduce the dose of radiation is called shield material; the choice of the material depends on the type of radiation. The greater the density of the shield material, the greater its radiation-shielding effect. There are several studies on the shielding properties of building materials [17-23].

MATERIALS AND METHODS

Radioactivity measurements. Forty-four building materials procured from different factories and enterprises in Turkey were used in the experiments. ORTEC's 905-4 (3" × 3") model NaI (Tl) scintillation detector-based gamma spectrometer system was used for measurements. The resolution of the system is 2% at 0.5 MeV and 1.3% at 2 MeV (for 1 μCi ^{137}Cs at a distance of 10 cm). The thickness of the detector's Al container is 0.5 mm. Standard RGU-1 uranium, RGTh-1 thorium, RGK-1 potassium sources, and point ^{60}Co source with known gamma energies, as referenced were used for calibration of the system. The activity concentration of ^{226}Ra radioactive isotope was calculated by selecting photo peak of ^{226}Ra (186 keV), ^{214}Pb (295 and 351 keV), and ^{214}Bi (609 keV) energy. The activity concentration of ^{232}Th radioactive isotope was calculated using photo peak of ^{228}Ac (911 keV) and ^{208}Tl (583 keV) gamma energies. The activity of ^{40}K radioactive isotope was calculated using photo peak of 1460 keV energy specific to this radioactive isotope. The activity concentration values obtained as a result of measurements are shown in Table 1.

TABLE 1
Activity concentration values measured in samples

Sample ID		Activity concentration in (Bqkg^{-1})		
		^{226}Ra	^{232}Th	^{40}K
Marble	Range	1.17-28.64	4.7-30.7	492.1-700.4
	Average	10.53	14.3	584.5
Granite	Range	4.9-290.9	6.5-128.5	698.6-1886.0
	Average	72.3	63.5	1024.7
Ceramic	Range	6.7-93.9	43.1-133.8	1154.3-1793.9
	Average	39.8	68.2	1383.7
Travertine	Range	3.1-8.0	5.5-26.8	317.2-812.2
	Average	5.9	9.9	410.6
Cimstone	Range	3.9-57.0	6.9-65.0	495.9-1088.1
	Average	6.7	26.9	649.7

Radium equivalent activity. Radium equivalent activity (Ra_{eq}) is a parameter used for evaluating radioactivity caused by radium, thorium, and potassium. The radium equivalent activity was calculated using Eq.(1) [24-25].

$$Ra_{eq}=C_{Ra}+1{,}423C_{Th}+0.077C_K \quad (1)$$

where C_{Ra}, C_{Th}, and C_K are the activity concentrations of ^{226}Ra, ^{232}Th, and ^{40}K radioactive isotopes in Bqkg^{-1}.

External and internal hazard index. To determine gamma radiation hazard, external (Iɣ) and internal hazard indices were calculated using the activity concentrations of ^{226}Ra in uranium decay series, and the activity concentrations of ^{232}Th and ^{40}K in thorium decay series. For building materials, external hazard index (Iɣ) was calculated using Eq.(2)

$$I\gamma = \frac{CTh}{200} + \frac{CRa}{300} + \frac{CK}{3000} \quad (2)$$

To evaluate the additional alpha radiation caused by inhalation of ^{222}Rn gas, internal hazard index (Iα) was calculated using Eq. (3) [26].

$$I\alpha = \frac{CRa}{200} \quad (3)$$

According to European Commission (EC) , the external hazard index (Iɣ) and the internal hazard index (Iα) used to evaluate the amount of radiation being exposed to due to the inhalation of radon gas must be less than 1 in order to meet the safety requirements of building materials. This can be achieved if the activity of ^{226}Ra is less than 200 Bqkg^{-1} [27]. The external and internal hazard indices and equivalent radium activity calculated using measured activities are shown in Table 2.

TABLE 2
Calculated radiological parameters

Sample	Ra_{eq} (Bqkg^{-1})	Activity index	
		I ɣ	Iα
Marble	75.93	0.26	0.05
Granite	240.04	0.85	0.36
Ceramic	241.89	0.93	0.19
Travertine	51.56	0.18	0.02
Cimstone	94.95	0.36	0.03

Gamma transmission technique. Using gamma transmission technique, the radiation attenuation effect of materials can be measured experimentally. This technique is based on the interaction of gamma rays with the material through which they pass [28]. Gamma rays lose part of their energy when they interact with materials; the linear attenuation coefficient (μ) of the material against gamma ray, mass attenuation coefficient (μ/ρ), and minimum thickness value (HVL) that the material must have to reduce the intensity of radiation by half are calculated and the count value is obtained as a function of energy and the density of the material. The radiation permeability of the material varies depending on its chemical content. The chemical content of ceramic, granite, and marble used in this study was determined using XRF technique and as shown in Table 3. The chemical content of cimstone and travertine was taken from the articles mentioned in Table 3. In this part of the study, the radiation attenuation effect

of marble, granite, ceramics, travertine, and cimstone was calculated using gamma energies of 121.78, 244.7, 344.28, 661.64, 778.9, 964.08, 1085.9, 1173.2, 1332.5, and 1408 keV obtained from Eu-152, Cs-137, and Co-60 point standard sources. The experimental results obtained were compared with the theoretical values obtained using WinXCom software [29]. Experimental apparatus based on gamma transmission technique is described in Figure 1, so that there would be a distance of 70 mm between the detector and the sample, and a distance of 175 mm between the standard point gamma ray source and the sample. To obtain a thin beam in apparatus, the collimator was designed to have a diameter 0f 30 mm. The materials were placed between the gamma ray source and the NaI(Tl) detector.

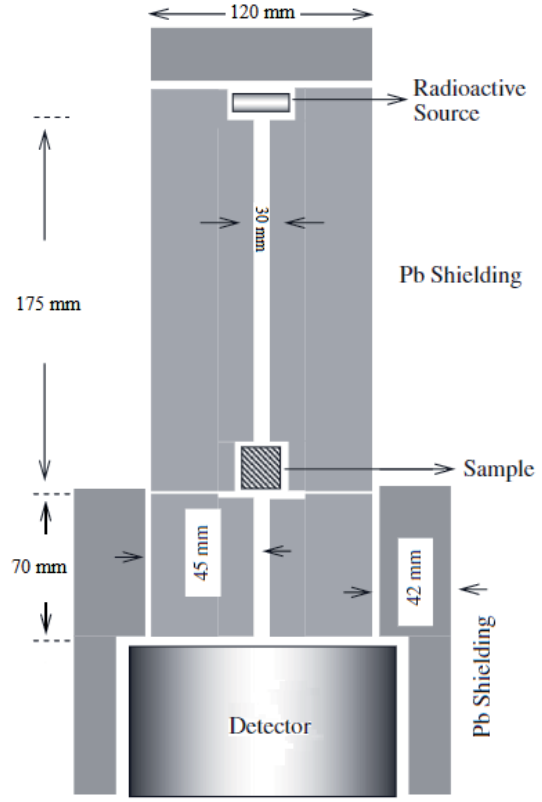


FIGURE 1
Schematic view of the experimental setup

RESULT AND DISCUSSION

Radiological evaluations. In the experiments performed using eight different marble samples, it was found that the activity concentration of ^{226}Ra ranged from 1.17 to 28.64 Bqkg^{-1}, while the average activity concentration of ^{226}Ra was 10.53 Bqkg^{-1}. In the same experiment, it was determined that the average activity concentration of ^{232}Th was 14.37 Bqkg^{-1}, while the average activity concentration of ^{40}K was 584.54 Bqkg^{-1}. In the experiments performed using ten different granite samples, it was determined that the average activity concentration of ^{226}Ra ranged between 4.91–290.08 Bqkg^{-1}, and the average activity concentration was 72.39 Bqkg^{-1}. It was found that the average activity concentration of ^{232}Th was 63.55 Bqkg^{-1}, ranging from 6.56 to 128.5 Bqkg^{-1}. In the granite samples, the average activity concentration of ^{40}K radioactive isotope was found to be 1024.73 Bqkg^{-1}.In the experiment performed using seven different ceramic samples, the average activity concentrations of ^{226}Ra, ^{232}Th, and ^{40}K radioactive isotopes were found to be 39.80 Bqkg^{-1}, 68.20 Bqkg^{-1}, and 1383.70 Bqkg^{-1}, respectively. In the experiment performed using nine different travertine samples, the average activity concentrations of ^{226}Ra and ^{232}Th radioactive trackballs were determined as 5.96 Bqkg^{-1} and 9.93 Bqkg^{-1}, respectively. In the same samples, the average activity concentration of ^{40}K radioactive isotope was found to be 410.67 Bqkg^{-1}.In the experiment performed using ten different cimstone samples, the average activity concentration of ^{226}Ra and ^{232}Th radioactive isotopes were found to be 6.78 Bqkg^{-1} and 26.9 Bqkg^{-1}, respectively, and the average activity concentration of ^{40}K radioisotope was found 649.77 Bqkg^{-1}. Based on UNSCEAR 2000 report values, it can be said that the average activity concentrations of ^{226}Ra and ^{232}Th radioactive isotopes detected for marble, ceramics, travertine, and cimstone were considerably smaller than the world average [30]. The granite measurements indicated that the average activity concentration of ^{226}Ra radioactive isotope was twice the world average, while the average activity concentration of ^{232}Th radioactive isotope was 1.5 times the world average. The measurements for ceramics and travertine indicated that the average activity concentration of ^{40}K radioactive isotope was below the world average. In the measurements for marble and cimstone, the average activity concentration of ^{40}K radioactive isotope was slightly above the world average, and the average concentration of activity of ^{40}K radioactive isotope was 2.5 times the world average. Radium equivalent activity caused by these activities was 21.6, 101.46, 32.29, 91.7, and 47.51 Bqkg^{-1} for marble, granite, travertine, ceramic, and cimstone, respectively. Radium equivalent activity value is 370 Bqkg^{-1}, as reported by the Nuclear Energy Agency (NEA) [31] . As it is seen in Table 2, the external hazard index (Iγ) and internal hazard index (Iα) indices are less than 1. In many countries, there are studies aimed at determining natural radioactivity levels in building materials. Table 4 summarizes the studies conducted in some countries. Comparing with the results of studies in different countries, it can be said that the average radioactivity concentration for many materials used in the construction industry in Turkey is lower than the limit values.

TABLE 3
Chemical contents (%by weight) of building materials

	Na_2O	MgO	$A_{l2}O_3$	SiO_2	P_2O_5	SO_3	Cl	K_2O	CaO	TiO_2	Fe_2O_3	Loss H_2O	Total
Ceramic T1200011390	2.4	0.85	18.14	71.44	-	-	-	3.62	1.02	0.55	-	1.75	0.2
Cimstone [32]	0,15	0.40	0.02	96.51	0.06	0.19	0.01	0.10	1.48	0.93	-	0.09	-
Granite T120001139	3.26	0.45	13.24	73.32	-	-	-	5.26	1.21	0.316	-	2.59	0.34
Marble T120001139	0.01	3.85	0.01	0.01	-	-	-	0.01	51.72	0.01	-	0.196	42.48
Travertine [33]	0.2	0.2	0.1	0.4	0.0	-	-	0.1	52.6	0.0	0.0	0.2	44.94

TABLE 4
Similar studies conducted in different countries

Sample	Country	Activity concentration in $Bqkg^{-1}$			Ra_{eq} ($Bqkg^{-1}$)	References
		^{226}Ra	^{232}Th	^{40}K	Ra_{eq}	
Marble	India	9.25	61.63	1366.85	202.63	[5]
	Saudi Arabia	5.8	2.3	33.7	11.6	[6]
	Turkey	5.4	4.9	49.7	54.88	[7]
	Tunis	33.24	8.01	116.98	-	[15]
	This paper	10.5	14.3	584.6 1	73	
Granite	India	6.17	4.62	39.17	23.49	[5]
	Egyptian	32.46	47.46	1314.82	-	[8]
	Saudi Arabia	54.5	43.4	667.7	168.7	[6]
	This paper	72.3	63.5	1024.7	240.0	
Cermaic	Egypt	51.12	40.52	682.6	-	[8]
	Saudi Arabia	47.18	80.7	590.2	207.2	[6]
	Turkey,	31±5	28±12	358±31	81	[10]
	Algerian	136	52.4	491.33	252.31	[9]
	Italy	50±2	59±2	520±22	-	[16]
	This paper	39.8	68.2	1338.7	242.8	
Travertine	Turkey	0.8	0.9	4.1	-	[7]
	Italy	5.4	13.5	65.6	75.2	[11]
	This paper	5.9	9.9	410.6	51.6	
Cimstone	Turkey	2.4	4.6	47.8	-	[7]
	This paper	6.78	26.9	649.7	99.9	

Investigation of mass attenuation coefficients. In this part of the study, gamma spectrometer system was used for attenuation coefficients measurements. The sample was placed between the gamma source and the detector. The radiation attenuation of ceramic, cimstone, granite, marble, and travertine samples produced in Turkey, were investigated. These materials are widely used as construction materials in public and commercial buildings. In this study, ceramic, cimstone, granite, marble, and travertine tiles measured 3–4 cm × 3–4 cm × 0.5–2 cm and their masses varied from 15 to 50 g. Content analysis of ceramic, granite, and marble was done using XRF technique with codes T1200011390, T1200011392, and T1200011391, respectively. The chemical contents of cimstone and travertine were taken from the studies indicated in Table 3 [32-33]. The mean density of ceramic, cimstone, granite, marble, travertine respectively is 2.36 $grcm^{-3}$, 2.15 $grcm^{-3}$, 2.6 $grcm^{-3}$, 2.78 $grcm^{-3}$, 2.44 $grcm^{-3}$.In this part of study, we investigate the gamma attenuation of building materials. Comparison of mass attenuation coefficients of gamma ray sources is as shown in Figures 2,3,4,5 and 6, respectively. The solid line shows the calculated results with WinXCom; the points shows experimental results obtained in this

study. In most cases, experimental and theoretical calculations were in good agreement. The differences between the mass attenuation coefficients are thought to be related to the chemical composition of the material. It can be said that the mass attenuation coefficient obtained experimentally decreases with increasing energy. With this study, experimental calculations showed that building materials can be used as an alternative material against radiation, especially at low energies.

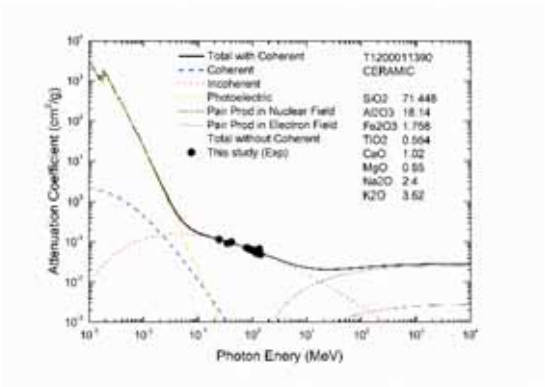


FIGURE 2
Comparison of mass attenuation coefficients of gamma ray sources of ceramic samples

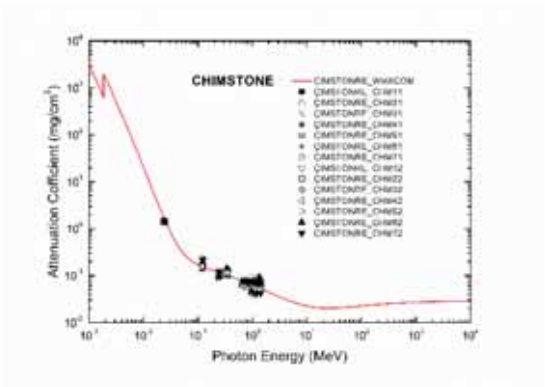


FIGURE 3
Comparison of mass attenuation coefficients of gamma ray sources of cimstone samples

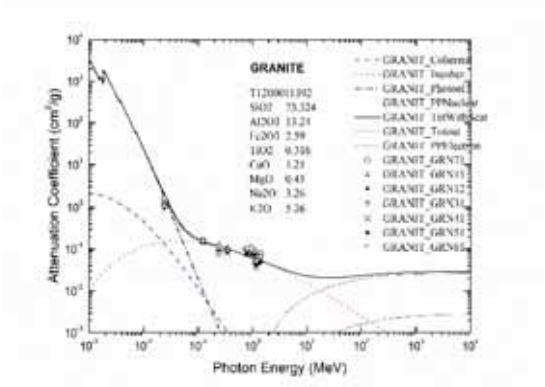


FIGURE 4
Comparison of mass attenuation coefficients of gamma ray sources of granite samples

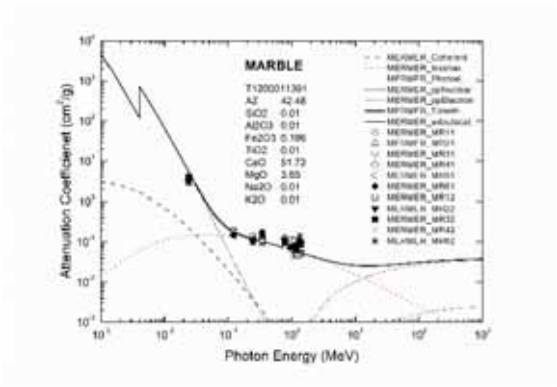


FIGURE 5
Comparison of mass attenuation coefficients of gamma ray sources of marble samples

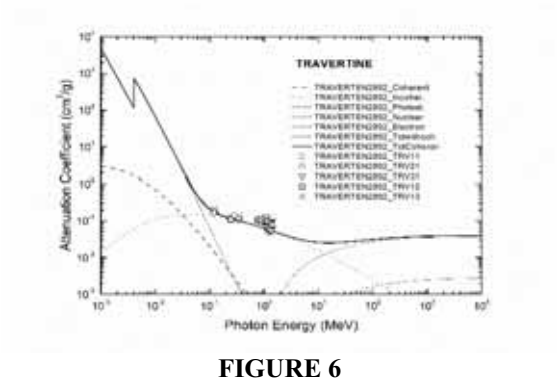


FIGURE 6
Comparison of mass attenuation coefficients of gamma ray sources of travertine samples

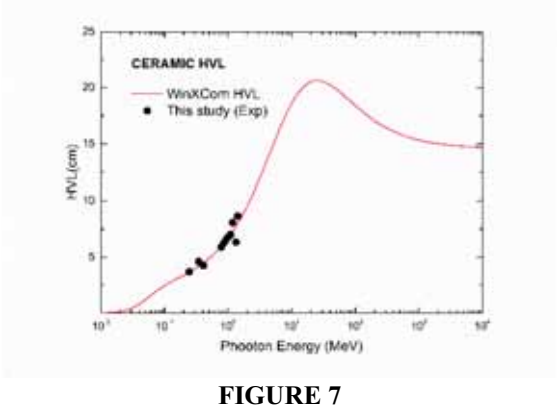


FIGURE 7
The plot of half value layers of ceramic.

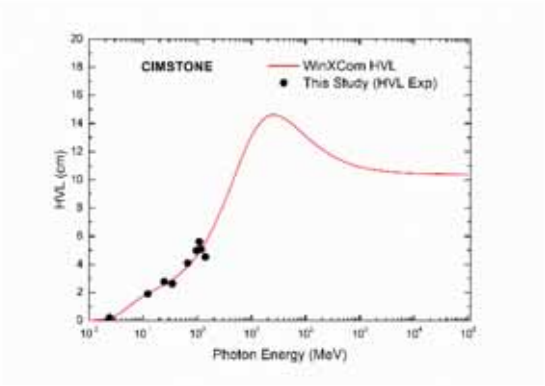


FIGURE 8
The plot of half value layers of çimstone.

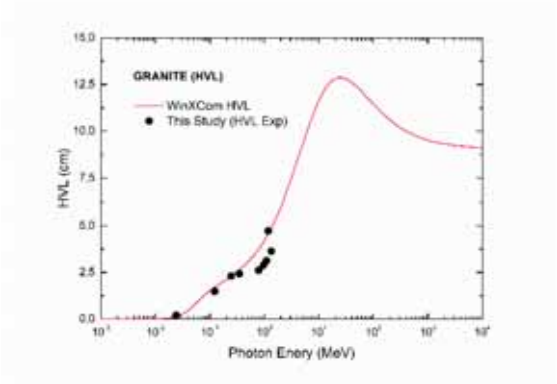


FIGURE 9
The plot of half value layers of granite

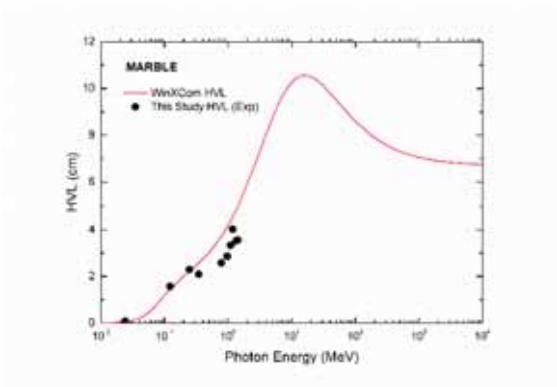


FIGURE 10
The plot of half value layers of marble

The measured and calculated half value layers (HVL) results for building materials are given in Figures 7,8,9,10 and 11, respectively. It can be seen that the experimental and theoretical values fit well as shown in these figures.

CONCLUSIONS

The activity concentrations of radionuclides building materials used in construction industry were determined using gamma spectrometric method. Radium equivalent activity indices as well as external and internal activity indices, which contribute to the protection of human health in the long term, were calculated based on the determined activity results. The results of the experiment were evaluated based on the standard data adopted by the UNSCEAR and EC commissions. The results of the study in different countries suggest that the activity and radiological parameter values in most building materials were lower than the limit values. In this study, the radium equivalent activity calculated for selected building materials was found less than the limit value of 370 $Bqkg^{-1}$. It was also seen that the materials used in the experiment met the requirement for the hazard index to be less than 1. On the contrary, it was seen that granite materials contained potassium activity above the limit value, which was because of its geological structure.

Experimental and theoretical studies were conducted to have an idea about the radiation permeability of building materials. Obtained results proved that the radiation permeability of materials exposed to different gamma energies shows similar changes.

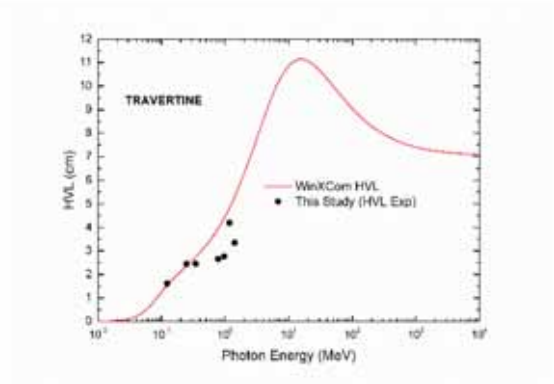


FIGURE 11
The plot of half value layers of travertine

ACKNOWLEDGEMENT

I would like to thank Esan Chemistry Laboratory of Eczacıbaşı for XRF measurements.

REFERENCES

[1] Kaynar, M., Tekinarslan, E., Keskin, S., Buldu, İ., Sonmez, M.G., Karatag, T. and Istanbulluoğlu, M.O. (2015) Effective radiation exposure evaluation during a one year follow-up of urolithiasis patients after extracorporeal shock wave lithotripsy. Central European Journal of Urology. 68, 348-52.

[2] Turhan, Ş., Yıldırım, A., Kurnaz, A., Hancerlioğulları, A., Altıkulaç, A., Atıcı, E., Varınlıoğlu, A. and Bassarı, A. (2018) A Survey on elemental distrubitions of volcanıc tuff quarıes in Turkey. Fresen. Environ. Bull. 26, 2087-2092.

[3] Turhan, Ş., Temirci, A.T., Kurnaz, A., Altıkulaç, A., Gören, E., Karataşlı, M., Kırısık, R. and Hançerlioğulları, A. (2018) Natural radiation exposure and radon exhalation rate of building materials used in Turkey. Nuclear Technology and Radiaiton Protection. 33, 159-166.

[4] Joel, S.H., Maxwell, O., Adewoyin, O.O., Eromosele, E.C., Embong, Z. and Saed, M.A. (2018) Assesment of natural radionuclides and its hazards from tiles made in Nigeria. Radiation Physics and Chemistry. 144, 43-47.

[5] Raviolsankar, R., Suganya, M., Vanasundari, K., Sivakumar, S., Senthilkumar, G., Chandramohan, J., P, Vijayagopal. and Venkatraman, B. (2011) Measurement of natural radioactivity in common building materials used in Tiruvannamalai, Tamilnadu, India. Radiation Protection and Environmental. 34, 171-177.

[6] Hamernah, I. F. A. (2017) Radiological hazards for marble, granite and ceramic tiles used in buildings in Riyadh Saudi Arabia. Environmental Earth Sciences. 76, 516-611.

[7] Turhan, Ş., Baykan, U.N., Şen, K. (2008) Measurement of the natural radioactivity in building materials used in Ankara and assessment of external doses. Journal of Radiological Protection. 8, 83-92.

[8] Shoeib, M.Y. and Thabayneh, K.M. (2014) Assessment of natural radiation exposure and radon exhalation rate in various samples of Egyptian building materials. Journal of Radiaton Research and Applied Sciences. 7, 174-181.

[9] Abdelfettah, B. and Tedjani, A. (2012) Natural Radioactivity Measurements for Some Algerian Building Materials. Journal of Physical Sciences and Application. 2, 171-174.

[10] Tufan, M.C. and Dışcı, T.(2013) Measurement of natural radioactivity in biulding materials used in Samsun, Turkey. Radiation Protection Dosimetry. 156, 87-92.

[11] Righi, S. and Bruzzi. L. (2006) Assesment of natural radiaiton expousure and radon exhalatıon in building materials used in Italian dwellings. Journal of Environmental Radioactivity 88, 158-70.

[12] Turhan, Ş., Akyürek, S., Erdoğan, M., Kurnaz, A. and Altıkulaç, A. (2017) Health hazards due to the exposure to radon in school of the Cappadocia Region. Nuclear Tehnology and Radiation Protection. 32, 174-179.

[13] Kayakökü, H., Karatepe, Ş. and Doğru, M. (2016) Measurement of radioactivity and dose assesments in some building materials in Bitlis, Turkey. Applied Radiation and Isotopes. 115, 172-179.

[14] Elnobi, S., Harb, S. and Ahmed, N.K. (2017) Influence of grain size on radionuclide activity concentrations and radiological hazard of building materials samples. Applied Radiation and Isotopes. 130, 43-48.

[15] Manai, K., Ferchichi, C., Oueslati, M. and Trabelsi, A. (2012) Gamma radiation measurements in Tunision marbles. World Journal of Nuclear Science and Technology. 2, 80-84

[16] Bruzzi, L., Baroni, M., Mozzat, G., Mele, R. and Righi, S. (2000) Radioactivity in raw materials and end products in the Italian ceramics industry. Journal of Environmental Radioactivity. 47, 171-181.

[17] Akman, F., Turan, V., Sayyed, M.I., Akdemir, F., Kaçal, M.R., Durak, R. and Zaid, M.H.M. (2019) Comprehensive study on evaluation of shielding parameters of selected soils by gamma and X-rays transmission in the range 13.94–88.04 keV using WinXCom and FFAST programs. Results in Phys. 15, 102751

[18] Salinas, I.C.P., Conti, C.C. and Lopes, R.T. (2006) Effective density and mass attenuation coefficient for building material in Brazil. Applied Radiation and Isotopes. 64, 13-18.

[19] Araz, S.O., Gümüş, H., Bayca, S.U. and Aydın, A. (2021) Investigation of gamma-ray attenuation coefficients for solid bronized 304L stainless stell. Applied Radiation Isotopes.170, 109605.

[20] Sharaf, J.M. and Saleh, H. (2015) Gamma-ray energy buildup factor calculations and shielding effects of some Jordanian building structures, Radiation Physics and Chemistry. 110, 87-95.

[21] Mavi, B.(2012) Experimental investigation of γ-ray attenuation coefficients for granits. Annals of Nuclear Energy.44, 22-25

[22] Medhat, M.E. (2009) Gamma-ray attenuation coefficients of some building materials available in Egypt, Annals of Nuclear Energy. 36, 849-852.

[23] Singh K., Singh S., Dhaliwal A.S. and Singh, G. (2015) Gamma radiation shielding analysis of lead-flyash concretes, Applied Radiation and Isotopes. 95, 174-179.

[24] Beretka, J. and Mathew, P. J. (1985) Natural radioactivity of Australian building materials, industrial wastes and by-products. Health Phys. 48, 87–95.

[25] Yang, Y.X., Wu, X.M., Jiang, Z.Y., Wang, W.X., Lu, J.G., Lin, J., Wang, L.M. and Hsia, Y.F. (2005) Radioactivity concentrations in soils of the Xiazhuang granite area, Chin. Applied Radiation and Isotopes. 63, 255-259.

[26] Trevisi, R., Risica, S., Alessandro, MD., Paradiso, D. and Nuccetelli, C. (2012) Natural radioactivity in building materials in the Europen Union: a database and an estimate of radiological significance. Journal of Environmental Radioactivity. 105,11-20.

[27] EC (European Commission) (1999) Radiation protection 112. Radiological Protection Principles Concerning the Natural Radioactivity of Building Materials, Directorate General Environment, Nuclear Safety and Civil Protection .

[28] Büyük, B. and Tugrul, B.A. (2015) Investigation on the behavıours of TiB_2 reinforced B_4C-SiC composites against Co-60 gamma radioısotopes source. Pamukkale University Journal of Engineering Sciences. 21, 24-29.
[29] Medhat, M.E. and Singh. V.P. (2014). Mass attenuation coefficients of composite materials by Geant4, XCOM and experimental data: comparative study. Radiation Effects and Defects in Solids. 169, 37-41.
[30] United Nations Scientific Committee on the Effects of Atomic Radiation (UNSCEAR). (2000) Sources and Effects of Ionizing Radiation, United Nations Scientific Committee on the Effects of Atomic Radiation, United Nations Publication, New York,USA. pp.1-21.
[31] Nuclear Energy Agency (NEA) (1979). Exposure to radiation from natural radioactivity in some building materials. Report by NEA Group of Experts, Organization for Economic Co-Operation and Development, Paris, France. 35-45
[32] Çelik, F. and Işık, İ. (2016) A preliminary study on the Use of waste silica in floor tile Production, UCTEA Chamber of Metallurgical & Materials Engineers, Proceedings Book. 18, 137-144.
[33] Çobanoğlu, I. and Çelik, S.B. (2012). Determination of strength parameters and quality assessment of Denizli travertines (SW Turkey). Engineering Geology. 129, 38–47.

Received: **08.04.2021**
Accepted: **17.05.2021**

CORRESPONDING AUTHOR

Aydan Altikulac
Mugla Sitki Kocman University,
Ula Ali Kocman Vocational School,
48640 Ula Mugla – Turkey

e-mail: aydanaltikulac@mu.edu.tr

© by PSP Volume 30– No. 09/2021 pages 10871-10879 Fresenius Environmental Bulletin

EFFECTS OF PHYSICOCHEMICAL FACTORS ON THE NITROGEN TRANSFORMATION FUNCTIONAL GENES OF MICROORGANISMS DURING THE INTERMITTENT AERATION IN POLLUTED RIVER

Hua Zhang[1,2], HaiTao Tao[1,2], Jian Huang[1,2], ShanShan Xi[1,2,*], JinHua Wang[1,2], Tao Luo[1,2], XueFeng Cao[1,2]

[1]Anhui Provincial Key Laboratory of Environmental Pollution Control and Resource Reuse, Hefei, 230601, P.R. China
[2]School of Environmental and Energy Engineering, Anhui Jianzhu University, Hefei, 230601, P.R. China

ABSTRACT

The nitrogen transformation functional genes in microbes are the basis of biological nitrogen removal. It is significant to study the effect of physicochemical factors in sediment on nitrogen transformation genes during the biological nitrogen removal. The fluorescence quantitative PCR was used to detect the abundance of nitrogen transformation genes. The redundancy analysis and the variation partitioning analysis were used to analyze the physicochemical factors affecting nitrogen transformation function genes. The abundance of nitrogen transformation functional genes showed that the short-cut biological nitrogen removal was achieved with the intermittent aeration method. During the short-cut nitrification stage, the ammonia monooxygenase (*amoA*) gene had an obvious growth trend, and that there was no significant change in the nitrous oxide reductase (*nxr*) gene, which indicated that ammonia nitrogen was mainly converted into nitrite nitrogen. During the short-cut denitrification stage, the copper type nitrite reductase gene (*nirK*) and the cytochrome nitrite reductase (*nirS*) genes increased significantly, but the nitrate reductase (*narG*) gene did not change much, which indicated that the transformation of nitrite nitrogen to nitric oxide is the main reaction in short-cut denitrification. Redundancy analysis showed that, during the short-cut nitrification stage, the amoA gene was positively correlated with the dissolved oxygen and the ammonia nitrogen; During the short-cut denitrification stage, the *nirK* gene, the *nirS* gene, the nitrous oxide reductase (*nosZ*) gene, the hydrazine synthase (*hzsA, hzsB*) gene and the hydrazine oxidase (*Hzo*) gene were negatively correlated with the dissolved oxygen. The results of the variance partitioning analysis showed that, during the short-cut nitrification stage, the dissolved oxygen, the ammonia nitrogen and the C:N (carbon to nitrogen ratio) were the main factors affecting the nitrogen transformation functional genes. However, the dissolved oxygen, the nitrite nitrogen and the total organic carbon were the main factors affecting the nitrogen transformation functional genes.

KEYWORDS:
Nitrogen transformation function gene, intermittent aeration, physical and chemical factors, redundancy analysis

INTRODUCTION

Excessive nitrogen destroys the ecological balance of water, and leads to water eutrophication in rivers [1-3]. As a result, it is urgent to control the pollution of the endogenous nitrogen when the exogenous nitrogen is under control [4]. Intermittent aeration is an energy-saving and high-efficiency technology to eliminate the endogenous nitrogen [5-6], which can effectively remove nitrogen in the river through biological nitrogen removal [7-9].

Under intermittent aeration, the nitrogen transformation is an important way to realize biological nitrogen removal in river. The nitrogen transformation functional genes are the basis of nitrogen transformation [10-12]. Studies have shown that the nitrogen transformation functional genes play an important role during the process of the biological nitrogen removal [13-15]. However, the nitrogen transformation functional genes are susceptible to the environment. Studies have shown that aeration of groundwater may bring about the enrichment of the nitrogen transformation functional genes[21]. Long-term fertilization in soil can also increase the abundance of nitrogen transformation functional genes [22]. However, there are few researches on the effect of physicochemical factors on nitrogen transformation function genes during the process of biological nitrogen removal.

Therefore, this study makes efforts to investigate the effects of different physicochemical factors on the nitrogen transformation functional genes [26-

28]. In this study, intermittent aeration was used to remove endogenous nitrogen in river. The polymerase chain reaction, agarose gel electrophoresis, and quantitative real-time PCR were used to analyze the abundance of the nitrogen transformation functional genes. The methods of the redundancy analysis and the variational partitioning were used to analyze the effects of different physicochemical factors on the nitrogen transformation functional genes [29-30]. This study may provide theoretical support for further study on the mechanism of biological nitrogen removal by intermittent aeration.

MATERIALS AND METHODS

Experimental device and design. In the experiment, the reactor was designed to simulate the river system. The reactor is a cuboid, with the length, width and height being 21cm, 20cm and 51 cm. The lower part of the reactor was covered with black opaque plastic film as light shading. The sediment and overlying water of the reactor were taken from the Shiwulihe River in Hefei city in China. The ratio of sediment to water is 1:3. The dissolved oxygen in overlying water is controlled at 5.5 mg/L by air pump and flowmeter. The dissolved oxygen was monitored by the on-line monitor of dissolved oxygen. The experiment lasted 138 days. The first 12th days were stable period, the 13-41th days, the 80-90th days, the 114-117th days and the 130-135th days were aeration periods, and the rest were non-aeration periods.

Collection and detection of water samples and sediment samples. The water samples were collected at the depth of 5 cm below the water surface. Each time three samples were taken at different locations, and then were mixed. Total nitrogen was measured by alkaline potassium persulfate digestion with Ultraviolet Spectrophotometry (HJ 636-2012), ammonia nitrogen was measured by Nessler's reagent spectrophotometry (HJ 535-2009), nitrate nitrogen was measured by ultraviolet spectrophotometry (HJ/T 346-2007), and nitrite nitrogen was measured by spectrophotometry (GB 7493-87).

During the short-cut nitrification stage, the sediment samples were taken from the aeration stage during the 13-41th days (the 13th day, the 21st day, the 26st day, the 32st day, and the 41st day). These days were tagged as SN1, SN2, SN3, SN 4 and SN5. During the short-cut denitrification stage, the sediment samples were taken during the 42-79th days (the 50th day, the 56th day, the 63th day, the 67th day, and the 79th day). These days were tagged as SD1, SD2, SD3, SD4 and SD5.

Quantitative analysis of functional genes. (1) Extraction and PCR amplification of total DNA. The total DNA was extracted by E.Z.N.A.™ Soil DNA Kit(50) kit. The extracted DNA samples were stored in -20°C freezer for fluorescence quantitative determination of functional gene abundance. The PCR amplification was performed by Stepone real-time PCR instrument (ABI, USA).(2) Fluorescence quantitative analysis. The abundance of 11 functional genes was determined by real-time fluorescent quantitative PCR (AB Applied Biosystems) and Kapa SYBR @ fast qPCR kit Master Mix universal (Kapa biosystems, Boston, USA). The primers of functional genes for nitrogen transformation are shown in Table 1.

Data analysis method. Redundancy analysis was implemented with R programming language (version 3.2.0) to study the physicochemical factors affecting nitrogen transformation function genes; The variation partitioning was used to analyze the effects of the physicochemical factors on the nitrogen transformation functional genes.

RESULTS AND DISCUSSION

Nitrogen transformation during intermittent aeration in overlying water. The nitrogen transformation during intermittent aeration is shown in Figure 1. As can be seen in Figure 1, during the stage of aeration (13-41 d), ammonia nitrogen concentration gradually decreased to 0.12 mg/L, the nitrite nitrogen gradually increased to 31.25 mg/L, and the nitrate nitrogen gradually increased to 0.37 mg/L. The results showed that nitrification occurred in the stage of aeration. However, during the stage of non-aeration (42-79 d), the ammonia nitrogen increased to 19.04 mg/L due to the release of sediment, the nitrite nitrogen gradually decreased to 0.14 mg/L, the nitrate nitrogen gradually decreased to 0.025 mg/L. The results showed that denitrification occurred in the stage of non-aeration. Finally, the total nitrogen decreased to 0.64 mg/L after repeated aeration and non-aeration, but the nitrate nitrogen changed little (0~0.38 mg/L). The results showed that the short-cut biological nitrogen removal was achieved with the method of intermittent aeration of overlying water in river.

TABLE 1
Primers of amplifying nitrogen transformation functional genes by real time PCR

Gene name	Primer	Primer sequence (5'→3')	Base number	Amplified fragment length	Initial copy number($\times 10^8$)
amoA (*Archaeal*)	Arch-amoAF Arch-amoAR	STAATGGTCTGGCTTAGACG GCGGCCATCCATCTGTATGT	20 20	635	1.59
amoA (*Bacterial*)	amoA1F amoA2R	GGGGTTTCTACTGGTGGT CCCCTCKGSAAAGCCTTCTTC	18 21	491	2.54
nxr	F1norA R2norA	CAGACCGACGTGTGCGAAAG TCCACAAGGAACGGAAGGTC	20 20	322	3.28
narG	narG1960m2f narG2050m2r	TAYGTSGGGCAGGARAAACTG CGTAGAAGAAGCTGGTGCTGTT	21 22	100	1.07
nirK	F1aCu R3Cu	ATCATGGTSCTGCCGCG GCCTCGATCAGRTTGTGGTT	17 20	473	3.25
nirS	R3cd Cd3aF	GASTTCGGRTGSGTCTTGA GTSAACGTSAAGGARACSGG	19 20	425	1.39
cnorB	cnorB2F cnorB6R	GACAAGNNNTACTGGTGGT GAANCCCCANACNCCNGC	19 18	389	2.21
nosZ	nosZ1F nosZ1R	WCSYTGTTCMTCGACAGCCAG ATGTCGATCARCTGVKCRTTYTC	21 23	259	8.30
hzsA	hzsA_382F hzsA_1353R	GGYGGDTGYCAGATATGGG ATAHCCTTCMACHTTCACCT	19 20	800	4.48
hzsB	hzsB_396F hzsB_742R	ARGGHTGGGGHAGYTGGAAG GTYCCHACRTCATGVGTCTG	20 20	300	5.12
hzo	hzocl1F1 hzocl1R2	TGYAAGACYTGYCAYTGG ACTCCAGATRTGCTGACC	18 18	470	1.31

Notes: Y: C/T; R: A/G; B:C/G/T; S: C/G; K: G/T; N: A/T/C/G; H: A/T/C; D: G/A/T; W: A/T; M: A/C; V:G/A/C.

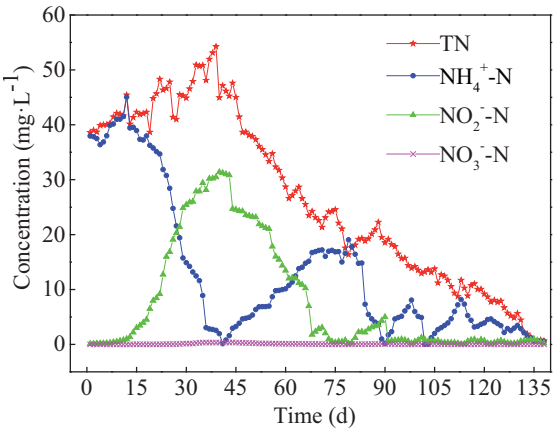


FIGURE 1
Changes of nitrogen during intermittent aeration

Abundance of nitrogen transformation functional genes during the short-cut biological nitrogen removal. The abundances of nitrogen transformation functional genes are shown in Table 2 and Table 3. Table 2 shows the abundance of nitrogen transformation functional genes in the short-cut nitrification stage. As can be seen in Table 2, the ammonia oxidation function gene (*amoA*) showed an obvious tendency of increase, which indicates that ammonia nitrogen gradually transformed into nitrite nitrogen in the short-cut nitrification stage. However, the change of nitrification function gene (*nxr*) was not significant, which indicates that less transformation of nitrite nitrogen to nitrate nitrogen in the short-cut nitrification stage. These results may account for the nitrite nitrogen accumulation in overlying water. As can be seen from Table 2, the functional genes of the *nirK, nirS, cnorB, nosZ, hszA, hszB* and *hzo,* which relate to short-cut denitrification, gradually reduced, indicating that these functional genes are inhibited under the condition of the high dissolved oxygen

TABLE 2
Abundance of nitrogen transformation functional genes in the short-cut nitrification stage

Function gene	Abundance (copies/g)				
	SN1	SN2	SN3	SN4	SN5
Archaeal-amoA	1.42×10^{8}	2.13×10^{8}	2.60×10^{8}	3.90×10^{8}	4.17×10^{8}
Bacterial-amoA	1.78×10^{6}	2.56×10^{6}	3.07×10^{6}	3.89×10^{6}	10.1×10^{6}
nxr	7.03×10^{6}	9.18×10^{6}	7.66×10^{6}	8.96×10^{6}	8.44×10^{6}
narG	9.48×10^{7}	8.55×10^{7}	6.81×10^{7}	3.23×10^{7}	2.79×10^{7}
nirK	9.25×10^{7}	5.54×10^{7}	4.53×10^{7}	4.49×10^{7}	3.02×10^{7}
nirS	2.32×10^{6}	1.84×10^{6}	1.58×10^{6}	1.11×10^{6}	0.877×10^{6}
cnorB	6.90×10^{7}	3.28×10^{7}	2.27×10^{7}	1.49×10^{7}	1.08×10^{7}
nosZ	2.21×10^{6}	1.75×10^{6}	1.28×10^{6}	1.19×10^{6}	1.03×10^{6}
hzsA	4.52×10^{5}	2.06×10^{5}	1.81×10^{5}	1.59×10^{5}	1.37×10^{5}
hzsB	10.7×10^{3}	7.47×10^{3}	6.27×10^{3}	6.00×10^{3}	4.48×10^{3}
hzo	3.72×10^{5}	3.56×10^{5}	2.99×10^{5}	2.20×10^{5}	1.97×10^{5}

Table 3 shows gradual decreases of the function genes of *amoA* and *nxr*, which are related to short-cut nitrification, indicating that the *amoA* and *nxr* were inhibited in the environment during the denitrification stage. However, there are obvious increases of the function genes of nitrite reduction (Cu type nitrite reductase *nirK*, cytochrome CD1 type nitrite reductase *nirS*), which indicating that the conversion of nitrite nitrogen to nitric oxide is the main reaction in the short-cut denitrification stage. The nitric oxide reduction gene, *cnorB,* also shows an obvious increase, which indicates that nitric oxide transformed into nitrous oxide. However, nitrous oxide reduction functional genes, *nosZ*, decreases, which suggests that nitrous oxide was rarely transformed into nitrogen. The anammox functional genes, *hszA*, *hszB* and *hzo,* increase significantly, which indicate that anammox was also the main pathway of nitrogen removal during the short-cut nitrification stage. However, the nitrate reduction function gene (*narG*) did not change much, which indicates that the full denitrification did not take place in this stage.

Effect of physicochemical factors on nitrogen transformation function genes in the short-cut nitrification stage. To investigate the main influencing factors of nitrogen transformation functional gene abundance in the short-cut nitrification stage, nine factors, that is, total nitrogen, ammonia nitrogen, nitrite nitrogen, nitrate nitrogen, total organic carbon, pH, carbon nitrogen ratio, dissolved oxygen and temperature were selected as the research variables. Since there may be strong linear correlation among the variables, the variation partition analysis was used to analyze the variables, and the collinear variables were deleted. The results of the variation partition analysis show that the combination of dissolved oxygen, the ratio of carbon to nitrogen and ammonia nitrogen can ensure that the variance expansion coefficient of all variables is less

TABLE 3
Abundance of function genes of nitrogen transformation in the short-cut denitrification stage

Function gene	Abundance (copies/g)				
	SD1	SD2	SD3	SD4	SD5
Archaeal-amoA	3.23×10^{8}	2.88×10^{8}	2.28×10^{8}	2.02×10^{8}	2.26×10^{8}
Bacterial-amoA	8.37×10^{6}	7.26×10^{6}	4.95×10^{6}	3.64×10^{6}	4.11×10^{6}
nxr	9.94×10^{6}	8.75×10^{6}	9.30×10^{6}	7.94×10^{6}	9.52×10^{6}
narG	8.43×10^{7}	10.2×10^{7}	11.2×10^{7}	12.4×10^{7}	9.74×10^{7}
nirK	1.90×10^{7}	2.43×10^{7}	2.80×10^{7}	3.81×10^{7}	5.85×10^{7}
nirS	0.61×10^{6}	1.01×10^{6}	1.18×10^{6}	1.26×10^{6}	1.58×10^{6}
cnorB	0.96×10^{7}	1.10×10^{7}	1.58×10^{7}	2.08×10^{7}	3.35×10^{7}
nosZ	9.84×10^{5}	6.47×10^{5}	5.13×10^{5}	3.92×10^{5}	3.40×10^{5}
hzsA	1.37×10^{5}	1.46×10^{5}	2.04×10^{5}	2.50×10^{5}	3.05×10^{5}
hzsB	4.48×10^{3}	4.89×10^{3}	7.36×10^{3}	10.2×10^{3}	6.04×10^{3}
hzo	1.49×10^{5}	1.79×10^{5}	2.17×10^{5}	2.63×10^{5}	3.13×10^{5}

TABLE 4
Explanatory variables of sediment in the short-cut nitrification

Chemical index	SN1	SN2	SN3	SN4	SN5
Dissolved oxygen (mg/L)	0.33±0.01	0.36±0.01	0.34±0.01	0.39±0.01	0.39±0.01
C:N (mg/kg)	0.57±0.04	0.15±0.02	0.18±0.01	0.20±0.02	0.41±0.05
Ammonia nitrogen (g/kg)	0.59±0.01	0.84±0.01	0.50±0.02	0.82±0.03	0.61±0.01

TABLE 5
Results of RDA ordination

Index	Sort axis			
	Axis 1	Axis 2	Axis 3	Axis 4
Characteristic value	0.7328	0.0595	0.0194	0.1057
Correlation between functional genes and physico-chemical factors	0.9767	0.8079	0.7396	0.0000
Cumulative percentage of functional genes	73.28	79.23	81.17	91.74
Cumulative percentage of relationship between functional genes and physicochemical factors	90.28	97.61	100.00	
Sum of all eigenvalues	0.8117			
Population characteristic value	1			
Correction factor R^2	0.76			

than 20 [31]. Therefore, the dissolved oxygen, the ratio of carbon to nitrogen (C/N) and ammonia nitrogen were selected as explanatory variables. The dissolved oxygen, C/N and ammonia nitrogen are shown in Table 4.

The relationships between the functional genes and physicochemical factors were studied during the short-cut nitrification stage with the redundancy analysis and the variance expansion factor analysis. The results of redundancy analysis are shown in Table 5: the characteristic values of the first two ordination axes are 0.7328 and 0.0595 respectively, and the correlation coefficients between functional genes and physicochemical factors are 0.9767 and 0.8079, respectively. These results indicate a good correlation between functional genes and physicochemical factors

The redundancy analysis is shown in Figure 2, which shows that *amoA* and ammonia are positively correlated with dissolved nitrogen, and that the abundance of the *amoA* is higher when dissolved oxygen and ammonia nitrogen are higher. There was a negative correlation between the anaerobic ammonium oxidation genes (*HzsA*，*HzsB*，*Hzo*) and the dissolved oxygen. The main reason is that anaerobic ammonium oxidation bacteria are very sensitive to dissolved oxygen, which significantly inhibits anaerobic ammonium oxidation bacteria. In addition, *HzsA*，*HzsB*，*Hzo* were negatively correlated with ammonia nitrogen. Ammonia nitrogen was the main substrate of anaerobic ammonium oxidation bacteria, but the activity of the anaerobic ammonium oxidation bacteria was inhibited by high concentration of ammonia nitrogen. The *nirK* and the *nirS* were positively correlated with C:N, which indicate that the abundance of *nirK* and *nirS* was higher when C: N was higher. Figure 3 shows the results of the variation partition analysis. According to Figure 3, the influence rates of dissolved oxygen, ammonia nitrogen and C: N are 34.50%, 14.90% and 8.90%, respectively. The variation partition analysis shows that the dissolved oxygen and C: N are the most important factor.

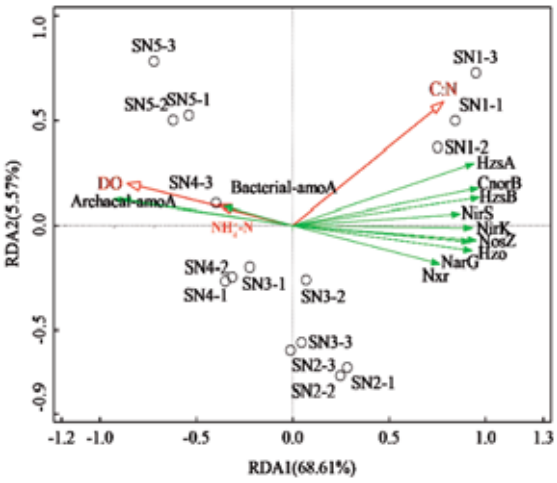


FIGURE 2
Redundancy analysis in the short-cut nitrification stage

TABLE 6
Physicochemical factors of the sediment in the short-cut denitrification stage

Physicochemical factors	SD1	SD2	SD3	SD4	SD5
Dissolved oxygen (mg/L)	0.02±0.01	0.01±0.01	0.01±0.01	0.01±0.01	0.02±0.01
Nitrite nitrogen (mg/kg)	0.12±0.01	0.29±0.02	0.22±0.04	0.39±0.04	0.46±0.04
Total organic carbon (g/kg)	0.77±0.02	0.77±0.13	0.71±0.04	0.41±0.03	0.39±0.06

TABLE 7
Sort axis of RDA

Index	Sort axis			
	Axis 1	Axis 2	Axis 3	Axis 4
Characteristic value	0.6831	0.2281	0.0341	0.0338
Correlation between functional genes and physicochemical factors	0.9869	0.9926	0.9530	0.0000
Cumulative percentage of functional genes	68.31	91.12	94.53	97.91
Cumulative percentage of relationship between functional genes and physicochemical factors	72.26	96.39	100.00	
Sum of all eigenvalues	0.9453			
Population characteristic value	1			
Correction factor R^2	0.93			

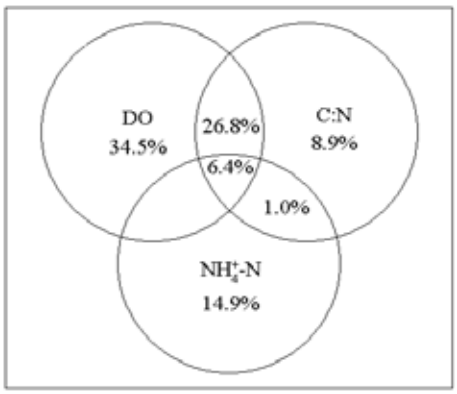


FIGURE 3
Analysis of the variance partitioning in the short-cut nitrification stage

Effect of physicochemical factors on nitrogen transformation functional genes in the short-cut denitrification stage. Variation partition analysis was conducted to probe into the collinearity among the total nitrogen, the ammonia nitrogen, the nitrite nitrogen, the nitrate nitrogen, the total organic carbon, the pH, the carbon nitrogen ratio, the dissolved oxygen, and the temperature. The results of the variation partition analysis show that the combination of the dissolved oxygen, the nitrite nitrogen, and the total organic carbon led to the results that the variance expansion coefficient of all variables is less than 20. Therefore, the dissolved oxygen, the nitrite nitrogen, and the total organic carbon were selected as explanatory variables. The data concerning dissolved oxygen, nitrite nitrogen and total organic carbon are shown in Table 6.

The relationship between nitrogen transformation functional genes and physicochemical factors was studied in the short-cut denitrification stage with redundancy analysis and variation partition analysis. The results of redundancy analysis are shown in Table 7: the characteristic values on the first two ordination axes are 0.6831 and 0.2281 respectively, and the correlation coefficients between functional genes and physicochemical factors are 0.9869 and 0.9926, respectively. The results indicate that there is a good correlation between functional genes and physicochemical factors.

The results of redundancy analysis are shown in Figure 4, which shows that, in the short-cut denitrification stage, *nirK* and *nirS* are negatively correlated with the dissolved nitrogen. The reduction reaction of the nitrite can play a better role in the anoxic or anaerobic environment, so the abundance of *nirK* and *nirS* is higher in the condition of the lower dissolved oxygen. In addition, *nosZ* can transform the nitrous oxide into nitrogen. There is a negative correlation between *nosZ* and dissolved oxygen,

which indicates that the *nosZ* is more abundant in the condition of low dissolved oxygen. *Hzsa, hzsb* and *Hzo* are also negatively correlated with the dissolved oxygen, indicating that the lower dissolved oxygen is beneficial to anaerobic ammonium oxidation. Therefore, the abundance of *hzsa, hzsb* and *Hzo* is higher when the dissolved oxygen is lower. Figure 5 shows the results of the variation partition analysis: the influence rates of the dissolved oxygen, nitrite nitrogen and total organic carbon are 68.9%，26.8% and 16.6%, respectively. The variation partition analysis shows that the dissolved oxygen is the most important factor in the short-cut denitrification stage.

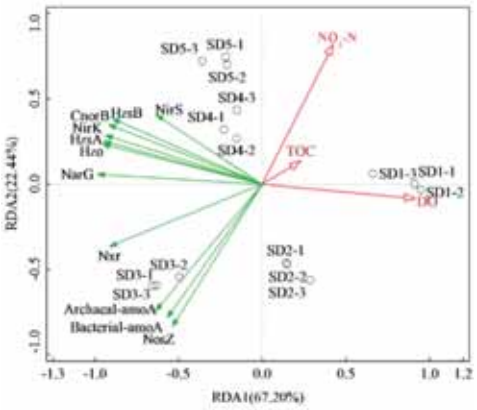


FIGURE 4
Redundancy analysis in the short-cut denitrification stage

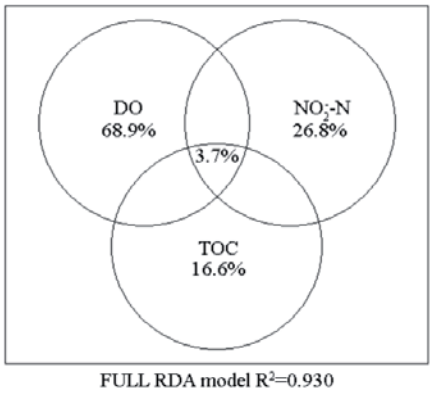


FIGURE 5
Variance partitioning in the short-cut denitrification stage

CONCLUSIONS

Nitrogen can be effectively removed from the river by intermittent aeration of overlying water. In the aeration stage, there is obvious increase of *amoA*, but *nxr* did not change significantly. Therefore, ammonia nitrogen was mainly converted into nitrite nitrogen, that is, short-cut nitrification occurred in the aeration stage; In the non-aeration stage, *nirK* and *nirS* increased significantly, while *narG* did not change much. Therefore, nitrite nitrogen was converted into nitric oxide at this stage, that is, short-cut denitrification occurred mainly in the non-aeration stage. The physicochemical factors of sediment have important effects on nitrogen transformation function genes. In the short-cut nitrification stage, *amoA* was positively correlated with the dissolved oxygen and ammonia nitrogen, while *HzsA, HzsB* and *Hzo* were negatively correlated with the dissolved oxygen and ammonia nitrogen. In addition, in this stage, dissolved oxygen, ammonia nitrogen, and C: N were the main factors affecting the nitrogen transformation function genes. In the short-cut denitrification stage, *nirK*, *nirS, NosZ*, *HzsA, HzsB* and *Hzo* were negatively correlated with the dissolved oxygen. The dissolved oxygen, nitrite nitrogen and the total organic carbon were the main factors affecting the nitrogen transformation function genes in the short-cut denitrification stage. In this study, the biological nitrogen removal in river was studied from the perspective of nitrogen transformation functional genes, which is hoped to motivate more in-depth study of biological nitrogen removal in river in the future.

ACKNOWLEDGEMENTS

This research was supported by Anhui Province Natural Science Foundation (1808085MB34, 1908085ME142), the Natural Science Project for Colleges of Anhui Province (KJ2019ZD52, KJ2020A0466), the Project of National key research and development program(2019YFC0408504), Ph.D. start-up foundation of Anhui Jianzhu University (2019QDZ64, 2019QDZ60).

REFERENCES

[1] Kim, H., Bae, H.S., Reddy, K.R., Ogram, A. (2016) Distributions, abundances and activities of microbes associated with the nitrogen cycle in riparian and stream sediments of a river tributary. Water Research. 106, 51-61.

[2] Ma, G.W., Wang, Y.Y., Bao, X., Hu, Y., Liu, Y.P., He, L.H., Wang, T.M., Meng, F.S. (2015) Nitrogen pollution characteristics and source analysis using the stable isotope tracing method in Ashi River, northeast China. Environmental Earth Sciences. 73(8), 4831-4839.

[3] Zhao, Y.Q., Xia, Y.Q., Ti, C.P., Shan, J., Li, B.L., Xia, L.L., Yan, X.Y. (2015) Nitrogen removal capacity of the river network in a high nitrogen loading region. Environmental Science and Technology. 49(3), 1427-1435.

[4] Zhang, H., Wang, K., Huang, X.H., Huang, J., Zhong, Y., Tao, Y. (2015) Nitrogen removal in overlying water by intermittent aeration and ammonia indirect measurement by fluorescence method. China Environmental Science. 35(11), 3275-3281.

[5] Huang, J., Liu, P.R., Sun, Q.Y., Zhang, H., Zhang, Y., Wang, K. (2017) Determination of total Nitrogen, Ammonia, and Nitrite in River Water by Near-infrared Spectroscopy and Chemometrics. Analytical Letters. 50(10), 1620-1629.

[6] Huang, J., Zhang, X., Sun, Q.Y., Zhang, H. (2017) Simultaneous Rapid Analysis of Multiple Nitrogen Compounds in Polluted River Treatment Using near-infrared Spectroscopy and a Support Vector Machine. Polish Journal of Environmental Studies. 26(5), 2013-2019.

[7] Fan, J.L., Zhang, B., Zhang, J., Ngo, H.H., Guo, W.S., Liu, F.F., Guo, Y.Y., Wu, H.M. (2013) Intermittent aeration strategy to enhance organics and nitrogen removal in subsurface flow constructed wetlands. Bioresource Technology. 141(7), 117-122.

[8] Ma, Y.J., Domingo-félez, C., Plósz, B.G., Smets, B.F. (2017) Intermittent Aeration Suppresses Nitrite-Oxidizing Bacteria in Membrane-Aerated Biofilms: A Model-Based Explanation. Environmental Science and Technology. 51(11), 6146-6155.

[9] Uggetti, E., Hughes-Riley, T., Morris, R.H., Newton, M.I., Trabi, C.L., Hawes, P., Garcíaa, J. (2016) Intermittent aeration to improve wastewater treatment efficiency in pilot-scale constructed wetland. Science of the Total Environment. 559, 212-217.

[10] Wu, Q.L., Ruan, X.H., Wu, Z.Z., Li, R.F., Wang, C.W., Wan, Y. (2015) Analyses of sources and transformation of nitrogen as a contaminant in the river and lake water in the western region of the Taihu Lake basin. Acta Scientiae Circumstantiae. 35(12), 3883-3889.

[11] Levy-Booth, D.J., Prescott, C.E., Grayston, S.J. (2014) Microbial functional genes involved in nitrogen fixation, nitrification and denitrification in forest ecosystems. Soil Biology and Biochemistry. 75, 11-25.

[12] Reyes, C., Schneider, D., Lipka, M., Thürmer, A., Böttcher, M.E., Friedrich, M.W. (2017) Nitrogen Metabolism Genes from Temperate Marine Sediments. Marine Biotechnology. 19(2), 175-190.

[13] Wang, H.L., Ji, G.D., Bai, X.Y., He, C.G. (2015) Assessing nitrogen transformation processes in a trickling filter under hydraulic loading rate constraints using nitrogen functional gene abundances. Bioresource Technology. 177, 217-223.

[14] Wang, H.L., Ji, G.D., Bai, X.Y. (2016) Distribution patterns of nitrogen micro-cycle functional genes and their quantitative coupling relationships with nitrogen transformation rates in a biotrickling filter. Bioresource Technology. 209, 100-107.

[15] Zhang, L.L., Sun, Z.Z., Xie, J., Wu, J., Cheng, S.P. (2018) Nutrient removal, biomass accumulation and nitrogen-transformation functional gene response to different nitrogen forms in enhanced floating treatment wetlands. Ecological Engineering. 112, 21-25.

[16] Wang, L.P., Zheng, B.H., Nan, B.X., Hu, P.L. (2014) Diversity of bacterial community and detection of nirS- and nirK-encoding denitrifying bacteria in sandy intertidal sediments along Laizhou Bay of Bohai Sea, China. Marine Pollution Bulletin. 88(1-2), 215-223.

[17] Chen, R., Deng, M., He, X.G., Hou, J. (2017) Enhancing Nitrate Removal from Freshwater Pond by Regulating Carbon/Nitrogen Ratio. Front Microbiol. 8, 1712-1721.

[18] Wu, L., Osmond, D.L., Graves, A.K., Burchell, M.R., Duckworth, O.W. (2012) Relationships between nitrogen transformation rates and gene abundance in a riparian buffer soil. Environmental Management. 50(5), 861-874.

[19] Lee, J.A., Francis, C.A. (2017) Spatiotemporal Characterization of San Francisco Bay Denitrifying Communities: a Comparison of nirK and nirS Diversity and Abundance. Microbial Ecology. 73(2), 271-284.

[20] Gu, Q., Zhang, X., Ye, D.H., Zheng, Y., Sun, J., Wei, Z., Zhou, Y. (2016) Quantitative analysis on the functional genes involved in biological transformation of carbon, nitrogen and sulfur in Fenghua sediments. Environmental Pollution Control. Environmental Pollution and Control. 38(11), 60-67.

[21] Sun, Y.F., Pan, J., Qi, S.Y., Fei, H.X. (2017) Effects of hydraulic loading rate and aeration mode on nitrogen removal and nitrogen functional gene abundances in subsurface wastewater infiltration systems. Water Science and Technology. 76(1), 210-218.

[22] Sun, R.B., Guo, X.S., Wang, D.Z., Chu, H.Y. (2015) Effects of long-term application of chemical and organic fertilizers on the abundance of microbial communities involved in the nitrogen cycle. Applied Soil Ecology. 95, 171-178.

[23] Ding, K., Zhong, L., Xin, X.P., Xu, Z.H., Kang, X.M., Liu, W.J., Rui, Y.C., Jiang, L.L., Tang, L., Wang, Y.F. (2015) Effect of grazing on the abundance of functional genes associated with N cycling in three types of grassland in Inner Mongolia. Journal of Soils and Sediments. 15(3), 683-693.

[24] Fuchslueger, L., Kastl, E.M., Baue, F., Kienzl, S. (2014) Effects of drought on nitrogen turnover and abundances of ammonia-oxidizers in mountain grassland. Biogeosciences. 11(21), 6003-6015.
[25] Zhi, W., Ji, G.D. (2014) Quantitative response relationships between nitrogen transformation rates and nitrogen functional genes in a tidal flow constructed wetland under C/N ratio constraints. Water Research. 64(7), 32-41.
[26] Graham, J.E., Wantland, N.B., Campbell, M., Klotz, M.G. (2011) Chapter Fourteen–Characterizing Bacterial Gene Expression in Nitrogen Cycle Metabolism with RT-qPCR. Methods in Enzymology. 496, 345-372.
[27] Kuzdraliński, A., Szczerba, H., Tofil, K., Filipiak, A., Garbarczyk, E., Dziadko, P., Muszyńska, M., Solarska, E. (2014) Early PCR-based detection of Fusarium culmorum, F. graminearum, F. sporotrichioides and F. poae on stem bases of winter wheat throughout Poland. European Journal of Plant Pathology. 140(3), 491-502.
[28] Ribbons, R.R., Levy-Booth, D.J., Masse, J., Grayaton, S.J., McDonald, M.A., Vesterdal, L., Prescott, C.E. (2016) Linking microbial communities, functional genes and nitrogen-cycling processes in forest floors under four tree species. Soil Biology and Biochemistry. 103, 181-191.
[29] Jiang, R., Wang, J.X., Huang, B., Yu, K.C., Zhang, P., Zheng, J.W., Liu, X.Z. (2016) Phylogenetic analysis of bacterial community composition in sediments with organic contaminants from the Jiaojiang estuary in China. Marine Pollution Bulletin. 109(1), 558-565.
[30] Liu, Q.H. (2015) Variation partitioning by partial redundancy analysis (RDA). Environmetrics. 8(2), 75-85.
[31] Braak, C.T., Šmilauer, P. (2002) CANOCO Reference Manual and Users Guide to Canoco for Windows. New York: Centre for Biometry Wageningen.

Received: **09.04.2021**
Accepted: **17.05.2021**

CORRESPONDING AUTHOR

ShanShan Xi
School of Environment and Energy Engineering,
Anhui Jianzhu University,
Hefei 230601 – China

e-mail: 52784255@qq.com

© by PSP Volume 30– No. 09/2021 pages 10880-10889 Fresenius Environmental Bulletin

STUDY ON DYNAMIC UPDATING ALGORITHM OF MARINE ALGAE STATISTICAL DATABASE

Lina Cui*

Basic Teaching and Research Department, Yingkou Institute of Technology, Yingkou, China

ABSTRACT

In order to solve the problems of long updating time, high packet loss rate, poor security and large storage space after updating, a dynamic updating algorithm of Marine algae statistical database is proposed. The wavelet packet is used to decompose the data three times, and the feature vector of the data is extracted by reconstructing the decomposition coefficient. Adopts adaptive threshold time cleaning stale data, using the reader to read data buffer queue, determine the data label is expected expiration time, current time is greater than or equal to a label expected expiration time, thinks that the label has expired, will delete the data, the complete statistical database of Marine algae cleaning and dynamic update for the first time. The extracted data characteristics were treated as individual, the data to be updated and its update weight were determined according to the matching contribution value of each individual, and the new data was used to replace the data with the large contribution value to obtain the dynamic update result of the Marine algae statistical database. Experiments show that the algorithm can reduce the updating time and packet loss rate of Marine algae statistical database, improve the storage space after updating, and the safety factor can reach up to 0.98.The proposed algorithm can greatly improve the feasibility of dynamic updating of Marine algae statistical database and provide reference for big data research.

KEYWORDS:
Tense, Marine algae statistics database, Dynamic update, Update weights

INTRODUCTION

The research on dynamic update of Marine algae statistical database began in the mid-1980s, and since the 1990s, it has attracted more and more attention and become an important field of modern Marine algae statistical database[1].The update of Marine algae statistical database requires the initiative to be integrated with the existing Marine algae statistical database in a unified way into a Marine algae statistical database system. Up to now, this mechanism is mainly realized by embedding some rules into the Marine algae statistical database system, and people's research work mainly focuses on the implementation model of the active Marine algae statistical database[2].At present, the update of Marine algae statistical database is manually operated by relevant personnel, and the update rules are not limited, resulting in the failure of timely update of Marine algae statistical database due to human factors[3].In view of the growing development in the field of Marine algae statistical database, many scholars have studied the dynamic update of Marine algae statistical database.

Literature[4] tries to interpret the importance of velocity and discuss how to deal with its challenges for big data analysis system. By comparing the different requirements of object processing, data flow and data analysis system on velocity, two recent studies are discussed from the perspective of the relationship between data update and big data analysis system. On the one hand, MaSM supports online data update in data warehouse system; On the other hand is LogKV, which supports high-speed log data inflow and time-based connection operations in the log processing system. The method can be attributed to the data online update, the poor quality of data cleaning in the process, resulting in a long update time. Literature[5] proposed a solution for rapid data update. By adding packet loss retransmission and packet confirmation mechanism, the transport layer UDP protocol is improved, and the data update protocol of the application layer is designed by using the multi-thread mechanism of data transmission in parallel between separate request and update ports. The security problem is not taken into account during the operation of the method. Literature[6] proposed a network-encoded cloud storage data update algorithm. The storage node only needs to update part of the code block according to the difference matrix sent by the server to complete the update of the whole file. This method has a high loss rate. Literature[7] proposed the use of genetic algorithm to update and query the statistical database of large Marine algae. The Marine algae statistical database cat-

alog manager is used to collect all kinds of cost information in real time, generate query processing tree of Marine algae statistical database, find out the optimal query execution plan, obtain the communication cost and local operation cost of single query plan, and carry out weighted processing. According to the fitness value in the problem domain, the selection, crossover, variation and other genetic operations are carried out, and different evolutionary adaptation plans are used in the update query phase to obtain the global optimal solution for the optimization target problem. Under this method, data update takes up a large storage space.

Aiming at the problems existing in the updating process of Marine algae statistical database, a temporal object-oriented dynamic updating algorithm based on Mean shift is proposed. The main structure is:

(1) wavelet packet decomposition was used to extract the data feature vectors from the statistical database of Marine algae.

(2) the adaptive time threshold method is adopted to clean the statistical database of Marine algae to remove expired data, so as to realize the initial update of the statistical database of Marine algae, reduce the data update time and the storage space occupied by the updated data.

(3) dynamic update of Marine algae statistical database was carried out by means of Mean shift algorithm to improve the updating security of Marine algae statistical database and reduce packet loss rate.

(4) the overall effect of the proposed algorithm is verified through experiments and analysis.

(5) summarize the full text and put forward the future development direction.

MATERIAL AND METHOD

Data feature extraction. In this paper, the data in the Marine algae statistical database are decomposed by wavelet packet and the data feature vectors are extracted.

Wavelet packet method is a fine orthogonal decomposition method, which determines the characteristic information of data at different locations according to the characteristics of the data being analyzed[8-9].In data eigenvector analysis, U_j^n represents the closure space of function $\mu_n(t)$, and $\mu_n(t)$ satisfies the following two-scale equation:

$$\mu_{2n}(t)=\sqrt{2}\sum h(k)*\varphi(t) \tag{1}$$

$$\mu_{2n+1}(t)=\sqrt{2}\sum g(k)*\phi(t) \tag{2}$$

Where, $h(k)$ and $g(k)$ represent orthogonal filter coefficients, $\varphi(t)$ represent scale functions, $\phi(t)$ represent wavelet functions, k represent translation parameters, n represent wavelet decomposition layers, j represent scale parameters, t represent wavelet decomposition time, and g and h represent orthogonal functions.

According to the two-scale equation, the wavelet packet space is obtained by scaling and translation of 1, and each data space is constituted by right angles of two subspaces larger than $\varphi(t)$ [10].Then the decomposition formula of data characteristics analysis is:

$$S_{h(k)}=\sum \mu_{2n}(t)*S_k \tag{3}$$

$$S_{g(k)}=\sum \mu_{2n+1}(t)*S_k \tag{4}$$

Where, S_k represents the decomposition function.

Suppose that, characteristic $f(t)\in U_j^n$ of the data itself, then the decomposition formula of wavelet is:

$$f(t)=\frac{\sum S_{g(k)}\cdot S_k}{\sqrt{2}}+\frac{\sum S_{h(k)}\cdot S_k}{\sqrt{2}} \tag{5}$$

Formula (5) shows that in wavelet decomposition, any data trait can be decomposed into two parts: one is the projection of data trait on $\mu_{2n}(t)$ after the low-pass filter; The other part is the projection of the data trait onto $\mu_{2n+1}(t)$ after it has been used by the high pass filter. The representation of wavelet decomposition results in terms of energy is called wavelet packet energy spectrum[11].In the wavelet transform, the original data trait $f(t)$ two norm is defined as:

$$\|f\|_2^2=\int|f(t)|^2 \tag{6}$$

According to formula (6), in the wavelet transform, the square of the data characteristic two norm is equivalent to the energy of the trait in the time domain. For the data in the statistical database of Marine algae, when the characteristic components of the data are different, the specific energy emitted by them is quite different.

The decomposition of equations (3) to (5) and the definition of equations (6) are used to decompose the data in the statistical database of Marine algae

into three-layer wavelet packets and extract the characteristic signals emitted by the data of 8 frequency components in the third layer from low to high frequency. The decomposition coefficient is reconstructed to extract data features[12].Reconstruct all data features of the third layer:

$$S = \left(S_{30} + S_{31} + \cdots + S_{37}\right) * \left\| f \right\|_2^2 \tag{7}$$

Where, S_{IJ} represents the J data in the I layer.

The total energy of the data trait signal is calculated.Assume that the corresponding energy of S_{3J} is E_{3J}, then: $E_{3J} = \int S_{3J} = \sum_{k=1}^{n} \left| x_{Jk} \right|^2$ (8)

Where, x_{Jk} represents the discrete point amplitude of S_{3J} of the reconstruction feature.

The data feature vector is constructed by formula (8) :

$$T = \left[E_{30}, E_{31}, \cdots, E_{37}\right] \tag{9}$$

The eigenvectors are normalized.When the feature energy increases, E_{3J} is usually a relatively large value. In order to reduce the computational complexity, the feature vector is improved and the data characteristics in the statistical database of Marine algae are normalized to:

$$E = \left(\sum_{j=0}^{7} \left| E_{3J} \right|^2 \right)^{\frac{1}{2}} \tag{10}$$

According to formula (10), the normalized data feature vector value is:

$$T' = \frac{1}{E}\left[E_{30}, E_{31}, \cdots, E_{37}\right] \tag{11}$$

According to the above steps, three-layer wavelet decomposition was performed on the data in the measured Marine algae statistical database by using wavelet packet, and the coefficients after decomposition were reconstructed to obtain the data feature vector. The data feature vectors obtained by normalization are extracted.

Data cleaning. In order to reduce the data update time, it is necessary to use adaptive time threshold to clean the expired data, i.e., preliminary update[13].

The cell format of the data label cache queue is defined as:

$$V^t = \left\{ \left[VID^t \right] \left[T_{end} \right] \left[N \right] \right\} \tag{12}$$

Where, VID represents the ID of the data tag, T_{end} represents the expected expiration time of the data transition, and N represents the number of times the data tag has been read.

Use the reader to read the data label cache queue and get VID .Determine whether the number of data labels in the cache queue is within the valid threshold range.If it is within the valid range, calculate the expected expiration time of data label information according to the time t' at the time when the data label is read and the time threshold T'' at this time:

$$T_{end} = \frac{\left(t' + T''\right)}{V^t} \tag{13}$$

If the number of data labels in the cache queue is not within the valid range of the threshold, then the new time threshold is calculated according to formula (14), and the threshold range is updated according to formula (15) :

$$T'' = \left[\frac{\ln\left(1/\delta\right)}{p_a^{avg}} \right] * T_{end} * T' \tag{14}$$

Where, δ represents confidence, and the higher the value, the higher the quality of data cleaning. p_a^{avg} represents the average reading rate for each data reader cycle.

$$\lambda = \frac{\left| N' - N \right|}{N} * T'' \tag{15}$$

Among them, N' represents the number of data labels in the cache queue at the last threshold change, and λ represents a confidence interval, which is used to represent an acceptable range of change.

Compare the VID recorded in the tag with the data label information in the cache queue to determine whether the label information already exists in the cache queue. If it already exists, add Nt' + 1 to the number of times the data label has been read, update the expected expiration time of the data label, and so on. The label information is transferred to the end of the cache queue, and the number of times that the data label is read is judged. If the number is greater than the set parameter θ, the label information is considered to be real information, and it is output to the upper module for marking. If it does not exist, the number of times the data label has been read is recorded as Nt' plus 1, and the information about the data label is inserted at the end of the cache queue.

The cache queue is updated, the length of the

cache queue is counted, and the count value is initialized to represent the first label information of the cache queue[14].Compare the expected expiration time of the first tag in the cache queue with the current time. If the current time has exceeded or is equal to the expected expiration time of the tag, the tag information is considered expired. Remove it from the cache queue and continue to update the cache queue. If the current time is not exceeded, or is equal to the expected expiration time of the tag, then the read operation is judged to have stopped. If stopped, then end the data cleansing; If it is not stopped, continue with the data cleansing operation to reduce the amount of storage space occupied by the updated data.

According to the above contents, the data cleaning results obtained are:

$$F\left(V^t\right)=\frac{\sum_{N} T_{end} * T''}{\lambda} \tag{16}$$

Based on the above, the data tag was repeatedly found by the reader multiple times during the entire existence period. When a new read occurs, the system queries the cache queue to determine whether it already exists in the cache queue. If it already exists, then based on the time and time threshold length at this time, the estimated expiration time of the tag is obtained, and the correlation of the tag is updated. Information, and put the tag information at the end of the queue; if it does not exist, insert the relevant information of the tag directly into the end of the cache queue, and query the cache queue in sequence at the same time, if the current time is greater than or equal to the expected expiration time of a tag, the tag is considered Expired, remove the tag from the cache queue.

RESULTS

According to the preliminary data update results, the Mean shift algorithm is used to update and analysis the data once.

Assuming that the initial target position is $F\left(V^t\right)_0$, the target model q_u is calculated according to equation (17) :

$$q_u=\frac{C\cdot\sum K\cdot\zeta}{F\left(V^t\right)_0} \tag{17}$$

Where, C represents the security coefficient in the process of data update, and the closer the coefficient is to 1, the higher the security of data update is K for kernel and ζ for Kronecker delta.

Equation (18) and equation (19) were used to calculate candidate target model $p\left(F\left(V^t\right)_0\right)$ and its similarity with the target model $\rho\left(F\left(V^t\right)_0\right)$:

$$p\left(F\left(V^t\right)_0\right)=C\cdot\frac{q_u}{h} \tag{18}$$

Where, h represents the kernel bandwidth.

$$\rho\left(F\left(V^t\right)_0\right)=\rho\left[\,p\left(F\left(V^t\right)_0\right)\right] \tag{19}$$

Where, ρ represents the data similarity.

Through the calculation of equation (18) and equation (19), equation (20) is used to calculate the data to update the weight value w, and equation (21) is used to determine the new position of the target $F\left(V^t\right)_1$:

$$w=\sum\sqrt{\frac{q_u}{\rho\left(F\left(V^t\right)_0\right)}}\zeta \tag{20}$$

$$F\left(V^t\right)_1=\frac{\sum w\left(F\left(V^t\right)_0/h\right)}{\sum wC} \tag{21}$$

It is assumed that the candidate target model $p\left(F\left(V^t\right)_1\right)$ of the new position $F\left(V^t\right)_1$ is known, and its matching degree with the target model is $\rho\left(F\left(V^t\right)_1\right)$ .If $\rho\left(F\left(V^t\right)_1\right)<\rho\left(F\left(V^t\right)_0\right)$, then let $F\left(V^t\right)_1\leftarrow\left(F\left(V^t\right)_0+F\left(V^t\right)_1\right)/2$, and re-determine the candidate target model of the new location, and its matching degree with the target model.

Formula (22) is used to calculate the matching contribution of each sub-model of the tracking result MCD_u:

$$MCD_u=\frac{\sqrt{q_u}}{\rho}\cdot F\left(V^t\right)_1\cdot T' \tag{22}$$

Select the data with high matching degree according to equation (23), and get the data update result. In order to avoid the deviation of the data model in the Marine algae statistical database caused by over-updating, the data model with a larger contribution is updated, that is, the data model with a higher consistency with the target model in the current data model is updated:

$$K=\arg\min\left(\sum MCD_u\right)\cdot\alpha,\ \rho\geq\gamma \tag{23}$$

Where, γ represents the reliability threshold of data tracking, which can effectively adjust packet

loss in the process of data update, and α represents the speed factor of data update. Equation (23) is the result of data update.

To sum up, the data characteristic model of each component as a separate individual[15], based on matching the contribution of each component, select the current statistics of Marine algae respectively in the database needs to update the data model of component and its update weights, using new data replace high similarity data, Marine algae statistical database dynamic updates. The data tracking reliability threshold can greatly reduce the packet loss in the update process of Marine algae statistical database.

RESULTS AND DISCUSSION

The experimental platform of dynamic update algorithm is: Windows 7 operating system, Intel (R) Core (TM) i3-4010u Duo @ 1.70uhz, and the simulation experiment is carried out in Visual Studio 2017 development platform. The algorithm is implemented in C++.The 6 data sets used in the algorithm test were all from the UCI Marine algae statistics database, as shown in Table 1.

Establishment of experimental indicators:

(1) update time of Marine algae statistical database;

(2) packet loss rate in the update process;

(3) update safety of Marine algae statistical database;

(4) the storage space occupied after the update.

Experiment (1): the update methods of different Marine algae statistical databases were respectively updated in the same data volume of Marine algae statistical databases, so as to verify the update duration of different update methods in different data volumes. The experimental results are:

Analysis of the experimental results in Figure 1 shows that the update time of the marine algae statistics database is different under different algorithms. The update of the marine algae statistics database based on network coding is time-consuming and tends to increase with the increase in the amount of data. Time consuming has a downward trend. The time-consuming update of the marine algae plant statistics database based on online updates continues to increase with the increase in the amount of data, which tends to be gradual when the amount of data is about 22 million. The marine algae plant statistics database based on Mean shift is time-consuming, and although it fluctuates slightly, it has remained below 80s. This is mainly because the marine algae plant statistics database was cleaned when the marine algae plant statistics database was officially updated. Reduce data update time. In addition, the data update speed factor also ensures the update speed of the marine algae plant statistics database.

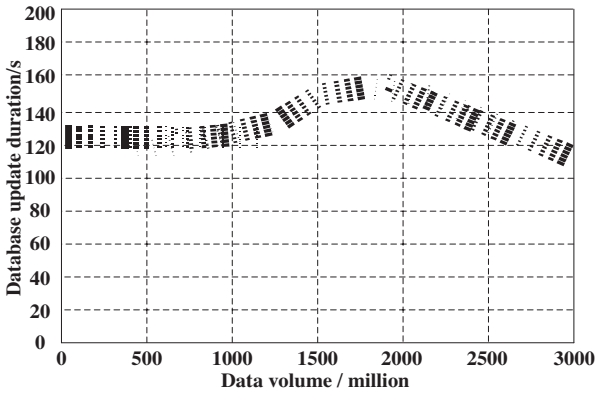
Experiment (2): Use different data update algorithms to implement the update operation in the marine algae plant statistics database with the same amount of data, and observe the packet loss of different algorithms.

As can be seen from Figure 2, the packet loss rate curve of the updated Marine algae statistical database based on the update protocol changed greatly, but after the data volume reached 6 million, the trend of decline was obvious and stable. The fluctuation of packet loss rate curve of Marine algae statistical database based on network coding is regular and the overall packet loss rate is the highest. The packet loss rate curve of Marine algae statistical database based on Mean shift fluctuates little up and down, and can be controlled at about 5% after the data volume reaches 5 million. The data tracking reliability threshold is set in the update algorithm of Marine algae statistical database based on Mean shift, which can effectively adjust the packet loss in the process of data update.

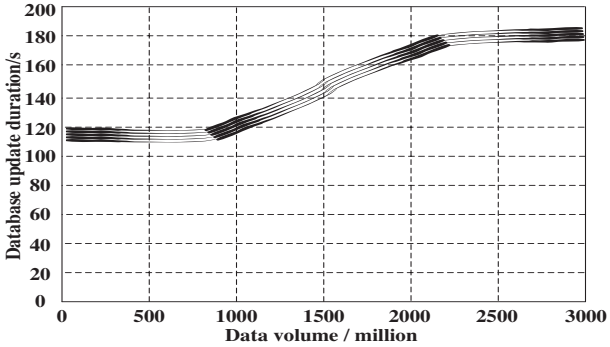
Experiment (3): the data volume and safety factor and iteration times were taken as the representative values of three-dimensional coordinates respectively to compare the safety of the update algorithm of Marine algae statistical database based on the update protocol and the update algorithm of Marine algae statistical database based on Mean shift.

TABLE 1
Experimental data

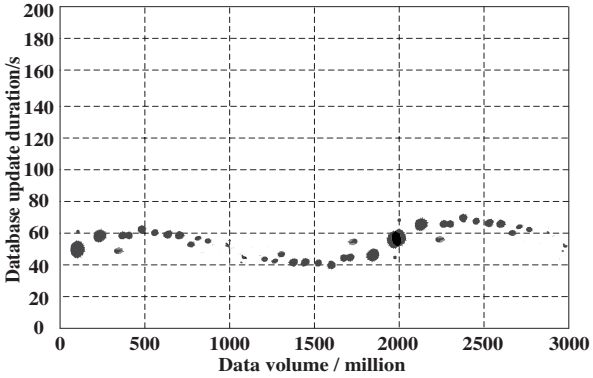
Data sets	Samples / million	Attrihutc sets
wine	1780	13
SPECT Heart	2670	23
car evaluation	1728	6
chess(king-rook vs. king-pawn)	3196	36
statlog	4436	38
mushroom	8125	23



(a) the time required to update the web-based statistical database of Marine algae



(b) time to update the Marine algae statistics database based on online updates

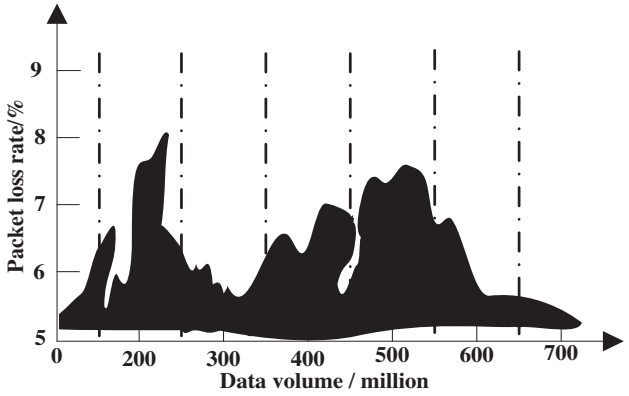


(c) Time-consuming update of marine algae statistics database based on Mean shift

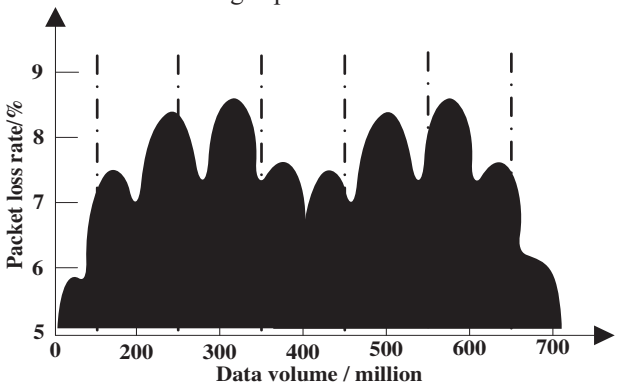
FIGURE 1
Comparison of the time taken to update the marine algae plant statistics database with different algorithms

According to the experimental results in Figure 3, it can be seen that the overall safety factor of the Marine algae statistical database update algorithm based on Mean shift is high, up to 0.98, while the safety of the Marine algae statistical database update algorithm based on the update protocol is poor.In this paper, the security control coefficient is arranged in the data update, which can effectively improve the security in the process of data update, making the algorithm in this paper more advantageous and reliable than the current update method.

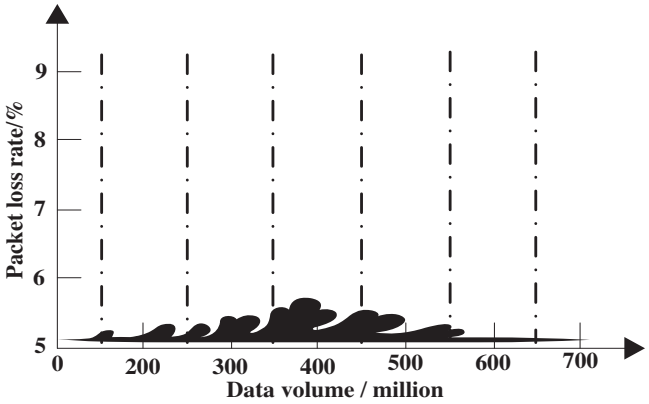
Experiment (4): different data updating methods were used to update the statistical database of Marine algae with different data volumes, so as to verify the storage space occupied by different data updating methods.



(a) Update packet loss rate of the marine algae plant statistics database based on the update protocol



(b) update packet loss rate of the network coding Marine algae statistical database

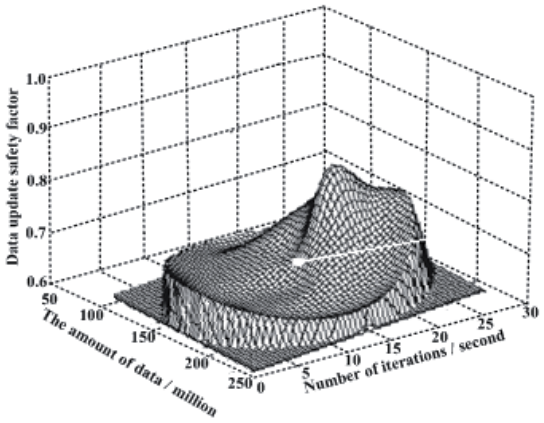


(c) update packet loss rate of Marine algae statistical database based on Mean shift

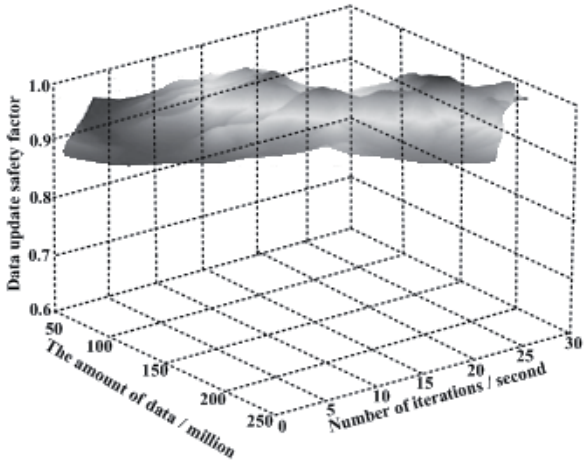
FIGURE 2

Comparison of packet loss rate of Marine algae statistical database updated by different algorithms

According to the analysis of the experimental results in Figure 4, the curve of storage space occupancy after the update of Marine algal statistical database based on genetic algorithm fluctuates slightly more than that based on Mean shift, and it keeps going up significantly. In order to reduce the storage space occupied by updated data of Marine algae statistical database, the algorithm in this paper makes a judgment on whether the reader will stop reading the data when the data is cleaned, and will not stop cleaning until the reader cleans all expired data in the Marine algae statistical database. This will greatly reduce the number of expired data in the Marine algae statistics database, which will make the storage space of the database larger.



(a) updating the safety factor of the Marine algae statistics database based on the update protocol



(b) Update safety factor based on Mean shift Marine algae statistical database

FIGURE 3

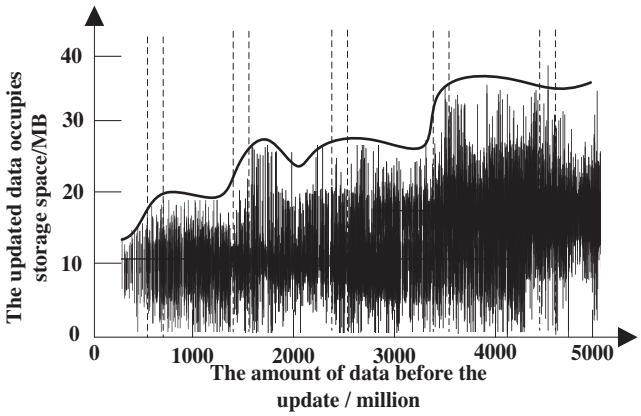
Comparison of safety of different algorithms for updating Marine algae statistical database

CONCLUSION

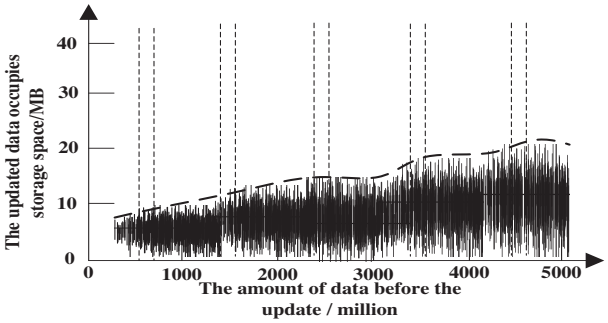
The amount of data in the temporal object-oriented Marine algae statistics database keeps increasing and changing. Therefore, it is necessary to update the data in the statistical database of Marine algae to improve the utilization rate of the data. In view of the problems existing in the current correlation updating method, a mean shift-based updating algorithm for Marine algae statistical database is proposed. The wavelet packet is used to decompose the data in three layers, and the decomposition coefficient is obtained. Through the decomposition coefficient, the data features are reconstructed, and the data feature vectors are obtained. The adaptive time threshold method was used to clean the statistical database of Marine algae, and the expired data was deleted to realize the initial dynamic update of the statistical database of Marine algae. The Mean shift algorithm is used to obtain the similarity between data models, so as to obtain the contribution value of individual component of data features, determine the data to be updated, and complete the dynamic update of data. Experiments show that the proposed algorithm is superior to the current algorithm in the aspects of updating time, packet loss rate, updating safety factor and storage space occupied by updated data. The development Suggestions for the proposed algorithm can be divided into the following two points:

(1) to further improve the security of the algorithm, the database of Marine algae statistics can be encrypted and updated;

(2) in the process of data update, new data should be continuously entered into consideration, so as not to delay the entry of new data as far as possible, but also to quickly complete the data update.



(a) storage space occupancy after updating the genetic algorithm-based statistical database of Marine algae



(b) storage space occupancy after the Mean shift-based statistical database of Marine algae is updated

FIGURE 4
Comparison of storage space occupied by different algorithms after updating Marine algae statistics database

REFERENCES

[1] Knuth, M., Reddy, D., Dimou, A., (2015) Towards Linked Data Update Notifications. Siam Journal on Numerical Analysis. 2, 408-427.

[2] Mahapatra, P.R., Zrnic, D.S. (2015) A physical basis for NEXRAD data update rates. Journal of Aircraft. 11, 840-850.

[3] Holger, D., Kim, V.R., Sushama, M., (2016) ELM 2016—data update and new functionality of the eukaryotic linear motif resource. Nucleic Acids Research. Database issue. D294-D300

[4] Chen, S.M. (2015) Big Data Analysis and Data Velocity. Journal of Computer Research and Development. 2, 333-342.

[5] Ye, W.F., Pan, G.F., Zhong, Z., (2016) Design of data update system based on elastic compute branch service. Video Engineering. 11, 25-29.

[6] H. Wu, C.Z. Lai, J.L. Fan, (2017) Data update algorithm based on secure network coding in cloud environment. Journal on Communications. 5, 121-127.

[7] Liu, Z. (2017) Real Time Query Optimization and Simulation of Large Database Demand Information. Computer Simulation. 1, 427-430.

[8] Athanassoulis, M., Chen, S., Ailamaki, A.(2015) Online Updates on Data Warehouses via Judicious Use of Solid-State Storage. Acm Transactions on Database Systems. 1, 1-42.

[9] Vizcaíno, J.A., Csordas, A., Deltoro, N, (2016) 2016 update of the PRIDE database and its related tools. Nucleic Acids Research. Database issue. D447-D456.

[10] Outrata. J. (2016) A lattice-free concept lattice update algorithm. International Journal of General Systems. 2, 1-21.

[11] Zong, W., Wu, F., Jiang, Z. (2017) A Markov-Based Update Policy for Constantly Changing Database Systems. IEEE Transactions on Engineering Management. 3, 287-300.

[12] Zhang, J.B., Li, T.R., Pan, Y., (2015) Parallel and incremental algorithm for knowledge update based on rough sets in cloud platform. American Journal of Pathology. 6, 827-834.

[13] Jing, T., Wei, X., Cheng, W., (2016) An Efficient Scheme for Tag Information Update in RFID Systems on Roads. IEEE Transactions on Vehicular Technology. 4, 1-1.

[14] Delhibabu, R., Behrend, A. (2015) A new rational algorithm for view updating in relational databases. Applied Intelligence. 3, 1-15.

[15] Liang, Y. (2019) Distributed Big Data Integration Conflict Resolution Simulation in Relational Database. Computer Simulation. 5, 399-402.
[16] Ogihara T. (2017) Tense and aspect. The Handbook of Japanese Linguistics. 326-348.
[17] Janda, L.A. (2019) Tense, aspect and mood. Cognitive Linguistics-Key Topics.
[18] Coghlan, D., Shani, A.B. (2017) Inquiring in the present tense: the dynamic mechanism of action research. Journal of Change Management. 17(2), 121-137.
[19] Xu, S.Y., Huang, X., Cheong, K.L. (2017) Recent advances in marine algae polysaccharides: Isolation, structure, and activities. Marine Drugs. 15(12), 388.
[20] Bilal, M., Rasheed, T., Sosa-Hernández, J.E., (2018) Biosorption: an interplay between marine algae and potentially toxic elements—a review. Marine Drugs. 16(2), 65.
[21] Berthon, J.Y., Nachat-Kappes, R., Bey, M., (2017) Marine algae as attractive source to skin care. Free Radical Research. 51(6), 555-567.
[22] Kraska, T., Alizadeh, M., Beutel, A., (2019) Sagedb: A learned database system//CIDR. Pages.
[23] Scott, L.C. (2020) Abstract C008: Descriptive analysis of Black/White disparities in triple-negative breast cancer for the United States—A population-based study from the United States Cancer Statistics database. Pages.
[24] Nahabedian, L., Braberman, V., D'Ippolito, N., (2018) Dynamic update of discrete event controllers. IEEE Transactions on Software Engineering.
[25] Keshet, E. (2018) Dynamic update anaphora logic: A simple analysis of complex anaphora. Journal of Semantics. 35(2), 263-303.
[26] Zhang, Q., Li, B., Yuan, Q., (2020) Database dynamic update management system for power system//Journal of Physics: Conference Series. IOP Publishing. 1550(5), 052001.
[27] Zong, W., Wu, F., Jiang, Z. (2017) A Markov-based update policy for constantly changing database systems. IEEE Transactions on Engineering Management. 64(3), 287-300.
[28] Boyer, F., Gruber, O., Pous, D. (2017) A robust reconfiguration protocol for the dynamic update of component-based software systems. Software: Practice and Experience. 47(11), 1729-1753.
[29] Slik, D., Altman, T., Ciapponi, A.F. (2020) Dynamic update to views of a file system backed by object storage: U.S. Patent 10,740,302. 2020-8-11.
[30] Huo, Z., Gu, B., Huang, H. (2018) Training neural networks using features replay//Advances in Neural Information Processing Systems. 2018, 6659-6668.
[31] Bailey, J.P., Piliouras, G. (2018) Multiplicative weights update in zero-sum games//Proceedings of the 2018 ACM Conference on Economics and Computation. 2018, 321-338.

Received: **09.04.2021**
Accepted: **17.05.2021**

CORRESPONDING AUTHOR

Lina Cui
Yingkou Institute of Technology
University Yingkou Institute of Technology
Yingkou – China

e-mail: mufang8385082170@163.com

© by PSP Volume 30– No. 09/2021 pages 10890-10898 Fresenius Environmental Bulletin

ASSESSMENT OF SOIL EROSION INTENSITY IN THE KUTINSKA RIVER BASIN IN THE PERIOD 1971-2016

Gocic Milena[1,*], Dragicevic Slavoljub[2], Zivanovic Stanimir[3], Ivanovic Radomir[4], Martic Bursac Natasa[1], Stricevic Ljiljana[1], Radivojevic Aleksandar[1], Zivkovic Jelena[1]

[1]Department of Geography, Faculty of Sciences and Mathematics, University of Niš, Serbia
[2]Faculty of Geography, University of Belgrade, Belgrade, Serbia
[3]Emergency Management Sector of Serbia, Belgrade, Serbia
[4]Faculty of Mathematics and Sciences, University of Priština With Temporary Head Office in Kosovska Mitrovica, Kosovska Mitrovica, Serbia

ABSTRACT

Soil erosion assessment plays an important role in the conservation of natural resources because soil degradation is a major problem in many parts of the world. This study explains the links between changes in arable land areas, rural population dynamics and soil erosion intensity. The Erosion Potential Method was used to determine spatial changes in erosion intensity and annual sediment yield in the Kutinska River Basin, Serbia. The analysis of proportional changes was used to determine demographic changes and arable land areas-land use patterns in the basin area. The period of the research is 1971-2016. During the research period, it was determined that there was a decrease in the soil erosion intensity and sediment yield as a consequence of land use changes, primarily due to the reduction of arable land areas, abandonment of arable land by the agricultural population, which caused economic and social changes. Land use changes have been identified as the most important factor in reducing the intensity of soil erosion in the basin. Results of research are the basis for water management, soil and environmental protection measures, argiculture and other human activities.

KEYWORDS:
Erosion Potential Method, Analysis of Proportional Changes, Case Study, Serbia

INTRODUCTION

Soil erosion is one of the most significant form of soil degradation and present serious environmental problem, which is particularly affected by human activity [1-5]. Relief, climate, vegetation, population-settlement and changes of land use are important factors that determine the development of erosion processes. The large number of studies have been caried out to emphasize the effects of demographic and land use changes on soil erosion at different scales [6-11]. Some studies indicate a strong influence of land use changes on soil erosion and sediment rates [12-16]. Land use are expected to change because of human activities in the future [17-19] so the potential effects of these change on soil erosion in the basin need to be determined.

Land degradation caused by soil erosion is a serious problem in the Republic of Serbia. According to [20] 65% of the territory of Serbia is affected by different categories of soil erosion. Therefore, it is very important to assess the current state of soil erosion in the basin in order to prevent further soil disturbance.

In our research we used the Erosion Potential Method (EPM) [21]. This method shows acceptable accuracy and allows the identification of the area that is most sensitive to the erosion process and can be used without climatic and spatial restrictions [22-27].

The main aim of this study was to determine the spatio-temporal change in the intensity of soil erosion during the research period and to determine the strength of the influence of demographic factors and land use changes in the Kutinska River Basin, Serbia.

MATERIALS AND METHODS

Study area. The Kutinska River Basin covers approximately 231 km^2 of the territory of the Republic of Serbia with a total length of 43.03 km (Figure 1). Basin area lies between 21°57′39″ and 22°13′29″ E longitude and 43°04′49″ and 43°18′14″ N latitude. The elevation ranges from 203 to 1810 m above mean sea level (Figure 2).

On the territory of the basin there are 31 rural settlements. In the period 1961-2011 the number of inhabitants decreased. The reduction in the number of inhabitants is present in settlements located in mountain areas that are distant from major roads and city centers.



FIGURE 1
Geographical position of the Kutinska River basin in the Republic of Serbia.

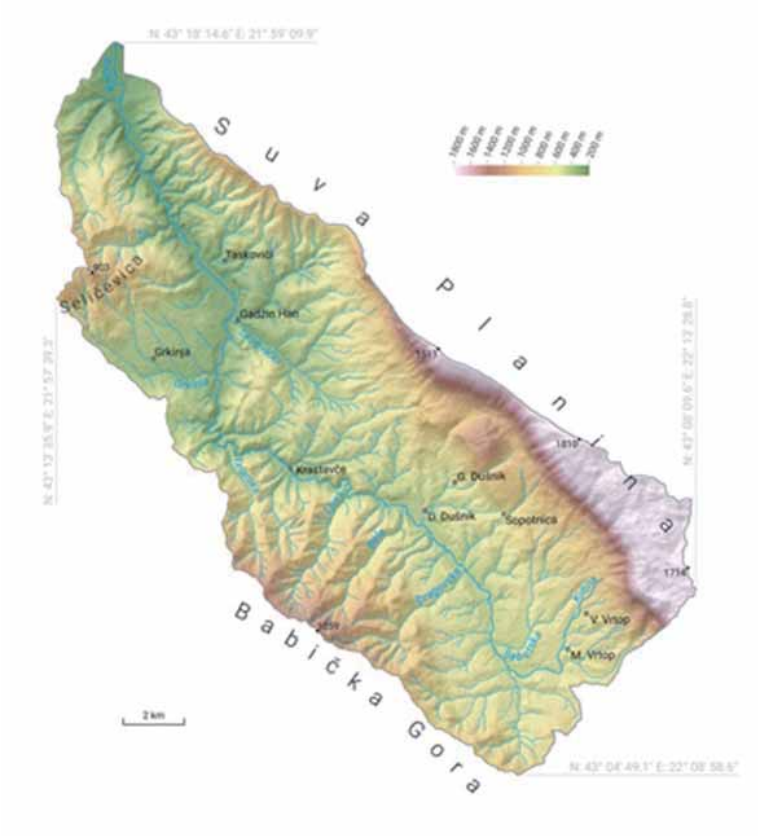


FIGURE 2
Relief map of the Kutinska River basin in the Republic of Serbia.

The demographic decline and depopulation of rural settlements have resulted in an aging population, the emergence of elderly households and a reduction in the working age population of the agricultural population, which over time has led to a reduction in the intensity of erosion in the basin.

The great variability of environmental and economic conditions makes the basin an appropriate area to study the implication of land use dynamics. The diversity of physical and social characteristics makes the Kutinska River Basin susceptible to soil erosion, mainly due to the intensive demographic, economic and land use changes.

Methodology. To calculate gross annual erosion and sediment yield in basin we used the EPM method. The equation 1 for the calculation of annual volume of detached soil due to surface erosion is:

$$W_{year} = T \times H_{year} \times \pi \times \sqrt{Z^3} \times F \quad (1)$$

where, W_{year} is the annual erosion (m^3/year), T is the temperature coefficient, H_{year} is the average yearly preticipation (mm), F is the basin area (km^2), Z is the erosion coefficient.

The temperature coefficient (T) is calculated:

$$T = \sqrt{t} / 10 + 0{,}1 \quad (2)$$

The soil erosion coefficient (Z) can be calculated from the equation 3:

$$Z = Y \times X \times (\varphi + \sqrt{I_{avg}}) \quad (3)$$

where X is the soil protection coefficient, Y is the coefficient of soil resistance, φ is the erosion and stream network development coefficient, I_{avg} is the average slope of the watershed (%) [21]. Five categories of erosion can be singled out according to the methodology: excessive, strong, medium, weak, very weak, and accumulation. The 1971 Erosion Map was used as a basis for quantifying the change in erosion intensity in the Kutinska River Basin.

In order to analyze the suitability of methodology for use with GIS tehniques, we had to prepare the following maps: geological, pedological, terrain slope, temperature and land use in digital form. A raster-based Geographic Information System (GIS) was applied to generate the Erosion Map. Digitization and mapping were done in QGIS 3.6. In orded to determine the changes in erosion intensity, the 1971 Erosion Map was digitized and compared with the 2016 Erosion Map. The differences between these two maps showed changes in the categories of erosive processes as well as sediment yield in the basin.

Analysis of changes in population dynamics and arable land areas for the period 1961-2011 can be determined on the bases on the following equations [28,29]:

$$AC_j = E_j^1 - E_j^0 \quad (4)$$

$$N_j = E_j^0 \times (T^1 / T^0) - E_j^0 \quad (5)$$

$$R_j = E_j^1 - E_j^0 \times (T^1 / T^0) \quad (6)$$

where, AC_j is spatial changes; E_j^1 population/arable land areas in rural settlements in 2011; E_j^0 population/arable land in rural settlements in 1961; N_j regional development component; T^1 total rural population/arable land areas in 2011; T^0 total rural population/arable land areas in 1961; R_j net of relative component.

The typology is based on the net relative change (R_j%). Based on the values of R_j, we have singled out three basic types and one sub-type: progressive, stagnant and regressive type and dominant regressive sub-type [28].

Settlements were the basic territorial level. In this paper we used data from different sources: Statistical Yearbooks of the Statistical Office of the Republic of Serbia (1961-2011) for the demographic data (number of inhabitants, the number of households, the population age, the share of the agricultural population in the total population) [30] and Census of Agriculture for land use data (1961 and 2011) [31].

RESULTS

The spatial and temporal distribution of the erosion coefficient Z indicates that erosion intensity decreased in the period 1971-2016 as shown in Table 1.

The erosion coefficient in the Kutinska River basin in 1971 was 0.556, the annual gross erosion of the sediment was 232306.42 m^3 and the specific annual erosion was 1050.02 m^3 km^{-2} $year^{-1}$ [32]. At that time, 57% of the basin area was affected by intensive and excessive erosion, medium 4.4%, weak 1.4% and very weak 36% as shown in Figure 3A. The most obvious changes in the period of investigation were related to excessive and intensive erosion intensities which in 1971 covered more than half area of the basin and in 2016 only 4% of the basin area. As areas under severe erosion decreased, areas under medium and weak erosion increased, from 38% in 1971 to 54.6% in 2016.

TABLE 1
Distribution of erosion process in the basin (1971 and 2016).

Erosion category	Erosion intensity	Range of Z	Range of W (m^3/km^2/year)	1971		2016	
				F (km^2)	F (%)	F (km^2)	F (%)
I	excessive	1.01-1.50	>3000	8.9	3.8	-	-
II	intensive	0.71-1.00	1200-3000	123.8	53.5	9.41	4.08
III	medium	0.41-0.70	800-1200	10.2	4.4	87.85	38.05
IV	weak	0.21-0.40	400-800	3.3	1.4	126.04	54.6
V	very weak	0.01-0.20	100-400	83.9	36.2	7.55	3.27
	accumulation			2.6	0.9	-	-

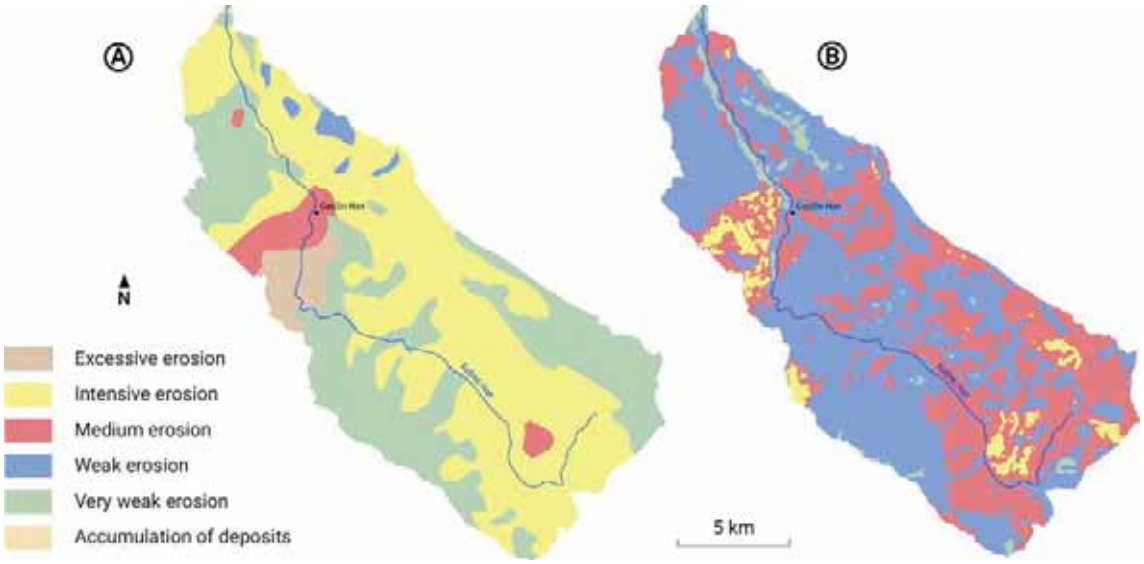


FIGURE 3
Soil erosion map of Kutinska river basin in 1971 (A) and 2016 (B).

Based on the applied methodology, in 2016 the erosion coefficient was 0.390, the annual gross erosion of the sediment was 117869.95 m^3 $year^{-1}$ and specific annual erosion 510.25 m^3 km^{-2} $year^{-1}$, which indicates that the production of the deposit in the basin decreased by 50%. The erosion map shows that in 2016, the entire basin territory was affected by some erosion intensity. Excessive erosion is not represented in the basin on the erosion map from 2016, and intensive erosion in only 4% of the basin territory. It presents a small area along the river, around settlements and important agricultural areas. The Figure 3 shows soil erosion map of Kutinska river basin in 1971 (A) and 2016 (B).

Emigration and demographic aging of the population from 1961 until today have caused changes related to land use. The most intensive agricultural production was at the time of the greatest concentration of the population (1960s). The population has been declining significantly from 21,191 in 1961 to 12,121 in 2011. Pronounced depopulation is present in the area over 500 m in which 30.3% of the total population lived in 1961 and only 8.5% in 2011. Also, comparing the data of the agricultural population from the census of 1961 and 2011, it was noticed that the the total agricultural population decreased from 84% to 11%. The analysis of the age structure also shows that there is an increasing population that can be classified into older age groups. According to the 2011 census, the share of the elderly population (over 65 years old) is 45.6%.

On the territory of all settlements in the basin, a decrease in arable land areas was observed (1961 - 5,232.9 ha; 2011 - 3,021.13 ha). The largest decrease in arable land areas was recorded in settlements at lower altitudes. Changes in the structure of land use in the basin caused changes related to the spatial distribution of erosion categories, so the largest decrease in erosion intensity was recorded in the area along the river and its larger tributaries.

The discrepancy in the periods taken for comparison, demographic and land use changes (1961-2011) and changes in the intensity of erosion (1971-2016), can be explained by the intense period of demographic and agrarian-geographical transformation of rural areas that began in the 1960s and its results became visible decades later, which was confirmed by other researches [6,7].

DISCUSSION

Some studies [33,34] have found an increase in the intensity of erosion caused by agricultural activities. On the other hand, in the Kutinska River Basin, there has been a decrease in the intensity of erosion as a consequence of demographic and land use changes. The reasons for the reduction of erosion should be analyzed in terms of indirect anthropogenic influences. They are the result of abandonment or cessation of agriculture due to migration of the population from rural to urban areas for economic reasons [9]. These impacts have proven to be significant in the basin and need to be analyzed in more detail to determine the level of change and the possible impact on erosion intensity. Findings from this research are in line with [35] who clearly demonstrate that the soil erosion intensity "is highly dependent on agriculture use". Furthermore, various research reports have shown the importance of depopulation [9] and land use changes [10,18,36] to the soil losses and erosion intenisty.

Analysis of proportional changes (1961-2011). Based on the analysis of proportional

changes, the following types and their characteristics were determined:

The progressive type of settlement has R_j value of the total population (R_j > 42.8%) and arable land areas (R_j > 78%). This type is characterized by a positive demographic trend. It is related to settlements located near major roads and cities. Settlements belong to suburban areas, so there is an increase in population. Most of the inhabitants of this type of settlement work in cities, give up agriculture and engage in non-agricultural activities. This leads to a situation where the areas under arable land are reduced. This type of settlement corresponds to a stagnant or regressive type of change of arable land areas.

The stagnant type is characterised by a R_j change in the total population (0 < R_j < 42.8%) and arable land areas (0 < R_j < 78%). Settlements belonging to this type are located in rural areas next to progressive type settlements. The characteristics of this type of settlement are favorable gender and age structure. Settlements of this type are characterized by a reduction in the number of people engaged in agriculture, which leads to reduced arable land areas that is cultivated. Land use changes have caused changes concerning the share of certain categories of land use as well as the economic structure of the population, the share of the agricultural population, the age structure.

The regressive type of total population (0 > R_j < -42.8%) and arable land (0 > R_j < -78%) show negative values. Due to intensive migrations of the rural population in the period 1961-2011, settlements belonging to regressive type recorded a drastic decline in population. These are mostly settlements that are located far away from cities, in sub-mountainous and mountainous parts of the basin, so they are usually characterized by an old population. The old population is no longer able to cultivate the arable land so over time it grows into grass and natural vegetation. In this way, there is a reduction in arable land areas in settlements of this type.

The dominant regressive sub-type of settlement has R_j values of total population (R_j% > - 42.8%) and arable land areas (R_j > -78%). This subtype is present in settlements located in peripheral, mountainous and border areas. It is characterized by negative demographic trends, a drastic decline in population, the old population, but the areas under arable land are not decreasing, but are stagnant and belong to the stagnant type. Figure 4 shows the types of settlements according to analysis of proportional changes in the number of inhabitants (C) and arable land areas (D) 1961-2011.

Land use changes (1961-2011). Structure of land use in rural settlements in the basin area were obtained by comparing data on each category of land use from the agricultural census for 1961 and 2011. The results are giving below in Table 2.

It is considered that arable land is under the greatest influence of people who, through inadequate management, create territories where the intensity of erosive processes is strongest.

During the research period, it was determined that there was a decrease in arable land areas (Table 2). The structure of arable land was dominated by the category of plough land and gardens (75.9% in 1961 and 57.5% in 2011). Other categories belonging to the category of arable land (vineyards, orchards, meadows) covered small areas in the basin and their changes during the research period are insignificant.

The share of areas under forests decreased from 2,183.63 ha (1961) to 1,586.9 ha (2011). This decrease can be explained by the uncontrolled use of wood for firewood and construction. In other circumstances, it could be expected that the reduction of arable land and the reduction of the population, considering the mountainous and sub-mountainous parts, will increase the area under forests, because the vegetation returns to its original state where there is no human influence.

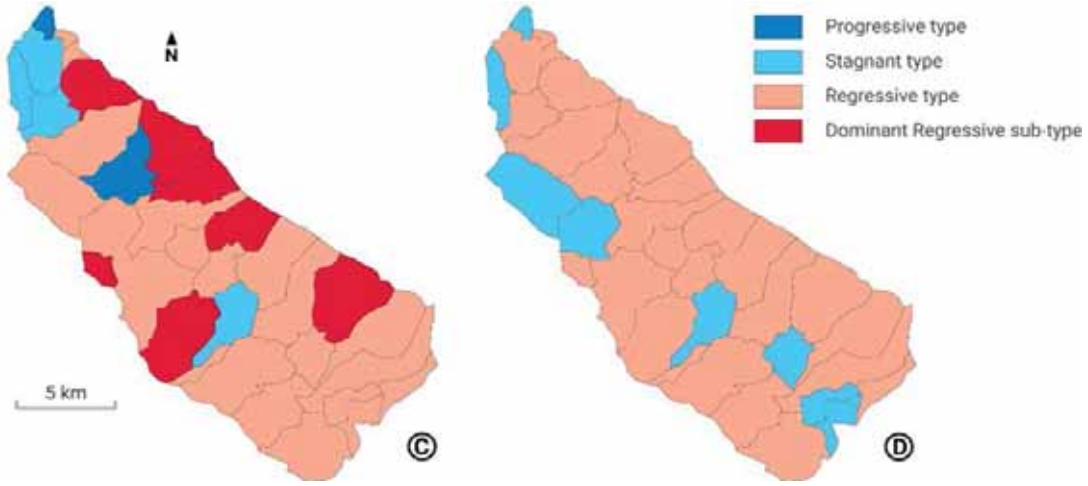


FIGURE 4
Types of settlements according to the change in the number of inhabitants (C) and arable land areas (D) 1961-2011.

TABLE 2
Structure of land use in rural settlements in the territory of the Kutinska River Basin in 1961 and 2011.

Land use	1961.	2011.
	F (ha)	
Plough land and gardens	3,972.3	1,738.4
Vineyards	117.6	68.16
Orchards	441.2	485.9
Meadows	701.8	728.67
Arable land	5,232.9	3,021.13
Forests	2,183.63	1,586.9
Pastures	1,165.3	1,206.86
Other	872.4	1720
Total	9,454.23	7,534.89

Key aspect to control the soil loss is agriculture, particulary the cultivation of certain crops [35] which over time leads to a decrease in erosion intensity because of vegetation recovery [36].

Research in Europe has concluded that the reduction of arable land areas leads to a large reduction in sediment production [7,18,33]. In the basin, the lower terrains are singled out as areas of agricultural production, where the majority of settlements and population are located, so these parts of the basin are with intensive erosive processes. On the other hand, parts of the basin at higher altitudes record a decline in population, which leads to the destruction of once arable land and conversion into meadows, and eventually to overgrowing in the forest, which leads to reduced sedimentation and erosion. However, areas under arable land at higher altitudes are small (due to the mountainous area), so erosion reduction is negligible.

Demographic change. The total population in all settlements in the basin decreased during the research period (1961-2011). The most intensive reduction was found in settlements far from cities and roads. Regarding the distribution of inhabitants by altitude zones, it was determined that the largest number of inhabitants is represented in the altitude zone of 300-500 m, as well as the largest number of settlements (Table 3). According to the latest census (2011), the largest number of inhabitants live in the altitude zone below 300 m (61.5% in 4 settlements). On the other hand, depopulation is present in the area of over 500 m (9 settlements), in which in 1961 lived 30.3% of the total population, and in 2011 only 8.5% [30].

The demographic recession and the unfavorable age structure of the population affected the extremely high participation of elderly households in rural settlements on the territory of the Kutinska River Basin. Despite the decrease in the number of inhabitants, the total number of households during the census years mostly increased. According to [37] the reason for this is "fragmentation of households due to the division of family cooperatives and modern trends of reducing the household to a close family". The analysis of the population of hypsometric zones indicates that depopulation is most intense in zones on higher altitude. The elderly population lives in hilly and mountainous areas, which over time leads to the disappearance of these rural settlements.

A direct consequence of the natural and mechanical movement of the population leads to a disruption of the age structure. The age structure of the population is a significant factor that shows the condition and quality of the population, which is indirectly related to land use in rural areas [38]. The analysis of the age structure of the population is based on the share of age groups: young population (up to 19 years); young middle-aged (20-39 years); older middle-aged (40-64 years) and old population (older than 65 years). The young population accounted 34.6% of the total population (1961) and only 14.8% in 2011. As shown in Figure 5 the percentage of the old population (over 65 years old) was 6.5% in 1961 and 45.6% in 2011.

TABLE 3
Altitude distribution of the population and settlements in the Kutina river basin, 1961-2011.

altitude zones (m)	number of settlements	number of inhabitants (1961)	number of inhabitants (2011)
201-300	4	4,056	7,245
301-400	7	4,533	2,095
401-500	10	6,175	1,572
501-600	6	4,763	947
601-700	3	1,174	202
701-800	1	490	60

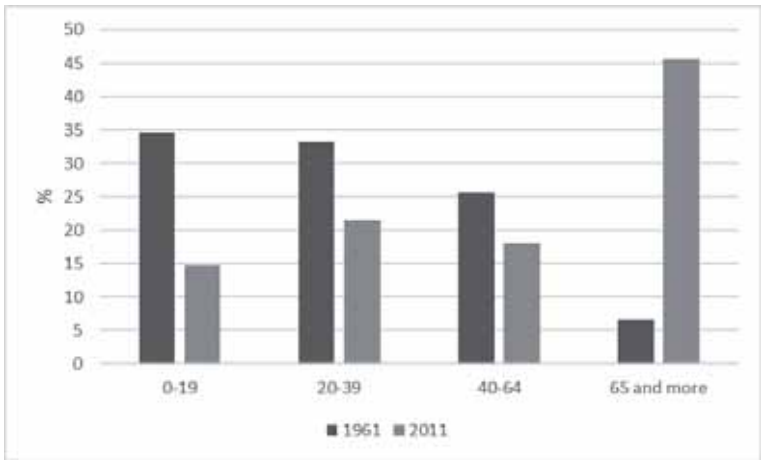


FIGURE 5
Population of rural settlements in the Kutinska River Basin by age groups in 1961 and 2011.

In the basin, in addition to demographic changes in the population structures, the process of deagrarization is also present. This process is related to the abandonment of agriculture by the population for whom it was the main activity and source of income. This has led to changes in the appearance of settlements, migration, disruption of gender and age structure as well as changes in land use. Based on the data from the agricultural census (1961 and 2011), we can conclude that the share of the agricultural population has decreased, from 84% to 11%. This decrease in the share of the agricultural population can be explained by the fact that a larger number of inhabitants in settlements located near cities are starting to engage in non-agricultural activities while agriculture remains as an additional activity. Also, the population of rural settlements is aging, so they are giving up agriculture, and thus the areas under arable land are being reduced.

The identified changes: population aging, the transition of the agricultural population to non-agricultural activities, changes in the economic structure of the population, indirectly caused changes in land use, which stands out as the most important factor in reducing erosion intensity in the basin.

CONCLUSIONS

This research represents an estimate of the change in erosion intensity in the Kutina River Basin in the period 1971-2016. Research has shown that human activities are the main cause of changes in the intensity of soil erosion.

The results show that in the Kutinska river basin a decrease in erosion intensity, sediment production as well as erosion coefficient was recorded. The decrease in the number of inhabitants in the settlements on the territory of the basin was accompanied by the abandonment of agriculture by people who were engaged in agriculture until then and the transition to non-agricultural activities, which led to a significant reduction in the share of agricultural population, from 84% to 11%. The decrease in the share of the agricultural population over time has led to changes in land use. The area under arable land was reduced, which together with demographic changes (reduction of the total population, reduction of the agricultural population, increase of the share of the elderly population in the total population) significantly reduced the erosion intensity in the basin.

The results generated from this study will be useful for determining the changes in soil erosion intensity influenced by land use and demographic changes at the basin level.

REFERENCES

[1] Van Rompaey, A., Govers, G., Puttemans, C. (2002) Modelling land use changes and their impact on soil erosion and sediment supply to rivers. Earth Surface Processes and Landforms. 27, 481-494.

[2] Životić, Lj., Perović, V., Jaramaz, D., Đorđević, A., Petrović, R., Todorović, M. (2012) Application of USLE, GIS and Remote Sensing in the Assessment of soil erosion rates in Southeastern Serbia. Polish Journal of Environmental Studies. 21 (6), 1929-1935.

[3] Serpa, D., Nunes, J. P., Santos, J., Sampaio, E., Jacinto, R., Veiga, S., Lima, J. C., Moreira, M., Corte-Real, J., Keizer, J. J., Abrantes, N. (2015) Impacts of climate and land use changes on the hydrological and erosion processes of two contrasting Mediterranean catchments. Sci Total Environ. 15 (538), 64–77.

[4] Khaledian, Y., Kiani, F., Ebrahimi, S., Brevik, E., Aitkenhead-Peterson, J. (2017) Assessment and monitoring of soil degradation during land use change using multivariate analysis. Land Degradation & Development. 28, 128-141.

[5] Uddin, K., Matin, M. A., Maharjan, S. (2018) Assessment of Land Cover Change and Its Impact on Changes in Soil Erosion Risk in Nepal. Sustainability. 10 (12), 4715.
[6] Kostadinov, S., Zlatić, M., Dragićević, S., Novković, I., Košanin, O., Borisavljević, A., Lakićević, M., Mlađan, D. (2014) Antropogenic Influence on Erosion Intensity Changes in Rasina River Watershed Area upstream from "Ćelije" Water Reservoir, Central Serbia. Fresen. Environ. Bull. 23 (1), 254-263.
[7] Manojlović, S., Antić, M., Sibinović, M., Dragicević, S., Novković, I. (2017) Soil erosion response to demographic and land use changes in the Nišava river basin, Serbia. Fresen. Environ. Bull. 26 (12), 7547-7560.
[8] Perović, V., Kadović, R., Đurdjević, V., Braunović, S., Čakmak, D., Mitrović, M., Pavlović, P. (2019) Effects of changes in climate and land use on soil erosion: case study of the Vranjska Valley, Serbia. Regional Environmental Change. 19 (4), 1035-1046.
[9] Tošić, R., Lovrić, N., Dragićević, S. (2019) Assessment of the impact of depopulation on soil erosion: Case study- Republika Srpska (Bosnia&Herzegovina). Carpathian Journal of Earth and Environmental Sciences. 14 (2), 505-518.
[10] Spalevic, V., Barovic, G., Vujacic, D., Curovic, M., Behzadfar, M., Djurovic, N., Dudic, B., Bıllı, P. (2020) The impact of land use changes on soil erosion in the river basin of Miocki Potok, Montenegro. Water. 12 (11), 2973.
[11] Manojlović, S., Sibinović, M., Srejić, T., Hadud, A., Sabri, I. (2021) Agriculture land use change and demographic change in response to decline suspended sediment in Južna Morava river basin (Serbia). Sustainability. 13 (6), 3130.
[12] Van Rompaey, A., Govers, G., Van Hecke, E., Jacobs, K. (2001) The impact of land use policy on the soil erosion risk: A case study in central Belgium. Agriculture Ecosystems & Environment. 83 (1), 83-94.
[13] Bakker, M., Govers, G., Kosmas, C., Vanacker, V., Van Oost, K., Rounsevell, M. (2005) A soil erosion as a driver of land use change. Agriculture, Ecosystems and Environment. 105, 467-481.
[14] Lopez-Vicente, M., Poesen, J., Navas, A., Gaspar, L. (2013) Predicting runoff and sediment connectivity and soil erosion by water for different land use scenarious in the Spanish Pre-Pyrenees. Catena. 102, 62-73.
[15] Ozsahin, E., Duru, U., Eroglu, I. (2018) Land Use and Land Cover Changes (LULCC), a Key to Understand Soil Erosion Intensities in the Maritsa Basin. Water. 10(3), 335.
[16] Almohamad, H. (2020) Impact of land cover change due to armed conflicts on soil erosion in the basin of the Northern Al-Kabeer River in Siria using the RUSLE Model. Water. 12(12), 3323.
[17] Sharma, A., Tiwari, K.N., Bhadoria, P. B. (2011) Effect of land use land cover change on soil erosion potential in an agricultural watershed. Environmental Monitoring and Assessment. 173(1-4), 789-801.
[18] Perović, V., Jakšić, D., Jaramaz, D., Koković, N., Čakmak, D., Mitrović, M., Pavlovıć, P. (2018) Spatio-temporal analysis of land use/land cover change and its effects on soil erosion (Case study in the Oplenac wine-producting area, Serbia). Environmental Monitoring and Assessment. 190 (11), 675.
[19] Ozsahin, E., Eroglu, I. (2019) Soil Erosion Risk Assessment due to Land Use/Cover Changes (LUCC) in Bulgaria from 1990 to 2015. Alinteri Journal of Agriculture Science. 34 (1), 1-8.
[20] Miljković, P., Belanovıć Sımıć S. (2020) Soil loss data comparation using USLE and WaTEM/SEDEM model in the Polomska River Catchment, Serbia. Fresen. Environ. Bull. 29, 5012–5020.
[21] Gavrılović, S. (1972) Torrential flow Engineering and Erosion Processes. - Izgradnja
[22] Haghizadeh, A., Teang Shui, L., Godarzi, E. (2009) Forecasting Sediment with Erosion Potential Method with Emphasis on land use changes at basin. Electronic Journal of Geotechnical Engineering. 14, 1-12.
[23] Solaimani, K., Modallaladoust, S., Lotfi, S. (2009) Investigation of land use changes on soil erosion process using geographical information system. Intenational Journal of Envoronmental Sciences and Technology. 6 (3), 415-424.
[24] Da Silva, R. M., Santos, C. A. G., Silva, A. M. (2014) Predicting soil erosion and sediment yield in the Tapacura Catchement, Brazil. Journal of Urban and Environmental Engineering. 8 (1), 75-82.
[25] Dragičević, N., Karleuša, B., Ožanić, N. (2016) A review of the Gavrilović method (erosion potential method) application. Građevinar. 68 (9), 715-725.
[26] Tošić, R., Lovrić, N. (2018) Assessment of soil erosion and sediment yield using erosion potential method: Case study- Vrbas River basin (B&H). Bulletin of the Serbian Geographical Society. 98 (1), 1-14.
[27] Gocić, M., Dragićević, S., Radivojević, A., Martić Bursać, N., Stričević, Lj. and Đorđević, M. (2020) Changes in soil erosion intensity caused by land use and demographic changes in the Jablanica River Basin, Serbia. Agriculture 10, 345.

[28] Antić, M., Šantić, D., Kašanin-Grubin, M., Malić, A. (2017) Sustainable rural development in Serbia –Relationship between population dynamicss and environment. Journal of Environmental Protection and Ecology. 18 (1), 323–331.
[29] Manojlović, S., Antić, M., Šantić, D., Sibinović, M., Carević, I., Srejić, T. (2018) Anthropogenic Impact on Erosion Intensity: Case Study of Rural Areas of Pirot and Dimitrovgrad Municipalities, Serbia. Sustainability. 10 (3), 826.
[30] Statistical Office of the Republic of Serbia (2014) Internet Site for Data on Census 1961-2011. online avilable on www.stat.gov.rs (last accessed 17/3/2019).
[31] Statistical Office of the Republic of Serbia (2014) Internet Site for Data on Agriculture Census 1961-2011. online avilable on www.stat.gov.rs (last accessed 17/3/2019).
[32] Lazarević, R. (1983) Erosion Map of SR Serbia. Scale 1:500000; Institute of Forestry: Belgrade, Serbia.
[33] Zorn, M., Komac, B. (2009) Response of soil erosion to land use change with particular reference to the last 200 years (Julian Alps, Western Slovenia)' In IAG Regional Conference on Geomorphology: Landslides, Floods and Global environmental change in mountian regions, Brasov, Romania, 39-47.
[34] Spalevic, V., Barovic, G., Fikfak, A., Kosanovic, S., Đurovic, M., Popovic, S. (2016) Sediment yield and Land use changes in the Northern Montenegrin Watersheds: Case study of Seocki Potok of the Polimlje Region. Journal of Environmental Protection and Ecology. 17 (3), 990–1002.
[35] Mohammadi, M., Khaledi Darvishan, A., Spalevic, V., Dudic, B., Billi, P. (2021) Analysis of the impact of land use changes on soil erosion intensity and sediment yield using the IntErO model in the Talar watershed of Iran. Water. 13, 881.
[36] Feng, T., Wei, W., Chen, L., Rodrigo-Comino, J., Die, C., Feng, X., Ren, K., Brevik, E. C., Yu, Y. (2018) Assessment of the impact of different vegetation patterns on soil erosion processes on semiarid loess slopes. Earth Surf. Process. Landf. 43, 1860-1870.
[37] Antić, M. (2016) Anthropogeographical studies of the settlement of Zaplanje. Belgrade, 1-358.
[38] Zlatić, M. (2002) Socio-Economic Aspects of Degradation and Soil Management for Sustainability in Mountainous Regions. Natural and Socio-Economic Effects of Erosion Control in Mountainous Regions, key note paper, Vrujci Spa, Serbia. 497-516.

Received: **09.04.2021**
Accepted: **17.05.2021**

CORRESPONDING AUTHOR

Gocic Milena
Department of Geography
Faculty of Sciences and Mathematics
University of Niš
Niš 18000 – Serbia

e-mail: milena.j.gocic@gmail.com

© by PSP Volume 30– No. 09/2021 pages 10899-10907 Fresenius Environmental Bulletin

OPTIMIZATION PROTOCOL FOR IN VITRO ESTABLISHMENT OF SELECTED APRICOT GERMPLASM

Farhat Ali Khan[1], Aftab Afzal[1], Shazia Erum[2], Shabana Irum[1,*], Haji Khan[3], Zahid Hussain[3], Hassan Sher[4], Nadia Bostan[5], Fazal Rabi[5]

[1]Department of Botany, Hazara University Mansehra, Khyber Pakhtunkhwa, Pakistan
[2]National Agricultural Research Centre, Islamabad, Pakistan
[3]Center of Biotechnology and Microbiology, The University of Swat, Khyber Pakhtunkhwa, Pakistan
[4]Department of Botany, The University of Swat, Khyber Pakhtunkhwa, Pakistan
[5]Department of Horticulture, The University of Agriculture Peshawar, Khyber Pakhtunkhwa, Pakistan

ABSTRACT

Novelty statement: During Apricot *in-vitro* propagation a lot of difficulties were faced during the experiment (high death rate and contamination).

Therefore, this work will have the best approach for the apricot establishment based on disinfectants. In the other treatments, the survival percentage was very low and with high contamination as compared to sodium hypochlorite 28% plus ethanol 70% which showed a high rate of survival with a little bit of contamination. This was the first work (surface sterilization) on the selected germplasm of apricot from Gilgit Baltistan and Quetta.

The main purpose of the presented study was to investigate the techniques for *in vitro* surface sterilization of Apricot selected germplasm (Trivet, Share, Aluchi wala, Castle bright, Habi sharot, Habi gulmet, and Pana sherqila). Shoot tips of the selected plants were used as a source of explants. The shoots were previously sterilized using six treatments. The disinfectant treatment was based on sodium hypochlorite 15, 20 and 25%, Ethanol 70%, and Sodium hypochlorite 28% with the combination of ethanol 70% and also with double distilled water 100% and inoculated in MS media supplemented with BAP 1mg/l. to eliminate microbial contamination and to increase the survival percentage of Apricot germplasm. Results showed that Sodium hypochlorite 28% plus ethanol 70% (15+1min) were the best results for survival percentage in Trivet (100%), Habi sharot, Gulmet, and Pana sherqila (80%), while fungal 20%, bacterial 40%, viral 40% and 60% deaths were naturally recorded, although in all other treatments high rate of contamination and naturally declined of explants were stared after some time as compared to control.

KEYWORDS:
In vitro establishment, *Prunus Armeniaca*. L, Surface sterilization, Disinfectants

INTRODUCTION

Apricot (*Prunus armeniaca* L) belongs to the family Rosaceae, genus *Prunus* L. and the section Armeniaca (Lam). The world's largest producers of apricots are Turkey and Iran accounting for 21.6% and 14.7% of world apricot production respectively, followed by Pakistan, Uzbekistan, Italy, Algeria, Japan, Morocco, Egypt, and Spain [1], Although Sendall *[2]* suggested that Pakistan total apricot production is approximately 300,000 tons of fresh apricot, making it the world's fourth-largest producer. According to Provincial Crop Reporting Service Centers (2015), production of apricot per year was recorded in Baluchistan was 157651 (t), Khyber Pakhtunkhwa 12606 (t), Punjab 247 (t) while, there is no production recorded in Sindh. Gilgit Baltistan (GB) and Baluchistan are the two main apricot growing regions in Pakistan where, planting density is only 230 trees/ha, which is much less than the recommended 750 trees/ha, due to apricots being planted around field edges, rather than orchards. There are many issues which are responsible for the reduction of apricot at a national and international level, for example, worldwide apricots losses due to some biotic factors like Bacterial, Viral, Fungal, Phytoplasmal and Nematodal diseases (The American Phytopathological Society). Abnormal galls and tumors were observed on the roots and crown regions of the apricot plants. Moreover, secondary wood rots were also observed in some of the infected apricot trees. Gummosis is associated with diseases, pests, and also with other abiotic factors such as high winds and snow. Pruning and grafting with unsterilized tools can also cause gummosis. Some researchers consider gummosis as the non-specific defensive response of trees against diseases and other differential stresses [3]. In Pakistan, especially in Gilgit Baltistan (GB), the production of apricots has dropped largely as a result of diseases such as gummosis, cankers, crown galls, grey mold, and shot hole disease [4]. Anyhow the disease has seriously affected thousands of apricot trees in Gilgit-Baltistan [5]. In Pakistan, most apricots are consumed domestically and only a minor proportion is exported fresh or dried. Only 1% of the land area in Gilgit is cultivated and the average farm size is less than 1(ha). The quality of apricots is the generally poor and low market value [2]. There is a growing demand for apricots and their products in

Chitral and outsides from Chitral where there are very poor transportation facilities to other parts of the country and outside the country [6].

There were a lot of problems faced during Peach establishment through *in vitro* propagation, therefore to established an appropriate protocol based on surface sterilization to reduce the loss of Apricot due to high mortality and due to fungal, viral, and bacterial diseases various disinfectants were tested.

MATERIALS AND METHODS

Preparation. Total seven germplasm of Apricot were collected from Gilgit and Quetta, Baluchistan (Trivet, Share, Aluchi wala, Castle bright, Habi sharot, Habi gulmet, and Pana sherqila) and ex-situ conserved in the living repository of BCI (Bio-resource conservation institute) in PGRP (Plant Genetic Resource Program) NARC (National Agricultural Research Centre), Islamabad (Table.1). Experiments were carried out at Plant Tissue Culture (*In-vitro*) Laboratory, Bio-resource Conservation Institute (BCI) NARC, Islamabad. Ex-plant from apical tips were collected and sterilization was carried out by washing them with running tap water for 40 minutes by adding some droplets of Tween-20 and detergent (dish-wash). After that, the explants were dis-infected with Sodium hypochlorite and with Ethanol solutions for 1 to 15 min in a laminar flow hood (Table. 2). Then the explants were washed with double distilled water (100%) 3 to 5 times each [7]. Explants were then cut at both ends under the aseptic condition to remove damaged edges.

Media preparation and inoculation. Explants were cultured in jars containing 40 ml of MS [8] medium supplemented with BAP 1 mg/l (6-benzyl amino purine), 30 (gm) sucrose, and 7 (gm) of agar. After the inoculation of ex-plant, the jars were sealed properly with caps and covered with para-film and then labeled, and were placed in the growth room with a photoperiod of (light/dark) 16/8 hours by using cool-white fluorescent lamps at 25 ± 2°C and light intensity (4000 Lux led) [9].

Study design and Statistical analysis. For each sterilization treatment, a complete randomized design (CRD) with five replications was used. Data were recorded on monthly basis by including the number of contamination (fungal, bacterial, viral, and naturally dead), and survived cultures were also noted after six months. Through statistics 8.1 software LSD and ANOVA were done and excel was used for making the graphs and descriptive state.

TABLE 1
Passport data of selected Apricot germplasm

S. No	Indigenous data	
1	Apricot trivet	Gilgit Baltistan
2	Apricot share	Gilgit Baltistan
3	Apricot aluchi wala	Gilgit Baltistan
4	Apricot castle bright	Quetta, Baluchistan
5	Apricot habi sharot	Gilgit Baltistan
6	Apricot habi gulmet	Gilgit Baltistan
7	Apricot pana sherqila	Ghizer Gilgit Baltistan

RESULTS

Total six treatments were used during the study. Current results showed that all the dis-infected treatments were shown the best results at the start but after some time it was started declined although 28% Sodium hypochlorite and 70% ethanol were best for survival percentage. It was suggested from the current work that 100 % survival percentage was recorded in Apricot trivet, 80% in Habi gulmet, Habi sharot and Pana sherqila, while 60% in castle bright, 40% in Aluchi wala, which was dis-infected with Sodium hypochlorite 28% plus ethanol 70 % (15+1) in

TABLE 2
The Treatment combination for sterilization

Treatment code	Treatment	Percent (%)	Exposure time (min)
T_0	Double distilled water	100	15
T_1	Sodium hypochlorite	15	15
T_2	Sodium hypochlorite	20	15
T_3	Sodium hypochlorite	25	15
T_4	Ethanol	70	3
T_5	Sodium hypochlorite + Ethanol	28+70	15+1

MS media supplemented with BAP 1mg/l as compared to (MS) control, and these plantlets were also survived after six months (Table. 3; Figure 6, 7 and 8 (a) and (b). The current result also revealed that Sodium hypochlorite 20% showed the best result (Habi sharot, 100%) in starting months (Figure 3), followed by Sodium hypochlorite 25% (Share and

Aluchi wala 80%) (Figure 4) and the very weak response showed by Sodium hypochlorite 15% (Figure 2) followed by Ethanol 70% (Figure 5) and 100% distilled water respectively (Figure 1). Very low contamination was recorded in selected Apricot germplasm in the treatment 28% Sodium hypochlorite and 70% ethanol as compared to control and other treatments. Fungal contamination was started at the 3rd month of culturing in Pana sherqila which was 20% (Figure 9 and 13. (a), otherwise bacterial contamination (Figure 10 and 13. (d) was found in month 2nd in Castle bright (20%) and at 5th month in Habi sharot and Habi gulmet (20%) and viral contamination at 2nd month was recorded in Aluchi wala (Figure 11 and 13. (b), while naturally, death (browning) occurred in genotypes Share 40% and Aluchi wala (20%) (Table 4. Figure 12 and 13. (c).

Analysis of variance showed that the viral and fungal contamination showed significant results, while others were non-significant (Table. 5), whereas LSD of the selected germplasm were non-significant results (Table. 3).

TABLE 3

(LSD) All pair-wise comparison (Mean) of the six treatments survival % in BAP (1mg/l) and in MS (control) media after six months; T0=100% Distilled water (control), Sodium hypochlorite T1= 15%, T2=20%, T3= 25%, T4= 70% ethanol and T5= sodium hypochlorite 28%+ethanol 70%

Treatments	T_0		T_1		T_2		T_3		T_4		T_5	
Genotypes	**Control**	**BAP**	**Control**	**BAP**	**Control**	**BAP**	**Control**	**BAP**	**Control**	**BAP**	**Control**	**BAP**
Apricot trivet	0	0	0.0A	0.2A	0.2AB	0.6A	0.2A	0.0B	0.0A	0.0A	0.4A	1.0A
Apricot share	0	0	0.2A	0.2A	0.2AB	0.4A	0.6A	0.8A	0.0A	0.0A	0.6A	0.6AB
Apricot aluchi wala	0	0	0.0A	0.4A	0.2AB	0.4A	0.4A	0.8A	0.0A	0.2A	0.4A	0.4B
Apricot castle bright	0	0	0.0A	0.2A	0.0B	0.4A	0.4A	0.8A	0.0A	0.0A	0.2A	0.6AB
Apricot habi sharot	0	0	0.2A	0.4A	0.4AB	0.6A	0.4A	0.6A	0.2A	0.0A	0.4A	0.8AB
Apricot habi gulmet	0	0	0.2A	0.2A	0.6A	0.4A	0.4A	0.6A	0.0A	0.0A	0.8A	0.8AB
Apricot pana sherqila	0	0	0.2A	0.4A	0.4AB	0.4A	0.6A	0.6A	0.0A	0.2A	0.6A	0.8AB
LSD (0.05)	-	-	0.4380	0.6384	0.5997	0.7096	0.6925	0.5997	0.2190	0.3097	0.6750	0.5997

TABLE 4

(LSD) All pair-wise comparison of Fungal, Bacterial, Viral and Mortality rate of selected apricot germplasm

Genotypes	Fungal	Viral	Bacterial	Mortality
Apricot trivet	0.0A	0.0B	0.0A	0.0B
Apricot share	0.0A	0.0B	0.0A	0.4A
Apricot aluchi wala	0.0A	0.4A	0.0A	0.2AB
Apricot castle bright	0.0A	0.0B	0.2A	0.0B
Apricot habi sharot	0.0A	0.0B	0.2A	0.0B
Apricot habi gulmet	0.0A	0.0B	0.2A	0.0B
Apricot pana sherqila	0.2A	0.0B	0.0A	0.0B
LSD (0.05)	0.2190	0.2682	0.3793	0.3462

TABLE 5

(ANOVA) Effect of sodium hypochlorite (28%) +Ethanol (70%), Mortality, Survival, Fungal, Bacterial and Viral contamination load (100% double distilled water) of apricot ex-plant after six months

Source of variation	DF	Fungal load	Bacterial load	Viral load	Mortality rate	Survival %
Genotypes	6	0.02857*	0.08571 ^{NS}	0.04286*	0.07143 ^{NS}	0.21429 ^{NS}
Error	28	-	-	-	-	-
Total	34	-	-	-	-	-
SS		0.17143	0.34286	0.68571	0.74286	1.14286
MS		0.02857	0.05714	0.11429	0.12381	0.19048
F		1.00	0.67	2.67	1.73	0.89
P		0.4448	0.6771	0.0357	0.1501	0.5162
CV		591.61	341.57	362.28	311.80	64.81

** = Significant at 1% α: * = Significant at 5% α: NS=Non-significant CV=Coefficient of variation: DF= degree of freedom: SS = Sum of squares: MS=Means of squares: P= probability

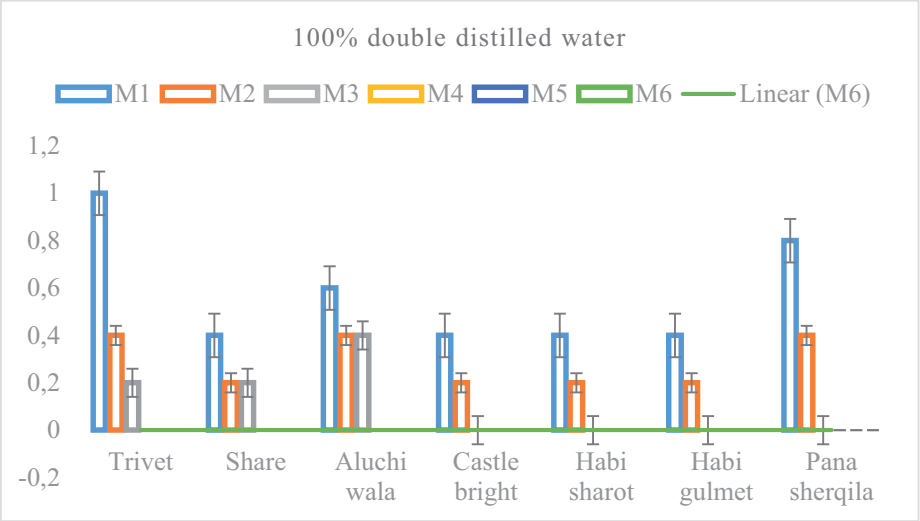


FIGURE 1
Survival percentage up to 6th Month (M=Month)

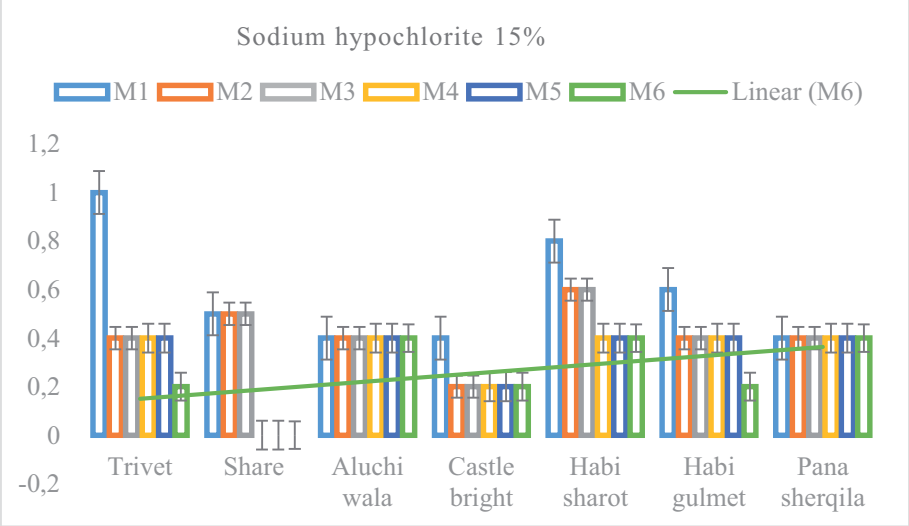


FIGURE 2
Survival percentage up to 6th Month (M=Month)

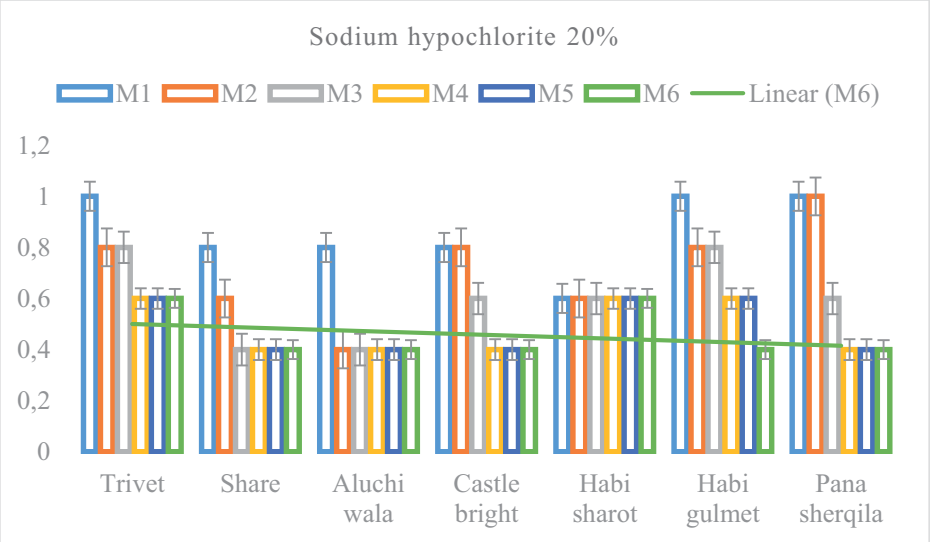


FIGURE 3
Survival percentage up to 6th Month (M=Month)

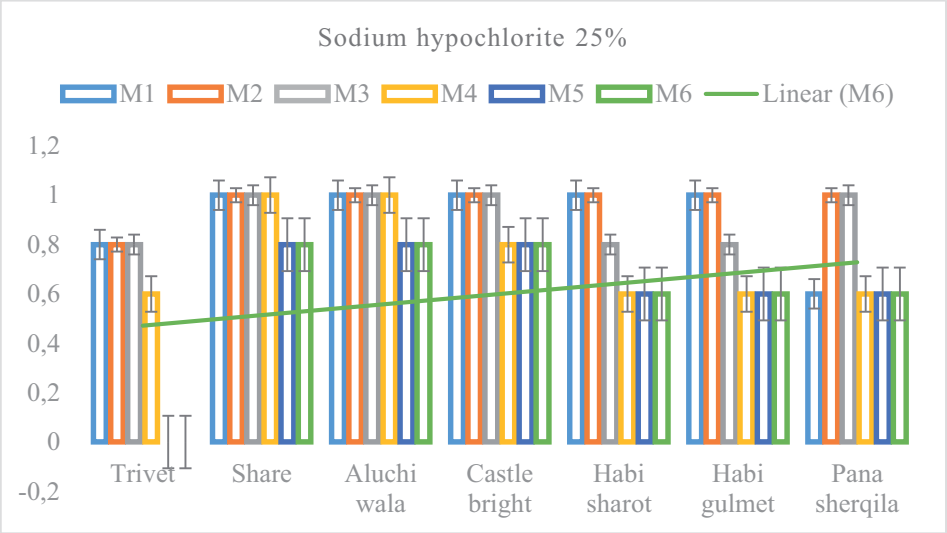


FIGURE 4
Survival percentage up to 6th Month (M=Month)

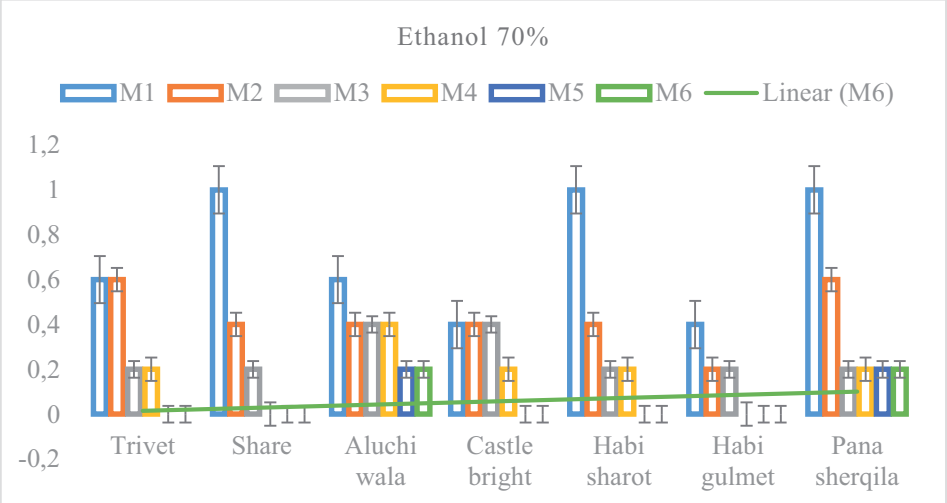


FIGURE 5
Survival percentage up to 6th Month (M=Month)

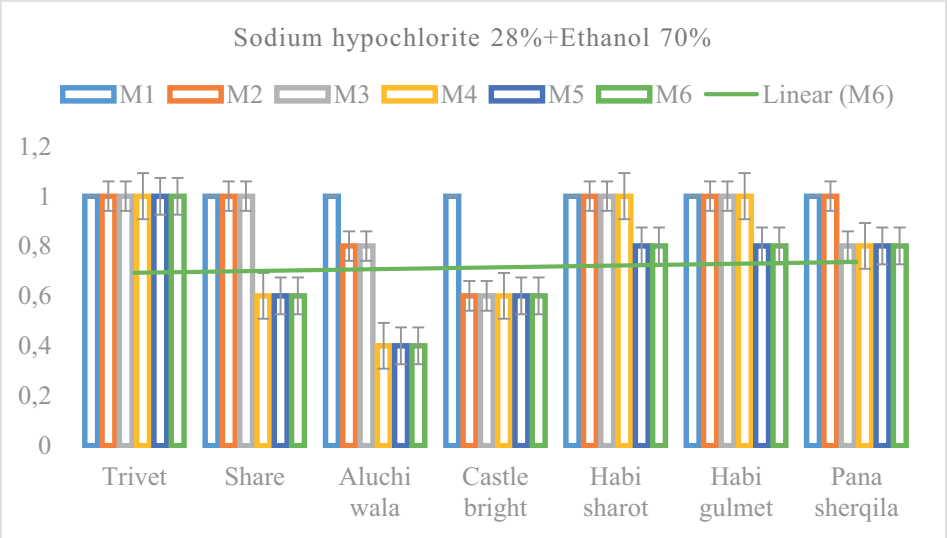


FIGURE 6
Survival percentage up to 6th Month (M=Month)

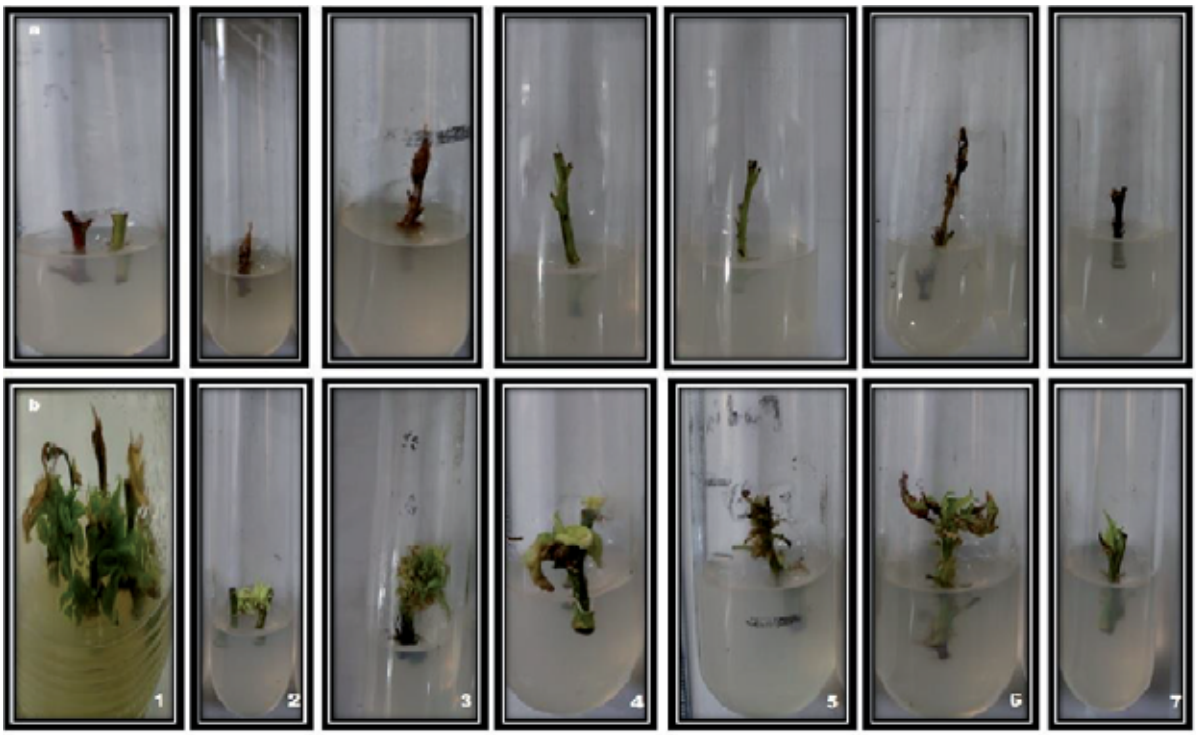


FIGURE 7
Survival percentage of Apricot germplasm after six-month (Sodium hypochlorote 28% + Ethanol 70%) (a) Control (b) Bap1mg/l
(1). Trivet (2). Share (3). Aluchi wala (4). Castle bright (5). Habi sharot (6). Habi gulmet (7). Pana sherqila

DISCUSSION

Our recent studies shows that the highest survival percentage was recorded in Apricot ex-plants when those were dis-infected with Sodium hypochlorite 28% for 15 min plus Ethanol (70%) for 1 min, which was supported Koubouris and Vasilakakis [10], according to the highest culture survival (62.5%) were recorded when ex-plants were dis-infected with 0.75% Sodium hypochlorite for 15 min, and with ethanol 1 min, therefore it was also concluded from the current research that 15 minutes treatment of Sodium hypochlorite and ethanol with 1 min treatment is beneficial for the higher survival rate of Apricot ex-plant. Our recent activity was also supported by Farag [11], who's suggested that Sodium hypochlorite was very effective for the establishment of apricot to give a 90% survival rate. Current work suggested that all other treatments were declined after some time due to natural death or due to contamination but those ex-plants which were disinfected with Sodium hypochlorite 28 % plus ethanol 70% were showed very low contamination as compared to other treatments, although recent work was in an agreement with Farag [11], according to the increasing or decreasing the duration reduced the survival percentage significantly to 70 and 60 %, respectively. lower concentrations of Sodium hypochlorite solution significantly resulted in a reduction in the survival percentage and used an increase in the contamination of ex-plants even with longer durations, up to 25 min. The recent result was also showed agreement with Yildirim [*12]* according to them 25 ± 2 °C, provided with a 16-hours photoperiod under cool white fluorescent light at 40 µ mol m-2 s-1, and transferred to fresh medium every 3-4 weeks (standard growing conditions).



FIGURE 8
Survival percentage of Apricot germplasm in BAP1mg/l (Sodium hypochlorite 28%+Ethanol 70% (a) Month 1st (b) Month 6th

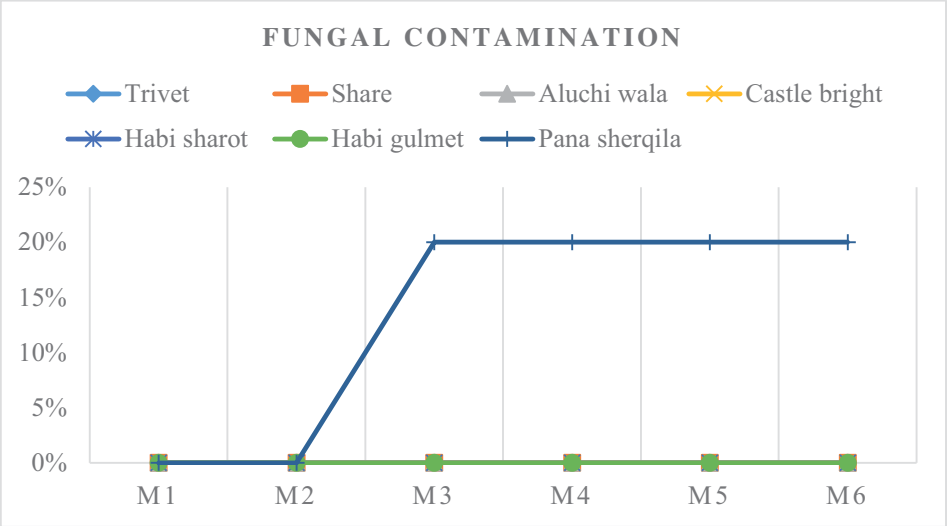


FIGURE 9
Fungal contamination up to 6th Month (M=Month)

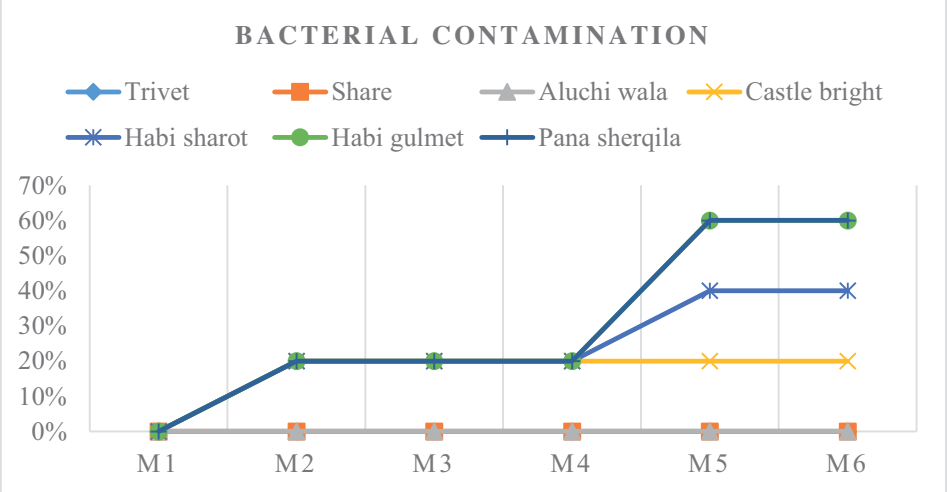


FIGURE 10
Bacterial contamination up to 6th Month (M=Month)

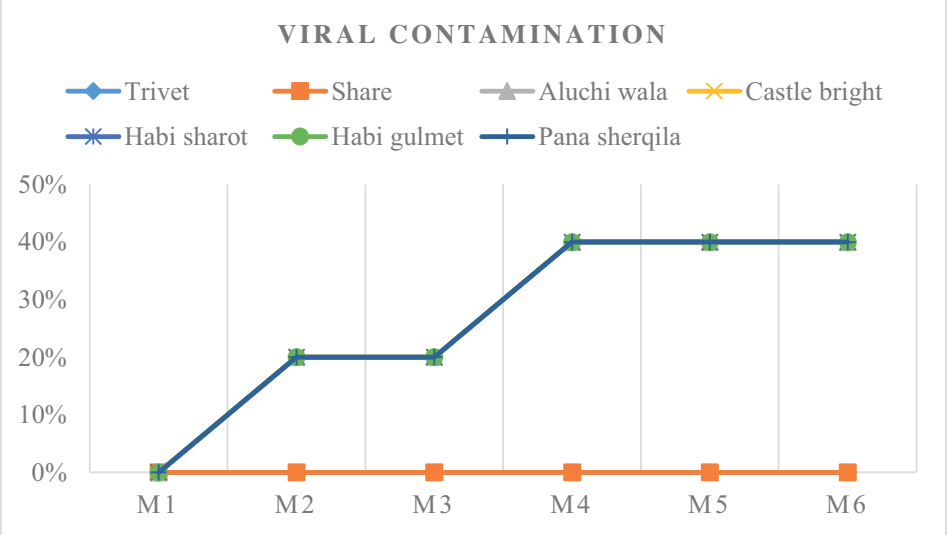


FIGURE 11
Viral contamination up to 6th Month (M=Month)

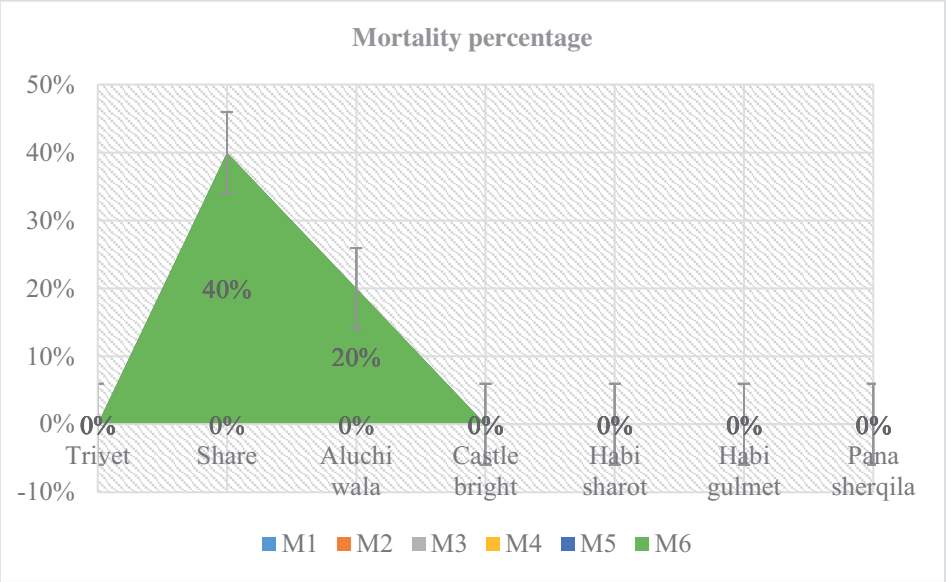


FIGURE 12
Mortality rate up to 6th Month (M=Month)



FIGURE 13
Contamination load in Apricot ex-plants
(a). Fungal infection (b). Viral infection (c). Naturally dead (d). Bacterial infection

CONCLUSIONS

From the current activity, it was concluded that Ethanol 70% + Sodium hypochlorite 28% were best dis-infected treatment for surface sterilization of shoot tips (ex-plants) from different Apricot germplasm, which were survived up to six months as compared to other disinfectants used in the present work, as all other plantlets of selected apricot germplasm were expired after six months. Very high Fungal, bacterial and viral contamination was found when the ex-plants were sterile with all other concentrations of ethanol and sodium hypochlorite as compared to Ethanol 70% + Sodium hypochlorite 28% which showed a very low contamination rate. It was also concluded from the present study that double distilled water (100%), were not enough treatment for Apricot ex-plants sterilization and their establishment. By using sodium hypochlorite with the combination of ethanol will be the best protocol for the establishment of apricot germplasm.

REFERENCES

[1] Fao, Food and Agriculture Organization, United Nations. (2010). Agriculture statistics: Apricot. FAOSTAT.
[2] Sendall, A., Mir, M., Khabir, A. (2013) Apricot Value Chain Assessment Final Report for the Agribusiness Project. USAD. 2-58.
[3] Li, H.Y., Cao, R.B., Mu, Y.T. (1995) In vitro inhibition of Botryosphaeria dothidea and Lasiodiplodia theobromae, and chemical control of gummosis disease of Japanese apricot and peach trees in Zhejiang Province, China. Crop Prot. 14(3), 187-191.
[4] Aqleem, A. (2017b) A report of grey mold disease on grapes caused by Botrytis cinerea in Gilgit-Baltistan, Pakistan. Clin. Biotechnol. Microbiol. 1 (3), 117-119.

[5] Moyo, P., Damm, U., Mostert, L., Halleen, F. (2018) Eutypa, Eutypella, and Cryptovalsa Species (Diatrypaceae) Associated with Prunus Species in South Africa. Plant Dis. 102 (7), 1402-1409.
[6] Hussain, S., Hussain, E., Partap, U. (2017) Strategies for apricot value chain development in Chitral, Pakistan. ICIMOD Working Paper 2017/21. Kathmandu: ICIMOD, 1-44
[7] Wolella, K.E. (2017) Surface sterilization and in vitro propagation of Prunus domestica L. cv. Stanley using axillary buds as explants. Journal of Biotech Research. 8 (1), 18-26
[8] Murashige, T. and Skoog, F. (1962) A Revised Medium for Rapid Growth and Bio Assays with Tobacco Tissue Cultures Physiologia Plantarum. 15 (3), 473–497.
[9] Arab, M.M., Yadollahi, A., Shojaeiyan, A., Shokri, S., Ghojah, M.S. (2014) Effects of nutrient media, different cytokinin types and their concentrations on in vitro multiplication of G. N15 (hybrid of almond peach) vegetative rootstock. Genet. Eng. Biotechn. 12 (2), 81–87
[10] Koubouris, G. and Vasilakakis, M. (2006) Improvement of in vitro propagation of apricot cultivar 'Bebecou'. Springer. 85 (2),173–180.
[11] Farag, K., Nagy, N., Soliman, H., Ahmad, M. (2012) In vito propagation of apricot (prunusnarmeniaca l.) growing at saint catherine valleys in sinai peninsula, Egypt. J.Agric. & Env. Sci. 11 (1), 1-35
[12] Yildirim, H., Onay, A., Ilkat, E., Akturk, Z. (2011) Micropropagation of the apricot (Prunus armeniaca L.) cv. Hacıhaliloglu by means of single node culture. Turk. J. Agric. 35 (1), 55-64.

Received: **09.04.2021**
Accepted: **17.05.2021**

CORRESPONDING AUTHOR

Shabana Irum
Department of Botany,
Hazara University Mansehra,
Khyber Pakhtunkhwa – Pakistan

e-mail: shabanairum911@gmail.com

© by PSP Volume 30– No. 09/2021 pages 10908-10924 Fresenius Environmental Bulletin

COMPARATIVE EVALUATION OF STAND-ALONE HYBRID POWER SYSTEM WITH DIFFERENT ENERGY STORAGES

Zafer Ozturk[1,*], Salih Tosun[1], Ali Ozturk[2], Onur Akar[3]

[1]Department of Electrical-Electronics Engineering, Institute of Science, Duzce University, Duzce, Turkey
[2]Department of Electrical-Electronics Engineering, Duzce University, Duzce, Turkey
[3]Department of Electric and Energy, Istanbul Gedik University, Istanbul, Turkey

ABSTRACT

Nowadays, increasingly technological improvements and population augmentation lead to searching for new energy resources. The limited energy resources against growing energy demand lead increase in the trend towards Renewable Energy Resources (RES) such as solar and wind. The lack of continuity in energy generation of RES due to weather conditions causes fluctuations in the power network. The energy surplus from RES can be charged, and then the stored energy can be discharged if needed to prevent the fluctuation. The utilization of storage increases energy costs. However, it is possible to reduce this cost thanks to proper energy management. Thus, it is of great importance to determine the most appropriate storage management according to generation and loading profile. In this study, management of a hybrid power system (HPS) is proposed for the facility location in Balıkesir, Turkey. The proposed HPS includes modeling of solar panels (PV), wind turbine (WT), diesel generators (DG), and six different battery types. The technical and economic performances of HPS configurations containing six different battery types are optimized. Besides, the sensitivity of the results is analyzed. A new approach for optimal battery selection is presented to increase the efficiency of HPS.

KEYWORDS:
Battery, HOMER, Hybrid Renewable Energy, Optimization, Sensitivity Analysis

INTRODUCTION

Fossil-based conventional energy resources cover 75.5% of the world's energy resources. In recent years, countries have been started to search for new alternative energy resources to meet the energy needs due to the depletion of conventional energy resources and increasing emissions of CO_2 and greenhouse gases. Thus, RES as a new alternative has been chosen widely [1]. An HPS is preferred for using RES effectively. These systems require energy management inevitably [2, 3]. An HPS can be controlled individually and independently or designed for connection to the network at the point of common coupling. The features and dimensions of the elements of HPS are of great importance. In particular, an HPS should be sized according to certain criteria for effective use. Determining and optimally dimensioning HPS components by the load characteristics provide many benefits in modeling. For this reason, an HPS should be analyzed in economic and technical terms and necessary optimization studies should be carried out [4-7]. Similar to the studies in the literature were carried out on HPSs containing PV, hydrokinetic and DG is in the Amazon city of Ecuador. Various optimization studies have been carried out for HPS using five different storage systems: lead-acid battery (LAB), lithium-ion (Li-Ion) battery, vanadium redox flow battery (VRFB), hydrogen storage, and hydrogen-VRFB. The timings of each storage system were sampled and the required sensitivities were examined. It has been shown that the VRFB system offers lower costs and the hydrogen tank and fuel cell have lower economic effects [8]. A sample study was conducted to remodel and plan economic analysis on a rural micro-grid on the island of Koh Jik in Thailand. Technical and economic analyzes of HPS containing PV, WT, DG in two different scenarios with two different battery types, Li-Ion and LAB, have been performed. Because of the analysis, it was understood that systems containing LAB generally lagged behind those containing Li-Ion and caused more environmental problems. However, it has been observed from the calculations that Li-Ion batteries are quite expensive in terms of investment cost. Besides, models were made with a limited battery [9]. Economic optimization and sizing analysis of the reverse osmosis off-grid plant operating as HPS in North Sinai, Egypt has been carried out. Eleven system models including WT, PV, DG, and LAB have been examined with simulations. As the result of the analyses, it has been observed that the PV/DG/battery system is more applicable, renewable, and economical than the others. However, these systems are modeled on a single storage unit [10]. To

meet the electrical energy demand of the desalination plant located in the village of Abo Ramad in the Red Sea region of Egypt, 11 different systems have been modeled for renewable energy system modeling, off-grid system optimization, techno-economic and environmental evaluations. DG, WT, converter, Li-Ion are used in the system. It has been observed that the best system modeling is achieved by using all system elements together and resulted in more environmentally friendly. However, these systems were also limited to a single storage unit [11]. WT, PV, biogas generator (BG), and Trojan L16P battery-powered system modeling were simulated in 8 different scenarios to examine the effects of the Hybrid Renewable Energy System (HYES) potential on energy consumption by taking a house as an example in Newcastle, UK. A cost-effective system that uses sun and wind sufficiently and saves 20% of BG has been designed [12]. In the coastal city of Bejaia in Eastern Algeria, a house was modeled to test the feasibility of the energy management strategy to be applied to the PV system, and the optimum system components were designed to provide the load of the house safely. PV power has been modeled using a fuzzy logic controller. In the system; fuel cell, electrolyzer, PV, hydrogen tank, and battery are used. The tests were handled under different meteorological conditions and the results were obtained. The operation of the system has been analyzed economically [13]. DG with internal combustion engines, PV and LAB, Li-Ion, VRFB were used in a micro-grid system having 10-50 houses in a town called Streaky Bay in South Australia. The system is designed as independent from the network. System modeling was made according to three different battery types, optimization and sensitivity analyzes were carried out to examine their effects on energy cost using various parameters. The results show that the LAB system is more expensive and less environmentally friendly than the other two battery systems, and has similarities with the Li-Ion battery system. On the other hand, VRFB is more affordable, environmentally friendly, and having a high renewable rate compared to the other two battery systems [14]. Energy profile and storage modeling study has been carried out in 25 different towns of Chad in Africa. In these regions, PV, WT, battery, converter, hydrogen tank, reformer, hydrogen load, electrolyzer, DG, and grid (on-grid) system were used. Under two different scenarios, the hydrogen & on-grid system and the battery & off-grid system were handled for all regions and economic, technical, and environmental analyzes were carried out. Cost-effective modeling has been calculated for all HPS combinations. As a result, it has emerged that the hydrogen system is more expensive [15]. An HPS modeling was designed to meet the electrical and thermal load demands of a rural house on the Greek island. PV, WT, hydrogen tank, electrolyzer, fuel tank, fuel cell, and battery are used in the system. It was analyzed in the optimization that the electricity and thermal load demand were met safely throughout a year [16]. The research was conducted on the potential of electricity and hydrogen generation from solar and wind energy resources in Dhahran, Riyadh, Jeddah, Abha, and Yanbu regions of the Kingdom of Saudi Arabia. Six different systems have been modeled using PV, WT, battery, electrolyzer, fuel cell, and hydrogen tank. Besides, whether the load demand is met or not is examined as a result of simulation analysis including economic conditions. According to the cost results, it has been shown that the optimum configuration is PV/WT/battery system [17]. An HPS model containing PV, WT, battery and hydropower has been conducted to determine whether the electricity load demand of the region in the rural village in the Southern part of India is met. As the result of optimizations, it has been shown that this hybrid combination is a cost-effective, sustainable, techno-economic, and environmentally friendly alternative to network expansion [18]. Studies in the reviewed literature generally focused on HPS modeling and energy optimization using different types of renewable or conventional energy resources. In addition, the number of batteries in studies is limited to a few in terms of compatibility and optimization. In this study, an energy management model has been created by considering different solid battery types for the system whose generation and demand values are given. The most suitable battery model has been determined by the cost analyses. Optimization studies have been carried out on different battery models in different scenarios. In the case that variables such as WT height, inflation rate, and diesel fuel cost take different values, sensitivity analyzes have been made and the results are evaluated. Thus, HPSs including different types of batteries have been modeled and the optimal battery has been selected according to the type of energy resource.

MATERIALS AND METHODS

Solar and wind potential in terms of having an appropriate area of Bandirma district of Balıkesir province in Turkey has been selected. The energy management plan of 50 kW peak power HPS has been implemented in this region. The system is off-grid and 30 kW PV, 10 kW WT and 50 kW DG are considered as energy generation resources. The hourly varying load model of the system, which can reach an annual average of 30 kW peak, has been taken into consideration.



FIGURE 1
The satellite position of the region.

Atmospheric parameters such as the region location, solar radiation, wind speeds, temperature values are necessary for optimization. The coordinates of the HPS are 40° 13' (north) latitude and 27° 50' (east) longitude. The region's location is the Mediterranean climate zone. Figure 1 shows the satellite position of the region.

Figure 2 shows the average value of the daily load consumption of the facility. The highest energy consumption is calculated as 30 kW on average between 15.00-18.00 hours, and the least energy consumption is calculated as 10 kW between 23.00-05.00 hours. The annual energy demand of this building is 472 kWh/day.

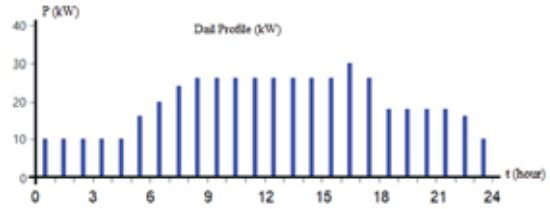


FIGURE 2
Load profile (July, 7).

Figure 3 shows the seasonal variation in average load consumption. In January, the maximum power consumption is seen as an average of 40.78 kW, the minimum power consumption as an average of 3.76 kW, the average daily maximum power consumption as 34.29 kW, the average daily minimum power consumption as 7.43 kW, and the average power consumption as 19.40 kW.

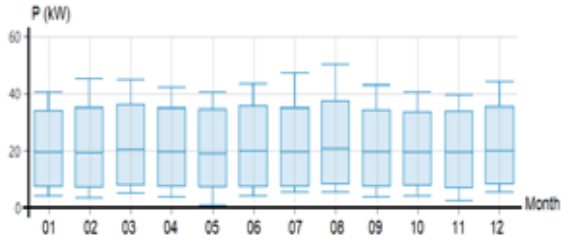


FIGURE 3
The seasonal average load consumption.

Photovoltaic (PV). Figure 4 shows the monthly average solar radiation data of the region taken from NASA POWER (Prediction of Worldwide Energy Resource) data [19].

The annual average solar radiation value is 4.17 kWh/m^2/day. For an economical Solar Power Plant (SPP) investment, there must be a solar radiation value above the threshold value of 1500 kWh/m^2/year and a sunshine duration of more than 2000 hours per year. Considering the annual data of the region, the region is suitable for the establishment of SPP. While solar radiation value takes its highest value in June and July, it takes its lowest value in December and January. The same is true for the clarity index. Under the standard test conditions of the PV system, the efficiency that converts sunlight into electricity while it is at the maximum power point is calculated in equation (1) [19].

$$\eta_{m,STC} = \frac{Y_{PV}}{A_{PV} \,.\, G_{T,STC}} \quad (1)$$

In equation (1),

$\eta_{m,STC}$ The efficiency of PV module under the standard test conditions (%),

Y_{PV} The nominal output power of PV module under the standard test conditions (kW),

A_{PV} The surface area of PV module (m^2),

$G_{T,STC}$ Radiation value under the standard conditions (kW/m^2).

Equation (2) is used to calculate the output power of PV array [20].

$$P_{PV} = Y_{PV}.f_{PV}.\left(\frac{G_T}{G_{T,STC}}\right).\left[1 + \propto_P .\ \left(T_C - T_{C,STC}\right)\right] \quad (2)$$

In equation (2),

P_{PV} The output power of PV array (kW),

Y_{PV} The nominal capacity of PV array (output power under the standard test conditions) (kW),

f_{PV} PV losses (reduction factor) (%),

G_T PV solar energy (incident radiation in PV) (kW/m^2),

$G_{T,STC}$ PV solar energy (under the standard test conditions) (kW/m^2),

$\propto_P$ Power temperature coefficient (%/°C),

T_C Cell temperature of PV (present time) (°C),

$T_{C,STC}$ Cell temperature of PV under the standard test conditions (°C).

Equation (3) is used to calculate the cell temperature of the PV array [21, 22].

$$T_C = T_a + G_T.\frac{T_{C,NOCT} - T_{a,NOCT}}{G_{T,NOCT}}.\left(1 - \frac{\eta_C}{\tau.\alpha}\right) \quad (3)$$

In equation (3),

T_C PV cell temperature (°C),

T_a Ambient temperature (°C),

G_T Striking solar radiation of PV arrays (kW/m^2),

$T_{C,NOCT}$ Cell temperature of PV under nominal operation (°C),

$T_{a,NOCT}$ Ambient temperature (20 °C),

$G_{T,NOCT}$ Solar radiation (0.8 kW/m^2),

η_C Electrical conversion (panel, maximum power point) efficiency of the PV array (%),

τ Solar permeability (%) of any panel on the PV array (%),

α Solar absorption of PV array (%) ($\tau.\ \alpha$= 0.9)..

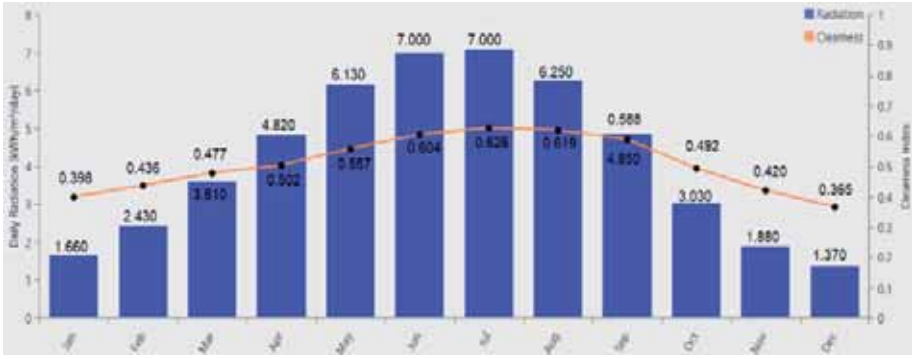


FIGURE 4
The monthly average solar radiation.

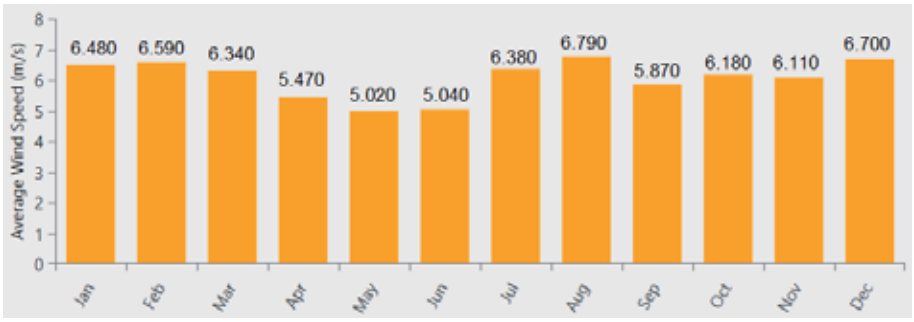


FIGURE 5
The monthly average wind speed.

Wind Turbine (WT). Figure 5 shows the monthly average wind speed data of the region taken from NASA POWER [19]

Weibull k parameter was determined as 2, autocorrelation factor 0.85, daily signal strength 0.25, and maximum wind speed hour 15:00. For an economical Wind Power Plant (WPP) investment, a wind speed of 7 m/s or greater and a capacity factor of 35% and higher are considered appropriate [23]. The annual average wind speed of the region is 6.08 m/s. These values are suitable for RES installation and utilization. Accordingly, the highest wind speeds are observed in August and December, while the lowest wind speeds are observed in May and June. Wind data for April, May, June, and September are below the monthly average wind speed.

The output power of WT is calculated in three stages. The first is the calculation of the wind speed, the second is the calculation of the power generation at the wind speed, and the third is the adjustment of the output power value. Equation (4) shows the WT power formula [24].

$$P_{WT} = \begin{cases} 0 & V(t) \le V_{cin} \; ya \; da \; V(t) \ge V_{cout} \\ P_R . \frac{V(t)-V_{cin}}{V_R-V_{cin}} & V_{cin} \le V(t) \le V_R \\ P_R & V_R \le V(t) \le V_{cout} \end{cases} \quad (4)$$

In equation (4),
P_{WT} The output power of WT (kW),
P_R The output power of single WT (kW),
$V(t)$ Wind speed at time t (m/s),
V_R Nominal wind speed (m/s),
V_{cin} Maximum wind speed (m/s),
V_{cout} Minimum wind speed (m/s),

Power curves determine WT performance under standard pressure and temperature conditions. The power value estimated by the power curve is calculated by multiplying by air density given in equation (5). Equation (6) shows the state of the wind speed [25].

$$P_{WTG} = P_{WTG,STG} . \left(\frac{\rho}{\rho_0}\right) \quad (5)$$

In equation (5),
P_{WTG} The output power of WT (kW),
$P_{WTG,STG}$ The output power of WT under standard temperature and pressure (kW),
ρ Real air density (kg/m^3),
ρ_0 Real air density under standard temperature and pressure (1.225 kg/m^3).

$$U_{hub} = U_{anem} . \left(\frac{Z_{hub}}{Z_{anem}}\right)^{\alpha} \quad (6)$$

In equation (6),
U_{hub} Wind speed at turbine height (m/s),
U_{anem} Wind speed at anemometer height (m/s),
Z_{hub} Hub height of WT (m),
Z_{anem} Anemometer height (m),
α Wind shear coefficient.

The Weibull factor k, which reflects the distribution of wind speed in width, is adapted to the wind speed data. While k is low in the wide range of wind,

k is high in the narrow range of wind. In most wind scenarios k is typically chosen 2. The two-parameter Weibull distribution is often used to characterize wind regimes. Wind speed and density function are shown in equations (7) and (8) [19].

$$f(v) = \frac{k}{c} . \left(\frac{v}{c}\right)^{k-1} . exp\left(-\left(\frac{v}{c}\right)^{k}\right) \quad (7)$$

In equation (7),
$f(v)$ Probability density function,
k Weibull shape parameter,
c Weibull scale parameter (m/s),
v Wind speed (m/s).

$$v_{ort} = c . \Gamma\left(1 + \frac{1}{k}\right) \quad (8)$$

In equation (8),
v_{ort} Average wind speed (m/s),
Γ Gama function.

Diesel Generator (DG). DG produces energy by consuming diesel fuel. DG capacity is calculated with a useful life of 15000 hours and a maximum loading rate of 25%. If the DG is operating at a certain time step, the fuel consumption rate for that time step is calculated using equation (9) [26].

$$F = F_0 . Y_{gen} + F_1 . P_{gen} \quad (9)$$

In equation (9),
F Fuel consumption rate (L/h),
F_0 Generator fuel curve intercept coefficient (L/hour/kW),
Y_{gen} Generator fuel curve slope (L/hour/kW),
F_1 Generator nominal capacity (kW)
P_{gen} The output power of DG in a certain time (kW).

DG fuel curve intercept coefficient is obtained by dividing the no-load fuel consumption of DG by the nominal capacity. [22].

Converter. The part provides power conversion between AC and DC buses. They are used as an inverter (DC/AC) and rectifier (AC/DC). The power of the converter is chosen depending on the peak value of the load. The power of the converter is given in Equation (10) [27].

$$P_{inv} = \frac{P_{peak}}{e_{inv}} \quad (10)$$

In equation (10),
P_{inv} The output power of converter (kW),
P_{peak} Peak power of load (kW),
e_{inv} The efficiency of the converter.

The inverter is used to connect the DC bus to the AC bus. The output power of an inverter is given in Equation (11) [28].

$$P_0 = P_i . \eta_{inv} \quad (11)$$

In equation (11),
P_0 The output power of inverter (kW),
P_i Input power of an inverter (kW),
η_{inv} The efficiency of the inverter.

Battery. Batteries can use energy whenever and wherever demanded. Batteries balance energy production and load demand. Batteries can store or discharge excess energy at the most appropriate time as possible as quickly. Figure 6 shows an example of energy management on batteries [29].

HPS integrated battery energy management graph is given in Figure 6, fluctuations in energy use according to energy storage and load demand are seen at certain time intervals. To meet the energy demand arising from energy fluctuations, the energy stored during the day or night will be returned to the system. Today, there are batteries can store energy in various forms. Classifications of batteries are shown in Figure 7 [30-32]. Technical characteristics of batteries used in the HPS are shown in Table 1 [30-35].

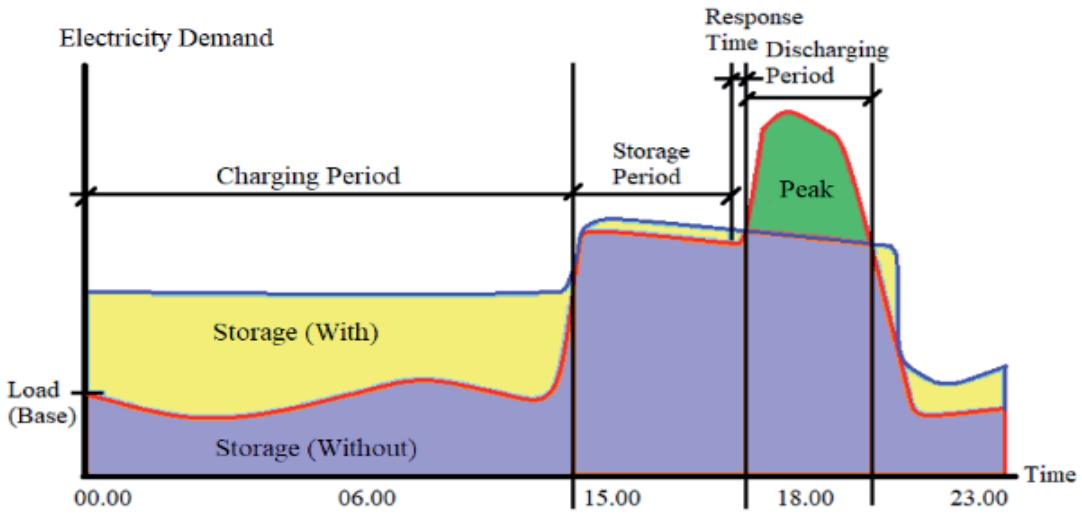


FIGURE 6
Energy management on a battery.

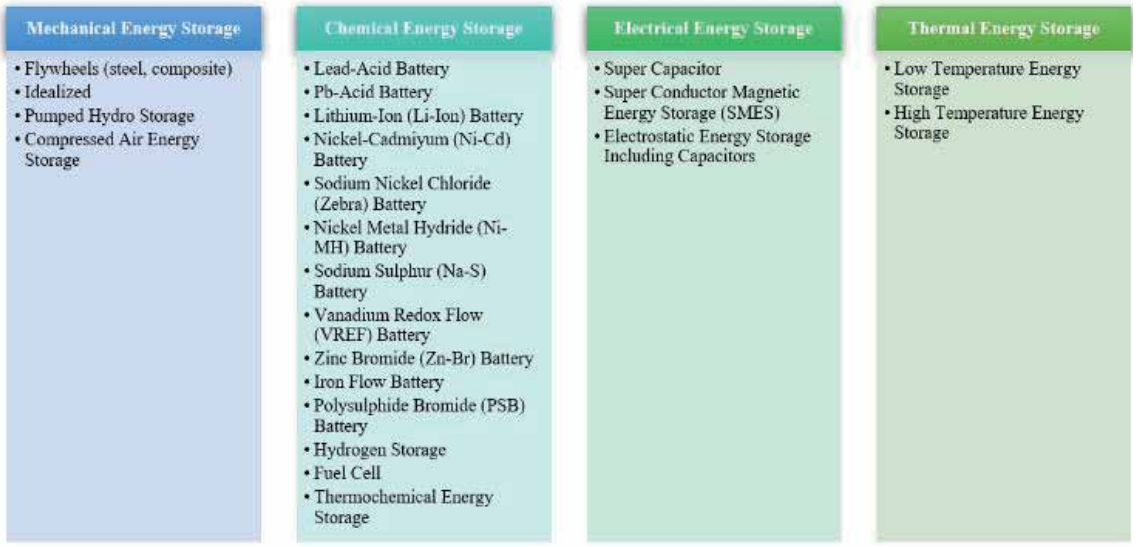


FIGURE 7
Classifications of batteries.

TABLE 1
Technical characteristics of six batteries.

Features	Flow Battery	Lead Acid Battery	Lithium-Ion Battery	VRFB Battery	Flywheel Battery	Zinc-Bromine Flow Battery
Mechanism	Electro Chemical	Electro Chemical	Electro Chemical	Electro Chemical	Mechanical	Electro Chemical
Energy Efficiency	60-70	70-80	70-85	20-80	95	65-75
Energy Density	20-30	20-35	100-200	25	5-30	20-35
Power Density	80-150	25	360	80-150	1000	100-150
Cycle Life (cycles)	>2000	200-2000	500-2000	>10000	>20000	>2000
Life Time (year)	>20	3-12	5-20	>20	>20	>20
Self-Discharge	High	Low	Medium	Medium	Very high	High
Capital cost	500-2000	300–600	1200-4000	600-1500	250-350	700-2500
Capital cost	100-1000	200–400	600-2500	150-1000	1000-5000	150-1000
Power rating	50 kW–1 MW	0–20 MW	0–100 kW	30 kW–3 MW	0–250 kW	50 kW–2 MW
Discharge time	Seconds & hours (10h)	Seconds & hours	Minutes & hours	Seconds & hours (10h)	Seconds (mili) & minutes	Seconds & hours (10h)
Self-discharge per	Small	0.1%–0.3%	0.1%–0.3%	Small	100%	Small
Suitable storage duration	Hours & Months	Minutes & Days	Minutes & Days	Hours & Months	Seconds & Minutes	Hours & Months

Maximum charge power variations of a storage system according to charge and discharge conditions are specified in equation (12) [14].

$$P_b(t) = \frac{k.Q_1(t).e^{-k.\Delta t} + Q(t).k.c.\left(1-e^{-k.\Delta t}\right)}{1-e^{-k.\Delta t} + c.\left(k.\Delta t - 1 + e^{-k.\Delta t}\right)} \quad (12)$$

In equation (12),
$P_b(t)$ Maximum power of the battery (kW),
k Storage rate constant (1/h),
$Q_1(t)$ Existing energy in storage at the beginning of time step (kWh) (40% for LAB, 20% for Li-Ion, 0% for VRFB),
$Q(t)$ The total energy in storage at the beginning of time step (kWh),
c Storage capacity rate,
Δt Time step (hour).

Equation (13) shows the maximum power that the storage bank can use for a certain period.

$$P_b(t) = \frac{-k.c.Q_{max}(t) + k.Q_1(t).e^{-k.\Delta t} + Q(t).k.c.\left(1-e^{-k.\Delta t}\right)}{1-e^{-k.\Delta t} + c.\left(k.\Delta t - 1 + e^{-k.\Delta t}\right)} \quad (13)$$

In equation (13),
$Q_{max}(t)$ Total storage capacity (kWh).

Equation (14) is used to calculate the battery storage energy cost at any time step [19].

$$C_{be,n} = \frac{\sum_{i=1}^{n-1} C_{cc,i}}{\sum_{i=1}^{n-1} E_{cc,i}} \quad (14)$$

In equation (14),
$C_{be,n}$ Energy storage cost for n time step ($/kWh),
$C_{cc,i}$ Storage cycle cost at time step i,
$E_{cc,i}$ Amount of energy flowing to storage bank at time step i (kWh).

Economic Analysis. All system components of HPS and their costs should be considered and analyzed for operation at optimal cost. Equations (15), (16), and (17) are used to obtain the configuration of this system [36, 37].

$$\min C = \sum \begin{pmatrix} N_{PV}.\ C_{PV,tot}, N_{WT}.\ C_{WT,tot}, \\ N_{batt}.\ C_{batt,tot}, C_{inv}, N_{DG}.\ C_{DG,tot} \end{pmatrix} \quad (15)$$

In equation (15),
$\min C$ The minimum cost of HPS ($)
N_{PV} Number of PV panels
$C_{PV,tot}$ PV panel cost ($)
N_{WT} Number of WT
$C_{WT,tot}$ WT cost ($)
N_{batt} Number of Battery
$C_{batt,tot}$ Battery cost ($)
N_{DG} Number of DG
$C_{DG,tot}$ DG cost ($)

$$N_{min} \leq \{N_{PV}, N_{WT}, N_{batt}, N_{DG}\} \leq N_{max} \quad (16)$$

In equation (16),
N_{min} Minimum number of component in HPS
N_{max} Maximum number of component in HPS

$$P_{load}(t) \leq P_{PV}(t) + P_{WT}(t) + P_{batt}(t) + P_{inv}(t) + P_{DG}(t) \quad (17)$$

In equation (17) [38],
$P_{load}(t)$Power of load at time t (kW)
$P_{PV}(t)$ Power of PV panel at time t (kW)
$P_{WT}(t)$ Power of WT at time t (kW)
$P_{batt}(t)$ Power of battery at time t (kW)
$P_{inv}(t)$ Power of inverter at time t (kW)
$P_{DG}(t)$ Power of DG at time t (kW)

Annual real interest rate is used in calculating annual cost or converting between annual costs. The annual real interest rate is calculated as in equation (18) [39, 40].

$$i = \frac{i'-f}{1+f} \quad (18)$$

In equation (18),
i Annual real interest rate
i' Nominal interest rate
f Expected interest rate

The life cycle cost is the net present cost of HPS. It constitutes the total of operating, installation, capital, renewal, maintenance, and repair costs incurred during the project period. In Equation (19), the net present cost value is given [41, 42].

$$NPC = \frac{C_{ta}}{CRF(i,n)} = \frac{C_{cap} + C_{rep} + C_{O\&M}}{CRF(i,n)} = C_{cap} + \sum_{t=1}^{N} \frac{C_F}{(1+i)^t} \quad (19)$$

In equation (19),
NPC Net present cost ($)
C_{ta} Total annual cost ($)
$CRF(i,n)$ Capital recovery factor
C_{cap} Capital cost ($)
C_{rep} Renewal cost ($)
$C_{O\&M}$ Operation and maintenance (O&M) cost ($)
C_F Amount of cash flow for year t ($)
t Number of years (year)
i Annual interest rate
N Project lifespan (year)

Levelized energy cost is given in Equation (20) [37, 43].

$$COE = \frac{C_{ann,tot} - C_{boiler}\ .\ H_{served}}{E_{served}} = \frac{TAC}{E_{served}} \quad (20)$$

In equation (20),
COE Levelized energy cost ($/kWh)
$C_{ann,tot}$ Total annual cost ($/year)
C_{boiler} Boiler marginal cost ($/kWh)
H_{served} Total served thermal load (kWh/year)
E_{served} Total served electrical load (kWh/year)
TAC Total annual cost ($/year)

The capital recovery factor (CRF) given in Equation (21) is used to find the NPV of annual income during the project period [44, 45].

$$CRF = \frac{i.\ (1+t)^t}{(1+t)^t - 1} \quad (21)$$

Renewable fraction (RF) is used to find the usage rate of RES and it is calculated from the formula in equation (22) [46].

$$RF = 1 - \frac{E_{nonren} + H_{nonren}}{E_{served} + H_{served}} \quad (22)$$

In equation (22),
RF Renewable fraction (%)
E_{nonren} Non-renewable electricity consumption (kWh/year)
H_{nonren} Non-renewable thermal consumption (kWh/year)
E_{served} Served total electric load (kWh/year)
H_{served} Served total thermal load (kWh/year)

RESULTS

System Modelling and and Optimization Results. Modeling of off-grid renewable HPS is shown in Figure 8. Six different models were created with six different battery types

The technical information of elements in HPS is shown in Table 2. Cost variables of the elements are given in Table 3 [8, 9, 19, 39, 40].

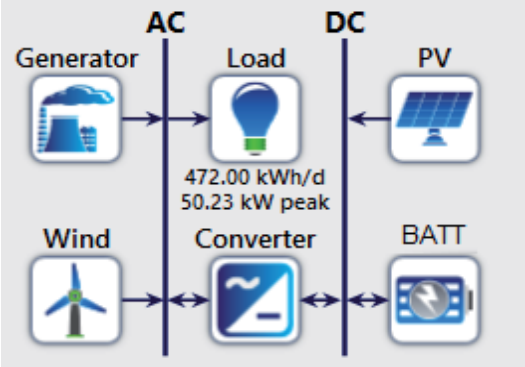


FIGURE 8
System Model.

Parameters of all elements in HPS are used in system modeling. Input parameters are evaluated by considering GHI solar energy, wind speeds, load demand, technical and economic data of system components, constraints, and sensitivity conditions. As a result, optimal sizing of the system, cost values, capacity problems, renewable rates, CO_2 emissions, fuel consumption, energy generation, and load demand is evaluated.

Table 4 shows the economical optimization results of six systems with different types of batteries. Because of the calculations, the most suitable system modeling for the NPC after 25 years is seen as the Zinc-Bromine Flow (Zi-Br) battery system with $ 987,694. Also, the fact that this system has the lowest fuel cost and the user gains -11,501 $ makes this system advantageous. However, the investment cost of the system is at the highest value of $ 733,884. It is noteworthy that the number of batteries used in the occurrence of this situation is high (10 pieces of 50 kWh batteries were used). Flywheel storage, on the other hand, is seen as negative because both the total and fuel costs are quite high, besides being the system that makes the most money for the users. LAB, the oldest type of battery, has the highest value in terms of total costs; however, capital investments are very low. When evaluated in terms of costs; the Zi-Br battery stands out, followed by the VRFB battery. Classical type LABs are the most costly and least profitable resources

.

TABLE 2
Technical information of elements in HPS modeling.

Compo-	Description	Data Description	Component	Description	Data Descrip-
Diesel	Capacity	50 kW	**Wind Tur-**	Capacity	10 kW
Genera-	Fuel	Diesel	**bine**	Lifetime	20 year
tor (DG)	Minimum Load	%25		Hub Height	16 m
	Lifetime	15,000.00 hour	**Lithium Ion**	Nominal volt-	600 V
PV	Capacity	30 kW	**Battery (L3)**	Nominal capac-	100 kWh
	Panel Type	Flat plate		Roundtrip effi-	%90
	Temperature Co-	-0.4100		Maximum	167 A
	Operating Tem-	45 ^{0}C		Maximum dis-	50 A
	Efficiency	%17.30		Throughput	300,000.00 kWh
	Derating Factor	%96		Lifetime	15 year
	Lifetime	25 year		Minimum/ini-	%20/%100
Con-	Capacity	100 kW	**Vanadium**	Nominal volt-	48 V
verter	Lifetime	15 year	**Redox Flow**	Nominal capac-	100 kWh –
	Efficiency	%95	**Battery**	Roundtrip effi-	%64
	Relative Capac-	%100	**(VRFB) (L4)**	Maximum	200 A
Flow Bat-	Nominal voltage	167 V		Maximum dis-	313 A
tery (L1)	Nominal capac-	142 kWh – 850 Ah –		Throughput	876,000.00 kWh
	Roundtrip effi-	%68		Lifetime	20 year
	Maximum	0.112 A/Ah		Minimum/ini-	%20/%100
	Maximum	110 A	**Flywheel**	Nominal volt-	825 V
	Maximum dis-	170 A	**Battery (L5)**	Nominal capac-	25 kWh – 30.3
	Lifetime	20 year		Roundtrip effi-	%85
	Minimum/initial	%20/%100		Maximum	121 A
Lead	Nominal voltage	12 V		Maximum dis-	121 A
Acid Bat-	Nominal capac-	51.6 kWh – 4.3E+03		Lifetime	20 year
tery (L2)	Capacity ratio	0.298		Minimum/ini-	%20/%100
	Rate constant	1.95 hour^{-1}	**Zinc Flow**	Nominal volt-	100 V
	Roundtrip effi-	%97	**Battery (L6)**	Nominal capac-	50 kWh – 500
	Maximum	1 A/Ah		Roundtrip effi-	%72
	Maximum	3.9E+03 A		Maximum	150 A
	Maximum dis-	4.6E+03 A		Maximum dis-	300 A
	Throughput	55,134.60 kWh		Lifetime	20 year
	Lifetime	15 year		Minimum/ini-	%20/%100
	Minimum/initial	%20/%100			

TABLE 3
Costs of elements in HPS.

Description	Capital Cost	Replacement Cost	Operation and Maintenance
PV System	3,000.00 $/kW	3,000.00 $/kW	10.00 $/year
Wind Turbine	20,000.00 $	20,000.00 $	500.00 $/year
Diesel Generator (DG)	1,000.00 $	1,000.00 $	0.5 $/op.hour
Converter	300.00 $	300.00 $	0.0 $/year
Flow Battery	40,000.00 $	0.00 $	800.00 $/year
Lead Acid Battery	6,630.00 $	12,574.00 $	6,518.00 $/year
Lithium-Ion Battery	70,000.00 $	70,000.00 $	1,000.00 $/year
VRFB Battery	10,000.00 $	300.00 $	1,000.00 $/year
Flywheel Battery	30,000.00 $	20,000.00 $	0.0 $/year
Zinc Flow Battery	40,000.00 $	40,000.00 $	0.0 $/year

TABLE 4
Optimization results (economic).

Type	Quantity	COE	NPC	Operating	Initial Cap-	Salvage	Fuel
Flow	3x142	0.138 $	1,130,922 $	14,286 $/yr	452,874 $	-7,138 $	6,237 $
Lead Acid Battery	1x51,6 kWh	0.210 $	1,717,210 $	30,149 $/yr	286,304 $	-6,835 $	15,099 $
Lithium-Ion Battery	2x100	0.156 $	1,272,079 $	17,246 $/yr	453,559 $	-9,209 $	7,333 $
VRFB	4x100	0.135 $	1,105,902 $	15,425 $/yr	373,811 $	-7,227 $	5,827 $
Flywheel	1x25	0.181 $	1,481,925 $	19,344 $/yr	563,863 $	-15,026 $	14,446 $
Zinc Flow Battery	10x50	0.121 $	987,694 $	5,348 $/yr	733,884 $	-11,501 $	4,321 $

TABLE 5
Optimization results (energy generation).

Type	Quantity	Production (Electrical) PV	DG	Wind	AC Primary Load	Excess Electricity	Renewable Fraction
Flow	3x142	75,763kWh/yr	22,475kWh/yr	162,782kWh/yr	172,280kWh/yr	83,776kWh/yr	%87.0
Lead Acid	1x51,6	69,034 kWh/yr	55,919 kWh/yr	139,527kWh/yr	172,280 kWh/yr	97,552 kWh/yr	%67.5
Lithium-Ion	2x100	75,763 kWh/yr	27,479 kWh/yr	139,527kWh/yr	172,280 kWh/yr	79,390 kWh/yr	%84.0
VRFB	4x100	75,763 kWh/yr	20,956 kWh/yr	162,782kWh/yr	172,280 kWh/yr	77,609 kWh/yr	%87.8
Flywheel	1x25	69,034 kWh/yr	66,446 kWh/yr	116,273kWh/yr	172,280 kWh/yr	74,038 kWh/yr	%61.4
Zinc Flow	10x50	75,763 kWh/yr	15,509 kWh/yr	162,782kWh/yr	172,280 kWh/yr	76,881 kWh/yr	%91.0

TABLE 6
Optimization results (diesel fuel consumption and CO_2 emission).

Type	Fuel Summary Total	Avg	Avg	Emissions CO_2	CO	Unburned	Particulate	Sulfur Di-	Nitrogen
Flow	8,785 L	24.1	1.00	22,999	144 kg/yr	6.33 kg/yr	0.861kg/yr	56.3 kg/yr	135 kg/yr
Lead Acid	21,267 L	58.3	2.43	55,674	347 kg/yr	15.3 kg/yr	2.08 kg/yr	136 kg/yr	327 kg/yr
Lithium-Ion	10,328 L	28.3	1.18	27,038	169 kg/yr	7.44 kg/yr	1.01 kg/yr	66.2 kg/yr	159 kg/yr
VRFB	8,208 L	22.5	0.937	21,486	134 kg/yr	5.91 kg/yr	0.804 kg/yr	52.6 kg/yr	126 kg/yr
Flywheel	20,348 L	55.7	2.32	53,267	332 kg/yr	14.7 kg/yr	1.99 kg/yr	130 kg/yr	313 kg/yr
Zinc Flow	6,087 L	16.7	0.695	15,934	99.5kg/yr	4.38 kg/yr	0.597 kg/yr	39 kg/yr	93.5

In Table 5, optimization results of six systems with different batteries are given in terms of electricity generation. As a result of the calculations, the system in which the minimum DG usage is required among three different electrical systems feeding a load with an annual demand of 172,280 kWh, is the Zi-Br battery system that produces 15,509 kWh of energy annually by DG and has the highest rate of RF 91%. It is followed by the VRFB battery system with 87.80%. The system with the lowest rate of 67.50% is the system with a LAB battery.

Table 6 shows the optimization results of six systems with different batteries in terms of diesel fuel consumption and CO_2 emission. The most suitable system with the hourly, daily, and total fuel consumption of 0.695 L/h, 16.70 L/day, and 6,087 L is the Zi-Br battery system, while the most expensive is LAB with 2.43 L/h, 58.30 L/day, and 21,267 L fuel consumption, respectively. VRFB and Flow Battery (FB) systems appear as the next systems with the lowest fuel consumption. The Zi-Br battery-powered system is seen as the most environmentally friendly, with an annual emission of 15,934 kg of CO_2 and 99.5 kg of CO.

In Figure 9, the monthly energy generation amounts of DG, WT and PV in six systems with different batteries are given in MWh. As seen in Figure 9, the highest generation of electricity from wind occurs in January and August, while the lowest generation rate is in April and May. The highest generation of electricity from the sun takes place between May and August, while the lowest is between November and March. DG generates electricity mostly in June and November and rarely in July, and the

most storage space is in the LAB.

Figure 10 shows power generation curves (July 7) of each element in the Zi-Br battery system. Figure 10 shows that the fastest charging and discharging of the battery take place between 14.00 and 16.00. Energy consumption is minimum with the value of 5.87 kW at 00.00, while it is maximum with the value of 38.96 kW at 16.00. DG was not necessary. The battery was charged at a maximum power of 29.82 kW and discharged at -11.67 kW. Stored energy from 02.00 to 09.00 and from 19.00 to 00.00 was used here. The energy generated in the system between 09.00 and 16.00 was effective in the load and charging of the battery. Using batteries gradually will be beneficial in keeping their life long. The power generated from WT was maximum with the value of 38.81 kW at 01:00, while it was minimum with a value of 0.97 kW at 23:00. The power generated from PV panels is maximum with a value of 29.98 kW between 10.00 and 12.00, while power generation is zero between 21.00 and 05.00.

Figure 11 shows the hourly variation of the power generation of each element in the Zi-Br battery system on February 9.

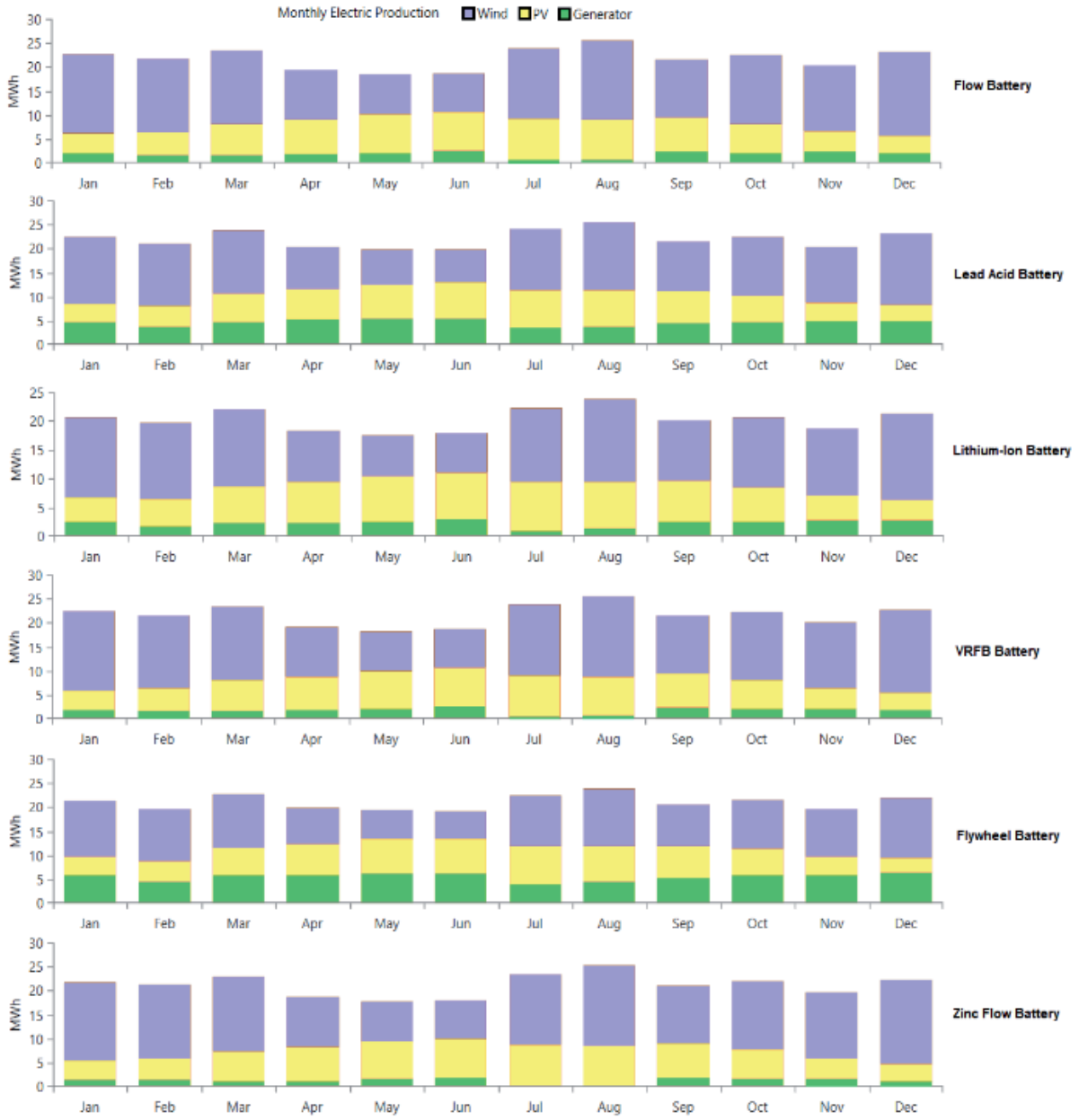


FIGURE 9
The monthly energy generation amounts of DG, WT, and PV in six systems with different batteries.



FIGURE 10
Daily load consumption in the system with Zi-Br battery (July 7).

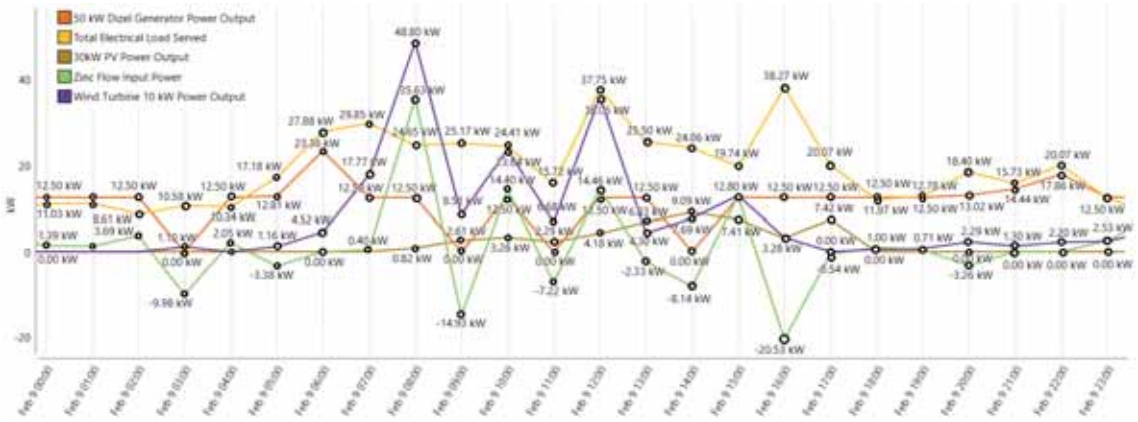


FIGURE 11
Daily load consumption in the system with Zi-Br battery (February 9).

As seen in Figure 11, the fastest charging and discharging occurs between 07.00 and 09.00. Besides, between 02.00 and 17.00 hours, charging and discharging are activated very often. It is seen that the energy consumption is minimum at 02.00 with a value of 8.61 kW and at 16.00 with a value of 38.27 kW. DG is used at certain power values during the day and the most fuel is consumed at 06.00 at 23.36 kW power value. Compared to July 7, more diesel fuel is consumed and fluctuations in production change suddenly.

Table 7 shows the optimization results of the battery technical features of six systems with different batteries.

Nominal and utilized capacity values in kWh are respectively 500 and 400 for Zi-Br, 426 and 341 for FB, 400 and 320 for VRFB, 200 and 160 for Li-Ion battery, 51.6 and 41.3 for LAB, 25 and 20 for flywheel storage. For Zi-Br batteries, the total amount of energy that can be charged and discharged during a 30-year lifetime is 1,511,728 kWh and for LAB, 55,135 kWh of energy can be charged and discharged in 4 years. The total energy amount through the storage system throughout one year can be listed in kWh as 50,931 for Zi-Br, 48,052 for VRFB, 46,001 for flywheel storage, 45,040 for FB, 35,444 for Li-Ion battery, and 13,540 for LAB. It is seen that Zi-Br batteries could store more energy than others and reflect them to the system throughout a year. Among the batteries, flywheel storage has an average cost of 0.2 $/kWh. In addition, Li-Ion and LAB batteries have high calendar aging costs, on average around 0.24 $/kWh.

Figure 12 shows the change of cost variables of two systems including Zi-Br and LAB over 25 years on the normal DG and the most optimal system (DG+ PV+ WT+ storage). As examining graphs in Figure 12, the situation changes linearly because of working with DG. If the system is operated optimally, the cost values may decrease at a certain value at the end of this period. The NPC of the DG-powered system is calculated as $ 2.36M, capital cost $ 1,000, O&M $ 49,776/year, and COE $ 0.289/kWh. Zi-Br and LAB batteries, NPCs $ 0.987M - $ 1.72M (difference $ 0.742M), capital costs $ 0.733M - $ 0.286M (difference $ 0.447M), O&M costs $ 5.348/year - $ 30,149/year (24,801 $/year) and COE is calculated as 0.121 $/kWh - 0.210 $/kWh. Accordingly, the Zi-Br battery-powered system with a capital cost of $ 447.58 more, the annual maintenance cost is $ 24,801 and the NPC is $ 0.742M less, and it saves the user $ 4,444 more money.

TABLE 7
Optimization results (battery technical features).

Specifications	Flow Battery	Lead Acid Bat-	Lithium-Ion	VRFB Battery	Flywheel Bat-	Zinc Flow
Batteries size	3	1	2	4	1	10
Capacity	142 kWh	51.6 kWh	100 kWh	100 kWh	25 kWh	50 kWh
Bus Voltage	167 V	12 V	600 V	48 V	825 V	100 V
Autonomy	17.3 hour	2.1 hour	8.14 hour	16.3 hour	1.02 hour	20.3 hour
Nominal Capacity	426 kWh	51.6 kWh	200 kWh	400 kWh	25 kWh	500 kWh
Usable Nominal Ca-	341 kWh	41.3 kWh	160 kWh	320 kWh	20 kWh	400 kWh
Lifetime	900,809 kWh	55,135 kWh	531,664 kWh	961,037 kWh	920,017 kWh	1,511,728
Expected Life	20 year	4.07 year	15 year	20 year	20 year	30 year
Energy In	54,257	13,736 kWh/yr	37,244 kWh/yr	59,728 kWh/yr	49,881 kWh/yr	58,992
Energy Out	37,141	13,336 kWh/yr	33,625 kWh/yr	38,441 kWh/yr	42,411 kWh/yr	42,758
Energy Losses	17,415	412 kWh/yr	3,730 kWh/yr	21,556 kWh/yr	7,483 kWh/yr	16,568
Annual Throughput	45,040	13,540 kWh/yr	35,444 kWh/yr	48,052 kWh/yr	46,001 kWh/yr	50,391

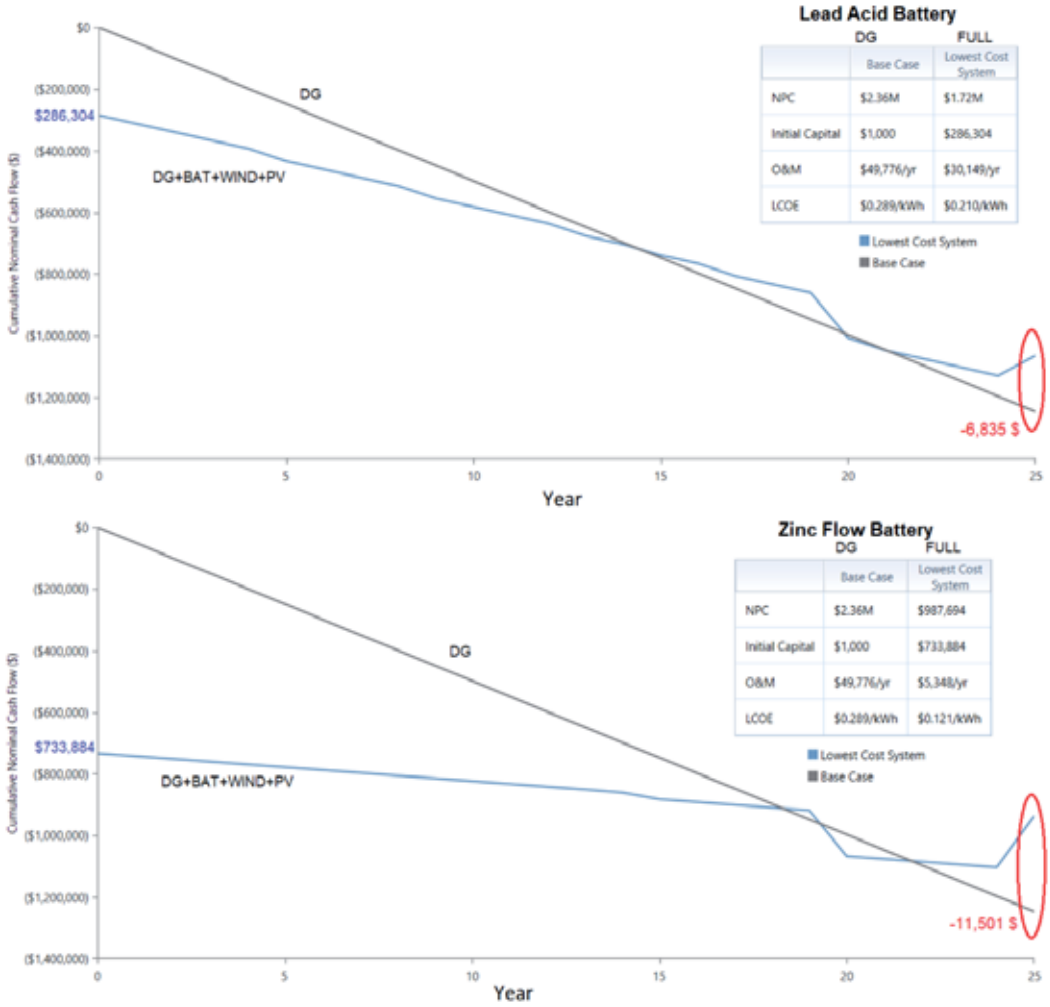


FIGURE 12
Cash flows of two systems with different batteries through 25 years.

Sensitivity Analysis. It was carried out using a single variable optimization. However, in the sensitivity analysis, variables are calculated by converting them into multiple and the results are given in detail. For example, in optimization, WT height 16 m, DG fuel cost 0.71 $/L, and inflation rate 13% are considered. In the sensitivity analysis, the values of WT height 16, 24, and 30 m, DG fuel cost 0.60, 0.71, and 0.80 $/L, and inflation rate 10%, 13%, and 15% were used.

Table 8 shows the sensitivity analysis results of six systems with different batteries according to WT heights. Because of the increase in WT heights, the renewability rate also increased, while the amount of fuel spent, COE, NPC and O&M, capital costs decreased.

Table 9 shows the sensitivity analysis results of six systems with different batteries according to different diesel fuels. According to the increase in DG fuel costs, RF, COE, NPC, O&M and capital costs

increased as the total fuel amount decreased.

Table 10 shows the sensitivity analysis results of six systems with different batteries according to different inflation rates. According to the increase in the inflation rate, RF, NPC, capital cost increased while COE, O&M cost and the total amount of fuel decreased.

Figure 13 shows sensitivity analysis of the Zi-Br battery system under various parameters. As DG fuel cost was 0.71 $/L and the inflation rate was 13%, it was obtained that 30 m WT height is the optimal modeling among three different WT heights. In this case, COE was $ 0.113, the 25-year NPC was $ 921,131, the RF rate was 91.40% and the total fuel consumption was 5,762 L. Because of the 14 m change in WT height, NPC costs $ 59,785, O&M costs $ 0.965 / year ($ 24,125 at the end of 25 years), capital cost $ 14,006 and fuel consumption decreased by 1,136 L while RF increased 1.70%. As a result of the increase in the price of diesel fuel from $ 0.60/L to $ 0.80/L during the process, nevertheless, total fuel consumption decreased by 1,747 L, but it caused an additional cost of around $ 69,084 for the NPC.

As the inflation rate increased from 10% to 15%, the NPC increased by $ 8,905 and the capital cost by $ 595,121, while the cost of capital decreased by $ 12,999 and the amount of fuel 7,156 L.

CONCLUSION

In this study, HPS modeling was examined together with different storage systems and technical and economic analyzes were made. Modeling was designed off-grid and the system design was rearranged according to each different battery structure. Optimizations were made under parameters such as economic costs, electricity generation, battery conditions, CO_2 emissions, renewability rates. As a re

TABLE 8
The results of sensitivity analysis (according to WT heights).

Battery	Wind	COE	NPC	Operating	Initial Capi-	Renew.	Total	Battery
Flow Battery (L1)	16 m	0.149 $	1.22M $	15,811 $/yr	466,069 $	%81.7	12,306 L	3
	24 m	0.140 $	1.15M $	14,623 $/yr	454,169 $	%84.1	10,664 L	3
	30 m	0.136 $	1.11M $	14,428 $/yr	430,039 $	%83.3	11,210 L	3
Lead Acid Battery (L2)	16 m	0.232 $	1.90M $	34,715 $/yr	251,379 $	%59.2	26,558 L	1
	24 m	0.247 $	2.02M $	37,441 $/yr	244,586 $	%40.1	39,704 L	1
	30 m	0.243 $	1.98M $	36,779 $/yr	237,791 $	%41.2	38,936 L	1
Lithium Ion Battery (L3)	16 m	0.184 $	1.50M $	22,904 $/yr	416,236 $	%72.8	17,633 L	2
	24 m	0.188 $	1.54M $	19,231 $/yr	624,856 $	%79.3	13,145 L	3
	30 m	0.187 $	1.53M $	27,287 $/yr	237,507 $	%58.6	25,633 L	1
VRFB Battery (L4)	16 m	0.134 $	1.10M $	13,692 $/yr	445,613 $	%89.5	7,006 L	4
	24 m	0.129 $	1.05M $	13,284 $/yr	422,028 $	%90.1	6,598 L	4
	30 m	0.126 $	1.03M $	12,992 $/yr	414,313 $	%90.7	6,264 L	4
Flywheel Battery (L5)	16 m	0.181 $	1.48M $	19,344 $/yr	563,863 $	%61.4	20,348 L	1
	24 m	0.175 $	1.43M $	18,262 $/yr	563,630 $	%64.2	18,901 L	1
	30 m	0.172 $	1.40M $	17,696 $/yr	563,552 $	%65.6	18,142 L	1
Zinc Flow Battery (L6)	16 m	0.120 $	980,916 $	6,016 $/yr	695,399 $	%89.7	6,898 L	8
	24 m	0.115 $	940,391 $	5,134 $/yr	696,739 $	%91.3	5,807 L	8
	30 m	0.113 $	921,131 $	5,051 $/yr	681,393 $	%91.4	5,762 L	8

TABLE 9
The results of sensitivity analysis (according to diesel fuel price).

Battery Type	Diesel Full	COE	NPC	Operating	Initial Capi-	Renew.	Total	Battery
Flow Battery (L1)	0.60 $/L	0.149 $	1.22M $	15,811 $/yr	466,069 $	%81.7	12,306 L	3
	0.71 $/L	0.156 $	1.28M $	16,688 $/yr	487,420 $	%83.6	11,017 L	3
	0.80 $/L	0.162 $	1.33M $	17,537 $/yr	494,075 $	%83.9	10,838 L	3
Lead Acid Battery (L2)	0.60 $/L	0.228 $	1.86M $	34,539 $/yr	223,580 $	%35.5	42,655 L	1
	0.71 $/L	0.232 $	1.90M $	34,715 $/yr	251,379 $	%63.8	26,558 L	1
	0.80 $/L	0.239 $	1.96M $	34,835 $/yr	303,518 $	%63.6	23,710 L	1
Lithium Ion Battery (L3)	0.60 $/L	0.180 $	1.47M $	20,895 $/yr	476,686 $	%65.3	21,650 L	2
	0.71 $/L	0.184 $	1.50M $	22,904 $/yr	416,236 $	%72.8	17,633 L	2
	0.80 $/L	0.168 $	1.37M $	18,443 $/yr	495,781 $	%84.4	10,101 L	2
VRFB Battery (L4)	0.60 $/L	0.129 $	1.06M $	13,383 $/yr	421,319 $	%87.3	8,498 L	4
	0.71 $/L	0.134 $	1.10M $	13,692 $/yr	445,613 $	%89.5	7,006 L	4
	0.80 $/L	0.138 $	1.12M $	14,107 $/yr	455,304 $	%89.9	6,729 L	4
Flywheel Battery (L5)	0.60 $/L	0.202 $	1.65M $	22,809 $/yr	566,783 $	%37.2	33,142 L	1
	0.71 $/L	0.181 $	1.48M $	19,344 $/yr	563,863 $	%61.4	20,348 L	1
	0.80 $/L	0.205 $	1.68M $	22,448 $/yr	613,023 $	%58.9	21,667 L	1
Zinc Flow Battery (L6)	0.60 $/L	0.115 $	941,966 $	5,490 $/yr	681,396 $	%88.0	8,017 L	8
	0.71 $/L	0.120 $	980,916 $	6,016 $/yr	695,399 $	%89.7	6,898 L	8
	0.80 $/L	0.123 $	1.01M $	6,140 $/yr	717,397 $	%90.6	6,270 L	8

TABLE 10
The results of sensitivity analysis (according to inflation rates).

Battery Type	Inflation	COE	NPC	Operating	Initial Capi-	Renew.	Total	Battery
Flow Battery (L1)	10%	0.203 $	1.12M $	27,139 $/yr	249,678 $	%54.4	29,102 L	2
	13%	0.149 $	1.22M $	15,811 $/yr	466,069 $	%81.7	12,306 L	3
	15%	0.130 $	1.41M $	14,593 $/yr	493,058 $	%83.9	10,854 L	3
Lead Acid Battery (L2)	10%	0.269 $	1.49M $	43,256 $/yr	100,777 $	%19.0	52,532 L	1
	13%	0.232 $	1.90M $	34,715 $/yr	251,379 $	%59.2	26,558 L	1
	15%	0.213 $	2.30M $	31,148 $/yr	351,481 $	%66.4	22,025 L	1
Lithium Ion Battery (L3)	10%	0.228 $	1.26M $	26,295 $/yr	417,282 $	%62.0	24,365 L	2
	13%	0.184 $	1.50M $	22,904 $/yr	416,236 $	%72.8	17,633 L	2
	15%	0.140 $	1.51M $	15,644 $/yr	529,225 $	%86.3	8,821 L	2
VRFB Battery (L4)	10%	0.162 $	0.894M $	14,843 $/yr	419,096 $	%87.2	8,576 L	4
	13%	0.134 $	1.10M $	13,692 $/yr	445,613 $	%89.5	7,006 L	4
	15%	0.118 $	1.27M $	12,858 $/yr	462,193 $	%90.2	6,556 L	4
Flywheel Battery (L5)	10%	0.262 $	1.44M $	28,860 $/yr	519,436 $	%33.3	35.174 L	1
	13%	0.181 $	1.48M $	19,344 $/yr	563,863 $	%61.4	20,348 L	1
	15%	0.167 $	1.80M $	18,722 $/yr	630,485 $	%60.9	20,603 L	1
Zinc Flow Battery (L6)	10%	0.165 $	911,384 $	9,857 $/yr	595,818 $	%85.2	9,900 L	6
	13%	0.120 $	980,916 $	6,016 $/yr	695,399 $	%89.7	6,898 L	8
	15%	0.085 $	920,289 $	-3,142 $/yr	1.12M $	%95.9	2,744 L	18

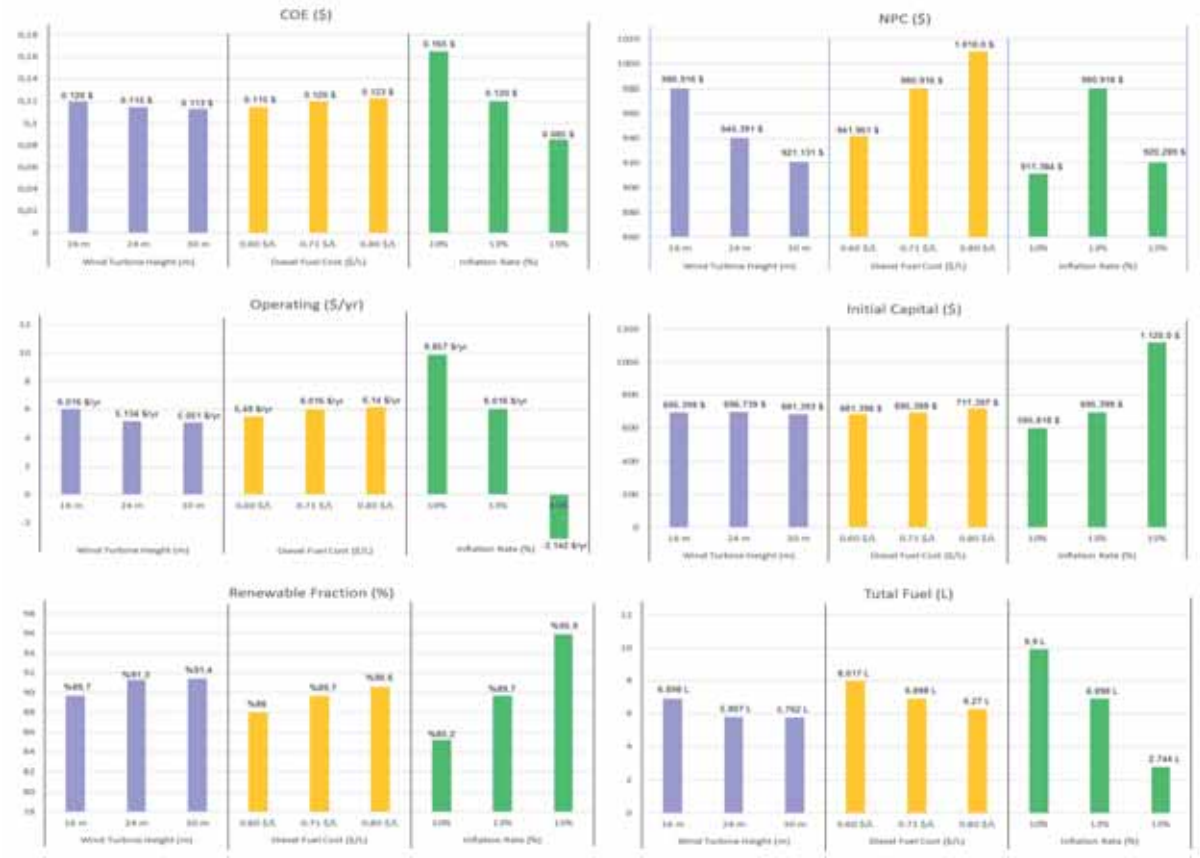


FIGURE 13
Sensitivity analysis of Zi-Br battery.

sult, 10 Zi-Br batteries with 50 kWh were determined as the most suitable battery model. It is seen that the total cost of this system after 25 years is $ 987,694. The advantage of the optimum model is that the fuel cost is the lowest and the gain to the user is -11,501 $. However, the investment cost of the system has the highest value of $ 733,884. Additionally, it is seen that flywheel storage is the most profitable system, but the fact that the NPC and fuel costs are quite high shows the situation negatively. LAB are batteries with the highest value and least return in terms of total costs, but their capital investment is extremely low. Cost evaluation shows that Zi-Br battery forefront and VRFB follows. These two batteries are more environmentally friendly, cause less CO_2 emission and diesel fuel consumption. It is concluded that very low diesel fuel is consumed because the RF ratio of the Zi-Br battery system is 91% due to RES. This situation is followed by the VRFB system with 87.8% RF. In the LAB system, RF is the

lowest with 67.5%. Nominal and utilization capacity values can be listed from highest to lowest as Zi-Br, FB, VRFB, Li-Ion, LAB, and flywheel storage.

Additionally, in this study, sensitivity analyzes of six systems with different batteries have been made. Sensitivity analyzes were carried out by considering the changes in WT heights, diesel fuel price, and inflation rate. The effects of each component on the system were examined and changes in costs according to the types of variables were observed.

The changes observed in costs are:

- As WT height increases, also RF increases, while the fuel consumption, COE, NPC and O&M, capital costs decrease.
- According to the increasing DG fuel costs, RF, COE, NPC, O&M and capital costs increased as the total fuel amount decreased.
- According to the increase in the inflation rate, RF, NPC, capital cost increased while COE, O&M cost, and the total amount of fuel decreased.

In this study, a preliminary evaluation is made to determine the most optimal storage system for HPS with different battery types and energy resources. As a result of this study, the battery model to be used especially in cases where the power demands of the load increase. Due to the advantages of Zi-Br and VRFB batteries, it is thought that it will create a prerequisite for designing a more economical model and comparing it with new generation storage resources (hydrogen, etc.).

REFERENCES

[1] Akar, O., Terzi, U.K., Tuncalp, B.K., Sonmezocak, T. (2019) "Determination of the Optimum Hybrid Renewable Power System: A case study of Istanbul Gedik University Gedik Vocational School", Balkan Journal of Electrical and Computer Engineering. 7(4), 456-463.

[2] Rehman, S., Natrajan, N., Mohandes, M., Alhems, L.M., Himri, Y., Allouhi, A. (2020) "Feasibility Study of Hybrid Power Systems for Remote Dwellings in Tamil Nadu, India". IEEE Access. 8, 143881–143890.

[3] Araujo, D., Batista, N., Carvalho, P., Reges, J., Costa, D., Dias, R., Freitas, D., Lima, S., Ramos, K., Ribeiro, S., Soares, F. (2020) "Renewable Hybrid Systems: Characterization and Tendencies", IEEE Latin America Transactions. 18(1), 102-112.

[4] Farret, F.A., Simões, M.G. (2006) "Integration of alternative sources of energy, 1st edition, IEEE press", Wiley. 1-408.

[5] Unamuno, E., Barrena, J.A. (2015) "Hybrid AC/DC microgrids-Part I: Review and classification of topologies". Renewable and Sustainable Energy Reviews. 52, 1251-1259.

[6] Djelailia, O., Kelaiaia, M.S., Labar, H., Necaibia, S., Merad, F. (2019) "Energy Hybridization PhotoVoltaic/Diesel Generator/ Pump Storage Hydroelectric Management Based on Online Optimal Fuel Consumption per kWh". Sustainable Cities and Society. 44, 1-15.

[7] Singh, M., Balachandra, P. (2019) "Microhybrid Electricity System for Energy Access, Livelihoods, and Empowerment", Proceedings of the IEEE. 107(9), 1995 – 2007.

[8] Arevalo, P., Benavides, D., Lata-Garcia, J., Jurado, F. (2020) "Energy control and size optimization of a hybrid system (photovoltaic hidrokinetic) using various storage technologies". Sustainable Cities and Society. 52, 101773, 1-17.

[9] Veilleux, G., Potisat, T., Pezim, D., Ribback, C., Ling, J., Krysztofinski, A., Ahmed, A., Papenheim, J., Pineda, A.M., Sembian, S., Churcerd, S. (2020) "Techno-economic analysis of microgrid projects for rural electrification: A systematic approach to the redesign of Koh Jik off grid case study". Energy for Sustainable Development. 54, 1-13.

[10] Atallah, M.O., Farahat, M.A., Lotfy, M.E., Senjyu, T. (2020) "Operation of conventional and unconventional energy sources to drive a reverse osmosis desalination plant in Sinai Peninsula, Egypt". Renewable Energy. 145, 141–152.

[11] Elmaadawy, K., Kotb, K.M., Elkadeem, M.R., Sharshir, S.W., Dan, A., Moawad, A., Liu, B. (2020) "Optimal sizing and techno-enviro-economic feasibility assessment of large-scale reverse osmosis desalination powered with hybrid renewable energy sources". Energy Conversion and Management. 224, 113377, 1-19.

[12] Miao, C., Teng, K., Wang, Y., Jiang, L. (2020) "Technoeconomic analysis on a hybrid power system for the UK household using renewable energy: A case study". Energies. 13 (12), 3231, 1-19.

[13] Hassani, H., Zaouche, F., Rekioua, D., Belaid, S., Rekioua, T., Bacha, S. (2020) "Feasibility of a standalone photovoltaic/battery system with hydrogen production". Journal of Energy Storage. 31, 101644, 1-18.

[14] Das, B.K., Zaman, F. (2019) "Performance analysis of a PV/Diesel hybrid system for a remote area in Bangladesh: Effects of dispatch strategies, batteries, and generator selection". Energy. 169, 263–276.

[15] Jahangiri, M., Soulouknga, M.H., Bardei, F.K., Shamsabadi, A.A., Akinlabi, E.T., Sichilalu, S.M., Mostafaeipour, A. (2019) "Techno-econo-environmental optimal operation of grid-wind-solar electricity generation with hydrogen storage system for domestic scale, case study in Chad". International Journal of Hydrogen Energy. 44(54), 28613-28628.

[16] Kalamaras, E., Belekoukia, M., Lin, Z., Xu, B., Wang, H., Xuan, J. (2019) "Techno-economic assessment of a hybrid off-grid DC system for combined heat and power generation in remote islands". Energy Procedia. 158, 6315-6320.
[17] Al-Sharafi, A., Sahin, A.Z., Ayar, T., Yilbas, B.S. (2017) "Techno-economic analysis and Optimization of solar and wind energy systems for power generation and hydrogen production in Saudi Arabia". Renewable and Sustainable Energy Reviews. 69, 33–49.
[18] Amutha, W.M., Rajini, V. (2016) "Cost benefit and technical analysis of rural electrification alternatives in southern India using HOMER". Renewable and Sustainable Energy Reviews. 62, 236–246.
[19] HOMER (2021) Using and Works, "https://www.homerenergy.com/ products/pro/docs/latest/index.html" (Accessed: 24 January 2021)
[20] Adaramola, M.S., Agelin-Chaab, M., Paul, S.S. (2014) "Analysis of hybrid energy systems for application in southern Ghana". Energy Conversion and Management. 88, 284-295.
[21] Duffie, J.A., Beckman, W.A. (1991) "Solar Engineering of Thermal Processes 2nd edition". Wiley, New York. 1-920.
[22] Rezk, H., Al-Dhaifallah, M., Hassan, Y.B., Ziedan, H.A. (2020) "Optimization and Energy Management of Hybrid Photovoltaic-Diesel-Battery System to Pump and Desalinate Water at Isolated Regions". IEEE Access. 8, 102512 – 102529.
[23] Ozturk, Z., Tosun, S., Ozturk, A. (2019) "Modeling a Hybrid Renewable Energy System with HOMER, Economical and Technical Analysis". Bayburt University Journal of Science. 2(2), 286 – 299.
[24] Ma, T., Yang, H., Lu, L., Peng, J. (2014) "Technical feasibility study on a standalone hybrid solar-wind system with pumped hydro storage for a remote island in Hong Kong". Renewable Energy. 69, 7-15.
[25] Das, I., Canizares, C.A. (2019) "Renewable Energy Integration in Diesel-Based Microgrids at the Canadian Arctic". Proceedings of the IEEE. 107(9), 1838 – 1856.
[26] Khalid, F., Dincer, I., Rosen, M.A. (2017) "Thermoeconomic analysis of a solar-biomass integrated multigeneration system for a community". Applied Thermal Engineering. 120, 645–653.
[27] Singh, S., Singh, M., Kaushik, S.C. (2016) "Feasibility study of an islanded microgrid in rural area consisting of PV, wind, biomass and battery energy storage System". Energy Conversion and Management. 128, 178-190.
[28] Rehman, S., Habib, H.U.R., Wang, S., Buker, M.S., Alhems, L.M., Garni, H.Z.A. (2020) "Optimal Design and Model Predictive Control of Standalone HRES: A Real Case Study for Residential Demand Side Management". IEEE Access. 8, 29767 – 29814.
[29] Chauhan, A., Saini, R. (2014) "A review on integrated renewable energy system based power generation for stand-alone applications: configurations, storage options, sizing methodologies and control". Renewable and Sustainable Energy Reviews. 38, 99-120.
[30] Molina, M.G. (2012) "Distributed Energy Storage Systems for Applications in Future Smart Grids". Transmission and Distribution: Latin America Conference and Exposition (T&D-LA), Sixth IEEE/PES, Uruguay.
[31] Chen, H., Cong, T.N., Yang, W., Tan, C., Li, Y., Ding, Y. (2009) "Progress in electrical energy storage system: a critical review". Progress in Natural Science. 19(3), 291–312.
[32] Vazquez, S., Lukic, S.M., Galvan, E., Galvan, E., Franquelo, L.G., Carrasco, J.M. (2011) "Energy storage systems for transport and grid applications". IEEE Transactions on Industrial Electronics. 57(12), 3881-3895.
[33] Barote, L., Weissbach, R., Teodorescu, R., Marinescu, C., Cirstea, M. (2008) "Stand-alone wind system with Vanadium Redox Battery energy storage". 11th International Conference on Optimization of Electrical and Electronic Equipment, August 2008, Romania.
[34] Huynh, C., Zheng, L., McMullen, P. (2007) "Thermal Performance Evaluation of a High-Speed Flywheel Energy Storage System". 33rd Annual Conference of the IEEE Industrial Electronics Society – IECON, Taiwan.
[35] International Flow Battery Forum (2019) https://flowbatteryforum.com/what-is-a-flow-battery/ (Accessed: 14 February 2021)
[36] Tsai, C.T., Beza, T.M., Molla, E.M., Kuo, C.C. (2020) "Analysis and Sizing of Mini-Grid Hybrid Renewable Energy System for Islands". IEEE Access Multidisciplinary. 8, 70013 – 70029.
[37] Hossain, M.S., Jahid, A., Islam, K.Z., Rahman, M.F. (2020) "Solar PV and Biomass Resources-Based Sustainable Energy Supply for Off-Grid Cellular Base Stations". IEEE Access. 8, 53817 – 53840.
[38] Al-Ammar, E.A., Habib, H.U.R., Kotb, K.M., Wang, S., Ko, W., Elmorshedy, M.F., Waqar, A. (2020) "Residential Community Load Management Based on Optimal Design of Standalone HRES With Model Predictive Control". IEEE Access. 8, 12542 – 12572.

[39] Javed, M.S., Song, A., Ma, T. (2019) "Techno-economic assessment of a stand-alone hybrid solar-wind-battery system for a remote island using genetic algorithm". Energy. 176, 704-717.
[40] Catuogno, G., Torres, L., Proietti, L., Garcia, G. (2019) "Methodology for the Selection and Sizing of an Isolated MicroGrid Based on Economic Criteria". IEEE Latin America Transactions. 17, 11, 1761-1770.
[41] Singh, R., Bansal, R.C. (2019) "Optimization of an Autonomous Hybrid Renewable Energy System Using Reformed Electric System Cascade Analysis". IEEE Transactions on Industrial Informatics. 15, 1, 399-409.
[42] Silva, L.M.R., Beluco, A., Daronco, G. (2020) "A Wind PV Diesel Hybrid System for Energizing a Sewage Station in Santa Rosa, in Southern Brazil". IEEE Latin America Transactions. 18, 4, 773-780.
[43] Clairand, J.M., Arriaga, M., Canizares, C.A., Alvarez-Bel, C. (2019) "Power Generation Planning of Galapagos' Microgrid Considering Electric Vehicles and Induction Stoves". IEEE Transactions on Sustainable Energy. 10, 4, 1916-1926.
[44] Habib, H.U.R., Wang, S., Elkadeem, M.R., Elmorshedy, M.F. (2019) "Design Optimization and Model Predictive Control of a Standalone Hybrid Renewable Energy System: A Case Study on a Small Residential Load in Pakistan". IEEE Access. 7, 117369-117390.
[45] Oladigbolu, J.O., Ramli, M.A.M., Al-Turki, Y.A. (2020) "Feasibility Study and Comparative Analysis of Hybrid Renewable Power System for off-Grid Rural Electrification in a Typical Remote Village Located in Nigeria" IEEE Access. 8, 171643-171663.
[46] Shafik, M.B., Rashed, G.I., Chen, H. (2020) "Optimizing Energy Savings and Operation of Active Distribution Networks Utilizing Hybrid Energy Resources and Soft Open Points: Case Study in Sohag, Egypt". IEEE Access. 8, 28704-28717.

Received: **10.04.2021**
Accepted: **17.05.2021**

CORRESPONDING AUTHOR

Zafer Ozturk
Department of Electrical-Electronics Engineering
Institute of Science
Duzce University
Duzce 81620 – Turkey

e-mail: zafer14034@ogr.duzce.edu.tr

© by PSP Volume 30– No. 09/2021 pages 10925-10932 Fresenius Environmental Bulletin

STUDY ON THE COUPLING AND COORDINATED DEVELOPMENT OF TOURISM ECONOMY AND ECOLOGICAL ENVIRONMENT IN GUIZHOU PROVINCE, CHINA

Wenlu Li, Li Luo*

School of Economics, Southwest Minzu University, Chengdu Sichuan 610041, China

ABSTRACT

At present, tourism has become an important industry in the overall economic development of China, people's demand for tourism is also increasing, and most people choose tourism as a way of entertainment during holidays. At the same time, the ecological environment has also been widely concerned by the society, and China pays more and more attention to the ecological environment protection. If tourism economy wants to get long-term development, it must be fully combined with environmental protection. This paper mainly takes Guizhou Province in the southeast of China as the research object, analyzes and measures the coupling relationship between tourism economic development and ecological environment protection through coupling coordination model. This study selects a relevant index as the establishment standard of the main evaluation index system to make an overall evaluation of tourism economic development and ecological environment protection in Guizhou Province. From the perspective of the coupling and coordinated development of tourism economy and ecological environment in Guizhou Province, the economic development coefficient showed a straight-line upward trend from 0.1509 in 2015 to 0.9472 in 2020. From 2018-2020, the coupling and coordinated development of economy and ecological environment in Guizhou province gradually changed into a high-level coupling and high-quality coordination stage. Through the comparative analysis of the coupling and coordinated development degree coefficient of tourism economy and ecological environment in Guizhou Province, the coupling and coordinated development degree of Guizhou Province has shown an obvious upward trend since 2015, and the upward trend in the past three years is relatively stable, which indicates that there is an obvious effect between the two systems of tourism economy and ecological environment.

KEYWORDS:
Guizhou Province, tourism economic development, ecological environment protection, coupling and coordinated development

INTRODUCTION

The rapid development of tourism industry in China provides sufficient impetus for regional economic development and promotes the development of urbanization process. In order to promote the development of tourism industry in an all-round way, we must pay more attention to the ecological environment [1]. The process of tourism industry development could have negative impact on the ecological environment, while the ecological environment impact will react with the development of tourism industry. How to promote the coordinated development of tourism economy and ecological environment is a key issue in the academic field [2].

In 1920, domestic and foreign experts and scholars carried out research on the relationship between tourism and environment [3-4], analyzed the impact relationship between tourism activities and environment in California Sequoia Park, and pointed out that the impact relationship between tourism and environment is mainly manifested in two aspects [5]. In the process of analyzing the interaction between convection activities and environment, it mainly studies the tourism planning environment and tourism environmental carrying capacity and other related fields [6]. In the process of studying the interaction between tourism and environment, experts and scholars mainly combined with quantitative research method to analyze the relationship between the two [7]. In the process of analyzing the impact relationship between tourism economy and ecological environment, the following evaluation methods can be adopted: first, they build the evaluation index system of tourism economy and ecological environment; second, they select the index related to tourism economy and ecological environment; third, they substitute the tourism economy index and ecological environment index into the evaluation model to get the conclusion of tourism economy and the change

of ecological environment under different indexes [9-10].

In the process of constructing the evaluation index system of tourism economy and ecological environment, it is necessary to fully combine the subjective will to build a framework of tourism economy and ecological environment evaluation system [11]. Then, they determine the weight of each index by combining the analytic hierarchy process and weight picking method, to show the influence degree of each index on tourism economy and ecological environment [12]. Through the analysis of the current research literature and data on the evaluation model of tourism economy and ecological environment, we can understand that the current evaluation models mainly include the system wild model and the coordination coefficient model, and the most widely used one is the coordination coefficient model [13]. Wang Hui, Weng gangmin, Liu Dinghui and Wang Lifang used the coordination coefficient model to analyze the relevant data of tourism economy and ecological environment in Dalian, Qinhuangdao, Anhui and Shanxi forest parks in recent years, and then rated the interaction between the two [14-17]. In the coordination coefficient model, the use of coordination degree and coordinated development to analyze the relationship between tourism economy and ecological environment, cannot be relatively clear and accurate to show the relationship between the two. The application of system evolution model in the actual research process is rare, and Hanzhen is one of the only scholars who used system evolution model. Compared with the first mock exam, the system evolution model can not fully show the relationship between the two models in the process of analyzing and discussing the interaction between them, which is also a main reason why this model is less used [18].

On the whole, there is a close interaction between tourism economy and ecological environment, mainly in the form of coupling. Guizhou Province is a typical karst region, which has laid a solid foundation for promoting the development of tourism industry. However, in the process of tourism economic development, Guizhou Province will also have a certain negative impact on the development of ecological environment. Therefore, it is necessary to comprehensively coordinate the coordinated development of regional tourism economy and ecological environment in order to promote the sustainable development of tourism economy.

MATERIALS AND METHODS

(1) Overview of the study area. In 1949, at the initial stage of the founding of the people's Republic of China, Guizhou's economic development was based on the primary industry, and its industrial structure was adjusted during the 13th Five Year Plan period (Figure 1). In 2020, the proportion of the three industrial structures was 14.2:34.8:50.9. Guizhou is rich in tourism resources, and its total tourism income is also increasing year by year. As can be seen from Figure 2, the total number of tourists in Guizhou Province in 2020 is 617.8149 million, an increase of 52.8% over the same period. The total tourism income is 578.509 billion yuan, accounting for 63.74% of the total value of the tertiary industry. In the regional national economic income, Guizhou's tourism industry has become an irreplaceable important part Points.

(2) Analysis of interaction mechanism between tourism economy and ecological environment. 1) Effect of tourism economy on ecological environment. By analyzing the positive role of tourism economic development, we can understand that in the process of tourism economic development, it can provide funds for ecological environmental protection to a certain extent, so as to comprehensively promote the improvement of ecological environment and lay a solid foundation for environmental protection. By analyzing the negative effects of tourism economic development, we can understand that in the process of tourism economic development, the ecological environment will be damaged and threatened to a certain extent.

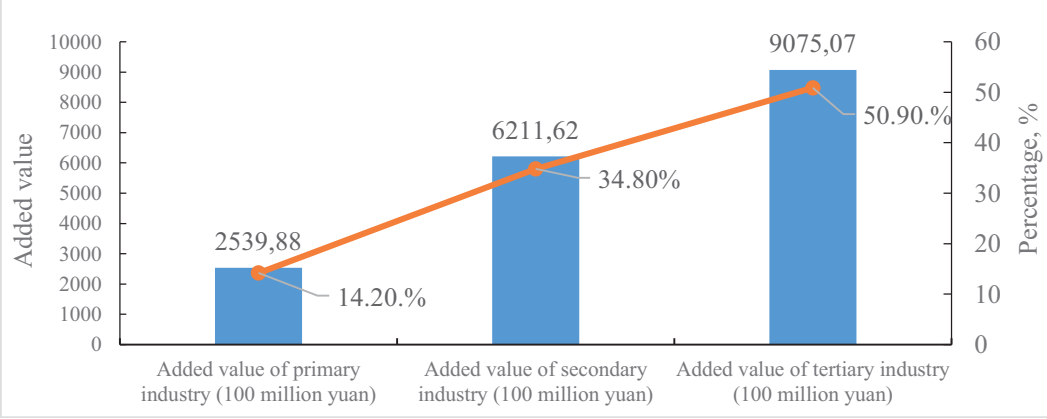


FIGURE 1
Industrial structure proportion of Guizhou Province in 2020.

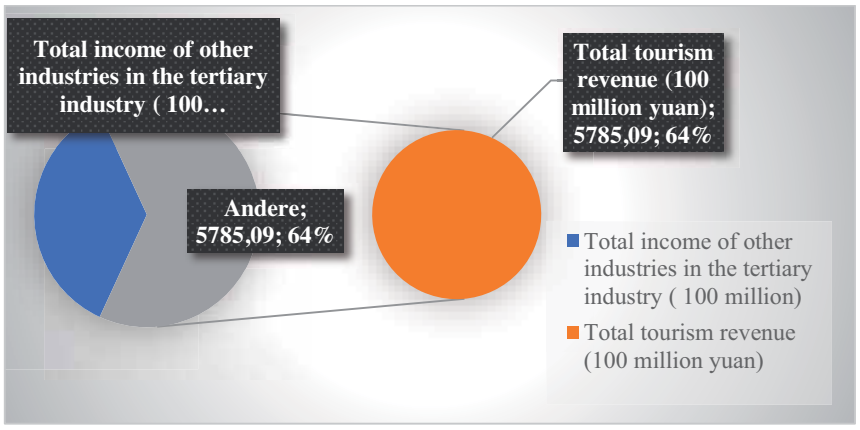


FIGURE 2
Statistics of the proportion of total tourism revenue in Guizhou Province in 2020.

(1) Tourism economy promotes the ecological environment. In the process of developing tourism in most areas of China, the actual development of tourism is relatively weak, so it is unable to effectively improve the tourism economy, which leads to the less investment in ecological environment protection in these areas and affects the regional ecological environment protection. If the tourism industry in the region has a strong development potential, it can provide sufficient financial support for the region, and can provide sufficient funds for the comprehensive promotion of the governance and development of the ecological environment. For example, in some regions with better tourism economic development, special funds for green sanitation and ecological restoration will be set up to protect the regional natural and cultural heritage and natural environment which can effectively protect the environment and promote the sustainable development of the ecological environment.

(2) Tourism economy has a stress effect on ecological environment. Through the analysis of the interaction between the tourism economy and the ecological environment, we can understand that the tourism economy also has a stress effect on the environment in the actual development process, which can be described from two aspects. Firstly, the tourism economy will affect the development of the ecological environment in the actual development process, because in the process of tourism resources development, it is bound to affect the ecological environment of the region. At the same time, some uncivilized behaviors of tourists will damage the ecological environment. Secondly, under the background of further expansion of tourism scale, many regions will pay more attention to the economic benefits brought by the development of tourism industry, thus ignoring the negative impact on the environment in the process of tourism resources development. Therefore, in the process of tourism economic development, excessive development and use of land resources will eventually lead to a series of phenomena, such as soil erosion or land hardening. In the short time, it can promote the development of tourism economy, but for the development of tourism products, it will have a serious impact on the development of the region.

2) The effect of ecological environment on tourism economy.(1) Ecological environment plays a bearing role in tourism economy. The ecological environment is not only an important guarantee for people's production and life, but also an important source for people to create economic value. The better the ecological environment of the region, the greater the external tourism attraction of the region. At this time, it can also attract more tourists. Therefore, in the process of the development of tourism, we must consider the ecological environment protection to realize the sustainable development of tourism economy.

(2) The ecological environment restricts the tourism economy. The natural environment and natural resources have the characteristics of limitation and vulnerability. If the region only pays attention to the economic benefits of the region in the process of tourism economic development and ignores the negative impact on the ecological environment in the process of tourism development, the ultimate tourism development intensity will exceed the bearing value of the ecological environment. At this time, it will cause serious environmental pollution. The self-regulation ability of the ecosystem can not effectively restore the pollution in the process of tourism development. At this time, the carrying capacity of the ecological environment for tourism activities will also be greatly reduced, which will eventually react on the tourism economy, leading to the weakening of the regional tourism economic development [19]. At this time, the cost of tourism economy will be further increased, which is not worth the loss for the sustainable development of tourism economy. Figure 3 shows the interaction between tourism economy and ecological environment.

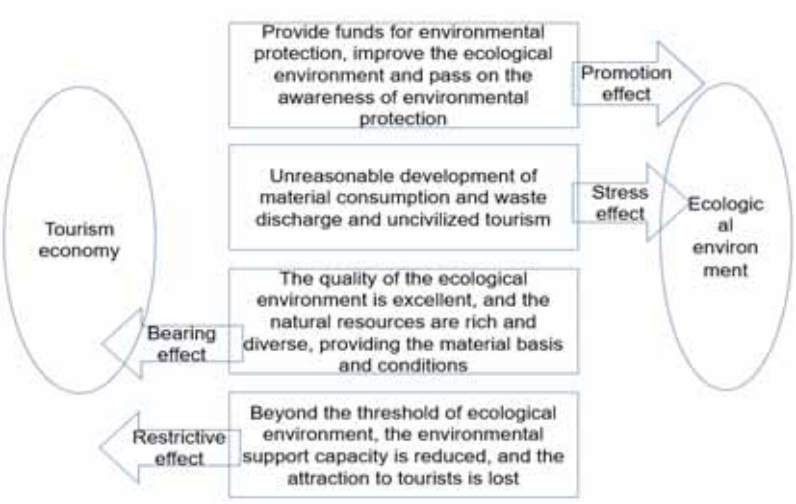


FIGURE 3
Schematic diagram of mechanism analysis of eco economic system and tourism economy.

RESULTS

(1) Construction of coupling coordination model of tourism economy and ecological environment. In order to fully reflect the coupling effect of a certain tourism and ecological environment, the multi factor comprehensive index evaluation method is used to obtain the comprehensive index of tourism and ecological environment (also known as the development level of comprehensive index) [20]. The comprehensive development degree of tourism economic system and ecological environment system is calculated by linear weighting method:

$$U_i = \sum_{j=1}^{n} \lambda_{ij} u_{ij}, \sum_{j=1}^{n} \lambda_{ij} = 1 \quad (1)$$

In formula (1), the comprehensive evaluation function is represented by U_i; the index weight is represented by λ_{ij}; the contribution degree of the index to the system is represented by u_{ij}.

(2) Coupling coordinated development model. 1) Coupling. The coupling degree model is mainly used to evaluate the degree of coupling coordination between the systems [21]. In this paper, the degree of influence between tourism economic system and ecological environment system is described by using the index. The specific coupling degree formula can be described as follows:

$$C = 2\left\{(u_1 \times u_2)/\left[(u_1 + u_2) \times (u_1 + u_2)\right]\right\}^{1/2} \quad (2)$$

Where C is the coupling degree, u_1 is the tourism economic development index and u_2 is the ecological environment development index, also known as the coupling coefficient. The larger C the system is, the closer the relationship between the systems is, the more coordinated the system is. The classification of coupling degree is shown in Table 1.

2) Coupling coordination. In order to better describe the coupling of economic and environmental conditions of Guizhou Province, this paper constructs a coupling model:

$$D = \sqrt{CT}, T = \alpha u_1 + \beta u_2 \quad (3)$$

Formula 3 is the coupling coordinated development degree, and the comprehensive development level evaluation function of the above two systems is T. α 、 β are two undetermined coefficients. Because the two systems are in the same important position, the coefficient value can be taken as 0.5. Coupling degree $C \in [0,1]$. A large value of coupling degree indicates a high degree of coupling. This index only indicates the related effect between the two systems. Therefore, the coupling coordinated development degree D is introduced, and the value range is the same. If the coordination data value is the same, it means that the coupling coordination degree of the two systems is good. The coupling coordination degree can be classified according to Table 2 below.

TABLE 1
Classification of coupling degree

Coupling degree	[0,0.3]	(0.3,0.5]	(0.5,0.8]	(0.8,1]
Grading	Low level coupling stage	Antagonistic stage	Running in stage	High level coupling stage

TABLE 2
Level division of coupling coordinated development degree

Coupling coordinated development degree	Level
[0, 0.09]	Extreme maladjustment
[0.10, 0.19]	Serious maladjustment
[0.20, 0.29]	Moderate maladjustment
[0.30, 0.39]	Mild maladjustment
[0.40, 0.49]	On the verge of maladjustment
[0.50, 0.59]	Barely out of balance
[0.60, 0.69]	Primary coordination
[0.70, 0.79]	Intermediate coordination
[0.80, 0.89]	Good coordination
[0.90, 1.0]	High quality coordination

TABLE 3
Evaluation system of tourism economy ecological environment index in Guizhou Province

System layer	Element layer	Index layer
Ecological environment	Ecological load	Ratio of cultivated land to construction land (%)
		Tourism environmental capacity saturation (%)
		Community pollutant emission rate (%)
	Ecological quality	Forest and grassland coverage (%)
		Air quality index excellent rate (%)
		Water environment quality (%)
	Ecological construction	Sewage centralized treatment rate (%)
		Garbage centralized treatment rate (%)
		Popularization rate of public environmental protection awareness (%)
		Total tourism income growth rate (%)
Economic benefits of Tourism	Economic performance	Total number of tourists growth (%)
		Proportion of tourism households (%)
	Resource level	Types and scale of tourism resources
		The value of tourism resources history and culture science education
	Tourism development	The influence of tourism resources infrastructure
		Tourism development potential

(3) Results. 1) Analysis of the comprehensive development level of tourism economy and ecological environment. According to formula (1), the comprehensive level system values of tourism economic system and ecological environment system development in Guizhou Province are obtained, as shown in Table 4. The statistics in the table show that the tourism economic benefit index of the province has been rising continuously in the six years, from 0.1509 in 2015 to 0.9472 in 2020. It shows that the tourism economy development trend of Guizhou Province is relatively good, which is closely related to the importance of tourism industry development in Guizhou Province.

It can be seen from the data in Figure 4 that the development of tourism economy depends on the development and utilization of tourism resources, and the ecological environment has a certain purification capacity. As long as the development intensity of tourism resources and the damage degree of tourism activities to the ecological environment do not exceed the carrying capacity of the ecological environment, the negative effects of these activities are still digestible. Therefore, the index data is relatively good.

TABLE 4
Statistics of comprehensive development level index of tourism economy and ecological environment in Guizhou Province

Year	Index of economic development level	Index of ecological environment development level
2015	0.1509	0.3004
2016	0.1786	0.3123
2017	0.3245	0.4563
2018	0.4081	0.5317
2019	0.8764	0.6725
2020	0.9472	0.7789

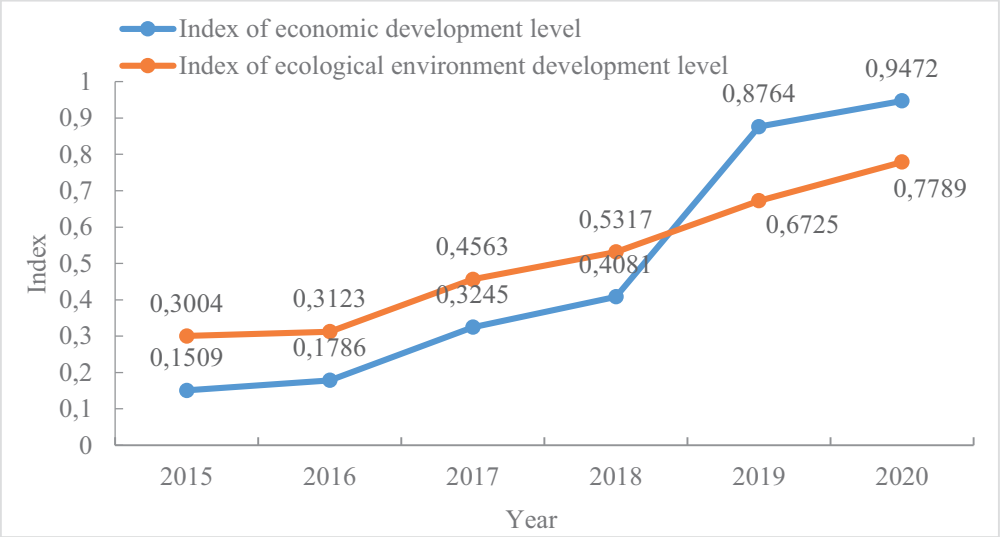


FIGURE 4
Comprehensive development index of tourism economy and ecological environment in Guizhou Province.

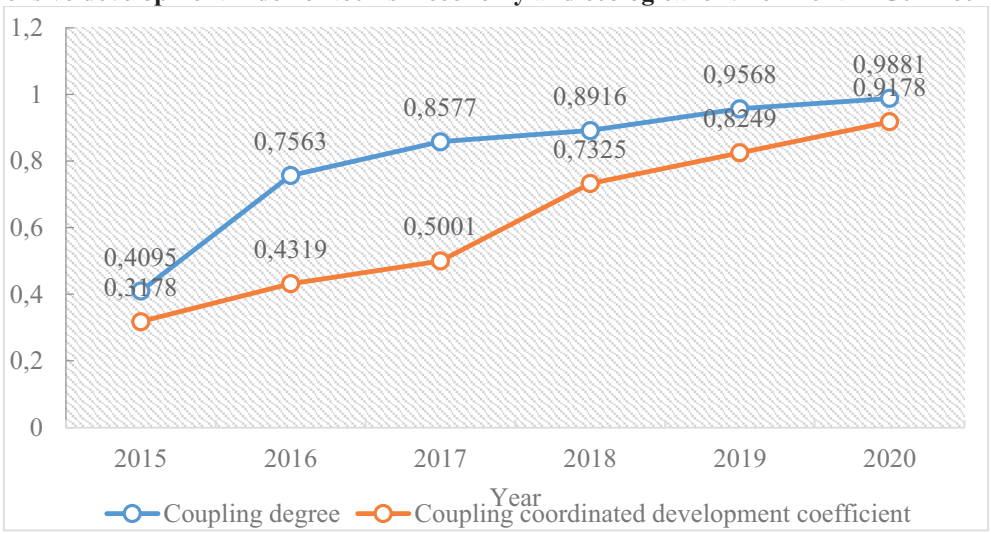


FIGURE 5
Coordinated development trend of tourism economy ecological environment in Guizhou Province from 2015 to 2020.

2) Coupling and coordinated development analysis. According to formula (2) and formula (3), the value of coupling degree coefficient and coupling coordination degree of tourism economy ecological environment in Guizhou Province are obtained. The division process of coupling coordination degree is realized through the statistics of the data. The specific statistical data are shown in Figure 5.

According to the data in Figure 5, the coupling coordination degree of tourism economy and ecological environment in Guizhou Province has been increasing gradually in recent 6 years, and there is no downward floating trend from the curve change range. The coupling coordination degree of the two systems increased from 0.3178 in 2015 to 0.9178 in 2020. According to Table 2, the development of coupling coordination degree of Guizhou Province from 2015 to 2017 has gradually changed from mild to barely unbalanced. Since 2018, the coupling coordination change of tourism economy and ecological environment in Guizhou Province has been stabilized, and the coefficient of coordination in three years has increased from 0.7325 to 0.9178 and achieved high-quality coordination in 2020.

CONCLUSIONS

(1) After a deep exploration of tourism economy and ecological environment in Guizhou Province, it is found that there is a relationship between them. For example, to a certain extent, the ecological environment can directly affect the decision behavior of tourists, and the climate environment can directly affect the tourists' choice of tourism areas. After the active development of tourism, Guiyang City in Guizhou Province has been developing towards reducing emission pollution and saving natural re-

sources in order to further promote the long-term development of tourism, such as aluminum industry, phosphorus mining industry and other related industries in Guiyang.

(2) People's tourism activities will have an impact on the water environment within the scope of the scenic area, which will lead to the loss of water resources in a certain area, and then increase the load bearing capacity of the water supply system. In addition, the water quality of the tourism area will be polluted by all kinds of garbage and sewage generated in the tourism activities. In the peak period of tourism activities, some tourism ships drive too frequently in the relevant tourism areas, and the pollutants discharged by them are much higher than the self purification capacity of the water body, which leads to the pollution of water quality.

(3) Through measurement and analysis, the overall tourism economic benefit index and ecological environment benefit index of Guizhou Province begin to increase year by year. At the same time, the coupling degree between tourism economy and ecological environment in Guizhou Province also shows a rising trend, which has been maintained stably after reaching a higher level. On the whole, the coupling degree between tourism economy and ecological environment in Guizhou Province was in the antagonistic stage (0.4095) in 2015, in the running in stage (0.7563) in 2016, and showed a high coupling degree from 2018 to 2020.

ACKNOWLEDGEMENTS

This work was supported by thekey research base of social sciences in Sichuan Province (expansion) national park research center project: study on the establishment of national park system in karst areas of south China(GJGY2019-ZC020).

REFERENCES

[1] Parolo, G., Ferrarini, A., Rossi, G. (2009) Optimization of tourism impacts within protected areas by means of genetic algorithms. Ecological Modelling. 220(8), 1138-1147.

[2] Liu, W.X., Coveney, R.M., Chen, J.L. (2003) Environmental quality assessment on a river system polluted by mining activities. Applied Geochemistry. 18(5), 749-764.

[3] Dann, P.M., Chambers, L. (2013) Ecological effects of climate change on little penguins Eudyptula minor and the potential economic impact on tourism. Climate Research. 58(1), 67-79.

[4] Yu, G., Schwartz, Z., Walsh, J.E. (2009) A weather-resolving index for assessing the impact of climate change on tourism related climate resources. Climatic Change. 95(3-4), 551-573.

[5] Atique, U., Iqbal, S., Khan, N., Qazi, B., Sherzada, S. (2020) Multivariate assessment of water chemistry and metals in a river impacted by tanning industry. Fresen. Environ. Bull. 29(4A), 3013-3025.

[6] Lacitignola, D., Petrosillo, I., Cataldi, M., Zurlini, G. (2007) Modelling socio-ecological tourism-based systems for sustainability. Ecological Modelling. 206(1-2), 191-204.

[7] Wu, B., Rui, Z., Cheng, S.P., Ford, T., Zhang, X.X. (2011) Risk assessment of polycyclic aromatic hydrocarbons in aquatic ecosystems. Ecotoxicology. 20(5), 1124-1130.

[8] Maciejewski, K., Kerley, G.I.H. (2016) Elevated elephant density does not improve ecotourism opportunities: convergence in social and ecological objectives. Ecological Applications. 24(5), 920-926.

[9] Su, L., Liu, J., Christensen, P. (2011) Spatial distribution and ecological risk assessment of metals in sediments of Baiyangdian wetland ecosystem. Ecotoxicology. 20(5), 1107-1116.

[10] Mengu, G.P., Akkuzu, E., Anac, S., Sensoy, S. (2011) Impact of climate change on irrigated agriculture. Fresen. Environ. Bull. 20(3), 823-830.

[11] Convery, J.J. (1994) Challenges to environmental engineers. Waste Management. 14(8), 661-670.

[12] Duian, L. (2017) Comparative assessment of heavy metals in agricultural soils under different land uses: a case study from China. Fresen. Environ. Bull. 26(8), 5323-5330.

[13] Molina, S. (1991) Ecological and environmental knowledge to be used in the training of human resources for tourism. Solid State Ionics. 228(24), 56-63.

[14] Kacar, A., Kucuksezgin, F. (2014) Profiles of some beaches on coastal bathing waters of Turkey in the eastern Mediterranean. Fresen.Environ. Bull. 23(10), 2466-2473.

[15] Wei, X., Huang, W.M., Liu, G.H., Liu, Y.D. (2009) Vertical distributions of size-fractionated iron in three typical bays of lake Dianchi (China). Fresen. Environ. Bull. 18(5), 624-627.

[16] Copeland, E. (1992) The role of airlines in the tourism and environment debate. Tourism Management. 13(1), 112-114.

[17] Prunier, E.K., Sweeney, A.E., Geen, A.G. (1993) Tourism and the environment: the case of Zakynthos. Tourism Management. 14(2), 137-141.

[18] Batra, G.S., Kaur, N. (1996) New vistas in reducing the conflicts between tourism and the environment: an environmental audit approach. Managerial Auditing Journal. 11(4), 3-10.

[19] Ypeij, J.L. (2007) Incatourism and the protection of the environment, landscape and cultural heritage. Australia Refugee Review Tribunal. 1(2), 218-259.

[20] Williams, A. (2007) Reconciling tourism and the environment: a task for international environmental law. Wiadomoci Parazytologiczne. 53(3), 203-211.
[21] Farrell, B.H., Mclellan, R.W. (1987) Tourism and physical environment research. Annals of Tourism Research. 14(1), 1-16.

Received: **10.04.2021**
Accepted: **17.05.2021**

CORRESPONDING AUTHOR

Li Luo
School of Economics,
Southwest Minzu University,
Chengdu Sichuan 610041 – China

e-mail: lbswllmxy@163.com

© by PSP Volume 30– No. 09/2021 pages 10933-10940 Fresenius Environmental Bulletin

THE EVALUATION OF COORDINATED DEVELOPMENT OF AGRICULTURAL ECONOMY AND RURAL ECOLOGICAL ENVIRONMENT TAKING SINO AFRICAN COOPERATION PROJECT AS AN EXAMPLE

Jiang Ou[1], Jie Wang[2,*]

[1]Changsha Yijingfang Education Technology Co., Ltd, Changsha Hunan 410000, China
[2]School of Economics, Hunan Agricultural University, Changsha Hunan 410000, China

ABSTRACT

From the way of free aid to the cooperation mode of aid, trade and investment, Sino African agricultural cooperation has made long-term progress. The modern agricultural production mode has accelerated the development of agricultural economy and greatly enriched people's material life. However, in the background of pursuing the rapid growth of agricultural economy, it also brings pollution and destruction to the rural ecological environment and threatens the long-term survival and development of people. Taking the Sino African cooperation project as an example, this paper qualitatively studies the current situation of agricultural economy and rural ecological environment in an African city, constructs the evaluation index system of agricultural economic system from two dimensions of economic strength and economic vitality, constructs the evaluation index system of rural ecological environment system from three dimensions of ecological quality, production environment and environmental pollution, and introduces the coefficient of variation measurement model. The coordinated development of agricultural economy and rural ecological environment in recent ten years is quantitatively evaluated. The results show that the overall development trend of agricultural economy and rural ecological environment in the study period is good. The degree of coordinated development is constantly improving, and the type of coordinated development transits from mild imbalance in the early stage to the verge of imbalance, and from the later stage to barely coordinated type.

KEYWORDS:
Agricultural economy, rural ecological environment, coordinated development, Sino African cooperation

INTRODUCTION

Over the past 20 years, agriculture, as a traditional field and an important interest intersection of Sino African cooperation, has also been continuously enriched and improved under the framework of the forum, and many new progress has been made: the mode of cooperation has changed from free aid to the combination of aid, trade and investment, the main body of cooperation has developed from government oriented to multi-agent and multi-channel participation, and the content of cooperation has expanded from the production link of food crops to the whole industrial chain. The form of cooperation has changed from fragmented project cooperation to institutionalized cooperation [1-2]. Sino African cooperation has led to the introduction of modern agricultural production mode, accelerated the pace of agricultural economic development, and greatly enriched the material life of the local people in Africa [3-4]. But in the context of the rapid pursuit of agricultural economic growth, it also brings pollution and destruction to the rural ecological environment, threatening people's long-term survival and development [5-6]. It is imperative to explore the coordinated development between agricultural economy and rural ecological environment.

Foreign researchers paid attention to the relationship between economic growth and environment earlier, and the research has already begun. But at the beginning of the study, most western economists focused on how to develop the economy quickly to enhance the comprehensive strength of the country, while ignoring the important role of ecological environment in economic development [7]. With the rapid economic growth, more and more ecological and environmental problems have emerged. In 1966, Bolding put forward the concept of ecological economics, and made a clear overview and explanation of its meaning and characteristics, which opened the way for researchers to study the relationship between ecological environment and economy.

Arrow (1995) and Hefner (1996) pointed out that after economic growth, the state will invest more money to improve and protect the ecological environment, and more scientific and high-quality treatment measures can more specifically solve environmental problems [9-12]. Domestic scholars have also done a lot of similar research. Jia Shijing [13]

(2008) from the perspective of the coordinated development of agricultural regional ecological environment and economy, selected the evaluation index of the two, analyzed the coordination degree of China's provincial economy and agricultural and rural ecological environment, and found that there were significant differences among provinces, and most of them were in the middle and high coordination degree. Ren Zhiyuan [14] (2011) evaluated the coordination degree of agricultural economy and rural ecological environment of 10 cities in Shaanxi Province, and the results showed that the coordination degree was low.

This paper selects a city under the cooperation between China and Africa as the research target, constructs the index evaluation system of agricultural economy and rural ecological environment, calculates the weight of each index by entropy weighting method, evaluates the coordinated development degree of agricultural economy and rural ecological environment by coordination degree model, and evaluates the actual situation of the target city objectively and scientifically.

MATERIALS AND METHODS

(1) Evaluation index system. As for agricultural economy, it is divided into two directions: agricultural economic strength and agricultural economic vitality. Agricultural economic strength is mainly composed of per capita grain output, per capita gross agricultural output value and per capita net income of farmers. In terms of agricultural economic vitality, four evaluation factors, namely rural power consumption, total power of agricultural machinery, the proportion of added value of agriculture, forestry, animal husbandry and fishery in total output value, and the proportion of primary industry in GDP, are considered to mainly reflect the activity of agricultural economic development modernization [15-17].

The rural ecological environment is described from three aspects: rural ecological quality, rural production environment, and rural environmental pollution. The rural ecological quality is mainly composed of two evaluation factors: forest coverage rate and annual actual water supply of water conservancy project, which mainly reflects the overall quality of ecological environment in rural areas. The three evaluation factors of per capita cultivated land area, per capita crop planting area and effective irrigation area mainly reflect the environmental conditions of agricultural production resources provided by rural areas. In terms of rural environmental pollution, the three evaluation factors are mainly the use of agricultural medicine, agricultural plastic film and chemical fertilizer. Evaluation factors mainly reflect the impact of the main pollutants produced in agricultural production on the ecological environment in rural areas. The details are shown in Table 1.

(2) Evaluation method. 1) Determination method of index weight. The advantage of subjective weighting method is that experts can distinguish the importance of indicators in practical application according to their own rich knowledge and experience. However, the results are too subjective and random, which also increases the burden of analysis and causes certain limitations. In order to make the evaluation results more real and avoid the deviation caused by subjective human factors as far as possible, the objective weighting method has stronger mathematical logic, which makes up for the above shortcomings. The entropy method is the most used objective weighting method [18-20], which is used in this study.

TABLE 1
Evaluation index of coordinated development of agricultural economy and rural ecological environment

Target layer	Criterion layer	Index layer
Agricultural economy	Economic strength	Grain output per capita
		Gross agricultural output value per capita
		Per capita net income of farmers
	Economic vitality	rural power consumption
		Total power of agricultural machinery
		Proportion of added value of agriculture, forestry, animal husbandry and fishery in total output value
		Proportion of primary industry in GDP
Rural ecological environment	Ecological quality	Forest coverage
		Actual annual water supply of water conservancy project
	Production environment	Per capita cultivated land area of primary industry employees
		Per capita sown area of crops for the first industry employees
		Effective irrigation area of farmland
	Environmental pollution	Pesticide usage
		Usage of agricultural plastic film
		Fertilizer usage

Entropy method uses the characteristics of the concept of uncertainty in complex science and reflects the discrete degree of the index by calculating entropy. If the index is more discrete, it shows the greater impact on the overall evaluation, and plays the role of objective empowerment of the index, to provide a scientific basis for the following comprehensive evaluation. According to the characteristics of this method, it is suitable to study the complex problems of agricultural economy and rural ecological environment in the target city. The detailed steps are as follows:

The first step is to standardize the indicators. In order to solve the problem of different dimensions and orders of magnitude of the original data, the extreme value method is used to convert the absolute value of the index into the relative value, so as to realize the homogenization of each value. Due to the difference between positive and negative indicators, formula (1) is used to calculate positive indicators, that is, the larger the value is, the better; formula (2) is used to calculate negative indicators, that is, the smaller the value is, the better.

$$r_{ij}{}' = \frac{r_{ij} - \min(r_{ij})}{\max(r_{ij}) - \min(r_{ij})} \quad (1)$$

$$r_{ij}{}' = \frac{\max(r_{ij}) - r_{ij}}{\max(r_{ij}) - \min(r_{ij})} \quad (2)$$

The second step is to calculate the information entropy of each index:

$$H_{ij} = -k \sum_{j=1}^{m} (f_{ij}\, In f_{ij}) \quad (3)$$

Where $f_{ij} = \frac{r_{ij}{}'}{\sum_{j=1}^{n} r_{ij}{}'}$, $k = \frac{1}{Inm}$, m represents the number of all indicators, assuming $f_{ij} = 0$, $f_{ij} In(f_{ij}) = 0$.

The third step is to calculate the weight of indicators:

$$W_{ij} = \frac{1 - H_{ij}}{m - \sum_{i=1}^{m} (H_{ij})} \quad (4)$$

Where H_{ij} is the information entropy of the index.

2) Evaluation method of coordination degree. The coordinated development model is used to quantitatively evaluate the coordination between agricultural economic system and rural ecological environment system. The measurement method of coefficient of variation mainly reflects the degree of variation through the concept and properties of coefficient of variation in mathematical statistics, and then obtains the coordination measure between two related systems, that is, the coordination coefficient. This paper uses this method to evaluate the coordination degree.

According to the concept of coefficient of variation measurement method, the calculation model of coefficient of variation is deduced. The comprehensive benefit indexes of agricultural economy and rural ecological environment in a certain period of time in a certain region are expressed as U1 and U2, respectively, the coefficient of variation is expressed as C, the standard deviation wis expressed as s, the average is expressed as $\bar{x}$, and the coefficient of variation is expressed as the ratio of standard deviation and average.

$$C = \frac{s}{\bar{x}} \quad (5)$$

The coordination degree measurement model of agricultural economy and rural ecological environment is defined as follows:

$$C_t = \left[\frac{U_1 \times U_2}{\left(\frac{U_1 + U_2}{2}\right)^2}\right]^k \quad (6)$$

Where: Ct is the coordination degree of agricultural economy and rural ecological environment in t period, K is the adjustment coefficient, K ≥ 2. According to the actual situation of the research object, the value of K is 2. It can be proved from the model that the value of Ct is between 0 and 1. The larger the value is, the better the coordination between them is. The smaller the value is, the worse the coordination is.

Coordination degree Ct is an important index to evaluate the coordination between agricultural economy and rural ecological environment, which has constraint and guiding significance in promoting the coordinated and healthy development of agricultural economy and rural ecological environment. However, in some cases, it is difficult to describe the overall function of agricultural economy and rural ecological environment, or the comprehensive level of both. There is a high degree of coordination between agricultural economy and rural ecological environment in two regions or in the same region in two different periods, but it may be coordinated at a higher level and a lower level, respectively. Therefore, based on the evaluation of the degree of coordination between the two, the concept of coordinated development degree Dt is introduced to evaluate the level of coordinated development. The specific calculation model is as follows:

$$D_t = \sqrt{C_t \times T} \quad (7)$$

$$T = \alpha \times U_1 + \beta \times U_2 \quad (8)$$

Where: Dt is the coordinated development degree, Ct is the coordinated degree, t is the comprehensive evaluation index of agricultural economic benefit and rural ecological environment benefit, which reflects the comprehensive benefit and level of agricultural economy and rural ecological environment. α, β is a specific weight. This study thinks that the development of agricultural economy is as important as the protection of rural ecological environment, so α and β take the same value as 0.5, respectively.

The coordinated development of agricultural economy and rural ecological environment is divided into three levels and 10 subcategories. The details are shown in Table 2.

TABLE 2
Classification criteria and types of coordinated development of agricultural economy and rural ecological environment

Coordination category	D	Coordination subclass
Maladjustment recession layer	0-0.09	Extreme disorders
	0.1-0.19	Serious disorders
	0.2-0.29	Moderate maladjustment
	0.3-0.39	Mild disorders
Overharmonic layer	0.4-0.49	On the verge of maladjustment
	0.5-0.59	Reluctantly coordinated
Coordinated development layer	0.6-0.69	Primary coordination
	0.7-0.79	Intermediate coordination
	0.8-0.89	Good coordination
	0.9-1	High quality coordination

U1 > U2: environment lag; U1 = U2: economy and environment synchronization; U1 < U2: economy lag

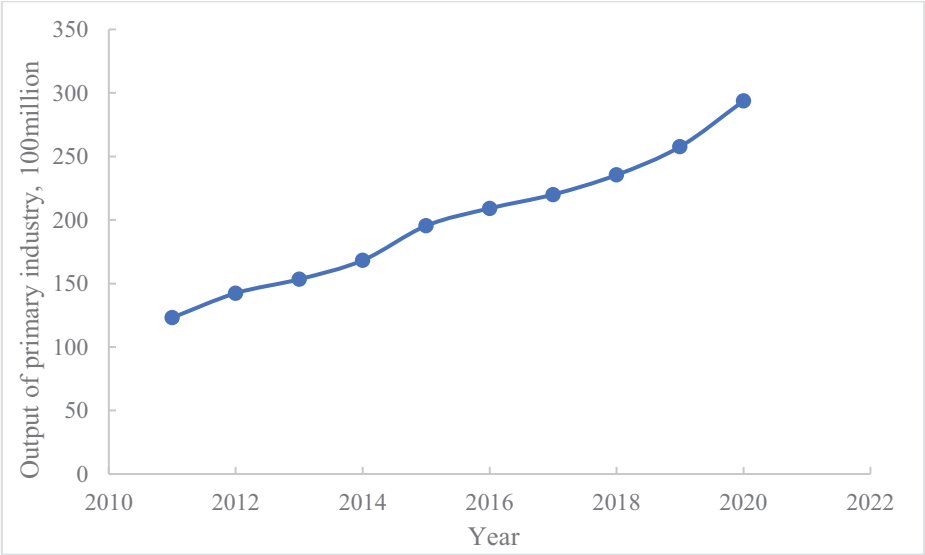


FIGURE 1
Changes of gross output value of primary industry.

RESULTS

(1) Economic analysis. In 2020, the city's GDP reaches 2019.30 billion yuan. In recent years, the city's agricultural economy has maintained a trend of medium and high-speed growth. The total output value of the primary industry reflects the overall effect of agricultural economic development, the grain output reflects the capacity of agricultural production, and the diversified agricultural industries promote the stability of agricultural economic development.

(1) The total output value of the first industry continues to increase, and the agricultural economy is developing steadily. The agricultural economy of the city presents a state of rapid development. The continuous growth of the total output value of the first industry during the research period reflects this development momentum. From 2011 to 2020, the output value increased from 12.314 billion to 29.372 billion yuan. Figure 1 reflects the specific changes.

(2) The increase of grain output plays a key role in ensuring the stable development of agricultural economy. The city's total grain output has been continuously stable at more than 1.5 million tons. In 2011, the city's total grain output was 1.532 million tons, and will increase to 1.736 million tons by 2020. Figure 2 shows the specific changes.

(2) Determine index weight. According to the formula (1) and formula (2) of the extreme value method, the original data is standardized,

Then, according to the calculation formula (3) and (4) of entropy method, the entropy value and weight of each index of agricultural economic system and rural ecological environment system are obtained. From the perspective of agricultural economic system, the proportion of primary industry in GDP and the weight of per capita agricultural output value are the highest, which are 0.0878 and 0.09, respectively. This shows that promoting the economic growth of the primary industry, increasing its proportion in the GNP, and taking various measures to promote the increase of farmers' per capita agricultural output value are conducive to improving the agricultural economic benefits.

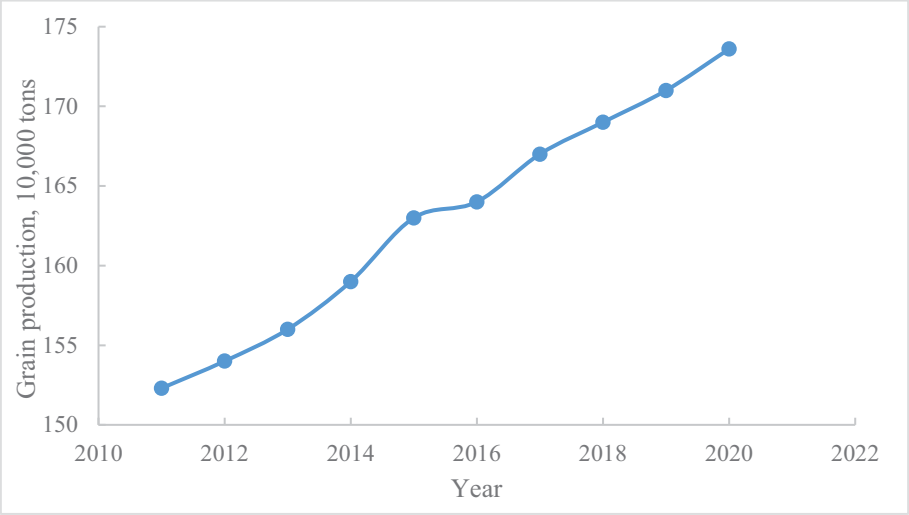


FIGURE 2
Changes of grain yield.

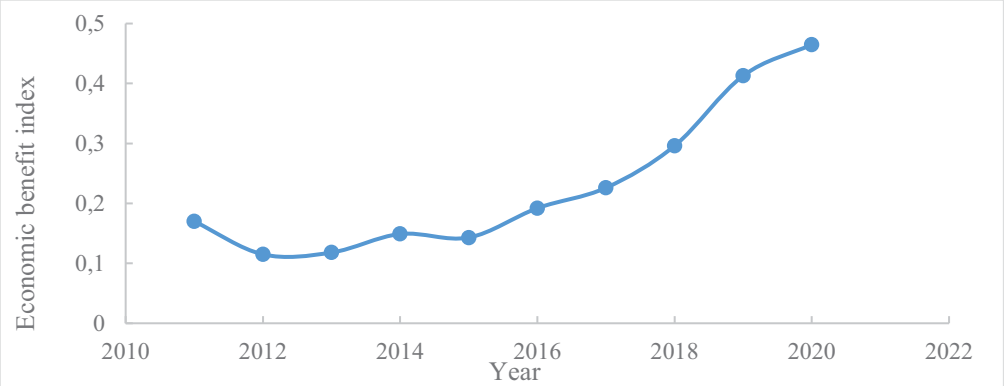


FIGURE 3
Trend of agricultural economic benefits.

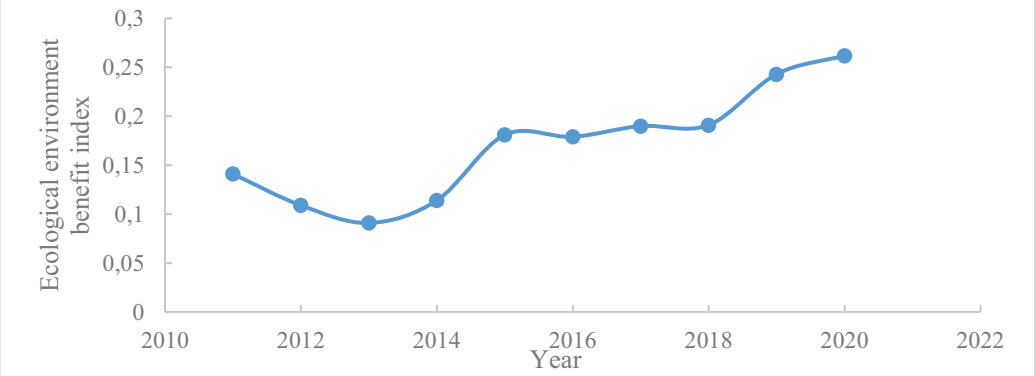


FIGURE 4
Trend of rural ecological environment benefit.

From the perspective of rural ecological environment system, the weight of the two indicators of per capita cultivated land area of the first industry employees in the agricultural production environment and the annual actual water supply of water conservancy projects in the ecological quality is the highest, which indicates that the quantity of cultivated land area and the water supply of water conservancy projects are the key factors to improve the rural ecological environment benefit. From the perspective of environmental pollution index, the weight value of chemical fertilizer application is greater than that of pesticide and agricultural film, which indicates that chemical fertilizer has the greatest impact on rural ecological environment among the three major pollutants of agricultural production in the target city in the study period.

(3) Analysis on the benefit of agricultural economy and rural ecological environment. Referring to the calculation formula of benefit index, the benefit analysis values of the city's agricultural economic system and rural ecological environment system are obtained. The results are shown in Figure 3 and Figure 4.

During the study period, the index of agricultural economy and rural eco-environmental benefits of the city shows a rising trend. From 2011 to 2015, the agricultural economy fluctuated greatly and declined overall, with a decrease of 0.027 and an average annual decrease of 0.0068 compared with 2011. From 2015 to 2020, the agricultural economy showed a good development trend, with the benefit index increasing year by year, with a total increase of 0.322 and an average annual increase of 0.054. The rural eco-environmental benefit index is in a fluctuating and slowly rising trend. From 2011 to 2013, the benefit index of rural ecological environment decreased by 0.05. From 2013 to 2015, the environmental benefit increased by 0.09. From 2015 to 2020, the overall benefit of ecological environment increased by 0.081, but there was a downward trend in some years, which was not stable.

Generally speaking, the benefit of rural ecological environment is lower than that of agricultural economy, and the benefit indexes of both are between 0-0.6, indicating that the overall benefit of both is low. In the process of rural development in the future, we should pay more attention to the protection of rural ecological environment and strive for the stable development of agricultural economy and rural ecological environment to present a high-level green coordinated development trend.

(4) Analysis on the coordinated development of agricultural economy and rural ecological environment. According to the above calculated benefit index of agricultural economic system and rural ecological environment system and referring to the calculation formula of coordination degree and coordinated development degree, the coordination degree and coordinated development degree between agricultural economy and rural ecological environment of the city are obtained. The results are shown in Figure 5 and Figure 6.

It can be seen from Figure 5 and Figure 6 that the coordination degree of agricultural economy and rural ecological environment presents a general trend of slight decline in fluctuation and then slow rise in fluctuation. From the perspective of coordination index, from 2011 to 2017, the state of the study period is relatively stable, and both are above 0.9, indicating that in this stage, the gap between the development speed of agricultural economy and rural ecological environment is small, showing a state of keeping pace with each other. The degree of coordination between 2017 and 2020 shows a downward trend, indicating that the gap between agricultural economy and rural ecological environment has expanded. In this period, the agricultural economic benefit index is higher than the rural ecological environment benefit index, which shows that with the rapid development of agricultural economy, the protection of rural ecological environment can not keep pace with it.

During the study period from 2011 to 2020, the coordinated development degree is on the rise, from 0.375 in 2011 to 0.575 in 2020. The coordination type between agricultural economy and rural ecological environment is changing from the mild imbalance in the early stage to the marginal imbalance in the later stage, which indicates that the coordinated development level of the two is evolving to a good trend. This benefits from the city's attention to rural ecological environment in recent years. In the coordination type, most years belong to the environmental lag type. Although the city's agricultural economy has developed rapidly, the rural ecological environment problems still need to be further solved. Therefore, it is urgent to take more effective measures to promote the coordinated development of agricultural economy and rural ecological environment in the city.

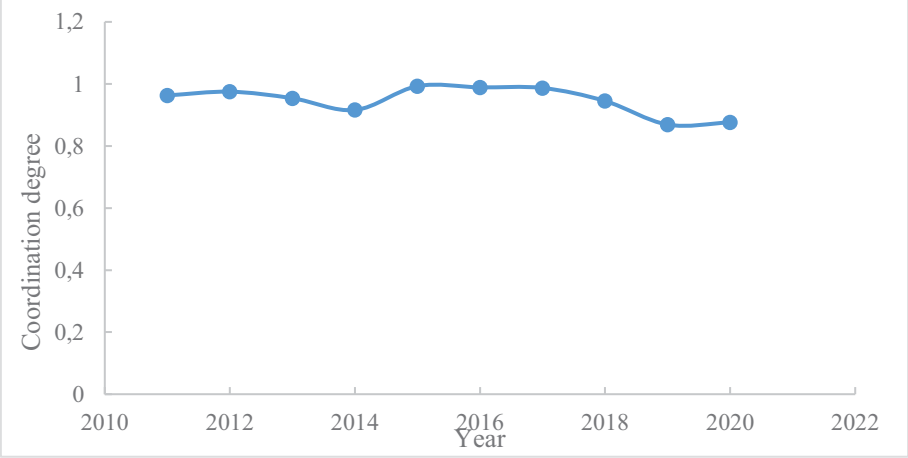


FIGURE 5
Trend of coordination degree of agricultural economy and ecological environment in the city.

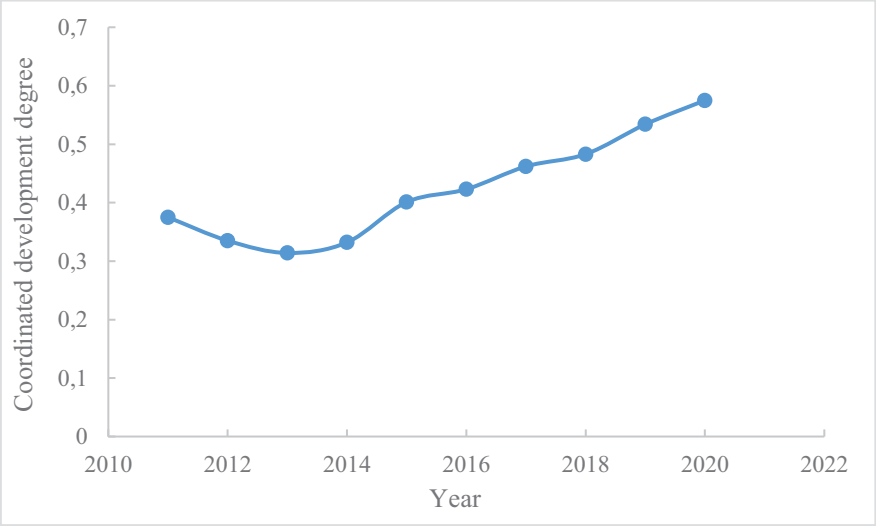


FIGURE 6
Trend chart of coordinated development degree of agricultural economy and ecological environment in the city.

CONCLUSIONS

(1) The interaction between agricultural economy and rural ecological environment can be divided into mutual competition and complementary. Under the mutual competition, the growth of agricultural economy is often achieved by sacrificing the rural ecological environment. Under the complementary relationship, the growth of agricultural economy promotes the construction and maintenance of the rural ecological environment.

(2) During the study period, under the cooperation between China and Africa, the comprehensive benefit index of agricultural economy and rural ecological environment of the city showed a common upward trend. From 2011 to 2020, the agricultural economic benefit index was higher than the rural ecological environment benefit index, and the rural ecological environment protection lagged behind the agricultural economic development. In the process of agricultural economic development, the prevention and control of rural ecological environment pollution and destruction can not be ignored. The degree of coordinated development between agricultural economy and rural ecological environment is gradually rising, and the type of coordinated development between the two is from mild imbalance in the early stage to barely coordinated in the later stage, which indicates that the level of coordinated development between the two is constantly evolving to a good trend.

(3) Sino African agricultural cooperation has made a lot of new progress with remarkable results. The cooperation of aid, trade and investment not only effectively shows the effect of China's agricultural technology on increasing the output and improving the quality of agricultural products, but also has a potential positive impact on Africa's politics, economy, and foreign relations.

ACKNOWLEDGEMENTS

This work was not supported by any funds. The authors would like to show sincere thanks to those techniques who have contributed to this research.

REFERENCES

[1] Parolo, G., Ferrarini, A., Rossi, G. (2009) Optimization of tourism impacts within protected areas by means of genetic algorithms. Ecological Modelling. 220(8), 1138-1147.
[2] Kacar, A., Kucuksezgin, F. (2014) Profiles of some beaches on coastal bathing waters of Turkey in the eastern Mediterranean. Fresen. Environ. Bull. 23(10), 2466-2473.
[3] Gu, W. (2012) Three essays on product design: incorporating capacity, remanufacturing, and environmental friendliness. Fresen. Environ. Bull. 21(9), 2656-2663.
[4] Tang, Z., Shi, C.B., Liu, Z. (2011) Sustainable development of tourism industry in China under the low-carbon economy. Energy Procedia. 5(1), 1303-1307.
[5] Porfiriev, B.N. (2019) The low-carbon development paradigm and climate change risk reduction strategy for the economy. Studies on Russian Economic Development. 30(2), 111-118.
[6] Li, D.X., Kang, T.W. (2012) Inspiration from green effect of south Korea's low-carbon economy development to China. Low Carbon Economy. 3(4), 154-159.
[7] Yang, C. (2006) Evolution analysis of coordinated development between economy and environment in Shenzhen. China Population Resources and Environment. 16(4), 84-89.

[8] Zheng, D., Zang, Z., Zhao, L., Sun, C. (2014) Analyzing the spatial-temporal correlation of the economic growth and resource-environment with the model of coordinated development degree. Journal of Glaciology & Geocryology. 36(3), 740-750.
[9] Wang, J., Xu, Z., Hu, X., Peng, X., Zhou, Y. (2010) Analysis of environmental efficiencies and their changes in china based on DEA theory. China Environmental Science. 30(4), 565-570.
[10] Tang, H., Yang, D., Qiao, X., Yang, L., Wang, G. (2009) Evaluation of coordination degree between regional development and eco-environment on the northern slope of the Tianshan Mountains. Progress in Geography. 28(5), 805-813.
[11] Nowak, P. (2009) The adoption of agricultural conservation technologies: Economic and diffusion explanations. Rural Sociology. 1307(4), 113-134.
[12] Armagan, G., Ozden, A. (2015) Food production and pesticide use: a dilemma in agriculture. Fresen. Environ. Bull. 24(12), 4364-4369.
[13] Ozden, A. (2016) Measurıng environmental efficiency in the EU agricultural sector "Considering Desirable and Undesirable Outputs". Fresen. Environ. Bull. 25(1), 240-248.
[14] Paping, R. (2004) Family strategies concerning migration and occupations of children in a market-oriented agricultural economy. History of the Family. 9(2), 159-191.
[15] Zhou, Z. (2004) China's experience with agricultural cooperatives in the era of economic reforms. China Agricultural Economic Review. 2(2), 238-257.
[16] Paulsen, A., Blase, M., Wagner, L., Matiashvili, V., Cherevko, G. (1995) Building agricultural economic teaching institutions in the newly independent states. American Journal of Agricultural Economics. 77(5), 1355-1356.
[17] Filloy, J., Grosso, S., Bellocq, M.I. (2015) Urbanization altered latitudinal patterns of bird diversity-environment relationships in the southern Neotropics. Urban Ecosystems. 18(3), 777-791.
[18] Maqbool, S., Zameer, M.N. (2018) Corporate social responsibility and financial performance: an empirical analysis of Indian banks. Future Business Journal. 4(1), 84-93.
[19] Chen, M., Lu, D., Zha, L. (2010) The comprehensive evaluation of China's urbanization and effects on resources and environment. Journal of Geographical Sciences. 20(1), 17-30.
[20] Kwon, Y.D., Yamauchi, H. (1993) Agricultural policy adjustments in the Korean rice economy. Agricultural Economics. 9(4), 335-346.

Received: **10.04.2021**
Accepted: **17.05.2021**

CORRESPONDING AUTHOR

Jie Wang
School of Economics,
Hunan Agricultural University,
Changsha Hunan 410000 – China

e-mail: wangj_0203@163.com

© by PSP Volume 30– No. 09/2021 pages 10941-10950 Fresenius Environmental Bulletin

ORGANIC AMENDMENTS AND NANO-MICRONUTRIENTS RESTORE SOIL PHYSICO-CHEMICAL PROPERTIES AND BOOST WHEAT YIELD UNDER SALINE ENVIRONMENT

Sobhy Sorour[1], Megahed Mohamed Amer[2], Dalia El Hag[1], Etab Ahmed Hasan[1], Mahrous Awad[3], Ferhat Kizilgeci[4], Ferhat Ozturk[5], Muhammad Aamir Iqbal[6], Ayman El-Sabagh[1,*]

[1]Agronomy Department, Faculty of Agriculture, Kafrelsheikh University, 33516 Kafrelsheikh, Egypt
[2]Soils, Water and Environment Research Institute, Agriculture Research Center, 33717 Kafr Elsheikh, Egypt
[3]Department of Soils and Water, Faculty of Agriculture, Al-Azhar University, Assiut 71524, Egypt
[4]Deparment of Plant and Animal Production, Kiziltepe Vocational School, Mardin Artuklu University, Turkey
[5]Department of Field Crops, Faculty of Agriculture, Sirnak University, Turkey
[6]Department of Agronomy, Faculty of Agriculture, University of Poonch, Rawalakot, AJK, Pakistan

ABSTRACT

Ensuring food security under climate change scenario requisites amending degraded soils and sustainably boost staple crops yield in a biologically viable way through effective plant nutrition management strategies. Two multi-year lysimeter experiments were conducted to investigate the impact of soil organic substances and foliar application of some nano-nutrients on soil properties and wheat yield under saline conditions. The experiment was executed in split plot with three replications. Treatments included organic amendments (molasses, compost tea, K-humate, molasses+ compost tea, molasses+K-humate, compost tea+ K-humate and molasses+K-humate+Compost tea and control) in main plots, while sub plots had nano-micronutrients (nano-selenium, nano-manganese and nano-silica) and a control treatment. The results showed that physio-chemical properties (bulk density, cation exchange capacity, electrical conductivity etc.) of the soil were significantly influenced by all organic amendments; however, co-application of molasses+K-humate+compost tea remained unmatched. The same treatment combination also remained effective in boosting nitrogen uptake and recovery along with wheat yield during both seasons. Among foliage applied nano micronutrients, silicon remained superior by recording the highest yield attributes and grain yield of wheat. Therefore, it is inferred that co-application of organic amendments and foliage applied nano-fertilization management could be developed as an effective approach to restore and conserve the soil and increase wheat productivity under saline environment of arid and semi-arid regions.

KEYWORDS:
Organic amendments, Compost tea, K-humate, Molases, Nano-Micronutrients

INTRODUCTION

The changing climate has multiplied the adverse effects of salinity which seriously deteriorate crops productivity and nutritional quality across the world [1, 2]. Salinity causes abrupt decline in the assimilation of essential nutrients which leads to specific ions toxicity and significant reduction in crops growth and yield [3, 4]. Wheat (*Triticum aestivum* L.) is one of the leading cereal crops in terms of area under cultivation, and deemed as strategic crop in Egypt [5]. However, there exists a wide gap regarding wheat consumption and production, which necessitates developing strategies to boost wheat yield on per unit area basis. Furthermore, fast growth of population and rapid urbanization have made it necessary to increase per acre yield of wheat and effective plant nutrition, and amending salt affected soil with organic substances can be used as a potential tools to achieve the goal of food and nutritional security [6,7,8]. Nanotechnology represents an opportunity to improve the use of mineral elements as a source of plant nutrients by utilizing nano-particles to fulfil plants nutrition needs.

Humic substances (HS) are the major components of soil organic matter and impart multiple benefits to the soil in terms of improved physico-chemical characteristics as well as higher microbial growth in the root zone of crop plants [9]. In addition, they enhanced macronutrients (N, P and K) uptake by improving soil bulk density, porosity, and lowering the pH of the soil [10]. It has been inferred earlier [11] that humic acid markedly increased the growth and nutritional parameters of wheat such as the plant height, spike length and 1000-grains weight along with grain and straw yields. It also effectively remained the nutritional quality of wheat grain especially protein content. Compost tea (CT) which is a compost extract brewed with a microbial food source like molasses, rock dust and humic-fulvic acids triggered the population growth of microbial community in the rhizosphere [12, 13]. It has been reported that

organic amendments such as compost tea, and molasses (sugarcane and sugar beet) contain organic acids, amino acids, humic and fulvic acids which have the potential role to boost the plant growth, nutrients uptake and wheat yield [14].

Micro-nutrients and trace elements applied as foliar sprays hold perspective for boosting wheat yield on saline soils, owing to rapid absorption of nutrients by plant leaves [15]. Selenium (Se) is trace element that modulates cellular metabolism, protects plants against oxidative damage and component of numerous vital enzymes [16]. Although abiotic stressed-plants tend to response to Se application, but dose optimization is needed keeping in view the close margin of safety for Se concentrations [17, 18]. In addition, silicon (Si) is the second most abundant trace element in the soil that has the potential influence to alleviate the adverse effects of abiotic stresses including salt, drought, chilling etc. in crop plants [19]. Nano-Si mediates the synthesis of protein, amino acids, nutrient uptake, and stimulates the antioxidant enzyme activity [20, 21]. The importance of nano-Si to improve plant growth by enhancing chlorophyll content, nitrogen uptake and nitrogen use efficiency of maize and faba bean has been previously reported [22]. However, research gaps exists regarding its effect on salt stressed-wheat crop, which necessitates conducting in-depth studies. In addition, manganese (Mn) is another trace nutrient that is involved in vital processes such as photosynthesis, respiration, and nitrogen (N) metabolism [23]. In addition to cellular-level roles, the agronomic benefits of Mn application have been demonstrated in maize, beans, soybean, wheat, and sugarcane [24, 25]. Foliar application of Mn nanoparticles enhanced the nitrogen metabolism [23] as well as increased grain yield by 22% in wheat [26].

The application of micro-nutrients in nano-formulations (1–100 nanometers in size) has recently emerged as effective exogenous source of plant nutrients [6, 27]. Considerable higher nutrient uptake by crop plants, greater nutrient use efficiency and negligible losses are few of the advantages offered by nano micronutrients over their bulky application [28-32]. Notably, nanoparticles are more reactive than their bulk-scale, and these materials may cause greater toxicity or beneficial effects on agricultural crops. Thus, with better understanding and management, the beneficial aspects of nano-enabled fertilizers can become a highly valued tool for addressing the problem of global food security [33].

It was hypothesized that solo or co-application of organic amendments can alleviate salt-affected soils along with exogenous application of nano micro-nutrients hold potential to boost growth and grain yield of wheat in saline soils. This work aimed to determine the effects of some humic substances and foliar spraying of nano-Se, -Mn, and -Si on physico-chemical properties of soil, nutrients uptake, nitrogen use efficiency as well as grain yield of wheat in salt affected soil.

MATERIALS AND METHODS

Experimental site. Two lysimeter (82 cm diameter x 110 cm depth) experiments were conducted at Sakha Agricultural Research Station Farm, Kafr El Sheikh, Egypt during two growing winter seasons to study the effect of soil organic amendments and foliar applied nano-nutrients on some soil properties, plant growth and yield of wheat. The experimental treatments of HS viz., i) T1: Check treatment, ii) T2: Molasses (M), iii) T3: Compost tea (CT), iv) T4: K-humate (KH), v) T5: M + CT, vi) T6: M + KH, vii) T7: CT + KH, viii) T8: M + CT + KH were arranged in main plots, and four nano-fertilizer treatments viz., i) N1: Check treatment, ii) N2: Nano-Selenium, iii) N3: Nano-Manganse, and iv) N4: Nano-Silica were placed in sub-plots in this study.

Molasses having pH 7.3 contained 48% sucrose, 14% water, 1% starch and polysaccharides, 3% dextrin and cellulose, 10% N content, 11% crude protein, 3.6% total potassium content, 0.6% calcium,0.11% magnesium, 1.4% sodium, 40µgkg-1 trace element, 2.5% glutamic acid, and some vitamins (as mg kg-1) including pyridoxine or B6 (5.0), thiamine or B1 (1.3), riboflavin or B2 (0.4). Some non-nitrogenous organic acids also are included in molasses such as lactic (1.3%), citric, glycolic, malic (0.8%), oxalic, succinic (0.2%), acetic (0.2%), propinic (0.2%), and putyric (0.2%). Compost tea manure of 20 was soaked into 200 liters of tap water with a dilution ratio 1:10 (w/v) in plastic tanks, and the mixture was turned daily and filtrated after 10 days. The chemical composition of compost extract of pH, EC (dSm-1), NO_3, NH_4, P, K, Ca, Mg, Na, Fe, Mn, and Zn were 8.11, 5.81, 67.0, 0.73, 21.0, 1.544, 463, 240, 58.0, 22.8, 1.18 and 0.93 mgl-1, respectively. The KH (pH 6.70) which have humic acid (75%), K_2O (10%), fluvic acid (4%) and iron (2 mg kg^{-1}). The used nano-Si, -Se and -Mn were provided by National Research Center (NRC), Egypt, and have characterized by specific surface area (300-330 m^2g^{-1}), pH (4.0-4.5), and mean diameter (10 nm).

Compost tea, K-humate and molasses were added at 400 $Lfed^{-1}$, 6 KgFed-1 and 30 $Lfed^{-1}$, respectively. All of the above substances were added equally with 1st irrigation and 2nd irrigation as a soil application, while nano-Si, nano-Se and nano-Mn were added as twice at 25 and 50 days after sowing (DAS) as a foliar application.

Wheat Experiment. In the winter seasons of 2017/18 and 2018/19, wheat seeds were sown in lines using flood irrigation method. The wheat plants were harvested at 135 days after planting during both seasons. All the agronomic practices were applied as per recommendations. Nitrogen (N) fertilizer was applied as urea (46.5% N) at rate of 75kg fed-1 in

two equal doses at 21 and 55 DAS with the first and second irrigation, respectively. The recommended dose of phosphorus as mono phosphate (15.5% P_2O_5) and potassium as potassium sulfate (48% K_2O), and fertilizers were applied to the wheat plants before planting (at final tillage) at rates of 15 KgP_2O_5 fed^{-1} and $30K_2O$ fed-1, respectively.

Data collection. Flag leaf area (cm^2) was measured using LAI 3000 meter and estimated at booting stage of wheat for each experimental. Total chlorophyll was measured at booting stage using spectrophotometer. Weight of 1000-grains, grain and straw yields were determined at harvesting stage for each experimental unit. Harvest index was calculated according to the following formulae [34]

Harvest index (%) = Grain yield/biological yield x 100

Plant analysis. Plant samples were taken at harvesting stage in each season, washed with distilled water. The plant samples were digested, and the digest was analyzed for measuring total N, P and K according the standard methods described by [35]. Apparent nitrogen recovery of fertilizer (%) was calculated according to the following equation [36]:

Nitrogen recovery (%) = (N-uptake from fertilizer-N-uptake from control)/ (N-applied from fertilizer)×100

Nitrogen use efficiency (NUE) was calculated as follows:

NUE (kg/kg N-applied) = Grain yield (kg fed-1) from fertilizer- grain yield from control/total N applied (kg fed-1)

Soil analysis. Soil samples were taken from each treatment from 0-20, 20-40 and 40-60 cm layers before experiment and after harvesting. Electrical conductivity (EC), soluble cations, and anions were determined in soil paste extract and cation exchange capacity (CEC), exchangeable sodium percentage (ESP) and organic matter (OM) content was determined using the Walkley and Black method according to [35]. Particle size distribution of soil was measured using pipette method according to [37]. Soil bulk density and total porosity were determined for each treatment according to [38]. Field capacity and permanent wilting point were calculated from soil moisture tension curve [39]. Some physical and chemical properties of the experimental soil are shown in Table 1 and Table 2.

Statistical analysis. The collected data were subjected to the statistical analysis, using the technique of analysis variance (ANOVA) in a split-split plot design according to [40]. The treatments means were compared by using the least significant differences (LSD) test employed at 5% probability level to determine the level of significance among the treatment means.

RESULTS AND DISCUSSION

Soil chemical properties. The effects of molasses, compost tea and K-humate on soil chemical properties are presented in Figure 1. The results revealed that the EC, ESP and CEC were significantly ($P \leq 0.05$) influenced by soil amendments applied individually or in combination with each other. It was observed that M+CT, and M+KH application significantly decreased the EC and ESP. The combined application of three organic materials (M+CT+KH) remained the most effective and superior treatment. These results may be attributed to decrease in the upward movement of saline water owing to co-application of organic amendments which delayed surface soil salinization. Similar results were observed by [10, 41]. The results indicated that the M, CT and KH remained effective in increasing CEC. Figure 1 pointed out that the CEC increased significantly ($P \leq 0.05$) with soil application of M, CT, KH, and their combination (M+CT+H) which recorded the highest values. This result was probably due to the effect of these organic materials on increasing the specific surface and thus increasing soil exchangeable capacity of the soil as reported by [42].

TABLE 1
Chemical characteristics of the experimental soil

Soil depth	pH	EC	ESP	CEC	OM	$CaCO_3$	N	P	K
(cm)		(dSm^{-1})	(%)	(mole kg^{-1})	(g kg^{-1})	(g kg^{-1})		mg kg^{-1}	
0-20	8.18	6.33	13.45	39.46	187	297	34	11.5	295
20-40	8.20	7.05	14.87	38.21	152	286	31	9.6	281
40-60	8.45	8.13	15.7	37.18	141	233	27	8.4	274
mean	-	7.17	14.70	38.28	160.0	270	30.7	9.8	283.3

TABLE 2
Physical characteristics of the experimental soil

Soil depth(cm)	Soil moisture characteristics					Particle size distribution (g/kg)			
	FC (%)	WP (%)	AW (%)	BD (kg m^{-3})	Total porosity,%	Sand	Silt	Clay	Soil texture
0-20	43.20	22.15	21.05	1.32	50.19	173.1	255.1	571.8	clay
20-40	40.60	20.46	20.14	1.35	49.06	188.5	247.6	563.9	clay
40-60	38.70	19.10	19.60	1.43	46.04	190.6	251.2	558.2	clay

pH: was determined in soil water suspension (1:2.5); EC: was determined in saturated soil paste extract; ESP: Exchangeable Sodium Percent; CEC: Cation Exchange Capacity. OM: Organic Matter. N, P and K: Available of nitrogen, phosphors and potassium. FC: Field Capacity; WP: Wilting Point; AW; Available Water; BD: Bulk Density

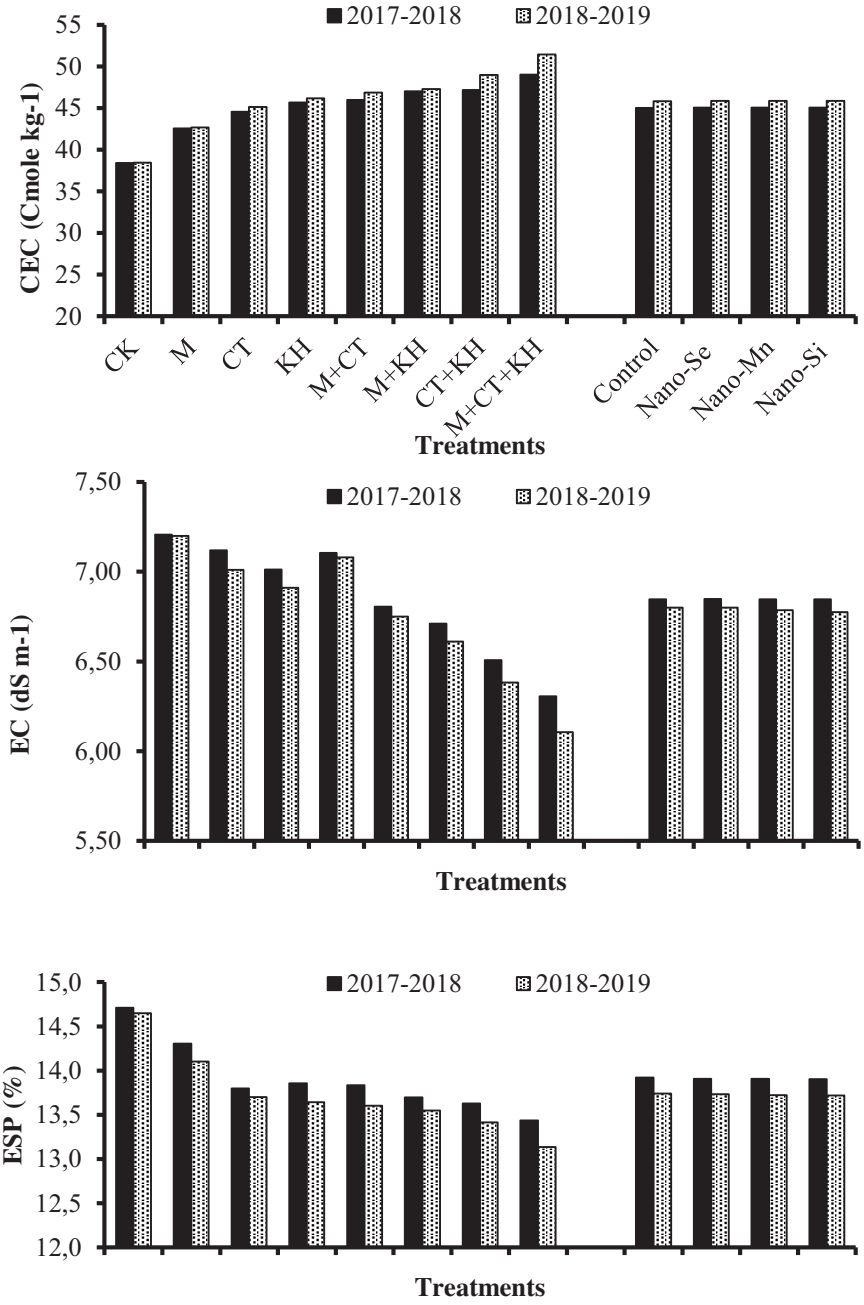


FIGURE 1
Electrical conductivity (EC), exchangeable sodium percentage (ESP), cation exchange capacity(CEC) as affected by organic amendments application after the growing seasons of 2017/18 and 2018/19.

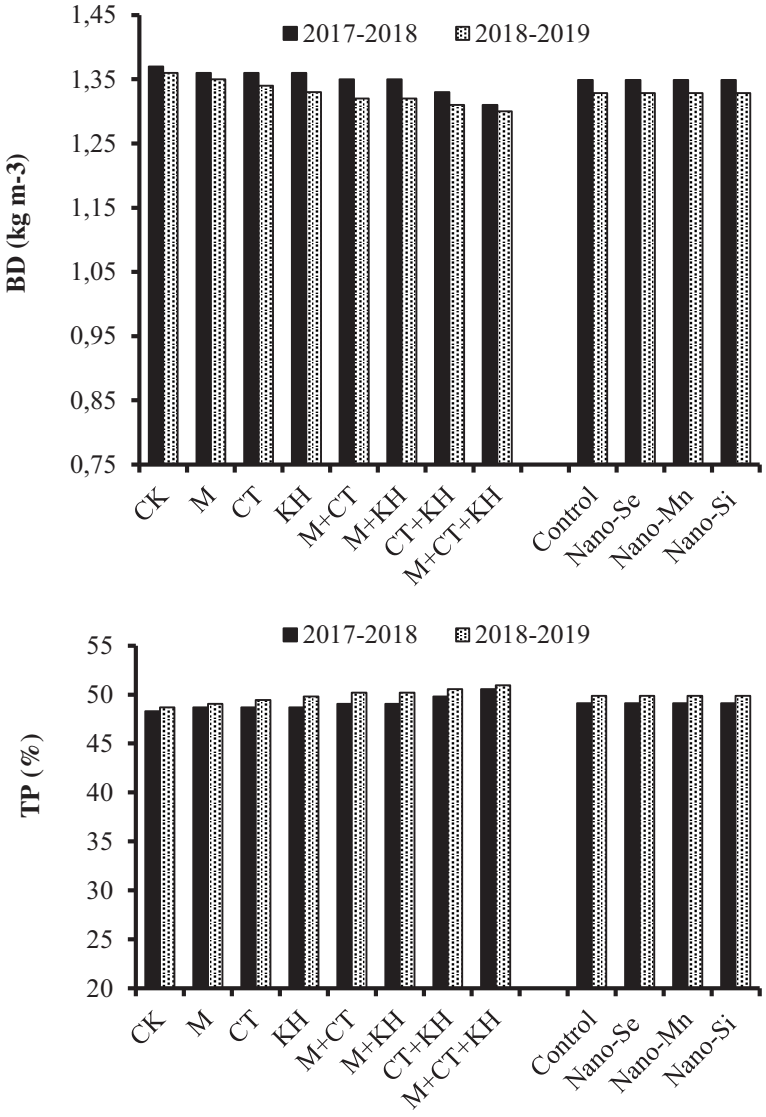


FIGURE 2
Bulk density (BD, a) and total porosity (TP, %) (b) as affected as affected by organic amendments application after the growing seasons of 2017/18 and 2018/19 .

Growth attributes. The data illustrated in Table 2 indicated that the leaf area index, flag leaf area (cm2) and chlorophyll content of wheat leaf were increased significantly ($p < 0.01$) by all organic amendments additions. The combined effect of M+CT+KH outperformed rest of treatments during both growing seasons. The foliar application of nano-Se, -Mn and -Si also significantly ($p < 0.01$) increased these parameters compared without application (control). The highest increment of the studied parameters was observed with foliar application of nano-Si treatments compared with other nano-Mn and -Se. The significant increment of leaf area index, flag leaf area (cm^2) and chlorophyll content may be due to an increase in the accumulation of nutrients, antioxidant enzymes activity by application of the nano-Si, thereby improving the tolerance of plants to abiotic stress. These results are supported by [21].

Yield of wheat. The soil applied organic amendments and foliage supplied nano-nutrients had significant effect on 1000-grains weight along with grain and straw yields of wheat (Table 3). The highest performing treatment was M+CT+KH while, the lowest values were obtained from the control treatment. Similar results were obtained by [11,14], who reported that combined application of organic manures was effective in boosting soil fertility and water holding capacity of the soil which led to higher nutrient use efficiency and grain yield. In addition, organic amendments were recorded to have abundant macro and micro nutrients [44, 45] which consequently triggered vegetative growth and robust yield attributes led to improve the yields of tomato and caraway. Regarding nano-nutrients, the highest values of 1000-grain weight, grain and straw yield of wheat were obtained by the foliar spraying of nano-

Si, while the lowest were observed in control treatment. These results are compatible with those observed by [11, 22]. The interaction effect between soil organic amendments treatment and foliar spraying of nano-micronutrients showed highly significant results for grain and straw yields of wheat during the two growing seasons, and the highest values were recorded with M + CT + combined with nano-Si application. These results were supported by [10]. The improvement in the grain and straw yield of wheat plants that were developed under saline stress conditions, partially due to the presence of an increment of photosynthetic pigments in the leaves, which can improve the photosynthetic capacity of the plants. These results are similar to those obtained by [31-33].

The harvest index of wheat was significantly increased due to the application of molasses, compost tea and potassium-humate and their combinations. The highest values were recorded by application of potassium-humate, while it remained unaffected by the nano-micronutrients application.

Uptake of some nutrients. The uptake of macro-nutrients (N, P and K) was significantly ($P \leq 0.05$) increased with soil applied organic amendments and foliar supplied nano-nutrients. The highest values were recorded with combined effect of M + CT + KH treatments in comparison to other treatments. These results are similar to those observed with [11, 14]. Addition of organic amendments plays an important role in soil ecosystem via increasing soil organic matter which provides substrates for decomposing microbes, improves soil structure consequently aeration system and water holding capacity thereby reflected on the plant growth [46]. Also [47] reported similar results for the effect of organic amendments on N, P, and K uptake by potato plants. Regarding nano-fertilizers spraying, nano-Si remained unmatched. Consequently, the N, P and K uptake by wheat plants as affected by the treatments can be arranged in the descending order M+CT+KH > CT+ KH > M +KH > M+CT > KH > CT > M >control. These results are supported by [22], who inferred that foliage application of micro and trace nutrients improved overall health of the crop plants and resultantly plants were able to extract higher quantities of nutrients from the soil solution.

The interaction between soil applied organic amendments and foliar spraying of nano-micronutrients recorded a significant increase in N uptake in both seasons, while P was significant in the 2nd season, and K was significant in the 1st season. Nonetheless, the highest N, P and K uptake by wheat plants were recorded due to the interaction effect between all organic materials together and nano-Si application (Table 4). Our results are in agreements with the findings of [31, 33, 48].

TABLE 3
1000-grain weight, grain yield, straw yield and harvest index as affected by organic amendments application after the tow growing seasons.

Application method	1000-grain weight		Grain yield		Straw yield		Harvest index	
	1st sea-	2nd sea-	1st sea-	2nd sea-	1st sea-	2nd sea-	1st sea-	2nd sea-
Soil application (SA):								
Control (C)	41.40 b	40.87 e	2.497 b	2.703 d	2.857 f	3.182 e	0.466 a	0.459ab
Molass (M)	41.92ab	41.16de	2.527 b	2.996 c	3.254 de	3.549 d	0.438 ab	0.458ab
Compost tea	42.31ab	41.47cd	2.543 b	3.026 bc	3.379 cd	3.840 c	0.430 bc	0.441abc
K-Humate	42.31ab	42.19 b	2.536 b	3.024 bc	3.178 e	3.513 d	0.444 ab	0.463a
M + CT	42.56 a	41.85bc	2.564 b	3.154 ab	3.499 bc	4.035 b	0.423 bc	0.439bc
M + KH	42.64 a	42.06 b	2.564 b	3.135abc	3.748 a	3.913 bc	0.407 c	0.445abc
CT + KH	42.74 a	42.29 b	2.576 b	3.164 ab	3.641 ab	4.048 b	0.415 bc	0.439bc
M + CT + KH	42.88 a	43.15 a	2.727 a	3.195 a	3.657 ab	4.226 a	0.427 bc	0.431c
F test	*	**	**	**	**	**	**	**
Foliar application (FA):								
Control (C)	42.13 a	41.34 b	2.529 b	2.937 c	3.307 b	3.575 c	0.434	0.451
Nano Se	42.30 a	42.27 a	2.558ab	3.032 b	3.425 ab	3.732 b	0.428	0.448
Nano Mn	42.43 a	41.42 b	2.579ab	3.086 b	3.363 b	3.868 ab	0.434	0.444
Nano Si	42.51 a	42.49 a	2.601 a	3.143 a	3.512 a	3.978 a	0.426	0.441
F test	*	**	**	**	**	**	NS	NS
Interaction SA*FA)	NS	NS	**	**	**	**	NS	NS

*, ** and NS indicate $p < 0.05$, < 0.01 and not significant, respectively. Means of each factor followed by the same letter are not significantly different at 5 % level according to Duncan's multiple range test

TABLE 4
Total nitrogen (N), phosphorus (P) and potassium (K) uptake as affectedby organic amendments application after the tow growing seasons.

Treatments	N uptake (kg/fed)		P uptake (kg/fed)		K uptake (kg/fed)	
	1st season	2nd season	1st season	2nd season	1st season	2nd season
Soil application (SA):						
Control	22.26 b	22.75 b	13.97 f	14.58 g	20.52 g	22.45 h
Molass (M)	26.58 ab	27.77 ab	15.39 e	17.36 f	23.57 f	26.45 g
Compost tea (CT)	26.73 ab	31.03 ab	16.06 d	18.66 e	25.03 d	28.97 e
K-Humate (KH)	27.61 ab	29.64 ab	15.78 de	19.17 d	24.34 e	27.57 f
M + CT	27.72 ab	31.87 ab	16.65 c	21.10 b	26.52 c	30.83 c
M + KH	29.03 a	31.42 ab	16.99 bc	20.53 c	27.44 b	29.70 d
C + KH	29.17 a	33.53 ab	17.23 b	20.98 b	27.15 b	31.47 b
M + CT + KH	29.96 a	37.90 a	19.01 a	22.94 a	29.30 a	33.77 a
F test	**	**	**	**	**	*
Foliar (FA):						
Control	26.87 b	27.20 c	15.33 c	17.61 c	23.51 c	26.22 c
Nano Se	26.92 b	32.17 a	16.26 b	19.57 b	26.20 ab	28.90 b
Nano Mn	27.39 b	30.82 b	16.64 b	19.73 b	25.65 b	29.87 a
Nano Si	28.36 a	32.78 a	17.31 a	20.75 a	26.58 a	30.61 a
F test	**	**	**	**	**	**
Interaction (SA x FA)	**	**	NS	**	**	NS

*, ** and NS indicate p < 0.05, < 0.01 and not significant, respectively. Means of each factor followed by the same letter are not significantly different at 5 % level according to Duncan's multiple range test.

TABLE 5
Nitrogen use efficiency (NUE) and recovery percentage (NRP) as affected by organic amendments application after the tow growing seasons.

Method	NUE (kg grain/kg N)		NR (%)	
	1st season	2nd season	1st season	2nd season
Soil application (SA):				
Control	5.37 c	7.94 b	13.49 b	15.39 d
Molass (M)	5.78 bc	10.17 ab	20.09 ab	19.87 cd
Compost tea (CT)	5.99 bc	9.74 ab	19.18 ab	24.50 bc
K-Humat (KH)	5.89 bc	10.54 a	19.24 ab	22.93 bc
M + CT	6.27 b	9.78 ab	20.49 ab	26.45 ab
M + KH	6.27 b	9.53 ab	21.68 a	25.58 bc
C + KH	6.42 b	10.75 a	21.87 a	26.72 ab
M+CT+KH	8.43 a	10.33 ab	24.88 a	31.70 a
F. test	**	*	**	*
Foliar application (FA):				
Control	5.80 b	9.81 ab	17.83 b	20.92 b
Nano Se	6.19 ab	10.24 a	20.12 a	24.21 ab
Nano Mn	6.47 a	10.13 a	20.46 a	24.21 ab
Nano Si	6.76 a	9.22 b	22.05 a	27.24 a
F. test	**	*	**	*
Interaction (SA x FA)	**	*	**	*

*, ** and NS indicate p < 0.05, < 0.01 and not significant, respectively. Means of each factor followed by the same letter are not significantly different at 5 % level according to Duncan's multiple range test.

Nitrogen use efficiency (NUE). The NUE of wheat was significantly increased with soil and foliar application of organic amendments and nano-nutrients (Table 5). The highest value of NUE (8.43kg grain /kg N) was given by the application of M+CT+KH during the first season, while the treatment C+KH remained outstanding result (10.75kg grain/kg N) for the second season. The foliar applied nano-Si remained superior (6.76 and 9.21kg grain /kg N) by giving the highest NUE during both seasons, respectively. The order of NUE of wheat due to soil application organic amendments were M+CT+KH > CT+KH > M+KH > M+CT > KH > CT > M > control. Data in Table 5 and Figure (2.a) showed that the interaction between soil application and foliar spraying of nano-micronutrients significantly increased the NUE of wheat in both seasons. However, the highest values of NUE of wheat were recorded with the interaction between M+CT+KH combined with nano-Mn application (Table 5).

Therefore, the response of NUE of wheat as affected by foliar spraying of nano-micronutrients could be ordered as Nano-Mn> Nano-Si > Nano-Se > control. This results may be attributed to the fact that the organic amendments has the ability to improve physio-chemical properties, including water holding properties, which may be retain the nutrient from leaching as long that is a source of nutrient supply which improves the nutrient use efficiency. These results are supported by [23, 49].

Recovery of nitrogen. The recovery of nitrogen (NR) by wheat was significantly increased with application of molasses, compost tea and potassium-humate and their combinations (Table 5). However, application of M+CT+KH recorded the highest values of NR (24.88 and 31.7% for 1st and 2nd season, respectively). It was also indicated that there was no significant difference between M+KH, C+KH and M+C+KH on NR. These results are supported [22]. The NR of wheat was increased significantly due to using nano-fertilizers in both seasons of the experiment. The highest values of NR of wheat (22.05 and 27.24%) were obtained by the foliar spraying of nano-Si for both two seasons, respectively, while the lowest values were obtained by control. Data in Table 5 and Figure (2.b) showed that the interaction between soil and foliar spraying of nano-micronutrients had a significant increase on NR of wheat in both seasons. While, the highest values of NR in wheat were recorded with the interaction effect between M+CT+KH combined with nano-Si application. The NR of wheat to foliar spraying of nano-micronutrients ordered as nano-Si >nano-Mn>nano-Se > control.

CONCLUSION

Our results were in line with the postulated hypothesis that organic amendments applied solely or in conjunction with each other, and exogenous application of nano micronutrients have the potential role to improve soil physico-chemical characteristics and boost wheat grain yield under saline environment. The results revealed that co-application of molasses+K-humate+compost tea outperformed other treatments in terms of improved bulk density, soil porosity, electrical conductivity, cation exchange capacity, N uptake and recovery, etc. Moreover, foliage applied silicon remained superior in terms of better yield attributes and grain yield of wheat grown on salt affected soil. However, further studies are needed to optimize dose of trace elements and these findings may serve as base line to evaluate the impact of other organic amendments and trace elements for alleviating the adverse effects of salinity on wheat crop under changing climate scenario for ensuring the nutritional security of rapidly increasing populace globally.

REFERENCES

[1] Yihdego, S.P.Y. (2017) Studies on nature and properties of salinity across globe with a view to its management - A review. Glob. J. Human-Social Sci. Res. 17(1), 31-37.

[2] El Sabagh, A., Hossain, A., Barutçular, C., Islam, M.S., Awan, S.I., Galal, A., Iqbal, M.A., Sytar, O., Yildirim, M., Meena, R.S., Fahad, S., Najeeb, U., Konuskan, O., Habib, R.A., Llanes, A., Hussain, S., Farooq, M., Hasanuzzaman, M., Abdelaal, K.H., Hafez, Y., Cig, F., Saneoka, H. (2019) Wheat (*Triticum aestivum* L.) production under drought and heat stress - adverse effects, mechanisms and mitigation: a review. App. Eco. Environ. Res. 17(3), 5571-5581.

[3] Kizilgeci, F., Ebrahim Pour Mokhtari, N., Hossain, A. (2020) Growth and physiological traits of five bread wheat (*Triticum aestivum* L.) genotypes are influenced by different levels of salinity and drought stress. Fresen. Environ. Bull. 29(9A), 8592-8599.

[4] Iqbal, M.A., Junaid, R., Wajid, N., Sabry, H., Yassir, K., Ayman, S. (2021) Rainfed winter wheat (*Triticum aestivum* L.) cultivars respond differently to integrated fertilization in Pakistan. Fresen. Environ. Bull. 30(4), 3115-3121.

[5] Karrou, M., Oweis, T., Abou El-Enein, R., Sherif, M. (2012) Yield and water productivity of maize and wheat under de0xFB01cit and raised bed irrigation practices in Egypt. Afr. J. Agric. Res. 7, 1755-1760.

[6] Iqbal, M.A. (2021) Nano-fertilizers for sustainable crop production under changing climate: a global perspective. In: Crop Production. Intechopen Ltd. United Kingdom. Retrieved on March 17.
[7] Siddiqui, M.H., Iqbal, M.A., Wajid, N., Imtiaz, H., Khaliq, A. (2019) Bio-economic viability of rainfed wheat (Triticumaestivum L.) cultivars under integrated fertilization regimes in Pakistan. Custos e Agronegocio. 15(3), 81-96.
[8] Kizilgeci, F., Yildirim, M., Islam, M.S., Ratnasekera, D., Iqbal, M.A., Sabagh, A.E. (2021). Normalized difference vegetation index and chlorophyll content for precision nitrogen management in durum wheat cultivars under semi-arid conditions. Sustainability. 13, 3725.
[9] Lobartin, J.C., Orioli, G.A., Tan, K.H. (1997) Characteristies of soil humic acid fractions separated by ultrafiltration //Communications in Soil Sci. Plant Analysis. 28, 787-796.
[10] Amer, M.M., El-Ramady, H. (2015) Alleviation soil salinity and sodicity hazard using some biochemical amendments for production of canola (*Brassica napus* L.) In north delta region. J. Soil Sci. Agric. Eng. Mansoura Univ. 6, 514-534.
[11] Antoun-Landa, W., Zakaria-Sahar, M., Rafla-Hanaa, H. (2010) Influence of compost, N-mineral and humic acid on yield and chemical composition of wheat plants. J. Soil Sci. Agric. Eng. Mansoura Univ. 1, 1131-1143.
[12] Meshref, H.A., Rabie, M.H., El-Ghamry, A.M., El-Agamy, M.A. (2010) Maximizing utilization of compost addition using foliar compost extract and humic substances in alluvial soil. J. Soil Sci. Agric. Eng. Mansoura. Univ. 1, 957-971.
[13] Shaban, K.A., Abd El-Kader-Mona, G., Khalil-Zeinab, M. (2012) Effect of soil amendments on soil fertility and sesame crop productivity under newly reclaimed soil conditions. J. Appl. Sci. Res. 8, 1568-1575.
[14] Amer, M.M. (2016) Effect of biochar, compost tea and magnetic iron application on some soil properties and productivity of some field crops under saline soils conditions at North Nile Delta. Egypt. J. Soil Sci. 56, 169-186.
[15] Faisal, M., Iqbal, M.A., Serap K.A., Abdul H., Nasir, R., Ayman, S., Abdul, K., Muzammil, H.S. (2020) Exogenously foliage applied micronutrients efficacious impact on achene yield of sunflower under temperate conditions. Pak. J. Bot. 52, 1215-1221.
[16] Reilly, C. (2006) Selenium in food and health. http://www.springer.com./978-0-387-33243-7
[17] Kabata-Pendias, A., Pendias, H. (2011) Trace Elements in Soils and Plants. 4th Edition, CRC Press, Boca Raton.
[18] Zahedi, H., Rad, A.H.S., Moghadam, H.R.T. (2011) Effects of zeolite and selenium applications on some agronomic traits of three canola cultivars under drought stress. Pesq. Agropec. Trop., Goiânia. 41, 179-185.
[19] Liang, Y., Sun, W., Zhu, Y.G., Christie, P. (2007) Mechanisms of silicon mediated alleviation of abiotic stresses in higher plants: A review. Environ. Pol. 147, 422-428.
[20] Li, B., Tao, G., Xie, Y., Cai, X. (2012) Physiological effects under the condition of spraying nano-SiO2 on to the Indocalamus barbatus McClure leaves. J. Nanjing Forest Uni. (Natural Sciences Edition). 4, 161-164.
[21] Siddiqui, M.H., AL-Whaibi, M.H., Faisal, M., Al Sahli, A.A. (2014) Nano-Silicon Dioxide Mitigates The Adverse Effects Of Salt Stress on *Cucurbita pepo* L. Environmental Toxicology and Chemistry. 33(11), 2429–2437.
[22] Amer, M.M., El- Emary, F. (2018) Impact of Foliar with Nano-silica in Mitigation of Salt Stress on Some Soil Properties, Crop-Water Productivity and Anatomical Structure of Maize and Faba Bean. Environ. Biodiv. Soil Security. 2, 25-38.
[23] Pradhan, S., Patra, P., Mitra, S., Dey, K.K., Jain, S., Sarkar, S., Roy, S., Palit, P., Goswami, A. (2014) Manganese nanoparticles: Impact on non-nodulated plant as a potent enhancer in nitrogen metabolism and toxicity study both in vivo and in vitro. J. Agric. Food Chem. 62, 8777-8785.
[24] Fageria, N.K. (2001) Adequate and toxic levels of copper and manganese in upland rice, common bean, corn, soybean, and wheat grown on an oxisol. Com. Soil Sci. Plant Anal. 32, 1659-1676.
[25] Dimkpa, C.O., Bindraban, P.S. (2016) Micronutrients fortification for efficient agronomic production. Agron. Sustain. Dev. 36, 1–26.
[26] Christian, O., Dimkpa, I.D., Singh, U., Adisa, I.O., Bindraban,P.S., Elmer, W.H., Gardea-Torresdey, J.L., White, J.C. (2018) Effects of manganese nanoparticle exposure on nutrient acquisition in wheat (*Triticum aestivum* L.). Agron. 8, 158.
[27] Sharifi, R.S., Razieh, K., Alireza, P., Sumera, A. (2020) Effects of biofertilizers and nano zinc-iron oxide on yield and physicochemical properties of wheat under water deficit conditions. Com. Soil Sci. Plant Anal. 51, 2511-2524.
[28] Rengel, Z. (2015) Availability of Mn, Zn and Fe in the rhizosphere. J. Soil Sci. Plant Nutr. 15, 397–409.
[29] Reddy, P.V.L., Hernandez-Viezcas, J.A., Peralta-Videa, J.R., Gardea-Torresdey, J.L. (2016) Lessons learned: Are engineered nanomaterials toxic to terrestrial plants? Sci. Total Environ. 568, 470–479.

[30] Du, W., Tan, W., Peralta-Videa, J.R., Gardea-Torresdey, J.L., Ji, R., Yin, Y., Guo, H. (2017) Interaction of metal oxide nanoparticles with higher terrestrial plants: Physiological and biochemical aspects. Plant Physiol. Biochem. 110, 210–225.
[31] Tolaymat, A., Genaidy, A., Abdelraheem, W., Dionysiou, D., Andersen, C. (2017) The effects of metallic engineered nanoparticles upon plant systems: An analytic examination of scientific evidence. Sci. Total Environ. 579, 93–106.
[32] Dimkpa, C.O., Bindraban, P. (2018) Nanofertilizers: New products for the industry? J. Agric. Food Chem. 66, 6462–6473.
[33] Raliya, R., Saharan, V., Dimkpa, C., Biswas, P. (2018) Nanofertilizer for precision and sustainable agriculture: Current state and future perspectives. J. Agric. Food Chem. 66, 6487–6503.
[34] Condon, A.G., Richards, R.A., Rebetzke, G.J., Farquhar, G.D. (2002) Improving intrinsic water-use efficiency and crop yield. Crop Science. 42, 122-131.
[35] Page, A.L., Miller, R.H., Keeny, D.R. (1982) Methods of Soil Analysis II. Chemical and Microbiological Properties. Soil Sci. Soc. Amer. Madison, Wisconsin.
[36] Crasswell. E.T., Godwin, D.C. (1984) The efficiency of nitrogen fertilizers applied to cereals in different climates. Adv. Plant Nutrition. 1, 1-55.
[37] Gee, G.W., Bauder, J.W. (1986) Particle-size Analysis. In Page, A.L. (ed.). Methods of soil analysis, Part 1, physical and mineralogical methods. 383-411.
[38] Klute, A. (1986) of Soil Analysis, Part 1, Physical and Mineralogical properties, Amer., Society, Agronomy, Monograph 9, 2nd ed. Madison, Wisc., USA.
[39] Black, C.A. (1965) Methods of soil analysis. Amer. Soc.Agro. Inc., Madison, Wisconsin, U.S.A. 117-174.
[40] Gomez, K.A., Gomez, A.A. (1984) Statistical procedures for agricultural research. John Wiley & Sons. Inc., Canada. 139-141.
[41] Awad, M., Moustafa-Farag, M., Wei, L., Huang, Q., Liu, Z. (2020) Effect of garden waste biochar on the bioavailability of heavy metals and growth of *Brassica juncea* (L.) in a multi-contaminated soil. Arab. J. Geosci. 13, 439.
[42] Amer, M.M., Gazia, E.A.E., Aboelsoud, H.M., Rashed, S.H. (2020) Management of irrigation water and organic matter application contribution in improving some soil properties and yields – water productivity of sugar beet and cotton in salt affected soil. Environ. Biodiv. Soil Security. 4, 7-18.
[43] Amer, M.M., Aiad, M., Rashed, S.H., El-Ramady, H. (2019) Sustainable Irrigation and Fertilization Management of Successive Cultivated Sugar Beet and Cotton under Salt-affected Soil Conditions Environ. Biodiv. Soil Security. 3, 227–239.
[44] Awad, M. (2016) Poultry manure and humic acid foliar applications impact on caraway plants grown on a clay loam. J. Soil Sci. Agric. Eng. 7, 1-9.
[45] Awad, M. (2001) Effect of Some Organic Compounds on Soil Properties and Plant Growth. Master's Thesis, Menoufia University, Al Minufya, Egypt.
[46] Rekaby, S.A., Awad, M.Y., Hegab, S.A., Eissa, M.A. (2020) Effect of some organic amendments on barley plants under saline condition. J. Plant Nutr. 43, 1840-1851.
[47] Ali, A.M., Awad, M.Y., Hegab, S.A., Gawad, A.M.A.E., Eissa, M.A. (2021) Effect of potassium solubilizing bacteria (*Bacillus cereus*) on growth and yield of potato. J. Plant Nutr. 44, 411-420.
[48] Dimkpa, C.O., Singh, U., Adisa, I.O., Bindraban, P.S., Wade, H.E., Jorge, L.G., Jason, C.W. (2018) Effects of Manganese Nanoparticle Exposure on Nutrient Acquisition in Wheat (*Triticum aestivum* L.). Agron. 8, 158.
[49] Rekaby, S., Awad, M., Hegab, S., Eissa, M.A. (2019) Effect of biochar application on barley plants grown on calcareous sandy soils irrigated by saline water. Sci. J. Agric. Sci. 1, 52-61.6.

Received: **11.04.2021**
Accepted: **17.05.2021**

CORRESPONDING AUTHOR

Ayman El-Sabagh
Agronomy Department,
Faculty of Agriculture,
Kafrelsheikh University,
33516 Kafrelsheikh, Egypt

e-mail: ayman.elsabagh@agr.kfs.edu.eg

© by PSP Volume 30– No. 09/2021 pages 10951-10960 Fresenius Environmental Bulletin

ECO-PHYSIOLOGICAL RESPONSE OF SELECTED FARM TREE SPECIES UNDER SALINE FIELD CONDITIONS AFTER TREATING WITH ORGANIC AMENDMENTS DURING NURSERY STAGE

Muhammad Talha Bin Yousaf[1], Muhammad Farrakh Nawaz[1,*], Sadaf Gul[2], Irfan Ahmed[1], Muhammad Rizwan[3], Ghulam Yasin[4], Taimoor Hassan Farooq[5]

[1]Department of Forestry and Range Management, University of Agriculture, Faisalabad, Pakistan
[2]Department of Botany, University of Karachi, Pakistan
[3]Department of Environmental Sciences and Engineering, Government College University, Faisalabad, Pakistan
[4]Department of Forestry, Range Management and Wildlife Management, The Islamia University of Bahawalpur, Pakistan
[5]College of Life Science, Central South University of Forestry and Technology, Hunan, China

ABSTRACT

Salinity is a global issue and afforestation of degraded soils is the most sustainable approach to combat salt toxicity but trees have to suffer during their early growth in these soils. Under local set of climatic conditions, organic soil amendments are reported to enhance the yield of cultivated crops but their effects and efficiency on trees during their establishment in saline soils is not reported yet. This study was designed to check the transferability of the effect of different organic amendments on tree establishment in salt affected soils. In the present study, various organic amendments applied at early growth stages, to assess the survival rate, morphological and physiological attributes of three selected agroforestry species: *Eucalyptus camaldulensis* Dehnh., *Vachellia nilotica* (L.) P.J.H.Hurter & Mabb. and *Dalbergia sissoo* Roxb., in saline field conditions. Six different types of organic amendments: farmyard manure (FYM), poultry manure (PM), slurry (SL), sugarcane bagasse biochar (SCB), woodchips biochar (WCB) and farmyard manure biochar (FYMB), were applied to check the response of selected tree species against salinity in field conditions. Survival rate was observed in the order of *E. camaldulensis* > *V. nilotica* > *D. sissoo* against all applied organic amendments. Maximum height increment was observed for FYMB in all tree species under saline conditions: 46.22 cm (*E. camaldulensis*), 18.63 cm (*V. nilotica*), 8.50 cm (*D. sissoo*) as compared to other treatments. Photosynthetic and transpiration rates were greater for FYM and were maximum in *E. camaldulensis* and minimum in *D. sissoo*, whereas, chlorophyll contents and stomatal conductance were higher for FYMB in *E. camaldulensis* as compared to other species and treatments. Higher amounts (mg g-1) of leaf Na+ and K+ were observed for control (6- 8.6) and FYMB (6.3-8.06), respectively as compared to other treatments. All types of biochar treatments showed more promising results and can be recommended for future afforestation programs.

KEYWORDS:
Agroforestry, Salinity, Biochar, Degraded Lands, Afforestation

INTRODUCTION

Salinity is a worldwide problem. It is reported that almost 75 countries of world are affected by salt toxicity in which 397 M ha are saline soils and 434 M ha are sodic [1]. In few countries, salt-induced land degradation accounts for more than 50% of the cultivated land [2]. Growth and biomass production of plants is badly affected in degraded lands which results in increasing the issue of food security for ever growing human population [3–5]. Among other approaches, afforestation of [6] salt affected soils is the most cost-effective, sustainable and efficient approach to reclaim these degraded lands [7].

Trees face lot of problems to establish in saline sodic soils at early growth stages [8]. At early-growth stages, salt-induced toxicity reduces the survival rate and growth rate of trees [9,10]. At early growth stages trees face nutrient toxicity, nutrient deficiency, high pH, reduced redox potential, increased osmotic stress and poor root zone aeration due to salinity [11–14]. Salinity results in damaged and poor root growth, reduced shoot growth, necrosis and even the death of the plant [15–18]. Though growing multipurpose trees species on salt affected soils result in reduced tree growth but, meanwhile, they have countless benefits [6]. Trees improve physical, chemical and biological properties of degraded lands [7,19,20]. Trees facilitate leaching of salts by improving water permeability [8], reduce electrical conductivity (EC), pH and exchangeable sodium percentage, and improve water holding capacity, hydraulic conductivity and cation exchange capacity (CEC) [21,22]. Trees enhance organic matter contents and recycling of important nutrients in soil [23,24].

Green manures, farmyard and poultry manures,

compost food processing wastes, cover crops and biochar are some of the examples of organic amendments which are very helpful in reclaiming the degraded soils including saline soils [25–30]. Organic amendments have several benefits to improve the quality of soil like increase in water holding capacity, soil fertility, organic carbon and cation exchange capacity (CEC) [21,31], decrease electrical conductivity (EC) [28,32], maintain structural stability of soil [33], reduce soil compaction [34] enhance enzymatic activities [35,36]. Environmental quality and sustainable production of land are directly related to good soil structure [37].

In literature, a detailed meta-analysis showed that plants have to face different climatic conditions like temperature and intensity of light under field conditions as compared to controlled conditions of glasshouse and growth chamber conditions of laboratory. So plant's response can be varied in field conditions from lab experiments [38].

Under controlled conditions, a lot of research work has been performed to check the effect of various organic amendments on the growth of different crops and trees in saline soils [39–43]. But, there is a gap of knowledge to check that whether the effects of organic amendments at early growth stages are transferable to field conditions. So, this study was designed to check eco-physiological response of selected farm tree species (*Eucalyptus camaldulensis* Dehnh., *Vachellia nilotica* (L.) P.J.H.Hurter & Mabb. and *Dalbergia sissoo* Roxb) under saline field conditions after treating with organic amendments (Farmyard manure, Poultry manure, Slurry, Sugarcane bagasse biochar, Woodchips biochar and Farmyard manure biochar) during nursery stage.

MATERIALS AND METHODS

Study location and experiment technique. This experiment was divided in two phases. In the first phase, plants were grown in pots in the experimental area of the Department of Forestry and Range Management (FRM), University of Agriculture Faisalabad (UAF) located at 31o 25'57" N, 73o 04' 21" E during the period of 2017-2018. After 4 months, these plants were transferred to field. Field experiment was conducted in the salt affected field of village of 467 G. B. in the suburbs of Tehsil Samundri (31° 4' 0" N, 72° 58' 0" E), district Faisalabad, Punjab, Pakistan. The field with poor fertility status and high EC was selected for this study. The other major attribute for selecting particular field was that it was accessible for planting of trees for field experiment. During the first phase, the soil was collected and transported from the same filed. Location of study sites are shown in Figure 1.

Soil and organic amendments preparation. Prior to experiment, soil was air dried and grounded with the help of wooden roller. After that it was passed through 2 mm sieve and prepared for further use and analysis. Different physicochemical characteristics of soil were determined according to the procedures described by the [44]. Initial physicochemical characteristics of soil are given in Table 1. Farmyard manure in the form of dung cakes, poultry manure, slurry and sugarcane bagasse were collected from farm area of Agronomy department of UAF and woodchips were collected from FRM, UAF. Farmyard manure biochar (FYMB), Sugarcane bagasse biochar (SCB) and woodchips biochar (WCB) were prepared under slow pyrolysis at 450˚C for the period of 3 hours in the Agro-climatology lab of UAF. All amendments were air dried (kept under shady place for one month), ground with Willy mill fitted with stainless steel blades, subjected to physicchemical analysis and stored in plastic containers until used in experiments.

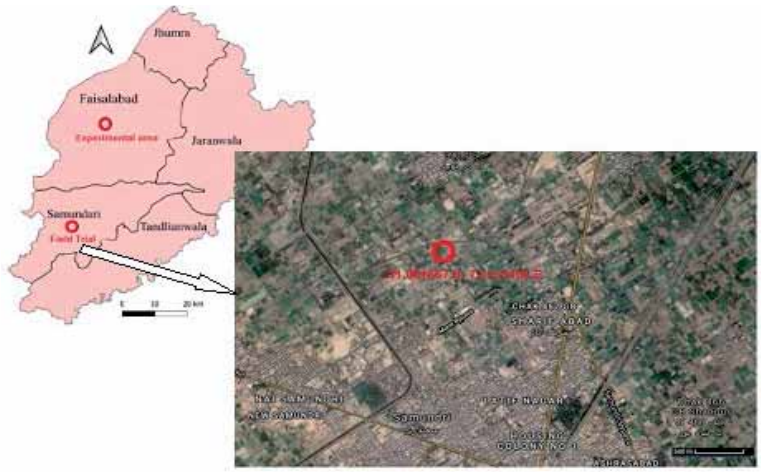


FIGURE 1
Study sites locations of experimental area and field trial in the District Faisalabad, Pakistan.

TABLE 1
Initial Physicochemical properties of soil and amendments used for the experiment

Parameters	Soil	FYM	PM	SL	FYMB	SCB	WCB
pH	8.5 ± 0.3	5.8± 0.2	6.3± 0.3	6.0± 0.3	7.0 ± 0.2	6.7 ± 0.2	6.8 ± 0.2
EC (dS/m)	20.5 ± 9	6.55± 2.5	7.31± 3.2	6.82± 3.8	2.08 ± 0.03	2.15 ± 0.02	2.10 ± 0.02
TSS(mg/kg)	205 ± 20	65± 5.8	73.1± 10.2	68.2±8.4	20.8 ± 1.8	21.5 ± 2.2	21 ± 2.3
CO_3^{2-}(mg/kg)	10 ± 2	(-)	(-)	(-)	(-)	(-)	(-)
HCO_3^- (mg/kg)	30 ± 4	10± 3.2	6± 3.8	12± 4.5	8 ± 1.5	10 ± 1.8	11 ± 2.1
Cl^- (mg/kg)	140 ± 19	8.0± 2.2	5± 3.2	5± 3.2	4 ± 0.8	6 ± 1.2	6.5 ± 1.3
$Ca^{2+} + Mg^{2+}$ (mg/kg)	12 ± 4.5	7.3± 4.2	6.3± 3.1	6.9± 2.5	13.2 ± 4.0	12.2 ± 3.6	12.5 ± 3.8
Na^+ (mg/kg)	160 ± 15.2	11.6± 1.8	15.2± 3.4	13.4± 2.5	3.4 ± 0.9	4.1 ± 1.2	4.0 ± 1.1
K^+(mg/kg)	47± 7	9.2± 2.7	8.8± 2.5	8.9± 2.9	7.2 ± 2.5	7.1 ± 2.8	7.4 ± 2.9
OM (%)	0.64 ± 0.03	60.8± 2.4	67.2± 5.5	65.4± 4.3	70.2 ± 0.12	73.1 ± 0.13	74.5 ± 0.09

Planting Material. Three agroforestry trees species: *E. camaldulensis*, *V. nilotica* and *D. sissoo* were selected for this study due to their salt tolerance potential and preference by farmers. Uniform sized seedlings of these species were collected from the nursery of Department of FRM. Due consideration was given to fact that seedlings should be healthy and free of disease. Pots were filled with the soil collected from field. After 4 months plants were transferred to field check their survival percentage and effect of organic amendments on morpho-physiological parameters of selected species. There were seven treatments for this experiment: T1 (Control), T2 (FYM), T3 (PM), T4 (SL), T5 (SCB), T6 (WCB) and T7 (FYMB).

At the time of transferring to the field, collar diameter (mm) and shoot length of the three selected species were measured with the help of digital vernier caliper and measuring tape. And then after six months these parameters were again measured. Photosynthetic rate (μ mol of CO_2 m^{-2} s^{-1}), transpiration rate (m mol O_2 m^{-2} s^{-1}), stomatal conductance (m mol H_2O m^{-2} s^{-1}) and sub-stomatal CO_2 concentration (μ mol of CO_2 mol^{-1} air) were measured using LCA-4 ADC portable infrared gas analyzer (Analytical Development Company, Hoddesdon, England) according to the procedures described earlier [30]

Ionic contents. The leaves of plants were collected and oven dried at 75○C till constant weight. Leaves were subjected to digestion according to the procedures described earlier [30]. After digestion, the mixture was cooled to room temperature and diluted to 25 mL with distilled water and stored in an air-tight bottle for ionic analysis. The ionic concentration for Na+ and K+ in plant samples was determined by Jenway PFP-7 flame photometer with the help of self-prepared standard solutions using reagent grade salt of NaCl and KCl, respectively.

Statistical Analysis. The data was analyzed by using factorial under CRD using computer based software Statistix 8.1. Tukey HSD was applied to differentiate the significant differences between treatments.

RESULTS

Survival rate and height of selected species. Results of the current study showed that after shifting of plants from nursery to field to conditions, some plants could not survive and survival rate of tree species (*E. camaldulensis*, *V. nilotica* and *D. sissoo*) against 7 different treatments T1 (Control), T2 (FYM), T3 (PM), T4 (SL), T5 (SCB), T6 (WCB), T7 (FYMB) is shown in Table 2. All plants were not able to tolerate the severe conditions of field. Survival of plants was different according to species and applied organic amendments. Maximum number of plants of *E. camaldulensis* survived, whereas, minimum plants of *D. sissoo* could survive. Treatment effect was also different for different species. Table 3 gives the information about the difference in height of selected plants species against seven different treatments. Although maximum shoot length was observed against T2 (FYM) treatment but maximum increment in shoot length was observed in the plants treated with biochar. Amongst biochars, T7 (FYMB) showed the best results. T5 (SCB) and T6 (WCB) also showed better results as compared to unprocessed organic amendments.

Shoot length and Diameter. Figure 2 depicts the results of morphological parameters of selected species against seven different treatments. Results of the current study revealed that when plants were transplanted from nursery to field maximum shoot length (186.4 cm) was found in the plants *E. camaldulensis* against T2 (FYM) whereas minimum shoot length (50.6 cm) was found in the plants of T1 of *D.*

TABLE 2
Survival percentage of selected agroforestry species under different treatments

Treatments	Survival (%)		
	E. camaldulensis	*V. nilotica*	*D. sissoo*
T1 (Control)	88.89	77.78	55.56
T2 (FYM)	100	88.89	66.67
T3 (PM)	88.89	77.78	66.67
T4 (SL)	88.89	77.78	55.56
T5 (SCB)	100	88.89	77.78
T6 (WCB)	100	100	66.67
T7 (FYMB)	100	100	77.78

TABLE 3
Difference in height of selected agroforestry species under different treatments

Treatments	Difference in Height (cm)		
	E. camaldulensis	*V. nilotica*	*D. sissoo*
T1 (Control)	11.00 ± 4.2	5.14 ± 2.2	1.71 ± 0.9
T2 (FYM)	16.40 ± 3.5	11.94 ± 4.4	3.40 ± 1.2
T3 (PM)	12.64 ± 2.3	10.68 ± 3.7	2.91 ± 1.1
T4 (SL)	12.93 ± 2.7	12.33 ± 4.7	3.12 ± 1.4
T5 (SCB)	33.49 ± 4.4	17.93 ± 5.2	6.40 ± 2.3
T6 (WCB)	30.69 ± 4.9	12.77 ± 4.3	7.27 ± 3.1
T7 (FYMB)	46.22 ± 6.7	18.63 ± 5.4	8.50 ± 3.5

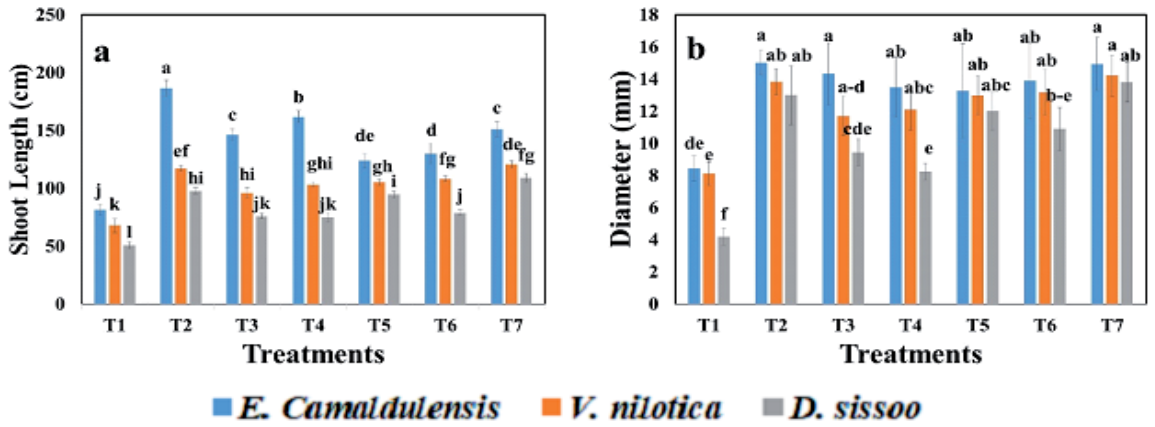


FIGURE 2
Shoot length and diameter of selected agroforestry species against seven different treatments where t1=control, t2=farmyardmanure, t3=poultrymanre, t4=slurry, t5=sugarcane bagasse biochar, t6=wood-chips biochar, t7=farmyardmanure biochar

sissoo. Maximum shoot diameter was found in the plants of T2 and T7 treatment whereas minimum shoot diameter was found in the plants of T1 of *D. sissoo*. The order of species for shoot length and shoot diameter against all treatments was *E. camaldulensis* > *V. nilotica* > *D. sissoo*.

Physiological attributes. Figure 3 depicts that physiological parameters of different species significantly vary from each other. The values for photosynthetic rate for all the species against all the treatments were found in the range of 7. 78 (μ moles CO_2 m^{-2} s^{-1}) to 26.52 (μ moles CO_2 m^{-2} s^{-1}). The values for stomatal conductance (gs) for all the species against all the treatments were found in the range of 0.014 (mol H_2O m^{-2} s^{-1}) to 0.14 (mol H_2O m^{-2} s^{-1}). General trend for three selected agroforestry species for photosynthetic rate and stomatal conductance against different organic amendments in saline field was found to be *E. camaldulensis* > *V. nilotica* > *D. sissoo*.

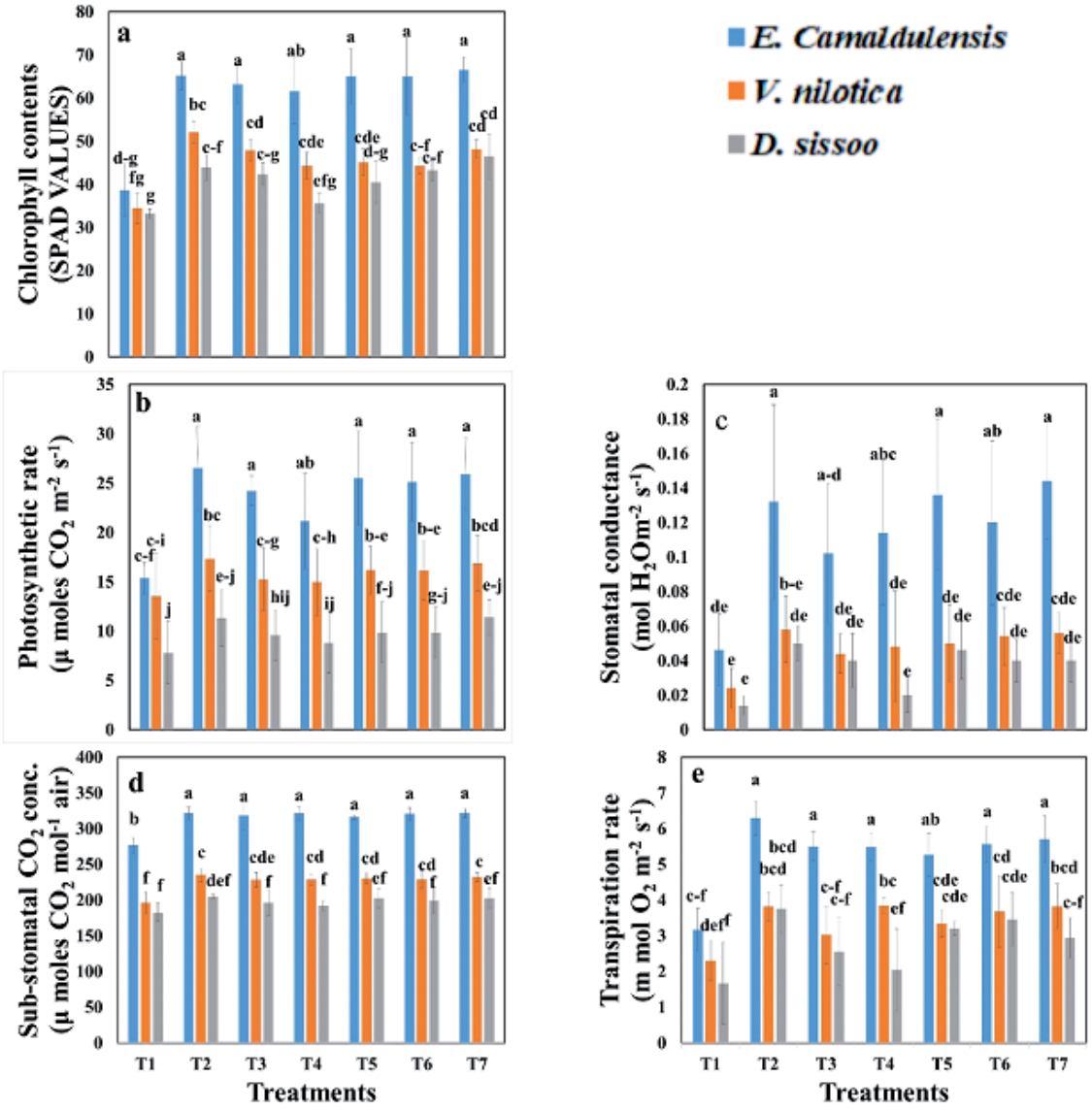


FIGURE 3
Physiological attributes of agroforestry species against seven different treatments where T1=Control, T2=Farmyardmanure, T3=Poultrymanre, T4=Slurry, T5=Sugarcane Bagasse Biochar, T6=Woodchips Biochar, T7=Farmyardmanure Biochar

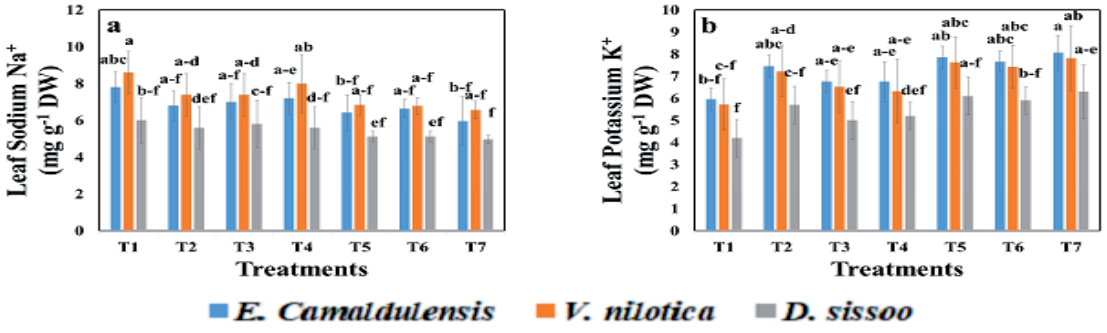


FIGURE 4
Ionic concentration in leaves of different agroforestry species against seven different treatments where T1=Control, T2=Farmyardmanure, T3=Poultrymanre, T4=Slurry, T5=Sugarcane Bagasse Biochar, T6=Woodchips Biochar, T7=Farmyardmanure Biochar

Concentration of sodium and potassium. Trees have excellent potential to remediate saline soils through phytoremediation. Results of this study revealed that different treatments showed significantly different results as compared to control for the concentration of sodium and potassium ions in leaves. Concentration of sodium and potassium in leaves of all three selected agroforestry species against seven different treatments is shown in figure 4. Leaf Na+ was observed maximum in the T1 (control) for all trees (6 – 8.6 mg g^{-1} DW) and minimum in T7 (4.9 to 6.5 mg g^{-1} DW). *V. nilotica* accumulated the maximum leaf Na+ concentrations in T1. Leaf K+ was observed maximum in the T7 for all trees (6.3 – 8.06 mg g^{-1} DW) and minimum in T1 (4.2 to 5.9 mg g^{-1} DW). *E. camaldulensis* accumulated the maximum leaf K+ concentrations in T7.

DISCUSSION

This study was designed to check survival and growth of three selected agroforestry species in salt affected soil under field conditions. These saplings of these species were grown under nursery conditions with different types of organic amendments including farmyard manure (T1), poultry manure (T2), slurry (T3), sugarcane bagasse biochar (T4), woodchips biochar (T5) and farmyard manure biochar (T6). At nursery stage, results were promising as compared to control for all the treatments. Unprocessed organic amendments showed better results as compared to biochar at nursery stage. Among three species, survival rate of *E. camaldulensis* was the maximum as compared to other tree species. Results indicated that *E. camaldulensis* was the best followed by *V. nilotica*. Least effective tree species was *D. sissoo* in terms of all morphological and physiological characteristics. Our results are in accordance with previous studies as authors have also discussed about the negative effects of salinity on the growth of plants and the potential of tree species to grow in salt degraded lands [9,45–49].

Almost all organic amendments showed better results than control. Results were different for field conditions as compared to nursery experiment. In literature, a detailed meta-analysis showed that plants have to face different climatic conditions like temperature and intensity of light under field conditions as compared to controlled conditions of glasshouse and growth chamber conditions of laboratory. So plant's response can be varied in field conditions from lab experiments[38,50] .

The most interesting results of this study was that in nursery experiments, unprocessed organic amendments showed more promising results in terms of all growth, morphological and physiological parameters as compared to biochar but in field condition the plants which were treated with biochar, especially, farmyard manure biochar showed more increment in shoot length, diameter and other gas exchange parameters of plants as compared to FYM, PM and SL. Biochar was found to be more effective as compared to vermicompost and farmyard manure in the growth of geranium (*Pelargonium graveolens* L.) as it showed lowest losses to harvest nutrient ratio [51].

The reason behind this is that biochar has the ability to release nutrients in slow fashion and supply it continuously which makes it better amendment than others. Biochar incorporation results in enhanced nutrient cycling and affects plants performance [50,52]. Large surface area and porous structure of biochar plays a very vital in slow release of biochar-bound nutrients [53]. Structure of biochar helps in slow release of nutrient thus enhancing nutrient use efficiency and increasing nutrient bioavailability which in turns increase growth and yield of crop [54]. Biochar prepared from solid municipal wastes (newspaper, cardboard, woodchips and landscaping residues) was found to be very effective enhancing nutrient use efficiency by reducing leaching of nutrients and releasing nutrients slowly [55]. In another study, it is suggested that chemical bonding to carbon molecules is another reason for this slow release of nutrients. In addition to that sorption capacity of some of the functional groups of biochar is very high which allows to concentrate nutrients in problematic soils and releases it slowly through slow desorption process into aqueous phase for plants [53,56].

It is reported that compost and biochar alone and their mixture increased soil water properties of sandy soil and resultantly increase the growth of *Eucalyptus torquata* [57]. It is reported that biochar showed more promising results as compared to farmyard manure and vermicompost when *W. somnifera* in alleviating the negative stress of heavy metal in field conditions. Almost 50% higher net profit was gained as compared to control by using biochar as an amendment [58].

Biochar is reported to have more potential as compared to compost to improve soil nutrient status and enhance maize yield [59]. Organic amendments prepared from commonly available organic wastes are reported to act as a very cost effective strategy to enhance vegetation cover of degraded lands [60]. Straw biochar is reported to enhance productive potential, economic and environmental benefits when applied in acidic soils [61]. Wheat straw residues at the rate of 5t ha^{-1} is reported to increase maize yield and raised 45% of economic benefits under semi-arid climatic conditions [62].

Biochar is reported to enhance crop yield by releasing nitrogen and phosphorus slowly when applied as an amendment in Illinois agricultural field [63]. Combined effect of gypsum with biochar, biosolid composts and green waste composts were tested and results indicate that biochar plus gypsum showed better results in ameliorating salt affected

soils as compared to other two organic amendments [64]. It is reported that hardwood biochar has more potential to increase crop yield of okra and reduce carbon mineralization when applied in acidic soils as compared to farmyard manure and vermicompost [65].

It is reported that stem elongation in urban tree species *Samanea saman* and *Surgeda multiflora* was more when treated with biochar as compared to compost. Although combined effect of biochar and compost gave better results [66]. Exhausted grape marc biochar prepared at different temperatures and applied at different application rates has showed potential to release nutrient (nitrogen, phosphorus and potassium) very slowly and recommended as a slow release biofertilizer [67]. Sorption capacity of biochar can provide a great hidden economic benefit to release nutrients slowly. Moreover, wastes of food industry can be converted into vital fertilizers [68].

Organic fertilizer based on rice straw biochar in combination with humic acid, bentonite, starch and adhesive agent showed very promising results in rice growth at laboratory and field experiments by releasing nutrients in slow fashion and providing them at heading and maturing stages [69]. Composite of biochar/truvite is reported to release nutrients slowly as compared to traditional chemical fertilizers and showed great potential for soil and environment remediation [70]. Oak based biochar along with other types of biochar are reported to have the capability of immobilizing nutrients and metal in soil water system and thus saving nutrients from leaching down and keeping them available for longer time and releasing them slowly according to plant's needs [71].

It is reported that raw poultry manure derived biochar released nutrients (phosphorus and potassium) very slowly as compared to unprocessed poultry manure. The amount of nutrients release was almost negligible from biochar as compared to manure at early stages [72].

CONCLUSION

According to the results of current study it was concluded that salinity negatively affected the growth of plants and physicochemical characteristics of soil. Moreover, growing the trees with the application of organic amendments was very useful in ameliorating salt affected soils. When trees were transferred to field conditions, *E. camaldulensis* showed the maximum survival rate for all treatments and biochar showed more promising results as compared to unprocessed organic amendment. Use of processed organic amendments and planting of *E. camaldulensis* is highly recommended on salt affected soils during future afforestation programs. Findings of this study can also be employed in modified Miyawaki methods which involve the use of different soil amendments to boost tree growth.

ACKNOWLEDGEMENTS

We are highly acknowledged to Higher Education Commission of Pakistan for providing funding to Mr. Muhammad Talha Bin Yousaf, under the program of Indigenous 5000 PhD Fellowship program PIN NO. 213-60808-2AV2-166 (50025747).

REFERENCES

[1] FAO. (2020) FAO Soils Portal.
[2] Hayat, K., Bundschuh, J., Jan, F., Menhas, S., Hayat, S., Haq, F., Shah, M.A., Chaudhary, H.J., Ullah, A., Zhang, D., Zhou, Y., Zhouy, P. (2020) Combating soil salinity with combining saline agriculture and phytomanagement with salt-accumulating plants. Crit. Rev. Environ. Sci. Technol. 50, 1085–1115.
[3] Akhtar, S.S., Andersen, M.N., Liu, F. (2015) Biochar Mitigates Salinity Stress in Potato. J. Agron. Crop Sci. 201, 368–378.
[4] Kukal, S.S., Chary, G.R., Virmani, S.M. (2017) Soil-Related Abiotic Constraints for Sustainable Agriculture. In Abiotic Stress Management for Resilient Agriculture. Springer Singapore. Singapore. 97–119.
[5] Shao, H., Chu, L., Lu, H., Qi, W., Chen, X., Liu, J., Kuang, S., Tang, B., Wong, V. (2019) Towards sustainable agriculture for the salt-affected soil. L. Degrad. Dev. 30, 574–579.
[6] Niazi, N.K., Bibi, I., Shahid, M., Ok, Y.S., Shaheen, S.M., Rinklebe, J., Wang, H., Murtaza, B., Islam, E., Nawaz, M. F., Luttge, A. (2018) Arsenic removal by Japanese oak wood biochar in aqueous solutions and well water: Investigating arsenic fate using integrated spectroscopic and microscopic techniques. Sci. Total Environ. 621, 1642–1651.
[7] Shahid, S.A., Zaman, M., Heng, L. (2018) Soil Salinity: Historical Perspectives and a World Overview of the Problem. In Guideline for Salinity Assessment, Mitigation and Adaptation Using Nuclear and Related Techniques, Springer International Publishing, Cham. 43–53.
[8] Awan, A.R., Mahmood, K. (2017) Tree plantation in problem soils. Text B. Appl. For. 140–159.
[9] Tewari, P., Saxena, A.K., Rao, O.P. (2006) Effect of sodicity and salinity on seedling growth of two early successional agroforestry tree species. Trop. Ecol. 47, 125–132.
[10] Dagar, J.C., Tewari, V.P. (2018) Agroforestry: Anecdotal to modern science. Agrofor. Anecdotal to Mod. Sci. Jagdish Chander Dagar, Vindhya Prasad Tewari (Eds.), Springer, Heidelberg Germany.

[11] Mehari, A., Ericsson, T., Weih, M. (2005) Effects of NaCl on seedling growth, biomass production and water status of Acacia nilotica and A. tortilis. J. Arid Environ. 62, 343–349.
[12] Ahmad, R., Azeem, M., Ahmed, N. (2009) Productivity of ginger (*Zingiber officinale*) by amendment of vermicompost and biogas slurry in saline soils. Pakistan J. Bot. 41, 3107–3116.
[13] Young, J., Udeigwe, T.K., Weindorf, D.C., Kandakji, T., Gautam, P., Mahmoud, M.A. (2015) Evaluating management-induced soil salinization in golf courses in semi-arid landscapes. Solid Earth. 6, 393–402.
[14] Hasanuzzaman, M., Hakeem, K.R., Nahar, K., Alharby, H.F. (2019) Plant abiotic stress tolerance: Agronomic, molecular and biotechnological approaches. Plant Abiotic Stress Toler. Agron. Mol. Biotechnol. Approaches. 1–490.
[15] Stiller, V. (2009) Soil salinity and drought alter wood density and vulnerability to xylem cavitation of baldcypress (*Taxodium distichum* (L.) Rich.) seedlings. Environ. Exp. Bot. 67, 164–171.
[16] Marcar, N. (2016) Prospects for Managing Salinity in Southern Australia Using Trees on Farmland. 49–71.
[17] Benjamin, J.J., Lucini, L., Jothiramshekar, S., Parida, A. (2019) Metabolomic insights into the mechanisms underlying tolerance to salinity in different halophytes. Plant Physiol. Biochem. 135, 528–545.
[18] Bano, A., Javed, H. (2021) Pgpr Assisted Bioremediation of Heavy Metals and Nutrient Accumulation In Zea Mays Under Saline Sodic Soil. 53, 31–38.
[19] Nawaz, M.F., Gul, S., Tanvir, M.A., Akhtar, J., Chaudary, S., Ahmad, I. (2016) Influence of NaCl-salinity on Pb-uptake behavior and growth of River Red gum tree (Eucalyptus camaldulensis Dehnh.). Turkish J. Agric. For. 40, 425–432.
[20] Yildiz, O., Altundağ, E., Çetin, B., Guner, Ş., Sarginci, M., Toprak, B. (2017) Afforestation restoration of saline-sodic soil in the Central Anatolian Region of Turkey using gypsum and sulfur. Silva Fenn. 51,1579.
[21] Trivedi, P., Singh, K., Pankaj, U., Verma, S.K., Verma, R.K., Patra, D.D. (2017) Effect of organic amendments and microbial application on sodic soil properties and growth of an aromatic crop. Ecol. Eng. 102, 127–136.
[22] Verma, E., Singh, S., Niveshika Mishra, A.K. (2019) Salinity-induced oxidative stress-mediated change in fatty acids composition of cyanobacterium Synechococcus sp. PCC7942. Int. J. Environ. Sci. Technol. 16, 875–886.
[23] Nawaz, M.F., Yousaf, M.T.B., Yasin, G., Gul, S., Ahmed, I., Abdullah, M., Rafay, M., Tanvir, M.A., Asif, M., Afzal, S. (2018) Agroforestry status and its role to sequester atmospheric CO2 under semi-arid climatic conditions in Pakistan. Appl. Ecol. Environ. Res. 16, 645–661.
[24] Yasin, G., Nawaz, M.F., Martin, T.A., Niazi, N.K., Gul, S., Yousaf, M.T.B. (2019) Evaluation of Agroforestry Carbon Storage Status and Potential in Irrigated Plains of Pakistan. Forests. 10, 640.
[25] Mekuria, W., Noble, A. (2013) The Role of Biochar in Ameliorating Disturbed Soils and Sequestering Soil Carbon in Tropical Agricultural Production Systems. Appl. Environ. Soil Sci. 1–10.
[26] Wang, L., Sun, X., Li, S., Zhang, T., Zhang, W., Zhai, P. (2014) Application of Organic Amendments to a Coastal Saline Soil in North China: Effects on Soil Physical and Chemical Properties and Tree Growth. PLoS One. (Bond-Lamberty, B., ed.) 9, e89185.
[27] Oo, A.N., Iwai, C.B., Saenjan, P. (2015) Soil Properties and Maize Growth in Saline and Nonsaline Soils using Cassava-Industrial Waste Compost and Vermicompost with or Without Earthworms. L. Degrad. Dev. 26, 300–310.
[28] Zheng, H., Wang, X., Chen, L., Wang, Z., Xia, Y., Zhang, Y., Wang, H., Luo, X.., Xing, B. (2018) Enhanced growth of halophyte plants in biochar-amended coastal soil: roles of nutrient availability and rhizosphere microbial modulation. Plant, Cell Environ. 41, 517–532.
[29] Tully, K.L., McAskill, C. (2019) Promoting soil health in organically managed systems: a review. Org. Agric. 10, 339-358.
[30] Yousaf, M.T.B., Nawaz, M.F., Khawaja, H.F., Gul, S., Ali, S., Ahmad, I., Rasul, F., Rizwan, M. (2019) Ecophysiological response of early stage Albizia lebbeck to cadmium toxicity and biochar addition. Arab. J. Geosci. 12, 134.
[31] Saifullah, Dahlawi, S., Naeem, A., Rengel, Z., Naidu, R. (2018) Biochar application for the remediation of salt-affected soils: Challenges and opportunities. Sci. Total Environ. 625, 320–335.
[32] Akbarimoghaddam, H., Galavi, M., Ghanbari, A., Panjehkeh, N. (2011) Salinity Effects on Seed Germination and Seedling Growth of Bread Wheat Cultivars. Trakia J. Sci. 9, 43–50.
[33] Diacono, M., Montemurro, F. (2015) Effectiveness of Organic Wastes as Fertilizers and Amendments in Salt-Affected Soils. Agriculture. 5, 221–230.
[34] Yazdanpanah, N., Mahmoodabadi, M., Cerdà, A. (2016) The impact of organic amendments on soil hydrology, structure and microbial respiration in semiarid lands. Geoderma. 266, 58–65.

[35] Luo, X., Liu, G., Xia, Y., Chen, L., Jiang, Z., Zheng, H., Wang, Z. (2017) Use of biochar-compost to improve properties and productivity of the degraded coastal soil in the Yellow River Delta, China. J. Soils Sediments. 17, 780–789.
[36] Leogrande, R., Vitti, C. (2019) Use of organic amendments to reclaim saline and sodic soils: a review. Arid L. Res. Manag. 33, 1–21.
[37] Cherubin, M.R., Chavarro-Bermeo, J.P., Silva-Olaya, A.M. (2019) Agroforestry systems improve soil physical quality in northwestern Colombian Amazon. Agrofor. Syst. 93, 1741–1753.
[38] Poorter, H., Fiorani, F., Pieruschka, R., Wojciechowski, T., van der Putten, W.H., Kleyer, M., Schurr, U., Postma, J. (2016) Pampered inside, pestered outside? Differences and similarities between plants growing in controlled conditions and in the field. New Phytol. 212, 838–855.
[39] Usman, A.R.A. (2015) Influence of NaCl-Induced Salinity and Cd Toxicity on Respiration Activity and Cd Availability to Barley Plants in Farmyard Manure-Amended Soil. Appl. Environ. Soil Sci. 1–8.
[40] Minhas, P.S., Dagar, J.C. (2016) Use of Tree Plantations in Water-table Drawdown and Combating Soil Salinity. 33–48.
[41] Chowdhury, S., Bhusan, D., Hashem, M.A., Hoque, M.A. (2019) Organic amendments for mitigating soil salinity in rice. Res. Agric. Livest. Fish. 6, 11–17.
[42] Mbarki, S., Skalicky, M., Talbi, O., Chakraborty, A., Hnilicka, F., Hejnak, V., Zivcak, M., Brestic, M., Cerda, A., Abdelly, C. (2020) Performance of Medicago sativa Grown in Clay Soil Favored by Compost or Farmyard Manure to Mitigate Salt Stress. Agronomy. 10, 94.
[43] Wichern, F., Islam, M.R., Hemkemeyer, M., Watson, C., Joergensen, R.G. (2020) Organic Amendments Alleviate Salinity Effects on Soil Microorganisms and Mineralisation Processes in Aerobic and Anaerobic Paddy Rice Soils. Front. Sustain. Food Syst. 4.
[44] McGeorge, W.T. (1954) Diagnosis and Improvement of Saline and Alkaline Soils. Soil Sci. Soc. Am. J. 18, 348.
[45] Madsen, P.A., Mulligan, D.R. (2006) Effect of NaCl on emergence and growth of a range of provenances of *Eucalyptus citriodora*, *Eucalyptus populnea*, *Eucalyptus camaldulensis* and *Acacia salicina*. For. Ecol. Manage. 228, 152–159.
[46] George, S.J., Harper, R.J., Hobbs, R.J., Tibbett, M. (2012) A sustainable agricultural landscape for Australia: A review of interlacing carbon sequestration, biodiversity and salinity management in agroforestry systems. Agric. Ecosyst. Environ. 163, 28–36.
[47] Abbas, G., Saqib, M., Akhtar, J., Basra, S.M.A. (2013) Salinity tolerance potential of two acacia species at early seedling stage. Pakistan J. Agric. Sci. 50, 683–688.
[48] Meir, M., Zaccai, M., Raveh, E., Ben-Asher, J., Tel-Zur, N. (2014) Performance of *Ziziphus jujuba* trees correlates with tissue mineral content under salinity conditions. Agric. Water Manag. 142, 47–55.
[49] Sharma, P.C., Singh, A. (2019) Reviving the Productivity of Salt-affected Lands: Technological Options, Constraints and Research Needs. In Research Developments in Saline Agriculture, Springer Singapore, Singapore. 591–627.
[50] Purakayastha, T.J., Bera, T., Bhaduri, D., Sarkar, B., Mandal, S., Wade, P., Kumari, S., Biswas, S., Menon, M., Pathak, H., Tsang, D.C. (2019) A review on biochar modulated soil condition improvements and nutrient dynamics concerning crop yields: Pathways to climate change mitigation and global food security. Chemosphere. 227, 345–365.
[51] Meena, M.D., Yadav, R.K., Narjary, B., Yadav, G., Jat, H.S., Sheoran, P., Meena, M.K., Antil, R.S., Meena, B. L., Singh, H.V., Meena, V.S. (2019) Municipal solid waste (MSW): Strategies to improve salt affected soil sustainability: A review. Waste Manag. 84, 38–53.
[52] El-Naggar, A., Lee, S.S., Rinklebe, J., Farooq, M., Song, H., Sarmah, A.K., Zimmerman, A.R., Ahmad, M., Shaheen, S.M., Ok, Y.S. (2019) Biochar application to low fertility soils: A review of current status, and future prospects. Geoderma. 337, 536–554.
[53] Xiao, X., Chen, B., Chen, Z., Zhu, L., Schnoor, J.L. (2018) Insight into Multiple and Multilevel Structures of Biochars and Their Potential Environmental Applications: A Critical Review. Environ. Sci. Technol. 52, 5027–5047.
[54] Gwenzi, W., Chaukura, N., Noubactep, C., Mukome, F.N.D. (2017) Biochar-based water treatment systems as a potential low-cost and sustainable technology for clean water provision. J. Environ. Manage. 197, 732–749.
[55] Randolph, P., Bansode, R.R., Hassan, O.A., Rehrah, D., Ravella, R., Reddy, M.R., Watts, D.W., Novak, J.M., Ahmedna, M. (2017) Effect of biochars produced from solid organic municipal waste on soil quality parameters. J. Environ. Manage. 192, 271–280.
[56] Yu, H., Zou, W., Chen, J., Chen, H., Yu, Z., Huang, J., Tang, H., Wei, X., Gao, B. (2019) Biochar amendment improves crop production in problem soils: A review. J. Environ. Manage. 232, 8–21.
[57] Somerville, P.D., Farrell, C., May, P.B., Livesley, S.J. (2019) Tree water use strategies and soil type determine growth responses to biochar and compost organic amendments. Soil Tillage Res. 192, 12–21.

[58] Nigam, N., Yadav, V., Khare, P., Singh, R.P., Das, P., Shanker, K., Sharma, R.S. (2019) Exploring the benefits of biochar over other organic amendments for reducing of metal toxicity in *Withania somnifera*. Biochar. 1, 293–307.
[59] Agegnehu, G., Bass, A.M., Nelson, P.N., Bird, M.I. (2016) Benefits of biochar, compost and biochar–compost for soil quality, maize yield and greenhouse gas emissions in a tropical agricultural soil. Sci. Total Environ. 543, 295–306.
[60] Forja´n, R., Asensio, V., Guedes, R.S., Rodríguez-Vila, A., Covelo, E. F.. Marcet, P. (2017) Remediation of Soils Polluted with Inorganic Contaminants: Role of Organic Amendments. In Enhancing Cleanup of Environmental Pollutants. Springer International Publishing, Cham. 313–337.
[61] Bi, Y., Cai, S., Wang, Y., Xia, Y., Zhao, X., Wang, S., Xing, G. (2019) Assessing the viability of soil successive straw biochar amendment based on a five-year column trial with six different soils: Views from crop production, carbon sequestration and net ecosystem economic benefits. J. Environ. Manage. 245, 173–186.
[62] Ali, S., Jan, A., Manzoor, Sohail, A., Khan, A., Khan, M.I., Inamullah, Zhang, J., Daur, I. (2018) Soil amendments strategies to improve water-use efficiency and productivity of maize under different irrigation conditions. Agric. Water Manag. 210, 88–95.
[63] Zheng, W. (2010) Using Biochar as a Soil Amendment for Sustainable Agriculture. Sustain. Agric. 7276.
[64] Chaganti, V.N., Crohn, D.M., Šimůnek, J. (2015) Leaching and reclamation of a biochar and compost amended saline–sodic soil with moderate SAR reclaimed water. Agric. Water Manag. 158, 255–265.
[65] Sarma, B., Borkotoki, B., Narzari, R., Kataki, R., Gogoi, N. (2017) Organic amendments: Effect on carbon mineralization and crop productivity in acidic soil. J. Clean. Prod. 152, 157–166.
[66] Ghosh, S., Ow, L.F., Wilson, B. (2015) Influence of biochar and compost on soil properties and tree growth in a tropical urban environment. Int. J. Environ. Sci. Technol. 12, 1303–1310.
[67] Ibn Ferjani, A., Jellali, S., Akrout, H., Limousy, L., Hamdi, H., Thevenin, N., Jeguirim, M. (2020) Nutrient retention and release from raw exhausted grape marc biochars and an amended agricultural soil: Static and dynamic investigation. Environ. Technol. Innov. 19, 100885.
[68] Maroušek, J., Strunecký, O., Stehel, V. (2019) Biochar farming: defining economically perspective applications. Clean Technol. Environ. Policy. 21, 1389–1395.
[69] Dong, D., Wang, C., Van Zwieten, L., Wang, H., Jiang, P., Zhou, M., Wu, W. (2019) An effective biochar-based slow-release fertilizer for reducing nitrogen loss in paddy fields. J. Soils Sediments. 1-14
[70] Hu, P., Zhang, Y., Liu, L., Wang, X., Luan, X., Ma, X., Chu, P.K., Zhou, J., Zhao, P. (2019) Biochar/struvite composite as a novel potential material for slow release of N and P. Environ. Sci. Pollut. Res. 26, 17152–17162.
[71] Van Poucke, R., Meers, E.. Tack, F.M.G. (2020) Leaching behavior of Cd, Zn and nutrients (K, P, S) from a contaminated soil as affected by amendment with biochar. Chemosphere. 245, 125561.
[72] Hadroug, S., Jellali, S., Leahy, J.J., Kwapinska, M., Jeguirim, M., Hamdi, H., Kwapinski, W. (2019) Pyrolysis Process as a Sustainable Management Option of Poultry Manure: Characterization of the Derived Biochars and Assessment of their Nutrient Release Capacities. Water. 11, 2271.

Received: **12.04.2021**
Accepted: **17.05.2021**

CORRESPONDING AUTHOR

Muhammad Farrakh Nawaz
Department of Forestry and Range Management,
University of Agriculture,
Faisalabad 38000 – Pakistan

e-mail: kf_uaf@yahoo.com

© by PSP Volume 30– No. 09/2021 pages 10961-10969 Fresenius Environmental Bulletin

FEATURE EXTRACTION METHOD OF ECOLOGICAL ENVIRONMENT LANDSCAPE REMOTE SENSING IMAGE BASED ON GIS TECHNOLOGY

Chunjie Wang*

Jincheng College of Sichuan University, Chengdu Sichuan 611731, China

ABSTRACT

With the rapid development of social economy, science and technology, the rapid development of Chinese cities has led to the great changes of regional society and economy. Reducing the adverse effects of economic growth and social progress on ecological environment landscape pattern and promoting the virtuous cycle of natural resource system and social economic system have become the social goals. Ecological environment landscape image feature extraction can provide timely and effective regional environment landscape information, which is important to analyze, predict and comprehensively evaluate the dynamic changes of landscape environment caused by the implementation of regional planning. In this paper, the Landsat-TM remote sensing images in 2010 and 2017 are used to extract and analyze the features of the remote sensing images by using the maximum likelihood classification method. The results show that the overall classification accuracy and kappa coefficient of TM images in 2010 are 89.2409% and 0.8532, respectively, and the overall classification accuracy and kappa coefficient of TM images in 2017 are 86.2134% and 0.8012, respectively. The deviation rate of classified data in 2010 and 2017 is not large. The deviation rate of woodland landscape is the smallest (2.89% for 2010 and 1.28% for 2017), followed by construction land landscape (3.54% for 2010 and 3.13% for 2017), and the deviation rate of other land landscape is the largest (7.85% for 2010 and 11.23% for 2017).

KEYWORDS:
GIS, Remote sensing image, Riverside area, Feature extraction, Ecological environment

INTRODUCTION

In order to reduce the adverse impact of economic growth and social progress on landscape pattern and promote the virtuous cycle of natural resource system and social economic system, it is particularly important to analyze, predict and comprehensively evaluate the dynamic change law of landscape environment caused by the implementation of regional Planning [1-3]. The core of landscape pattern research is landscape ecology. Landscape ecology takes landscape as the research object. Through the exchange and transmission of energy flow, material flow, species flow and information flow on the earth surface, it studies the spatial structure, ecological function, internal function of landscape, and the relationship between time and space [4-5].

With the rapid development of science and technology, especially the development of remote sensing technology and geographic information system, the research of modern landscape pattern has developed from qualitative description to quantitative analysis. The dynamic change of landscape pattern has become an important research field of landscape ecology [6-7]. Before the 1980s, landscape pattern research was mainly based on qualitative analysis. In recent years, many foreign countries have carried out research on regional landscape pattern. Mande and rob H. gjongman [8] studied the human factors in the rural landscape change in central and Northern Europe under the guidance of sustainable development. R. D. swetraam et al [9] established an ecological model by using GIS modeling analysis function to simulate the change process of landscape pattern. Hannes palang et al [10] used diversity index to study the change characteristics of landscape diversity in Estonia in the 20th century, and pointed out that there were regional differences in the change of landscape diversity. K.A.Ulbricht and W.D.Heckendo [11] studied the relationship between land use change and landscape pattern change in the coastal zone of Joao Pessoa in Northeast Brazil by using remote sensing images in 1988 and 1996. JohnT.Lee et al [12] used GIS technology to study the human factors of landscape pattern change in Chiitern mountains. Hietala [13] used landscape area ratio, average patch area, patch density, average shape index and boundary length to study the change of agricultural landscape structure in Yiane, Finland in 39 years. Kristensen [14] used GIS technology to study the impact of agricultural activities on the regional landscape pattern of rostrup in Danmai from 1973 to 1995. Michael B. Usher [15] demonstrated theoretically and experimentally that human factors

and natural factors can promote the change of landscape structure, composition, and function. Michael F. Thomas [16] studied the temporal and spatial characteristics of landscape sensitivity and pointed out that the different anti-interference sensitivity of different landscape components led to the spatial differentiation of Landscape. In China, Ding Shengyan and Liang Guofu used remote sensing images in 1987 and 2002 to study and analyze the evolution of landscape pattern along the Yellow River in Henan Province [17-18]. Ding Shengyan and Zhang Mingliang used landscape index to analyze the landscape dynamic change of Kaifeng City [19].

As a concentrated area of economic development, Jiangsu riverside area is an important area of national economic and cultural development, which plays an irreplaceable role in Jiangsu and even the whole country [20]. The development of advanced regional economy, design theory and market, long history and typical cultural characteristics of Jiangnan jointly determine that the research on the current situation and development trend of local landscape planning has typical representative significance. In this paper, the remote sensing image along the Yangtze River is taken as the research object. By using the maximum likelihood classification method to extract and analyze the features of remote sensing image, the types, quantities, and locations of various changes along the Yangtze River are obtained.

MATERIALS AND METHODS

Study area. Jiangsu Province has a population of about 25 million people and an area of 2.47 million square kilometers. The whole area along the Yangtze River is located at the junction of China's coastal areas. The terrain along the Yangtze River in Jiangsu Province is generally high in the west, low in the east. The strata of each geological age in the territory are relatively complete, from the oldest Archean metamorphic rock series to the latest Quaternary sedimentary rocks. The landform is mainly plain, and the area of hills and mountains is very small. Between the foothills of low mountains and plains, there are loess hillock in the southwest and metamorphic rock hillock in the northeast, accounting for less than 10% of the total land area. The area along the Yangtze River in Jiangsu Province is located in the transition zone from subtropical zone to warm temperate zone, with mild climate, moderate rainfall and four distinct seasons. The average temperature is 13-16 °C and the annual rainfall is about 1000 mm.

Data collection. The main data sources of this paper include four different periods of Landsat-TM remote sensing image mosaic as the first phase data image on May 25, 2010, July 26, 2010, and September 27, 2010, and four different periods of Landsat-TM remote sensing image mosaic as the second phase data image on June 14, 2017, July 25, 2017 and October 14, 2017. TM is the imaging equipment installed on Landsat satellite which can be used to image the earth's surface.

TM image is better than MSS image in spectral resolution, radiation resolution and ground resolution. In terms of spectral resolution, it uses seven bands to record the target information obtained by the remote sensor. In terms of radiation resolution, TM uses two-way scanning to improve the accuracy of radiation measurement. The spectral characteristics of different ground objects are described by 256 radiance levels after analog-to-digital conversion of ground object simulation signal. In terms of ground resolution, the ground resolution corresponding to TM instantaneous field of view is 30m.

Research data processing. Geometric correction. The purpose of geometric correction is to correct the image deformation caused by system and non-system factors, so as to realize the geometric integration with standard image or map. Image geometric correction needs to determine the appropriate geometric correction method according to the nature of image geometric deformation, available correction data and image application purpose. The polynomial correction method avoids the spatial geometric process of remote sensing imaging and simulates the remote sensing image itself. Because of its simple principle and uncomplicated implementation, it is widely used. In this paper, cubic polynomial is used as the transformation model. Two phases of remote sensing images were corrected by geometric precision. The projection is set by orthorectification in envi4.4 software. 22 actual control points are selected (the points with excessive error should be removed in the process of point selection). The error accuracy of the corrected TM remote sensing image is no more than 0.5 pixels, that is, 15 meters, which met the accuracy requirements. Then the cubic polynomial function is constructed for image correction, and resampling is performed to obtain two matched corrected images.

Radiometric correction. Radiometric correction generally includes radiometric correction, illuminance correction and atmospheric correction. Generally, the data provided to users by satellite ground stations are corrected by system radiation, that is, the radiation error caused by the change of sensor performance is removed. Illumination correction is generally used for comparative study of different time phase images or mosaic of images in different regions.

Image mosaic and clipping. Image mosaic is a process of simultaneous interpreting and matching multiple overlapped images (which may be obtained from different time, different viewpoints or different

sensors) in space. Image mosaic technology is a large seamless high-resolution image technology. Image clipping sergio draws the boundary according to the vector map of the area along the river and uses the Subset Data via ROIs tool under ENVI to clip the image.

Extraction of landscape type information. Remote sensing image classification methods are mainly divided into two kinds: one is visual interpretation, which is mainly used to judge the types of ground objects from the brightness, tone, position, structure and other characteristics of the image by professionals based on spectral characteristics, geological laws and experience. The other is computer interpretation, which is the specific application of pattern recognition technology in the field of remote sensing technology, combined with artificial intelligence technology to analyze the earth surface. The information of surface and its environment in the remote sensing image can be identified and classified by attribute recognition, so as to recognize and distinguish the actual features corresponding to the image information and achieve the purpose of extracting the required feature information.

Maximum likelihood classification [21]. Computer classification of remote sensing image has gradually become the main means of remote sensing classification because of its fast and objective characteristics. Because the maximum likelihood method is considered to be the most stable and robust classifier and the internal algorithm has few defects and high reliability, this paper mainly uses the maximum likelihood method to classify images.

Maximum likelihood classification is a method to classify a pixel into the category with the maximum probability of belonging. The maximum likelihood method assumes that the spectral characteristics of the ground objects in the training area, like most random phenomena in nature, approximately obey the normal distribution. Using the training area, the characteristic parameters such as mean value, variance and covariance can be obtained, thus the prior probability density of the whole population can be obtained.

For multi band images, the probability density function is processed by matrix method. If m variables are taken for each pixel in a remote sensing image to be classified, the pixel value can be expressed by vector.

$$X = \begin{bmatrix} x_1 \\ x_2 \\ \vdots \\ x_m \end{bmatrix} \quad (1)$$

When all kinds of population are multivariate normal population $N(\mu_i, \Sigma_i)$.The probability density of the pixel eigenvector x is expressed as in Eq. 2:

$$p(x/w_i) = \frac{1}{(2\pi)^{m/2}|\Sigma_i|^{1/2}} \exp\left[-\frac{1}{2}(x-\mu_i)^T \sum_i^{-1}(x-\mu_i)\right. \quad (2)$$

Where $\mu_i = \begin{bmatrix} \mu_{i1} \\ \mu_{i2} \\ \vdots \\ \mu_{im} \end{bmatrix}$ and $\Sigma_i = \begin{bmatrix} \sigma_{i1}^2 & \sigma_{i12} \cdots & \sigma_{i1m} \\ \sigma_{i21} & \sigma_{i2}^2 \cdots & \sigma_{i2m} \\ \vdots & \vdots & \vdots \\ \sigma_{im1} & \sigma_{im2} & \sigma_{im}^2 \end{bmatrix}$

Where, $\mu_i$and $\Sigma_i$is the mean vector and covariance matrix of the i-th population. $|\Sigma_i|$is the determinant value of the covariance matrix. $\Sigma_i^{-1}$is expressed as the inverse of the covariance matrix.

If the unknown measure vector x comes from class w_i, then the maximum likelihood criterion becomes: $x \in w_i$. That is, if and only if $p(x|w_i) \times p(w_i) \geq p(x|w_j) \times p(w_j)$, it is considered that the point should be classified. However, in practice, we rarely use the prior information to determine which kind of image is more likely to appear than other kinds of people. This kind of information is called the prior probability information of the class. Therefore, in the application, it is assumed that the probability of each class in the landscape is equal.

In order to divide an unknown pixel measure vector into a certain class, the maximum likelihood classification method obtains the probability density function value by calculating the statistical value of the sample, and then divides the unknown pixel into the class with the largest probability density function value.

Classification accuracy analysis. In order to analyze and compare the classification methods and effects of remote sensing images, it is necessary to evaluate the classification accuracy. Classification accuracy refers to the degree to which pixels in thematic classification images of remote sensing images are correctly classified. At present, the most widely used method to measure classification accuracy is confusion matrix method [22]:

$$M = \begin{bmatrix} m_{11} & m_{12} \cdots & m_{1n} \\ m_{21} & m_{22} \cdots & \sigma_{2n} \\ \vdots & \vdots & \vdots \\ m_{n1} & m_{n2} & m_{nn} \end{bmatrix} \quad (3)$$

Where, $m_{ij}$is the total number of pixels belonging to i in the experimental area which are divided into j categories, and N is the number of categories. The larger the diagonal elements in the confusion matrix, the higher the classification accuracy. The larger the non diagonal elements in the confusion matrix, the more serious the misclassification.

The main indexes of classification accuracy are production accuracy, user accuracy, omission errors, commission errors and kappa coefficient.

1. Production accuracy (PA) refers to the proportion of correct classification number of a certain category in the total number of pixels of that category in the inspection data. On the contrary, the proportion of wrong classification number in the total number of pixels of that category in the inspection data is the omission error (OE):

$$PA = \frac{m_{jj}}{\sum_{j=1}^{n} m_{ij}} \quad (4)$$

$$OE = 1\text{-}PA \quad (5)$$

2. User accuracy (UA) refers to the proportion of the number of correct classifications in the total number of pixels divided into a certain category, while the number of wrong classifications in the total number of pixels divided into a certain category is the misclassification error (CE):

$$UA = \frac{m_{ii}}{\sum_{j=1}^{n} m_{ij}} \quad (6)$$

$$OE = 1\text{-}UA \quad (7)$$

3. Overall accuracy (OA) refers to the proportion of the total number of correct classifications to the total number of samples, which reflects the overall accuracy of classification results:

$$OA = \frac{\sum_{i=1}^{n} m_{ii}}{\sum_{j=1}^{n}\sum_{i=1}^{n} m_{ij}} \quad (8)$$

4. Kappa coefficient:

$$k = \frac{N\sum_{i=1}^{n} m_{ij} - \sum_{i=1}^{n}(m_{i+}m_{+j})}{N^2 - \sum_{i=1}^{n}(m_{i+}m_{+j})} \quad (9)$$

Where: n is the number of rows and columns of the classification matrix, m_{ij} is the element value of row i and column j in confusion matrix, m_{i+} and m_{+j} denote the row sum and column sum of the classification confusion matrix, respectively, N is the total number of pixels used for accuracy evaluation, that is, the sum of all elements in the mixing matrix.

RESULTS AND DISCUSSIONS

Determination of landscape types. Landscape pattern analysis needs to be carried out on the basis of classification, and the determination of classification type should also consider the needs of landscape pattern. The classification of landscape element type is to define the object area as several relatively homogeneous land ecological units according to certain characteristics. It is a multi-level and detailed structural system. The detailed level of type definition is determined not only by the recognition degree that can be achieved by data and technical means, but also by the classification level required by the work goal. The classification of landscape types is one of the bases of landscape ecology research. Due to the different understanding of the definition of landscape, there are different classification systems: landscape classification based on human impact intensity, landscape classification based on land use, landscape classification based on natural degree, and landscape classification based on vegetation type or geomorphic characteristics.

The classification of landscape ecology should follow certain principles. Usually, first of all, we must make clear the grade of landscape units, and determine the basic units of classification according to the requirements of different spatial scales or graphic scales. Secondly, landscape classification should reflect the spatial differentiation and combination of landscape, that is, different landscapes are independent and interrelated. Landscape classification should reflect the main factors controlling the formation process of landscape. The division of landscape elements in this paper is based on the study of land use landscape pattern, revealing land use landscape pattern, ecological environment, and dynamic change process. According to the characteristics of land use landscape classification, the landscape types of the study area are mainly divided into five categories: cultivated land, forest land, construction land, water area and other land. Among them, the distribution area of cultivated land is the largest, and occupies an absolute advantage, followed by construction land, water area and water conservancy facilities (Table 1).

Selection of training area. The selection of training area is the premise and key of remote sensing image supervised classification, which directly affects the quality and accuracy of classification. Training and district selection should be representative and meet the following requirements of classification: ① in terms of time, the mapping date of the topographic map should be as close as possible to the image imaging date (the color and shape of vegetation and other ground features are different in each season), so as to ensure the accuracy and typicality of the ground feature types; ② in terms of space, the possibility of spectral feature changes with the change of spatial position should be considered for each ground feature type, and the selection method should be adopted. The training area should be able to reflect this change, but also to ensure the uniform distribution of training sample points; ③the training sample trees should at least meet the requirements of establishing the classification and discrimination function. In this paper, the selection of training area is mainly based on the reference of Jiangsu Province Yearbook, Google Earth and Landsat TM image supervision classification, and through manual selection of representative sample points of the training area with synthetic images.

Classification accuracy evaluation results. The confusion matrix of precision evaluation is established, and the sampling points are determined. The timing categories of random sampling and real pixel points in the graph are compared. This paper evaluates the accuracy through the post classification fusion matrix in classification under the classification module of ENVI, as shown in Table 2 and Table 3.

TABLE 1
Landscape classification of land use.

Landscape types	Type code	Types of land use included
Landscape of cultivated land	1	Paddy field, dry land and vegetable field
Woodland landscape	3	Woodland, shrubbery, sparse woodland, orchard, grassland
Landscape of construction land	7	Rural residential land, urban residential land, industrial and mining land
Landscape of water area and water conservancy facilities land	11	Rivers, reservoirs, inland beaches, lakes and ponds
Landscape of other land use	12	Bare land, wasteland, etc

TABLE 2
Confusion matrix of TM images in 2010.

Type	Cultivated land	Wood-land	Land used for construction	Water area and water conservancy	Other land	Test sample 数	Mapping
Cultivated land	3423	49	85	23	0	3523	95.23%
Woodland	775	2245	109	27	0	3108	71.69%
Land used for construction	189	68	2386	126	4	2723	86.41%
Water area and water conservancy facilities land	105	0	0	3302	0	3354	96.59%
Other land	6	0	0	0	72	76	93.03%
Test sample	4423	2385	2673	3467	76	12754	
Mapping accuracy	77.32%	96.12%	93.74%	95.67%	94.69%		

Overall Accuracy = 89.2409% Kappa Coefficient = 0.8532.

TABLE 3
Confusion matrix of TM images in 2017

Type	Cultivated land	Wood-land	Land used for construction	Water area and water conservancy	Other land	Test sample 数	Mapping
Cultivated land	4654	125	452	55	0	5321	88.54%
Woodland	772	1572	8	0	0	2416	67.34%
Land used for construction	195	35	2104	34	0	2504	88.51%
Water area and water conservancy facilities land	68	0	15	1368	0	1512	94,74%
Other land	0	0	0	0	100	100	100%
Test sample	5669	1798	2544	1495	100	11572	
Mapping accuracy	81.23%	91.03%	82.17%	94.95%	100%		

Overall Accuracy = 86.2134% Kappa Coefficient = 0.8012.

Classification post processing. There is still a certain gap between the classification results and the requirements of landscape analysis, so it is necessary to carry out a series of post-processing for the classified images according to the requirements of landscape analysis. In this paper, the processing methods after classification mainly include: ① Cluster analysis and filter analysis of remote sensing image by using clump and sieve under ENVI software is used to remove a large number of broken small patches and isolated points in the classified image. ② The classified image is masked, and most of the pixels belong to the correct area and the wrong area. ③ Using visual interpretation, we correct the wrong pixel classification, and get a more correct classification result. After a series of classification processing, the overall image classification accuracy in 2010 increases from 85.132% to 94.562%, and the overall image classification accuracy in 2017 also increases from 87.246% to 91.932%. Finally, the classified images are vectorized to calculate the area of each type and compared with the actual land use data, as shown in Figure 1-4.

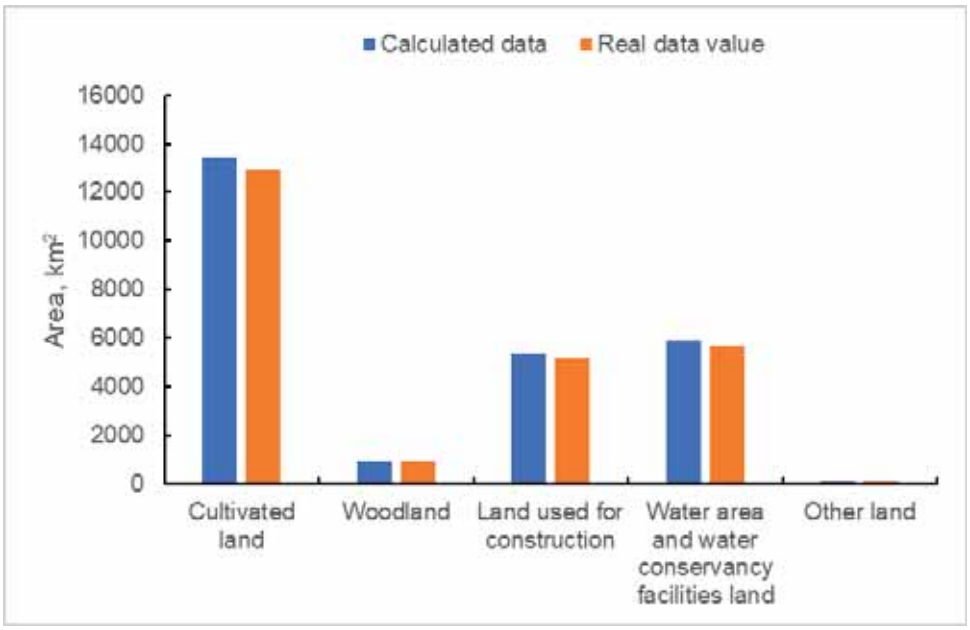


FIGURE 1
Comparison of remote sensing image classification data and actual land use data (2010).

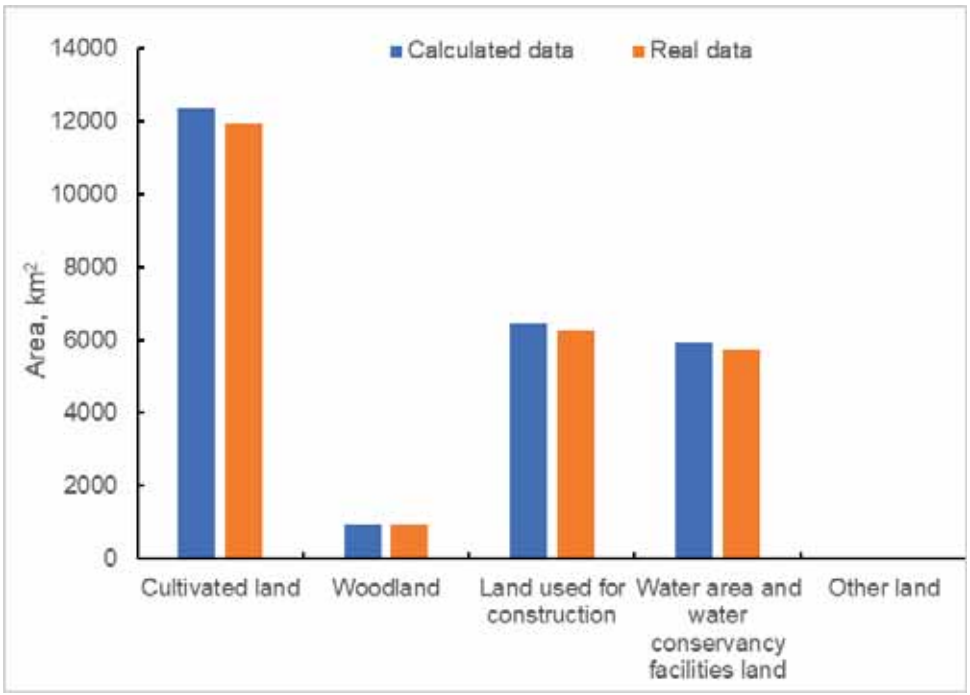


FIGURE 2
Comparison of remote sensing image classification data and actual land use data (2017).

It can be seen from Figure 3 and Figure 4 that the deviation rates of classified data in 2010 and 2017 are not large. Among them, the deviation rate of woodland landscape is the smallest, which is 2.89% (2010) and 1.28% (2017), respectively, followed by construction land landscape. The biggest deviation rate is other land landscape, but because the proportion of other land landscape in remote sensing image is very small, it has little significance in practical application. From the comparison of these data, the area of each landscape type is effective and available. Water area and water conservancy facilities land, cultivated land, construction land and woodland are of great significance in practical application, and the deviation rate will not have a great impact on the research results.

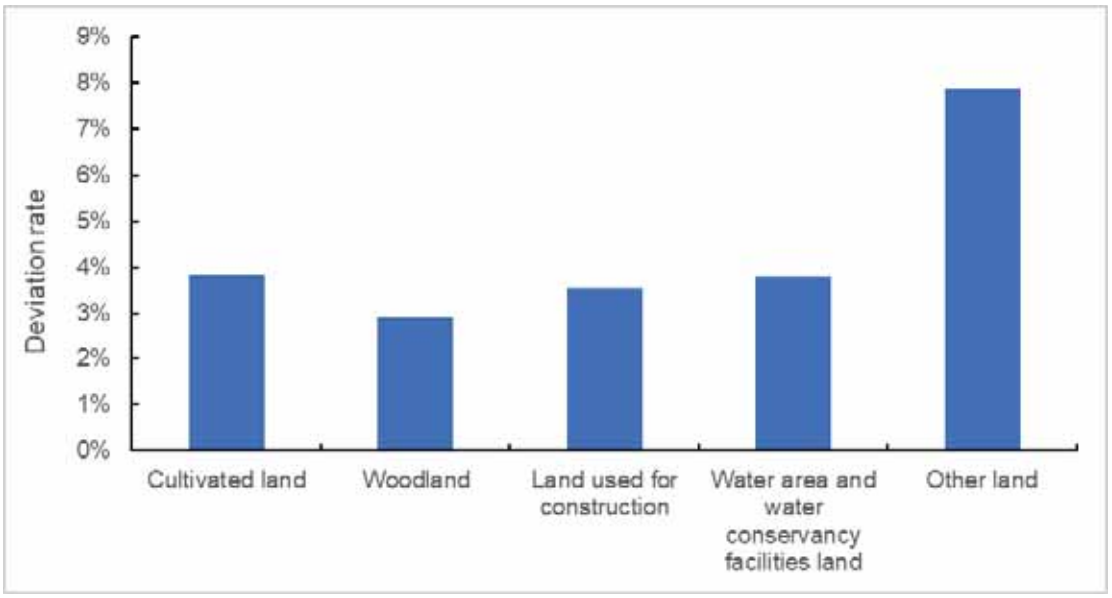


FIGURE 3
Deviation rate between remote sensing image classification data and actual land use data (2010).

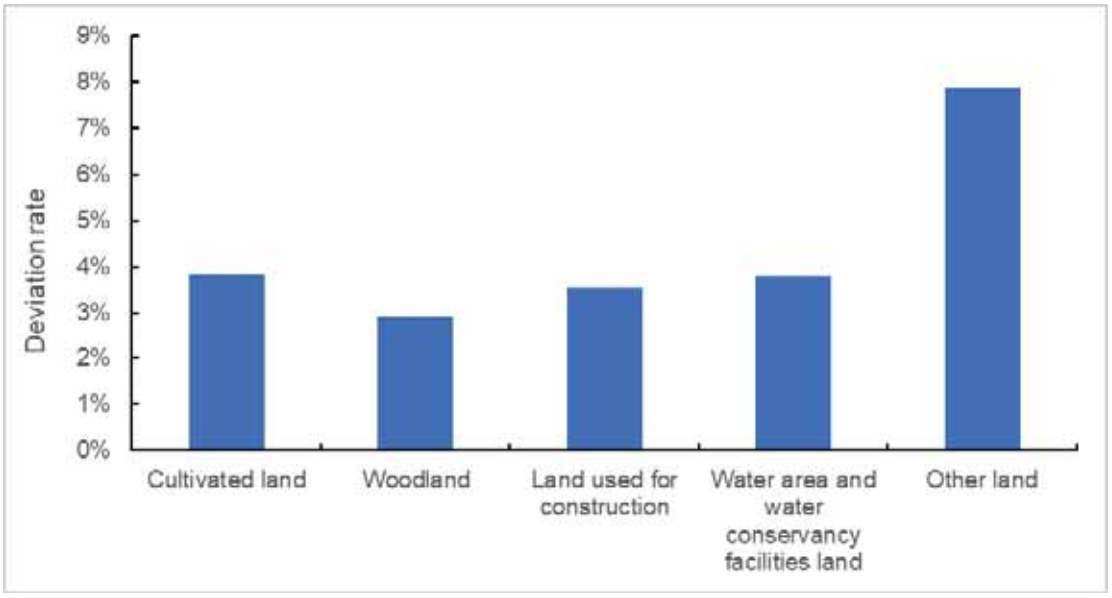


FIGURE 4
Deviation rate between remote sensing image classification data and actual land use data (2017).

CONCLUSION

(1) In this paper, the LandsatTM data in 2010 and 2017 are used as the information source, remote sensing and GIS technology are used to preprocess the data, and some theoretical knowledge of landscape ecology is used as the analysis basis to extract and analyze the landscape type information along the Yangtze River in Jiangsu Province.

(2) The maximum likelihood method is used to classify the image, and good classification results are obtained. Among them, the overall classification accuracy and kappa coefficient of TM images in 2010 are 89.2409% and 0.8532, respectively, and the overall classification accuracy and kappa coefficient of TM images in 2017 are 86.2134% and 0.8012, respectively.

(3) The deviation rate of classified data in 2010 and 2017 is not large. Among them, woodland landscape has the smallest deviation rate, followed by construction land landscape, while other land landscape has the largest deviation rate. However, due to the small proportion of other land landscape in remote sensing image, it has little significance in practical application.

ACKNOWLEDGEMENTS

This work was not supported by any funds. The authors would like to show sincere thanks to those techniques who have contributed to this research.

REFERENCES

[1] Samer, M. (2013) Towards the implementation of the green building concept in agricultural buildings: a literature review. Agricultural Engineering International: The CIGR E-journal. 15(2), 25-46.
[2] Hatch, L.T., Fristrup, K.M. (2009) No barrier at the boundaries: implementing regional frameworks for noise management in protected natural areas. Marine Ecology Progress. 395, 223-244.
[3] Aditjandra., Teguh, P. (2013) The impact of urban development patterns on travel behaviour: lessons learned from a British metropolitan region using macro-analysis and micro-analysis in addressing the sustainability agenda. Research in Transportation Business & Management. 7, 69-80.
[4] O'Neill, R.V., Riitters, K.H., Wickham, J.D., Jones, K.B. (2001) Landscape pattern metrics and regional assessment. Ecosystem Health. 5(4), 225-233.
[5] Dorner, B., Lertzman, K., Fall, J. (2002) Landscape pattern in topographically complex landscapes: issues and techniques for analysis. Landscape Ecology. 17(8), 729-743.
[6] Musaoglu, N., Seker, D.Z., Kabdasli, S., Kaya, S., Duran, Z. (2004) Using remote sensing and GIS for the assessment of visual attributes: a case study of the south coastal zone of Turkey. Fresen. Environ. Bull. 13(9), 854-859.
[7] Efe, R., Soykan, A., Soenmez, S., Cuerebal, I. (2008) Quantifying the effect of landuse change on olive tree cultivation in the vicinity of Edremit between 1979 and 2006 using GIS and RS techniques. Fresen. Environ. Bull. 17(6), 696-704.
[8] Mander, L., Jongman, R. (1998) Human impact on rural landscapes in central and northern Europe. Landscape & Urban Planning. 41(3-4), 149-153.
[9] Carone, M.T., Simoniello, T., Coppola, R., D 'Emilio, M., Macchiato, M. (2010) Analysis of landscape structure and connectivity at watershed scale. Fresen. Environ. Bull. 19(10), 2361-2366.
[10] Yildirim, M., Topkaya, B. (2006) Pollution potential of ground-water resources in Antalya city. Fresen. Environ. Bull. 15(9A), 981-988.
[11] Alexakis, D.D., Agapiou, A., Hadjimitsis, D.G., Retalis, A. (2012) Optimizing statistical classification accuracy of satellite remotely sensed imagery for supporting fast flood hydrological analysis. Acta Geophysica. 60(3), 959-984.
[12] Lee, J.T., Elton, M.J., Thompson, S. (1999) The role of GIS in landscape assessment: using land-use-based criteria for an area of the chiltern hills area of outstanding natural beauty. Land Use Policy. 16(1), 23-32.
[13] Abdullah, S.A., Nakagoshi, N. (2006) Changes in landscape spatial pattern in the highly developing state of Selangor, peninsular Malaysia. Landscape and Urban Planning. 77(3), 263-275.
[14] Demirel, Z., Oezer, Z., Oezer, O. (2010) Nitrogen and phosphate contamination stress of groundwater in an internationally protected area, the Gksu Delta, Turkey. Fresen. Environ. Bull. 19(11), 2509-2517.
[15] Usher, M.B. (2001) Landscape sensitivity: from theory to practice. Catena. 42(2-4), 375-383.
[16] Bahceci, I., Topkaya, B. (2008) Landfill site selection using GIS methods. Fresen. Environ. Bull. 17(11), 1859-1867.
[17] Baker, F., Smith, C. (2019) A GIS and object based image analysis approach to mapping the greenspace composition of domestic gardens in Leicester, UK. Landscape and Urban Planning. 183, 133-146.
[18] Niren, T. (1999) An impact analysis of shifting cultivation in the forest of northern Laos using GIS and satellite image. Hydrology & Earth System Sciences Discussions. 6(1), 1197-1231.
[19] Shibasaki, R. (1991) Comparison of functions of GIS software in using image information. Journal of the Japan Society of Photogrammetry. 30(6), 54-64.
[20] Azuma, E., Furusawa, T., Kojima, K., Watanabe, T., Ohgishi, T. (1987) High photosensitivity frame transfer CCD image sensor. Itej Technical Report. 10, 25-30.
[21] Baban, S., Yusof, K.W. (2001) Mapping land use/cover distribution on a mountainous tropical island using remote sensing and GIS. International Journal of Remote Sensing. 22(10), 1909-1918.
[22] Gisolf, F., Malgoezar, A., Baar, T., Geradts, Z. (2013) Improving source camera identification using a simplified total variation based noise removal algorithm. Digital Investigation. 10(3), 207-214.

Received: **12.04.2021**
Accepted: **17.05.2021**

CORRESPONDING AUTHOR

Chunjie Wang
Laboratory XYZ
Jincheng College of Sichuan University
Chengdu Sichuan 611731 – China

e-mail: 16004500@qq.com

© by PSP Volume 30– No. 09/2021 pages 10970-10975 Fresenius Environmental Bulletin

GROWTH PERFORMANCES OVER A SLOPE RANGE IN NATURAL REPRODUCTIONS OF ANATOLIAN BLACK PINE

Yunus Eser*

Atabey Vocational School of Isparta University of Applied Sciences, Isparta, Turkey

ABSTRACT

Seedling height (SH), root-collar diameter (RCD), and number of reproductions (NR) were examined in two years natural regeneration areas sampled over a slope (S) range (low, S<15%; middle, 30%>S>15%; high, S>30%) of Anatolian black pine [*Pinus nigra* Arnold. subsp. *pallasiana* (Lamb.) Holmboe] to contribute to silvicultural practices of the species in this study.

Large differences supported also by analysis of variance (ANOVA) were found for SH, RCD and NR among slope ranges and within range. Middle slope showed highest SH (14.49 cm) and RCD (5.32 mm) performances, while they were lowest (11.87 cm and 4.69 mm) in the highest slope. Numbers of reproduction were ordered, 0.58 /m^2, 0.27 and 0.18 seedlings from low to high slope.

Results of ANOVA showed statistically significant ($p<0.05$) differences among slope ranges and within range for SH and RCD. Positive and significant ($p<0.05$) relations were found between SH and RCD in sampled areas and slope range.

Results of the study were discussed based on climate change, and silvicultural practices of the species.

KEYWORDS:
Climate, *Pinus nigra*, regeneration, seedling, silviculture

INTRODUCTION

Natural regeneration and artificial regeneration included afforestation or reforestation by plantation and seeding are main methods of sustainable forestry and conversion of degraded forest to productive forest. The regeneration methods and their combinations have advantage and disadvantage against each other such as transmitting of present genetic diversity to next generation naturally, and increasing of forest productivity by artificially. It is well discussed based on climate change for sustainable forestry recently to establish forest resistance to biotic and a-biotic damages recently. Many environmental and biological factors could be effective on success of the methods, sustainable forestry and forestry practices [i.e., 1, 2, 3, 4, 5, 6, 7, 8]. Anatolian black pine [*Pinus nigra* Arnold. subsp. *pallasiana* (Lamb.) Holmboe] is one of the most important commercial and ecological tree species used afforestation practices widely, which has 2.84 million ha productive and totally 4.35 million ha natural distribution in 22.74 million ha in Turkish forestry according to the latest forest inventory [9]. The species is used widely in afforestation practices in Turkish forestry [10]. Besides, Black pine (*Pinus nigra* Arnold.) has wide natural spread around the world at 40° east longitude in Turkey, west longitude 5° in Spain and Morocco, 35° north latitude in Morocco and Cyprus island, between latitude 35° north in Crimea and 48° north in Austria [11]. Climate change could be more effective on the species because of its large distribution, sustainability, and its decision on regeneration methods. Shelter wood method of cutting, which included preparatory, seed, light and removal cuttings, is suggested for natural regeneration in productive forests of the species by 80-120 seed tree/ha, and clear cutting method for degraded forest area [2]. Similar methods are also suggested by Odabaşı et al. [4]. However, while many studies were carried out on artificial regeneration practices included afforestation and nursery techniques [i.e., 5, 6, 8, 12, 13, 14, 15, 16], there were limited studies on natural regeneration practices [i.e., 3, 17, 18, 19, 20].

It was aimed to contribute natural regeneration practices, and to compare to early results of afforestation practices, and to discuss based on global warming in the study.

MATERIALS AND METHODS

Natural regeneration area. Studied natural regeneration area was selected from natural distribution of Anatolian black pine at southern part of Turkey in a restricted area to minimize effect of other biotic and a-biotic factors (Figure 1). The area was divided into three slope (S) ranges as low (S<15%), middle (30%>S>15%) and high (S>30%). Three areas, which was 300 m^2 (30 m x 10 m) each, were sampled chosen randomly from each slope range (Figure 2, Table 1).

Data collection. Height (SH) and root-collar diameter (RCD) of all natural reproductions were

measured at each sampled areas of slope range, together with counting of total and deformed numbers of reproductions (NR) (Figure 3) at end of growing period of 2020.

Data analysis. Collected morphological data (SH and RCD) was analyzed by one-way analysis of variance (ANOVA) to compare sampled areas and slope range. Sampled areas and slope range were grouped by Duncan's multiple range' test [21] for SH and RCD. Pearson' phenotypic correlation analysis was performed to estimate relation between SH and RCD.

RESULTS AND DISCUSSION

Seedling height (SH) and root-collar diameter (RCD). SH and RCD showed large differences among slope ranges and among sampled areas within slope range (Table 2, Figure 4). SH (14.49 cm) and RCD (5.32 mm) showed highest growth performances in middle slope, while they were lowest (11.87 cm and 4.69 mm) in the highest slope. They were between 13.21 cm (L2) and 27.41 cm (M2) for SH, and ranged from 4.03 mm (H1) to 10.72 mm (M2) for RCD in individual sampled areas (Table 2, Figure 4). The variation showed importance of mother tree and local forestry practices. Averages height and root collar diameter were 253 cm and 78 mm at 11 years in natural regeneration areas of the species, 23 cm and 7.8 mm annual height and annual increment [20]. Averages of seedling height and root-collar diameter were 13.3 cm and 27.6 cm; 5.2 mm and 6.33 mm at 2+0 and 3+0 year of bare-root seedlings of Anatolian black pine, respectively [22].

RCD had higher variation than SH in all slope range and sampled areas except of L2, M2 and M3 (Table 2). It showed mother tree were more effective on RCD than SH. RCD was an important morphological characteristics for absorbing water from ground and to establish resistance forest to climate change based on natural selection, and sustainable forestry.



FIGURE 1
Natural regeneration area at middle slope

TABLE 1
Geographic information of the sampled areas

Slope	Sampled area	Latitude (N)	Longitude (E)	Altitude (m)	Aspect
Low (S<15%)	L1	41°98'36"	28°29'83"	1410	Northeast
	L2	41°98'32"	25°30'41"	1445	Northeast
	L3	41°98'28"	25°30'19"	1395	Northeast
Middle (30%>S>15%)	M1	41°98'37"	25°25'14"	1455	Northwest
	M2	41°98'36"	25°25'42"	1475	Northwest
	M3	41°98'40"	25°25'69"	1460	Northwest
High (S>30%)	H1	41°98'41"	25°25'92"	1520	North
	H2	41°98'37"	25°26'92"	1490	North
	H3	41°98'36"	25°26'51"	1510	North



FIGURE 2
Some of sampled areas in the study

TABLE 2
Averages and coefficient of variation (CV %) of SH and RCD in sampled areas

Sampled areas	SH		RCD	
	Average	CV	Average	CV
L1	20.04[b]	86.48	6.73[b]	101.52
L2	13.21[a]	42.01	4.09[a]	40.59
L3	16.69[ab]	66.45	5.19[a]	73.99
Low	**16.78[a]**	**30.10**	**5.42[a]**	**93.17**
M1	20.18[b]	62.83	6.91[b]	64.83
M2	27.41[c]	64.76	10.72[c]	61.47
M3	20.98[b]	59.83	7.73[b]	55.89
Middle	**22.38[b]**	**64.75**	**8.18[b]**	**65.04**
H1	14.26[a]	28.47	4.03[a]	34.24
H2	15.36[a]	42.64	4.20[a]	50.24
H3	20.33[b]	85.98	7.07[b]	99.43
High	**16.81[a]**	**70.61**	**5.21[a]**	**90.02**
General	**18.25**	**73.97**	**6.11**	**85.27**

*; The same letters showed not significantly different at p>0.05



FIGURE 3
Measured natural reproductions in the sampled areas

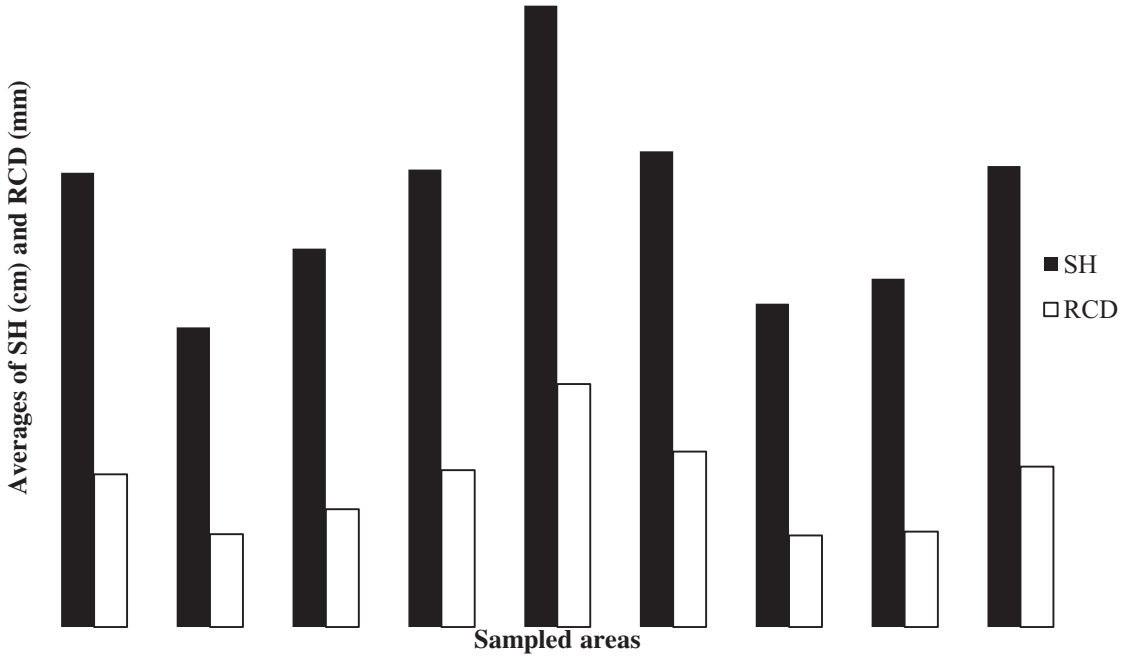


FIGURE 4
Averages of SH and RCD in the sampled areas

Statistically significant ($p<0.05$) differences were found among slope ranges and within range according to analysis of variance. Middle slope range and M2 sampled area were different than others based on results of Duncan's multiple range' test (Table 2). Significant ($p<0.05$) differences among sampled plots were also reported in natural regeneration areas of the species for height, root collar diameter terminal shoot height [20]. Many factors could be effective on growth performances of natural reproductions such as natural distribution of the species [1], canopy [17].

Positive and significant ($p<0.05$) relation between SH and RCD were estimated in slope range and sampled areas, and their combinations by analysis of correlation. It was also found among height, root collar diameter in natural reproduction of Anatolian black pine [20], and 2+0 and 3+0 year of bare-root seedlings of Anatolian black pine, respectively [22].

TABLE 3
Number of seedlings (NS) in sampled areas

Sampled areas	Deformed reproductions (%)	NS/m^2	NS
L1	2.24	0.74	223
L2	1.49	0.67	201
L3	2.04	0.33	98
Low	**1.92**	**0.58**	**522**
M1	3.60	0.37	111
M2	-	0.22	67
M3	1.52	0.22	66
Middle	**2.05**	**0.27**	**244**
H1	-	0.20	61
H2	2.33	0.14	43
H3	-	0.21	62
High	**0.60**	**0.18**	**166**
General	1.72	0.35	932

Number of reproductions (NR). Number of natural reproductions could play important roles in future tending process (e.g., thinning) in forestry for artificial selection by foresters or natural selection by global warming or other biotic and a-biotic factors. Averages of numbers of reproduction per m^2 were 0.58 in low slope, 0.27 in middle and 0.18 in high, and 0.35 in polled sampled areas (Table 3). It could be said that low slope was close to successful regeneration practices [23]. It was emphasized importance of seeding support and other artificial regeneration practices for middle and high slope. Number of natural reproductions was reported 0.36 in natural regeneration areas of the species at regeneration stage [20]. However, percentages of degraded reproductions were 1.92, 2.05 and 0.60 in low, middle and high slope, respectively (Table 3). It was found 28%, 46% and 19% in natural regeneration areas of Anatolian black pine [20]. However, there could be many environmental and biological factors on number of reproductions such as good seed year [3, 18]. NR could be balanced by combination of natural and artificial regeneration practices.

CONCLUSIONS

Variation of SH, RCD and NR among sampled areas within slope range emphasized importance of mother tree or also called seed tree. Differences among slope ranges showed obligation of local forestry practices. Insufficient NR could be supported by artificial regeneration practices.

There could be many factors effective on growth performance and number of natural reproductions. However, present study was conducted only on slope range. New studies should be carried out on effect of regeneration practices of other environmental and biotic factors such as aspect, altitude, genetic structure of mother tree.

ACKNOWLEDGEMENTS

The author thank to PhD. student Samet Dirlik for their help during data collection.

REFERENCES

[1] Saatcioglu, F. (1976) Silviculture-I. Forestry Faculty of Istanbul University press, Istanbul. 1-423.
[2] Ata, C. (1995) Silviculture Technique. Bartin Forestry Faculty of Zonguldak Karaelmas University press, Bartin. 1-281.
[3] Guner, S.T. (2001) An evaluation on the natural regeneration works at the stands of Anatolian black pine in Afyon forest district. Journal of Forestry Faculty of Suleyman Demirel University. 2, 61-74.
[4] Odabasi, T., Caliskan, A. and Bozkus, H.F. (2007) Silviculture Technique (Silviculture-II). Forestry Faculty of Istanbul University press, Istanbul. 1-314.
[5] Ozkan, K., Gulsoy, S. and Mert, A. (2008) Interrelations between height growth and site characteristics of *Pinus nigra* Arn. subsp. *pallasiana* (Lamb.) Holmboe. J. the Malaysian Forester. 71, 9-16.
[6] Ozel, H.B., Ertekin, M. and Tufanoglu, G.C. (2010) Investigation of relationship between some climate factors and height increment in Black pine (*Pinus nigra* Arnold. ssp. *pallasiana* (Lamb.) Holmboe) and Scotch pine (*Pinus sylvestris* L.) afforestarions in the Devrek-Akcasu district. Ecological Life Science. 5(4), 376-389.
[7] Gulsoy, S., Suel, H., Celik, H., Ozdemir, S. and Ozkan, K. (2014) Modelling site productivity of Anatolian black pine stands in response to site factors in Buldan District, Turkey. Pakistan Journal of Botany. 46(1), 213-220.

[8] Guner, S.T., Comez, A., Ozkan, K., Karatas, R. and Celik, N. (2016) Modelling the productivity of Anatolian black pine plantations in Turkey. Journal of the Faculty of Forestry Istanbul University. 66(1), 159-172.
[9] General Directorate of Forestry (OGM) (2019) Forestry Statistics-2019. www.ogm.gov.tr. 1-17. (Date of Access: 11.04.2021).
[10] Ayan, S., Yer, E.N. and Gulseven, O. (2017) Evaluation of Taurus cedar (*Cedrus libani* A. Rich.) afforestation areas in Turkey in terms of climate type. Artvin Coruh University Journal of Forestry Faculty. 18(2), 152-161.
[11] Critchfield, W.B. and Little, E.L. (1966) Geographic Distribution of the Pines of the World. USDA Forest Service, Misc. Publication, Washington. 1-97.
[12] Kizmaz, M. (1993) Research on the determination of quality classifications of Crimean pine seedlings. Technical Bullettin of Forest Research Institute. 7(36), 238-241.
[13] Dirik, H. (994) Ecophysiological analysis of transpiration attitudes of three native pine (*Pinus brutia* Ten., *Pinus nigra* Arn. ssp. *pallasiana* Lamb. Holmboe, *Pinus pinea* L.) Species. Journal of the Faculty of Forestry Istanbul University. 44, 111-121.
[14] Ucler, A.O., Gulcu, S. and Bilir, N. (2000) Interaction between seed sources and seedling properties on Brutian pine (*Pinus brutia*) and Black pine (*Pinus nigra*). Second Seedling Symposium. Ege University, 25-29 September, Izmir, Turkey. 39-45.
[15] Gulcu, S. and Ucler, A.O. (2008) Genetic variation of Anatolian black pine (*Pinus nigra* Arnold. subsp. *pallasiana* (Lamb.) Holmboe) in the lakes district of Turkey. Silvae Genetica. 57, 1-5.
[16] Akcakaya, M. (2011) Genetic diversity of forestation trials with ten populations of Anatolian balck pine (*Pinus nigra* Arnold. subsp. *pallasiana* (Lamb) Holmboe) (9 year results), Graduate School of Natural and Applied Science, Suleyman Demirel University, MSc. Thesis, Isparta, Turkey.
[17] Genc, M. (1994) Growth characteristics of advanced regeneration of Black pine (*Pinus nigra* Arnold. subsp. *pallasiana*). Tubitak Turkish Journal of Agriculture and Forestry. 18, 487-493.
[18] Boydak, M., Caliskan, F. and Bozkus, H.F. (2002) Seed crop and its variation of *Pinus nigra* Arnold. subsp. *pallasiana* in Dursunbey-Alacam locality. Journal of the Faculty of Forestry of Istanbul University. 52(2), 1-26.
[19] Yilmaz, M. and Kalkan, M. (2019) Application of the seed tree regeneration method in Anatolian Black Pine (*Pinus nigra* subsp. *pallasiana*), the case of Tandir-Eskisehir. Turkish Journal of Forest Science. 3(1), 24-36.
[20] Ertugrul, G.S. and Bilir, N. (2020) Evaluation on natural regenerations in Kutahya-Simav district of Anatolian black pine. Artvin Coruh University Journal of Forestry Faculty. 21(1), 75-81.
[21] Duncan, D.B. (1955) Multiple range and multiple F tests. Biometrics. 11, 1-42.
[22] Tebes, N.T., Seyedi, N. and Bilir, N. (2015) Morphological characteristics and quality in Black pine (*Pinus nigra* Arn. ssp. *pallasiana*) seedlings. International Journal of Latest Research in Science and Technology. 4(6), 7-9.
[23] Eler, U., Genek, A. and Yildirim, K. (1988) Effects of early final cutting and (*Pinus nigra* Arnold.) regenerations. Forest Research Institute press. Technical Report No.42, Ankara. 1-42.

Received: **14.04.2021**
Accepted: **24.05.2021**

CORRESPONDING AUTHOR

Yunus Eser
Atabey Vocational School of Isparta University of Applied Sciences,
Isparta – Turkey

e-mail: yunuseser@isparta.edu.tr

© by PSP Volume 30– No. 09/2021 pages 10976-10982 Fresenius Environmental Bulletin

CYTOGENETICS ANALYSES OF THE GENUS SPERMOPHILUS CUVIER 1825 (MAMMALIA RODENTIA) DISTRIBUTED IN TURKEY

Safak Bulut[1,*], Cemil Arslan[2]

[1]Department of Molecular Biology and Genetics, Hitit University, Corum, Turkey
[2]Kiziltepe Anadolu Imam Hatip High School, Kiziltepe, Mardin, Turkey

ABSTRACT

Cytogenetic analysis were studied on three species of the genus *Spermophilus* distributed in Turkey (*S. citellus, S. xanthoprymnus* and *S. taurensis*). Different chromosomal features occurring in different subpopulations of *S. xanthoprymnus*, which has a wide distribution area in Anatolia and the lack of Turkey's population of banded chromosome studies in *S. citellus* and the fact that different chromosome morphologies are still encountered in the *S. taurensis* population led us to carry out this study. In this study, G, C and Ag-NORs banding of *S. xanthoprymnus*, sampled from Bolkar Mountains, and *S. citellus* from Turkish Thrace were performed. The C-banding patterns and Ag-NORs chromosome features was given for the first time from the samples of *S. citellus* from Turkey. In addition, new chromosomal features of *S. taurensis*, an endemic species, were also presented.

In this study, diploid chromosome number of *S. xanthoprymnus* was 2n=42, fundamental chromosome number (NF) was 82, autosomal chromosome number (NFa) was 78, while C banding revealed a heterochromatin region in one chromosome. Because of Ag-NOR staining of *S. xanthoprymnus*, eight NOR stains were determined in the male sample, and we detected six NOR stains in the female sample. The diploid chromosome number of S. citellus species was determined as 2n=40, NF=77, NFa=74, while C banding revealed a heterochromatin area in two chromosomes. As a result of Ag-NOR staining of *S. citellus* species, seven NOR staining were detected. *S. taurensis* species, diploid chromosome number was determined as 2n=40, NF=80 and NFa=76.

The G, C banding patterns and Ag-NORs chromosome features was given for the first time from the samples of *S. citellus* obtained from Turkish Thrace. In addition, new chromosomal features of *S. taurensis*, an endemic species, were also presented.

KEYWORDS:
Spermophilus, Ag-NORs, C-banding, Karyotype

INTRODUCTION

169 mammal species living in Turkey, 66 of them belong to the rodent order of these mammals [1]. The genus of Eurasian sciurids *Spermophilus* Cuvier, 1825 has 12 species that are endemic to Eurasia [2-4]. Three species are distributed in Turkey which *S. xanthoprymnus* is wide-distributed over the Anatolia [5] and recently described *S. taurensis* is endemic to Turkey [6,7], and *S. citellus* is known from Turkish Thrace [8,9].

The genus Spermophilus was first named Mus by Linneus in 1766, *Citellus* by Oken in 1816, and *Spermophilus* by Cuvier in 1825. While Ellerman and Morrison-Scott [10] claimed that the use of the name *Citellus* was necessary, Corbet [11] noted that the date Oken was given the name *Citellus* in 1816 was not accepted, and the name was *Spermophilus*, given by Cuvier in 1825 [10,11]. Bennet (1835) was described a new species named *Citellus xanthoprymnus* from Turkey in Erzurum province, then Ellerman and Morrison-Scott [10] and Corbet [11] stated that only *Spermophilus citellus* was distributed in Turkey and they considered that species as *Spermophilus citellus xanthoprymnus* subspecies [10,11]. It was argued that *S. xanthoprymnus* was a different species, claiming that *S. xanthoprymnus* has a different karyological feature than *S. citellus* [10]. Doğramacı et al. [8] revealed that *Spermophilus citellus* with 2n=40 chromosomes in Thrace, and S. xanthoprymnus species with 2n=42 chromosomes in Anatolia [8].

According to Özkurt et al. *S. xanthoprymnus* with 2n=40 was found in the Akseki (Antalya province) population [13]. Later, Yiğit [14] evaluated the biometric and genetic differences on these population differences, which Özkurt [13] were suggestted. They suggested conducting chromosome banding studies of the Akseki population [14]. Arslan [15] carried out karyological studies (C-banded and Ag-NORs) on *S. xanthoprymnus* samples collected from Anatolia (Konya) [15]. With these data, we observed that the fundamental number of autosomal arms was not the same in samples from Thrace (NFa=66) and Taurus (NFa=72) [9]. Gündüz et al. [6], *S. citellus* is in the Turkish Thrace but also in Central and Eastern

Anatolia have observed that there is *S. xanthoprymnus*, has also been named as a new species *S. taurensis* with 2n=40 from Akseki [6]. At the same time, *S. torosensis* were recognized as a new species from Akseki [7]. Gündüz et al. [16] later showed that *S. torosensis* species and *S. taurensis* species have subjective synonyms and stated that the current name of the species is *S. taurensis* [16]. Later, G and C banded chromosome features [17] and C-banding and Ag-NORs banded chromosome features were studied of Taurus ground squirrel [18]. Arslan et al. [19], a difference was detected in the Y chromosomes of Gümüşhane and the Bitlis populations of *S. xanthoprymnus*. In addition, different C positive bands were observed in the autosomes and X chromosomes, and it was determined that this difference might be because of intrachromosomal translocation [19].

Two different karyotypes were determined as 2n=40, NF=78, NFa=74 and 2n=40, NF=69, NFa=76 in S. citellus [2, 5, 6, 7, 9]. Chassovnikarova et al. [20] compared the sex chromosome variances in S. citellus species in the southeast of the Balkan Peninsula. They observed that the Y chromosome appears to be a dot, with the exception of a few small and medium-sized acrocentric and metacentric chromosomes in most of the sample [20].

Different chromosomal features occurring in different subpopulations of *S. xanthoprymnus*, which has a wide distribution area in Anatolia and the absence of Turkey's population of banded chromosome studies in S. citellus and the fact that different chromosome morphologies are still encountered in the S. taurensis population led us to carry out this study. With this study, G, C and Ag-NORs banding of *S. xanthoprymnus*, sampled from Bolkar Mountains, and S. citellus was performed. The G, C banding patterns and Ag-NORs chromosome features was given for the first time from the samples of *S. citellus* obtained from Turkish Thrace. In addition, new chromosomal features of *S. taurensis*, an endemic species, were also presented.

MATERIALS AND METHODS

Samples of *S. xanthoprymnus* were collected from Meydan Plateau of Bolkar Mounts (Niğde Prov.); of *S. taurensis*, endemic to Anatolia; from Mt. Central Taurus (Karaman Prov.); and of *S. citellus*, Enez District (Edirne Prov.) between 2018 and 2019, using Tomahawk live traps (Figure 1). All samples were prepared as standard museum vouchers and deposited in the Mammalogy Collection of Hitit University. This study was approved by the Ethics Committee of Niğde University (approval no. 86837521-50.99-E.387)

Karyotypes were prepared using Ford and Hamerton's Colchicine Hypotonic Citrate technique to avoid false diagnoses by looking at their morphology and to determine their karyological traits [21]. Chromosomes were extracted from bone marrow cell suspensions stained with a 4% Giemsa solution by a standard air-drying method modified from Lee and Elder [22]. Ag-NOR bands were obtained by the modified technique of Howell and Black [23], and C bands by the technique of Sumner [24]. The number of diploid chromosomes (2n), the number of fundamental chromosome arms (NF) and the number of autosomal chromosome arms (NFa) were determined by examining approximately 20 metaphase spreads of each sample with the 100x immersion objective. Photographs of suitable metaphase spreads were taken and karyological traits were determined. Karyotypes were arranged in pairs according to their size and centromere position from the best metaphase spreads. The number of fundamental chromosome arms (NF) and number of autosomal chromosome arms (NFa) were computed by counting bi-armed autosomes as two arms and acrocentric autosomes as one arm. Chromosome morphologies were determined according to the centromere position as Acrocentric (a), Subtelocentric (st), Submetacentric (sm) and Metacentric (m) chromosomes were subtracted [25].



FIGURE 1

Localities of the collected material of *Spermophilus*. *S. xanthoprymnus* (●):1. Niğde Prov., Meydan Plateau; *S. taurensis* (■): 2. Karaman Prov., Büyük Yayla; *S. citellus* (▲): 3. Edirne Prov., Enez.

RESULTS

***Spermophilus citellus* (Linnaeus, 1766) European Souslik.** Diploid chromosome number obtained from male individual of *S. citellus* was determined as 2n = 40. The fundamental chromosome arm number (NF) was 77 and the autosomal chromosome arm number (NFa) was 74. Y chromosome was recorded acrocentric and point-shaped, X chromosome submetacentric (Table 1).

Heterochromatin area was detected on two chromosomes of *S. citellus* sample (subtelocentric chromosome number 11 and acrocentric chromosome number 17).

As a result of NOR banding performed with sample taken from a male individual of the *S. citellus*, 7 NOR staining was detected on chromosome 14, 16, 17th pairs and one on chromosome 15th (Table 2).

***Spermophilus xanthoprymnus* (Bennett, 1835) Anatolian Souslik.** Diploid chromosome number was determined as 2n = 42 after karyotype analysis with male and female individuals taken from *S. xanthoprymnus*. The fundamental chromosome arm number (NF) was 82, and the autosomal chromosome arm number (NFa) was 78. The X chromosome was double-armed and metacentric, while the Y chromosome was the smallest and point-shaped (Table 1).

As a result of C banding, a heterochromatin area (subtelocentric chromosome number 12) was detected. As a result of NOR banding performed with a female sample taken from male individuals, a total of 8 NOR staining was detected in pairs of 9, 10, 11, and 12nd chromosomes (Table 2).

***Spermophilus taurensis* (Gündüz et al., 2007) Taurus Souslik.** In the analysis performed with the female sample of *S. taurensis*, the diploid chromosome number was determined as 2n = 40, the fundamental chromosome arm number (NF) was 80 and the autosomal chromosome arm number (NFa) was 76. The X chromosome was recorded as double-armed and metacentric (Table 1).

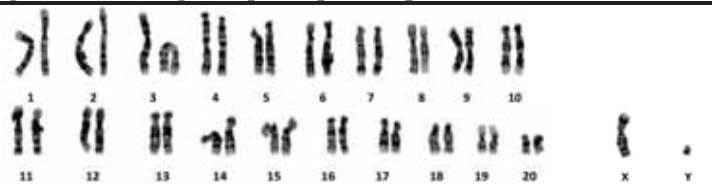
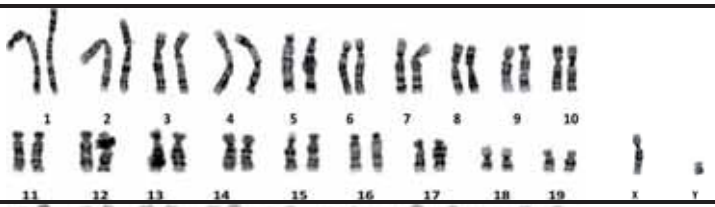
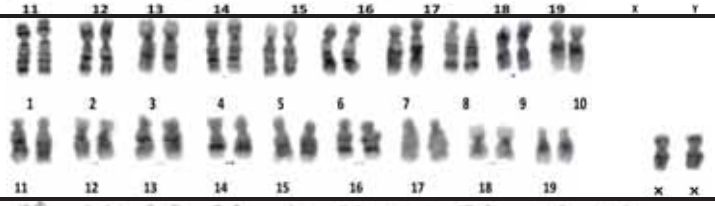
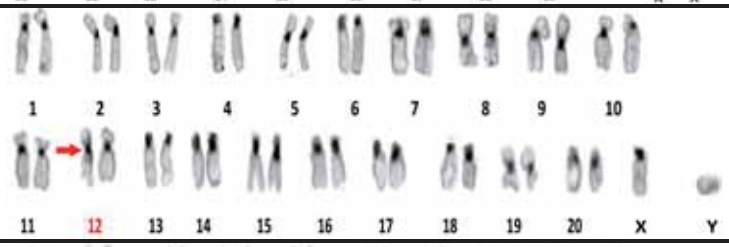
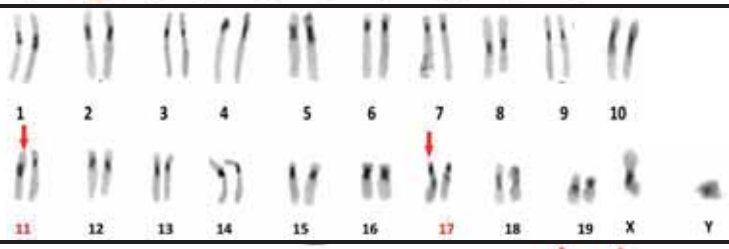
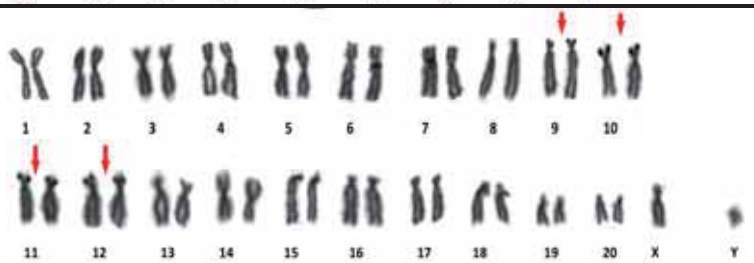
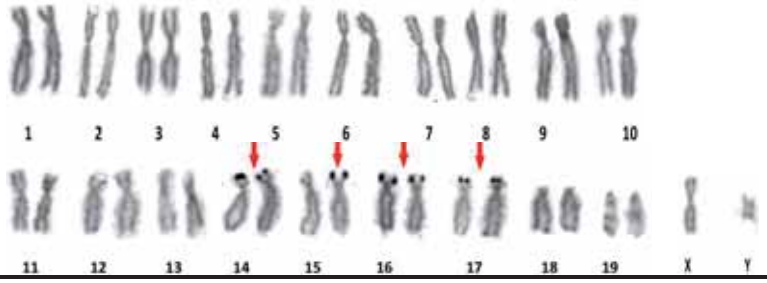
DISCUSSION

In chromosomal studies performed on Anatolian Souslik, the number of chromosomes 2n = 42 was recorded [13, 14, 6, 19]. Arslan [15] found the diploid chromosome number as 2n = 42 and the fundamental chromosome number (NF) as in previous studies with the *S. xanthoprymnus* sampled from Konya (Selçuk) province in the Central Anatolia, using C banding and Ag-NOR banding techniques and recorded the number of autosomal arms (NFa) as 78.

TABLE 1
Chromosome features of *Spermophilus* species distributed in Turkey

	S. citellus ♂	*S. xanthoprymnus* ♂	*S. taurensis* ♀
1	sm	sm	sm
2	sm	sm	sm
3	sm	sm	sm
4	sm	st	sm
5	st	st	sm
6	st	st	st
7	sm	st	st
8	m	sm	st
9	sm	m	m
10	sm	st	sm
11	st	st	st
12	st	st	sm
13	st	st	st
14	st	st	sm
15	st	sm	st
16	st	st	st
17	a	st	st
18	m	st	m
19	sm	m	st
20	-	a	-
X	sm	sm	m
Y	a	a	-

TABLE 2
G, C and Ag-NOR bandings of *Spermophilus* species distributed in Turkey

	S. xanthoprymnus♂	
G banded	*S. citellus* ♂	
	S. taurensis ♀	
	S. xanthoprymnus♂	
C banded	*S. citellus* ♂	
	S. xanthoprymnus	
Ag-NORs	*S. citellus* ♂	

It was observed that *S. xanthoprymnus* had 2 metacentric, 7 submetacentric, 10 subtelocentric, one acrocentric chromosomes. X chromosome was determined submetacentric and Y chromosome was determined acrocentric. Arslan [15] found the heterochromatin region in all autosomes as a result of C banding, and pericentromeric heterochromatin area on the X chromosome. As a result of Ag-NOR staining, he recorded that NOR stain in 3 pairs of autosomal chromosomes. As a result of our C

banding findings, one heterochromatin area was determined in female and male *S. xanthoprymnus* samples, while in our Ag-NOR staining result, NOR staining was detected in 4 pairs of chromosomes. When we compared the results, it was seen that his C banding and Ag-NOR banding results were different from our banding results [15].

Arslan et al. [19] found differences in some chromosomes in their karyotype analysis comparisons with *S. xanthoprymnus* samples where they obtained from Gümüşhane and Bitlis provinces. They recorded the diploid number of chromosomes as 2n = 42, the fundamental chromosome number (NF) as 84 and the number of autosomal arms (NFa) as 80. It was observed that *S. xanthoprymnus* had 2 metacentric, 9 submetacentric and 9 subtelocentric chromosomes in the chromosome morphology sequence. X chromosomes are medium-sized and submetacentric. While the Y chromosome was observed as a point in Bitlis samples, the Y chromosome in Gümüşhane samples was determined as two-armed and subtelocentric [19]. In our study, it was observed that the Y chromosome morphology was similar to the samples of the Bitlis province, and it was different from the population samples of Gümüşhane province. The fundamental chromosome number (NF) was determined as 82 and the autosomal chromosome number (NFa) as 78, and 2 metacentric, 5 submetacentric, 12 subtelocentric and one acrocentric chromosome were detected.

It was recorded that diploid chromosome number as 2n= 40, NF= 80 and NFa= 76 in cytogenetic studies performed with *S. taurensis* species. It was observed that there were 3 metacentric, 10 submetacentric, 6 subtelocentric chromosomes in the chromosome morphology sequence of *S. taurensis*. X chromosome was determined metacentric, and Y chromosome was determined acrocentric [13, 17, 18]. It has also been noted that the Y chromosome heterochromatin of *S. taurensis* is similar to that of the *S. citellus* species [18]. In our study with *S. taurensis* species, 2 metacentric, 8 submetacentric and 9 subtelocentric chromosomes were detected in chromosome morphology, and it was observed that it was different in terms of chromosome morphology. Since our C banding and Ag-NOR banding analysis results could not result in *S. taurensis* species.

Chassovnikarova et al. [20] found new data in their study by taking into account the sex chromosomes of samples taken from *S. citellus*. They determined differences in sexual chromosomes using G banding, C banding, special fluorescent dye and FISH techniques. Three different morphologies were observed for both the X and Y chromosomes. X chromosomes are classified as acrocentric, subtelocentric or submetacentric. In most of the analyzed samples, the Y chromosomes were identified as small or medium, but while several morphologies of the Y chromosomes were acrocentric and metacentric, other samples were observed similar to the point. While all autosomes and centromeric regions of the X chromosomes have heterochromatin blocks of different sizes, it has been noted that all Y chromosome variants are completely heterochromatic. Chassovnikarova et al. [20] attributed all these differences to variation between different populations. In our study with the *S. citellus* samples, while the X chromosome was submetacentric, the Y chromosome was determined as acrocentric and dot. In addition, we found heterochromatin region in one subtelocentric chromosome. When the results of Chassovnikarova et al. [20] were compared with our results, it was seen that although the X and Y chromosome morphologies were similar, the C banding results were different.

Doğramacı et al. [8] recorded the diploid chromosome number as 2n = 40, the fundemantal chromosome number (NF) as 78 and the autosomal arm number (NFa) as 74 in the karyological studies on *S. citellus* individuals obtained from Turkish Thrace. It was observed that *S. citellus* had 2 metacentric, 12 submetacentric, 4 subtelocentric and 1 acrocentric chromosome in chromosome morphology sequence. He determined the X chromosome metacentrically and the Y chromosome as two-armed and the smallest. In our study, the diploid chromosome number of *S. citellus* was found to be 2n = 40. The fundamental chromosome number (NF) was 77 and the number of autosomal arms (NFa) was 74. In our study, chromosome morphology sequence was determined as 2 metacentric, 8 submetacentric, 8 subtelocentric and 1 acrocentric chromosome. Doğramacı et al., [8] and our study, although the diploid chromosome number is similar, there are differences in chromosome morphologies, basic chromosome arm number and autosomal chromosome arm number. In addition, the Y chromosomes in our examples are acrocentric and point-shaped, not two-armed.

As a result of our study, no satellite was found in any chromosome. At the same time, no anomalies were found in any of the chromosomes. Unlike previous studies, different NOR numbers and regions with different heterochromatin in some chromosomes were detected in the chromosomes of species. In addition, non-similar numbers were detected in chromosome arm numbers. The reason for the differences in NOR differences detected between species, C positive heterochromatin area differences, fundamental chromosome arm number (NF) difference and autosomal chromosome arm numbers (NFa) may be related to mutations such as inversion, deletion and translocation. These numbers may vary because of these and similar mutations. In addition, geographical isolation or habitat difference may cause this difference.

TABLE 3
Karyological characteristics of genus *Spermophilus* species distributed in Turkey

Species	Localities and References	2n	NF	NFa	m	sm	st	a	X	Y
S. citellus	Yugoslavia [26, 27, 28], Moldavia [29], Bulgaria [30]	40	-	66	2	12 (sm or st)		5	biarmed or a	sm
	Czech Republic [12]	40	-	-	2	13 (sm or st)		4	D	biarmed
	Turkish Thrace [8]	40	78	74	2	12	4	1	m	biarmed and small
	Turkish Thrace [13]	40	69	66	2	12	-	5	sm	a
	This study	**40**	**77**	**74**	**2**	**8**	**8**	**1**	**sm**	**a**
S. taurensis	Akseki [13]	40	76	72	2	15	-	2	m	m
	Mut and Hadim [13]	40	76	72	2	15	2	-	m	a
	Hadim [17, 18]	40	80	76	3	10	6	-	m	a
	This study	**40**	**80**	**76**	**2**	**8**	**9**	**-**	**m**	**-**
S. xanthoprymnus	Ermenia [29, 31]	42	70	66	13	-	-	7	m	biarmed and small
	Bayburt, Çorum, Erzurum, Malatya ve Sivas [8]	42	67	64	1	7	4	8	m	the smallest
	Polatlı, Maden and Erzurum [13]	42	81	78	2	17	-	1	m	a
	Konya (Selçuklu) [15]	42	81	78	2	7	10	1	sm	a
	Bitlis [19]	42	84	80	2	9	9	-	sm	a
	Gümüşhane [19]	42	84	80	2	9	9	-	sm	st
	This study	**42**	**81**	**78**	**2**	**5**	**12**	**1**	**sm**	**a**

REFERENCES

[1] Özkurt, Ş.Ö., Bulut, Ş. (2020). Mammals of Turkey. Panama Publishing, Ankara. 456 pp. ISBN: 9786057739575 (in Turkish).

[2] Helgen, K.M., Cole, F.R., Helgen, L.E., Wilson, D.E. (2009). Generic revision in the holarctic ground squirrel genus *Spermophilus*. Journal of Mammalogy. 90(2), 270-305.

[3] Thorington Jr, R.W., Koprowski, J.L., Steele, M.A., Whatton, J.F. (2012). Squirrels of the world. JHU Press.

[4] Sinitsa, M.V., Pogodina, N.V. (2019). The evolution of early *Spermophilus* in eastern Europe and the antiquity of the Old World ground squirrels. Acta Palaeontologica Polonica. 64(3).

[5] Gür, M.K., Gür, H. (2010) *Spermophilus xanthoprymnus* (Rodentia: Sciuridae). Mammalian Species. 42(1), 183-194.

[6] Gündüz, İ., Jaarola, M., Tez, C., Yeniyurt, C., Polly, P.D., Searle, J.B. (2007a). Multigenic and morphometric differentiation of ground squirrels (*Spermophilus*, Scuiridae, Rodentia) in Turkey, with a description of a new species. Molecular Phylogenetics and Evolution. 43, 916-935.

[7] Özkurt, Ş., Sözen, M., Yiğit, N., Kandemir, I., Çolak, R., Gharkheloo, M.M., Çolak, E. (2007). Taxonomic status of the genus *Spermophilus* (Mammalia: Rodentia) in Turkey and Iran with description of a new species. Zootaxa. 1-15.

[8] Doğramacı, S., Kefelioğlu, H., Gündüz, I. (1994). Karyological analysis of the genus, *Spermophilus* (Mammalia: Rodentia) in Turkey. Tr. J. Zoology. 18, 167-170.

[9] Kryštufek, B., Vohralík, V. (2005). Mammals of Turkey and Cyprus. Rodentia I: Sciuridae, Dipodidae, Gliridae, Arvicolinae, Knjiznica Annales Majora, Koper, Slovenia. 1-292.

[10] Ellerman, J.R., Morrison-Scott, T.C.S. (1951) Checklist of Palaeartic and Indian Mammals 1758 to 1946. London. 1- 808.

[11] Corbet, G.B. (1978). The Mammals of the Palaearctic Region: a Taxonomic Review. British Museum (Natural History), Cornell University Pres, London and Ithaca.
[12] Zima, J., Kral, B. (1984). Karyotypes of European Mammals II. Acta Sc. Nat. Brno. 18, 1-62.
[13] Özkurt, Ş., Yiğit, N., Çolak, E. (2002). Karyotype variation in Turkish populations of *Spermophilus* (Mammalia: Rodentia). Mammalian Biol. 67, 117 –119.
[14] Yiğit, N., Neumann, K., Özkurt, S. (2005). Biometric and genetic evaluation of *Spermophilus* (Mammalia: Rodentia) populations in western Turkey. Israel J. Zool. 51, 191–198.
[15] Arslan, A. (2005). Cytogenetic studies on *Spermophilus xanthoprymnus* (Rodentia: Sciuridae) in Central Anatolia. Folia Zoologica. 54-3, 278-284.
[16] Gündüz, I., Jaarola, M., Tez, C., Yeniyurt, C., Polly, P.D., Searle, J.B. (2007b). Spermophilus torosensis Özkurt et al., 2007 (Sciuridae, Rodentia) is a subjective junior synonym of *Spermophilus taurensis* Gündüz et al., 2007, a newly described ground squirrel from the Taurus Mountains of southern Turkey. Zootaxa. 1663(1), 67-68.
[17] Matur, F. (2009). A cytogenetic study on the Taurus Ground Squirrel, *Spermophilus taurensis* Gündüz et al., 2007 (Mammalia: Rodentia), in Turkey. Zoology in the Middle East. 48(1), 103-105.
[18] Arslan, E., Arslan, A. (2010). Heterochromatin distribution and nucleolar organizer regions (NORs) in chromosomes of the Taurus ground squirrel. *Spermophilus taurensis* Gunduz et al., 2007 (Mammalia: Rodentia), in Turkey. Turk. J. Zool. 34, 105-110.
[19] Arslan, A., and Toyran, K., Gözütok, S. (2020). The Karyotype of Anatolian Ground Squirrel *Spermophilus xanthoprymnus* (Bennett, 1835) (Rodentia: Sciuridae) from two localities in Anatolia, Turkey. Acta Zool. Bulg. 72(3), 363-367.
[20] Chassovnikarova, T., Rovatsos, M., Atanasov, N., Koshev, J. (2015). Sex chromosome variability of *Spermophilus citellus* (Linnaeus, 1766) in the Southeastern part of the Balkan Peninsula. Mammalian Biology. 80, 365-371.
[21] Ford, C.E., Hamerton, J.L. (1956). A colchicine, hypotonic citrate, squash sequence for mammalian chromosomes. Stain Technology. 31(6), 247-251.
[22] Lee, M.R., Elder, F.F.B. (1980). Yeast stimulation of bone marrow mitosis for cytogenetic investigations. Cytogenetic and Genome Research. 26(1), 36-40.
[23] Howell, W.T. and Black, D.A. (1980). Controlled silver-staining of nucleolus organizer regions with a protective colloidal developer: a 1-step method. Experientia. 36(8), 1014-1015.
[24] Sumner, A.T. (1972). A simple technique for demonstrating centromeric heterochromatin. Exp. Cell Res. 75, 304-306.
[25] Hillis, D.M., Moritz, C. (1990). Molecular systematics. Sinauer Associates Inc. 159. Zivkovic, S., Soldatovic, B., Milosevic, M., Savic, I. (1968). Analysis of the chromosomes of the three populations of ground squirrel (Citellus citellus) from Serbia Zool. Anz. 181, 3–4, 181–185 (in Dutch).
[26] Savic, I., Milosevic, M., Zivkovic, S. (1971). Chromosomes of ground squirrel (*Citellus citellus* Linnaeus, 1766) from Yugoslavia. Arch. Biol. Nauka 23, 1–2, 35–37.
[27] Hsu, T.C., Benirschke, K. (2013). An Atlas of Mammalian Chromosomes: Volume 10 (Vol. 10). Springer Science and Business Media.
[28] Vorontsov, N.N., Lyapunova, E.A. (1969). The chromosomes of Palaearctic ground squirrels (*Citellus*, Mamotinae, Scuridae, Rodentia). In The Mammals (Evolution, Karyology, Taxonomy, Fauna). Edited by NN Vorontsov. Materials for the II All-Union Mammalogy Conference (Moscow, December, 1969), Novosibirsk (pp. 41-47).
[29] Belcheva, R.G., Peshev, D.T. (1979). Intersubspecific sex chromosome difference in *Citellus citellus* L.(Rodentia, Sciuridae). Experientia. 35(5), 595-596.
[30] Orlov V.N., Rodova M.A. Kotenvoka E.A. (1969). Chromosomal differentiation of the ground squirrels subgenus *Citellus*. Mat. II. vsesoj. sov. Po mlekopit. 48–49 (in Russian)

Received: **15.04.2021**
Accepted: **25.05.2021**

CORRESPONDING AUTHOR

Safak Bulut
Department of Molecular Biology and Genetics
Hitit University
Çorum 19040 – Turkey

e-mail: safakbulut@hitit.edu.tr

© by PSP Volume 30– No. 09/2021 pages 10983-10988 Fresenius Environmental Bulletin

A RESEARCH ON IMPROVING SEED QUALITY (PELLETING) IN TRUE POTATO OF 101 (NIF) GENOTYPE

Zeynep Dumanoglu[1,*], Gulsum Ozturk[2]

[1]Bingol University, Faculty of Agriculture, Department of Biosystem Engineering, 12000, Bingol, Turkey
[2]Ege University Faculty of Agriculture, Department of Field Crops, 35100, Izmir, Turkey

ABSTRACT

True potato is one of the most preferred crops in human diet. Mechanization is widely used in the production of potato which is reproduced vegetatively using its tubers. Generative reproduction, on the other hand, is done using potato seeds which are referred to as real potato seeds (RPS). This study aims at identifying the general features of the 101 (Nif) real potato seeds and the seed quality with pelleting which is known as a technique for increasing seed quality. Organic and inorganic materials were used as pelleting materials. Several physical (form, size, area, sphericity, thousand-grain-weight), physiological (seedling emergence and time), and mechanical (natural accumulation angle) quality parameters were examined. It was found that the pelleting technique increased the seed size by 1-1.5 times and the seed weight by 1.5 times in true potato seeds. Moreover, the pelleted seeds germinated (81.33%) more than the control group.

KEYWORDS:
True Potato Seed, *Solanum tuberosum* L., seed pelleting, seedling emergence

INTRODUCTION

Potato (*Solanum tuberosum* L.), an annual cash crop that belongs to the Solanaceae family, is native to the Andes in South America. Its tubers have an important place in human diet with the starch, proteins, minerals, and Vitamin C they include. Besides, it is processed and marketed as a food and industry raw material in different forms [1, 2]. Potato is produced both vegetatively (using its tubers) and generatively (using its seeds). While tubers are used in industrial potato production, seeds are not preferred in cultivation as they are very small and light. Although it is suggested that seeds be coated and then planted to overcome this shortcoming, no satisfying result has been achieved yet in this regard [3].

The technique of pelleting, one of the recent techniques used for enhancing seed quality, has been implemented on various plant seeds to increase the plantability of small, light, and amorphous seeds. Thanks to this technique, seeds get heavier and larger and take a homogeneous form [4]. Various materials are used in the pelleting process. It is of prime importance that seeds are coated homogenously [5] and coating does not prevent the seed from germination [6].

In a study carried out at National Honam Agricultural Experiment Station (NHAES) (1998) in Korea, sesame (*Sesamum indicum* L.) seeds were pelleted to make them fit for mechanical cultivation, and it was reported that this application (coating with organic and inorganic materials) increased the diameter of the sesame seeds up to 3 mm. It was also reported that a delay was observed in the plant emergence times, but the farmers enjoyed a net income increase by 11-20% [7].

In a previous study, Sesame (*Sesame indicum* L.) seeds were pelleted and then planted using the single-piece cultivation method as an alternative to the broadcasting seeding method. Three seed types (Muganli-57, Ozbek-82, Golmarmara) were pelleted and mechanically cultivated using this method [8; 9].

In his study, Karakuzu (2015) planted both the seedlings obtained from basil (*Ocimum Basilicum* L.) seeds and the pelleted seeds. Using sand, clay, and silica, the researcher coated the seeds until they reached a diameter of more than 3 mm. It was reported that the basil plants reached the same height after 70 days in both methods, and the planting by machine was more advantageous [10].

In this study, small and light true potato seeds were pelleted to prevent any undesired outcomes such as displacement of seeds in the seed bed due to being dragged. The seeds were planted into viols in a controlled manner, and it was tried to identify their seedling emergence and time. The data was recorded using MS Excel and analyzed using SPSS V.18 in accordance with the Randomized Blocks Trial Design. The statistical significance was set at $p<0.05$.

MATERIALS AND METHODS

The study was conducted in the laboratories of the Department of Agricultural Engineering and Technologies and the Department of Field Crops, Faculty of Agriculture, Ege University between 2016 and 2018. True potato seeds of the genotype 101 (Nif)

were used in the study.

Organic (pod of pinto bean, corn cob, pea pod and artichoke leaf powder), inorganic (clay), and binding materials (sugared water) were used as pelleting materials [11]. Previous analyses revealed that setting the dry material ratio of the organic materials as 89-95% has a positive effect in that the water-holding capacity of the pelleting material increases, which provides the humidity that the seed needs for germination.

The general features of the true potato seeds were identified, and then all the seeds were brought together to be divided into the control group and the group of the pelleted seeds. Each test was triplicated by randomly selecting seeds from the heaps of seeds.

The form and structure of each seed constitute its unique characteristics. These characteristics affect many agricultural processes such as seed cleansing, packaging, and sowing. Seed characteristics are length (a), width (b), and thickness (c) [12]. Table 1 shows the classification of the potato seeds by their characteristics. 100 grains were picked randomly and their basic features were identified using a Nexius Zoom stereo microscope (Image Focus 4.0 V2.4) and its software. Identifying the surface area of the seeds is especially important for deciding the amount of material to be used for pelleting. A Nexius Zoom stereo microscope (Image Focus 4.0 V2.4) was used to identify the surface area of the seeds [13]. Moreover, in order to obtain a healthy set of values, the projection areas (mm2) of the seeds were calculated using the formula below and compared with the surface areas [14]. Another basic feature of seeds is the sphericity. The sphericity of the potato seeds was calculated using the formula below [14; 15; 16].

Projection area (mm2):

A: (π*L*W)/4 (1)

L : Seed grain length (mm)

W : Seed grain width (mm)

π : 3.14

Sphericity:

Φ = [Do / L] (2)

Φ : Seed sphericity Value

Do : Seed Average Geometrical Diameter (mm)

L : Seed Length (mm)

The seed grains were divided into two groups: control group and the group of pelleted seeds. 1000 seeds were randomly selected from each group three times in accordance with ISTA (2007) rules [17]. Then, they were counted and weighed using a Precisa digital scale with precision of 0.001 g [18].

The seeds were germinated for 14 days (08-22 February 2017) in viols under controlled conditions (24°C, approximately %70 humidity) in accordance with ISTA (2007) rules. The viols were filled with a standard mixture (sandy soil, turf, manure at the ratio of 2:1:1) and the seeds in the control group and the pelleted seeds were planted in this mixture. The data was recorded using MS Excel.

Natural accumulation angle is an important parameter in transportation, storage, silo building, and the design of transportation machinery, especially in terms of granulated products. This angle is the angle formed between the horizontal plane and the lateral surface of the pile formed when the products are poured from a certain height [19]. In Dumanoglu (2016)'s thesis study, a device was produced using a 3D printer (Makerbot) to identify the characteristics of small and light seeds. This device was used to identify the accumulation angle of the true potato seeds.

The true potato seeds (control seeds and pelleted seeds) were poured on three different surfaces (standard germination paper, wood, and rubber) from three different heights (10, 15, and 20 mm) three times, and the data obtained was recorded using MS Excel. In addition, the heaps of the seeds were photographed and transferred to Solid Works 2012 software after each test to finalize the measurement. Then, the natural accumulation angle of the potato seeds were calculated using the formula below [20; 21; 22];

$$\alpha = \arctan \frac{2.h}{\ddot{d}-d} \quad (3)$$

h : Cone height (mm) (the height between the base plate and the cone bottom edge)

$\ddot{d}$: The arithmetic average of the 4 diameter values measured at the bottom with an angle of 90o to each other(mm)

di : Internal diameter of cone exit(mm)

RESULTS

Hundred true potato seeds were randomly selected and their basic features were identified using a Nexius Zoom stereo microscope and its software (Figure 1). In this study, seeds belonging to 101 potato genotype were used. The basic measurements of the seeds were identified using a stereo microscope before and after pelleting.



FIGURE 1
Seeds belonging to 101 potato genotype (control seeds and pelleted seeds)

TABLE 1
Classification of seeds according to their geometric characteristics and shapes

Geometric characteristics	Grain width/Grain length (b/a) (mm)	Shape	Length (a), Width (b), Thickness (c) (mm)
Long	0.6	Round	$a \approx b \approx c$
Medium	0.6 – 0.7	Oval	$a/3 < b \approx c$
Short	> 0.7	Long	$c < b < a/3$

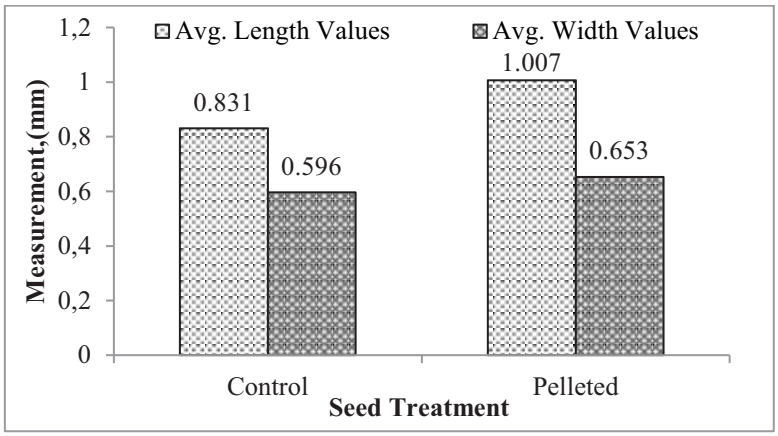


FIGURE 2
The average length and width of the true potato seeds (control seeds – pelleted seeds)

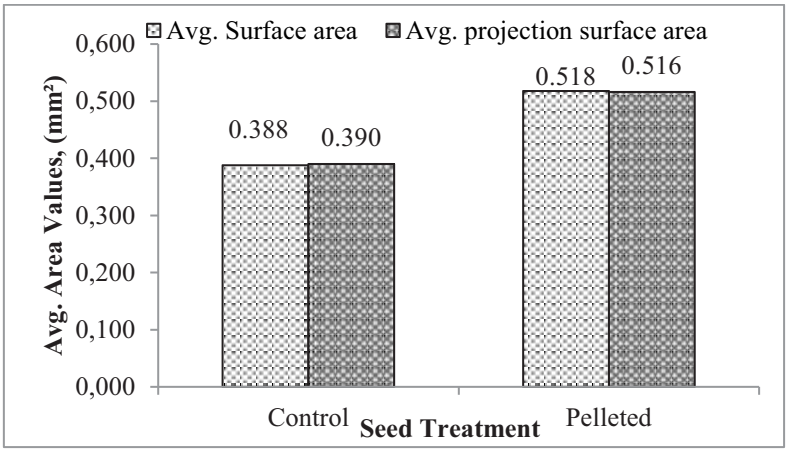


FIGURE 3
The average surface area of potato seeds (mm^2)

The average length and width of the seeds in the control group were 0.831 mm and 0.596 mm, respectively. On the other hand, the average length and width of the pelleted seeds were 1.007 mm and 0.653 mm, respectively. It was found that the pelleting increased the basic measurements of the seeds (Figure 2). Based on this data and other studies, the true potato seeds could be classified as "medium grain" in geometrical terms. It was also found that form of the seeds did not change after the pelleting, and the seeds still remained in the medium grain class.

Hundred true potato seeds (control – pelleted) were selected randomly and examined. The projection areas (mm^2) of the seeds were calculated and compared with the projection areas (mm^2) identified under the stereomicroscope. Figure 3 shows the surface areas of the true potato seeds before and after pelleting. As can be seen in the Figure 3, the surface area and projection area of the seeds in the control group were 0.388 mm^2 and 0.390 mm^2, respectively. On the other hand, the surface area and projection area of the pelleted seeds were 0.518 mm^2 and 0.516 mm^2, respectively (Figure 3). The measured surface area and projection area of the seeds were remarkably close to those calculated, which indicates the reliability of the obtained data.

The general surface area of the control group was 0.833 mm^2, while that of the pelleted seeds was 0.513 mm^2, which shows that the pelleting increased the surface area by about 1.5 times. Also, the average projection values were similar to the surface area values, which indicates the correctness of the measurements.

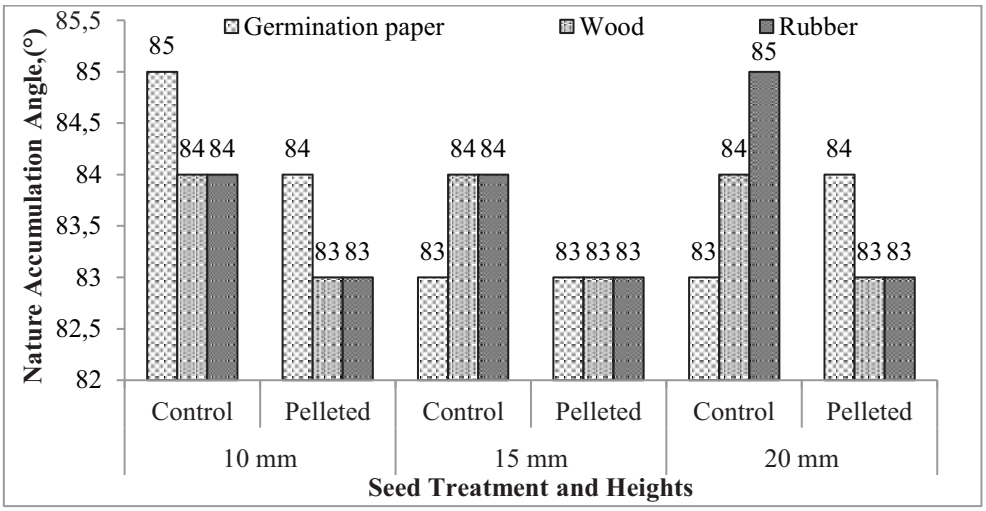


FIGURE 4
The natural accumulation angles of the true potato seeds (control-pelleted) on different surfaces and at different heights

TABLE 2
Geometrical diameter and sphericity of the potato seeds

True Potato Seeds	Average Geometrical Diameter (mm)	Average Length (mm)	Average sphericity
Control	0.101	0.831	0.120
Pelleted	0.144	1.007	0.143

Sphericity of the 101 (Nif) seeds (control-pelleted) was calculated using their mean length (L) and geometrical diameter (Do). The mean values were calculated for 100 seeds from each group. It was found that that the 101 (Nif) potato genotype seeds attained a more round form after the pelleting. While the mean sphericity was 0.120 in the control group, it was 0.143 in the pelleted group (Table 2).

Thousand true potato seeds (control-pelleted) were selected randomly three times and weighed. While the 1000-seed-weight was 48 g in the control group, it was 748 g in the pelleted seeds. The pelleting increased the weight of the seeds by 1.5 times.

True potato seeds (control-pelleted) were tested three times in three different heights (10, 15 and 20 mm). Despite different heights and surfaces, similar values were obtained (Figure 4). Despite different surfaces and heights, similar values were observed in the control group and the pelleted group (Table 3). When the data was analyzed using the DUNCAN test in SPSS V.18, it was found that there were significant relationships between the seed situation, surface, and height ($p<0.05$).

The potato seeds in the control group and the pelleted potato seeds were germinated in viol under controlled conditions for 14 days. The seeds were observed on a daily basis, and their seedling emergence was identified in both groups. It was found that the mean germination was 81.33% in the pelleted seeds and 72% in the control group (Figure 4). This shows that the pelleting had a positive effect on the seedling emergence of the potato seeds. On the other hand, there was no difference between the control group and the pelleted seeds in terms of germination time; so, the seeds in both groups germinated on the same day (Figure 5).

This is a basic study designed to identifying the basic features of the seeds of potato, which is one of the important plant products in Turkey. There is a limited number of studies that show pelleting increases the seed quality. Therefore, pelleting was tested on 101 (Nif) potato genotype in this study. First, the size and form of these small and light seeds were determined, and then they were pelleted and measured. Since in daily farming life seeds are transported from one place to another by pouring from one surface to another, it is important to identify their behavior as response to these conditions. So, the seeds were tested on three different surfaces (germination paper, wood, and rubber) at different heights (10, 15 and 20 mm). Moreover, after the pelleting, the seeds were planted in viols to identify their seedling emergence and time. As in previous studies, it was found that the size and surface area of the seeds increased with pelleting. Very similar results were obtained from the tests carried out on three different surfaces and heights, and it was found that there were significant relationships between all the following three parameters: seed situation, surface and height ($p<0.05$). One of the most important results was the percentage of seedling emergence. The pelleting was found to increase the seedling emergence. This indicates that the seed can obtain the humidity and nutrients that it needs from the pelleting materials. This study will help other researchers to carry out more studies on true potato seeds under greenhouse and farmland conditions.

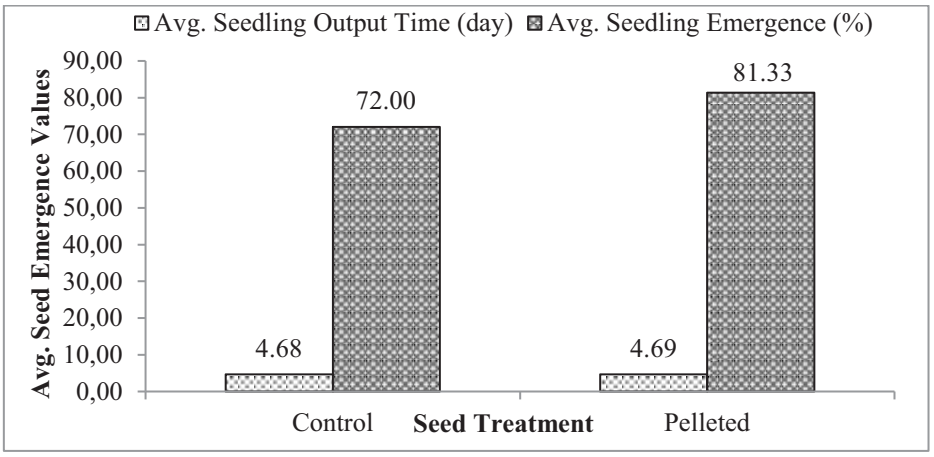


FIGURE 5
The seedling emergence ratios of the true potato seeds (control – pelleted)

REFERENCES

[1] Yıldırım, M.B. and Yıldırım, Z. (2002). Potato Breeding and Biotechnology Textbook, Ege University Faculty of Agriculture Publications, Izmir.

[2] Yıldırım, Z. and Ozturk, G. (2015). A research on determination of yield and quality characteristics of meristem-based clones used in basic seed production in potato, Ege University of Scientific Research Project (2012-ZRF-013), Izmir.

[3] Mıdıkoglu, N. (1998). Studies on coating of potato seed, Ege University Institute of Field Crops, Master's Thesis, Izmir.

[4] Kavak, S. and Eser, B. (2005). Investigation on the Elimination of Negative Effects of Some Polymers Used in Film Coating of Seeds on Germination and Output, Turkey II. Seed Congress (9-11Nov), Adana. 76-81.

[5] Cavuslar, F. and Eser, E. (2002). A Research on Film Coating Technique in Tomato Seeds, Turkey I. Seed Congress (11-13 Sep.2002), Izmir. 191-200.

[6] Dumanoglu, Z. and Cakmak, B. (2017). The Effect of Coating and Pelleting on Quality of Lemon Balm (*Melissa officinalis* L.) Seeds, Journal of Agricultural Machinery Science. ISSN 1306-0007. 13(2), 87-92.

[7] NHAES (National Honam Agriculture Experiment Station). (1998). The Integrated Mechanization System Used Palletting Sesame seed, Iksan, South Korea (www.nhaes.go.kr/english/research_upland3.htm). (Accessed date: June 2016).

[8] Dogan, T., Aykas, E., Tuvay, N.H. and Zeybek, A. (2005). A Study on Pelleting and Planting Sesame (*Sesame indicum* L.). Asian Journal of Plant Sciences. 4(5), 449-454.

[9] Dogan, T. and Zeybek, A. (2009). Improving the Traditional Sesame Seed Planting with Seed Pelleting. African Journal of Biotechnology. 8(22), 6120-6126.

[10] Karakuzu, E. (2015). Sowing Possibilities of Basil (*Ocimum Basilicum* L.) Seed, Adnan Menderes University Institute of Science and Technology Department of Agricultural Machinery, Master's Thesis, Aydın.

[11] Dumanoglu, Z. (2016). The Determination of Appropriate Coating and Pelleting Methods for Some Medical and Aromatic Plant's Seeds, Ege University Institute of Science and Technology Department of Agricultural Machinery and Technologies Engineering, PhD Thesis, Izmir.

[12] Yagcıoglu, A. (2015). Product Processing, Ege University Faculty of Agriculture Publications No: 517 (Extended 2nd Edition), Izmir. p:403

[13] Dumanoglu, Z., Çaçan, E. and Kökten K. (2021). Determination of Physical Properties Seeds of Sainfoin (*Onobrychis viciifolia* Scop.). Genotypes Journal of Anatolian Environmental and Animal Sciences. 6(1), 18-24.

[14] Kara M. (2012). Physical Properties of Biological Products, Atatürk University Faculty of Agriculture Publications No: 242, Erzurum, p:327.

[15] Mohsenin, N.N. (1970). Physical Properties of Plant and Animal Materials. Gordon and Breach Science Publishers. p:881.

[16] Alayunt, F.N. (2000). Knowledge of Biological Materials, Ege University Faculty of Agriculture Department of Agricultural Machinery Textbook, Ege University Faculty of Agriculture Publications No:541. ISBN:975-483-464-4

[17] International Rules for Seed Testing (ISTA). (2007). International Rules for Seed Testing Book.

[18] Dumanoglu, Z. and Geren, H. (2020). An Investigation on Determination of Seed Characteristics of Some Gluten-Free Crops (*Amarantus mantegazzianus, Chenopodium quinoa Willd., Eragrostis tef* [Zucc] Trotter, *Salvia hispanica* L.). Turkısh Journal of Agriculture-Food Science and Technology. 8(8), 1650-1655.

[19] United Nations Industrial Development Organization (UNİDO) and International Fertilizer Development center (IFDC). (1998). Fertilizer Manual, Kluwer Academic Publishers, The Netherlands. ISBN 0-7923-5032-4.
[20] Rutland, D.W. (1986). Manual for Determining Physical Proterties of Fertilizer, Reference Manual IFDC-R-6, International Fertilizer Development Center Muscle Shoals, Alabama, USA.
[21] Miserque, O. and Pirard, E. (2004). Segregation of The Bulk Blend Fertilizers (http://www.ekolojimagazin.com). (Accessed date: June 2016).
[22] Alayunt, F.N., Onal, I. and Aykas, E. (2009). Some Physical Properties of Mineral Fertilizers and Methods for Measuring Them, 25. National Agricultural Mechanization Congress, ISBN 978-9944-452-31-1, Isparta. 225-232.

Received: **19.04.2021**
Accepted: **06.06.2021**

CORRESPONDING AUTHOR

Zeynep Dumanoglu
Department of Biosystem Engineering,
Faculty of Agriculture,
Bingol University,
12000 Bingol – Turkey

e-mail: zdumanoglu@bingol.edu.tr

© by PSP Volume 30– No. 09/2021 pages 10989-11001 Fresenius Environmental Bulletin

IMPACT OF CHITOSAN PMAA-NPK NANO COMPOSITE AND TRADITIONAL MINERAL-NPK FERTILIZERS ON GROWTH, YIELD AND BIOCHEMICAL PARAMETERS OF EGYPTIAN COTTON CV.GIZA 94 (*Gossypium barbadense* L.)

Abdel Hamed Omar[1], Mohamed El-Menshawi[2], Samira El-Okkiah[3,*], Khaled Farroh[4], Samir El-Okkiah[5]

[1]Department of Agronomy, Fac. Agric. Kafrelsheikh Univ., Egypt
[2]Department of Cotton Physiology, CRI. Sakha, Agric. Res. Sta., Kafrelsheikh, Egypt
[3]Department of Agriculture Botany, Fac. Agric. Kafrelsheikh Univ., Egypt
[4]Nano-Tech. & Advanced Materials Central Lab. (NAMCL) ARC Giza, Egypt
[5]Department of Cotton Physiology, CRI. ARC., Sakha, Agric. Res. Sta., Kafrelsheikh, Egypt

ABSTRACT

Nanotechnology is the engineering of functional systems at the molecular scale, deals with particles sizes between 1 and 100 nanometers at least one dimension. The preparation of chitosan nanoparticles was carried out using methacrylic acid (MAA). All preparation steps were carried out at Nanotechnology & Advanced Materials Central Lab. (NAMCL), Agric, Res. Center – Giza, Egypt. The properties of Cs-PMAA nanoparticles were studied by particle size analyzer, Zeta potential, transmission electron microscopy (TEM) and size distribution of nanoparticles by dynamic light scattering (DLS). An experiment on Egyptian cotton cultivar Giza 94 Long-Staple (LS) was conducted at Sakha, Agric., Res. Station, Cotton Res. Inst., Agric. Res. Center, Egypt, during the two growing seasons 2018 and 2019. The experiment was laid out in the Randomized Complete Block Design with nine fertilizer treatments and three replications. The purpose of this current study was comparing the effects of traditional mineral NPK fertilizer and Cs-PMAA-nanoparticles loaded with NPK composite fertilizer, besides the combination mixed treatments with various percent between them. The results of study showed that nano-NPK composite treatments significantly enhanced growth parameters, Results also showed that the highest seed cotton yield, lint cotton yield and yield components were resulted from either 100 % nano-NPK composite fertilizer treatment or mixed treatments nano-NPK with traditional NPK mineral. The use of nano- NPK fertilizers leads to an increase in the efficiency of the consumption of nutrient elements.. Hence it could be concluded that nano- NPK fertilizers could use as an alternative to traditional mineral NPK fertilizers and could be recommended use in the commercial area of cotton crop in clayey soils in Nile Delta of Egypt.

KEYWORDS:
Nanotechnology, nanoparticles, chitosan, Zeta potential, Tem, DLS, Cotton, biochemical, foliar application, clayey

INTRODUCTION

Cotton is the most important cash crop of Egypt; it is still play a vital role in Egyptian economic. It is supplying the national and international market demands with the highest quality of lint cotton (Extra fine and Extra-long-staple).

It is also considered the main cash crop for most growers, besides it is one of the main sources of the hard currency for the national income. Nowadays the cotton crop occupies about 3.5 – 4.0 % of the total cultivated area in Egypt. The total area of cotton was retreated from about two millions feddans during the fifties of the nineteen century to the minimum area, ranged from 200000 to 350000 feddans annually. The retreating area is due to mainly; 1- The prices of cotton are not rewarding for the farmers, and consequently refrain grow cotton. 2- The costs of inputs are very high expensive especially fertilizers, pesticides and labor wages.

Cotton production occupies a very unique position among all other field crops in Egypt. No doubt that cotton production as for other crops could be easily maximized through appropriate cultural practices; one of these is controlled slow release NPK fertilizers, throughout the application of recent nanotechnology. The term 'Nanotechnology' has been defined as the branch of science that deals with matter at the dimensions of about 1-100 nm (a nanometer nm is one billionth 10^9 of a meter). The

Nano fertilizers mainly delay the release of the nutrients and extend the fertilizer effect period [1].

Indeed, nanotechnology has provided the feasibility of exploiting nanoscale or nanostructured materials as fertilizer carriers or controlled release vectors for building of so-called "Smart fertilizer" as new facilities to enhance nutrient use efficiency and reduce costs of environmental protection [2].

Fertilizers are chemical compounds applied to promote plant and fruit growth [3]. Fertilizers are usually applied either through the soil (for uptake by plant roots) or by foliar feeding (for uptake through leaves). Meanwhile, The total fertilizer nutrient ($N+P_2O_5+K_2O$) consumption all over the world is estimated to be 199.00 million tonns for 2019 [4]. In the meantime, total loss in nitrogen fertilizer application is about 60-75 % [5]. Therefore, a greater part of nitrogen fertilizers are not absorbed, and they consequently pollute both underground and surface water. N (nitrogen) promotes leaf growth and forms proteins and chlorophyll. P (phosphorus) contributes to root, flower and fruit development. K (potassium) contributes to stem and root, also improve the quality properties of cotton fiber, and the synthesis of proteins [6].

Overuse of fertilizers is one of the causes for degradation of environment and soil, besides causing not only substantial economic and resource losses but also very serious environmental pollution [7] and [8].

For avoiding the adverse effects of an overuse of fertilizers, recently, the use of slow release fertilizers (SRFs) has become a new trend to save fertilizer consumption and to minimize environmental pollution [9] and [10]. Therefore, the method of encapsulation of fertilizers components in polymeric nanoparticles is relatively novel with potential commercial applications.

The use of Nano fertilizer leads to an increased efficiency of the elements. Reduce the toxicity of the soil, to at least reach the negative effect caused by the consumption of excessive applications of fertilizers and reduce the frequency of application of fertilizer [11]

The evaluation of nanotechnology and the emergence of novel Nano devices and nanomaterial open up new trends in agriculture and biotechnology. Nanoparticles are molecules that are so small to fall within the nanometric range, with at least one of their dimensions being less than a few hundred nanometers. This small size rather brings about marvelous changes in their physical properties with respect to observed in bulk materials. The ability of controlling nanoparticles size is highly favorable for most applications in nanotechnology [12].

Nowadays, nanotechnology has opened up a large scope to revolutionize the agriculture and food sectors with new concepts, ideas and tools by maximizing the productivity and reduce the poverty in coming years.

Three main macronutrients (NPK) are the predominant fertilizer which has been used to improve yield and quality of crop where soil supplies are limited [13].

The aim of the use of nanomaterial (NMs) in the field of agriculture is to improve the efficiency and sustainability of agricultural practices by putting less input and generating less waste than conventional products and approaches [14] .

The main objectives of this investigation were to evaluate in comparison studies; the effect of foliar spraying with nano-NPK, and ordinary application of mineral (NPK) fertilizers on the growth, yield, yield components and fiber properties of the Egyptian cotton cultivar (*Gossypium barbadense* L.), Giza 94 Cv.

MATERIALS AND METHODS

Site of the experiment. The field experiment was conducted at the farm of Sakha Agriculture. Research Station (SARS), Cotton Research Institute (CRI), Agricultural Research Center (ARC), Egypt, during the two growing seasons 2018 and 2019, to evaluate in comparison studies "the effect of foliar spraying with nano and ordinary application of mineral NPK-fertilizers on the growth, yield, yield components and biochemical of the Egyptian cotton cultivar "Giza 94".

Giza 94 is a new commercially available long-staple cotton cultivar (Gossypiuam barbadense, L.) was used as a plant material in the present study, and it is grown commercially at the North of Nile Delta of Egypt, Kafr El-Sheikh District. Fiber quality characteristics of G. 94 cultivar are shown in Table (1)

The soil texture of the research area was clayey, clay ranged between 51.27 – 54.14 % for 2018 and 2019 seasons, respectively Table (2)

Table (3) is shown mechanical and chemical analysis of soil sample for macro and micro-elements of the experiment during 2018 and 2019 growing seasons.

Experimental Design. A randomized complete block design with three replicates was devoted. Plots in each replicate were randomly assigned to the nine studied fertilizer treatments; Sowing was done on 28 April and 25 April for the first and second seasons respectively.

Times of fertilizer application:

a. The first: at the seedling stage 40 DAS.
b. The second: at initial of squaring stage 60 DAS.
c. The third: at beginning of flowering stage 80 DAS.

After 40 days from both the second and third fertilization, (at 100 and 120 DAS) four guarded

plants as a sample were randomly taken from each plot to measure growth parameters.

All other cultural practices were done according to the recommendations of Ministry of Agriculture and Land Reclamation. The recommended rate of traditional mineral NPK fertilizers for cotton plants per one feddan is (45kg N + 30kg P_2O_5 + 48kg K_2O) as soil application (side dressing) or foliar application (spray on leaves).

Fertilizer treatments. Nine fertilizer treatments were studied in the current research, as follow:

(T1) 100% foliar application with Cs-NPK-NPs fertilizer (500ppm N: 60ppm P: 400ppm K).

(T2) 100% foliar application of recommended rate (RR) with traditional NPK fertilizer (control).

(T3) 100% soil application of recommended rate(RR) with traditional NPK fertilizer.

(T4) 75% foliar application with Cs-NPK-NPs fertilizer + 25% traditional NPK fertilizer as soil application.

(T5) 50% foliar application with Cs-NPK-NPs fertilizer + 50% traditional NPK fertilizer as soil application.

(T6) 25% foliar application with Cs-NPK-NPs fertilizer + 75% traditional NPK fertilizer as soil application.

(T7) 75% foliar application with traditional NPK fertilizer + 25% traditional NPK fertilizer as soil application.

(T8) 50% foliar application with traditional NPK fertilizer + 50% traditional NPK fertilizer as soil application.

(T9) 25% foliar application with traditional NPK fertilizer + 75% traditional NPK fertilizer as soil application.

Experimental Materials. In this study, chitosan nanoparticles were obtained by polymerizing methacrylic acid (PMAA) for the incorporation of NPK fertilizers.

The interaction and stability of chitosan nanoparticles (CsNPs) suspensions containing N, P and K were evaluated by size particles analysis, zeta-potential and net charge on its surface by dynamic light scatter (DLS), Also transmission electron microscope (TEM) gave an information on the particle shape and the determination of particle size .

Chitosan (Cs) MW 71.3 KDa, degree of deacetylation 85% was purchased from Sigma-Aldrich (Germany). All other reagents devoted here were of analytical grade and were sourced from Sigma-

TABLE 1
Fiber quality characteristics of G. 94 an Egyptian cotton cultivar

Cultivars	color	Values of color attributes		Micronaire values	Maturity ratio	Fiber length		Filer strength	
						UHM	uniformity	strength	Elongation
		Brightness (Rd%)	Yellowen (+b)	Mic.	MR.	(mm)	(Uni Index)	g/tex	%
Giza 94 (LS)	White	79.5	8.6	4.2	0.9	34.2	86.8	43.0	7.1

TABLE 2
Soil texture & particle size distributions %.

seasons	*Soil mechanical analysis*			*Soil texture*	*PH*	*E.C ds m^{-1}*
	Clay%	Silt%	Sand%			
2018	51.27	28.29	20.44	Clayey	8.06	2.95
2019	54.14	26.82	19.04	Clayey	7.6	1.61

TABLE 3
Chemical analysis of experimental soil samples for macro and micro elements during 2018 and 2019 growing seasons

seasons	*Depth cm*	*Macro–elements of soil profiles (ppm).*			*Micro–elements of soil profiles (ppm).*			
		N	P	K	Fe	Zn	Mn	Cu
2018	0-30	162.50	7.00	287.04	16.74	3.00	13.69	3.84
	30-60	162.50	5.00	351.78	16.12	2.34	13.63	3.92
	60-90	169.00	3.00	315.12	14.29	2.35	14.14	3.06
2019	0-30	50.40	7.00	270.00	15.84	2.81	13.79	3.60
	30-60	33.60	5.00	229.00	15.41	2.44	13.55	3.74
	60-90	33.61	2.00	230.00	13.91	2.37	13.94	3.11

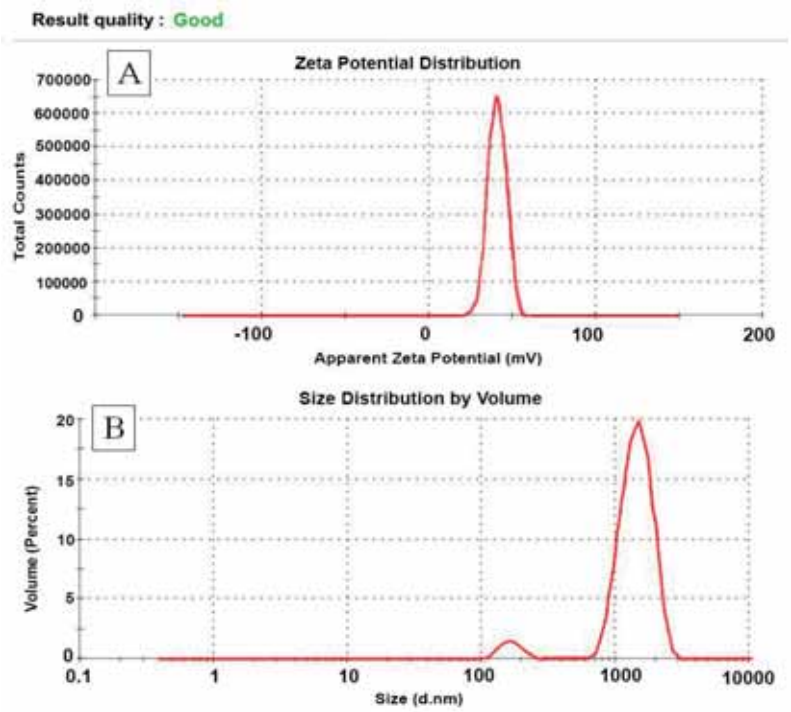


FIGURE 1
DLS analysis of CsNPs,Zeta potential (A) Particle size (B)

Aldrich (Germany) and used as received, potassium persulfate (k_2 S_2 O_8), calcium phosphate Ca (H_2 P_4)2. H_2O, urea $Co(NH_2)2$, potassium chloride kCl and methacrylic acid (MAA).

Preparation of Cs-PMAA-nanoparticles Materials. According to the method developed by [15] and [16] Cs-PMAA nanoparticles were obtained by polymerizing MAA in Cs solution as described by [12]. All preparation steps were carried out at Nanotechnology and Advanced Materials Central Lab, (NAMCL), Agric. Res. Center, Giza, Egypt.

Description of Cs-PMAA nanoparticles with NPK fertilizers. The morphology shape and size of the Cs-PMAA nanoparticles were measured using a JEOL 1010 transmission electron microscope at 80 KV (JEOL, Japan). One drop from each solutions (Cs-PMAA nanoparticles only and Cs-PMAA suspension nanoparticles with entrapment of NPK fertilizers) was taken separately and spread onto a carbon-coated copper grid and was subsequently dried at room temperature for transmission electron microscopy (TEM) analysis , The zeta potential and particle size distribution measurements were carried out in Zetasizer Nano ZS (Malvern Instrument, Woreestershire UK) at Electron Microscopy Unit EMU, El-Mansoura Univ., Egypt. ..

Growth parameters/ yield parameters. At the beginning of flowering stage (at 100 and 120 days after sowing) samples were taken for estimation of growth parameters (plant height, leaf area, leaf area index) Leaf area per plant: was calculated in square decimeters (dm2) using ci-202 portable Instr. Laser leaf area meter SB 3.01-12006. Plant samples were collected randomly from each plot for recording the following seed cotton yield, lint cotton yield and yield components.

Total chlorophyll and biochemical analysis of cotton leaves and seeds. Chlorophyll a, chlorophyll b and Total chlorophyll in the fresh leaves were determined according to the method described by [17]

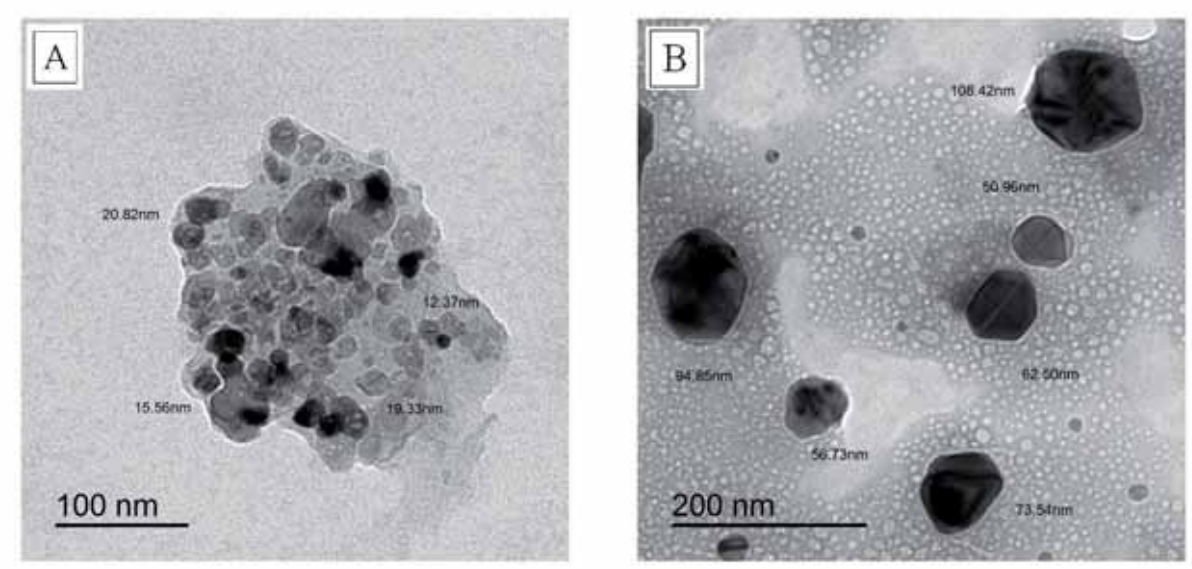
A nutrient element such as nitrogen was estimated in the digestion product, using the official Micro-Kjeldahl Method as described in [18]

Total phosphorus was estimated by ascorbic acid method using the calorimetric method as described by [19]

Total potassium was also estimated by using flame photometer according to [20].

Seed oil was estimated by the method described by [21] and seed protein was estimated by [18]

Statistical analysis. The data were subjected to an analysis of variance using, COSTAT statistic program according to [22].The differences among the different treatments were tested using Duncans 'Multiple Range method outlined by [23].



A:TEM image of Cs-PMAA nanoparticles B:TEM image of Cs-NPK nanocomposite particles

FIGURE 2
Transmission Electron Microscope (TEM)

RESULTS AND DISCUSSION

Dynamic light scattering analysis (DLS). The DLS pattern of suspension of NPK nanoparticles synthesized using Cs-PMAA for foliar application of G. 94 (LS) cotton cultivar with the chitosan NPK nanoparticles composite were characterized by TEM, Zeta potential and size distribution. The results showed that size distribution was from 166.9 – 1473 nm, Zeta potential was 40.7 (mV), Z-average size was 1024 (dnm) and polydisperese index (PD1) chitosan nanoparticeles suspension was 0.853 indicating that synthesized particles are good and uniform sizes with spherical shape and in nano- scale (Figure 1 and 2) . The Zeta potential of NPs came out to be higher positive values, which showed high stability of nanoparticles in aqueous solution in the present study [24].

Effect on growth parameters. Plant height cm. There were significant differences among the nine studied fertilizer treatments (Table 4). Application of 100% nano NPK - fertilizer gave the tallest cotton plants at both growing stages 100 and 120 DAS of G. 94 Cv. in both seasons. T1 (100 % nano-NPK) was ranked first for most growth parameters, as well as the fertilizer treatments T4, T5 and T6 involved nano fertilizer mixed in combinations with traditional mineral NPK came out after T1. Several studies revealed that an exogenous application of some NPK-nanoparticles could be significantly improve plant growth due to plant cells growth increase under NPK-NPs might be a reason for plant height rise, [25-29] obtained the same results and with the same trend.

Total fresh and dry weights (gm) / plant. Table (4) show that regarding of both fresh and dry weights for the whole cotton plant (roots, leaves, main stem and reproductive organs) of G. 94 cotton Cv. at 100 and 120 DAS were significantly affected by different nano-NPK and traditional mineral ones. The highest means of fresh and dry weights were resulted from the treatment which received 100% nano-NPK fertilizer (T1). Additionally, the fertilizer treatments involved nano-NPK mixed in combinations with traditional mineral NPK fertilizer T4 and T5 directly came out after T1. Similar findings were recorded by [30] who found that nano NPK fertilizer were absorbed into the plants, thus the dry matter production was also increment.

Total leaf area / plant (dm^2) and leaf area index (LAI). There were significant differences among the nano –NPK fertilizer and traditional mineral ones regarding the total leaf area per plant and leaf area index at 100 and 120 DAS of G. 94 cotton cv. in 2018 and 2019. With an exception at 120 DAS in 2019 (Table 5). The highest LA and LAI was in favor of 100 % nano-NPK (T1), however, the fertilizer treatments included nano-fertilizer mixed in combinations with traditional ones (T4, T5 and T6) gave higher means of both LA and LAI compared with control. The magnitude of LA and LAI in relation to plant metabolic processes (photosynthesis) is generally known. Cotton plant LA and LAI were significantly affected by both the fertilizer treatments under study and growth stages of cotton plant. Nano-NPK fertilizer as foliar application boosted the photosynthetic rate, leaf expansion and leaf persistency. As leaf area directly relates to the photosynthetic rate, as

TABLE 4
Effect of different fertilizer treatments of nano – NPK, traditional mineral NPK and its coordination of both on plant height and total fresh weight and dry weights at 100 and 120 DAS of G.94 cotton cultivar in 2018 and 2019 seasons.

seasons	*Treatments*	*Plant height (cm)*		*Total fresh weigh(g/p)*		*Total dry weigh(g/p)*	
	(T)	(at 100 DAS)	(at 120DAS)	(at 100 DAS)	(at 120DAS)	(at 100 DAS)	(at 120DAS)
2018	T1	127.67a	158.01a	447.83a	595.8a	95.84	135.53a
	T2	111b	132.34cd	265.57b	521.9ab	56.96	115.52ab
	T3	119bc	144.65b	306.33b	516.96ab	64.54	113.89ab
	T4	113.65bc	138.38bc	346.4b	471.34b	66.31	106b
	T5	108.35c	133.01cd	301.83b	434.76b	60.91	98.51b
	T6	108.32c	126.68d	248.43b	440.89b	54.1	96.8b
	T7	106.62c	132.3cd	271.02b	435.75b	60.52	99.64b
	T8	104.68c	127.01d	232.67b	453.3b	48.93	101.97b
	T9	96d	114.01e	226.58b	422.5b	48.43	95.28b
Treatments mean		110.59	134.04	294.07	477.02	59.62	107.02
Test of significance by (DMRT)		**	**	**	*	n.s	*
Coefficient of Variation (C.V.%)		4.44	2.99	17.59	13.75	16.24	13.29
2019	T1	155.33a	163.01a	706.93a	1032.49a	167.11a	214.13a
	T2	139.33de	145.17de	495.04bc	752.02bcd	128.86cd	187.97ab
	T3	148.17bc	150.83bcd	487.03ab	853.4ab	139.28bc	186.29ab
	T4	148.17b	157.33ab	624.32a	888.84ab	155.19ab	185.83ab
	T5	143.17cd	150.33cd	475.2bc	839.06 bcd	119.92cde	157.75bc
	T6	145.67bc	151.33bcd	479.09bc	648.93cd	116.92cde	145.29bc
	T7	144cd	153.67bc	487.77bc	625.59d	124.25cd	133.7cd
	T8	144.33bcd	152.17bc	445.59c	568.44de	103.49de	129.64cd
	T9	134.83e	142.33e	411.27c	413.73e	96.84e	94.12d
Treatments mean		144.96	151.8	523.58	735.84	127.95	159.42
Test of significance by (DMRT)		**	**	**	**	**	**
Coefficient of Variation (C.V.%)		2.03	2.31	12.62	14.38	10.70	14.31

duration of leaf expansion, so LAI finds to be sensitive to N availability to crop plants [31]. Nano-fertilizer enhance growth parameters (plant height, leaf area index, total fresh and dry weights production and net assimilation production which translocated to reproductive parts of the plant [32] and [26]

Effect on yield and yield components parameters. Seed cotton yield K/fed. Seed cotton yield in kentars / feddan was significantly affected by fertilizer treatments of G. 94 cotton Cv. in both 2018 and 2019 seasons, (Table 6). The highest yield of seed cotton was resulted from the treatment (T_1) 100% nano-NPK incorporated into Cs-PMAA-NPs. This treatment was significantly ranked first among the nine studied treatments and gave an increases in yield was estimated with 14.78 and 25.89% over the control in 2018 and 2019 growing seasons, respectively, and with average yield improvement over two seasons 20.34% . As well as T_4 and T_5 which involved nano-NPK mixed in combination with used mineral traditional NPK were ranked second and fourth, respectively. The treatment (T_1) 100% nano-NPK fertilizer contains higher concentrations of N and K (500 ppm N: 60 ppm P: 400 ppm K) which led to higher production in flower numbers /plant, higher boll setting number and higher opened bolls. The same findings were obtained by [33]., Also higher concentration of N and K in nano – NPK fertilizer in the current study promoted photosynthic rate, consequently net assimilation rate production and accumulation that

TABLE 5

Effect of different fertilizer treatments of nano – NPK, traditional mineral NPK and its Coordination of both on total leaf area /plant (dm^2) and leaf area index at 100 and 120 DAS of G.94 cotton cultivar in 2018 and 2019 seasons.

	Treatments (T)	*Total leaf area /p (dm^2)* (at 100 DAS)		*Total leaf area /p (dm^2)* (at 120DAS)		*Leaf area index (LAI)* (at 100 DAS)		*Leaf area index (LAI)* (at 120DAS)	
2018	**T1**	103.62	a	106.12	a	7.40	a	7.58	a
	T2	78.53	bcd	93.54	abc	5.61	bcd	6.68	abc
	T3	96.40	ab	104.09	ab	6.89	ab	7.44	ab
	T4	82.00	bcd	98.73	abc	5.79	bcd	7.05	abc
	T5	78.61	bcd	89.82	bc	5.62	bcd	6.42	bc
	T6	69.43	cd	89.76	bc	5.17	cd	6.41	bc
	T7	68.01	cd	94.27	abc	4.86	cd	6.74	abc
	T8	63.26	d	87.40	c	4.52	d	6.24	c
	T9	87.12	abc	86.44	c	6.22	abc	6.18	c
Treatments mean		**80.78**		**94.46**		**5.79**		**6.75**	
Test of significance by (DMRT)		**		*		**		*	
Coefficient of Variation (C.V.%)		**13.84**		**8.87**		**13.31**		**8.87**	
2019	**T1**	104.99	a	132.31		7.50	a	9.44	
	T2	82.63	cd	97.03		5.90	cd	6.93	
	T3	98.36	ab	113.37		7.03	ab	8.13	
	T4	100.38	ab	117.02		7.17	ab	8.36	
	T5	86.91	bcd	86.12		6.21	bcd	6.15	
	T6	90.14	bcd	100.07		6.44	bcd	7.15	
	T7	95.05	abc	109.13		6.79	abc	7.80	
	T8	87.40	bcd	109.53		6.24	bcd	7.83	
	T9	76.02	d	79.10		5.43	d	5.65	
Treatments mean		**91.32**		**104.89**		**6.52**		**7.49**	
Test of significance by (DMRT)		**		**n.s**		**		**n.s**	
Coefficient of Variation (C.V.%)		**8.14**		**13.05**		**8.15**		**12.95**	

TABLE 6

Effect of different fertilizer treatments of nano – NPK, traditional mineral NPK and its coordination of both on Seed cotton yield k/fed, Lint cotton yield k/ fed, and earliness % of G.94 cotton cultivar in 2018 and 2019 seasons.

seasons	*Treatments (T)*	*Seed cotton yield **k/*fed*		*Lint cotton yield **k/*fed*		*Earlines*	*%*
2018	**T1**	12.81	a	16.58	a	84.70	a
	T2	11.16	ab	14.68	ab	74.89	b
	T3	11.74	ab	16.07	ab	83.79	a
	T4	12.56	ab	15.32	ab	84.68	a
	T5	11.68	ab	15.30	ab	84.23	a
	T6	10.38	ab	13.62	ab	82.98	a
	T7	10.53	ab	13.46	ab	82.92	a
	T8	9.80	b	12.84	b	78.28	ab
	T9	10.13	ab	13.28	ab	81.44	a
Treatments mean		**11.20**		**14.57**		**81.41**	
Test of significance by (DMRT)		*		*		**	
Coefficient of Variation (C.V.%)		**8.72**		**8.61**		**3.02**	
2019	**T1**	14.83	a	20.22	a	93.97	a
	T2	11.78	bcd	15.52	cd	84.91	bc
	T3	13.51	abc	17.68	abc	88.78	abc
	T4	13.80	ab	18.42	ab	92.92	ab
	T5	12.96	abc	17.16	bc	89.68	abc
	T6	11.65	cd	15.36	cd	89.27	abc
	T7	10.64	d	13.80	d	87.33	abc
	T8	12.45	bcd	16.24	bcd	85.49	bc
	T9	11.54	cd	14.86	cd	84.13	c
Treatments mean		**12.57**		**16.85**		**88.50**	
Test of significance by (DMRT)		**		**		**	
Coefficient of Variation (C.V.%)		**8.67**		**8.78**		**4.71**	

*one feddan=4200m^2 **one kentar seed cotton=157.5 kg **one kentar lint cotton=50 kg

ultimately boosted final seed cotton yield. These results were supported by [34-35]and [28] & [29].

Lint cotton yield K/fed. Lint cotton yield in kentars / fed of G. 94 cotton cv. was significantly affected by different nano and traditional NPK fertilizer treatments in both seasons. (Table 6) showed that 100 % nano- NPK (T1) was superior over control with 12.94 and 30.28 % in 2018 and 2019 seasons respectively. The same findings were obtained by [36-37] and [38] who pointed out that controlled release fertilizers increased crop yields and nutrient use efficiency in a number of production systems. they also found that results have demonstrated that yield of cotton was increased by 12.4-34.5% using controlled release N fertilizer compared with common urea treatment, on the other hand, [26] on cotton; [27] on rice crop and [28- 29]on cotton obtained similar findings and in the same trend

Earliness of crop maturity Earliness of cotton crop maturity of G. 94 cotton cv. was significantly affected by the different fertilizer treatments in both 2018 and 2019 growing seasons (Table 6). Results showed that cotton plants were treated with 100 % nano-NPK fertilizer were earlier in its maturity than control. As well as, the mixed treatments of nano-NPK in combinations with used traditional NPK fertilizer (T4, T5 and T6) gave an earlier cotton plants compared with control and other traditional NPK fertilizer. These findings might be due to that traditional common NPK fertilizer abundantly foliar spraying has given an excessive vegetative growth causing too late in crop maturity, consequently late harvesting. On the other hand, nano – NPK fertilizer treatments powered by the system of controlled – release fertilizer (CRFs) which increase crop yields and nutrient use efficiency (NUE) in a number of production systems [35] and [37] who illustrated that the application of controlled – release urea enhanced soil N supply in the late cotton growth period and consequently late in the harvest time.

(No. of flowers /p, No. of total bolls setting/ p and No. of opened bolls/ p). With an exception, number of opened bolls per plant in 2018 season, the others yield components parameters in (Table 7) were significantly affected by different nano-NPK, traditional NPK fertilizers and coordination of both in the two seasons. The highest mean values of these yield parameters in (Table 7) were produced from the nano-fertilizer treatments in both seasons. The increases in flower number per plant might be interpretation on the basis of the genotype of cotton cv. and its response to the increase of N and K elements in nano-fertilizer which N enhancement the formation of amino acids which are essential component of protein and also reducing the shedding of cotton squares, causing rise flower number and K accelerated mobility of photosynthesis from source to sink. These results were in close agreement with those obtained by [39], [26] and [28-29]. The present results indicated that nano-NPK fertilizer enhanced an increase in number of opened bolls number / plant might be due to the increment in number of boll setting / plant and reduce both squares and young bolls shedding. These results were in parallel with those obtained by [31]

Effect on chlorophyll content in cotton leaves. Results in (Table 8) revealed that chlorophyll a, b and total chlorophyll were not significantly affected by different Nano- NPK and common fertilizer treatments, with an exception chlorophyll b in only 2019 season. It is clear from the data that chlorophyll content in the cotton leaves (a, b and total) were decreased at 120 DAS compared to at 100 DAS. The general means of chlorophyll a, b and the total over the fertilizer treatments were (11.69 & 10.18), (5.62 & 2.61) and (19.25 & 15.73) at 100 DAS & 120 DAS and (10.86 & 8.84), (2.25 & 1.65) and (15.03 & 12.12) in 2018 and 2019 respectively. This is logic according to the changes of leaf chlorophyll fluorescence throughout the different growth stages and K rate application in Nano – NPK fertilizer. These findings were in agreement with those obtained by [40] who recorded that chlorophyll concentration in cotton leaves were reduced from the boll - setting stage to maturity stage might be due to an increasing leaf number senescence.

Effect on biochemical analysis of cotton leaf. There were significant differences among the studied fertilizer treatments for macro elements N, P and K percentages in cotton leaf content of G. 94 cotton cv. in 2018 and 2019 growing seasons. It is obvious from the data in (Table 9) that the highest leaf content of N and K were in favor of 100 % Nano – NPK fertilizer treatment (T_1). Also mixed Nano – NPK in combinations with traditional NPK (T4 and T_5) gave higher percent of N and K in both 2018 and 2019 seasons compared to control. The average leaf N content % and leaf K content % over fertilizer treatments were (5.40 & 5.24 %) and (5.31 & 5.54 %) respectively.

These results in the current study are in accordance with same other works on using chitosan nanoparticles and nano-fertilizers [41- 42] who reported that using N nano fertilizer based on chitosan nanoparticles and meth acrylic acid possessed a higher N use efficiency compared to using free urea in the control, because of chitosan acting as a potent fertilizer due to its high concentration in nitrogen , On the other hand, The highest leaf P content was resulted from the traditional mineral NPK fertilizer (recommended dose) as soil application (T_3) which gave higher values (0.093 and 0.107%) compared to control in 2018 and 2019 seasons, respectively [43] concluded that

TABLE 7

Effect of different fertilizer treatments of nano – NPK, traditional mineral NPK and its coordination of both on number of flowers/plant, number of total boll setting/p, number of opened bolls/p and earliness % of G.94 cotton cultivar in 2018 and 2019 seasons.

seasons	*Treatments (T)*	*Number of Flowers/plant*		*No .of total boll setting/p*		*No. of opened bolls/plant*	
2018	**T1**	38.30	a	19.44		17.58	a
	T2	29.20	bc	17.07		14.00	ab
	T3	29.97	bc	17.62		14.60	ab
	T4	35.27	ab	19.40		15.86	ab
	T5	33.30	abc	19.06		14.62	ab
	T6	26.73	bc	18.71		13.97	ab
	T7	27.73	bc	17.37		14.38	ab
	T8	24.53	c	15.96		12.60	b
	T9	26.37	bc	16.82		13.39	ab
Treatments mean		**29.04**		**17.94**		**14.56**	
Test of significance by (DMRT)		**		**n.s**		*	
Coefficient of Variation (C.V.%)		**11.50**		**9.41**		**11.49**	
2019	**T1**	45.87	a	40.33	a	33.67	a
	T2	37.97	cd	32.33	de	26.83	cd
	T3	40.57	abcd	36.00	bcd	28.50	bcd
	T4	44.20	ab	38.33	ab	31.00	ab
	T5	41.27	abc	36.67	abc	28.83	bc
	T6	40.57	abcd	36.33	abcd	28.17	bcd
	T7	38.33	cd	32.67	cde	25.50	cd
	T8	38.97	bcd	35.67	bcd	28.00	bcd
	T9	35.50	d	31.33	e	25.17	d
Treatments mean		**40.36**		**35.52**		**28.41**	
Test of significance by (DMRT)		*		**		**	
Coefficient of Variation (C.V.%)		**7.33**		**6.20**		**6.41**	

TABLE 8

Effect of different fertilizer treatments of nano – NPK, traditional mineral NPK and its coordination of both on Chlorophyll a, ,chlorophyll b and Total chlorophyll mg/dm² at 100 and 120 DAS of G.94 cotton cultivar in 2018 and 2019 seasons

seasons	*Treatments (T)*	*Chlorophyll A mg/dm²*		*Chlorophyll B mg/dm²*		*Total chlorophyll mg/dm²*	
		(at 100 DAS)	**(at 120 DAS)**	**(at 100 DAS)**	**(at 120 DAS)**	**(at 100 DAS)**	**(at 120 DAS)**
2018	**T1**	12.81	10.84	5.97	2.40	19.28	16.50
	T2	10.80	9.74	5.65	3.12	19.30	15.74
	T3	12.50	10.43	6.24	3.24	21.78	16.88
	T4	12.61	10.75	5.33	2.66	17.37	15.97
	T5	12.51	10.64	5.94	2.45	20.42	16.31
	T6	10.86	9.73	5.68	2.46	19.29	15.37
	T7	11.89	9.95	4.78	2.17	18.36	15.91
	T8	11.67	10.09	5.51	2.65	19.48	15.44
	T9	9.59	9.43	5.51	2.38	17.94	13.45
Treatments mean		11.69	10.18	5.62	2.61	19.25	15.73
Test of significance by (DMRT)		n.s	n.s	n.s	n.s	n.s	n.s
Coefficient of Variation (C.V.%)		12.07	13.88	15.95	17.25	12.02	13.64
2019	**T1**	12.32	9.95	2.71	2.24	17.11	14.22
	T2	11.33	8.49	1.91	1.75	15.16	11.79
	T3	10.64	9.10	2.32	1.69	14.99	12.33
	T4	12.00	9.27	2.22	1.67	16.05	12.89
	T5	10.43	8.86	2.18	1.53	14.52	11.91
	T6	9.87	8.00	2.06	1.46	13.60	10.98
	T7	11.86	9.98	2.75	2.07	16.80	13.92
	T8	11.14	8.96	2.77	1.84	15.65	12.41
	T9	8.19	6.97	1.66	0.64	11.37	8.63
Treatments mean		**10.86**	**8.84**	**2.25**	**1.65**	**15.03**	**12.12**
Test of significance by (DMRT)		**n.s**	**n.s**	**ns**	**n.s**	**n.s**	**n.s**
Coefficient of Variation (C.V.%)		**15.07**	**13.51**	**11.51**	**14.87**	**16.08**	**14.92**

TABLE 9
Effect of different fertilizer treatments of nano – NPK, traditional mineral NPK and its coordination of both on Leaf N content %, Leaf P content % and Leaf K content % of G.94 cotton cultivar in 2018 and 2019 seasons.

seasons	*Treatments (T)*	*Leaf N content %*		*Leaf P content %*		*Leaf K content %*	
	T1	7.30	a	.070	bc	5.93	a
2018	**T2**	4.77	d e	.053	cd e	5.07	abc
	T3	4.93	d	.093	a	5.60	ab
	T4	6.27	b	.047	de	4.49	ab
	T5	6.10	b c	.070	bc	5.50	ab
	T6	5.07	d	.063	bc d	5.49	abc
	T7	5.33	c d	.050	cd e	4.94	bc
	T8	4.87	d e	.077	ab	5.25	abc
	T9	4.00	e	.040	e	4.52	c
Treatments mean		**5.40**		**0.060**		**5.31**	
Test of significance by (DMRT)		**		**		*	
Coefficient of Variation (C.V.%)		**9.07**		**19.17**		**8.89**	
2019	**T1**	7.07	a	.050	c	6.32	a
	T2	4.63	c d	.057	bc	5.34	bcd
	T3	5.03	c	.107	a	5.82	ab
	T4	5.77	b	.050	c	5.88	ab
	T5	5.83	b	.060	bc	5.62	bc
	T6	4.90	c d	.077	b	5.45	bcd
	T7	4.97	c d	.047	c	5.48	bc
	T8	4.73	c d	.070	bc	5.10	cd
	T9	4.23	d	.077	b	4.85	d
Treatments mean		**5.24**		**0.070**		**5.54**	
Test of significance by (DMRT)		**		**		**	
Coefficient of Variation (C.V.%)		**7.36**		**19.39**		**5.98**	

application of nano-fertilizer improved 17.04 % nitrogen, 16.31 % phosphorous and 67.50 % potassium content in the leaves of treated plots compared to the control on coffee crop.

Effect on biochemical analysis of cotton seed. There were significant differences among the studied fertilizer treatments for macro elements N, P and K percentages in cotton seed content of G. 94 cotton cv. in 2018 and 2019 growing seasons. It is clear from the results in table 10 that the highest oil, Pr. and N percents in cotton seed were resulted from 100% nano – NPK fertilizer treatment (T_1) in both seasons. Also higher values of oil, Pr. and N percents in cotton seed were resulted from mixed treatments in combinations with nano-fertilizers and traditional one (T_4 and T_5) compared to control as well as nitrogen N % increase in case of application of 100 % nano-fertilizer and mixed nano with traditional NPK (T_4 and T_5). It could be suggested that nano-fertilizer considerably influenced the biochemical composition of both cotton seeds and cotton leaves for N, P and K percent [44] [45]; [32], found that the activity of water after adding nanomaterials was increased, and the elements N, P and K were absorbed into the plants, thus the macro elements N, P and K were also increased.

CONCLUSIONS

In the current study, application of 100 % chitosan – nanoparticles loaded with NPK-nanofertilizer composite has given the highest growth and yield performance parameters compared to the other foliar of traditional mineral NPK fertilizer and soil applications with recommended fertilizer dose (RFD) in the commercially of cotton areas . As well as, mixed of nano-NPK fertilizer with used traditional minertal NPK treatments significantly enhanced the most of growth, yield, yield components, earliness of crop maturity compared with control. Additionally, the leaf content of macro elements (N, P and K%) and the seed content of oil, protein, and nitrogen % were significantly increment in case of foliar application of nano-NPK fertilizer or nano coordinated with traditional NPK. It could be concluded that nano – fertilizer are the unique better substitute for traditional mineral NPK fertilizers in the developing countries. Nano –

TABLE 10
Effect of different fertilizer treatments of nano – NPK, traditional mineral NPK and its coordination of both on seed oil content %, seed prot. content % and seed N content % of G.94 cotton cultivar in 2018 and 2019 seasons.

seasons	*Treatments (T)*	*Seed oil content %*		*Seed prot. content %*		*Seed N content %*	
	T1	23.93	a	25.07	a	4.39	a
2018	**T2**	20.49	bc	22.63	b	3.84	ab
	T3	21.95	ab	22.37	b	3.74	ab
	T4	23.82	a	24.20	a	3.87	ab
	T5	22.16	ab	22.87	b	4.05	ab
	T6	18.87	c	22.57	b	3.84	ab
	T7	21.64	ab	21.67	b c	3.46	b
	T8	21.08	bc	22.17	b	3.52	b
	T9	20.52	bc	20.50	c	3.30	b
Treatments mean		**21.61**		**22.67**		**3.78**	
Test of significance by (DMRT)		**		**		*	
Coefficient of Variation (C.V.%)		**5.81**		**3.18**		**11.30**	
2019	**T1**	23.65	a	24.71	a	3.70	a
	T2	22.72	abc	23.40	a b c	3.07	c
	T3	22.07	cd	22.07	c	3.13	c
	T4	23.41	ab	24.14	a b	3.75	a
	T5	22.09	cd	23.41	a b c	3.63	a
	T6	21.89	cde	23.19	a b c	3.19	bc
	T7	22.47	bcd	23.20	a b c	3.51	ab
	T8	21.48	e	22.49	c	3.16	bc
	T9	20.83	e	22.87	b c	2.91	c
Treatments mean		**22.29**		**23.28**		**3.34**	
Test of significance by (DMRT)		**		*		**	
Coefficient of Variation (C.V.%)		**2.64**		**3.54**		**6.04**	

fertilizer causes an increase in their efficiency through controlled – release – fertilizers (CRF), reduces soil toxicity, minimizes the potential negative effects associated with over dosage of common fertilizers and reduces the frequency of the applications. Nano – fertilizers mainly delay the release of the nutrients and extends the fertilizer effect period. According to the findings, it could be proposed the chitosan-nanoparticles is the best candidate for agricultural application.

ACKNOWLEDGEMENTS

This study was a part of Ph. D. Thesis entitled "Effect of foliar spraying of nano and ordinary application of mineral NPK fertilizer on growth, yield, yield components and fiber properties of two Egyptian cotton (Gossypium barbadense L.) cultivars" The authors would like to express their deep gratitude due to Emeritus Prof. Dr. Ahmed Fouad H.El-Okkiah (previous) Vice Director of Cotton Res. Inst. Agric. Res. Center for valuable help and conductive criticism during the writing and preparation of this manuscript . The authors wish to express their sincere gratitude and appreciation to all staff of Nano-Technology and Advanced Materials Central Lab. (NAMCL). Agric. Res. Center (ARC). Giza, Egypt .

REFERENCES

[1] Naderi, M. R. and Danish Shahraki, A. (2013). Nano-fertilizer and their roles in sustainable agriculture. Int. J. Agric. Crop. Sci. 5. (19), 2229-2232.

[2] Veronica, N., Guru, T., Thatikunta, R., Narander Reddy, S. (2015).Role of nanofertilizers in agricultural farming. Int. J. Environ. Sci. Tech. 1(1), 1-3.

[3] Behera, S.K., Panda, R.K. (2009). Integrated management of irrigation water and fertilizes for wheat crop using field experiments and Simulation modeling. Agric. Wat. Manag. 96, 1532-1540.
[4] FAO (2019).The world fertilizer trends and outlook to 2019.
[5] FAO (2013).The total loss in nitrogen fertilizers application in 2013.
[6] Mandal, K.G., Hati K.M., Mista, A.K (2009). Biomass yield and energy analysis of soybean production in relation to fertilizer. NPK and organic manure. Biomass and Bioenergy, 33, 1670-1679 (2009).
[7] Trenkel, M.E. (1997). Controlled - release and stabilized fertilizers in agriculture Int. Fert. Indust. Assoc. Paris (1997).
[8] Saigusa, M. (2000), Broadcast application versus band application of polyolefin coated fertilizer on green peppers grown on andisol. Jounal of Plant Nutrition. 23, 1485-1493.
[9] Wu, L. and Lui, M. (2008). Preparation and properties of chitosan-coated NPK compound fertilizer with controlled-release and water retention. Carbohydrate Polymers. 72, 240-247.
[10]Guo, M.Y., Liu, M.Z., Zhan, F.L. and Wu, L. (2005). Preparation and Properties of a slow-release membrane- encapsulated urea fertilizer with superabsorbant and moisture preservation. 'Indust. Engin. 'Chem. Res. 44, 4206- 4211.
[11]Naderi, M.R. and Danesh Shahraki, A. (2011). TiO2, nano-particles affected on Maize (*Zea mays* L.)In 2nd. J. Nanotech. 11(1), 18-26.
[12]de Moura, M.R., Aouda, F.A., Mattose, L.H.C. (2008). Preparation of chitosan nanoparticles using methacrylic acid. J. Colloid. Interface Sci. 321, 477-483.
[13]Westermann, D.T. (2005). Nutritional requerments of potatos. American Journal of Potato Research. 82, 301-307.
[14]Singh, A., Bagri, S. K. Jha, J., Pandey, G.K. (2015). ABA inducible rice protein Phosphatase 2C confers ABA insensitivity and abiotic stress tolerance in Arabidopsis. Plos One. l0 (4), e 0125168.
[15]Corradini, E., de Mora , M.R., Mattoso L. H. C., (2010). A preliminary study of the incorporation of NPK fertilizes into chitosan nanoparticles. Express Polymer Letters. 4(8), 509-515.
[16]Hussien, M.M., El-Ashry, S.M., Haggag, W.M., Mubarak, D.M. (2015). Response of mineral status to nano-fertilizer and moisture stress during different growth stages of cotton plants. Inter.J. Chem Tech. Res. 8 (12), 643-650.
[17][Moran, R. (1982). Formula for determination of chlorophyllous pigments extracted with N.N.dimethylformamide. Plant Physiol. 69, 1371-1381.
[18]AOAC. (1995). Official Methods of Analysis of Association of Official Analytical Chemist. AOAC International. Virginia USA.
[19]Murphy, J., and Riley, J.P. (1962) A modified single-solution method for the determination of phosphorus in natural waters: Analytica Chimica Acta. 27, 31-36.
[20]Jackson, M. L.(1967): Soil Chemical Analysis Prentice Hall of India Pvt. Ltd., New Delhi. pp. 205
[21]Kates, M. (1972). Techniques of Lipidology (Isolation Techniques in Biochemistry and Molecular Biology Eds Ti's.T.S. Work& E. Work) P.350 Amsterdam North Holland Publishing.
[22]Snedecor, G.W. and Cochran, W.G. (1990) Statistical Methods. 8th Edition, Iowa State University Press, Ames.
[23]LeClerg, E. L. (1962) Field Plot Techniques (2nd. Ed.), Burgess, Mineapolis. 373 pp.
[24] Kazemi, N.M. and Salimi, A, A.(2019). Chitosan nanoparticles for loading and release of nitrogen, potassium, and phosphorus nutrients. Iran J. Sci. Tech. Trans. Sci (2019) 43, 2781-2786.
[25]Song. U., M. Shin, G. Lee, J. Roh, Y.Kim, E.J. Lee (2013). Functional analysis of TiO2, nanoparticle toxicity in three plant species. Biological Trace E. 155(1), 93-103.
[26][Eleyan Sohair, E.D., Abodahab, A A Abdallah Amany, M. and Rabeh Hauda,A (2018). Effect of nitrogen, phosphorus and potassium nano fertilizer with different application times, methods and rates on some growth parameters of Egyptian Cotton(Gossypium barbadense L) Bioscience Research. 15 (2), 549-564.
[27]Rathnayaka, R.M.N.N, Mahendran, S., Igbal, Y. B., Rifnas, L. M. (2018). Influence of urea and nano- nitrogen fertilizers on the growth and yield of Rice (Oryza sativa L.) cultivar a (Bg 250) Int. J. Res. Publ. 5(2), 1-7.
[28][Kanjana, D. (2019). Foliar study on effect of iron oxide nano-particles As an alternate soirce of iron pestilizes to Cotton. Inter J. Chem. Studies. 7(3), 4374_4379.
[29]Kanjana, D. (2020).Evaluation of foliar application of different types of nanofertilizers on growth,yield and quality parameters and nutrient concentration of cotton under irrigated condition.Int. J.Curr.Microbial APP.Sci. 9(7), 429-441.
[30]Ghormade, V., Deshpande, M. V., Paknikar. K.M. (2011). Perspectives for nano-biotechnology enabled protection and nutrition of plants Biotechnol. Adv. 29, 792-803.
[31]Wajid,A.,A.Ahmed,M.Awais,M.Hbib-ur-Rahman, A.Sammar, U. Bashir, M. N.Arshad, Sana Ullah, M.Irfan and U.Gull (2017). Nitrogen requirements of promising cotton cultivars in arid climate of Multan. Sarhad J.of Agric. 33(3),397-405.

[32]Meena. D. S., Chirag, G., Prakash, P.OM., Mohan, M. H., Prakasha, G. and Vishwa, J. (2017) Nano fertilizers is a new way to increase nutrients use efficiency in cop production. Int. J. Agric. Sci. 9 (7), 3831-3833.

[33]Tarafdar, J.C., R. Raliya: H. Mahawar and I. Rathore (2014). Development of zinc nanofertilizer to enhance crop production in pearl millet (Pennisetum americanum). Agric. Res. 3(3), 257-262-

[34]Kumbhar, A.M., Buriro, U. A., Junejo, S., Oad, F.C., Jamro, G.H., Kumbhar, B.A. and Kumbhar, S.A (2008). Impact of different nitrogen levels on cotton growth, yield and N-uptake planted in legume rotation. Pakistan J. Bot. 40, 767-778.

[35]Zakzok, A.K.M.E. (2018). Effect of organic and mineral fertilization by nano- technology on yield and lint characters of Egyptian cotton. M. Sc. Thesis, Fac. Agric. Ain Shams Univ.

[36]Ovalle, J.F., Arellano, E.C., Ginocchio R and Becema P. (2016). Fertilizar location modifies root zone salinity, root morphology, and water stress resistance of the seedlings according to the watering regime in a dry land reforestation. J. Plant Nutr. Soil Sci. 179, 223-233.

[37]Shoji, S., Delgado, J., Mosier, A. and Miura, Y. (2001). Use of controlled release fertilizers and nitrification, inhibitors to increase nitrogen use efficiency and to conserve air and water quality. Commun. Soil Sci. Plan. 32, 1051 -1070.

[38]Geng, J, Ma, Q., Zhang, M., Li, C., Liu, Z., Lyu, X., Zheng, W. (2015). Synchronized relationships between nitrogen release of controlled release fertilizes and nitrogen requirements of cotton. Field Crop. Res. 184, 9-16.

[39]Liu, J., Zhang, Y.D. and Zhang, Z.M (2009). The application research of nano- biotechnology to promote increasing of vegetable production. Hubei. Agric. Sci. 1,123-127. (in Chinese with English abstract).

[40]Xiao Fei, T., Cheng, L.L., Zhang, M., Yan, Y.L., Yan, L.G. and Long, F.L. (2017). Effect of controlled, release potassium fertilizer on available potassium, photosynthetic performance and yield of cotton. J. Plant Nut. Soil Sci. 180, 505-515.

[41]Nguyen, V.S.,. Dinh, M. H. and. Nguyen, A. D. (2013). Study on chitosan nanoparticles on biophysical characteristics and growth of Robusta coffee in green house. Biocatalysis and Agric. Biotechen.:2(4), 289-294.

[42]Ledezma Delgadillo, A., Conzalez, R.C., San Martin, E., Fonseca, M.R.J. and Lopez, M.A.C. (2016). Rev. Mex. Ing. Quim. 15, 423 2016.

[43]Chau Ha, N.M., Nguyen, T.H., Wang, S.L. and Nguyen, A.D. (2019). Preparation of NPK nanofertilizer based on chitosan nanoparticles and its effect on biophysical characteristics and growth of coffee in green house. Res. Chem. Intermediates. 45, 51-63.

[44]Gao, J., Xu, G., Qian, H., Liu, P., Zhao, P., and Hu, Y. (2013). Effects of nano.TiO2 on photosynthetic characteristics of Ulmus elongata Seedlings. Environmental Pollution. 176,63-70.

[45]]Morteza, E., Moaveni, P., Farahani, H. A. and Kiyani, M. (2013) Study of photosynthetic pigments changes of maize (*Zea mays* L.) under nano TiO2, spraying at various growth stages. Springer Plus. 2(1),1-5

Received: **22.12.2020**
Accepted: **23.05.2021**

CORRESPONDING AUTHOR

SamiraEl-Okkiah
Department of Agriculture Botany,
Faculty of Agriculture,
Kafr El-Sheikh University,
33516 Kafr El-Sheikh, Egypt

e-mail: samira.fouad@agr.kfs.edu.eg

© by PSP Volume 30– No. 09/2021 pages 11002-11008 Fresenius Environmental Bulletin

EVALUATION OF ANTIMICROBIAL, ANTIOXIDANT AND ENZYME INHIBITORY POTENTIAL OF FIXED OIL EXTRACTED FROM STEM BARK OF *Acacia stenophylla*

Nadia Khan[1], Arshad Iqbal[1], Khushnood Ur Rehman[1], Muhammad Hamayun[2], Farooq Shah[3], Amjad Iqbal[4], Anwar Hussain[2], Jamshaid Ahmad[5], In-Jung Lee[6,*]

[1]Department of Botany, Islamia College Peshawar, Pakistan
[2]Department of Botany, Abdul Wali Khan University Mardan, Pakistan
[3]Department of Agronomy, Abdul Wali Khan University Mardan, Pakistan
[4]Department of Food Science & Technology, Abdul Wali Khan University Mardan, Pakistan
[5]Centre of Biotechnology & Microbiology (COBAM), University of Peshawar, Pakistan
[6]School of Applied Biosciences, Kyungpook National University, Daegu, Korea

ABSTRACT

The current research was planned to determine the antimicrobial, antioxidant and enzyme inhibitory activity of fixed oil extracted from stem bark of *Acacia stenophylla.* Antimicrobial activities were determined by disc-diffusion and macro dilution methods. The results revealed that maximum zone of inhibition (bacteria and fungi) was measured by fixed oil against 12 mm and 5 mm, respectively. MIC values recorded by fixed oil were 0.5 mg/ml, 1.0 mg/ml, 2.0 mg/ml, 4.0 mg/ml and 8.0 mg/ml against different bacterial and fungal strains tested. Acetylcholinesterase and lipooxygenase inhibitory activity were measured by spectrophotometric methods. Fixed oil of *Acacia stenophylla* inhibited acetylcholinesterase by 247.1 mg/ml (IC_{50}). Similarly, antioxidant potential of fixed oil was measured by two different models, i.e ABTS radical scavenging and ferric reducing/antioxidant power (FRAP) assay. The reduction in ABTS radical scavenging activity depended on the concentration of the extract. Maximum percent inhibition was shown by fixed oil at 800 µg/ml. In case of ferric reducing/antioxidant power assay, plant sample showed inhibition of 671.3 µg/ml. It is concluded that fixed oil of *Acacia stenophylla* has strong antimicrobial, enzyme inhibitory and antioxidant potential.

KEYWORDS:
Acacia stenophylla, Fixed oil extraction, Antimicrobial, Antioxidant, ACE inhibition

INTRODUCTION

Plants, animals and microbes can be used as one of the best sources of potent compounds [1-3]. The potents compounds, includes poly phenols, flavonoids, oils and someother compounds that have antimicrobial and/or antioxidative properties [4-10] Fixed oil from plant species are fragrant oily fluids that consists of phenolic compounds, terpenoids, alcohols, aldehydes [11]. Fixed oil also contains stearic, linoleic, linolinic acids and palmitic acid. In human diet oleic acid helps to reduce levels of LDL-cholesterol, total cholesterol and glycemic index [12]. Essential oils are rich in terpenoids, some species have large amounts of phenylpropanoids, which give specific flavour and odour to the plants. Monoterpenes and sesquiterpenes are also present in essential oils [13].

Pharmacological ability of the essential oil is due to the presence of secondary metabolites [14]. Variety of essential oil and their components are reported recently to show antimicrobial activity against fungi and bacteria [15]. Essential oils have been use to overcome infectious microorganisms and to control predominant multi-drug resistant microorganisms [16]. Thymol, carvacrol and eugenol are essential oils obtained from plants containing phenolic compounds that exhibited antibacterial properties [17].

MATERIALS AND METHODS

Fixed oil extraction: Approximately, 7 gm material of *A. stenophylla* bark was taken in 250 ml flask. It was then mixed in water and hexane (2:1 v/v). The sample was shaken vigorously for 2-3 minutes. The upper layer (hexane) was taken in another tube and 1 ml hexane was then added. The hexane layer was shaken and separated. The collected hexane layer was heated on water bath to obtain the oil extracted from the plant material.

Antimicrobial activity. Initial screening (Zone of inhibition): The antimicrobial activities were carried out by performing the disc-diffusion

method of Reller, et al. [18]. Crude extract of *A. stenophylla* bark extract (10 mg) was dissolved in 1 ml of DMSO (10%) in a tube. The selected microbial cell suspension culture (10^5 CFU/ml) was inoculated individually on Muller-Hinton Agar plates and the plates were allowed to dry under sterile conditions. During this time sterile paper discs were soaked in 100 µl of the *A. stenophylla* bark extract. In case of antibacterial assay, streptomycin (10 µg/ml) was used as a positive control, whereas amphotericin B (10 µg/ml) or miconazole (10 µg/ml) were used as a positive control in antifungal assay. The plates were covered an sealed after placing the discs in each plate to prevent any evaporation. The sealed plates were left on the bench top for 30 minutes at room temperature to allow diffusion. After 30 minutes, the plates were transferred to the incubator operated at 37 °C for one day. On the next day, zone of inhibition was measured as antimicrobial activity of the test solution.

Determination of MIC: The test sample (8, 4, 2, 1 and 0.5 mg) was mixed with 1 ml of DMSO (10%). The mixture was filtered through a 0.45 µm thick filter membrane. The inoculum of the tested bacterial or fungal strains was then mixed in Muller-Hinton broth to end up with 10^5 CFU/ml. The Microplates in a laminar flow cabinet were then filled with the 150 µl of the diluted tested sample mentioned above. The bacterial or fungal inoculum (50 µl) was then inoculated into the different wells and the microplate was incubated for 24 hours at 37 °C. On the next day, tetrazolium was added to each well. A dim colour confirmed the antimicrobial activity and the lowest concentration that showed inhibition was set as minimum inhibitory concentration. The standards used for comparison were streptomycin, amphotericin B and miconazole [19].

Acetyl cholinesterase inhibitory activity: The modified spectrophotometric method of Khan, et al. [20] was used for the determination of the AChE inhibitory activity. A solution mixture was made that consisted of 150 µL of sodium phosphate buffer (100 mM, pH 8.0), 10 µl of DTNB [5,5-Dithiobis (2-nitrobenzoic acid)], 10 µl of *A. stenophylla* bark extract and 20 µl of acetylcholinesterase. The mixture was incubated for 15 minutes at 25 ºC. The reaction was then initiated by adding 10 mL of acetylthiocholine to the mixture. A yellow coloured compound, 5-thio-2-nitrobenzoate anion was formed by the enzymatic hydrolysis of acetythiocholine, which was measured after 15 minutes at 412 nm using spectrophotometer. The reaction was conducted in 96-well micro-plate. The percentage inhibition of AChE was calculated by using the following formula:

$$\%\ Inhibition = \frac{(E - S)}{E} \times 100$$

Where,

E is the activity of the enzyme without test sample; S is the activity of enzyme with the test sample.

Lipoxygenase assay: The modified spectrometric method of Khan, et al. [21] was used for lipoxygenase assay. The reaction mixture consisted of 160 µL of sodium phosphate buffer (0.1 mM; pH 7.0), *A. stenophylla* bark extract (10 mL) and lipoxygenase solution (20 mL). After mixing the solution thoroughly, it was incubated at 25 ºC for 5 minutes. Added, 10 µL of the linoleic acid as a substrate and the reaction was initiated. The absorbance was monitored at 234 nm for 10 minutes. Baicalein was utilised as a positive control.

Radical scavenging activity: The stock solutions was prepared by mixing 2.5 ml of 7 mM ABTS [2,2-azino-bis(3-ethylbenzothiazoline-6-sulponic acid)] and 2.4 mM potassium persulfate. The mixture was allowed to stand in cool and dark place for 16 hours. Distilled water was added to adjust the optical density (OD) of the ABTS and potassium persulfate mixture to 0.706 ± 0.1. The OD of the mixture was monitored through spectrophotometer operated at 734 nm [22]. For the reaction 1 ml of the *A. stenophylla* bark extract was added to the ABTS mixture solution and the absorbance was measured after 7 minutes at 734 nm by spectrophotometer. Butylated hydroxytoluene (BHT) was used as a standard. The percentage inhibition was measured by comparing BHT with ABTS scavenging capacity of the *A. stenophylla* bark extract by using the following formula:

$$ABTS\ _{activity\ (\%)} = [(Abs_1 - Abs_2)/Abs_1] \times 100$$

where, Abs_1 is the absorbance of ABTS radical + methanol; Abs_2 is the absorbance of ABTS radical + sample extract /standard.

Ferric Reducing/Antioxidant Power (FRAP) Assay: FRAP assay was determined by using the modified method of Benzie and Strain [23]. Solution 1: Acetate buffer (pH 3.6) was prepared by adding 3.1 g of $C_2H_3NaO_2 \cdot {}_3H_2O$ to 16 ml of $C_2H_4O_2$. Solution 2: TPTZ (2, 4, 6-tripyridyl-*s*-triazine) solution (10 mM) was made in 40 mM HCl and 20 mM $FeCl_3.6H_2O$. The FRAP working solution was made by mixing 30 ml of acetate buffer, 3 ml TPTZ, and 3 ml $FeCl_3 \cdot 6H_2O$. The working solution was kept at 37 ºC before use. About, 75 µl of the *A. stenophylla* bark extract was mixed with 1425 µl of the FRAP solution and the mixture was kept in dark for 30 minutes. After the incubation, the absorbance was measured at 593 nm. Ascorbic acid was used as a standard for comparison.

RESULTS

Oil analysis of *A. stenophylla*: The crude extract of *A. stenophylla* stem bark was screened by GCMS for the presence of fatty acid (Table 1). The analysis confirmed the presence of fatty acid. The main fatty acids were: C12:0; lauric acid, methyl ester (0.00%), C14:0; myristic acid, methyl ester (0.00%), C14:1c; myristoleic acid, methyl ester (0.02%), C16:0; palmitic acid, methyl ester (0.04%), C18:1c; oleic acid, methyl ester (0.02%), C18:2c; linoleic acid, methyl ester (0.12%), C18:2t; octadecadienoic acid, ethyl ester (0.07%) and C18:3n6; γ-linolenic acid, methyl ester (0.08%), respectively.

Antibacterial activity of fixed oil from stem bark of *A. stenophylla*: The data about zone of inhibition and minimum inhibitory concentration (MIC) of fixed oil extracted from stem bark of *A. stenophyla* has been given in Table 2. The results declared that the standard drug streptomycin and the test sample (fixed oil) showed variable inhibition against different bacterial strains tested. Streptomycin revealed maximum zone of inhibition against *S. flexienari*. Similarly, plant sample showed maximum zone of inhibition against *B. subtils*, which was 12 mm. *P. aeruginosa* and *S. typhi* were not inhibited by the test sample. The results further reveal a different inhibitory concentration (MIC) values of standards and test sample. Minimum inhibitory concentration (MIC) measured for streptomycin (0.002 µg/ml) against *E. coli.* Similarly, plant sample showed MIC of 0.5 mg/ml, 1.0 mg/ml, 2.0 mg/ml and 4.0 mg/ml against *S. subtils*, *S. aureus, E. coli* and *S. flexienari*, respectively. No MIC values were measured against *P.aeruginosa* and *S.typhi* by the test sample (Table 2).

Antifungal activity of fixed oil from stem bark of *A. stenophylla*: Data about zone of inhibition and minimum inhibitory concentartion of *A. Stenophyla* stem bark is shown in Table 3. Application of the standard drugs (miconazole and amphotericin B) or selected plant (fixed oil) extract revealed different zone of inhibition against the different tested fungal strains. Miconazole and amphotericin B revealed highest zone of inhibition against *C. glabrata*. Similarly, *A. stenophylla* bark extract exhibited the highest zone of inhibition (5 mm) against *C. albicans*. Whereas, *A. stenophylla* bark extract failed to inhibit the growth of *A. flavus, M. canis* and *T. longifusus*. The results further demonstrated different MIC values for standard drugs and tested plant sample. MIC for miconazole was 0.0005 mg/ml against *C.glabrata*. Similarly, the selected plant revealed MIC values of 4.0 mg/ml against *C. albicans*, *E. solani* and *C. glabrata*, while 8.0 mg/ml against *C. glabrata*, respectively. No MIC values were observed against *A. flavus*, *M. canis* and *T. longifusus* by tested plant sample.

TABLE 1
Quantitative analysis of stem bark oil

S.No	Name	R.Time	Area	Conc. (%)
1.	C12:0; Lauric acid, methyl ester	8.522	1552	0.00
2.	C14:0; Myristic acid, methyl ester	10.951	1931	0.00
3.	C14:1c; Myristoleic acid, methyl ester	11.549	1702	0.02
4.	C16:0; Palmitic acid, methyl ester	14.614	18864	0.04
5.	C18:1c; Oleic acid, methyl ester	20.146	1814	0.02
6.	C18:2c; Linoleic acid, methyl ester	21.334	13080	0.12
7.	C18:2t; Octadecadienoic acid, ethyl ester	21.722	8339	0.07
8.	C18:3n6; g-linolenic acid, methyl ester	23.080	5582	0.08

TABLE 2
Antibacterial activity of fixed oil from stem bark of *Acacia stenophylla*

Microbes	Zone of inhibition (mm)		MIC (mg/ml)	
	Streptomycin	AS	Steptomycin	AS
E. coli	28	8	0.002	2.0
B. subtils	26	12	0.005	0.5
S. flexienari	29	6	0.003	4.0
S. aureus	27	9	0.009	1.0
P.aeruginosa	28	NA	0.021	NA
S. typhi	24	NA	0.014	NA

AS = *Acacia stenophylla*

TABLE 3
Antifungal activity of fixed oil from stem bark of *Acacia stenophylla*

Microbes	Zone of inhibition (mm)		Minimum inhibitory concentration, MIC (mg/ml)	
	Standard (Miconazole/ Amphotericin B	AS	Standard (Miconazole/Amphotericin B	*Acacia stenophylla*
C. albicans	23[1]	5	0.0017[1]	4.0
A. flavus	21[2]	NA	0.0024[2]	NA
M. canis	22[1]	NA	0.0017[1]	NA
F. solani	26[1]	2	0.0011[1]	8.0
C. glabrata	29[1]	3	0.0005[1]	8.0
T. Longifusus	24[1]	NA	0.0014[1]	NA

[1]= Miconazole,[2]=Amphotericin B, AS = *Acacia stenophylla*

TABLE 4
Acetycholinesterase and lipoxygenase inhibitoy activity of fixed oil from stem bark of Acacia *stenophylla*

Enzyme	IC_{50} (µg/ml)		
	AS	Standard	
Acetycholinesterase	247.1±0.04	0.0017±0.0001	Galanthamine (Standard)
Lipoxygenase	61.41±0.004	0.08251±0.001	Baicalein (Standard)

AS = *Acacia stenophylla*

TABLE 5
ABTS radical scavenging assay of fixed oil from stem bark of *Acacia stenophylla*

Sample	Percent inhibition (%)				IC_{50} (µg/ml)
	100 µg/ml	200 µg/ml	400 µg/ml	800 µg/ml	
AS	63.22±0.16	69.05±0.23	74.08±0.27	89.91±0.14	<0.1
AA (standard)	76.61±0.62	78.89±0.42	79.26±0.91	81.72±0.97	<0.1

AS = *Acacia stenophylla*, AA = Ascorbic Acid

Acetycholinesterase and lipoxygenase inhibitory activity of fixed oil from stem of *Acacia stenophylla*: The data concerning the acetylcholinesterase and lipoxygenase inhibitory activity of fixed oil extracted from stem bark of *A. stenophyla* is given in the Table 4. The results showed that the standard (Galanthamin) or test sample (fixed oil) showed different inhibitory activity against acetycholinesterase. The recorded IC_{50} for acetylcholinesterase by the *A. stenophylla* bark extract was 247.1µg/ml, whereas the standard drug (Galanthamine) showed IC_{50} value of 0.0017µg/ml.

The IC_{50} of *A. stenophylla* bark extract against the lipoxygenase activity was 61.41 µg/ml, while the standard drug (Baicalein) shoed 0.08251 µg/ml of the lipoxygenase inhibitory activity (Table 4).

ABTS (2, 2-azino-bis (3-ethylbenothiazoline-6-sulphonic acid) radical scavenging assay of fixed oil from stem of *A. stenophylla*: The antioxidant activity of *A. stenophylla* stem bark and ascorbic acid (standard) are shown in Table 5. The data revealed 100% inhibition against the different concentrations (100, 200, 400, 800 µg/ml) of ABTS.

Ferric Reducing/Antioxidant Power (FRAP) Assay of fixed oil from stem bark of *A. stenophylla*: The antioxidant activity of the *A. stenophylla* stem bark and ascorbic acid (standard) are shown in Table 6. The *A. stenophylla* stem bark extract revealed maximum inhibitory activity of 671.3, while the antioxidant activity of AA was 1642.8.

DISCUSSION

The *Acacia stenophylla* stem bark showed the presence of poly unsaturated fatty acid of omega class. This poly unsaturated fatty acid of omega class is useful for cardiac diseases. This helps in preventing cardiac arrhythmia and thus preventing sudden cardiac death of human [24]. Omega-3 fatty acids are a type of polyunsaturated fat (like omega-6), which are considered as essential fatty acids because it cannot be synthesised by the body [25]. As a result, people must obtain omega-3 fatty acids from foods, such as fish, nut, and plant-based oils (canola oil and sunflower oils).

Essential oils or its components are very effective against a variety of organisms, such as fungi [26] and bacteria [27]. Thymol, carvacrol and eugenol essential oils obtained from plants contain phenolic compounds that are having antibacterial properties and are best against pests and microbes [17]. Essential oil obtained from garlic, ginger, clove, black pepper and green chilli showed antibacterial

TABLE 6
Ferric reducing/ antioxidant power (FRAP) assay of fixed oil from stem of *A. stenophylla*

Sample	FRAP (Expressed in units of µmol Fe (II)/g)
AS	671.3±26.97
Ascorbic acid (standard)	1642.8±19.9

activity against different bacterial strains, such as *Bacillus sphaericus, Enterobacter aerogenes*, *E. coli*, *P. aeruginosa*, *S. aureus*, *S. epidermidis*, *S. typhi* and *Shiguella flexneri* [28].

Lipoxygenases are non-heme iron-containing dioxygenases [29]. Lipoxygenase is enzyme that catalyses the oxygenation of polyunsaturated fatty acids to fatty acid hydro peroxides. In cells, the accumulation of free fatty acids is limited and thus, LOX substrates have to be liberated from cellular stores by ester lipid hydrolyzing enzymes [30]. Acetylcholine can also help in the transmission of massages in neuron. In the presence of enzyme acetyl cholinesterase, acetylcholine can be hydrolysed into choline and acetyl group. Acetyl cholinesterase inhibitors are commonly used for therapy of Alzheimer's disease to improve central cholinergic neurotransmitter [31]. The essential oils and extracts from *Salvia* are very helpful in the protection of neurodegenerative disorders, because of their potential acetylcholinesterase inhibitory and antioxidant activities [32]. From above study it is concluded that fixed oil of the stem bark of *A. stenophylla* showed the inhibition against AChE and LOX, which are useful in the curing of many disorders and diseases.

Oxidative stress involved in cellular and extracted- lunar metabolic processes, cause metabolic stress and nitrosamine stress. During biological conditions reactive nitrogen intermediate and reactive oxygen intermediate are continuously formed, which is indeed critical events in the living organisms. Antioxidative defence mechanisms are the most operative way to combat the free radicals that can cause oxidative stress. Antioxidants can in fact disrupt the free radicals by blocking the reactions by which they can be produced in the body [33]. The reactive oxygen species can lead to many disorders, including cancer, cardiac disorders, Alzheimer's disease, aging, inflammation, degenerative disorders of nervous system, atherosclerosis, and optical diseases. Vegetables and fruits have natural occurring antioxidants are very operative in the treatment of cancer and heart diseases [6-9, 34-36].

CONCLUSION

The present research work consists of three major activities. The fixed oil of *Acacia stenophylla* stem bark revealed good antioxidant potential. The antimicrobial activity of the fixed oil showed good activity against the tested bacterial and fungal strains. The plant fixed oil also demonstrated promising enzyme inhibition activity. On the basis of the results, we concluded that the fixed oil from the bark of *A. stenophylla* can be used in foods as a health promoting neutracuticals.

REFERENCES

[1] Iqbal, A. and Fry, S. C. (2012), Potent endogenous allelopathic compounds in *Lepi-dium sativum* seed exudate: effects on epidermal cell growth in *Amaranthus caudatus* seedlings. Journal of Experimental Botany. 63(7), 2595-2604.

[2] Iqbal, A., Miller, J. G., Murray, L., Sadler, I. H. and Fry, S. C. (2016), The pectic disaccharides lepidimoic acid and β-d-xylopyranosyl-(1→ 3)-d-galacturonic acid occur in cress-seed exudate but lack allelochemical activity. Annals of Botany. 117(4), 607-623.

[3] Iqbal, A., Shah, F., Hamayun, M., Khan, Z. H., Islam, B., Rehman, G., Khan, Z. U., Shah, S., Hussain, A. and Jamal, Y. (2019), Plants are the possible source of allelochemicals that can be useful in promoting sustainable agriculture, Fresen. Environ. Bull. 28(2 A), 1052-1061.

[4] Iqbal, M., Amin, M., Iqbal, Z., Bibi, H., Iqbal, A., Din, Z.-u., Suleman, M. and Shah, H. U. (2014) Antimicrobial, cytotoxic and phytotoxic potency of ethyl acetate extract of *Rhizopus stolonifer* culture. Tropical Journal of Pharmaceutical Research. 13(1), 87-92.

[5] Jan, I., Rab, A., Sajid, M., Iqbal, A., Shinwari, Z. K. and Hamayun, M. (2016), Effect of calcium salt on soft rot, bitter pit and physicochemical properties of stored apples. Pakistan Journal of Botany. 48(4), 1415-1420.

[6] Qadri, R., Ubaid, Z., Saleem, A., Iqbal, A., Khan, M. M., Feroz, A., Azam, M. and Yang, Y. (2018), Phenotypic diversity among peach cultivars grown under environmental conditions of Pothohar (salt range) Pakistan. Fresen. Environ. Bull. 27(12 A), 9289-9299.

[7] Qadri, R., Yang, Y., Abid, A., Iqbal, A., Khan, M. M., Shah, F. and Iqbal, M. (2018), Genetic Diversity Of The Productive Jujube Cultivars From Punjab-Pakistan on the basis of morphological and biochemical characteristics. Fresen. Environ. Bull. 27(3), 1742-1748.

[8] Rehman, G., Hamayun, M., Iqbal, A., Ul Islam, S., Arshad, S., Zaman, K., Ahmad, A., Shehzad, A., Hussain, A. and Lee, I. (2018), In Vitro Antidiabetic Effects and Antioxidant Potential of *Cassia nemophila* Pods. BioMed. Research International. 2018, 1-6.

[9] Rehman, G., Hamayun, M., Iqbal, A., Zaman, K., Arshad, S., Hussain, A., Shah, M., Gul, S., Kang, S.-M. and Lee, I.-J. (2018) Hypoglycemic effect of *Cassia nemophila* pods extract in STZ-induced diabetic mice. Fresen. Environ. Bull. 27(12 A), 9329-9335.

[10] Rehman, G., Arshad, S., Hamayun, M., Iqbal, A., Shams, W. A., Hussain, A., Zaman, K., Ahmads, A., Shah, M. and Gul, S. (2019) Novel bioactivities of *Cassia nemophila* pods against diabetic nephropathy: In vitro and in vivo study. Fresen. Environ. Bull. 28, 2656-2663.

[11] Goni, P., López, P., Sánchez, C., Gómez-Lus, R., Becerril, R. and Nerín, C. (2009), Antimicrobial activity in the vapour phase of a combination of cinnamon and clove essential oils. Food Chemistry. 116(4), 982-989.

[12] Brouwer, I. A., Wanders, A. J. and Katan, M. B. (2010), Effect of animal and industrial trans fatty acids on HDL and LDL cholesterol levels in humans–a quantitative review, PloS one, 5(3), e9434.

[13] Bakkali, F., Averbeck, S., Averbeck, D. and Idaomar, M. (2008), Biological effects of essential oils–a review. Food and Chemical Toxicology. 46(2), 446-475.

[14] Sartoratto, A., Machado, A. L. M., Delarmelina, C., Figueira, G. M., Duarte, M. C. T. and Rehder, V. L. G. (2004), Composition and antimicrobial activity of essential oils from aromatic plants used in Brazil. Brazilian Journal of Microbiology. 35(4), 275-280.

[15] Vasinauskienė, M., Radušinė, J., Zitikaitė, I. and Survilienė, E. (2006), Chemical composition and antimicrobial activity of the essential oils of Gentiana asclepiadea, L. Agronomy Res. 4, 1-12.

[16] Mulyaningsih, S., Youns, M., El-Readi, M. Z., Ashour, M. L., Nibret, E., Sporer, F., Herrmann, F., Reichling, J. and Wink, M. (2010), Biological activity of the essential oil of Kadsura longipedunculata (Schisandraceae) and its major components. Journal of Pharmacy and Pharmacology. 62(8), 1037-1044.

[17] Kim, J., Marshall, M. R. and Wei, C.-i. (1995), Antibacterial activity of some essential oil components against five foodborne pathogens, Journal of Agricultural and Food Chemistry. 43(11), 2839-2845.

[18] Reller, L. B., Weinstein, M., Jorgensen, J. H. and Ferraro, M. J. (2009) Antimicrobial susceptibility testing: a review of general principles and contemporary practices. Clinical Infectious Diseases. 49(11), 1749-1755.

[19] El-Hawary, S., Taha, K., Kirillos, F., Dahab, A., Saleh, N. and El-Mahis, A. (2015), Molecular identification, GC/MS and antimicrobial activity of the essential oils and extracts of three Podocarpus species, Int. J. Pharmacog. Phytochem. 30(2), 1360-1369.

[20] Khan, I., Nisar, M., Shah, M. R., Shah, H., Gilani, S. N., Gul, F., Abdullah, S. M., Ismail, M., Khan, N. and Kaleem, W. A. (2011), Anti-inflammatory activities of Taxusabietane A isolated from Taxus wallichiana Zucc. Fitoterapia. 82(7), 1003-1007.

[21] Khan, I., Nisar, M., Khan, N., Saeed, M., Nadeem, S., Ali, F., Karim, N., Kaleem, W. A., Qayum, M. and Ahmad, H. (2010), Structural insights to investigate Conypododiol as a dual cholinesterase inhibitor from *Asparagus adscendens*. Fitoterapia. 81(8), 1020-1025.

[22] Valantina, R. S. and Neelamegam, P. (2015), Selective ABTS and DPPH-radical scavenging activity of peroxide from vegetable oils. International Food Research Journal. 22(1), 289.

[23] Benzie, I. F. and Strain, J. J. (1996), The ferric reducing ability of plasma (FRAP) as a measure of "antioxidant power": the FRAP assay. Analytical Biochemistry. 239(1), 70-76.

[24] Leaf, A., Kang, J. X., Xiao, Y.-F. and Billman, G. E. (2003) Clinical prevention of sudden cardiac death by n-3 polyunsaturated fatty acids and mechanism of prevention of arrhythmias by n-3 fish oils. Circulation. 107(21), 2646-2652.

[25] Amjad Khan, W., Chun-Mei, H., Khan, N., Iqbal, A., Lyu, S.-W. and Shah, F. (2017), Bioengineered plants can be a useful source of omega-3 fatty acids. BioMed Research International. 2017, 1-9.

[26] Hammer, K., Carson, C. and Riley, T. (2003), Antifungal activity of the components of Melaleuca alternifolia (tea tree) oil. Journal of Applied Microbiology. 95(4), 853-860.

[27] Akthar, M. S., Degaga, B. and Azam, T. (2014), Antimicrobial activity of essential oils extracted from medicinal plants against the pathogenic microorganisms: A review. Issues in Biological Sciences and Pharmaceutical Research. 2(1), 1-7.

[28] Arora, D. S. and Kaur, J. (1999), Antimicrobial activity of spices. International Journal of Antimicrobial Agents. 12(3), 257-262.

[29] Schneider, C., Pratt, D. A., Porter, N. A. and Brash, A. R. (2007), Control of oxygenation in lipoxygenase and cyclooxygenase catalysis. Chemistry & Biology. 14(5), 473-488.

[30] Schaller, A. and Stintzi, A. (2009), Enzymes in jasmonate biosynthesis–structure, function, regulation. Phytochemistry. 70(13), 1532-1538.

[31] Wszelaki, N., Kuciun, A. and Kiss, A. (2010), Screening of traditional European herbal medicines for acetylcholinesterase and butyrylcholinesterase inhibitory activity, Acta Pharmaceutica. 60(1), 119-128.
[32] Şenol, F. S., Orhan, I., Celep, F., Kahraman, A., Doğan, M., Yilmaz, G. and Şener, B. (2010), Survey of 55 Turkish Salvia taxa for their acetylcholinesterase inhibitory and antioxidant activities. Food Chemistry. 120(1), 34-43.
[33] Uttara, B., Singh, A. V., Zamboni, P. and Mahajan, R. (2009), Oxidative stress and neurodegenerative diseases: a review of up-stream and downstream antioxidant therapeutic options, Current Neuropharmacology. 7(1), 65-74.
[34] Lobo, V., Patil, A., Phatak, A. and Chandra, N. (2010), Free radicals, antioxidants and functional foods: Impact on human health. Pharmacognosy Reviews. 4(8), 118.
[35] Rehman, G., Hamayun, M., Iqbal, A., Khan, S. A., Khan, H., Shehzad, A., Khan, A. L., Hussain, A., Kim, H.-Y. and Ahmad, J. (2017), Effect of methanolic extract of dandelion roots on cancer cell lines and AMP-activated protein kinase pathway. Frontiers in Pharmacology. 8, 1-6.
[36] Viyar, A. H., Qadri, R., Iqbal, A., Nisar, N., Khan, I., Bashir, M. and Shah, F. (2017), Evaluation of unexplored pomegranate cultivars for physicochemical characteristics and antioxidant activity. Journal of Food Science and Technology. 54(9), 2973-2979.

Received: **20.02.2020**
Accepted: **23.11.2020**

CORRESPONDING AUTHOR

In-Jung Lee
School of Applied Biosciences,
Kyungpook National University,
Daegu – Korea

e-mail: ijlee@knu.ac.kr

© by PSP Volume 30– No. 09/2021 pages 11009-11010 Fresenius Environmental Bulletin

NOTICE

CONTENT AND SAFETY OF FOUR MAIN HEAVY METALS IN HARD GELATIN CAPSULE SHELL

Jin Xiaoli, Wang Lei, Zhu Huanlei*

Yantai Yuhuangding Hosp, Yudong Rd 20, Zhifu District 26400, Shandong Province, P.R. China

ABSTRACT

Capsules are widely used in pharmaceutical packaging. As a substance entering human body by taking medicine, the safety of capsule should be as important as that of food. The contents of four main heavy metals in capsule shell were studied by ICP-MS. The results show that the standards of different countries and regions are different, and some of the heavy metals used exceed the standards, while others do not. It is necessary to establish the limit standard of heavy metals in the hard gelatin capsule shell suitable for Chinese medicine according to the amount of capsules eaten by Chinese people and the daily allowable intake of heavy metals.

KEYWORDS:
Heavy metals, Safety, Gelatin capsule shell, ICP-MS

INTRODUCTION

Capsule is one of the main dosage forms of oral solid preparations. In China, the production of hard capsule dosage forms accounts for about 20% of the total production of oral solid preparations [1]. Medicinal gelatin hard capsule shell is a kind of container used for drug packaging. It is not a food, but it should be taken orally with the drug into the human body. Although it is not a effective ingredient, it should still be limited to the level required the same as the food. Therefore, it is very important to study the content of heavy metals in the capsule shell of drugs sold on the market. In this paper, the contents of heavy metals (CD, Pb, Hg, Cr) in gelatin hard capsule shells sold in pharmacies in Shandong and Beijing of China were determined by ICP-MS.

MATERIALS AND METHODS

Samples. Gelatin hard capsules were randomly selected from ten regular pharmacies in Shandong and Beijing. The remaining capsule shell was rinsed with deionized water for 3 times after removing the intermediate drug components.

Determination Methods. ICP-MS method is used for the detection equipment, and the specific method is referred to the literature of wipe possibility test [2-5].

RESULTS AND DISCUSSIONS

The limit of heavy metal content in capsule shell is the most noticeable problem.If the packaging containers used for Chinese patent medicines refer to

TABLE 1
Content of heavy metals in ten capsule samples

No.	Cd		Pb		Cr		Hg	
	Content	RSD(%)	Content	RSD(%)	Content	RSD(%)	Content	RSD(%)
1	0.26±0.003	2.91	6.35±0.219	1.07	0.52±0.004	2.16	0.09±0.005	3.19
2	0.18±0.004	1.95	8.57±0.246	1.51	0.57±0.005	2.31	0.11±0.003	2.56
3	0.25±0.002	0.87	7.26±0.310	1.78	0.64±0.003	1.78	0.23±0.005	1.33
4	0.37±0.002	3.28	12.49±0.156	0.91	0.83±0.007	3.32	0.25±0.013	2.17
5	0.30±0.004	2.37	9.29±0.095	0.76	0.72±0.007	2.19	0.17±0.004	2.19
6	0.26±0.003	3.21	11.75±0.177	0.58	0.59±0.004	0.95	0.21±0.007	1.47
7	0.15±0.001	1.99	10.83±0.218	0.45	0.81±0.009	1.57	0.19±0.005	2.81
8	0.19±0.004	1.25	9.81±0.129	1.62	0.66±0.045	1.72	0.12±0.004	1.99
9	0.17±0.002	0.72	7.66±0.114	0.33	0.52±0.005	2.43	0.25±0.015	1.77
10	0.19±0.003	1.27	6.39±0.172	0.95	0.61±0.017	1.76	0.14±0.008	2.15

the provisions of the green industry standard for the import and export of medicinal plants and preparations [6] issued by the Ministry of foreign trade and economic cooperation of the people's Republic of China, some heavy metals in the samples measured this time exceed the standard. If it is clearly stipulated in the EU food hygiene standard [6-7], only lead exceeds the standard; cadmium, mercury and the rate of exceeding the standard are 0 (Table 1).

But the capsule is different from the food, because the capsule is generally only eaten when it is sick, unlike the food, which should be eaten every day, and the capsule is not easy to exceed the daily allowable intake. Heavy metals, as the currently recognized harmful elements to human body, seriously affect human health. It is necessary to establish the limit standard of heavy metals in the hard gelatin capsule shell suitable for Chinese medicine according to the amount of capsules eaten by Chinese people and the daily allowable intake of heavy metals.

ACKNOWLEDGEMENTS

We thank Dr. Xu Fang from Beijing Forestry University for determining the samples. Jin Xiaoli and Wang Lei made the same contribution to the work.

REFERENCES

[1] Zheng, Q., Cheng, Q., Yang, M., Wang, S. (2007) Progress on Study of Empty Capsules and Thinking of How to Resolve the Problem in Hard Capsules of Traditional Chinese Medicine. Journal of Jiangxi University of TCM. 19(6), 74-77.

[2] Yang, J., Jiang, F., Ma, C., Rui, M., Adeel, M., Cao, W., Xing, B. (2008) Alteration of Crop Yield and Quality of Wheat upon Exposure to Silver Nanoparticles in a Life Cycle Study. Journal of Agricultural and Food Chemistry. 66(11), 2589-2597.

[3] Shi, R., Zou, C., Rui, Y., Zhang, X., Xia, X., Zhang, F. (2009) Application of ICP-AES to Detecting Nutrients in Grain of Wheat Core Collection of China. Spectroscopy and Spectral Analysis. 29(4), 1104-1107.

[4] Rui, Y.-K., Shen, J.-B., Zhang, F.-S. (2008) Application of ICP-MS to Determination of Heavy Metal Content of Heavy Metals in Two Kinds of N Fertilizer. Spectroscopy and Spectral Analysis. 28(10), 2425-2427.

[5] Rui, Y., Qu, L., Kong, X. (2008) Effects of soil use along Yellow River basin on the pollution of soil by heavy metals. Spectroscopy and Spectral Analysis. 28(4), 934-936.

[6] Xie, X., Li, Y., Mai, J., Chen, J. (2010) Study on Content of Heavy Metal in Medical Gelatin Hard Capsule Shells. Pharmacy Today. 20(1), 28-30.

[7] Dong, Z., Feng, K., Zhang, L., Zhang, Y., Song, Y., Cao, J., Zhang, Q., Wang, G. (2012) Determination of Chromium in Soft Capsule Shells by Microwave Digestion-Graphite Furnace Atomic Absorption Spectrophotometry. Chinese Pharmaceutical Journal. 47, 9717-719.

Received: **26.03.2020**
Accepted: **17.05.2021**

CORRESPONDING AUTHOR

Zhu Huanlei
Yantai Yuhuangding Hosp.,
Yudong Rd 20, Zhifu District 26400,
Shandong Province – P.R. China

e-mail: jxlxyq2004@126.com

© by PSP Volume 30– No. 09/2021 pages 11011-11024 Fresenius Environmental Bulletin

NOTICE

GREEN REMANUFACTURING EVALUATION MECHANISM BASED ON FAULT DIAGNOSIS OF ELECTRIC SPINDLE FROM THE PERSPECTIVE OF ENVIRONMENTAL PROTECTION

Haixiang Yu[1,*], Meng Wang[2]

[1]Tianjin Transportation Technical College, Tianjin, 300110, China
[2]School of Applied Foreign Languages and International Communication, Tianjin Sino-German University of Applied Science, Tianjin, 300350, China

ABSTRACT

Scrap cars and their disassembled parts contain a variety of heavy metals, chemical liquids, plastics and other substances. If they are not handled properly, they will cause serious air, water and soil pollution, and huge waste of energy and resources, which will affect Sustainable development of society. In order to build a resource-saving and environment-friendly society, the automobile, aerospace and other industries have proposed the development direction of realizing parts remanufacturing, green manufacturing, and intelligent manufacturing. Effectively evaluate the remanufacturability of electric spindle products, which can support the formation of green redesign and remanufacturing schemes for electric spindle products. Combined with the five decision attributes of green manufacturing technology, quality, economy, resources and environment. This paper first uses wavelet packet decomposition and reconstruction algorithm to remove the noise in the non-linear and unstable signal, and uses empirical mode analysis to extract the eigenvalues in the signal; Secondly, the time domain and frequency domain features in the extracted signal are used as input, and the BP neural network fault diagnosis model is used to verify the effectiveness of the system algorithm; Then from the five perspectives of remanufacturing capability, remanufacturing quality, remanufacturing time, remanufacturing environmental impact, and remanufacturing cost, the comprehensive influencing factors of electric spindle remanufacturing are extracted and the evaluation index system is constructed. Finally, the experiment shows that when the remanufacturability of the electric spindle is λ=0.721, that is, the electric spindle has a higher remanufacturing degree and can obtain a better comprehensive effect of remanufacturing.

KEYWORDS:
Environmental protection, green remanufacturing, sustainable development, electric spindle, fault diagnosis

INTRODUCTION

In recent years, the manufacturing industries of various countries have developed rapidly. Taking the automobile industry as an example, the major industrial countries in the world are gradually developing into a mature automobile society [1]. The vigorous development of the automobile industry has stimulated the development of industries such as steel and petroleum, but it has also caused many problems in countries such as resource consumption, environmental degradation, and ecological destruction. According to data released by the country Association of Automobile Manufacturers each year, global automobile production reached 80 million in 2012. By the end of 2012, the global car ownership reached 1 billion, and the number of scrapped vehicles reached 40.176 million. Among them, China's car ownership is 78.02 million vehicles, and the number of scrapped vehicles is 3.506 million. It is estimated that by 2020, China's car ownership will reach 200 million [2]. Corresponding to the huge inventory is the same huge amount of scrapped automobiles. Scrapped automobiles and their disassembled parts contain a variety of heavy metals, chemical liquids, and plastics [3]. If it is not handled properly and does not enter the formal recycling and remanufacturing channels, it will cause serious air, water and soil pollution, as well as a huge waste of energy and resources, and affect the sustainable development process.

Electric spindle has become a hot issue in the research of high-speed CNC systems at home and abroad [4], and its performance has become a symbol of the level of CNC technology. China proposes to cover the urgent needs of key areas in the 'Made in China 2025', and strive to take into account the needs of key emerging industries such as robots,

which have recently developed rapidly in technology and the market. It is necessary to condense the key core technologies, concentrate on breaking through the key common technologies of high-end CNC systems and other products, and form the industry's sustainable innovation capabilities. my country's manufacturing industry is constantly changing and changing, both in terms of equipment and concepts. In 2015, Premier Li Keqiang proposed the national strategy of "Made in China 2025". More than a hundred academicians have jointly designed the development thinking of China's manufacturing industry in the next 10 years. The goal is to promote China's basic industrialization by 2025 and become a manufacturing power. "Made in China 2025" is to move from traditional machinery manufacturing to "Intelligent manufacturing", "Internet + industry", and "Big data + industry". This idea puts forward 5 key projects, including the construction of a national manufacturing innovation center, intelligent manufacturing, strong industrial base, green manufacturing, and high-end equipment innovation. As the core component of CNC machine tools, the electric spindle belongs to the ranks of high-end equipment. CNC machine tools have become the most widely used processing tool in the manufacturing industry due to their high productivity and high processing accuracy[5]. In addition, the application industries of CNC machine tools are very wide, including automobiles, national defense, textiles, precision instruments and other fields. And every year, the demand for CNC machine tools in various manufacturing industries continues to rise at a rate of 17% [6-8].

In order to better realize the remanufacturing technology, on the one hand, it is to use the remanufacturing technology to put it back into use after the parts fail [9-10]. On the other hand, predictive diagnosis can be used to detect component failures in advance, and use remanufacturing technology to maintain equipment [11]. Predictive diagnosis not only uses remanufacturing technology, but also an advancement in maintenance methods. Different from traditional corrective maintenance and preventive maintenance, predictive maintenance belongs to prefailure maintenance. It integrates equipment status monitoring, fault prediction, fault diagnosis, maintenance decision support and maintenance activities [12-14]. Greatly improve maintenance efficiency and equipment stability.

RELATED WORK

The research and development of electric spindle fault diagnosis technology at home and abroad can be roughly divided into four directions: fault mechanism and characterization, signal acquisition and sensing technology, signal analysis and processing, identification classification and intelligent decision-making.

Literature [15] uses variational modal decomposition combined with the maximum correlation kurtosis deconvolution method to isolate the fault characteristics from the strong interference signal. And use this method to successfully extract the correct fault signal from the simulated disturbed fault signal. Finally, it is compared with the separation result of ensemble empirical mode decomposition to verify its superiority. Literature [16] proposed a fault feature extraction method based on wavelet packet fuzzy entropy combined with support vector machine. It aims to solve the shortcoming that multiscale fuzzy entropy cannot capture the amount of high-frequency components when analyzing the complexity of time series. This method can simultaneously obtain the signal components of the high-frequency group and the low-frequency group, and provides a more comprehensive and accurate feature extraction method for analyzing nonlinear and non-stationary signals. Literature [17] proposed a fault characteristic frequency identification method based on Fourier decomposition and singular value difference spectrum. The method first uses Fourier decomposition to decompose non-stationary signals into multiple intrinsic frequency band signals. Then use the cross-correlation method to reconstruct the decomposed signal and use the singular value to reduce the noise of the reconstructed signal. Finally, the Hilbert envelope spectrum is used to analyze the signal. Literature [18] proposed a fault diagnosis method based on evidence fusion based on the multi-sensor fusion for the situation that the fault state of the equipment is incorrectly estimated when the sensor fails. This method uses evidence distance and conflict quality as antilogs to measure the size of conflicts between evidences, and then uses the D-S method to fuse data from multiple sensors to obtain complete and reliable equipment failure signals.

In terms of green effectiveness evaluation, literature [19] uses data envelopment method and independent component analysis method to construct a green performance evaluation model. Literature [20] uses a combination of principal component analysis and data envelopment methods to evaluate the green performance of energy bureau projects. The combination of multiple methods is more effective and scientific than the single use of data envelopment method for performance evaluation. Literature [21] chooses the matrix method to calculate the relative weight of the influencing factors in the green performance evaluation system in the overall situation. Literature [22] selects indicators from the perspectives of carbon dioxide emissions, energy consumption, raw material consumption, and net economic benefits to evaluate the green performance of the industrial symbiosis network. Literature [23] uses the structural equation model method to calculate the factor analysis of green policy and the factor analysis of port green performance and competitive-

ness from the perspective of green supply chain management, and evaluate the port green performance. Literature [24] extracts system control factors from the perspectives of process, technology, subject, information, organization, capital and control. Select the system's green performance output factors from the perspectives of economy, resources, environment, and human factors. Construct a system dynamics model to study the impact of recycling and remanufacturing green performance.

There are some flaws in the above research. The complexity of modern equipment has greatly increased, making it difficult to construct mathematical and mechanical models. However, the study of failure mechanism requires a large amount of experimental analysis, and it is difficult to obtain results in a short time. Many characteristic information of complex faults are coupled with each other, making it difficult to determine the source of the fault. At present, most of the researches in the laboratory environment are single and few failures. The main research contents of this paper are as follows:

(1)The wavelet packet decomposition and reconstruction algorithm is used to remove the noise in the non-linear and unstable signal, and the empirical mode analysis is used to extract the eigenvalues in the signal.

(2)The time domain and frequency domain features of the extracted signal are used as input, and the BP neural network fault diagnosis model is used to verify the effectiveness of the system algorithm.

(3)From the five perspectives of remanufacturing capability, remanufacturing quality, remanufacturing time, remanufacturing environmental impact, and remanufacturing cost, the comprehensive influence factors of electric spindle remanufacturing are extracted and the evaluation index system is constructed.

GENERAL STRUCTURE INTRODUCTION

A complete high-speed electric spindle of a machine tool includes the rotating shaft, bearings, motor stator, motor rotor and cooling subsystem, lubrication subsystem, and spindle housing with internal integrated broaching mechanism. It is a highly integrated complex electro-hydraulic coupling system. When one part or component fails, the parameters of other parts will change. For example, when the bearing gap of the electric spindle is too large, the axis trajectory of the spindle will change significantly, and the rotor of the motor fixedly connected with the spindle will also jump accordingly. Then the air gap between the stator and rotor of the original motor is changed, and the internal magnetic field will change accordingly. According to the principle of electromagnetic induction, the change of the magnetic field will further affect the three-phase alternating current. Therefore, a simple fault with too large bearing clearance will not only cause a change in the vibration signal, but also a change in the current signal. For vibration signals that contain a lot of noise interference, they contain less characteristic information. In particular, the signals used for the early stage of failure warnings contain less characteristic information and are difficult to extract effectively. If only one signal source is used as the input variable for the fault warning, the information at the initial stage of the fault will not be effectively extracted. Only when the fault develops to a certain extent can the difference of the signal be distinguished, which delays the prime time for timely detection of potential faults and arranging repairs, resulting in direct or indirect economic losses. In addition, after a long-term tracking study, it is found that for complex electro-hydraulic coupling systems like electro-spindles, as the faults in parts or components gradually intensify, the changes in vibration, current, temperature, noise and other signals are often different. If only relying on a single signal source to provide early warning of failures of components or systems, its credibility, comprehensiveness and accuracy need to be further verified.

Therefore, the characteristics of single signal characteristic information is not obvious, incomplete, and the evolution law of each signal is different in the evolution of the electrical spindle fault. This article adopts the electric spindle fault early warning method based on multi-signal fusion such as three-phase current and radial vibration commonly used in rotating machinery. Failure early warning mainly includes three steps, namely feature quantity extraction, feature quantity analysis, health trend prediction and remaining life assessment. The fault warning method proposed in this paper is as follows: First, the three-phase current signal and the two-way (rotation axis radial XY direction) vibration signal are respectively analyzed by wavelet packet decomposition and reconstruction and empirical mode decomposition. Remove noise and extract energy entropy distribution matrix as eigenvalues. Secondly, the multi-dimensional characteristic signal is used to reduce the dimensionality of the signal and extract its principal components through the fault diagnosis method based on BP neural network to form a comprehensive health index. Finally, input the obtained data into the green remanufacturing evaluation mechanism of the electro-spindle. The flowchart is shown in Figure 1.

PROPOSED FAULT DIAGNOSIS METHOD OF ELECTRIC SPINDLE

Signal noise reduction and feature extraction. After long-term tracking and collection of various signals of the electro-spindle, the author found that for the electro-spindle, an electro-hydraulic coupling system that works in complex conditions, both

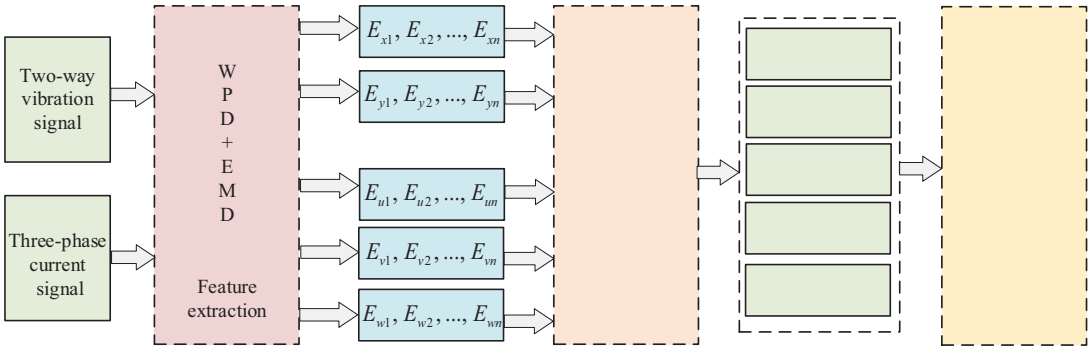


FIGURE 1
Flow chart of failure warning method

the vibration signal and the current signal are nonlinear and unstable with strong noise interference State signal. Noise interference must be removed before feature extraction. The wavelet packet decomposition and reconstruction algorithm developed on the basis of wavelet analysis can effectively remove the noise in nonlinear and unstable signals.

For the finite energy signal containing the analysis wavelet, the continuous wavelet change is obtained by convolution with the conjugate wavelet function:

$$W_f(a,b) = \frac{1}{\sqrt{a}} \int_{-\infty}^{+\infty} x(t) \psi^* \left(\frac{t-b}{a} \right) dt \quad (1)$$

Where, $W_f(a,b)$ is the wavelet coefficient of the signal, a and b are scale parameters and translation parameters respectively, $\psi^*(t)$ is the mother wavelet. The mother wavelet $\psi^*(t)$ has a short duration and needs to meet the admissible conditions:

$$C_\psi = \int_0^{+\infty} \frac{|\hat{\psi}(\omega)|^2}{\omega} d\omega < +\infty \quad (2)$$

The signal $x(t)$ can be reconstructed with the generated wavelet coefficients after wavelet transformation, the formula is as follows:

$$x(t) = \frac{1}{C_\psi} \int_0^{+\infty} \frac{da}{a^2} \int_{-\infty}^{+\infty} Wf(a,b) \psi_{a,b}(t) db \quad (3)$$

It can be seen from formula (3) that wavelet transform is a time-frequency analysis. The difference from Fourier transform is that it includes not only frequency domain characteristics but also time domain characteristics.

If the translation parameter b and scale parameter a of the continuous wavelet transform are discretized, the discrete wavelet transform can be obtained. Among them, this paper uses $a = 2^j$, $b = na$, where $n \in Z$. The analysis wavelet calculation formula is as follows:

$$\psi_{j,n}^*(t) = 2^{\frac{-j}{2}} \psi\left(2^{-j} t - n\right) \quad (4)$$

The discrete wavelet transform can be expressed as the following form:

$$W_{j,n} = \int_{-\infty}^{+\infty} x(t) \psi_{j,n}^*(t) dt \quad (5)$$

Where * means conjugate, $x(t)$ represents the vibration or current signal being analyzed, $W_{j,n}$ represents the discrete wavelet coefficients of the analyzed signal.

Compared with the Fourier transform, the classic dual-band wavelet transform adds a time dimension, which allows us to know not only that the feature quantity appears, but also when the feature quantity appears. But the classic dual-band wavelet transform will form an exponential frequency band result. The low frequency band window is very narrow, so the low frequency signal can be well decomposed, and its feature quantity can be well extracted. However, the signal window of the high frequency band is relatively wide, and its feature quantity can only achieve limited extraction. In order to overcome this difficulty, on the basis of wavelet decomposition, a wavelet packet decomposition which can effectively decompose signals in all frequency bands is established. Another advantage of wavelet packet decomposition is that its structure is diverse, which can adapt to the singular signals of electro-mechanical-hydraulic coupling systems like electro-spindles working in complex conditions.

The specific algorithm steps of wavelet packet decomposition and reconstruction are as follows:

According to multi-resolution analysis and biorthogonal wavelet, the positive scaling function $\varphi(t)$ and its corresponding wavelet function $\psi(t)$ satisfy the following two-scale relationship:

$$\begin{cases} \varphi(t) = \sqrt{2} \sum_{k=-\infty}^{+\infty} h(k) \varphi(2t-k) \\ \psi(t) = \sqrt{2} \sum_{k=-\infty}^{+\infty} g(k) \varphi(2t-k) \end{cases} \quad (6)$$

Where, the conjugate filter coefficients $h(k)$ and $g(k)$ are:

$$\left\{ \begin{array}{l} h(k) = \left\langle \frac{1}{\sqrt{2}} \varphi\left(\frac{t}{2}\right), \varphi(t-k) \right\rangle \\ g(k) = (-1)^k h(1-k) \end{array} \right\} \quad (7)$$

Now for further derivation, let $u_0(t)=\varphi(t)$ and $u_1(t)=\psi(t)$ then get:

$$\left.\begin{aligned} u_{2_p}(t)&=\sum_{k\in Z}h(k)u_p(2t-k)\\ u_{2_{p+1}}(t)&=\sum_{k\in Z}g(k)u_p(2t-k)\end{aligned}\right\} \quad (8)$$

$u_n(t)$, $n=2p$ or $n=2p+1$, $p=0,1,\cdots,n$ are defined as wavelet packets of orthogonal scaling function $\varphi(t)$.

The wavelet analysis and the generation of wavelet packet are briefly introduced. When the wavelet packet is generated, the last step is to use wavelet packet decomposition and reconstruction for signal denoising. The specific algorithm is as follows:

According to the theory of multi-resolution decomposition [24], if $U_j^0=V_j$, $U_j^1=W_j$, formula (6) can be transformed into:

$$U_j^0=U_{j+1}^0\oplus U_{j+1}^1 \quad (9)$$

Similarly, the formula (8) can be written as:

$$U_j^n=U_{j+1}^{2n}\oplus U_{j+1}^{2n+1} \quad (10)$$

Where, $p=0,1,\cdots$, if the wavelet packet u_n is subjected to binary translation and scaling, the following equation can be obtained:

$$u_{j,n,k}=2^{\frac{-j}{2}}u_n\left(2^{-j}t-k\right) \quad (11)$$

The wavelet library $\left\{u_{j,n,k}(t)\right\}_{j\in Z,k\in Z,n\in Z^+}$ can be obtained by formula (11),

If it is necessary to decompose the wavelet function space W_j, then set $n=1$ and iterate (11) repeatedly to obtain the decomposition formula of the wavelet space:

$$W_j=U_{j+n}^{2^n}\oplus U_{j+n}^{2^n+1}\oplus U_{j+n}^{2^n+2}\oplus\ldots\oplus U_{j+n}^{2^{n+1}-1} \quad (12)$$

In the same way, the scale space V_j can be expressed as follows:

$$V_j=U_{j+n}^0\oplus U_{j+n}^1\oplus U_{j+n}^2\oplus\ldots\oplus U_{j+n}^{2^n-1} \quad (13)$$

Where, $j+n$ indicates that the scale is 2^{j+n}.

From the above analysis, we can see that when $\forall x(t)\in L^2(R)$, $x(t)\in V_0$, it can be decomposed according to formula (13) to get:

$$V_0=U_n^0\oplus U_n^1\oplus U_n^2\oplus\ldots\oplus U_n^{2^n-1} \quad (14)$$

In order to restore the signal, the signal needs to be reconstructed after wavelet packet decomposition:

$$\begin{aligned} d_{j,n}(k)=&\sum_l h(k-2l)d_{j+1,2n}(l)\\ &+\sum_l g(k-2l)d_{j+1,2n+1}(l)\end{aligned} \quad (15)$$

From the above specific algorithm, it can be seen that wavelet packet analysis has far greater signal decomposition and reconstruction capabilities than wavelet analysis. In particular, the high-frequency components in the early precursor signals of equipment failure can be effectively processed. Therefore, we use wavelet packet analysis instead of simple wavelet analysis when performing fault early warning analysis of complex systems. Wavelet packet analysis has been used in many aspects of fault diagnosis and fault early warning, especially in signal denoising. In addition, wavelet packet decomposition can also be used to describe the time-to-time division of the signal and decompose the detailed characteristics of the signal into frequency bands. However, it also has many shortcomings, mainly in:(1)It is difficult to select wavelet basis functions. Professionals with in-depth understanding of wavelet transform are required to select suitable wavelet basis functions, which is not conducive to engineering applications;(2)Once the wavelet basis function is selected, it cannot automatically change with time and signal characteristics;(3)The resolution is constant. When a standard function and conversion scale are selected, the resolution is also determined, and it cannot change with the size of the signal. Therefore, wavelet packet analysis can be used for the decomposition and reconstruction of multi-dimensional signals to remove noise and interference. Due to its own shortcomings, it is not suitable as a method for extracting the characteristic quantities of nonlinear and unsteady signals of complex rotating machinery.

Empirical Mode Decomposition (EMD) is a mathematical method proposed by Huang et al. to effectively extract the eigenvalues of unsteady and nonlinear random fluctuation signals. As an adaptive time-frequency-domain signal analysis method, EMD usually analyzes fluctuating signals as characteristic quantities. Its Intrinsic Mode Function (IMF) can show different intrinsic modes in the form of fluctuations. Many studies have shown that EMD has more obvious advantages than traditional signal analysis methods and can extract the eigenvalues of complex time-varying and nonlinear signals in electromechanical coupling systems. At the same time, the signal must meet the following assumptions when performing EMD decomposition on the signal:(1)The signal has at least two extreme values;(2)The characteristic time scale is defined by the local maximum and minimum values appearing in the signal;(3)If the signal has no extreme values but contains inflection points, it can be decomposed one or more times to extract extreme values.

EMD decomposes the signal into a series of IMF and signal residuals. After wavelet packet decomposition and reconstruction, the noise-eliminated signal can be formed into an empirical mode and its residual:

$$x(t)=\sum_{i=1}^{n}c_i(t)+r_n(t) \quad (16)$$

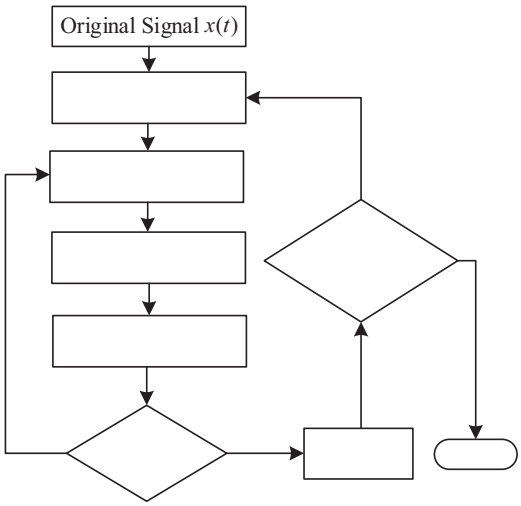


FIGURE 2
EMD algorithm flow chart

Where, $r_n(t)$ is the residual function, $c_i(t)$ is each IMF from high frequency to low frequency.

When the electric spindle is in different working states, the energy spectrum of the signal changes with the change of the frequency spectrum. Usually we use EMD energy entropy to explain the change of signal $x(t)$ energy. For n IMFs, the energy E_i, $i=1,2,3\cdots n$ are:

$$E_i = \int_{-\infty}^{+\infty} |c_i(t)|^2 \, dt \tag{17}$$

The corresponding EMD energy entropy can be obtained by the following formula:

$$H_i = -\sum_{i=1}^{M} p_i \log p_i \tag{18}$$

Where, $P_i = E_i / (E_1 + E_2 + E_3 + \cdots E_n)$ is the energy of signal $c_i(t)$ as a percentage of all signal energy. Generally, for n IMFs, the first m IMFs contain most of the fault characteristic information. But for different types of signals, such as vibration signals and current signals, the value of m needs to be determined according to the characteristics of the specific signal. These m IMFs with different frequency characteristics and energy distribution: The energy entropy distribution matrix of $c_1(t)$, $c_2(t)$, $c_3(t)$, $\cdots\cdots$ $c_m(t)$ is:

$$T(t) = [H_1(t) H_2(t) \cdots H_m(t)] \tag{19}$$

Fault diagnosis based on BP neural network. The main idea of BP neural network learning method is to divide network learning into two processes, forward propagation and back propagation. If the desired output is obtained in the forward direction, the algorithm ends. Otherwise, go to reverse propagation, and calculate the error signal in reverse according to the original connection path. The weights of neurons in each layer are adjusted by the gradient descent method to reduce the error. Before the BP neural network makes predictions, it needs to pass data training to make the network have associative memory and prediction capabilities. The BP neural network training process is as follows:

(1)Network initialization. According to the input and output sequence (X,Y), determine the number of input layer nodes n, hidden layer nodes l, and output layer nodes m. Initialize the connection weights between the input layer, hidden layer and output layer neurons to ω_{ij}, ω_{jk}. Initialize the hidden layer threshold value a, the output layer threshold value b, given the learning rate and neuron activation function.

(2)Hidden layer output calculation. According to the input vector X, the connection weight ω_{ij} between the input layer and the hidden layer, and the hidden layer threshold a, the hidden layer output H is calculated. The calculation method is as follows.

$$H_j = f\left(\sum_{i=1}^{n} \omega_{ij} x_i - a_j\right) i = 1,2,\ldots,n \quad ; \quad j = 1,2,\ldots,l \tag{20}$$

(3)Output layer output calculation. According to the hidden layer output H, connect the weight ω_{jk} and the output layer threshold b to calculate the predicted output O.

$$O_k = \sum_{j=1}^{l} H_j \omega_{jk} - b_k \quad k = 1,2,\cdots,m \tag{21}$$

(4)Error calculation. According to the network predicted output O and the expected output Y, calculate the network prediction error e.

$$e_k = Y_k - O_k \quad k = 1,2,\cdots,m \tag{22}$$

(5)Weight update. Update the network connection weights ω_{ij} and ω_{jk} according to the network prediction error e.

$$\omega_{ij} = \omega_{ij} + \eta H_j (1 - H_j) x(i) \sum_{k=1}^{n} \omega_{jk} e_k \quad i = 1,2,\cdots,n \quad j = 1,2,\cdots,l \tag{23}$$

$$\omega_{jk} = \omega_{jk} + \eta H_j e_k \quad j = 1,2,\cdots,l \quad k = 1,2,\cdots,m \tag{24}$$

(6)Threshold update. Update the network node thresholds a and b according to the network prediction error e.

$$a_j = a_j + \eta H_j (1 - H_j) x(i) \sum_{k=1}^{m} \omega_{jk} e_k \quad j = 1,2,\cdots,l \tag{25}$$

$$b_k = b_k + e_k \quad k = 1, 2, \cdots, m \tag{26}$$

(7)Judgement. Judge whether the iteration of the algorithm is complete, if not, return to step (2).

When performing neural network fault diagnosis, the first step is to establish an effective fault diagnosis model. Determine the number of input feature vectors and the number of output feature vectors according to the actual situation. When designing a BP neural network, comprehensive consideration and design should be made from the aspects of the number of network layers, the number of neurons in each layer, the initial value, and the learning method.

The feature parameter space dimension of BP neural network is composed of time domain and frequency domain, totaling 16 dimensions. There are 5 types of faults to be identified: normal, outer ring, inner ring, rolling element and cage. For the selection process of the number of hidden layer nodes, refer to Principle 101 of the method for selecting the number of hidden layer nodes. According to the degree of non-linearity of input and output and the pros and cons of the debugging state, the selection is 16, that is, the number of input layer nodes, the number of hidden layer nodes, and the number of output layer nodes are 16, 16, and 5 respectively. Finally, the expected output values of the BP neural network are set as: no fault, hidden trouble, minor fault, moderate fault, and severe fault.

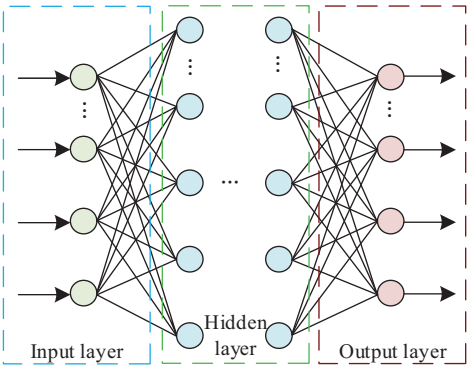


FIGURE 3
Topological structure of BP neural network

GREEN REMANUFACTURING EVALUATION INDEX OF ELECTRIC SPINDLE

Index selection principle. In the practical application of influencing factor evaluation, a scientific and reasonable evaluation index system plays a vital role in guaranteeing. Therefore, in order to establish a systematic and scientific indicator system to provide a basis for the green performance evaluation of remanufacturing enterprises. The construction of the indicator system needs to follow the following principles:

(1)Systematic principle. The scope of work of remanufacturing companies includes multiple processes such as recycling, remanufacturing, and sales, and their behavior involves many subjects such as the government, remanufacturing companies, and consumers. The comprehensive influencing factors cover multiple dimensions such as remanufacturing capacity, recycling capacity, economic benefits, ecological benefits, and internal green management systems. Therefore, only by systematically and logically selecting evaluation indexes to construct an index system, and striving to construct an index system covering all aspects of remanufacturing enterprises, can the scientificity and validity of the evaluation results be guaranteed.

(2)Scientific principle. The scientific principle is one of the basic principles for constructing the evaluation index system. Only by following the economic and ecological laws of remanufacturing enterprises, fully understand the connotation of remanufacturing. Comprehensively refer to the existing remanufacturing enterprise evaluation theoretical research results and combine the actual development situation to construct an index system based on science. Ability to scientifically reflect the internal relationship between the overall evaluation system and various factors.

(3)Independence principle. Because the selection of evaluation indicators for the influencing factors of remanufacturing enterprises involves multiple dimensions. Therefore, the various factors of the criterion level must avoid duplication and omission, and maintain their independence from each other, in order to effectively influence the evaluation object from all angles.

(4)Testability principle. In actual situations, many indicators have difficulties in obtaining data or the indicators are qualitative factors. Therefore, in the process of constructing the index system, it is necessary to consider whether each factor is easy to quantify and whether the data is highly available. Reduce the difficulty of subsequent calculation operations and ensure the validity and scientificity of the calculation results of the constructed evaluation system. This provides a theoretical basis for making decisions.

Index selection process. Constructing an index system is the basis and prerequisite for the subsequent evaluation work. On the basis of following the principle of index selection, the evaluation index must be selected through scientific and reasonable methods to ensure the effectiveness of the index system. Based on the summary of the literature, this article uses Delphi to further extract the collected indicators and build an indicator system.

1.Overview of Delphi Method. The Delphi method is also called the expert survey method. The problems that need to be resolved are sent to the members of the expert group through communication to ask for their opinions. Summarize the feedback of the experts to obtain comprehensive opinions and use them as reference materials, and then send them to the expert group for comments. The experts analyzed and judged based on the comprehensive opinions, put forward new feedback, and then summarized again. If the opinions of the experts differ greatly, the opinions will be consulted again, and after many iterations, until a relatively stable and consistent opinion result is obtained.

The Delphi method seeks expert opinions back-to-back and anonymously. That is to say, experts must not discuss with each other or communicate horizontally. Therefore, it has the advantage that the opinions collected only come from the experts' own ideas and are not influenced by others. It is widely used in the field of scientific research.

2.Basic steps of the Delphi method. The specific steps are as follows:

(1) Establish an expert group. The expert group has 8 members, including remanufacturing research experts from universities and management-level employees of remanufacturing enterprises. All team members are engaged in related research and work, have a deep understanding of the remanufacturing industry and remanufacturing companies, and each team member does not know the identity of other members.

(2) Construct a preliminary index system. Sort out the content of existing research literature and combine it with the current development status of the remanufacturing industry. On the basis of following the principle of index selection, extract the factors affecting the green performance of remanufacturing enterprises, and try to avoid duplication and omission.

(3) Design a research survey. Design a questionnaire for the initially constructed indicator system, see Appendix B for details. The questionnaire consists of 4 parts:①Survey description, including research background, significance, and description of how to fill out the questionnaire;②The main text is the indicator system constructed in Step 2. Including 20 influencing factors selected from 5 dimensions. A 0-4 point scoring system is adopted. The higher the score, the higher the importance of the corresponding indicator factor. A score of 0 indicates the lowest importance and it is recommended to delete;③Suggestions are open-ended questions. Experts put forward specific opinions on the construction of evaluation indicators of the questionnaire, such as duplication and omission of influencing factors;④Fill in basic information, and each group member will fill in basic personal information.

(4) Distribute and return questionnaires. Distribute questionnaires to experts through E-mail. Set the time limit for recycling feedback to one week, collect the questionnaire on time, and summarize the opinions of experts. The aggregate score uses the mean method.

(5) Design a follow-up questionnaire. According to the expert opinions summarized in the previous step, the evaluation indicators with a mean value less than 1 are deleted. If there are experts in the open opinion column that there are missing indicators in the questionnaire, the missing indicators will be added to the indicator system. Construct a new indicator system and design it into a questionnaire.

(6)Distribute and collect tracking questionnaires. Distribute the newly designed tracking questionnaire to all team members. Experts are still required to score the newly constructed evaluation indicators on the tracking questionnaire on a 0-4 point scoring system. Return the questionnaire on time after 1 week and summarize the feedback from the questionnaire. If the opinions of the experts still differ, continue to repeat step 5 until a more consistent opinion is obtained and all group members agree.

(7) Build an indicator system. According to the final opinions of the expert group, an indicator system of influencing factors of green performance of remanufacturing enterprises is constructed.

Comprehensive Evaluation Model of Green Remanufacturing. The purpose of the comprehensive evaluation of green remanufacturing of electric spindle products is to qualitatively and quantitatively assess whether electric spindle products are suitable for remanufacturing and how remanufactured. It needs to evaluate all factors that affect the remanufacturing of electric spindle products. Since remanufacturing is a green manufacturing model, the five major decision-making attributes of green manufacturing "TQCRE" should be comprehensively considered in the remanufacturing evaluation of electric spindle products. Since remanufacturability firstly depends on technical factors, the five decision-making attributes of green manufacturing are applied to remanufacturing on the premise of considering technical factors. That is, T represents remanufacturing time (time), Q represents remanufacturing product quality (quality), C represents remanufacturing cost (cost), R represents remanufacturing resource consumption (resource), E represents remanufacturing environmental impact (environment).

TABLE 1
Comprehensive evaluation index system for green product remanufacturing of electric spindle

First level indicator	Secondary indicators	Weight	Evaluation method
Technical indicators	Removable assembly	0.3	Expert evaluation
	Manufacturability	0.3	Expert evaluation
	Performance upgradeability	0.2	Expert evaluation
	Processing difficulty	0.2	Expert evaluation
Economic indicators	Economic benefit	0.4	Data calculation
Environmental indicators	Environmental protection	0.1	Statistics
Resource indicators	Save resources	0.1	Statistics
Time index	Manufacturing time	0.1	Data calculation
Quality index	Service years	0.3	Data calculation

Comprehensive evaluation index system for green remanufacturing of electric spindle products. The factors that affect the remanufacturing characteristics of electric spindle products are complex. After inductive analysis, it can be seen that the influencing factors such as technology, economy, resources, environment, quality and time of remanufacturing comprehensively determine the remanufacturing characteristics of electric spindle products, and they also influence each other. Comprehensively considering the actual situation of electric spindle electric products, a comprehensive evaluation index system for electric spindle product remanufacturing has been established as shown in Table 1.

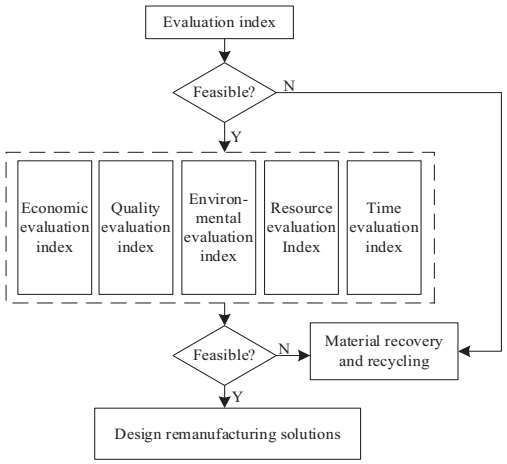


FIGURE 4
Flow chart of comprehensive evaluation of green remanufacturing of electric spindle products

As shown in Figure 4, it is the comprehensive evaluation framework process for green remanufacturing of electric spindle products. The comprehensive evaluation of electric spindle product remanufacturing is to evaluate the remanufacturability of electric spindle products. The remanufacturability λ of electric spindle products can be expressed by the following formula:

λ = Technical index × (economic index × weight + quality index × weight + resource index × weight + environmental index × weight + time index × weight)

(1)Technical index $\lambda_{technology}$

$$\lambda_{technology}=\begin{cases}\sum_i \lambda_i\alpha_i & 0<\lambda_i\le 1;\ i=1,2,3,4\\ 0 & \lambda_i=0;\ i=1,2,3,4\end{cases} \tag{27}$$

Where, λ_i ($i=1,2,3,4$)is the assemblability index, remanufacturing processability index, performance upgradeability index and processing difficulty index respectively; α_i ($i=1,2,3,4$)is its corresponding weight. The steps of technical feasibility evaluation using expert system fuzzy comprehensive evaluation method are as follows.

1) Establish a comment set and calculate the degree of membership A_{ij}.

The comment set is a collection of various evaluation results made by the evaluator on the evaluation object. Combining the characteristics of the technical feasibility of electric spindle product remanufacturing, the comment set is taken as {good, better, fair, bad}, and the evaluation index set {removable assembly, remanufacturing processability, performance upgradeability, processing difficulty }. The calculation formula of membership degree is:

$$A_{ij}=a_{ij}\Big/\sum_{j=1}^{n}a_{ij} \tag{28}$$

2) Calculate the technical comprehensive evaluation value μ from the membership matrix $\mathbf{R}$

Membership matrix $\mathbf{R}=\begin{Bmatrix}A_{11} & \cdots & A_{1n}\\ \vdots & \vdots & \vdots\\ A_{1n} & \cdots & A_{nn}\end{Bmatrix}$.

Suppose the index weight vector is W_F, and the index comment set is W_E, then the technical comprehensive evaluation value $\mu=W_E\left(W_F\mathbf{R}\right)^T$.

(2)Economic index λ_C

$$\lambda_C=\begin{cases}\left(C_m-C_1-C_2\right)/C_m & C_m-C_1-C_2>0\\ 0 & C_m-C_1-C_2\le 0\end{cases} \tag{29}$$

Where, C_m is the added value of remanufactured electromechanical products; C_1 is the remanufacturing cost; C_2 is the cost of obtaining electric spindle products.

(3)Quality index λ_Q

$$\lambda_Q = \begin{cases} \dfrac{T'_{residual}}{T''_{residual}} & \dfrac{T'_{residual}}{T''_{residual}} > a \\ 0 & 0 \le \dfrac{T'_{residual}}{T''_{residual}} \le a \end{cases} \tag{30}$$

Where, $T'_{residual}$ is the service life of remanufactured electromechanical products; $T''_{residual}$ is the service life of the new product; a is a limit value for judging the feasibility of remanufacturing quality. Here, set the value to 0.5.

(4)Resource index λ_R

λ_R is the resource index, which is the resource and energy conservation index. Resource conservation mainly refers to the conservation of energy and materials. λ_R takes the average of the two saving rates.

(5)Environmental index λ_E

λ_E is the environmental index, that is, the environmental protection index. Environmental protection mainly includes air pollution reduction and water pollution reduction. λ_E is the average of the reduction rates of the two aspects.

(6)Temporal index λ_T

$$\lambda_T = \begin{cases} \dfrac{T''_{Produce} - T'_{Produce}}{T''_{Produce}} & 0 < \dfrac{T'_{Produce}}{T''_{Produce}} < 1 \\ 0 & \dfrac{T'_{Produce}}{T''_{Produce}} \ge 1 \end{cases} \tag{31}$$

Where, $T'_{Produce}$ is the remanufacturing time of the electric spindle product; $T''_{Produce}$ is the time to produce a new product. In the index of technology, economy, quality, resource, environment and time, the value of each individual index is between 0 and 1. The larger the value, the better. When the value is 1, it means the index represented by the index is the best, and when it is 0, it means the index represented by the index is the worst. Except for the technical index, which is obtained through fuzzy comprehensive evaluation, all other indexes can be obtained through accurate calculation and data statistics.

After the above index is obtained, the factors of economy, quality, resources, environment and time are comprehensively measured, and the corresponding weights are respectively 40%, 10%, 10%, 10% and 30%. Finally, calculate the remanufacturability λ of the electric spindle product, namely:

$$\lambda = \lambda_{technology}\left(0.4\lambda_C + 0.1\lambda_R + 0.1\lambda_E + 0.1\lambda_T + 0.3\lambda_Q\right) \tag{32}$$

After discussion by experts, unanimous voting stipulates that when the value of λ is between 0 and 0.3, it is considered that the degree of remanufacturing is low, and there is no need to invest in a remanufacturing program with too high value; When the value of λ is between 0.3 and 0.65, the degree of remanufacturing is considered to be medium, and appropriate remanufacturing investment can be made to obtain optimal economic benefits; When the value of λ is between 0.65 and 1, it is considered that the degree of remanufacturing is high and it is worth making great efforts to remanufacture. After remanufacturing, significant comprehensive benefits can be obtained.

EXAMPLE VERIFICATION AND RESULT DISCUSSION

Experimental environment. Due to the fact that the machine tool in this study is in service and the project time is short, enough sample data can not be provided. Therefore, the data of bearing life cycle experiment [20] downloaded from NASA website is used in this chapter, which is provided by the intelligent maintenance system center of University of Cincinnati. The schematic diagram of the experimental device is shown in Figure 5.

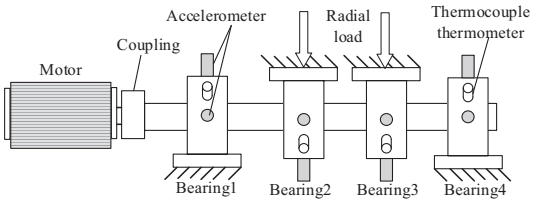


FIGURE 5
Schematic diagram of experimental device

Experimental verification. The mean value of the signal is often not directly used for diagnosis, it can only reflect the steady-state part of the signal. But it is often used when calculating other parameters for zero-average processing; the effective value reflects the magnitude of the signal energy, which is often used for the evaluation of vibration intensity; Skewness is the symmetry of the probability density function of the signal amplitude, that is, the uneven distribution of the time domain signal on both sides of the time axis; Kurtosis represents the concentration of the probability density of signal amplitude, that is, the degree to which time-domain signals are concentrated on the time axis. Generally, a kurtosis of 3 is defined as zero kurtosis, a kurtosis greater than 3 is defined as positive kurtosis, and a kurtosis less than 3 is defined as negative kurtosis. When a fault occurs, the mean value, effective value, peak to-peak value, kurtosis, etc. will increase. The kurtosis is

most sensitive to the amplitude and is suitable for diagnosing pulse-shaped faults. In order to increase the universality of parameters, the dimensionless parameters are obtained by processing the dimensionless parameters. The dimensionless parameters only depend on the probability density function of the signal and are not affected by the frequency amplitude. That is, it is separated from the specific motion parameter relationship, which can directly reflect the state transition information, and the application range is wider. The kurtosis index is very sensitive to early weak failures, but its stability is not good, and it will decline to a certain extent when the failure occurs; The effective value has good stability, but it is not sensitive to early weak faults; the pulse index can monitor pulse faults well.

To this end, the three indicators are used to divide the state of the system, and the indicator change curve is shown in Figure 6. From top to bottom is the change curve of effective value, impulse index, and kurtosis index. The ordinate is the parameter size and the abscissa is the sample number (arranged in chronological order, the range is 1 to 1000). Observing the kurtosis index, we can find that there is a small change in the range of 1 to 690, a sharp rise at 690, a slight fluctuation at 690 to 920 but little change, a rapid fluctuation at 920, and a small amount rise quickly after delay. The changes in the effective value, the change in the impulse index and the kurtosis index are very similar, and the corresponding mutation points can be found. Therefore, 690 is used as the starting point of early failures and 920 is used as the starting point of serious failures.

According to the above-mentioned neural network fault diagnosis model training, 15 groups of data of vibration signals of 5 types of faults and 3 channels are collected respectively, and two segments of each are intercepted, totaling 60 groups. Extract 50 groups from it as the training set of the neural network, and test the other 10 groups (one for each fault type) as the test set. During the test, select one group of each of the 5 fault types for testing, and the output results are shown in Table 2. It can be seen from the experimental diagnosis results that the 10 sets of data used can basically diagnose the corresponding faults more clearly, but the recognition rate in the cage fault group is not obvious enough, which has a certain relationship with the intercepted data. Therefore, the overall diagnosis result is ideal.

Among them, R1, R2, R3, R4, R5 respectively represent no fault, hidden trouble, minor fault, moderate fault, and severe fault. Through the fault diagnosis of the experimental data BP neural network model, it is verified that the model can identify and diagnose different fault types during the use process. The feasibility of the fault diagnosis method provided under the condition that the parameters and fault categories of the electric spindle of the later machining center are clear is verified.

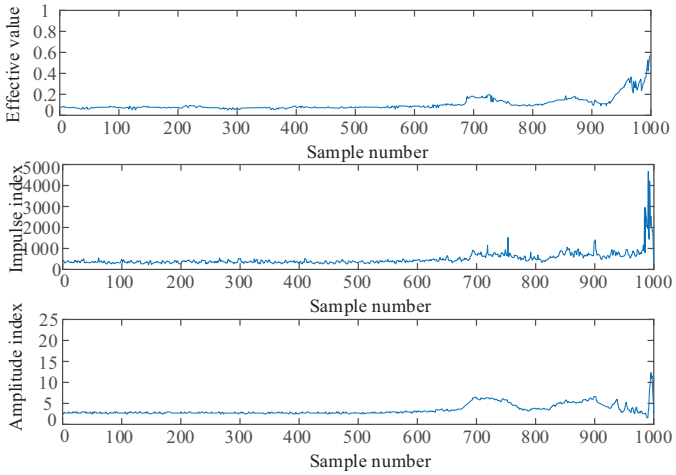


FIGURE 6
Output results of BP neural network

TABLE 2
The output of BP neural network

Expected output	Actual output					Diagnostic result
	R1	R2	R3	R4	R5	
0001	0.733	0.102	0.052	0.115	0.076	No faults
0010	0.175	0.650	0.203	0.085	0.157	Hidden faults
0011	0.214	0.222	0.726	0.111	0.121	Minor faults
0100	0.115	0.236	0.093	0.645	0.088	Moderate faults
0101	0.277	0.143	0.122	0.065	0.548	Severe faults

Through the change of the trend chart, we need to extract useful data information from it, perform feature extraction and fault diagnosis, so as to realize the monitoring and diagnosis function of the whole process. In the trend chart, we should focus on the data in the early warning stage. Because this is to find out the trend information of the failure before the failure occurs, it is very important for the next judgment of the type of failure and preventive measures in advance. The vibration waveforms in the early warning phase and the alarm phase are shown in Figure 9 and Figure 10 below.

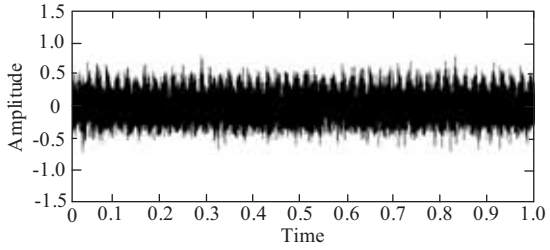


FIGURE 9
The original signal diagram of the early warning stage

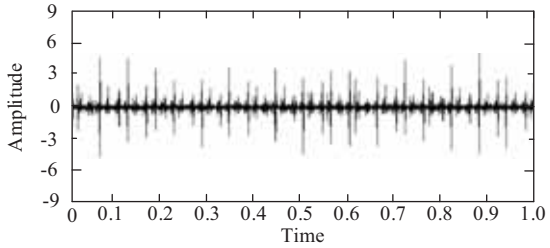


FIGURE 10
The original signal diagram of the alarm stage

As can be seen from the figure 10, the signal amplitude in the early warning stage is low and there is some shock, while the signal vibration amplitude in the warning stage is obviously larger, and there are obvious shocks that are suspected to be periodic. Therefore, we can extract the fault feature information in the early warning stage based on this feature, determine the faulty components and fault locations in advance, and formulate maintenance plans in advance.

According to the comprehensive evaluation model, the remanufacturability of the electric spindle is evaluated, and the technical index of the electric spindle is evaluated by the evaluation method proposed in this paper. According to the previous model algorithm, the quality index $\lambda Q=0.883$, the resource index $\lambda R=0.768$, the environmental index $\lambda E=0.795$, the time index $\lambda T=0.604$, and the remanufacturing cost index $\lambda C=0.668$. Finally, according to the formula, the degree of remanufacturing of the electric spindle is calculated as $\lambda=0.721$, that is, the electric spindle has a higher degree of remanufacturing and can obtain a better comprehensive effect of remanufacturing.

CONCLUSION

This paper proposes a fault diagnosis method of electric spindle based on neural network, and evaluates the remanufacturing of electric spindle by integrating remanufacturing time, remanufacturing product quality, remanufacturing cost, remanufacturing resource consumption and remanufacturing environmental impact. Use wavelet packet decomposition and reconstruction algorithm to remove the noise in the non-linear and unstable signal, and use empirical mode analysis to extract the eigenvalues in the signal; Secondly, the time domain and frequency domain features in the extracted signal are used as input, and the BP neural network fault diagnosis model is used to verify the effectiveness of the system algorithm; Then from the five perspectives of remanufacturing capability, remanufacturing quality, remanufacturing time, remanufacturing environmental impact, and remanufacturing cost, the comprehensive influencing factors of electric spindle remanufacturing are extracted and the evaluation index system is constructed. This paper has made certain research results in the green evaluation mechanism of electric spindle remanufacturing. But there are still some unresolved problems. In the future, it can be calculated which factors have a greater impact on the resource saving rate, and the development direction can be adjusted to improve the resource saving rate.

REFERENCES

[1] Ghobakhloo, M. (2018) The future of manufacturing industry: a strategic roadmap toward Industry 4.0. Journal of Manufacturing Technology Management. 20(1), 15-25.

[2] He, Z.C., Wang, J., Cao, W. M. (2018)Industrial Map of China Automotive Industry and Determinants of Industrial Distribution. Scientific Decision Making. 8(2), 1000-1013.

[3] Olabi, A. G., Wilberforce, T., Abdelkareem, M. A. (2020) Fuel cell application in the automotive industry and future perspective. Energy. 2(14), 118-130.

[4] Li, B., Tian, X., Zhang, M. (2019)Thermal error modeling of machine tool spindle based on the improved algorithm optimized BP neural network. The International Journal of Advanced Manufacturing Technology. 105(4), 1497-1505.

[5] Niaz, H., Sultan, M., Khan, A. A., Mahmood, M. H., Feng, Y., Khan, Z. M., Yasir Niaz, E. D., Mahmood, M. H., Ali, I., Imran, M. A. (2019) Study on evaporative cooling assisted desiccant air conditioning system for livestock application in Pakistan. Fresen. Environ. Bull. 28(11), 8623-8633.

[6] Kizilgeci, F., Mokhtari, N. E. P., Hossain, A. (2020)Growth and physiological traits of five bread wheat genotypes are influenced by different levels of salinity and drought stress. Fresen. Environ. Bull. 29(004), 8592-8599.

[7] Ozkan, A. (2020) Effect of Gold Nanoparticle Functionalized Multi-Walled Carbon Nanotubes on the Properties of Na-Bentonite Water Based Drilling Fluid. Fresen. Environ. Bull. 29(1), 143-151.

[8] Guo, H., Yang, X., Wang, S., Dai, Z. M. (2020) Research on the application of multiplication dimension reduction method in global sensitivity analysis of CNC machine tools. AIP Advances. 10(1), 015-029.

[9] Liu, C., Zhu, Q., Wei, F., Rao, W. Z., Liu, J. J., Cai, W. (2019) A review on remanufacturing assembly management and technology. The International Journal of Advanced Manufacturing Technology. 105(11), 4797-4808.

[10] Kafuku, J. M., Saman, M. Z. M. (2019) Application of Fuzzy Logic in Selection of Remanufacturing Technology. Procedia Manufacturing. 33(9), 192-199.

[11] Zhao, J., Wang, C., Xu, L. (2019) Decision for pricing, service, and recycling of closed-loop supply chains considering different remanufacturing roles and technology authorizations. Computers & Industrial Engineering. 132(21), 59-73.

[12] Wang, J., Liang, Y., Zheng, Y., Gao, R. X., Zhang, D. L. (2020) An integrated fault diagnosis and prognosis approach for predictive maintenance of wind turbine bearing with limited samples. Renewable Energy. 145(11), 642-650.

[13] Asiri, H. F. M., Idris, A. M., Said, T. O. (2020) Monitoring and health risk assessment of some pesticides and organic pollutants in fruit and vegetables consumed in Asir Region, Saudi Arabia. Fresen. Environ. Bull. 29(1), 615-625.

[14] Niaz, H., Sultan, M., Khan, A. A., Mahmood, M. H., Feng, Y., Khan, Z. M., Yasir Niaz, E. D., Mahmood, M. H., Ali, I., Imran, M. A. (2019) Study on evaporative cooling assisted desiccant air conditioning system for livestock application in Pakistan. Fresen. Environ. Bull. 28(11), 8623-8633.

[15] Wan, S., Zhang, X., Dou, L. (2018) Research on the separation method of rolling bearing composite fault under the interference of strong noise sources. Journal of Central South University. 25(8), 16-29.

[16] Zhao, H. Y., Han, H., Wang, J. D. (2018) Research on fault feature extraction method of reciprocating compressor bearing based on wavelet packet fuzzy entropy. Noise and Vibration Control. 38(4), 18-22.

[17] Fu, X., Gao, G. (2018) Rolling bearing fault diagnosis method based on Fourier decomposition and singular value difference spectrum. Acta Metrology. 39(5), 688-692.

[18] Chen, B., He, Y., Yao, B. (2018) Sparse multiclass intelligent fault diagnosis of vibration data of transmission components of spacecraft. Spacecraft Environmental Engineering. 35(4), 359-364.

[19] Lin, T., Chiu, H. (2013) Using independent component analysis and network DEA to improve bank performance evaluation. Economic Modelling. 32(12), 608-616.

[20] Fu, H., Ou, J. (2013) Combining PCA With DEA to Improve the Evaluation of Project Performance Data: A Taiwanese Bureau of Energy Case Study. Project Management Journal. 44(1), 94-106.

[21] Wu, J., Wu, Z., Hollaender, R. (2012) The application of Positive Matrix Factorization (PMF) to eco-efficiency analysis. Journal of Environmental Management. 98(8), 11-14.

[22] Park, H., Behera, S. (2014) Methodological aspects of applying eco-efficiency indicators to industrial symbiosis networks. Journal of Cleaner Production. 64(1), 478-485.

[23] Wu, Z., Sheng, Y., Zhou, X. (2015) Research on the Performance Evaluation of Green Supply Chain from the Perspective of Low Carbon. Management and Technology of Small and Medium-sized Enterprises. 2015(01), 74-80.

[24] Deng, Q., Li, W., Li, X. (2015) Correlation simulation model of green impact factors in mechanical product recycling and remanufacturing system. China Mechanical Engineering. 12(11), 2000-1028.

Received: **28.01.2021**
Accepted: **17.02.2021**

CORRESPONDING AUTHOR

Haixiang Yu
Tianjin Transportation Technical College,
Tianjin 300110–China

e-mail: yuhx2000@126.com

© by PSP Volume 30– No. 09/2021 pages 11025-11026 Fresenius Environmental Bulletin

LETTERS TO THE EDITOR

Rebuttal to:

MAPPING OF HEXAVALENT CHROMIUM REMOVAL RESEARCH: A BIBLIOMETRIC ANALYSIS OF RESEARCH OUTPUTS FROM 1975 TO 2012

Baogang Zhang[1,*], Ye Liu[1], Wenli Huang[2], Jiaxin Li[1], Chuanping Feng[1], Weiwu Hu[1]

[1]Key Laboratory of Groundwater Circulation and Evolution, School of Water Resources and Environment, China University of Geosciences Beijing, Ministry of Education of China, Beijing 100083, China
[2]College of Environmental Science and Engineering, Nankai University, Tianjin 300071, China

vol. 24, pp 4834–4841
Yuh-Shan Ho
Trend Research Centre, Asia University, No. 500, Lioufeng Road, Wufeng, Taichung County 41354, Taiwan
E-mail: ysho@asia.edu.tw

Recently, Zhang et al. [1] published the paper entitled "Mapping of hexavalent chromium removal research: A bibliometric analysis of research outputs from 1975 to 2012". In 2. DATA SOURCES AND METHODOLOGY, authors mentioned that "Documents used in this study were based on the online database of the Science Citation Index (SCI), retrieved from the ISI Web of Science, Philadelphia, USA." which is the same from an earlier article entitled "Assessment of world aerosol research trends by bibliometric analysis" [2]. There is no more ISI Web of Science but Thomson Reuters Web of Science only. Authors also noticed that "According to Journal Citation Reports (JCR), it indexed 8411 major journals with citation references across 186 scientific disciplines in 2013." In fact, there were 8539 journals in Science Citation Index Expanded across 176 Web of Science categories in 2013. In addition, the most parts of "2. DATA SOURCES AND METHODOLOGY" copied from "A review of published wetland research, 1991-2008: Ecological engineering and ecosystem restoration" [3] and "Trends in research on global climate change: A Science Citation Index Expanded-based analysis" [4].

Again, in 2. DATA SOURCES AND METHODOLOGY, authors noticed that "To study the recent tendency intensively, all keywords, both those reported by authors and those assigned by ISI, as well as words in the title in the just past 22 years were identified and separated into 5 spans (1991-1995, 1996-2000, 2001-2005, 2006-2010, and 2011- 2012, respectively), then their ranks and frequencies were calculated, and different words with identical meaning and misspelled keywords were grouped and considered as a single keyword." In last decade, my co-workers and I have reported on examining the distribution of words in article titles, abstracts, keywords, and *KeyWords Plus* at different time periods, for example 2-year [5], 4-year [6], 5-year [7], and 6-year [8] interval, in order to evaluate trends in research topics [6,9-11]. Furthermore, similar rebuttals have also been published in *Environmental Earth Sciences* [12] and *Scientometrics* [13].

In 3.1. Characteristics of publication outputs, authors mentioned "From this research, 13 document types were found among the total 12324 publications during the 38-year study period, and the most frequent document type was articles (11083), which were responsible for 89.9% of the total publications." In fact, 182208 publications were found in 19 document types and the most frequent document type was articles (167655) using the same method as mentioned in the original paper [1]. It is clear that all results in this study are incorrect and discussions are not appropriate.

In 3.1. Characteristics of publication outputs, authors presented Fig. 1 that shows "World SCI-EXPANDED journal publications with chromium or (Cr) or (chrome) in titles during 1975-2012." This overlooks the fact since 1991, abstract information has been included in it the SCI-EXPANDED database [8]. In 1990, only 20% articles had abstract information in SCI-EXPANDED. However, since 1991 more than 90% of articles include abstract information [14]. Analysis of publications before 1991 is not appropriate for investigating publication trends [14]. It is thus clear that analysis of publications before 1991 is not appropriate for investigating publication trends [13]. Therefore, results and discussions about Fig. 1 in the original paper [1] is not appropriate. The same rebuttals were also reported for "A bibliometric study of earthquake research: 1900-2010" [15] and "Progress in global parallel computing research: a bibliometric approach" [16] in *Scientometrics* [13,14]. This type of results by database bias can be also found in earlier publication [14]. There is no more such bias in Ho's publications after that. This type of error could be avoided if authors have had paid more attentions to details about the method from the original paper [14].

It is accepted that citing the original paper is not only respecting authors who presented a novel idea in research but also to read the original idea in detail of the work [17]. An evidence was reported that the original papers even published about 100 years ago, still have extremely high citations in the recent years [18,19]. When a scientific publication duplicate previously published idea, text, equations, or figures without any citations, it frequently is regarded as a sign of possible plagiarism [20,21]. In my view, Zhang et al. [1] should have cited the original paper for what they mentioned in their paper and thereby provided greater accuracy and information details about the idea and the methods that they employed.

REFERENCES

[1] Zhang, B.G., Liu, Y., Huang, W.L., Li, J.X., Feng, C.P. and Hu, W.W. (2015), Mapping of hexavalent chromium removal research: A bibliometric analysis of research outputs from 1975 to 2012. *Fresen. Environ. Bull.*, 24 (12C), 4834-4841.

[2] Xie, S.D., Zhang, J. and Ho, Y.S. (2008), Assessment of world aerosol research trends by bibliometric analysis. *Scientometrics*, 77 (1), 113-130.

[3] Zhang, L., Wang, M.H., Hu, J. and Ho, Y.S. (2010), A review of published wetland research, 1991-2008: Ecological engineering and ecosystem restoration. *Ecological Engineering*, 36 (8), 973-980.

[4] Li, J.F., Wang, M.H. and Ho, Y.S. (2011), Trends in research on global climate change: A Science Citation Index Expanded-based analysis. *Global and Planetary Change*, 77 (1-2), 13-20.

[5] Fu, H.Z., Long, X. and Ho, Y.S. (2014), China's research in chemical engineering journals in Science Citation Index Expanded: A bibliometric analysis. *Scientometrics*, 98 (1), 119-136.

[6] Li, J.F., Zhang, Y.H., Wang, X.S. and Ho, Y.S. (2009) Bibliometric analysis of atmospheric simulation trends in meteorology and atmospheric science journals. *Croatica Chemica Acta*, 82 (3), 695-705.

[7] Ho, H.C. and Ho, Y.S. (2015), Publications in dance field in *Arts & Humanities Citation Index*: A bibliometric analysis. *Scientometrics*, 105 (2), 1031-1040.

[8] Ho, Y.S., Satoh, H. and Lin, S.Y. (2010), Japanese lung cancer research trends and performance in Science Citation Index. *Internal Medicine*, 49 (20), 2219-2228.

[9] Zhang, G.F., Xie, S.D. and Ho, Y.S. (2010), A bibliometric analysis of world volatile organic compounds research trends. *Scientometrics*, 83 (2), 477-492.

[10] Mao, N., Wang, M.H. and Ho, Y.S. (2010), A bibliometric study of the trend in articles related to risk assessment published in Science Citation Index. *Human and Ecological Risk Assessment*, 16 (4), 801-824.

[11] Fu, H.Z., Wang, M.H. and Ho, Y.S. (2013), Mapping of drinking water research: A bibliometric analysis of research output during 1992-2011. *Science of the Total Environment*, 443, 757-765.

[12] Ho, Y.S. (2016a), Rebuttal to: "A bibliometric review on carbon cycling research during 1993–2013" by Zhi et al. (Environ Earth Sci 2015, 74 (7): 6065–6075). *Environmental Earth Sciences*, 75 (9), 819.

[13] Ho, Y.S. (2016b), Rebuttal to: "Progress in global parallel computing research: A bibliometric approach"; Liu et al., Vol. 95, pp 967-983. *Scientometrics*.

[14] Ho, Y.S. (2013), Comments on "A bibliometric study of earthquake research: 1900-2010". *Scientometrics*, 96 (3), 929-931.

[15] Liu, X.J., Zhan, F.B., Hong, S., Niu, B.B. and Liu, Y.L. (2012), A bibliometric study of earthquake research: 1900-2010. *Scientometrics*, 92 (3), 747-765.

[16] Liu, Z.Q., Liu, Y.L., Guo, Y.J. and Wang, H. (2013), Progress in global parallel computing research: A bibliometric approach. *Scientometrics*, 95 (3), 967-983.

[17] Ho, Y.S. (2014), Comments on "Adsorption characteristics and behaviors of graphene oxide for Zn(II) removal from aqueous solution". *Applied Surface Science*, 301, 584.

[18] Ho, Y.S. and Kahn, M. (2014), A bibliometric study of highly cited reviews in the Science Citation Index Expanded™. *Journal of the Association for Information Science and Technology*, 65 (2), 372-385.

[19] Fu, H.Z. and Ho, Y.S. (2014), Top cited articles in adsorption research using Y-index. *Research Evaluation*, 23 (1), 12-20.

[20] Hunter, T.B. (1994), Point-counterpoint. Plagiarism: What is it, whom does it offend, and how does one deal with it? *Academic Radiology*, 1 (2), 191-193.

[21] Noè, L.F. and Batten, D.J. (2006), 'Publish or perish': The pitfalls of duplicate publication. *Palaeontology*, 49 (6), 1365-1367.

Received: **25.05.2017**
Accepted: **01.05.2019**

AUTHOR INDEX

A

Aatif, H. M. 10841
Abbas, H. T. 10841
Abdelmotaleb, I. A. 10782
Abdullah 10790
Acar, C. 10633
Afsheen, Z. 10790
Afzal, A. 10899
Ahmad, I. 10474
Ahmad, J. 11002
Ahmad, R. 10728
Ahmed, I. 10951
Akar, O. 10908
Akpinar, A. 10515
Aksu, A. 10825
Aleem, M. 10728
Aleksandar, R. 10890
Ali, Q. S. 10474
Ali, S. 10474
Altikulac, A. 10863
Amer, M. M. 10941
Arslan, C. 10976
Arslan, D. 10515
Attaullah 10790
Avci, O. 10836
Awad, M. 10941

B

Basit, A. 10474
Bibi, A. 10790
Bibi, P. 10790
Bin-Yousaf, M. T. 10951
Bostan, N. 10899
Bulut, O. 10836
Bulut, S. 10976

C

Caglar, A. 10586
Caglar, N. B. 10825
Cao, C. 10602
Cao, X. 10871
Carlak, H. F. 10754
Cebe, G. E. 10505
Chen, C. 10625, 10849
Chen, K. 10449, 10772
Chen, X. 10797
Chen, Y. 10652, 10849
Cui, D. 10551
Cui, H. 10530
Cui, L. 10880

D

Dai, B. 10712
Deng, H. 10690
Der, G. 10505
Dik, I. 10836
Din, S. U. 10474
Dong, M. 10856
Dou, Z. 10559
Du, H. 10718
Du, K. 10797
Du, L. 10592
Dumanoglu, Z. 10983
Duru, A. A. 10435

E

Elmalı, D. A. 10435
El-Menshawi, M. E. 10989
El-Nagar, A. B. 10782
El-Okkiah, S. A. F. 10989
El-Sabagh, A. 10941
Erdogan, M. A. 10505
Erum, S. 10899
Eser, Y. 10970

F

Farooq, T. H. 10951
Farroh, K. Y. 10989
Fazal-i-Wahid 10474
Fu, X. 10763

G

Gao, H. 10602
Gecer, E. N. 10441
Gokmen, S. 10586
Gul, S. 10951
Guo, L. 10815
Guo, X. 10411
Gurer, T. 10515
Guvenc, S. 10568

H

Habib, A. 10841
Hacioglu, A. 10522
Hag, D. E. 10941
Hamayun, M. 11002
Han, J. 10482
Han, M. 10705
Han, Z. 10712
Hanif, S. 10728
Hao, Q. 10849
Hasan, E. A. 10941
Hatipoglu, R. 10463
He, F. 10690
Hegazy, R. A. 10782
Hu, G. 10797
Hu, R. 10559
Huan, C. 10690
Huang, J. 10871
Huang, L. 10643
Huang, X. 10849
Huanlei, Z. 11009
Hussain, A. 11002
Hussain, Z. 10728, 10899

I

Ijaz, M. 10841
Ikram, K. 10841
Imran, M. A. 10728
Inal, I. 10463
Iqbal, A. 11002
Iqbal, M. A. 10941
Irum, S. 10899
Isik, E. 10492

J

Jan, S. A. 10790
Jelena, Z. 10890
Jiang, C. 10602
Jiang, M. 10807
JingYu 10738

K

Kan, Y. 10559
Kandemir, K. 10754
Karakaya, H. 10530
Karapinar, S. 10427
Karhan, M. 10522
Kaya, C. 10441
Khalid, I. 10841
Khalil, S. K. 10474
Khan, F. A. 10899
Khan, H. 10899
Khan, I. H. 10474
Khan, M. 10790
Khan, N. 11002
Khan, Z. M. 10728
Kilinc, E. 10505
Kiremitci, S. A. 10505
Kizilgeci, F. 10941
Kompe, Y. O. 10530
Kong, F. 10797
Kong, P. 10602
Konyalioglu, S. 10505
Korkmaz, N. E. 10825
Kula, H. O. 10568
Kutay, H. 10435

L

Lee, I.-J. 11002
Lei, W. 11009
Li, G. 10849
Li, H. 10690
Li, J. 10602, 10675, 10690
Li, L. 10610
Li, M. 10411
Li, P. 10482
Li, Q. 10763
Li, S. 10690, 10748
Li, W. 10925
Li, Z. 10718
Liang, N. 10763
Liaudanskiene, I. 10576
Lin, L. 10665
Liu, C. 10610
Liu, H. 10449, 10748
Liu, X. 10807, 10856
Liu, Z. 10602
Ljiljana, S. 10890
Lu, N. 10797
Lu, Q. 10625
Lucas, J. S. 10515
Luo, L. 10925
Luo, T. 10871
Luo, Y. 10690
Lv, J. 10705

M

Ma, F.	10482	Meng, C.	10592
Mahmood, M. H.	10728	Milena, G.	10890
Mansha, M. Z.	10841	M-Omar, A. H.	10989
Mansoor, M. Z.	10841	Moussa, W. M.	10782
Mao, H.	10856	Mubin, S.	10790
Mehmood, T.	10728	Mutlu, V. A.	10530
Memon, M. S.	10449		

N

Natasa, M. B.	10890	Niu, J.	10592
Nawaz, M. F.	10951		

O

Ou, J.	10933	Ozturk, F.	10941
Ou, L.	10849	Ozturk, G.	10983
Ozturk, A.	10908	Ozturk, Z.	10908

P

Peng, H.	10545	Peter, M.	10449
Peng, W.	10772		

Q

Qian, L.	10849	Qiu, X.	10772
Qiang, Y.	10610		

R

Rabi, F.	10899	Ren, S.	10807
Radomir, I.	10890	Riaz, M.	10790
Rehman, K. U.	11002	Rizwan, M.	10951

S

Sajid, M.	10474	Slavoljub, D.	10890
Salman, M.	10790	Song, N.	10592
Segmenoglu, M. S.	10685	Soomro, S. A.	10449
Sessiz, A.	10449	Soomro, Z. A.	10449
Shah, F.	11002	Sorour, S.	10941
Shah, M.	10790	Stanimir, Z.	10890
Shah, S. T.	10474	Sultan, M.	10728
Sher, H.	10899	Sun, A.	10690
Simsek, A.	10836	Sun, L.	10772
Siyal, A. A.	10449		

T

Tao, H.	10871	Tosun, S.	10908
Taseer, Y. R.	10728	Tugan, V.	10492
Topcuoglu, H.	10685	Turgut, K.	10522
Topkara, E. F.	10457		

U

Ullah, A.	10728	Unal, N.	10522
Ullah, I.	10474	Unlusayin, M.	10754
Ullah, O.	10790	Uzunali, A.	10633

V

Varol, M. I.	10515	Velykis, A.	10576

W

Wagan, B. 10449
Wang, B. 10602, 10856
Wang, C. 10961
Wang, G. 10797, 10856
Wang, J. 10871, 10933
Wang, M. 10602, 11011
Wang, Q. 10411
Wang, R. 10602
Wang, W. 10530, 10856
Wang, Y. 10705
Wu, G. 10482
Wu, S. 10643

X

Xi, S. 10871
Xia, C. 10610
Xiaoli, J. 11009
Xing, W. 10482
Xing, X. 10643
Xiong, R. 10482
Xu, L. 10675
Xu, Z. 10482, 10856
Xue, B. 10675

Y

Yang, J. 10748
Yang, Q. 10602
Yang, X. 10705, 10712
Yang, Z. 10449
Yapici, O. 10836
Yasin, G. 10951
Yavru, S. 10836
Yengin, C. 10505
Yi, K. 10690
Yildiz, M. 10522
Yu, H. 11011
Yu, M. 10763
Yu, Y. 10652
Yuan, W. 10659
Yucel, C. 10463
Yucel, D. 10463
Yucesan, Z. 10427
Yuksel, O. 10435
Yuncu, A. 10515

Z

Zhang, B. 10797
Zhang, H. 10871
Zhang, Q. 10643
Zhang, S. 10610
Zhang, Y. 10675, 10697, 10748
Zhao, D. 10610
Zhao, W. 10856
Zhao, X. 10772
Zheng, Z. 10610
Zhou, W. 10856
Zhou, Y. 10551, 10748
Zukaitis, T. 10576

SUBJECT INDEX

A

Acacia stenophylla 11002
ACE inhibition 11002
Acetyl-CoA Carboxylase (ACCase) 10797
Afforestation 10951
Ag-NORs 10976
Agricultural economy 10933
Agroforestry 10951
AHP 10718
Alleviate burden 10705
Anacamptis laxiflora 10535
Analysis 10551
Analysis of Proportional Changes 10890
Analytic hierarchy process 10712
Animal feed 10782
anthocyanins 10441
Anthropogenic 10568
Antimicrobial 11002
Antioxidant 10505, 11002
antioxidant activity 10441
Apical dominance 10474
Apriori algorithm 10807
Automobile radiator 10492
Avena fatua 10797

B

Bacillus thuringiensis 10457
Battery 10908
Benzyl Amino Purine 10474
Biochar 10951
biochemical 10989
Biochemical parameters 10836
biological toxicity 10697
Black seed oil 10685
Black spot 10841
Block MJG-60 10856
BP neural network 10559
building layout 10625
building material 10863
bullvain 10690
BVDV 10836

C

cadmium concentration 10690
Cancer-related fatigue 10705
Carbon dioxide fixation 10411
Carbonized steel slag 10411
Carrot 10441
Case Study 10890
C-banding 10976
chitosan 10989
chopping power 10782
City Silhouette 10633
Clay loam soil 10576
clayey 10989
Climate 10970
coalbed methane 10602
Complex environment 10807
Compost tea 10941
Conservation 10535
Construction 10551
Consumption 10457
cooking processes 10441
coordinated development 10933
copper-sulfur mining area 10849
Cotton 10989
countermeasures 10665
coupling and coordinated development 10925
Coupling coordination degree 10712
Coupling development 10551
Crataegus monogyna 10505
crop residue 10782
Cutaneous leishmaniasis 10790

D

Debris Flow 10610
Degraded Lands 10951
Dianthus 10474
Digitization of Esthetics 10633
Diplocarpon rosae 10841
Discriminant indicators 10675
diversity 10568
DLS 10989
Drinking water source 10728
Dynamic update 10880

E

ecological adaptability 10763
ecological building 10763
Ecological civilization 10551, 10659
ecological efficiency 10665
Ecological 10625, 10718, 10738, 10961
ecological environment protection 10925
Ecological footprint 10665
ecological fragility 10559
Ecological perspective 10545
Ecological tourism 10659
Ecology 10652
economic development 10545, 10712, 10815
Economic growth 10652
Economy 10530
Ecosystems 10530
Eddy current tool 10748
electric spindle 11011
Energy consumption 10652
Entropy 10633
environmental Kuznets curve 10815
Environmental protection 10697, 10807, 11011
environmental quality 10738, 10815
environmental resources 10665
Epidemiological status 10790
epiphytic lichen 10568
Erosion Potential Method 10890
Evaluation index 10530
experimental field 10690

F

fault diagnosis 11011
Feature extraction 10961
Fenoxaprop-p-ethyl Resistance 10797
Fish freshness 10754
Fish species 10825
Fixed oil extraction 11002
Floriculture 10474
flow regulator 10697
fluent 10748
Flume experiments 10675
foliar application 10989
Forage Quality 10463
Forage Yield 10463
Fourier transform with Nuttall window 10643
fracturing 10602
Fungicide 10841
Fuzzy Comprehensive Evaluation 10610
Fuzzy evaluation 10738

G

Gas field 10748
gastrointestinal 10685
gel oil displacement agent 10856
Gelatin capsule shell 11009
GIS 10961
GIS tools 10728
Golden Horn Estuary 10825
Green energy-saving building 10807
green remanufacturing 11011
Groundwater quality maps 10728
Growth retardants 10474
Guizhou Province 10925

H

Harvest times 10522
Head and neck tumors 10705
Heat transfer 10492
heavy metal accumulation 10690
heavy metal pollution 10690, 10849
Heavy metals 10728, 11009
Henan Province 10815
hepatotoxicity 10685
heterogeneity 10602
histopathology 10685
HOMER 10908
HPLC 10505
Hybrid Renewable Energy 10908
hydrochemistry 10772

I

ICP-MS 11009
image processing 10754
In vitro establishment 10899
Industrial CT 10592
Innovative research 10545
Intercropping 10463
intermittent aeration 10871
Inverse distance weighted 10728
Istanbul 10825

K

Karyotype 10976
K-humate 10941

L

landscape 10559
Leaf positions 10522
Leishmania 10790
lime sludge 10576
Liquid loading 10748
Loading rate 10449
local binary pattern 10754
Lycosidae 10515

M

machine learning 10754
Maize 10463
Malakand 10790
Malic acid 10435
Mantı 10586
Marine algae statistics database 10880
mass attenuation coefficient 10863
MDA 10836
Mechanical properties 10411, 10449
Mental resilience 10705
methotrexate 10685
methyleneblue 10482
microclimate 10568
Mitochondrial Cytochrome Oxidase I (COI) 10515
Moisture 10449
Molases 10941
Monte Carlo Simulation 10610
Multi-criteria Decision-making 10610
Municipal sewage 10643
Mutation Points 10797
Mycorrhiza 10535
Mytilus galloprovincialis 10825

N

nano silicone 10856
Nanofluid 10492
Nano-Micronutrients 10941
nanoparticles 10989
Nanotechnology 10989
National Park 10568
Natural radioactivity 10863
natural reverse 10559
Neuroprotective 10505
Nitrogen transformation function gene 10871

O

old residential area 10625
Optimization 10908
Orchid reintroduction 10535
Orchidaceae 10535
Ordos Basin 10856
Organic amendments 10941
Oriental beech 10427
Orthogonal experiment 10748

P

P. italica 10515
P. tatarica 10515
Pardosa proxima 10515
Path 10545
PCR 10790
persistently infected 10836
Pharmaceuticals 10825
phenolics 10441
Phenoloxidase 10457
Photocatalyst 10482
physical and chemical factors 10871
Physico-chemical 10728
Pinus nigra 10970
planning method 10625
planning strategy 10625
Plant resources 10559
Post-traumatic growth 10705
precommercial thinning 10427
Prefabricated building 10763
principal component analysis 10815
probability and statistics method 10718
productivity 10602
Prunus Armeniaca. L 10899

Q

Qinshui Basin 10602

R

radiation shielding 10863
railway construction 10718
Rebaudioside A 10522
reduced tillage 10576
redundancy analysis 10871
regeneration 10970
Remote sensing image 10961
reservoir plugging 10856
reservoir reconstruction 10856
Resource utilization 10411
Resources 10659
Rice straw 10449
Risk Assessment 10610
River patterns 10675
River simulation 10675
Riverside area 10961
Rose Black spot 10841
rural ecological environment 10933
Rural tourism 10738

S
Safety 11009
Salinity 10951
Sampling 10728
Saturated hydraulic conductivity 10592
Secondary compound 10457
seed pelleting 10983
seedling 10970
seedling emergence 10983
Sensitivity Analysis 10908
sensory quality 10586
Serbia 10890
Shallow groundwater 10772
shared space 10625
Silage quality 10435
Silhouette 10633
Silhouette Analysis 10633
silviculture 10970
Sim 10474
Single straight tube coriolis flowmeter 10643
Singular value decomposition 10643
Sino African cooperation 10933
Skyline 10633
soil 10849
soil macropore 10592
soil organic carbon 10576
Solanum tuberosum L. 10983
source 10849
Southern Anhui residential 10763
Sowing Pattern 10463
Soybean 10463
spatial and temporal characteristics 10665
Spermophilus 10976
Stevia rebaudiana 10522
Stevioside 10522
storage 10586
Surface 10899
Survival 10457
Sustainable development 10659, 11011

T
TAC 10836
Tem 10989
temperature resistance 10697
Tense 10880
thinning intensity 10427
thiobarbutiric acid 10586
Tourism 10665, 10712
tourism economic development 10925
Tracer method 10849
True Potato Seed 10983

U
Uludağ 10568
Ulva laccuta 10825
Update weights 10880
UV-C 10586

V
Variety 10449
Vetch 10435
visible light irradiation 10482

W
water infiltration 10592
water quality assessment 10772
water-based drilling fluid 10697
water–rock interaction 10772
wavelet transform 10754
Whey 10435

X
XRF 10863

Z
Zeta potential 10989

1,2,3,……0
3-D characteristics 10592

FEB – GUIDE FOR AUTHORS

General

FEB accepts original papers, review articles, short communications, research abstracts from the entire sphere of environmental-chemistry,-biology,-microbiology,- technology, -biotechnology and-management, furthermore, about residue analysis/ and ecotoxicology of contaminants.

Acceptance or no acceptance of a contribution will be decided, as in the case of other scientific journals, by a board of reviewers. Papers are processed with the understanding that they have not been published before (except in form of an abstract or as a part of a published lecture, review or thesis);that they are not under consideration for publication elsewhere; that their publication has been approved by all co-authors, if any, as well as- tacitly or explicitly- by the responsible authorities at the institute where the work has been carried out and that, if accepted, it will not be published elsewhere in the same form, in either the same or another language, without the consent of the copyright holders.

Language

Papers must be written in English. Spelling may either follow American (Webster) or British (Oxford) usage but must be consistent. Authors who are less familiar with the English language should seek assistance from proficient colleagues in order to produce manuscripts that are grammatically and linguistically correct.

Size of manuscript

Review articles should not exceed 30 typewritten pages. In addition up to 5 figures may be included.

Original papers must not exceed 14 typewritten pages. In addition up to 5 figures may be included.

Short-Communications should be limited to 4 typewritten pages plus not more than 1 illustration.

Short descriptions of the authors, presentation of their groups and their research activities (with photo) should together not exceed I typewritten page. Short research abstracts should report in a few brief sentences (one-fourth to one page) particularly significant findings. Short articles by relative newcomers to the chemical innovation arena highlight the key elements of their Master and PhD-works in about I page.

Book Reviews are normally written in-house, but suggestions for books to review are welcome.

Preparation of manuscript

Dear authors,

FEB is available both as printed journal and as online journal on the web. You can now e-mail your manuscripts with an attached file. Save both time and money. To avoid any problems handling your text please follow the instructions given below:

When preparing your manuscripts have the formula K/SS (Keep It Simple and Stupid) in mind. Most word processing programs such as MS-Word offer a lot of features. Some of them can do serious harm to our layout. So please do not insert hyperlinks and/or automatic cross-references, tables of contents, references, footnotes, etc.

1. Please use the standard format features of your word processor (such as standard.dot for MS Word).
2. Please do not insert automatisms or secret link-ups between your text and your figures or tables. These features will drive our graphic department sometimes mad.
3. Please only use two fonts for text or tables "Times New Roman" and for graphical presentations "Arial".
4. Stylesheets, text, tables and graphics in shade of grey
5. Turn on the automatic language detection in English (American or British)
6. Please - check your files for viruses before you send them to us!!

Manuscripts should be uploaded on our website prt-parlar.de

Thank you very much!

STRUCTURE OF THE MANUSCRIPT

Title page: The first page of the manuscript should contain the following items in the sequence given: A concise title of the paper (no abbreviations). The names of all authors with at least one first name spelled out for every author. The names of Universities with Faculty, City and Country of all authors.

Abstracts: The second page of the manuscript should start with an abstract that summarizes briefly the contents of the paper (except short communications). Its length should not exceed 150-200 words. The abstract should be as informative as possible. An extended repetition of the paper's title is not considered to be an abstract.

Keywords: Below the Summary up to 6 key words have to be provided which will assist indexers in cross-indexing your article.

Introduction: This should define the problem and, if possible, the frame of existing knowledge. Please ensure that people not working in that particular field will be able to understand the intention. The word length of the introduction should be 150 to 300 words.

Materials and methods:
Please be as precise as possible to enable other scientists to repeat the work.

Results: Only material pertinent to the subject must be included. Data must not be repeated in figures and tables.

Acknowledgements: Acknowledgements of financial support, advice or other kind of assistance should be given at the end of the text under the heading "Acknowledgements". The names of funding organisations should be written in full.

References: Responsibility for the accuracy of references rests with the authors. References are to be limited in number to those absolutely necessary. References should appear in numerical order in brackets and in order of their citation in the text. They should be grouped at the end of the paper in numerical order of appearance. Abbreviated titles of periodicals are to be used according to Chemical or Biological Abstracts, but names of lesser known journals should be typed in full. References should be styled and punctuated according to the following examples:

ORIGINAL PAPERS:
l. Author, N.N. and Author, N.N. (Year) Full title of the article. Journal and Volume, first and last page.

BOOK OR PROCEEDING:
2. Surname, N., Surname, N.N., Surname, N.N., Surname, N. (Year) Title of the contribution. In: Title of the book or proceeding. Volume, Publisher, City, first and last page

DOCTORAL THESIS:
3. Author, N.N. (Year) Title of the thesis, University and Faculty, City

UNPUBLISHED WORK:
Papers that are unpublished but have been submitted to a journal may be cited with the journal's name followed by "in press". However, this practice is acceptable only if the author has at least received galley proofs of his paper. In all other cases reference must be made to “unpublished work" or "personal communication".

Discussion and Conclusion: This part should interpret the results in reference to the problem outlined in the introduction and of related observations by the author/s or others. Implications for further studies or application may be discussed. A conclusion should be added if results and discussion are combined.

Corresponding author: The name of the corresponding author with complete postal address